studies in surface science and catalysis

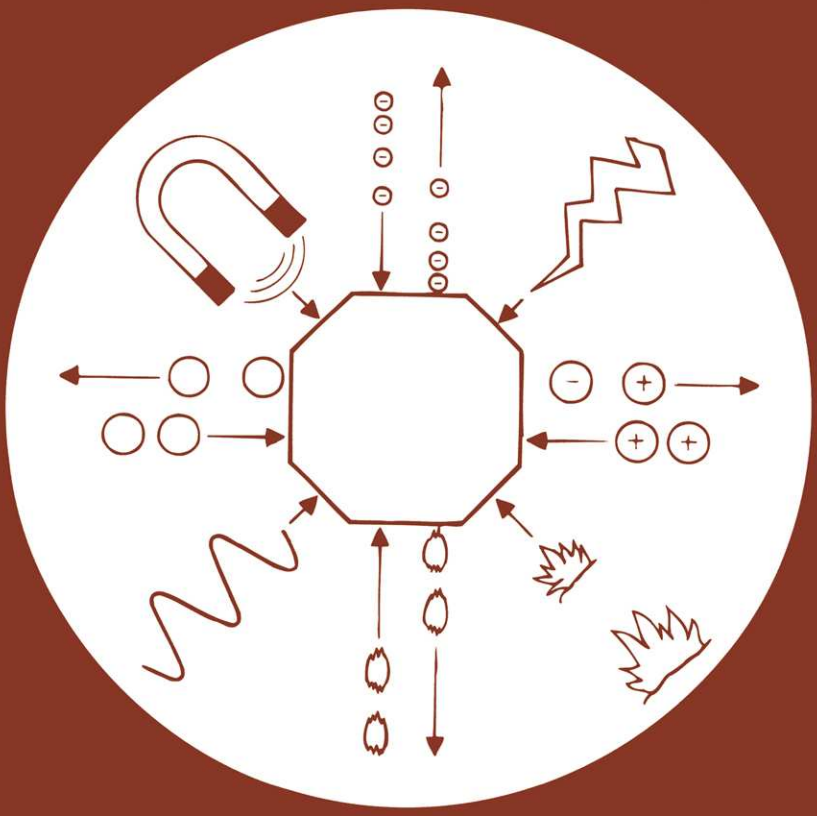

99

ADSORPTION ON NEW AND MODIFIED INORGANIC SORBENTS

A. Dąbrowski
V.A. Tertykh
(editors)

elsevier

Studies in Surface Science and Catalysis 99

ADSORPTION ON NEW AND MODIFIED INORGANIC SORBENTS

This Page Intentionally Left Blank

Studies in Surface Science and Catalysis

Advisory Editors: B. Delmon and J.T. Yates

Vol. 99

ADSORPTION ON NEW AND MODIFIED INORGANIC SORBENTS

Editors

A. Dąbrowski
Faculty of Chemistry, Maria Curie-Skłodowska University, Lublin, Poland

V.A. Tertykh
Institute of Surface Chemistry, Academy of Sciences of Ukraine, Kiev, Ukraine

1996

ELSEVIER
Amsterdam — Lausanne — New York — Oxford — Shannon — Tokyo

ELSEVIER SCIENCE B.V.
Sara Burgerhartstraat 25
P.O. Box 211, 1000 AE Amsterdam, The Netherlands

ISBN 0-444-82179-1

This book is printed on acid-free paper.

Printed in The Netherlands

PREFACE

A need for a profound book on adsorption and chemisorption on inorganic sorbents has existed for a long time. Justification for such a book results from the biological, environmental and technological importance of inorganic sorbents and significance of adsorption phenomena at the solid/gas as well as solid/liquid interfaces. The range of the work has been determined by the attributes of the above mentioned fields of science. As the themes to be considered refer to such a wide spectrum, no single author could write a critical review or paper on more than a very limited number of problems. That is why this book includes chapters written by authoritative specialists. We would like to present a study including papers and critical reviews describing theories and experiments, systems and methods used in the investigations and in many cases the examples of their applications. Moreover, we would like to point out problems and questions already solved but requiring further researches.

The sorbents discussed in this book are first of all synthetic mineral ones. Such materials as zeolites and organic carriers will not be considered as they have already been discussed in numerous monographs. Each contribution deals with a problem critically showing its development and presenting a summary of the latest results.

The book is divided into three sections consisting of chapters arranged in a consistent order, though some chapters could be put in the second or third section. On the other hand, a uniform treatment and style cannot be anticipated in the book that represents the efforts of many authors. Despite this, the presented works provide the comprehensive, high standard and modern study on the structure, investigations, preparation of inorganic sorbents, their numerous applications and deal with the adsorption on new and chemically modified inorganic solids.

Section 1 considers the methods of synthesis and physico-chemical properties of new types of inorganic sorbents (complex carbon-mineral sorbents, co-precipitated hydroxides, functional polysiloxane sorbents, porous glasses with controlled porosity, colloidal silicas, aluminium oxyhydroxide colloids, apatites). These sorbents are widely used in scientific investigations, in chemical practice and are important from a technological point of view. The presented results provide additional possibilities for the preparation of inorganic sorbents possessing unique adsorption and catalytic properties. Moreover, Section 1 presents the possibilities of the computational studies on the design of synthetic materials for selective adsorption of different substances.

By chemical modification of the oxide surfaces it has become possible to design new, reliable, highly-specified adsorbents, selective catalysts, polymer extenders, efficient thickeners of dispersive media. The interest in the modified oxides has increased for a few years as a result of favourable perspectives for their application for various kinds of the chromatographic separation, preparation of grafed metal complex catalysts, immobilized enzymes and other biologically active compounds. Introduction of the surface

modified silicas into practice of the high-performance liquid chromatography both in the reversed and normal phases was the most pronounced.

Section 1 presents the studies both on the structure of the formed surface compounds and the main regularities of the chemisorption processes and on kinetics of chemisorption from the gas phase on oxide surfaces. Prospective ways for the immobillization of different active compounds have been also proposed.

The next stage of the presented investigations shows the elaboration of the physicochemical approaches for the quantitative prediction of the alternations in the properties of the compound after its chemisorption on the solid surface. This is important to improve the experimental possibilities for the characterization of the interactions of the active surface sites with the grafed compound. Moreover, it is necessary to take into account the influence of the residual structural hydroxyl groups practically always remaining modified oxide surface. The mutual influence of the neighbouring molecules anchored on the oxide surface should be taken into account as well. Elucidation of the chemical modification influence on the alterations in the porous structure of the oxide matrices, working out the principles of the mosaic surface modification for the creation of different sites on the surface and some practical objectives are of significant importance.

The principal aim of Sections 2 and 3 dealing with the adsorption from gaseous and liquid phases is to present various approaches for investigating the surface characteristics of inorganic sorbents. For this to reach the following methods have been presented:

- adsorption studies assuming the well-defined models of adsorption systems,
- calorimetric studies of adsorption phenomena,
- chromatographic studies for examining the surface properties of original and modified solid sorbents,
- experimental techniques, such as NMR techniques, X-ray analysis, IR spectra, etc.,

for measuring surface parameters, where this seems useful. Moreover, in many cases the calorimetric and apparatus techniques are discussed and related to the analysis of the adsorption investigations.

In Section 2 the phenomenon of the phase transitions in the layers adsorbed on solid sorbents is also discussed.

Section 3 presents the chapters both on adsorption from nonelectrolyte mixtures and on ion adsorption at the oxide/electrolyte interface. This interface is probably the most important in science, life and technology. Moreover, the ionic surfactant adsorption, mainly from aqueous solutions onto various inorganic sorbents has been considered.

It should be pointed out that only a few chapters of the book present the problems including carbonaceous sorbents. It results from the fact that (e.g. Chapter 2.10) the micropore filling mechanism for carbon porous sorbents is relatively well known and therefore this knowledge can be a basis for analogous considerations on inorganic sorbents. On the other hand, in Chapter 3.10 concerning the chromatography of fullerenes, the silicas with bonded fullerenes are used for the separation of organic compounds by the reversed phase liquid chromatography.

In some chapters of Sections 2 and 3 the adsorption and desorption kinetics is discussed in terms of the phenomena including inorganic sorbents.

Many areas in which technological novelty has involved this kind of substances and surface phenomena related to them, have been developed to be more of an art than science. From this point of view, understanding of the scientific backgrounds is very important for a large group of research workers both in academic institutes and industrial laboratories, whose professional activity is related to the fields of surface chemistry, inorganic chemistry, adsorption, ion-exchange, catalysis, chromatography and spectroscopy of the surface phenomena. This book is meant for the above mentioned potential readers and for the students of graduate and postgraduate courses.

It should be emphasized that each of 34 chapters gives not only brief, current knowledge about the studied problem but is also a source of topical literature on it. Thus, each chapter can constitute a literature guide for a given subject and encourage the reader to get to know a problem and develop the own studies in this exciting area of surface chemistry.

A. Dąbrowski

This Page Intentionally Left Blank

AUTHOR INDEX

1. E.V.Aksenenko – Institute of Colloid Chemistry and Chemistry of Water, Academy of Sciences of Ukraine, pr.Acad.Vernadsky 42, 252680 Kiev, Ukraine

2. V.Bakaev – Department of Chemistry, 152 Davey Laboratory, Penn State University, University Park, PA 16802, U.S.A.

3. H.Ballard – Centre de Recherches sur la Physico-Chimie des Surface Solides, 24 avenue du President Kennedy, 68200 - Mulhouse, France

4. J.Barrow – CSIRO, Division of Soils, Private Bag, Wembley, WA 6014, AUSTRALIA

5. L.A.Belyakova – Institute of Surface Chemistry, Academy of Sciences of Ukraine, pr. Nauki 31, 252022 Kiev, Ukraine

6. V.I.Bogillo – Institute of Surface Chemistry, Academy of Sciences of Ukraine, pr. Nauki 31, 252022 Kiev, Ukraine

7. S.V.Bondarenko – Institute of Colloid Chemistry and Chemistry of Water, Academy of Sciences of Ukraine, pr.Acad.Vernadsky 42, 252680 Kiev, Ukraine

8. T.Borowiecki – Faculty of Chemistry, Maria Curie-Skłodowska University, 20031 Lublin, Poland

9. J.-Y.Bottero – Laboratoire Environnement et Mineralurgie, URA 235 CNRS, ENSG, INPL, BP 40, 54501 Vandoeuvre Cedex, France

10. J.Cases – Laboratoire Environnement et Mineralurgie, URA 235 CNRS, ENSG, INPL, BP 40, 54501 Vandoeuvre Cedex, France

11. G.F.Cerofolini – Istituto Guido Donegani EniChem, Via G.Fauser 4, 28100 Novara NO, Italy

12. R.Charmas – Faculty of Chemistry, Maria Curie-Skłodowska University, 20031 Lublin, Poland

13. A.Dawidowicz – Faculty of Chemistry, Maria Curie-Skłodowska University, 20031 Lublin, Poland

14. V.Ya.Davydov – Laboratory of Adsorption and Gas Chromatography, Department of Chemistry, Moscow State University, Leninskije Gory, 119899 Moscow, Russia

15. A.Dąbrowski – Faculty of Chemistry, Maria Curie-Skłodowska University, 20031 Lublin, Poland

16. I.Dekany – Department of Colloid Chemistry, Attila József University, Szeged, Aradi Vertanuk tere 1, H-6720 Hungary

17. S.D.Dubrovensky – Department of the Solid Chemistry of the St.Petersburg Technological Institute, Moscow St.26, 198013 St.-Petersburg, Russia

18. A.Yu.Fadeev – Laboratory of Organic Catalysis, Department of Chemistry, Moscow State University, Leninskije Gory, 119899 Moscow, Russia

19. J.K.Garbacz – Faculty of Chemical Technology and Engineering, Polytechnical and Agriculture University, 85326 Bydgoszcz, Poland

20. M.D.Garcia – Departamendo de Quimica Inorganica, Facultad de Granada, Universidad de Granada, 18071 Granada, Spain

21. F.J.L.Garzón – Departamendo de Quimica Inorganica, Facultad de Granada, Universidad de Granada, 18071 Granada, Spain

22. T.C.Golden – Air Products and Chemicals, Inc., 7201 Hamilton Boulevard, Allentown, PA, 18195, U.S.A.

23. J.Goworek – Faculty of Chemistry, Maria Curie-Skłodowska University, 20031 Lublin, Poland

24. T.Ishikawa – Osaka University Education, School of Chemistry, 4-898-1 Asahigaoka, Kaishiwara-shi, Osaka-fu 582, Japan

25. M.Jaroniec – Department of Chemistry, Kent State University, Kent, Ohio 44242, U.S.A.

26. N.Kallay – Laboratory of Physical Chemistry, Faculty of Science, University of Zagreb, 41000 Zagreb, Croatia

27. K.Kaneko – Chiba University, Department of Chemistry, Faculty of Science, 1-33 Yayoi, Inage, Chiba 263, Japan

28. M.Katagiri – Department of Molecular Chemistry and Engineering, Faculty of Engineering, Tohoku University, Aoba, Aramaki, Aoba-ku, Sendai 980, Japan

29. I.Kobal – Department of Physical and Environmental Chemistry, J.Stefan Institute, 61000 Ljubljana, Slovenia

30. V.S.Komarov – Institute of General and Inorganic Chemistry, Byelorussian Academy of Sciences, Syrganova Str.,9, 220606 Minsk, Byelorussia

31. S.Kondo – Fukui Institute of Technology, 12-24 Uzumasa-Midoriga-Oka, Neyagawa-shi 572, Japan

32. L.Koopal – Wageningen Agricultural University, Department of Physical and Colloid Chemistry, Dreijenplein 6, 6703 HB Wageningen, The Netherlands

33. M.Kubo – Department of Molecular Chemistry and Engineering, Faculty of Engineering, Tohoku University, Aoba, Aramaki, Aoba-ku, Sendai 980, Japan

34. R.Leboda – Faculty of Chemistry, Maria Curie-Skłodowska University, 20031 Lublin, Poland

35. G.V.Lisichkin – Laboratory of Organic Catalysis, Department of Chemistry, Moscow State University, Leninskije Gory, 119899 Moscow, Russia

36. A.A.Malkov – Department of the Solid Chemistry of the St.-Petersburg Technological Institute, Moscow St.26, 198013 St.-Petersburg, Russia

37. A.A.Malygin – Department of the Solid Chemistry of the St.-Petersburg Technological Institute, Moscow St.26, 198013 St.-Petersburg, Russia

38. A.Miyamoto – Department of Molecular Chemistry and Engineering, Faculty of Engineering, Tohoku University, Aoba, Aramaki, Aoba-ku, Sendai 980, Japan

39. P.Nikitas – Faculty of Sciences, Department of Chemistry, Laboratory of Physical Chemistry, 54 006 Thessaloniki, Greece

40. E.Papirer – Centre de Recherches sur la Physico-Chimie des Surfaces Solides, 24 avenue du President Kennedy, 68200 - Mulhouse, France

41. R.V.Parish – University of Manchester, Institute of Science and Technology, Department of Chemistry, Manchester M60 1QD, U.K.

42. S.Partyka – Laboratoire des Agregats Moleculaires et Materiaux Inorganiques, Universite des Sciences et Techniques du Languedoc, pl.E.Bataillon, 34095 Montpellier Cedex 05, France

43. A.Patrykiejew – Faculty of Chemistry, Maria Curie-Skłodowska University, 20031 Lublin, Polan

44. M.B.Rao – Air Products and Chemicals , Inc., 7201 Hamilton Boulevard, Allentown, PA, 18195, U.S.A.

45. J.Rayss – Faculty of Chemistry, Maria Curie-Skłodowska University, 20031 Lublin, Poland

46. W.Rudziński – Faculty of Chemistry, Maria Curie-Skłodowska University, 20031 Lublin, Poland

47. S.Sircar – Air Products and Chemicals , Inc., 7201 Hamilton Boulevard, Allentown, PA, 18195, U.S.A.

48. W.Steele – Department of Chemistry, 152 Davey Laboratory, Penn State University, University Park, PA 16802, U.S.A.

49. H.Takaba – Department of Molecular Chemistry and Engineering, Faculty of Engineering, Tohoku University, Aoba, Aramaki, Aoba-ku, Sendai 980, Japan

50. Yu.I.Tarasevich – Institute of Colloid Chemistry and Chemistry of Water, Academy of Sciences of the Ukraine, pr.Acad.Vernadsky 42, 252680 Kiev, Ukraine

51. V.A.Tertykh – Institute of Surface Chemistry, Academy of Sciences of Ukraine, pr. Nauki 31, 252022 Kiev, Ukraine

52. R.Vetrivel – Catalysis Division, National Chemical Laboratory, Pune-411008, India

53. A.Voelkel – Poznań University of Technology, Institute of Chemical Technology and Engineering, Pl.M.Skłodowskiej-Curie 2, 60-965 Poznań, Poland

54. V.V.Yanishpolskii – Institute of Surface Chemistry, Academy of Sciences of Ukraine, pr. Nauki 31, 252022 Kiev, Ukraine

55. J.Zajac – Laboratoire des Agregats Moleculaires et Materiaux Inorganiques, Universite des Sciences et Techniques du Languedoc, pl.E.Bataillon, 34095 Montpellier Cedex 05, France

56. S.Zalac – Laboratory of Physical Chemistry, Faculty of Science, University of Zagreb, 41000 Zagreb, Croatia

57. Yu.L.Zub – Institute of Surface Chemistry, Academy of Sciences of Ukraine, pr. Nauki 31, 252022 Kiev, Ukraine

CONTENTS

Preface v

Author Index ix

Section 1
Preparation, Structure and Properties of New and Modified Inorganic Sorbents 1

Chapter 1.1
Computational studies on the design of synthetic sorbents for selective adsorption of molecules
R. Vetrivel, H. Takaba, M. Katagiri, M. Kubo and A. Miyamoto 3

Chapter 1.2
Controlled porosity glasses (CPGs) as adsorbents, molecular sieves, ion–exchangers and support materials
A.L. Dawidowicz 31

Chapter 1.3
Influence of pH of precipitation of hydroxides on the structure of co–precipitated adsorbents
V.S. Komarov 57

Chapter 1.4
Colloidal silicas
S. Kondo 93

Chapter 1.5
Complex carbon–mineral adsorbents: preparation, surface properties and their modification.
R.Leboda and A.Dąbrowski 115

Chapter 1.6
Solid-phase hydrosilylation reactions with participation of modified silica surface
V.A.Tertykh and L.A.Belyakova 147

Chapter 1.7
Structure and molecular organization of bonded layers of chemically modified silicas
A.Yu.Fadeev and G.V.Lisichkin 191

Chapter 1.8
The chemical basis of surface modification technology of silica and alumina by molecular layering method
A.A. Malygin, A.A. Malkov and S.D. Dubrovenskii 213

Chapter 1.9
Kinetics of organic compounds chemisorption from the gas phase on oxides surface
V. I. Bogillo 237

Chapter 1.10
Functionalized polysiloxane sorbents:
preparation, structure, properties and use
Yu. L. Zub and R. V. Parish 285

Chapter 1.11
Surface structure and molecular adsorption of apatites
T. Ishikawa 301

Chapter 1.12
Surface chemistry and adsorption properties of Al_{13} colloids
J.Y. Bottero and J.M. Cases 319

Section 2
Adsorption from Gaseous Phase 333

Chapter 2.1
Computer simulation of adsorption on amorphous oxide surface
V. Bakaev and W. Steele 335

Chapter 2.2
On the nature of the energetic heterogeneity of water/oxide interface in adsorption phenomena occurring at oxide surfaces
W. Rudziński, R. Charmas and T. Borowiecki 357

Chapter 2.3
Energetic heterogeneity of porous inorganic oxides:
Adsorption and chromatographic studies
M. Jaroniec 411

Chapter 2.4
Adsorption kinetics on real surfaces
G.F. Cerofolini 435

Chapter 2.5
Inverse gas chromatography in the examination of acid–base and some other properties of solid materials
A. Voelkel 465

Chapter 2.6
Chemical and morphological characteristics of inorganic sorbents with respect to gas adsorption
E. Papirer and H. Balard 479

Chapter 2.7
Structure and properties of the films formed by organic substances on silica gel surface. Investigations by inverse gas chromatography (IGC)
J. Rayss 503

Chapter 2.8
The use of gas chromatography to study the adsorption from gaseous phase at the infinite dilution
F. J. López Garzón and M. Domingo Garcia 517

Chapter 2.9
Molecular statistic and gas chromatographic study of hydrocarbons adsorption on the modified layer silicates and silica in the Henry region
Yu.I.Tarasevich, E.V.Aksenenko and S.V.Bondarenko 539

Chapter 2.10
Micropore filling mechanism in inorganic sorbents
K. Kaneko 573

Chapter 2.11
Phase transitions in adsorbed layers
A. Patrykiejew 599

Chapter 2.12
Drying of gases and liquids by activated alumina
S. Sircar, M. B. Rao and T. C. Golden 629

Section 3
Adsorption from Solution 647

Chapter 3.1
Characterization of inorganic sorbents by means of adsorption at the liquid – solid interface
A. Dąbrowski, R. Leboda, J. Goworek and J.K. Garbacz 649

Chapter 3.2
Study of adsorption from solutions by chromatography
V.Ya.Davydov 673

Chapter 3.3
Equilibria of adsorption from solutions on the silica surface
V. A.Tertykh and V. V.Yanishpolskii 705

Chapter 3.4
Adsorption from dilute solutions – some novel aspects
P. Nikitas 729

Chapter 3.5
Ion adsorption on mineral oxide surfaces
Luuk K. Koopal 757

Chapter 3.6
Recent progress in the studies of adsorption of ionic surfactants from aqueous solutions on mineral substrates
J. Zajac and S.Partyka 797

Chapter 3.7
The reaction of anions and cations with metal oxides as models for their reaction with soil
N. J. Barrow 829

Chapter 3.8
Problems in modelling the electrical interfacial layer in metal/oxide aqueous systems
N. Kallay, S. Zalac and I. Kobal 857

Chapter 3.9
Adsorption and immersional wetting on hydrophilic and hydrophobic silicates
I. Dékány 879

Chapter 3.10
Liquid chromatography of fullerenes and study of adsorption properties of fullerenes crystals
V.Ya.Davydov 899

Subject Index 915

This Page Intentionally Left Blank

Section 1

PREPARATION, STRUCTURE AND PROPERTIES OF NEW AND MODIFIED INORGANIC SORBENTS

This Page Intentionally Left Blank

A. Dąbrowski and V.A. Tertykh (Editors)
Adsorption on New and Modified Inorganic Sorbents
Studies in Surface Science and Catalysis, Vol. 99

Chapter 1.1
Computational studies on the design of synthetic sorbents for selective adsorption of molecules

R. Vetrivel[a], H. Takaba[b], M. Katagiri[b], M. Kubo[b] and A. Miyamoto[b]

[a]Catalysis Division, National Chemical Laboratory, Pune - 411008, India

[b]Department of Molecular Chemistry and Engineering, Faculty of Engineering, Tohoku University, Aoba-ku, Sendai 980-77, Japan

1. INTRODUCTION

Selective adsorption of molecules are of paramount importance in the gas phase separation technology. Conventionally zeolite catalysts are widely used as molecular sieves and shape selective catalysts [1]. However, the extra framework cations, particularly the protons in zeolites are source of unwanted reactions in selective adsorption and separation of molecules. Recently, crystalline aluminophosphates having microporous structures are reported [2]. Aluminophosphates (AlPOs) are having neutral framework with regularly alternating $[AlO_4]^-$ and $[PO_4]^+$ tetrahedra. The AlPOs do not have extra framework cations and they can be synthesized with novel pore shapes and sizes. Carbon molecular sieves have also been known to be inert and applicable to gas separation applications for reasonably long time [3]. Recent discovery of molecular carbon structures such as carbon nanotubes[4] has provided impetus to search for new selective adsorption applications of such materials. The selective adsorption of molecules over ceramics and extraction with supercritical fluids is also an emerging technology[5].

In this chapter, we present the results of computational studies on the above mentioned novel inorganic systems namely AlPOs, carbon nanotubes and supercritical fluid extraction from the adsorbed phase over ceramics. Multi-technique computational methods such as Computer Graphics (CG), molecular mechanics (MM), quantum chemistry (QC) and molecular dynamics (MD) were applied. The attempts made to design synthetic sorbents at molecular level are reviewed.

2. COMPUTATIONAL METHODOLOGY

2.1. Computer graphics (CG) and molecular mechanics (MM)

The structures of typical aluminophosphates, namely $AlPO_4$-11[6] and VPI-5[7] were generated from the reported crystal structures. adsorption of probe molecules such as water and ammonia, as well as the template organic molecules and larger molecules were

studied. The equilibrium geometry of the molecules were obtained from energy minimization MM calculations.

Standard force fields were used in the energy minimization calculations[8]. All geometrical degrees of freedom such as bond length, bond angle, and dihedral angles were varied. In this process all atoms were moved and the molecule reaches a final geometry, where the molecular potential energy is minimum. From these calculations we obtain the dimensions of the molecules at their minimum energy conformations. We also calculate the strain energy involved in the conformational changes from their equilibrium geometry.

2.2. Quantum chemical technique

Semi-empirical quantum chemical calculations using the MNDO (modified neglect of differential overlap) technique [9] was used to study the electronic structure of the amines, cluster models of $AlPO_4$-11 framework, and the ammonia as well as water adsorption complexes over the oxygen sites in $AlPO_4$-11. The values of the electronic and total energies are used to decide the favourable adsorption sites; the analysis of molecular orbital energy as well as the contributions of various atomic orbitals to molecular orbitals and the electron distribution and partial charges calculated are also useful to determine the nature of interaction between molecules and framework.

2.2.a. Dimer cluster models

There are 11 possible bridging oxygen sites which are crystallographically distinct in the ordered $AlPO_4$-11 structure[6]. The geometry of the repeating unit cell containing six unique T sites and the 11 oxygens attached to them is shown in Fig. 1. The inset shows the lattice of $AlPO_4$-11 formed by the presence of such repeating units. All 11 unique oxygen sites in $AlPO_4$-11 are simulated by suitable cluster models. Dimer cluster models [$(OH)_3$-T1-O-T2$(OH)_3$] where T1 = P and T2 = Al were selected to model all the bridging oxygen sites in the $AlPO_4$- 11. The hydrogen atoms needed to maintain neutrality of the clusters are located at the nearest-neighbour T sites. A typical cluster model is shown in Fig. 2a. Electronic structures of these clusters are calculated by the MNDO method. Cluster models, their total energies, and the electron densities on the bridging oxygens are calculated. The net electron density on the bridging oxygen atom is found to increase with increasing T-O-T angle and decreasing T-O distance.

2.2.b. Monomer cluster models

Structure of each tetrahedral units (either AlO_4 or PO_4) are also obtained from the crystal structure reported[6] for $AlPO_4$-11. The unsaturated valency of the oxygen atoms in the tetrahedra is balanced by bonding a hydrogen atom to them, and the positions of these hydrogen atoms are those of the adjacent T atoms in the $AlPO_4$-11 structure. For each of the tetrahedra, the different possibilities of water approaching the T site through its oxygen end is considered. The calculations were carried out for the water molecule, the bare tetrahedral cluster (Td), and tetrahedral clusters with water molecules adsorbed (adsorption complex). The adsorption energy of water (ΔH_{ads}) at different sites is calculated as mentioned below:

$$\Delta H_{ads} = TE_{complex} - (TE_{Td} + TE_{water}) \quad (1)$$

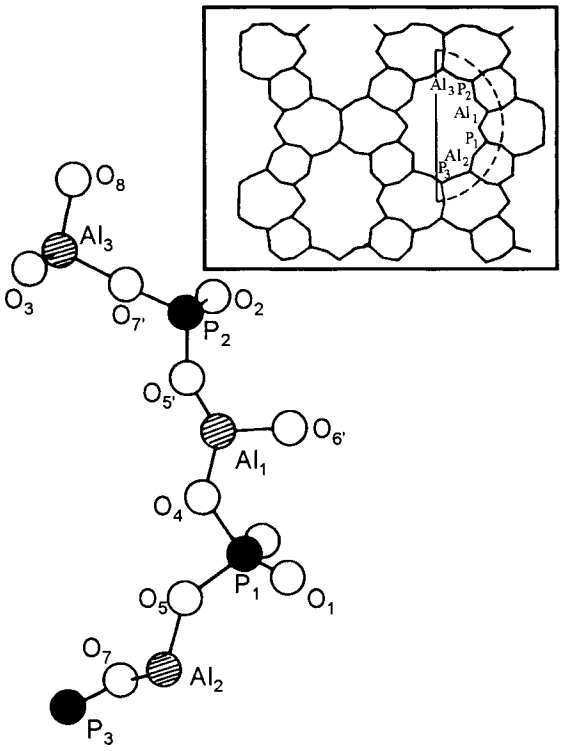

Figure 1. A repeating unit cell of the ordered $AlPO_4$–11structure. The inset is the schematic representation of the $AlPO_4$–11 lattice which is formed by several such repeating units and their mirror images.

In all the adsorption complexes, the distance between the tetrahedral atom and the oxygen of a water molecule (T atom of H_4TO_4 and oxygen of H_2O) is kept at 1.5Å uniformly.

2.3. Molecular dynamics method

The molecular dynamics (MD) simulations for carbon nanotubes were carried out using the Discover module of the commercial software package supplied by Biosym Technologies Inc., USA in SiliconGraphics–IRIS 4D/30 workstation. The motion of the nuclei on the potential energy surface of the system with energy E(R) is described by Newton's equation of motion as follows:

$$dE/dR = m \cdot d^2R/dt^2 \qquad (2)$$

The MD code derives the solution to equation (2), using an empirical fit to the potential energy surface for the motion of all atoms in the system. This equation is numerically integrated using small ($\sim 10^{-15}$ s) time steps, producing a trajectory of the system. The empirical fit to the potential energy is performed using suitable force field. We choose the

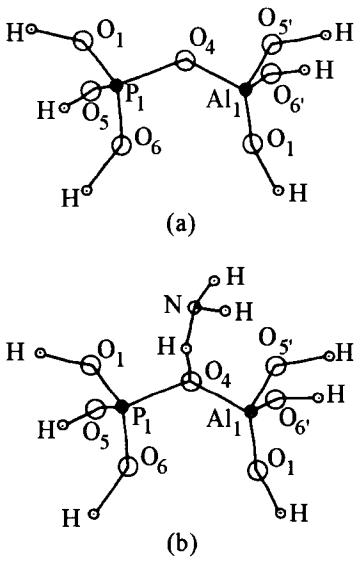

Figure 2. (a) A typical representative dimer cluster model showing the bridging oxygen site, O4. (b) The geometry of the dimer cluster–ammonia adsorption complex.

consistent valence force field (CVFF) reported by Dauber–Osguthorpe et al.[10] which include parameters for variety of functional groups. The algorithms for minimization and the functional forms of force fields used to evaluate the potential energy are described in detail elsewhere[11]. The procedure includes finding the equilibrium structures and their relative energy values over a period of time. In all the calculation, static energy minimization was carried out prior to the MD simulation. The interval of each MD simulation step was typically $2.0 \cdot 10^{-15}$s and the simulation was carried out for typically 5000 time steps. All calculations were carried out at 300K using NVT ensembles.

The MD calculation to study supercritical fluid extraction from ceramics was performed with the XDORTO program developed by Kawamura[12]. The Verlet algorithm was used for the calculation of atomic motions, while the Ewald method was applied to the calculation of electrostatic interactions. Temperature was controlled by means of scaling the atom velocities under 3–dimensional periodic boundary condition. The calculations were made for 40000 time steps with the time increment of $2.5 \cdot 10^{-15}$ seconds. The two body central force interaction potential, as shown in equation (3) was used for all the calculations:

$$u(r_{ij}) = Z_i Z_j e^2/r_{ij} + f_0(b_i + b_j)\exp\left[(a_i + a_j - r_{ij})/(b_i + b_j)\right] + \\ + D_{ij}\left\{\exp\left[-2\beta_{ij}\left(r_{ij} - r_{ij}^*\right)\right] - 2\exp\left[-\beta_{ij}\left(r_{ij} - r_{ij}^*\right)\right]\right\} \quad (3)$$

First, second, and third terms in the equation (3) refer to Coulomb potential, exchange repulsion interaction potential, and Morse potential, respectively. Z_i is an atomic charge, e is an elementary electric charge, r_{ij} is an interatomic distance, and f_0 is a constant. The parameters a and b in Eq. (3) represent the size and stiffness of the atoms, respectively, in

the exchange repulsion interaction, while D_{ij}, r_{ij}^{*} and β_{ij} represent bond energy, equilibrium bond distance and stiffness, respectively in the Morse interaction. The parameters of equation (3) for solids were determined to reproduce the structures of various metal oxides and metal crystals.

The calculations were performed with SiliconGraphics IRIS–4D/25TG and Hewlett Packard 9000 series 710 workstations, while the visualization was made with BIOSYM Insight II code in SiliconGraphics IRIS–4D/25TG workstation. The dynamic features of the supercritical fluid on adsorbed phase were also investigated by using the real time solid modeling visualization with MOMOVIE code developed in our laboratory on OMRON LUNA88K workstation.

3. STUDIES ON AlPOs

Microporous AlPOs are believed to nucleate around organic molecules during synthesis, however the actual interactions between the organic molecules acting as templates and AlPOs are not yet understood. Prasad and Vetrivel[13] predict the location and conformation of the secondary amine template molecules inside the pores of $AlPO_4$–11 molecular sieve. The results obtained by molecular modelling and the semi–empirical quantum chemical calculations are used as tools for this purpose. The geometric and electronic requirements of the amines to be a successful structure– directing species for the synthesis of $AlPO_4$–11 are reported. The results of ^{13}C magic angle spinning (MAS) NMR studies help to identify the nature of the occluded species, which supports the results derived by modelling studies. It is shown that the relation between the pore architecture and the structural as well as electronic properties of templates could be interpreted. These interpretations are essential to design synthetic sorbents and the details are given in the following sections.

3.1. Organic template guest – $AlPO_4$–11 host interactions

It was found by several authors[14–16] that the secondary amine molecules are the efficient templates for the synthesis of $AlPO_4$–11. MNDO calculations were carried out on different amine molecules in order to study the electronic factors involved in the specificity of secondary amines as structure–directing species. The electron charge density on nitrogen increases in the order primary $\sim$ secondary $<$ tertiary amines. We notice that the absence of hydrogen attached to nitrogen in the case of a tertiary amine and almost zero charge on the hydrogens of methylene and methyl groups of tertiary and primary amines are partial reasons for their failure to act as templating agents for the synthesis of the $AlPO_4$–11 framework.

The net charge on nitrogen in secondary amines is found to be – 0.30, independent of the dimension and nature of the alkyl groups. However, the n–alkyl groups are more efficient than the isoalkyl groups in withdrawing electrons from the hydrogen attached to nitrogen. Among all the atoms, the hydrogen attached to the nitrogen is the atom with maximum positive charge and hence it is expected to have strong bonding interactions with the oxygen atoms of the $AlPO_4$–11 framework. The electron distributions among the methylene and methyl groups are almost constant for all the secondary amines. Overall, these amines are less polar with a typical dipole moment value of $\sim$ 1.25 D and hence are expected to be weakly bound to the framework. Tapp and et al.[16] reported that the

template molecules desorbed at $\sim$ 200°C, which is in agreement with the weak binding predicted by the above calculations.

The electronic structure of amines indicates that the major interaction of the amine with the framework is expected to occur through the hydrogen attached to nitrogen and its nearest neighbours. Hence, ammonia adsorption over different oxygen sites in $AlPO_4$-11 will have corollary results as far as electronic interactions are concerned. A neutral ammonia molecule adsorbed through one of its hydrogen atoms onto the bridging oxygen site of the $AlPO_4$-11 cluster is considered. Ammonia is positioned in such a way that the O-HNH_2 bond lies at the center of the T-O-T angle on the obtuse side. The typical cluster model representing the ammonia adsorption complex is shown in Fig. 2b. The binding energy values of ammonia to the 11 different oxygen sites in the $AlPO_4$-11 lattice are calculated and given in Table 1. The binding energy values of ammonia to the oxygen sites are calculated as follows:

$$BE_{ammonia} = TE_{complex} - (TE_{dimer\ cluster} + TE_{ammonia}) \tag{4}$$

where BE and TE are the binding energy and total energy, respectively. The binding energy of ammonia is a positive value, which is an artifact of the small cluster model. However, the binding energy gives the trend in the strength of adsorption of ammonia at various oxygen sites, which is expected to be the same for the amine molecules also. The analyses of molecular orbitals of the cluster models show that the highest occupied molecular orbitals (HOMO) are contributed by the 2p orbitals of oxygen and aluminum, while the lowest unoccupied molecular orbitals (LUMO) are contributed by the 1s orbital of hydrogen and 2p orbitals of oxygen and phosphorus. The 1s orbital of hydrogen in ammonia is contributing to the frontier HOMO in the adsorption complex. Since PO_4 groups have unoccupied orbitals, electron donation from amines to the PO_4 group is expected to occur.

The favourable adsorption sites for ammonia are found to be 04, 05, 05′, and 06′. Indeed, the values of the T-O-T angles for these oxygen sites are having minimum values (Table 1). The ammonia prefers to adsorb on oxygen sites where the steric hindrance for ammonia to approach the oxygen site is minimum, and this argument is applicable to the secondary amines also. The amine molecule may undergo multiple site adsorption with the hydrogen atoms of the alkyl groups having interactions with other oxygen atoms of the framework.

The topographic analysis of the various oxygen atoms and the silicon substitution sites were reported based on MNDO calculations[17]. The results indicated that P1 and Al1 are the crystallographic sites where silicon substitution is energetically favourable. Incidentally, the favourable oxygen sites for the adsorption of ammonia mentioned above, are all bonded to P1 and Al1 as shown in Fig. 1.

The substitution process of silicon in $AlPO_4$-11 lattice is considered as follows:

$$(OH)_3Al - O - P(OH)_3 + Si(OH)_4 \longrightarrow [(OH)_3Al - O - Si(OH)_3]^{-1} + [P(OH)_4]^{+1} \tag{5}$$

$$(OH)_3Al - O - P(OH)_3 + 2Si(OH)_4 \longrightarrow [(OH)_3Si - O - Si(OH)_3] + [Al(OH)_4]^{-1} + [P(OH)_4]^{+1} \tag{6}$$

Table 1
The results of MNDO calculations on the cluster models of the AlPO4-11 lattice and the ammonia adsorption complexes

No.	cluster model	T-O-T angles (deg)	total energy of the cluster(eV)	charge density on the bridging oxygen	tot. energy for ammonia adsorption complex(eV)	adsorption energy of ammonia(eV)	charge density on ammonia
1	P1-O1 -Al1	167	-2519.21	-0.63	-2767.16	2.29	-0.04
2	P1-O4 -Al1	131	-2519.86	-0.50	-2768.69	1.41	-0.02
3	P1-O5 -Al2	140	-2519.85	-0.61	-2768.44	1.65	-0.05
4	P1-O6 -Al2	152	-2517.75	-0.63	-2766.24	1.75	-0.06
5	P2-O2 -Al2	174	-2521.07	-0.66	-2768.36	2.95	0.00
6	P2-O7′-Al3	168	-2524.15	-0.62	-2772.22	2.17	-0.02
7	P2-O5′-Al1	147	-2519.14	-0.62	-2767.78	1.60	-0.02
8	P2-O6′-Al1	140	-2519.59	-0.64	-2768.18	1.65	-0.04
9	P3-O3 -Al3	172	-2518.78	-0.66	-2766.03	2.99	-0.05
10	P3-O7 -Al2	166	-2517.38	-0.68	-2765.21	2.32	-0.05
11	P3-O8 -Al3	175	-2518.38	-0.69	-2765.24	3.38	-0.04

The substitution energy(SE) of silicon for phosphorus and aluminum in the above processes are calculated according to the equation:

$$SE = TE_{products} - TE_{reactants} \quad (7)$$

The negative charge in the $[(OH)_3Al\text{-}O\text{-}Si(OH)_3]^{-1}$ cluster is compensated by adding a hydrogen at the bridging oxygen (O_b) to form $(OH)_3Al\text{-}OH\text{-}Si(OH)_3$. The hydrogen ($H_b$) is attached to the bridging hydroxyl group on the obtuse side of the Al–O–Si angle. The hydrogen is placed in such a way that the angle $Al\text{-}O_b\text{-}H_b$ is equal to the angle $Si\text{-}O\text{-}H_b$ and the $O_b\text{-}H_b$ distance is 1.0Å. When the protons are linked to O4, O5, O5′ and O6′, ammonia adsorbing on these sites will form ammonium cations in $SAPO_4$–11, which is silicoaluminophosphate analog of $AlPO_4$–11. It is encouraging to note that our findings are in correspondence with the studies on the crystal structure analysis of the as–synthesized $MnAPO_4$–11 material, which show that the diisopropylamine is located inside the pore in such a way that nitrogen lies closer to O4 and O5 of the framework.

The ^{13}C cross polarization (CP) magic angle spinning (MAS)–NMR spectroscopic studies of $AlPO_4$–11 with secondary amine template molecules in as–synthesized and calcined forms are reported in detail elsewhere[13]. In the as– synthesized $AlPO_4$–11 with di–n–butylamine, the template is chemically in–tact. When the as–synthesized samples are dried at higher temperatures, the NMR spectrum shows a split in the methyl group signal. Such a solid–state splitting could be due to environmental changes or due to conformational changes occurring in the occluded species. Conformational changes between the two alkyl groups are expected to cause splitting in the methyl as well as the methylene group signals.

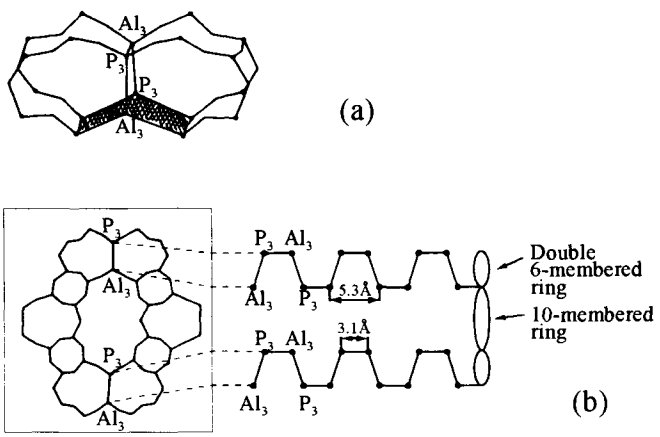

Figure 3. (a) The geometry of the side pocket which is a double 6–member ring. The access to this side pocket from the 10–member ring is shown by shading. (b) The schematic view of the channels along the c axis (box) and the perpendicular a axis.

However, since in the observed spectrum, the splitting occurs only in the signal of the methyl group, the fact that the terminal methyl group alone is present in a different

environment is brought out. In this context, it is relevant to note a unique feature of the structure of $AlPO_4$–11, namely the presence of interconnected double 6–member side pockets. There is access to these side pockets from the 10– member channel. The geometry of the side pocket and the schematic view of channels of $AlPO_4$–11 from two perpendicular directions are shown in Figs. 3a and 3b, respectively. The non bonded distance between A13 and P3 is 5.30Å. When 0.86Å for the ionic radii of Al^{3+} (0.51Å) and P^{5+}(0.35Å) is left out, the free dimension across the 6–member ring aperture is 4.44Å. This is an unusually large aperture for a 6–member ring compared to those in other molecular sieves, and this provides a hint to explain the cause of the split in the signal of the methyl group. On heating, the weakly bound amine molecule shifts its interaction site, resulting in the movement of the –CH fragment of the terminal methyl group into the 6–member side pocket, and thus exists in a different environment. These results indicate that the template molecules are still chemically intact and they possess the freedom that allows the dynamic behaviour inside the neutral $AlPO_4$–11 framework. It i s shown that the selective sorbent property of $AlPO_4$–11 is due to the presence of 6–member ring side pockets which can accommodate the methyl groups. Thus even large template molecules could still play the structure directing role.

3.2. $AlPO_4$–11 framework – water interactions

The phase transitions in molecular sieves on calcination is a phenomenon connected with the role of water. It is noted that the water brings about certain reversible and irreversible structural changes. The calcined $AlPO_4$–11 is capable of adsorbing water, and the results of many experimental techniques[18,19] such as IR, NMR, and TGA–DTA have shown that $AlPO_4$–11 undergoes structural change reversibly on adsorption of water including overall reduction in the unit cell volume and pore volume[18]. Quantum chemical technique with no greater sophistication have been applied to study $AlPO_4$–11 — water interactions. The results shed light on the causes of changes occurring in the XRD pattern and MAS NMR profiles due to hydration[20].

Electronic structure calculations are undertaken to locate the preferred sites of adsorption for water inside the $AlPO_4$–11 framework. Further, it is revealed that quantitative correlation exists between the additional NMR signals due to water adsorption and change in the environment of T sites. The total energy calculated for the six crystallographically distinct T sites (3Al and 3P) modeled by the H_4TO_4 cluster is given in Table 2. Calcined and dehydrated $AlPO_4$–11 shows a tendency for rapid uptake of water molecules. Different modes of adsorption of water molecule over TO_4 sites are considered. It was reported that the adsorption of water in the plane of O–T–O with the oxygen atom of the water molecule towards T site is the energetically favoured configuration. The interaction of water with all the six TO_4 groups given in Table 2 were analyzed in detail.

When the net negative charge on the framework oxygen atoms and the net positive charge on the aluminum atom are maximum, the adsorption is favoured. Oxygen of the water molecule gains the maximum negative charge in this case. The adsorption of water is found to take place by the transfer of electrons from the TO_4 group. The net charges on various atoms themselves are found to depend on the geometry of TO_4. The average adsorption energy of water obtained indicate that A13 and P3 are the preferred sites among the various aluminum and phosphorus sites, respectively, for the adsorption of water. The water molecules are expected to be mobile around the T3 site; hence the ad-

Table 2
The electronic properties of H_4TO_4 (where T = Al or P) clusters representing different sites in the $AlPO_4$-11 framework

T site	oxygen sites	total energy (eV)	net charge on T site
Al1	O1, O3 , O5′, O6′	-1380.32	0.91
Al2	O2, O5 , O6 , O7	-1380.73	1.01
Al3	O3, O7′, O7′, O8	-1383.31	0.91
P1	O1, O4 , O5 , O6	-1476.03	1.47
P2	O2, O5′, O6′, O7′	-1477.97	1.65
P3	O3, O7 , O7 , O8	-1473.84	1.81
free H_2O		-351.41	—

sorption energies calculated for the water molecule in more than one plane are comparable in magnitude.

The geometric reasons for the preference for these T sites is obvious since these sites have the largest T-O-T angles, thus possessing minimum steric hindrance to the approaching water molecules. In addition to the steric factor, the electronic factor is also favourable where the T-O-T angles are maximum and the T-O distances are minimum. It has also been shown that the charge separation between T and O sites in the $AlPO_4$-11 framework is maximum at sites where T-O distances are short and T-O-T angles are large[13]. The polarity and hence the electrostatic field play a significant role in the adsorption process. Although charge separation occurs inside water, still it remains intact and there is no indication of its dissociation from the calculated bond order values. Topologically, Al3 and P3 sites occur at the junction of 10-membered and two 6-membered rings. Statistically, T3 sites represent 20% of the T sites (where T is either Al or P) since there are two T1 and T2 sites each for every single T3 site.

In the ^{27}Al MAS NMR spectrum of hydrated $AlPO_4$-11 sample, there are signals in the region 20 to 35 ppm corresponding to tetrahedrally coordinated T-site[20]. In addition to the peaks in the tetrahedral region, a broad peak appeared in the high field region of -15 to -25 ppm in the hydrated sample. A peak in this region is characteristic of a 6-coordinated Al species in the framework and has been reported in the case of related materials such as $AlPO_4$-5, $AlPO_4$-17, VPI-5, $AlPO_4$-11 as well as SAPO-34. It is attributed to interaction of water molecules with the AlO_4 tetrahedron[21] and is recognized as evidence for the presence of chemisorbed water in the hydrated sample. Nearly 20% of the total framework aluminum could be assigned an octahedral coordination in the hydrated form. Significantly, the fraction corresponds to the fraction of Al3 sites which are favoured sites for the location of water molecules on the basis of MNDO energy calculations. Thus the quantum chemical calculations are shown useful to bring out the local structural changes occurring in molecular sieve frameworks due to adsorption of water molecules.

3.3. VPI–5 framework – water interactions

VPI–5 is an aluminophosphate framework with very large one–dimensional pores defined by 18–member ring[22]. The crystal structure report[7] of synthesized VPI–5 revealed the possible role of water molecules as templates. The use of VPI–5 as a molecular sieve and as a catalyst primarily depend on the removal of the occluded water molecules without the destruction of the framework structure. Prasad et al.[23] reported from their TGA experiment that the seven distinct types of water molecules could be desorbed from VPI–5 in a step–wise fashion, in the temperature range of 35 to 60°C. The cluster model calculations[24] have revealed the actual electronic interaction of water molecules with VPI–5 framework. CG technique also indicated that the void volume in VPI–5 could be controlled by the partial removal of water molecules.

The cluster models to represent the framework were generated by the same procedure as for the $AlPO_4$–11[20] and the interaction energy of water with several sites were studied. VPI–5 also has three crystallographically distinct Al as well as P sites. The total energy calculated for the three crystallographically distinct Al and P sites modeled by the H_4TO_4 clusters (where T = Al or P) are given in Table 3. The geometry of different T sites, the O sites which are attached to each of the T sites, and the net electron density on T sites are included. The results of the calculation on the water molecule is also given in Table 3. The charges on T sites given in Table 3 show that the variations are too small to distinguish the crystallographically distinct T sites. The interaction of the water molecule with different T sites is dependent on the O–T–O angle (shown in Table 3), and the net electron density values are an indication of the strength of this interaction.

The interaction of water with each of these Al site was studied. The average interaction energy of water is more favourable for the Al1 site rather than the Al2 and Al3 sites, although all the values are positive. The observed positive values for adsorption energy may partly be due to an artifact of the small cluster size considered to represent the tetrahedral sites and the representative T–water distance of 1.5Å uniformly used here. However, we are comparing the same parameter calculated for different sites on a relative basis. The incoming water can approach the Al1 site through three planes, namely, 413, 412, and 312. Out of these three modes, the approach of water along the 413 plane, where the O–Al–O angle is a maximum of 169°, is the most favourable mode of adsorption. The hydrogen atom of the water molecule lies parallel to the O3–Al1–O4 bonds. The experimental position of the water molecules shows that there are simultaneously two water molecules present leading to octahedral coordination at Al1 as shown in Fig. 4. As far as the A12 and A13 sites are concerned, the average O–Al–O angles are larger than in the Al1 site and there is no significant variation in the O–T–O angles of different planes in these sites as in the case of the Al1 site. Thus, the results of our calculation confirm that the water molecule is located near the Al1 site and it approaches the Al1 site specifically through the 413 plane.

Similar calculations were also carried out to study the interaction between the water molecules and the three crystallographically distinct P sites. The average interaction energy of water is more favourable for the P2 site than the P1 and P3 sites. Unlike in the Al1 site, none of the O–P–O angles are large enough to lead to octahedral coordination. The results of these quantum chemical calculations are in correspondence with the T....H_2O distances obtained from XRD studies. Further ^{31}P MAS NMR studies led to contradicting assignments by different research groups[25,26]. The interaction energy

Table 3
The geometry and the electronic properties of H_4TO_4 (where T = Al or P) clusters representing different sites in the VPI-5 framework

T site	oxygen sites	average T–O distance(Å)	average O–T–O angle(deg)	average T–O–T angle(deg)	total energy(eV)	net charge on T site
			H_4AlO_4 clusters			
Al1	O1, O2, O3, O4	1.83	105.80	150.51	-1379.54	0.96
Al2	O5, O7, O8, O9	1.73	109.44	151.82	-1381.98	1.00
Al3	O6, O10, O11, O12	1.76	109.41	143.84	-1382.63	0.93
			H_4PO_4 clusters			
P1	O1, O2, O5, O6	1.52	109.42	154.62	-1475.47	1.58
P2	O3, O7, O8, O10	1.51	109.46	146.09	-1476.29	1.55
P3	O4, O9, O11, O12	1.52	109.46	145.53	-1475.55	1.51
			water			
		O–H = 0.96	H–O–H = 104.5		-351.41	-0.32*

*net charge on oxygen of water molecule

values support the assignments made by Grobet et al.[25]. The formation of octahedrally coordinated aluminum by the interaction of two water molecules with the All site has been proved beyond doubt by ^{27}Al MAS NMR studies. From the average net charges calculated for the T sites, it is possible to qualitatively correlate the MAS NMR chemical shift to the polarizability. The net charges on oxygen atoms of the framework, which lie close to the water molecules, have less charge and hence cause more polarization around TO_4. Thus the cluster calculations are able to clarify the doubts arising, while interpreting the MAS NMR spectroscopic results. They also lead to new structural insights of the synthetic sorbents with novel structure.

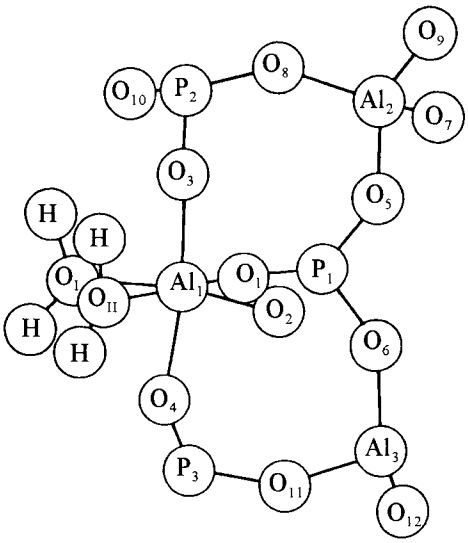

Figure 4. Energetically favourable mode of adsorption of a water molecule over the Al1 site leading to octahedral coordination as reported in Ref. [7].

3.4. VPI–5 framework – porphyrin interactions

Here, a typical case study where the density function theory quantum chemical (DFT–QC) technique has revealed the important structural aspects involved in catalytic functioning of microporous sorbents is reported[27]. The possibility of anchoring organometallics, namely porphyrins and metalloporphyrins with 'enzyme– like' active sites, were studied. The analysis of the 3–d contours of electron density and molecular electrostatic potential maps corresponding to various porphyrin systems and the cluster models representing VPI–5 framework brought out the probable locations for porphyrins inside VPI–5, as well as the molecular recognition existing between the guest sorbate molecule and host sorbent lattice. This study probes the possible design of a biomimicking catalyst containing porphyrin encapsulated in the large pore of VPI–5 molecular sieve. DFT–QC calculations[28] were performed using the DMOL package of Biosym Technologies, Inc., USA. The calculations were carried out using a numerical basis set[29] and JMW type local correlation functional were used for exchange correlation energy terms in the total

energy expression. The modeling approach and the procedure for cluster generation are essentially the same as described in our earlier study[20].

The CG picture of the structure of the water network in VPI–5 molecular sieve as reported by the high resolution synchrotron powder diffraction study[7] is shown in Fig. 5. As mentioned earlier, quantum chemical cluster model calculations by MNDO method have also shown that the energetically favourable sites for the adsorption of water is in correspondence with the experimental reports.

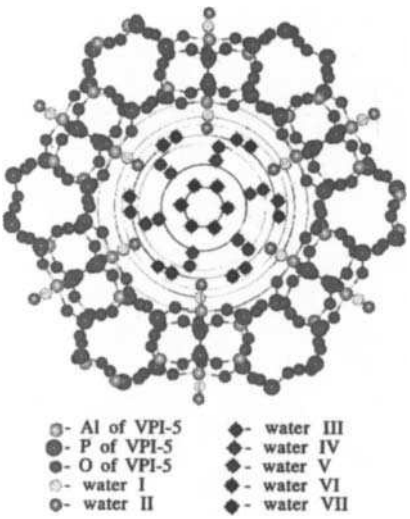

Figure 5. The seven kinds of water molecules in the hydrated VPI–5 molecular sieve. Only the oxygen atoms of the water molecules are shown. The concentric circles represent the void space generated in the 18–member pore due to the step–wise thermal desorption of water.

Of all the catalysts known, biological catalysts, namely enzymes are the most efficient ones. The aim of the study reported below is to mimic these catalysts by designing a structurally and electronically similar catalysts. With this aim, the electronic structure calculations were carried out to study the encapsulation of enzyme–like active sites into porous inorganic mantles. Porphyrins have a significant role in the biological actions such as photosynthesis, oxygen carrier and decomposition of water. Although, porphyrin based catalysts undergo oxidative dimerization as well as degradation, their encapsulation inside microporous materials extend their catalytic life[30] and enhance their catalytic activity[31] and selectivity[32]. Earlier, metalloporphyrins were synthesized inside the sub-nano space of zeolite cages and they were reported[33] to catalyze many novel reactions. The phthallocyanine type complexes are known to get encapsulated inside VPI–5, leading to a catalyst with superior stability[31]. However, there are no studies on the incorporation of porphyrins inside VPI–5. We report here the possible structure and design of such a catalyst system based on the 3–d contour of electron density [ED] and molecular electrostatic potential [MEP] maps derived from DFT QC calculations.

The electronic structure calculations by DFT method were performed for the porphyrin as well as for the metalloporphyrin, where the two protons of porphyrin are replaced by bivalent metals such as Mg, Fe, Ni and Zn. Fig. 6 shows the 3-d contour electron density (ED) map calculated for the 5,10,15,20-tetramethyl porphyrin. The ED maps for the unsubstituted porphyrins had the same overall features with less directional, but a smoothened contour of the ED maps at the substitution sites. The substitution of the imine protons by various other metals practically showed no visible changes in the ED on the periphery of the porphyrin complex. The most distinct feature of the ED contour is the 12 regions, where the electron density is high and these regions are adjacent to the methyl groups or hydrogen atoms on the periphery, which are essentially electron-deficient sites. Thus the 'electron-rich' and 'electron-deficient' regions are regularly alternating and there are 24 such regions, as schematically pointed out in Fig. 6 as − and + symbols, respectively. The ED contour also shows the delocalization of the electrons over the porphyrin ring.

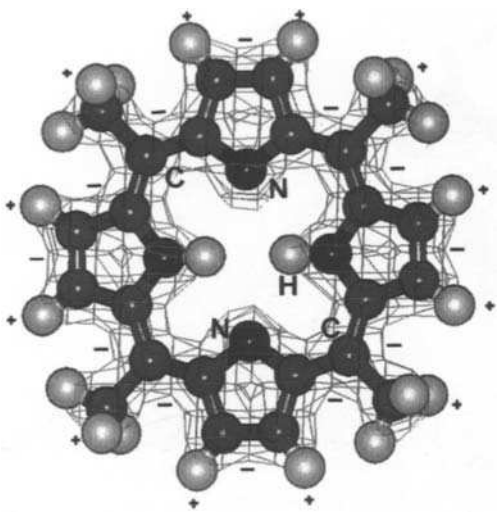

Figure 6. The 3-d contour electron density map of 5,10,15,20-tetramethyl porphyrin.

The molecular electrostatic potential [MEP] generated by the porphyrin complex was also calculated. The MEP maps indicate the positive and negative potentials occurring in space around the molecule. A cubic space consisting the molecule and 3Å from its outermost atoms in all directions is considered. The cubic space is divided into 25 equal spaced regions in all the three directions. The molecular electrostatic potential [MEP], V(R) between the molecular electronic and nuclear charge distribution as well as an external proton at all the points formed by a grid of $25 \times 25 \times 25$ points are calculated by the method proposed by Tomasi[34] according to the equation:

$$V(\vec{R}) = -\int \frac{\rho(\vec{r})}{\left|\vec{R}-\vec{r}\right|} dr + \sum_{\alpha=1}^{N} \frac{Z_\alpha}{\left|\vec{R}-\vec{R}_\alpha\right|} \tag{8}$$

where $\vec{R}, \vec{r}$, and $\vec{R}_\alpha$ are the coordinates of the external proton, electron and nucleus, respectively. Z_α is the nuclear charge and $\rho(\vec{r})$ is the molecular electronic charge density. The isopotential points are connected to form a contour and the positive potential contours (electrophilic sites) and negative potential contours (nucleophilic sites) are shown as dark and light shades, respectively. Fig. 7 shows the MEP map around the 5,10,15,20-tetramethyl porphyrin molecule. The MEP maps are in correspondence with the ED maps shown in Fig. 6. There are alternating electrophilic and nucleophilic regions

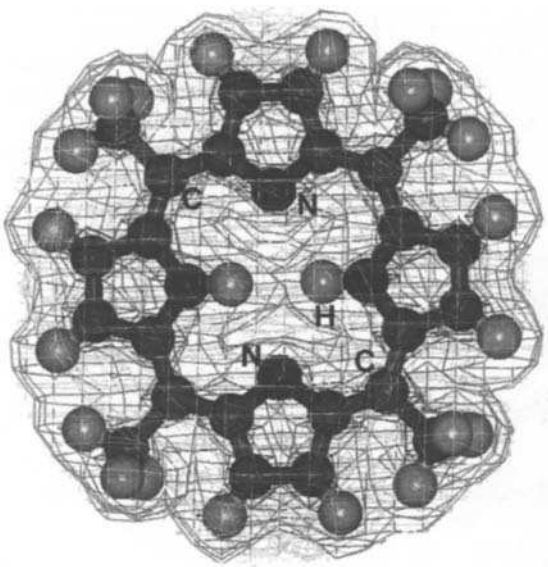

Figure 7. The 3-d contour molecular electrostatic potential of 5,10,15,20-tetramethyl porphyrin; the positive and the negative potential contours are shown as dark and light shades, respectively.

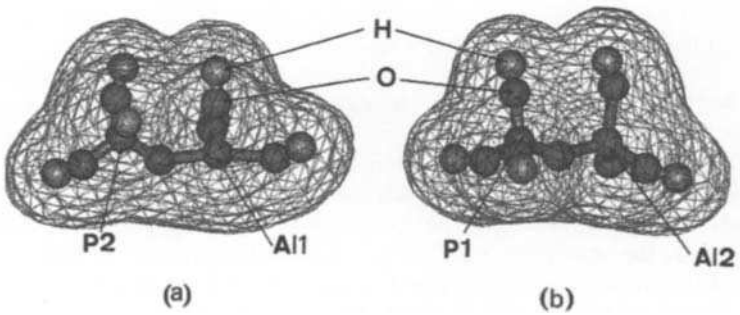

Figure 8. Typical dimer cluster models of Al1-P2 sites (a) and P1-Al2 sites (b) used to represent the sites in VPI-5 and the 3-d contour of electron density map around them.

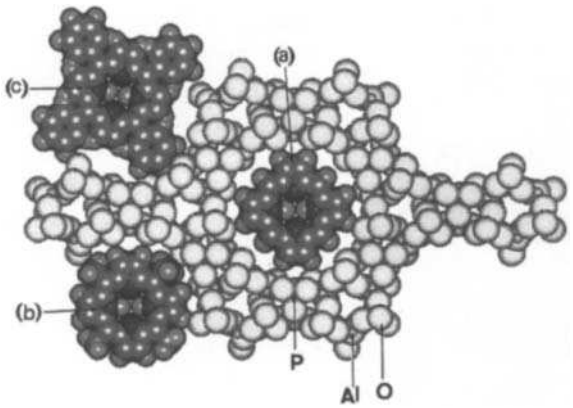

Figure 9. The relative sizes of the CPK models of porphyrin (a), 5,10,15,20–tetramethyl porphyrin (b) and 5,10,15,20–tetraphenyl porphyrin (c) molecules with respect to the diameter of the 18–member pore of VPI–5.

and the total projections on the periphery amounted to 24 such regions. For fundamental electronic properties such as binding energy and net charges on various atoms, the detailed report[27] may be referred.

A localized cluster model approach was adopted to study the electron density distribution in the pores of VPI–5. The calculations were carried out on cluster models containing two TO_4 groups, where T = P and Al. Typical cluster models centered at Al1–P2 and P1–Al2 sites are shown in Fig. 8. Nine such cluster models were generated to represent the 18–member pore of VPI–5. Fig. 8 also includes the 3–d contour of the electron density map around the cluster models. It was observed that there were electron–rich spaces around each TO_4 group and they were connected continuously. However, nearer to the oxygen which bridges the two TO_4 groups, there was a small electron–deficient region. Hence, the simulated electron density map of the 18–member pore in VPI–5 will have 18 electron–rich regions and 18 electron–deficient regions, regularly alternating. The MEP maps calculated for the framework cluster models showed alternating electrophilic regions around each $[PO_4]^+$ group and nucleophilic regions around each $[AlO_4]^-$ group, which was expected based on electrostatic principles. Comparing the ED and MEP maps of porphyrin with those of cluster models of VPI–5, it appears that the electron– rich and electron–deficient regions are regularly alternating in both porphyrins and VPI–5. However, the number of such polarized regions are greater in number for the porphyrin molecule compared to the pore of VPI–5. In Fig. 9, the molecular fitting of porphyrin and substituted porphyrins inside the pores of VPI–5 are shown as CG pictures. It is observed that the phenyl substituted porphyrins are too large to get encapsulated in VPI–5, while the methyl substituted porphyrin and unsubstituted porphyrin are tightly fitting in. When the distance between the electrophilic and nucleophilic centers in both porphyrins and VPI–5 are compared and an empirical fitting of the molecule inside pores were tried by CG technique, it was obse-

rved that the orientation of the molecule inclined at 45 degrees as shown in Fig. 10, rather than an orientation perpendicular to the 18- member pore(Fig. 9) leads to a perfect fit.

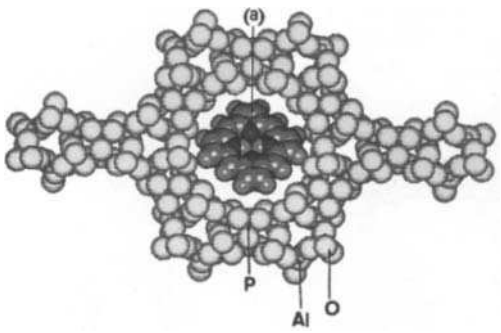

Figure 10. The molucelar fitting of CPK model of the porphyrin molecule (a) inside the pores of VPI-5. The molecular plane of porphyrin is inclined at 45 degress along the axis which passes through the pore of VPI-5.

In this inclined configuration (Fig. 10), the top portion of the molecule is in contact with the upper layer of VPI-5 channel, while the bottom portion of the molecule is in contact with the lower layer of VPI-5 channel. Thus by judicial use of the knowledge derived from cluster calculations, it is possible to solve the structures of even large complex molecules inside the microporous solvents.

4. STUDIES ON CARBON NANOTUBES

Carbon nanotubes are a new generation of sorbent materials with great potential for selective adsorption and shape selective separation. We report the studies on the MD simulation of structure of the carbon nanotube and the dynamic behaviour of aromatic molecules such as benzene, alkylated benzenes as well as alkylated naphthalenes[35]. The interest is to design effective molecular sieves for the bulk separation of hydrocarbon molecules of industrial importance.

4.1. The structure of carbon nanotubes

The model of the carbon nanotube is generated by rolling a sheet of graphitic layer of dimensions 25Å·10Å. This led to a open ended tube containing nearly 12 hexagonal rings lengthwise and 6 hexagonal rings on the circumference. The inner diameter of the tube after accounting for the van der Waals radii of carbons was 7.3Å and the computer graphics (CG) picture of the model in longitudinal and cross-sectional views are shown in Fig. 11a. The unsaturated valency of the carbon atoms on the circumference are saturated by adding hydrogen atoms. The hydrogen atoms have charges of +0.1 and the carbon atoms to which they are attached have charges of -0.1. Thus the carbon nanotube is a overall chargeless neutral structure. The aromatics such as benzene, the three isomers of xylene and two typical isomers of methyl naphthalene as well as dimethyl naphthalene were considered

in their equilibrium configurations. Their dimensions were obtained from the CPK model CG pictures. Initially, the MD simulations were performed for the carbon nanotube in the absence of any molecules. Both the longitudinal and cross–sectional configurations of the carbon nanotube after 2000 time steps of simulation are shown in Fig. 11b. Rarely any structural differences are noticed during this simulation and hence the chemical validity of the model is established. Our results indicate that such nanotubes are stable structures at 300K and their properties could be studied by simulation techniques.

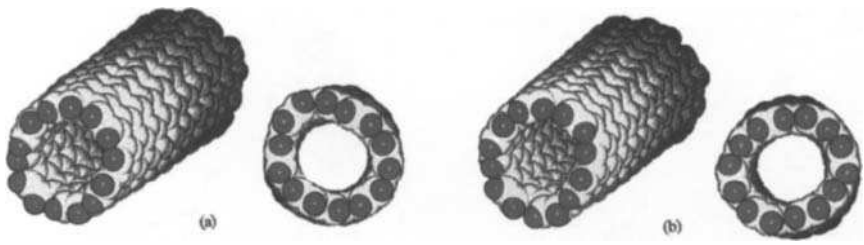

Figure 11. CG picture of the longitudinal and cross–sectional views of the carbon nanotube model considered for simulation (a) at 0 steps and (b) after 2000 steps of MD simulation at 300K.

4.2. Carbon nanotube: aromatics interaction

Studies to simulate the dynamic behaviour of benzene were carried out as the first step in the analysis of diffusion of various aromatics inside the carbon nanotube. The benzene molecule is ingested into the tube and it makes a smooth sailing towards the other end of the tube. The analysis of the potential energy of the system showed that the system has a favourable energy when the molecule is inside the tube and it has to cross the activation energy barrier to enter and exit the tubes. The dynamics of xylene molecules were studied, where the separation of isomers are industrially important and currently their isomerization– cum–separation are commercially carried out over zeolite molecular sieves[36]. It was observed that all these molecules could enter the tube and remain inside. Their overall dynamic behaviour is similar to the benzene molecule. The ingestion of all the isomers inside the tube in spite of the differences of their dimensions was surprising. We analyzed the results of the calculation in more detail to understand the rather interesting phenomenon. The variation in the pore width, measured as the largest diameter of the tube near the ingesting molecule, during the ingestion of the molecules are studied. This measurement indicates that there is widening of the pore due to the presence of the molecule. The tube itself is very flexible; the diameter increases to the extent of $\sim$ 1.5Å.

The next step of the investigation deals with the study of the behaviour of still larger molecules, namely mono and dimethyl naphthalenes. It was observed that the smaller naphthalenes could diffuse into the tube, while the larger naphthalenes is unable to enter the mouth of the tube. 2,6–dimethyl naphthalene (DMN) is a valuable intermediate for the preparation of monomer to produce thermotropic liquid crystalline polymers, altho-

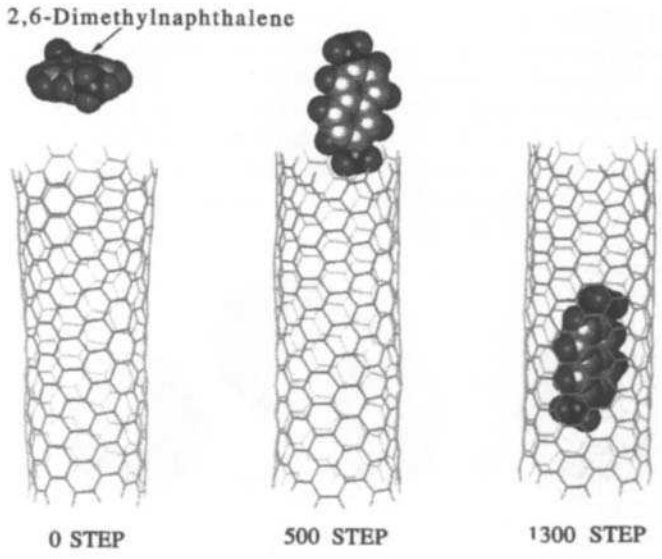

Figure 12. The dynamic behaviour of 2,6-dimethylnaphthalene at various time intervals during the simulation of the ingestion process into a carbon nanotube at 300K.

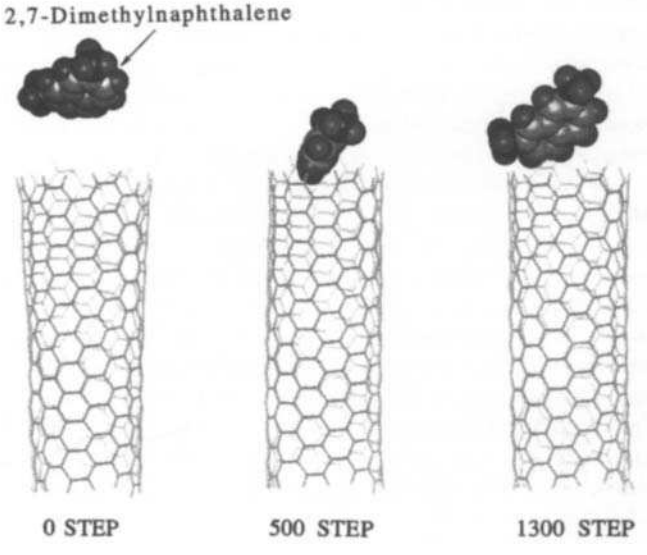

Figure 13. The dynamic behaviour of 2,7-dimethylnaphthalene at various time intervals during the simulation of the ingestion process into a carbon nanotube at 300K.

ugh nine other isomers of this compound with closely related dimensions are of no use to produce such engineering plastics. Liquid phase alkylation of naphthalene and monomethyl naphthalene lead to the selective formation of 2,6- and 2,7-DMN isomers[37]. The results of our simulations on the dynamic behaviour of these two isomers inside the carbon nanotube indicate that carbon nanotube could serve as useful molecular sieve for this separation. The results of the simulation studies of 2,6-DMN during the various time steps at 300K are shown in Fig. 12. It can be seen that the ingestion of the molecule takes place as in the case of benzene or xylenes. However, the same is not true in the case of 2,7-DMN as can be seen in Fig. 13, where the results of simulation during the various time steps at 300K are shown. The molecule clearly faces a greater activation energy and it is unable to enter the mouth of the tube.

The carbon nanotubes can be useful in the separation of molecules not only with different sizes (monomethyl naphthalenes) but also those with different shapes (dimethyl naphthalenes) as demonstrated with a tube of inner diameter of 7.3Å. The above results have clearly indicated that the application of carbon nanotubes for gas separation is in very early stage of a technology with far-reaching consequences. The important point brought out is the fact that computational techniques such as MD and CG methods are efficient for screening and designing of carbon nanotubes for selective adsorption and separation of molecules.

5. STUDIES ON SUPERCRITICAL FLUID EXTRACTION

The supercritical fluid extraction, for example - the use of supercritical CO_2 as the extracting solvent in place of organic solvents is becoming popular. The supercritical CO_2 has the following advantages: non-toxic, environmentally friendly, cheap, non-flammable and applicable on large scales[38]. The intrinsic mechanisms involved in the increased solubility of solute at supercritical conditions[39] as well as the enhancement effect imposed by the catalytic amounts of water[40] known as entrainer effect are studied.

5.1. Supercritical fluid extraction from adsorbed phase

The dynamics of adsorbed species over MgO(001) surface was studied by MD method. The migration of the adsorbed species was found to depend on the morphology of MgO and the thermal vibration of surface atoms in MgO lattice. Further, the situation where the supercritical fluid and adsorbed species exist together was simulated. The collision of supercritical fluid with the adsorbed species was identified as the primary cause of extraction. Additionally, the supercritical fluid form clusters around the desorbed species avoiding the readsorption. Thus, clustering is the secondary cause for the increased efficiency of supercritical extraction even above the critical conditions. The details of these simulation studies are given in the following section.

MgO solid was used as adsorbent to simulate solid surface and micropore systems, because of its chemical inertness and stability. Solid surface system was constructed with the dimensions of a = 33.04Å, b =16.62Å and c = 42.11Å, including 192 fluid molecules, 256 Mg atoms and 256 O atoms in a unit cell. Solid surface and micropore (diameter = ~4Å) systems were constructed with the dimensions of a = 37.90Å, b = 24.64Å and c = 72.10Å, including 350 fluid molecules, 768 Mg atoms and 768 O atoms in a unit

cell. Although these methods are applicable to investigate various supercritical fluids and adsorbed molecules, the fluid and adsorbed species are treated as rare–gas type model molecules to derive the basic information on the supercritical fluid extraction of adsorbed phase. The critical points of this fluid, namely T_c and P_c, are equal to 338 K and 132 atm, respectively. The two–body interactions of fluid–fluid, fluid–MgO, fluid–adsorbed species, and adsorbed species–MgO are represented by suitable Morse type potentials[39]. In the following sections we use the reduced units to represent temperature(T) and pressure (P) of the conditions. These are defined as: $T_r = T/T_c$ and $P_r = P/P_c$.

The dynamics of the adsorbed species were studied as a function of temperature. At 300K, the adsorbed species were almost static over Mg^{2+} ions on MgO surface, while at 1100K the migration of the adsorbed species from one Mg^{2+} to other Mg^{2+} ions were observed. At higher temperatures, such as 2200K, the desorption of adsorbed species was observed. The structure and dynamics of the supercritical fluid on MgO(001) were also investigated. The dynamics of the supercritical fluid was studied by MD simulation under the supercritical condition at 340K and 135 atm ($T_r = 1.01$, $P_r = 1.02$). Supercritical fluid molecules also undergo adsorption on MgO(001) surface, and a monolayer of supercritical fluid was formed on the surface. The adsorbed supercritical fluid molecules on MgO(001) surface at 0 time step were exchanged with others after 40000 time steps. This result suggests that the supercritical fluid molecules underwent reversible adsorption and desorption on solid surfaces under the thermal equilibrium conditions.

The supercritical extraction process of a model adsorbed species as described earlier from the MgO(001) surface was investigated on the basis of above MD calculations. Fig. 14 shows the dynamic behaviour of the fluid and adsorbed species on MgO(001) surface at 300K and 88.9atm which is not supercritical condition ($T_r = 0.89, P_r = 0.67$). Although the adsorbed species thermally vibrated on MgO(001) surface and slightly migrated on the surface, it was not extracted from the surface.

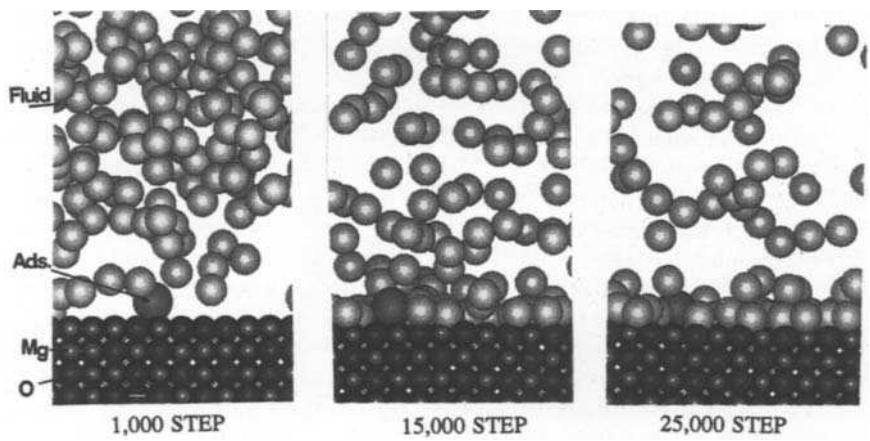

Figure 14. The dynamic behaviour of adsorbed species on MgO(001) surface with fluid at 300K and 88.9atm, which is *not* a supercritical condition.

The dynamic behaviour of the supercritical fluid and adsorbed species on MgO(001) surface under the supercritical condition at 400K and 198 atm ($T_r = 1.18, P_r = 1.50$) is shown in Fig. 15. After the supercritical fluid molecules condensed around the adsorbed species, the adsorbed species was extracted from MgO(001) surface by supercritical fluid after nearly 3000 time steps. In the system containing both supercritical fluid and adsorbed species, the extraction of adsorbed species occurred at low temperatures compared to the situation in the absence of fluid system.

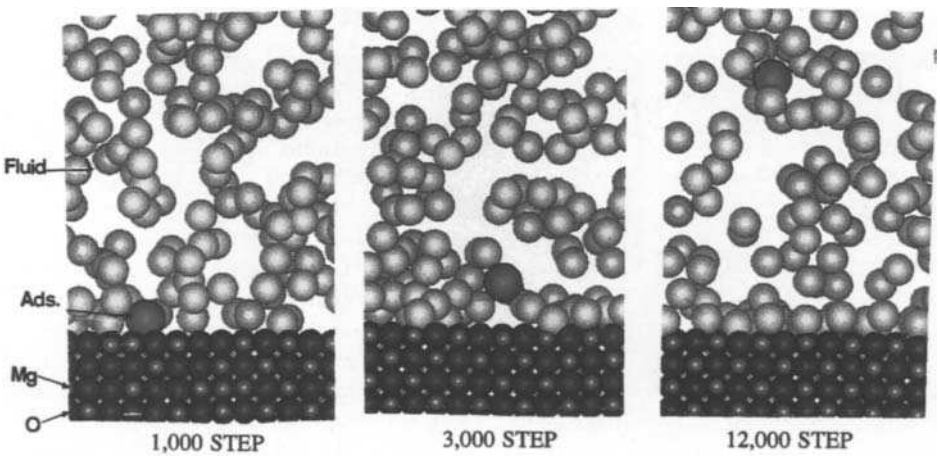

Figure 15. The extraction process of adsorbed species from MgO(001) surface under the supercritical condition at 400K and 198atm.

The detailed understanding of the role of supercritical fluid in the extraction process was studied by considering one adsorbed species and one fluid molecule on MgO(001). The desorption of adsorbed species never occurred unless the fluid molecule underwent direct collision with the adsorbed species. Further, the structure and dynamics of supercritical fluid inside a micropore generated on Mg(001) surface was studied. The dynamic behaviour of the supercritical fluid was studied for 40000 time steps under the supercritical condition at 340 K and 135 atm ($T_r = 1.01$, $P_r = 1.02$). The density of supercritical fluid in the micropore was higher than that in the fluid phase, which indicates that the supercritical fluid molecules are condensed in the micropore of MgO. The behaviour of adsorbed species inside the micropore in the presence of supercritical fluid was also studied. Fig. 16 shows the dynamic behaviour of a model adsorbed species in the micropore of MgO in the presence of the fluid at 300 K and 84.5 atm which is below supercritical condition ($T_r = 0.89$, $P_r = 0.64$). The adsorbed species moved to MgO(001) surface from the micropore along the surface after 3000 time steps, however it was not extracted from the surface during 40000 time steps. The dynamic behaviour of adsorbed species in the micropore under the supercritical condition at 340 K and 135 atm ($T_r = 1.01, P_r = 1.02$) is shown in Fig. 17. After 3000 time steps, the adsorbed species was extracted from the micropore directly to the fluid phase. Thus, it was indicated that the presence of supercritical fluid is crucial for the ready extraction from the micropore of solids. Another

interesting feature observed in the CG pictures of the snapshots during MD simulation is that the adsorbed species after extraction is wrapped by fluid molecules in the form of a cluster (Fig. 17). Thus the simulation studies in addition to explaining the behaviour of the supercritical fluids, they throw some light on the actual mechanism of the process.

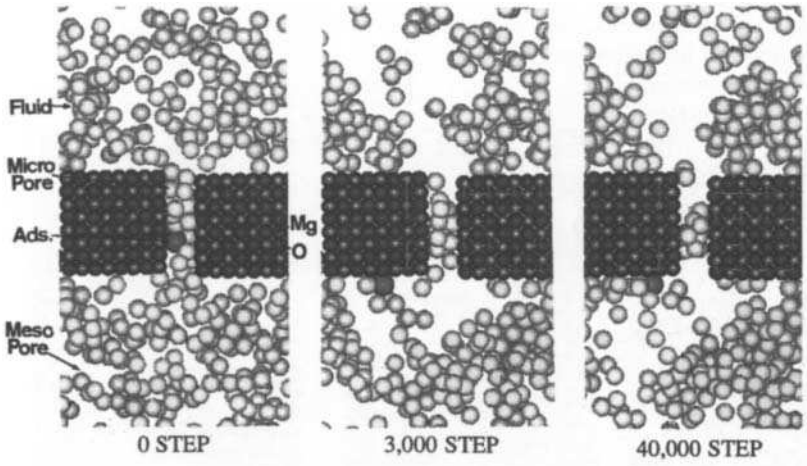

Figure 16. The dynamic behaviour of adsorbed species and the fluid molecules over solid surface and micropores of MgO at 300K and 84.5atm, which is *not* a supercritical condition.

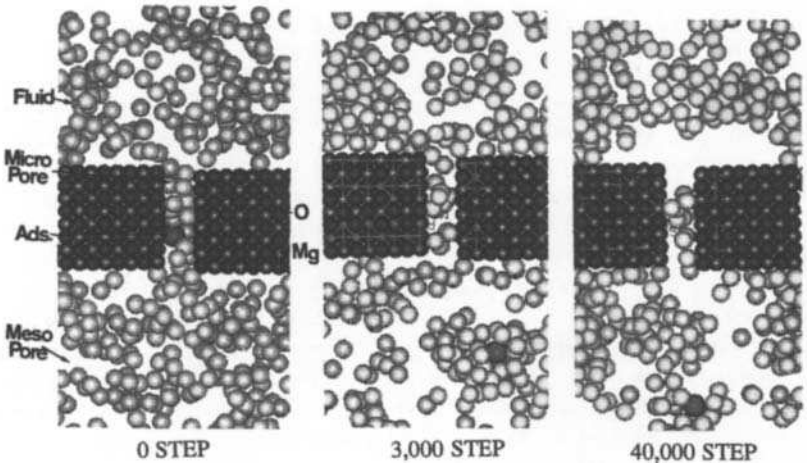

Figure 17. The dynamic behaviour of adsorbed species and the fluid molecules over solid surface and micropores of MgO under the supercritical condition at 340K and 135atm. Under these conditions, the dynamic behaviour led to the extraction of the adsorbed species from the micropore of MgO.

5.2. Role of entrainers in the supercritical extraction

Although CO_2 is the most commonly used supercritical fluid for extraction, the solubility of certain solutes in CO_2 is usually low and causes an inconvenience. The remedy for this problem is to add some entrainers such as water to facilitate the extraction. In this background, the MD simulations were carried out to study the supercritical extraction of nicotine by CO_2 in the presence and absence of water as entrainer[40]. In the tobacco leaf, nicotine molecule is bonded to other organic molecules and forms organic acid salts. The malic salts of nicotine was chosen as the model with nicotine bonded to two malic molecules by hydrogen bonds[41]. It is assumed that when malic salts of nicotine are extracted from tobacco leaf, supercritical CO_2 or entrainer molecule attacks the hydrogen bonds and decomposes the salt into three molecules.

The role of water as entrainer in the extraction of nicotine by supercritical CO_2 fluid was studied by MD simulation. The following three systems were studied in detail:

a) nicotine molecule and CO_2 fluid

b) malic salts of nicotine and CO_2 fluid

c) malic salts of nicotine, CO_2 fluid and water molecules.

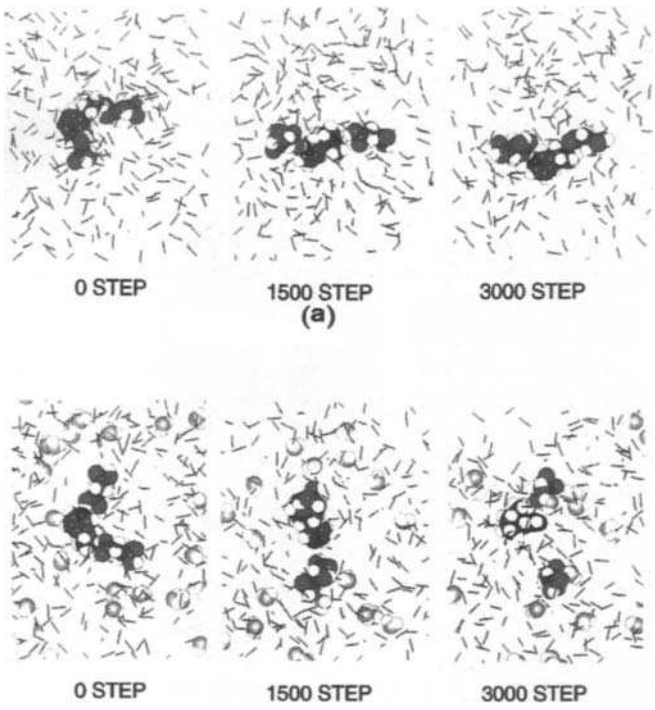

Figure 18. The dynamic behaviour of (a) malic salts of nicotine and CO_2 fluid, as well as (b) malic salts of nicotine, CO_2 fluid and water molecules.

The dynamic behaviour of the system b (nicotine salt and CO_2 supercritical fluid) and the system c (system b plus entrainer molecules) is shown in Figs. 18a and 18b, respectively. It can be seen from these CG pictures that the malic salts of nicotine keeps its configuration even on interaction with the supercritical CO_2 and the two hydrogen bonds remain stable during the simulation (Fig. 18a). On the contrary, the separation of nicotine from its malic counterparts develops in the presence of entrainer molecules and hydrogen bonds become finally broken (Fig. 18b).

The selective breaking of hydrogen bond in the presence of entrainer molecules is also clearly brought out by monitoring the hydrogen bond distance during the MD simulation. Similar monitoring of the distance between the water molecule and the nitrogen of nicotine indicated that water molecules form a hydrogen bond with nicotine by replacing the malic residue. Further, the formation of a cluster of fluid around the malic salts of nicotine was also observed. This is similar to the behaviour of supercritical CO_2 around the adsorbed species in the example shown in the previous section. The formation of a cage surrounding the adsorbate or solute, and the dynamic nature of this cage seems to be a common phenomenon. The formation of such an dynamic cage prevents the smooth mobility of the solute or adsorbate, thus increasing the solubility or extraction, respectively.

6. SUMMARY

The contents of the above reports could be summarized to conclude that the computational studies are having a substantial impact on our understanding of synthetic sorbents at present and will have enormous predicting power in the not too distant future. The tactics needed to attack the problems lie in judicial use of different combination of computational techniques. In this chapter, it has only been possible to highlight the studies on a few specific synthetic sorbents. The reader can find a comprehensive survey of the application of computational methods for zeolite studies in the book edited by Catlow[42]. All those methodologies are essentially applicable to any other synthetic sorbents and essentially reminds us that a great deal remains to be done. Future explorations should deal with the elimination of some of the approximations that are often being made, such as semi-empirical QC methods. Particularly with the advent of limitless computing power, more accurate QC and MD calculations will become feasible in the foreseeable future. Thus the computational methods are poised to make a strong impact in the design of sorbents for selective adsorption and separation technology.

REFERENCES

1. D.W. Breck, Zeolite Molecular Sieves; Structure, Chemistry and Use, Wiley, New York, 1974.
2. S.T. Wilson, B.M. Lok, C.A. Messina, T.R. Cannan and E.M. Flanigen, J. Am. Chem. Soc., 104 (1982) 1146.
3. P.L. Walker, Jr., T.G. Lamond and J.E. Metcalfe, in: Proc. 2nd Conf. Industrial Carbon Graphite, Society of Chemical Industry, London, 1966, p.7.
4. S. Iijima, Nature, 354 (1991) 56.

5. R.W. Shaw, T.B. Brill, A. Clifford, C.A. Eckert and E.U. Franck, Chem. Eng. News, 69 (1991) 26.
6. J.W. Richardson, Jr., J.J. Pluth and J.V. Smith, Acta Crystallogr., B44 (1988) 376.
7. L.B. McCusker, Ch. Baerlocher, E. Jahn and M. Bulow, Zeolites, 11 (1991) 308.
8. Molecular modeling package - Quanta and CharmM - Release 2.1; Polygen Corporation: Waltham, USA, 1990.
9. M.J.S. Dewar and W. Thiel, J. Am. Chem. Soc., 99 (1977) 4899.
10. P. Dauber-Osguthorpe, V.A. Roberts, D.J. Osguthorpe, J. Wolff, M. Genest and A.T. Hagler, Proteins: Struct. Funct. Genet., 4 (1988) 31.
11. Molecular modeling package - Insight and Discover - Version 3.1, Biosym Technologies Inc., San Diego, U.S.A., 1993.
12. K. Kawamura, in F. Yonezawa (ed.), Molecular Dynamics Simulations, Springer-Verlag, Berlin, 1992, p.88.
13. S. Prasad and R. Vetrivel, J. Phys. Chem., 96 (1992) 3092.
14. S.T. Wilson, B.M. Lok and E.M. Flanigen, Crystalline Metallophosphate Composition, U.S. Patent 4310440, 1982.
15. I. Balakrishnan and S. Prasad, Appl. Catal., 62 (1990) L7.
16. N.J. Tapp, N.B. Milestone and D.M. Bibby, Zeolites, 8 (1988) 183.
17. S. Prasad and R. Vetrivel, J. Mol. Catal., 84 (1993) 299.
18. N.J. Tapp, N.B. Milestone, M.E. Bowden and R.H. Meinhold, Zeolites, 10 (1990) 105.
19. R. Khouzami, G. Coudurier, F. Lefebvre, J.C. Vedrine and B.F. Mentzen, Zeolites, 10 (1990) 183.
20. S. Prasad, I. Balakrishnan and R. Vetrivel, J. Phys. Chem. 96 (1992) 3096.
21. D. Muller, I. Grunze, E. Hallas and G. Ladwig, Z. Anorg. Allg. Chem., 500 (1983) 80.
22. M.E. Davis, C. Saldarriga, C. Montes, J.M. Garces and C.E. Crowder, Nature, 331 (1988) 698.
23. S. Prasad, S-B. Liu and R. Vetrivel, Stud. Surface Sci. Catal., 90 (1994) 291.
24. S. Prasad and R. Vetrivel, J. Phys. Chem., 98 (1994) 1579.
25. P.J. Grobet, J.A. Martens, I. Balakrishnan, M. Mertens and P.A. Jacobs, Appl. Catal., 56 (1989) L21.
26. G. Engelhardt and W. Veeman, J. Chem. Soc., Chem. Comm., 7 (1993) 622.
27. A. Miyamoto, M. Katagiri, M. Kubo and R. Vetrivel, Res. Chem. Int., 21 (1995) 151.
28. W. Kohn and L.J. Sham, Phys. Rev., A140 (1965) 1133.
29. B. Delley, J. Chem. Phys., 92 (1990) 508.
30. Y.W. Chan and R.B. Wilson, ACS Prep. Div. Petr. Chem., 33 (1988) 453.
31. R.F. Parton, L. Uytterhoeven and P.A. Jacobs, Stud. Surface Sci. Catal., 59 (1991) 395.
32. M. Nakamura, T. Tatsumi and H. Tominaga, Bull. Chem. Soc. Jpn., 63 (1990) 3334.
33. R. Parton, D. De Vos and P.A. Jacobs, in: Zeolite Microporous Solids: Synthesis, Structure and Reactivity, E.G. Derouane, F. Lemos, C. Naccache and F.B. Ribeiro (eds.), NATO ASI Ser. C., Kluwer Academic Publishers, Amsterdam, 1992, p.555.

34. J. Tomasi, in: Chemical Applications of Atomic and Molecular Electrostatic Potentials, P. Politzer and D.G. Truhlar (eds.), Plenum Press, New York, 1981, p.151.
35. H. Takaba, M. Katagiri, M. Kubo, R. Vetrivel and A. Miyamoto, Microporous Materials, 3 (1995) 449.
36. W.O. Haag and F.G. Dwyer, AIChE 8th meeting, Boston, MA, August 1979, American Institute of Chemical Engineering, New York, 1979.
37. D. Fraenkel, M. Cherniavsky, B. Ittash and M. Levy, J. Catal., 101 (1986) 273.
38. G. Kaupp, Angew. Chem., Int. Ed. Engl., 33 (1994) 1452.
39. H. Takaba, M. Katagiri, M. Kubo, R. Vetrivel and A. Miyamoto, unpublished results.
40. H. Takaba, M. Katagiri, K. Mizukami, R. Miura, E. Broclawik, M. Kubo and A. Miyamoto, Proc. I. Int. Conf. Solvo-thermal Reactions, (in press).
41. M. Dezelic and B. Nikolin, Spectrochimica Acta, 23 (1967) 1149.
42. C.R.A. Catlow (ed.), Modelling of Structure and Reactivity in Zeolites, Academic Press, London, 1992.

A. Dąbrowski and V.A. Tertykh (Editors)
Adsorption on New and Modified Inorganic Sorbents
Studies in Surface Science and Catalysis, Vol. 99

Chapter 1.2
Controlled porosity glasses (CPGs) as adsorbents, molecular sieves, ion–exchangers and support materials

A.L. Dawidowicz

Department of Chemical Physics and Physicochemical Separation Methods,
Faculty of Chemistry, University of Maria Curie-Skłodowska, 20-031 Lublin, Poland.

Among siliceous materials which play the role of adsorbents, support materials and molecular sieves in chromatographic processes controlled porosity glasses (CPGs) deserve special attention. The popularity of these materials results from their widespread utilization for biomolecule separation (by means of affinity chromatography) and, earlier, for macromolecule separation (by means of size exclusion chromatography). However, a range of properties such as hardness, chemical and thermal resistance, very good permeability and surface chemistry indicate possibilities of their wider application. Although the structure of CPGs is composed of almost pure silica (94-99 % SiO_2; 1-6 % B_2O_3; 0.05-0.3 % Na_2O), they are obtained from glass, and this is why the name "porous glasses" was historically accepted. The possibility to produce porous glasses with *a priori* desired properties (mean pore diameter, pore volume, specific surface area), the high reproducibility of these materials with similar properties in subsiquant preparation procedures, and especially a narrow pore size distribution additionally justify the name of controlled porosity glasses commonly given to porous glasses.
Fundamental properties and examples of CPGs applications are the subject of numerous papers [1-5]. Therefore, apart from a general description of CPGs, an effort is made in this chapter to present other, rarely discussed features which differentiate these materials from the most popular chromatographic sorbents – silica gels.

1. GLASS AS A SOURCE OF POROUS SILICA

The history of porous glasses preparation goes back to the year 1926 when Turner and Winks [6] published a paper on leaching boric oxide containing glasses with hydrochloric acid. The researchers reported that glasses in the $Na_2O - B_2O_3 - SiO_2$ system became very soluble in HCl solution when B_2O_3 content exceeded 20 %. The leachability of the glasses was selective since the acid left behind a porous skeleton composed of almost pure silica. The finding of Turner and Winks was the starting point for Nordberg and Hood [7] to develop a process (the so called Vycor process) for making porous objects from which, after sintering, high silica glass objects could be produced. In their patents [7-9] Nordberg and Hood described how - after heat treatment - glass composition in a certain region of

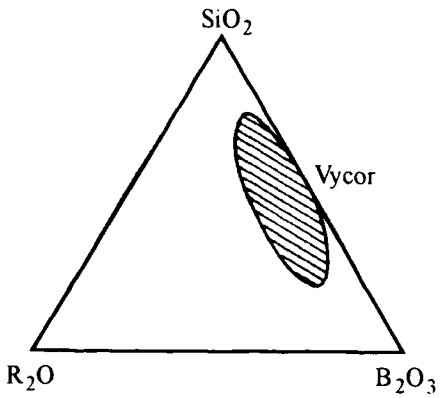

Figure 1. Vycor glass zone in the $R_2O-B_2O_3-SiO_2$ system.

the ternary system $R_2O-B_2O_3-SiO_2$, where R_2O means Na_2O or K_2O or Li_2O (Fig. 1), separates into two interconnected (continuous and mutually penetrated) phases. One of these phases is very rich in silica and is insoluble in acids, while the second is soluble in acids and may be leached out of and away from the insoluble phase leaving the latter in a rigid cellular structure which maintains the orginal shape of the initial glass. In the Vycor process high silica glass objects are produced by sintering porous objects, yet the porous structure of the intermediate product (i.e. of porous object) was not point of interest for the autors of Vycor process. Only further experiments with alkali-boro-silicate glasses, especially the works of Dobychin 10,11], Poray-Koshits [12], Molchanova [13] and Zhdanov [14] (who summarized the results of their work [15]), showed the influence of thermal treatment and composition of this kind of glasses on the dimension of alkaliborate heterogeneities and, consequently, on the diameter of the pores formed in the siliceous residue. These finding were the basis for the investigations by Haller [16,17], who worked out a preparation procedure of porous glasses differing in mean pore diameter which can be applied as sorbents in chromatography.

The making of controlled porosity glasses involves a three-step procedure:

A) Preparation of raw material. Melting a suitable glass composition [2,3,7-9,16,17], for instance from the area patented by Nordberg and Hood (see Fig. 1). To obtain best results, melting should be done in platinum containers under stirring and observance of all practices to obtain a highly homogeneous glass. After the melting process the glass is quench-cooled to minimize any phase separation.

B) Thermal treatment of glass obtained in stage A. The glass (in pieces or as crushed and sieved powder) is reheated for several hours to several days [16,17] to achieve phase separation and to increase the microheterogeneities which are the alkali-borate phase. The thermal history determines the later size of the CPG pores. The separation process for alkali-borate glasses occurs in the temperature range from about 500 to 700°C.

C) Leaching process of thermally treated glass. In this stage the glass, when heated in the form of pieces, is crushed and sieved to the desired particle-size fraction and leached at first with hot acid (e.g. 3 N HCl or H_2SO_4 at 60 to 100°C for 6-10 hrs) and then (after washing with water) with alkali solution (e.g. 0.5 N NaOH at 20°C for 2 to 6 hrs) [16,17].

The acid leaching removes alkali-borate heterogeneities and produces the porous material which can contain colloidal silica or secondary silica network in its pores [12,16]. These silicas are removed from the pores by alkali solution. The timing of this stage is rather critical, otherwise the prepared CPG is destroyed or the unremoved fine silica decreases the pore volume of the final product, thus interfering with its later use.
The properties of CPGs obtained from the same glass composition and under the same conditions of thermal treatment and leaching process are very similar, which proves the reproducibility of the preparation procedure. However, it should be stressed that each step has to be well mastered as small differences in the process can lead to materials of undesirable properties. For example, small deviations in the composition of the initial glass, particularly its impurities, cause changes in the phase-separation kinetics. Similarly, small differences in the thermal treatment (temperature, time), which is responsible for the degree of the demixture process and the dimension of alkali-borate heterogeneities, bring about the formation of CPGs of various physicochemical parameters. The details of CPG preparation can be found in [2,3,7-9,15-17].

The materials prepared by Electro-Nucleonics, Inc., (USA) under the name CPG-10 [4,18] are the most popular commercial controlled porosity glasses used for chromatography and/or for enzyme immobilization. These packings in the form of free-flowing powders consisting of non-spherical rigid porous particles are available in three standard particle sizes d_p:125-177, 74-125, and 37-74 μm. They differ in the mean pore diameter D (from 7.0 to 400.0 nm), specific surface area S_{BET} (from 4 to 370 m^2/g), and pore volume V_p (between 0.6 and 1.1 cm^3/g). In fact a wider assortment of CPGs for chromatography can be obtained. There are no problems, for example, to produce CPGs of smaller particle sizes (ca. 5, 10 μm) [19] or CPGs whose particles have a spherical shape [20-22]. Similarly CPGs of higher porosity (exceeding 1.5 cm^3/g) can also be prepared [23], but due to the lower mechanical stability their usefulness (especially for HPLC) is limited.

2. STRUCTURE OF CPGs

The phenomenon of phase separation in alkali-boro-silicate glasses (which is the principal process in CPG production) is responsible for the structure of the siliceous network obtained after leaching of thermally treated raw material. Contrary to silica gel (the most popular siliceous sorbent used in chromatography), the structure of CPG resembles a sponge [5] composed of almost pure SiO_2, whereas the porous structure of most silica gels is built of $(SiO_2)_n \times (H_2O)_m$ globules [24]. The electronomicrographs of both materials are shown in Fig. 2.

Although the porous lattice of CPG and silica gel is made of the same component (SiO_2), silica gel demonstrate lower resistance to temperature.
As seen in Fig. 3 illustrating the effect of heat treatment of CPG and silica gel, the structure of CPG does not change till 650°C.

Further temperature increase brings about the decrease of the mean pore diameter and porosity. In silica gel, significant changes in its structure are observed above 550°C. In consequence, porous glass contaminated with organic material can be cleaned by heating it up to 650°C or by oxidation in hot concentrated nitric acid without any change in pore size distribution. Such cleaning procedure is almost impossible for silica gel.

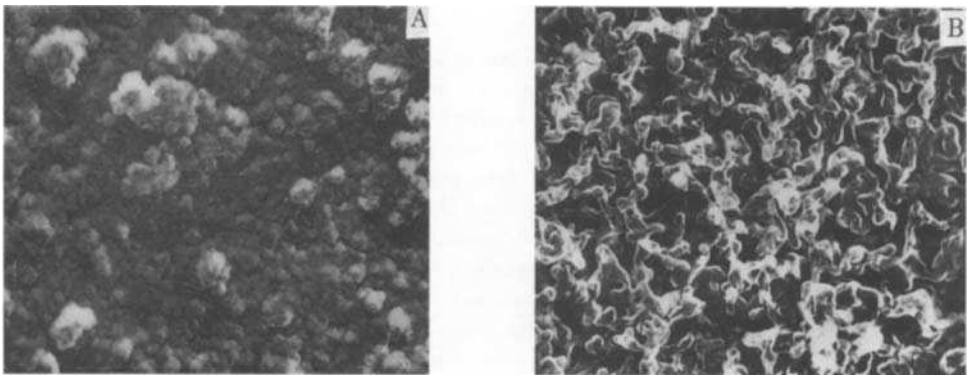

Figure 2. Microscope photos of silica gel (mean D = 58.0 nm) (A) and of porous glass (mean D = 60.0 nm) (B). Multiplication 42000 x.

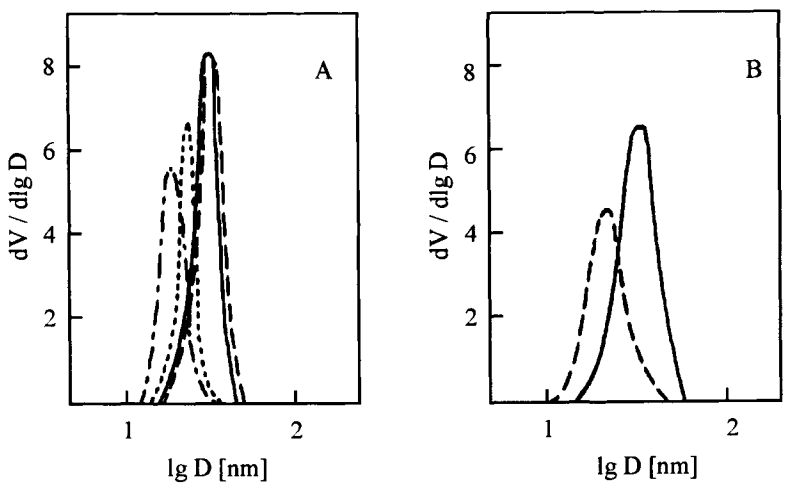

Figure 3. Pore size distribution functions (mercury porosimetry data) for: A) initial CPG (D = 30.5 nm) (solid line) and the same material heated for: 20 hrs at 650°C (dashed line); 20 hrs at 720°C (dotted line); 20 hrs at 805°C (dash-dotted line), B) initial silica gel (D = 32.8 nm) (solid line) and the same material heated for 20 hrs at 580°C.

The sponge-like structure of CPG probably also explains why its resistance to pH is a little higher than that of silica gel. The solublity of SiO_2 increases with pH, but in the case of CPG this process rarely interferes with normal laboratory operation unless pH exceeds 9.0 or even 9.5. For silica gel pH above 8.0 is significant – see Fig. 4.

The characteristic feature of controlled porosity glasses is a very narrow pore size distribution [2,3,5,16], well seen when compared with silica gel or other porous materials produced by polymerization or by crosslinking of monomers – cf. Fig. 5.

The breadth of the pore diameters distribution in CPGs is usually less than 10 %.

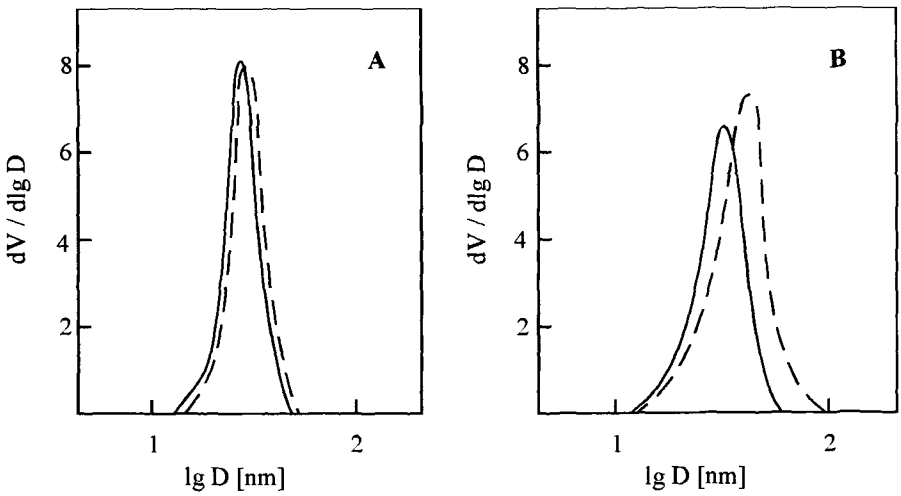

Figure 4. Pore size distribution functions (mercury porosimetry data) for: A) initial CPG (D = 29.6 nm) (solid line) and the same material after leaching by carbonate buffer, pH 9.0, over 5 hrs (dashed line), B) the same for silica gel (D = 32.8 nm).

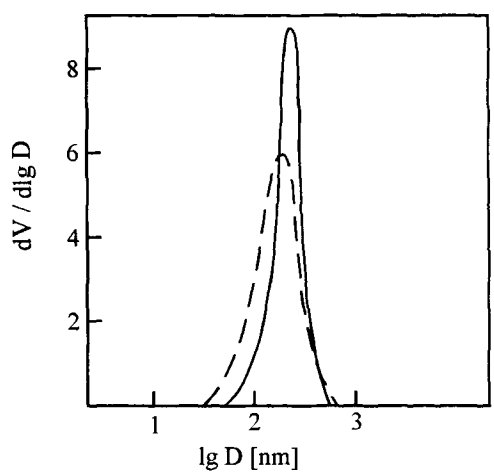

Figure 5. Pore size distribution functions (mercury porosimetry data) for CPG (D = 60.0 nm) (solid line) and silica gel (D = 58.0 nm) (dashed line).

The customary definition of this distribution is that 80 % of pore volume consists of pores whose size fall within 10 % of the average pore size. Such narrow pore size distribution results from the narrow size distribution of alkali-borate heterogeneities formed in alkali-boro-silicate glasses during their thermal treatment. The uniformity of the kinetics

of the phase separation process is also proved by almost the same pore size at the surface of the product as in its centre.

The rigidity of controlled porosity glasses as well as their sharp pore size distribution suggested their applicability as macromolecular sieves for size exclusion chromatography (SEC) - the separation method based on the ability of the penetration of pores by molecules differing in diameter [2-5,21,22,25,26]. Among siliceous materials controlled porosity glasses demonstrate a very good separation ability of macromolecules, which is reflected by the flat run of the calibration curves resulting exactly from the narrow pore size distribution. The calibration curves for exemplary columns packed with CPG and silica gel of similar physicochemical properties are illustrated in Fig. 6.

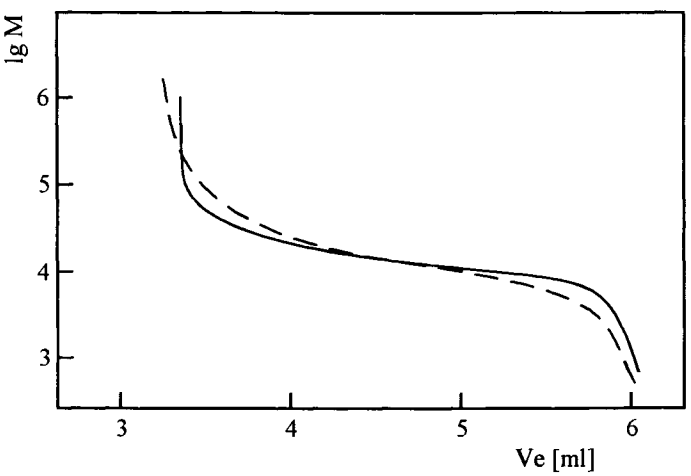

Figure 6. Calibration curves for SEC columns packed with CPG (D = 31.0 nm; $V_p = 1.12\,cm^3/g$; $d_p = 12\,\mu m$) (solid line) and silica gel (D = 29.1 nm; $V_p = 1.09\,cm^3/g$; $d_p = 10\,\mu m$) (dashed line). Column 300 x 6 mm. Polystyrene calibration standards. Mobile phase - tetrahydrofuran.

Although a number of packings of organic origin for SEC are now produced [27], in the 1960s and 70s CPGs played one of the most important roles in the field of macromolecules separation and purification by means of SEC. They are still applied for this purpose today. Ideally, in size exclusion chromatography, one desires a minimum of adsorptive or repulsive interactions between purified molecules and sorbent. With CPGs this goal is very often difficult to achieve due to the presence of strong adsorption sites on their surface (see Chemistry of CPG Surface below). The application of a proper mobile phase composition (with components blocking the adsorption sites) or CPG surface modification helps remove obstacle [3,18,22,28,29].

3. CHEMISTRY OF CPG SURFACE

Alongside investigations dealing with preparation and structure of controlled porosity glasses research works of the chemistry of the CPG surface were carried out. Although at first the surface of CPG was identified with the surface of silica gel, it was soon realized that CPGs showed stronger adsorption properties than silica gels (Fig. 7).

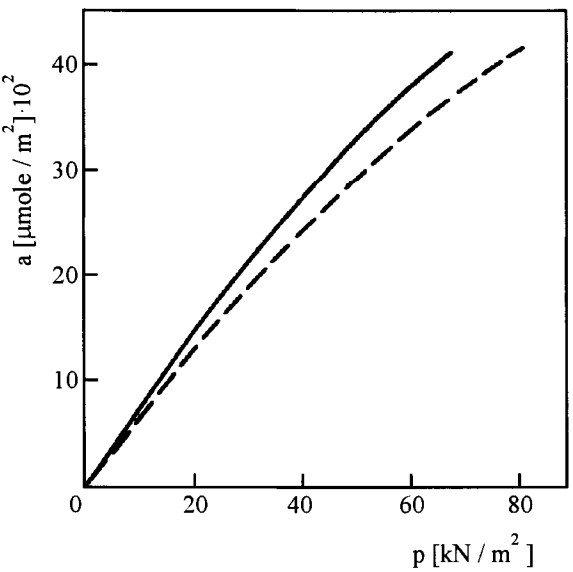

Figure 7. The adsorption isotherms of benzene on CPG ($S_{BET} = 298\,m^2/g$) (solid line) and silica gel ($S_{BET} = 269\,m^2/g$) (dashed line).

The same conclusion was drawn from the confrontation of silica gel and CPG used as adsorbents in HPLC columns [19]. Indeed the separation of simple compounds on columns filled with both mentioned materials is similar (see Fig. 8) [19], but the comparison of these compounds for their capacity factors calculated per $1\,m^2$ of the sorbent area in the chromatographic column (Table 1) points out a stronger interaction of the separated molecule with the CPG surface.

Stronger adsorption properties of CPG are especially evident for polar molecules with electron-donating atoms [30,31], and they cannot results only from the presence of silanol groups, which play the role of adsorption sites on the silica gel surface.

Already in the 1950s Sidorov [32] showed a difference between silica gel and the CPG surface. He proved that in the CPG surface there exist, beside silanol groups, boron atoms and hydroxyl groups bonded with surface boron atoms. Their presence results from the residue of B_2O_3 (1-6 %) which remains in the siliceous structure of CPG after its preparation procedure. More information was supplied by the investigations in 1960s and 1970s in which CPGs, CPGs with adsorbed molecules and CPGs with chemically modified surface groups were examined by means of infrared spectroscopy [33-48].

Table 1
Values of the capacity factors calculated for one square meter of a sorbent in HPLC column. Packings: LiChrosorb Si 100 ($S_{BET} = 318\ m^2/g$; $V_p = 1.32\ cm^3/g$; $D = 16.0$ nm) and CPG ($S_{BET} = 347\ m^2/g$; $V_p = 1.16\ cm^3/g$; $D = 13.4$ nm). Mobile phase: hexane

Substance	CPG	LiChrosorb Si 100
Benzene	0.09	0.09
Naphthalene	0.18	0.16
Diphenyl	0.26	0.21
Anthracene	0.33	0.27
Nitrobenzene	1.88	1.59

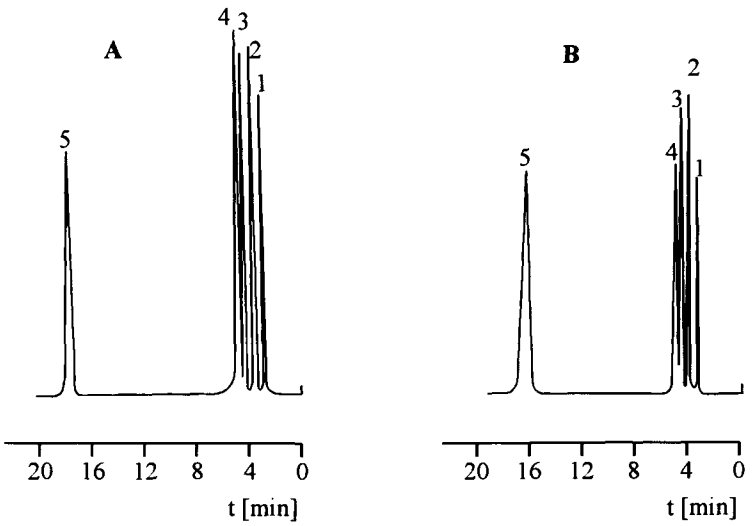

Figure 8. Chromatograms of testing mixture obtained on the columns: A) filled with CPG ($S_{BET} = 347\ m^2/g$; $D = 13.4$ nm; $V_p = 1.16\ cm^3/g$), B) packed with LiChrosorb Si-100 ($S_{BET} = 318\ m^2/g$; $D = 16.0$ nm; $V_p = 1.32\ cm^3/g$). Column: 250 x 4 mm. Mobile phase: hexane at 1 ml/min. Peaks: 1 = benzene; 2 = naphthalene; 3 = diphenyl; 4 = anthracene; 5 = nitrobenzene.

They allowed to visualize an image of the CPG surface chemistry which appears to be more complex than silica gel surface. The conclusions from these works are as follows:

1) The infrared spectroscopy shows the presence of surface SiOH groups [35,36]. Infrared spectra also reveal the surface B-OH groups but only after degasing of CPG at elevated temperatures under vacuum conditions [32-34,37]. Geminal OH structures bonded with Si as well as B atoms can be detect among hydroxyl groups [38].

2) The CPG surface is covered by adsorbed water. The desorption of water takes place at about 200°C [39].
3) When CPG is heated in the temperature above 400°C its surface gets enriched in boron atoms migrating from
the interior of the siliceous CPG skeleton [35,40-44]]. The surface boron concentration increases with time and temperature. The infrared investigations suggest the formation of borate clusters on the surface of long thermally treated CPG [43]. B-O-B bridges formed on the surface of heated CPG hydrolyse much easier than B-O-Si or Si-O-Si bonds [35,43,43]. The Si-O-Si connections on CPG surface also hydrolyse much easier than the analogous silioxane bridges on the surface of silica gel thermally treated in the temperature above 400°C. Such behaviour results from the influence of the adjacent boron atoms [35,42]. The water formed from silanol condensing at elevated temperatures hydrolyses B-O-B bridges appearing on the CPG surface as the result of boron migration from the interior of the CPG skeleton [43]. Consequently, the concentration of B-OH groups increases in this reaction. The condensation of hydroxyl groups bonded with silica atoms starts above 200°C, whereas the B-OH groups are much more resistent thermally and condense above 600°C.
4) Kirutenko, Zhdanov, Bobrov et al. [43,45,46] proved the presence of hydroxyl groups bonded not only with three-coordinated but also with tetra-coordinated boron atoms.
5) Beside boron atoms bonding hydroxyl groups, the CPG surface contains free boron atoms of strong electroacceptor properties [32,35,42,47,48].

The schematic picture of the CPG surface and the processes occuring during its thermal treatment can be illustrated as in Fig. 9.

Investigations of surface free energy (SFE) of controlled porosity glasses and silica gels carried out more recently showed certain similarity in the properties of bare materials and important differences caused by thermal treatment [49-56]. Dispersive interactions expressed as dispersive component of SFE (γ_s^d) and polar interactions expressed as polar component of SFE (γ_s^p) measured by means of hexane and toluene respectively are similar for both materials. The average value of γ_s^d for silica gel equals 35.6 mJ/m^2 and for CPG 35.0 mJ/m^2. The mean values of γ_s^p for silica gel and CPG are 159.8 mJ/m^2 and 159.2 mJ/m^2, respectively. The thermal treatment of both materials leads to a small increase of dispersive interactions and simultaneously causes a significant drop of polar interactions.

The investigations of γ_s^p changes resulting from the rehydroxylation process show that thermally treated CPGs are easily rehydroxylated (by water vapour), whereas silica gels require stronger hydroxylation, such as treating with diluted alkaline solutions.
The kinetics of the suface rehydroxylation process depends on the boron content on the CPG surface: the bigger surface boron concentration, the quicker the rehydroxylation process.

Adsorption of ions from aqueous solutions on CPGs and their surface charge are very sensitive to the solution pH. In this respect, the behaviour of CPG is similar to silica gel and other oxides and different from most aluminosilicates showing a fixed surface charge and low sensitivity to pH. Negative surface charge density (σ_o) of CPG over a wide pH range promotes adsorption of cations, while adsorption of anions is generally low. The pH dependence of adsorption of multivalent cations on CPG is typical for oxides [57]. The uptake is negligible at low pH values and then it increases from 0 to 100 % within

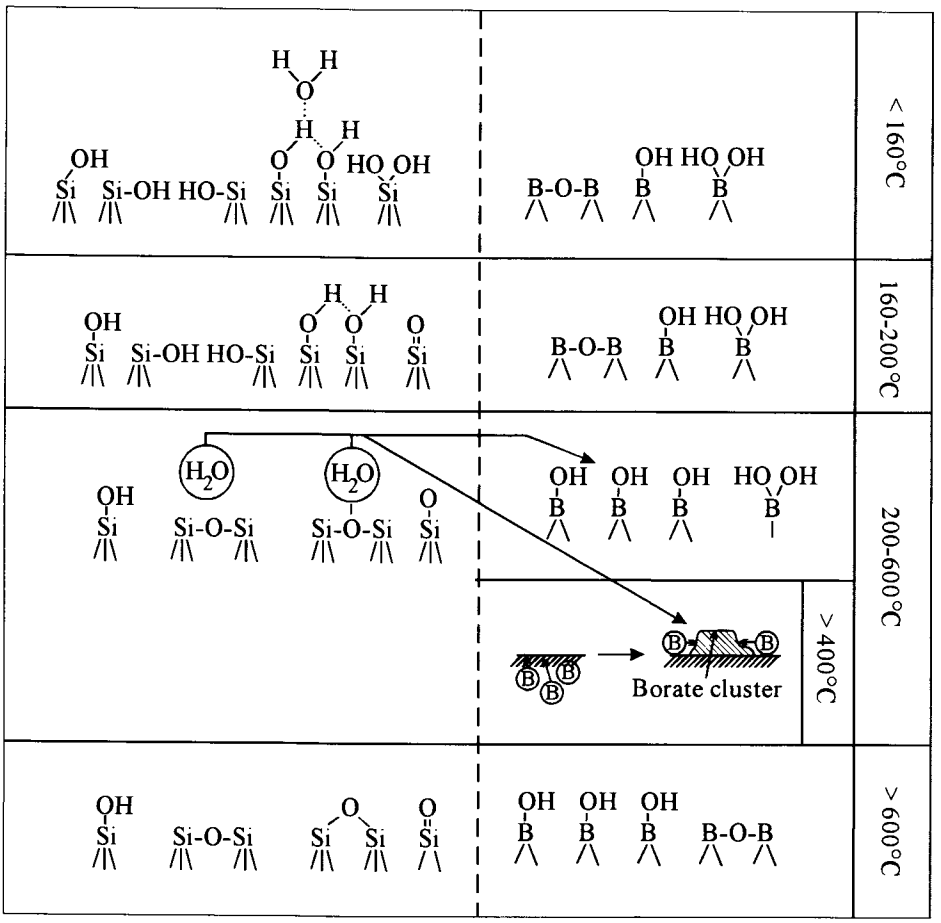

Figure 9. A schematic picture of the CPG surface.

about 2 pH units (typically around pH = 6.0) [58]. Thus, CPGs are good adsorbents of multivalent cations from neutral or basic solutions. This adsorption is reversible and pre-adsorbed cations can be easily removed by means of strong acids.

The ζ potentials of CPGs are negative over the entire available pH range; thus, the isoelectric point (IEP) falls at pH $\cong$ 2 [59]. This pH value is even lower than IEP of silica gel. The ζ potentials of CPGs are low in spite of high σ_o. This property is due to compensation of σ_o by adsorbed cations. This explanation was confirmed in direct measurements. Analogously with silica gel and unlike other oxides [60], σ_o of CPGs (and thus counterion adsorption) at given pH and ionic strength increases in the series Li < Na < K < Rb < Cs. It is convenient to introduce the coefficient

$$K_{Cs/Na} = \frac{[Cs_{adsorbed}]\,[Na_{solution}]}{[Na_{adsorbed}]\,[Cs_{solution}]} \qquad (1)$$

to express the selectivity of cesium adsorption [61-63]. For silica the values of $K_{Cs/Na}$ range from 1.5 to 6 and depend on the porous structure. Modifying the composition of raw glass (from which CPG is prepared) and the conditions of demixion process and leaching, one can obtain CPG showing the $K_{Cs/Na}$ selectivity factor as high as 60. Such CPGs have a very high S_{BET} and, probably, very narrow pores. They may be applied to concentrate Cs-137 contained in rain or in fresh water for analytical purpose [64-66].

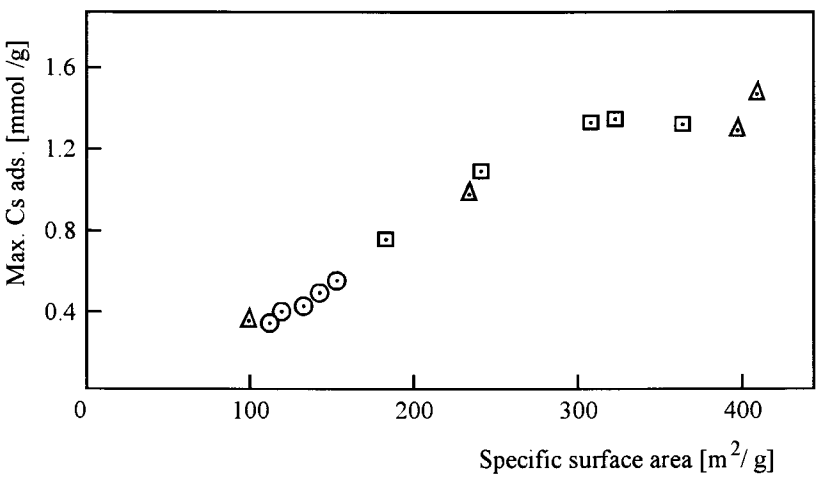

Figure 10. Dependence between specific surface area and adsorption capacity in relation to CsOH for the following adsorbents: CPGs (rings), CPGs heated at 700°C for 2 hrs (squares) and silica gels (triangles).

Cation adsorption capacities of CPGs and silica gels (in mmol/g) are approximately proportional to the S_{BET} (Fig. 10) [62]. Adsorption capacity of CPG and silica gel with respect to CsOH determined from Fig. 10 equals ca. 4 μmol/m^2 and it is little sensitive to the thermal and chemical treatment of CPG.

This result confirms that surface hydroxyl groups are responsible for the creation of surface charge on CPG as it is the case of silica gel. The number of these groups per nm^2 is similar for both adsorbents. However, due to neighbouring boron atoms, hydroxyl groups on CPG surface are more acidic than those on silica gel. By means of infrared measurements the pK_a value of the acidic groups of silica was estimated to be about 7.1 ± 0.5 [67]. In Altug and Hair [68], pK_a of Si-OH groups on CPG surface equals 7, whereas B-OH surface groups are more acid with $pK_a = 5.1$.

Investigations of the thermal treatment of CPG by means of infrared spectroscopy proved the enrichment of its surface in boron atoms and suggested the formation of borate clusters on the CPG surface after its long heating. The presence of these clusters has been proved by means of small angle X-ray scattering (SAXS) [69,70] and differential thermal analysis [71]. Is well known today that during the CPG heating in the temperature range 500-700°C a self-cleaning process of silica building the porous CPG structure takes place. Boron and sodium atoms remaining in CPG (as well as other elements polluting the

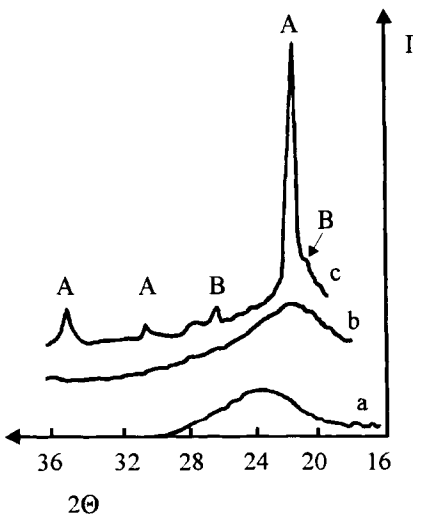

Figure 11. X-ray patterns for: silica gel heated at 700°C over 100 hrs (curve a), CPG (curve b) and CPG heated at 700°C during 105 hrs (curve c). (A) peaks correspond to α-cristobalite, (B) peaks correspond to α-quartz.

siliceous skeleton of CPG) are "thrown out" of the CPG structure and accumulate on the surface.

The siliceous CPG structure tends towards regularity. Diffractometric investigations [72] allowed to identify cristalites of α- and β-cristobalite and even α-quartz in thermally treated glass. They also showed that the structure of the non-heated CPG was amorphous (see Fig. 11). In borate clusters which are formed on the surface of a heated CPG complex forms of $(Na_2O)_i$ x $(B_2O_3)_j$ system can be found (e.g. $Na_2[(B_4O_6)(OH)]x3H_2O$, [71]). The presence of surface borate clusters negatively influences the effect of the investigation of heterogeneity distribution in CPG by means of SAXS [69,70]. The SAXS method cannot be applied to the investigation of the pore size distribution in thermally treated glasses containing borate clusters. Borate clusters decrease the intensity of the X-ray scattering resulting from the presence of pores in CPG and suggest the absence of pores in the examined material, whereas porosimetry investigations indicate its significant porosity. The removal of borate clusters from CPG pores (e.g. by dissolution in acid) restores the X-ray scattering ability of the system (Fig. 12).

4. SPECIFIC PROPERTIES OF THE SURFACE OF THERMALLY TREATED CPGs

The presence of B-OH and B atoms on the CPG surface and the varied behaviour of CPG at elevated temperatures are the main features differentiating this material from silica gel. Although the surface of the initial CPG can sometimes be perceived as similar to silica gel surface, such similarity is very distant after their thermal treatment. It is

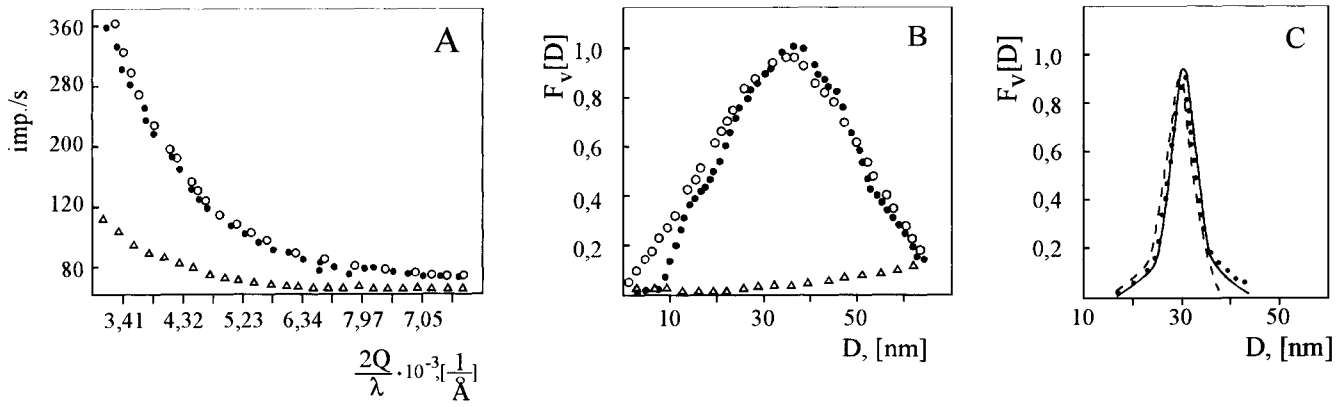

Figure 12. A) SAXS scattering curves, B) size heterogeneity distribution functions $F_v = f(D)$ obtained from SAXS data and C) pore size distribution functions obtained by means of mercury porosimetry for: CPG (mean D = 31.8 nm) (white rings or solid line); CPG heated at 650°C over 100 hrs, (mean D = 28.1 nm) (white triangles or dashed line) and CPG heated at 650°C over 100 hrs and then leached to remove borate clusters (mean D = 28.0 nm) (black rings or dotted line).

especially evident when a thermally treated CPG is used as a support of adhesively deposited and chemically bonded stationary phases or as a support of carbon deposit for carbosils preparation.

4.1. Adsorption properties of thermally treated CPG

Experiments with CPGs subjected to progressive thermal treatment leading to partial dehydroxylation of the surface and its enrichment in boron atoms showed specific adsorption properties of these materials differentiating them from silica gels [30,31,73]. It was found that depending on the type of adsorbate two trends in the adsorption behaviour of heated CPG can be observed [30,31]. The increase of thermal treatment time leads to the increase of CPG adsorption properties in relation to water, chloroform or hexane [30] (e.g. see Fig. 13).

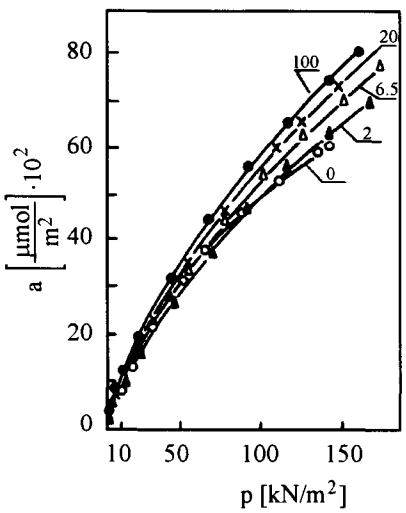

Figure 13. The adsorption isotherms of chloroform on CPG heated at 700°C for different periods of time. The values at curves mean the period of time heating in hrs.

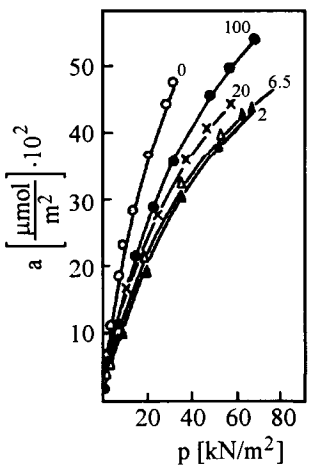

Figure 14. The adsorption isotherms of diethyl ether on CPG – see Fig. 13.

The adsorption of diethyl ether or tetrahydrofurane decreases for shortly heated glasses in comparison to non-heated ones and increases for longer heated CPG (e.g. see Fig. 14). This can be attributed to the described processes occuring on the CPG surface during its thermal treatment (dehydroxylation of Si-OH groups, creation of B-OH groups, increase of surface boron and sodium concentration, borate cluster formation). Each of these processes differently influences the adsorption properties of CPG. The adsorption properties of silica gel treated thermally in the same conditions (above 400°C) significantly decrease as the result of surface dehydroxylation.

Additional information about energetic heterogeneity of the thermally treated CPG surface was supplied by measurements of isosteric heats of adsorption (Q^{ST}) [73]. These investigations also partly confirmed the results obtained by means of infrared spectroscopy.

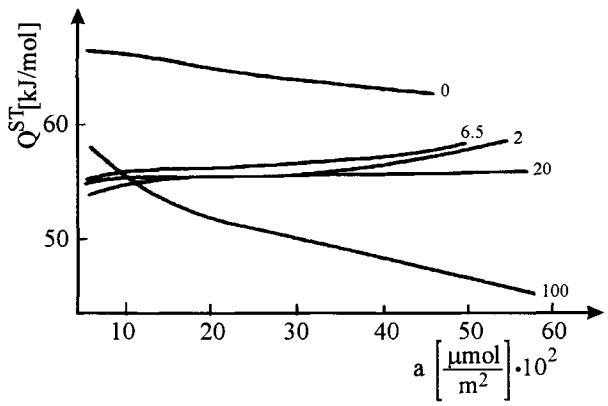

Figure 15. The isosteric heat of adsorption for diethyl ether adsorbed on CPG heated over different periods of time (see - Fig. 13) at 700°C.

Fig. 15 illustrates the changes of the isosteric heats of adsorption of diethyl ether as a function of adsorption amount for CPG heated over a longer and longer period of time.

The molecules of diethyl ether seem to be particularly suitable for the study of adsorption on surfaces with varying concentrations of boron atoms. The diethyl ether molecule has a donor electron-pair on the oxygen atom and in consequence it can specifically interact with boron atoms (which are electron acceptors) or hydroxyl groups of acidic character. Amines or pyridine, for example, have similar properties but, according to a preliminary study, their retention times in chromatographic columns filled with CPG particles are very long and a remarkable contribution of chemisorption has been found. As seen in Fig. 15, diethyl ether adsorption on the initial glass (curve 0) indicates that the surface is heterogenous (a diminution of Q^{ST} vs. adsorption amount). The run of this dependence is understandable if one takes into account different types of hydroxyl groups bonded with Si or B atoms and free B atoms present in the CPG surface (see above). An increase in the time of heating (curves 2 and 6.5) has only a minor influence of the heat of adsorption, though a small increase in Q^{ST} is observed. The surface seems to be a little more homogenous than that of the initial glass. This can be explained by a partial condensation of less thermally resistant OH groups existing on the CPG surface. Further heating of the glass for 20 and 100 hrs leads to a gradual increase of the CPG surface heterogeneity, which is connected with the enrichment of the surface of this material in boron atoms and with borate clusters formation.

4.2. Thermally treated CPG as support of adhesively deposited phases

The presence of boron atoms in CPG surfaces frequently influences the properties of stationary phases adhesively deposited on CPG used as support. It is especially well evidenced for phases whose molecules form a monolayer in which they are parerely oriented towards a support surface in the gas/solid or phase/solid interface [74]. The properties of

the mentioned monolayer depend frequently not only on the temperature but also on the properties of the support [75]. n-Octadecanol (n-ODL) deposited on silica gel surface is an example of such system [75,76]. This alcohol (like other long-chain aliphatic alcohols) forms two phases on the silica gel surface (Fig. 16): a) monomolecular film of the oriented n-ODL molecules and b) three dimensional drops in equilibrium with this monolayer. Because of autophobicity occuring in the system the drops do not wet the monolayer.

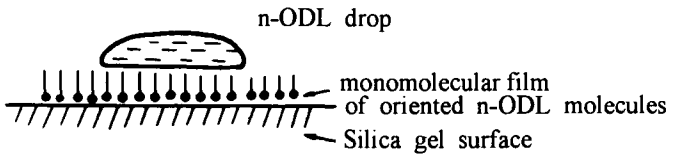

Figure 16. The distribution model of n-ODL deposited on silica gel.

The monolayer may exist in two basic physical states: as a solid condensed phase and, in higher temperatures, as a liquid expanded phase. For example, in the n-octadecanol monolayer on silica gel surface the phase transition between these phases takes place at 81-82°C. As a result, the surface occupied by a single molecule in the monolayer, (ω) increases from $\omega = 0.21$ to $\omega = 0.27$ nm^2 [74,76]. Phase transitions occuring in the n-ODL deposit can be investigated by means of inverse gas chromatography (on the basis of the shape of log V_s vs. $1/T$ dependence, where V_s and T are a retention volume and temperature in K, respectively) [77-79] or by the differential thermal analysis (DTA) [77,80]. Fig. 17 (thermogram A) illustrates a typical DTA curve for the discussed system. Investigations of analogous systems in which CPGs with differently boron-enriched surfaces were employed instead of silica gel [77-80] showed that:

1) the ODL monolayer is also present on boron eriched CPG surfaces;
2) the temperatures of the phase transitions occuring in the ODL monolayer depend on the degree of boron enrichment of the CPG surface;
3) the boron-enriched CPG surface is better wetted by n-ODL. A better distribution of the n-ODL phase leads to a bigger number of theoretical plates for chromatographic columns packed with sorbent in which n-ODL is deposited in boron enriched surface than for columns filled by silica gel with n-ODL on the surface [78].

Boron enriched CPG surfaces manifest also specific properties agains Carbowax, another popular stationary phase. Sorbents with non-extractable layer of Carbowax (which is immobilized on the surface, for example, to deactivate its adsorption properties) show a relatively high thermal stability, do not demand pre-column application and, contrary to materials modified with alkylsilanes, are wettable by aqueous solutions [81-84]. According to Aue et al. [85], Carbowax chains in this non-extractable layer are placed on the surface in the form of an extended spiral in which a part of oxygen atoms interacts with adsorption sites of the support material (with Si-OH groups in the case of silica gel). Such Carbowax layer deposited on the silica gel surface is less polar than pure Carbowax [86]. The physicochemical investigations of analogous sorbents based on CPG show that the increase of surface boron concentration brings about a higher extention of Carbowax

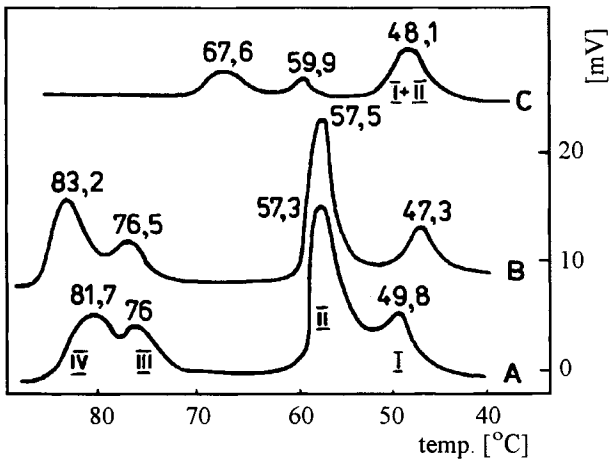

Figure 17. Thermograms of n-ODL films deposited on: A) silica gel; B) CPG; C) CPG heated at 700°C for 20 hrs. Peak I represents the heat of the $\gamma \rightarrow \alpha$ polymorphic transition occuring in solid n-ODL; Peak II – the melting of n-ODL not bonded with monolayer; Peak III is connected with phase transition in the part of the monolayer covered by melted n-ODL; Peak IV corresponds to the phase transition in the part of monolayer in contact with gas.

spiral [87]. This phenomenon resembles the increase of the wettability of CPG with boron enriched surface by n-ODL.

4.3. Thermally treated CPG as support of chemically bonded phases

Sorbents with chemically bonded alkyl phases are usually prepared by the chemical reaction which occurs between groups existing on the surface of support and a proper modifying agent. Among numerous sorbents of such type silica gels with chemically bonded octadecyl radicals are most widely applied in chromatography. As it was described above, a boron-enriched CPG surface (for example by heating CPG at 600°C) is covered with a larger amount of hydroxyl groups bonded mainly with surface boron atoms than the surface of silica gel thermally treated at the same conditions. Due to the presence of surface hydroxyl groups CPG with a boron-enriched surface can also play the role of a support of chemically bonded alkyl phases. The investigations of Morel and Serpinet [88,89] showed that in C_{18} films chemically bonded to silica gel surface a phase transition takes place in the temperature range 18-28°C, i.e. in the range in which most chromatographic measurements are performed. This transition is connected with the change of the bend of the chemically bonded radicals towards the surface and can be reflected as deviation from linearity of the log $V_s = 1/T$ relationship in the mentioned temperature range (see Fig. 18).

As a results of the described phase transition a change of the chromatographic properties of sorbent is observed. Investigations of sorbents with C_{18} radicals chemically bonded with the boron-enriched CPG surface [90,91] prove the absence of phase transition in the

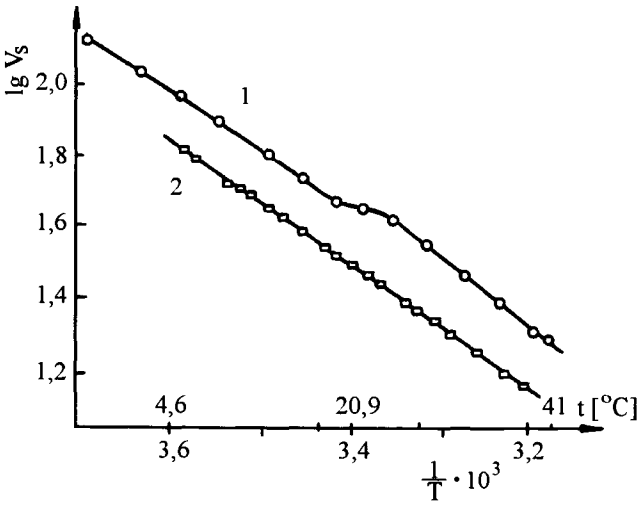

Fiure 18. Relationship between log V_s of n-heptane and the reciprocal column temperature, 1/T for sorbents: 1) C_{18} radicals chemically bonded with CPG; 2) C_{18} radicals chemically bonded with CPG whose surface was enriched with boron atoms.

mentioned temperature range (Fig. 18). The structure of the bonded film is so rigid that phase transition does not occur below 90°C [91]. Thus, to obtain high reproducibility of the retention data of an analyte a very precise temperature controll is not necessary.

4.4. Thermally treated CPG as support of carbon deposit

Materials with carbon on the surface used as column packings for chromatography include carbosils, which are prepared mainly by pyrolysis of aliphatic alcohols [92], aromatic hydrocarbons [93], chloroalkanes [94], and other organic compounds on the surface of silica gel. The carbon deposit obtained under the standard pyrolysis conditions is amorphous and possesses different physicochemical properties than graphitized carbon blacks. The transformation of such amorphous carbon deposit to graphitized carbon black on a silica gel surface is not possible because of the high temperature of the graphitization process (ca. 3000 K).

Investigations of carbosils obtained by pyrolysis of alcohols on CPGs revealed specific carbon deposit properties resulting from the presence of boron on the support surface [95,96]. They can be summarized in the following points:

1) the amount of carbon deposit is proportional to the amount of surface boron atoms,
2) pyrolysis of alcohol takes place mainly on boron centres,
3) the carbon formed by alcohol pyrolysis on boron-enriched surface is unreactive both with hydrogen and with a precusor of isobutane,
4) the results of hydrogenization of carbosils prepared on CPG with boron-enriched surface show the formation of carbon deposit with a highly regular structure,
5) X-ray diffraction measurements prove the presence of graphite cristallites in the carbon deposit formed by alcohol pyrolysis on the boron-enriched CPG surface (cf. Fig. 19).

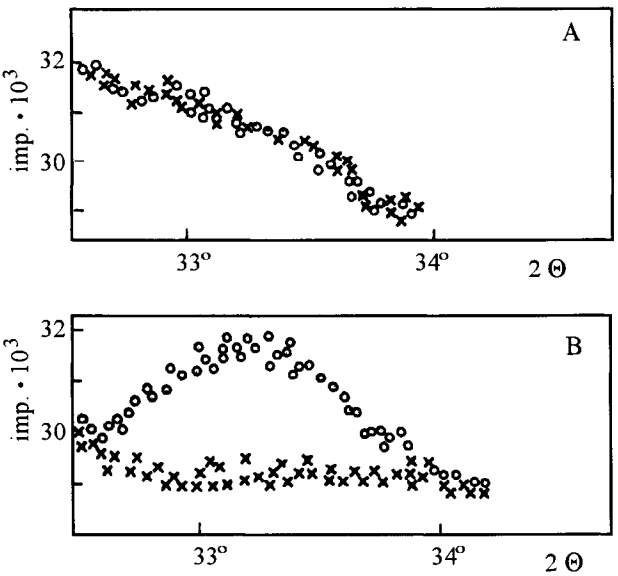

Figure 19. X-ray patterns (iron tube with manganese filter) for the following materials: A) × = CPG and ● = carbosil obtained using this CPG; B) × = CPG with the boron enriched surface and ● = carbosil obtained using CPG with boron enriched surface.

5. CPGs AS SUPPORTS OF BIOLIGANDS AND ENZYMES

The wide application of CPGs as supports of ligands for affinity chromatography or as matrices of immobilized enzymes used in various biotransformation processes [2-4,97-104] results from the described properties of CPG, namely: the possibility of CPG preparation in a wide range of mean pore diameter; its excellent premeability resulting from narrow pore size distribution; hardness; thermal stability up to 650°C; resistance towards pH higher than that of silica gel, and the presence of surface hydroxyl groups allowing its surface modification. Systems with immobilized ligands or enzymes are prepared by covalent attachment of a ligand (substance bioselectively interacting with separated biomolecules) or enzyme with the CPG surface. Because the hydroxyl groups present on the siliceous surface are rather unsuitable for direct bonding of ligands and enzymes, and because a highly polar CPG surface is very often responsible for deactivation or even for denaturation of biological materials (ligands, enzymes, purified substances), ligands and enzymes are covalently coupled with the modified surface. For this purpose CPGs modified by γ-aminopropyltriethoxysilane or γ-glycidoxypropyltrimethoxysilane are mostly used [3]. The amino and epoxy groups allow the bonding of a great number of biological and biologically active species but they are frequently not so effective as other reactive groups. This is why on the basis of these two materials a series of the reactions were worked out leading

to CPG derivatives with benzoylazide, bromoacetamide, azidoaryl, aldehyde, carboxylic acid, acid chloride, isothiocyanate, iminocarbonate etc. groups. Methods, reaction conditions and examples of their application for ligand bonding and enzyme immobilization are the subject of many publications and reviews [3,97,105] which will not be discussed in this chapter. However, some properties are worth noticing which differentiate CPG from silica gel as support of ligands and enzymes. Due to the high cost of enzymes and most ligands and due to the cost of reactions involved in the preparation of sorbents and biocatalysts these materials are exceptionally expensive. They are often exposed to atacks by microorganisms and polluted by impurities typical for natural samples. Negligent work frequently leads to their wast. These considerations are extremally important from the economic point of view when such materials are employed in large scale processes. The application of CPG as a support of a biological material allows to diminish the losses resulting from the system deactivation.

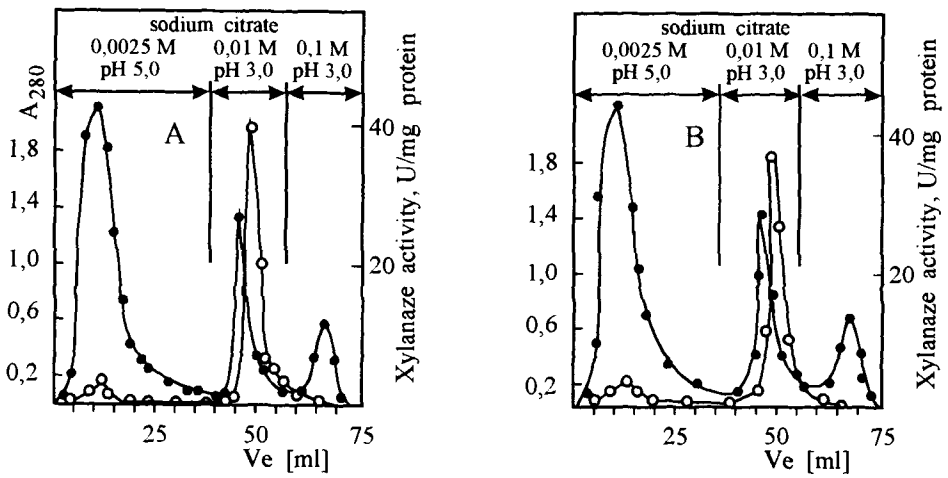

Figure 20. Affinity chromatography of xylanase on CPG with bonded xylan. A) Xylan bonded with initial CPG; B) Xylan bonded with regenerated CPG. Xylanase activity – open rings; absorbance at 280 nm – black rings. Column: 6 x 1 cm.

Due to the thermal resistance of CPG this support material can be recovered form the deactivated material and reused to synthetise a new one. It is enough to burn up the organic compounds bonded with CPG surface, for example by heating the affinity sorbent or biocatalyst in the presence of air or oxygen in the temperature range 550-650°C. Chromatograms illustrated in Fig. 20 present the result of such operation.

Almost every work dealing with the application of CPG as support for affinity chromatography or enzyme immobilization emphasizes the possibility of a negative influence of the surface boron atoms on the purified biomolecule or on the immobilized ligands and enzymes. However, there are chromatographic data showing the resolution increase resulting from the increase of surface boron atoms on the surface of CPG used as a support of affinity ligands [106]. A good example is the separation of fungal proteins on sorbents in which vanillin as bioligand is chemically bonded with CPG surface and a boron-enriched

CPG surface. As appears from the comparison of the elution profiles illustrated in Fig. 21, the sorbent prepared on CPG with boron enriched surface (chromatogram B) allows to separate partly the proteins of fraction III eluted by $(NH_4)_2SO_4$ gradient, whereas the analogous material prepared from the initial CPG (with the surface not enriched in boron atoms) does not give a such possibility.

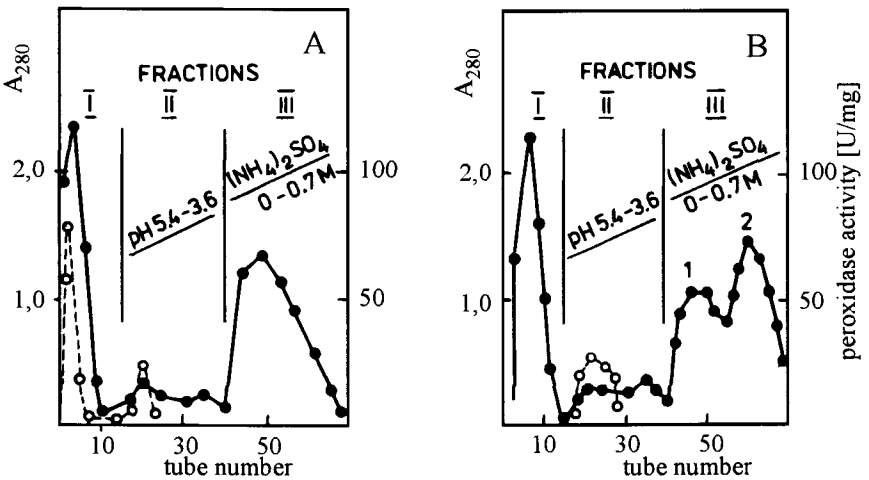

Figure 21. Affinity chromatography of fungal proteins on columns packed with sorbent: A) vanillin chemically bonded with the CPG surface; B) vanillin chemically bonded with the boron-enriched CPG surface. Peroxidase activity – open rings; absorbance at 280 nm – black rings.

6. HYDROTHERMAL TREATMENT OF CPG

The characteristic feature of most silica gels is their globular structure [24]. The porous network of these materials is formed by mutual contact of non porous spherical particles $(SiO_2)_nx(H_2O)_m$. The geometric parameters and physicochemical properties of silica gels are determined by the packing density and diameter of the $(SiO_2)_nx(H_2O)_m$ spheres. Possibile modifications of the silica gel porous structure have been investigated for a long time. Particularly worth-while are the investigations of silica gel rebuilding by hydrothermal treatment. Hydrothermal rebuilding of silica gel is performed by its heating (usually above 100°C) in the presence of water or water vapour. This rebuilding is connected with the growth of larger $(SiO_2)_nx(H_2O)_m$ spheres and the dissolution of smaller ones because of their different solubility in water [107]. In this process the physicochemical properties of silica gel change due to the changes occuring in the globular structure. The increase of the time and temperature of the hydrothermal modification leads to the drop of the specific surface area and to the increase of the mean pore diameter.

As it was described above, the siliceous structure of CPG resembles a sponge-like structure. Because it differs from the globular structure of silica gel the question appeared about its resistance and behaviour in hydrothermal modification [108,109]. The conclusions from the investigation of hydrothermally treated CPGs can be divided into two groups: one dealing with the changes of CPG structure and the other with the changes of the CPG surface properties.

CPG does undergo hydrothermal modification and the observed changes depend on time and temperature of the modification process. Like in silica gel, the structural changes in hydrothermally treated CPGs are caused by the dissolution of SiO_2 in one place and its condensation in another. In CPG, silica dissolves in large pores and precipitates in small ones. As a result hydrothermal treatment the mean pore diameter in CPG increases.

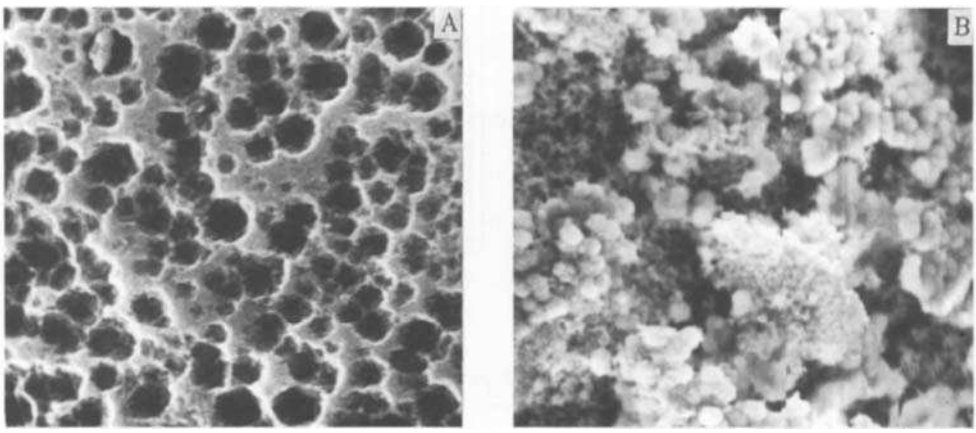

Figure 22. Scanning-microscopy photos of: A) CPG; B) CPG which underwent hydrothermal modification at 300°C.

A secondary structural phenomenon occuring during hydrothermal process can be observed in modified CPG: the formation of globular silica structures. On the flatter and flatter CPG surface huge globules made of SiO_2 are formed (see Fig. 22).

The rebuilding of CPG structure in hydrothermal process causes a significant enrichment of the surface of the final product in boron atoms [109]. Moreover, the thermogravimetric analysis of modified CPGs suggests the formation of micropores, the amount of which increases with the temperature and time of hydrothermal treatment. Such micropores can result from the washing away of components building the walls of CPG pores or are present in the globular structures formed in CPG after its hydrothermal treatment. In consequence of these two phenomena, the hydrothermal treatment of CPG leads to the increase of the adsorption properties of the material surface (Fig. 23).

As indicated at the beginning, the presented discussion of CPG is selective. It focuses on the many properties distinguishing CPGs from silica gels. These differences are found in the porous structures of these materials and - mainly - in their surface properties. Both are built of SiO_2 and have surface covered with hydroxyl groups, but boron residue remaining

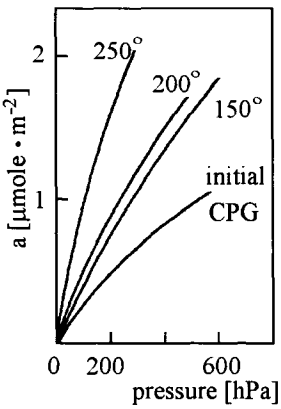

Figure 23. The adsorption isotherms of chloroform on CPG hydrothermally treated for 6 hrs at different temperatures.

on the surface and in the silica skeleton of CPGs gives these materials specific surface properties strongly evident after thermal treatment.

REFERENCES

1. M.B. Volf, Technical Glasses, Isaac Pitman and Sons, Ltd., London, 1961, chapter 10.
2. F. Janowski, W. Heyer, Poröse Gläser, Herstellung, Eigenschaften und Anwendung, VEB Deutscher Verlag für Grundstoffindustrie, Leipzig, 1982.
3. W. Haller, in: vol.66, Chemical Analysis: A Series of Monographs on Analytical Chemistry and its Applications, P.I. Elving, J.D. Winefordner, (eds.), John Wiley and Sons, New York 1983, chapter 11.
4. CPG, Bibliography on Controlled-Pore Glass Chromatography and Related Subjects. Subject listing, literature references, authors edited by Electro-Nucleonics, Inc., 368 Passaic Avenue, Fairfield, N. J., 07006, USA.
5. A.R. Cooper, A.R. Bruzzone, J.H. Cain, E.M. Barrall II, J. Appl. Polym. Sci., 15 (1971) 571.
6. W.E.S. Turner, F. Winks, J. Soc. Glass Tech., 10 (1926) 102.
7. H.P. Hood, M.E. Nordberg, Treated Borosilicate Glass, U.S. Patent N 2106744 (1934).
8. H.P. Hood, M.E. Nordberg, Method of Treating Borosilicate Glasses, U.S. Patent N 2215039 (1940).
9. H.P. Hood, M.E. Nordberg, Borosilicate Glass, U.S. Patent N 2221709 (1940).
10. D.P. Dobychyn, Dokl. AN SSSR, 113 (1957) 372.
11. D.P. Dobychyn, Zhurn. Prikl. Khimii, 35 (1962) 51.
12. E.A. Poray-Koshits, Izv. AN SSSR, Ser. Fiz., 15 (1951) 195.
13. O.S. Molchanova, Steklo i Keramika, 14 (1957) 5.

14. S.P. Zhdanov, Dokl. AN SSSR, 92 (1953) 597.
15. S.P. Zhdanov, Structure of Glass, Consultants Bureau, New York, 1955.
16. W. Haller, J. Chem. Phys., 42 (1965) 686.
17. W. Haller, Material and Method for Performing Steric Separations, U.S. Patent N 3549524 (1970).
18. Advertasing Materials about Controlled Porosity Glasses, edited by Electro-Nucleonics, Inc., 386 Passaic Ave., Fairfield, N. J., 07006, USA.
19. I. Choma, A.L. Dawidowicz, Chromatographia, 33 (1992) 122.
20. A. Waksmundzki, Z. Suprynowicz, J. Gawdzik, A.L. Dawidowicz, Chem. Anal., 19 (1974) 1033.
21. A.L. Dawidowicz, A. Waksmundzki, Z. Suprynowicz, Chem. Anal., 21 (1976) 917.
22. A.L. Dawidowicz, A. Waksmundzki, S. Sokołowski, Separat. Sci., 12 (1977) 573.
23. B. Biliński, A.L. Dawidowicz, W. Wójcik, Progr. Colloid Polym. Sci., 97 (1994) 46.
24. K.K. Unger, Porous Silica – its Properties and use as Support in Column Liquid Chromatography. J. Chromatogr. Library, vol. 16, Elsevier Scientific Publishing Comp., Amsterdam 1979, chapter 2.
25. A. Waksmundzki, P. Pryke, A.L. Dawidowicz, J. Chromatogr., 168 (1979) 234.
26. A.L. Dawidowicz, Chromatographia, 20 (1985) 487.
27. G. Glöckner, Polymer Characterization by Liquid Chromatography. vol. 34, in: J. Chromatogr. Library, Elsevier, Amsterdam, 1987, chapters 11 and 12.
28. A.L. Dawidowicz, S. Sokołowski, Chromatographia, 18 (1984) 579.
29. F.E. Regnier, R.E. Noel, J.Chromatogr.Sci., 14 (1976) 316.
30. A.L. Dawidowicz, I. Choma, Mater. Chem. Phys., 8 (1983) 323.
31. A.L. Dawidowicz, Mater. Chem. Phys., 11 (1984) 504.
32. A.N. Sidorov, Zhurn. Fiz. Khimii, 30 (1956) 995.
33. N. Sheppard, Spectrochim. Acta, 14 (1959) 249.
34. M. Folman, D.J.C. Yates, Trans. Faraday Soc., 54 (1958) 429.
35. M.J.D. Low, N. Ramasubramanian, J. Phys. Chem., 71 (1967) 730.
36. M.L. Hair, W. Hertl, J. Phys. Chem., 73 (1969) 2572.
37. M.J.D. Low, N. Ramasubramanian, P. Ramamurthy, J. Vac. Sci. Technol., 4 (1967) 111.
38. M.L. Hair, W. Hertl, J. Phys. Chem., 77 (1973) 1965.
39. T.H. Elmer, I.D. Chapman, M.E. Nordberg, J. Phys. Chem., 66 (1962) 1517.
40. A.V. Kiselev, V.I. Lygin, K.L. Shchepalin, Kinetika i Kataliz, 12 (1971) 185.
41. M.J.D. Low, N. Ramasubramanian, J. Phys. Chem., 70 (1966) 2740.
42. M.J.D. Low, N. Ramasubramanian, J. Phys. Chem., 71 (1967) 3077.
43. V.M. Kirutenko, A.V. Kiselev, V.I. Lygin, K.L. Shchepalin, Kinetika i Kataliz, 15 (1974) 1584.
44. I.D. Chapman, M.L. Hair, Trans. Faraday Soc., 62 (1965) 1507.
45. S.P. Zhdanov, Dokl. AN SSSR., 217 (1974) 581.
46. V.S. Bobrov, A.P. Kalashnikova, Sh. Shulc, Zhurn. Prikl. Khimii, 38 (1965) 766.
47. Y. Kozirowski, M. Folman, Trans. Faraday Soc., 60 (1964) 1532.
48. M.J.D. Low, P.L. Bartner, Canad. J. Chem., 48 (1970) 7.
49. B. Biliński, W. Wójcik, A.L. Dawidowicz, Appl. Surf. Sci., 47 (1991) 99.
50. B. Biliński, W. Wójcik, A.L. Dawidowicz, Appl. Surf. Sci., 52 (1991) 125.
51. B. Biliński, Appl. Surf. Sci., 63 (1993) 251.
52. B. Biliński, Colloids Surf., 70 (1993) 61.

53. B. Biliński, A.L. Dawidowicz, Appl. Surf. Sci., 74 (1994) 277.
54. B. Jańczuk, E. Chibowski, I. Choma, A.L. Dawidowicz, T. Białopiotrowicz, Mater. Chem. Phys., 25 (1990) 185.
55. B. Jańczuk, T. Białopiotrowicz, E. Chibowski, A.L. Dawidowicz, A. Kliszcz, J. Material Sci., 25 (1990) 1682.
56. B. Jańczuk, I. Choma, A.L. Dawidowicz, A. Kliszcz, T. Białopiotrowicz, Chromatographia, 30 (1990) 382.
57. D.G. Kinniburgh, M.L. Jackson, Adsorption of Inorganics at Solid-Liquid Interfaces, M.A. Anderson, A.J. Rubin, (eds.), Ann Arbor, 1981, chapter 1.
58. M. Kosmulski, J. Szczypa, J. Radioanal. Nucl. Chem., Letters, 144 (1990) 73.
59. M. Kosmulski, J. Szczypa, J. Jabłoński, P. Gołkiewicz, J. Radioanal. Nucl. Chem., Articles, 150 (1991) 456.
60. J. Lyklema, Fundamentals of Interface and Colloid Science, Academic Press, London, 1991.
61. M. Kosmulski, J. Radioanal. Nucl. Chem., Letters, 118 (1987) 209.
62. M. Kosmulski, J. Radioanal. Nucl. Chem., Articles, 129 (1989) 149.
63. M. Kosmulski, A.L. Dawidowicz, J. Szczypa, J. Radioanal. Nucl. Chem., Articles, 131 (1989) 377.
64. M. Kosmulski, A.L. Dawidowicz, J. Szczypa, A. Waksmundzki, Separation Sci. Techn., 25 (1990) 952.
65. J. Szczypa, A.L. Dawidowicz, M. Kosmulski, Method of Estimation of Cesium Existing in Trace Amounts, Patent RP, No. 159851 (1993).
66. J. Szczypa, A.L. Dawidowicz, M. Kosmulski, Estimation of Cesium and Especially its Radioactive Isotopes Existing in Trace Amounts, Patent RP, No. 159853 (1993).
67. M.L. Hair, W. Hertl, J. Phys. Chem., 74 (1970) 91.
68. I. Altug, M.L. Hair, J. Phys. Chem., 71 (1967) 4260.
69. A.L. Dawidowicz, St. Pikus, Appl. Surface Sci., 17 (1983) 45.
70. St. Pikus, A.L. Dawidowicz, Appl. Surface Sci., 24 (1985) 274.
71. A.L. Dawidowicz, P. Staszczuk, J. Therm. Anal., 30 (1985) 793.
72. A.L. Dawidowicz, St. Pikus, J. Therm. Anal., 32 (1987) 409.
73. A.L. Dawidowicz, I. Choma, A. Patrykiejew, K. Pilorz, Mater. Chem. Phys., 8 (1983) 531.
74. J. Rayss, J. Colloid Interface Sci., 91 (1983) 376.
75. J. Rayss, K. Surowiec, A. Waksmundzki, Chromatographia, 17 (1983) 491.
76. J. Serpinet, J. Chromatogr., 68 (1972) 9.
77. J. Rayss, A.L. Dawidowicz, Z. Phys. Chem., 266 (1985) 624.
78. A.L. Dawidowicz, J. Rayss, K. Surowiec, Z. Phys. Chem., 267 (1986) 401.
79. J. Rayss, A.L. Dawidowicz, Z. Phys. Chem., 267 (1986) 113.
80. A.L. Dawidowicz, J. Rayss, Z. Phys. Chem., 266 (1985) 1210.
81. M.M. Daniewski, W.A. Aue, J. Chromatogr., 147 (1978) 119.
82. I. Choma, A.L. Dawidowicz, R. Lodkowski, J. Chromatogr., 600 (1992) 109.
83. I. Choma, A.L. Dawidowicz, R. Dobrowolski, St. Pikus, J. Chromatogr., 641 (1993) 205.
84. I. Choma, A.L. Dawidowicz, J. Chromatogr., 641 (1993) 211.
85. W.A. Aue, C.R. Hastings, S. Kapila, J. Chromatogr., 147 (1978) 395.
86. W.A. Aue, M.M. Daniewski, J. Chromatogr., 151 (1978) 11.
87. A.L. Dawidowicz, I. Choma, W. Buda, Z. Phys. Chem., 268 (1987) 273.

88. D. Morel, J. Serpinet, J. Chromatogr., 200 (1980) 95.
89. D. Morel, J. Serpinet, J. Chromatogr., 214 (1982) 202.
90. A.L. Dawidowicz, J. Rayss, Z. Suprynowicz, Chromatographia, 17 (1983) 157.
91. A.L. Dawidowicz, J. Rayss, Chromatographia, 20 (1985) 555.
92. A. Waksmundzki, R. Leboda, Z. Suprynowicz, M. Waksmundzka-Hajnos, Method of Carbosil Preparation, Patent RP, No. 182 171 (1978).
93. H. Colin, G. Guiochon, J. Chromatogr., 126 (1976) 43.
94. A.L. Dawidowicz, A. Gierak, A. Waksmundzki, Chromatographia, 17 (1983) 627.
95. A.L. Dawidowicz, D. Nazimek, St. Pikus, J. Skubiszewska, J. Anal. Appl. Pyrolysis, 7 (1984) 53.
96. A.L. Dawidowicz, St. Pikus, D. Nazimek, J. Anal. Appl. Pyrolysis, 10 (1986) 59.
97. W.H. Scouten, in: vol. 59, Chemical Analysis: A Series of Monographs on Analytical Chemistry and its Application, P.I. Elving and J.D. Winefordner, (eds.), John Wiley and Sons, New York, 1981, chapters 2 and 3.
98. J. Łobarzewski, A.L. Dawidowicz, Phytochemistry, 22 (1983) 2427.
99. J. Rogalski, J. Szczodrak, A.L. Dawidowicz, Z. Ilczuk, A. Leonowicz, Enzyme Microb. Technol., 7 (1985) 395.
100. M. Wojtaś-Wasilewska, J. Luterek, A. Leonowicz, A.L. Dawidowicz, Biotechnol. Bioeng., 32 (1988) 507.
101. J. Rogalski, A.L. Dawidowicz, Acta Biotechnol., 9 (1989) 275.
102. J. Rogalski, A.L. Dawidowicz, J. Fiedurek, A. Leonowicz, Acta Biotechnol., 10 (1990) 283.
103. A.L. Dawidowicz, T. Rauckyte, J. Rogalski, Chromatographia, 37 (1993) 168.
104. A.L. Dawidowicz, T. Rauckyte, J. Rogalski, J. Liquid Chromatogr., 17 (1994) 817.
105. H.H. Weetal, in: Methods in Enzymology, vol. 44, K. Moosbach, (ed.), Academic Press, New York, 1976, p.134.
106. A.L. Dawidowicz, J. Łobarzewski, Chromatographia, 18 (1984) 389.
107. R.K. Iler, The Chemistry of Silica, Wiley, New York, 1979.
108. A.L. Dawidowicz, E. Mendyk, Mater. Chem. Phys., 21 (1989) 463.
109. E. Mendyk, A.L. Dawidowicz, Mater. Chem. Phys., 24 (1989) 13.

A. Dąbrowski and V.A. Tertykh (Editors)
Adsorption on New and Modified Inorganic Sorbents
Studies in Surface Science and Catalysis, Vol. 99

Chapter 1.3
Influence of pH of precipitation of hydroxides on the structure of co–precipitated adsorbents

V.S. Komarov

Institute of General and Inorganic Chemistry, Academy of Sciences,
220072, Minsk, The Republic of Belarus

1. INTRODUCTION

Formation of the structure of co–precipitated adsorbents depends on many factors, among which the pH of precipitation of mixture components is one of the most important factors. It should be noted that porosity of the co–precipitated adsorbents is a function of the pH of initial and final precipitation of hydrogels: in the case of hydrogels, the pH of initial and final co–precipitation is different, adsorbents formed have a maximum in the sorption capacity (V_s) – composition curve; and, vice versa, when the pH of co–precipitated hydrogels coincides, adsorbents produced have the sorption capacity directly proportional to V_s of the components in mixture. It cannot be excluded that the phenomenon revealed is of a general nature and occurs in natural conditions with the appropriate combination of the pH of the medium and the presence of suitable salts. In the present work universality of the found relationship will be proved by numerous examples. This relationship is extremely useful in the synthesis of complex adsorbents with the predicted structural parameters. From the sorption capacities of individual components it is also possible to calculate the mixture composition corresponding to the maximum sorption capacity of porous materials produced.

2. THE STRUCTURE OF ADSORBENTS WITH THE COMPONENTS HAVING THE SAME pH OF PRECIPITATION

Among the various methods for controlling the porous structure of adsorbents [1–3], one of the most popular is synthesis of co–precipitated adsorbents with the structure depending on the pH of the initial and final precipitation of hydroxides. This method has not been yet developed and grounded theoretically.

In view of characteristic features of each of the components in the mixture, co–precipitation of hydroxides from binary solutions can be divided into four distinctive cases:

1) the pH of the initial and final co–precipitation of the components coincides;
2) the hydroxide of one of the components precipitates at a lower pH than the second does, while pH values of complete precipitation of the components are the same;

3) the pH values of the initial and final co-precipitation of the hydroxides do not coincide;
4) the pH of the initial precipitation of hydroxides concides while pH values of the complete precipitation do not.

Each of the enumerated cases of co-precipitation of hydroxides has its distinctions in forming the porous structure of the adsorbents produced.

In paper [4] the first case is considered. The fact that the compositions of the solution and hydroxide remain the same from the beginning to the end is its distinction. This is caused by coincidence of the pH values of the initial and complete precipitation of components that is accompanied by implantation of one hydroxide into the network of the other to produce a mixed structure. Properties of the final product depend on the size of hydroxide particles and their capability of isomorphic substitution.The character of these substitutions and the type of their mutual penetration change substantially with alterations in composition of the components.

Here two cases can be distinguished. The first case: the shape and size of hydroxide particles are the same. In the samples produced no substantial differences in the porous structure are observed, i.e., the adsorption-structural properties of the individual or co-precipitated hydrogels should not differ substantially. In this case porosity is characterized by one type of particles or a mixture of particles different in nature but equal in size, which introduce no changes into the skeletal architecture of the co-precipitated gel and its structural parameters. This is corroborated by the sorption capacity of a sample of the $Cr(OH)_3$ - $Zn(OH)_2$ system, whose components, in addition to the coincidence of the pH values of the initial and complete co-precipitation of hydrogels, have also almost equal sorption capacities at $P/P_s = 1$ (Fig.1, curve 1).

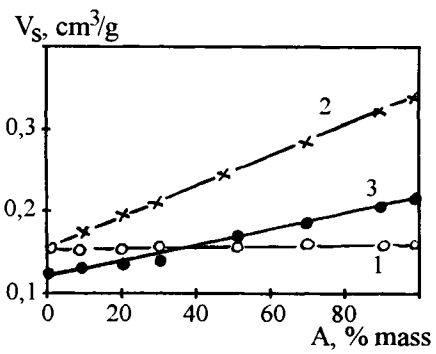

Figure 1. The limiting sorption capacity - composition curves for the following systems: 1 - $Cr(OH)_3$ - $Zn(OH)_2$; 2 - $Zn(OH)_2$ - $Cu(OH)_2$; 3 - $Ni(OH)_2$ - $Co(OH)_2$ (A - content of the second component of the system).

The second case: the shape and size of particles for co-precipitated hydrogels are different. As a result, the probability of mutual arrangement of particles increases, which results in formation of the samples with a sorption capacity that changes linearly in the direction from a less to a more adsorbing component, depending on the composition. As mentioned earlier, such a behaviour of the V_s-composition curves is typical for binary

systems, in which pH values of the initial and complete precipitation of hydroxides of the first and the second components coincide (Table 1).

Table 1
The pH values of precipitation of metal hydroxides

Hydroxide	pH of the initial precipitation [5]	pH of the complete precipitation [6]
$Zn(OH)_2$	5.2	8–10
$Cu(OH)_2$	5.3	8–10
$Ni(OH)_2$	6.7	9–10
$Co(OH)_2$	6.6	9–14
$Cr(OH)_3$	5.3	6–11

Adsorption–structural properties of co–precipitated specimens of the $Zn(OH)_2$–$Cu(OH)_2$ and $Ni(OH)_2$–$Co(OH)_2$ and other systems, whose components meet the indicated requirements, can serve a good confirmation to the aforesaid. In this case the structure–formation mechanism does not involve exhibition of any unpredictable changes leading to a maximum or minimum of the V_s – composition curve.

Just as for the samples produced from different mixtures of a similar type, the linear dependence of V_s on their composition is general. Samples for the study were synthesized under conventional conditions and pH of 9.5 was assumed. Under these conditions the effect of pH on formation of the porous structure was eliminated. Adsorption structural properties of the gels after washing–out salts, granulation and drying were found from adsorption of CCl_4 in vacuum. The results of the study are presented in Fig.1 (curves 2,3) and Table 2. One can see that V_s of the samples can be calculated at any point of the curve as the sum of the products of the sorption capacity (V_1 and V_2) for each of the hydroxides by its percentage content in the mixture (c_1 and c_2):

$$V_s = \frac{V_1c_1 + V_2c_2}{100} \qquad (1)$$

With sorption capacities of the initial hydroxides known, it is possible to calculate V_s of the co–precipitated samples from formula (1) or to evaluate it from the straight line connecting the sorption capacities of individual hydroxides without experimentation. Irrespective of the number of components involved, the mechanism of forming such structures consists in the fact that the compositions of the solution and co–precipitated hydroxides are equal at every point, i.e., equality of the pH of co–precipitation does not result in selective removal of particular components from the mixture. The structure of the co–precipitated hydrogels is characterized by uniform volume distribution of particles forming the skeleton of porous body. In this case, the content of a particular component changes in a sample depending on the composition, but the contribution of each to the adsorption properties of the sample produced does not change. It is likely that the particles of the first or second component substitute each other in an isomorphic way to form a common framework, whose architecture depends on the particle size and packing. Here two types of contacts are possible: at a low concentration of the component in the mixture its particles only interact with those of the second component. At medium or close

Table 2
Data on adsorption of CCl_4 vapour by co-precipitated hydroxide samples calcinated at different temperatures (t°C)

Composition, %mass of hydroxide			t°C	p/p_s at	Sorption capacity of CCl_4 (cm^3/g) at p/p_s of					S_{sp} (m^2/g)
I	II	III		i.p.h.*	0.1	0.3	0.6	0.9	1.0	
$Zn(OH)_2$–$Cu(OH)_2$										
100			120	0.36	0.022	0.018	0.032	0.125	0.153	28
			400	0.35	0.024	0.020	0.036	0.132	0.172	32
10	90		120	0.30	0.052	0.052	0.065	0.320	0.341	82
			400	0.30	0.061	0.061	0.072	0.333	0.363	84
30	70		120	0.26	0.045	0.051	0.061	0.235	0.296	80
			400	0.26	0.050	0.058	0.070	0.245	0.318	88
50	50		120	0.28	0.031	0.035	0.061	0.230	0.255	75
			400	0.28	0.034	0.041	0.068	0.240	0.271	80
70	30		120	0.26	0.030	0.031	0.041	0.182	0,214	70
			400	0.27	0.034	0.035	0.052	0.211	0.232	77
80	20		120	0.34	0.025	0.020	0.082	0.145	0.193	37
			400	0.30	0.024	0.024	0.090	0.156	0.215	54
90	10		120	0.30	0.012	0.012	0.025	0.128	0.179	33
			400	0.30	0.014	0.014	0.028	0.132	0.192	45
	100		120	0.30	0.035	0.035	0.051	0.252	0.360	66
			400	0.30	0.040	0.040	0.053	0.275	0.380	71
$Ni(OH)_2$–$Co(OH)_2$										
100			120	0.28	0.019	0.022	0.032	0.111	0.132	52
			400	0.30	0.025	0.025	0.036	0.122	0.142	50
10	90		120	0.26	0.026	0.027	0.038	0.190	0.214	51
			400	0.26	0.028	0.029	0.040	0.208	0.230	60
30	70		120	0.26	0.027	0.032	0.048	0.169	0.181	51
			400	0.27	0.029	0.036	0.052	0.182	0.210	57
50	50		120	0.28	0.012	0.014	0.030	0.149	0.165	23
			400	0.29	0.016	0.019	0.041	0.162	0.182	32
70	30		120	0.30	0.023	0.023	0.038	0.122	0.143	30
			400	0.28	0.025	0.031	0.042	0.141	0.165	40
90	10		120	0.31	0.040	0.039	0.048	0.112	0.130	44
			400	0.30	0.042	0.042	0.055	0.129	0.151	50
	100		120	0.28	0.036	0.044	0.065	0.205	0.225	81
			400	0.28	0.040	0.052	0.072	0.222	0.240	88
$Cu(OH)_2$–$Cr(OH)_3$–$Zn(OH)_2$										
10	45	45	120	0.26	0.081	0.086	0.111	0.153	0.165	100
20	40	40	120	0.28	0.092	0.104	0.142	0.176	0.186	110
30	35	35	120	0.27	0.046	0.049	0.078	0.192	0.240	75
50	25	25	120	0.30	0.047	0.047	0.091	0.212	0.252	77
70	15	15	120	0.32	0.048	0.045	0.112	0.258	0.300	58
90	5	5	120	0.32	0.050	0.047	0.125	0.265	0.320	62
	100		120	0.26	0.029	0.032	0.051	0.124	0.151	67

*i.p.h. – initial point of hysteresis

to medium concentrations, each of the components forms its own space network and, as a result, homogeneous particles contact both with one another and with the particles of the other component. Moreover, intermediate types of particle interaction cannot be excluded and their probability increases with the number of components in the mixture. The character of the interaction of gel particles in the structure is also determined largely by concentration fluctuations of atoms in the solution which results in forming aggregates of gel–like structures of both mixed composition and those enriched with particles of one type.

Moreover, the structure of gels produced depends substantially on precipitation conditions and is determined by the precipitation temperature, pH of the medium, initial composition of solution, its concentration, of sequential mixing of solutions or conditions of introduction of precipitating agent [7]. It should be noted here that even in the production of one–component gel, periodicity of precipitation gives a product with a non–homogeneous structure which, as a rule, forms adsorbents with a set of pores different in size. Therefore, strict observance of all the conditions of sample synthesis enumerated above is absolutely necessary.

Calcination of specimens has not changed the general regularity of their sorption capacity, except for a slight increase in V_s caused by an increase in the pore volume due to removal of hydrate water (Table 2).

The linear V_s composition relationship obtained for the binary co–precipitated systems was confirmed with the samples synthesized from a three–component mixture containing different amounts of copper, chromium and zinc salts (Table 2). The results suggest that the V_s – composition relationship found is general. This generality is confirmed by the samples obtained from three–component systems, and therefore, using formula (2), similar to Eq. (1), it is possible to calculate the adsorption capacity of the sorbent at any point of compositions:

$$V_s = \frac{V_1c_1 + V_2c_2 + V_3c_3}{100} \qquad (2)$$

The studies have shown that irrespective of the composition of the initial mixture, as a result of uniform distribution of components in the structure of samples, the shape of their adsorption isotherms is transformed gradually from the typical isotherm for one individual component to the isotherm for the second component. In this case, as the content of the second component, having a higher sorption capacity, increases, transitional isotherms accumulate features inherent in its structure: the micro– and mesopore volume, limiting sorption capacity V_s, and specific surface area S_{sp} increase. The latter increases because of the fact that along with development of porosity of samples, their more open structure accessible to adsorbate molecules is formed.

To conclude the section it should be noted that the mechanism of formation of the porous structure of co–precipitated adsorbents from binary or multicomponent systems with components having the same pH values of the initial and final precipitation of hydroxides follows the cooperative type determined by the contribution of each of the components to the total sorption capacity of the specimen.

3. THE MECHANISM OF STRUCTURE FORMATION OF CO-PRECIPITATED ADSORBENTS

In spite of a number of relevant publications [8–11], the mechanism of formation porous structure of co-precipitated adsorbents has not been theoretically substantiated yet and it comes mainly to a protective action of components in the mixture relative to one another. This does not facilitate the development of scientific basis for understanding of porosity formation process of co-precipitated solids, and for predicting their structure and component composition that would ensure necessary properties.

Komarov, Repina and Skurko [12] studied the regularities of structure formation for the samples obtained from binary and three-component solutions of salts with coinciding pH of the initial and complete precipitation of hydrogels. This is the simplest case of synthesis of adsorbents, virtually the same as mechanical mixing of hydroxides.

Binary mixtures, whose components have different pH of initial and complete precipitation of gels, are the most interesting both from theoretical and practical standpoints (Table 3).

Table 3
The pH of precipitation of metal hydroxides [14]

Hydroxide	pH values of			
	initial precipitation (concentration of precipitating ion 1 M)	complete precipitation (residual concentration $< 10^{-5}$ M)	initial dissolution of precipitate	complete dissolution of precipitate
$Fe(OH)_3$	1.5	4.1	14.0	
$Mg(OH)_2$	9.4	12.4		
$Cr(OH)_3$	4.0	6.8	12.0	15.0
$Cd(OH)_2$	7.2	9.7		
$Al(OH)_3$	3.3	5.2	7.8	10.8
$Mn(OH)_2$	7.8	10.4	14.0	

Authors of paper [13] considered the systems, in which the pH of complete precipitation of one component differs from the pH of initial precipitation of the other. In particular, in mixtures of 5% solutions of iron and magnesium, chromium and magnesium sulfates, the differences between the pH of final precipitation of $Fe(OH)_3$ – $Cr(OH)_3$ and the pH of initial precipitation of $Mg(OH)_2$ is 6.4 and 4.5 pH – units, respectively. In the $Fe(OH)_3$ – $Cd(OH)_2$ system this difference is 3.1, and in the system $Fe(OH)_3$ – $Cr(OH)_3$ it is zero. This set of systems characterized by succession of gelation of components should lead to adsorbents with composition represented by a mechanical mixture of individual hydroxides. As is known [12], depending on composition, the sorption capacity of such porous bodies must be expressed by a straight line connecting sorption capacities of individual components. However, real curves of limiting sorption capacites have maxima (Table 4, Figs. 2 and 3).

This suggests that in spite of substantial distinctions in composition of co-precipitated gels, the process of their structure formation is accompanied by building-up of particles

Table 4
Adsorption–structural properties of co–precipitated metal hydroxides

Composition, % mass of hydroxide			V_s	S_{sp}	r^*_{eff}
	I	II	(cm^3/g)	(m^2/g)	(nm)
$Fe(OH)_3$ – $Mg(OH)_2$	100	0	0.225	290	1.6
	90	10	0.255	295	1.7
	80	20	0.283	300	1.9
	70	30	0.312	310	2.0
	60	40	0.341	310	2.2
	50	50	0.358	300	2.4
	40	60	0.352	280	2.5
	30	70	0.336	250	2.7
	20	80	0.300	205	2.9
	10	90	0.265	160	3.3
	0	100	0.244	86	5.7
$Cr(OH)_3$ – $Mg(OH)_2$	100	0	0.151	67	4.5
	90	10	0.182	80	4.6
	80	20	0.210	89	4.7
	70	30	0.243	97	5.0
	60	40	0.265	103	5.1
	50	50	0.281	107	5.3
	40	60	0.300	105	5.7
	30	70	0.310	100	6.2
	20	80	0.298	95	6.3
	10	90	0.271	90	6.0
	0	100	0.244	86	5.7
$Cd(OH)_2$ – $Fe(OH)_3$	100	0	0.078	27	5.7
	90	10	0.085	35	4.8
	80	20	0.096	50	3.8
	70	30	0.121	60	3.2
	60	40	0.148	75	3.9
	50	50	0.195	85	4.6
	40	60	0.265	102	5.2
	30	70	0.252	130	3.9
	20	80	0.242	165	2.9
	10	90	0.230	260	1.8
	0	100	0.225	290	1.6
$Cr(OH)_3$ – $Fe(OH)_3$	100	0	0.151	67	4.5
	90	10	0.185	115	3.2
	80	20	0.220	143	3.1
	70	30	0.255	160	3.2
	60	40	0.280	170	3.3
	50	50	0.275	180	3.1
	40	60	0.270	190	2.8
	30	70	0.265	200	2.7
	20	80	0.250	220	2.3
	10	90	0.240	240	2.0
	0	100	0.225	290	1.6

*r_{eff} – effective size of particles

of hydrogel that was precipitated first and as seen in Fig.2, the effect of its exhibition on the increase in the sorption volume of the samples dominates over the contribution of the V_s of the component with a higher sorption capacity. The succession of precipitation of hydrogels results in a change of both homogeneity and structure of the samples.

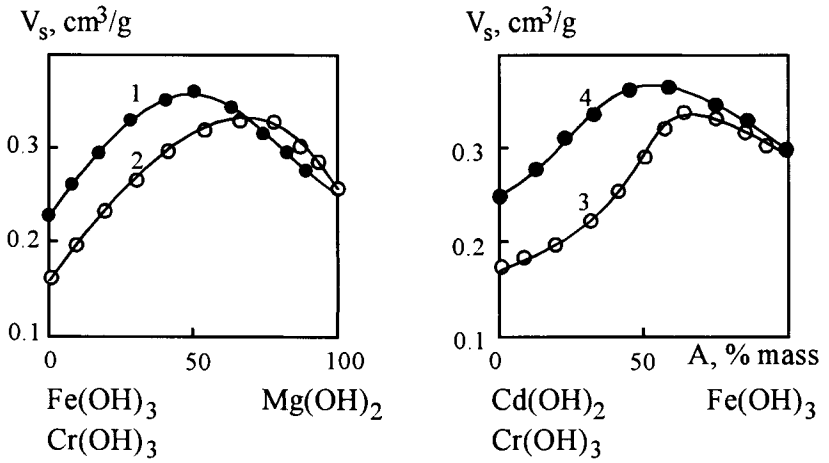

Figure 2. The limiting sorption capacity – composition curves for the systems: 1 – $Fe(OH)_3$ – $Mg(OH)_2$; 2 – $Cr(OH)_3$ – $Mg(OH)_2$; 3 – $Cd(OH)_2$ – $Fe(OH)_3$; 4 – $Cr(OH)_3$ – $Fe(OH)_3$.

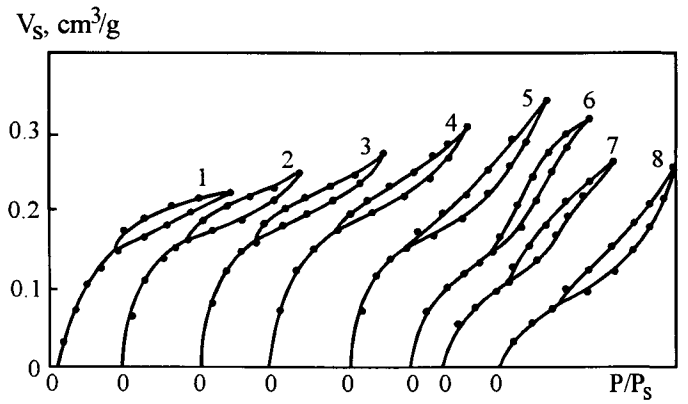

Figure 3. Isotherms of CCl_4 vapour adsorption by the samples of the composition (% mass): 1 – 100% $Fe(OH)_3$; 2 – 90% $Fe(OH)_3$ + 10% $Mg(OH)_2$; 3 – 80% $Fe(OH)_3$ + 20% $Mg(OH)_2$; 4 – 70% $Fe(OH)_3$ + 30% $Mg(OH)_2$; 5 – 50% $Fe(OH)_3$ + 50% $Mg(OH)_2$; 6 – 30% $Fe(OH)_3$ + 70% $Mg(OH)_2$; 7 – 10% $Fe(OH)_3$ + 90% $Mg(OH)_2$; 8 – 100% $Mg(OH)_2$.

Two types of structure formed were found. One is associated with the hydrogel of the component with a lower pH of precipitation and with adsorption of the other component ions on the surface of its particles. The second type consists in formation hydrogel of

the component with a higher pH–precipitation. In this final stage of hydroxide precipitation, the porous structure is determined by the size and mutual arrangement of particles. Moreover, changes in concentration of the compound in solution also contribute to the mechanism of structure formation. As a result, hydrogels obtained in the final precipitation stage are hydrated substantially, and, as is known, their drying is accompanied by large volume shrinkage, resulting in formation of fine porous structure. Consequently, it is evident that hydrogels of such systems are highly diverse in composition and structure. Therefore, adsorption–structural properties of a sample produced from solution of a particular concentration are the sum of properties of the various microstructures formed during co–precipitation of hydroxides. As the composition of initial solutions changes, the character of the microstructures and, consequently, the sorption capacity of samples produced will change too. In particular, as the content of the component with a higher pH of initial precipitation of hydroxide increases, the accretion in V_s due to growing of hydrogel particles precipitated first, increases (Table 4, Fig. 2) and reaches the highest value in the sample synthesized from the mixture with an optimal component ratio, i.e., when the content of the component with a higher pH of precipitation is quite sufficient for limiting adsorption on the surface of particles of the gel precipitated first.

This process depends essentially on the concentration of cations of the component precipitated as the second, for example, in the systems studied at low concentration of Mg^{2+} adsorbed completely by the surface of iron or chromium hydrogel particles. The latter are encapsulated by magnesium hydroxide. The thickness of this coating depends on both the nature of cation and its valence. As the Mg^{2+} content in the solution rises further, i.e., above the capacity of the potential– controlling layer of particles of the hydrogels mentioned above, two independent processes occur: increase in the amount of homogeneous material ($Mg(OH)_2$) in the encapsulated particles and formation of individual magnesium hydroxide particles. The former is aimed at increasing the sorption capacity of samples obtained and the latter, at its decreasing.

In other words, after the first stage of co–precipitation of hydrogels, further formation of the structure of samples is subjected to counteracting effects, the result of which is expressed in deviation of the V_s –composition curve from the additive straight line, connecting sorption capacities of individual components, in formation of maxima, and determination of their position on the composition axis. In this process, the pH of precipitation of hydrogels and the difference in V_s of individual components of the mixture, depending on which, the maximum in the V_s–composition curve can be shifted towards one or the other component, are of great importance. Between the extreme cases of the synthesis of co–precipitated samples other combinations of compositions, responsible for the behaviour of the V_s–composition curve, can occur. Therefore, with suitable selection and combination of the components in solution with different pH of initial and complete precipitation of hydrogels, the samples different in composition and position of the maximum in the curve can be synthesized. This takes place both for binary and ternary systems. The only difference is that the probability of varying the structure in multicomponent systems increases much due to a suitable combination of properties of their components and complication of the mechanism of the porosity formation of the samples produced.

Analysis of the results on the structural and adsorption properties of $Fe(OH)_3$ –$Mg(OH)_2$ and $Cr(OH)_3$ –$Mg(OH)_2$ systems has shown that in the V_s –composition curves there are

maxima, whose positions on the composition axis do not coincide, in spite of uniformity of the systems studied. For example, for the samples containing $Fe(OH)_3$ the maximum in the curve is shifted leftward and lies at a concentration of $Fe(OH)_3$ of 55% mass, while for $Cr(OH)_3$ – $Mg(OH)_2$ systems with a differing nature of the threevalent ion, it occurs at 30% mass of $Cr(OH)_3$ and 70% mass of $Mg(OH)_2$. This difference in positions of the maxima is caused by different dispersities of hydroxide particles and distinction in pH of their complete precipitation.

All binary mixtures represented by hydroxides with different pH of initial and complete precipitation are such systems. These systems differ from those discussed above only in the fact that, as mentioned earlier, depending on the order of precipitation of components, the height and position of the maximum in the V_s –composition curve will be determined by the properties of the solution. However, the mechanism of porosity formation and factors that cause departure of the sorption capacity of the samples produced from additivity are the same. Undoubtedly, each of the cases mentioned [12] has its specificities introduced by components to the structure – formation mechanism and a common characteristic of passing the V_s –composition curves through a maximum.

Adsorption characteristics of co–precipitated samples with the composition $Fe(OH)_3$ – $Cd(OH)_2$ and $Fe(OH)_3$ – $Cr(OH)_3$ confirm this statement and generality of the regularity found follows from the structural formation mechanism considered. This regularity inherent in all two– and multicomponent systems with different pH of initial and complete precipitation of components opens a broad perspective for scientifically justified and purposeful selection of conditions for the synthesis of adsorbents with the given structure and catalysts with the component precipitated first being a carrier and the other, an active phase.

4. DEPENDENCE OF THE STRUCTURE OF ADSORBENTS ON pH OF CO–PRECIPITATED HYDROGELS

In papers [12,13] the extreme cases of structual formation of binary and ternary systems, whose pH of precipitation of components occupy diammetrically opposite positions, are considered and the mechanism of porosity formation and its connection with different properties and composition of solutions has been studied.

Apart from these, binary mixtures of salts with components whose pH of precipitation are overlapping (pH of complete precipitation of one component is higher than pH of initial precipitation of the other) are also of certain interest [15]. In co–precipitation of hydrogels from such systems a section of simultaneous precipitation of hydroxides of the first and second components is inevitable.

In this case, the mechanism of the porous structure formation can be subdivided into several stages that differ from one another by the gel particle size, composition of gel, and particle arrangement. Undoubtedly, these parameters will change with composition of the solution. In particular, at a high concentration of the first component (with a lower pH of precipitation) and insignificant content of the second, completely adsorbed on gel particles, precipitated by the first component, the structure of the adsorbent obtained will be represented by gel partially encapsulated by the other component. As the concentration of the second component increases, the number of encapsulated particles will

Table 5
Adsorption–structural properties of co–precipitated metal hydroxides

Composition, % mass of hydroxide			V_s	S_{sp}	r_{eff}
	I	II	(cm^3/g)	(m^2/g)	(nm)
$Ni(OH)_2$ – $Cr(OH)_3$	100	0	0.130	52	5.0
	90	10	0.181	65	5.6
	80	20	0.225	79	5.7
	70	30	0.264	91	5.8
	60	40	0.300	101	5.9
	50	50	0.326	110	5.9
	40	60	0.351	124	5.7
	30	70	0.340	120	5.6
	20	80	0.292	108	5.4
	10	90	0.215	88	4.9
	0	100	0.151	67	4.5
$Mn(OH)_2$ – $Zn(OH)_2$	100	0	0.169	26	13.0
	90	10	0.232	33	14.6
	80	20	0.290	52	11.1
	70	30	0.333	74	9.0
	60	40	0.351	80	8.8
	50	50	0.350	82	8.5
	40	60	0.312	78	8.0
	30	70	0.291	67	8.7
	20	80	0.230	48	9.6
	10	90	0.200	37	10.8
	0	100	0.153	28	10.9
$Al(OH)_3$ – $Fe(OH)_3$	100	0	0.332	210	3.2
	90	10	0.362	240	3.0
	80	20	0.375	260	2.9
	70	30	0.380	290	2.6
	60	40	0.386	310	2.5
	50	50	0.372	330	2.2
	40	60	0.350	340	2.1
	30	70	0.332	335	2.0
	20	80	0.300	325	1.8
	10	90	0.272	315	1.7
	0	100	0.221	290	1.5

rise and at concentrations exceeding the sorption capacity of the gel, apart from completely encapsulated particles, individual particles of the second component will appear in the mixture.

In view of the fact that concentrations of components in the mixture exceed the sorption capacities of hydrogels present,in the section of co–precipitated gels, the structure–

formation mechanism of samples produced consists both in growing particles of both components and in the structure formation of the prevailing hydrogel.

As the concentration of the component with a higher pH of complete precipitation increases, the composition of the precipitate will be represented by grown particles of hydrogel with a lower pH of complete precipitation and individual particles of the second component (Tables 1 and 3). As the ratio of components changes further, the mentioned trend changes towards increase in the concentration of particles of the second component and decrease in the sorption capacity of the adsorbents produced (Table 5, Fig.4).

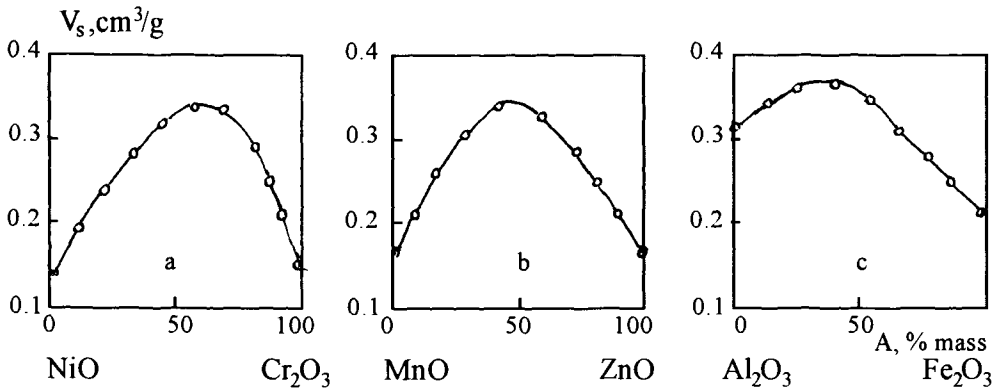

Figure 4. Limiting sorption capacity V_s – composition curves for the systems: a – NiO – Cr_2O_3; b – MnO – ZnO; c – Al_2O_3 – Fe_2O_3.

Analysis of the results obtained shows that in the systems studied the greatest departure of the V_s –composition curve from additivity is observed for NiO – Cr_2O_3 and MnO – ZnO samples with very close sorption capacities of individual components. In the systems, whose sorption capacities differ markedly from each other (Al_2O_3 – Fe_2O_3), the effect of building-up of hydrogel particles is masked slightly by the contribution to V_s of the portion of the oxide with the highest sorption capacity. As a rule, in this case the position of the maximum in the V_s –composition curve is shifted towards the component with a higher sorption capacity and its height is exhibited less distinctly as compared to the NiO – Cr_2O_3 and MnO – ZnO specimens.

Of course, it does not mean that in this case the effect of building-up of particles on the growth of the sorption capacity is exhibited to a smaller extent. The main reason seems to be the fact that two main factors that make contributions different quantitatively but having the same directions are involved here. In particular, excess of the absorption capacity of Al_2O_3 over that of Fe_2O_3 is 0.111 cm^3/g, which itself makes a substantial contribution to the growth of the total sorption capacity of the samples, when they are enriched with aluminium oxide. Nevertheless, this contribution is markedly lower than the increase in V_s of the samples due to hydrogel particles building- up (Fig.4), though in this system the effect of this factor is not very great as compared to the other systems studied. This can be explained by the fact that fine iron hydroxide particles that are

precipitated first, when built–up by aluminium hydroxide, are not substantially increased in volume. As a result, as the specimens become enriched with iron oxide and especially when the free phase of Fe_2O_3 with a lower sorption capacity is formed, accretion in V_s of the specimens is aimed at fine–porous structures formation that, as formation is known, do not facilitate the increase in the sorption capacity.

Analysis of the structure formation mechanism of the studied systems and others with maxima in the V_s –composition curves has revealed their similarity, which suggests uniformity of processes involved in porosity formation of co–precipitated adsorbents. Analogy is also seen in the determination of sample composition in maxima in the V_s –composition curves in terms of sorption capacities of components [2]:

$$C_1 = \frac{V_{s_1} \cdot 100}{V_{s_2} \cdot 2} \qquad (3)$$

Such systems and the mechanism of the adsorbent porous structure formation can be used for purposeful modification of the nature of their surfaces and the value of their sorption capacity. In this case, during calcinating of a sample, the modifying additive can interact with the prevailing component, forming a new crystalline compound with properties differing essentially from those of the initial compounds. This fact opens unrestricted possibility of changing the chemical nature of the solid surfaces and, consequently, their adsorption and catalytic properties.

This matter will be considered in more detail later here, and now it should be noted that as is shown by calculations, the value of the shift of the maximum in the V_s –composition curve towards the component with a higher sorption capacity follows the relationship: the larger the difference between the sorption capacities of individual components,the greater the shift of the maximum towards the most active component and the maximum is exhibited at a smaller content of the second component. In should be noted here that as a result of insignificant growing of particles and increase of their size, the height of the maximum drops continuously and the sorption capacity of the sample produced approaches V_s of the individual component.

Thus, apart from pH of initial and complete precipitation of hydrogels responsible for growing of particles, the formation of the structure of specimens is also affected by sorption capacities of individual components, which do not affect the gel structure formation mechanism, but distort the shape of the V_s –composition curve and to some extent, create illusive impression of effective growth of the particle size and V_s of the sample in the process of co–precipitation of hydroxides.

Apart from the changes in the sorption capacity of samples, other parameters of their structure also change in a specific way. In particular, the curves of the specific surface area and the average effective pore radius are similar in shape to the V_s –composition curves, especially, with equal or relatively similar values of S_{sp} of individual components in the mixture.

The reason for these changes and causative factors will be considered in more detail later here. Therefore, we will not dwell on this matter and only note that apart from the factors considered, the character of the porous structure formation is affected essentially by the nature of hydroxide, the shape of its particles, tendency for crystallization, etc. In other words, the action of the controlling factor (the pH of hydroxide precipitation), responsible for structure formation and shape of the V_s–composition curve, is also affected

by the nature of hydroxide, which is exhibited by the value of sorption of samples and the chemical nature of their surface. Depending on combination of components in a mixture, conditions of precipitation and drying of hydroxides, the action of surfactants, etc., the efficiency of these factors can be directed towards increase of the structural parameters of samples produced or towards their decrease.

In this connection it should be noted that varying the porous structure of solids by various combinations of components with different pH of the initial and complete precipitation of hydrogels (and these combinations are innumerable and diverse, especially in multicomponent systems), it is possible to carry out purposeful synthesis of porous bodies not only with a prescribed structure but also with prescribed properties. Moreover, it may be possible to predict the presence of a maximum in the V_s –composition curve and the behaviour of the structure of precipitated materials with variations of relative contents of the components from sorption properties of individual components in the mixture designed.

5. THE EFFECT OF THE SOLUTION CONCENTRATION AND pH OF PRECIPITATION OF HYDROGELS ON THEIR STRUCTURE

Apart from the investigations of the mechanism of structure formation of adsorbents by successive building–up of hydrogel particles [16], it seems of interest to make these studies specific, in particular, to elucidate the effect of concentrations of initial solutions on the behaviour of the porous structure of adsorbents produced. Solution of this problem is of basic importance both as regards finding the regularities of changes in the sorption capacity and the shape of the V_s –composition curve as well as changes in the sorption capacity of co–precipitated materials as a function of their composition and concentrations of initial solutions.

Studies have been carried out with the binary mixture $Ni(OH)_2$ – $Cr(OH)_3$ with 5, 10, and 15% concentrations of initial solutions and with the component compositions ranging from 0 to 100% mass. Because of this, it was possible to obtain a sufficiently complete picture of the behaviour of the properties of synthesized materials as a function of the composition and concentration of the solution.

In Table 6 and Fig.5 it can be seen that concentrations of initial solutions and the calcination temperature of the samples do not change the shape of the V_s –composition curve but only promote the growth of the sorption capacity of the products, as shown in some works [2,17,18]. The reason for it has been considered in detail in papers [2,19], the authors of which have ascribed it to the presence of association complexes, the size and complexity of which increase with the concentration of the solution.

As shown by calculations, changes in V_s of the products in the process of building–up of particles are more effective in more diluted solutions. It seems probable that this can be explained by the fact that every building–up of fine gel particles, the number of which per unit volume is larger than that of large particles, is accompanied by formation of a structure with a larger pore size, excluding formation of macropores. On the contrary, changes in the size of initial gel particles obtained from more concentrated solutions that slightly increase in size during building–up inevitable result in appearance of macropores

Table 6
Sorption of CCl_4 vapour by co–precipitated hydroxides

Sample composition, % mass		Obtained from 5% salt solution				Obtained from 10% salt solution				Obtained from 15% salt solution			
		Calcination temperature, °C											
		120		500		120		500		120		500	
$Ni(OH)_2$	$Cr(OH)_3$	V_s (cm^3/g)	S_{sp} (m^2/g)	V_s (cm^3/g)	S_{sp} (m^2/g)	V_s (cm^3/g)	S_{sp} (m^2/g)	V_s (cm^3/g)	S_{sp} (m^2/g)	V_s (cm^3/g)	S_{sp} (m^2/g)	V_s (cm^3/g)	S_{sp} (m^2/g)
100		0.130	52	0.175	68	0.180	63	0.241	80	0.220	70	0.270	80
90	10	0.181	65	0.202	81	0.231	78	0.292	94	0.270	87	0.325	94
80	20	0.225	79	0.250	96	0.280	91	0.332	110	0.322	102	0.371	110
70	30	0.264	90	0.305	110	0.325	105	0.370	125	0.355	115	0.410	120
60	40	0.300	104	0.340	121	0.360	120	0.409	138	0.390	127	0.451	135
50	50	0.326	110	0.379	131	0.380	125	0.439	146	0.410	135	0.480	146
40	60	0.361	124	0.405	134	0.401	135	0.481	150	0.420	140	0.500	150
30	70	0.340	110	0.375	122	0.385	130	0.440	145	0.415	135	0.475	145
20	80	0.292	96	0.325	108	0.340	120	0.409	140	0.365	126	0.425	140
10	90	0.215	80	0.255	91	0.290	110	0.335	121	0.320	115	0.375	126
	100	0.151	67	0.200	75	0.235	96	0.292	110	0.261	103	0.341	120

in the structure of the sample, which are not filled by condensed vapour in the sorption process. This is evidenced by the value of the total sorption capacity, which, as was shown experimentally, for the products obtained from 10 and 15% solutions with composition (60% mass of Cr_2O_3) corresponding to the maximum in the V_s –composition curve, differs from V_s of compounds synthesized from 5% solution by 0.04 and 0.06 cm^3/g, respectively, i.e., the maxima differ in height from each other by 0.04 and 0.02 cm^3/g. In other words, at the points of maxima, sorption capacities of the samples drop as the concentrations

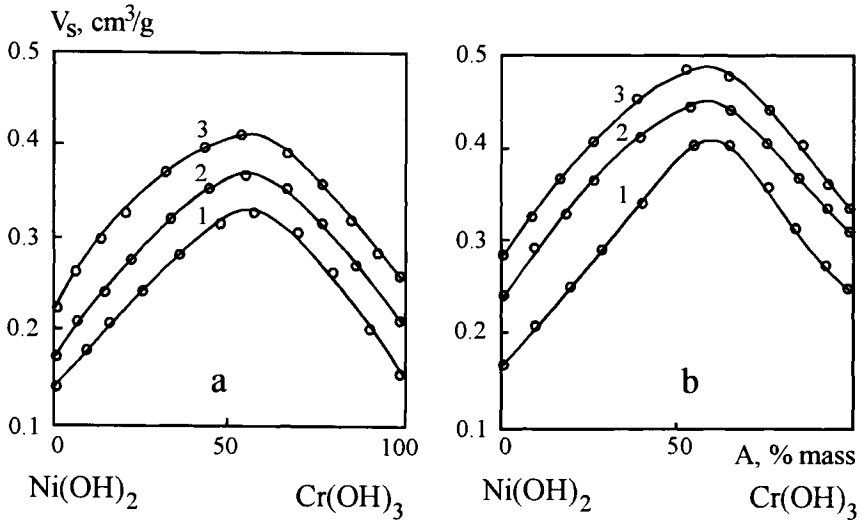

Figure 5. The V_s –composition curves for the system $Ni(OH)_2$ – $Cr(OH)_3$ obtained: from 5 (1), 10 (2) and 15% salt solutions (3). Calcination temperature is 120°C (a) and 500°C (b).

of salts in solutions decrease, while the difference between the total sorption capacity of compounds with compositions indicated and V_s increases. This implies that in the structure of materials, obtained from more concentrated solutions, accumulation of macropores occurs, which is known not to promote the growth of the sorption capacity of the materials. It is important that the position of the maximum in the V_s composition curve does not change, while its height does, which suggests that the mechanism of its formation is the same. In other words, building-up of hydrogel particles is of general character and any changes in experimental conditions may affect its course only partially. Moreover, it is of interest to follow out the structural changes in thermally treated specimens. Depending on the properties of individual components, nature and composition of the built-up compound and the presence of phases of individual components, several cases can be distinguished: 1) one of the components in the mixture has a high thermal resistance, the other is easily sintered; 2) all components of the mixture are heat resistant; 3) components are not stable under the temperature effect, etc.

Of course, in each of the above cases, the interaction of components with each other, at high temperatures producing new crystal structures with properties that differ substantially from those of the initial compounds, cannot be excluded. In other words, a new ther-

modynamically stable phase is formed which encapsulates the surface of the component that is precipitated first. It should be noted that as the compositions of co-precipitated hydrogels change, not only the composition of the encapculated phase changes but also the ratio of the components as well, which will result in prevalence of one or the other component. Therefore, in order to understand the essence of the processes and to predict the behaviour of the structure of co-precipitated compounds subjected to calcination, each of the above cases must be considered in every detail.

The first case can be implemented in two versions: the component that is precipitated first is thermosensitive or, on the contrary, thermostable. In the first version, hydrogel particles are encapsulated by the thermostable compound. As a result, in calcination of such a globule, its inner part decreases substantially, while the outer shell remains almost unchanged. This leads to formation of intraparticle porosity and, as shown by the experimental results, increase in the sorption capacity of the compounds after they were calcinated at the temperature of intense sintering of the component contained inside the globule.

The situation changes essentially when components are co-precipitated in the inverse order, i.e., when a thermostable component is inside the globule and the easily sintered component, which at a high temperature on the surface of the particle "core" forms a nonporous layer with a low or zero sorption capacity, in its outer shell.

Results of the adsorption-structural studies on building-up of iron hydroxide particles by aluminium hydroxide followed by calcination have shown that with account of phase and structural changes, the sorption capacity of the samples increases with the calcination temperature and content of Fe_2O_3 in their composition (Table 7, samples 5–8).

This behaviour of the sorption capacities of the samples indicates that the value of the volume shrinkage of thermally treated iron hydroxide is noticeably higher than the accretion in its sorption capacity. As it was mentioned above, this is caused by forming an additional pore volume inside the built-up globule.

The inverse order of building-up of hydrogels (Table 7, samples 9–12) results in a reduction of the sorption capacity of both initial and calcinated samples. These changes are caused by the fact that when being calcinated, $Fe(OH)_3$ occurring on the surface on a built-up $Al(OH)_3$ particle forms a sufficiently dense porous material that excludes formation of additional intraglobular porosity, a source of growth for the sorption capacity of adsorbents obtained.

Comparison of sorption capacities V_s of built-up samples with the additive quantities of sorption (V_s add.) shows that depending on the composition and thermal treatment, the latter vary from 0.32 to 0.39 cm^3/g, i.e., they are substantially lower than the experimental values. However, in reality, in the case of mechanical mixing of individual hydroxides of iron or aluminium V_s values must coincide since the sorption capacity is a statistical mean determined by the particle size of the components mixed and their arrangement. In the present case one of these conditions is violated as the particle size increases substantially as a result of building-up of particles. This is the main reason for the differences between V_s of the samples obtained and the additive sorption capacities (V_s add.). Moreover, shrinkage of hydroxide components in the process of drying and calcination makes a noticeable contribution to this process, which is observed especially distinctly for the samples of iron hydroxide built-up by aluminium hydroxide (Table 7).

It is doubtless that between the extreme cases considered intermediate versions are

Table 7
Adsorption-structural characteristics of samples obtained by building-up of gel particles

Composition of sample	Calcination temperature °C	V_s (cm^3/g)	S_{sp} (m^2/g)	r_{eff} (nm)	V_s add. (cm^3/g)
$Al(OH)_3$	120	0.440	250	3.5	–
	500	0.491	210	4.7	–
$Fe(OH)_3$	120	0.225	212	2.1	–
	500	0.250	180	2.8	–
42% $Fe(OH)_3$ + 58% $Al(OH)_3$	120	0.690	195	7.1	0.350
	500	0.725	121	12.0	0.390
45% $Fe(OH)_3$ + 55% $Al(OH)_3$	120	0.750	167	9.0	0.341
	500	0.885	149	11.8	0.380
42% $Al(OH)_3$ + 58% $Fe(OH)_3$	120	0.512	168	6.1	0.316
	500	0.537	99	10.8	0.350
44% $Al(OH)_3$ + 56% $Fe(OH)_3$	120	0.538	134	8.0	0.320
	500	0.570	103	11.0	0.355

possible, determined by thermostability of components in the mixture, i.e., with a high stability of one component, the other may have most different sintering temperatures. Because of this, it is possible to control the intraglobular porosity within certain ranges,thus controlling also the sorption capacity of samples obtained.

In adsorbents of the second type, i.e., in the case of equal thermostability of components, no essential changes proceed during calcination. The present system is indifferent to the fact which of the components is in the core and which is on the surface of the particle. However, when properties of one of the components do not meet the conditions enumerated above, the mechanism of formation of the porous structure of calcinated samples will follow the scheme considered in the first case.

In systems of the third type i.e., in combination of substantially sintered components, the behaviour is slightly different as the structure of the samples is reduced. As a rule, such systems are useless in practice, especially in catalytic processes occurring at high temperatures, in which unstability of the structure of the catalysts is exhibited, which is accompanied by changes in their size and chemical nature of the surface, activity, selectivity and kinetic characteristics.

It should be noted here that systems of the first version are preferable as with the same particle size they ensure the highest development of porosity and specific surface area of the samples obtained. Depending on conditions of usage, components ratios of these systems can be extremely diverse but must satisfy the condition: at a specified temperature, the volume shrinkage of either component must be noticeably higher than that of the other. When components in the system interact chemically to produce the layers of crystalline compound, impermeable for adsorbed molecules, at the interface, the sorption capacity will be smaller by an "intraparticle" volume.

In the second type systems, irrespective of the succession of settling of the components, the behaviour of the structure of samples with components that do not interact chemically

is similar to that of individual components in the system studied. However, this does not concern the chemical nature of the surface, the behaviour of which is specific for each of the components. Thus, it is important, which of the components is superposed, especially, when a catalytic active metal or metal oxide is used as a superposed material.

6. THE MECHANISM OF STRUCTURE FORMATION OF CO-PRECIPITATED ADSORBENTS FROM THREE- AND FOUR-COMPONENT SYSTEMS

Apart from examination the porous structure formation of binary co-precipitated adsorbents as a function of pH of initial and final precipitation of hydroxide components [4,15,20] it was interesting to investigate more complex compositions and the mechanism of their structure formation. Komarov, Repina and Skyrko [21] studied the three-component systems $Fe(OH)_3$ - $Zn(OH)_2$ - $Cu(OH)_2$, $Fe(OH)_3$ - $Al(OH)_3$ - $Zn(OH)_2$ and $Fe(OH)_3$ - $Cr(OH)_3$ - $Ni(OH)_2$. The fact that in the first of the systems the pH of initial and final co-precipitation of zinc and copper coincide is a characteristic feature of these systems. In this case the V_s -composition curve is represented by a straight line connecting the sorption capacities of individual components [15]. In the first and third systems pH values of initial and final precipitations of hydroxide of all the components of the mixture do not coincide (Tables 1 and 3). This selection of compositions allows the mechanism of co-precipitation of hydroxide components and relations of porous structure formation of adsorbents obtained to be followed.

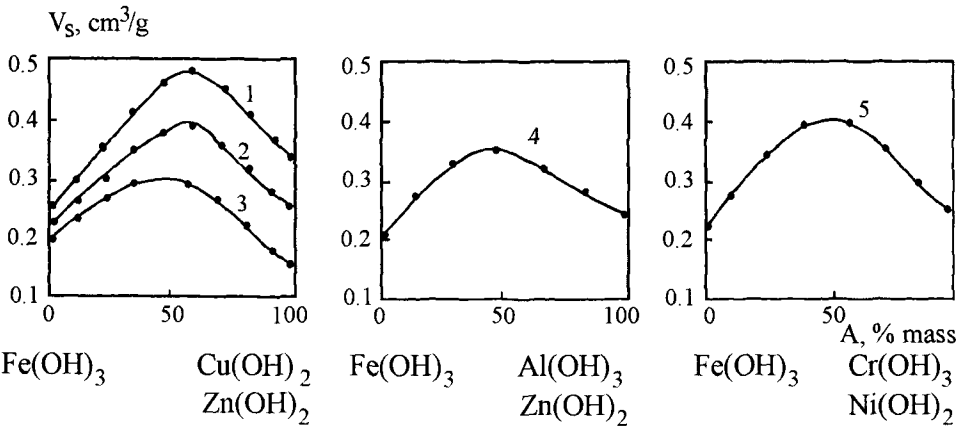

Figure 6. The limiting sorption capacity V_s -the composition curves for the following systems: 1 - $Fe(OH)_3$ - $Cu(OH)_2$; 2 - $Fe(OH)_3$ - $Cu(OH)_2$ - $Zn(OH)_2$; 3 - $Fe(OH)_3$ - $Zn(OH)_2$; 4 - $Fe(OH)_3$ - $Al(OH)_3$ - $Zn(OH)_2$; 5 - $Fe(OH)_3$ - $Cr(OH)_3$ - $Ni(OH)_2$.

Thus, for the system $Fe(OH)_3$ - $Zn(OH)_2$ - $Cu(OH)_2$ the co-precipitation of components follows the mechanism of a two-component mixture since, as mentioned earlier, zinc and copper hydroxides are co-precipitated simultaneously. Therefore, in the

three-component mixture considered and binary mixtures $Fe(OH)_3$ - $Cu(OH)_2$ or $Fe(OH)_3$ - $Zn(OH)_2$; the V_s -composition curves only differ by the fact that sorption capacities of $Cu(OH)_2$ and $Zn(OH)_2$ are not equal and consequently, in the V_s -composition curves the sorption maxima are shifted towards the most actively sorbed component (Fig.6).

In this case the arithmetical mean of V_s of binary systems studied follows almost exactly the V_s -composition curve of the ternary system $Fe(OH)_3$ - $Zn(OH)_2$ - $Cu(OH)_2$, thus indicating identity of the structure formation. The only difference is that in the ternary system, because of equality of pH of precipitation of zinc and copper gels, particles are built-up by two components simultaneously, while in the case of binary systems, by only one component. It is this component that determines the position of the V_s -composition curve relative to this curve of a ternary system.

Because of a genetic relation between the V_s -composition curves of the systems studied, with a common component of $Fe(OH)_3$, it is possible from the sorption data of the ternary system and those of binary systems to calculate the V_s -composition curve for the second binary system or from these data for two binary systems to calculate the V_s -composition curve for a ternary system containing the same components.

The fact that iron hydroxide particles are built-up by a mixture of zinc and copper ions not selectively but in the same ion and quantitative proportion which is prescribed in the initial solution is a characteristic feature of the ternary system $Fe(OH)_3$ - $Zn(OH)_2$ - $Cu(OH)_2$. Alternatively, i.e., when this condition is not observed, the V_s -composition curve of the three-component mixture cannot be calculated from the sorption data for two-component systems.

The mixtures $Fe(OH)_3$ - $Al(OH)_3$ - $Zn(OH)_2$ and $Fe(OH)_3$ - $Cr(OH)_3$ - $Ni(OH)_2$, in which the pH of initial and complete precipitation of metal hydroxides do not coincide (Table 8), are an example of such systems. In this connection, building-up of iron hydroxide particles precipitated first follows a more complicated scheme since the component and concentration composition of the mixture building-up a colloid particle continuously change. In a four-component system containing iron, chromium, aluminium and nickel hydroxides, i.e., the same components that occur in various combinations in compositions of two- and three-component mixtures, the mechanism of these changes is almost the same. Because of this, from the analysis of simpler systems it is possible to find relations of the structure formation, to reveal the mechanisms of the processes involved in coprecipitation of metal hydrogels and to determine the general character of the interaction of components in the mixture, in particular, the effect of their ions on building-up of colloid particles precipitated first.

Knowledge of the effect of composition of initial mixtures and the pH of initial and final precipitation of their components on the formation of porous bodies will allow to understand deeply the processes involved in co-precipitation of multicomponent samples and to suggest a mechanism of their structure formation.

It should be noted that irrespective of complexity of a system, its component composition and properties, the principle of formation of porosity of adsorbents found for binary mixtures holds for more complicated systems too. The only difference is final results, i.e., the shape of the V_s composition curves that is different from those of the adsorption curves of samples synthesized from binary systems. Several explanations can be suggested for this difference but the main reason is sorption characteristics of the components, which can be identical, slightly or substantially different from one another. As reported

Table 8
Structural parameters of co-precipitated adsorbents from three and four-component systems

Composition, % mass of hydroxide				V_s	S_{sp}
I	II	III	IV	(cm^3/g)	(m^2/g)
$Fe(OH)_3$–$Zn(OH)_2$–$Cu(OH)_2$					
100				0.225	290
90	5	5		0.271	278
80	10	10		0.306	267
70	15	15		0.341	251
60	20	20		0.372	217
50	25	25		0.391	193
40	30	30		0.400	158
30	35	35		0.375	135
20	40	40		0.332	83
10	45	45		0.290	71
50	50			0.255	75
$Fe(OH)_3$ – $Al(OH)_3$ – $Zn(OH)_2$					
90	5	5		0.262	259
70	15	15		0.315	190
50	25	25		0.340	160
30	35	35		0.310	130
10	45	45		0.263	81
50	50			0.238	76
$Fe(OH)_3$ – $Cr(OH)_3$ – $Ni(OH)_2$					
90	5	5		0.281	234
70	15	15		0.350	181
50	25	25		0.390	167
30	35	35		0.381	160
10	45	45		0.320	121
50	50			0.282	110
$Fe(OH)_3$ – $Cr(OH)_3$ – $Ni(OH)_2$ – $Al(OH)_3$					
		50	50	0.245	104
5	5	45	45	0.275	117
10	10	40	40	0.300	140
15	15	35	35	0.305	148
20	20	30	30	0.280	170
25	25	25	25	0.250	162
30	30	20	20	0.215	148
35	35	15	15	0.175	130
40	40	10	10	0.150	123
45	45	5	5	0.125	92
50	50			0.102	86

in papers [4,15,20], the shape of the V_s –composition curves is determined by individual characteristics of the processes involved in co–precipitation of hydroxides.

The four–component system $Fe(OH)_3$ – $Cr(OH)_3$ – $Ni(OH)_2$ – $Al(OH)_3$ is not an exclusion from the general mechanism of structure formation, especially, because the mechanism of building–up of gel particles is similar to that of the process occurring in co–precipitation of simpler systems, except for some peculiarities.

A distinctive feature of this four–component system is that the quantitative composition of components is chosen in such a way that each pair of them in the mixture constitutes from 10 mass% (5 mass % of each component) to 100 mass% (50 mass % of each component). Because of this it was possible to avoid diversity of concentration combinations of the components and to investigate it in the simplest case of a mixture of two binary components $Fe(OH)_3$ – $Cr(OH)_3$ and $Ni(OH)_2$ – $Al(OH)_3$ containing 50% mass of each of the oxides. Equality of the compositions and conditions of co–precipitation of components in binary mixtures implies equality of sorption capacities of the adsorbents obtained. Therefore, upon mechanical mixing of hydrogels of these binary mixtures the V_s –composition curve is a straight line. However, in reality, because of interaction of hydroxides during their co–precipitation a structure is formed which differs essentially in its parameters from the structure of samples synthesized from the binary mixtures considered from a mechanical mixture of their hydroxides (Fig. 7).

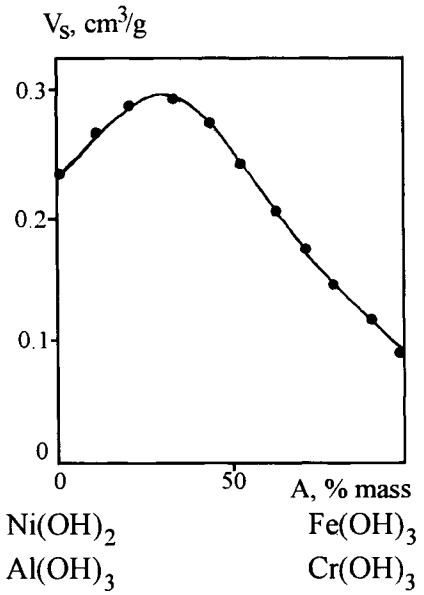

Figure 7. The limiting sorption capacity V_s –the composition curve for the four–component system $Ni(OH)_2$ – $Al(OH)_3$ – $Fe(OH)_3$ – $Cr(OH)_3$.

In order to understand the porous structure formation of adsorbents co–precipitated from both three and four–component systems, succession of formation of hydrogels and

accompanying processes will be considered. Analysis of the data in Tables 1 and 3 shows that proceeding from the pH of its initial precipitation, iron hydroxide is formed first, sorbing Cr^{3+}, Al^{3+} and Ni^{2+} ions on its particle surfaces. Among the ions just enumerated, aluminium ion is preferred that has the lowest size and a high charge and a lower pH of the initial precipitation of hydrogel is preferable. Because of this, aluminium functions as a component building-up iron hydroxide particles. As the pH in the solution increases further, chromium-modified iron and aluminium hydroxides co-pricipitate. In the final stage of co-precipitation of hydroxides the individual phase of nickel hydroxide is developed.

Undoubtedly, in multicomponent mixtures the structure-formation process obeys a more complicated scheme, the essence of which can be described as follows. When the modifying component is present in the mixture in excess, it becomes an object of modification by ions of different metals with a higher pH of precipitation of hydroxides. Cases of simultaneous precipitation of two or three hydroxides with the same or different pH of their complete precipitation cannot be excluded. Other combinations of components, whose properties determine the shape of the V_s composition curve and the order of their modifying action, are possible.

The scheme of successive reactions involved in co-precipitation of hydrogels of multicomponent systems only gives a general idea about the mechanism of structure formation, and a detailed analysis of a particular problem for a given mixture must be carried out proceeding from individual properties of its components. It should be noted that any quantitative change in the mixture makes a certain contribution to the mechanism of structure formation of the products, leaving the order of gelation unchanged. For example, when the composition of the initial solution is enriched with the component with a high sorption capacity, V_s of porous bodies obtained increases due both to the presence of a hydroxide with a high sorption capacity and to building-up of particles. The latter depends functionally on many factors, primarily, on ion-exchange capacity of colloid particles, the valence of ions and their size. Moreover, the initial composition of a colloid particle and the nature of the built-up compounds are also important. These are only some of the reasons that determine the mechanism of the growth of colloid particles that are probably of a vital importance for the increase of their size.

In spite of complexity of building-up of colloid particles, especially in co-precipitation of hydrogels out of multicomponent mixtures, where these factors impose over one another, it is possible to simplify this process essentially by dividing it into binary systems according to the pH of precipitation of hydroxides of individual components and the whole path of the structural formation of the adsorbents obtained can be followed.

When two components with the same pH of initial and complete precipitation of hydroxides are present in the mixture, the situation changes essentially and in the presence of three such components with the same pH, a four-component mixture becomes similar to a binary system in the structure formation mechanism.

To conclude the section, it should be noted that the new approach to understanding the mechanism of the porous structure for co-precipitated hydrogels considered in [4,15,20] may be extremely useful for the purposeful selection of component compositions and their percentage in the solution to ensure a maximum sorption capacity of the porous material synthesized.

7. THE EFFECT OF FREEZING AND TEMPERATURE OF CO-PRECIPITATION OF HYDROGELS ON THE STRUCTURE OF ADSORBENTS PRODUCED

Apart from the investigations of the relations governing the porous structure formation of coprecipitated adsorbents in terms of the pH of initial and complete precipitation of hydrogels, it was of interest to find out how the temperature of co-precipitation of hydrogels and freezing of salt solutions and hydrogels affects the structure of adsorbents produced.

Komarov et al. [22] have carried out such investigations with the systems $Zn(OH)_2$ - $Cu(OH)_2$, $Fe(OH)_3$ - $Mg(OH)_2$ and $Cr(OH)_3$ - $Mg(OH)_2$. For the first system, the V_s - the composition curve is a straight line with a maximum which is located in the composition axis at different concentrations of the components.

Since the structure formation mechanism is described in detail in [4,13,15,20], I will not dwell on the reasons for the changes in the sorption capacity of the adsorbents obtained.

The present studies were carried out to investigate formation of a porous structure of coprecipitated adsorbents as a function of their composition and physical effects. With this aim, 5% salt solutions and hydrogels were frozen at - 8°C, then defrosted at room temperature and brought to 20°C. Then hydrogels were precipitated, washed to remove salts, shaped as rods, dried at room temperature for 24 h and finally in a drying cabinet at 120°C.

Studies of the adsorption structure of the materials produced (Table 9, Fig.8) show that after freezing their sorption capacity is much higher than that of the initial materials. The difference is that the sorption capacity of materials synthesized from frozen solutions is preferable over that of frozen hydrogels.

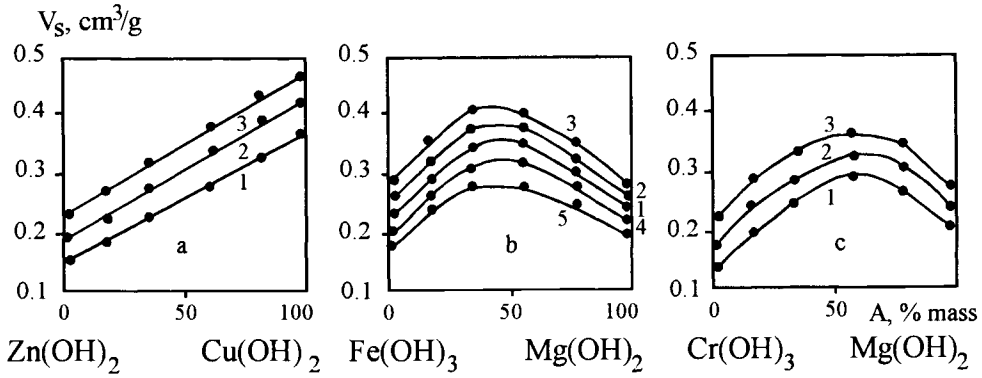

Figure 8. The limiting sorption capacity V_s -composition curves for the systems $Zn(OH)_2$ - $Cu(OH)_2$ (a); $Fe(OH)_3$ - $Mg(OH)_2$ (b); $Cr(OH)_3$ - $Mg(OH)_2$ (c): 1 - initial samples; 2 - frozen gels of the samples; 3 - obtained from frozen solutions; 4 - obtained at 50°C; 5 - obtained at 80°C.

As mentioned in monograph [2], the reason for these differences is that the structure formation mechanism of hydrogel produced from frozen solution is essentially different

Table 9
Adsorption–structural characteristics of co-precipitated adsorbents obtained from frozen solutions and hydrogels

Composition % mass of hydroxide		Initial samples		Samples obtained from Frozen solutions		Samples obtained from Frozen gels	
I	II	V_s (cm^3/g)	S_{sp} (m^2/g)	V_s (cm^3/g)	S_{sp} (m^2/g)	V_s (cm^3/g)	S_{sp} (m^2/g)
$Zn(OH)_2$ – $Cu(OH)_2$							
100	0	0.153	28	0.223	38	0.200	35
20	80	0.321	80	0.440	82	0.395	82
40	60	0.275	77	0.382	79	0.352	78
60	40	0.235	73	0.330	75	0.300	74
80	20	0.193	37	0.282	57	0.250	50
0	100	0.360	66	0.487	88	0.450	80
$Fe(OH)_3$ – $Mg(OH)_2$							
0	100	0.244	86	0.291	116	0.260	100
20	80	0.300	205	0.350	207	0.310	213
40	60	0.352	280	0.402	328	0.362	294
60	40	0.341	310	0.395	330	0.362	324
80	20	0.283	300	0.340	325	0.306	320
100	0	0.225	290	0.260	310	0.235	302
$Cr(OH)_3$ – $Mg(OH)_2$							
0	100	0.244	86	0.280	116	0.260	100
20	80	0.298	95	0.371	122	0.362	112
40	60	0.300	105	0.366	120	0.355	115
60	40	0.265	103	0.335	115	0.315	109
80	20	0.211	89	0.270	100	0.250	96
100	0	0.151	67	0.210	81	0.190	75

from that of hydrogel having a prescribed porosity.

While in the first case ions associate in the solution and their size and composition are responsible for porous structure, in the second and third cases formation of the porous structure is caused by already formed colloid particles and their conglomerates. These two processes differ substantially in the mechanism of structure formation, but the directions of their actions coincide and both of them promote the increase of the sorption capacity of the adsorbents produced.

A distinctive feature of the processes occurring in the systems studied is the fact that in spite of their complexity and physical effects, the shape of the V_s –composition curves and the position of the maximum in the composition axis remain unchanged. This suggests that as a result of internal changes, salt solution and hydrogel subjected to freezing differ from the initial state only by qualitative indices, i.e., the factor of ion association in the solution subjected to freezing plays a main role and its contribution to the structure formation mechanism constitutes 15 to 40%, depending on the nature of the systems obtained.

For hydrogels this effect is noticeably lower, which is caused by a lower possibility of aggregation of already aggregated particles into larger ones. It is interesting to note that for each of the mixtures, the increase of V_s is approximately the same, which suggests uniformity and correlation of changes of both association of ions in the solution and agglomeration of hydrogel particles in the course of their freezing. Undoubtedly, individual properties of the systems affect, to a certain extent, the course of these processes determined by the size, polarizability and charge of ions and especially, by the increase of their association as the temperature decreases.

The fact that the reasons responsible for the structure formation of adsorbents produced when freezing solutions are plausible is confirmed by the results of co-precipitation of gels at temperatures 50 and 80°C, i.e., under the conditions when the ion association in solution is minimum. In such solutions gelation is characterized by a rather small size of particles, which fully or partially lose the stability factor (the double electric layer, solvate shell, etc.) and stack to one another, forming compact aggregates. Having reached a certain size, these aggregates form a dense coagulate, which, as shown by X-ray analysis, has a crystalline or pseudocrystalline structure. As a result, the particles stacking to one another at these sites, form a spatial network, meshes of which contain disperse material; removal of this material is accompanied by development of porosity.

Adsorbents, co-precipitated at 80°C, whose sorption capacity is 20–25% lower than that of the initial compounds and the specific surface area is 1.4 to 1.7 times lower, are an example of the systems of the first type (Table 10). Moreover, a substantial difference is found in the shape of the sorption isotherms, which have a smoother rise at low relative pressures and narrow hysteresis loops as compared to the initial materials.

Table 10
Adsorption-structural characteristics of $Fe(OH)_3$–$Mg(OH)_2$ systems co-pricepitated at various temperatures

Composition of sample % mass of hydroxide		Co-precipitation temperature, °C					
		20		50		80	
$Fe(OH)_3$	$Mg(OH)_2$	V_s (cm^3/g)	S_{sp} (m^2/g)	V_s (cm^3/g)	S_{sp} (m^2/g)	V_s (cm^3/g)	S_{sp} (m^2/g)
0	100	0.244	86	0.220	75	0.200	70
20	80	0.300	205	0.275	130	0.247	120
40	60	0.352	280	0.315	180	0.275	162
60	40	0.341	310	0.300	200	0.255	190
80	20	0.283	300	0.250	220	0.220	205
100	0	0.225	290	0.200	210	0.170	200

Adsorption-structural properties of adsorbents obtained at 50°C have intermediate indices, lower than those of the initial materials and slightly higher than those of the samples formed at a temperature of 80°C which corresponds to strong destabilization of the interlayer of a disperse material between the particles, leading to formation of the strongest but simultaneously, the most brittle structures (Table 10, Fig.8).

It is undoubted that co-precipitation of hydrogels at a higher temperature is accompanied by other reactions aimed at decreasing the structural parameters of porous materials

synthesized. One of these processes is hydrothermal aging of gel, which, as shown by some authors [1,23], has great importance. The essence of the aging can be described as follows. If in the same vessel, under the solution there are simultaneously fine and coarse particles of some compound, the fine particles are dissolved gradually and the coarse ones grow. This can be ascribed to different thermodynamic properties of fine particles that differ substantially from the properties of coarser ones or the macrophase. An increased vapour pressure of fine droplets or an increased solubility of fine solid particles is an example of this statement. Consequently, solutions saturated relative to coarse particles are yet unsaturated relative to fine particles. The latter are dissolved, the concentration of the solution increases, and a part of the compound dissolved is deposited on the surface of larger particles. Theoretically this process can continue for a very long time until one large particle or several particles of the same size and volume are formed.

The increased pressure of vapor of fine particles can be calculated from the Kelvin's equation [24]:

$$RT \ln \frac{P_r}{P_\infty} = -\frac{2\sigma}{r} \cdot V \tag{4}$$

where P_r is the pressure of a droplet with the radius r, P_∞ is the pressure of vapour over a flat surface, σ is the surface tension, V is the molecular volume of the liquid. The equation relating an increase in the vapour pressure to the surface curvature and consequently, to the size of droplets of liquid can be applied, to crystals and amorphous solid particles. Since real crystals are shaped as polyhedra, whose surfaces are characterized by different surface tensions, the question arises here about the values of σ and r to be used here.

Wulff's theorem [25] states that σ/r is invariant for all faces. Therefore, the result obtained from the Kelvin's equation must be independent of the choice of a face.

Thus, the results of studies on sorption properties of adsorbents synthesized at elevated temperatures are affected by some factors whose action, as shown by the analysis, is directed towards reducing parameters of the structure of adsorbents produced. It is more difficult to answer the question about the contribution of each of them to this process and to estimate their effects. The difficulty consists in the fact that the effects of these factors are simultaneous and it is impossible to neglect at least one of them. It is only possible to suggest that the following two factors are the most effective: decrease of association in solution that is responsible for formation of fine disperse particles and destabilization of their aggregative state, which facilitates formation of the crystal phase. It is a joint action of these factors that largely determines properties of the materials synthesized.

8. SYNTHESIS OF CO–PRECIPITATED ADSORBENTS ON THE BASIS OF TWO BINARY SYSTEMS

As shown in [21], complexity of forming the structure of multicomponent adsorbents consists in selection of suitable components of the mixture that would provide successive building–up of hydrogel particles during their precipitation. In this case several combinations of components are possible, among which the following can be distinguished:

1. Two components in the mixture have equal pH of initial precipitation of hydrogels and the pH of the third component is different. According to the mechanism of structure formation, the mixture can be considered binary. In the presence of the fourth component whose pH differs from the others' ones, the mixture is ternary.
2. If the mixture consists of four components with different pH of initial precipitation of hydroxides, the system is a four-component mixture according to formation of its structure.
3. When the pH of three components of the mixture coincide and the pH of the fourth component is different, the system behaves as binary. A similar situation is observed in mixtures, in which two components have equal pH of initial and complete precipitation and the pH of the two other components differ from those of the two first components but coincide between each other.

In other words, irrespective of the number of components, whose pH of initial and complete precipitation coincide, the components behave as one component with a certain sorption capacity. Therefore, their participation in forming a porous structure of co-precipitated adsorbents can increase or decrease, to a certain extent, the optimum sorption capacity of the synthesized material, depending on the size and shape of hydrogel particles.

Of course, these examples do not exhaust the whole diversity of combinations of components in a mixture, especially, if we take into consideration differences in the pH of initial and complete precipitation of their hydrogels. Nevertheless, it is quite sufficient for confirmation of reasonability of the above suggestions.

Komarov and Repina [26] investigated the structure formation in three- and four-component systems, in which binary mixtures with compositions corresponding to the maximum of the sorption capacity in the V_s -composition curve, function as individual components.

A characteristic feature of these mixtures consists in selection of individual components, whose pH of precipitation promotes increasing the size of colloid particles in co-precipitation of hydroxides. In order to satisfy this condition it is necessary that pH of initial precipitation of hydroxides in the mixture do not coincide and that the component composition of the samples differ at the sorption maximum. Moreover, the use of other compositions of binary systems cannot be excluded. However, in this case the highest structure forming effect is not achieved. In spite of the fact that such systems are multicomponent, the mechanism of forming porosity is almost the same as the mechanism of structure formation in binary mixtures [13,15]. The difference only consists in the number of built-up components and the order of their deposition onto colloid particles precipitated first.

The behaviour of ΔV at the maximum of four-component systems depends on the sorption capacity of binary systems taken for synthesis. There are several reasons for it and all of them are caused by the sorption capacity of adsorbents obtained from binary systems, the presence of micropores in their structure and deceleration of the particle growth. Moreover, the increase of the sorption capacity of four-component systems depends on the combination of its components. Therefore, not optimum mixtures of binary systems providing the highest sorption capacity of the products are presented here but it is only shown that development of porous structure of adsorbents synthesized is possible

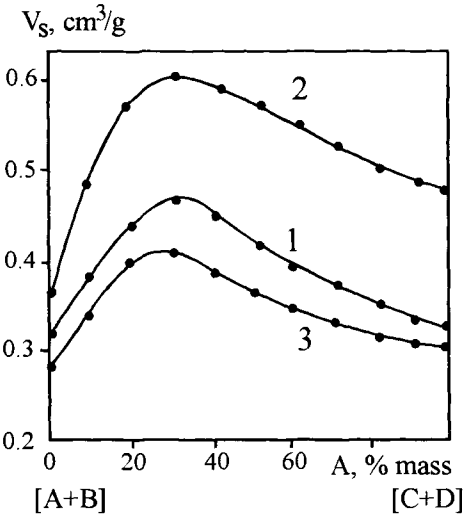

Figure 9. The V_s composition curves for the systems [A+B] – [C+D]:
1 – [40% $Ni(OH)_2$ + 60% $Cr(OH)_3$] – [50% $Mn(OH)_2$ + 50% $Zn(OH)_2$];
2 – [60% $Al(OH)_3$ + 40% $Fe(OH)_3$] – [40% $Fe(OH)_3$ + 60% $Cu(OH)_2$];
3 – [60% $Fe(OH)_3$ + 40% $Cr(OH)_3$] – [60% $Co(OH)_2$ + 40% $Mn(OH)_2$].

in principle. In this case binary systems are of vital importance in formation of structural parameters of the products. The systems are selected in such a way that in one of them [60%$Al(OH)_3$ – 40%$Fe(OH)_3$] – [40%Fe $(OH)_3$ – 60%$Cu(OH)_2$] one component (Fe) is common, because of which it can be considered as a three-component system with a high content of iron and the two others, as four-component ones. The results of adsorption-structural studies show that (Fig.9) the V_s -composition curves have a maximum, the height of which is markedly higher than the sorption capacity of the corresponding binary systems. It should be also noted that the character of structure formation in these systems is peculiar [21] and therefore determination of the component composition formed at the maximum of the sorption capacity from equation (3) is impossible. The thing is that structure formation in such a complex mixture depends on many factors, which (together with the process of growing particles) are responsible for structure formation of synthesized adsorbents and for appearance and the height of a maximum in the V_s -composition curve.

Apart from the reasons enumerated above, the efficiency of these factors depends on the conditions of co-precipitation of hydrogels promoting more complete implementation of the mechanism of growing of hydrogel particles [16].

Analysis of the results obtained shows that the sorption capacity of samples of the systems studied increases at the maximum by 36.0–65.9% as compared to that of binary systems. It is quite possible that depending on the component composition of the systems, the figures will be higher or lower. The amount of these changes is determined by the values of V_s of binary systems: the higher the sorption capacity of both binary systems used in the mixture, the lower the increment ΔV of four-component adsorbents, and vice versa, the lower the V_s of binary systems at a maximum, the higher the probability of obtaining

multicomponent samples with a higher ΔV.

Porous materials of this type are interesting as regards possibility of modifying their composition, structure, chemical nature of the surface and its kinetic properties favourable for sorption, activity and selectivity of catalysts.

In other words, the present studies based on of the relationships of the porous stucture formation of binary systems are promising for synthesizing porous materials from components with different surface properties and sorption parameters. This allows researchers to change properties of porous materials, enhancing the useful functions and suppressing active surface sites responsible for by-processes.

More thorough and comprehensive studies of multi-component porous materials will be extremely useful for synthesis of new adsorbents and catalysts with a prescribed structure and nature of the surface and sorption as well as catalytic properties.

9. DEPENDENCE OF THE SPECIFIC SURFACE AREA OF CO-PRECIPITATED ADSORBENTS ON THEIR COMPOSITION

The surface area and chemical nature of the surface of adsorbents and catalysts are their most important characteristics. However, the behaviour of the specific surface as a function of composition of samples has not been studied inadequately so far. There are only fragmentary data on the effect of some factors on the specific surface area of binary systems, whose structure-formation mechanism differs essentially from that of individual porous materials. It is impossible to extend the regularities of porosity formation and specific surface area of individual hydroxides to co-precipitated systems.

For example, as one can see in Fig.10, the specific surface area passes through a maximum, whose position coincides with that of the maximum in the V_s -composition curve. Before considering this problem, it is necessary to answer the question: what determines the value of the specific surface area? It is generally known that S_{sp} depends on the method and conditions under which adsorbents are obtained and is mainly determined by the nature of the hydroxide itself. Under the same conditions of production, hydroxides have different values of specific surface areas. This question is answered, to some extent by Berestneva and Kargin [27]. It appears that each metal hydroxide has a certain crystallization period determined by the rate of formation of ordered areas inside the amorphous phase and by the number of these areas. It cannot be excluded that the size and shape of various hydroxides differ from one another. Moreover, the specific surface area is a relative value that does not reflect the reality. The thing is that real densities (d) of adsorbents sometimes differ substantially and therefore, commensurable values of the surface areas can be obtained only if they are based not on gramm but on cm^3 in this way:

$$S_{sp} \cdot d = S, \quad m^2/cm^3 \tag{5}$$

This expression of the surface area seems the most covenient as it gives a realistic characteristic of any adsorber or a catalytic reactor.

Moreover, even if all conditions of precipitation of hydroxides (temperature, concentration, nature of the precipitant, etc.) are observed, the hydroxides are not identical as each of them has individual pH of initial and final precipitation, solubility, shape of particles and calcination temperature. It is well known that different hydroxides calcinated under

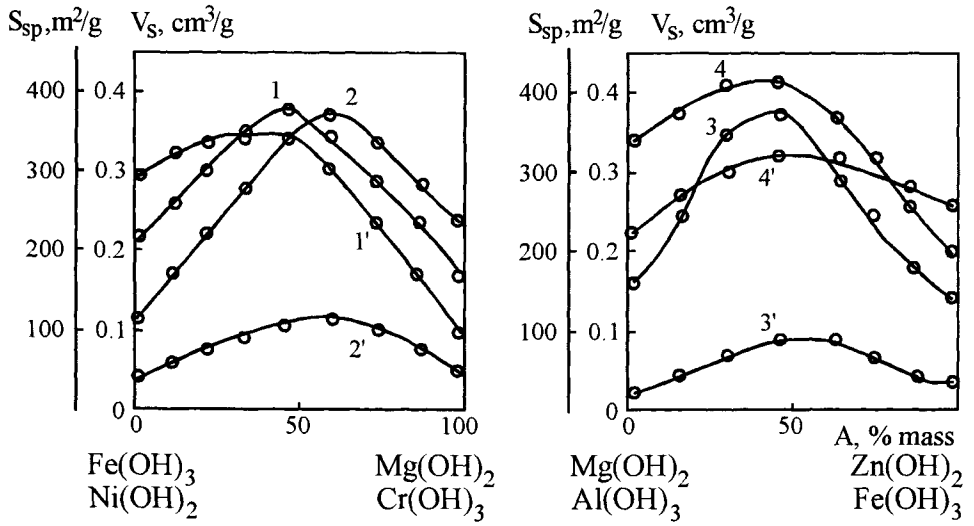

Figure 10. The V_s –composition (1 – 4) and S_{sp} – composition (1′ – 4′) curves for systems: 1, 1′– $Fe(OH)_3$ – $Mg(OH)_2$; 2, 2′ – $Ni(OH)_2$ –$Cr(OH)_3$, 3, 3′ – $Mg(OH)_2$ – $Zn(OH)_2$; 4, 4′ – $Al(OH)_3$ – $Fe(OH)_3$.

the same conditions contain different amounts of bound water. A similar situation is observed with sintering 50 of the hydroxides, which, according to the Tamman's rule, occurs at different temperatures, which may probably be attributed to the structure and energy of crystal lattice, surface energy and surface tension of oxide and hydroxide particles.

Thus, the specific surface area of synthesized adsorbents and catalysts is a quantity depending on many factors and in its explanation it should be borne in mind that none of the factors determines definitely the value of the specific surface area of adsorbents synthesized. In this connection, the structure formation of each of the hydroxides should be considered only individually and all components of this process should be analyzed. Moreover, manifestation of a particular factor is different for other hydrogels. It is most likely that only the joint effect of all the factors under required conditions determines the final structure of synthesized porous materials. Therefore, it is unnecessary to seek for some general relationships describing the structure–formation process. In this case some individual factors that make the most appreciable contributions to the behaviour of the structure can be indicated.

Moreover, even though the precipitation conditions are observed most strictly, the process is periodical because it is unsteady in its nature and occurs, as a rule, with changing conditions of precipitation. For example, if at the beginning of precipitation the system is supersaturated,at the end it has different parameters. As a result, hydrogel particles or crystals that were formed upon initial precipitation can have different sizes, especially because for many hydroxides the pH of initial and final precipitation occur in the acid region, i.e., pH < 7, while for others, the pH of initial precipitation lie in the acid medium and those of the final precipitation, in the alkaline medium, etc.

Hence, peculiarities of precipitation and structure formation of hydroxides and their effect on physico-chemical properties of porous materials (sorption capacity and surface area) are evident.

All the said above on the effect of the various factors on S_{sp} of individual hydroxides cannot be extended automatically to co-precipitated hydroxides, whose structure formation follows different laws, in spite of certain analogy with the individual hydroxide.The essence of these laws consists in the fact that in co-precipitation of hydroxides, the specific surface area of samples produced increases in comparison with those of individual components [2,13,15,28-30].

Milligan et al. [31,32] have shown in many works that in precipitation of hydroxides they prevent crystallization of one another and as a result, materials are produced that are amorphous according to X-ray analysis. Milligan has ascribed this effect to adsorption of one oxide on the surface of another. "The mutual protection" must be accompanied by an increase of the specific area. This view is shared by many authors, in spite of the fact that it neglects the nature of components in the mixture and their interaction and, which is most important, does not clear up the mechanism and compositions necessary for the development of the most extensive specific surface area.

The reason is that in co-precipitation of hydroxides with different pH of initial gelation, particles of the hydrogel that is precipitated first are built-up [13,15,27]. As a result, the process of increasing the particle size prevents, to a certain extent, or minimizes origination of new finer colloid formations, thereby preventing polydispersity of the systems and consequently, their dense packing. It is well known that if the space between larger particles is filled with finer ones, a packing is formed, some of the inner surface of which is inaccessible for adsorbate molecules. On the contrary, particles on which the second component is deposited are more uniform in size and form a porous structure with the surface that is the most accessible for the adsorbate molecules. In this case maximum development of micro- and macropores in the structure of co-precipitated adsorbents is the limit for the growth of the specific surface area and sorption capacity.

In this case, as shown by numerous studies, the largest specific area corresponds to the maximum in the V_s -composition curve and, as mentioned above, the condition of manifestation of the maximum is noncoincidence of the pH of initial co-precipitation of hydroxides of components in the mixture.

Because of this we can argue with Klyachko-Gurvich and Rubinstein [33] who suggested that there was a relation between the specific surface area and phase composition of the system and that this relation was general for binary oxide systems.

This view based on reciprocal solubility of the components of the mixture contradicts recent experimental results [2,13,15,22,28-30]. In particular, there are some binary systems, whose structure-forming mechanism does not involve any unpredictable changes leading to the presence of maxima in the V_s -composition and S_{sp} -composition curves [4].

In this case, depending on the composition of the initial mixture, only the content of a particular component in the sample changes, not disturbing the additive contribution of each of them to the sorption capacity and specific surface area (Fig. 11).

Of course, in many binary systems, with certain concentrations of components and under appropriate conditions, a phase of solid solutions or a chemical compound may be produced. Each of these phases differs in its physico-chemical and crystallographic properties from the initial components, which affects, to a certain extent, the values of

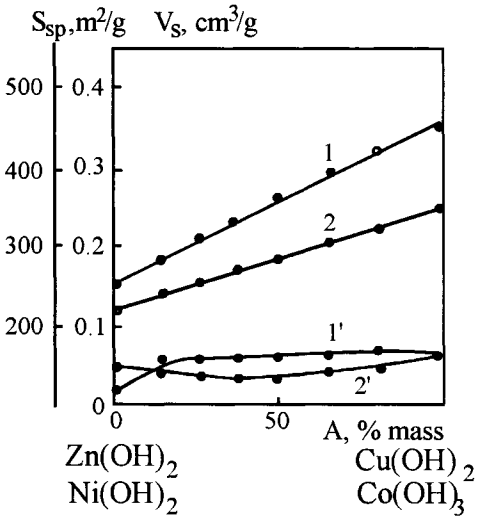

Figure 11. The V_s –composition (1, 2) and S_{sp} –composition (1′, 2′) curves for systems $Zn(OH)_2$ – $Cu(OH)_2$ – (1, 1′) and $Ni(OH)_2$ – $Co(OH)_2$ – (2, 2′).

the specific surface area. It is only unclear if these phase changes facilitate growth of the surface.

Bearing in mind that spontaneous formation of chemical and crystalline formations is accompanied by a decrease of the free energy of the system, which can be much smaller than its initial value (φ_1), especially when the newly produced compound is more stable than the mixture of initial components. The inverse case of $\varphi_2 \gg \varphi_3$ is seldom encountered (nitrogen oxide or $N_2 + O_2$ mixture) or when $\varphi_2 = \varphi_1$ (HI or $H_2 + I_2$ mixture). As a rule, for porous materials phase transformations are accompanied by reduction of their specific surface area.

In view of the above said, it is difficult to realize that the factors considered are connected with formation of new phases, chemical compounds or isomorphic substitutions of ions in the crystalline lattice, etc. and aimed at substantial changing the specific surface areas of synthesized samples. Therefore, without any extensive hypotheses, we will formulate conditions that should be satisfied by the initial binary system providing the most extensive surface and a high sorption capacity of the samples.

These conditions are presented in this work and require that the relation between the pH of precipitation of hydroxides binary system and the specific surface area samples be general. This statement is consistent with the mechanism porous samples and formation of their structural parameters.

In this case the position of maxima in the S_{sp} –composition curve fully coincides with those in the V_s –composition curves of synthesized porous materials. Depending on the value of the sorption capacity, the positions of maxima in the composition axis can be shifted towards the most sorbed component or be in its center when the sorption capacities of individual components in a binary mixture are equal.

Thus, the present analysis of the dependence of the specific surface area on the composition of samples shows that the area of co-precipitated porous materials is higher than that of each of the components only in the case when the pH values of precipitation of hydroxides in the mixture are different. This condition is a part of the mechanism of formation of the structure of co-precipitated materials with the most extensive porosity. Of course, under the action of the various factors affecting the process of structure formation, the absolute value of S_{sp} can both increase and decrease, but the general trend in S_{sp} remains unchanged and persists for all binary systems meeting the requirements listed above.

REFERENCES

1. V.S.Komarov, I.B.Dubnitskaya, Physicochemical Fundamentals of Controlling the Porous Structure of Adsorbents, Minsk, 1981 (in Russian).
2. V.S.Komarov, Structure and Porosity of Porous Adsorbents and Catalysts, Minsk, 1988 (in Russian).
3. I.E.Neimark, R.Yu.Sheinfain, Silica Gel: Its Production, Properties and Use, Naukova Dumka, Kiev, 1973 (in Russian).
4. V.S.Komarov, N.S.Repina, O.F.Skurko, Vesti AN BSSR, Ser. Khim. Nauk, No. 2 (1990) 22.
5. B.A.Bolotov, V.S.Komarov, T.V.Nizovkina, Practical Works in Organic Catalysis, Moscow, 1959 (in Russian).
6. Handbook of a Chemist, Moscow, 1965, p.57.
7. I.I.Ioffe, L.M.Pismen, Engineering Chemistry of Heterogeneous Catalysis, Moscow, 1965 (in Russian).
8. Yu.A.Eltekov, K.I.Slovetskaya, A.M.Rubenshtein, Kinetika i Kataliz, 1 (1960) 169.
9. A.M.Rubinshtein, A.O.Klyachko-Gurvich, V.M.Akimov, Izv. AN SSSR, Otd. Khim.Nauk, No. 5 (1961) 780.
10. N.F.Ermolenko, G.G.Korunnaya, Vesti AN BSSR, Ser. Khim. Nauk, No. 5 (1968) 95.
11. R.E.Tugushev, S.M.Rakhovskaya, L.A.Illina, L.A.Vereshchagina, Inorgan. Materials, 95 (1989) 276.
12. V.S.Komarov, N.S.Repina, O.F.Skurko, Vesti AN BSSR, Ser. Khim. Nauk, No. 2 (1990) 22.
13. V.S.Komarov, N.S.Repina and O.F.Skurko, Vesti AN BSSR, Ser. Khim. Nauk, No. 3 (1990) 7.
14. Yu.Yu.Lurjie, Handbook of Analytical Chemistry, Moscow, 1990 (in Russian).
15. V.S.Komarov, O.F.Skurko, N.S.Repina, Vesti AN BSSR, Ser. Khim. Nauk, No. 1 (1991) 11.
16. V.S.Komarov, O.F.Skurko, N.S.Repina, Vesti AN BSSR, Ser. Khim. Nauk, No. 5 (1990) 13.
17. V.A.Dzisko, in: Production, Structure and Properties of Adsorbents, Leningrad, 1983, p.311 (in Russian).
18. V.S.Komarov, I.B.Dubnitskaya, Vesti AN BSSR, Ser. Khim Nauk, No. 3 (1969) 109.

19. V.S.Komarov, N.S.Repina, O.F.Skurko, Vesti AN BSSR, Ser. Khim. Nauk, No. 3 (1985) 14.
20. V.S.Komarov, N.S.Repina, O.F.Skurko, Vesti AN BSSR, Ser. Khim. Nauk, No. 2 (1991) 3.
21. V.S.Komarov, N.S.Repina, O.F.Skurko, Vesti AN BSSR, Ser. Khim. Nauk, No. 3 (1991) 10.
22. V.S.Komarov, E.E.Bogdanova, O.F.Skurko, N.S.Repina, Vesti AN BSSR, Ser. Khim. Nauk, No. 3–4 (1992) 14.
23. V.M.Chertov, V.M.Shamrikov, V.V.Tsyrina, V.I.Malkiman, Ukr. Khim. Zhurn., 56 (1990) 1166.
24. S.J.Gregg and K.S.W.Sing, Adsorption, Surface Area and Porosity, Academic Press, London, 1982.
25. M.M.Dubinin, Physicochemical Fundamentals of Sorption Technique, Goskhimtekhizdat, Moscow, 1932 (in Russian).
26. V.S.Komarov, N.S.Repina, Vesti AN Belarusi, Ser. Khim. Nauk, No. 2 (1995) 15.
27. Z.Ya.Berestneva and V.A.Kargin, Uspekhi Khimii, 24 (1955) 249.
28. V.I.Kvashonkin, D.A.Agievskii, V.A.Pronin, L.I.Kolchanova, Kinetika i Kataliz, 26 (1985) 1213.
29. V.S.Komarov, N.S.Repina, S.L.Dulko, O.F.Skurko, Vesti AN BSSR, Ser. Khim. Nauk, No. 5 (1991) 9.
30. V.S.Komarov, O.F.Skurko, N.S.Repina, S.L.Dulko, Vesti AN BSSR, Ser. Khim. Nauk, No. 1 (1992) 35.
31. W.O.Milligan, J.Holmes, J. Am. Chem. Soc., 63 (1941) 149.
32. M.Watt, W.O.Milligan, J.Phys. Chem., 57 (1953) 883.
33. A.O.Klyachko-Gurvich, A.M.Rubinshtein, in: Problems of Kinetics and Catalysis, No. 11, 1996, p.96 (in Russian).

This Page Intentionally Left Blank

A. Dąbrowski and V.A. Tertykh (Editors)
Adsorption on New and Modified Inorganic Sorbents
Studies in Surface Science and Catalysis, Vol. 99

Chapter 1.4
Colloidal silicas

S. Kondo

School of Applied Physics and Chemistry, Fukui Institute of Technology,
Gakuen, Fukui 910, Japan

1. INTRODUCTION

Silicas and silicates are the most abundant solid materials on the earth and there are various forms of natural and synthetic colloidal silicas which have numerous applications. In this chapter, the term *colloid* is used for the gaseous and liquid dispersions and/or their aggregates of silica particles, the diameter of which ranges from about 10^{-5} to 10^{-9} m. This term also includes glasses such as porous silicas which usually have a high surface area and porosity. Also, *adsorption* is used not only as the adsorption of gases on the solid surface but also as the physical and chemical interactions of materials at the solid–solid and solid–liquid interfaces. The silica mentioned here has 3 dimensional networks. There are no compounds having 1 or 2 dimensional networks such as the silicate clay minerals or organosilicone compounds. The properties of silicas from the chemical point of view were described in detail, particularly on silica sol by R.K. Iler[1,2]. Some recent aspects of silica research and development were reported [3,4].

In nature, there are large deposits of silica–rich volcanic ashes in coarse amorphous colloidal particles, some of which are fairly pure and quite readily soluble to alkali solutions. They are used often as an industrial source of silica. Impure volcanic ash which contains alumina is used as a detergent, filter aid and mild ion–exchange agent after alkali or acid treatment and as a raw material for the synthesis of zeolite and porous glass.

There is macroporous silica *diatomite or diatomeceous earth* as biological deposits of sea algae "diatom". This is used as an industrial filter aid and heat insulator. The inside space of the bamboo stems and the rice straws contain silicas of high purity.

Quartz *silica sand* of high purity is used as the most important source of silica and glass in industry, although most of them are coarse granules and difficult to dissolve in the alkali solution at normal pressure. The jewel stone opal is made of very densely packed periodic precipitate of monodispersed silica particles.

There are numerous industrial products of colloidal silicas in various forms. The methods of industrial synthesis and main applications are briefly surveyed as follows. Ultrafine particles of nanometer order such as *aerosil* (commercial name) are produced by the hydrolysis of tetrachlorosilane in air. A similar material can be obtained from oxidation of tetralkoxysilane in a gas phase. The former is used as a thixotropic additive of composite materials, heat insulator and etc.

Fine powders being composed of particle aggregates such as *precipitated silicas* or *white carbon* are made by the decomposition of sodium silicate by sulfuric acid in an aqueous phase at high temperature. This material has microporosity as well as macroporosity due to a rapid growth and aggregation of primary particles as will be discussed later. These are used as rubber filler, paper sizing and etc.

Silica sol which is a stable sol of monodispersed particles is made by the decomposition of sodium silicate at low concentration under controlled pH and surface treatment and then evaporation of water. A stable floccular aggregates of silica particles are made by the peptization of dilute hydrogels under controlled pH. The former material is used as fiber and paper sizing, binder and the latter is used for water treatment.

Particle aggregates with high and low packing densities such as silica hydro– and xerogels are obtained in industry by the decomposition of sodium silicate by sulfuric acid of medium concentration and in controlled pH and temperature. They have a wide variety of surface area and porosity and are used as hydrophilic and acid– resistant adsorbents, catalyst carriers, composite materials and etc. Since this material contains various impurities, the material obtained by the hydrolysis of tetraethoxysilane is sometimes used for research purposes because of its purity.

The so called porous silica is made by the acid etching of annealed sodium borosilicate glass. The bulk structure is glass mainly of silica and has a uniform pore size distribution in the mesopore region. These are used as a source of silica glass.

Porous silica fiber was synthesized by the acid etching of sodium silicate fiber of molar ratio 3 [5,6]. This material has ultramicropores and adsorbs water and alkali ions in the acidic environment and can be used for the removal of water from acid and of alkali radioisotope ions such as Cs^+, from the environment.

High silica zeolite crystal is synthesized by the hydrothermal reaction of tetralkylaminosilane. The crystal thus grown consists of the ordered 3–dimensional network of siloxane bonds having a host amine compound in the network. This material is then calcined to burn off the organic compound and only silica network remains keeping the original regular structure. These have uniform micropores with hydrophobic surface and are used as hydrophobic adsorbents and catalyst carriers. Recently, *mesoporous silica crystals* were synthesized from long–chain alkyltrimethylaminosilane which forms cylinder–shaped micelles as a template [7,8]. Silicate ions precipitate around these micelles forming a tubular siloxane network, and these tubes aggregate to each other and precipitate as a honeycomb structure. This material is then calcined and the template organic compound is oxidized, leaving the skeleton silica tubes. They have uniform and ordered tubular or cylindrical mesopores with the hydrophobic surface.

This article presents the research on amorphous colloidal silica aggregation.

2. THE ATOMIC ORBITAL OF SILICON AND OXYGEN ATOMS

Silicon atom belongs to group IV of the periodic table and its orbitals consist of $1s^2$ $2s^2$ $2p^6$ $3s^2$ $3p^2$ similar to carbon. The outer electrons form covalent tetrahedral sp^3 and octahedral sp^3d^2 hybrid orbital with other atoms such as silane and potassium silicone hexafluoride respectively, but no stable sp or sp^2 hybrid orbitals are found. Since the electronegativity of Si atom is smaller than that of carbon, the bond between Si and

heteroatoms such as oxygen having greater electronegativity is more ionic than that of carbon. This allows for a slight variation of both the bond angles and distances as well as the internal rotation of Si–O σ–bond, depending upon the overall structural stability such as in silicate minerals and some of the organosilicone molecules. This would be also true for the stability of the polymorphism of natural crystals such as α– and β–cristobalites, α– and β–quartz, various forms of tridymites, keatites, coesites and stishovites and the amorphous or glassy silica as well. The colloidal silicas are usually composed of highly amorphous silica particles because of the rapid growth of solid phase as in the industrial processes in contrast to the natural processes. This gives rise to an initial formation of not only an amorphous structure but also of a very fine particle size of nanometer order.

The atomic orbitals of oxygen are $1s^2\ 2s^2\ 2p_x^2\ 2p_y^1\ 2p_z^1$. The covalent bond with heteroatoms is made of the unpaired electrons of $2p_y^1 2p_z^1$. The bond angle thus formed, however, is greater than 90°. They have the tendency to hybridize with 2 sets of lone pair of electrons to create sp^3 orbital. This situation is more clearly seen in the structure of ice where oxygen atoms take diamond–like tetrahedral positions and the hydrogen–bonding H–atoms are located in double minimum positions on the straight line connecting oxygen atoms. Thus the hydrogen bond is composed of not only the ionic bond but also the covalent bond orbital between the donating $2p_y^2$ and/or $2p_z^2$ electrons of oxygen atom and adjacent protons of neighboring molecules, keeping the tetrahedral orientation and straight line relation of O–H$\cdots$O bond. This structure may be applied to other hydrogen–bonding systems involving oxygen atoms and should be taken into account while considering the steric relation of hydrogen bond between silanol groups and water molecules or other electron–donating and electron–seeking molecules.

3. TETRAHYDROXYSILANE

Colloidal silica consist of primary particles of nanometer order. Sometimes, these can grow to a much larger size as a stable discrete particle and form silica sol in a liquid phase. The polymerization starts from tetrahedral *tetrahydroxysilane* or *orthosilicic acid* $Si(OH)_4$.

A physical identification of silanol groups is made by the IR spectra, and recently by ^{29}Si NMR chemical shift. The former method is based on the frequency and intensity changes of the stretching and bending vibrations in the fundamental and overtone regions of O–H band, which can be identified by H–D isotope exchange by, for example, adsorption of heavy water. IR spectroscopic measurement can be made easily in situ. The stretching, bending, combination and first overtone vibration frequencies of free silanol groups are 3740, 810, 4556, 7316 cm^{-1} respectively. It is recommended to use the combination and overtone region in near the IR region in order to distinguish the silanol groups from other hydroxyl groups such as water and alcohol. High resolution NMR is based on the chemical shift of ^{29}Si nuclear resonance influenced by the change of atomic orbital surrounding the respective Si nucleus and can analyze the environment of Si nuclei in a *very short range*. Therefore, one must be very careful to interpret the chemical shift for the identification and assignment of the functional surface groups bonded to the oxygen atom.

Both the Si–O and O–H bonds in silanol groups are more ionic than C–O and O–H groups in carbinol groups. Both the proton or hydroxyl ion can be easily released from the

silanol group depending upon its environment such as pH. The isoelectric point of colloidal silica is about 3, above and below which the silica surface has negative and positive charges, respectively. Silanol groups act as both the electron-acceptor (proton) and electron-donor (2 lone electron pairs of oxygen). The name orthosilicic "acid" originates in the weak Brönstead acidity of this surface.

The plural number of hydroxyl groups can be attached to a single silicon atom in the aqueous phase or perhaps in the water vapour phase where the hydrogen-bonding of water can stabilize such a structure. However, it is not known to what extent twin [=$Si(OH)_2$] or even triplet [-$Si(OH)_3$] hydroxyl groups are stable in the gas phase. It should be difficult to form a stable *intramolecular* hydrogen bond between these hydroxyl groups, due to the linear bonding principle as mentioned above. The same must be true for the hydrogen bond between the *vicinal* silanol groups on the surface. It is difficult to assume such a configuration both from chemical and structural points of view.

The solubility of amorphous silica is roughly 100 ppm at ambient temperature and neutral pH, although its solubility in pure water depends very much on the structure of the surface and the particle size of silica. The solubility increases exponentially by temperature increase, for instance to about 1000 ppm at 100°C. It also increases drastically by increasing pH as shown in the solubility-pH relation in Fig. 1. This behaviour is used for the hydrothermal reaction of silica and related compounds in industry or in the geothermal reaction in nature.

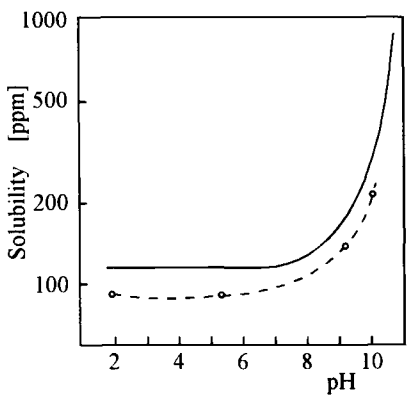

Figure 1. The solubility of amorphous silica against pH at 303 K. The full and dotted lines show the original and alkali-treated materials, respectively.

In most industrial processes, tetrahydroxysilane is prepared by the decomposition of aqueous sodium silicate of the molar ratio about 3 by sulfuric acid as mentioned below. The particle size would be smaller or larger if the decomposition were carried out in the acidic or alkaline environment, respectively. The final product by this method contains a lot of impurities such as alkali, alkali earth, Al, Ti, Zr and etc. depending on the raw materials used. It is rather difficult to remove these impurities completely by acid washing. Therefore, in order to obtain a high purity silica, distilled tetraethoxysilane is hydrolyzed by water at controlled pH, temperature and concentration.

The electrolysis of sodium silicate in the dilute solution may produce tetrahydroxysilane

at the anode. When this compound is produced by the hydrolysis of tetrachlorosilane or the oxidation of tetraethoxysilane in the gas phase, the polymerization reaction may take place successively and instantly, since in the gas phase, tetrahydroxysilane is not stable.

The high temperature heating of silica with carbon in the electric arc or plasma produces fine powder silica called *pyrogenic silica* which is hydrophobic.

4. SILICA POLYMER – SILICA PRIMARY PARTICLE

The hydroxyl groups of tetrahydroxysilane monomer can form intermolecular hydrogen-bond easily with other adjacent monomers and then dehydroxylate to dimer or oligomer forming siloxane bond and releasing water in the aqueous or gas phase such as:

$$Si(OH)_4 + Si(OH)_4 = (OH)_3Si - O - Si(OH)_3 + H_2O \quad (1)$$

when its concentration is increased to more than a few hundred ppm. Since the reaction product such as in Eq. (1) still has many silanol groups, the dehydroxylation and condensation reaction continues to produce cyclic and/or spherical oligomers. There are two different ways of polymerization from these oligomers. (a) When the concentration of oligomers is low and the separation between oligomers is too long for them to join, the oligomer continues to grow to a larger spherical polymer of various sizes having a few pores inside the bulk of the polymer, as is in an ordinary condition. (b) When the concentration of oligomers is high, these oligomer units aggregate and form a polymer of nanometer size including small spaces or ultramicropores inside the polymer. After drying, they are ultramicroporous polymers having a pore diameter of less than 1 nm. This reaction is carried out in a special environment such as in the aqueous solution in a confined space of water-in-oil microemulsion [10]. Both particles are siloxane polymers, but they are different in bulk structures.

These polymers still hold quite many silanol groups on the surfaces and possibly a little amount in the bulk structure. These silanol groups act as the binder of polymer particles with the hydrogen bond. The stronger covalent siloxane bond is formed after dehydroxylation of these hydrogen-bonding silanol groups. When the concentration of these polymers is low and hence the distance between polymers is long, and the protons of surface silanol groups are ion-exchanged to cations, (that is, positively charged) or the hydroxyl groups are modified with hydrophobic functional groups to make the surface hydrophobic, the aggregation of these polymers is prevented and the polymer becomes a stable silica sol. The silica concentration of silica sol by weight thus produced can reach as much as 40 %.

5. THE AGGREGATION OF SILICA POLYMERS

The silanol groups on the polymer particle surface play a very important role upon the particle aggregation such as the interparticle hydrogenbonding and the hydrothermal reaction thereafter. The hydrogen bond between these particles is about 5 times stronger than that of electrostatic and van der Waals forces, but weak enough to be broken by a mechanical force in such cases as the thixotropic behaviour of aerosil powder mixed in

the hydrophobic organic solvent and the peptization of dilute hydrogel to flocculent silica. However, these hydrogen bonds can be transformed to the covalent siloxane bonds easily by dehydroxylation and the interparticle bond becomes much stronger than the hydrogen bond.

The aggregation will commence between particles if the concentration of the polymers is high and/or there are no hindering factors against aggregation such as the surface modification of the silanol groups of the particles. As the aggregation proceeds, the viscosity of the sol becomes higher and, finally, the sol is set to a hydrogel or jelly. The rate of aggregation depends upon (1) the concentration of primary particles, (2) temperature, (3) pH, and to a less extent (4) the nature of the solute such as inorganic ions or organic solvents.

5.1. The effect of concentration

When the concentration of the particles is low, there appear at first fairly dense and independent groups of aggregation such as floc called primary aggregation. These primary aggregates join together and make the viscosity higher. If the reaction is rapid in such cases as the high temperature decomposition of fairly dilute sodium silicate by sulfuric acid in alkali environment, these primary aggregates may be precipitated as a white carbon. This product has a microporosity as well as macroporosity. When the aggregation is carried out at ambient temperature, a dilute jelly or hydrogel is made and it can be peptized by heating in a weakly alkali solution when it is fresh. It is stable as a flocculent sol as mentioned above. The IR spectroscopic observation shows that these hydrogels possess a lot of free silanol groups and hydrogen-bonded silanol groups as well, after exchanging water contained in hydrogel to, for instance, carbon tetrachloride.

When a very dilute hydrogel is aged, or hydrothermally treated at temperatures above 100°C or at pH higher than about 10 for a suitable time, the interparticle hydrogen bond changes to the siloxane bond. In this hydrothermal treatment the convex surface of particles is ready to dissolve and the solute thus made precipitate into the concave contact points of the interparticle bond because of the high solubility as shown in Fig. 1 and the solubility difference of the convex and concave surface. Thus the particle contacts are filled with the siloxane structure and the silica surface becomes more homogeneous. The linking of the interparticle bond both inside the primary aggregates and between primary aggregates becomes stronger by 3-dimensional network and becomes more and more rigid. The material cannot be peptized any more. When this material is dried very slowly near or above the critical temperature and pressure in an autoclave, or when the water is exchanged to a volatile solvent, the shrinking of the hydrogel and the destruction of the whole structure do not occur during dehydration. Then a silica aerogel is formed with a density as low as 0.02 g/cm^3 and a very large macroporosity which was occupied before by water is produced between primary aggregates. This mechanism may be the origin of macropores of silica gel . This material is used to measure the intensity of high energy radiation.

It is obvious that the higher the concentration of silica primary particles is the denser primary and secondary aggregations and heavier density of the hydro- and xerogels.

5.2. The effect of hydrothemal treatment

The hydrothermal treatment (called HTT) or the hydrothermal reaction process can be observed more clearly with hydrogels of higher concentration of silica particles [11-13]. A hydrogel was obtained by the hydrolysis of 1 mole of redistilled tetraethoxysilane in 10 moles of water (about 33 % SiO_2 in water by weight) at pH 2.0 and 70°C for about 100 min. This condition produces silica polymer with a small particle size. Silica sol thus obtained was cooled immediately to 0°C and was set to hydrogel in 24 h at 17°C as a thin film. This hydrogel was washed sufficiently to remove alcohol and chloride ion, stored in a refrigerator before the use as a raw material of HTT. HTT was carried out by keeping a necessary amount of hydrogel film samples in a pyrex ampoule with water being adjusted to a fixed pH=5.9 or other values, when necessary. This was placed in an autoclave, if necessary, and heated at desired temperatures for mostly 2 h. After HTT, the hydrogel was dried slowly at about 10°C for 48 h in the refrigerator in order to minimize the change of the structure of the sample during drying. The samples obtained were used for the measurements of the nitrogen adsorption isotherms, IR spectra, thermodilatometry, Vicker's hardness and etc.

The longer the time of HTT was the larger the pore volumes (ml/g), whereas the surface area increased to maximum at about 2 h and then decreased slowly. This result indicates that the longer HTT time strengthened the particle aggregation by burying the concave space of interparticle contact with siloxane as mentioned in the end of the previous section. Therefore, the period of HTT was set to 2 h in order to compare the effect of HTT at different pH and temperature conditions.

5.2.1. The effect of temperature

The rate of shrinkage of hydrogels during drying decreases as the temperature of HTT increases because of the reinforcement of the silica skeleton structure. This makes the pore size and pore volume of xerogels larger by higher temperature of HTT. This process then gives the variety of adsorption isotherms as illustrated in Fig.2. The aging is immature by low temperature HTT and the hydrogel shrinks distinctly by drying and results in a microporous and mechanically brittle or fragile gel. The temperature increase of HTT to 100 and 163°C gives mesoporous gels. The drastically high temperature HTT produces macroporous and mechanically strong gels.

The change of the shape of the isotherms in Fig.2 is discussed in terms of the change of BET specific surface area, A_s, and pore volume V_p computed from these isotherms (Fig. 3.).

The pore volume increased as the HTT temperature was raised. This is reasonable considering the mechanism of HTT. However, the strength of the interparticle binding is smaller at the beginning but rises above 100°C as seen in the Vicker's hardness per particle contact point in Fig. 4 in which the curve shows a mild HTT below 100°C.

It is interesting to see that the A_s increased up to 100°C and then decreased gradually. The reason for this change can be interpreted as follows. A moderate HTT may contribute mainly to the strengthening of the particle contact (siloxane bond) and not to the particle growth. Therefore, the shrinkage by drying becomes smaller, making the pore size wider and keeping the original particle size. This would make more nitrogen molecules possible to access to the silica surface of this material than that by low HTT and would give a larger apparent specific surface area than that at low HTT. In other words, the area of

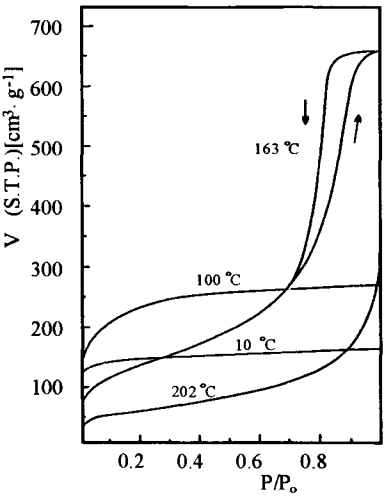

Figure 2. The nitrogen adsorption isotherms of silica gels hydrothermally treated at different temperatures for 2 h.

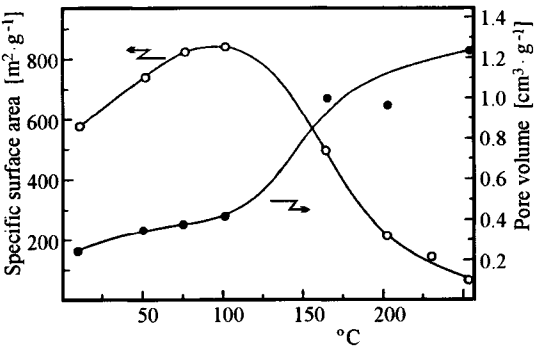

Figure 3. The specific surface area and the pore volume of silica gels versus the temperature of HTT for 2 h.

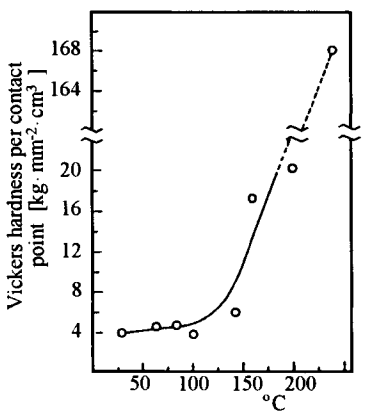

Figure 4. The Vicker's hardness per interparticle contact point versus the HTT temperature.

surface approached by nitrogen becomes close to the real surface area.

The microporous gel may have a fraction of micropores so narrow that nitrogen molecules cannot enter and cover the total silica particle surface. This would result in the smaller apparent specific surface area than the real area because we use nitrogen molecule as the probe. This shows that the surface area estimated by the gas adsorption method is dependent on the size of the probe molecule even in case of nitrogen.

An estimation of the real surface area A_{total} was made from the measured A_s m^2/g

(the apparent surface area covered by nitrogen molecules), pore volume, V_p ml/g, the coordination number, N, of particle contact points; the number of contact points of a particle calculated from the density of irregular packing of uniform spherical particles [14], the size relation between nitrogen molecule, and radius of the primary particle, r nm, as shown in Table 1 [15].

Table 1
The relation between the HTT temperature and the specific surface area A_s, pore volume V_p, coordination number N, particle radius r, total surface area A_{total} and the surface area obtained from the OH concentration of free silanol groups (A_{OH})

HTT °C	A_s (m^2/g)	V_p (ml/g)	N	r (nm)	A_{total} (m^2/g)	A_{OH} (m^2/g)
10	580	0.25	8.8	1.23	1107	1073
50	742	0.35	7.0	1.24	1104	1052
100	839	0.42	5.9	1.24	1100	1038
163	495	1.02	3.9	2.48	551	552
201	214	0.97	4.0	6.04	226	220
253	64	1.17	3.8	21.1	65	88

It is interesting to see that A_{total} from 10 to 100°C of HTT where HTT is mild, is almost the same. The total number of silanol groups of each HTT material, which can be measured by ignition loss, divided by the apparent specific surface area, A_s gives the apparent OH concentration as shown in Fig.5. This curve shows a peculiar behaviour.

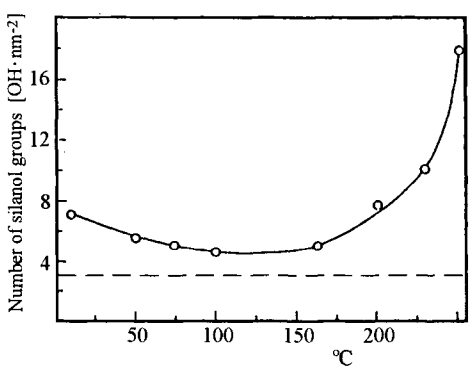

Figure 5. The number of OH groups per A_s (full line) and A_{total} (dotted line) vs. the HTT temperature.

At low HTT, this value is about 5.5/nm^2 and decreases to about 4 at 100°C, but then increases finally to a surprisingly high value of about 18. The reason for the initial increase is because A_s approaches A_{total} by HTT. Therefore, the value 4/nm^2 should be close to the real OH concentration. The marked rise afterwards is because the inlet of nitrogen to the pores becomes narrower and narrower by the drastic HTT, leaving the silanol

groups inside the pores which are the *inner* OH *groups*. Thus A_s becomes smaller and the apparent concentration of OH groups per A_s becomes very large.

The number of free silanol groups on the *outer surface* of silica per surface area can be obtained from the intensity analysis of IR OH bands which contains various kinds of OH groups at different frequency on each HTT material. These values are shown by the dotted line in Fig.5. It is interesting to see that this value is much smaller than the number of total OH/A_s and is nearly equal to 3. These free silanol groups produce interparticle hydrogen-bonded and inner silanol groups. This value $N_{free} \approx 3/nm^2$ agrees very well with other studies of concentration of free silanol groups such as those measured by surface alkoxylation [16], ion exchange [17], and adsorption of water and alcohol [18], all made by IR spectroscopy, and by heat of immersion [19]. Under the assumption that the whole silica surface is covered with free silanol groups with $N_{free} \approx 3/nm^2$, the total OH groups of the material per gram divided by N_{free}, gives the total surface area covered with free silanol groups, and is, as expected, nearly equal to A_{total}, as listed in the last column of Table 1. Both values are in excellent agreement taking into account the degree of approximation. It is not unreasonable to assume that all the surface of amorphous silica which have silanol groups before the thermal treatment would have the similar structure being basically composed of free silanol groups with $N_{free} \approx 3/nm^2$.

The change of surface silanol groups during HTT was studied by the IR transmission spectroscopy [11]. All the samples were vacuum dried at 150°C before measurement. The shape of OH band at the fundamental stretching region changes by the HTT temperature as shown in Fig.6. The analysis of the IR spectra such as the spectral deconvolution of heat-treated [20], surface-modified [19 ,21], ion-exchanged [22], and H-D

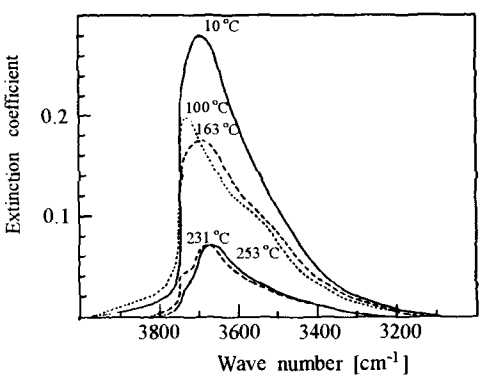

Figure 6. The IR spectra of silanol groups of silica gels in the OH stretching region at the different HTT temperature.

isotope-exchanged silica gels showed that this band consists mainly of a sharp *free* silanol band, very broad *interparticle hydrogen-bonded* silanol band and skewed *inner* silanol band which are located inside closed pores and even water cannot enter, as revealed by the H-D isotope exchange with heavy water as listed in Table 2.

The sample by low temperature HTT had a very small fraction of free OH, a large fraction of interparticle OH and a small amount of inner OH groups. This would be

Table 2
The wave numbers of silanol groups in fundamental stretching ν_f, bending ν_b, combination ν_c and first overtone ν_0 vibration modes

	ν_f	ν_b	ν_c	ν_0
Free OH	3748	810	4556	7316
Inner OH	3670	–	–	–
Interparicle OH	3500	–	–	–
Surface H-bonded OH	3500			
Water (gas) assym.	3756	1595	5332	7252
Water (gas) sym.	3652	–	–	–
Methanol (gas)	3682	1340	4410	–

because the HTT is immature and the interparticle bond is weak and hydrogel shrinks greatly. Therefore, this microporous gel has a high packing density (the high coordination number) and has a large number of interparticle OH and possesses a small fraction of closed pores due to a dense packing. This is the reason for the comparatively small A_s and pore volume, as shown in Fig.3, and a fairly high total OH concentration in the left part of the full line in Fig.5.

The medium HTT gives a fairly strong interparticle bond. The hydrogel shrinks less and produces mesopores and a larger pore volume. Hence, the relative amount of free OH becomes larger and these of interparticle OH and inner OH are smaller. A_s of this material becomes larger and approaches A_{total}. The same is true for the fraction of free OH to total OH groups.

The intense HTT makes the interparticle binding very strong as shown in Fig.4, but the A_s becomes smaller, because the apparent particle size becomes bigger close to the size of primary aggregates as described below. The fraction of both free OH and interparticle OH is greatly decreased but that of inner OH is large as shown in the spectrum of HTT at 253°C in Fig.6. This is because this drastic HTT would close small pores of primary aggregation holding silanols inside and thus the apparent particle size becomes rapidly large and the OH concentration per apparent surface area A_s becomes astonishingly high as seen in Fig.5.

5.2.2. The effect of pH

The change of aggregation state by HTT of different pH is very similar to that of temperature mentioned above. For instance, HTT at low pH gives an immature gel which has microporosity and high pH HTT gives a larger pore size.

However, HTT at pH higher than 10 gives a different kind of surface property than that of pH lower than 10 from where the solubility of silica rises sharply in Fig. 1. HTT of hydro–, xerogel and aerosil at pH = 11 adjusted with either sodium hydroxide or ammonia at 100°C gives a new perturbed OH band at about 3500 cm^{-1} with interesting physical and chemical properties, as illustrated in Fig.7 [13]. This band disappears by vacuum heating at 400°C, but revives again easily by the adsorption of water with no change of surface area, in contrast to other kinds of hydrogen–bonded silanol groups which show an irreversible behaviour by sintering. This band shifts to OD band easily by H–D exchange

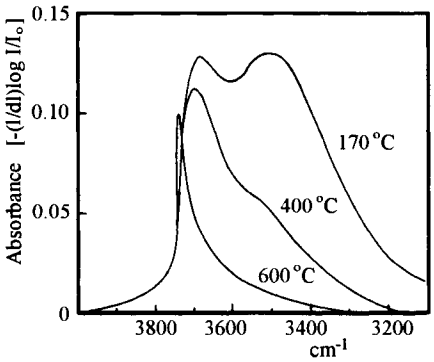

Figure 7. The IR spectrum of silica gel by HTT at pH 11.2 for 2 h and its change by heating in vacuum at different temperatures.

but cannot be cation-exchanged with Co^{2+}, similar to other kinds of hydrogen-bonded silanol groups. Therefore, this hydrogen-bonded OH group must be located on the surface, but may not be the so called geminal silanol groups. A reasonable model of such a kind of silanol groups is that on the (110) plane of cristobalite, where adjacent Si atoms can have OH groups which make a zigzag chain of hydrogen bonds without strain. The solubility of this material is half that of medium HTT and almost similar to that heat-treated at 1473 K as shown in Fig.1 by a dotted line [23].

6. THE PROPERTIES OF SILICA ADSORBENTS

In this section, not only some of the physical and chemical properties of silica adsorbents, but also some of their industrial applications are described when necessary.

6.1. Thermal stability

The surface of adsorbents must be cleaned before the use in order to adsorb desired molecules. The ordinary procedure is to heat the material at a suitable temperature and time in the flow of carrier inert gas or under vacuum, in order to give the adsorbate molecules the thermal energy larger than that of adsorption enough to desorb from the adsorbent surface. The temperature of desorption must be chosen to be high enough to desorb the adsorbate completely and yet must preserve the original surface and bulk structure of the adsorbent which can be easily destroyed.

Silica adsorbents have free silanol groups both acting as the electron-donor and acceptor adsorption sites as well as the adsorption potential of ultamicro- and micropores. When they have both sites, the energy of adsorption is quite high so that the evacuation temperature should be higher than 100°C. However, they tend to sinter easily by heating, since silica adsorbents are the colloidal aggregates of fine particles. This sintering phenomenon is enhanced by the presence of impurities and surrounding gas. Commercial grade colloidal silica such as precipitated silicas contain a lot of Na^+ ion, in contrast to a high purity silica gel after sufficient HTT.

The sintering effect to the properties of silica adsorbent has been studied using silica gels synthesized from tetraethoxysilane and impregnated with various amounts of Na^+ ion and heated in various atmospheres [24]. Figs. 8, 9, 10 and 11 show the change of specific surface area with the samples loaded with various amounts of Na^+ impurity, and atmosphere, the thermogravimetry and the thermodilatometry of the sample with the

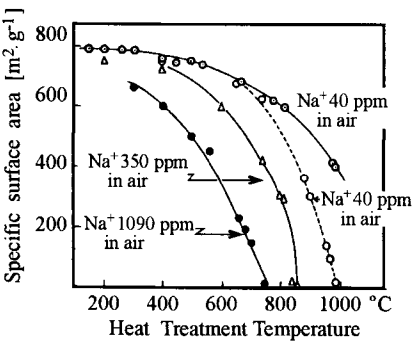

Figure 8. The specific surface area of silica gel containing various amounts of Na^+ impurities versus the temperature of heating.

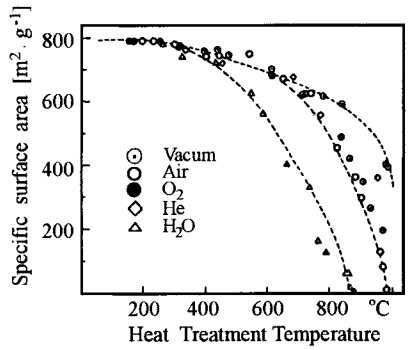

Figure 9. The specific surface area of silica gel containing 40 ppm of Na^+ versus the temperature of heating under various atmospheres.

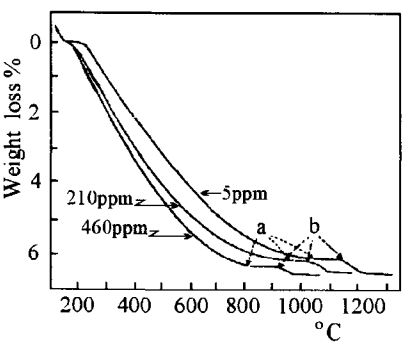

Figure 10. The weight loss of silica gel containing various amounts of Na^+ impurity against temperature.

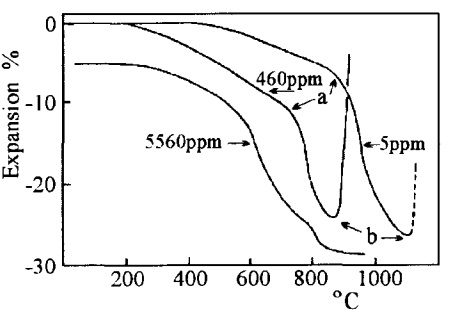

Figure 11. The dilatometry of silica gel containing various amounts of Na^+ impurity.

different amount of Na^+ impurities with a heating rate of 5°C/min in air, respectively. The change of specific surface area in Figs. 8 and 9 depends very much on the amount of Na^+ impurity and the kind of atmosphere. As the amount of Na^+ ion increased, the decrease of surface area started at as low as 200°C, whereas in case of 5 ppm Na^+, the area starts to decrease at about 500°C. Therefore, silica can be used as a catalyst carrier at temperatures as high as 500°C. The heating in steam decreases the surface area. This indicates that during the heating of silica adsorbent even under vacuum, pores would be filled with steam evolved from the pore surface and would damage the surface to some extent. That is to say, one should be careful enough to increase the temperature slowly enough to remove the steam from the pore before temperature evaluation. The weight

begins to decrease at temperatures as low as 200°C in Fig.10. It is sometimes difficult to distinguish the desorption of water from the dehydroxylation of surface silanol groups when the temperature of sintering is low. This difference can be identified by the near IR spectroscopy using the frequency difference of bending and/or combination band of silanol groups and water.

Water may be desorbed from the micropores at about 150~170°C. The dilatometry in Fig.11 shows that high purity silica starts to shrink or sinter at as high as about 500°C. There are changes of the curves at points a and b. After point a, bubbles appear in the bulk

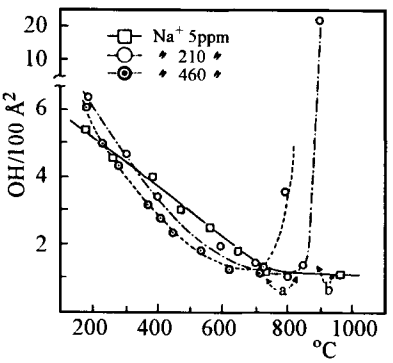

Figure 12. The OH concentration of silica gel containing various amounts of Na^+ against the temperature of heating.

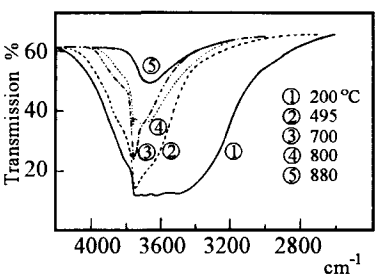

Figure 13. The IR spectra of silanol groups heated at various temperatures.

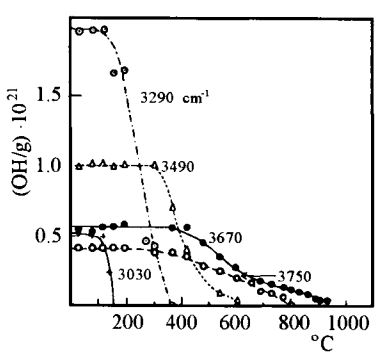

Figure 14. The intensity change of 5 bands deconvoluted from the spectra in Fig.13.

structure as shown in Photo 1 of the optical transmission microscope photograph, which shows the expansion of *closed pores* mentioned above by the steam pressure of heating. SEM photos 2, 3 and 4 show the silica gel after point b. One can see the outburst of the bubbles which appeared above the point a. The material now looks like white bread. Photo 4 shows the crystal growth. Points a and b are shown in other figures when it is necessary. The concentration of silanol groups as measured from the weight loss decreases as the

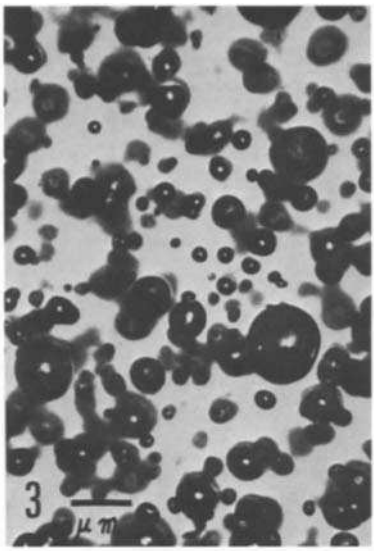

Photo 1

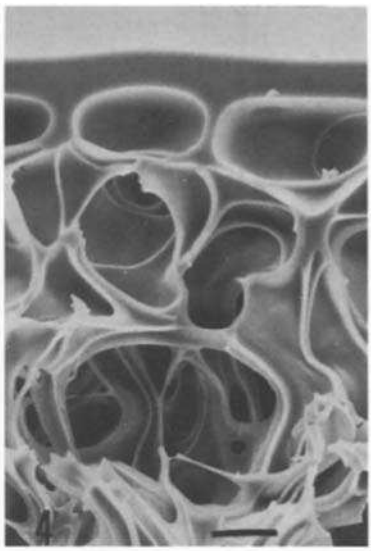

Photo 2

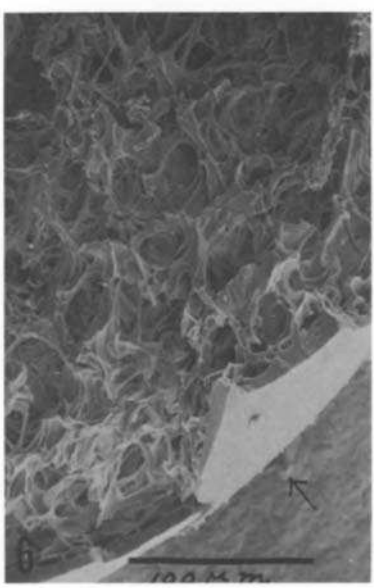

Photo 3

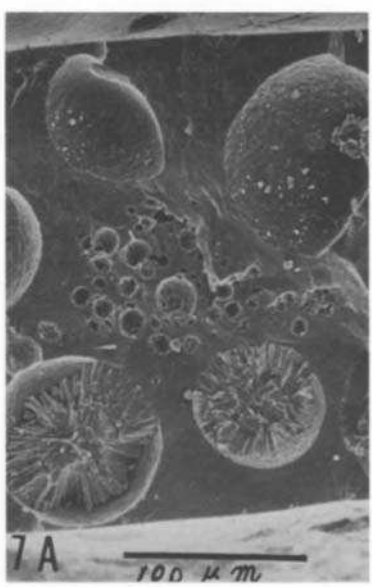

Photo 4

temperature of heating is raised as shown in Fig.12. At the point a, the OH concentration seems to increase because of the generation of closed pores.

The change of various kinds of silanol groups can be studied in more detail by IR spectra as shown in Fig. 13. Not only the intensity but also the shape changed markedly by heating. These curves can be deconvoluted approximately into roughly 5 component bands at 3750 (free), 3670 (inner), 3490+3290 (interparticle) and 3030 (water) cm^{-1} as illustrated in Fig.14. The 3030 cm^{-1} band disappeared, first the 3290 and 3490 cm^{-1} band decreased accompanied by the sintering and these at 3750 and 3670 cm^{-1} remained at high temperature.

6.2. The impurities

This section deals with the impurities which are present in the silica adsorbent as small amounts in the bulk structure and/or on the surface of silica. These impurities have usually their origin in the raw materials and in the environment during synthesis and adsorption– desorption cycles.

In the industrial process sodium silicate is made of natural silica sand and natural and synthetic sodium carbonate. They contain impurities such as Ti, Zr, Al, Ca, Mg and etc. depending upon the area. Alkali and alkali earth impurities can be removed fairly easily from silica gel by acid washing to as low as 50 ppm. Other kinds of impurities than these go to the final product. They remain not only inside the bulk structure but also on the surface. The heating of the material would make the diffusion of these impurities faster and thus there would be more fraction of these on the surface than in the bulk. The foreign atoms on the surface have different ionic valence and/or electronegativity from those of Si atom. Therefore, these impurities may act as Brönstead or Lewis acid sites for catalytic reactions. On the other hand, the impurities such as aluminum which can form the stronger covalent bond than mono or divalent atoms retard the sintering and increase the mechanical strength. If this kind of adsorbent is used in the presence of organic compounds, however, this adsorbs and decomposes the adsorbed organic molecules, leaving the carbon atoms inside the pore. This residual carbon may change the surface area and porosity at least.

The purification of fine powder precipitated silica is difficult by this method. In some applications of white carbon such as a rubber filler, a certain amount of Na^+ cation remains in order to adjust the acidity of the surface to achieve a better dispersion of particles. The silica products are fairly pure when $SiCl_4$ and $Si(OC_2H_5)_4$ purified by distillation are used.

6.3. Mixed oxides

A larger amount of foreign atoms than that mentioned above can be introduced on purpose as a form of mixed oxide such as silica– alumina. This material is produced by mixing silica sol and alumina sol in a molar ratio about 1:1 and used as the Lewis acid type oil cracking catalyst. The mixed oxide can be obtained also by the hydrolysis of the mixed solution of metal alkoxides. Various kinds of metal cations can be impregnated into the pores of silica adsorbent. In a dilute solution, these ions can exchange the proton of free silanol groups [24]. The exchange ratio of divalent cation was one cation to 2 free silanol groups. This property can be used for the ion exchange trapping of, for instance, long half

life radio isotopes of very low concentration, after which material can be made to glass [22].

When a larger amount of metal ions is doped and dried, excess electrolyte remains as crystals in the pore as in the case of blue-colored silica gel as a humidity indicator. This is obtained by the immersion of hydro- or xerogel in the cobalt chloride solution and they have cobalt complex salt in the pore. The impregnation of silver compound produces the adsorption sites of organic halides [24]. They are also used as a sterilizer by surface coating of various fibers, clothes, and plastics such as a telephone receiver. There are numerous applications of silica gels as the carrier of transition metal catalysts in the acidic atmosphere such as the oxidation of sulphur oxide in sulfuric acid production by vanadium pentaoxide, of carbon monoxide etc. The temperature resistance of high purity and macroporous gels is now up to 600°C. In these cases, metallic compounds in the pores are usually reduced to metallic clusters on the surface by hydrogen.

6.4. The adsorption interaction

The surface of silica taking part in the adsorption of molecules consists of mostly free silanol groups in varied surface concentrations and siloxane bonds. The silanol groups act as both an electron acceptor and donor such as the hydrogen bond with OH and NH groups and the lone pairs of nitrogen- and oxygen-containing molecules and electron transfer interaction with electron-donating molecules such as unsaturated and aromatic compounds forming weak adsorption complex molecules. These potentials are usually stronger than that of van der Waals potentials. Therefore, the adsorption of these molecules is "quasi" irreversible in the sense that they have to be desorbed at higher temperature than that of adsorption, although there are few chemical reactions on the surface at an ambient temperature.

One cannot estimate the surface area of polar surface such as silica having silanol groups by means of the adsorption of polar molecules, since the effective molecular adsorption cross section of these molecules varies depending on the concentration of free silanol groups. The structure of the adsorbed layers is complex compared with that of the homogeneous surface which has no specific adsorption sites. The orientation of molecules of the first layer depends on the configuration of silanol groups and that of second layer depends on the molecular configuration of the first layer and so on. Perhaps the structure above the third layer would be a little similar to that of liquid. Because of the hydrophilic surface surrounding the adsorbed water, the structure of this water would be more *structure-breaking* or less ordered (higher density) than that of bulk water or that which is surrounded by the pores of hydrophobic surface such as graphitic carbon and is structure-forming. From a colloid chemical viewpoint, the surface is more hydrophilic when there are more free silanol groups.

There are also pores in silica adsorbents which act as fairly strong adsorption potentials. Ultramicropores can adsorb only water molecules due to the relative size fitting of the pore and adsorptive molecule. Micropores can adsorb molecules such as nitrogen and these having similar molecular diameter. These pores exhibit the enhanced van der Waals force from the surrounding wall. The diameter of these pores can be estimated by the t- or α_s-method. When there are free silanol groups inside these pores and the adsorption interaction is of the electron transfer type, the energy of adsorption is quite strong. The above mentioned characteristics of adsorption interaction is used to adsorb selectively

the hydrogen-bonding molecules from non hydrogen-bonding molecules, and polar from nonpolar molecules. Mesoporous silica with a high surface area is used as a low humidity desiccant in such applications as the desiccation of dual glass window, the storage of food and drug, antiblocking of dry powder etc.

The pores can be used in such a wide range of applications as mentioned below. The mesoporous silica can control the air humidity to a medium humidity range at the ambient temperature because the water adsorption isotherm of mesopores rises fairly sharply in the medium of the relative humidity. They adsorb water when the air humidity goes up and release adsorbed water when the humidity goes down. This mechanism lasts almost forever, and is used for the adjustment of the humidity in the medium relative humidity range inside the precious music instruments, sculptures, and paintings etc. made of wood and fabrics, so that these fine arts are not exposed to the dew drops in the aircraft or ocean transportation, for instance. There is an interesting application of charcoal to dry the underneath of the floor above the ground in ancient Japan when silica gel was not available. Today silica gel is used to speed up the construction time, to keep the wall, floor and room of the living section and kitchen of houses and ocean-going ships away from high humidity. They also restrict the growth of fungi and insects. They can be used to fix enzymes in the pores for biological application. Powder porous silicas of controlled particle size are used as antiblocking agents of polymer films and printing ink for the efficient process. They are also mixed with paint and varnish to decrease the gloss of the coating surface to give a natural look and to retard the reflection of light, due to the minute roughness of the painted surface. They are made so fine that they cannot be detected with human touch and bare eyes. Since these paint liquids are adsorbed in the pores of silica, the refractive index of silica becomes almost equal to that of the liquid. This makes the silica particles not observable.

Silica adsorbents with controlled macropores in the form of xerogel and hydrogel can adsorb proteins and high polymers selectively by size difference. This mechanism is used for the removal of unnecessary proteins from the edible fermented liquids such as beer, wine, vinegar and etc. (Japan Patents 1242401, 1277849, 1630838, 1792050). This selective adsorption can help preserve the quality of the liquid and yet prevents the liquid from the turbidity caused by the coagulation of proteins during the storage. This can make the time of aging and filtration short and easy.

The enthalpy of adsorption of silica has been studied to some extent. However, it takes a long time to reach the equilibrium compared with the fluctuation of the temperature of measuring instrument in static and flow types owing to the slow diffusion of adsorbate into the pore. Therefore, most studies were carried out on the enthalpy of immersion (wetting), which can look into some aspects of adsorption energetics especially when the heat of adsorption is large. Fig.15 illustrates the heat of immersion of silica gel heat-treated at various temperatures into various liquids [19]. In this figure the OH concentration per A_s is shown in a horizontal axis instead of heating temperature. The heat of immersion of nonpolar hexane was small and did not change by the concentration of silanol groups but those of aromatic toluene and polar chloroform were proportional to the OH concentration of 3-4/nm^2. The same tendency was observed for water and various aliphatic alcohols. These results indicate that the adsorption interaction would be mainly caused by the free silanol groups and their maximum number would be about 3-4/nm^2.

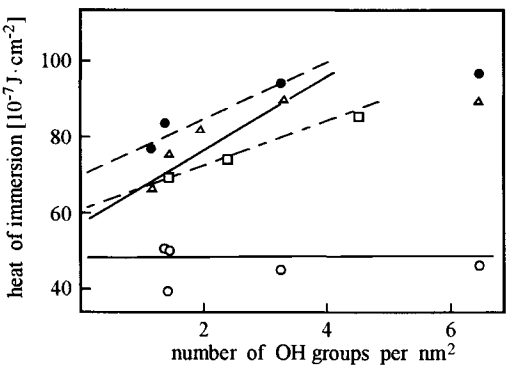

Figure 15. The heat of immersion of silica gel with 40 ppm Na^+ and having different surface free silanol concentrations into cyclohexane (○), benzene (△), toluene(●) and chloroform (□).

6.5. The surface modification

Silica is used to coat the surface of other particles such as titania and organic and glass fibers. The surface of titania pigment is modified by a thin layer of silica to decrease the photocatalytic reaction on the surface. Glass and organic fibers are coated with silica sol to increase the surface roughness so as to make the weaving easy by the adsorption of silica particles on their surface. Synthetic fiber stockings and cloths are coated with silica in order to keep the humidity in the medium range and thus to prevent the surface from the electrostatic charge. Silica particles are sometimes coated with other oxides such as titania to improve the cosmetic properties.

The surface of newly made silica is hydrophilic. There are many applications where less hydrophilicity is required such as in adsorption–separation of various kinds of polar, and nonpolar compounds, and in mixing silica with hydrophobic materials. In these cases, it is rather easy to modify the free silanol groups by substitution to other functional groups by heating at the ambient or high pressure.

$$\equiv Si - OH + XY = \equiv Si - O - Y + HX \qquad (2)$$

The compound XY can be alcohol, organosilicon or reactive alkali alkyl, and alkyl–halosilane compounds. These so called coupling agents can change the silanol groups to other functional groups such as short or long chain normal and branched alkyl, amino, carbonyl and other groups. However, not all the free silanol groups can be substituted to other functional groups owing to the steric hindrance between the substituted groups. There seems to be no way to substitute the hydrogen–bonded and inner silanol groups. The stability of these substituted groups is not long enough compared with the price of these materials due to the hydrolysis of these groups to silanol groups. There are many attempts to elongate their life by polimerization of the substituted functional groups to oligomer or polymer so that these surfaces would last longer and become more hydrophobic.

One of the most important applications is the gas and liquid chromatography. In this application, not only the chemical nature of their surface but also the particle size distribution, pore size distribution and the packing density, influence the separation efficiency such as resolution and retention time significantly.

7. SUMMARY

Occurrence, synthesis, properties and applications of silica adsorbents are presented. The surface characterization of the materials are described in detail. Same attention was given to the use of pores of silica adsorbents.

REFERENCES

1. R.K. Iler, The Colloid Chemistry of Silica and Silicate, Cornell Univ. Press, 1955.
2. R.K. Iler, The Chemistry of Silica, Wiley Interscience, New York, 1979.
3. E.H. Bergna (ed.), The Colloid Chemistry of Silica, Advances Chem. Ser., Am. Chem. Soc., 1994.
4. Ullmann's Encyclopedia of Industrial Chemistry, A23 (1993) 583.
5. S. Kondo, T. Tamaki and Y.Ozeki, Langmuir, 3 (1987) 349.
6. S. Kondo, Chem. Express, (1986) 240.
7. T. Yanagisawa, T. Shimazu, K. Kuroda and C. Kato, Bull. Chem. Soc. Jpn., 63 (1990) 988.
8. J. S. Beck, J.C. Vartuli, J.W. Roth, M.E. Leonowicz, C.T. Kresege, K.D. Schmitt, C.T-W. Chu, D.H. Olson, E.W.Sheppard, S.B. Mc Cullen, J.B. Higgins and J.B. Schlenker, J. Am. Chem. Soc., 114 (1992) 10843.
9. G. B. Alexander, W.M. Heston and R.K. Iler, J. Phys. Chem., 58 (1954) 153.
10. H. Yamauchi, T. Ishikawa and S. Kondo, Colloids Surf., 37 (1989) 71.
11. S. Kondo, K. Tomai and C. Pak, Bull. Chem. Soc. Jpn., 52 (1979) 2046.
12. S. Kondo, Y. Saito, T. Ishikawa and H. Yamauchi, in: J. Rouquerol and S.K. Sing (eds.), Adsorption at the Gas–solid and Liquid–solid Interface, Elsevier, Amsterdam 1982.
13. S. Kondo, H. Yamauchi, Y. Kajiyma and T. Ishikawa, J. Chem. Soc., Faraday Trans. 1, 80 (1984) 2033.
14. W.O. Smith, P.D. Foote and P.F. Busang, Phys. Rev., 34 (1929) 1271.
15. K. Naoki, J. Mineyama, K. Tomoi and S. Kondo, Mem. Osaka Univ. Education, III, 27 (1979) 131.
16. S. Kondo, T. Ishikawa, N. Yamagami and K. Yoshioka, Bull. Chem. Soc. Jpn., 60 (1987) 95.
17. T. Ishikawa, E. Amano, H.Yamauchi, M. Takasu and S. Kondo, Mem. Osaka Kyoiku Univ., III 35 (1986) 29.
18. H. Yamauchi and S. Kondo, Colloid Polym. Sci., 266 (1988) 855.
19. S. Kondo, H. Fujiwara, T. Ichii and T. Tsuboi, J. Chem. Soc., Faraday Trans. 1, 68 (1979) 646; S. Kondo, H. Fujiwara, E. Okazaki and T. Ichii, J. Colloid Interface Sci., 75 (1980) 328.

20. S. Kondo, F. Fujiwara and M. Muroya, J. Colloid Interface Sci., 55 (1976) 421.
21. T. Ishikawa, N. Yamagami and S. Kondo, Bull. Chem. Soc. Jpn., 59 (1986) 3729.
22. S. Kondo, T. Ishikawa, H. Yamauchi, H. Yamaoka, E. Amano, A. Fukushima and M.Ono, J. Chem. Soc. Japan, Nihon Kagakukaishi, (1983) 612.
23. S. Kondo, M. Igarashi and N. Nakai, Colloids Surf., 63 (1992) 23.
24. T. Ishikawa, S. Kondo, H. Yamaoka and M. Muroya, Ads. Sci. Tech., 3 (1984) 93.

This Page Intentionally Left Blank

A. Dąbrowski and V.A. Tertykh (Editors)
Adsorption on New and Modified Inorganic Sorbents
Studies in Surface Science and Catalysis, Vol. 99

Chapter 1.5
Complex carbon–mineral adsorbents: preparation, surface properties and their modification.

R.Leboda and A.Dąbrowski

Faculty of Chemistry, Maria Curie–Skłodowska University, 20031 Lublin, Poland

1. INTRODUCTION

It is known that the adsorption processes play an important role in numerous fields of modern technique, in medicine, analytical chemistry etc. In the initial period mainly carbon adsorbents and silica gels were used. Later the metal oxides mainly Al_2O_3, mixed oxides prepared on the basis of Al_2O_3 as well as zeolites became to be more and more widely used as adsorbents and catalysts. These are not obviously all materials needed for carrying out different adsorption and catalytic processes. There exists constant the need for new materials. Such materials should be characterized by high efficiency in different adsorption and catalytic processes as well as by high mechanical resistance especially to oxidizing media.

Carbon–mineral adsorbents represent a new type of materials containing two components: mineral and carbonaceous. Their properties depend on the amount of carbon deposited on the mineral matrix. In different adsorption processes occurring on the surface of such adsorbents it can utilize the advantages of either carbonaceous or mineral components. Silica, porous glass, aluminum oxide, aluminosilicates, zeolites, diatomites and other natural and synthetic adsorbents are the most popular mineral components of such adsorbents. The original surface properties of carbon–mineral adsorbents can predict very promising future for them. Our paper presents the analysis of current state of art related to preparation, physicochemical properties and application of carbon–mineral adsorbents. Preparation of carbon–silica adsorbents (carbosils) possessing a regular topography of adsorption sites is of special interest. Moreover, the effects of topography on thermodynamic properties of various adsorption systems is shown.

The studies on preparation of carbon–mineral adsorbents, modification of their surface properties as well as application carried out up to 1990 were presented in two comprehensive review papers [1,2]. Tarasevich published also an interesting paper on application of complex adsorbents in water purification technology [3]. The papers by Kamegawa and Yoshida [4,5], Kyotani et al. [6], Sonobe et al. [7–10], Fenelonov and Okkel [11], Bandosz et al.[12–16], Putyera et al. [17], Vissers et al. [18] as well as Baumgart and co–workers [19] are worth mentioning as they constitute a new trends in the studies and application of complex carbon–mineral adsorbents.

2. PREPARATION METHODS

From the literature review the following methods of complex adsorbents preparation could be distinguished [1]:

1) mechanical mixing of the graphitized carbon black particle or active carbon with the mineral adsorbent particles;

2) incorporation of the carbon adsorbent particles between the gel particles (usually silica gel or alumina) by the addition of carbon particles to the sol before gelation;

3) total or partial carbonization of organic substances previously bonded physically or chemically with the surface of the mineral adsorbent;

4) the process of carburization of adsorbents and catalysts.

The adsorbents produced by the latter two methods are the most interesting from either a practical or cognitive view-point. The processes of carbon matter formation from organic substances are in generally very complex, and depend on many factors [20]. The most general picture of the carburization process can be presented by the following scheme of the cracking of hydrocarbons [21]:

paraffins ⟶ olefins ⟶ high-molecular olefins and naphthenes ⟶ unsaturated cyclic hydrocarbons ⟶ aromatic hydrocarbons ⟶ high molecular condensed aromatic hydrocarbons ⟶ asphalt-like substances ⟶ carboids ⟶ coke. (1)

Formation of coke from hydrocarbons is determined by different thermodynamic factors and by kinetic characteristics of the process [21]. The thermodynamic characteristics of the process indicate the reality of the process and its general trends consisting in the shift of the process towards formation of defined condensation products including the graphite-like structures. Kinetic characteristics determine not only the rate of the process but also its peculiarities, accumulation of different intermediate products as well as the full course of the reaction.

The process of carbon deposit formation in complex carbon-mineral adsorbents may be initiated and terminated in any stage or stages of scheme 1. This is dependent on the chemical nature of the carbonized substance, porous structure and chemical nature of adsorption and catalytic sites of the mineral matrix, etc. For this reason, the complex adsorbents prepared by the third and fourth methods have the carbon deposits consisting of the substances of different chemical and physical structure formed during the defined stages of Scheme 1.

3. MORPHOLOGY AND CHEMICAL COMPOSITION OF CARBON DEPOSIT

In general the following types of carbon which may be formed during the carburization of adsorbents and/or catalysts can be distinguished [21]:

1) polycrystalline graphite;

2) tube-like graphite fibers;

3) dendrites;

4) carbon blacks;
5) carbon films and pyrocarbon layers.

The formation of carbon–mineral adsorbents containing carbon deposits in the form of dendrites, whiskers or carbon black is not advantageous because of the poor mechanical properties of these deposits. The morphology of the coke depends on the mechanism and conditions of its formation on the mineral surface. Two main mechanisms of formation of carbon deposits can be distinguished: consecutive reactions and carbide–forming. The latter mode consists in the thermal decomposition of hydrocarbons.

From the view–point of the expected properties of carbon–mineral adsorbents the cokes formed in the consecutive reactions are more interesting than those formed in a carbide cycle because in such reactions it is mostly the carbon deposits characterized by good mechanical properties that are obtained, although these deposits are less homogeneous and more poorly ordered than the cokes formed during the carbide cycle. However, they are characterized by a stronger adhesion to the mineral matrix. In practice, independently of formation condition, these deposits are usually mixtures of different types of carbon. As a result they are too small or to a greater extent morphologically heterogeneous.

Thus we will consider coke formation on the surface of the adsorbent/catalyst as the polycondensation of starting organic substances or the products of an earlier reaction of these substances which are capable of further reactions [13]. The process of formation of polycondensation products cannot be presented by only one chemical reaction (Scheme 1 illustrates only the general mechanism of coke formation.) This process can be imagined as a multitude of different polycondensation reaction processes leading to hypermolecular structure of the condensation products.

It is obvious that chemical composition of carbon deposit depends not only on the conditions in which pyrolysis is carried out but also on the chemical composition of carbonized organic substances on the surface of the solid carrier. As a result, carbon matter deposited on the surface of mineral carrier, besides C and H , can contain heteroatoms (S,N,O). The problem was discussed in the paper [2]. Similarly, the morphological composition depends on the conditions in which carbonization reaction is carried out. Gierak and Leboda showed [22], that it was possible to obtain graphitized carbon deposit of good mechanical properties under very mild conditions. The obtained adsorbents are applicable in chromatography in separation of polar substance mixtures [22,23].

4. CARBOSILS AS THE MODEL ADSORBENTS

4.1. Gas–solid adsorption systems

It is known [24,25] that the theory of adsorption on heterogeneous solid surfaces distinguishes two main models of distribution of energetic sites. The first model of the surface assumes the so–called patch–wise topography distribution of adsorption sites, and the second one random topographical distribution of the energetic sites. The transmission electron microscopy (TEM) investigations of carbosil demonstrate that its surface satisfy the conditions imposed upon adsorbents possessing a patch–wise distribution of adsorption sites, and some among them also correspond to the second model [26–28]. Carbosils, therefore become excellent model sorbents (because they are real and it is possible to regulate the size and properties of "carbon patches") in the studies of vapours, gases and

liquids adsorption.

Figure 1 illustrates differential distributions of the adsorption energy of n-hexane on partially dehydroxylated silica gel (1) and on carbon-silica adsorbents prepared through the pyrolysis of n-heptyl (2) and benzyl (3) alcohols and their different mixtures (4–6) on the solid surface. The energy distribution function X(E) of n-hexane was measured chromatographically from the pressure dependence of the retention volume [24,25].

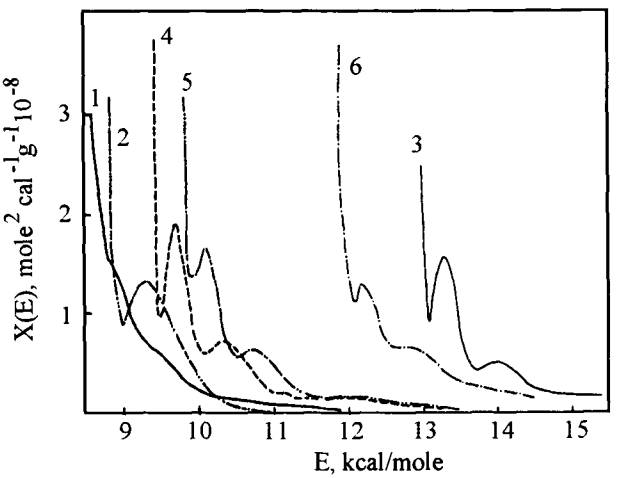

Figure 1. Energy distribution X(E) of n-hexane adsorbed on partially dehydroxylated silica gel (1) and on the carbon-silica adsorbents (2–6) (see text).

Distribution of adsorption centers on the surface of a non-modified silica gel is rather exponential, while in the case of carbon-silica adsorbents it is double or triple gaussian. Correlations were found between the topography and morphology of carbon deposits and the adsorption properties of carbosils (magnitudes of q^0_{st}, shape of the function X(E) and TEM photographs)[15–17]. Topography of the carbosils is of an evident patch-wise type, which is indicated by the distinct peaks in the X(E) curves. It also follows from the fact that the global function X(E) for such surfaces may be expressed as [29]:

$$X(E) = \sum_{k=1}^{r} X_k(E) \tag{2}$$

Here, X(E) denotes the distribution function for each subsurface k, and is defined in the following way:

$$X_k(E) = \begin{cases} X_k(E) & \text{for } E \in \Delta_k \\ 0 & \text{for } E \in \Omega - \Delta_k \end{cases} \tag{3}$$

where Ω represents the range of possible values of the adsorption energy, E, on the adsorbent surface, and Δ_k represents the range of the adsorption energy on a "homogeneous" k-th subsurface (patches).

As follows from Eqs. (2) and (3) the shape of the X(E) function depends on the local heterogeneity, Δ_k , of the particular patches of a heterogeneous surface. If the subsurfaces (patches) existing on the surface of the adsorbent radically differ in the Δ_k values, i.e. $\Delta_{k-1} \notin \Delta_k$ then there are clear maxima in the global X(E) curve, as in the case of carbon–silica adsorbents (Fig. 1). However, if $\Delta_{k-1} \in \Delta_k$, the X(E) function can assume the shape of an exponential distribution, or become similar to the distribution X(E) for a non–modified silica gel (Fig.1). The X(E) function for this adsorbent can also be a superposition of several local quasi–gaussian functions.

Using two chemically different alcohols and their mixtures in the pyrolysis made it possible to change both the size of carbon "patches" on the silica substrate surface and chemical structure of carbon deposit (see Scheme 1).

From IR spectroscopic and reaction gas chromatographic data it results that the carbon deposits prepared by pyrolysis of aliphatic and aromatic alcohols and their mixtures contain either aliphatic or aromatic segments and are to a considerable extent hydrogenated [30]. The larger the content of aliphatic substances in the pyrolyzed mixture, the more hydrogenated carbon depositis. It results there in a simple correlation between the characteristics of the carbosil surface and the composition of pyrolyzed mixture [26–28,30], which is also connected with the amount of carbon obtained. It was shown also, that the differences in the surface properties of the complex adsorbents are reflected in their resolution ability in gas chromatographic separation of organic substances [26,31–34].

The method of adsorption sites topography regulation discussed here does not permit to prepare the adsorbents of "random" type topography due to a poor transformation of alcohols into carbon matter. Another noteworthy type of reaction consists in the decomposition of methylene chloride on the surface of mineral adsorbents [35,36]:

$$CH_2Cl_2 \xrightarrow{\text{temp.}} C + 2HCl \qquad (4)$$

The ease of formation of carboneous substance in the above reaction results from the stoichometry of this reaction as well as the high energy of HCl formation. Reaction (4) performed on the surface of a solid adsorbent permits to obtain practically any amount of carbon [36]. Owing to that both "patch–wise" and "random" topography of carbosil adsorption sites can be easily regulated.

The carbon deposits obtained in the decomposition reaction of methylene chloride on the silica surface possess of completely different properties. IR measurements showed [30] that such deposits might consist of pure carbon and were characterized by a globular structure [35,36]. The adhesion of carbon deposit to the silica gel surface is very strong in this case. Moreover, such carbosils are characterized by high hardness. The silica matrix tightly screened by the carbon layer is inaccessible for small HF molecules. Such matrices are useful for application in researches and practice [37–39]. The paper [40] presents some interesting properties (among others, electrical ones) of carboaerosils prepared in reaction (4) carried out on the pyrogenic silica surface.

4.2. Efect of the mosaic surface on properties of liquid phases

4.2.1. Gas–solid–liquid systems

In the papers [41,42] the thermodynamic properties of polyethylene glycol PEG 4000 and silicone oil DC 550 of different quantities deposited on the heterogeneous surface of carbosils were investigated. The surfaces of tested adsorbents were similar to those described by the patch-wise model including local energetic heterogenities.

A complex adsorbent (carbosil) was prepared by n-octanol pyrolysis on the surface of silica gel (a particle size 0.15–0.20 mm, POCh, Gliwice, Poland) [41]. Alcohol pyrolysis was carried out in a steel autoclave of 0.3 l capacity at 500°C for 6 hrs. 1 ml of octanol was used per 1g of silica gel. The obtained carbosil contained 7.72 mass%C. Various amounts of polyethylene glycol with molecular mass of 4000 (PEG 4000) were deposited on the adsorbent surface (carbosil and initial silica gel). Some adsorption properties of the discussed systems, obtained from gas chromatography and sorptomatic measurements, are presented in Figs. 2-4.

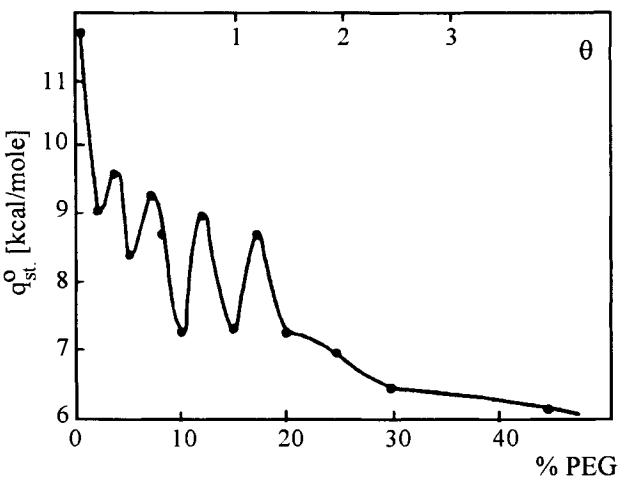

Figure 2. Adsorption heat of n-hexane as a function of polyethylene glycol percentage on carbosil surface and degree of carbosil coverage (Θ) corresponding to this percentage.

The nature of adsorption sites of an adsorbent surface (silica gel, carbosil) and the properties of deposited liquid phase (PEG 4000), which partially or completely block the sites, influence the thermodynamic properties of investigated systems. Surface hydroxyl groups of various kinds and narrow pores, which are the source of energetic heterogeneity, are the adsorption sites on non-modified silica gels. Pyrolytic processes that take place during the carbosil preparation change the nature of silica energetic sites. A part of the initial silica gel adsorption sites is blocked by formed pyrogenic carbons which become energetic sites of a new type. Physical heterogeneity on the surface of carbon patches, which is responsible for non-specific adsorption, is connected with the fluctuation of carbon film thickness [41]. Chemical heterogeneity, which is the source of specific adsorption, is connected with unsaturated bonds and aromatic elements of carbon deposit [30].

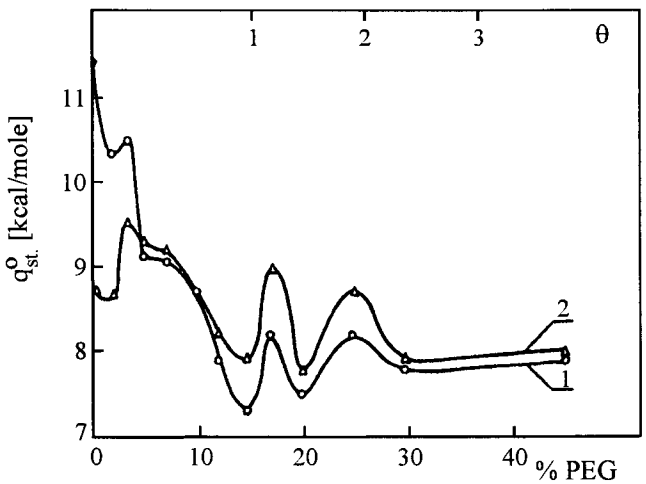

Figure 3. Adsorption heat of benzene as a function of polyethylene glycol percentage on carbosil surface at 160 (2) and 200°C (1) and degree of carbosil coverage (Θ) corresponding to this percentage.

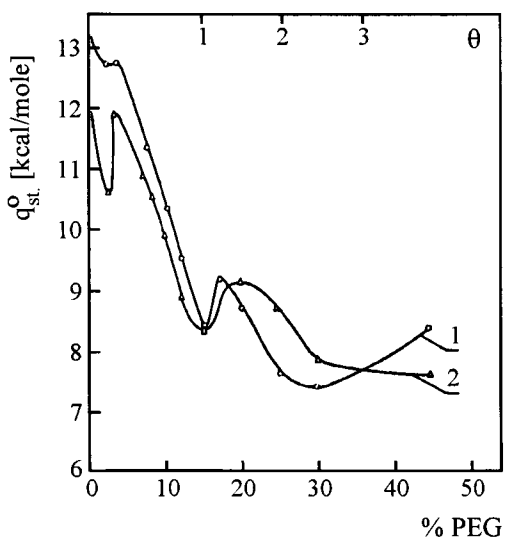

Figure 4. Adsorption heat of acetone as a fuction of polyethylene glycol percentage on carbosil surface at 160 (2) and 200°C (1) and degree of carbosil coverage (Θ) corresponding to this percentage.

On the surface of silica gel these are narrow pores and different kinds of hydroxyl groups, respectively [43]. Active sites of PEG 4000 phase are: –OH groups, situated at chain ends and oxygen from ether groups $-CH_2-O-CH_2-$. These are energetic sites capable of specific interactions. They can block the most active carbosil adsorption sites

through short-distance interactions, i.e. hydrogen bonds with surface -OH groups and π-complexes with unsaturated elements of carbon deposit.

Figures 2 - 4 show substantial, though various or individual test compounds drop of heat of adsorption values caused by the addition of very small amount (about 2% mass) of PEG 4000; when PEG 4000 amount on the carbosil surface is higher the relationship becomes more complex. Extremes occur on the plots of the investigated relationships $q_{st}^0 = f(\%PEG)$ in a similar way as in the case of graphitized black covered with PEG 1500 [44,45]. The occurrence of maxima and minima on the discussed type of plots was explained by the authors of the referred papers by formation of successive monolayers of liquid phase on the surface of carbon adsorbent. From the above and the well known [26,30,35] fact that heats of adsorption are usually higher on carbosils than on the non-modified surface of silica gel one would expect that the first portions of PEG 4000 are adsorbed on the surface of carbosil carbon patches. The fact that pores can on the surface of non-modified silica are narrower than on a carbosil surface [27] seems to confirm such a conclusion indicating reduction of adsorption site number on the silica surface. Thus the sequence of liquid phase deposition would be the following: first on the carbon patches and then on the uncovered silica surface.

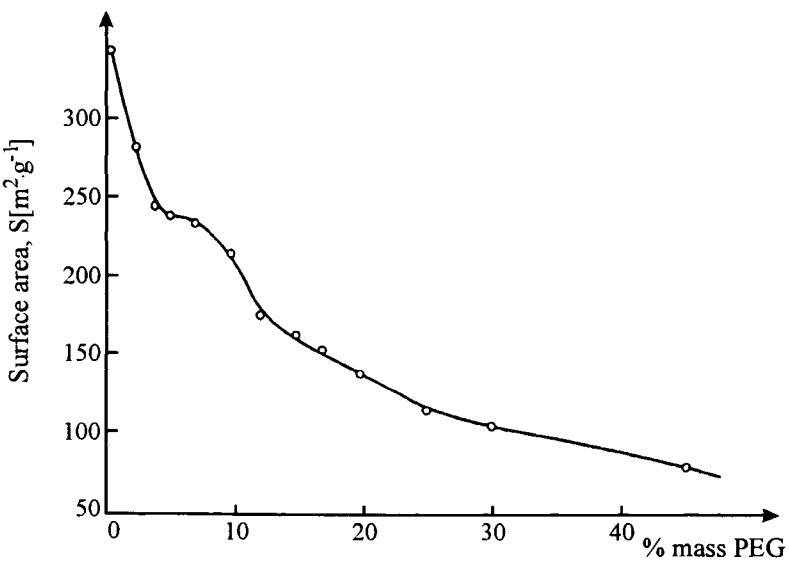

Figure 5. The dependence of specific surface area of carbosil modified with PEG 4000 on liquid phase percentage.

The degree of carbosil coverage Θ with a liquid phase corresponding to successive theoretical monolayers which were estimated approximately on the basis of Di Corcia's [45] and Kiselev's [46] data are marked in Figs. 2-4. According to the above data it was assumed that 0.5 mass % of liquid phase was necessary to cover the surface of 1 m^2 with a monolayer. So the adsorbent surface should be covered with a monolayer of liquid phase when the polyethylene glycol content is about 15 mass%. But the first minima on the plots of the relationship $q_{st}^0 = f(\%PEG)$ appear when the PEG content is as low as 2-2.5%. In

the case of hexane adsorption on the surface of modified carbosil only weak specific van der Waals forces operate. Owing to hexane disability for specific interactions its plot of the relationsip $q_{st}^0 = f(\%PEG)$ can be employed in the following physical heterogeneity changes of binary adsorbent surface as a result of modification with a liquid phase.

A sharp drop of heat adsorption value that can be seen at the beginning of the plot indicates that PEG adsorption is initiated not only on chemically heterogeneous areas but also on geometrically heterogeneous ones. A sudden decrease of effective adsorbent surface - about 60 m^2/g for the first 2% of a liquid phase (Fig.5), pore distribution analysis and investigation of the character of geometric heterogeneity of carbon film [41] lead to a conclusion that the first molecules of PEG 4000 block micropores of carbosil silica patches. The seemingly energetically unfavourable situation is confirmed by the fact that the energy of hydrogen bonds between glycol hydroxyl groups and silanol groups, which are formed (bonds) during adsorption on silica patches, is higher than the energy of analogous bonds between glycol hydroxyl groups which are formed during adsorption on carbon patches. Analogous situation takes place in the case of ether bridges; specific interactions between polyethylene glycol molecules are not possible here at all. So the first portions of PEG 4000 are adsorbed on the hydroxylated area of carbosil surface.

A close investigation of the plots in Figs. 2 – 5 leads to the conclusion that the position of minimum depends on the type of sorbate molecule. In paper [47] the effect was connected with the size of van der Waals radii of sorbate molecules. It indicates that in the gas chromatography retention process sorbate molecules interact with the adsorbent surface through the layer of liquid phase and, what more, it turns out [47] that for high degree of carbosil coverage with PEG – up to 45 mass% – the support has a substantial influence on heat of sorption of the analyzed compounds which proves that carbosil active sites are only partially blocked. Quite a different situation takes place in the case of a surface with low heterogeneity e.g. diatomite surface [47]. Covering of such a surface with a few monolayers (0.2%) of liquid phase causes homogenization of the support – liquid phase system and formation of linear sorption isotherms of polar compounds. Also in the case of Carbopack (an adsorbent of graphitized black type) [47] covering its surface with five monolayers of liquid phase causes a complete screening of active sites of the adsorbent surface. It proves a relatively high activity of carbosil adsorption sites.

4.2.2. Distribution of polyethylene glycol on solid surface

It is obvious that the mechanism of liquid phase deposition on the adsorbent surface depends on energetic properties of the surface and the kind of liquid phase. Generally speaking, a modifying agent causes homogenization of an adsorbent surface. In the carbosil–polyethylene glycol 4000 system the adsorbent surface is (qualitatively) double–patchy and each of the two patches is capable of various specific and non–specific interactions and glycol is also capable of the two types of interactions. Both kinds of carbosil surface patches are somehow heterogeneous and their relative heterogeneity depends on the type of adsorbate (because of non–specific interactions). It seems that in the discussed systems the sum of interaction energies between PEG and silica is higher than the sum of interaction energies between PEG and pyrogenic carbon. In consequence, the silica patches have the priority of modifying agent adsorption but only until the interaction energies of two kinds of surface patches become equal as a result of progressive screening of energetic

sites of the patches covered with PEG. Unquestionably, the influence of adsorption sites is a few layers of liquid phase deep so the presence of heterogeneous area on the surface of a binary adsorbent leads to lower or higher intensity of multilayer deposition of liquid phase macromolecules on the strong adsorption sites before formation of the first closely packed surface monolayer. From the above statements the concept of monolayers resulting from the relationship between the heat of adsorption and the amount of liquid phase does not correspond with the facts. PEG 4000 molecules are relatively big and they have many energetic sites. That is why the presence of only a few molecules on a given surface can substantially change its energetic parameters. The distribution of PEG molecules is not uniform. They are adsorbed locally with the preference of one kind of patches over the other one.

It is conceivable that a liquid phase is not yet deposited on the surface of carbon patches while there are already several monolayers on silica gel. So we come to a conclusion that the PEG 4000 monolayer which is being formed has a static character although it is formed as a result of localized adsorption.

Assuming that the above considerations are true we can suggest a pattern of formation of successive maxima and minima on the curves in Figs. 2–4. Heat of adsorption on adsorbents with the patchy structure can be expressed by the formula:

$$q_{st}^0 = \sum_i S_i q_{st,i}^0 \tag{5}$$

where: S_i denotes the surface of i patch; $q_{st,i}^0$ denotes the adsorption energy on this patch.

In relation to this additivity we can assume that successive maxima and minima on the curves of heat of adsorption changes along with the increase of adsorbent surface coverage with a liquid phase are the result of consecutive surface homogenization and heterogenization. Deviations of n–hexane curve (also chloroform and benzene curves for small amounts of a modifying agent and methanol and acetone curves virtually in the whole range) from a model curve seem to confirm anti–coincidence of monolayers formation on individual patches which is manifested during adsorption of compounds with different polarities.

According to a multilayer adsorption theory developed by Champion and Halsey such adsorption on a homogeneous surface leads inevitably to step like isotherms and isotherm continuity should be explained by surface heterogeneity [48]. Differences in the relationship course $q_{st}^0 = f(\%PEG)$ between non–polar hexane, polar chloroform, π–complexing benzene, acetone and methanol which are capable of hydrogen bonds formation become comprehensible in view of the fact that specific and non–specific interactions, having different adsorption energies, take part in the adsorption process. Formation of distinct extreme on hexane heat of adsorption curve can be explained by hexane non–polarity – hexane gas chromatography retention can be a good measure of surface homogeneity changes because of its incapability for specific interactions. The possibility of EDA complexing interactions [49] in the discussed adsorption systems (chromatographic columns) in the following donor–acceptor systems: benzene–OH groups and polyalcohol ether bridge–chloroform explains different behavior of the compounds than that of model hexane. At the same time their similar affinity for EDA complex formation [50] explains the similar course of their curves in spite of differences in the retention mechanism. In the case of methanol and acetone we deal with short distance interactions, i.e. hydrogen bonds. Existence of bonds with several times, surely at least twice, higher energy in

such systems [51] causes further independence of the course of the discussed curves of the successive homo- and heterogenization of a complex adsorbent surface. The differences in the course of the discussed functions result from different mechanisms of interactions between molecules. Non-specific adsorptive interactions that exist in all discussed cases cause similar changes of function monotonicity for all sorbates.

Energetic activity of silica gel and hence of carbosils and discussed adsorption systems (gas-liquid-solid-chromatographic packing) depends on the type of adsorbate. That is why the whole adsorption system should be taken into account and not only the non-modified adsorbent surface. Beside adsorptive interactions there is also a partition mechanism analogous to that in gas-liquid-chromatography and consistent with the rule "similia similibus solventur"; adsorption contribution to the column process depends on liquid phase and sorbent polarity. Even when a modifying agent content is higher than 10% adsorption can retain a considerable amount of a compound [52].

4.2.3. Separation properties

The retention volume of a chromatographied compounds can be expressed by a simple relationship:

$$V_{Ng} = \text{const.} \exp(-q^0_{st}/RT) \tag{6}$$

where the constant (const.) is connected, among other things, with the number of energetic sites or adsorbent specific surface area and entropy changes of a compound in the chromatographic process. The relationship between the specific surface area and the liquid phase content (Fig.5) is a decreasing function. So we can state that entropic effects play an important role in the retention (sorption) mechanism of the discussed compounds, especially in a stationary polyethylene glycol monolayer on carbosil surface.

Characteristic features of some of the studied chromatographic columns and, for comparison, of corresponding packings prepared from the initial silica gel are presented in Table 1. Values of α are a measure of thermodynamic differences in distribution of the two compounds in the compared adsorption systems (chromatographic columns). The differences result mainly from the specific interactions of benzene molecules. The greater the interactions influence on retention (sorption) the greater the differences Δ (ΔG). Thus, higher values of free energy increments on silica gel result from a greater number of hydroxyl groups on its surface. There is a specific interaction between benzene molecules and these groups and EDA complexes are formed.

Interaction energies (heats of adsorption) of test compounds on carbosil change in a sequence characteristic of graphitized blacks [43] with which the compounds interact in a non-specific way: $q^0_{st,H} > q^0_{st,B}$. That is why higher values of a were obtained in case of silica gel. PEG deposition on silica surface, however, causes selectivity decrease whereas the coefficient α increases on carbosil modified with glycol (Table 1). A considerable increase is observed after polyethylene glycol monolayer formation on the complex adsorbent surface.

The studied adsorbents showed considerable differences in separation processes of mixtures of compounds with different chemical nature. For example, aliphatic alcohols were not separated on non-modified silica gel and on silica gel modified with PEG but they were successfully separated on carbosil deactivated with small amounts of polyethylene glycol monolayer. Ketones and esters were well separated on silica gel containing 30 mass% PEG

but just 3.5–5% of stationary phase is sufficient to separate these compounds on carbosil. Aliphatic hydrocarbons C_{10}–C_{16} were separated both on non–modified silica (analysis time about 40 min) and on silica modified with polyethylene glycol (15 mass% PEG, analysis time – 7 minutes).

Table 1
Comparison of adsorption thermodynamic parameters of the test compounds – n–hexane and benzene – on the studied adsorbents

Adsorbent		q^0_{st} [kcal·mole^{-1}]		α [l]		$\Delta(\Delta G)$ [cal·mole^{-1}]		$\Delta(\Delta S)$ [kcal(mole·K)$^{-1}$]	
		C_6H_{14}	C_6H_6	433 K	473 K	433 K	473 K	433 K	473 K
Carbosil		11.7	11.4	1.78	1.98	499	566	–1.84	–1.83
Silica gel		8.4	9.4	2.88	2.28	911	783	0.20	0.46
Carbosil	+5% PEG	8.4	9.1	1.82	1.04	518	269	0.42	0.70
Silica gel	+5% PEG	8.4	9.6	2.20	1.93	678	618	1.20	1.23
Carbosil	+10% PEG	7.3	8.7	1.81	1.07	510	368	2.05	2.18
Silica gel	+10% PEG	8.0	8.1	1.73	1.67	471	480	–0.86	–0.80
Carbosil	+15% PEG	7.3	7.3	1.83	1.78	519	543	–1.20	–1.15
Silica gel	+15% PEG	7.7	11.7	1.89	1.30	546	245	7.98	7.94
Carbosil	+30% PEG	6.5	7.6	2.23	2.08	690	688	0.95	0.87
Silica gel	+30% PEG	7.5	8.6	1.53	1.48	365	366	1.70	1.55
Carbosil	+45% PEG	6.2	7.9	2.80	2.67	886	933	1.88	1.62
Silica gel	+45% PEG	7.6	7.7	1.72	1.80	497	552	–0.92	–0.95

Notations: q^0_{st} = heat of adsorption, $\alpha = t_{r,B}/t_{r,H}$ the measure of thermodynamic differences in benzene and hexane partition on the investigated column, $\Delta(\Delta G)$ = increments of free energy changes (differences in free adsorption energy between benzene and hexane), $\Delta(\Delta S)$ = entropic effects which accompany adsorption process. Reprinted from: R.Leboda, P.Grochowicz, A.Łodyga, A.Gierak, Polish J. Appl. Chem, 36(1992)123.

Examples of chromatograms of hydrocarbons C_{10}–C_{16} separation on carbosil are presented in Fig.6. It shows that very short analysis time (2 min) was obtained on carbosil with 5% PEG addition but peaks of some analyzed compounds are assymmetric which indicates that the investigated column is heterogeneous one.

The role played by non–volatile molecules of liquid phase adsorbed on adsorbent surface is very important from the chromatographic point of view. The main criterion of liquid phase choice is the necessity for blocking heterogeneous surface sites of an active support. Thus a modifying agent functions as a "band broadening reducer" removing abnormal surface sites (Fig.6 A and B) when the surface concentrations are low. Eluate molecules start to interact with liquid molecules as the surface coverage increases. In this stage the liquid phase functions as a "selectivity modifier" because the initial retention mechanism is now substantially changed (Figs.6 B and C). At the same time the coverage growth leads to a retention volume decrease (Fig.6 D) due to a effective sorbent surface decrease. Continuation of modifying agent addition results in formation of a thick surface film which leads to (partial) screening of adsorption sites of the active support. Eluate

retention in such column is the result of simultaneous occurrence of two phenomena: eluate sorption in a high-molecular film and adsorption on its surface. Separation properties of such film are different from those of a volumetric phase because forces operating at adsorbent–liquid phase and the liquid phase–carrier gas interface change magnetic and electrostatic orientation of intermediate layers [53–55]. In reality it means that selectivity decreases once again for most separations. Table 1 contains some results obtained for silica gel (random topography) and carbosil (patch-wise topography).

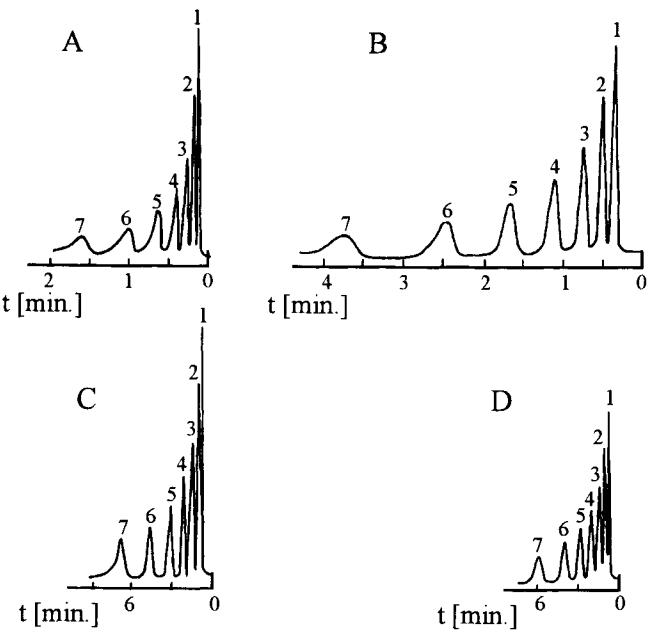

Figure 6. Examplary chromatograms of hydrocarbons C_{10}–C_{16} separation (1–7 respectively) on carbosil modified with various amounts of liquid phase. Liquid phase (PEG 4000) percentages are the following: A = 5 %, B = 15 %, C = 25 %, D = 45 %.

From the presented experimental data it can be seen that adsorption mechanism of sorbate molecules on the gas–liquid–solid chromatographic packing with an adsorbent having a mosaic surface is more complex than that with homogeneous adsorbents or those having statistical topography. The influence of support active sites extends even over the multilayer coverage with the liquid phase. A much larger amount of the liquid phase than that in the known [47] cases of diatomities or graphitized carbon blacks is necessary to reduce a long-distance operation of carbosil adsorption forces because of the high activity of its surface. The modifier (static liquid phase) monolayers being formed are of a statistic nature with the initial preference for silica gel patches. The mechanism of formation of successive liquid phase layers on the carbosil patchy surface is quite different from that on the homogeneous surface or surface with random distribution of adsorption sites. The utilization of specific interaction sites of PEG 4000 molecules (–OH and $-CH_2-O-CH_2-$ groups) in adsorption (retention) processes is fuller with carbosil as the support because

the sites are "consumed by strong interaction forces with hydroxyl groups in the surface of silica gel. When carbosil is used the number of "consumed" active sites is smaller and can be adjusted by carbon percentage on the carbosil surface. Entropic effects play an important part in the compounds retention (separation) process on the column packed with carbosil modified with PEG.

4.2.4. Liquid–solid systems

Unique properties of mosaic carboaerosils were pointed out in the further studies on carbon–silica adsorbents by ^{1}H NMR [56]. Thickness of benzene and water solvation shells near the surface of three adsorbents (Table 2) differing in adsorption site topography and their chemical nature was studied.

Table 2
Thickness of water and benzene solvation shells near the surface of carbosil, aerosil and carbon black particles

Adsorbent:	Carbosil		Carbon black		Aerosil
	water	benzene	water	benzene	water
I/I_0	0.008	0.12	0.03	0.08	0.03
d	1.0	7.8	2.0	2.4	3.0

I/I_0 – the intensity ratio of signals in the frozen and liquid state; d – the thickness of solvation shell. Reprinted from: V.V.Turov, R.Leboda, V.I.Bogillo, J.Skubiszewska–Zieba, Langmuir, 11(1995)935.

From Table 2 it appears that on passing from carbon black and aerosil to carbosil the thickness of the solvation shell of benzene increases and the hydration film decreases. The studies of changes of chemical potential of water molecules at the adsorbent/bonded water/ice interface depending on water layer thickness are presented in another paper [57]. For the initial silica the surface effect is confined to the adsorbent water monolayer. Poor carbonization of aerosil surface causes the increase of water layer thickness to 40–50 molecular diameters. With the increase of carbon constituent part on the complex adsorbent surface, the thickness of interfacial water layer decreases to 15 molecular diameters.

5. MODIFICATION OF THE SURFACE PROPERTIES

Methods of modification of surface properties of complex carbon–mineral adsorbents distinguishing those used on the commercial scale and on the laboratory scale are presented in the review paper [2]. However, not all methods can be applied in both cases. Some attention is paid to the latest publications not included in the quoted paper.

5.1. Hydrothermal treatment

One of the most effective methods of modification of porous structure and chemical nature of adsorbents and catalyst surface is their hydrothermal treatment with water

vapour under high pressure [58]. The water under these conditions, particularly above 200°C, changes its properties due to disappearance (decomposition) of its original tetrahedral structure. As a result its capability of dissolving solids increases. Silica gels are particularly susceptible to water vapour [58]. The mechanism of hydrothermal treatment (HTT) of carbon–silica adsorbents is complex. It depends on carbon deposit topography on the silica surface. Modification of both mineral and organic parts (of carbon deposit) should be taken into account. Silica mineral deposit modification depends on the silica initial structure, amount of carbon deposit, physicochemical properties of pyrolyzed substance and carbonizate deposition conditions.

High temperature (800°C), pressure–free hydrothermal treatment of carbosil prepared by pyrolysis of methylene chloride was studied in the paper [38]. The results of hydrothermal treatment of such adsorbents under the conditions without pressure (800°C) and high pressure of water vapour (250–500°C) are presented in another paper [59].

Table 3
Surface properties of carbon–silica adsorbents modified with water vapour

Adsorbent, modifier	Pyrolized substance	C (wt.%)	S_{BET} (m^2/g)	Heat of Adsorption, q^0_{st}·kcal/mole	
				n–hexane	benzene
Carbosil C	CH_2Cl_2	14.5	286	19.7	18.5
$C(H_2O)$ 250°C		14.0	280	8.6	8.9
$C(H_2O)$ 500°C		13.2	185	10.6	8.8
Carbosil B	n–octanol	3.75	385	9.0	9.6
$B(H_2O)$ 250°C		3.09	90	14.0	13.6

Reaction conditions: 0.2 l autoclave, temperature 250 and 500°C, time 6 h, 15 ml water for 5 g adsorbent. Reprinted from: R.Leboda, A.Gierak, B.Charmas, A.Łodyga, React.Kinet. Catal.Lett. 50(1993)63.

Carbon deposits prepared from CH_2Cl_2 possess the most heterogeneous structure [35,36]. At the same time they are strongly energetically heterogeneous and possess their own porous microstructure. At low temperatures (250–500°C, Table 3.) homogenizing of these deposits takes place which is shown among others, in the q_{st} decrease. At high temperatures (800°C, Table 4) the adsorbents with such deposits can be activated by developing a microporous system in them, which can be seen in the increase of W_0 and E_0 value and the decrease of R value (Table 4). Moreover, the total pore volume V_p and mesopore volume V_{meso} increase significantly and mesopore surface S_{meso} increases slightly. In Table 4, W_0 and E_0 are the parameters of the Dubinin equation [60]:

$$W = W_0 \exp[-(A/\beta E_0)] \tag{7}$$

where W is the volume of adsorbate condensed in the micropores at the temperature T and the relative pressure p/p_0, W_0 is the total volumes of micropores, $A = RT \ln(p/p_0)$, R is

the universal gas constant, β is the similarity coefficient characterizing the sorbate structural properties (for benzene $\beta = 1$), and E_0 is the characteristic sorption energy of the system under investigation. For n = 2, Eq. (7) gives the well-known Dubinin–Radushkevich (D–R) equation usually used to approximate adsorption in sorbents having a homogeneous micropore system [61]. E_0 is the characteristic sorption energy of the system under investigation.

Table 4
Pore parameters of Carbosil E and their activation product (Carbosil E/A). (The data from the adsorption and desorption isotherms of benzene vapours measured at 25 C)

Adsorbent	C mass%	S_{BET} m^2/g	S_{mezo} m^2/g	V_p cm^3/g	V_{mezo} cm^3/g	W_0 cm^3/g	R nm	E_0 kcal/mole
Carbosil E	40.2	95.3	82.4	0.266	0.266	0.037	5.6	1.74
Carbosil E/A	20.1	320.3	98.8	0.462	0.376	0.178	2.9	2.00

Reaction conditions: quartz flow reactor, passing overheated water vapour through the sample, temperature 800°C, the reaction was carried out till half of the carbon deposit was gasified. Reprinted from:A.Gierak,F.Czechowski, R.Leboda, Mater.Chem.Phys.,36(1994)264.

The presented data show possibilities of activation at high temperatures of carbon–silica adsorbents, i.e. microporous structure creation and change of chemical nature of the surface adsorption sites. As an illustration, adsorption from the aqueous solutions of chlorophenols and methane trihalotanes was discussed [37–39]. Activation and deactivation of carbosils (in physical and chemical adsorption) through their HTT under the water vapour high pressure conditions and at moderate temperatures (250–500°C) were discussed [59]. Some results are presented in Figs. 7 – 10.

Figs.7 and 8 present absolute adsorption isotherms of n–hexane and chloroform on pure silica gel, on nonmodified carbosil prepared on its basis, and on this carbosil hydrothermally modified at 250°C (carbosil B, Table 3). The adsorption heats of the adsorbates mentioned on the above adsorbents are given in Table 3. The data indicate that a sharp increase in the physical adsorption (and an appropriate increase in the adsorption heats) of both pairs of substances occurs for hydrothermally treated carbosils. The same effects for carboaerosil gels treated hydrothermally with water and 5% H_2O_2 water solution can be seen in Figs.9 and 10. The adsorbates here are ammonia and water vapours. This also confirms the formation on the surface of carbon deposits of functional groups with an acidic character on their surface. The groups of this type (strongly and weakly acidic) are formed during oxidation of carbon adsorbents with hydrogen peroxide solution [62]. Carbosils, presented in Figs.9–12, containing 5–36 mass% pyrogenic carbon, were prepared according to the procedure described in Ref. 63 by pyrolysis of methylene chloride at 500°C in a nitrogen stream in a dynamic reactor [64]. All of these carbosils were subjected to hydrothermal treatment with pure water or 5% hydrogen peroxide at the temperatures in the range 100–350°C for 5 h. All HTT processes were performed in an autoclave under the saturated water vapour conditions corresponding to given temperatures [65].

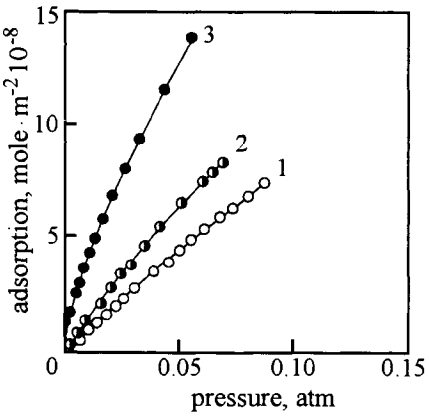

Figure 7. Absolute adsorption isotherms of n-hexane on (1) silica gel, (2) carbosil prepared on the basis of this silica gel, and (3) the same carbosils undergone hydrothermal treatment with water at 250°C.

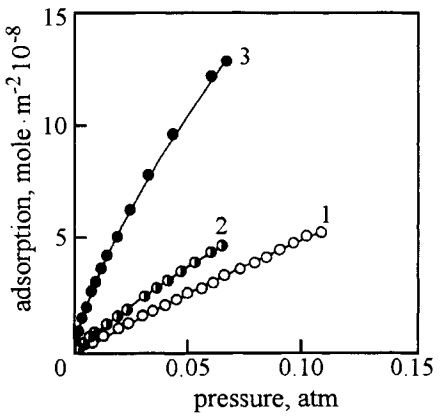

Figure 8. Absolute adsorption isotherms of chloroform. Symbols are the same as in Fig. 7.

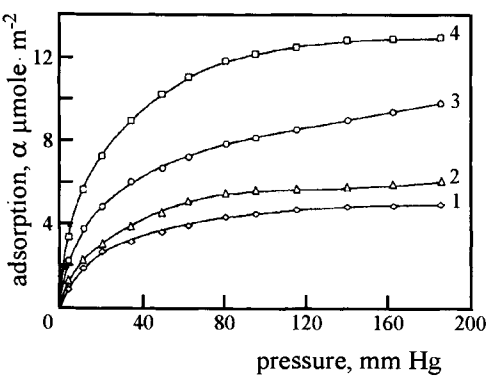

Figure 9. Absolute adsorption isotherms of ammonia at 20°C on (1) aerosil modified with water at 250°C, and on the carboaerosils: (2) carboaerosil 5 %C; (3) carboaerosil 5 % C, HTT, H_2O, 250°C; (4) carboaerosil 19.6 %C HTT, H_2O, 350°C.

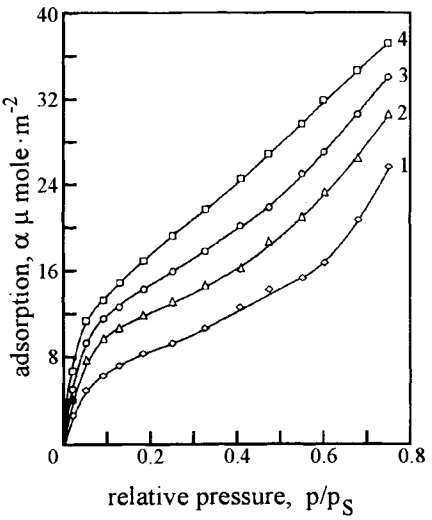

Figure 10. Absolute adsorption isotherms of water vapour on (1) aerosil modified hydrothermally (HTT) with water at 250°C, and on the following carboaerosils: (2) carboaerosil 5 % C, HTT, 250°C, H_2O; (3) carboaerosil 5 % C, HTT, 100°C, 5% H_2O_2; (4) carboaerosil 19.6 % C, HTT, 350°C, H_2O.

A new method of carbosil HTT, namely using H_2O_2, was applied in the discussed paper [65]. Owing to that modification is great and its conditions are milder than in the case of

H_2O. It should be noted that carbosil HTT improves the kinetics of sorption–desorption of organic substances from the aqueous solution which is important e.g. in separation and preconcentration of substance trace amount by means of the solid–phase–extraction method [25].

5.1. Mechanism of HTT of carbon–silica adsorbents

In hydrothermal treatment of carbosils and silica (water steam), a decrease in the specific surface area with the increasing temperature is generally observed (Figs. 11 and 12). Regarding carboaerosils, the higher their pyrocarbon content, the smaller the S_{BET} area decrease at a given temperature (Fig.11, 12). Thus, in carbosil containing 36 % pyro-

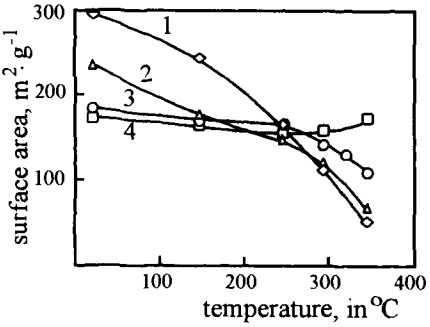

Figure 11. Dependence of the specific surface area of carboaerosil on the temperature of hydrothermal treatment with water: (1) aerosil; (2) carboaerosil 5 % C; (3) carboaerosil 19.6 % C; (4) carboaerosil 36 % C.

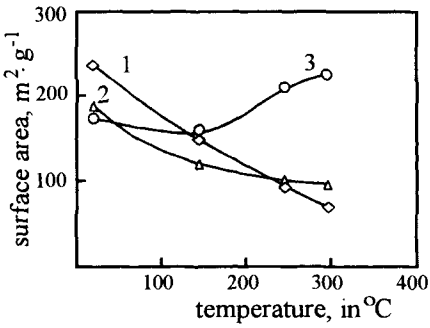

Figure 12. Dependence of the specific surface area of carboaerosil on the temperature of hydrothermal treatment with a 5% solution of hydrogen peroxide: (1) carboaerosil 5 % C; (2) carboaerosil 19 % C; (3) carboaerosil 36 % C.

carbon, the specific surface area practically does not change at 350°C. A comparison of the course of respective curves in Figs. 11 and 12 shows the effect of the stronger oxidizer (H_2O_2) on the process of hydrothermal modification of carbosils containing different pyrocarbon amounts. In hydrothermal treatment in vapours of a 5% water solution of hydrogen peroxide (Fig. 12), for the samples containing 5 and 19.6 % carbon, the rate of S_{BET} decrease is higher than in the case of the analogous sample treated with pure water. This difference may result from the fact that hydrothermal treatment in the oxidizing atmosphere always leads to liberation of a large surface area from carbon and, as a consequence, to intensification of silica transport during depolimerization and recondensation. As already known [58], the reactions of this type are the basis of the hydrothermal modification of silica gels. In this case water interacts with the silica surface causing its simultaneous hydration and depolymerization [66]:

$$(SiO_2)_n + 2H_2O \longrightarrow (SiO_2)_{n-1} + Si(OH)_4 \qquad (8)$$

Mainly the small globules undergo dissolution. The newly formed silicic acid is deposited on large globules and builds a polymeric structure. However, the process of hydro-

thermal treatment of carbon–silica adsorbents must be considered as a complex process because either the carbon deposit or silica may react with water vapour.

The basic reaction of carbon with water vapour is endothermal and may be illustrated by the following stoichiometric equation:

$$C + H_2O \longrightarrow H_2 + CO + 130\ kJ \tag{9}$$

The rate of the oxidation process is determined by the reactivity of the starting carbon and oxidizer. The greater the reactivity of the substrates the lower the temperature of the process in which uniform formation of the pores in the granules is observed. In the case of carbonaceous materials the cokes of brown coals show the greatest reactivity, and the cokes of hard coals the smallest activity. The cokes of pit coals show an intermediate reactivity. This is connected with the earlier mentioned "ordering" of the crystallographic structure of carbon, which is of significant importance in the case of modification of carbon deposits contained in the carbon–mineral adsorbents in which the carbonaceous compound may be characterized by a differentiated chemical and physical structure. Thus the surface properties of hydrothermally modified complex adsorbents are defined by the course of three processes:

a) modification of mineral background;
b) gasification of carbon deposit causing gradual disclosing of pores;
c) formation of different oxygen groups of specific activity on the deposit surface.

Carbon deposits largely block the narrowest pores of the modified silica; on such pores formed by small globules reaction (8) is the most effective. Generally, the course of processes **(b)** and **(c)** under the given conditions depends on the chemical structure of carbon deposits resulting from the kind of pyrolyzed substance and temperature (see Scheme 1 and Table 3 and 4).

During the oxidation of carbon deposit the water vapour attacks mainly the most active elements of this deposit (the least ordered), i.e. hydrogenated parts, small particles of the carbon and edges. This can cause a partial homogenization of deposit surface obtained from CH_2Cl_2 pyrolysis (decrease of q_{st} – Table 3). In case of carbosil B in Table 3 adsorption heats increase because its carbon deposit is more susceptible to oxidation. Then carbon deposits capable of strong specific and non–specific interactions are formed.

In the sample with a high carbon content (36 %), the specific surface area is observed to increase over 150°C (Fig. 12). This may be due to microporosity developed in a relatively thick layer of carbon deposited on the surface of aerosil particles (according to the data [40], the carbon layer is about 40Å thick). Similar effects observed are in Table 4, but in that study a high temperature (800°C) was used in the hydrothermal process. As indicated by the data in Tables 3 and 4, the carbon content in the samples distinctly decreases with the increasing temperature, and, as expected, it decreases even more strongly when the sample is treated with hydrogen peroxide. Such gasification of carbon, the influence of oxidizers (water or hydrogen peroxide) finally results not only in geometrical modification and morphological changes in the carbon layer deposited on the silica surface, but also, as shown, in the increased concentration of active adsorption sites on the surface, which is an essential change in its chemical structure [65]. The consequence of these changes is the increased activity of hydrothermally treated carbosils in physical and chemical adsorption.

5.3. Chemical modification

It follows from the works [30,67,68], devoted to the study of the properties of modified carbon–silica adsorbents by means of IR spectroscopy, that the modification of the original silica gel by the pyrolysis products of alcohols does not result in the disappearance of hydroxyl groups on the surface. This makes a chemical modification of the surface of carbosils possible [30,59,65,68]. Chemically modified carbosils (with a patch–wise topography) have specific structure of active (adsorption) sites called a "topographic–architectonic structure" [28].

5.3.1. Modified adsorbents

There are many methods of chemical modification of silica gels [69]. The modification can be carried out by esterification or by reacting the surface hydroxyl groups with organosilicon compounds. From the practical point of view the latter way is of greater importance because it makes possible to prepare a chemically modified adsorbent of higher thermostability and resistance to a negative action the of mobile phase (hydrolysis, solvolysis etc) compared to the esterified compounds. The modification can be carried out using organosilicon compounds containing one or several, different, functional groups, which makes further reactions on the surface of the modified adsorbents possible; in this way selective adsorbents can be prepared. The results of the studies on surface properties of carbosils modified by octadecyltrichlorosilane (ODS) and hexamethyldisilazane (HMDS), trimethylchlorosilane (TMCS) and HMDS as well as aliphatic alcohols are presented in the papers [30,59,65,68].

Some surface characteristics of the unmodified and chemically modified with silane carbosils and initial silica gel are given in Table 5.

Table 5
Surface characteristics of unmodified adsorbents (A,B,C) and adsorbents silanized with ODS (AI, BI, CI) and ODS+HMDS (AII, BII, CII). A – the starting silica gel; B – and C – the carbosils obtained by pyrolysis of n–heptane (B) and benzyl alcohol (C) on the surface of adsorbent A [70]

Adsorbent	Content of		Adsorption heat kcal/mole	
	carbon mass%	hydrogen mass%	hexane	CH_3Cl
A – initial silica gel			9.1	10.2
AI – ads. A modified with ODS	9.38	2.16	7.4	8.4
AII – ads. AI modified with HMDS	11.82	2.60	7.0	6.1
B – carbosil	2.30	0.72	9.2	8.9
BI – ads. B modified with ODS	2.80	0.76	7.1	7.5
BII – ads. BI modified with HMDS	6.10	1.42	6.7	6.1
C – carbosil	4.30	0.70	13.9	12.5
CI – ads. C modified with ODS	8.82	1.21	8.4	9.0
CII – ads. CI modified with HMDS	9.92	1.39	7.9	8.2

Reprinted from: R.Leboda, Chromatographia, 11(1980)703.

Silanization of silica gels generally results in a decrease of the adsorption heat of various substance and in an improvement of peak resolution of the adsorbents [70] such a change of adsorption heats is also observed in this case (Table 5).

A strong decrease of the adsorption heats of the tested hydrocarbons takes place already after the first stage of chemical modification of the adsorbents. ODS, chemically bonded to the surface of carbosils, first of all blocks strong sites of specific adsorption (OH groups) as well as other more active adsorption sites by screening them with the long $C_{18}H_{37}$ radical. Further modification of the adsorbents in question by HMDS results in further screening of their active sites. Hence after the second stage of silanization a further decrease of adsorption heat of the tested substances is observed.

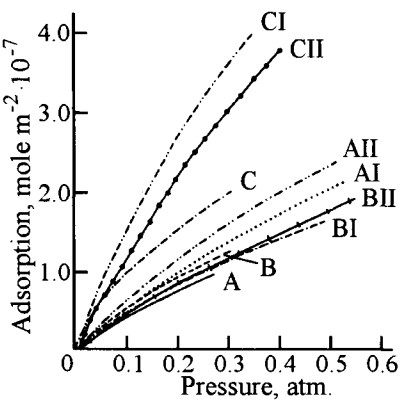

Figure 13. Absolute adsorption isotherm of n-hexane for the adsorbents listed in Table 5.

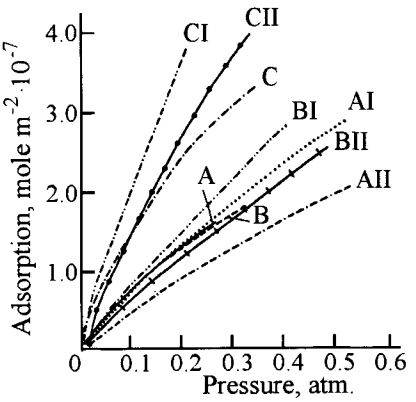

Figure 14. Absolute adsorption isotherm of chloroform for adsorbents listed in Table 5.

The changes in the chemical character of the adsorption sites of the adsorbents are also reflected in the adsorption capacity. Isotherms of n-hexane and chloroform for the adsorbents listed in Table 5 are compared in Figs. 13 and 14. Comparison of the respective curves in these figures leads to the conclusion that the adsorption capacity i.e. amount of substance adsorbed at a given pressure on the adsorbents increase after their chemical modification, particularly after silanization (ODS). Nevertheless the adsorption capacity of such adsorbents is higher than that of the chemically unmodified ones. There are small differences in the course of adsorption isotherms of n-hexane (Fig.13) and chloroform (Fig. 14) on the adsorbents. According to the classification of adsorbate and adsorbent molecules given by Kiselev [43] the molecules of n-hexane can interact only in a non-specific way (dispersive forces), while the interaction of chloroform molecules can be non-specific and specific, e.g. by formation of hydrogen bonds. Hence, there are differences in the course of the adsorption isotherms of both the substances. For example, n-hexane molecules exhibit a minimum adsorption capacity on the unmodified silica gel (curve A, Fig. 13), while chloroform molecules show a minimum adsorption capacity on this adsorbent modified first by ODS, and then by HMDS (curve AII, Fig. 14). In this case the adsorption on unmodified, starting silica gel is significantly higher because the latter contains surface hydroxyl groups capable of specific interactions.

On the other hand, adsorbents A and B modified with ODS and adsorbent C unmodified or modified with ODS as well as with ODS+HMDS exhibit higher adsorption capacity. Benzene shows similar adsorption behavior [68]. The above facts are due to the specific structure of adsorption sites which is formed after the chemical modification of the adsorbents. Adsorption energy sites constitute of spacially arranged CH, CH_2 and CH_3 groups of the octadecyl radical, chemically bonded to the surface of the silica gel and, in the case of carbosils of components of the carbon deposit (i.e. CH, CH_2, CH_3) "planary" distributed on the surface of the supporting material. There is an essential difference in the mechanism of the molecular adsorption on chemically modified and unmodified adsorbents [30]. The surface of chemically unmodified adsorbents can be considered as planar, i.e. two-dimensional, while that of the modified sorbents as three-dimensional.

In the latter case the adsorption sites (energy sites) show spatial arrangement and form architectonic compositions similarly to the case of silica gels esterified by alcohols [28]. The problems connected with the mechanism of molecular retention on such adsorbents as well as with testing unmodified and chemically modified adsorbents have been dealt with in many works [28,30,68,71].

The observed increase of adsorption capacity results from the location of the adsorbate molecules between the organosilane radicals, favoured by the moderate degree of silanization of the adsorbent surface. This is obvious because the starting silica gel has been hydroxylated only partly and the carbosils obtained from it have only partly been coated with pyrolytic carbon. It is assumed here that the carbon deposit does not react with silanes. Using the nomenclature proposed [28] silanized carbosils constitute architectonic and topographic compositions. Owing to this fact, they exibit higher adsorption capacity with respect to hydrocarbons. Silanization of carbosils results in a significant improvement of their separation properties in chromatography [28,68].

5.3.2. Effect of HTT

As mentioned earlier HTT of carbosils caused not only the change of their activity in the physical adsorption processes but also causes the increase of their chemisorptive activity. The results of the studies on HTT of carbosils modified chemically in the reactions of silanes and aliphatic alcohols are presented in the papers [25,59,65,72]. To prepare the carbon–silica adsorbents, silica gels [25,59,72] and aerosils [65] were used. Some results obtained for carboaerosils [65] chemically modified with n–butanol whose properties were discussed earlier are presented here. For comparison the data are presented in Table 6. From the analysis of these data it follows that for carboaerosils modified with water and a 5% water solution of hydrogen peroxide, the concentration of surface–bonded butoxy groups reaches 8.45 μmol m^{-2} at a 16 % carbon content in the sample. At smaller and bigger carbon contents in the aerosilogel the concentration of bonded groups decreases; however, it may also exceed that of free silanol groups on the surface of maximally hydroxylated silicas 4.6–4.8 μmol m^{-2} [70,73]. As the content of oxygen–containing functional groups on the carbon surface (also oxidized) does not exceed this value [62,74], it is of course the surface structure of carbosils, particularly of those treated hydrothermally, that causes the occurrence of such abnormally high concentrations of bonded groups. It is possible that for such complex adsorbents synergism of their properties is revealed. Similar results were obtained when carbosils

prepared from silica gels modified with silanes were used in HTT modification [72].

Table 6
Effect of hydrothermal treatment on surface properties of carboaerosils

No.	Adsorbent, conditions of modification	S_{BET} m^2/g	%C mass	α $\mu mole/m^2$
I	Aerosil (A)	295	–	(3.43)
II	Adsorbent I modified with $C_4H_9OH/250°C$	203	–	3.88
III	Adsorbent I modified with $H_2O/250°C$(HTT)	167	–	(4.58)
IV	Adsorbent III modified with $C_4H_9OH/250°C$	101	–	4.88
V	Carbosil 5% mass C (C-5%)	236	5.0	–
VI	Adsorbent V modified with $C_4H_9OH/250°C$	196	4.9	2.10
VII	Adsorbent V modified with 5% $H_2O_2/100°C$ (HTT)	202	3.2	–
VIII	Adsorbent VII modified with $C_4H_9OH/250°C$	178	3.8	6.40
IX	Adsorbent V modified with $H_2O/250°C$ (HTT)	151	4.0	–
X	Adsorbent IX modified with $C_4H_9OH/250°C$	91	3.9	5.27
XI	Adsorbent V modified with $H_2O/350°C$ (HTT)	71	3.1	–
XII	Adsorbent XI modified with $C_4H_9OH/250°C$	60	3.0	7.30
XIII	Carbosil 19.6% mass C (C-19.6%)	188	19.6	–
XIV	Adsorbent XIII modified with $C_4H_9OH/250°C$	180	19.4	0.15
XV	Adsorbent XIII modified with $H_2O/350°C$ (HTT)	111	16.3	–
XVI	Adsorbent XV modified with $C_4H_9OH/250°C$	93	16.1	8.45
XVII	Carbosil 36% mass C (C-36%)	176	36.0	–
XVIII	Adsorbent XVII modified with $C_4H_9OH/250°C$	172	35.8	–
XIX	Adsorbent XVII modified with 5%$H_2O_2/250°C$(HTT)	210	22.3	–
XX	Adsorbent XIX modified with $C_4H_9OH/250°C$	190	22.0	3.70
XXI	Adsorbent XVII modified with $H_2O/350°C$(HTT)	177	30.7	–
XXII	Adsorbent XXI modified with $C_4H_9OH/250°C$	161	30.4	1.52

In the parentheses there are given the concentrations of free OH groups on silica surface, determined on the basis of the results of the reaction with hexamethyldisilazane. Reprinted from: R.Leboda, V.V.Sidorchuk, J.Skubiszewska-Zieba, Mater.Chem. Phys., 39(1994)136.

5.4. Secondary pyrolysis

As shown earlier, pyrolysis of methylene chloride on the surface of a mineral adsorbent is an effective way of preparation of complex adsorbents containing any amount of carbon and characterized by good mechanical properties. However, during the pyrolysis of CH_2Cl_2 different heterogeneous carbon particles of different sizes are formed [36]. Such globules of very different sizes (from tens to a few thousand Å) [36] contain geometrically heterogeneous micropores or even ultramicropores. The narrow pores are very strong adsorption sites owing to the increase of the potential of non-specific (dispersive) interactions. In

consequence, such adsorbents are strongly energetically heterogeneous and can adsorb a lot of substances irreversibly. The studies [63,72] show that these heterogeneities can be eliminated by additional pyrolysis of an organic substance on the surface of a complex adsorbent. This is illustrated by the data listed in Table 7 in which the effect of modification of two adsorbents (X and Y) containing different amounts of carbon are compared. The following characteristics were determined for the individual adsorbents: the specific surface area, S_{BET}, the radius of the dominating pores at the maximum pore distribution, R_{dom}, and the carbon content, mass % C. Furthermore, the adsorption isotherms and the heats of adsorption of n-hexane and chloroform used as testing substances were determined by gas chromatography.

Table 7
Surface properties of unmodified carbon-silica adsorbents (carbosils X, H, B, Y) and the same adsorbents modified with the products of pyrolysis of n-heptanol (H) and benzyl alcohol (B) in an autoclave (A) and dynamic reactor (R). The carbosils were prepared by the pyrolysis of methylene chloride (adsorbents X and Y), n-heptyl alcohol (H) and benzyl alcohol (B) on the silica surface

Adsorbent	Specific surface area S_{BET} (m^2/g)	Pore radius R_{dom} (Å)	% C mass	Adsorption heat (kcal/mole)	
				n-hexane	CH_3Cl
Nonmodified silica gel	382	27; 34	–	7.9	7.3
Adsorbent X	370	27; 31	2.46	8.7	7.3
Adsorbent X_{H-A}	300	34	10.63	8.5	7.3
Adsorbent X_{B-A}	246	32	15.95	13.1	11.0
Adsorbent X_{H-R}	422	28	3.76	8.0	7.6
Adsorbent H	331	39	2.30	8.0	8.6
Adsorbent B	286	68	4.60	10.4	10.0
Adsorbent Y	61	200	30.46	very high	
Adsorbent Y_{H-A}	19	260	32.46	12.0	10.2
Adsorbent Y_{H-R}	23	205	31.68	10.0	7.3

Reprinted from: R.Leboda, Chromatographia, 14(1981)524.

The relatively high carbon content of Adsorbent X (2.46 %) does not cause any significant changes in the porous structure of the modified initial silica gel. Adsorbent H obtained through the pyrolysis of n-heptanol contains, in fact, the same amount (2.3 %) of carbon as Adsorbent X, but, in spite of this, as shown by Table 7, the adsorbents clearly differ in their surface characteristics. The n-heptanol carbonization products block more effectively the narrow pores of the modified silica than the carbon produced in the pyrolysis of dichloromethane. This is confirmed by the differences in the specific surface area of both adsorbents (Table 7).

Additional modification of Adsorbent X with n-heptyl and benzyl alcohols (Adsorbents

X_{H-A} and X_{B-A}) causes a fundamental change in the geometrical structure of its pores and in the chemical nature of the adsorptive sites. The data listed in Table 7 show that this process is reflected in the specific surface area of these adsorbents, in their carbon contents, as well as in the adsorption heats of the substances used for testing. The size of the dominating pore radius, are similar for the adsorbents prepared on the basis of Adsorbent X. These adsorbents, however, differ from each other in the capacity of the pores with given radii. Figure 15 compares the nitrogen adsorption and desorption isotherms and the pore volume distribution curves according to their radii.

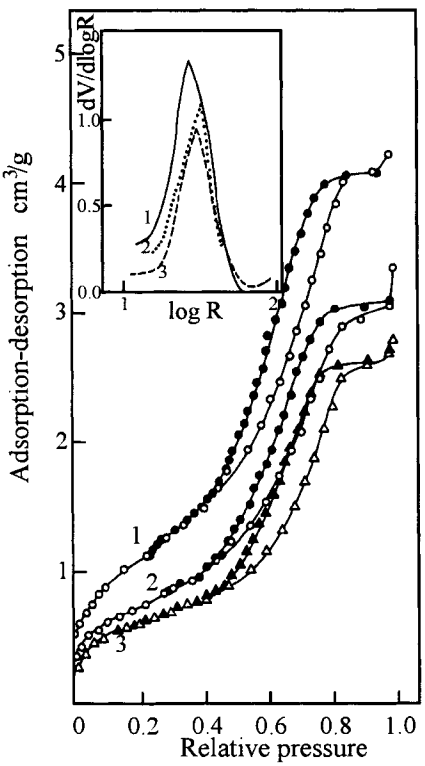

Figure 15. Adsorption and desorption isotherm of nitrogen on the following adsorbents: (1) X_{H-R}, (2) X_{H-A}, (3) X_{B-A}. Inserted diagram: differential pore size distribution as a function of pore radius (R) for the same adsorbents.

Adsorbent Y contains a considerable amount of pyrogenic carbon (30.46 %). It is characterized by high adsorption heats of hydrocarbons, which thus will be practically unmeasurable by gas chromatography using a thermal conductivity detector. Therefore it can never be used for chromatographic separation. At a relatively high temperature, i.e. at about 200°C, even the saturated and aromatic hydrocarbons are adsorbed irreversibly or very strongly on this adsorbent. After modifying Adsorbent Y with n-heptanol its surface properties are radically changed. As shown in Table 7, the adsorption heats of the test substances do not have very high values. It follows from the data of Table 7 that the surface

properties of Adsorbent Y depend on the method by which its additional modification was performed. The reaction products of n-heptanol carbonization carried out under dynamic conditions block less effectively the narrow pores of the modified adsorbent than in the case when the carbonization is carried out in an autoclave. This is reflected in the observation that the adsorbent modified in the reactor does not change the size of the dominating pore radius (R_{dom} = 205 Å), whereas the products of the n-heptanol pyrolysis reaction carried out in the autoclave block the initial dominating pores (R_{dom} = 200 Å) of modified Adsorbent Y, leaving out wider pores (R_{dom} = 260 Å). The increase in the carbon content deposited on the surface of the modified adsorbent by the static method (in the autoclave) always causes volumetric filling or blocking of its narrowest pores [26,30,75]. Figure 16 compares differential curves of pore volume distribution according to their radii both for unmodified and modified Adsorbent Y.

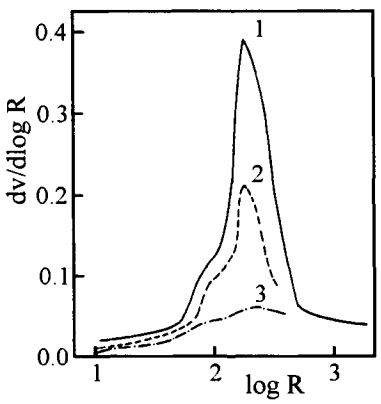

Figure 16. Differential pore size distribution function of pore radius (R) for the following adsorbents: (1) Y, (2) Y_{H-R}, (3) Y_{H-A}.

The method described permits to enrich the chromatographic properties of carbon–silica adsorbents prepared through the pyrolysis of dichloromethane. Figure 17 shows the extent to which the resolution capability of such an adsorbent can be improved. A considerable progress has been achieved here compared to the adsorbents prepared through the pyrolysis of alcohols in an autoclave [26,76], since Adsorbent X_{H-A}, having a high carbon content (10.63 %), is characterized by a good resolution ability and a short analysis time, producing symmetrical peaks. On the other hand, carbon–silica adsorbents, having a similar carbon content but prepared through the pyrolysis of alcohols, are characterized by a poor resolution ability and strong adsorptive properties [26,75–78].

Applying modification of substances having different chemical nature and different methods to deposit their pyrolysis products one can obtain adsorbents with differentiated surface properties and thus showing different chromatographic resolution abilities. The data in Table 7 and Figs. 17–20 confirm this statement. Figs. 17–20 show adsorption isotherms while Table 7 lists characteristic data of n-heptane and chloroform adsorption on Adsorbent Y as well as on the same adsorbent but modified with n-heptanol in an autoclave and in a rotary reactor. Similarly to the experiments described in papers

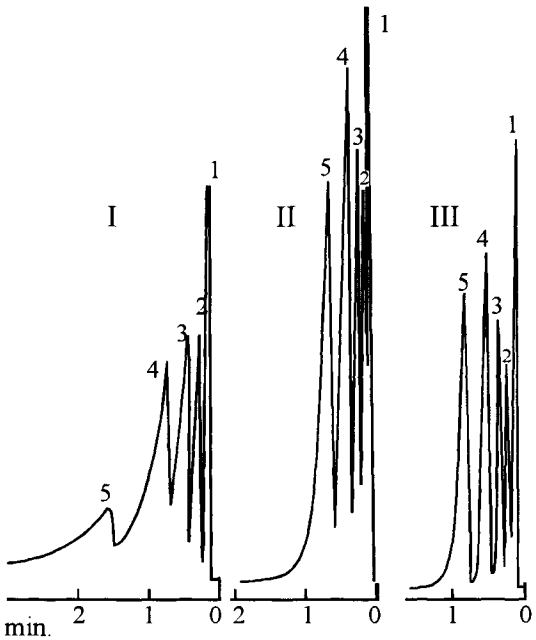

Figure 17. Chromatograms of saturated hydrocarbons at 200°C on the following adsorbents: (I) X, (II) X_{H-R},(III) X_{H-A}. Peaks: (1) n-pentane, (2) n-hexane, (3) n-heptane, (4) n-octane,(5) n-nonane. Chromatographic conditions: glass column (0,4 m×2,5 mm i.d.), carrier gas - hydrogen, flow rate 32 cm^3/min. Thermal conductivity detector, sample size 1 μl.

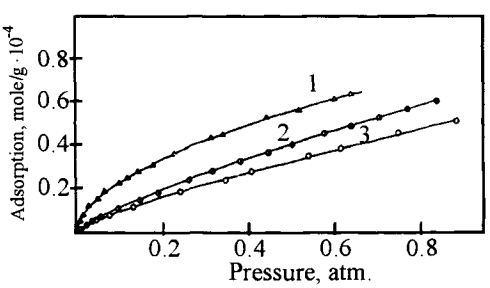

Figure 18. Adsorption isotherms of n-hexane at 170°C on the following adsorbents: (1) Y, (2) Y_{H-A}, (3) Y_{H-R}.

[26,30,78] the narrow pores of the modified adsorbent are, in this case, also more effectively blocked by the products of the pyrolysis of an aromatic (benzyl) alcohol than by those of an aliphatic (n-heptyl) alcohol. Moreover, as shown in Table 7, the modification of the carbon-silica adsorbent with an aliphatic alcohol generally results in a decrease of the adsorption heats of the test substances, whereas the use of an aromatic alcohol strongly increases the adsorption heats. This can be accounted for by the differences in

the physicochemical properties of both alcohols, i.e. by shape and size of their molecules and by their adsorptive affinity. Besides, there are difference in the chemical structure of the carbon deposits obtained through the pyrolysis of n-heptyl and benzyl alcohols [30,79].

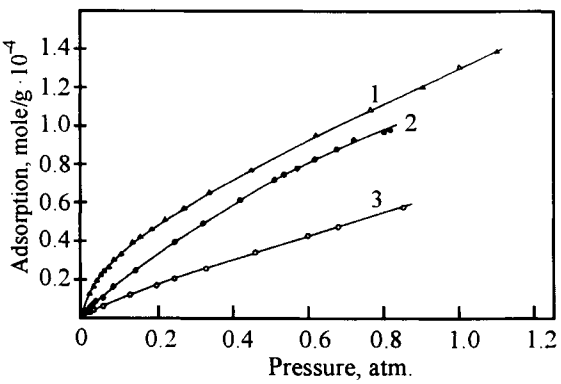

Figure 19.Adsorption isotherms of chloroform at 170°C on the folowing adsorbents: (1) Y, (2) Y_{H-A}, (3) Y_{H-R}.

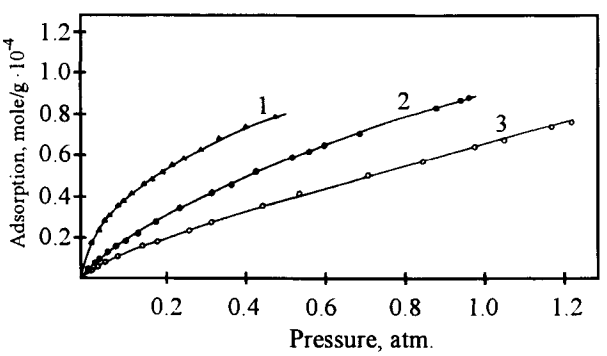

Figure 20. Adsorption isotherms of benzene at 170°C on the following adsorbents: (1) Y, (2) Y_{H-A}, (3) Y_{H-R}.

It should be added that the method presented here also permits us to obtain adsorbents with an increased specific surface area as compared to the initial carbon–silica adsorbent. This process can be easily accounted for if one takes into consideration the fact that the vapours of the pyrolysed substance transport by the carrier gas, with its adequately high flow rate over the modified carbon–silica adsorbent, may not diffuse into the narrow pores on time but will undergo decomposition either in wide and more easily accessible pores or on active, catalytically acting, corners and walls of the carbon agglomerates formed in the process of pyrolysis of dichloromethane. (Diffusion is a rather slow process, slower than adsorption.) Thus the size of the specific surface area of silica gels modified by dichloromethane may be increased or slightly changed (e.g. Adsorbent X, see Table 7).

This substance may form agglomerates around the pores thus increasing their capacity [64]. In contrast to this process, the adsorbent modified in an autoclave is more thoroughly wetted by the vapours of the pyrolysed substance which, before destruction, can penetrate the respective pores continuing the change of their structure. It follows from the data listed in Table 7 that the silica gel modified with n–heptanol in an autoclave (Adsorbent H) is considerably different in S_{BET} surface area values compared to a similar adsorbent prepared in the rotary reactor (Adsorbent X_{X-R}).

It is the advantage of the rotary reactor that during the pyrolysis of alcohols and other substances only slight amounts of pitch–like substances are formed on the surfaces of the modified adsorbents. Moreover, in the set–up shown in [63,64] one can subject the directly prepared carbon–silica adsorbents to a further thermal modification in the atmosphere of various gases thus obtaining adsorbents with the required properties [35].

6. CONCLUSION

The paper presents only some studies of preparation and properties of surface carbon–silica adsorbents. The application of these materials as model adsorbents in investigations of various adsorption processes is discussed. They can be also used for testing the theories describing adsorption and catalytic processes on the heterogeneous surfaces. The influence of such surfaces on the properties of adsorbed gases and liquids as well as their application have been studied.

Papers [1–3] cited in introduction discuss more widely the complex (carbon–mineral) adsorbents including a large number of carbonized mineral carriers and describe various applications such as: catalysts and their carriers, ion–exchangers, polymer filling materials, chromatographic and extraction column packings, as sorbents for purification of water and other media. Possibilities of further development of studies on preparation and application of carbon–mineral adsorbents are also presented. However, the survey of the literature data shows that neither papers [1–3] nor the present one include all interesting publications. There are others dealing with:

- an original method of preparation of carbon–silica adsorbents from esterified silica gel [4] as well as determination of their surface properties [4,5];
- formation of highly oriented graphite from polyacrylanite by using a two–dimentional space between montmorillonite lamellae [6–10];
- studies of carbon deposit distribution on the surface of adsorbents and catalysts as well as its effect on the porous structure of complex adsorbent (catalysts) [11,18,19];
- preparation and sorption properties of carbon composite materials formed from layered clay minerals [12–17];
- estimation of applicability of carbon–covered alumina carrier materials for their use as a support for different catalytic reactions [18,19] as well as their physicochemical characteristics [18,19,80];
- new possibilities of carbon–mineral adsorbents in the adsorption processes from solution in which favourable properties of both, carbon and mineral components are used [81].

Only some of the interesting publications are mentioned above. Those and future works require a different approach to complex adsorbents/catalysts from that presented in this papers which will be a subject of further investigations.

REFERENCES

1. R.Leboda, Mater. Chem. Phys., 31(1992)243.
2. R.Leboda, Mater. Chem. Phys., 34(1993)123.
3. Yu.I.Tarasevich, Khimiya i Tekhnol. Wody, 9(1989)699.
4. K.Kamegawa, H.Yoshida, Bull. Chem. Soc. Jpn., 63(1990)3683.
5. K.Kamegawa, H.Yoshida, J. Colloid. Interface Sci., 159(1993)324.
6. T.Kyotani, N.Sonobe, A.Tomita, Nature, 331(1988)331.
7. N.Sonobe, T.Kyotani, A.Tomita, Carbon, 29(1991)61.
8. N.Sonobe, T.Kyotani, A.Tomita, Carbon, 28(1990)483.
9. N.Sonobe, T.Kyotani, A.Tomita, Carbon, 26(1988)573.
10. N.Sonobe, T.Kyotani, Y.Yoshihiro, M.Shiraishi, A.Tomita, J.Phys.Chem., 92(1988)7029.
11. V.B.Fenelonov, L.G.Okkel, Zhurn. Fiz. Khimii, 67(1993)2095.
12. T.J.Bandosz, K.Putyera, J.Jagiełło, J.A.Schwarz, Carbon, 32(1994)659.
13. T.J.Bandosz, J.Jagiełło, K.A.G.Amankwah, J.A.Schwarz, Clay Minerals, 27(1992)435.
14. T.J.Bandosz, J.Jagiełło, B.Andersen, J.A. Schwarz, Clay Minerals, 40(1992)306.
15. T.J.Bandosz, K.Putyera, J.Jagiełło, J.A.Schwarz, Microporous Materials, 1(1993)73.
16. T.J.Bandosz, S.Gomez-Saleras, K.Putyera, J.A.Schwarz, Microporous Materials, 3(1994)177.
17. K.Putyera, T.J.Bandosz, J.Jagiełło, J.A.Schwarz, Clay and Clay Minerals, 42(1994)1.
18. J.P.R.Vissers, F.P.M.Merex, S.M.A.Bouwens, V.H.J.de Beer, R.Prins, J. Catal., 114(1988)291.
19. J.Boumgart, Y.Wang, W.R.Ernst, J.D.Carruthera, J. Catal., 126(1990)477.
20. E.Fitzer, K.Mueller, W.Schaefer, in: P.L.Walker, Jr.(ed.), Chemistry and Physics of Carbon, vol.7, Marcel Dekker, New York, p. 237.
21. R.A.Buyanov, Coking of Catalysts, Nauka, Novosibirsk, 1983 (in Russian).
22. A.Gierak, R.Leboda, J.Chromatogr., 486(1989)197.
23. A.Gierak, R.Leboda, Chem. Anal. (Warsaw), 32(1987)957.
24. M.Jaroniec, R.Madey, Physical Adsorption on Heterogeneous Solids, Elsevier, Amsterdam, 1988.
25. W.Rudziński, D.H.Everett, Adsorption of Gases on Heterogeneous Surfaces, Academic Press, New York, 1992.
26. R.Leboda, Chromatographia, 9(1980)549.
27. R.Leboda, A.Łodyga, J.Anal.Appl.Pyrol., 14(1988)203.
28. R.Leboda, S.Sokołowski, A.Łodyga, A.N.Korol, Teoret. i Eksperim. Khimiya, 6(1990)698.
29. A.Waksmundzki, J.Toth, M.Jaroniec, W.Rudziński, Ann.Soc.Chim.Pol., 49(1975)1003.

30. R.Leboda, Chromatographia, 11(1980)703.
31. R.L.Mendyk, A.Łodyga, Polish J.Appl. Chem., 32(1988)423.
32. R.Leboda, J.Skubiszewska, E.Mendyk, A.N.Korol, Chem. Anal. (Warsaw), 30(1985)737.
33. R Leboda, Chem. Anal. (Warsaw), 25(1980)783.
34. R.Leboda, Chem. Anal. (Warsaw), 25(1980)979.
35. A.Gierak, R.Leboda, Mater.Chem.Phys., 19(1988)503.
36. A.Gierak, E.Tracz, R.Leboda, J.Anal.Appl.Pyrol., 13(1988)89.
37. W.Rudziński, A.Gierak, R.Leboda, A.Dąbrowski, Fresenius Z.Anal.Chem., 352 (1995)667.
38. A.Gierak, F.Czechowski, R.Leboda, Mater.Chem.Phys., 36(1994)264.
39. R.Leboda, A.Gierak, P.Grochowicz, Ochrona Środowiska (Wrocław), Nos.2-3(1987)61.
40. R.Leboda, J.Skubiszewska-Zieba, V.V.Sidorchuk, V.A.Tertykh, V.I.Zarko, J.Non-Cryst.Solids, in press.
41. R.Leboda, P.Grochowicz, A.Łodyga, A.Gierak, Polish J.Appl.Chem., 36(1992)123.
42. A.Gierak, R.Leboda, in: Postepy chromatografii w Polsce w ostatnich latach. Mater. Symp., UMCS, Lublin, 1984, p. 145.
43. A.V.Kiselev, Ya.I.Yashin, Gas-adsorption Chromatography, Nauka, Moscow, 1967 (in Russian).
44. A.Di Corcia, A.Liberti, in: Advances in Chromatography, M.Dekker, New York, 1976, vol.14, p.305.
45. A.Di Corcia, A.Liberti, in: Advances in Chromatography, A.Zlatkis (ed.), University of Houston, 1973, p.25.
46. A.V.Kiselev, Ya.I.Yashin, Gas- and Liquid-Adsorption Chromatography, Khimiya, Moscow, 1979 (in Russian).
47. R.Leboda, A.Łodyga, A.N.Korol, Zhurn. Anal. Khimii, 45(1990)711.
48. K.M.Champion, G.D.Halsey, J.Phys.Chem., 57(1953)646.
49. G.Briegleb, Elektron-Donator-Acceptor-Komplexe, Springer-Varlag, Berlin, 1961.
50. R.P.Rostagi, Indian J. Chem., 8(1970)541.
51. G.Briegleb, Zwishchenmolecular Kraefte, Verlag Braun, Karlsruhe, 1949.
52. T.Czajkowska, J.Chromatogr., 241(1982)9.
53. J.C.Neniker, Rev.Mol.Phys., 21(1949)322.
54. D.E.Martire, R.L.Pecsok, J.H.Purnell, Trans.Faraday Soc., 61(1965)2496.
55. V.G.Berezkin, J.Chromatogr., 65(1972)227.
56. V.V.Turov, R.Leboda, V.I.Bogillo, J.Skubiszewska-Zieba, Langmuir, 11(1995)935.
57. V.V.Turov, R.Leboda, V.I.Bogillo, J.Skubiszewska-Zieba, Langmuir, submitted for publication.
58. R.Leboda, Mater.Chem.Phys., 27(1991)189.
59. R.Leboda, A.Gierak, B.Charmas, A.Łodyga, React.Kinet.Catal.Lett., 50(1993)63.
60. M.M.Dubinin, Carbon, 21(1983)359.
61. M.M.Dubinin, H.F.Stoeckli, J. Colloid Interface Sci., 75(1980)34.
62. I.A.Tarkovskaya, Oxidated Coal, Naukova Dumka, Kiev, 1981 (in Russian).
63. R.Leboda, Chromatographia, 14(1981)524.
64. R.Leboda, Inżynieria chemiczna i procesowa, 3(1982)343.
65. R.Leboda, V.V.Sidorchuk, J.Skubiszewska-Zieba, Mater.Chem.Phys., 39(1994)136.

66. I.E.Neimark, Synthetic Mineral Adsorbents and Catalyst Carriers, Naukova Dumka, Kiev, 1982 (in Russian).
67. R.Leboda, Polish J.Chem., 54(1980)2305.
68. R.Leboda, J.Skubiszewska, B.Buszewski, Chem. Anal. (Warsaw), 29(1984)267.
69. V.A.Tertykh, L.A.Belyakova, Chemical Reaction Involving Silica Surface, Naukova Dumka, Kiev, 1991 (in Russian).
70. Modified Silicas in Sorption, Catalysis and Chromatography, G.V.Lisichkin (ed.), Khimiya, Moscow, 1986 (in Russian).
71. R.Leboda, S.Sokołowski, J.Skubiszewska, Annales UMCS, 36(1981)1.
72. R.Leboda, A.Gierak, E.Mendyk, A.Lichaczewski, Polish J. Appl. Chem., 32(1988)219.
73. C.I.Brinker, G.W.Scherer, Sol-Gel Science: The Physics and Chemistry of Sol-Gel Processing, Academic Press, San Diego, 1990.
74. H.P.Bohem, Hig.Temp.-High Pressures, 22(1990)275.
75. R.Leboda, A.Waksmundzki, Chromatographia, 4(1979)207.
76. R.Leboda, Chem. Anal. (Warsaw), 25(1980)979.
77. A.Gierak, R.Leboda, Chem. Anal. (Warsaw), 33(1988)735.
78. R.Leboda, Polish J.Appl.Chem., 32(1988)229.
79. R.Leboda, J.Skubiszewska, E.Mendyk, Chem. Anal. (Warsaw), 30(1985)615.
80. C.A.Leon y Leon, A.W.Sarini, L.R.Radovic, J. Colloid. Interface Sci., 148(1992)1.
81. Yu.I.Tarasevich, E.A.Nechaev, K.M.Rudenko, L.G.Ivanova, B.M.Kats, Kolloid Zhurn., in press.

A. Dąbrowski and V.A. Tertykh (Editors)
Adsorption on New and Modified Inorganic Sorbents
Studies in Surface Science and Catalysis, Vol. 99

Chapter 1.6
Solid-phase hydrosilylation reactions with participation of modified silica surface

V.A.Tertykh and L.A.Belyakova

Institute of Surface Chemistry, National Academy of Sciences of the Ukraine,
252022 Kiev, Ukraine

1. INTRODUCTION

The development of methods of producing chemical compounds on silica surface (chemical modification of surface) is essential for the creation of new highly specific adsorbents, selective heterogeneous catalysts, active fillers of polymeric materials, effective thickeners of dispersive media. Of prime importance for many practical applications of modified silicas is hydrolytic and chemical stability of surface chemical compounds. For example, the chemical compounds formed upon the interaction between silanol groups and alcohols by the reaction:

$$\equiv SiOH + ROH \longrightarrow \equiv SiOR + H_2O$$

are bound to the surface by Si–O–C bonds which are easily splitted under the action of water especially in acidic and basic media. At the same time, modifying coating should rather often possess a high hydrolytic stability providing a basis for the long–term and repeated use of modified matrices without the deterioration of properties. In this respect, surface chemical compounds with Si–C bonds have obvious advantages.

The method most frequently applied for producing such compounds involves using the appropriate halo– or alkoxyorganosilanes, organosilazanes or organosiloxanes for the chemical modification of silica surface [1]. In this case the Si–C bond is not formed on the surface, but is introduced into a modifying layer together with a molecule of a previously synthesized organosilicon compound which already has the Si–C bond, for example :

$$\equiv SiOH + XSi(CH_3)_3 \longrightarrow \equiv SiOSi(CH_3)_3 + HX$$

where X is a halogen, alkoxy or other group reactive with respect to surface silanol groups.

Side by side with this, the application of organosilicon compounds where organic radicals are bound to silicon atoms through Si–C bonds for chemical modification is in very many cases hampered by the absence of a corresponding modifier or by its low reactivity relative to surface sites. As a consequence, of great importance is the development of methods of the synthesis of surface chemical compounds with Si–C bonds directly on silica surface.

This work considers the state of the art with reference to the problem of the synthesis of surface chemical compounds with Si–C bonds directly on silica surface with the main accent being given to reactions of solid-phase hydrosilylation. In recent years the major regularities of such processes were the subject of numerous researches and the results obtained allow us to classify the solid-phase hydrosilylation reaction as the basis for promising methods of chemical modification of silica surface.

2. EVOLUTION OF RESEARCHES INTO THE SYNTHESIS OF COMPOUNDS WITH Si–C BONDS DIRECTLY ON SILICA SURFACE

The data obtained in the field of producing surface chemical compounds with Si–C bonds directly on silica surface may be classified into three main groups:
- reactions of the previously chlorinated silica surface with the Grignard reagent and other organometallic compounds;
- reactions of the previously chlorinated silica surface with benzene in the presence of aprotic acids;
- addition reactions of unsaturated compounds through ≡SiH groups attached to silica surface (solid-phase hydrosilylation).

2.1. Reactions of the chlorinated silica with organomagnesium and organolithium compounds

Though the first organosilicon compounds with Si–C bonds were prepared [2] using organic compounds of zinc and mercury, for example:

$$SiCl_4 + 2Zn(C_2H_5)_2 \longrightarrow Si(C_2H_5)_4 + 2ZnCl_2$$

it is organomagnesium compounds that are the most commonly used for this purpose. F.Kipping succeeded in synthesizing a great number of organosilicon compounds making use of the Grignard reagent according to the general scheme:

$$SiX_4 + RMgX^1 \longrightarrow RSiX_3 + MgXX^1$$

where X and X^1 are halogen atoms and R is an organic radical.

In the early 1960's Deuel [3], Spenser and Gieseking [4] were the first to show the possibility of effecting this reaction on the chlorinated montmorillonite surface. At the first stage of the process the mineral surface was treated with thionyl chloride :

$$\equiv SiOH + SOCl_2 \longrightarrow \equiv SiCl + HCl + SO_2$$

then the ≡SiCl groups attached to the surface entered into the reaction with ethyl- [3] or phenyl magnesium bromide [4]:

$$\equiv SiCl + RMgBr \longrightarrow \equiv SiR + MgBrCl \quad (R = C_2H_5, C_6H_5)$$

Deuel [3] pointed the principal possibility of bringing about similar reactions on the silica gel surface previously chlorinated with $SOCl_2$ or $SiCl_4$. The surface chemical compounds formed have a high hydrolytic stability. According to the data of Ref.[4] even the

boiling in 35% aqueous solution of KOH for 30 minutes failed to remove completely all the attached phenyl groups.

In conformity with some sources [3,5] when considering the reactions with the Grignard reagent it is necessary to allow for the breaking of the lattice siloxane bonds:

$$\equiv SiOSi\equiv + RMgBr \longrightarrow \equiv SiR + \equiv SiOMgBr$$

though such a reaction is more characteristic of organolithium compounds.

The reaction of the chlorinated silica with the Grignard reagent was also used for the synthesis of various organosilicas [6–10].

The organolithium reagents for producing organosilicon compounds with Si–C bonds were proposed by Gilman and Massie [11]. In accordance with Refs.[12–17] phenyl and butyl lithium were used for reactions with the chlorinated silica:

$$\equiv SiCl + RLi \longrightarrow \equiv SiR + LiCl \quad (R = C_4H_9, C_6H_5)$$

The formation of the grafted phenyl groups under the action of phenyl lithium on the chlorinated silica gel was corroborated by IR absorption spectra [12–17] and chemical analysis data [15]. The analysis performed showed [15] that on the surface of the chlorinated matrix with the $\equiv SiCl$ group content of 0.85 mmol/g with the help of phenyl lithium it is possible to attach phenyl groups up to 0.73 mmol/g. The silica modified in this way was treated with 4N KOH, and the data obtained showed that the treatment involved the formation of phenylpolysiloxane in the solution [12–14]. The phenyl groups attached to the surface can be subjected to sulfonation [14] and nitration with the subsequent followed by the reduction of nitro groups and diazotization [18]. The reactions of organolithium compounds with the chlorinated silica were used for attachment of pyridine [8] and long–chain hydrocarbon radicals [19].

Boehm and his co–authors [15,17] paied attention to the fact that C_4H_9Li and C_6H_5Li could also react with the starting silica surface to form attached n–butyl and phenyl groups (0.04–0.13 mmol/g). In all probability, this occurs due to the breaking of siloxane bonds on the silica matrix surface:

$$\equiv SiOSi\equiv + RLi \longrightarrow \equiv SiR + \equiv SiOLi$$

Indeed, from the IR spectroscopy data by Chmielowiec and Morrow [9] it follows that C_4H_9Li is chemisorbed on the starting silica, and after the hydrolysis of a modified sample the absorption in the range of the O–H stretching vibrations increases but the absorption in the range of ν_{CH} does not change. The possibility of the addition of organolithium compounds through siloxane bonds should be taken into account when using such compounds for determining the silanol groups concentration on the silica surface.

The serious disadvantage of the use of the reactions of the chlorinated silica with organometallic compounds is caused by the high sensitivity of the Grignard reagent and organolithium compounds to the action of water, side reactions with the participation of surface siloxane bonds, and problems of removing metallic impurities from the surface of modified matrices. The difficulties mentioned explain why this approach to the synthesis of surface chemical compounds with Si–C bonds finds limited application.

2.2. Reactions of the chlorinated silica with benzene in the presence of Lewis acids

Earlier, the attempts to effect reactions of hydrocarbons and silicon compounds with Si–Cl bonds in the presence of $AlCl_3$ and other aprotic acids (Friedel–Crafts reactions) were successful only at high temperatures and pressures. Thus, the reaction with benzene according to scheme:

$$C_6H_6 + SiCl_4 \xrightarrow{AlCl_3} C_6H_5SiCl_3 + HCl$$

proceeds at 300–350°C and pressure $3.65 \cdot 10^6$ Pa [2]. Saturated hydrocarbons interact with $SiCl_4$ according to this scheme under even more severe conditions [2].

Meanwhile, in the study by Deuel [3] it was already reported that he succeeded in effecting the Friedel–Crafts reaction on the chlorinated montmorillonite surface:

$$\equiv SiCl + AlCl_3 + C_6H_6 \longrightarrow (\equiv Si^+C_6H_6 \cdots AlCl_4^-) \longrightarrow \equiv SiC_6H_5 + AlCl_3 + HCl$$

It was pointed out that many phenyl groups were formed on the sample surface. This might result from the destruction of the mineral structure and the appearance of new reactive sites on the surface. Owing to the efforts mainly by Deuel and his co–workers [3,12,14,20-24] the interest to this reaction was held for several years but then suddenly waned. The formation of the grafted phenyl groups was verified by the IR absorption spectra, DTA and chemical analysis data, the possibility of sulfonation of grafted groups with chlorosulfonic acid, the stability of surface compounds under the action of solvents, acids and alkalis, the variation of adsorption properties of modified matrices. As follows from the data presented in Ref.[21], the reaction proceeds under unusually mild conditions (70°C). It was also established that the increase of the $AlCl_3$ content (from 0.06 to 0.30 g per 1g of the chlorinated mineral) led to the increase of the carbon concentration in surface compounds (from about 3.6 to 19% wt.).

Effecting the Friedel–Crafts reaction in a surface layer of silicas (especially under mild conditions) is of a considerable practical interest. However, there is doubt as to such a sharp difference in the temperature conditions of the proceeding of processes for individual silicon compounds and $\equiv SiCl$ groups on silica surface. It is well known that C–Cl and Si–Cl bonds differ substantially both in the sensitivity to the action of nucleophilic reagents (due to a higher effective charge of a silicon atom in comparison with a carbon atom) and in the degree of ionization and binding energy. It is these differences that, most likely, lead to the situation when the Friedel–Crafts reaction through C–Cl bonds (including these bonds in the structure of organosilicon compounds) proceeds under substantially milder conditions than through Si–Cl bonds. On account of this the possibility of effecting the Friedel–Crafts reaction on the chlorinated silica surface and the mechanism and optimum conditions for its proceeding need further studies.

2.3. Reactions of solid–phase hydrosilylation

The synthesis of compounds with Si–C bonds often involves the hydrosilylation reaction consisting in the addition of unsaturated organic compounds through Si–H bonds under the action of catalysts and heat [2]. It has been specially pointed out [25,26] that effecting such a reaction on silica surface is of indubitable interest for producing surface chemical

compounds with Si–C bonds. The proceeding of the process according to the scheme:

$$\equiv SiH + CH_2 = CHR \longrightarrow \equiv SiCH_2CH_2R$$

where R is a suitable organic radical with various functional groups, can be regarded as a hydrosilylation reaction in which the modified silica matrix containing ≡SiH groups acts as a heterogeneous hydrosilylating agent. This kind of reactions where one of the interacting participants is fixed on a solid surface should be classified as solid–phase hydrosilylation processes. It is also known that there hydrosilylation reactions proceeding with the participation of catalysts supported on a solid matrix and of suitable hydrosilanes and olefins in a liquid phase. However, the surface chemical compounds with Si–C bonds can be obtained only in the case when silicas with attached ≡SiH or olefin groups are used. Though separate attempts to carry out solid–phase hydrosilylation processes were made as early as 1952 by Wagner and Pines [27], the detailed consideration of such reactions and their use for chemical modification of silica surface became possible only recently. Before discussing the results of researches into characteristics of solid–phase hydrosilylation reactions it is expedient to analyze briefly the experience gained in the field of the production of modified silica matrices bearing attached silicon hydride and olefin groups.

3. SILICA MATRICES WITH ATTACHED ≡SiH GROUPS

3.1. Polyhydrosiloxanes

The first silica matrices bearing ≡SiH groups were prepared as a result of the hydrolysis of trichloro– and triethoxysilane in organic solvents. Wagner and Pines [27] carried out the hydrolysis of $HSiCl_3$ in mixtures containing benzene, ether or dioxane and obtained polyhydrosiloxane whose general formula is $(HSiO_{3/2})n$, specific surface area amounts to about 200 m^2/g, and content of ≡SiH groups reaches 91.5% of the theoretical value. Muller [28,29] was the first to describe production of polyhydrosiloxane by hydrolysis of $HSi(OC_2H_5)_3$. Adsorption and reduction properties of polyhydrosiloxane xerogels prepared by hydrolysis of $HSi(OC_2H_5)_3$ were later considered in detail in series of papers by Slinyakova, Budkevich, Neimark and their co–authors [30–41]. Matrices have been obtained with a hydrogen content of ≡SiH groups of 1.82% wt. which is close to a predicted value under the assumption that every silicon atom of the space network is bound to a hydrogen atom. It has been shown [35] that the porous structure of polyhydrosiloxane xerogels which is created by contacting globules can be formed depending on the intermicellar liquid nature. The adsorption of methanol and water vapours on polyhydrosiloxane decrease in comparison with silica gel having a similar surface area and analogous porous structure. At the same time the adsorption of hexane vapours is practically the same for both adsorbents [30]. As compared to silica gel in the case of polyhydrosiloxane the adsorption of acetone, dioxane and benzene from solutions in hexane as well as the adsorption of benzene, nitrobenzene, benzaldehyde, phenol, and chlorobenzene from solutions in CCl_4 substantially decreases [36]. The data [33] on the adsorption of acetic, propionic, butyric, and valeric acids from their aqueous solutions give evidence for a highly organophilic nature of polyhydrosiloxane adsorbents.

The stretching vibrations of Si–H in polyhydrosiloxanes are related to the IR absorption band at 2260 cm^{-1} [42]. According to the data of Refs.[31,37] the heating of polyhydrosiloxane in the air at 265°C leads to a decrease in the content of ≡SiH groups by about 50%, and as a result of the oxygen addition one can observe an increase in the adsorbent mass. However, in the case of the heating at 230°C the oxidation of ≡SiH groups does not occur yet. The heating of polyhydrosiloxanes under vacuum [38] above 200°C is accompanied by the evolution of atomic hydrogen, and the gaseous phase exhibits the formation of monosilane SiH_4 already at 230°C.

One of the interesting characteristics of polyhydrosiloxaness is the presence of pronounced reduction properties. From the data by Muller [28,29] polyhydrosiloxane reduces salts of mercury, copper, and gold as well as organic dyes. Besides, he reported that in presence of fluorine ions the reduction is accelerated. Wagner and Pines [27] observed the reduction of Ag^+ and palladium salts to corresponding metals and of the MnO_4^- anion to MnO_2. Budkevich et al. [32] showed that when polyhydrosiloxanes are in contact with aqueous solutions of salts of various metals the cations in terms of their ability to be reduced on adsorbent surface are arranged in the order similar to the sequence of the arrangement of metals according to the value of their electrode potential in electrolytic solutions. Thus, in the case of salts of potassium, sodium, zinc and cobalt the reduction of metals was not observed; for salts of nickel, lead, and copper one can observe a partial reduction of metals which is discontinued upon acidification of solutions. For salts of palladium, platinum, silver, and mercury the reduction of metals occurs even in highly acidic solutions, for example:

$$\equiv SiH + Hg^{2+} + H_2O \longrightarrow \equiv SiOH + Hg + 2H^+$$

This reaction makes the basis for the application of polyhydrosiloxanes for purifying waste waters of mercury [42–44].

Wagner and Pines [27] effected the first reactions of polyhydrosiloxane with some alkenes. It was shown that the reaction can proceed according to the scheme:

$$HSiO_{3/2} + RCH = CH_2 \longrightarrow RCH_2CH_2SiO_{3/2}$$

The reaction with ethylene and cyclohexene was effected at 350°C or above and that with 1–pentene at 80°C in the presence of benzoyl peroxide. Though the degree of the ≡SiH group participation in this reaction was not high (3–6% of the ≡SiH group number) [27], in essence it was the first successful attempt to effect a solid–phase hydrosilylation reaction.

3.2. Silicas with a deposited layer of polyhydrosiloxane

Wagner and Pines [27] carried out the hydrolysis of trichlorosilane on the previously wetted silica surface with a specific surface area of about 300 m^2/g and obtained samples containing from 7.4 to 16.7 % wt. of $HSiO_{3/2}$. The surface of the silica modified in this way exhibits properties inherent in polyhydrosiloxane, namely hydrophobic nature, ability to evolve hydrogen under the action of an alkali, to reduce silver ions and other ions, and to add alkenes at high temperatures (about 450°C). Thus, in the case of the silica surface with a deposited layer of polyhydrosiloxane the chemisorption of ethylene, pentene, octene, cyclohexene, and butadiene has been carried out.

The authors of Refs. [45,46] performed the hydrolysis of triethoxysilane in a surface layer of various silicas with a specific surface area from 90 to 375 m^2/g and average pore diameter from 38.5 to 9.0 nm making suitable selection of solvents, amounts of water, and catalytic amounts of 0.1 M HCl so as to deposit a monolayer of ≡SiH groups on the surface. It is assumed that the produced silanetriol $HSi(OH)_3$ condenses with the silica silanol groups forming polyhydrosiloxane coating chemically bound with the surface. At the same time, as follows from the IR absorption spectra [46] a substantial part of silanol groups is retained in the modifying coating. The attained concentrations of attached ≡SiH groups (8–18 $\mu mol/m^2$) are significantly higher than the amounts of isolated silanol groups on the starting silica surface as might be inferred in the case of the formation of a polymeric siloxane film. The solid-state NMR spectra of modified silica on ^{29}Si nuclei with cross-polarization and magic angle spinning display signals at –84 and –74 ppm due to $HSi^*(OSi\equiv)_3$ [47] and, most probably, to $HSi^*(OH)(OSi\equiv)_2$. The same chemical shifts are also observed in the NMR spectra of a pure polyhydrosiloxane produced by the acid hydrolysis of triethoxysilane. Although the process of the silanetriol polymerization in a silica surface layer is rather difficult to control, Chu et al.[46] succeeded in producing hydride-modified silicas practically with a monolayer coating. The evidence for it is the fact that when using moderate amounts of triethoxysilane for the hydrolysis the specific surface area and pore sizes of the starting and modified silica matrices differs slightly. The ≡SiH group content in such dense monolayers of chemically bound polyhydrosiloxane is 8–10 $\mu mol/m^2$. Characteristically, similar ≡SiH group contents in a monolayer (10 $\mu mol/m^2$) were also measured by Baigozhin, Sergeev and Fattakhov [48,49] when treating the surface of optical glasses with solutions of $HSiCl_3$ in benzene. According to the data of Ref.[46] the optimum conditions for the formation of monolayer films involve the use of dioxane as a solvent, the HCl solution concentration of about 0.1 M, reaction time of 1– 2 hr, reaction temperature of 101°C (corresponding to a gentle reflux). In this case the reaction is carried out by slow (dropwise) addition of a triethoxysilane / dioxane solution into a silica / dioxane suspension containing an aqueous catalyst solution. In all probability, a similar procedure of the polyhydrosiloxane film formation may be extended to surfaces of other inorganic oxides as well.

At the same time a more reliable control over the process of the polyhydrosiloxane film formation on the surface is possible through sequential treatments of silica with vapours of $HSiCl_3$ and water. The modification – hydrolysis procedures, when repeated many times, lead to the formation of polyhydrosiloxane coverings with different ≡SiH group contents on the silica surface. The procedure of this kind, conventionally referred to as the molecular layering method, was applied by the authors of Refs.[25,50–55] for manufacturing hydride-modified silica matrices. For example, in accordance with the data of Koltsov, Kuznetsova, Aleskovskii [52] a large-porous silica gel (260 m^2/g) dried at 180°C and treated at this temperature with $HSiCl_3$ vapours in a dry nitrogen flow after the removal of hydrogen chloride and of the excess of trichlorosilane has the surface with a ≡SiH group content of 8 $\mu mol/m^2$. The subsequent procedure *hydrolysis of surface compounds / modification with* $HSiCl_3$ *vapours* results in the formation of a product whose content of silicon hydride groups amounts to 10 $\mu mol/m^2$. In the final cycle of the hydrolysis / modification procedure the authors of Ref.[52] succeeded in attaching additional silicon hydride groups to surface increasing their content by about 1 $\mu mol/m^2$.

It is interesting that approximately the same content of silicon hydride groups on the

silica surface was also achieved by Wagner and Pines [27], and in this case the silica (300 m^2/g, 100 g) after the wetting with water (8 cm^3), treatment with an excess amount of $HSiCl_3$, and evacuation has a silicon hydride group content of about 9–10 $\mu mol/m^2$. In all likelihood, these figures are rather close to those in the case of a monolayer, if it is assumed that the surface area per one fragment of $HSiO_{3/2}$ is equal to 0.122 nm^2.

3.3. Introduction of ≡SiH groups by chemisorption of silanes of various structures

The widest application for the synthesis of silicas with attached ≡SiH groups is enjoyed by methods of chemical modification of surface with various silanes.

Besides the above-mentioned researches into the hydrolysis of $HSiCl_3$ in a surface silica layer [27,45,46,48,49] and reactions of molecular layering [25,50–55] there are many studies designed to establish the mechanism of chemisorption of trichlorosilane, to elucidate the structure of the formed surface compounds and their behaviour at elevated temperatures and in the subsequent chemical transformations [25, 56–65]. It was shown by Chuiko et al. [25] that on the surface of aerosil prepared at 400°C and above $\equiv SiOSi(H)Cl_2$ groups are predominantly formed since the distance between free silanol groups is about 0.7 nm, and, consequently, the simultaneous participation of two Si–Cl bonds in the reaction is unlikely. After the silica modified in this way has been treated with water vapours at low temperatures, approximately a half of the closely spaced silanol groups is condensed and the remaining surface hydroxyls can enter into the subsequent chemical reactions. As for the case when the silica bearing on the surface $\equiv SiOSi(H)Cl_2$ groups has been subjected to a treatment with vapours of ethyl alcohol, one observes the formation of diethoxysilyl groups [56]. The complex processes proceeding during the reaction of ammonia with trichlorosilylating silica have been already considered in a number of references [58,64,65].

According to data of Refs.[50–53] after the reaction of trichlorosilane with the surface of hydrated silica prepared at moderate temperatures the ratio of chlorine and hydrogen contents (Cl : H) in surface compounds is 1 : 1. The authors of Refs.[50–53] are of the opinion that this result gives evidence for the fact that one molecule of $HSiCl_3$ reacts with two closely spaced surface silanol groups:

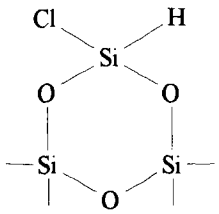

At the same time there are spectroscopic data as well as results of chemical analyses and researches on the kinetics of reactions with chlorosilanes [1] which give evidence for the fact that during the chemisorption of $HSiCl_3$ on the hydrated silica one observes, most probably, the predominant formation of surface compounds with the following structure:

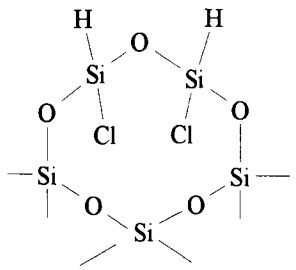

In this case the Cl : H ratio in the surface compounds is 1:1; the chemisorption value obtained is determinated by the isolated silanol groups content, and the decrease in the activation energy for the process on the hydrated surface is related to the participation of coordinately bonded water (3550 cm^{-1}) in this reaction.

The comparison of activities of $HSiCl_3$, methyldichlorosilane, and dimethylchlorosilane with respect to surface silanol groups showed [25] the decrease in the activity of the above-mentioned modifying reagents as additional methyl groups are introduced into the structure of the molecule. The high sensitivity of the Si–H stretching vibrations band to the nature of substituents at a silicon atom manifests itself clearly during the chemisorption of the mentioned organosilanes [25]. Later on this effect was employed in Refs.[56–60,64–69] for establishing the structure of the formed surface compounds.

When using silicas prepared under vacuum at 400°C, after the modification with vapours of methyldichlorosilane and hydrolysis of surface compounds Chuiko et al. [25] observed a practically complete condensation of the formed silanol groups:

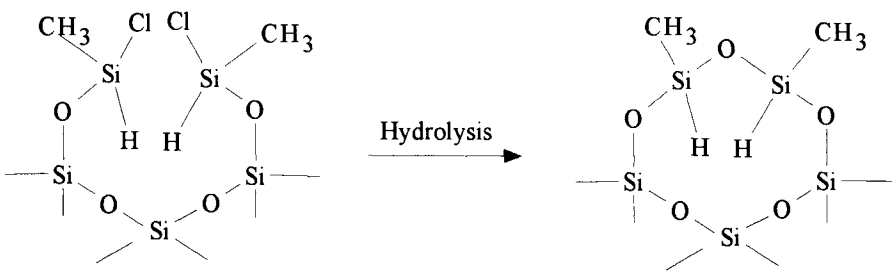

The highly characteristic and symmetric shape of the absorption band attributed to the Si–H stretching vibrations and its sufficiently convenient position in the spectral region (2100 – 2300 cm^{-1}) make it possible to apply IR spectroscopy for the quantitative determination of the ≡SiH groups on the hydride-modified silica surface as it was proposed by Sobolev, Tertykh, and Chuiko [54]. Yoshinaga et al. [70] proposed to use the band ν_{SiH} for determining the concentration of free silanol groups on the silica surface. In order to do it at first the chemisorption of dimethylchlorosilane on the surface was effected. The reaction was carried out in dry chloroform in the presence of triethylamine and these conditions the chemisorption of $ClSi(CH_3)_2H$ proceeded at room temperature. Then they determined the content of ≡SiH groups (2148 cm^{-1}) by the diffuse reflectance FTIR spectroscopy.

The introduction of dimethylsilyl groups into a surface layer is easily carried out at room temperature when using dimethyl(dimethylsilyl)amine $H(CH_3)_2SiN(CH_3)_2$ as well [71]. Golding, Barry and Burke [72] synthesized ethyl–, octyl–, and octadecyldihydrochlorosilanes, and it showed that the mentioned reagents are chemisorbed on the silica surface to a considerably greater extent than the similar alkyldimethylchlorosilanes. Really, in conformity with the data by Meiouet et al. [73] the achieved silica surface coverages with organic groups when using $C_8H_{17}Si(CH_3)_2Cl$ and $C_8H_{17}SiH_2Cl$ amount to 2.68 and 4.24 $\mu mol/m^2$ respectively.

Besides the researches on the triethoxysilane hydrolysis on the silica surface which were discussed earlier [45,46], there are studies [56,69,74] concentrating upon the chemical reactions of $HSi(OC_2H_5)_3$ with silanol groups. It was established by Petrova, Tertykh, and Pavlov [56] that this chemical reaction is accelerated not only in the presence of organic bases but also in the case of the introduction of hydrogen chloride into the reaction volume. The possible causes of the catalytic effect of electron– and proton–donors on the proceeding of chemical reactions in a silica surface layer has been discussed in more detail in our monograph [1].

The introduction of $\equiv SiOSiH_3$ groups (2217 cm^{-1}) to the silica surface for the reaction of silanol groups with SiH_4 at 250°C was discussed by Ganyuk [75]. In the case of higher temperatures (350°C) the formation of $=SiH_2$ groups was observed (2275 cm^{-1}). In Low's opinion [76] the wave number for Si–H bands in surface chemical compounds should also decrease in the order:

$\equiv SiH > =SiH2 > -SiH_3$

3.4. Reduction with inorganic hydrides

Hydride–modified silicas can be produces by reduction with an inorganic hydrides of a silica surface whose silanol groups have been previously converted to $\equiv SiCl$ groups. The same approach was proposed and implemented by Sandoval and Pesek [77] using a solution of lithium aluminum hydride in ether:

$$\equiv SiOH + SOCl_2 \longrightarrow \equiv SiCl + SO_2 + HCl$$

$$\equiv SiCl + LiAlH_4 \longrightarrow \equiv SiH + LiCl + AlH_3$$

The data by IR spectroscopy provide evidence for the fact that on the silica surface subjected to the chlorination and subsequent reduction, besides $\equiv SiH$ groups (2260 cm^{-1}) there are also $=AlH$ groups absorbing at somewhat lower wave numbers. The presence of aluminum and chlorine on the reduced silica surface is also corroborated by the ESCA data [77]. Surface alane species may be decomposed under the exposure to 0.1 M HCl for 1 hr. As follows from ESCA spectra the acid treatment removes aluminum, chlorine, and traces of organic groups from the surface. In investigating these phenomena Sandoval and Pesek [77] established an interesting fact related to the transformation of a part of alane groups into silane groups. It is appropriate to mention here that the formation of $\equiv SiH$ groups on the silica surface was observed by Mashchenko [78] and Gillis–D'Hamers et al.[79] during the treatment with diborane. The surface silane groups seem to appear as a result of the addition reaction of BH_3 through siloxane bridges:

$$\equiv SiOSi\equiv + BH_3 \longrightarrow \equiv SiH + \equiv SiOBH_2$$

As it was pointed out by the authors [77] themselves, a serious limitation of the chlorination / reduction method is its extreme sensitivity to moisture both at the chlorination and reduction steps resulting in time-consuming and labor-intensive procedures. Additionally, it is necessary to point out the potential difficulties associated with the presence of chemisorbed aluminum in reduced silicas.

3.5. Thermal destruction of methoxy groups

The formation of ≡SiH groups on the silica surface in the process of the vacuum thermal destruction of attached methoxy groups was observed for the first time by Morterra and Low [80–82]. The stretching vibrations of the Si–H bonds in compounds formed give the absorption band with a peak at 2300 cm^{-1}. The formation of the hydride compounds on the silica surface is related by Morterra and Low [81,82] to a possible homolytic breaking of Si–O bonds and the subsequent addition of hydrogen from gaseous products of pyrolysis. The formation of free radicals after the destruction of methoxysilica was also registered by ESR method [83]. At the same time the vacuum thermal destruction of attached ethoxy or butoxy groups does not detect the appearance of ≡SiH groups on the surface as it might be expected for similar homolytic processes (the breaking of Si–O bonds in $\equiv SiOC_2H_5$ and $\equiv SiOC_4H_9$ groups and addition of hydrogen from decomposition products). By the IR spectroscopy method [84] it was shown that during the destruction of ester compounds (beginning with C_2) the reduction of silanol groups and the release of a corresponding olefin occurred, for instance:

$$\equiv SiOC_2H_5 \xrightarrow{t^0} \equiv SiOH + CH_2 = CH_2$$

Chuiko et al. [84] made the assumption that the formation of such considerable numbers of ≡SiH groups during the destruction of methoxysilica is attributed not to homolytic reactions which scarcely characteristic of silicon compounds but to elimination processes, for example:

$$\equiv SiOCH_3 \xrightarrow{t^0} \equiv SiH + H - CHO$$

The mass spectrometric analysis of the evolved gas composition carried out by Brei et al. [85] detected most intensive lines corresponding to 28, 30, 31, and 2 amu (CO^+, H_2CO^+, and H_2^+) which is presumed by the proceeding of the methoxy group destruction in accordance with the scheme:

$$\equiv SiOCH_3 \xrightarrow{t^0} \equiv SiH + H - CHO \longrightarrow \equiv SiH + H_2 + CO$$

The calculations of potential energy surface profiles done in Ref.[85] showed as well that the main route of decomposition is consistent with the evolution of formaldehyde and upon a further temperature increase – with that of CO and H_2. However, it is not ruled out that at high temperatures of the grafted organic group destruction there are both heterolytic and homolytic processes.

4. SILICA MATRICES WITH ATTACHED OLEFINS

There are many methods that are used for the production of silica matrices with olefins attached through Si–C bonds. The widest application is enjoyed by the methods based

on reactions of surface chemical modification with appropriate chloro- or alkoxyorganosilanes containing vinyl, allyl, or other unsaturated hydrocarbon groups [7,86–101]. It was assumed [7,86, 89–95] that the attached olefin groups made the basis for one of the promising routes to form a bridge between applicable groups of polymeric macromolecules and silica filler surface. Really, in this case the authors of Refs.[7,86,89,90,93–95,101] observed a substantial improvement of physico-mechanical properties of polymeric systems filled with olefinorganosilicas. It was supposed [7, 93, 95] that the opening of double bonds during polymerization leads to the formation of a cross-linked polymer. Later on the results obtained by ESR method authors of Refs.[96,98] corroborated the conclusion that γ-irradiation provided the formation of free radicals stabilized by chemical bonds with surface.

In most cases in order to carry out chemical modification of surface it is advantageous to use vapours of suitable olefinorganosilanes or their solutions in organic solvents. When the surface treatment involves the application of aqueous solutions of vinyltriethoxysilane, for example, the deposited coatings often have non-reproducible properties which is due to the difficulties in controlling polymerization of the formed vinylsilanetriol [89,100,102–106]. In conformity to the data of Refs.[107,108] the application of vinyltrichlorosilane for chemical modification of silica provides higher contents of attached olefin groups than the treatment of hydrated surface with vinyltriethoxysilane.

The attachment of olefin groups through Si–C bonds can be also carried out with the aid of the reaction of the previously chlorinated silica surface with allylmagnesium bromide. For the first time the approach of this kind was employed by Neimark, Chuiko, and Slinyakova [7]:

$$\equiv SiCl + BrMgCH_2CH=CH_2 \longrightarrow \equiv SiCH_2CH=CH_2 + MgBrCl$$

Afterwards a similar approach was applied by Pesek and Swedberg [10] for grafting allyl groups to silica treated with thionylchloride. As shown in Refs. [7,109] grafted allyl groups as well as vinyl groups can be subjected to bromination with a bromine solution to form 1,2-dibromopropyl groups. As a result of the addition of HBr one observes the formation of grafted 2-bromopropyl groups [109].

Silicas with chemically attached C=C groups can be used as intermediate matrices for graft polymerization with appropriate functional olefins. Thus, the organosilicas with grafted carboxyl groups were produced due to the attachment of methacrylic acid [94,99] and maleic anhydride [110] to vinylsilica surface. Carboxyorganosilica can be obtained as well by the reaction of attached allyl groups with ozone [111]. A more strong cationite was produced with the aid of the addition of bisulfite through attached allyl groups in the presence of azobisizobutyronitrile as a catalyst [112]. A weak anion exchanger was obtained as a result of a catalytic addition of N-methylpyrrolidone to the same matrix [113]. Engelhardt et al. [114] prepared various matrices through addition of olefins with functional groups characterized by chirality or high anion-cation-exchanging properties to the vinyltrichlorosilane-modified silica surface. Besides, some experience has been gained to use attached olefin groups for hydrosilylation reactions. Thus, Stuurman, Kohler and Schomburg [115] applied a matrix with previously attached olefin groups in order to bind (in the presence of chloroplatinic acid) siloxane bearing a ≡SiH groups and quinine (Q) according to the scheme:

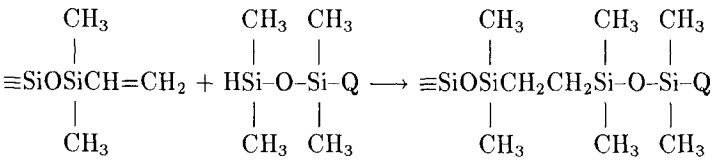

Pesek and Rashet [116] used attached allyl groups for the hydrosilylation reaction with dimethylphenylsilane in the presence of chloroplatinic acid. The conclusion about the grafting of phenyl groups was corroborated by IR spectroscopy. However, in most studies a hydrosilylation reaction is usually used to produce a suitable modifying reagent. In order to do it one can carry out a catalytic addition of an appropriate olefin to dimethylchlorosilane (see, for instance, Refs.[117,118]) and the reaction product with a necessary functional group is used for attachment to inorganic matrix surface.

Below we shall consider some experience acquired in carrying out reactions of catalytic and thermal solid-phase hydrosilylation with the participation of hydride-modified silicas, simple terminal olefins, and a number of functional compounds with double bonds.

The results presented provide strong evidence that the method based on the application of hydrosilylation reactions for producing hydrolytically stable Si–C bonds is very promising. The broad experience has been acquired in the field of the introduction of ≡SiH groups and olefin radicals into a surface layer of silica by various procedures. A large body of basis for carrying out systematic researches into the formation Si–C bonds on silica surface by catalytic and thermal hydrosilylation reactions. The results obtained during the last decade of the studies on the solid-phase hydrosilylation reactions with the participation of modified silica surface are discussed in Refs. [119–137].

5. RESEARCHES ON THE INTERACTION BETWEEN HYDRIDE–MODIFIED SILICAS AND SIMPLE TERMINAL OLEFINS

The interaction between hydride –modified silicas and simple terminal olefins C_6 – C_{18} (Table 1) was studied under conditions of liquid-phase catalytic reaction. The catalyst, namely 0.1N solution of H_2PtCl_6 in isopropyl alcohol (Speier catalyst), is the most active compound in homogeneous hydrosilylation processes [138]. The pyrogenic silicon dioxide (aerosil) with a specific surface area of 300 m^2/g as to methanol was used as a starting silica. Hydridesilica was produced by the interaction between dehydrated silica and methyldichlorosilane vapours in a vacuum cell with walls of CaF_2 glass (spectrophotometer IKS-29, LOMO, Russia, region 4000 – 1200 cm^{-1}; pressed silica plates, 10 – 15 mg/cm^2, compression pressure $1.72 \cdot 10^8$ Pa). The silica evacuated at 400°C for 3 hr (Fig.1, spectrum 1) was brought into contact with $Cl_2Si(CH_3)H$ vapours at 25 – 300°C and held for 2 hr. Then the excess of silane and gaseous reaction products were removed by evacuation at 300°C for 2 hr. The reaction is already initiated at 25°C, and effective chemisorption of methyldichlorosilane takes place at 300°C (Fig.1, spectrum 2). In this case the IR spectrum exhibits an absorption band at 2204 cm^{-1} attributed to the stretching vibrations of Si–H bonds and absorption bands attributed to asymmetric (2984 cm^{-1}) and symmetric (2931 cm^{-1}) stretching and bending (1400 cm^{-1}) vibrations of C–H bonds of methyl groups.

Table 1
Some physico-chemical parameters of simple terminal olefins and obtained values of attached C_nH_{2n+1}-group concentrations on silica surface as a result of the solid-phase catalytic hydrosilylation

1-Olefin	Molecular mass	$t_{boil.}$ (°C)	n_D^{20}	d_4^{20} (g/cm^3)	Obtained value of chemisorption C_nH_{2n+1}-group (μmol/m^2)
Hexene	84.16	63.4	1.3879	0.673	3.47
Octene	112.21	121.6	1.4087	0.712	3.01
Decene	140.26	170.6	1.4215	0.740	2.05
Tetradecene	196.36	243.0	1.4365		0.99
Hexadecene	224.42	274.0	1.4410	0.787	0.88
Octadecene	252.47	186.0*	1.4449	0.790	0.71

* at $2.7 \cdot 10^3$ Pa

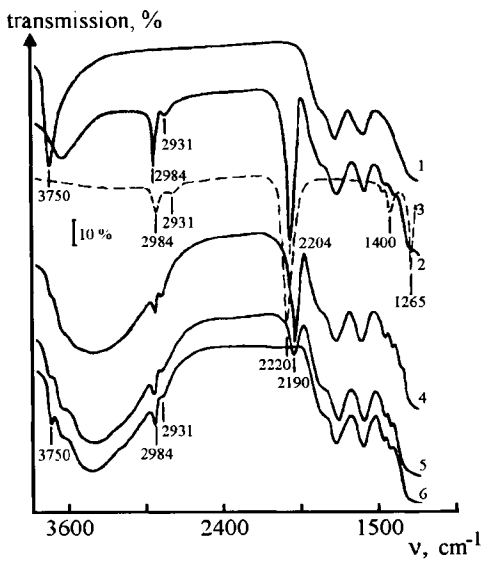

Figure 1. IR spectra of silica prepared under vacuum at 400°C for 3 hr (1), after the interaction with methyldichlorosilane at 300°C for 2 hr and evacuation at the reaction temperature (2), after contact with air at 25°C for 30 days (4), with water at 100°C for 1 hr (5), with water in the presence of H_2PtCl_6 at 100°C for 1 hr (6). (3)-IR spectrum of methyldichlorosilane.

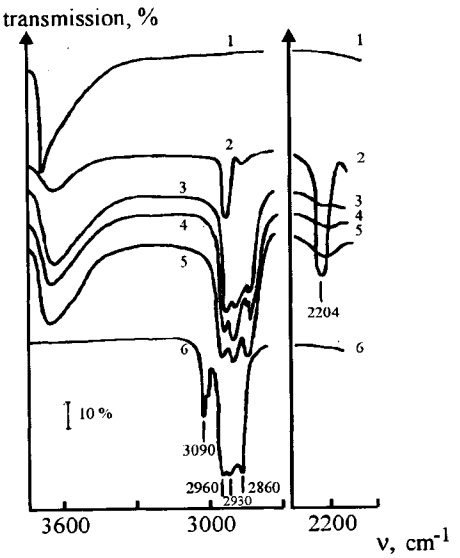

Figure 2. IR spectra of silica prepared under vacuum at 400°C for 3 hr (1), after the methyldichlorosilane chemisorption at 300°C for 2 hr (2), after the interaction of hydridesilica with 1-hexene, 1-decene, 1-octadecene and evacuation at 300°C for 1hr (spectra 3, 4, 5 respectively). The IR spectrum for 1-decene is also shown (6).

In the IR spectrum of methyldichlorosilane (Fig.1, spectrum 3) there are also absorption bands at 2984, 2931, and 1400 cm^{-1}. Besides, in the spectrum of $Cl_2Si(CH_3)H$ there is an absorption band for Si–C bond (1265 cm^{-1}). In the spectrum of hydridesilica the last band is masked with silica core absorption band, and band for Si–H bond is at 2220 cm^{-1} unlike hydridesilica whose absorption band for Si–H bond is shifted to 2204cm^{-1}.

The frequency of the Si–H bond stretching vibrations is sensitive to the nature of substituents at a silicon atom [25,68]. If the wave number of the Si–H band during chemisorption of methyldichlorosilane on silica surface is 2204 cm^{-1}, one observes the formation of $\equiv SiOSi(CH_3)(Cl)H$ groups. But if the absorption band maximum is shifted to 2190 cm^{-1}, one can regard this as evidence for the proceeding of hydrolysis with the formation of $\equiv SiOSi(CH_3)(OH)H$ groups.The results presented in Fig.1 (spectrum 4) provide evidence for the formation of $\equiv SiOSi(CH_3)(Cl)H$ groups on silica surface and for their slow hydrolysis in the air. Besides, the hydrolysis of Si–Cl bonds in contact with water the partial hydrolysis of Si– H bonds occurs as well. In the IR spectrum there appears an absorption band for isolated silanol groups at 3750 cm^{-1} (Fig.1, spectrum 5). In the presence of the Speier catalyst the hydrolysis proceeds even more vigourously (Fig.1, spectrum 6): the hydridesilica does not practically contain $\equiv SiH$ groups. Thus, the hydrolysis of the $\equiv SiOSi(CH_3)(Cl)H$ groups attached to the silica surface can be regarded as a side process leading to a decrease of the $\equiv SiH$ group content. This circumstance should be taken into account when studying the interaction between hydridesilica and simple terminal olefins in the presence of the Speier catalyst.

The interaction of 1–olefins with the hydridesilica produced as a result of the methyldichlorosilane chemisorption was studied using liquid–phase reactions at 25 – 100°C in sealed glass ampoules. All the reagents were thoroughly dehydrated and the hydridesilica was preliminarily subjected to a thermal evacuation. After carrying out catalytic reactions a decrease in the intensity of absorption band for Si–H bonds was observed. At 100°C a substantial decrease (by 90 – 95%) of the intensity of the absorption band at 2204 cm^{-1} (Fig.2, spectra 3–5) occurred. The $\equiv SiH$ groups concentration variation which is a measure of the intensity of the chemical process proceeding in a silica surface layer was determined in terms of the ratio of optical densities $D_{SiH} = Dexp._{SiH}(2204)/Dexp._{SiOSi}(1860)$ in order to eliminate the effect of the silica plate mass as well instrument errors during the spectra recording [139,140]. Besides, the IR spectra exhibit an increase in the intensity of absorption bands related to the stretching vibrations of C–H bonds in methyl groups (2980, 2930 cm^{-1}) and the appearance of absorption bands for methylene links (2900, 2855 cm^{-1}). The increase in the surface concentration of C–H bonds manifests itself in the region of the bending vibrations of CH_3 and CH_2 groups (1500–1300 cm^{-1}). The IR spectra of the modified silicas (Fig.2, spectra 3–5) are characterized by the absence of the absorption band for the stretching vibrations of C–H bonds in $H_2C{=}CH–$ groups (3090 cm^{-1}) which clearly manifests itself in the IR spectra for 1–olefins (Fig.2, spectrum 6). The band for isolated silanol groups is also absent (Fig.2, spectra 3–5) which can provide evidence for the absence of hydrolysis of the hydridesilica $\equiv SiH$ groups under the conditions of the experiment. By independent experiments it was shown that 1–olefins (in the absence of the catalyst) and isopropyl alcohol do not enter into a reaction with hydridesilica under these conditions. Upon the contact with 1–olefins in the presence of the Speier catalyst the starting silica displays the absorption in the region of 3000 – 2800 cm^{-1} that is related to the strong retention of 1–olefins on surface seemingly in the form of platinum – olefin

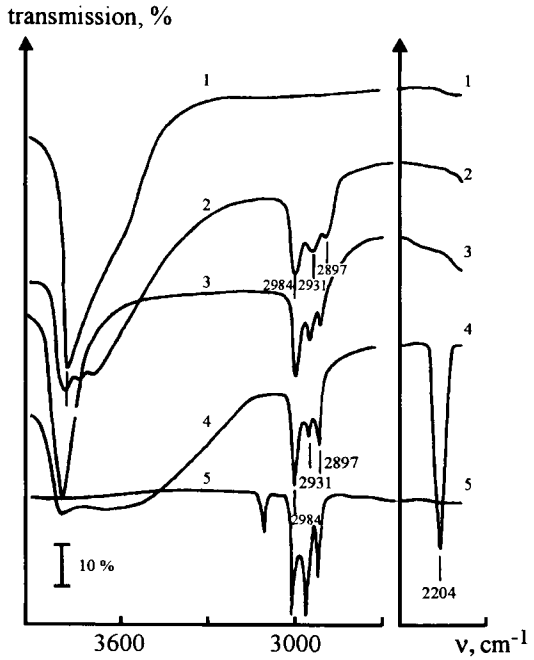

Figure 3. IR spectra for the silica prepared under vacuum at 400°C for 3 hr (1), after the interaction with 1-octene at 100°C for 1 hr in the presence of H_2PtCl_6 (2), after contact with methyldichlorosilane at 25°C for one day (4). The IR spectrum for 1-octene (5) is also shown.

complexes, since the band at 3090 cm^{-1} in the spectrum is absent and silanol groups (3750 cm^{-1}) do not participate in the reaction and interact with methyldichlorosilane (Fig.3). Therefore the observed spectral pattern gives evidence for the proceeding of the chemical reaction of the hydrosilylation of 1-olefins on the hydridesilica surface according to following scheme:

$$\equiv SiOSi(CH_3)-H + H_2C=CH(CH_2)_nCH_3 \rightarrow \equiv SiOSi(CH_3)CH_2CH_2(CH_2)_nCH_3 + \equiv SiOSi(CH_3)-CH(CH_2)_nCH_3 \quad (CH_3)$$

Thus, using modified silicas whose surface contains ≡SiH groups makes it possible to carry out reactions of solid-phase hydrosilylation with the attachment of terminal simple

olefins having different lengths of the hydrocarbon chain (C_6– C_{18}). These processes result in the organosilicas with hydrolytically stable Si–C bonds. The formation of Si–C bonds is also supported by the absence in the IR spectra for C_6– C_{18} – silicas after the contact with pyridine and water vapours for one day. Under similar conditions the chemical bonds Si–O–C become completely broken [141].

Sandoval and Pesek [142] performed the solid–phase hydrosilylation of 1–octene and 1–octadecene on the surface of the hydridesilica obtained through chlorination with the help of $SOCl_2$ and reduction with $LiAlH_4$. In order to do it 1–olefin was brought into contact with a fresh–prepared solution of chloroplatinic acid in 2–propanol and heated at 60–70°C for 1 hr. Then the hydridesilica dried at 110°C for 6 hr was added and the reaction was allowed to proceed for at least 24 hr at 100°C. The infrared analysis detected the appearance of strong absorption bands in the 3000–2800 cm^{-1} region concomitant with a substantial decline of the Si–H stretching band at 2260 cm^{-1}. It clearly indicates chemical bonding to the silica surface. Another way of proving that the olefins indeed undergo Si–H addition at the silica surface is solid–state NMR spectroscopy. ^{13}C CP–MAS NMR spectra of the octyl– and octadecyl–bonded phases are virtually the same for both silicas with the only change in intensity due to the difference in chain lengths. The peak near 12 ppm can be assigned to the combined contributions from the terminal methyl group of the alkyl chain and the methylene group which is directly attached to the surface silicon atom, i.e. the carbon involved in the direct bonding of the terminal olefin to the silicon hydride in the hydrosilylation reaction. By ^{29}Si CP–MAS NMR spectroscopy it was possible to gain a further insight into the structure of the hydride intermediate as well as the C_8– and C_{18}–product phases. The spectrum of the hydridesilica shows five distinct peaks. There are the peaks at -110.4 ppm, which represents framework $Si^*(OSi{\equiv})_4$ structures, -100.9 ppm, which represents surface single silanols, $HOSi^*(OSi{\equiv})_3$ structures, and -80.3 ppm, which represents surface geminal silanols, $(HO)_2Si^*(OSi{\equiv})_2$. The peak at - 85.3 ppm in the spectrum can be assigned to the hydride $HSi^*(OSi{\equiv})_3$ species; fifth peak at -74.8 ppm can be tentatively assigned to the $HSi^*(OH)(OSi{\equiv})_2$ group. For the C_8– (or C_{18}–) product there are the three peaks at -110.2; -100.8; and -89.9 ppm as described above. The peaks near -85 and -75 ppm have virtually disappeared due to the bonding reaction. Two new peaks at -66.2 and -54.6 ppm have now appeared in the spectra. These signals have been previously assigned to $CSi^*(OSi{\equiv})_3$ and $C(OH)Si^*(OSi{\equiv})_2$ groups respectively.

6. REACTIONS OF SOLID–PHASE CATALYTIC HYDROSILYLATION WITH THE PARTICIPATION OF HYDRIDE–MODIFIED SILICAS AND SOME FUNCTIONAL OLEFINS

The attachment of functional olefins to the hydridesilica offers new scope for the production of corresponding organosilicas. This section presents the results of researches on the interaction between hydridesilicas and various functional compounds (Table 2).

The studies of the interaction with these compounds were carried out using the hydridesilicas obtained through the chemisorption of methyldichlorosilane. The ≡SiH groups content was 2.4 $\mu mol/m^2$. The interaction between hydridesilicas and functional olefins was studied at the boiling temperature (82.4°C) of the solvent in the presence of the Speier catalyst. In order to do it a hydridesilica sample was placed into the glass reactor

Table 2
Physico–chemical characteristics of the studied functional olefins

Olefin	Chemical formula	Molecular mass	$t_{boil.}$ (°C)	n_D^{20} (g/cm^3)	d_4^{20}
Vinyltrimethylsilane	$H_2C{=}CHSi(CH_3)_3$	100.24	55	1.3920	
Vinyltrichlorosilane	$H_2C{=}CHSiCl_3$	161.49	90	1.4360	
Acetyl acetone	$H_3CCOCH_2COCH_3$	100.12	139–140	1.4513	0.972
	↑↓		($t_{melt.}$ − 23)		
	$H_3C(HO)C{=}CHCOCH_3$		($t_{melt.}$ − 9)	1.4609	
Vinyl acetate	$H_2C{=}CHOOCCH_3$	86.09	72.7	1.3953	0.934
Acrylamide	$H_2C{=}CHCONH_2$	71.08	215		1.122
Styrene	$H_2C{=}CHC_6H_5$	104.15	145	1.5470	0.909
			($t_{melt.}$ − 31)		

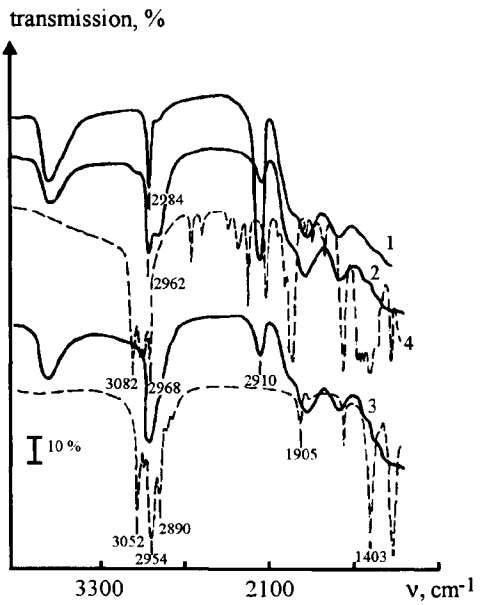

Figure 4. IR spectra for hydridesilica with ≡Si–O–Si–H groups (1), treated with vinyltrichlorosilane (2) or vinyltrimethylsilane (3) in the presence of the Speier catalyst and evacuated at 300°C for 1 hr. Curves (4) and (5) are IR spectra for vinyltrichlorosilane and vinyltrimethylsilane respectively.

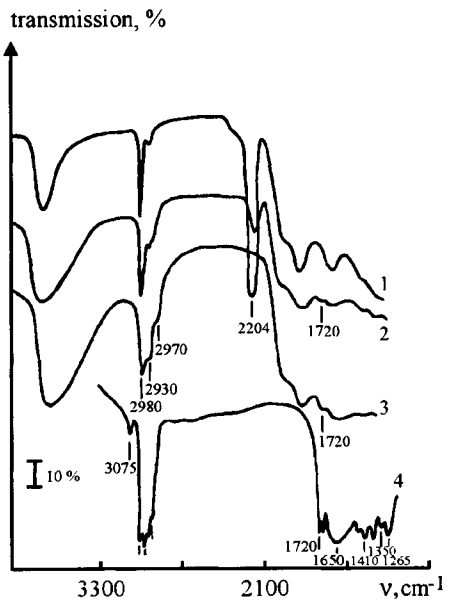

Figure 5. IR spectra of hydridesilica (1), treated with acetyl acetone in the presence of the Speier catalyst and evacuated at 300°C for 1 hr (2), after the treatment with water and pyridine vapours at a room temperature for 17 hr and evacuation at 300°C for 1 hr (3). The IR spectrum for acetyl acetone is also shown (4).

containing isopropyl alcohol and one of the functional olefins and then several drops of the catalyst were added, upon which the mixture was subjected to boiling with refluxing for 4–5 hr. After this procedure the organosilica produced was filtered, washed with isopropanol and acetone and dried in the air. The proceeding processes were controlled using IR spectroscopy. The attached organic group content was determinated through performing gravimetric thermal analysis [143].

Vinylsilanes. Upon the interaction between vinylsilanes and hydridesilica the IR spectra of modified silicas (Fig.4, spectra 2,3) display a substantial decrease (by 80–85%) in the intensity of the absorption band attributed to stretching vibrations of Si–H bonds (2204 cm^{-1}). Besides, there appear absorption bands assigned to asymmetric and symmetric stretching vibrations of C–H bonds in methyl groups (2872, 2853 cm^{-1}), and in the case of vinyltrimethylsilane one can also observe an increase in the intensity of ν_{CH} bands for methyl groups (2962, 2926 cm^{-1}). Furthermore, in the IR spectra of silicas modified with vinylsilanes there are not ν_{CH} absorption bands for double bonds (3100–3000 cm^{-1}) and $\nu_{C=C}$ absorption band (at 1600 cm^{-1}) which can be observed in the IR spectra for the studied silanes, namely 3082, 3032, and 1602 cm^{-1} for vinyltrichlorosilane and 3052, 3010, and 1596 cm^{-1} for vinyltrimethylsilane (Fig.4, spectra 4,5). The above-mentioned variations in the IR spectra provide evidence that the catalytic transformation of ≡Si–H groups into ≡Si–C≡ groups at the expense of hydrosilylation reaction proceeded in a surface layer of hydridesilica can be observed under mild conditions already:

$$\equiv SiOSi-H + H_2C=CHSiX_3 \longrightarrow \equiv SiOSiCH_2CH_2SiX_3 + \equiv SiOSi-CH(CH_3)-SiX_3$$

where X is –Cl or $-CH_3$.

Acetyl acetone and vinyl acetate have electron-seeking groups at carbon atoms with double bonds, which may decrease their reactivity during hydrosilylation processes since it is known [144,145] that the reactivity of olefins depends on the electron density of the C=C bond. Besides, C=O groups can also take part in homogeneous hydrosilylation reactions [138,145]. In this case a silicon atom is added to a more electronegative atom with the formation of Si–O–C bonds. By experiment it has been established that the interaction between hydridesilica and acetyl acetone in the presence of the Speier catalyst leads to a decrease (by 77%) in the intensity of the ν_{SiH} absorption band (2204 cm^{-1}) and appearance the absorption bands for stretching vibrations of methylene groups (2870, 2850 cm^{-1}) and carbonyl groups (1720 cm^{-1}). In addition, one can observe an increase in the intensity of absorption bands of ν_{as} and ν_s for C–H bonds at 2980 and 2930 cm^{-1} assigned to methyl groups (Fig.5, spectra 1,2). The treatment of acetyl acetone-modified silica with water and pyridine vapours does not result in any change of its IR spectrum (Fig.5, spectrum 3), which provides evidence for a high hydrolytic stability of the chemical bonds formed on the surface [141]. Thus, it may be concluded that the interaction between hydridesilica and acetyl acetone proceeds by the following mechanism:

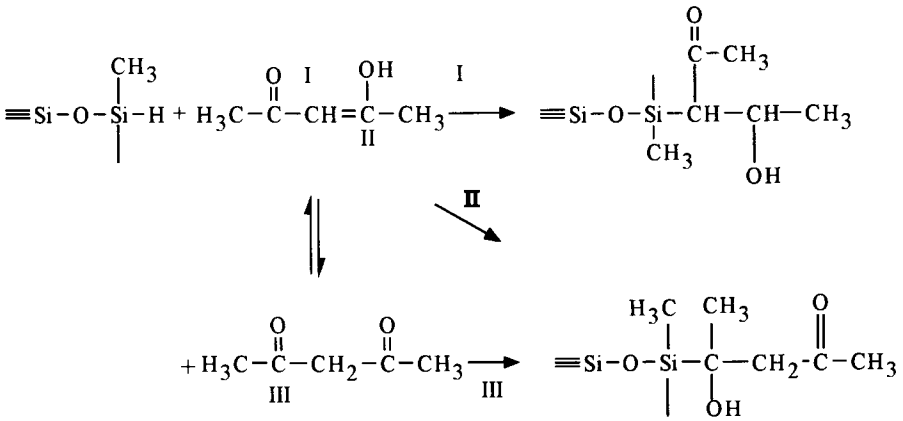

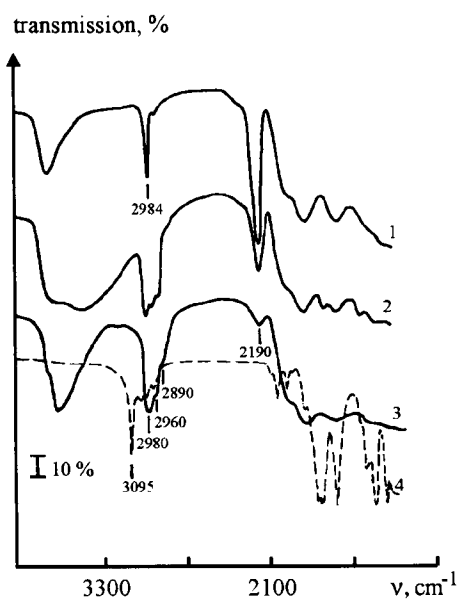

Figure 6. IR spectra for hydrifesilica (1), treated with vinyl acetate in the presence of the Speier catalyst and evacuated at 300°C for 1 hr (2), after the treatment with water and pyridine vapours at room temperature for 17 hr and evacuation at 300°C for 1 hr (3). The IR spectrum of vinyl acetate is also shown (4).

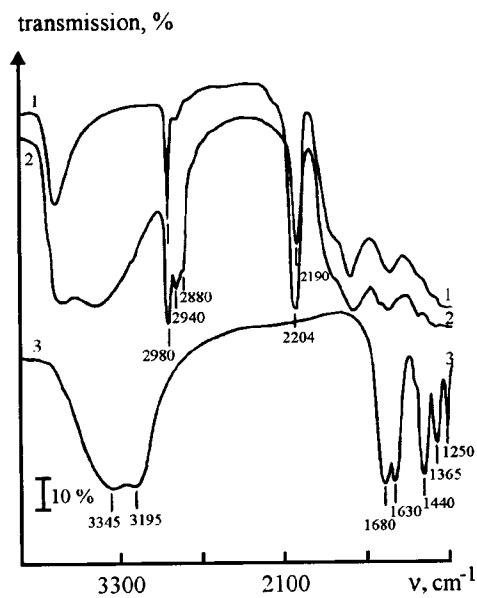

Figure 7. IR spectra of hydridesilica (1), after the interaction with acrylamide in the presence of the Speier catalyst and evacuation at 300°C for 1 hr (2). (3)–IR spectrum of acrylamide.

The attachment of acetyl acetone to hydridesilica through oxygen atoms is unlikely since in this case the hydrolytic stability of the product would be not high due to the formation of Si–O–C bonds:

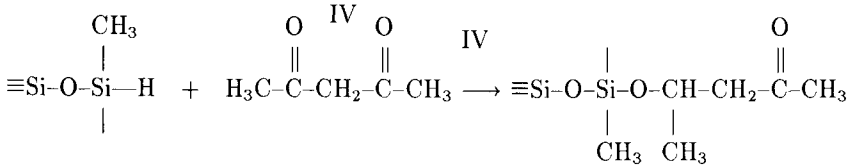

The contact of *vinyl acetate* (under the same conditions) with the hydridesilica surface does not lead to the embracing participation of the ≡SiH groups in the reaction (Fig.6, spectra 1,2), however, just as in the case of acetyl acetone one can observe a decrease in the absorption band intensity for stretching vibrations of Si–H bonds, appearance of absorption bands for C–H bonds of methylene groups, and an increase in the intensity for ν(C–H) of methyl groups. The high hydrolytic stability of silica modified with vinyl acetate, the absence (in the IR spectrum) of the absorption bands attributed to vinyl groups, and the decrease in the intensity of the absorption band for ν(Si–H) (Fig.6, spectra 1–4) make it possible to conclude that the solid- phase hydrosilylation of vinyl acetate proceeds in accordance with the following scheme:

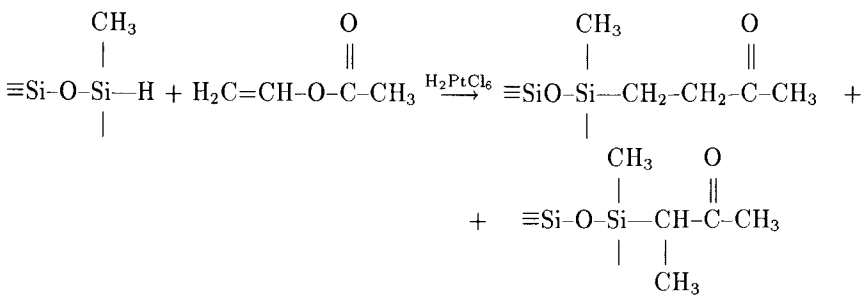

Acrylamide. During the interaction the hydridesilica one can observe a decrease (by 32%) in the ν(Si–H) band; besides, there appear absorption bands attributed to methylene, carbonyl, and amine groups (2940, 1680, 3345, and 3185 cm^{-1}). The absorption bands for C–H stretching vibrations at a C=C double bond (3100–3000 cm^{-1}) and C=C stretching vibrations (1630 cm^{-1}) are absent in the IR spectrum (Fig.7), which may give evidence for the solid-phase hydrosilylation according to the following scheme:

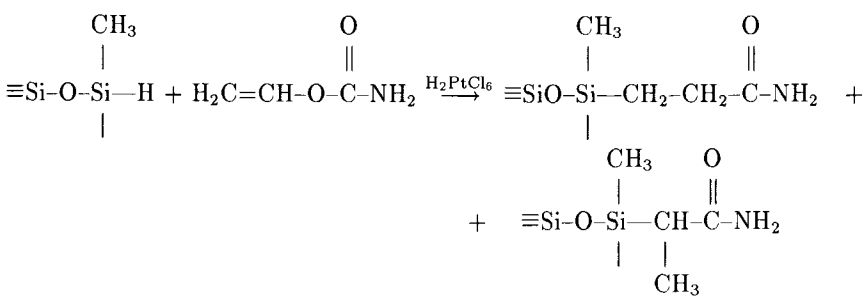

Styrene. The attachment of styrene on silica surface through a solid-phase hydrosilylation reaction to produce functional organosilicas is of special interest. This is due to easiness of the introduction of some functional groups (-SO_3H, -COOH, -OH, -NO_2, -NH_2) into benzene rings.

The hydrosilylation reaction was effected using a liquid-phase process without any solvent, without access for light at 100°C for 3 hr in the presence of the Speier catalyst. Then the modified silica was washed with carbon tetrachloride for 1hr in a Sohxlet apparatus and evacuated at 300°C for 2 hr. As a result of this reaction the IR spectrum of the modified silica (Fig.8, spectrum 2) displayed a considerable decrease in the intensity

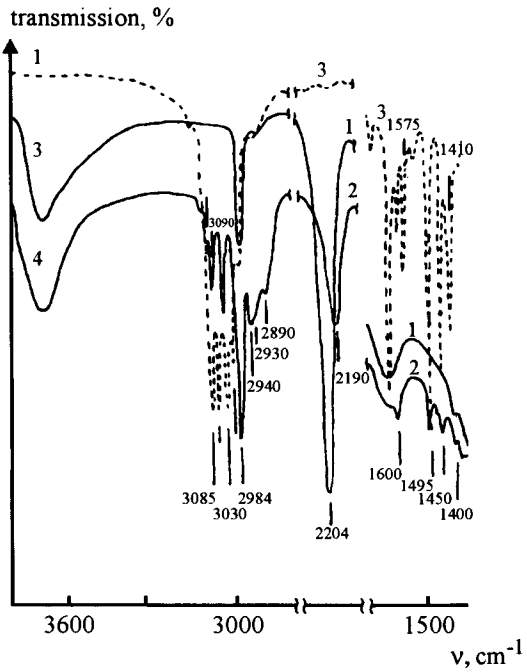

Figure 8. IR spectra of hydridesilica (1), after the interaction with styrene in the presence of the Speier catalyst and evacuation at 300°C for 1 hr (2). (3)-IR spectrum of styrene.

of the absorption band for Si-H bonds. The peak maximum of this absorption band was shifted into the region of 2190 cm^{-1} as a consequence of the partial hydrolysis of Si-Cl bonds [25,68] upon the contact of the modified silica with air moisture during its washing. The formation of silanol groups is accompanied with the appearance of the absorption band at 3750 cm^{-1}. Besides, in the spectrum there are absorption bands at 3090, 3072, and 3035 cm^{-1} for stretching vibrations of C-H bonds of benzene rings. At the same time the spectrum does not contain the band at 1630 cm^{-1} (characteristic of styrene) for stretching vibrations of C=C bonds of vinyl groups and the band at 1575 cm^{-1} for in-plane vibrations of benzene rings, which manifests itself only upon the conjugation of π-electrons of a double bond or with an unshared electron pair of a substituent [146]. In addition, there appears a substantial increase in the intensity of the absorption bands at

2984, 2930, and 2890 cm^{-1} for stretching vibrations of C–H bonds in methyl, methylene, and methine groups [146]. The results obtained provide evidence that styrene entered into the reaction of the catalytic hydrosilylation with Si–H bonds of hydridesilica:

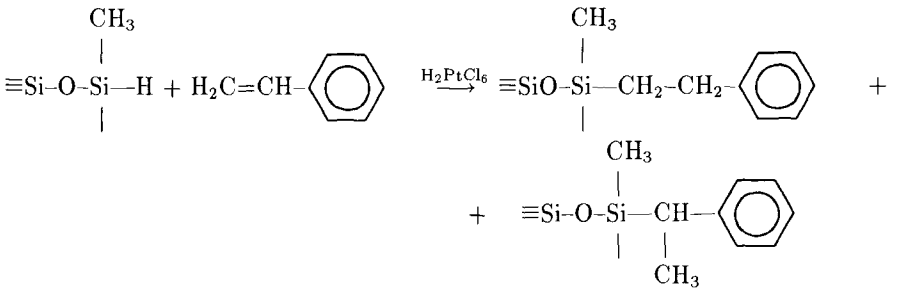

The degree of completeness of this reaction is 64%. The content of grafted phenyl ethyl groups amounts to 0.46 mmol/g.

Thus, the research on the interaction between various functional olefins and hydridesilica surface in the presence of chloroplatinic acid has shown that the solid-phase hydrosilylation provides a lower yield than in the case of simple terminal olefins. As to their reactivity the olefins studied can be arranged in the following order: simple terminal olefins > vinylsilanes > acetyl acetone > vinyl acetate > styrene > acrylamide. The decrease in the reactivity of olefins in the solid-phase hydrosilylation processes may be related to the decrease of the electron density on C=C bonds of reagent molecules since in the case of unsaturated compounds this density is determined by the mesomeric effect of substituents. The most substantial decrease in the reactivity is observed for functional olefins whose molecules contain conjugated double bonds. From these standpoints it becomes possible to explain practically the same reactivity of vinylsilanes with electron-donating and electron-seeking substituents in whose molecules the delocalized π-orbitals are absent. The inductive effect of substituents is characteristic of unsaturated groups and compounds and is observed only at small distances, while mesomeric effects may be transferred from one end of comparatively large molecules to the other in the presence of the conjugation.

It should be noted that as distinct from the hydrosilylation reactions in homogeneous media in the case of the solid-phase catalytic hydrosilylation there are no processes involving carbonyl groups of acetyl acetone, vinyl acetate, and acrylamide, therefore the attachment of olefins to hydsridesilica surface is effected only by the formation of Si–C bonds between silica and a functional compounds. The discovered effect which consists in increasing selectivity of catalytic reactions proceeding on solid surfaces can be applied for synthesizing monofunctional organosilicas with hydrolytically stable Si–C bonds.

In the patent specification [147] there data on the chemical attachment to hydridesilica surface in the presence of the Reney nickel, chloroplatinic acid or metallic platinum deposited on activated carbon as a catalyst of the following unsaturated functional compounds: divinylbenzene, ethylene glycol diacrylate, acetylene, allyl alcohol, allyl glycidyl ether, allyl isocyanate, acrylic acid. The chemical reactions result in the transformation of Si–H bonds of hydridesilica surface into Si–C bonds. Such transformations may be also classified as processes of solid-phase catalytic hydrosilylation of functional olefins.

7. TRANSFORMATION OF ATTACHED METHOXY GROUPS INTO SURFACE COMPOUNDS WITH Si–C BONDS

As it was mentioned above, hydridesilica may be produced without use of chloro- or alkoxysilanes, for instance, through thermodestruction of methoxysilica. Carrying out processes of methoxylation, subsequent thermal decomposition of grafted methoxy groups, and formation of attached ≡SiH groups and then a reaction of solid-phase catalytic hydrosilylation with olefins makes it possible, as we assumed [123], to produce chemical compounds with Si–C bonds on silica surface without use of organosilicon reagents. At the same time the proceeding of these chemical reactions in accordance with the assumed scheme required experimental corroborations. The results obtained are presented below.

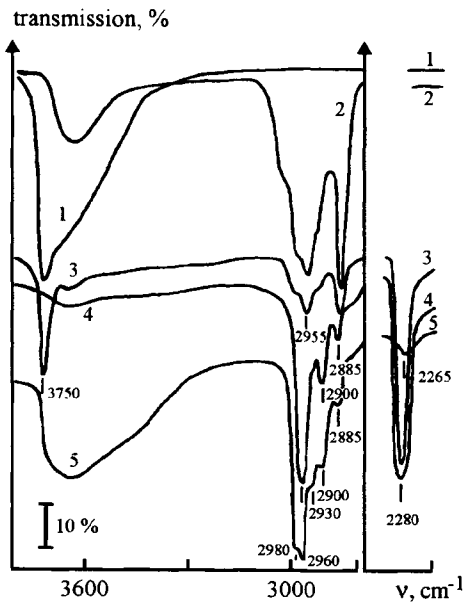

Figure 9. IR spectra of silica evacuated at 400°C for 2 hr (1), after the treatment with methyl alcohol at 380°C for 3 hr and evacuation at 300°C for 1 hr (2), after thermoevacuation at 700°C for 40 min (3), treated with hexamethyldisilazane at 100°C for 1 hr and evacuated at 400°C for 1 hr (4), after the treatment with 1-octene in the presence of the Speier catalyst and evacuation at 300°C for 1 hr (5).

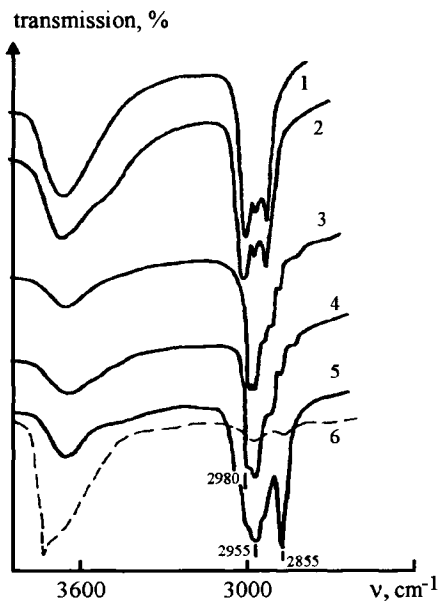

Figure 10. IR spectra of organosilicas with attached ≡Si–O–Si–C_8H_{17}, ≡Si–C_8H_{17}, and ≡Si–OCH_3 groups before (1,3,5) and after (2,4,6) hydrolysis in the presence of pyridine at 25°C for 1 hr and evacuation at 300°C for 1 hr.

Methoxysilica was prepared in the way discussed in Ref.[148,149]. 1-Octene purified applying procedure described in Ref.[150] and dried from water with the aid of molecular sieves NaX [151] was used as an olefin. The silica previously evacuated at 400°C (Fig.9,

spectrum 1) was treated with methyl alcohol vapours at 380°C so as to ensure that all the isolated silanol groups entered into reaction. The chemisorption of methanol on the silica surface was monitored and judged by the appearance of characteristic absorption bands for isolated groups (3750 cm^{-1}) (Fig.9, spectrum 2). As a result of the thermovacuum pumping-out of methoxysilica at 700°C the IR spectrum exhibits a sharp decrease in the intensity of absorption bands for methoxy groups, appearance of a sufficiently strong absorption band at 2280 cm^{-1} attributed to stretching vibrations of Si–H bonds and of a middle intensity band at 3750 cm^{-1} (Fig.9, spectrum 3). The side effects associated with the appearance of silanol groups were eliminated by the end-capping of hexamethyldisilazane at 100°C. In doing so the intensity of the absorption band at 2280 cm^{-1} does not change, the absorption band at 3750 cm^{-1} disappears, and in the IR spectrum there appear absorption bands for asymmetric and symmetric vibrations of C–H bonds in attached trimethylsilyl groups (Fig.9, spectrum 4). The hydrosilylation reaction results in a substantial decrease (by 97%) in the intensity of the absorption band attributed to ≡SiH groups (Fig.9, spectrum 5). The disappearance of these groups is accompanied with an increase of the intensity of absorption bands assigned to stretching vibrations of C–H bonds in methylene and methyl groups. This fact corroborates the conclusion about the transformation of ≡SiH groups formed upon the thermal decomposition of methoxysilica into chemically attached hydrocarbon radicals.

An additional corroboration of the formation of Si–C bonds on silica surface is provided by the data on the hydrolytic stability of organosilicas produced as a result of the solid-phase hydrosilylation reaction. The treatment of these organosilicas with water vapours in the presence of pyridine [141] does not lead to any variation in the character of their IR spectra (Fig.10, spectra 1– 4). At the same time in the case of methoxysilica under similar conditions one can observe the destruction of Si–O–C bonds and formation of silanol groups (Fig.10, spectra 5,6) which is evidenced for by the decrease in the intensity of the absorption bands in the region of 3000 – 2800 cm^{-1} attributed to ether groups, and by the appearance of the band 3750 cm^{-1}.

The results presented support the possibility for carrying out the solid-phase hydrosilylation reaction of olefins on the silica surface with ≡SiH groups with the formation of Si–C bonds directly on the silicon dioxide surface without using organosilicon compounds. The solid-phase hydrosilylation process seems to involve ≡SiH groups of any structure produced by various methods including the polycondensation method of the hydrosiloxanes synthesis. However, their reactivities is likely to be different as it is the case for the homogeneous hydrosilylation of silanes of various structures [2,138,145,150,152]. The approach suggested may be applied for the synthesis of organosilicas with thermally and hydrolytically stable Si–C bonds between silica carrier and functional organic groups.

8. HYDROSILYLATION REACTIONS INVOLVING VINYL GROUPS ATTACHED TO SILICA SURFACE

As it was mentioned above, olefin groups attached to silica surface under conditions of γ-irradiation or in the presence of benzoyl peroxide enter into the reaction of copolymerization with unsaturated acids, styrene, methyl methacrylate, acrylonitrile, and other compounds whose molecules have unsaturated bonds [1,91,101,108,109,153–155]. The au-

thors of Ref.[115] effected the chemical addition reaction between the silica surface with vinyl groups and the chiral modifier attached to polymethylhydrosiloxane through catalytic hydrosilylation. The interactions between olefinorganosilicas and residual ≡SiH groups of polymer modifier may be classified as solid-phase hydrosilylation processes.

In order to elucidate the nature of the possible influence of the phase state (in a solution or on surface) of $H_2C{=}CH-$ groups on the hydrosilylation reaction we carried out the studies [123,129] of the interaction between silica with attached $\equiv SiCH{=}CH_2$ groups and methyldichlorosilane using the Speier catalyst.

The silica with vinyl groups was prepared through the interaction between dehydrated silicon dioxide and vinyltrichlorosilane (fig .11, spectra 1,2). The IR spectrum displays the

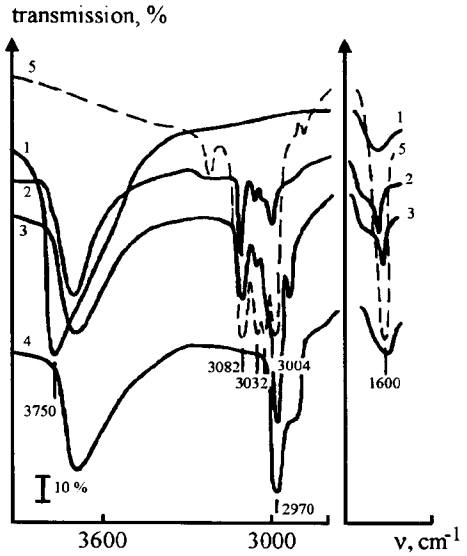

Figure 11. IR spectra of silica evacuated at 400°C for 2 hr (1), after the treatment with vinyltrichlorosilane at 380°C for 3 hr and evacuation at 300°C for 1 hr (2), treated with hexamethyldisilazane at 100°C for 1.5 hr and evacuated at 300°C for 1 hr (3), after boiling with methyldichlorosilane for 2 hr in the presence of the Speier catalyst and evacuation at 300°C for 1 hr (4). The IR spectrum for vinyltrichlorosilane is also shown (5).

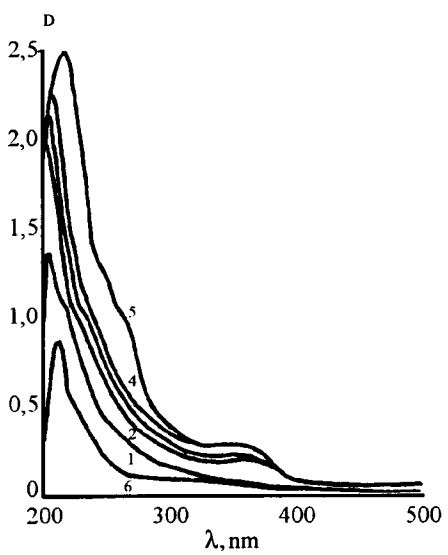

Figure 12. Transmission electronic spectra for the system *hydridesilica + Speier catalyst* (silica plate 30 mg, l=2 mm; 0.001 N solution of H_2PtCl_6 in isopropyl alcohol) in 5 (1), 15 (2), 25 (3) and 35 min (4) after the addition of the catalyst; 35 min after the addition of 1-decena to the system *hydridesilica + Speier catalyst* (5). Spectrum (6) corresponds system *starting silica + Speier catalyst* on 35 min.

appearance of absorption bands at 3082, 3032, 3004, and 1602 cm^{-1} attributed to ν(C–H) at a double bond and to ν(C=O) [156]. The absorption band intensity for isolated silanol groups substantially decreases. After the treatment of vinylsilica with hexamethyldisilazane (to eliminate residual silanol groups) in the IR spectrum there appear intense absorption bands at 2970 and 2910 cm^{-1} assigned to stretching vibrations of C–H bonds

in trimethylsilyl groups (Fig.11, spectrum 3). As a result of the interaction between the prepared organosilica and methyldichlorosilane the absorption bands for $H_2C{=}CH-$ groups (3082, 3032, 3004, and 1602 cm^{-1}) are not observed in the IR spectrum; the line of ν(Si–H) is also absent. The IR spectrum exhibits only the bands for stretching vibrations of C–H bonds in methyl and methylene groups (Fig.11, spectrum 4). Therefore the results obtained allow us to draw a conclusion that the chemical transformation of attached groups on silica surface can be represented by the following scheme:

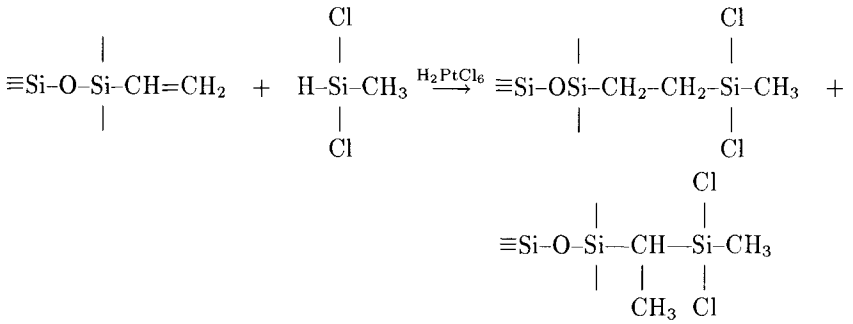

Differences in the reactivity of silicas containing vinyl or ≡SiH groups have not been detected, i.e. the reaction of the solid-phase catalytic hydrosilylation resulting in the formation of surface compounds with Si–C bonds involves practically all functional groups of the modified silicas. The results obtained by us earlier [119–127] and the literature data presented in Refs. [115,138,145,152] make it possible to assume that the solid-phase catalytic hydrosilylation with the participation of silanes containing unsaturated groups will proceed with a lower reaction product yield.

9. INVESTIGATION OF MECHANISM SOLID-PHASE CATALYTIC HYDROSILYLATION

It is known [138,157] that the homogeneous catalytic hydrosilylation is characterized by two main schemes of the reaction proceeding:
- through initial activation of Si–H bonds of silane by a platinum catalyst;
- through formation of platinum–olefin active complex.

However, as a result of researches into reactions of solid-phase catalytic hydrosilylation involving hydridesilica or silica with grafted vinyl groups it has not been found any distinctions in the behaviour of these processes of chemical addition [123]. And so, it was logical to assume that in the case of a solid-phase hydrosilylation the Speier catalyst activates both reagents. Indeed, by IR spectroscopy (spectrophotometer IKS–29, Russia, region 4000–400 cm^{-1}, pressed silica plates 10–15 mg/cm^2) it has been established that as a result of the contact of hydridesilica with 0.1N solution of chloroplatinic acid in 2-propanol the absorption band at 2204 cm^{-1} attributed to ≡SiH groups weakens (or disappears) and the bands at 3070 and 1650 cm^{-1} for $H_2C{=}CH-$ groups in the IR spectrum of vinylsilica are not observed, which may be the consequence of the activation by

the Speier catalyst both of Si–H and C=C bonds in the modified silicas.

The electron spectra presented in Fig.12 give evidence that upon the contact of hydridesilica with a chloroplatinic acid solution the adsorption of the Speier catalyst on the solid surface occurs, which may promote the formation of coordination complexes responsible for the proceeding of the solid-phase hydrosilylation processes. It should be noted that the coordination of platinum on hydridesilica ($\equiv$Si$\cdots$H$\cdots$Pt) in the case of platinum acetylacetonate was established on the basis of the shift of ν(Si–H) absorption band from 2204 to 2175 cm^{-1}. Thus, the preliminary results of the researches into the solid-phase hydrosilylation providing evidence for the possibility of the simultaneous activation by the Speier catalyst hydridesilica and 1-decene [127]. Hydridesilica was prepared by the interaction between pyrogenic dehydrated silica and methyldichlorosilane. 1-Decene was subjected to an additional purification and stored over molecular sieves in order to prevent the ingress of moisture. 2-Propanol and chloroplatinic acid were stored under conditions ruling out the contact with air. Electron spectra were recorded with the aid of a PU 8800 instrument for the region of 600–200 nm using quartz cells (L=2 mm) with caps. Pressed plates of hydridesilica were fixed on one the cell walls with the help of a solvent ensuring the adherence to a cell wall and enhancement of the silica transparency in the region under study. Such recording of electron spectra does not require an introduction of vaseline oil or similar liquid as an immersion medium, which in this case is extremely undesirable in view of the fact that the systems studied are multicomponent. The expansion of absorption electronic spectra in terms of Gauss components was performed using a personal computer HP-85 by the sequential differentiation and subtraction of absorption bands from an integral spectrum [158]. As follows from the data obtained, in the electronic

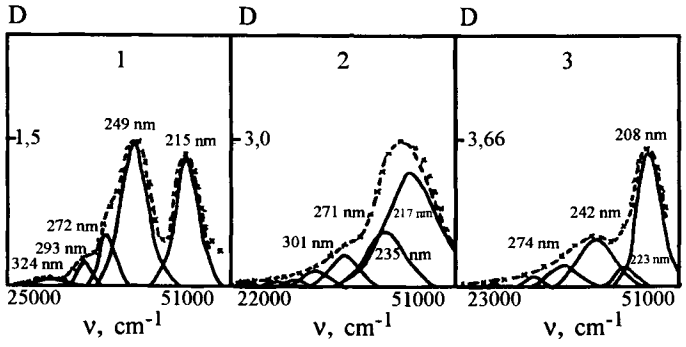

Figure 13. Electronic spectra of the *Speier catalyst* (1) and of the system *Speier catalyst + 1-decene* (2) and *Speier catalyst + hydridesilica* (3) (+++ experimental spectrum; — differential components; - - - integral envelope).

spectrum of the Speier catalyst (Fig.13, spectrum 1) there are five absorption bands. The band with peak maximum at 272 nm is attributed to Pt(IV), and those with maxima at 249 and 324 nm are assigned to Pt(II) [159]. The bands at 272 and 249 nm are due to charge-transfer transitions $\pi\gamma_4 \rightarrow 3d\gamma_3$ and d $\rightarrow$ p respectively [160]. The absorption band with a maximum at 293 nm is attributed to acetone coordinated with one of the platinum compounds.

The contact of the Speier catalyst with hydridesilica and / or 1-decene leads to the

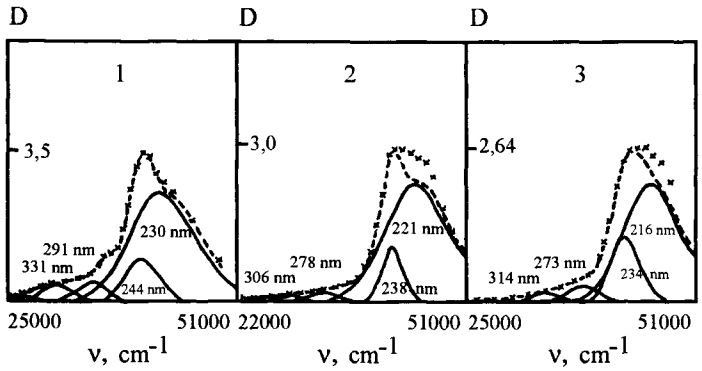

Figure 14. Electronic spectra of *1-decene* (1) and of the system *1-decene + hydridesilica* (2) and *hydridesilica + 1-decene + Speier catalyst* (3) (+++ experimental spectrum; — differential components; - - - integral envelope).

broadening and hypsochromic shift by 1000–2600 cm^{-1} of the 249 nm band attributed to Pt(II) that is responsible for the catalytic hydrosilylation process (Fig.13, spectra 2,3; Fig.14, spectrum 3). Such a change of the electronic spectrum of chloroplatinic acid may be caused by the substitution of one of the ligands in the $[PtCl_4]^{2-}$ complex for a more massive ligand or a ligand with a high electron density [159]. Therefore, it is quite logical to assume that the hypsochromic shift of the 249 nm band is caused by the coordination of the Speier catalyst through Si–H bonds of hydridesilica and C=C bonds of 1-decene.

With allowance for the obtained spectral results the scheme of the solid-phase hydrosilylation process may be visualized as follows. Upon the contact with the Speier catalyst the hydridesilica forms complex I on its surface, then complex becomes coordinated with a molecule of 1-olefin, which gives structure II:

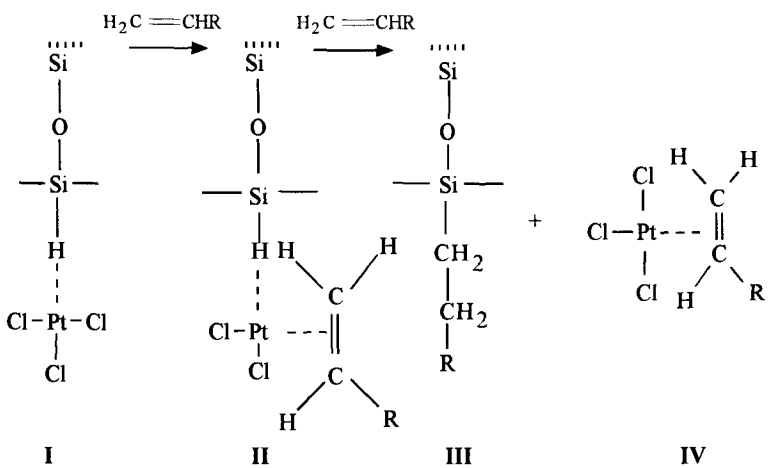

The intracomplex transformations on the silica surface result in the formation of product III of the hydrosilylation, and the catalyst is displaced by another molecule of 1-olefin that is coordinated with platinum. Since the electronic spectra of the system containing the catalyst and olefin (Table 3) display the shift of the charge-transfer band from 249 to 235 nm, the formation of platinum – olefin complexes IV in the solution seems to be quite probable.

Table 3
Transmission differentiated electronic spectra for systems containing hydridesilica, Speier catalyst, and 1-decene

System under study	λ_{max} of absorption bands (nm) (Half-width of absorption bands, Δ, cm^{-1})
Speier catalyst	215 (1766); 249 (2044); 272 (1185); 293 (961); 324 (2334)
Speier catalyst + + 1-decene	217 (4231); 235 (3000); 271 (1879); 301 (1786); 334 (1704); 368 (1517); 411 (1498)
Speier catalyst + + hydridesilica	208 (1896); 223 (1183); 242 (2738); 274 (2366); 305 (1264); 388 (1517)
1-Decene	228 (4901); 244 (977); 291 (1776); 331 (2062); 376 (1040)
1-Decene + + hydridesilica	221 (5041); 238 (1462); 278 (712); 306 (2474); 353 (2299); 406 (1579)
Speier catalyst + + 1-decene + + hydridesilica	216 (4455); 234 (2212); 273 (2493); 314 (2390); 347 (486); 369 (1600); 417 (993)

It is known [138] that platinum-olefin complexes can be active catalysts of homogeneous hydrosilylation. Therefore, quite feasible may be also another scheme of solid-phase hydrosilylation on the hydridesilica surface (when the catalyst is added after 1-olefin), namely the scheme involving the coordination of the platinum-olefin complex IV (that is formed in the solution) on hydridesilica surface, the effecting of which provides the formation of structure II and its subsequent rearrangement into hydrosilylation product III. A similar scheme for the proceeding of solid-phase catalytic hydrosilylation of 1-olefins has been suggested by Sandoval and Pesek [142]. The authors [142] consider the mechanism of hydrosilylation for the case when at first a catalyst is added to 1-olefin and then hydridesilica is. During the induction period a catalytically active (olefin)·Pt(II) complex is formed. Oxidative addition of the silicon hydride to the metal produces an (olefin)·Pt(II)·(HSi≡) intermediate. Hydride addition to the olefin then gives an (alkyl)·Pt(IV)·(-Si≡) complex, presumably stabilized by coordination of more olefin. Finally, reductive elimination of alkylsilane occurs, regenerating the starting (olefin)·Pt(II) complex:

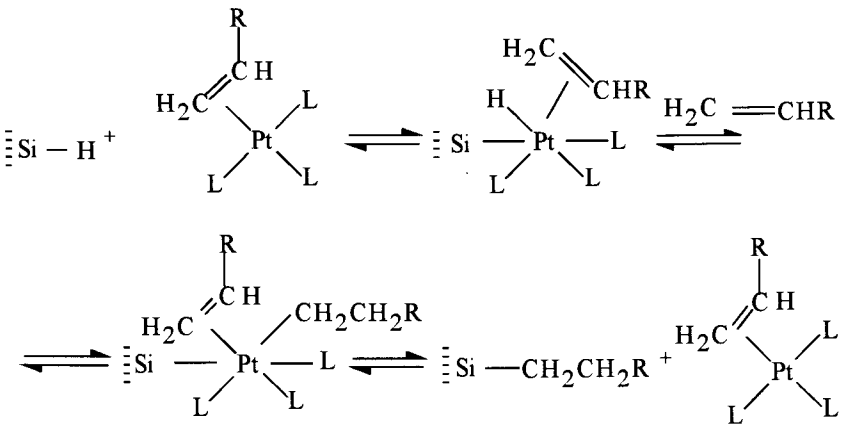

The authors of Ref.[142] believe the whole process to take place around the coordination sphere of the transition-metal catalyst. Most experimental facts related to olefin hydrosilylation (predominance of the terminal adduct, olefin isomerization, stereochemistry ot the silicon atom, reductive catalyst deactivation) have been explained in terms of the proposed mechanism.

Attempts to study the system $\equiv SiOSiCH{=}CH_2$ + *Speier catalyst* + *hydridesilica* by electron spectroscopy failed for the impossibility to carry out experiments on hydridesilane in cells of optically transparent quartz. However, the IR spectroscopy data about the possibility of coordinating the Speier catalyst on the silica surface with vinyl groups and the results obtained when studying the mechanism of solid-phase catalytic hydrosilylation on silica surface allow us to suggest the following schemes of the catalytic hydrosilylation with the participation of vinyl-containing silica:

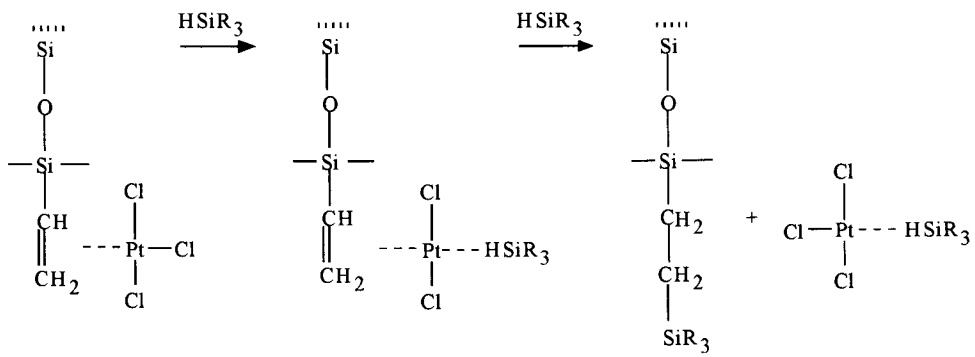

In the case of the reverse order of addition of the catalyst and silane:

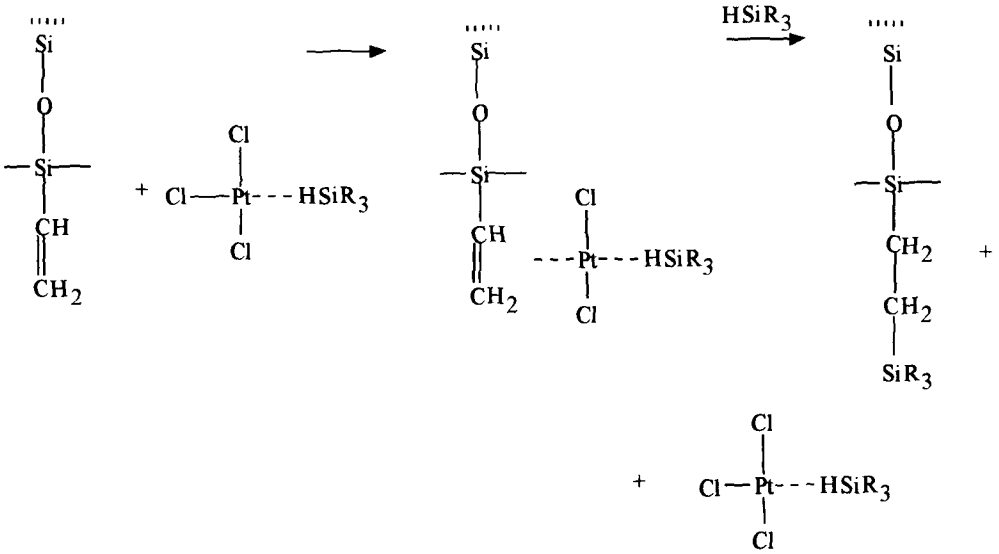

Thus, irrespective of the order of addition of the catalyst and reagents for the solid-phase catalytic hydrosilylation reaction to proceed, the appearance of an active intermediate compound containing both of the reagents and catalyst is necessary:

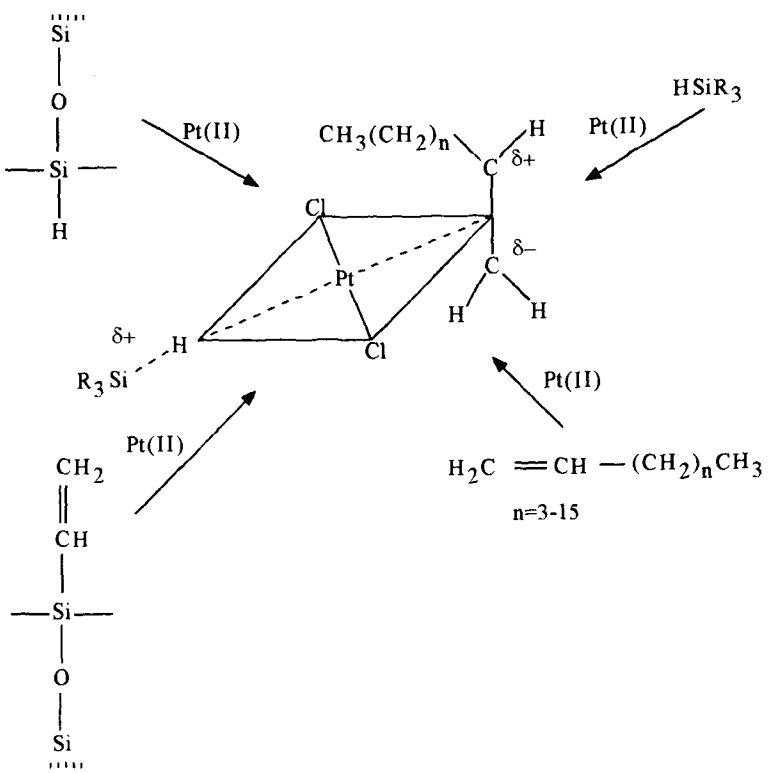

The consideration of the intermediate complex structure permits us to draw a conclusion that the intracomplex transformations leading to products of solid-phase hydrosilylation may be classified as processes of nucleophilic addition through silicon atom. In general, an increase of the electrophility of a silicon atom in hydridesilica (or hydridesilane) and an increase of the complexation capacity of olefin (or olefinosilica) must lead to a rise in the solid-phase hydrosilylation product yield. A special note should be made of the indubitable role of the modified silica surface in the simultaneous activation by the Speier catalyst both of Si-H and C=C bonds as well as of the increasing significance of steric factors and adsorption interactions during the formation of intermediate complexes leading to products of solid-phase hydrosilylation. From these standpoints it becomes possible to understand the enhancement of selectivity of solid-phase hydrosilylation of functional olefins in comparison with a homogeneous process: the formation of a catalytically active intermediate compound involves the participation of only C=C bonds of olefin; it is these bonds that determine the hydrosilylation product yield. The higher is the electron density of C=C bonds of a functional olefin, the higher is the possibility of the formation of an intermediate active compound and its transformation into a solid-phase product of the reaction. Thus, the fact that one of the present reagents is attached to the silicon dioxide surface leads to a change in the hydrosilylation reaction mechanism.

10. THERMAL ADDITION OF 1-OLEFINS TO HYDRIDESILICA

The establishment of the fact that it possible to form Si-C bonds directly on silica surface by the catalytic hydrosilylation reaction of 1-olefins opens up new prospects for the synthesis of various hydrolytically stable functional organosilicas. At the same time the presence of a homogeneous catalyst inevitably leads to the contamination of reactions products and to the catalyst loss. Besides, it is known [138] that the hydrosilylation reaction is very sensitive to the chemical nature of catalysts used. The most active in homogeneous hydrosilylation reactions is the Speier catalyst. Its replacement by transitional metal compounds causes a decrease in the product yield and an increase of the contribution of side processes to catalytic transformations. That is why the ideal solution to the problem would be a non-catalytic solid-phase hydrosilylation. The most promising approach to solving this task consists in the application of elevated temperatures or high-energy radiation to effect interactions between reagents containing silicon hydride and olefin groups.

In literature there are data on the homogeneous thermal addition of trichlorosilane to aliphatic and cyclic alkenes as well as to alkodienes with isolated and conjugated double bonds which proceeds under high pressures at 280-300°C [161-163]. Voronkov et al. [164] succeeded in carrying out the thermal addition of trichlorosilane to phenylacetylene in a polar solvent at 200°C while without the solvent the reaction proceeds at 500°C. The authors of Refs.[27,165] have performed the addition of ethylene, propylene, butene, butadiene, octene to silica surface at elevated temperatures. These chemical processes may be referred to as reactions of solid-phase thermal hydrosilylation. Unfortunately, these works have not received a large development effort.

By IR spectroscopy we have studied [128,129,131] the interaction between 1-olefins and silica surface bearing silicon hydride groups at elevated temperatures and pressures.

The researches were conducted using hydridesilicas produced by the thermodestruction of methoxysilica (hydridesilica I) and modification of silica with methyldichlorosilane vapours (hydridesilica II):

≡Si–H	≡Si–O–Si(CH_3)(Cl)H
Hydridesilica I	Hydridesilica II

The interaction between 1–olefins and hydridesilicas at high pressures was effected in the autoclave of stainless steel with a volume of 45 cm^3 equipped with quartz inserts. A 1–olefin sample was put on the bottom of the autoclave for the modification to proceed in a vapour phase [128]. After this the autoclave was held in an electric furnace at the required temperature. Then the hydridesilica plate was placed in a quartz cell and evacuated at 300°C for 2hr in order to remove the adsorbed reagent and possible products of the reaction.

The calculation of the modifier equilibrium pressure at a given temperature was done by the Antoine empirical equation [166]:

$$\lg P = A - \frac{B}{t + C}$$

where P – is the equilibrium pressure, mm Hg;
A, B, C – are constants having specific values for each compound;
t – is the temperature, °C.

In order to calculate the amount of modifier necessary to set a designed pressure in the autoclave (including the equilibrium one) a use was made of the real–gas equation [167]:

$$PV = ZnRT$$

where : P – pressure (atm); V – volume (l); Z – gas compressibility coefficient; n – amount of gas (mol); R – universal gas constant (0.082 l·atm/mol·K); T – temperature (K). The gas compressibility coefficient, Z, was determined in terms of reduced parameters (pressure and temperature) using the Hougen – Watson – Ragatz diagram. The equilibrium pressures of the studied 1–olefins in the interval of 200–400°C are listed in Table 4.

Figure 15 displays the IR spectra of hydridesilicas treated with 1–hexene at 200°C. It is seen that during the interaction between hydridesilica I and olefin a distinct decrease in the intensity of the absorption band at 2280 cm^{-1} is observed providing evidence for the participation of hydride groups in the reaction (Fig.15, spectrum 2). Side by side with this the IR spectrum exhibits absorption bands for stretching vibrations of C–H bonds in attached hydrocarbon groups at 2970, 2940, and 2880 cm^{-1}, but the absorption band at 3080 cm^{-1} ascribed to vibrations of C–H bonds in $H_2C{=}CH-$ groups is absent from this spectrum [146]. Thus, on the basis of these IR spectral data it is possible to make a conclusion that in a surface layer of hydridesilica I a noncatalytic hydrosilylation reaction takes place:

$$\equiv SiH + H_2C = CH - (CH_2)_3 - CH_3 \rightarrow \equiv Si - CH_2 - CH_2 - (CH_2)_3 - CH_3 +$$
$$+ \equiv Si - CH(CH_3) - (CH_2)_3 - CH_3$$

At the same time the contact of hydridesilica II with 1–hexene vapours under the same conditions does not lead to any hydrosilylation of the surface: the intensity of the absorption band at 2190 cm^{-1} does not practically change. It should be noted that the

Table 4
Equilibrium pressures of 1-olefins at various temperatures

Temperature (°C)	Pressure in the autoclave (10^5·Pa)	
	1-Hexene ($t_{boil.}$ = 63.4°C)	1-Decene ($t_{boil.}$ = 170.6°C)
100	3	
150	8	
200	19	2
300	63	12
350	97	22
400	142	37

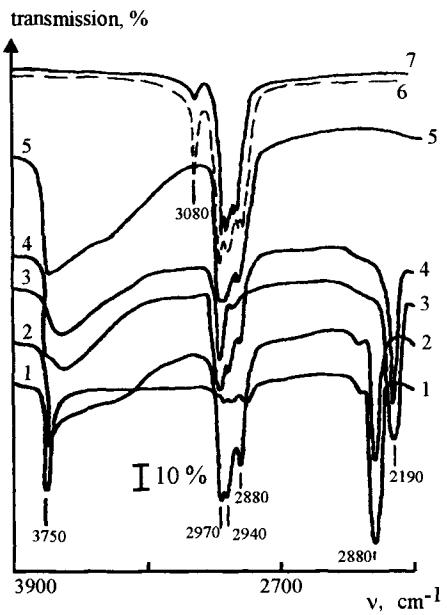

Figure 15. IR spectra of hydridesilicas I (1) and II (3), after the treatment with 1-hexene vapours in an autoclave at 200°C for 3 hr spectra (2) and (4) respectively). (5)-IR spectrum of hydrosilylated silica after the autoclave treatment with 1-hexene vapours at 200°C for 3 hr. The figure also shows the IR spectra of 1-hexene (l=0.01 mm) before (6) and after the autoclave treatment at 350°C (7).

appearance of the absorption band at 3750 cm^{-1} in the IR spectrum of hydridesilica II and the shift of the peak maximum of the absorption band for Si–H bonds into a low-frequency region are caused by the hydrolysis of Si–Cl groups [25,121] proceeding at the time of the transfer of a hydridesilica sample from the vacuum cell into the autoclave. Nevertheless, the IR spectrum of hydridesilica II (Fig.15, spectrum 4) exhibits absorption bands in the region of 3000–2800 cm^{-1} attributed to the attached hydrocarbon radicals. Hence, the immobilization of 1-hexene takes place at 200°C. During the interaction between 1-hexene and silica bearing only structural silanol groups under similar conditions the chemisorption of 1-olefin takes place as well (Fig.15, spectrum 5). It may be assumed that the reaction involves the participation of surface siloxane bonds and the formation of the attached oligomer [168].

With increasing interaction temperature the degree of the participation of silicon hydride groups in the hydrosilylation reaction increases, and the activity of ≡SiH groups of hydridesilica I in the reaction with 1-olefins becomes higher than that of hydridesilica II over the whole studied interval of temperatures (Fig.16 and 17). At 350–400°C the hydrosilylation reaction is accompanied with the thermal oligomerization of 1-olefin

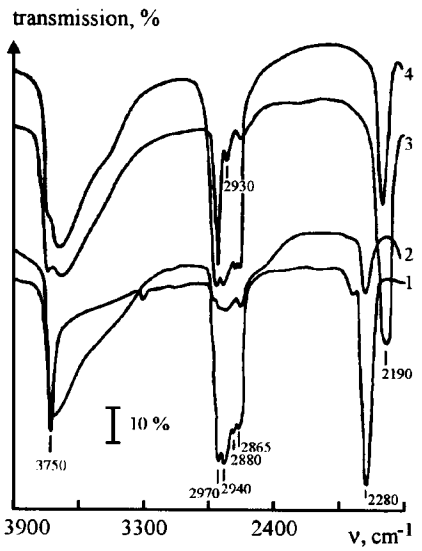

Figure 16. IR spectra of hydridesilicas I (1) and II (3) and those of hydridesilica modified with 1-hexene vapours in an autoclave at 300 (2) and 350°C (4) respectively.

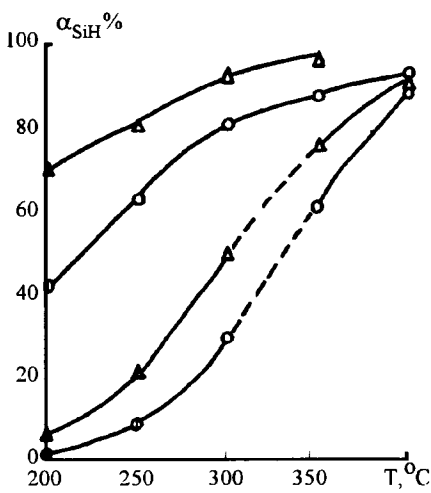

Figure 17. Dependence of the degree of the participation of silicon hydride groups I (—) and II (- - -) in the reaction with 1-hexene (○) and 1-decene (△) on the interaction temperature.

within the autoclave followed by the immobilization of the oligomer formed on the silica surface. This conclusion is corroborated by variation of the IR spectrum of 1-hexene (as compared to that of the starting 1-hexene) after the reaction in the autoclave above 300°C: there is observed a marked decrease in the intensity of the absorption bands at

3080 and 1640 cm^{-1} ascribed to stretching vibrations of C–H bonds in CH_2=CH– groups and to those of C=C bonds respectively.

One of the possible explanations of the higher activity of hydridesilica I in comparison with hydridesilica II in the hydrosilylation reaction of 1–olefins may be the induction effect of electron–seeking substituents on the value of the effective positive charge of a silicon atom of hydridesilica. Thus, the rate of the reaction of homogeneous hydrosilylation of 1–heptene in the presence of chloroplatinic acid decreases with increasing electron density on a hydrogen atom of hydridesilanes: $HSiCl_3 > C_2H_5SiHCl_2 > (C_2H_5)_2SiHCl > (C_2H_5)_3SiH$ [145]. In other words, the presence of electron–seeking substituents at a silicon atom increases the activity of hydridesilanes in the reaction with 1–heptene. Similar results for solid–phase hydrosilylation reaction of 1–olefins are presented here. The inference that the degree of completeness of the solid–phase hydrosilylation reaction depends on the electrophilicity of a silicon atom is corroborated by the data about the hydrolytic stability of Si–H bonds. The presence of electron–seeking groups in a molecule substantially increases the rate of the hydridesilane hydrolysis [150]. Therefore, the hydrolysis of Si–H bonds in hydridesilica I must proceed easier than in the case of hydridesilica II. Really, after boiling hydridesilica I in water for 1 hr its IR spectrum does not practically exhibit the band of ≡SiH groups, while in the case of hydridesilica II this band remains rather intense. Thus, the activity of modified silicas bearing the attached ≡SiH groups in the solid–phase hydrosilylation reaction seems to decrease in the order:

$$\equiv SiH > \equiv SiOSi(Cl_2)H > \equiv SiOSiCl(CH_3)H > \equiv SiOSi(CH_3)_2H$$

which agrees with the data obtained experimentally for the first and third members of the above–mentioned sequence. The activity of silicas modified with trichlorosilane and dimethylchlorosilane in reactions of solid–phase hydrosilylation has not been studied yet.

As is seen from Fig.17, the reactivity of 1–decene in the solid–phase hydrosilylation reaction is higher than that of 1–hexene. This can be accounted for by a higher electron density on a terminal carbon atom of a double bond of 1–decene since alkyl radicals are electron donors. For example, the positive induction effect of octyl groups is higher than that of butyl groups [144].

Thus, the researches on reactions of thermal solid–phase hydrosilylation (without a catalyst and a solvent) in a surface layer of hydridesilica I and II made it possible to reveal the distinctions in the reactivity both of 1–olefins and hydridesilicas. It has been established that the activity of 1–olefins is symbate to the electron density on a carbon atom of double bonds, and the reactivity of hydridesilicas increases with the electron–accepting ability of substituents at silicon atoms.

The fact that in principle it is possible to carry out solid–phase hydrosilylation reaction was also demonstrated in the case of other terminal simple olefins (1–octene, 1–tetradecene, 1–hexadecene, 1–octadecene) as well as of some functional compounds (acetyl acetone and vinyl acetate). In all the cases one can observe a process of oligomerization of reagents progressing with increasing interaction temperature, which manifests itself by high concentrations of organic groups attached to silica surface as compared to monomeric grafting. The derivatographic investigations of such modified silicas display the thermal destruction of organic groups in a range of 450–600°C, which is characteristic of polymers. The organosilicas produced have a high hydrolytic stability.

11. CONCLUSIONS

Up to the present a substantial experience has been gained in the field of the formation of modified silicas with attached silicon hydride and olefin groups. Matrices with attached silicon hydride groups can be produced as a result hydrolysis and polycondensation of trichloro- and triethoxysilane (including on silica surface), during chemical modification of silica with various organosilanes containing Si–H bonds or by means of the molecular layering method. The hydridesilicas can be produced by the reaction between inorganic hydrides and ≡SiCl groups of the chlorinated silica surface or as a result of the thermal destruction of methoxysilica. Matrices with attached silicon hydride groups can be successfully applied for carrying out processes of catalytic solid-phase hydrosilylation of simple terminal and functional olefins. Reactions of catalytic hydrosilylation proceed also with participation of attached olefin groups and hydrosilanes in a gaseous or liquid phase. The attachment of one of the participants of the hydrosilylation process to solid surface provides more convenient and favourable standpoints and approaches to researches into reaction mechanism. The experimental data give evidence that solid-phase catalytic hydrosilylation reactions involve the formation of intermediate complexes containing both of the reagents and the Speier catalyst. The possibility has been also established of effecting a non-catalytic reaction of solid-phase hydrosilylation of olefins at high pressures and temperatures. The modifying coatings obtained using solid-phase hydrosilylation reactions have a rather high hydrolytic stability and reproducible properties. This allows us to regard the reaction of solid-phase hydrosilylation as to the basis for one of promising methods of producing surface chemical compounds with Si–C bonds.

REFERENCES

1. V.A.Tertykh and L.A.Belyakova, Chemical Reactions with Silica Surface Participation, Naukova Dumka, Kiev, 1991 (in Russian).
2. K.A.Andrianov, Methods of Organoelement Chemistry. Silicon, Nauka, Moscow, 1968 (in Russian).
3. H.Deuel, Kolloid-Z., 124 (1951) 164.
4. W.F.Spenser and J.E.Gieseking, J.Phys.Chem., 56 (1952) 751.
5. H.Kautsky and B.Bartoche, Z.Naturforsch., 10b (1955) 422.
6. R.Yu.Sheinfain and I.E.Neimark, in Preparation, Structure and Properties of Sorbents, Gostekhizdat, Leningrad, 1959, p.136 (in Russian).
7. I.E.Neimark, A.A.Chuiko and I.B.Slinyakova, Vysokomolek. Soed., 3 (1961) 711.
8. V.A.Semikolenov, V.A.Likholobov and Yu. I.Ermakov, Kinetika i Kataliz, 18 (1977) 1294.
9. J.Chmielowiec and B.A.Morrow, J. Colloid Interface Sci., 94 (1983) 319.
10. J.J.Pesek and S.A.Swedberg, J.Chromatogr., 361 (1986) 83.
11. H.Gilman and S.Massie, J. Am. Chem.Soc., 68 (1946) 1128.
12. J.Wartmann and H.Deuel, Chimia, 12 (1958) 82.
13. H.Deuel and J.Wartmann, Helv.Chim.Acta, 42 (1959) 1166.
14. H.Deuel, Makromolekulare Chem., 34 (1959) 206.
15. H.P.Boehm and M.Schneider, Z.Anorg.Allg. Chem., 301 (1959) 326.
16. J.J.Fripiat, J.Uytterhoeven, U.Schobinger and H.Deuel, Helv.Chim.Acta, 43 (1960) 176.

17. H.P.Boehm, M.Schneider and H.Wistuba, Angew.Chem., 77 (1965) 622.
18. N.Fery, R.Hoene and K.Hamann, Angew.Chem., 84 (1972) 359.
19. T.B.Tennikova, L.V.Vinogradova, V.N.Zgonnik and B.G.Belenkii, Izv. AN SSSR, Ser.Khim., No. 2 (1987) 352.
20. H.Deuel and G.Huber, Helv.Chim.Acta, 34 (1951) 1697.
21. H.Deuel, G.Huber and Hs.H.Gunthard, Helv.Chim.Acta, 35 (1952) 1799.
22. H.Deuel and R.Iberg, Helv.Chim.Acta, 36 (1953) 808.
23. R.Gentily and H.Deuel, Helv.Chim.Acta, 40 (1957) 106.
24. K.H.Ebert, Monatsh. Chem., 88 (1957) 275.
25. A.A.Chuiko, V.A.Tertykh, V.A.Khranovskii, Yu.P.Egorov and L.M.Roev, Teoret. i Eksperim. Khimiya, 2 (1966) 247.
26. Modified Silicas in Sorption, Catalysis and Chromatography, G.V.Lisichkin (Ed.), Khimiya, Moscow, 1986 (in Russian).
27. G.H.Wagner and A.N.Pines, Ind. Eng.Chem., 44 (1952) 321.
28. R.Muller, Chem. Techn., 2 (1950) 7.
29. R.Muller, Chem. Techn., 2 (1950) 41.
30. I.B.Slinyakova, G.B.Budkevich and I.E.Neimark, Dokl. AN SSSR, 154 (1964) 692.
31. I.B.Slinyakova, G.B.Budkevich and I.E.Neimark, Kolloid.Zhurn., 27 (1965) 758.
32. G.B.Budkevich, I.B.Slinyakova and I.E.Neimark, Kolloid.Zhurn., 28 (1966) 21.
33. I.B.Slinyakova and G.B.Budkevich, Ukr. Khim. Zhurn., 33 (1967) 157.
34. I.B.Slinyakova and A.N.Korol, Ukr. Khim. Zhurn., 33 (1967) 373.
35. G.B.Budkevich, I.B.Slinyakova, E.F.Polstyanov, M.M.Dubinin and I.E.Neimark, Izv. AN SSSR, Ser. Khim., No. 3 (1968) 467.
36. G.B.Budkevich, I.B.Slinyakova and I.E.Neimark, Kolloid. Zhurn., 32 (1970) 17.
37. G.B.Budkevich, I.N.Slinyakova, I.E.Neimark and Ya.V.Zhigailo, Ukr. Khim. Zhurn., 37 (1971) 429.
38. L.N.Ganyuk, I.B.Slinyakova and I.E.Krot, Teoret. i Eksperim. Khimiya, 7 (1971) 109.
39. I.B.Slinyakova, L.I.Kurennaya and I.E.Neimark, Fiz.–Khim. Mekh. Liofilnost Dispersnykh Sist., No. 2 (1971) 313.
40. L.I.Kurennaya and I.B.Slinyakova, Kolloid. Zhurn., 37 (1975) 178.
41. I.B.Slinyakova and T.I.Denisova, Organosilicon Adsorbents. Preparation, Properties, Application, Naukova Dumka, Kiev, 1988 (in Russian).
42. G.B.Budkevich, V.Ya.Momot, I.I.Sirenko, Yu.A.Tarasenko and I.A.Sheka, Ukr. Khim. Zhurn., 40 (1974) 364.
43. G.B.Budkevich, V.Ya.Momot, I.I.Sirenko and Yu.A.Tarasenko, Khim. Tekhnologiya, No. 6 (1973) 50.
44. G.B.Budkevich, V.Ya.Momot, I.I.Sirenko, Yu.A.Tarasenko and I.A.Sheka, Zhurn. Prikl. Khimii, 47 (1974) 2217.
45. J.J.Pesek, J.E.Sandoval, C.–H. Chu, M.Auvenin and P.Visser, Abstracts of Intern. Conf. Oxide Surface Chemistry and Reaction Mechanisms, vol.1, Kiev, 1992, p.40.
46. C.–H.Chu, E.Jonsson, M.Auvinen, J.J.Pesek and J.E.Sandoval, Anal. Chem., 65 (1993) 808.
47. G.Engelhardt, H.Jancke, E.Lippmaa and A.Samoson, J.Organomet. Chem., 210 (1981) 295.
48. A.Baigozhin and L.V.Sergeev, Vysokomolek. Soed., 4 (1962) 972.
49. L.V.Sergeev, A.Baigozhin and S.G.Fattakhov, Vysokomolek. Soed., 4 (1962) 977.

50. S.I.Koltsov, Zhurn. Prikl. Khimii, 38 (1965) 1384.
51. S.I.Koltsov, G.N.Kuznetsova and V.B.Aleskovskii, Zhurn. Prikl. Khimii, 40 (1967) 2774.
52. S.I.Koltsov, G.N.Kuznetsova and V.B.Aleskovskii, Izv. AN SSSR, Neorg. Mater., 3 (1967) 894.
53. S.I.Koltsov and V.B.Aleskovskii, Zhurn. Fiz. Khimii, 41 (1967) 665.
54. V.A.Sobolev, V.A.Tertykh and A.A.Chuiko, Zhurn. Prikl. Spektroskopii, 10 (1969) 928.
55. V.V.Strelko and V.A.Kanibolotskii, Kolloid. Zhurn., 33 (1971) 750.
56. L.F.Petrova, V.A.Tertykh and V.V.Pavlov, in: Surface Phenomena in Dispersed Systems, Naukova Dumka, Kiev, 1975, p.46 (in Russian).
57. M.J.D.Low and A.G.Severdia, J.Catal., 54 (1978) 219.
58. M.J.D.Low, A.G.Severdia and J.Chan, J.Catal., 71 (1981) 144.
59. M.J.D.Low and A.G.Severdia, J. Mol. Struct., 80 (1982) 209.
60. M.J.D.Low, A.G.Severdia and J.Chan, J. Colloid Interface Sci., 86 (1982) 111.
61. A.G.Severdia, C.Morterra and M.J.D.Low, J. Colloid Interface Sci., 99 (1984) 208.
62. P.Van der Voort, I.Gillis-D'Hamers and E.F.Vansant, J. Chem. Soc., Faraday Trans., 86 (1990) 3751.
63. P.Van der Voort, I.Gillis-D'Hamers, K.C.Vrancken and E.F.Vansant, J. Chem. Soc., Faraday Trans., 87 (1991) 3174.
64. P.Van der Voort, J.Swerts, K.C.Vrancken and E.F.Vansant, J. Chem. Soc., Faraday Trans., 89 (1993) 63.
65. P.Van der Voort, K.C.Vrancken, E.F.Vansant and J.Riga, J. Chem. Soc., Faraday Trans., 89 (1993) 2509.
66. P.M.Vainschtein, S.I.Koltsov, Yu.K.Ezhovskii and V.B.Aleskovskii, Dokl. AN SSSR, 258 (1981) 927.
67. P.M.Vainschtein, Yu.K.Ezhovskii and S.I.Koltsov, Zhurn. Fiz. Khimii, 55 (1981) 394.
68. P.M.Vainschtein, S.I.Koltsov, Yu.K.Ezhovskii and E.A.Ivanova, Zhurn. Fiz. Khimii, 57 (1983) 1728.
69. P.M.Vainschtein, S.I.Koltsov and Yu.K.Ezhovskii, Zhurn. Fiz. Khimii, 57 (1983) 1733.
70. K.Yoshinaga, H.Yoshida, Y.Yamamoto, K.Takakura and M.Komatsu, J. Colloid Interface Sci., 153 (1992) 207.
71. A.Tuel, H.Hommel, A.P.Legrand and E.Sz.Kovats, Langmuir, 6 (1990) 770.
72. R.D.Golding, A.J.Barry and M.F.Burke, J.Chromatogr., 384 (1987) 105.
73. F.Meiouet, G.Felix, H.Taibi, H.Hommel and A.P.Legrand, Chromatographia, 31 (1991) 335.
74. L.N.Ganyuk, Adsorbtsiya i Adsorbenty, 1 (1972) 101.
75. L.N.Ganyuk, Adsorbtsiya i Adsorbenty, 1 (1972) 98.
76. M.J.D.Low, J. Catal., 103 (1987) 496.
77. J.E.Sandoval and J.J.Pesek, Anal. Chem., 61 (1989) 2067.
78. A.I.Mashchenko, Kinetika i Kataliz, 15 (1974) 1015.
79. I.Gillis-D'Hamers, J.Philippaerts, P.Van der Voort and E.Vansant, J. Chem. Soc., Faraday Trans., 86 (1990) 3747.
80. C.Morterra and M.J.D.Low, Chem. Commun., No. 4 (1968) 203.
81. C.Morterra and M.J.D.Low, J.Phys.Chem., 73 (1969) 321.

82. C.Morterra and M.J.D.Low, J.Phys.Chem., 73 (1969) 327.
83. T.V.Voskoboinikov, M.V.Vishnetskaya, A.Yu.Loginov and B.V.Romanovskii, React. Kinet. Catal. Lett., 39 (1989) 387.
84. A.A.Chuiko, V.V.Pavlov, A.I.Scherstyuk and V.A.Tertykh, Kolloid. Zhurn., 36 (1974) 1012.
85. V.V.Brei, V.M.Gunko, V.D.Khavryuchenko and A.A.Chuiko, Kinetika i Kataliz, 31 (1990) 1164.
86. J.Bjorksten, L.L.Yaeger and J.E.Hennig, Ind. Eng. Chem., 46 (1954) 1632.
87. B.M.Vanderbilt, Mod. Plastics, 37 (1959) 125.
88. B.M.Vanderbilt and J.P.Simko, Mod. Plastics, 38 (1960) 135.
89. W.Moebes and A.Wende, Plaste und Kautschuk, 9 (1962) 232.
90. I.E.Neimark, A.A.Chuiko, G.A.Blokh, T.R.Gendler and A.D.Chugai, Izv. Vyssh. Ucheb. Zaved., Tekhn. Legk. prom., No. 2 (1962) 60.
91. A.A.Chuiko and I.E.Neimark, Izv. Vyssh. Ucheb. Zaved., Tekhn. Legk. prom., No. 5 (1962) 32.
92. I.B.Slinyakova and I.E.Neimark, Kolloid. Zhurn., 24 (1962) 220.
93. A.A.Chuiko, I.E.Neimark, I.M.Landa, E.V.Tsipenyuk and E.A.Chuiko, Kauchuk i Rezina, No. 6 (1963) 31.
94. A.A.Chuiko and E.A.Chuiko, in: Synthesis and Physico–chemistry of Polymers, Naukova Dumka, Kiev, 1964, p.83 (in Russian).
95. E.A.Chuiko and A.A.Chuiko, in: Synthesis and Physico–chemistry of Polymers, Naukova Dumka, Kiev, 1966, p.129 (in Russian).
96. T.N.Burushkina and A.A.Chuiko, Teoret. i Eksperim. Khimiya, 1 (1965) 394.
97. T.N.Burushkina, A.A.Chuiko, N.V.Khaber and L.V.Manchenko, Teoret. i Eksperim. Khimiya, 4 (1968) 570.
98. V.A.Tertykh, T.N.Burushkina and A.A.Chuiko, in: Modification of Properties of Polymers and Polymeric Materials, Naukova Dumka, Kiev, 1965, p.85 (in Russian).
99. A.A.Chuiko, G.E.Pavlik, V.A.Tertykh, E.A.Chuiko, V.A.Artemov, I.E.Neimark and E.V.Tsipenyuk, Ukr. Khim. Zhurn., 32 (1966) 371.
100. S.N.Nikonova, L.I.Golubenkova, A.N.Shabadash and M.S.Akutin, Plast. Massy, No. 3 (1966) 45.
101. A.A.Chuiko, T.N.Burushkina, V.A.Sobolev, D.B.Boguslavskii, Kh.N.Borodushkina, T.R.Gendler, G.I.Levit, G.A.Blokh and V.Ya.Vasilenko, Kolloid.Zhurn., 31 (1969) 777.
102. J.L.Koenig, P.T.K.Shin and P.Lagally, Mater.Sci. Eng., 20 (1975) 127.
103. M.E.Abu–Zeid, G.S.Mahmoud, A.A.Anani, A.F.Halasa and A.A.Mobasher, J. Photochem., 16 (1981) 279.
104. D.Gorski, E.Klemm, P.Fink and H.–H.Horhold, J. Colloid Interface Sci., 126 (1988) 445.
105. M.Chaimberg and Y.Cohen, J. Colloid Interface Sci., 134 (1990) 576.
106. A.Iarena, M.U.de la Orden and J. Matinez Urreaga, J. Colloid Interface Sci., 149 (1992) 34.
107. L.B.Zubakova, V.N.Borisova, S.K.Koroleva, K.G.Gileva, E.S.Gryaznova and L.A.Nakhapetyan, Zhurn. Prikl. Khimii, 59 (1986) 1182.
108. V.N.Borisova, S.A.Akhnazarova, S.K.Koroleva, L.B.Zubakova, K.G.Gileva and E.S.Gryaznova, Zhurn. Prikl. Khimii, 61 (1988) 1663.
109. J.J.Pesek, P.Mahabadi and Shih–Jen Chen, Chromatographia, 23 (1987) 3.

110. V.V.Yanishpolskii, V.A.Tertykh and G.V.Lyubinskii, Ukr. Biokhim. Zhurn., 31 (1979) 324.
111. J.J.Pesek and Wan Ying Wey, Chromatographia, 25 (1988) 969.
112. J.J.Pesek and G.Guiochon, J. Chromatogr., 395 (1987) 1.
113. J.J.Pesek, E.L.Tarver and A.Lange, Chromatographia, 24 (1987) 815.
114. H.Engelhardt, H.Low, W.Engelhardt and M.Mauß, Chromatographia, 27 (1989) 535.
115. H.W.Stuurman, J.Kohler and G.Schomburg, Chromatographia, 25 (1988) 265.
116. J.J.Pesek and W.Rashet, Chromatographia, 30 (1990) 442.
117. H.S.Hsien, S.D.Fazio, S.A.Tomellini, J.B.Crowther and R.A.Hartwick, Chromatographia, 20 (1985) 161.
118. J.J.Pesek and T.Cash, Chromatographia, 27 (1989) 559.
119. A.V.Simurov and L.A.Belyakova, Abstracts of Conf. on Surface Chemistry of Dispersed Solids, Slavsko, 1989, p.134.
120. V.A.Tertykh, L.A.Belyakova and A.V.Simurov, Abstracts of Intern. Conf. Structure and Reactivity of Organosilicon Compounds, Irkutsk, 1989, p.154.
121. V.A.Tertykh, L.A.Belyakova and A.V.Simurov, Zhurn. Fiz. Khimii, 64 (1990) 1410.
122. V.A.Tertykh, L.A.Belyakova and A.V.Simurov, Abstracts of ACS Meeting and Fourth North American Chemical Congress, New York, 1991, p.94.
123. V.A.Tertykh, L.A.Belyakova and A.V.Simurov, Dokl. AN SSSR, 318 (1991) 647.
124. V.A.Tertykh, L.A.Belyakova and A.V.Simurov, Mendeleev Commun., 2 (1992) 46.
125. L.A.Belyakova, A.V.Simurov, D.Yu.Lyashenko and V.A.Tertykh, Ukr. Khim. Zhurn., 58 (1992) 630.
126. A.V.Simurov, L.A.Belyakova and V.A.Tertykh, Abstracts of Intern. Conf. Oxide Surface Chemistry and Reaction Mechanisms, vol.2, Kiev, 1992, p. 226.
127. L.A.Belyakova and A.V.Simurov, Ukr. Khim. Zhurn., 60 (1994) 1400.
128. A.M.Varvarin, L.A.Belyakova and V.A.Tertykh, Ukr. Khim. Zhurn., 59 (1993) 272.
129. V.A.Tertykh and L.A.Belyakova, Zhurn. Fiz. Khimii, 67 (1993) 2116.
130. V.A.Tertykh, L.A.Belyakova, A.V.Simurov and D.Yu.Lyashenko, Abstracts of X-th Intern.Symp. on Organosilicon Chemistry, Poznań, 1993, p.111.
131. L.A.Belyakova, A.V.Simurov and V.A.Tertykh, Ukr. Khim. Zhurn., 60 (1994) 201.
132. L.A.Belyakova and A.M.Varvarin, Abstracts of XIII European Chemistry at Interfaces Conference, Kiev, 1994, p.123.
133. L.A.Belyakova, A.V.Simurov, V.G.Ivanova, V.V.Sidorchuk and V.A.Tertykh, The Method for Silica Modification, SSSR Patent No. 1724574 (1992).
134. L.A.Belyakova, A.V.Simurov, V.V.Sidorchuk and V.A.Tertykh, The Method for Silica Modification, SSSR Patent No. 1742208 (1992).
135. L.A.Belyakova, V.G.Ivanova, D.Yu.Lyashenko, A.V.Simurov and V.A.Tertykh, The Method for Preparation of Silica Sorbent, SSSR Patent No. 1776433 (1992).
136. L.A.Belyakova, V.G.Ivanova, D.Yu.Lyashenko, A.V.Simurov and V.A.Tertykh, The Method for Preparation of Sorbent, SSSR Patent No. 1825651 (1993).
137. L.A.Belyakova, V.G.Ivanova, A.V.Simurov and V.A.Tertykh, The Method for Preparation of Modified Silica, SSSR Patent No. 1791384 (1993).
138. V.P.Yur'ev and I.M.Salimgareeva, Hydrosilylation Reaction of Olefins. Metallocomplex Catalysis in the Processes of Hydrosilylation, Stereochemistry and Mechanism of Reactions, Nauka, Moscow, 1982 (in Russian).
139. A.Ahmed and E.Gallei, Appl.Spectrosc., 28 (1974) 430.

140. D.Gorski, E.Klemm, P.Fink and H.–H.Horhold, J. Colloid Interface Sci., 126 (1988) 445.
141. A.N.Terenin and A.N.Sidorov, Optiko–mekhan. promyshlennost', 1 (1959) 1.
142. J.E.Sandoval and J.J.Pesek, Anal. Chem., 63 (1991) 2634.
143. E.V.Alekseevskii, R.K.Gol'ets and A.P.Musakin, Quantitative Analysis, Izd–vo khim. lit., Leningrad, 1955 (in Russian).
144. P.Sykes, A Guidbook to Mechanism in Organic Chemistry, Longmans, London, 1967.
145. E.Ya.Lukevits, Uspekhi Khimii, 46 (1977) 507.
146. L.J.Bellamy, Advances in Infrared Group Frequencies, Methuem, Suffolk, 1968.
147. G.Greber and H.Gruber, The Method for Preparation of Modified Aerosil, Germany Patent No. 38349493 (1990).
148. V.A.Tertykh, L.A.Belyakova, A.M.Varvarin, L.A.Lazukina and V.P.Kukhar, Teoret. i Eksperim. Khimiya, 18 (1982) 717.
149. V.A.Tertykh and V.M.Ogenko, Teoret. i Eksperim. Khimiya, 11 (1975) 827.
150. A.D.Petrov, B.Ph.Mironov, V.A.Ponomarenko and E.A.Chernyshov, Synthesis of Organosilicon Monomers, Izd. AN SSSR, Moscow, 1961 (in Russian).
151. A.J.Gordon and R.A.Ford, A Handbook of Practical Data, Techniques and References, John Wiley and Sons, New York–London–Sydney–Toronto, 1972.
152. E.Ya.Lukevits and M.G.Voronkov, Hydrosilylation, Hydrogermylation and Hydrostannylation, Izd. AN Latv.SSR, Riga, 1964 (in Russian).
153. B.B.Wheals, J. Chromatogr., 107 (1975) 402.
154. J.–P.Lefevre, A.Divry, M.Caude and R.Rosset, Analysis, 3 (1975) 533.
155. M.Chaimberg, J.Cohen, J.Colloid Interface Sci., 134 (1990) 576.
156. N.A.Chumaevskii, Vibrational Spectra of Elementoorganic Compounds of IV B and V B Groups, Nauka, Moscow, 1971 (in Russian).
157. I.L.Speier, Adv. Inorganometallic Chem., 17 (1979) 407.
158. K.B.Yatsimirskii and T.V.Malkova, in: Spectral Methods in Chemistry of Complex Compounds, Khimiya, Moscow–Leningrad, 1964, p.102 (in Russian).
159. A.B.P.Lever, Inorganic Electronic Spectroscopy, Elsevier, Amsterdam–Oxford–New York–Tokyo, 1984.
160. V.B.Pukhnarevich, B.A.Trophimov, L.I.Kopylova and M.G.Voronkov, Zhurn. Obshch. Khimii, 43 (1973) 2691.
161. M.G.Voronkov, N.G.Romanova and L.G.Smirnova, Chem. Listy, 52 (1958) 640.
162. M.G.Voronkov and N.G.Romanova, Chem. Listy, 28 (1958) 2122.
163. M.G.Voronkov and V.B.Pukhnarevich, Izv. AN SSSR, Ser. Khim., No. 5 (1982) 1056.
164. M.G.Voronkov, S.P.Sushchinskaya, V.B.Pukhnarevich and O.I.Randin, Zhurn. Obshch. Khimii, 49 (1979) 1281.
165. G.H.Wagner, Active Silica, US Patent No. 2705222 (1955).
166. M.Kh.Karapetyants and Chang–Gyang–Yua, Boiling Temperature and Pressure of Hydrocarbons Saturated Vapour, Gostoptekhkhimizdat, 1961 (in Russian).
167. M.Kh.Karapet'yants, Chemical Thermodynamics, Khimiya, Moscow, 1975 (in Russian).
168. L.A.Belyakova, A.M.Varvarin, V.V.Sidorchuk, A.V.Simurov and V.A.Tertykh, Ukr. Khim. Zhurn., 58 (1992) 30.

This Page Intentionally Left Blank

A. Dąbrowski and V.A. Tertykh (Editors)
Adsorption on New and Modified Inorganic Sorbents
Studies in Surface Science and Catalysis, Vol. 99

Chapter 1.7
Structure and molecular organization of bonded layers of chemically modified silicas

A.Yu.Fadeev and G.V.Lisichkin

Laboratory of Organic Catalysis, Chemical Department, M.V.Lomonosov Moscow State University, 119899 Moscow, Russia

1. INTRODUCTION

The science of solid–state surface, as well as molecular biology, is at present one of the most progressively developing area of natural science. Among many divisions of surface science, chemistry of solid–state surface and chemical modification of inorganic surfaces play an important role. The progress in these areas arises from the following. Materials, which contain surface bonded organic, inorganic, organometallic or natural compounds are widely used in different areas of modern technology. Objects with modified surfaces possess physical properties of solid support, whereas their chemical properties are mainly determined by the nature of bonded compounds. At the same time, these materials may acquire new valuable properties.

Pioneer investigations in chemical modification of mineral surface were performed by Kiselev and his colleagues [1]. The observed irreversible adsorption of methyl alcohol vapours on silica was associated with substitution of surface silanols with methoxy groups. At the same time, Deuel and co–workers [2–4] have performed surface modification of some clays. They used reactive organic compounds, which can readily react with surface hydroxyls. It is important that even in the early studies the goal of surface chemical modification was the directed changes of adsorptional and adhesive properties of solids.

The intensive progress of chemical modification of mineral surfaces started in the seventies. Practice required a design of immobilized metallocomplexes, the methods of immobilization of enzymes and other biopolymers and, in particular, the methods for preparation of stationary phases for high performance liquid chromatography.

The number of *surface modified mineral materials* described in literature is progressively growing. By now, the methods for fixation of not less than one thousand of individual compounds has been developed. It is not overestimation to say that synthetic methods of surface science allow for covalent immobilization of practically any of chemical compounds or functional groups on a mineral surface.

There is no question that new scientific domain in surface chemistry – *the chemistry of surface bonded compounds* has recently appeared. This scientific domain appeared at the interfaces between chemistry of solids, colloid chemistry, adsorption, macromolecular chemistry and topochemistry. The isolation of this domain is well founded, since it has

its own unique subject for study and can not be reduced to the above mentioned fields of science.

The subject matter of the chemistry of surface bonded compounds constitutes a solid mineral support with, covalently attached on its surface, layer of either individual molecules or their aggregates, or even different particles. In most cases, the bonded layer is significantly distinguished from the support by chemical nature. It is important that skeleton of support remains practically unchanged after chemical modification of its surface, while bonded molecules form strong (covalent) bonds with the functional groups of surface. The above conditions are met for a wide range of inorganic supports, a wide variety of modifier molecules and various reactions of surface modification.

Clearly, the borderlines between the interdisciplinary sciences in question are vague. Thus, one can gradually go on from typical organic polymer swelling in the appropriate solvent via highly cross-linked non-swelling plastics up to carbon black, coal, graphite and next to rigid solid oxide-based supports. There is no clear threshold also between chemical reactions on surface and physical adsorption, and adhesion.

2. TERMINOLOGY

The chemistry of surface bonded compounds, being only a forming area of surface chemistry, has no fully accepted terminology. Terms and conceptions taken from the related areas are usually used. Sometimes this results in confusions and misunderstanding. Therefore, we suggest determination of the basic terms used in our previous publications and present paper.

Support (carrier, matrix) - the solid matter, the participant of chemical modification. Support might be both mono or polycrystalline, amorphous, more or less dispersed and pelicular. There are inherent (structural) functional groups on the surface of support. The latter are responsible for the reactivity of surface. Normally, inorganic oxides or metals covered with oxide films are used as supports. Not less than 90% of studies in this field is performed on a silica surface. This comes from the following facts. Firstly, silica has "soft" surface hydroxyls; secondly, silica is commercially available in a wide range of pore, particle sizes and specific surface areas.

Modifier, substance to be bonded - molecule, oligomer, polymer, particle - the participant of chemical modification. Modifier reacts chemically with the surface functional groups. The basic types of surface reactions are given below (S - support; X, Y - modifiers, X_s, Y_s-surface bonded groups; inherent surface functional groups are not shown):

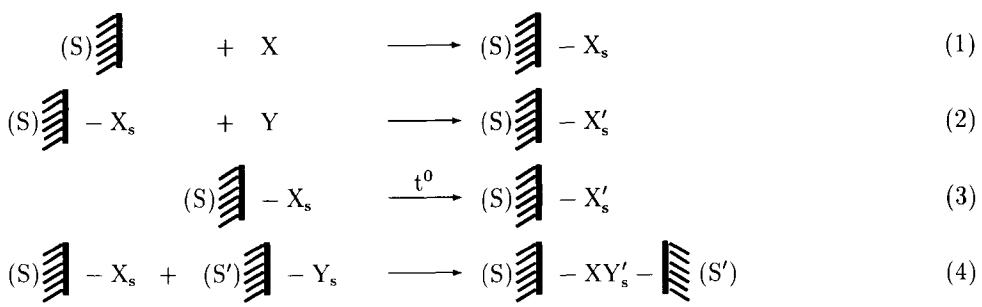

The reaction between the modifier and the structural groups of surface resulting in a fixation of the modifier on a surface is referred to as *immobilization reaction*, Eq. (1). Transformation of already bonded groups is referred to as *the surface assembly reaction*, Eq. (2). Decomposition, release, hydrolysis and other transformations of already bonded groups, that is surface chemical modifications without clear participation of the modifier, are also possible, Eq. (3). Besides, the interaction between two chemically modified supports is rather possible, Eq. (4).

One of the most popular sort of modifiers is organosilicon compounds. This is due to the fact that certain of organosilicon modifiers are commercially available and many of them can be synthesized in laboratory. On the other hand, rather stable chemical bonds Me–O–Si–C are formed after the interaction between the silanes and the surface hydroxyls. Especially stable linkage Si–O–Si–C appears when silica is modified with silanes.

Bonded layer – a collection of bonded compounds formed upon chemical modification and fixed on the surface. Bonded layer is the central issue in the surface chemistry of chemically modified solids. Indeed, it is composition, structure and other properties of bonded layer that mainly determine the surface properties of chemically modified support.

Bonding density (surface concentration) – a number of bonded molecules, particles per unit of surface area accessible for a given molecule. Two comments are worth mentioning here. The amount of functional groups in the sample should be related to the unit of surface different from the unit of mass of support:

$$c_s[\text{mol/sq.m}] = m_s/S \tag{5}$$

Then the surface concentration is an informative value if only the surface accessible toward the molecules under study is known. In practice, the accessible surface is markedly decreased as the size of a modifier is increased. The surface areas accessible toward a selection of adsorbates and modifiers on silica are presented in Table 1.

Table 1
Specific surface area of silicas (sq.m per g) determined using adsorbates of different sizes [5]

Adsorbed (bonded) molecule	Cross-sectional area, sq.nm	Silica gel KSS-3 (D=2.90)	Silica gel Silasorb L (D=2.33)	Aerosilogel Silokhrom S-120 (D=2.14)
N_2	0.162	484 ± 50	449 ± 50	169 ± 20
CH_3OH	0.199		347 ± 35	
Me_3Si–	0.416	383 ± 43	339 ± 42	183 ± 33
Ph_2EtSi–	0.727	240 ± 17	308 ± 16	159 ± 26
$(C_6H_{13})_3Si$–	1.450	224 ± 24	289 ± 24	135 ± 22

Using the idea of surface fractality [6–8] one can determine the accessible surface fractal dimension toward molecules of a given size (σ_1):

$$S(\sigma_2)/S(\sigma_1) = (\sigma_2)^{(2-D)/2} \tag{6}$$

D is the surface fractal dimension ($2 \leq D < 3$), $S(\sigma_i)$ – the specific surface determined by molecules with the cross-section σ_i. D is close to two for the geometrically smooth, uniform surface and it is close to three for geometrically nonuniform, narrow-pored surface.

Along with bonding density, the *extent of surface coverage* with a given bonded compound is an important characteristics of the surface modified solids. By definition, this is the ratio of surface concentration of bonded molecules to the maximum surface concentration for this bonded compound on a geometrically uniform, flat surface. The maximum surface concentration for a given bonded compound is determined with the size and structure of the modifier and with the surface concentration of functional groups of the surface. The latter depends on the crystalline structure of a support and on its history. The maximum surface concentrations for selected organosilicon modifiers on amorphous silica are given in Table 2.

Table 2
Maximum surface concentration of silanes on silica gels

Modifier	Maximal bonding density,		References
	groups/nm^2	μmol/m^2	
n-Alkyldimethylsilanes (C_1-C_{18})	2.4–2.8	4.0–4.7	[9 – 12]
Triethoxysilanes	1.4–1.6	2.3–2.7	[12, 13]
Triphenylsilanes	1.3–1.5	2.2–2.5	[13]

It should be noted that in surface chemistry, unlike the adsorption, the term "extent of surface coverage" means the yield of surface chemical reaction. Therefore, this notion should be used only with simultaneous specification of the modifier structure. For example, modification of silica with methyltrichlorosilane yields about 2.4 bonded methyl groups per sq.nm, whereas modification with methyltriethoxysilane yields not more than 1.6 bonded methyl groups per sq.nm. At the same time, both reactions achieve 100% yield of surface reactions and, therefore, the complete coverage of surface.

Pointing out not rigorous definition of this notion, we do not recommend it to be used without a special need.

3. DISTRIBUTION OF BONDED MOLECULES

There are *dense (monolayer) bonded layers* and *bonded layers with submonolayer coverages*. By definition, the former have bonding density close to the maximal limit, the latter have surface coverage significantly lower than the unit, e.g. from zero up to 0.3. The most important property of chemically modified support with submonolayer coverage is the *organization of bonded molecules throughout the surface.*

The problem of distribution of bonded molecules over the surface is among the most significant issues for understanding the structure of bonded layer of chemically modified supports. Character of the distribution of bonded molecules might exert an essential in-

fluence on the properties of modified supports. If some surface is modified by two or more modifiers [14–16], it is of interest whether they are mixed uniformly over the surface. Properties of such "multiphases" would differ from those of mechanical mixtures of packings of each kind, only if the distribution is uniform.

A few papers on experimental investigation of the character of distribution of bonded groups have been published [17–21], and we shall discuss their results in a due place.

3.1. Basic types of distribution of bonded molecules on the silica surface

Chemical modification can presumably lead to three basic types of the distribution of bonded modifier molecules over the surface, namely random, island–like, and uniform (Fig.1) [22]. Different types of distribution correspond to different mechanisms of surface

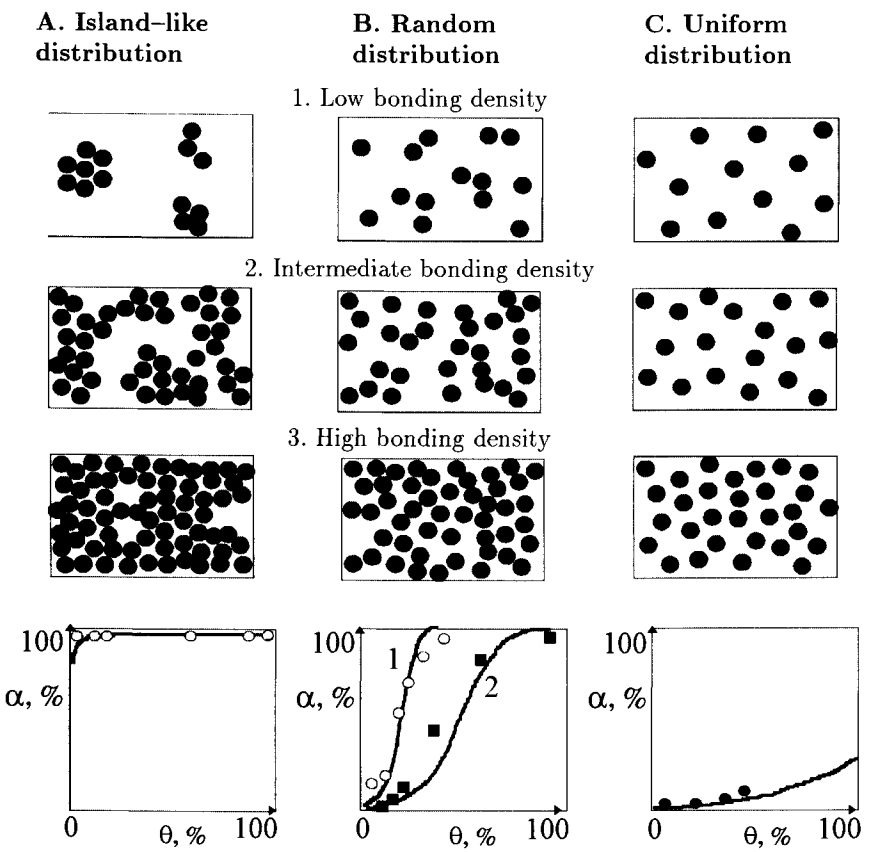

Figure 1. Distribution of bonded molecules along the surface at low, intermediate and high bonding densities for island–like (A), random (B) and uniform (C) types of distribution. Bottom row: dependencies between the amount of bonded molecules in clusters (α) and the extent of surface coverage (θ) for the corresponding types of distributions. Points correspond to the following experimental data: ○ — 3–bromopropyldimethylchlorosilane on silica; ■ — lysine on tosyl–activated silica; ● — n–octadecylamine on epoxy–activated silica (this work); ○ — [3–(3–pyrenyl)propyl]–dimethylchlorosilane on silica [20]. Solid curves 1 and 2 are calculated for l=1.2d and 2.0d respectively (see explanation in the text).

coverage by modifier. For a while we will leave aside the problem why one or another mechanism occurs, and devote our attention to basic features of different types of distribution and the respective mechanisms of surface coverage.

Random distribution. Molecules of modifier react with the surface independently. Mechanism of surface coverage might be called random. For distribution of such sort the bonded layer composition is polydispersed. Bonded molecules might be either isolated or form clusters of two or more species. Since bonded molecules are not engaged in lateral motions, dense monolayer coverage could not be achieved due to unavoidable gaps (Fig.1, middle column).

Size of these gaps could amount to the value of surface requirement for anchor groups of the modifier, namely 0.35–0.45 sq.nm for dimethylsilanes, 0.6– 0.7 sq.nm for triethoxysilanes. Published data [23] and our computation results show that the maximum surface coverage in this case is only 51–56% of the theoretical limit (see below).

Island–like distribution. Bonded molecules favour other molecules to be bound nearby (positive neighbour effect). The mechanism of surface coverage is described by formation and development of islands of bonded molecules. As long as the extent of surface coverage is small, the bonded layer consists of clusters of variable size, isolated molecules being scarce. With the increase of the extent of coverage growing clusters would coalesce to form a dense monolayer coverage with a limited number of faults (Fig.1, left column).

Uniform distribution. Modifier molecules do not tend to react with the surface within some region from the bound molecules (negative neighbour effect). With a small extent of surface coverage the bonded layer consists mostly of lone molecules. Increase in the surface coverage results in retardation of modification reaction, making high extents of coverage not feasible (Fig.1, right column).

It is noteworthy that for assignment of the type of distribution the ratio of areas, occupied by a reactive site on which modifier is bound, and by modifier itself should be taken into account. If this ratio is greater than unity the result of extensive modification would not depend on the coverage mechanism and type of distribution respectively.

For simplicity, below we neglect possible energetic inhomogeneity of the surface. However, this factor might be crucial for realization of one or another type of distribution of bonded molecules.

3.2. General requirements for the methods applicable to probing surface distribution of bonded groups

Distribution of bonded molecules may be examined by means of any physico- chemical method sensitive to intermolecular interactions, e.g. luminescence or ESR. Here we are not going to discuss the use of electronic microscopy and scanning tunnelling microscopy for the investigation of the spatial organization of bonded layers. The first method needs "heavy atoms" in the bonded layer, the second – electroconductive and, where possible, smooth or monocrystalline supports.

Two possible routes may be proposed to deal with the problem. The first, put forward in [19,20] utilises a modifier carrying some kind of labels, e.g. luminescent ones. In the alternative approach the labels are generated after completion of the modification process by treatment with appropriate developer agents [17,18]. The latter approach is advantageous since it allows for the investigation of practical samples, though the development procedure itself should be chosen to meet a number of restrictions.

The relative amount of proximate bonded molecules estimated for small extents of surface coverage serves as a quantitative criterion for distinguishing between different types of distributions. Indeed, differences between distributions are especially marked for small loading (Fig.1).

It is noteworthy that the notion of "proximity" might differ for different methods of investigation. In papers [20,21] 3-(3-pyrenyl)-propyldimethyl- chlorosilane was used as a modifier and fluorescence spectroscopy – as a method of investigation. Type of distribution of bonded molecules was inferred from the observation of a new signal in spectra assigned to the excimer emission from the pairs of bonded molecules. The authors [20,21] believed that the intensity of excimer emission is propotional to the amount of proximately bonded molecules. It was demonstrated that excimers might arise in case when the separation between the points of binding of bonded molecules is in the range 1.12–1.84 nm.

The authors [19] used nitroxide radicals for spin labelling followed by ESR spectroscopy. It is known that ESR spectra of nitroxide radicals are very sensitive to the distance between labels when the distance is less than 4 nm.

In our studies we have employed anion–radicals of tetracyanoquino- dimethane (TCNQ) as paramagnetic labels for ESR measurements. We have supposed that the amount of proximately bonded molecules is proportional to the area of exchange singlet in ESR spectra. A spin exchange between paramagnetic labels is feasible if bonded molecules are separated by 1–1.5 nm between points of fixation.

Therefore, in each particular case of experimental investigation of bonded molecules distribution relevant notions and values should be carefully discussed.

3.3. Quantitative criterion of classification of reactions of chemical modification by the type of distribution

In order to establish the quantitative criterion we have carried out computer simulation of surface coverage by the modifier molecules in the case of random distribution. The following model assumptions have been used in computations:

1) Silica surface is a uniform layer of silanol groups, which are situated at nodes of a regular triangular grid with an edge of 0.45 nm, that corresponds to the average distance between silanol groups in exclusively hydroxylated silicas [24];
2) Modifier molecules were approximated by disks with a diameter d. The value was taken to be equal to the anchor organosilicon group diameter;
3) A square $30d \times 30d$ is cut from the surface;
4) Coordinates $[x_i, y_i]$ of disks are randomly taken from the segment [0,30d];
5) Disks centres which hit within a diameter of disks having fallen before are discarded;
6) Sampling is continued up to some predefined value of coverage;
7) A cluster of size M is defined as a set of M disk centres which could be connected with a polygonal line (possibly branched) with segments not longer than a predefined length l.

Computer simulation was aimed at determination of dependence between the amount of clustered bonded molecules (α) and coverage extent (θ). Note, that it is the value of l that directly reflects differences of physico-chemical methods in determination of clustering. In fact, different methods reveal different clusters.

Dependence between the amount of molecules in clusters with size M $\geq$ 2 and the extent of surface coverage is given in Fig.1 for l equal to 1.2d=0.78–0.84nm (curve 1) and 2d=1.30–1.40nm (curve 2), where d=0.65–0.70 nm, (Fig. 1).

The data of Fig.1 show that within one and the same random type of distribution, the experimental procedures employing physico–chemical methods with different characteristic values of l would reveal markedly different values of the same extent of surface coverage. Moreover, even the type of distribution might be assigned erroneously. For instance, the authors [20] ascribed large values of $\alpha \simeq 50\%$ with a coverage extent 10–20% in the case of 3–PPS modifier to the island–like type of distribution. However, the experimental data given in Fig.1 conform reasonably to the curve for random distribution with l=1.3–1.4nm. Such a value falls within the range of values of l=1.12–1.84 nm given in the cited reference. Thus, in the work under discussion, it is the random and not island–like distribution that was really observed.

This example shows that the assignment of a certain distribution to one or another type requires a careful selection of simulated curve of distribution corresponding to characteristic value of l for the system under study. Then, if the experimental dependence between α and the extent of surface coverage θ is located over the simulated curve $\alpha(\theta)$ for random distribution, the distribution studied belongs to the island–like type. If the experimental dependence is located below the curve $\alpha(\theta)$, the distribution studied is most likely uniform.

It should be mentioned that this simple reasoning cannot comprehend all experimentally observable curves of the type $\alpha = \alpha(\theta)$. E.g., some kind of borderline behaviour is feasible and is not covered by the present model scheme. Nevertheless, the present classification allows to reveal three basic types of distribution of bonded molecules, which, in our opinion, are random, uniform and island–like.

4. TETRACYANOQUINODIMETHANE (TCNQ) AS A REAGENT FOR STUDYING OF ORGANIZATION OF BONDED MOLECULES

Potential applicability of TCNQ for studying the organization of bonded molecules was discussed in detail in our previous articles [17,18]. In the present chapter only the key features of the TCNQ method will be mentioned in brief.

The method is based on the ability of TCNQ to react with bonded nitrogen compounds (secondary, tertiary amines) to form stable ion–radical salts (IRS) under mild conditions and with high yields. Completeness of formation of stable IRS has been monitored by ESR and electronic spectroscopy. One of the most important features of this method is the formation of two–dimensional phase by TCNQ anion–radicals on the surface, if bonded donor molecules are fixed at a small distance between their anchoring points, i.e. when separation between points of fixation is in the range 1–1.5 nm. ESR spectra of such samples contain an exchange–narrowed singlet with $\Delta H = 0.5 - 1.1$ Gs, and g–factor 2.0025. Such spectra are typical for crystalline samples of IRS of TCNQ [25]. If bonded donor molecules are separated by as much as 2 nm or more, a distinct phase of TCNQ IRS is not formed. ESR spectra of such samples reveal either dipole–dipole broadening or hyperfine structure.

Particular features of the interaction of TCNQ with the bonded amino groups men-

tioned above have become the basis of a method examining the organization of bonded molecules. Paramagnetic labels emerge only upon treatment of a sample with TCNQ, that is the main advantage of the stated method. Sophisticated procedures of synthesis of specially designed molecules with labels are not needed. The method is suitable for studying practical samples of bonded silicas.

In the further discussion we shall demonstrate that "TCNQ method" can be applied for examining the organization of some non–amine modifiers, if the amine group can be somehow introduced in their molecules, e.g. as in the case of haloalkylsilanes. Sometimes the organization of even non–functional modifiers such as alkylsilanes can be estimated.

Before we proceed to the discussion of applications of the method, one more characteristic feature deserves mentioning. Exchange–narrowed singlet is assigned to occurrence of the TCNQ IRS phase on the surface, that is to clusters of bonded molecules with $M \geq 3$. This feature is an essential difference of the "TCNQ method" from the methods using luminescent or nitroxyl labels, in which the response is changed already in the case of occurrence of pairs of closely spaced molecules. Unfortunately, the theory of ESR spectra of IRS of TCNQ cannot predict how many species are sufficient to form the phase. In the present work triples of neighbouring molecules were believed to suffice.

Furthermore, having taken l=1.25 nm, we simulated the curve $\alpha = \alpha(\theta)$ for the clusters with $M \geq 3$ for random distribution for bonded molecules (see below). Figure 2 shows that if the distribution follows a random type the exchange–narrowed singlet can be observed for loading $\theta \geq 60\%$, in other words, when clusters of bonded molecules mostly consist of more than 3 species. Loading of 10 up to 50% should lead to superposition of exchange–narrowed and dipole–dipole broadened ESR spectra, whereas for loading less than 10% the contribution of exchange singlet can be neglected.

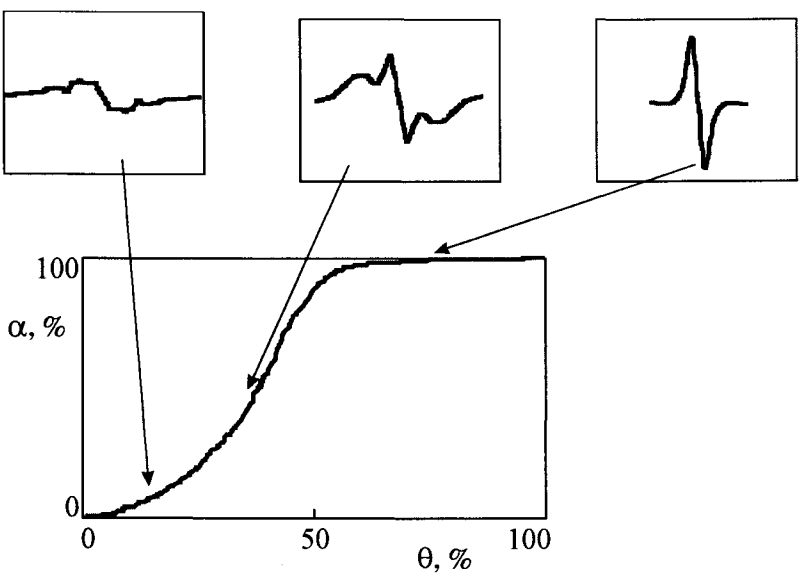

Figure 2. Dependence between the amount of bonded molecules in the clusters with size $M \geq 3$ (α) and the extent of surface coverage (θ) for random distributions. Typical ESR spectra of samples treated with TCNQ for the different values of α are shown in the upper line.

5. DISTRIBUTION OF ORGANOSILICON MODIFIERS IN THE IMMOBILIZATION REACTIONS

To study the type of distribution of organosilicon modifiers on silica surface the following transformation in the bonded layer has been used. If the starting modifier contains amino groups, the immobilization reaction, Eq. (7), was followed by the treatment with TCNQ, Eq. (8), recording and analysis of ESR spectrum. The modifier was taken in quantities sufficient to achieve the required surface coverage. Macroporous aerosilogel Silokhrom S–80 (Russia) has been used as a support. The average pore diameter and specific surface area, estimated by benzene adsorption were equal to 45 nm and 70 sq.m per gram respectively.

$$\equiv SiO_2 - OH + (CH_3O)_3Si(CH_2)_3N(C_2H_5)_2 \longrightarrow \equiv SiO_2 - OSi(CH_2)_3N(C_2H_5)_2 \quad (7)$$

$$\equiv SiO_2 - OSi(CH_2)_3N(C_2H_5)_2 + \underset{(TCNQ)}{NC_4H_2(CN)_2(CN)} \xrightarrow{[H^+]} \equiv SiO_2 - OSi(CH_2)_3NH^+(C_2H_5)_2^{\bullet} \quad (8)$$
$$(TCNQ^-)$$

If the starting modifier contained bromoalkyl groups, after immobilization reaction, Eq. (9), these groups were transformed into aminogroups according to the reaction Eq. (10).

$$\equiv SiO_2 - OH + ClSiR_2(CH_2)_nBr \longrightarrow \equiv SiO_2 - OSiR_2(CH_2)_nBr \quad (9)$$

$$\equiv SiO_2 - OSiR_2(CH_2)_nBr + HN(C_2H_5)_2 \longrightarrow \equiv SiO_2 - OSiR_2(CH_2)_3N(C_2H_5)_2 \quad (10)$$

Titrimetric determination established quantitative substitution of bromine by the diethylamine group. Sorbents obtained on (10) were treated with TCNQ according to (8).

Investigation of distribution of modifiers upon modification with alkylchlorosilane–bromoalkylchlorosilane mixtures was run similarly: bromoalkyl groups were transformed into amines via (10) which interact with TCNQ (8).

Table 3
Distribution of bonded modifier molecules on silica surface in the immobilization reactions

No.	Modifier	Range of concentration, group/nm^2	Studied surface coverage extent, %	Type of distribution
1.	$(MeO)_3Si(CH_2)_3NEt_2$	0.10–1.60	6.2–100	Random
2.	$Cl_3Si(CH_2)_3Br$	0.05–2.10	2.3–100	Island-like
3.	$ClMe_2Si(CH_2)_3Br$	0.10–2.00	5.0–100	Island-like
4.	$ClMe_2SiCH_2Br$	0.02–2.10	0.9–100	Island-like

The obtained results are given in Tables 3 and 4. Data in the tables show there are differences in mechanisms of surface coverage by organosilicon modifiers. Indeed, while in

Table 4
Distribution of modifier molecules on the silica surface in competing immobilization reactions

No.	Mixture of modifiers	Molar ratio in mixture	Surface concentration of bonded bromoalkyl groups, groups/nm^2	Type of distribution of bromoalkyl groups
1.	$ClSiMe_3$: $ClMe_2SiCH_2Br$	10 : 1	0.1	Island–like
2.	$ClSiMe_3$: $ClMe_2SiCH_2Br$	120 : 1	0.1	Island–like
3.	$Cl_3SiC_3H_7$: $Cl_3Si(CH_2)_3Br$	10 : 1	0.2	Island–like
4.	$Cl_3SiC_8H_{17}$: $Cl_3Si(CH_2)_3Br$	10 : 1	0.2	Island–like

the case of trimethoxysilane (No.1, Table 3) random distribution is realised, chlorosilyl derivatives of methyl and propyl bromides act as island like modifiers. Moreover, this finding is valid not only for trichlorosilanes, but also to monochlorosilanes, which are not capable of polycondensation.

In the cases of superposition of exchange singlet and dipole– broadened one, a portion of bonded molecules in clusters was believed to be proportional to the area of exchange singlet, which had been estimated using a routine procedure of deconvolution of complex signals into two gaussian components. Luckily, in most of the cases given in Tables 3, 4 as well as in those discussed below, the type of distribution can be distinguished by qualitative features alone. Thus, in the case of sample 3 (Table 3) we observed only an exchange singlet for loadings not exceeding 1%, revealing sharply the pronounced island–like organization of bonded molecules.

In attempt to "dilute" bromoalkyl residues in the bonded layers, modification with mixtures of alkylchlorosilane–bromoalkylchlorosilane (Table 4) was performed. This process is similar to that employed in the so– called "multiphase" generation. Alkylsilanes taken in excess were believed to result in formation of bonded layer with isolated bromoalkyl groups. However, experimental evidence shows that even with a huge excess of trimethylchlorosilane bromomethylchlorosilane reacts with silica surface by the island–like mechanism. This result is most likely related to enhanced reactivity of bromoalkylchlorosilanes compared to alkylchlorosilanes. To put it in other words, alkylchlorosilane fails to interfere in formation of bonded layer by bromoalkyl groups (Table 4).

6. DISTRIBUTIONS OF AMINES IN THE REACTIONS WITH MODIFIED SILICAS

This section describes the main results obtained on surface distributions of amines in the reactions with chemically modified silicas. Characteristics of the modified silicas

Table 5
Chemically modified silicas studied in the reactions with amines

No.	Surface bonded functional groups	Concentration of bonded functional groups, groups/nm^2	d_{av}, nm	Des.
1.		0.55	1.45	Epoxy
2.		1.25	0.95	Tosyl
3.	$-(CH_2)_3Br$	2.00	0.76	Bromopropyl

studied are given in Table 5.

The reaction between the amines and surface functional groups was as follows:

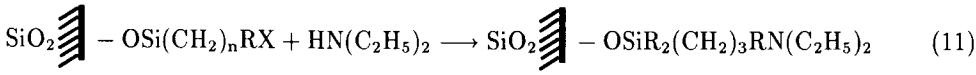

$$SiO_2 - OSi(CH_2)_nRX + HN(C_2H_5)_2 \longrightarrow SiO_2 - OSiR_2(CH_2)_3RN(C_2H_5)_2 \qquad (11)$$

X = epoxy; tosyl; bromopropyl

by thorough washing of the sorbent and removal of unreacted amine. Then the sorbents were treated with TCNQ according to Equation 8. The results obtained are given in Table 6.

It is seen that all three known types of distribution are observed experimentally. One can see that the nature of surface bonded groups of initial modified silica plays an important role. Namely, reactions between the amines studied and the bromopropyl-modified silica run according to the island-like mechanism. Whereas, both random and uniform coverages are more frequent for the tosyl- and the epoxy-modified silicas.

Noteworthy, that distribution in the reactions studied is very sensitive to the reaction conditions. For example, within the range of pH=3-9 ethylenediamine reacts with tosyl-silica according to the island-like mechanism, whereas at pH=1 and pH=11 the resulting distribution is random (Table 6, No. 12). Another example is the following. Diethylamine reacts with epoxy-silica according to the uniform mechanism. However, in the presence of 1M NaCl this reaction is the island-like one (Table 6, No. 2,3).

Summarising the data in Table 6, one can see that both the activity of amine in nucleophilic substitution of bonded groups Eq. (11) and the surface concentration of bonded groups (Table 5) are the key factors that control the mechanism of surface coverage. In other words, the higher the activity of amine and the concentration of surface bonded groups are the greater the probability of island-like coverage mechanism is. Possible explanations of these results will be given below.

7. STUDY OF ALKYLCHLOROSILANE DISTRIBUTION

Alkylsilanes lack functional groups which can be easily transformed to aminogroups and developed by TCNQ. However, the evidence on surface distribution of alkylsilanes may be inferred from the data on heavily loaded surfaces.

Table 6
Distribution of aminocompounds in the reactions with chemically modified silicas

No.	Functional groups of initial silica. Des.as in Tab.5	Amine	Range of concentration, group/nm^2	Reaction conditions	Type of distribution of amines
1.	Epoxy	n-$C_3H_7NH_2$	0.01–0.10	Water, 20°C	Island-like
2.	Epoxy	$(C_2H_5)_2NH$	0.05–0.41	Water, 20°C	Uniform
3.	Epoxy	$(C_2H_5)_2NH$	0.01–0.05	Water, 20°C, 1M NaCl	Island-like
4.	Epoxy	n-$C_{12}H_{25}NH_2$	0.05–0.20	DMFA, 100°C	Uniform
5.	Epoxy	n-$C_{18}H_{37}NH_2$	0.01–0.30	Ethyl alcohol, 20°C	Uniform
6.	Epoxy	$H_2N(CH_2)_4CHNH_2$ | COOH	10^{-4}–0.4	Water, 20°C	Uniform
7.	Tosyl	n-$C_3H_7NH_2$	0.01–0.05	Water, 20°C	Island-like
8.	Tosyl	$(C_2H_5)_2NH$	0.01–1.30	Water, 20°C	Island-like
9.	Tosyl	$(C_2H_5)_2NH$	0.05–0.10	Water, 20°C, Triethylamine	Random
10.	Tosyl	n-$C_{18}H_{37}NH_2$	0.01–0.30	Ethyl alcohol, 20°C	Uniform
11.	Tosyl	$H_2N(CH_2)_4CHNH_2$ | COOH	0.05–0.9	Water, 20°C	Random
12.	Tosyl	$H_2N(CH_2)_2NH_2$	0.01–0.05	Water, 20°C pH=1; 11; pH=3–9	Random Island-like
13.	Bromo-propyl	n-$C_3H_7NH_2$	0.01–2.10	Ethyl alcohol, 70°C	Island-like
14.	Bromo-propyl	$(C_2H_5)_2NH$	0.02–1.0	Ethyl alcohol, 70°C	Island-like
15.	Bromo-propyl	$(C_2H_5)_2NH$	0.01–1.0	Water, 20°C	Island-like

Indeed, computer simulation demonstrates that for the random distribution of modifier maximum surface coverage does not exceed 56% of maximum coverage owing to unavoidable gaps. The simulated value of maximal coverage for dimethylchloro- and trichlorosilanes is 2.3–2.8 groups per sq.nm [26,27]. On the other hand, there is a reasonable experimental evidence that bonding density of 2.2–2.8 groups per sq.nm can be achieved

only in the presence of organic bases [11,12,28,29] or using dimethylaminosilyl modifiers [9,10]. Modification in the absence of organic bases affords bonding density not exceeding 1.3–1.8 groups per sq.nm even with a huge excess of reagents and prolonged treatment [11,12,29].

Analysis of the published results has led us to a conclusion that the base catalysts alter the mechanism of coverage. Namely, in the presence of organic bases alkylchlorosilanes react with silica by island–like, while non–catalyzed reaction follows random mechanism.

In order to substantiate this conclusion the following experiments were done. Consider close to maximum coverage by alkylsilane, say 90%. Then, for island–like organization of modifier distribution of remaining vacant sites should be also island–like. Otherwise, random distribution of modifier accounts for the random distribution of vacant sites. The experiment was performed in the following manner. Organic base catalyzed modification was run with insufficient amount of modifier to achieve the surface coverage of 2.0– 2.1 groups per sq.nm, that is ca. 90% from the maximum coverage. The remaining free surface was covered with γ–bromopropyltrichlorosilane. Further procedures were as described above – aminogroups were introduced and TCNQ added (Eqs. 10,8).

Modification in the absence of base was performed with an excess of alkylchlorosilane. Surface coverage in this case amounted to 1.6–1.8 groups per sq.nm. Next, similarly as above, samples were treated with γ–bromopropyl trichlorosilane, amino groups introduced and TCNQ added. It is worth noting here that the limiting coverages of random distribution for alkylsilane and γ–bromopropyltrichlorosilane are not the same. Greater reactivity and smaller steric requirements of the latter allow to bind it to accessible sites.

Table 7
Distribution of n–alkylchlorosilane modifiers on the silica surface in the immobilization reactions

No.	Modifier	Presence of organic base (pyridine)	Concentration of bonded n–alkyl groups, group/nm^2	Surface coverage extent of n–alkyl groups, %	Type of distribution of n–alkyl groups
1.	$ClSiMe_3$	+	2.10	91	Island–like
2.	$ClSiMe_3$	–	1.75	76	Random
3.	$Cl_3SiC_8H_{17}$	+	2.15	93	Island–like
4.	$Cl_3SiC_8H_{17}$	–	1.65	72	Random
5.	$ClMe_2SiC_{12}H_{25}$	+	2.00	87	Island–like
6.	$ClMe_2SiC_{12}H_{25}$	–	1.60	69	Random

Table 7 presents the data on distribution of alkylchlorosilanes. The data clearly show that the role of base catalyst is crucial in determining which type of mechanism the modification process will follow. Recently [30], there have been obtained the direct spectral evidences that the mechanism of surface silanization changes in the presence of organic base. Thus, the conditions of modification process provide the key to govern the organization of bonded species on the surface. E.g. to produce ODS–stationary phases for

separation of proteins, where octadecyl tails are to be sparse and isolated, it is reasonable to apply non-catalyzed modification until the required coverage extent is reached, followed by the extensive screening of free surface with silanization agents. Oppositely, to produce dense monolayer coverage with as few defects as possible and maximum bonding density, modification should be accomplished in the presence of organic base or using dimethylamino-derivatives of chlorosilanes.

8. WHY DOES THE MODIFICATION OF SURFACE OCCUR BY DIFFERENT MECHANISMS?

The experimental data gathered until recently are not sufficient to make solid conclusions on the reasons of realization of one or another mechanism of surface coverage. However, some speculations concerning the mechanism can be given.

The analysis of published material shows that modification of macroporous stationary phases by dimethylaminosilanes affords loading near to a theoretical limit [9,10]. According to reasoning applied here such bonding density can be reached only in the case of island-like coverage. Here, the following description of the mechanism might apply. After the first molecule of modifier is attached to the surface, interaction of the liberated dimethylamine with the nearest silanol group renders enhanced reactivity in comparison with other silanol groups. Another modifier molecule reacts with the activated silanol group to release an adsorbed molecule of dimethylamine and give out still another molecule of dimethylamine. Thus, the concentration of organic base grows in the proximity of the developing cluster.

In the case of modification by alkylchlorosilanes in the presence of organic base the activation of neighbour sites might be a result of local destruction by hydrochloride of the organic adsorbed solvent layer formed in the process. The resulting defect in the adsorption layer is likely to be preferable reactive site of bonding of the next molecule. A chain length of alkylsilane being bonded might in general be another factor affecting the mechanism of coverage. For instance, a situation when a defect of adsorbed layer vanishes (integrity of adsorbed layer is restored) before another molecule of modifier hits the surface, is altogether feasible – and thus the island-like mechanism might be impaired. Note that in modification by chlorosilanes the order of addition of reagents is of importance: organic base should be introduced prior to the modifier. Otherwise a part of modifier would react by the random mechanism and the subsequent addition of base could not fix up defects in parts of the layer formed before.

Island-like organization of bonded species in the case of bromoalkylchlorosilane modifiers is likely to be associated with an influence of a dipole moment of the C–Br bond on the neighbouring surface silanol groups. "Stretching" of OH-bond is similar to the action of organic base.

In the cases of surface assembly reactions with the participation of amines, unlike the immobilization reactions, the researcher have much more factors affecting the resulting distribution.

The data in Table 6 show that the resulting distributions can change from one type to another depending on the reaction conditions or on the nature of surface bonded groups of modified silica. The island-like coverages are more likely observed in the reactions

with the participation of high nucleophilic amines. The higher the nucleophilic activity (basic conditions, amine with short alkyl substitutes) is, the higher the surface concentration of surface bonded groups is, the smaller chances are to obtain uniform or random distributions.

To our mind, the island-like mechanism is more likely associated with the redistribution of electronic density of the nearest bonded electrtophilic groups by a lone electronic pair of nitrogen. Possibly, this promotes the nucleophilic attack of the other amines nearby with those already bonded.

The following examples support the mechanism suggested. First, the reaction between diethylamine and epoxy-silica runs according to uniform distribution. Whereas, this reaction in the presence of electrolyte (1M NaCl) runs according to the island-like distribution. Indeed, the reaction between amine and electrophilic groups goes through the charged intermediates. Electrolyte promotes the charged intermediates produced in the reaction and, thus, facilitates the positive neighbour effect. Let us give one more example: the reaction between diethylamine and tosyl-silica runs according to the island-like type of distribution. At the same time, in the presence of excess of triethylamine this reaction runs according to the random distribution. The excess of physically adsorbed triethylamine cancels the positive neighbour effect of bonded diethylamine.

Thus, as the nucleophility of amine is decreased (acid conditions, long chain substitutes), the probability of realization of random or uniform distribution of bonded molecules is increased. Promotion and stabilization of intermediate ionic structures (electrolyte) facilitates the island-like mechanism of surface coverage.

Different reasons account for the occurrence of one or another type of surface coverage. Here only the most probable factors are mentioned. In conclusion we would like to say that factors determining the reasons for realization of one or another mechanism of surface coverage are far from ultimate clarity. No doubt, understanding of this matter would allow for both improvement of the known methods of surface modification and development of nanomaterials of new generation.

9. OUTLOOK FOR SURFACE MODIFICATION OF SOLIDS

In this section we would like to consider the most promising and actual problems of the chemistry of surface bonded compounds concerning the organization of bonded layer.

Quite a few experimental and theoretical studies have been devoted to the study of supramolecular organization of bonded layers. However, the very early studies have already demonstrated that these problems are very important both from the point of view of fundamental science and practical application of the surface modified solids.

The tendency arising in this field can be defined as the "design of bonded layer". This means the controlled preparation of supramolecular structures that are formed from molecules covalently bounded with the surface and possibly with each other.

Below, we shall discuss the basic published results and summarise the experimental approaches that may permit the preparation of nanostructures on the chemically modified surfaces. In this section we are not going to consider the methods concerning "remote" actions on the surface. Among them, this can be an action with the needle of scanning tunnelling microscope, "writing" from different source of radiation over photo-, radiation-

or electron- sensitive bonded layer. The methods listed seem to be very promising for the chemistry of bonded compounds, but they require special consideration. Next, we shall discuss "pure chemical methods" for preparation of nanostructures of surface bonded molecules.

9.1. Islands of bonded molecules. The method of molecular templates (imprints)

Polyakov [31] has a priority in preparation of the sorbents in the presence of molecular imprints. The sorbents obtained show specificity toward the substance that is used as an imprint. Since then the molecular imprinting methods has been successfully used in adsorption [32,33] and catalysis [34–37].

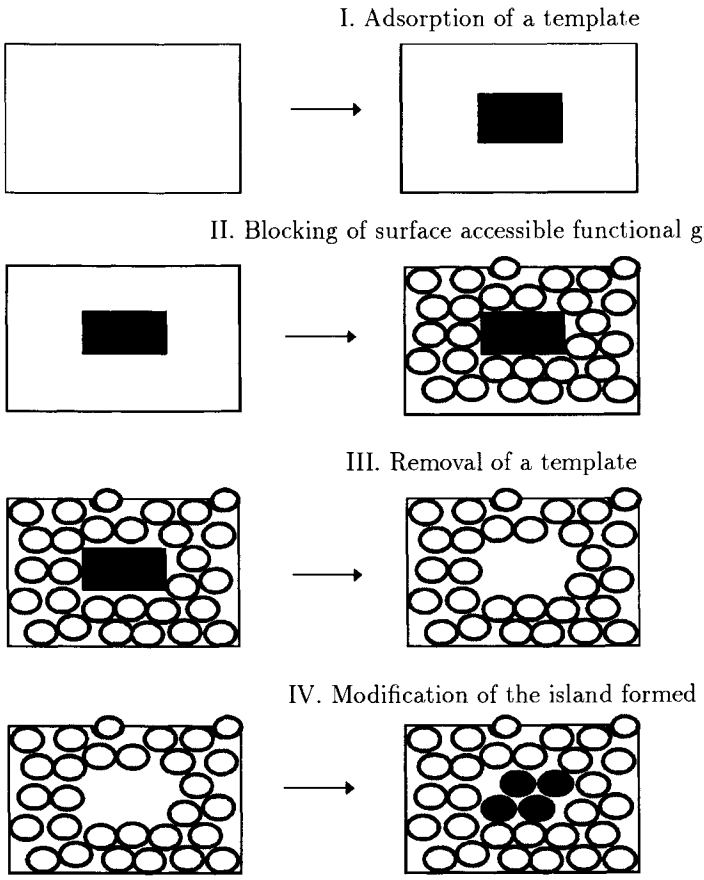

Figure 5. Method of molecular templates in the surface chemical modification.

The use of chemical modification for the "fixation" of imprints was proposed by one of the author of this paper in 1986. The idea is clear from Figure 5. In the first stage template molecules are adsorbed in small concentration on the surface, say the surface of

silica. It is important that templates adsorb in a random or uniform way. This leads to the presence of predominantly isolated adsorbed molecules. Other important requirements for the template are uniqueness of the adsorption complex and negligible lateral diffusion. The latter is true for many adsorbates containing functional groups, which are capable of interacting specifically with the surface silanols. The second stage involves the blockage of surface silanols, which are not covered with adsorbed templates (Fig.5). The use of hydrophilic water-soluble templates in the first stage and organic solvents in the stage of chemical modification seems not to disturb the distribution of adsorbed templates. In the third stage the templates adsorbed are removed and the islands of nonmodified silica can be modified by the modifier of another type (Fig.5).

Evidently, the size of an island is closely related to the cross-sectional area of a template.

9.2. "Mosaic structures." Bonded molecules are situated in the sets of a regular lattice

In order to obtain the mosaic bonded structures the following approach may be suggested. The surface is covered with a dense monolayer of large flat molecules covalently bonded to the surface along the axial anchor group (Fig.6). Conceivably the oxidative destruction of the bonded molecules or modification of the exposed reactive groups might result in regular network of bonded molecules in the surface. This idea can be realized, for example, by immobilization of phthalocyanine of silicon or aluminium on the surface of a crystalline silica.

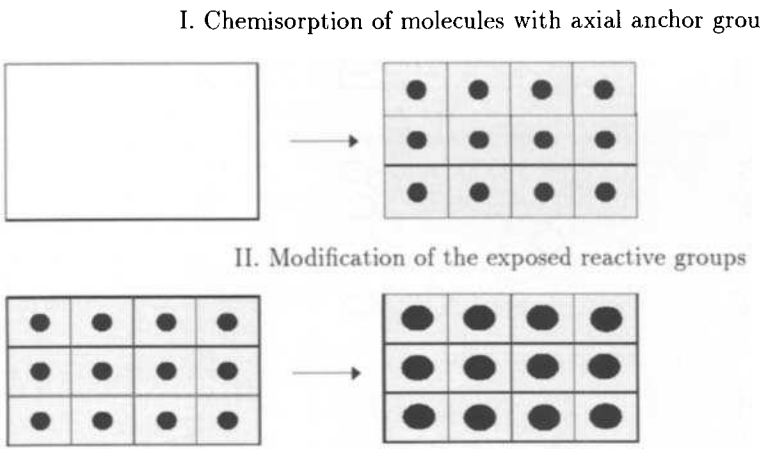

Figure 6. Scheme for preparation of a regular lattice from bonded molecules.

The following method can be also used for the preparation of mosaic bonded layers with a regular structure [38]. At first, the surface is covered with a dense monolayer of bulky, spherical molecules (Fig.7). Thereafter the surface acquires the mosaic structure due to unavoidable gaps, distribution of which depends on the crystalline structure of a support, the nature of modifier and other factors. Under certain conditions this distribution appears to be a regular with the lattice parameter equal to the diameter of adsorbed molecule.

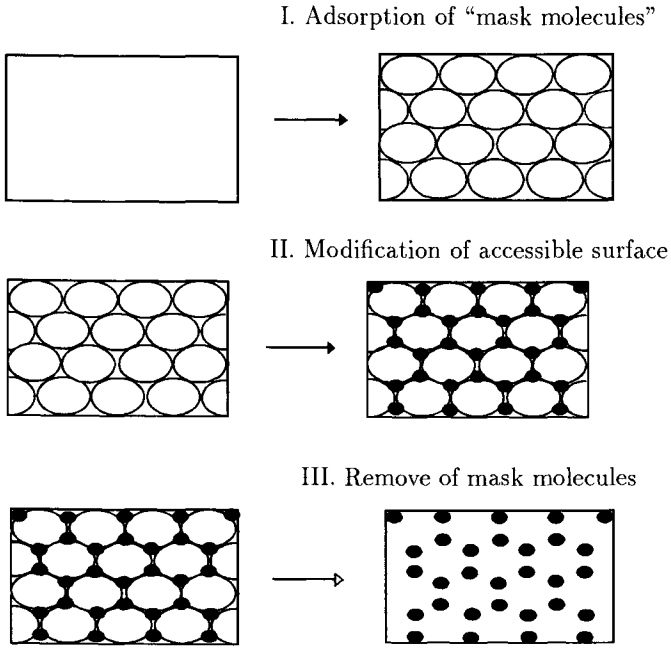

Figure 7. Scheme for preparation of mosaic structures on the surface.

This idea has been realized in the excellent study [39]. The quasi- crystalline monolayer of the protein from the thermophilic bacterium *Sulfolobus acidocaldarius* was prepared on the flat support. Then the deposition of metal (Ta/W) on the obtained layer of adsorbed protein was followed by the removal of both the protein and the metal deposited on the protein using the ion bombardment. As a result the regular network of metal islands with the lattice parameter 22 nm equal to the distance between the centres of the adsorbed proteins was obtained. The islands of metal have a diameter of 15 nm and a thickness of 1nm.

To our mind, a similar scheme can be applied for chemical modification of surface as follows. In the first stage organosilicon modifiers with bulky substitutes such as triphenyl, triisopropyl etc. should be used. In the second stage the sample is modified with a proper modifier penetrating the original surface of a support through the gaps.

9.3. Pairs of bonded molecules separated by a fixed distance

The idea of this method is clear in Figure 8. This method was used in the study [40]. Organosilicon derivative of phenylboronic acid was used as a modifier of silica, while bis-NAD I and bis-NAD II were used as spacers. Residues of phenylboronic acid were supposed to be separated by 0.7 and 1.5nm respectively. The stationary phase obtained exhibits higher retention of spacer used in comparison with other related biopolymers. Evidently, this method is appropriate only for the preparation of bonded layers with a low density of bonded groups.

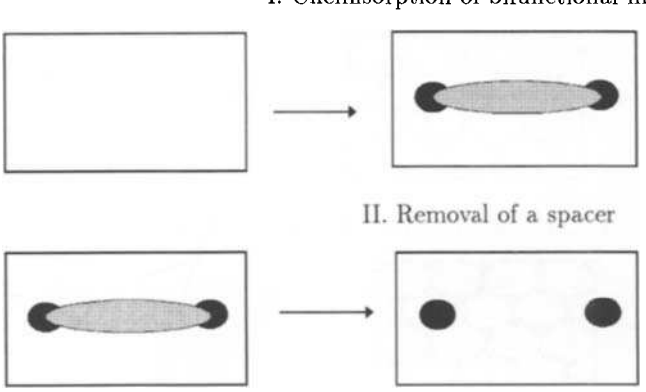

Figure 8. Scheme for preparation of modified surfaces containing pairs of bonded molecules situated at a fixed distance.

To our mind, except for bivalent biopolymers, the terminally functionalyzed conformational-rigid molecules such as polyphenylenes, polyacetylenes, perfluoroalkyls etc. seem to be promising spacers for this procedure.

Finally, we list in brief the most important fields of the potential use of materials with chemically bonded nanostructures.

Nanoelectronics and nanolithography may become an important area of the application of nanostructured surface materials. Since the use of nanoscale surface bonded materials allows one to achieve the ultimate level of miniaturization of electronic devices.

In *catalysis* one may expect the appearance of heterogeneous metallo-complex catalysts containing active centres distributed by "the required way". This can result in preparation of highly selective catalysts for structurally sensitive reactions.

The distribution of bonded molecules is a very important parameter for *bioaffinity sorbents*. Evidently, biospecific binding is dramatically dependent not only on the spatial disposition of bonded affinity ligands, but even on the number of ligand-surface bonds (one - or more) [41].

Among the *stationary phases for modern liquid chromatography* one should mention multiphase sorbents. It is clear that the adsorptional properties of such sorbents are closely related to the uniformity of mixing of bonded molecules in a bonded layer.

Recently, the so-called diphylic stationary phases, or more correctly - *heterosurfaced sorbents*, introduced by Pinkerton and co-workers [42] have received a wide acceptance in liquid chromatography of biological liquids [43]. These sorbents have different bonded groups on the internal surface than on the external surface of the particle.

The problems of supramolecular organization and distribution of bonded molecules are of great importance not only for the materials with a low surface coverage. These are also important for the preparation of the most dense bonded layers with the maximum shielding of the surface. Indeed, the complete modification of silica with alkylsilanes and preparation of *superhydrophobic surfaces* [44,45] are only possible under the conditions of island-like coverage of the surface with a modifier.

The above mentioned examples do not cover all the fields of possible application of

nanoscale surface bonded materials. However, just now one can see the potential usefulness of this tendency in modern surface chemistry.

Financial Support.

This paper is part of a project supported by the International Science Foundation (ISF). Grant MEL 000.

REFERENCES

1. O.M. Dzhigit, A.V.Kiselev and N.N.Mikos–Avgul, Dokl. AN SSSR, 70(1950)441.
2. H.Deuel, G.Huber and R.Iberg, Helv. Chim. Acta, 33(1950)1229.
3. H.Deuel and G.Huber, Helv. Chim. Acta, 34(1951)1697.
4. H.Deuel, Kolloid Z., 124(1951)164.
5. A.Fadeev, O.R.Borisova and G.V.Lisichkin, Zhurn.Fiz.Khimii, in press.
6. P.Pfeifer and D.Avnir, J.Chem.Phys., 79(1983)3558.
7. P.Pfeifer, D.Avnir and D.Farin, J.Chem.Phys., 79(1983)3666.
8. D.Avnir (ed.), The Fractal Approach to Heterogeneous Chemistry, Wiley, New York, 1992.
9. K.Szabo, N.L.Ha, P.Schneider, P.Zeltner and E.Kovats, Helv. Chim. Acta, 67(1984)2128.
10. D.Morel, K.Tabar, J.Serpinet, P.Claudy and J.M.Letoffe, J.Chromatogr., 395(1987)73.
11. B.Buszewski, A.Jarasek, J.Garaj, L.Nondek, I.Novak and D.Berek, J.Liquid Chromatogr., 10(1987)2325.
12. G.V.Lisichkin (ed.) Modified Silicas in Adsorption, Catalysis and Chromatography, Khimiya, Moscow, 1986 (in Russian).
13. K.K.Unger, Porous Silica, its Properties and Use as Support in Column Liquid Chromatography, J.Chromatogr. Library, vol.16, Elsevier, Amsterdam, 1979.
14. B.Feibush, M.L.Cohen and B.L.Karger, J.Chromatogr., 282(1983)3.
15. B.Growther, S.D.Fasio and R.A.Hartwick, J.Chromatogr., 282(1983)619.
16. B.Growther and R.A.Hartwick, Chromatographia, 16(1982)349.
17. G.V.Lisichkin, S.M.Staroverov, V.B.Golubev and A.Yu.Fadeev, Dokl. AN SSSR, 294(1987)1165.
18. S.M.Staroverov, A.Yu.Fadeev, V.B.Golubev and G.V.Lisichkin, Khimicheskaya Fizika, 7(1988)93.
19. L.D.Hall and J.C.Waterton, J.Am.Chem.Soc., 101(1979)3697.
20. C.H.Lochmuller, A.S.Colborn, M.L.Hunnicutt and J.M.Harris, Anal.Chem., 55(1983)1344.
21. C.H.Lochmuller, A.S.Colborn, M.L.Hunnicutt and J.M.Harris, J.Am.Chem.Soc., 106(1984)4077.
22. S.M.Staroverov and A.Yu.Fadeev, J.Chromatogr., 544(1991)77.
23. D.W.Cooper, J.Colloid Interface Sci., 119(1987)442.
24. R.K.Iler, The Chemistry of Silica, John Wiley & Sons, New York, 1979.
25. D.B.Chesnut and W.D.Phillips, J.Chem.Phys., 35(1961)1002.
26. G.E.Berendsen, Ph.D. Thesis, Delft University, Delft, 1980.
27. D.W.Sindorf and G.E.Maciel, J.Phys.Chem., 86(1982)5208.

28. G.E.Berendsen and L.De Galan, J.Chromatogr., 196(1980)21.
29. J.N.Kinkel and K.K.Unger, J.Chromatogr., 316(1984)193.
30. C.P.Tripp and M.L.Hair, J.Phys.Chem., 97(1993)5693.
31. M.V.Polyakov, Zhurn.Fiz.Khimii, 2(1931)799; ibid 4(1933)454; ibid 10(1937)100.
32. F.H.Dickey, Proc.Nat.Acad.Sci. USA, 35(1949)227.
33. V.V.Patrikeyev, A.F.Sholin and I.A.Nikiforova, Izv. AN SSSR, Otd.Khim.Nauk, No. 6(1963)1031.
34. G.F.Huttig, in: Handbuch der Katalyse III, Vien, 1943, p.318.
35. V.V.Patrikeyev, A.A.Balandin, E.I.Klabunovskii, Yu.S.Mardashev and G.I.Maksimova, Dokl. AN SSSR, 132(1960)850.
36. Y.S.Mardashev, G.N.Toropkina and V.M.Brovtseva, Zhurn.Fiz.Khimii, 49(1975)2016.
37. V.V.Vazhev, Zhurn.Fiz.Khimii, 58(1984)2783.
38. F.L.Carter, Toward Computing at the Molecular Level, in: Microelectronics Structure and Complexity, R.Dingle, (ed.), Plenum Press, New York, 1983.
39. K.Douglas, N.A.Clark and K.J.Rothschild, Appl.Phys.Lett., 48(1986)676.
40. O.Norrlow, M.O.Mansson and K.Mosbach, J.Chromatogr., 396(1987)374.
41. A.Yu.Fadeev, P.G.Mingalyov, S.M.Staroverov, E.V.Lunina, G.V.Lisichkin, A.V.Gaida and V.A.Monastyrskii, J.Chromatogr., 596(1992)114.
42. H.I.Hagestam and T.C.Pinkerton, Anal.Chem., 57(1985)1757.
43. T.C.Pinkerton, J.Chromatogr., 544(1991)13.
44. V.A.Yeroshenko and A.Yu.Fadeev, Kolloid. Zhurn., in press.
45. V.A.Yeroshenko and A.Yu.Fadeev, Zhurn.Fiz.Khimii, in press.

A. Dąbrowski and V.A. Tertykh (Editors)
Adsorption on New and Modified Inorganic Sorbents
Studies in Surface Science and Catalysis, Vol. 99

Chapter 1.8
The chemical basis of surface modification technology of silica and alumina by molecular layering method

A.A. Malygin, A.A. Malkov, S.D. Dubrovenskii

Department of Chemical Technology of Materials and Devices for Electronic Industry, St.-Petersburg State Technological Institute Technical University, 198013 St.-Petersburg, Russia

1. INTRODUCTION

The molecular layering method (ML) and its main principles were formulated on the basis of solid substance chemistry using the "skeleton hypothesis" of Aleskovskii made in the fiftieth [1].The first publication presenting the main rules of ML method is the article by Aleskovskii and Koltsov, submitted to the Technological Institute in Leningrad in 1963 [2]. The detailed account of the results of the chemical aspects of the ML method is found much later (1968–1978) in articles, inventions, monographs and textbooks of Aleskovskii, Koltsov, Volkova, Malygin et al. [3–25]. Just in this period qualitative accumulation of theoretical and experimental data, as well as quantative ones, prepared the transition of researches to another level – evaluation of the most perspective areas of application of the new method of synthesis and creation of scientific principles of ML technology and its subsequent development.

In the period mentioned above the most known world centers of the studies of chemical reactions on silica and alumina surfaces were USSR, Germany, Bulgaria. But since 1977 after the patent [26] had been published and later in the eightieth as well as at present the number of publications in this field has increased in various countries [27–39]. It should be noted, that some authors use another names for the synthesis like the ML method for example, atomic layer epitaxy (ALE) [30], chemical surface coating [31], grafting [32],elementary surface reactions of CVD method [33].

According to paper [30], including a list of main laboratories in the world and their first publications, it is possible to think, that since 1980–1982 the interest in the new synthesis method has increased greatly. The application of chemical principles of ML method to study the reactions between porous silica and alumina and elements of II–VIII groups of the Periodic Table chlorides has allowed, at first, to justify the principles of ML, experimentally and, secondly, to define its realization as the one of perspective areas for creation effective inorganic sorbents and heterogeneous catalysts. The purpose of this paper is generalization from the present results on study of chemical conversions on surfaces of inorganic sorbents (silica and alumina) in reactions with phosphorus, vanadium, chromium, titanium, chlorides etc.

2. THE MAIN CHEMICO–TECHNOLOGICAL FACTORS AND THEIR INFLUENCE ON CHEMISORPTION OF CHLORIDES

The synthesis by ML method is executed by repeated and alternate processing of solid state surfaces by surplus of appropriate reagents with removal of non–acted ones and forming gaseous products after each stage of processing [2,3,13]. For each cycle of ML reactions no more than one monolayer of new structural units joins the surface, thus the monoatomic assembly of the solid substance is realized on the chosen matrix.

The basic feature of the chemical assembly process of the surface by ML method, unlike the majority of conventional ways of solid substances formation, is the execution of synthesis in conditions, far from the equilibrium state [2,3,13]. The realization of the principle mentioned has been executed experimentally, for example, by permanent transport of the excess amount of the reagents to matrix surface by flow of gas carrier, and removal of collateral gaseous products from reaction zones.

The researches carried out both on study of reaction mechanisms in ML processes on silica, and synthesis of oxides and other structures on the surfaces of matrices of various chemical nature have shown, that in all cases it is necessary for the certain sequence of the same physico–chemical stages to be realized [13,15,40,41]:

- preparation of matrix surface (formation of functional groups, thermotreatment);
- chemical reaction of appropriate low–molecular reagent with surface functional groups;
- desorption of the surplus not–acted reagent and gaseous products of reaction.

The mentioned stages can be repeated a proper number of times. So, the ML method from a technological point of view represents a multistage heterogeneous process in the gas(liquid) – solid system, including a stage of chemisorption and desorption of reagents and products of reaction, quantity and sequence of which are set by program of synthesis, made in view of requirements for target products (chemical nature and concentration of components in the solid phase, thickness of synthesized layer, mutual arrangement of monolayers etc.) [13,41].

The chemical composition, structure, and, hence the properties of products with modified surface are determined both by observing the required sequence of operations, and chosen chemico–technological parameters of process: the chemical nature of reagents (volatile and solid), temperature (in stages of preparation of surface, chemisorption and desorption), concentration of reagents (in gas phase and functional groups on surfaces of substrate), hydrodynamics of the process (rate of transport and removal of reagents, mobility or stationary condition of disperse solid phase).

The present article submits the results, obtained in the experiments with various fractions of large–pore silica gel with a specific surface area (S_{sp}) 250 m^2/g, contents of OH–groups (C_{OH}) 3,46 mmol/g and γ–Al_2O_3 with S_{sp}= 200 m^2/g and C_{OH}=5,22 mmol/g. All the synthetic experiments conducted in a tubular gas–flow reactor at the atmospheric pressure by the known technique [2,3,13]. Chlorides and oxychlorides (PCl_3, $POCl_3$, $VOCl_3$, CrO_2Cl_2, $TiCl_4$) were applied as the volatile reagents, in the reaction chamber with a flow of dried gas - carrier (nitrogen, air).

In literature the significant number of submitted data is devoted to the processing of reactions of volatile halogenides with OH–groups on surfaces of silica and alumina in the temperature range of sample preparation 200–800°C [3,5,42–44]. The interaction in the

stage of chemisorption proceeds according to:

$$m(-M-OH) + EO_kCl_n \rightarrow (-M-O-)_mEO_kCl_{n-m} + mHCl \quad (1)$$

where M – is the surface silicon or aluminum atom in SiO_2 or Al_2O_3; E – is an atom of vanadium, chromium, titanium or phosphorus in appropriate chloride or oxychloride.

The magnitude of factor m is defined by nature of reagent, concentration of OH–groups on surfaces, concentration of halogenide in the gas phase (C_g) and $1 \leq m \leq n$.

So at $C_{POCl_3} = 3.2 \cdot 10^{-4}$ mol/l the reaction of silica gel with $POCl_3$ is completed in 4 hours, the amount of phosphorus in the sample does not exceed $C_P = 0.40$ mmol/g, and m=3. As C_{POCl_3} increases to $7 \cdot 10^{-4}$ mol/l the value of C_P changes to 1.06 mmol/g, m=3 and m=2 for 29 and 71% surface ($\equiv Si-O-)_mPOCl_{3-m}$ groups accordingly [6]. The kinetic study of the vanadium oxychloride interaction with silica gel at different C_{VOCl_3} has shown, that with the increase of concentration of oxychloride in the gas phase the degree of surface coverage by vanadium–oxide groups grows [45–47]. Thus, the predefined (threshold) value of $VOCl_3$ concentration in the gaseous flow for the given linear speed of gas–carrier, provided the fluidized state, exists, above which the kinetic curve does not change, but below which decreasing of both $VOCl_3$ chemisorption rate and the maximum possible vanadium content in the final product is observed (Figure 1).

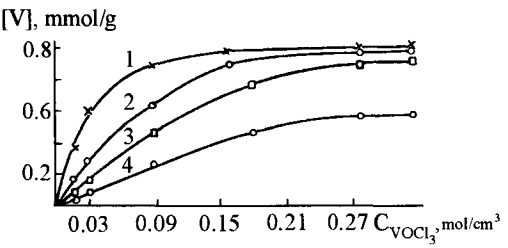

Figure 1. The vanadium oxychloride concentration in the gas flow influence on the chemisorbed amount. Gas flow rate 0.05 m/s; reaction time: 1 – 7200 s, 2 – 900 s, 3 – 420 s, 4 – 180 s.

The temperature makes an essential influence on the structure and composition of surface structures both in the stage of preliminary heat treatment of oxide (To), and in chemisorption (Ts) and desorption (Td) stages. As the study of reactions of chlorides of vanadium, phosphorus, titanium, chromium with silica gel surface, dehydroxylated at temperatures 200–800°C, has shown, the quantity of the chemisorbed reagent is reduced with the increase of To [3,42–44]. In this case the value of factor m decreases (see reaction 1) and interaction of chlorides by the nucleophilic mechanism practically does not take place, including oxygen in –Si–O–Si– groups. In Fig. 2 typical dependencies of To influence on the surface groups chemical composition are presented, taking as an example the interaction of $VOCl_3$ with silica. To increase from 180 to 700°C causes the decrease of surface OH–groups content. Some other features were observed in the research on chemical structure of reaction products of chlorides with surface of alumina, annealed at 200–1000°C (Table 1).

The analysis of results included in Table 1, as well as of literature data on the reaction of $TiCl_4$ with γ–Al_2O_3 [43] testifies, that the chemical nature of halogenide predetermines

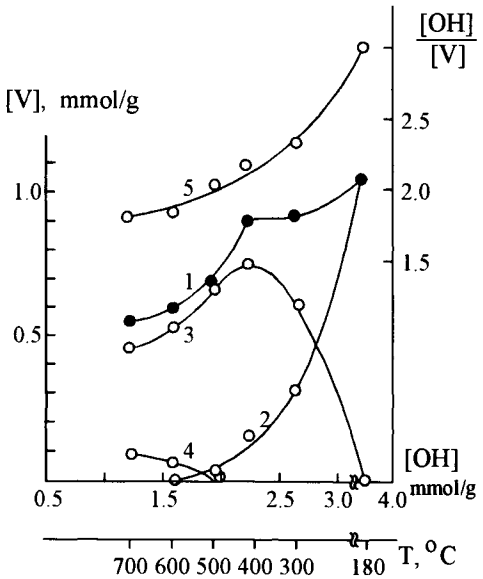

Figure 2. Dependencies of $VOCl_3$ chemisorption on the OH-group content on the silica surface: 1 – total vanadium content; 2 – 4 – amount of vanadium-containing groups bonded with surface by 3, 2 and 1 bonds respectively; 5 – [OH]/[V] ratio.

Table 1
The influence of preliminary heat treatment temperature of alumina on chemical structure of products of chemisorption of vanadium and phosphorus oxychlorides

To,°C	Contents, mol/g		Cl/V	Contents, mmol/g		Cl/P
	V	Cl		P	Cl	
200	0.87	1.67	1.90	1.20	2.26	1.89
300	0.95	1.55	1.63	1.05	2.42	2.31
400	0.84	1.52	1.81	0.99	2.37	2.39
500	0.59	1.54	2.61	0.96	2.41	2.51
600	0.56	1.46	2.60	0.86	2.41	2.80
700	0.48	1.35	2.80	0.66	2.43	3.66
800	0.48	1.08	2.27	0.65	2.18	3.33

the To value, at which the nucleophilic affiliating of molecule begins to proceed. In the range $POCl_3$ – $VOCl_3$ – $TiCl_4$ appreciable chlorinating of alumina is observed at To 300 (Cl/P=2.31), 500 (Cl/V=2.61), 900°C (Cl/Ti=2.61), accordingly.

The study of To influence was carried out with the model of the chemisorption of $TiCl_4$ by silica. It was shown in [44], that with the increase of To from 200 to 800°C the number of bonds forming titanium-oxychloride groups with surface increased (factor m grows) while titanium concentration in the samples decreases. Authors [44] associate the

increase of m with reorganization of surface as a result of interaction between mono- and bifunctionally connected groups, for example, in scheme:

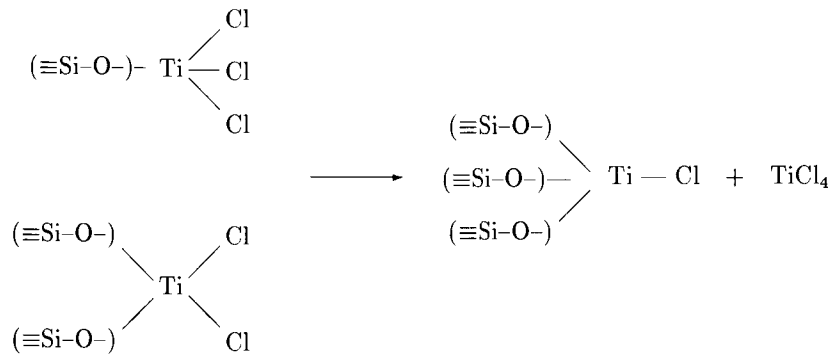

(2)

In contrast to SiO_2, during the interaction of γ-Al_2O_3 with $TiCl_4$ (Figure 3) in the same range of Ts magnitudes at 800°C alongside with the reaction of electrophilic substitution of proton in OH-groups the interaction, the increase of titanium content in the samples (Figure 3 B, curve 4) and weight gain in the process of gravimetric control were observed.

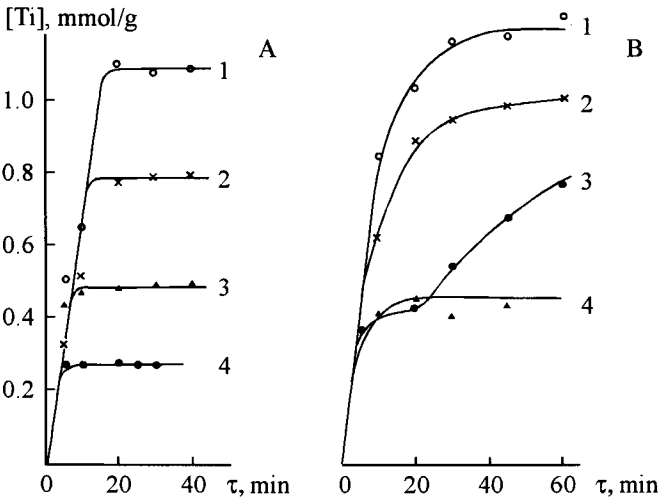

Figure 3. Titanium content dependencies on the chemisorption time at different temperatures: 1 – 200; 2 – 400; 3 – 600; 4 – 800°C; A – SiO_2; B – Al_2O_3.

The temperature regulation in the desorption stage can result in its essential intensification, as shown by the study of reaction of vanadium oxychloride with silica [48]. But it is necessary to take into account the properties of surface groups, in particular, their thermal stability. The latter, as it is known from the papers [49,50], can essentially influence the structural conversions of solid matrix.

In Figure 4 the data of annealing temperature influence on the specific surface area of both the initial and containing vanadium- and chromium-oxide surface groups silicas are presented.

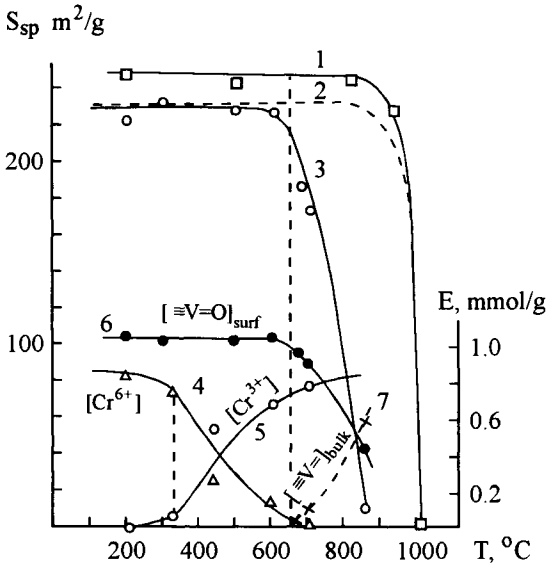

Figure 4. The thermal stability of vanadium- and chromium- containing silica. 1,2,3 -are specific surface area dependencies on temperature of annealing of initial (1), vanadium (2) and chromium (3) containing silica gels. 4,5 - are temperature dependencies of Cr(+6) and Cr(+3) content; 6,7 - are the temperature influence on the surface/bulk vanadium distribution.

Comparison of the modified silica gel thermal stability has shown, that characteristics mentioned are connected with the melting point of corresponding oxides. The elements can be distributed into three groups: 1) those which do not influence the silica gel thermal stability (Ti, Al) because of their melting point T_m is significantly higher than the temperature of silica gel sintering; 2) those which reduce the temperature of silica gel sintering (V,P,B) by the reason of low oxide melting point ($T_m < 800°C$); 3) those which do not change the temperature of silica gel sintering (Cr^{6+}) because during the surface groups destruction, for example, $(\equiv Si\text{-}O\text{-})_2CrO_2$ groups, the new Cr^{3+}-containing groups of stable in the considered temperatures range oxide are formed.

It is necessary to note, that the use of solid (hard-volatile) chlorides ($ZnCl_2$, $CdCl_2$, $TaCl_5$ etc.) requires the execution of chemisorption process at temperatures, close to the point of boiling or sublimation of the above mentioned compounds to achieve their optimum concentration in the gas phase [40].

Taking into account, that the collateral product of ML reactions with the use of element chlorides is the hydrogen chloride, stability of groups $(\equiv Si\text{-}O\text{-})_mEO_nCl_{n-m}$ for this effect as well as influence of HCl concentration in the gas phase on processing of modifying reactions were investigated [38,40,51].

Under identical conditions of processing (temperature, concentration and rate of HCl submission) the stability effect of hydrogen chloride correlates with the value of binding

energy $E_{M\text{-}O}$ (M=Cr, V, P, Ti) [51].

The interaction of vapour mixture $VOCl_3$–HCl with silica gel was investigated at 180±5°C. The concentration $VOCl_3$ in the gas phase was constant: 0.43±0.02 mmol/m^3. The HCl contents in $VOCl_3$–HCl mixture changed in the range appropriate to a molar ratio (α) C_{HCl}/C_{VOCl_3} from 0.35 to 2.0. Characteristics of vanadium–oxide layer on the silica gel dependending on α are submitted in Figure 5.

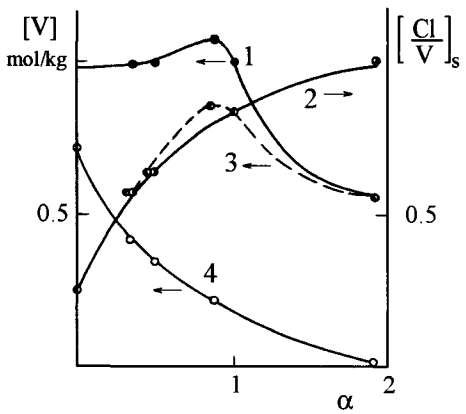

Figure 5. Dependencies of the chemical composition of vanadium–containing groups at the silica surface on the [HCl]/[$VOCl_3$] gaseous concentration ratio (α): 1 –is the total vanadium content; 2 – is the [Cl]/[V] ratio in the solid phase; 3,4 – are the amount of vanadium–containing groups bonded with the surface by 1 and 2 bonds respectively.

The obtained results show that with the increase of vanadium concentration in product (curve 1) not only changes, but also the ratio $[Cl/V]_s$ in the solid phase (curve 2) increases, i.e., the ratio of groups $(\equiv Si-O)_2VOCl$ (curve 3) and $(\equiv Si-O)_3VO$ (curve 4) on surface changes.

The analysis of experimental data permits to assume, that during synthesis the gradual destruction of three–functional groups $(\equiv Si-O)_3VO$ with the increase of α and T_s and formation of $(\equiv Si-O)_2VOCl$ takes place. And at $\alpha > 1$ the total breakage of Si–O–V bonds with educing of $VOCl_3$ into the gas phase is observed.

The interaction of silica gel with $VOCl_3$ was considered to be an opportunity for mathematical model construction of the process of volatile halogenides chemisorption on the disperse silica surface.

Developing the model the following factors, affecting distinctions in behaviour of active sites of surface and in structures of forming new functional groups were accepted: 1. Availability on the silica surface of various active sites – hydroxyl groups, isolated and connected by hydrogen bonds, siloxane bridges, coordinately linked water, stabilized radicals and charging states etc. [34,52–60]; 2. Opportunity of occurrence of gradient of low–molecular reagent concentration due to diffusion breaking in bulk layer and in porous space of grain; 3. Influence of HCl – the collateral product of reaction.

Assuming diversity of active sites, the characteristics of reactivity of silica surface may be the distribution function of active centers by the parameters of reactivity. It was

shown, that the free energy of transient complex (ΔG) was the most convenient parameter, connected with the rate constant of reaction (k) by the well known equation:

$$\Delta G = -RT \cdot \ln(k) \tag{3}$$

Thus based on approximation, not accounting diffusion breaking and HCl influence, dependence of contents of modifier in the solid phase on the time of chemisorption A(t) is possible to be presented as:

$$A(t) = \int_{\Delta G_{min}}^{\Delta G_{max}} \left[1 - \exp\left(-\exp\left(-\frac{\Delta G}{RT}\right) \cdot C \cdot t\right)\right] \cdot \psi(\Delta G) \cdot d(\Delta G) \tag{4}$$

where C – is the concentration of low-molecular reagent in the gas phase; ψ – is the distribution function of surface active sites upon the reactivity.

This equation was used to estimate the reactivity of silica gel surface at interaction with $VOCl_3$ vapour in the flow system in conditions of avoiding the diffusion moderation at the thickness of material in one grain [10]. On the basis of experimental kinetic data the function of distribution, submitted in Figure 6 was obtained. The account was conducted by numerical decision of the reverse task (4) by the Tikhonov regularization method with the use of the projector of conjugate gradients in the areas of non-negative magnitude of function ψ [61].

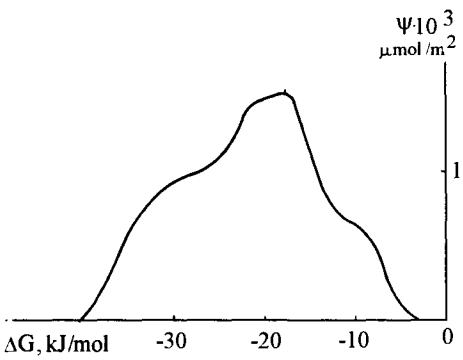

Figure 6. The calculated distribution function of silica surface sites on the reactivity in the interaction with $VOCl_3$.

From the submitted data it follows, that for the considered system the exactly expressed inhomogeneity of surface sites on reactivity is not observed. The reliability of the results is confirmed by the model calculations, demonstrating restorations of function of distribution, consisting of several peaks, with an error of 5–10%. Therefore for the considered system inhomogeneity of silica gel surface is possible to be neglected as the first approximation.

The account of influence of diffusion moderation is connected first of all with the concentration factor and the influence of hydrogen chloride. As shown earlier [40], in the

presence of HCl in the gas phase together with $VOCl_3$ on the silica gel surface the following reactions are possible:

$$3(\equiv Si - OH) + VOCl_3 \rightarrow (\equiv Si - O)_3VO + 3HCl \quad (5)$$

$$(\equiv Si - O)_3VO + HCl \rightarrow (\equiv Si - O)_2VOCl + (\equiv Si - OH) \quad (6)$$

$$(\equiv Si - O)_2VOCl + 2HCl \rightarrow 2(\equiv Si - OH) + VOCl_3 \quad (7)$$

Then the process kinetics can be described by the system of differential equations:

$$\frac{dC_1}{dt} = k_1 \cdot [VOCl_3] \cdot (A_0 - C_1 - C_2) - k_2 \cdot [HCl] \cdot C_1 + k_3 \cdot C_2$$

$$\frac{dC_2}{dt} = k_2 \cdot [HCl] \cdot C_1 - k_3 \cdot C_2 - k_4 \cdot [HCl] \cdot C_2$$

$$A_0 = [\equiv Si - OH]/3 + C_1 + C_2 \quad (8)$$

where C_1, C_2 are the concentrations in the solid phase of groups $(\equiv Si\text{–}O)_3VO$ and $(\equiv Si\text{–}O)_2VOCl$, accordingly, A_0 – is the concentration of the "hydroxyl triads" on the initial surface.

Estimation of parameters of the given system on the basis of experimental data on kinetics of silica gel interaction with gas mixture of HCl and $VOCl_3$ in conditions of avoiding the diffusion moderation [40], demonstrating adequacy of the proposed model, was performed. Influence of diffusion stages of heterogeneous process (5–7) equations (8) should be complemented by differential diffusion equations for gas components in pore space of silica grains:

$$\frac{\partial[VOCl_3]}{\partial t} - D_{VOCl_3}\frac{\partial^2[VOCl_3]}{\partial x^2} = -B \cdot \left(\frac{\partial C_1}{\partial t} + \frac{\partial C_2}{\partial t}\right)$$

$$\frac{\partial[HCl]}{\partial t} - D_{HCl}\frac{\partial^2[HCl]}{\partial x^2} = B \cdot \left(\frac{\partial C_1}{\partial t} \cdot 3 - \frac{\partial C_2}{\partial t}\right)$$

$$x = 0: \quad \frac{\partial[VOCl_3]}{\partial x} = 0; \quad \frac{\partial[HCl]}{\partial x} = 0;$$

$$x = R: \quad [VOCl_3] = C_{VOCl_3}; \quad [HCl] = 0;$$

$$t = 0: \quad [VOCl_3] = 0; \quad [HCl] = 0; \quad (9)$$

where:

D_{VOCl_3},D_{HCl} – are the gas diffusion coefficients of $VOCl_3$ and HCl accordingly;

R – is the linear size of material grain;

B – is the translation factor of surface concentration C_1, C_2 in volume ones;

C_{VOCl_3} – is the concentration of $VOCl_3$ in the gas flow;

The obtained system of parities (8–9) represents the nonlinear task. It was resolved numerically for various values of R and C_{VOCl_3}.

As a result of carried out calculations it was shown, that the HCl accumulation in pore space results in occurrence of gradient both of the concentration, and functionality of vanadium–oxide groups on the depth of separate grain. The value of a given gradient is determined by boundary conditions in equation (7). In Figure 7 the dependencies of

chemical composition of final solid product of interaction upon the reagent concentration in the gas phase and the geometrical sizes of particles are submitted. From the submitted data it follows, that for silica gel the ratio of concentrations of chlorine and vanadium can considerably vary depending on the conditions of synthesis. That can explain the spread of data of experimental value of a given parameter, obtained by various authors. So, the account of diffusion moderation permits to evaluate the results of surface modification more adequately and to build the mathematical models, necessary for technological realizations of similar processes.

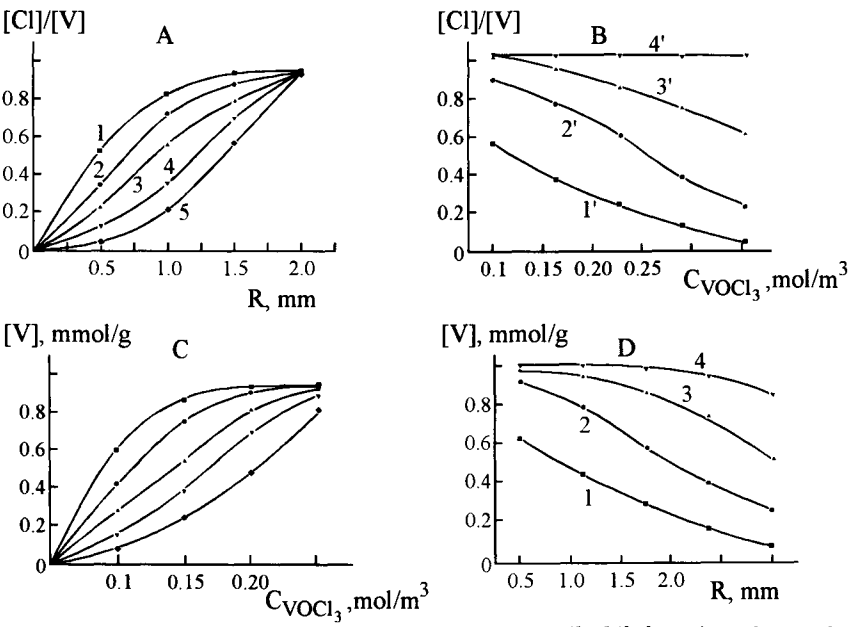

Figure 7. Dependencies of the stoichiometric ratio ([Cl]/[V],A,B) and vanadium content ([V],C,D) upon the gaseous concentration of $VOCl_3$ (0.1 (1′); 0.15 (2′); 0.20 (3′); 0.25 (4′); 0.30 (5′) mol/m^3) and grain size R (0.25(1); 0.5(2); 1.0(3); 1.5(4); 2.0(5) mm).

The study of macrokinetics of reaction $VOCl_3$ with silica gel has shown also, that the process proceeds in outside diffusion area. The significant intensification of interaction is observed during the synthesis in the fluidized regime of solid phase [10,45].

3. FORMATION OF MULTICOMPONENT MONOLAYERS OF A GIVEN COMPOSITION AND STRUCTURE ON SILICA SURFACE

From the ML principles and analysis of experimental data on stability of Si–O–E bonds to effect hydrogen chloride it was possible to distinguish the following ways of multicomponent monolayers synthesis:

a) consecutive processing of silica by vapour of halogenides of such elements as E1, E2, E3 and etc., that halogenides of E2, E3 interact with OH-groups, not taking part in the reaction with compounds of E1, E2, respectively;

b) the replacement of surface E1–containing groups by E2–containing groups ($E_{E1-O} < E_{E2-O}$), thus halogenide of element E1 is educed into the gas phase;
c) processing of silica by mixture of halogenides of E1 and E2, differed by reactivity in relation to the surface OH–groups.

Some main results on realization of the mentioned variants will be considered.

By the interaction of silica with phosphorus oxychloride the phosphorus–containing silica were synthesized, with the increase of phosphorus content from 0 to 0.95 mmol/g the amount of OH–groups in the samples decreases from 3.62 to 1.42 mmol/g. Obtained P–silica were treated by titanium and vanadium chlorides. The content of bonded at the expense of reaction with silanols of titanium– and vanadium–containing groups decreases from 1.08 to 0.35 (Ti, Table 2) and from 1.11 to 0.31 mmol/g (V, Table 3) accordingly [62,63].

Table 2
Chemical composition of PTi – silica. Time of $TiCl_4$ processing – 30 min

Composition of initial P–silica, mmol/g				Composition of PTi–silica, mmol/g						
P	Cl	Cl/P	OH	P	Ti	P/Ti	Cl	ΔCl	ΔCl/Ti	OH
–	–	–	3.62	–	1.08	–	1.52	1.52	1.41	0.82
0.13	–	–	3.23	0.13	0.97	0.13	1.58	1.58	1.63	0.93
0.20	0.02	0.10	3.04	0.20	0.89	0.22	1.53	1.51	1.70	0.99
0.34	0.08	0.22	2.67	0.34	0.74	0.46	1.55	1.47	1.99	1.18
0.45	0.14	0.32	2.41	0.45	0.63	0.72	1.46	1.32	2.10	1.21
0.61	0.30	0.49	2.08	0.61	0.47	1.30	1.36	1.06	2.26	1.25
0.95	0.65	0.68	1.42	0.95	0.35	2.71	1.49	0.84	2.40	0.86

Table 3
Chemical composition of PV–silicas. Processing time $VOCl_3$ – 30 min

Composition of initial P–silica, mmol/g				Composition of PV–silica, mmol/g						
P	Cl	Cl/P	OH	P	V	P/V	Cl	ΔCl	ΔCl/V	OH
–	–	–	3.62	–	1.11	–	0.42	0.42	0.38	0.71
0.08	–	–	3.32	0.08	1.02	0.08	0.46	0.46	0.45	0.78
0.28	0.05	0.18	2.83	0.28	0.83	0.34	0.55	0.50	0.60	0.84
0.37	0.10	0.27	2.61	0.37	0.73	0.51	0.76	0.66	0.91	1.08
0.69	0.37	0.54	1.92	0.69	0.42	1.64	0.77	0.40	0.95	1.06
0.81	0.51	0.63	1.70	0.81	0.34	2.38	0.89	0.38	1.12	1.06
0.92	0.62	0.67	1.48	0.92	0.31	2.96	0.98	0.36	1.16	0.91

The data of spectroscopic researches (ESCA, ESDR), submitted in work [63], testify to the transference of electronic density on a titanium atom and increase of the coordination number of titanium in the PTi–samples, that is stipulated by formation of donor–acceptor

P=O→Ti bond in the structure of surface groups. In PV-silica in connection with inclination of V(+5) to reduce the transference of electronic density on a vanadium atom with formation of P=O→V bond results in vanadium reducing to V(+4), that is confirmed by EPR data [62].

The reactions of replacement of vanadium-, titanium- and chromium-containing groups on silica surfaces are investigated when processing by vapour of $POCl_3$, $TiCl_4$, $VOCl_3$, as well as chemical composition and interfunctional interactions in formed vanadium-phosphorus (VP-), titanium-phosphorus(TiP-), vanadium-titanium (VTi-), chromium-vanadium (CrV-) and chromium-titanium (CrTi-) containing silica [63,64,65]. During the synthesis of TiP- and VP-samples on the surface the reactions of replacement with formation of $(\equiv Si\text{-}O\text{-})_2POCl$ groups and allocation of $TiCl_4$ and $VOCl_3$ proceed in the gas phase. The relation $P/\Delta Ti$ and $P/\Delta V$ makes accordingly 1.42 ± 0.05 and 1.20 ± 0.03, that testifies the partial interaction of $POCl_3$ with OH-groups, concentration of which grows on the surface with decreasing of titanium and vanadium contents in initial V- and Ti-silica, with formation of $(\equiv Si\text{-}O\text{-})POCl_2$, as well as owing to the partial destruction of Si-O-M bonds (M=Ti, V) and formation of Si-O-P bonds. In TiP- and VP-silica similarly to PTi- and VP-samples of the same chemical composition donor-acceptor P=O→Ti and P=O→V bonds in the two-component monolayer are formed.

The $POCl_3$ chemisorption rate in replacement reactions is found out to be above, that is in the interaction of $POCl_3$ with OH-groups of silica [64,66].

In the synthesis of VTi- and TiV-silica (Tables 4 and 5) in final products the ratios $Ti/\Delta V$ and $V/\Delta Ti$ are observed to be close to 1.

Table 4
Chemical composition of VTi-silica

No.	Proccessing time, min	Content, mmol/g							
		V	Ti	Cl	Ti/V	ΔV	Ti/ΔV	Cl_{calc}	Cl/Cl_{calc}
1	Initial	1.11	–	0.42	–	–	–	–	–
2	2	0.61	0.52	0.89	0.84	0.50	1.04	0.94	1.06
3	3	0.47	0.65	1.05	1.38	0.64	1.02	1.07	1.02
4	5	0.27	0.84	1.23	3.10	0.84	1.00	1.26	1.02
5	8	0.11	1.00	1.38	9.08	1.00	1.00	1.42	1.03
6	10	0.04	1.07	1.50	24.8	1.06	1.01	1.48	0.99
7	15	0.01	1.10	1.53	110.0	1.10	1.00	1.52	0.99

Thus the interfunctional interactions in the monolayer are absent, on the surface $(\equiv Si\text{-}O\text{-})_3TiCl$ or $(\equiv Si\text{-}O\text{-})_2VOCl$ groups are formed, and $VOCl_3$ or $TiCl_4$ is educed to the gas phase.

By obtaining CrV- and CrTi-silica the ratio $V/\Delta Cr$ and $Ti/\Delta Cr$ in the final products makes 1.63 and 1.94, i.e., together with the replacement of the interaction of $VOCl_3$ and $TiCl_4$ with residual OH-groups of Cr^{6+}-silica proceeds. In the composition of CrTi-samples the significant quantity of Cr^{3+}, stipulated, obviously, by reducing of Cr^{6+} to Cr^{3+} on the surface under the action of HCl, educed during reaction is present [51].

The interaction of $TiCl_4$-$VOCl_3$ mixture with silica (samples TiV) had been carried

Table 5
Chemical composition of TiV– silica

No.	Proccessing time, min	Content, mmol/g							
		Ti	V	Cl	V/Ti	ΔTi	V/ΔTi	Cl_{calc}	Cl/Cl_{calc}
1	Initial	1.08	–	1.52	–	–	–	–	–
2	60	0.85	0.24	1.33	0.28	0.23	1.04	1.28	0.96
3	120	0.67	0.41	1.12	0.61	0.41	1.00	1.11	0.99
4	240	0.50	0.59	0.89	1.18	0.58	1.02	0.93	1.04
5	420	0.39	0.70	0.87	1.80	0.69	1.01	0.82	0.94
6	540	0.36	0.72	0.85	2.00	0.72	1.00	0.80	0.94

out at the molar ratio of chlorides in the gas phase $TiCl_4/VOCl_3$=0.6 (Figure 8 A) and 1.5 (Figure 8 B). The total concentration of chlorides was 0.40 mol/m^3.

The analysis of the experimental data has shown, that on the silica surface the consecutive - parallel reactions of silanol groups with $VOCl_3$ and $TiCl_4$, as well as $(\equiv Si–O–)_2VOCl$ with $TiCl_4$ with escaping of $VOCl_3$ into the gas phase proceed. It follows from the data in Figure 8 that at enough large time of interaction $TiCl_4$ is, practically, selectively chemisorbed on silica. It permits to assume the opportunity for employment of the similar processes for separating and purification of chlorides.

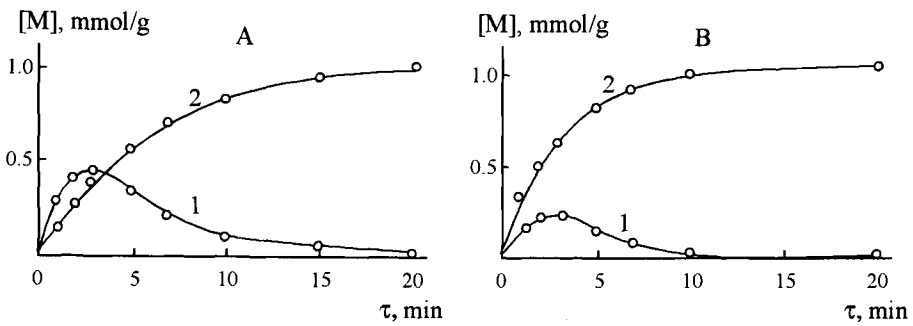

Figure 8. The kinetic curves of silica gel interactions with the mixture of vapours of $VOCl_3$ and $TiCl_4$. A–$TiCl_4/VOCl_3$=0.6; B–$TiCl_4/VOCl_3$=1.5; 1, 2 are the vanadium and titanium content [M] accordingly.

By the treatment of PTi–silica by vapour of $VOCl_3$ the PTiV–silica was synthesized and the interfunctional interactions in the three–component phosphorus–titanium–vanadium–oxide monolayer were studied [67]. It was found that the formation of P=O→Ti bond in PTi–silica ($P/Ti \leq 1$) prevents the interaction of P=O groups with vanadium atoms when processing of PTi–silica by $VOCl_3$, as a result on silica gel surface three–component phosphorus–titanium– vanadium–oxide monolayer (PTiV–silica) is formed. At $P/Ti > 1$ the part of groups P=O is not connected with titanium atoms and formation of P=O→V bonds becomes possible.

Thus, synthesis of monolayers, containing the given number of heteroatoms, has to be

executed both in view of nature of initial reagents, and properties of surface structures formed.

4. THE GROWTH OF OXIDE AND OXYGEN–FREE COATINGS ON THE SURFACES OF SiO_2 AND Al_2O_3

Literature presents numerous data on the syntheses by ML method of oxide layers of titanium, aluminum, chromium, phosphorus, tantalum and series of other elements on silica and alumina surfaces, when appropriate chloride and vapour of water are used as initial reagents [13,35,18,42]. The synthesis thus proceeds without the change of oxidation state of elements. But the stability of Si–O–M bonds in the process of gaseous treatment of element-chloride surface structures is of significant importance. Our researches have shown [44,68], that the strength of Si–O–M bonds is influenced by the thermal stability of element–oxide–chloride groups, quantity of their bonds with surfaces (factor m) and series other ones. The reason for the destruction is the hydrogen chloride which educes in the process of vapour hydrolysis [68].

The further researches have shown, that the temperature of synthesis and the nature of solid matrix render the appreciable influence on composition and structure of the oxide layer forming in the ML process. In Figure 9 the data on changes of titanium contents on silica and alumina surfaces in the ML process at the temperature of synthesis at the 200–600°C are shown. As results from the submitted dependencies, escalating

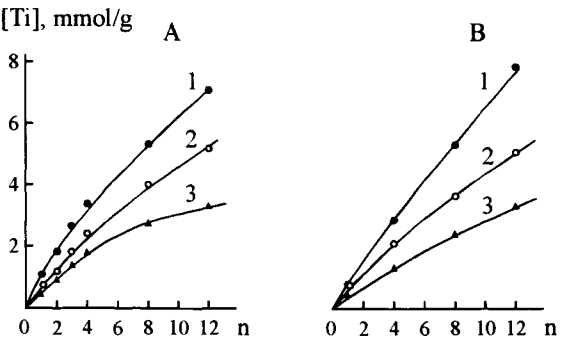

Figure 9. Dependencies of titanium content in the oxide layer on the number of ML cycles (n). Temperature of synthesis: 1 – 200, 2 – 400, 3 – 600°C; A – SiO_2, B – Al_2O_3.

titanium–oxide layer proceeds in regular intervals at all considered temperatures Ts. At the same time, the gain of titanium amount for each ML cycle with the increase of Ts from 200 to 600°C is reduced with 0.78 to 0.44 and with 0.68 to 0.27 mmol/g SiO_2 and Al_2O_3 accordingly. The tendency to stipulate was found, on one hand, by the decrease of quantity of active hydroxyl groups both on initial surface, and formed during the synthesis as a result of dehydroxylation. On the other hand, with the increase of temperature the conversions in structures of formed titanium–oxide– chloride groups took place as shown earlier in work [44]. The obtained surface structures by XRD data are the polycrystalline formations whose phase structure depends both on chemical nature of matrix, and on

temperature of the chemisorption stage (Figure 10). On the surface of silica up to 350°C the single-phase structure is formed, adequate anataze modification of TiO_2. At Ts≥350°C

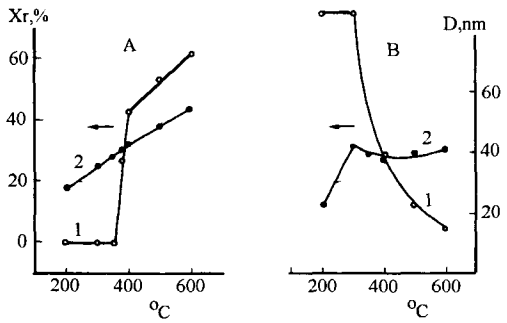

Figure 10. The rutile phase part Xr (1) and crystallite size D (2) dependencies upon the synthesis temperature (A–SiO_2, B–Al_2O_3).

alongside with anataze the rutile modification is proceeds, a part of which is increased with the increase of Ts and at 600°C makes 89 %. On the surface of alumina, on the contrary, a biphase structure is formed at low temperature. And with the increase of Ts the part of anataze form of TiO_2 grows, up to 100 % at 600°C.

The application in the ML processes of such compounds, as the chromium dioxydichloride and vanadium(5+) oxychloride (oxidators), the phosphorus trichloride (reductor) permits to expand the set of chemical interactions on surfaces in the synthesis of polymolecular layers. For the first time in work [14] the process of formation of oxide layer of phosphorus(5+) on silica gel was carried out with application of oxidizing-reducing reactions:

$$3(\equiv Si - OH) + PCl_3 \rightarrow (\equiv Si - O-)_3P + 3HCl \quad (10)$$

$$(\equiv Si - O-)_3P + Cl_2 \rightarrow (\equiv Si - O-)_3PCl_2 \quad (11)$$

$$(\equiv Si - O-)_3PCl_2 + 2H_2O \rightarrow (\equiv Si - O-)_3P(OH)_2 + 2HCl \quad (12)$$

Further reactions (10–12) appear again in the given sequence.
Using the oxidizing property of compounds of chromium(6+) in $(\equiv Si\text{-}O\text{-})_2CrO_2$ groups, for reception on surface hydroxyl groups, capable to enter further in the reaction with CrO_2Cl_2, chromium(6+)-containing sample was processed by the reductor – the molecular hydrogen. Thus the reaction on the surface at 180°C proceeds as follows [11]:

$$(\equiv Si - O-)_2CrO_2 \xrightarrow[-H_2O]{+3/2H_2} (\equiv Si - O-)_2CrOH \quad (13)$$

For the growth of chromium(3+)-oxide layers of given thickness on the silica surface the processing of Cr^{6+}-silica obtained by recurrence of cycles of ML reactions: 1– reduction by H_2; 2– processing by vapour of CrO_2Cl_2; 3–processing by aqueous vapour [12].

It follows from Table 6, which adduces the chemical composition of ML products that the repeated alternation of reactions mentioned results in the regular increase of chromium(3+) content in samples.

Table 6
Chemical composition of products of repeated alternate processing of silica gel by vapour of CrO_2Cl_2, H_2O (samples "a") and hydrogen (samples "b")

Sample	Content, mmol/g					v_s,	S_{sp},
	Cr(+6)	Cr(+3)	Cr_0	ΔCr_0	$[OH]_E$	cm^3/g	m^2/g
–	–	–	–	–	3.57	0.96	246
1a	1.03	0	1.03	1.03	1.50	–	–
1b	0	1.04	1.04	–	2.47	0.79	229
2a	1.03	1.01	2.04	1.00	2.29	–	–
2b	0	2.04	2.04	–	2.18	0.77	209
3a	1.12	2.11	3.23	1.19	2.29	–	–
3b	0	3.19	3.19	–	2.14	0.64	193
4a	1.32	3.54	4.86	1.67	2.36	–	–
4b	0	4.84	4.84	–	2.15	–	166
5a	1.44	5,07	6.51	1.67	2.36	–	–
5b	0	6.32	6.32	–	2.25	0.54	155
6a	1.57	6.44	8.01	1.69	2.42	–	–
6b	0	8.23	8.23	–	2.34	–	133

Thus the total volume of pores in silica gel and value of specific surface area with the increase of a number of ML cycles decreases.

For the first time with the use of oxidizing-reducing properties of surface groups and low-molecular reagents the synthesis of oxide layers, consisting of monolayers of various chemical composition, was carried out [51]. The study of interaction of groups $(\equiv Si\text{-}O\text{-})_3VO$ with PCl_3 and $(\equiv Si\text{-}O\text{-})_3P$ with $VOCl_3$ allowed to obtain on silica surface a two-component oxide layer, in which as a result of processing of oxidizing-reducing reactions vanadium and phosphorus are in three and five-valent states accordingly. The samples of, practically, identical chemical composition, differ by mutual arrangement of vanadium- and phosphorus - containing monolayers, connected by $\Delta\pi - \pi\pi$ bonds.

When processing Cr^{6+}-silica by vapour of PCl_3, alongside with oxidizing-reducing reaction between $(\equiv Si\text{-}O\text{-})_2CrO_2$ groups and PCl_3 with formation of Cr-O-P bonds, the affiliating PCl_3 to the surface Si-O-P bonds takes place [7]. Repeated and alternate processing of silica gel by vapour of CrO_2Cl_2, PCl_3 and H_2O leads to the regular increase of chromium and phosphorus contents in the samples [21].

The important factors, corroborating the generality of the principles of ML method for obtaining various kinds of surface structures, are the consequences, according to which, in appropriate stages of synthesis of the required reagents, it is possible to form on a surface not only oxide structures. In works [69–73] on the surface of silica, alumina and other solid matrices carbon (with the use of CCl_4 and CH_4), sulfide (from $ZnCl_2$ and H_2S or $Zn(OC_2H_5)_2$ and H_2S), nitride (processing, for example, vapours of $TiCl_4$ and NH_3) structures or their compositions were synthesized. The integrated outline of ways of chemical assembly of surface of solid by ML method has been presented in Fig. 11.

In summary we note the following: irrespective of the chemical nature and structure of disperse matrix the technological operations, hardware registration of process of synthesis

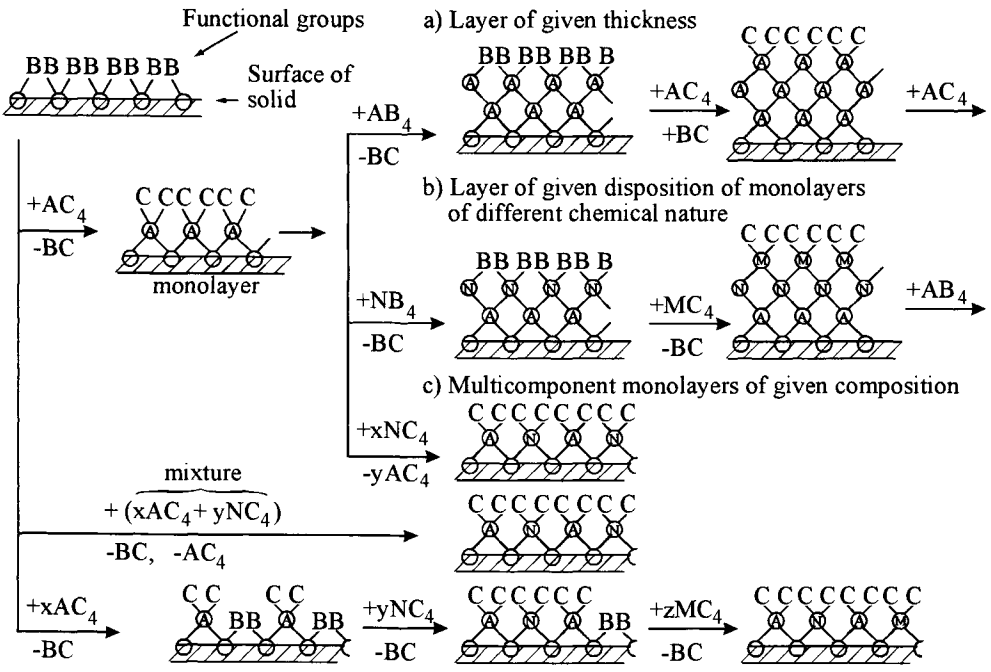

Figure 11. Solid surface chemical assembling scheme.

in all the cases is identical [41,42,72]. Only the technological regimes (temperature, concentration, the rate of gas – carrier) change, which are defined by properties of low–molecular reagents and initial matrix surface, physico–chemical characteristics of forming modified products, as well as operational requirements for them. So, using, practically, identical hardware it is possible to execute the production of materials of various target purposes of required properties.

5. THE MODIFICATION OF STRUCTURAL AND ADSORPTION CHARACTERISTICS OF SILICA AND ALUMINA BY THE MOLECULAR LAYERING METHOD

The investigation of properties of products obtained by the ML method allowed to find out three fundamental features that define new technology:

1) the monolayer effect, i.e. sharp, spasmodic change of matrix characteristics of new structure units;
2) the matrix overlap effect;
3) the effect of mutual concordance of matrix structure and formed layer [13,75]

On the basis of these effects and possibility to form multicomponent mono– and polylayers we considered the most perspective application fields of the ML method technology.

It is very good to use a "monolayer effect" (ME) in such cases when it is necessary to distribute uniformly and to bind in a strong way small quantities (from parts of monolayer to several monolayers) of alloy additions on a developed surface (from one to hundred m^2/g). Catalysts, sorbents, pigments, ceramic powders, fillers of compositional materials and some others are considered to be such materials. In different papers one can find information about application of the ML method basically for creation of highly active and selective catalysts [25,29,76,77], but the number of solid phase materials where ME could be applied is much greater. For example, uniform distribution of monolayer with elements combinations which change their colouring under the influence of surroundings can be used for raising of sorbents-indicators sensitive to the vapours H_2O, NH_3, H_2S, NO_2 and other harmful components in many technological processes. One of the best examples is a coloured humidity indicator which was created on the basis of vanadium-containing silica gel.

It is known that V_2O_5 in dependence on crystallohydrate water content has different colouring [78]. But in literature there is no information about using vanadium compounds for visual control of humidity in gas media because of very low rate of colour changing and contrast. At the same time the data presented in Table 7 show the great dependence of colouring of vanadium-containing silica gel on humidity of air stream. The edge of sensibility for IVS-1 in the contact with air stream (expenditure 0.5 l/min.) is -40°C according to a dew-point and the sample acquires even yellow colouring in 30 minutes. It should be noted that the sensitivity of IVS-1 approximately ten times higher in comparison with industrial cobalt-containing silica gel (Table 7), this is a reversible sorbent-indicator on water vapours and may be regenerated at 200-400°C. As shown IVS-1 can be used in control of industrial gases on vapours of ammonia in the concentration range 30-400 mg/m^3 (yellow colour), of SO_2 at 360-1400 mg/m^3 (blue colour), H_2S at 20-140 mg/m^3 (violet colour). It should be noted that the synthesis of the second monolayer of vanadium-containing groups on silica gel and the formation of samples by the impregnation method does not allow to receive products with indicator properties on water vapours.

Table 7
Sorbent-indicator of the H_2O vapour

Relative humidity (%)	0.5	1.6-4.6	6-10	10-13	15-45	48-95
Dew-point (°C)	-40	-30 – 20	-18 – 13	-12 – 10	-9 + 6	+8 + 19
Color of the external layer IVS-1* TU 6-10-1971-84	lemon	bright yellow	light orange	dark orange	from red to dark	brown

* IVS-1 can be used as a humidity indicator in the presence of NH_3, SO_2, NO_2.

Speaking about "matrix overlap effect" (MOE) it should be noted that it could be used in all the cases mentioned above. The ML technology allows to control the surface layer composition down to one monolayer. But the most interesting aspect of the use of this effect is creation of kernel pigments and fillers. It means that we use as a kernel the particles of cheap materials (desirably industrial waste materials) and form on their surfaces a jacket of optically active product (for example TiO_2, ZnO in creation of white

pigments). By the ESCA data it was shown that the intensity of Si2p peak (matrix) constantly decreased during the growing of titanium oxide layers on the SiO_2 surface (white soot BS-30), and $Ti2p^{3/2}$ peak in its energy parameters corresponds to the same one in the standard TiO_2. The samples of the white soot BS-30 with the TiO_2 jacket were tested as a white pigment. The mechanical mixture of SiO_2 and TiO_2 with the same ratio of components was used for comparison. It was shown that at the ratio SiO_2:TiO_2=9:1 (calculated thickness of TiO_2 jacket ~2 nm) the coverage of white pigment was ~78 g/m^2 vs. ~166 g/m^2 for a mechanical mixture.

On the basis of the white soot BS-100 with the ZnO jacket (~20% in calculation for ZnO) a new activator of rubber mixtures vulcanization was made. On the one hand, it substitutes ZnO, on the other it has better characteristics in comparison with a mechanical mixture of the same composition [79].

The possibility of coloured casing pigments and fillers creation was demonstrated on the basis of SiO_2 (Aerosil 175) with chromium(III) oxide jacket (~15% wt. in calculation for Cr_2O_3) [80].

The received data show the expediency of MOE application from the point of view of deficit raw materials great saving (for example ZnO), solving ecological problems (waste materials as kernels of casing products) and increasing of pigments and fillers output without great enlargement of raw materials' base. It should be noted, however, that because of many stages in the ML technology one needs serious economical estimate in realization of "thick layers" synthesis. At the same time, as it is known from literature and experimental data, there are ways to make the ML process in its combination with traditional methods much cheaper.

Thus, the ML method and MOE can be the basis for creation of the new resource saving technology for casing pigments and fillers.

The effect of mutual concordance of matrix structure and formed monolayer (EMC) is much less discussed in literature than the previous ones. But the very first experiments demonstrated that the above mentioned EMC could influence in a great way the phase transformations of both matrix and grafted layer increasing their velocity and decreasing power consumption [81,82]. The results obtained in [81,82] allow one to forecast with enough confidence their application in the processes of compacting high-dispersed products, for example in the ceramic technology.

One more interesting perspective of the ML method is in its possibility to form practically any artificial multicomponent nanostructures with any composition as shown in Figure 11 (schemes B and C).

Taking into account the above mentioned ME and MOE one can distinguish three main directions in realization of such artificial structures:

a) formation of clusters with a different known ratio of different atoms;
b) introduction into the surface structure composition different atoms increasing the influence of basic alloy additions;
c) chemical assembling of coverings possessing polyfunctional properties.

In Figure 12 the technological scheme of silica gel modification by the vanadium is submitted [41,74].

Preliminary dried silica is loaded into the section I by the loader 9 from vessel 10 on the gas-distribution plate 13 to be dried and heated up to 200°C. The air injected by the compressor 2 is used as a carrier gas. It is dried by the NaX zeolite up to a dew-point

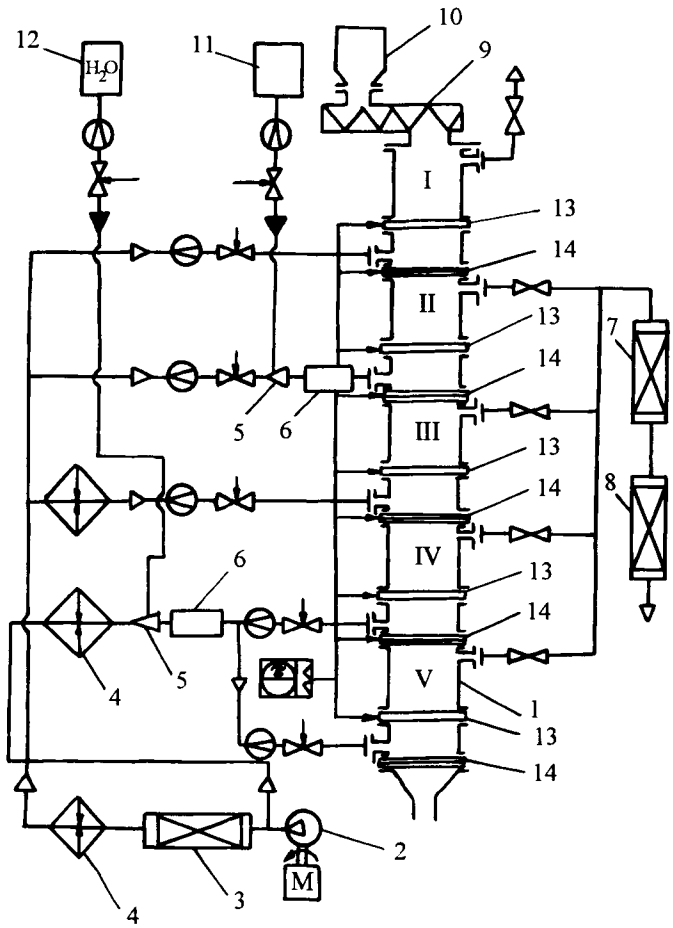

Figure 12. The technological scheme of gaseous obtaining of V–silica gel. Details are: chemical reactor (1), compressor (2), absorber (3), calorifer (4), injector (5), commingler (6), barboters (7,8), loader (9), vessels (10,11,12), gas–distributor plate (13), isolating device (14).

−50, −60°C into the adsorbers 3 and then is heated passing the calorifers 4. After the isolating device 14 has been opened, silica gel moves into section II, where it is treated by the $VOCl_3$ vapour. In section III the removal of the main part of non–reacted $VOCl_3$ by the air flow takes place at the temperature 300–500°C. Sections IV and V are used to desorbe $VOCl_3$ by the aqueous vapour–air mixture. The air is saturated by the $VOCl_3$ and H_2O vapours in the injectors 5 and in the comminglers 6. The $VOCl_3$ and H_2O vapours are absorbed at the reactor outlet into the barboters 7,8.

The mathematical description and the methods of technological calculations of $VOCl_3$ chemisorption by the fluidized silica gel process were proposed. For this purpose the exact

dependence of vanadium content on synthetic parameters and physicochemical properties of acted phases as well as on the processing time have been found:

$$a = a(C_{in}, w, H_0, D_g, d_{av}, \rho_{app}, A, \tau) \tag{14}$$

where H_0 is the height of silica layer; D_g is the gas diffusion coefficient; ρ_{app} is the apparent density; A is the maximum possible vanadium content for given silica gel; d_{av} is the average silica gel grain diameter; w is the gas flow rate; C_{in} is the vanadium concentration in the gaseous flow inlet the reactor; τ is the processing time.

Mathematical model was based on the dimension analysis method. The obtained dependence of silica gel surface conversion degree on the process parameters can be presented as:

$$\Theta = 1 - [1 - \Theta^*]^{1 - \exp\left[-\alpha_0 \left(\frac{wH_0}{D_g}\right)^{\alpha 1} \left(\frac{D_{av}}{H_0}\right)^{\alpha 2} \left(\frac{D_g \tau}{d_{av}^2}\right)^{\alpha 3}\right]} \tag{15}$$

where Θ^* is the maximum coverage of silica surface by the vanadium–containing groups under the experimental conditions.

The experimental data were treated by the least square method. As a result the numerical values of $\alpha 1$, $\alpha 2$, $\alpha 3$, $\alpha 4$ were obtained. To found the magnitude of Θ^* the empirical equation was proposed:

$$\Theta^* = 1 - e^{-27C_{in}} \tag{16}$$

The average relative error of Θ, Θ^* parameters estimation according to equations (15,16) does not exceed 10%.

The proposed mathematical model was taken as a basis of chemisorption process calculations for a semi–permanent action apparatus, used for the V–silica gel synthesis.

REFERENCES

1. V.B. Aleskovskii, Thesis, Technological Institute, Leningrad 1952.
2. S.I.Koltsov and V.B.Aleskovskii, in: Abstracts of Sci.–Tech. Conf., Goskhimizdat, Leningrad, 1963, p.37.
3. S.I. Koltsov, V.B. Aleskovskii, Zhurn. Fiz. Khimii, 42 (1968) 1210.
4. A.N. Volkova, A.A. Malygin, V.M. Smirnov, S.I. Koltsov and V.B. Aleskovskii, Zhurn. Obshch. Khimii, 42 (1972) 1431.
5. S.I. Koltsov, A.A. Malygin, A.N. Volkova, V.B. Aleskovskii, Zhurn. Fiz. Khimii, 47 (1973) 988.
6. A.N. Volkova, A.A. Malygin, S.I. Koltsov, V.B.Aleskovskii, Zhurn. Obshch. Khimii, 43 (1973) 724.
7. A.N. Volkova, A.A. Malygin, S.I. Koltsov, V.B.Aleskovskii, Zhurn. Obshch. Khimii, 45 (1975) 3.
8. A.N. Volkova, A.A. Malygin, S.I. Koltsov, N.N.Stafeeva and V.B. Aleskovskii, Method of Molibdenium–containing Silica Synthesis, USSR patent No. 440338 (1974).
9. A.N. Volkova, A.A. Malygin, S.I. Koltsov, V.B.Aleskovskii, Zhurn. Obshch. Khimii, 46 (1976) 2166.

10. V.F. Dergachev, A.A. Malygin, S.I. Koltsov, Zhurn. Prikl. Khimii, 54 (1981) 1972.
11. A.N. Volkova, A.A. Malygin, S.I. Koltsov, V.B.Aleskovskii, Zhurn. Obshch. Khimii, 47 (1977) 3.
12. A.A. Malygin, S.I. Koltsov, V.B.Aleskovskii, Zhurn. Prikl. Khimii,51 (1978) 2447.
13. V.B. Aleskovskii, Stoichiometry and Synthesis of Solid Compounds, Nauka, Leningrad, 1976 (in Russian).
14. A.N. Volkova, A.A. Malygin, V.M. Smirnov, V.B.Aleskovskii, Zhurn. Prikl. Khimii, 47 (1974) 1974.
15. V.B. Aleskovskii, Chemistry of Solid Substances, Vysshaya Shkola, Moscow, 1978 (in Russian).
16. V.B.Aleskovskii, Zhurn. Prikl. Khimii, 47 (1974) 2145.
17. V.B Aleskovskii, Vestnik AN SSSR, No. 6 (1975) 48.
18. S.I. Koltsov, V.B. Kopylov, V.M. Smirnov, V.B.Aleskovskii, Zhurn. Prikl. Khimii, 49 (1976) 516.
19. N.A. Stepanova, V.M. Smirnov, S.I. Koltsov, V.B.Aleskovskii, Zhurn. Prikl. Khimii, 50 (1977) 2567.
20. A.N. Volkova, A.A. Malygin, S.I. Koltsov ,V.B. Aleskovskii, Method of Ammonia Separating from Gaseous Mixtures, USSR Patent No. 356242 (1972).
21. A.N. Volkova, A.A. Malygin, S.I. Koltsov, V.B.Aleskovskii, Method of Synthesis of Cr(III) and P(V)-oxide Layer on the Silica Surface, USSR Patent No. 422446 (1976).
22. A.N. Volkova, A.A. Malygin, S.I. Koltsov, V.B.Aleskovskii, Method of Preparation of Vanadium Oxide Catalyst for Organic Compounds Oxidation, USSR Patent No. 42447 (1976).
23. B.I. Laskorin, V.V. Strelko, D.N. Strazhesko, V.I. Denisov, Silica Sorbents in: Radiochemistry. Chemical Properties. Applications, Atomizdat, Moscow, 1977 (in Russian).
24. G. Bliznakov, M. Majdraganova-Khrusanova, Izv. Khim. Bolg. AN, No. 4 (1976) 668.
25. D. Damyanov, D. Mekhandziev, Izv. Khim. Bolg. AN, No. 9 (1976) 294.
26. T. Suntola, M.J. Antson, "Solid state" Tyypinen Ionisolektivinen Electrod; ja sen Valmistusmenetelma, Finland Patent No. 51742 (1977).
27. J. Geyer-Lippmann, Ph. D. Thesis, Free University of Berlin, 1981.
28. B. Horvath, J. Strutz, J. Geyer-Lippmann, E.G. Horvath, Z. Anorg. Allg. Chem., 483 (1981) 181.
29. G. Ohlmann, Izv. Khim. Bolg. AN, No. 13 (1980) 48.
30. T. Suntola, in: Atomic Layer Epitaxy Materials. Science Reports, Holland Amsterdam, Dec. 1989, vol. 4, No. 7(1989) 261.
31. P. Van Der Voort, E.F. Vansant, Ceramic Industries International, (1994) 17.
32. Wei Zhaobin, Xin Qin, Guo Xiexian, Appl. Catal., 63(1990) 305.
33. Kei Inumaru, Toshio Okuhara, Makoto Misono, J. Phys. Chem., 95(1991) 4826.
34. G.V. Lisichkin (ed.), Modified Silicas in Sorption, Catalysis and Chromatorgraphy, Khimia, Moscow, 1986 (in Russian).
35. A.A. Malygin, Chemical Assembling of Materials with Predicted Properties, Student Course of Technological Institue, Leningrad, 1986 (in Russian).
36. Yu. I. Ermakov, A.A. Zakharov, B.N. Kuznetsov, Immobilized Complexes on Oxide Carriers in Catalysis, Nauka, Novosibirsk, 1980 (in Russian).

37. A.I. Lystsov, N.I. Shcherbin, Lakokrasochnye materialy i ikh primenenie, No. 1 (1980) 48.
38. A.N. Volkova, A.A. Malygin, S.I. Koltsov, V.B.Aleskovskii, Zhurn. Obshch. Khimii, 42 (1972) 2373.
39. H.G. Jerschkevitz, K. Wencke, W. Hanke, E. Schreter, React. Kinet. Catal. Lett., 18 (1981) 443.
40. S.D. Dubrovenskii, A.A. Malygin, Zhurn. Obshch. Khimii, 64 (1994) 177.
41. A.A. Malygin, in: Controllable Synthesis of Solids, vol.2, V.B. Aleskovskii (ed.), Leningrad, 1987 (in Russian).
42. A.A. Malkov, S.A. Sosnov, A.A. Malygin,in: Controllable Synthesis of Solids, vol.3, V.B. Aleskovskii (ed.), St. Petersburg, 1993, p.10 (in Russian).
43. A.A. Malkov, L.I. Petrova, A.A. Malygin, Zhurn. Prikl. Khimii, 64 (1991) 763.
44. S.A. Sosnov, A.A. Malygin, Zhurn. Prikl. Khimii, 61 (1988) 29.
45. S.V. Yakovlev, A.A. Malygin, S.I. Koltsov, Izv. VUZ'ov. Khimiya i Khimicheskaya Tekhnologia, No. 22 (1979) 1343.
46. A.A. Malygin, V.F. Dergachev, S.I. Koltsov, Zhurn. Prikl. Khimii, 59 (1986) 430.
47. A.A. Malygin, Yu.K. Ezhovskii, in: Apparatus of Chemical Assembling Process, Technological Institute, Leningrad, 1987, p.58 (in Russian).
48. V.F. Dergachev, A.A. Malygin, Zhurn. Prikl. Khimii, 61 (1988) 1231.
49. A.A. Malygin, S.I. Koltsov, A.N. Volkova, V.B. Aleskovskii, Izv. VUZ'ov. Neorganicheskie materialy, No. 8 (1974) 1518.
50. A.A. Malygin, S.I. Koltsov, A.N. Volkova, V.B. Aleskovskii, Kinetika i Kataliz, 16 (1975) 1023.
51. A.A. Malygin, S.I. Koltsov, in: Controllable Synthesis of Solids, vol.1, V.B. Aleskovskii (ed.), Leningrad, 1983 (in Russian).
52. A.A. Chuiko, Teoret. i Eksperim. Khimiya, 23 (1987) 597.
53. V.I. Lygin, I.A. Lygina, Zhurn. Fiz. Khimii, 59 (1985) 1180.
54. H.L. Krauss, D.Z. Naumann, Z. Anorg. Allg. Chem., 430 (1977) 23.
55. V.V. Strelko, Adsorbtsiya i Adsorbenty, No. 2 (1974) 65.
56. Yu.I. Gorlov, V.G. Golovatyi, M.M. Konoplya, A.A. Chuiko, Teoret. i Eksperim. Khimiya, 16 (1980) 202.
57. V.A. Radtsig, V.A. Khalif, Kinetika i Kataliz, 20 (1979) 705.
58. J.B. Kinney, R.H. Staley, J. Phys. Chem., 87 (1983) 3735.
59. A.A. Chuiko, V.A. Tertykh, K.P. Kazakov, V.V. Pavlov, S.O. Shimanovskii and R.V. Sushko, Adsorbtsiya i Adsorbenty, No. 5 (1980) 39.
60. D. Damyanov, M. Velikova, Iv. Ivanov, L. Vlaev, J. Non–Cryst. Solids, 105 (1988) 107.
61. A.N. Tikhonov, A.V. Goncharskii, V.V. Stepanov and A.G. Yagola (eds.), Regularizing Algorithms and a Priori Information, Nauka, Moscow, 1983 (in Russian).
62. S.I. Koltsov, A.V. Evdokimov, A.A. Malygin, Zhurn. Obshch. Khimii, 55 (1985) 983.
63. S.I. Koltsov, A.V. Evdokimov, A.A. Malygin, Zhurn. Prikl. Khimii, 58 (1985) 2358.
64. S.I. Koltsov, A.V. Evdokimov, A.A. Malygin, Zhurn. Prikl. Khimii, 59 (1986) 650.
65. S.I. Koltsov, A.V. Evdokimov, A.A. Malygin, Zhurn. Prikl. Khimii, 60 (1987) 749.
66. S.I. Koltsov, A.V. Evdokimov, A.A. Malygin, Method of Synthesis of Water Vapour Sorbent, USSR Patent No. 1219132 (1986).

67. S.I. Koltsov, A.V. Evdokimov, A.A. Malygin, Zhurn. Obshch. Khimii, 57 (1987) 2191.
68. O.V. Osipenkova, A.A. Malkov, A.A. Malygin, Zhurn. Obshch. Khimii, 64 (1994) 549.
69. V.B. Aleskovskii (ed.) Controllable Synthesis of Solids, vol.1, Leningrad, 1983 (in Russian).
70. V.B. Aleskovskii (ed.) Controllable Synthesis of Solids, vol.2, Leningrad, 1987 (in Russian).
71. N.A. Stepanova, V.D. Kupriyanov, A.A. Malygin, Izv. VUZ'ov. Neorganicheskie materialy, No. 3(1987) 1518.
72. A.A. Malkov, E.A. Sosnov, V.I. Zaporozets, A.A. Malygin, Zhurn. Prikl. Khimii, 62 (1989) 1467.
73. N.A. Stepanova, V.D. Kupriyanov, A.A. Malygin, Zhurn. Prikl. Khimii, 63 (1990) 1157.
74. A.A. Malygin, S.V. Kucherov, V.F. Dergachev, I.O. Protodyakonov, Yu.P. Yulenets, Khimicheskaya promyshlennost, No. 7 (1987) 428.
75. V.B. Aleskovskii, Course of Chemistry of Supramolecular Compounds, Leningrad State University, 1990 (in Russian).
76. Yu.I. Ermakov, V.A. Zakharov, B.N. Kuznetsov, Immobilized Complexes on Oxide Carriers in Catalysis, Nauka, Novosibirsk, USSR, 1980.
77. G. Ohlmann, Z. Chem., 24(1984) 161.
78. A.Yu.Polyakov, A.M. Samarin, Uspekhi Khimii, 19 (1960) 565.
79. N.A. Stepanova, E.Yu. Popova, A.A. Malygin, V.B.Aleskovskii, USSR Patent No. 1420012 (1989).
80. A.M. Postnova, N.A. Stepanova, A.A. Malkov, A.A. Malygin, Izv. VUZ'ov. Khimiya i Khim. Tekhnologiya, 31 (1988) 94.
81. N.V. Dolgushev, V.V. Gusarov, A.A. Malkov, Zhurn. Prikl. Khimii., 65 (1992) 1117.
82. V.V. Gusarov, A.A. Malkov, A.A. Malygin, E.V. Polyakova, L.I. Petrova, S.A. Suvorov, Zhurn. Prikl. Khimii, 66 (1993) 1234.

A. Dąbrowski and V.A. Tertykh (Editors)
Adsorption on New and Modified Inorganic Sorbents
Studies in Surface Science and Catalysis, Vol. 99

Chapter 1.9
Kinetics of organic compounds chemisorption from the gas phase on oxides surface

V. I. Bogillo

Institute of Surface Chemistry of National Academy of Sciences, 252022 Kiev, Ukraine

1. INTRODUCTION

Organic compounds chemisorption on Si, Al, Ti, Zr and other element oxides surface is a decisive stage in oxide modification and various catalytic processes proceeding on the surface of these solids [1–4]. Modification of the parent and mixed oxides surface by organic compounds is widely used in preparation of chromatographic supports [5–7], substrates for making chiral reagents for enantiometric separations [8], molecular recognition [9], extraction/detection of metal ions [10], dispersed fillers of polymer materials [5,11], immobilization of biomolecules such as enzymes [12], DNA [13] and antibodies [14], thickeners of dispersive media [1] and modified electrodes [15]. To select appropriate conditions of synthesis of modified oxides, it is essential to know the kinetic parameters of the processes involved and the laws governing the effects of preliminary thermal treatment of materials, structure of gaseous reactants and oxides on these parameters. From the kinetic study there may be determined the optimal parameters for modified oxide synthesis; that is reaction time, temperature of reaction and surface pretreatment, pressure of gaseous reactant as well as established the most optimal structure of reactant and catalytic additives for this process.

Problems of justification for correct kinetic model, limiting stage and reaction mechanism often arise in the investigation of organic compounds interaction with active sites of the solid surface. Such conclusions can be deduced from a kinetic study for series of related reactants with the solid surface and from well-known relations and postulates of physical organic chemistry [16–21]. However, the surface properties of the oxides are generally not identical to those of the bulk solid structure. The Brönsted and Lewis acid–base sites are the main types of active sites on SiO_2, TiO_2, Al_2O_3 and other parent and mixed oxides surface in different chemisorption and catalytic transformations of organic compounds. The properties of such acid–base sites strongly depend on their geometry and will generally display a distribution of the surface on the reactivity parameters. Furthermore, the induced surface heterogeneity may result from the lateral interaction between chemisorbed species at high surface coverage or due to the reconstruction of the surface during chemisorption. Same difficulties emerge when the application of physical organic chemistry methods to study of the reaction mechanism with active sites of the heterogeneous oxides surface is considered. The central problem concerns difficulties of description of reaction

kinetics using models of homogeneous surface. Kinetic models of such reactions should account for the effects of chemical and structural heterogeneities of the oxide surface.

So far, kinetics of various chemisorption reactions, mainly organosilicon compounds on the Si, Ti and Al oxide surface has been investigated. Kinetics of organic compounds reactions with hydroxyl groups of silica surface is one of the best investigated of these oxides [4,22]. Chemical properties of high surface area silica are now fairly well understood from adsorption, infrared, XPS and NMR studies [1,2,4,6,22]. Kinetic studies in the area were initiated by Evans and White [23] as well as by Hair and Hertl [24,25] over 25 years ago and are being continued by other investigators [4,22,26,27]. Most examples of organic compounds chemisorption on the oxide surface considered in the present review are given also for the above systems. At the same time, considerable advances have been made in the theory of elementary reaction kinetics on the solid, especially, on single crystal surface [28–32]. This is caused by development of new spectral techniques for the surface analysis as well as by a wide use of powerful computers for simulation of surface processes by Monte Carlo and molecular dynamics methods [33] and for solution of forward and opposite problems of reaction kinetics on the heterogeneous surface using modern numerical methods. As the review devoted to description of the organic compound chemisorption using well justified models is lacking in the literature, comparison of organic species or oxides surface active sites reactivity and following progress in the field of surface chemical modification is not possible. Most discussed studies are concerned with reaction kinetics from the gaseous phase on the oxides surface. However, some regularities presented in the review are likely to be true for chemisorption from the liquid phase, especially, from nonpolar or slightly polar media on the oxides surface.

A main purpose of proposed models and solutions presented in the review is to provide feasibility to describe the chemisorption kinetics in a wide range of experimental conditions and to determine the optimal conditions and structure of reactants for the oxides surface modification.

2. TYPES OF REACTION SITES ON THE OXIDES SURFACE

Understanding the mechanism of organic compounds chemisorption on a molecular scale means defining the active sites of oxides surface and the elementary steps of the overall process. Depending on the structure of initial reactants, preparation method and temperature of metal oxides pretreatment, different types of active sites may exist on their surface. Mainly, there are Brönsted and Lewis acid–base sites. Metal oxide surfaces have a surface density of about 4–5 hydroxyl groups/nm^2. These can be grouped into sets of surface hydroxyl groups with varying acidities [34–36]. For example, on the surface of silica, such Brönsted acid sites may be represented by single, vicinal and geminal OH groups [37–39]. Thermal and chemical treatment of the silica alter the degree of clustering of the silanol functionality present on the surface [1,40]. When silica surfaces are dehydroxylated in vacuum above 650°C, highly reactive surface sites, as edge–shared tetrahedral dimers, are created [41]. The highly strained Si–O–Si bonds in the dimers are destroyed "instantaneously" via dissociative chemisorption reactions [42–44]. For the formed defects, the strained silicon site is a Lewis acid since it possesses an unoccupied d–orbital which is available as an electron acceptor. The lone pair of electrons on the

bridging oxygen can function as a Lewis or Brönsted base (electron-donor).

It is known that several types of hydroxyl sites are present on the surface of γ-alumina [3,45]. Pretreatment or heating alumina at high temperatures leads to dehydroxylation of the surface hydroxyl groups and the formation of Lewis acid sites on the surface. During dehydration at high pretreatment temperatures (> 300°C), OH groups which have low acidity combine with hydrogen atoms from the neighbouring sites with stronger acidity, forming water molecules. This process creates an anion vacancy (Lewis acid site) which exposes coordinatively unsaturated aluminum cations and a cation vacancy,i.e., coordinative by unsaturated oxygen. The single and bridged OH groups are identified on the pyrogenic titania surface, except that the Lewis sites of the hydroxylated surface are capable to charge-transfer interaction with specific functional groups of adsorbed molecules [46]. Also, at lower temperatures of oxides surface pretreatment, the reactivity of active sites is influenced by the physically adsorbed water [4,22].

3. MECHANISMS OF ORGANIC COMPOUND REACTIONS WITH OXIDES SURFACE SITES

3.1. Reactions with hydroxyl groups

Since hydroxyl groups and element-oxygen bonds are key active sites on the Si, Ti and Al oxides surface at moderate temperature of a surface pretreatment [1-4,6,22], the most organic compounds interact with these sites during chemisorption according to the following mechanisms.

3.1.1. Electrophilic substitution of hydrogen (S_Ei)

Scheme of electrophilic substitution mechanism of surface OH group proton by organic residue at interaction of the organic compound RX with a single group of oxide (M^{n+}-OH) can be presented as follows [47-49]:

$$M^{n+}\text{-OH} + RX \rightleftharpoons M^{n+}\text{-O}:\overset{\overset{H}{\cdot\cdot}}{\underset{\underset{R}{\cdot\cdot}}{}}:X \rightleftharpoons M^{n+}\text{-OR} + HX \qquad (1)$$

Diborane (B_2H_6), organosilanes, organosiloxanes, Si, Ti, Al, B and P halogenides, organometallics and other chemical compounds possessing high electron-acceptor properties and low donor ability interact in accordance with the above mechanism [4,22,47-49]. Hence, one molecule from the gas phase interacts with one hydroxyl group and its kinetics is simply first order. In case of bi- and trifunctional compounds,e.g. $(CH_3)_2SiCl_2$, CH_3SiCl_3, $SiCl_4$, $AlCl_3$, $TiCl_4$, BCl_3, etc. interaction with the paired hydroxyl groups of oxides surface (geminal or vicinal) the next step of the transformation is reaction of surface product with the second OH group

$$\underset{R_1}{\begin{matrix}OH\ldots OH\\ |\quad\ |\\ M^{n+}\text{-O-}M^{n+}\end{matrix}} + \underset{R_2}{RX_2} \xrightarrow[HX]{k_1} \underset{P_1}{\begin{matrix}OH\ldots ORX\\ |\quad\ |\\ M^{n+}\text{-O-}M^{n+}\end{matrix}} \xrightarrow[HX]{k_2} \underset{P_2}{\begin{matrix}O\text{—}R\text{—}O\\ |\quad\ |\\ M^{n+}\text{-O-}M^{n+}\end{matrix}} \qquad (2)$$

This reaction has a stoichiometric coefficient equal to 2 with respect to the surface OH groups. It must be emphasized that different reaction order cannot be equated to a stoichiometric coefficient but must be obtained from the kinetics data. For example, for the above reaction we can write the equation for a loss of surface OH groups

$$d[OH]/dt = -k_1[OH] - k_2[OH]^2 \tag{3}$$

After integration of Eq. (3) we get:

$$\ln\left\{\frac{[OH]_0(k_1 + k_2[OH])}{[OH](k_1 + k_2[OH]_0)}\right\} = k_1 \cdot t \tag{4}$$

where k_1 and k_2 are the rate constants of the steps and t is the reaction time. Also, approximate solution of Eq. (3) may be obtained by putting $\varphi = [OH]_0/[OH]$ and its expanding into a power series [50]

$$[OH]_0 = (\varphi - 1)/k_2 t - \varphi k_1/k_2 \tag{5}$$

Apparent order of the above process consisting of the mixed first- and second-order reactions lies between 1 and 2 and it is a function of the first- and second-order transformations (k_1 and k_2). At a simultaneous RX_2 interaction with the paired OH groups ($k_2 \gg k_1$) we have simple second-order reaction kinetics

$$[OH] = [OH]_0 (1 + 2k_1 t[OH]_0)^{-1} \tag{6}$$

The consecutive reaction of RX_2 with the paired hydroxyl groups is a more probable process than its simultaneous interaction. When $[R_2] \gg [R_1]$, and $k_2 \approx k_1$, kinetics of P_2 formation is first-order and solution of differential equations set may be written as:

$$[P_2] = [R_1]_0 \left\{1 - (k_2 - k_1)^{-1} [k_2 \exp(-k_1 t) - k_1 \exp(-k_2 t)]\right\} \tag{7}$$

where $[R_1]$ is the initial concentration of the paired groups on the surface.

3.1.2. Nucleophilic substitution of hydrogen (S_Ni)

$$M^{n+}{-}OH + RX \rightleftharpoons M^{n+}{-}O : \underset{\underset{R}{|}}{\overset{H}{\overset{|}{\ddot{}}}} : X \rightleftharpoons M^{n+}{-}R + HX \tag{8}$$

This mechanism is more probable for the interaction of organic compounds possessing high electron-donor ability, i.e. alcohols, amines, water, hydrogen halides, diazomethane, etc. [4,22,51-54]. Also, at alkoxysilane chemisorption by the S_Ei mechanism with alcohol formation, the following step of transformation includes its interaction with the surface OH groups by the S_Ni mechanism

$$M^{n+}OH + RX \xrightarrow{k_1} M^{n+}OR + HX \tag{9a}$$

$$HX + M^{n+}OH \xrightarrow{k_2} M^{n+}X + H_2O \tag{9b}$$

The differential equations set describing reaction kinetics may be written at $[RX]_0 \gg [OH]_0$

$$d[OH]/dt = -k_1'[OH] - k_2[OH][XH] \tag{10a}$$

$$d[RX]/dt = k_1'[OH] - k_2[OH][XH] \tag{10b}$$

where $k_1' = k_1[RX]$.

The solution of this set can be obtained only for k_1'/k_2 ratio [55]. It equals the stationary concentration of XH. From this solution it follows that XH concentration does not decrease to zero when OH groups are completely consumed and it reaches a limiting value $[OH] = k_1'/k_2$.

The most effective way of oxides surface modification by organosilicon compounds is their reaction in the presence of minor concentrations of the third component. Ternary and secondary aliphatic amines, ammonia, heterocyclic nitrogen-containing compounds (pyridine, morpholine, etc.), water and other compounds possessing high electron-donor ability are effective catalysts of organosilanes and organosiloxanes reaction with the silica surface OH groups [1,4,5,6,22,56 and references therein]. Formation of a hydrogen-bonded complex between the surface OH group and catalyst molecule leads to the increase of electron donor ability of oxygen atom of this group and to enhancement of its reactivity in the S_Ei process. Another function of the catalysts possessing free hydrogen atoms, i.e. primary and secondary amines is assistance for removal of OH group proton by departing the alkoxy group. For example, catalytic efficiency in chemisorption of trimethoxymethylsilane on hydroxylated or dehydroxylated non-porous silica (Cab-O-Sil) surface decreases in the following series: ethylamine > diethylamine > ammonia > triethylamine > pyridine [56].

Let us consider kinetic scheme of such a transformation. A catalyst molecule (C) forms a hydrogen-bonded complex with the surface OH group (OH_s) in the first step

$$OH_s + C \underset{k_-}{\overset{k_+}{\rightleftharpoons}} OH_s \cdots C \tag{11a}$$

with the equilibrium constant $K = k_+/k_- = [OH_s \cdots C]/([OH_s][C])$. The compound RX (at $[RX]_0 \gg [OH_s]_0$) reacts with this complex and free OH groups

$$RX + OH_s \cdots C \xrightarrow{k_1} RO_s + HX + C \tag{11b}$$

$$RX + OH_s \xrightarrow{k_2} RO_s + HX \tag{11c}$$

Initial rates of RO_s formation and OH_s disappearance are described by following equations:

$$(d[RO_s]/dt)_{t\to 0} = \frac{(k_2' + k_1'K)[OH_s]_0}{(1+K)} \tag{12a}$$

$$(d[OH_s]/dt)_{t\to 0} = -\frac{k_2'[OH_s]_0}{(1+K)} \tag{12b}$$

where $k_1' = k_1[RX]_0$, $k_2' = k_2[RX]_0$ and $[RX]_0$ is the RX initial concentration. At $K \ll 1$ and $k_1' \gg k_2$ the kinetics is presented by the third-order equation with an apparent rate constant $k_{app} = k_1K[C]_0$.

3.2. Reactions with Lewis acid–base sites

3.2.1. Electrophilic or nucleophilic addition to Lewis sites

In accordance with donor–acceptor properties of organic compound, it interacts with the element–oxygen bond of oxide surface with an attack toward the Lewis base site (oxygen atom)

$$RX + M^{n+}O^{2-} \longrightarrow RX\cdots O^{2-}M^{n+} \tag{13}$$

or toward Lewis acid site (coordinative unsaturated metal ion)

$$RX + M^{n+}O^{2-} \longrightarrow RX\cdots M^{n+}O^{2-} \tag{14}$$

These reactions are often accompanied by dissociation of metal–oxygen bond (A_di process). For example, the element–oxygen bond (e.g., siloxane bond in silica) is cleaved readily by nucleophilic or electrophilic reactants

$$(M^{n+})_2O + R{-}X \longrightarrow M^{n+}{-}OR + M^{n+}{-}X \tag{15}$$

When X = H, a new Brönsted surface site is formed in the last step

$$RH + M^{n+}O^{2-} \longrightarrow RH\cdots O^{2-}M^{n+} \longrightarrow R{-}M^{n+}OH^{-} \tag{16}$$

The best known example for creating the site is hydratation of the oxide surface.

Reactions of organosilicon compounds with active sites of silica surface proceed via S_Ei mechanism [4,57]. Nevertheless, it has been established that, apart from the occurrence of chemisorption by the S_Ei mechanism, dissociation of silica surface siloxane bonds occurs by the A_di mechanism at interaction of such compounds, as $(CH_3)_3SiX$ (X = N_3, NCS and NCO) [58–61]

$$(CH_3)_3SiX + {-}SiOSi{-} \longrightarrow (CH_3)_3SiOSi{-} + {-}SiX \tag{17}$$

Kinetics of both reactions was observed by IR spectroscopy and gravimetry [57–61]. From scheme 1 it follows that kinetics measured by a decrease in intensity of stretching vibration band of the surface OH group on the reaction time corresponds to the S_Ei mechanism [2]. Dissociative addition (Scheme 17) can be defined by kinetics derived from measurements of the increasing intensity of stretching vibration band of surface SiX group [58–61]. Kinetic data derived from the increase in the intensity of valence vibration band of surface $Si(CH_3)_3$ group or from the gravimetric measurements (increasing of solid samples mass on the time) display the formation of a product by two parallel reactions and they can be described as:

$$\frac{d[Me]_t}{dt[Me]_{max}} = k_1' \frac{[OH]_0}{[Me]_{max}} \exp(-k_1't) + k' \frac{[{-}SiOSi{-}]_0}{2[Me]_{max}} \exp(-k_2't) \tag{18}$$

where $[Me]_t$ is the surface concentration of the chemisorbed $(CH_3)_3Si$ groups at instant time, while $[Me]_{max}$ is that observed on completion of the reaction, $[OH]_0$ and $[-SiOSi-]_0$ are the concentrations of the OH groups and the reactive siloxane bonds on the surface at $t = 0$, $[Me]_{max} = [OH]_0 + [-SiOSi-]_0$, $k_1' = k_1[RX]$, $k_2' = k_2[RX]$; k_1 and k_2 are the rate constants of reactions occurring by the S_Ei and A_di mechanisms, respectively and [RX] is the concentration of organosilicon compound in the gas phase.

It is clear that with a main chemisorption route proceeding through the S_Ei mechanism (i.e. at $k_1 \gg k_2$), kinetics of the process derived from the change in concentrations of the surface OH and $(CH_3)_3Si$ groups should match. At $k_2 \gg k_1$, kinetics derived from the increase in the $(CH_3)_3Si$ groups concentration with smaller t values will approximate to that of the increasing concentration of SiX surface group, characteristic for the A_di mechanism.

A more complex scheme of chemisorption including S_Ei and A_di mechanisms was considered by Mertens and Fripiat [62] for the silica gel methoxylation

$$Si-O-Si + CH_3OH \underset{k_{-1}}{\overset{k_1}{\rightleftharpoons}} Si-OCH_3 + SiOH \tag{19a}$$

$$Si-OH + CH_3OH \underset{k_{-2}}{\overset{k_2}{\rightleftharpoons}} Si-OCH_3 + H_2O \tag{19b}$$

$$Si-O-Si + H_2O \underset{k_{-3}}{\overset{k_3}{\rightleftharpoons}} 2Si-OH \tag{19c}$$

Kinetic parameters of the surface esterification were determined from the analysis of surface OH groups and chemisorbed methoxy species concentrations during the reaction assuming that $k_{-1} = k_3 = 0$: $E_1^{\neq} - E_2^{\neq} = 27.5$ kJ · mole^{-1}; $k_1/k_2 = 0.33$ at 150°C and 0.64 at 190°C; $k_{-3} = 1.3 \cdot 10^{-4}$ g · mole^{-1} · hour^{-1} at 150°C and $1.6 \cdot 10^{-4}$ g · mole^{-1} · hour^{-1} at 190°C. Thus, cleavage of the siloxane bridge is a less likely reaction than S_Ni reaction of alcohol with the surface OH groups. It should be noted that very low activation energy for silica surface dehydroxylation ($E_3^{\neq} = 8.4$ kJ · mole^{-1}) has been calculated from the temperature dependence of k_3. This value is in contradiction with a high temperature of such a process beginning (> 400°C [63]). This may be due to high errors in determination of the rate constants.

3.2.2. Redox reactions with Lewis sites

Such reactions are possible at interaction of transition metal oxide surface in the redox reactant/surface site pairs possessing low electron transfer free energy and lead to formation of radical-ions from the reactant molecules [64]

$$RX + M^{n+}O^{2-} \longrightarrow RX^{\bullet -} + O^{2-}M^{(n+)-1} \tag{20}$$

$$RX + M^{n+}O^{2-} \longrightarrow RX^{\bullet +} + M^{(n+)+1}O^{2-} \tag{21}$$

Following stages of the transformation are dissociation of the radical-ions and recombination of reaction product (anion from radical-anion, or proton from radical-cation) with surface sites. These reactions may be first steps in catalytic transformations of organic compounds with participation of the oxygen atom of oxides lattice.

Also, elimination reactions (mostly, free radical elimination E_R) are widespread in thermal decomposition of organic residue on the modified oxides surface. Degradation of organosilicon cover of modified silica surface at high temperatures presents an example of such transformation [65].

Majority of studies concerning organic compounds chemisorption kinetics on oxides surface are performed for the reaction mechanisms described by Schemes 1, 8 or 15 and mainly, for the first mechanism of organosilicon compounds interaction with OH groups of non-porous silica surface.

4. MAIN STAGES OF CHEMISORPTION ON THE OXIDES SURFACE

Models of homogeneous kinetics, Eqs. (3–7, 10, 12, 18, 19), describe badly the experimental kinetics of organic compounds chemisorption on the several oxides surface in the whole range of reactant concentrations, surface coverage at different temperatures. It may be connected with parallel chemical reactions on different mechanisms as well as with change of rate limiting stage at variations in the experimental conditions. Usually one of such stages is much slower than the others and it mainly determines the overall reaction rate. The chemisorption process can include the following stages.

4.1. External and internal pore diffusion

This process may be a rate limiting stage at high concentration of reactant in the gas phase. Its influence on the adsorption kinetics has been considered in detail by Unger [6] and Jaroniec and Madey [29]. The following simultaneous diffusion-adsorption model may be applied to the experimental kinetic data in order to derive effective diffusion coefficients [66]:

$$\frac{\partial C}{\partial t} = \frac{1}{r^2}\left\{\frac{\partial}{\partial r}\left[r^2 D\left(\frac{\partial C}{\partial r}\right)\right]\right\} - \frac{\partial a}{\partial t} \tag{22a}$$

where C and a are the adsorbate concentration in the gas phase and on the adsorbent surface, respectively, r is the equivalent radius of spherical adsorbent particles and D is the diffusion coefficient. This nonlinear partial differential equation is a modified version of Fick's second law of diffusion, which includes a nonlinear sorption term, and it can be solved using appropriate boundary conditions and assumptions [67–69]. The corresponding solution has the general form

$$C/C_0 = \exp(-Dt/r^2) \tag{22b}$$

where C_0 is the initial adsorbate concentration. At interaction with non-porous or macroporous oxides, chemisorption kinetics is determined mainly by external diffusion and chemical reaction. This diffusion stage is fast enough so that its influence on the chemisorption rate may be neglected. For example, Knudsen diffusion flow may be observed in

the volume of non-porous silica (Aerosil 300 with a radius of secondary pores 20 Å) at the reactant pressure higher than 1880 torr.

The diffusion coefficient in the solid layer of thickness l is connected with time ($t_{1/2}$) required to observe a half of bulk concentration of the surface product $p_t = 0.5p_\infty$ by Crank's equation

$$D = 0.049\ l^2 t_{1/2}^{-1} \tag{23}$$

Conclusions about a rate limiting stage of methanol chemisorption on the microporous Xerogel were performed by Mertens and Fripiat [62] from the comparison of a self-diffusion coefficient of physically adsorbed methanol ($D = 1.5 \cdot 10^{-6}$ cm$^2 \cdot$ s^{-1} at 25°C or $1.5 \cdot 10^{-5}$ cm$^2 \cdot$ s^{-1} at 150°C) with a range of its reaction rate constants on the Aerogel determined from the infrared data ($5 \cdot 10^{-11} < D < 4 \cdot 10^{10}$ cm$^2 \cdot$ s^{-1}). Hence, the second value is five orders of magnitude lower than the first one and reaction rate is not limited by diffusion.

4.2. Adsorption of reactant and formation of intrinsic precursors

Adsorption of reactant from the gas phase on the surface and formation of intrinsic or extrinsic precursors is a following stage of chemisorption. Precursor state models are built based on the notion that before chemisorbing, a molecule becomes trapped temporarily in a weakly bound, mobile, molecular state, which arises due to a long range physisorption interaction. Every chemisorption involves a passage through a precursor state, since all molecules have a long range attraction, and molecules will pass through a region where this interaction is effective on their way to the surface. As mentioned above, kinetics of organic compound reactions with the hydroxyl groups of silica surface occurs through two (S_Ei and S_Ni) main mechanisms. Formation of precursors (linear hydrogen-bonded or cyclic donor-acceptor complexes between organic molecules and surface groups) have been proposed in the first stage of these reactions [4,22,47–49,51–54]. Overall activation energy, rate and selectivity of surface reactions strongly depend on the precursor stability. These effects as well as relationships between electronic, structural properties of organic reactants and Brönsted, Lewis acid-base sites of oxides surface and heats of the complex formation as well as reaction activation energies are studied in [47–49,70].

4.2.1. Hydrogen-bonded complexes

Quantum chemical computations of potential energies surface sections along the reaction pathway (PEES) for interaction of typical electrophiles (halogensilanes H_3SiX (X = F, Cl, Br, I), trimethylchlorosilane [48,49], acetyl chloride [51]) and nucleophiles (hydrogen halides HX (X = F, Cl, Br, I), water, aliphatic amines, aliphatic alcohols [52], amino acids [53] and substituted phenols [54]) with the silica OH group in a cluster approach using semiempirical AM1, NDDO, MNDO and MNDO/H methods were performed. Representative PEES is shown in Fig.1.

The first minimum on the potential curve conforms to formation of linear hydrogen-bonded complex between the surface OH group and most electron donor atoms of organic molecule in the absence of steric restrictions. From the calculated heats of such complex formation (Q) with OH groups of parent and mixed Si, Ti and Al oxides surface clusters (by MNDO/H and NDDO methods [49]) it follows that steric restrictions have some influence on the stability of H complexes in case of H_3SiCl ($Q = 7.7$ kJ $\cdot$ mole^{-1}) and

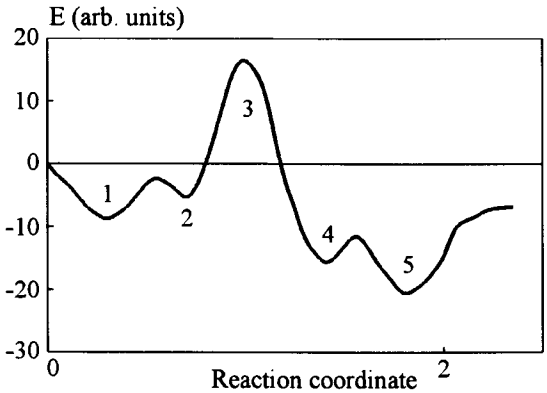

Figure 1. Potential energies surface sections along the reaction pathway for substitution of hydroxyl group on oxide surface by organic residue. Figure taken from [49].
(1)–linear H–complex between reactants; (2)–cyclic donor–acceptor complex between reactants; (3)–transition state; (4)–cyclic donor–acceptor complex between reaction products; (5)–linear H–complex between reaction products.

$(CH_3)_3SiCl$ ($Q = 5.8$ kJ · mole^{-1}) interaction with the silica OH group. Heat of H complex formation between NH_3 molecule and OH group increases at transition from single Si–OH to bridged Si–OH–Al and Ti–OH–Ti groups on the oxides surface. Also quantum chemical computations of bond dissociation energies of the element–OH groups, charges on the O and H atoms of OH group and O–H distances for several oxides clusters were carried out in [49]. Apparently, useful characteristics which determined proton donor ability of the surface OH group to form hydrogen bond with electron donor molecules will be deprotonation energy and charge on the H atom. It was established that deprotonation energy decreases and charge on the H atom increases in the series of single and bridged OH groups of Si, Ti and Al oxides [49].

Quantum chemical computations of H complexes heats formation in case of interaction of large organic molecules lead to high errors. A more perspective way is the use of well known relations of physical organic chemistry for this purpose. These equations allow to predict the heats of hydrogen-bonded or donor–acceptor complexes formation on the basis of donor (base) and acceptor (acid) empirical parameters. There are Drago and Weyland's equation [71]

$$Q = E_A E_B + C_A C_B \tag{24}$$

or the linear expression between Q value and Gutman parameters for organic solvents [72]

$$Q = DN_B AN_A \tag{25}$$

where E_A and E_B are the electrostatic and C_A and C_B are the covalent contributions of acid (A) and base (B) in the heat formation; DN and AN are the donor and acceptor numbers of base and acid, respectively. For instance, Eq. (26) was used for calculation of adsorption heats of organic bases on the surface of dehydrated silica [73]

$$Q = 20.33\ E_B + 1.16\ C_B + 1.41\ P_B + 5.36\ \mu_B \tag{26}$$

where P_B and μ_B are the molar deformation polarization and dipole moment of the base. Also, electrostatic and covalent contributions of sites of silica and silica–alumina mixed adsorbents surface to differential adsorption heats were determined using Eq. 24 [74]. Firstly, the use of Eq. (24) for characterization of polymers or their fillers surface was proposed by Fowkes [75]. Eq. (25) was successfully employed for determination of acid–base parameters of several silica surfaces from correlation of specific interaction contributions to their free surface energy with DN and AN values of test adsorbates [76]. However, the acid–base parameters of Eqs. (24) and (25) are not known for most typical organic reactants used for modification of oxides surface.

Linear relationships between quantum chemical indexes (maximum negative (q^-_{max}) and positive (q^+_{max}) charges) as well as energies of highest occupied molecular orbital ($E_{HOMO} = -IP$, where IP is the vertical ionization potential) and lowest unoccupied molecular orbital (E_{LUMO}) and the empirical donor–acceptor parameters of organic molecules were established in [49]. Parameters of the relationships are presented in Table 1.

Table 1
Parameters of linear equations Y = A X + B connecting empirical donor– acceptor parameters of organic molecules (Y) (Eqs. 24 and 25) with their quantum chemical indexes (X) from [49]

Empirical donor–acceptor parameter	Quantum chemical index	A	B	Mean square deviation	Number of compounds
C_B	E_{HOMO}	2.30	29.90	103.40	14
C_A	E_{LUMO}	- 8.90	0.80	4.90	18
E_B	q^-_{max}	0.71	0.80	0.91	14
E_A	q^+_{max}	8.20	2.40	77.90	18
DN	q^-_{max}	90.80	4.10	17.40	8

Hence, from these data one would expect the linear relationships between the quantum chemical indexes and heats of H complexes formation. However, thermodynamic functions of such complexes are absent for most organic reactants. As observed by IR spectroscopy method, the formation of H complexes between adsorbed compounds and oxides surface OH group at low temperatures is attended by a shift of valence vibration band of these groups in the direction of low frequencies ($\Delta\nu_{OH}$), to the widening and reduction of its intensity [2,77]. The $\Delta\nu_{OH}$ values for interaction of several organic bases and organosilicon compounds with the silica surface OH groups are presented in [2,77,78]. They are connected with heats of H complexes formation by the following expression [77,78]:

$$Q = 1.255\ (\Delta\nu_{OH} - 40)^{0.5} \tag{27}$$

Following linear dependencies between $\Delta\nu_{OH}$ on the silica surface and q^-_{max} as well as E_{HOMO} of organic compounds have been established [49]: for small organic molecules possessing basic properties

$$\Delta\nu_{OH} = 84.5\ E_{HOMO} + 1268\ q^-_{max} + 1025; \qquad S = 199; \quad n = 7 \tag{28a}$$

and for organosilicon compounds

$$\Delta\nu_{OH} = 92.8\ E_{HOMO} + 1264; \qquad S = 116; \quad n = 19 \qquad (28b)$$

The better correlation of $\Delta\nu_{OH}$ with E_{HOMO} than with q^-_{max} values in case of organosilicon compounds adsorption may be explained by more softness of these compounds in comparison with the small organic bases. The dependencies between $\Delta\nu_{OH}$ and quantum chemical indexes are presented in Fig. 2.

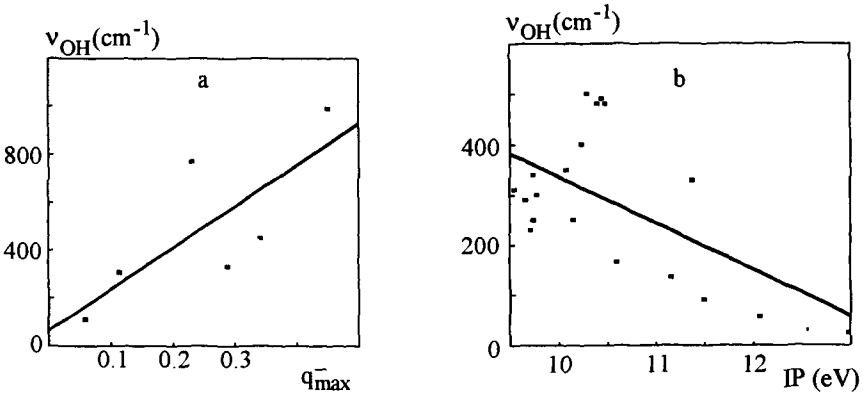

Figure 2. Dependencies of shift of valence vibration band of silica surface hydroxyl groups at adsorption of small organic bases (a) and organosilicon compounds (b) on the maximum negative charge of the bases (a) and on the ionization potential of organosilicon compounds (b).

A simple expression for the observed chemisorption activation energy ($E^{\neq}_{obs}$) with consideration of H complex formation prior to a slow chemical reaction can result from application of the quasi-steady-concentration for H complex medthod:

$$E^{\neq}_{obs} = E^{\neq}_{chem} - (Q + \Delta Q_{nsp}) \qquad (29)$$

where $E^{\neq}_{chem}$ is the activation energy of proton transfer stage and ΔQ_{nsp} is the contribution of nonspecific interaction to the overall adsorption heat. This contribution to the adsorption heat on the dehydrated silica surface can be estimated from its dependence on the molar deformation polarization Eq. (26). In such a manner the adsorption heats of organosilicon compounds on this surface can be calculated on the basis of their E_{HOMO} and P values Eqs. (26, 27, 28b). Using these data and Eq. (29), the activation energies for interaction of wide series of organosilicon compounds with OH groups of silica surface were estimated. These data are presented in Table 2.

It is obvious from this table that the change of structure of the organosilicon compounds can have a more pronounced effect on the activation energy of chemical stage than on the heat of H complex formation. Moreover, steric effects of substituents at Si atom in these compounds have a more dominant role in the chemical interaction than in the complex stability. This is apparent from comparison of the Q_{ads} change at adsorption of alkoxysilanes with the observed chemisorption energies. The $E^{\neq}_{corr}$ increases at enhancement (the absolute value) of a steric constant of the alkoxy substituent at Si atom.

Table 2
Activation parameters of the organosilicon compounds reactions with OH groups on the pyrogenic silica surface ($A^{\neq}$, pre-exponential factor and $E^{\neq}_{obs}$, observed activation energy on "free" surface) [79–81], the estimated heat of adsorption complex formation (Q_{ads}) and activation energy of proton transfer ($E^{\neq}_{corr}$) from [49]

Compound	$A^{\neq}$	$E^{\neq}_{obs}$	Q_{ads}	$E^{\neq}_{corr}$
	($cm^3 \cdot molecule^{-1} \cdot s^{-1}$)		($kJ \cdot mole^{-1}$)	
$(CH_3)_3SiCl$	$2.5 \cdot 10^{-12}$	105	54	159
$(CH_3)_3SiBr$	–	23*	57	80
$(CH_3)_3SiI$	–	20*	60	80
$(CH_3)_2SiCl_2$	$2.7 \cdot 10^{-13}$	76	52	128
CH_3SiCl_3	$1.2 \cdot 10^{-13}$	70	49	119
$SiCl_4$	$2.2 \cdot 10^{-16}$	50	42	92
$(CH_3)_3SiOSi(CH_3)_3$	$2.4 \cdot 10^{-11}$	129	59	188
$(CH_3)_3SiN(CH_3)_2$	$7.8 \cdot 10^{-14}$	43	61	104
$(CH_3)_3SiCN$	$5.0 \cdot 10^{-17}$	29	53	82
$(CH_3)_3SiN_3$	$8.2 \cdot 10^{-14}$	78	61	139
$(CH_3)_3SiNCO$	$1.1 \cdot 10^{-16}$	77	57	134
$(CH_3)_3SiNCS$	$4.7 \cdot 10^{-16}$	32	61	93
$(CH_3)_3SiOCH_3$	–	23*	58	81
$(C_2H_5)_3SiOCH_3$	–	24*	58	82
$(CH_3)_3SiOC_2H_5$	–	60*	58	118
$(CH_3)_3SiOC_3H_7$	–	62*	58	120
$(CH_3)_3SiOC(CH_3)_3$	–	62*	59	121
$(CH_3)_3SiOCH_2C_6H_5$	–	63*	–	–
$(CH_3)_3SiOCOCF_3$	–	13*	–	–
$[(CH_3)_2SiO]_4$	$2.2 \cdot 10^{-16}$	55	61	116
$[(CH_3)_2SiO]_3$	$3.0 \cdot 10^{-16}$	64	62	126
$[(CH_3)(CH_2{=}CH)SiO]_3$	$1.1 \cdot 10^{-17}$	34	61	95

*Activation energy was estimated on the basis of the time for given coverage achievement at certain temperature [80]. Temperature of preliminary preparation of the non-porous silica samples (Aerosil 175 or 300) ranges from 673 to 923 K in vacuum for 2 h.

4.2.2. Donor–acceptor complexes and reaction of proton transfer

Subsequent transformations of the above H complexes are affected by a way of temperature or reactant concentration enhancement as well as by addition of the third donor or acceptor component (catalyst) [4,47,48]. Quantum chemical computations of a section of potential energies surface along the reaction pathway for some S_Ei and S_Ni processes with silica OH group reveal that the linear H-complex with this group formed in the first reaction stage reactions thereafter transform to a cyclic donor–acceptor complex. The second minimum on the potential curve (Fig. 1) is due to formation of a cyclic donor–acceptor complex (DA_R) which is recognized for S_Ei and S_Ni reactions [49].

In case of large organic molecules interaction (for example, with $(CH_3)_2CHOH$ and $(CH_3)_3SiCl$), this minimum often missing from a potential curve and the DA_R complex is consistent with the reaction transition state. The heat of such complexes formation varies from 8 to 40 kJ·mole^{-1}. Relationships between activation energies of these reactions and quantum-chemical indexes of organosilicon compounds were established in [49,82]. Electron donor ability of surface sites and electron acceptor ability of gas reactant play a leading part in the rate of S_Ei reaction, while opposite properties of reactants affect the precursor stability. It increases with enhancement of proton donor ability of the surface OH group (B-acidity) and electron donor ability of the reactant molecule. By contrast to the above mechanism, the height of activation barrier of S_Ni reaction decreases with the increase of electron acceptor ability of Si or metal atom on the surface and with enhancement of electron donor ability of the gas phase reactant. Dependencies of precursors stability on the electronic structure of the gas phase reactant and OH surface group are closely allied for the S_Ni and S_Ei mechanisms. In such a manner the surface sites reactivity in S_Ni reactions will increase with the enhancement of their electron acceptor ability. The latter property (Lewis acidity) may be associated with their proton donor ability (Brönsted acidity) of mixed oxides surface [83].

4.3. Surface diffusion of reactant

This is a rate limiting stage at higher surface coverage in case of fast chemical reactions, due to the lateral interactions between precursor and chemisorbed organic species. Since the mobility of the adsorbed molecules is greatly restricted in the adsorbed state, the energy of adsorption acts as an additional barrier to rotation, vibration, or translation of reactant. Diffusion on the homogeneous and heterogeneous solid surfaces has been widely studied recently [84-88]. From the simulation studies it follows that surface diffusion is strongly affected by adsorptive energy correlations through the induced correlations on activation barriers as well as through the influence of adsorbate cluster morphology. From numerical calculations of diffusion coefficient dependence on the surface coverage taking into consideration the effects of chemical heterogeneity and lateral interactions between the activated complex and adsorbed particle as well as between the adsorbed molecules themselves it follows that this coefficient increases up to a surface coverage equal to 0.5 and decreases below this value in case of chemical heterogeneous surface without lateral interactions, while it decreases at enhancement of surface coverage with attractive interactions between the activated complex and adsorbed particle or repulsive interactions between adsorbed molecules [87]. The diffusion coefficient of methylmetacrylate on the non-porous silica surface increases from $1 \cdot 10^{-6}$ cm^2·s^{-1} to $3 \cdot 10^{-5}$ cm^2·s^{-1} with the change of surface coverage from 0.2 to the whole monolayer [89]. Only at $k > 2.5 \cdot 10^8$ l·mole^{-1}·s^{-1} (a rate constant for the second-order kinetics) the surface diffusion has an essential effect on the chemisorption reaction [89]. A diffusion coefficient of pyrene on the silica surface was determined to be $1.2 \cdot 10^8$ l · mole^{-1} · s^{-1} at room temperature and the apparent diffusion activation energy is 20 kJ · mole^{-1} [90].

A following stage of chemisorption process on the solid surface is a chemical reaction of the reactant immediately from the gas phase (Eley-Rideal mechanism) or between the intrinsic precursor and active sites (Langmuir-Hinshelwood mechanism). Possible mechanisms of these reactions and formal kinetic equations have been discussed previously.

Of course, the Eley–Rideal mechanism is a likely pathway at high reaction temperature, whereas the Langmuir–Hinshelwood mechanism is realized at low temperature, when the precursor concentration remains sufficient. The importance of reactant preadsorption on a given surface can be probed by the use of a Langmuir–Hinshelwood kinetic model [91–93]. With the assumptions for this model the surface coverage (Θ) is related to the initial pressure of reactant (P) and to the apparent adsorption equilibrium constant K:

$$\Theta = KP/(1 + KP) \tag{30}$$

The rate of product (R) formation can be written as:

$$d[R]/dt = kKP/(1 + KP) \tag{31}$$

where k is the apparent chemical reaction rate constant. The linearity of a plot of $(d[R]/dt)^{-1}$ versus $(1/P)$ tests the validity of this model. Subsequent desorption of reaction products may be rate limiting in the following catalytic transformations and thus it will influence on reversibility of overall chemisorption process.

5. MAIN REASONS FOR HETEROGENEITY OF OXIDES SURFACE

A rate constant and activation energy of organic compounds chemisorption on the oxides surface in the most cases depend on the surface coverage. It may be connected with different heterogeneity types of oxide surfaces. The reasons for oxides surface heterogeneity are as follows.

5.1. Geometric heterogeneity

It is connected with the amorphous structure of surface layer of most oxides. The results of numerical simulations of the adsorption equilibria of some gases on the surface of amorphous solids, i.e., hydrogen on amorphous ice [94] and argon on amorphous oxide simulated by a dense random packing of solid balls [95] allow for the conclusion that the distribution function of surface sites on the adsorption energy is a set of smeared peaks unlike narrow peaks characteristic for the surface of single crystals at low surface coverage. It has been shown experimentally [96] that the distribution curve of the pyrogenic silica surface on adsorption energy of n-octane is two smeared peaks in contrast to a narrow peak on the similar curve for the crystalline silica surface. If the chemisorption reaction is proceeded through formation of intrinsic precursor on the surface, then the distribution on adsorption energy may result in the distribution on the chemisorption activation energy. The reactant is in a random reaction field of amorphous surface and it leads to broadening of active sites distribution function on the interaction potential, for instance, Morse potential, and on rate constants. This is possible due to the difference in the M^{n+}–O bond distances and M^{n+}–O–M^{n+} bridge angles of oxide surface layer as well as to clustering of its OH groups in the micropores or in secondary pores. For example, adsorption ability and reactivity of bridged Si–OH–Al groups of alumina–silica surface depends on the Si–O and Al–O bond distances as well as on the Si–OH–Al bridge angle. Quantum chemical calculations [97–100] have evidenced a dependence of the O–H dissociation energy and stretching frequency on both Si–O and Al–O distances and the bridge angle. The reaction kinetics on amorphous surface may be described by integral equation

with a single distribution function on rate constants. Such equations for kinetic isotherms including normal, Gamma, Beta and other distribution functions on rate constants are presented in Section 6.6.

5.2. Chemical heterogeneity

That is the existence of several active site types on oxides surface (various single, geminal, vicinal, bridged OH groups and those placed in different coordination surroundings of metal ions, element–oxygen bonds and also ion, radical Lewis acid and base sites) which has been discussed previously. Quantum chemical computations of deprotonation energies and partial charges on the oxygen atom of OH groups on model surface clusters of SiO_2, TiO_2, Al_2O_3 and mixed oxides of these elements display a considerable range of variation of these parameters which may well cause different reactivity of these groups in the chemisorption processes [22,97–101]. Reaction kinetics on such a surface is described by a model of discrete heterogeneous surface

$$\frac{d\Theta}{dt} = \sum_{i=1}^{l} k_{app(i)} f_i \exp\left(-k_{app(i)} t\right) \tag{32}$$

where l is the number of different sites, f_i and $k_{app(i)} = k_{(i)} P$ are their relative concentration and apparent rate constant of the interaction with i–th site of the surface, and under the following condition

$$\sum_{i=1}^{l} f_i = 1 \tag{33}$$

Already at $l = 2$, this model describes well enough the kinetics of chemisorption of CH_3OH, CH_3NH_2, H_2O and NH_3 on the dehydroxylated silica surface at a constant temperature [26]. The use of Eq. 32 to describe the organosilicon compounds chemisorption kinetics on the silica surface is presented in Section 6.2.

5.3. Lateral interactions between chemisorbed species

The lateral interactions between chemisorbed particles or between these particles and activated complexes should be taken into consideration describing the chemisorption kinetics on the solid surface. This interaction is determined by a distance between neighbouring active sites (r). The account for the lateral interaction is possible on a single crystal surface in quasi- chemical or mean–field approximations [30,32]. Let us write the common expression for chemisorption kinetics on the homogeneneous surface with the account for lateral interactions between chemisorbed particles:

$$d\Theta/dt = f(N_A) k_0 (1 - \Theta)^n F(\Delta E_c, T, \Theta) \tag{34}$$

where $f(N_A)$ is the function of reactant concentration (N_A) in the gas phase, k_0 is the rate constant of the reaction on the "free" surface, e.g., at $\Theta \rightarrow 0$, n is the reaction order with respect to the surface active sites, $F(\Delta E_c, T, \Theta)$ is the function allowing for the change in the configuration contribution into free energy of the activated complex with the Θ varying. With $F = 1$ and $f(N_A) = N_A$, this equation describes well enough the chemisorption on a homogeneous surface in the absence of lateral interactions between

particles while with $F = \exp(-z\omega\Theta/RT)$ it describes the chemisorption with lateral interactions between chemisorbed particles in the mean–field approximation (z is the lattice coordination number and ω is the lateral interaction energy between neighbouring active sites; $\omega > 0$ for repulsive and $\omega < 0$ for attractive interactions). This model postulates the independence of $[(RT)^{-1} \ln F]$ parameter on the reaction temperature and linear increase of apparent activation energy with enhancement of surface coverage in case of repulsive interactions between chemisorbed species. Taking into consideration the lateral interactions on a single crystal surface in a quasi–chemical approximation, the calculations may be performed using the following expressions [102]:

$$F(\Delta E_c, T, \Theta) = \left\{ \frac{1 + ux}{1 - u + u\exp(z\omega/RT)} \right\}^z \tag{35a}$$

$$u = \frac{\delta - 1 + 2\Theta}{\delta + 1} \tag{35b}$$

$$\delta = \left\{ (1 - 2\Theta)^2 + 4\Theta(1 - \Theta)\exp(-z\omega/RT) \right\}^{1/2} \tag{35c}$$

$$x = \exp(-z\omega/RT) - 1 \tag{35d}$$

In contrast to the mean–field approximation, consideration of the lateral interaction in the quasi–chemical approximation takes into account possible correlation effects between localization of the adsorbed particles and predicts the correct diagrams of phase transitions on the surface [32]. This approach predicts the increase of apparent chemisorption activation energy with the growth of surface coverage and S–shaped dependence of the energy on the coverage. The Monte Carlo simulation technique has been used to elucidate the main features of the surface layer evolution during chemisorption of tetrachlorosilane on the hydroxylated silica surface (111 face of β–crystobalite). The S–shaped dependencies of apparent activation energy on the surface coverage, similar to those obtained in the quasi–chemical approximation, have been reached if the lateral interactions between chemisorbed species (repulsive or attractive) interactions are taken into account [103].

Unlike the single crystal surface, characterized by a constant distance between neighbouring active sites (r), on the surface of amorphous oxides there should exist a wide distribution of the active site pairs with respect to the distances between them. As it follows from the results of Monte Carlo simulation of adsorption kinetics of Lennard–Jones gas on the amorphous solid surface represented by a normal distribution of the neighbouring active sites on the distances between them and with the account of repulsive lateral interactions described by the Lennard–Jones potential, apparent chemisorption activation energy depends but insignificantly on Θ at its low value (< 0.5), while over this value the energy increases abruptly [104]. From the Monte–Carlo simulation it follows that the dependence of apparent activation energy on Θ can be approximated as [80]:

$$E_\Theta^{\neq} = E_0^{\neq} + \gamma\Theta^\nu \tag{36}$$

where $\nu > 1$. Approximate analytical solutions of kinetic isotherm equations, including distributions on the chemisorption rate constants and on the distance between neighbouring

sites on an amorphous random and patchwise heterogeneous surface [105] are presented in Section 6.8.

6. KINETIC MODELS USED FOR DESCRIPTION OF CHEMISORPTION ON OXIDES SURFACE

Organic compounds commonly interact with silica and other oxides surface at high temperatures. Ratio of surface site number of the types that undergo reaction (n_t) to the total number of the sites present before (n_0) is the relative surface coverage

$$\Theta = n_t/n_0 \tag{37}$$

Also, the conversion degree may be calculated from the kinetic data determined by the gravimetric method or from the data of elemental analysis during the surface reaction

$$\Theta_c = [p]_t/[p]_\infty \tag{38}$$

where $[p]_t$ and $[p]_\infty$ are the concentrations of chemisorption product at a time t and finally of irreversible reaction at maximum temperature. The latter value is limited by decomposition temperature of the surface compound. Also, it is suggested that the only monomolecular layer of organic groups is formed on the oxides surface. The conversion is limited by the maximum number of active sites that are accessible to the reactant. According to the Unger's definition [6], the surface coverage of silica OH groups can be estimated as

$$\Theta = \alpha_{exp}/\alpha_{max} = (wA_mN_A)/(10^{18}MS_a) \tag{39}$$

where w is the mass of chemisorbed species in grams per gram of solid, M is the molecular mass of this species and S_a is the specific surface area of the initial silica corrected by the weight increase due to modification, A_m is the mean cross-sectional area occupied by one OH group and N_A is the Avagadro's number. An analogous definition may be applied to a relative coverage of other active sites on the oxides surface. In the absence of sterical restrictions for chemical reaction and at high temperature of decomposition of the surface compound, both quantities Θ and Θ_c are coincident to each other.

The following models are used for description of organic compound chemisorption kinetics on oxides surface.

6.1. Homogeneous surface

This model is intended for description of alkylchlorosilanes and alkoxysilanes reaction kinetics with the OH groups of dehydrated non-porous silica surface [106,107]

$$d\Theta/dt = k_{app}(1 - \Theta)^n \tag{40}$$

where k_{app} is the apparent reaction rate constant including the reactant concentration on the surface and n is the reaction order with respect to the number of surface active sites interacting in a rate limiting stage. The fractional order obtained has been related to parallel reactions of chlorosilanes with the single and geminal OH surface groups

[25,106,107]. Infrared studies of kinetics of methylchlorosilanes chemisorption reveal that trimethylchlorosilane follows the first-order kinetics, while 1.5 ± 0.2 order kinetics were established in case of dimethyldichlorosilane and methyltrichlorosilane interactions, suggesting that 50% silane molecules react monofunctionally and 50% difunctionally. This model describes the reaction kinetics within a limited region of the surface coverage, i.e., at Θ from 0.3 to 0.8. A possible reason for the high fractional reaction orders in respect to the surface OH groups obtained by Hertl and Hair for organosilicon compound chemisorption ($n = 1.7$ for trimethylmethoxysilane, $n = 3.0$ for trimethoxysilane, $n = 2.2$ for dimethoxymethylsilane, $n = 2.0$ for hexamethyldisilazane [106,107]) may be chemical and geometric surface heterogeneity. The dependence of reaction order on the temperature provides a useful check on the surface heterogeneity. For example, at chemisorption of cyclic and linear organosiloxanes on the non-porous silica (Aerosil 300) surface [108,109] the reaction order in most cases decreases with enhancement of reaction temperature (Table 3), while the linear dependence in the logarithmic coordinates of integrated solution of Eq. (40) is observed with a high correlation coefficient at the constant temperature. It must be emphasized that rate constants at different temperatures obtained using Eq. (40) are poor parameters of siloxanes reactivity. The best way may be the calculation of these constants using some models of heterogeneous surface.

Table 3
Parameters for Eq. (41) describing the organosiloxanes chemisorption kinetics on non-porous silica surface [108,109]

Compound	Temperature (°C)		Reaction order $(1/\eta)$	ln k_{app}	Correlation coefficient
	Pretreatment	Reaction			
$[(CH_3)_2SiO]_3$	700	350	4.2	− 1.55	0.992
	–	410	2.6	− 2.50	0.999
	–	450	1.3	− 2.51	0.994
	460	270	2.8	− 4.74	0.999
	–	350	2.9	− 2.51	0.995
	–	450	1.5	− 2.87	0.985
$[(CH_3)_2SiO]_4$	460	350	2.2	− 3.59	0.997
	–	390	2.0	− 3.16	0.999
	–	410	1.4	− 3.75	0.999
	–	450	1.4	− 2.15	0.977
$[(CH_3)(CH_2{=}CH)SiO]_3$	460	200	6.7	− 3.87	0.994
	–	250	4.8	− 2.87	0.999
	–	275	3.1	− 3.44	0.999
	–	310	2.3	− 3.26	0.998
$(CH_3)_3SiOSi(CH_3)_3$	460	350	8.0	− 5.49	0.994
	–	390	1.4	− 5.89	0.990
	–	420	4.5	− 4.27	0.999
	–	450	5.5	− 2.24	0.999
	–	490	1.1	− 3.38	0.997

With a high number of different active sites the rate of chemisorption on heterogeneous surface can be described using a simpler Crickmore–Wojciechowski equation

$$d\Theta/dt = kP(1-\theta)^{1/\eta} \tag{41}$$

where k is the rate constant averaged over the entire heterogeneous surface and η is a parameter that characterizes the surface heterogeneity. For $\eta = 1$ this equation reduces to Eq. (40). Eq. (41) is an approximate representation of the chemisorption rate on the discrete surface

$$d\Theta/dt = P\sum_{i=1}^{l} f_i k_i (1-\theta_i) \tag{42}$$

where θ_i is the local surface coverage of the active sites of i–th type. Efficiency of this approximation was demonstrated for the discrete heterogeneous surface at $l = 5$ [110]. The expression for kinetic chemisorption isotherm can be obtained from Eq. (41) for $\eta < 1$

$$(1-\Theta)^{(\eta-1)/\eta} = (1/\eta - 1)kPt + 1 \tag{43}$$

and for $\eta = 0.5$ Eq. (43) transforms to the Ritchie equation which describes well the chemisorption kinetics of hydrogen, water vapour and carbon monoxide on various adsorbent surfaces [112]

$$(1-\Theta)^{-1} = kPt + 1 \tag{43a}$$

This is a simple second–order equation which usually applies to description of dissociative chemisorption from the gas phase on the homogeneous surface. However, Eq. (43a) describes well only an initial part of kinetic chemisorption isotherm for interaction of trimethylchlorosilane on dehydrated pyrogenic silica [113] and mixed alumina–silica and titania–silica [114] surface. At the same time, whole kinetic chemisorption isotherms are described using equations derived for the heterogeneous surface. Thus, high fractional reaction orders in respect to the silica surface OH groups obtained by Hertl and Hair for chemisorption of silanes and siloxanes [106,107] and in other studies [113,114] may be explained by heterogeneity of the oxides surface.

Isosteric activation energies of several organosilicon compound chemisorption on pyrogenic silica surface have been determined by the method also involving the surface homogeneity but with the unknown reaction order [4,22,23]. To reduce and integrate Eq. (40), using the Arrhenius equation, we can obtain the expression for calculation of isosteric chemisorption activation energy from the dependence of t on T at Θ = const.

$$E_\Theta^{\neq} = R\frac{d(\ln t)_\Theta}{d(1/T)} \tag{44}$$

However, as it follows from Fig.3, the isosteric chemisorption activation energy of organosiloxane interaction with the surface sites of pyrogenic silica depends strongly on the surface coverage. Dependencies similar to those in Fig. 3 are inherent in the chemisorption of some other organosilicon compounds on the surface of parent and mixed pyrogenic oxides of Si, Ti and Al. This indicates an energetic heterogeneity of the oxides surface in the chemisorption processes.

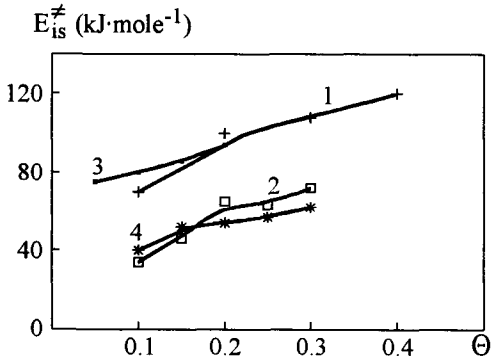

Figure 3. Dependencies of isosteric activation energy of organosiloxanes chemisorption on the pyrogenic silica surface (Aerosil-175) versus the surface coverage. Figure taken from [80]. (1) $(CH_3)_3SiOSi(CH_3)_3$; (2) $[(CH_3)(CH_2{=}CH)SiO]_3$; (3) $[(CH_3)_2SiO]_4$; (4) $[(CH_3)_2SiO]_3$.

6.2. Discrete heterogeneous surface

This model was discussed previously, Eq. (32). It applies kinetic description of chemisorption of CH_3OH, H_2O and NH_3 on the dehydroxylated silica surface at the constant temperature [26]. For most reactants, the kinetics results are best fit assuming two parallel and independent first order reactions. Although only one type of defect is apparent in the FTIR spectra, two distinct defect reactions with water molecules are observed: a rapid reaction ($k = 0.5\ min^{-1}$) which mainly produces isolated silanols, and a slower reaction ($k = 0.015\ min^{-1}$) which produces hydrogen bonded silanols. The reaction between surface defects and methanol is similar to that observed for water. The rate limiting step in the chemical dissociation of Si–O bonds in the surface defect sites could be either acid–base reactions leading to the adsorption gases onto the defect, or subsequent dissociative chemisorption reaction. Also, the organosilicon compound chemisorption kinetics on the surface of pyrogenic oxides is described well enough at T = const. by this model Eq. (32) at l = 2. It has been found, however, that the calculated relative concentrations of active sites (f_i) vary with T, while, for example, for the reaction of trimethylchlorosilane with dehydrated silica surface (temperature of pretreatment of the surface is 873 K), the f_i increases from 0.2 to 0.7 with T varying within 593 to 693 K which is in contradiction to the model used [80]. Thus the model of discrete surface heterogeneity at l = 2 or 3 fails to describe adequately the chemisorption kinetics under consideration at various temperatures.

6.3. Uniformly heterogeneous surface

Kinetics of several organosilicon compound chemisorption from the gas phase on the non-porous silica (Cab-O-Sil M5) surface is described by the well-known Elovich equation [27]:

$$d\Theta/dt = a\exp(-b\Theta) \tag{45}$$

where a and b are the empirical coefficients. Proceeding from the calculated a and b values, rate of the transformations has been determined at different surface coverage, temperatures and the dependencies of chemisorption activation energies on concentration of reacted

surface OH groups have been plotted. From the above dependencies it follows that activation energy at $\Theta \to 0$ ranges from 50 to 70 kJ·mole^{-1} at the temperature of silica pretreatment ($T_p = 673$ K) and from 40 to 46 kJ·mole^{-1} at $T_p = 873$ K. The difference between activation energies at $\Theta = 1$ and $\Theta = 0$ (this value ranges from 90 to 180 kJ·mole^{-1}) decreases in the following series: methyltrichlorosilane > trimethylchlorosilane > tetrachlorosilane > dimethyldichlorosilane at $T_p = 673$ K and trimethylchlorosilane > dimethyldichlorosilane > tetrachlorosilane > methyltrichlorosilane at $T_p = 873$ K. Eq. (45) results from the kinetic model of the heterogeneous surface with a uniform distribution function on the activation energy.

The equation for kinetic isotherm on the uniformly heterogeneous surface was derived by Temkin [115] for the middle region of surface coverage

$$\Theta = (\alpha f)^{-1} \ln\left(\frac{\alpha\pi k_0 P}{\sin(\alpha\pi)}\right) + (\alpha f)^{-1} \ln\left(t + \frac{\sin(\alpha\pi)}{\alpha\pi k_0 P}\right) \tag{46}$$

where $\alpha = \Delta E^{\neq}/\Delta H$ and $f = \left(E_\Theta^{\neq} - E_0^{\neq}\right) \cdot (RT) \cdot (\alpha\Theta)^{-1}$; k_0 and $E_0^{\neq}$ are the rate constant and activation energy at $\Theta \to 0$, while ΔH is the reaction enthalpy. At $\alpha\pi k_0 P \gg \sin(\alpha\pi)$ the linear dependence of Θ on the $\ln t$ should be observed for chemisorption kinetics. Eq. (46) at high $\gamma' = \alpha f$ coincides with the solution of Eq. (34) for kinetics on homogeneous surface with the account for lateral interactions between chemisorbed species in the mean-field approximation. Calculation of activation parameters for organosilicon compound chemisorption on the Si and Al pyrogenic oxides surface has shown that the mean square deviation between the calculated and experimental Θ values on the kinetic isotherms at different temperatures (S_M) decreases by more than an order of magnitude coming from $F = 1$ to $F = \exp(-\gamma'\Theta/RT)$. However, both latter models Eqs. (34) and (46) postulate the independence of γ' parameter of the T. It has been defined that, depending on the structure of reactant, oxide and temperature of surface pretreatment, the γ' values decrease, get constant or increase with increasing the T. Such changes in γ' with T are probably related to improper selection of the "apparent" distribution function on the activation energy.

6.4. Exponentially heterogeneous surface

The exponential distribution function on chemisorption activation energy conforms to Howar and Taylor's, Banham and Burt's as well as to Kwan's equations. They were used long ago for the description of small molecule chemisorption kinetics on oxide surfaces [116]. It is suggested that apparent rate constant depends on the coverage heterogeneous surface as follows [117]:

$$k_\Theta = k_1 \Theta^{-\alpha n} \tag{47}$$

where k_1 is the apparent rate constant at $\Theta \to 1$, $n = C/RT - n_0$; $n_0 = m/R$; C and m are the coefficients of dependencies of chemisorption enthalpy and entropy on the relative surface coverage

$$H_\Theta = H_1 - C \ln \Theta \tag{48a}$$

$$S_\Theta = S_1 + m \ln \Theta \tag{48b}$$

Thus, the expression for chemisorption kinetic isotherm on this surface may be written as:

$$\Theta = (\alpha n k_1)^{1/\alpha n}\, t^{1/\alpha n} \qquad (49)$$

6.5. Powerly heterogeneous surface

All the above-mentioned models described poorly the kinetics in a whole range of surface coverage at different temperatures. This conclusion is confirmed by isochrones given in Fig. 4 plotted using the kinetic data for chemisorption of some organosilicon compounds on the pyrogenic oxides surface. A type of distribution function on the activation energy may be determined from the dependencies of Θ maximum value (Θ_{max}) on T at a considerably fixed time of the reaction, that is, from the dependence of the "plateau" height of kinetic isotherm on T [118,119].

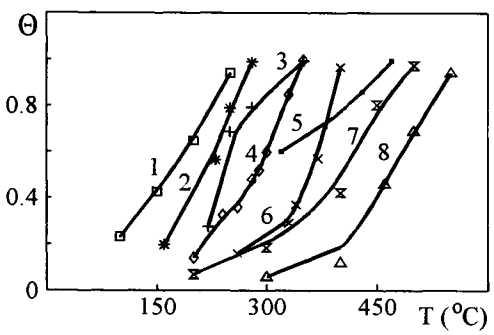

Figure 4. Isochrones of organosilicon compounds chemisorption on the pyrogenic oxides surface pretreated at different temperature (T_p). Figure taken from [80]. (1) $(CH_3)(CH_2CH)SiCl_2$ + SiO_2 (523 K); (2) $SiCl_4$ + SiO_2 (673 K); (3) CH_3SiCl_3 + SiO_2 (673 K); (4) $(CH_3)_2SiCl_2$ + SiO_2 (673 K); (5) $(CH_3)_3SiOSi(CH_3)_3$ + TiO_2 (923 K); (6) $(CH_3)_3SiCl$ + SiO_2 (673 K); (7) $(CH_3)_3SiNCS$ + SiO_2 (973 K); (8) $(CH_3)_3SiNCO$ + SiO_2 (973 K).

Fig. 4 shows that these dependencies are characterized by different signs of the second derivatives $d^2\Theta_{max}/dT^2$. Among simple distribution functions (exponential, inverse exponential, hyperbolic, uniform and power functions [119]), only the last function is valid with Θ varying in the range from 0 to 1, and, depending on the exponent, resulting in different signs of the second derivatives $d^2\Theta_{max}/dT^2$ or $d^2E_\Theta^{\neq}/d\Theta^2$. Therefore, Eq. (34) is written as follows:

$$d\Theta/dt = f(N_A)k_0(1-\Theta)^n \exp\{-\gamma\Theta^\nu/(RT)\} \qquad (50)$$

The numerical simulations show that, with a larger γ value, the activation energies calculated agree with both n = 1 and n = 2 due to the predominant effect of the exponential term in Eq. (50). Thus, in calculating the kinetic parameters of the reactions, it is possible to confine to n = 1.

To determine the parameters ν, γ and k_0 of Eq. (50) the following procedure has been used with the kinetic isotherms $\theta = f(t)$ at different T. The quasi-Newton procedure has been used in the first step to determine γ' in the mean-field approximation ($\nu = 1$) and k_0 corresponds to a minimum of mean-square deviation at T = const. The differential

equation has been integrated by the "prediction and correction" method. Then, proceeding from the γ' values obtained, the dependence of difference between $E_\Theta^{\neq}$ and $E_0^{\neq}$ on Θ was approximated at several M temperatures

$$\Delta E_i^{\neq} = E_i^{\neq} - E_0^{\neq} = \sum_{i=2}^{M} \gamma'_{i-1} \left(\Theta_i^{min} - \Theta_{i-1}^{min}\right) \tag{51a}$$

and the exponent ν has been calculated from the linear expression

$$\ln \Delta E_i^{\neq} = \nu \ln \Theta_i + \ln \gamma' \tag{51b}$$

The main chemisorption activation parameters, that are the pre-exponential factor ($A^{\neq}$) which does not depend on Θ and activation energy on the "free" surface ($E_0^{\neq}$) have been calculated, proceeding from the temperature dependence of k_0 on T, by the Arrhenius equation.

At high values of $\gamma \geq 3RT$, i.e., for the broad distribution on $E^{\neq}$, the approximate solution of the corresponding integral equation for chemisorption kinetics including the reaction of the first-order with active sites and power distribution function on $E^{\neq}$ obtained by the Roginskij method [119], can be used to determine k_0, γ and ν parameters of Eq. (50):

$$\Theta^{\nu} = \frac{\gamma}{RT} \ln \frac{k_0 N_A \gamma}{0.7\ RT} + \frac{RT}{\gamma} \ln t \tag{52}$$

The parameters of power distribution function are connected with those in Eq. (50) as follows: $\rho(E^{\neq}) = H(E^{\neq})^{\beta}$; $\beta = (1/\nu) - 1$; $H = \left\{\nu(E_1^{\neq} - E_0^{\neq})^{1/\nu}\right\}^{-1}$ where $(E_1^{\neq} - E_0^{\neq})$ is the difference between the activation energies at $\theta = 1$ and $\theta = 0$.

Comparison of the paramaters of Eq. (52) calculated from the kinetic isotherms simulated using exactly Eq. (50) showns that at a relatively wide distribution function on $E^{\neq}(\gamma \geq 50\ kJ \cdot mole^{-1})$, Eq. (52) may well be used for determination of Eq. (50) parameters. However, the γ values obtained for chemisorption of organosilicon compounds on the pyrogenic oxides surface lie within the limits from 10 to 50 $kJ \cdot mole^{-1}$, and the calculations made by Eq. (52) result normally in unthinkable values of k_0 and γ at reasonable values of ν and vice versa.

For the power dependence of $E^{\neq}$ on Θ, the variation in γ' calculated in the mean-field approximation is obviously related to the ν value, that is γ' increases with increasing T at $\nu > 1$ and decreases with $\nu < 1$. If the lateral interactions between chemisorbed particles on the amorphous surface mainly contribute to the "apparent" distribution function on $E^{\neq}$, then with the account for the results of Monte Carlo simulations [104], we can expect $\gamma > 1$ and low γ' values at low Θ. If the contribution of chemical heterogeneity of active sites dominates, then $\nu < 1$.

Chemical heterogeneity of the parent and mixed oxides surface contributes significantly to their overall heterogeneity. Because of this, the comparison of the parameters of Eq. (32) and Eq. (50) at $\nu = 1$ was performed. It has been found that the γ values vary non-linearly with T, while the dependence of k_0 on T is not described by the Arrhenius equation and, hence, is in contradiction with the dependence of these parameters on T as obtained on the basis of kinetic data for chemisorption on the Si, Ti and Al oxides surface [80].

6.6. Heterogeneous surface with the uniform, Gamma–, Beta and sinusoidal distribution functions on rate constants

The common integral equation for kinetic chemisorption isotherm on the heterogeneous surface taking into account the distribution function on the apparent rate constants (k) may be written as:

$$1 - \Theta(T,t) = \int_{k_{min}}^{k_{max}} \{(1 - \theta(T,t,k)\}\, \rho(k)dk \tag{53}$$

where $\{(1 - \theta(T,t,k)\}$ is the local concentration of the active sites possessing the rate constant k; $\rho(k)$ is the distribution functions on the k, k_{min} and k_{max} are the lower and upper limits of integration.

Exact analytical solutions of Eq. (53) for some distribution functions on k are presented in Table 4.

Table 4
Solutions for chemisorption isotherm containing some distribution functions of heterogeneous surface on the rate constants (k), Eq. (53)

Distribution function	Solution for $1 - \theta(t)$
Uniform:	
$\begin{cases} A \quad \text{at } \lvert k - k_m \rvert \le 1/2A \\ \text{or} \\ 0 \quad \text{at } \lvert k - k_m \rvert > 1/2A \end{cases}$	$(2A/t) \cdot \exp(-k_m t)\ \sinh(t/2A)$ or $(A/t) \cdot \exp(-k_0 t)\{1 - \exp(-t/A)\}$
Gamma:	
$\frac{b^a}{\Gamma(a)}(k - k_0)^{a-1}\ \exp\{-b(k - k_0)\}$	$\exp(-k_0 t)\left(\frac{b}{b - t}\right)^a$
Beta:	
$a^n \exp\{-(k - k_0)\}[1 - \exp\{-a(k - k_0)\}]^{n-1}$	$\exp(-k_0 t)\frac{\Gamma(n+1)\Gamma(t/a+1)}{\Gamma(n+t/a+1)}$
Sinusoidal:	
$\begin{cases} (A/2) \cdot \sin[A(k - k_0)], \text{ at } k_0 < k < k_0 + \pi/A \\ \text{or} \\ 0, \text{ at } k < k_0;\ \ k > k_0 + \pi/A \end{cases}$	$\frac{\exp(k_0 t)\{1 + \exp(-\pi t/A)\}}{2(1 + t^2/A^2}$ or $\exp(-k_m t)\ \cosh(\pi t/2A)(1 + t^2/A^2)^{-1}$

k_0 and k_m are the minimum and mean values of the rate constants.

Transformation of the above functions on k to the distribution functions on the logarithms k by the relation:

$$F(\ln k) = \{\rho(k)\}/k \tag{54}$$

should be adopted for the following structure–reactivity relationships in the chemisorption reactions. Examples of such correlations are presented in Section 7.1.

6.7. Application of the regularization method

From the mathematical point of view, Eq. (53) is a linear Fredholm integral equation of the first kind, where the integral kernel represents the local concentration of the active sites $\{(1-\theta(T,t,k)\}$. Many attempts have been undertaken to invert Eq. (53) with respect to $\rho(k)$. The disadvantages of the analytical integrating of Eq. (53) are that: 1) it is unknown whether the assumed shape of $\rho(k)$ is correct and 2) often a variety of different analytical functions can be used to describe a given data set with about the same degree of accuracy. Thus, the calculation of $\rho(k)$ from Eq. (53) is a numerically ill-posed problem; i. e. small changes in $\Theta(T,t)$ caused by experimental errors can distort significantly the calculated $\rho(k)$. The ill-posedness is mainly a mathematical numerical problem. Theoretical foundations for solving numerically unstable problems were developed by Tihonov [120,121], who introduced the regularization method. This method was successfully applied to the description of gas adsorption on the heterogeneous solid surface [122,123]. The fundamental idea of numerical regularization is to replace the ill-posed problem of minimizing the select function by a well posed one which smooths the calculated distribution function and distorts the origin problem insignificantly. The following functional $\psi\{\rho(k)\}$ can be minimized at $\rho(k) \geq 0$ for Eq. (53):

$$\left[\int_{k_{min}}^{k_{max}} \{\exp(-kt)\}\,\rho(k)dk + \Theta(t) - 1\right]^2 + \lambda \int_{k_{min}}^{k_{max}} \rho^2(k)dk = \psi\{\rho(k)\} \tag{55}$$

where λ is the regularization parameter. This parameter is usually chosen through a series of trials by an interactive judgment about the solution. A detailed description of strategies for finding the optimal λ value in adsorption applications is given in [124]. The λ value, shape and number of peaks on the calculated distribution curve depend strongly on the accuracy of experimental data. Unfortunately, the concentrations of chemisorbed species or unreacted active sites during chemisorption process on the oxides surface are determined from the spectral data or by gravimetry and elements analysis with a moderate accuracy. Then, the simpler methods, based on the assumption of analytical distribution functions (Table 4), can be used. One example of application of the regularization procedure for description of chemisorption kinetics is calculation of the distribution functions $\rho(k)$ on the basis of the simulated chemisorption kinetic isotherms on the amorphous heterogeneous solid surface, taking into account the distributions both on the k and on the distances between neighbouring particles [105].

6.8. Amorphous heterogeneous surface taking lateral interactions between species into consideration

The surface of most oxides provides an excellent example of amorphous heterogeneous solid surface. Various types of active sites determine the chemical heterogeneity (k). The difference in distances between these sites in the amorphous layer (r) estimates geometric heterogeneity of the surface. The recent Monte Carlo study of Lennard-Jones gas adsorption on the amorphous surface demonstrated that adsorption isotherms are very sensitive both to energetic and geometric heterogeneity [125]. One could expect that the geometric heterogeneity has a significant effect on the chemisorption kinetics on the heterogeneous amorphous solid surface. A simple approach to description of chemisorption kinetics on

the random and patchwise heterogeneous amorphous solid surface has been developed in [105]. A common equation for kinetic chemisorption isotherm on heterogeneous surface taking into account the distribution functions on k and on r in the absence of correlation between them may be written as:

$$1 - \Theta(T,t) = \int_{k_{min}}^{k_{max}} \int_{r_{min}}^{r_{max}} \{1 - \theta(T,t,k,r)\}\rho(k)\rho(r)dk\,dr \tag{56}$$

where $\{1 - \theta(T,t,k,r)\}$ is the local concentration of active sites possessing the apparent rate constant $k_{app} = kF(N_A)$ (under isobaric conditions) and with lateral interaction energy depending on the distance between them r; $\rho(k)$ and $\rho(r)$ denote the distribution functions on k and on r. Eq. (56) is an oversimplified expression and strongly, local surface coverage θ_i should be a function of $r_1, r_2, \ldots r_z$, where r_i are the distances between the site in question and each one of their z neighbours, if only the first–order neighbouring sites were allowed to interact.

Studies of adsorption phenomena on heterogeneous surface have revealed two main limiting types for the topography of the adsorption sites [126,127]: the random site distribution, i. e. when the sites with different adsorption energy are randomly distributed over the lattice, and patchwise site distribution, where the sites of equal energy are present in groups. Unlike the physical adsorption, where adsorption potential of the sites plays a crucial role in adsorption rate and equilibria, the chemisorption free energy (ΔG^0) is the fundamental quantity in the chemisorption process. This is connected with the chemisorption rate constant for the series of related sites by Brönsted–Temkin free–energy relation [115]

$$\Delta G^{\neq} = -RT \ln k = \alpha \Delta G^0 + \beta \tag{57}$$

where $\Delta G^{\neq}$ is the difference between free energies of chemisorption activated complex and reactants, α and β are the constants for given reaction series. Then, the k variation determines the "intrinsic" heterogeneity and type of surface topography, when α and β coefficients are fixed for all the surface sites.

Let us assume the patchwise topography for active sites and take into account the lateral interactions between the neighbouring chemisorbed species in the mean–field approximation [32]. Then, the interaction potential between the first–order neighbouring sites $(1/RT)\sum_{i=1}^{z}\varphi(r)$ is approximated by $z\varphi(r)/(2RT)$, where r is a kind of effective, mean distance between the site and each one of its z neighbours. Local surface coverage may be calculated from Eq. (58)

$$dy/dt = -ky \exp\{\omega(y-1)\} \tag{58}$$

under the initial condition: $y(0) = 1$, $y = 1 - \theta$; $\omega = z\varphi(r)/(2RT)$, where $\varphi(r)$ is an interaction potential between neighbouring particles on the surface. The solution of Eq. (58) is derived using the perturbation procedure for ω value

$$y = y_0 + \omega y_1 + \omega^2 y_2 + \omega^3 y_3 + \ldots \tag{59}$$

Only repulsive interactions between the chemisorbed species as their exponential dependence on the distance between them was taken into consideration. Assuming the Gamma distribution for $\rho(k)$ and Gamma–, uniform or normal distribution for $\rho(r)$ functions, approximate solutions of Eq. (56) for the reaction on patchwise and random topography have been obtained by its sequential integration as a long algebraic series [105].

These expressions make it possible to study the influence of distribution parameters $\rho(k)$ and $\rho(r)$ of an amorphous heterogeneous surface on the chemisorption kinetic isotherms as well as on the moments of distribution on the observable rate constants, $(k_{(0)})$. The 'apparent' distribution function on the observable rate constants is derived from the experimental chemisorption kinetic isotherms at a constant temperature. The first-order kinetic equation Eq. (40) is commonly used to denote the local concentration of surface active sites. Opposite kinetic problem is conventionally solved using the regularization procedure or from the expressions in Table 4. The regularization procedure was used for the calculation of the distribution functions $\rho(k_{(0)})$ on the basis of simulated kinetic isotherms, taking into account both $\rho(k)$ and $\rho(r)$ functions. The average value, $(\bar{k}_{(0)})$ and variance $(\sigma^2(k_{(0)})$ of $\rho(k_{(0)})$ function were calculated. The influence of average value r $(\bar{r})$, standard deviation of r (σ_r) and k (σ_k) on the profiles of kinetic isotherms as well as on the distribution functions $\rho(k_{(0)})$ was investigated with the following parameters of repulsive potential: $\varphi_0 = 5.36 \cdot 10^5$ kJ $\cdot$ mole^{-1}, $\gamma = 3.7$ Å and T = 500 K. The calculated dependencies of $\bar{k}_{(0)}$ and $\sigma^2(k_{(0)})$ on the average value and standard deviation of r are presented in Fig. 5.

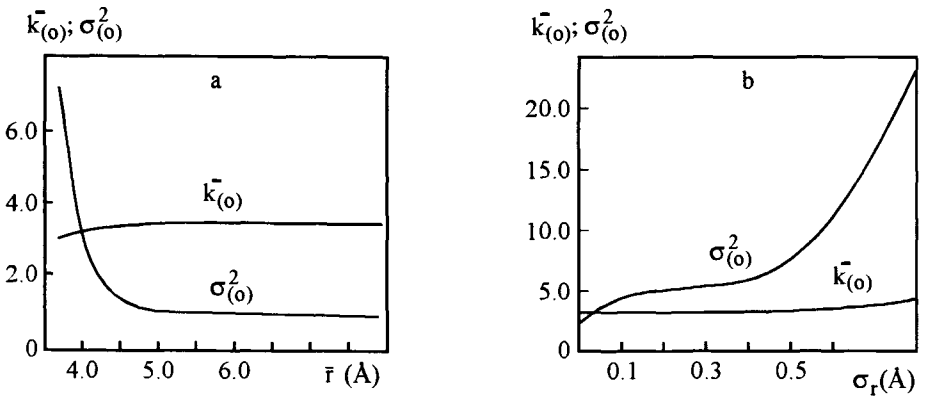

Figure 5. Dependencies of average observable rate constant $(k_{(0)})$ and its variance $(\sigma^2_{(0)})$ on the (a): mean-square deviation on the distance between the neighbouring surface sites with the initial parameters of Gamma distribution function on $\bar{k}$ value: $\bar{k} = 1.0$; $\sigma = 1 \cdot 10^{-5}$ and uniform distribution function on r value at $\bar{r} = 4$ Å and (b): on the average distance between neighbouring surface sites at $\sigma_r = 0.01$ Å. Figures taken from [105].

It was established that the increase of σ_r and decrease of $\bar{r}$ results in lowering the reaction rate in an intermediate part of the kinetic isotherm and leads to lower conversion degree of the reaction with the equal values of t/k. A more pronounced effect was observed with increasing of σ_k. From Fig. 5a and 5b it follows that $\sigma(k_{(0)})$ increases at enhancement

of σ_r. The lowering of $\bar{r}$ leads to the same broadening of the $\rho(k_{(0)})$ function. Also, the influence of heterogeneous amorphous surface topography (random and patchwise) with distributions on k and r on the parameters of $\rho(k_{(0)})$ function was studied.

It was found that with the initial parameters $k = 12.0$; $\sigma_k = 11.9$; $\bar{r} = 4.3$ Å; $\sigma_r = 1 \cdot 10^{-5}$ Å, the $k_{(0)}$ and $\sigma(k_{(0)})$ values increase from random (11.174 and 12.64) to patchwise (11.57 and 14.21) surfaces, respectively.

Variation of the r value on heterogeneous amorphous surface under the experimental conditions may be performed, for instance, by elimination of the active sites at high temperature. Thermal dehydroxylation of silica surface is the typical example of this process [1,63]. The kinetic data for the reaction of hexamethylcyclotrisiloxane with OH groups of silica surface pretreated at two different temperatures were used [108]. As the temperature of the surface pretreatment increases, the number of OH groups decreases and accordingly the average distance between them enhances. From the data obtained it follows that increasing temperature of the surface pretreatment from 733 K to 973 K leads to decreasing $\sigma(k_{(0)})$ from 0.173 to 0.095 min^{-1} (kinetics is measured at 723 K). This result correlates well with predicted theoretically decreasing of the $\sigma(k_{(0)})$ with enhancement of the average distance between neighbouring surface sites.

6.9. Heterogeneous surface with distributions both on the pre–exponential factor and on activation energy

Pre–exponential factor independence of the coverage of heterogeneous surface has been postulated at the above calculation of distribution functions on chemisorption activation energies on the basis of kinetic isotherms measured at different temperatures. However, it appeared to be in contradiction with some experimental data and theoretical conclusions [128]. Compensation relationship is commonly observed for the catalytic processes proceeding on the heterogeneous surface [129]

$$\ln A^{\neq} = B + eE^{\neq} \tag{60}$$

where $e = (RT_{is})^{-1}$, T_{is} is the isokinetic temperature and B is the logarithm of the rate constant at this temperature.

It is apparent that such dependence is possible at varying surface coverage of the heterogeneous surface, since reactivity of the sites reduces as Θ increases. An approach for calculation of the surface distribution functions on $\ln A^{\neq}$ and on $E^{\neq}$ values from chemisorption kinetic isotherms measured at different temperatures has been developed in [70,130,131]. Distribution functions on $\ln k$ at different T can be found, for example, using the regularization procedure or expressions from Table 4. If $\ln A^{\neq}$ and $E^{\neq}$ values are connected by Eq. (60), the expression connecting cumulant of $\ln k$ distribution with the sum of cumulants of $\ln A^{\neq}$ and $E^{\neq}$ distributions is changed for cumulants of the second order as [132]:

$$\sigma^2(\ln k) = \sigma^2(E^{\neq})/(RT)^2 + \sigma^2(\ln A^{\neq}) - 2R\sigma(E^{\neq})/RT\ \sigma(\ln A^{\neq}) \tag{61}$$

where R is the correlation coefficient. Parameters of distribution function on $\ln A^{\neq}$ in this case can be determined from $\overline{E^{\neq}}$ and $\sigma^2(E^{\neq})$ as well as from B and e coefficients of Eq. (60)

$$\sigma\left(\ln A^{\neq}\right) = e\sigma(E^{\neq}) \tag{62a}$$

$$\overline{\ln A^{\neq}} = B + e\overline{E^{\neq}} \tag{62b}$$

where $\overline{\ln A^{\neq}}$ and $\overline{E^{\neq}}$ are the averages and $\sigma(\ln A^{\neq})$, $\sigma(E^{\neq})$ are the mean-square deviations of $\ln A^{\neq}$ and $E^{\neq}$ values.

The above approach was applied for calculation of distribution functions of pyrogenic silica surface on the dimethyldichlorosilane chemisorption activation parameters [22,133]. Dependence of variance of distribution function on $\ln k$ versus $1/T$ is presented in Fig. 6.

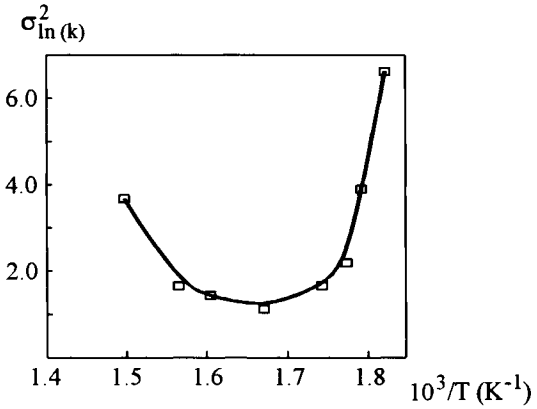

Figure 6. Dependence of variance of the logarithm of the rate constant on the inverse temperature for chemisorption of dimethyldichlorosilane on the pyrogenic silica surface, pretreated at 673 K. Figure taken from [130].

As shown, this dependence agrees well with Eq. (61) (R = 0.99978). The following parameters of distribution on the chemisorption parameters are obtained:

$\overline{E^{\neq}} = 139.8\ \text{kJ} \cdot \text{mole}^{-1}$; $\sigma(E^{\neq}) = 169.1\ \text{kJ} \cdot \text{mole}^{-1}$

$\overline{\ln A^{\neq}} = -21.2$; $\sigma(\ln A^{\neq}) = 33.0$ ($A^{\neq}$, in $\text{cm}^3 \cdot \text{molecule}^{-1} \cdot \text{s}^{-1}$)

The B and e coefficients of Eq. (60) are equal to -48.46 and 0.195 respectively, then $T_{is} = 617$ K.

The $\overline{E^{\neq}}$ value agrees well with isosteric activation energy ($\overline{E^{\neq}_{\theta}} = 126\ \text{kJ} \cdot \text{mole}^{-1}$) for this reaction calculated in [57]. However, the high $\sigma(E^{\neq})$ value testifies to high energetic heterogeneity of pyrogenic silica surface OH groups. The $\overline{\ln A^{\neq}}$ value lies in the range of "normal" pre-exponential factors predicted by the transition state theory for unimolecular adsorption $\{\ln A^{\neq} = (-20.7) \div (-36.8)\}$ [128]. The range of $\ln A^{\neq}$ varying $\{-54.2 \div 11.8\}$ obtained from $\ln A^{\neq}$ and $\sigma(\ln A^{\neq})$ values is far in excess of that, predicted by this theory. It may be explained by more complex reaction mechanism including, for instance, the formation of intrinsic precursor (H complex between silane and the surface OH group) at low temperature.

Let us suppose that $\rho(E^{\neq})$ function is described by the Gamma distribution. Then, the expression similar to Eq. (53) (substituting $\rho(E^{\neq})$ instead of $\rho(k)$ function) may be

written using Eq. (60)

$$1 - \Theta(t) = \frac{b^a}{\Gamma(a)} \int_0^\infty \exp\left\{-t\left[\exp\left(B + (e - 1/RT)E^{\neq}\right)\right]\right\} E^{\neq a-1} \exp\left(-bE^{\neq}\right) dE^{\neq} \qquad (63a)$$

A final approximate solution of Eq. (63a) can be obtained in the form

$$1 - \Theta(t) = \exp\{-t[\exp(b)]\}\left[1 + tb^{-1}\exp(B)R(T - T_{is})/(TT_{is})\right]^{-a} \qquad (63b)$$

The T_{is}, B, a and b parameters for distribution functions of pyrogenic oxides surface on chemisorption activation energy of some organosilicon compounds are presented in Table 5. The T_{is} value conforms to the temperature, at which the rate constants with several active sites coincide, that is surface becomes homogeneous. This implies that heterogeneity of surface active sites is irrelevant at T_{is}. This is due to high energy of reactant molecules from the gas phase which do not distinguish different active sites. It is in agreement with the results about reduction of energetic heterogeneity at sufficiently high temperatures [135].

Table 5
Isokinetic temperatures (T_{is}), logarithms of apparent rate constants at this temperature (B) and parameters of Gamma–distribution function (a and b) of some pyrogenic oxides surface on chemisorption activation energy of organosilicon compounds calculated from the kinetic isotherms obtained in [4,134] and activation energies on "free" surface from [79]

Organosilicon compound	Oxide	B min^{-1}	T K	a	b	$E_0^{\neq}$ $kJ \cdot mole^{-1}$
$[(CH_3)_2SiNH]_3$	Al_2O_3	– 9.74	293	0.176	$2.30 \cdot 10^{-10}$	1.2
$(CH)_3SiCN$	SiO_2	– 3.24	476	0.162	$0.20 \cdot 10^{-3}$	28.9
$[(CH_3)_3Si]_2O$	SiO_2 (30% TiO_2)	– 9.86	538	0.788	$0.25 \cdot 10^{-4}$	76.4
$[(CH_3)_3Si]_2O$	SiO_2 (30% Al_2O_3)	– 13.00	615	2.065	$0.48 \cdot 10^{-5}$	127.0

The B coefficient corresponds to the logarithm of the rate constant at T_{is}, i.e. to the reaction proceeding on the "pseudo–homogeneous" surface. It is likely, that T_{is} and B constants may be useful characteristics of heterogeneous surface active sites reactivity towards a "test" gas reactant. For example, as it follows from Table 5, T_{is} value increases with enhancement of the chemisorption activation energy for interaction of organosilicon compounds with the "free" surface of pyrogenic parent and mixed oxides.

7. CONNECTION BETWEEN THE STRUCTURE OF ORGANIC COMPOUNDS AND THEIR REACTIVITY IN CHEMISORPTION ON THE OXIDES SURFACE

7.1. Free energy relationships on heterogeneous surface

Chemisorption rate constants and activation energies are the basis for the following quantitative analysis of the reaction mechanism on the oxides surface. The examples of

such analysis with application of Taft's, Polanyi's and Klopman's equations are illustrated in [49,57,70,82,136–138].

A main task of chemisorption kinetics theory is prediction of activation parameters on the basis of physicochemical properties of reactant and surface active sites. One of the most widespread methods used for homogeneous media is application of the linear models

$$\Theta_j = \sum_{i=1}^{n} x_{ij} a_i \tag{64}$$

where Θ_j are the $\ln k$ or $E^{\neq}$ quantities, x_{ij} is the i–physicochemical property of reactant j; a_i is the parameter, characterizing active site property to the i–th type of interaction in the transition state determined by the property of reactant j. This model used, for instance, in relationships between logarithms of rate constant for the organic compounds reactions and substituent constants of these compounds in the Hammet's and Taft's equations [18–21].

Surface of most oxides is heterogeneous, and properties of its active sites should be described by means of the distribution on parameters a_i. Approach to calculation of distribution functions $\rho(a_i)$ on the basis of chemisorption kinetic data on heterogeneous surface was developed in [132].

Let us denote the parameters of Eq. (53) as follows: $\Phi = 1 - \Theta(T,t)$; $Q = E^{\neq}$ or $\ln k$; $\phi(Q) = \{(1 - \theta(T,t,k)\}$ and $F(Q)$ is the distribution function on Q. Let us take the distribution function $F(Q)$ calculated by the regularization procedure or other means from the experimental data for m reactants (j ranges from 1 to m). Random Q values, according to Eq. (64), are a linear combination of a_i . In this case $m \geq n$. It is necessary to define the distribution function $\rho(a_i)$. For this purpose the random values $y_{ij} = x_{ij}\ a_i$ can be introduced. Their distribution functions $f(y_{ij})$ are connected with $\rho(a_i)$ as:

$$f(y_{ij}) = (x_{ij})^{-1} \rho(a_i) \tag{65}$$

In accordance with Eq. (65), cumulants of $f(y_{ij})$ and $\rho(a_i)$ are connected by the ratio

$$K_{ij,r} = x_{ij}^{r} \kappa_{i,r} \tag{66}$$

where $K_{ij,r}$ is the cumulant of order r of y_{ij} and x_{ij}^{r} is x_{ij} in the exponent r, $\kappa_{i,r}$ is the cumulant a_i of order r. Since each Q_j equals to the sum y_{ij} $(i = 1,n)$, in accordance with the well-known theorem of probability theory [139], the cumulant of Q_j equals to y_{ij} cumulants sum, i.e.

$$R_{j,r} = \sum_{i=1}^{n} K_{ij,r} = \sum_{i=1}^{n} x_{ij}^{r}\ \kappa_{i,r} \qquad (j = 1,m;\ r = 1,\ \infty) \tag{67}$$

where $R_{j,r}$ is the Q_j cumulant of order r. For each r value there will be m equations for n values $\kappa_{i,r}$. Since the distributions $F(Q_j)$ are known, $R_{j,r}$ values may be calculated on the basis of set of Eq. (67). If the set of Eq. (67) is possible to solve for each r, cumulants $\kappa_{i,r}$ can be calculated and the distribution $\rho(a_i)$ can be restored. Let us introduce a standardized value

$$g_i = \{(a - M(a_i)\}\ /\sigma(a_i) \tag{68}$$

where $M(a_i)$ is the first central moment of a_i distribution and $\sigma(a_i)$ is the mean-square deviation of this distribution. If the consideration is limited by the cumulants of the second order then the distribution function $\varphi(g_i)$ presents the normal distribution

$$\varphi(g_i) = (2\pi)^{-0.5} \exp(-g_i^2/2) \tag{69}$$

Hence, the determination of distribution function $\rho(a_i)$ includes approximation of distribution curves F(Q) and calculation of their first and second moments (μ_1 and μ_2); distribution cumulants on the basis of the moments ($R_1 = \mu_1$; $R_2 = \mu_2 - \mu_1^2$); cumulants $\kappa_{i,r}$ on the basis of R_{ij} and x_{ij} from Eq. (67) and $\varphi(g_i)$ from Eq. (69).

This approach was applied to the determination of silica surface distribution functions on reaction constants of organosilicon compounds chemisorption using the Gamma distribution on k (Table 4). The distribution functions on ln k were calculated on the basis of chemisorption kinetic isotherms for methylchlorosilanes $(CH_3)_{4-n}SiCl_n$ (n from 1 to 4) and for the compounds $(CH_3)_3SiX$ { X = Cl, CN, N_3, NCO, NCS, $OSi(CH_3)_3$} on the non-porous dehydrated silica surface [4,22]. As shown in [57] the correlation is observed between the logarithms of rate constants with the sum of inductive constants of substituents at Si atom in $(CH_3)_{4-n}SiCl_n$ compounds (σ_I)

$$\ln k = \rho \sum \sigma_I + b \tag{70}$$

The following average values and mean-square deviations of ρ and b constants are obtained: $\bar{\rho} = 5.51$; $\sigma_\rho = 4.14$; $\bar{b} = 6.22$; $\sigma_b = 0$. The positive sign of $\bar{\rho}$ conforms with the proposed S_Ei reaction mechanism [57] and higher value of σ_ρ reflects the considerable heterogeneity of silica surface OH groups. For the $(CH_3)_3SiX$ compounds it was established that their reactivity increases with the enhancement of electron acceptor ability of X substituent (σ_I) and with the decrease of Si–X bond strength (E^{Si-X}) [81]. Then the following linear equation can be written:

$$\ln k = a_1\sigma_I + a_2E^{Si-X} + a_3 \tag{71}$$

The average and mean-square deviation of silica surface distribution functions on the parameters of Eq. (71) are : $\bar{a}_1 = 5.88$; $\sigma_{a1} = 39.2$; $\bar{a}_2 = -0.0257$; $\sigma_{a2} = 0$; $\bar{a}_3 = 27.6$; $\sigma_{a3} = 10.2$. The positive value of $\bar{a}_1$ and negative $\bar{a}_2$ agree with the S_Ei mechanism of the reactions, and higher value of σ_{a1} also characterizes the distribution of surface OH groups on their reactivity.

Thus, the proposed approach for determination of heterogeneous oxides surface distribution functions on the coefficients of linear models may be useful for the description of chemisorption kinetics of organic compounds.

7.2. Reactivity of organosilicon compounds toward silica surface active sites

The parameters of Eq. (50) proposed above allow to determine the dependence of the concentration of chemisorbed organosilicon compounds on the oxides surface on the reaction time at various temperatures over the entire range of the surface coverage.

Earlier, the chemisorption kinetic isotherms of alkylchlorosilanes [4,57,133,140], cyclic and linear organosiloxanes [108,109] and trimethylsilylpseudohalogenides [4,58–61] on the pyrogenic silica surface have been obtained.

Table 6
Kinetic parameters of Eq. (50) for organosilicon compounds chemisorption on pyrogenic silica surface

Compound	$E_0^{\neq}$ kJ·mole^{-1}	$A^{\neq}$ cm^3·molecule^{-1}	ν	γ kJ·mole^{-1}	S_M
Kinetics measured by the decrease in the surface OH groups absorption intensity and by the gravimetry method (see also Table 2)					
$(CH_3)_3SiCl$*	35.6	$7.80 \cdot 10^{-18}$	0.33	20	0.0232
$(CH_3)_2SiCl_2$*	38.8	$1.20 \cdot 10^{-17}$	0.43	18	0.0150
CH_3SiCl_3*	36.9	$3.90 \cdot 10^{-17}$	0.40	24	0.0208
$(CH_3)(CH_2CH)SiCl_2$*	36.8	$1.30 \cdot 10^{-17}$	0.50	12	0.0221
Kinetics measured by the increase in the surface –SiX groups absorption intensity					
$(CH_3)_3SiN_3$	57.2	$2.86 \cdot 10^{-15}$	0.61	42	0.0230
$(CH_3)_3SiNCS$	21.8	$2.25 \cdot 10^{-17}$	1.15	60	0.0072
$(CH_3)_3SiNCO$	60.3	$1.06 \cdot 10^{-15}$	1.18	84	0.0120
Kinetics measured by the increase in the surface –$Si(CH_3)_3$ groups absorption intensity					
$(CH_3)_3SiCN$	12.5	$2.15 \cdot 10^{-18}$	1.34	30	0.0166
$(CH_3)_3SiN_3$	75.8	$4.79 \cdot 10^{-14}$	1.46	52	0.0163
$(CH_3)_3SiNCS$	62.7	$9.49 \cdot 10^{-15}$	1.12	50	0.0105
$(CH_3)_3SiNCO$	64.0	$5.38 \cdot 10^{-16}$	0.90	44	0.0161

*Temperature of silica surface pretreatment is 523 K. In other cases this temperature is 923 K.

Reactions of these compounds with OH groups of pyrogenic silica surface proceed via the S_Ei mechanism [4,57,108,109,133,140]. Nevertheless, it has been disclosed that, apart from the occurrence of chemisorption by the S_Ei mechanism, the dissociation of silica surface Si–O bonds occurs by the A_di mechanism in the interaction of such compounds as $(CH_3)_3SiX$ (X = N_3, NCS and NCO) [4,58–61].

Kinetics of both reactions was observed by IR spectroscopy and gravimetry. The parameters of Eq. (50) which are calculated on the basis of kinetic isotherms are presented in Tables 2 and 6.

It is obvious from Tables 2 and 6 that for the reaction of $(CH_3)_3SiCN$ running only by the S_Ei mechanism, the difference in $E_0^{\neq}$ values calculated from the change in the surface OH and $(CH_3)_3Si$ groups concentrations is minimal and reaches 16 kJ·mole^{-1}. However, the reactions of $(CH_3)_3SiX$ (X = N_3 and NCO) compounds correspond to both the S_Ei and A_di mechanisms, because of a low potential barrier of the latter process, by close $E_0^{\neq}$ values measured in kinetics of the increase of SiX and $Si(CH_3)_3$ groups concentration. It follows from the data listed in Table 2 that reactivity of the $(CH_3)_3SiX$ compounds relative to the silica surface OH groups, decreases in the series of X substituents:

$$I > Br > CN > NCS > N(CH_3)_2 > NCO > N_3 > Cl > (CH_3)_3SiO$$

In the dissociative addition to siloxane bonds of silica surface, the reactivity decreases in

the following series:

$NCS > N_3 > NCO$

Reactivity of organosiloxanes, in the interaction with the surface OH groups, decreases in the series:

$[(CH_3)(CH_2 = CH)SiO]_3 > [(CH_3)_2SiO]_3 > [(CH_3)_2SiO]_4 > (CH_3)_3SiOSi(CH_3)_3$

and reactivity of alkylchlorosilanes with these groups decreases as:

$SiCl_4 > CH_3SiCl_3 > (CH_3)_2SiCl_2 > (CH_3)_3SiCl$

7.2.1. Structure–reactivity relationships

Organosilicon compounds act, while interacting with the silica surface OH groups, as electrophilic agents. Therefore, the main properties of these compounds governing the height of a reaction potential barrier are likely to be an electrophilic ability of reactants and strength of Si–X bond that becomes weakened in the transition state. Since there are no data on most organosilicon compounds under analysis, as far as the strength of Si–X bond (E^{SiX}) is concerned, these quantities for $(CH_3)_3SiX$ compounds have been calculated by the Sanderson method [141] for various substituents X. The inductive constants of the substituents X (σ_I) were selected to make quantities describing electrophilic ability of these compounds [142]. The computed energies of Si–X bonds and σ_I constants for the series $(CH_3)_3SiX$ compounds are listed in Table 7. The correlation analysis of the linear dependencies of $E_0^{\neq}$ values for interaction of $(CH_3)_3SiX$ compounds with OH groups of pyrogenic silica surface on the E^{SiX} and σ_I parameters has disclosed that activation energies decrease with lowering the bond energy and with enhancement of inductive constant of substituent X. This dependence is described by the linear relation [79,81]

$$E_0^{\neq} = 0.29\ E^{SiX} - 274.5\ \sigma_I + 62.9\ \text{kJ} \cdot \text{mole}^{-1} \quad (n = 6;\ \sigma^2 = 318.3) \tag{72}$$

Similar regularities are observed also on comparing apparent activation energies of the conversion at the surface coverages $\Theta = 0.5$ and 1.0 with the above parameters of the $(CH_3)_3SiX$ compounds [81].

Using the parameters of Eq. (72), it is possible to estimate in a satisfactory way the change in chemisorption activation energy with organosiloxane structure varying (Table 2). Thus, $E_0^{\neq}$ can increase in coming from $(CH_3)_3SiOSi(CH_3)_3$ to $[(CH_3)_2SiO]_4$ ($\Delta E_{0\ exp}^{\neq} = 65\ \text{kJ} \cdot \text{mole}^{-1}$), which is associated with the decrease of the Si–O bond energy and the increase of electron acceptor ability of the siloxane Si atom observed with the decrease in the number of electron donor CH_3 substituents at this atom ($\Delta E_{0\ calc}^{\neq} = 25\ \text{kJ} \cdot \text{mole}^{-1}$) [65]. The difference in activation energies of cyclic organosiloxanes $[(CH_3)_2SiO]_4$ and $[(CH_3)_2SiO]_3$ interaction ($\Delta E_{0\ exp}^{\neq} = 9.6\ \text{kJ} \cdot \text{mole}^{-1}$; $\Delta E_{0\ calc}^{\neq} = 6.6\ \text{kJ} \cdot \text{mole}^{-1}$), is related to the increase of energy of strain of siloxane cycle for the last compound (23 kJ·mole^{-1}).

The decrease of $E_0^{\neq}$ in coming from $[(CH_3)_2SiO]_3$ to $[(CH_3)(CH_2{=}CH)SiO]_3$ is well explained by the increase of the siloxane Si atom electron acceptor ability observed when a CH_3 substituent is replaced by the $CH_2{=}CH$ substituent, possessing higher electron acceptor ability ($\Delta E_{0\ exp}^{\neq} = 20.6\ \text{kJ} \cdot \text{mole}^{-1}$; ($\Delta E_{0\ calc}^{\neq} = 27.5\ \text{kJ} \cdot \text{mole}^{-1}$).

A main simple way of separating a thermodynamic (enthalpy of reaction) and kinetic (internal barrier caused by, in particular, polar effects in the reaction) contributions into the potential barrier of the interaction is the Evans–Polanyi linear relation [21]

$$E_0^{\neq} = \alpha\Delta H + \beta \tag{73}$$

where ΔH is the enthalpy of reaction and β coefficient approximates the reaction potential barrier at $\Delta H = 0$. The α coefficient can describe the location of transition state on the reaction coordinate ($1 \geq \alpha \geq 0$). It seemed interesting to check up on the applicability of Eq. (73) to description of the reactions of organosilicon compound chemisorption on the silica surface. There are no data on enthalpy of such interface reactions. For the reactions of structurally similar $(CH_3)_3SiX$ compounds, the calculation of the reaction enthalpy difference is not that difficult because the product of the reaction with the surface OH groups, $Si(CH_3)_3$, is identical for all these reactants. Therefore, the reaction enthalpy proceeding by the S_Ei mechanism equals

$$\Delta H = D_{RSiX} - D_{H\text{-}X} + B \tag{74}$$

where D_{RSiX} and $D_{H\text{-}X}$ are the energies of homolytic dissociation of the Si–X and H–X bonds in the reactant and product of the interaction, B is the constant for the entire series of $(CH_3)_3SiX$ compounds. Table 7 lists the calculated ($\Delta H - B$) values for the series of organosilicon compounds, incorporating experimentally found D_{RSiX} and $D_{H\text{-}X}$ parameters [143], and those determined by the Luo and Benson's method using electronegativity of X substituents (V_X) [144].

The comparison of the data listed in Table 2 shows that the decrease in $(CH_3)_3SiX$ compounds reactivity observed in coming from X = Cl to X = $OSi(CH_3)$ ($\Delta E_{0\ exp}^{\neq}$ = 24 kJ · mole^{-1}) is caused primarily by a significant increase in the reaction enthalpy (ΔH = 229 kJ · mole^{-1}). If X is the halogen atom (Cl, Br, I), then the reaction enthalpy increases as the main quantum number of the halogen decreases. However, the difference in activation energies observed in passing from X = Cl to X = Br ($\Delta E_{0\ exp}^{\neq}$ = 72 kJ · mole^{-1}) cannot be attributed solely to the decrease in the reaction enthalpy in the series (ΔH = 12.5 kJ · mole^{-1}). It is likely that the main contribution into the decrease of height of the reaction potential barrier is made by the decrease in the energy of the lowest unoccupied molecular orbital of the silane corresponding to the σ^* of Si–X bond in coming from X = Cl to X = Br, and by the decrease in β coefficient.

It follows from Table 6 that the $E_0^{\neq}$ values, calculated for a dissociative addition to siloxane bonds of silica surface at the interaction with $(CH_3)_3SiX$ (X = N_3, NCS and NCO) compounds, are by 10 to 20 kJ·mole^{-1} lower than the activation energies of reactions of these reactants with the silica surface OH groups. The lowest $E_0^{\neq}$ value in the A_di process is displayed by the reaction with X = NCS that features the weakest Si–X bond and a substituent with the highest electron acceptor ability, while the reactions with X = NCO and X = N_3 occur to the close activation energies, which, probably, is related to the close strength of Si–X bond in these reactants.

Using Eq. (73) for chemisorption of the $(CH_3)_3SiX$ compounds on silica surface, the difference in activation energies of the reactions occurring by the S_Ei and A_di mechanisms can be related by the expression between the bond dissociation energies in the reactants and products

$$\Delta E_0^{\neq} = \alpha(D_{SiO\text{-}H} - D_{SiO\text{-}Si} + D_{Si\text{-}X} - D_{H\text{-}X}) + \Delta\beta \tag{75}$$

Table 7
The energies of Si–X bond in the $(CH_3)_3SiX$ compounds ($kJ \cdot mole^{-1}$) calculated by Sanderson method [141] (E^{SiX}), inductive σ_I constants of substituent X [142], energies of homolytic dissociation of HX compound ($D_{H\text{-}X}$) [143] and Si–X bond ($D_{RSi\text{-}X}$) calculated by Luo and Benson method [144] and relative reaction enthalpy ($\Delta H - B$) ($kJ \cdot mole^{-1}$) for reaction with surface OH group from [81]

Substituent X	E^{SiX}	σ_I	$D_{RSi\text{-}X}$	D_{HX}	$\Delta H - B$
F	555.5	0.46	648.9	565.7	83.3
Cl	597.9	0.47	474.0	427.6	46.4
Br	331.8	0.45	397.5	362.3	35.2
I	275.1	0.40	322.6	294.6	28.0
OH	340.2	0.34	536.0	498.7	37.3
SH			407.5	384.9	22.6
N_3	455.6	0.43			
NCO	496.2	0.38			
NCS	374.0	0.44			
CN	374.5	0.55			
$OSi(CH_3)_3$	467.8	0.36	811.7	536.0	275.7
OCH_3	490.8	0.27			
CH_3	308.8	– 0.05	376.6	435.1	– 58.6
SiH_3			325.9	387.0	– 61.1
$Si(CH_3)_3$			338.9	377.4	– 38.5
H	402.1	0.00	377.4	432.2	– 54.8
$CONH_2$	326.4	– 0.13			
NH_2	420.1	0.12	470.7	438.1	32.6
PH_2	272.0	0.07	544.8	284.1	260.7
$NHSi(CH_3)_3$			318.8	334.7	– 15.9
$NHCH_3$			196.6	364.8	– 168.2
$N(CH_3)_2$			209.2	359.8	– 150.6
$N(C_2H_5)_2$			548.1	448.9	99.2

where $\Delta E_0^{\neq} = E_0^{\neq}(S_Ei) - E_0^{\neq}(A_di)$, $D_{SiO\text{-}H}$, $D_{Si\text{-}OSi}$ and $D_{Si\text{-}X}$ are the energies of homolytic dissociation of OH, SiO and SiX bonds in the SiO–H, Si–OSi and Si–X surface groups of the initial and modified silica, $\Delta\beta$ is the difference between internal barriers of the S_Ei and A_di routes. The above relation shows that the difference in activation energies of two reactions will be at maximum for organosilanes with maximum $D_{Si\text{-}X} - D_{H\text{-}X}$ difference. By assuming that $D_{Si\text{-}X}$ of surface species varies like $D_{Si\text{-}X}$ for $(CH_3)_3SiX$ compounds does on varying the X substituent nature in these compounds, we can easily put down the trend in the $D_{Si\text{-}X} - D_{H\text{-}X}$ variation using the data in Table 7. It is obvious that the maximum $\Delta E_0^{\neq}$ value is observed in the case of lowest reactivity of organosilanes in the S_Ei process. This explains the observed maximum of $\Delta E_0^{\neq}$ at interaction of $(CH_3)_3SiNCO$ and $(CH_3)_3SiN_3$ as compared with $(CH_3)_3SiNCS$ having a high reactivity at interaction with both OH groups and siloxane bonds of the silica surface.

The $D_{SiO-H} - D_{Si-OSi}$ difference in Eq. (75) can be estimated proceeding from the homolytic dissociation energy by the appropriate bonds of the $(CH_3)_3SiO-H$ and $(CH_3)_3Si-OSi(CH_3)_3$ ($\Delta D = -275$ kJ · mole^{-1}). This negative ΔD value indicates that the reaction of $(CH_3)_3SiX$ compounds with main active sites of the dehydrated silica surface preferably occurs by the S_Ei as compared with the A_di route. The latter is likely to be realized at interaction of $(CH_3)_3SiX$ compounds with the stressed siloxane bridges formed due to dehydroxylation of silica surface at a high temperature of its pretreatment. Moreover, the decrease in the activation energy of A_di process on the silica surface is also possible in case a large polar contribution increases into the height of a potential barrier of the reaction due to the interaction of organosilanes with electron donor (Lewis base) active sites of the surface, that are formed during silica dehydroxylation.

The data obtained in [79–81] allow for the conclusion that organosilicon compounds, exhibiting the highest reactivity at interaction with the main active sites of dehydrated silica surface, should have a low strength of the Si–X bond and contain X substituents with high acceptor ability. Also, reactivity of the compounds increases as the reaction enthalpy decreases.

7.3. Interaction of frontier orbitals of reactants in the chemisorption on silica surface

The static quantum chemical indexes of the reactivity may be used for description of kinetics of double exchange reactions which occur through the transition state with high charges separation [17]. If a barrier height of the surface reaction is controlled by frontier orbitals interaction, then the following correlation may be fulfilled:

$$E_0^{\neq} = a_1 / \left(E_{HOMO(OH)} - EA_{LUMO(RSiX)}\right) + a_2 \qquad (76)$$

where $E_{HOMO(OH)}$ is the energy of the highest occupied molecular orbital of surface OH group cluster and $EA_{LUMO(RSiX)}$ is the energy of the lowest unoccupied molecular orbital of organosilicon molecule. Furthermore, according to the Koopmans' theorem the frontier orbital energies are given by $-E_{HOMO} = IP$; $-E_{LUMO} = EA$, where IP is the ionization potential, and EA is the electron affinity [145]. These values for organosilicon compounds and clusters of silica surface OH group were calculated by the semi-empirical quantum chemical AM1 and MNDO methods in [82].

The linear dependencies of $E_0^{\neq}$ values of the organosilicon compound chemisorption on the silica surface (Table 2) on the quantum chemical indexes of these compounds (reaction enthalpy, charges on the Si and X atoms, their electron affinity and ionization potential, electronic polarizability and dipole moment) were compared in [82]. From these data it follows that the best correlation is observed between the organosilicon compounds reactivity and their electron affinity or parameters which include EA values. According to the data obtained the relationship (76) is satisfied most often. It was found that the following linear dependence between the activation energies of the organosilicon compounds chemical reaction with the silica surface OH groups corrected for adsorption complex formation Eq. (29) ($E_{corr}^{\neq}$) and their EA values is obeyed [49]:

$$E_{corr}^{\neq} = \frac{-1.48 \cdot 10^5}{IP_{SiOH} - EA_{RSiX}} + 251 \qquad (S_M = 27.8) \qquad (77)$$

This dependence is shown in Fig. 7.

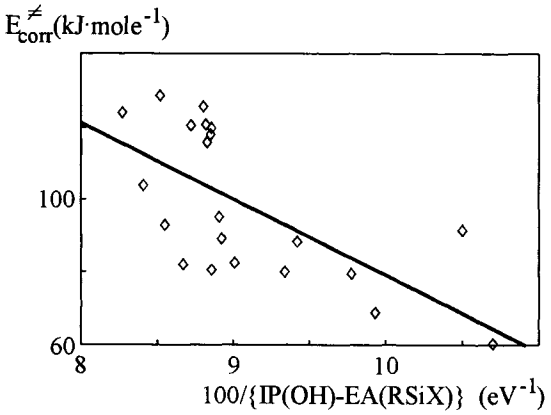

Figure 7. Dependence of organosilicon compounds chemisorption energy on the silica surface corrected for OH precursor formation on the inverse difference between ionization potential of silica surface cluster and electron affinity of the compounds. Figure taken from [49].

If the $E_0^{\neq}$ is controlled by charge transfer, then it can be determined on the basis of reactants electronegativity comparison as a surface reaction occurs through the S_Ni or S_Ei mechanisms. If inequality

$$(IP + EA)_{OH} > (IP + EA)_{RX} \tag{78}$$

is satisfied, then the reactants from the gas phase are nucleophiles, but at

$$(IP + EA)_{OH} < (IP + EA)_{RX} \tag{79}$$

ones are electrophiles. Allowance for these inequalities with the IP and EA values of the organosilicon compounds and silica clusters demonstrates that inequality (79) is satisfied and these compounds are electrophiles in the reactions with the silica surfaces. The electronegativities obtained, for the NH_3, $N(CH_3)_3$, H_2O, CH_3OH, C_2H_5OH, n-C_3H_7OH, n-C_4H_9OH fall within the interval 5.9÷8.6 eV. According to inequality (78) these compounds are nucleophiles in substitution reactions with the silica surface OH groups. These conclusions agree with the obtained correlation equations connecting logarithms of rate constant of organosilicon compound chemisorption on the silica surface with the inductive constant of substituents at the Si atom in these compounds [133], and with the quantum chemical calculations of potential energy surface profiles along a reaction pathway [47,48].

7.4. Influence of oxides structure and their temperature pretreatment on chemisorption kinetics of organosilicon compounds

In such a manner the main parameters of electronic structure of silica surface OH groups controlling precursors stability and height of activation barrier in the S_Ei or S_Ni reactions are the positive and negative maximum charges on the atoms of surface cluster and their frontier orbital energies. The identical approach with these parameters can be used for the description of organic compounds chemisorption on the parent and mixed Si, Ti and Al oxides surface. The activation energies, pre-exponential factors and other parameters

of Eq. (50) for chemisorption of various organosilicon compounds on the pyrogenic TiO_2, Al_2O_3 and mixed oxides surface [79,134] are presented in Table 8. It is seen (Tables 6 and 8), that the highest values of γ parameter are observed in these reactions. It evidences for considerable surface heterogeneity. The lower values of $E_0^{\neq}$ on Al_2O_3 surface are probably due to considerable contribution of strong complex formation between the reactant and Lewis surface sites to the measured $E_0^{\neq}$ values, Eq. (29).

It was established that in the presence of adsorbed water on the silica surface (T = 250°C) the activation energy of alkylchlorosilanes chemisorption is reduced (Table 7), probably due to interaction of water dipoles with the polar activated complex in these reactions.

Pyrogenic Al_2O_3 and TiO_2 surfaces are more reactive with respect to the organosilicon compound chemisorption than the SiO_2 surface is. It may be explained by the presence of strong Lewis acid sites on these surfaces. The addition of 30% Al to the silica matrix changes insignificantly the activation energy of hexamethyldisiloxane chemisorption; however the addition of Ti reduces the activation energy of this reaction. It may be explained by the lowered reactivity of Al–O bonds as compared to Ti–O bonds and by the absence of Al–OH groups on the surface of the mixed oxide at a high temperature of the surface pretreatment. Addition of Al or Ti to the silica matrix was found not to influence the activation energies of $(CH_3)_3SiCl$ reaction with silanol groups of mixed silicas surface as compared to the parent silica [114].

Table 8
Kinetic parameters of Eq. (50) for organosilicon compound chemisorption on the pyrogenic oxides surface

Compound	Oxide	T_p	$E^{\neq}$	γ	ν	$A^{\neq}$
		°C	$kJ \cdot mole^{-1}$			$cm^3 \cdot molecule^{-1}$
$(CH_3)_3SiOSi(CH_3)_3$	TiO_2	650	30.1	40	0.58	$1.1 \cdot 10^{-17}$
$(CH_3)_3SiOSi(CH_3)_3$	*TiSiO	650	76.4	20	0.80	$7.8 \cdot 10^{-14}$
$(CH_3)_3SiOSi(CH_3)_3$	*AlSiO	650	127.0	26	0.65	$2.2 \cdot 10^{-11}$
$[(CH_3)_2SiO]_4$	Al_2O_3	650	-0.2	34	0.34	$4.2 \cdot 10^{-20}$
$(CH_3)_3SiN(CH_3)_2$	Al_2O_3	650	12.2	22	0.78	$1.2 \cdot 10^{-17}$
$(CH_3)(CH_2{=}CH)SiCl_2$	Al_2O_3	650	-3.3	28	0.74	$2.7 \cdot 10^{-20}$
$[(CH_3)_2SiNH]_3$	Al_2O_3	650	1.2	22	0.21	$3.4 \cdot 10^{-18}$

*mixed oxides containing 30% mass Ti or Al in the SiO_2 matrix; T_p is the temperature of surface pretreatment in vacuum for 2 hours. Experimental data at different temperatures were obtained by the gravimetric method in [134].

Correlation of the parameters of heterogeneous surface active sites or its distribution functions on these parameters with activation parameters of organic compound chemisorption on the oxides surface is required for establishment of the reaction mechanism (for example, S_Ei or S_Ni). An approach for calculation of distribution functions of heterogeneous surface active sites on the donor, acceptor and polarization components of organic compounds adsorption energy using the nonlinear inverse gas chromatography

of test adsorbates possessing different donor-acceptor properties has been proposed in [146–148]. A more correct mathematically method for calculation of these distribution functions of parent and mixed Si, Ti and Al pyrogenic oxides surface is presented in [149]. It includes calculation of distribution function (sum of two uniform distribution functions) parameters on adsorption energy and cumulants of the distribution immediately from the chromatographic peak without intervening approximation and integration. The average values of distribution functions on the adsorption energies present the sum of specific (donor–acceptor or H–bond) as well as of nonspecific (mainly, dispersive) interactions between surface active sites and adsorbate molecules. The donor (DN) and acceptor (AN) numbers are the convenient parameters which determine the adsorbate ability to form the donor–acceptor or H complexes with the surface sites (acid–base parameters)

$$E_{sp} = A_2\ DN + A_3\ AN \tag{80}$$

where E_{sp} is the contribution of specific interaction into adsorption energy; A_2 and A_3 are the coefficients determining the acceptor (acid) and donor (base) parameters of surface active sites. The first central moments of distribution function on these parameters for several pyrogenic oxides surface were determined from the data of nonlinear chromatography [149].

As shown previously, the silica surface OH groups manifested as nucleophiles at the interaction with organosilicon compounds. On the hypothesis that reaction mechanism is invariant in going from the silica surface to parent and mixed Ti or Al oxides, then one would expect the decrease of chemisorption activation energy with enhancement of the surface sites donor ability parameter.

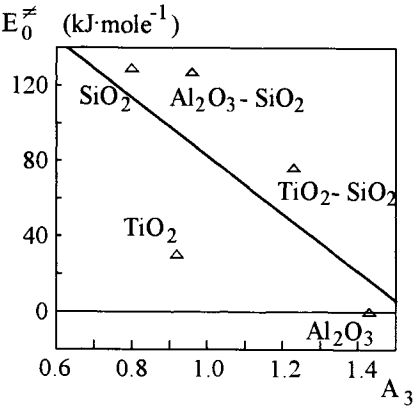

Figure 8. Dependence of hexamethyldisiloxane chemisorption activation energy on the pyrogenic oxides surface versus the first central moment of distribution on donor contribution of the surface sites to adsorption energy of organic compounds (A_3).

As can be seen from Fig. 8 the above mentioned dependence is obeyed for the hexamethyldisiloxane chemisorption on the oxides surface. Hence the most likely mechanism of the organosilicon compound chemisorption on this surface is the S_Ei mechanism.

8. CONCLUSION

Hence, the models of chemisorption kinetics on the homogeneous and discrete heterogeneous surfaces describe poorly the kinetic isotherms of organic compounds in a whole range of surface coverage at different temperatures. Isosteric activation energies of these processes strongly depend on the surface coverage. This is due to different heterogeneity types of oxide surfaces. The proposed empirical equation including the power dependence of chemisorption apparent activation energy on the surface coverage allows to describe the chemisorption kinetics of various organosilicon compounds on the Si, Ti and Al pyrogenic oxides surface in a wide range of experimental conditions and to determine the activation energy and pre-exponential factor for surface modification.

Effects of heterogeneous surface layer disordering and its topography can be studied using the solutions of simplified integral equations including the Gamma-distribution function on the chemisorption rate constants as well as the Gamma, normal or uniform distribution functions on the distances between neighbouring sites with the account for lateral interactions between chemisorbed species in the mean-field approximation. A satisfactory qualitative agreement has been found between the present model predictions and the experimental kinetic data obtained for the organosilicon compound chemisorption on the pyrogenic silica surface.

The best way to correct determination of chemisorption activation parameters on heterogeneous oxides surface includes the calculation of its both distribution functions on the activation energy and on logarithms of the pre-exponential factor and their central moments from the kinetic isotherms measured at different temperatures. Obtained from such calculations the isokinetic temperature and logarithm of rate constant at this temperature reflect the gaseous organic compound reactivity toward active sites of the heterogeneous oxides surface.

Activation energy of electrophilic substitution of silica surface OH group by organic residue decreases with the enhancement of acceptor ability of organosilicon compound and with the decrease of Si–X bond energy. The best correlation is observed between the organosilicon compounds reactivities and their electron affinities or parameters which include these values. Conclusions about the chemisorption reaction occurring through the S_Ni or S_Ei mechanisms at the Si atom of silica surface can be made on the basis of gaseous reagents and surface active site cluster electronegativities comparison. This conclusion may be spread on the chemisorption mechanisms on the surface of other element oxides.

As it follows from the quantum chemical calculations, two minima on the potential curves for the interaction of organic molecules with the silica surface OH group are due to formation of linear hydrogen-bonded and following cyclic donor-acceptor complexes prior to the transition state for proton transfer in these reactions. In case of large molecules interaction, the second minimum often missing from the potential curve and the donor-acceptor complex is consistent with the transition state of proton transfer reaction.

Simple linear relationships developed between the quantum chemical indexes of organic molecules (their maximum charges and energies of the frontier orbitals) and their empirical donor-acceptor parameters as well as the heats of the hydrogen-bonded complexes formation with silica surface OH groups or the chemisorption activation energies on this surface may be used for estimation of the complexes stability and reactivity of organic compounds towards Bronsted sites of other oxide surfaces. The electron donor ability of

surface site and electron acceptor ability of gas reactant play a leading part in the rate of electrophilic substitution of hydrogen atom of the surface OH groups, whereas the opposite properties of these reactants affect the stability of hydrogen–bonded precursors in these reactions. The overall activation reaction barrier reduces with the increase of preliminary adsorption complex stability and overall reaction rate grows.

One of the main problems of organic compound reactions proceeding on the heterogeneous oxide surfaces is possible dependence of their mechanism on the surface coverage. For instance, this deduction follows immediately from different variance of distribution functions of oxide surfaces on the donor and acceptor properties of the active sites [147–148], which determines their nucleophilic and electrophilic abilities to interact with organic compounds from the gas or liquid phase.

ACKNOWLEDGMENT

The author thanks Mr V. P. Shkilev for the technical assistance. Thanks are extended to Dr. V. M. Gunko for providing the quantum chemical calculations of organosilicon compounds and clusters of oxide surfaces; Dr. E. F. Voronin, Dr. A. M. Varvarin, Dr. G. Ya. Guba, Prof. A. A. Chuiko and Prof. V. A. Tertykh for providing the presentation of original kinetic isotherms of organosilicon compounds chemisorption from the gas phase on the pyrogenic oxide surfaces. The author also acknowledges Sherwin–Williams Co. (Ohio, USA) for the financial support of this work.

REFERENCES

1. R.K.Iller, The Chemistry of Silica, Wiley, New York, 1979.
2. M.I.Hair, Infrared Spectra of Surface Compounds, Wiley, New York, 1975.
3. H. Knozinger, P. Ratnasamy, Catal. Rev.–Sci. Eng., 17 (1978) 31.
4. V. A. Tertykh and L. A. Belyakova, Chemical Reactions with Participation of Silica Surface, Kiev, Naukova Dumka, 1991 (in Russian).
5. E.P.Plueddemann, Silane Coupling Agents, Plenum Press, New York, 1982.
6. K.K.Unger, J.Chromatogr.Library, vol.16, Elsevier, Amsterdam, 1979.
7. J. Nawrocki and B. Buszewski, J. Chromatogr. Rev., 449 (1988) 1.
8. W. H. Pirkle and T. C. Pochapsky, Chem. Rev., 89 (1989) 347.
9. W. M. Heckl, F. M. Marassi, K. M. R. Kallury, D. C. Stone and M. Thompson, Anal. Chem., 62 (1990) 32.
10. C. Airoldi and E. F. Alcantara, Colloids Surf., 39 (1989) 291.
11. A. C. Zettlemoyer, F. T. Micale, K. Klier, in: Water in Dispersed Systems, F. Franks (ed.), Plenum, New York, , vol. 5, 1975.
12. H. Muramatsu, J. M. Dicks, E. Tamlya and I. Karube, Anal. Chem., 59 (1987) 2760.
13. M.D. Matteucci and M.H.Caruthers, J.Am.Chem. Soc., 103 (1981) 3185.
14. E.Barastel, D.Blanchi, G.Rialdi, Pure Appl. Chem., 63 (1991) 1483.
15. P. R. Moses, L. Weir and R. W. Murray, Anal.Chem., 45 (1975) 1882.
16. J. N. Bronsted, Chem. Rev., 6 (1928) 231.

17. G.Klopman (ed.), Chemical Reactivity and Reaction Paths, Wiley, New York, 1974.
18. J. E. Leffler and E. Grunwald, Rates and Equilibria of Organic Reactions, Wiley, New York, 1963.
19. G. S. Hammond, J. Am. Chem. Soc., 77 (1955) 334.
20. F. H. Westheimer, Chem. Rev., 61 (1961) 265.
21. A. Pross, Adv. Phys. Org. Chem., 14 (1977) 69.
22. A. A. Chuiko and Yu. I. Gorlov, Chemistry of Silica Surface: Surface Structure, Active Sites and Adsorption Mechanisms, Kiev, Naukova Dumka, 1992 (in Russian).
23. B. Evans and T. E. White, J. Catal., 11 (1968) 336.
24. M. L. Hair and W. Hertl, J. Phys. Chem., 73 (1969) 2372.
25. W. Hertl, J. Phys. Chem., 72 (1968) 1248.
26. B. C. Bunker, D. M. Haaland, T. A. Michalske and W. L. Smith, Surf. Sci., 222 (1989) 95.
27. F.Buzek and J.Rathousky, J.Colloid Interface Sci., 79 (1981) 47.
28. G. A. Somorjai, Chemistry in Two Dimensions Surfaces, Cornell University Press, Ithaca, New York, 1981.
29. M. Jaroniec and R. Madey, Physical Adsorption on Heterogeneous Solids, Elsevier, Amsterdam, 1988.
30. Yu. Tovbin, Theory of Physicochemical Processes at Gas–Solid Interface, Mir Publishers: Moscow, and CRC Press, Inc.: Boca Raton, FL., 1991.
31. E. Shustorovitch, Adv. Catal., 37 (1990) 101.
32. V. P. Zdanov, Elementary Physicochemical Processes on Solid Surfaces, Plenum, New York, 1991.
33. D. Nicholson and N. G. Parsonage, Computer Simulation and the Statistical Mechanics of Adsorption, Academic Press, London, 1982.
34. P. Pichat, M. N. Mozzanega, H. Courbon, J. Chem. Soc. Faraday Trans., 83 (1987) 697.
35. T. Yamanaka and K. Tanabe, J. Phys. Chem., 79 (1975) 2409.
36. K. Kobayakawa, Y. Nakazawa, M. Ikeda, Y. Sato and A. Fujishima, Ber. Bunsen-Ges. Phys. Chem., 94 (1990) 1439.
37. D.F.Sindorf and G.E.Maciel, J.Am.Chem. Soc., 105 (1983) 1487.
38. C. E. Bronnimann, R. C. Ziegler and G. E. Maciel, J. Am. Chem. Soc., 110 (1988) 2023.
39. D. W. Sindorf, and G. E. Maciel, J. Phys. Chem., 86 (1982) 5208.
40. P. de Mayo, Pure Appl.Chem., 54 (1982) 1623.
41. B. C. Bunker, D. M. Haaland, K.J. Ward, T. A. Michalske, W. I. Smith, J. S. Binkley, C. F. Melius and C. A. Balfe, Surf. Sci., 210 (1989) 406.
42. B. A.Morrow and I. A. Cody, J. Phys. Chem., 80 (1976) 1995.
43. B. A.Morrow and I. A. Cody, J. Phys. Chem., 80 (1976) 1998.
44. B. A.Morrow, I. A. Cody and L. S. M. Lee, J. Phys. Chem., 80 (1976) 2761.
45. J. B. Peri and R. B. Hannan, J.Phys.Chem., 64 (1960) 1526.
46. P. V. Kamat, S. Das, K. G. Thomas and M. V. George, Chem. Phys. Lett., 178 (1991) 75.
47. V. M. Gunko, E. F. Voronin, E. M. Pakhlov, and A. A. Chuiko, A. A. Langmuir, 9 (1993) 716.

48. E. F. Voronin, V. M. Gunko, E. M. Pakhlov and A. A. Chuiko, in: Chemistry, Physics and Technology of Surface, vol. 1, Naukova Dumka, Kiev, 1993 (in Russian).
49. V. I. Bogillo and V. M. Gunko , Langmuir (in press).
50. K. B. Yerrick and M. E. Russell, J.Phys.Chem., 68 (1964) 3752.
51. V. M. Gunko, Kinetika i Kataliz, 32 (1991) 1124.
52. V. M. Gunko, Kinetika i Kataliz, 32 (1991) 322.
53. V. M. Gunko, V. A. Basuyk and T. V. Chernyavskaya, Ukr. Khim. Zhurn., 56 (1990) 571.
54. V. M. Gunko, S. S. Silchenko and V. I. Bogomaz, Teoret. i Eksperim. Khimiya, 27 (1991) 715.
55. S. W. Benson, J.Chem.Phys., 20 (1952) 1605.
56. J. P. Blitz, D. S. Shreedhara and D. E. Leyden, J. Colloid Interface Sci., 126 (1988) 387.
57. V. A. Tertykh, V. V. Pavlov, K. I. Tkachenko and A. A. Chuiko, Teoret. i Eksperim. Khimiya, 11 (1975) 823.
58. V. A. Tertykh, L. A. Belyakova, A. M. Varvarin, L. A. Lazukina and V. P. Kuhar, Teoret. i Eksperim. Khimiya, 18 (1982) 717.
59. A. M. Varvarin, L. A. Belyakova, V. A. Tertykh, L. A. Lazukina and V. P. Kuhar, Teoret. i Eksperim. Khimiya, 24 (1988) 496.
60. A. M. Varvarin, L. A. Belyakova, V. A. Tertykh, L. A. Lazukina and V. P. Kuhar, Teoret. i Eksperim. Khimiya, 23 (1987) 117.
61. A. M. Varvarin, L. A. Belyakova, V. A. Tertykh, L. A. Lazukina and V. P. Kuhar, Dokl. AN SSSR, 293 (1987) 1390.
62. G.Mertens and J.J.Fripiat, J.Colloid Interface Sci., 42 (1973) 169.
63. L. T. Zhuravlev, Colloids Surf., A, 74 (1993) 71.
64. Kyung Byung Yoon, Chem. Rev., 93 (1993) 321.
65. M. G. Voronkov, V. P. Mileshkevich and Yu. A. Yuzhelevskii, Siloxane Bond, Nauka, Novosibirsk, 1976 (in Russian).
66. J.Crank, The Mathematics of Diffusion, Clarendon Press, London, 1965.
67. V.L.Snoeyink and W.J. Weber, Jr., Adv. Chem.Ser., 79 (1968) 112.
68. J. Hanika, V. Machek, V. Nemec, V. Ruzicka, and J. Kunz, J. Catal., 77 (1982) 248.
69. W. J. Albery, P. N. Bartlett, C . P. Wilde and J. R. Darwent, J. Am. Chem. Soc., 107 (1985) 1854.
70. V. I. Bogillo, V. P Shkilev and V. M. Gunko, in Proc. of 400 Anniv. Symp. "Advances in the Measurement and Modelling of Surface Phenomena", San Luis, Argentina, 1994.
71. R. S. Drago, Coord.Chem.Rev., 33 (1980) 251.
72. V. Gutman, The Donor–Acceptor Approach to Molecular Interaction, Plenum Press, New York, 1978.
73. V. I. Bogillo, Ukr. Khim. Zhurn, 57 (1991) 1274.
74. N. Cardona–Martinez, J. A. Dumesic, J. Catal., 128 (1991) 33.
75. F. M. Fowkes, J. Adhesion, 5 (1972) 155.
76. A. Vidal, E. Papirer, W. M. Jiao and J. B. Donnet, Chromatographia, 23 (1987) 121.

77. G. Curious, V. Ya. Davydov, A. V. Kiselev, S. A. Kiselev and B. A. Kuznetsov, J. Colloid Interface Sci., 48 (1974) 58.
78. V. Ya. Davydov, A. V. Kiselev, and B. V. Kuznetsov, Zhurn. Fiz. Khimii, 39 (1965) 2058.
79. V. I. Bogillo, React. Kinet. Catal. Lett., 50 (1993) 75.
80. V. I. Bogillo, Ukr. Khim. Zhurn., 58 (1992) 144.
81. V. I. Bogillo and A. A. Chuiko, Ukr. Khim. Zhurn., 59 (1993) 920.
82. V. M. Gunko, V. I. Bogillo and A. A. Chuiko, Acta Chem. Hung. Models in Chemistry, 131 (1994) 561.
83. J. Sauer, J. Mol. Catal., 54 (1989) 312.
84. G. E. Murch, and A. S. Nowick, Diffusion in Crystalline Solids, Academic Press, New York, 1984.
85. A. G. Naumovets and Yu. S. Vedula, Surf. Sci. Rept., 4 (1985) 365.
86. V.Pereyra, G.Zgrablich and V.P.Zdanov, Langmuir, 6 (1990) 691.
87. V. Pereyra and G. Zgrablich, Langmuir, 6 (1990) 118.
88. D. W. Bassett, in: Surface Mobilities on Solid Materials, V. T. Binh (ed.), Wiley, New York, 1983.
89. S. A. Pavlov and M. A. Bruk, Dokl. AN SSSR, 271 (1983) 387.
90. J.Stahlberg, M.Almgren and J.Alsins, Anal. Chem., 60 (1988) 2487.
91. C. S. Turchi and D. F. Ollis, J. Catal., 122 (1990) 178.
92. I. Langmuir, Trans. Faraday Soc., 17 (1921) 621.
93. B. Jenny and P. Pichat, Langmuir, 7 (1991) 947.
94. R. Smoluchowski, J. Phys. Chem., 87 (1983) 4229.
95. V. A. Bakaev, Surf. Sci., 198 (1988) 571.
96. J. Jagiello, G. Ligner and E. Papirer, J. Colloid Interface Sci. 137 (1990) 128.
97. S. Beran , J. Mol. Catal., 23 (1984) 31.
98. S. Beran, Z. Phys. Chem. Neue Folge, 137 (1983) 89.
99. K. P. Shroder, J. Sauer, M. Leslie and C. R. Catlow, Zeolites, 12 (1992) 20.
100. G. M. Zidomirov and V. B. Kazanski, Adv. Catal., 34 (1985) 131.
101. Yu. I. Gorlov, V. I. Zaets and A. A. Chuiko, Teoret. i Eksperim. Khimiya, 22 (1987) 533.
102. Yu.K.Tovbin and V.K.Fedyanin, Kinetika i Kataliz, 19 (1978) 1202.
103. D.V.Kundirenko, L.A.Rykova and A. A. Chuiko, Dopov. AN USSR, Ser.B. No. 9 (1989) 41.
104. D.V.Kundirenko, Ph.D. Thesis, Institute of Surface Chemistry, Kiev, Ukraine, 1990.
105. V. I. Bogillo and V. P. Shkilev , Langmuir (in press).
106. W. Hertl, J. Phys. Chem., 72 (1968) 3993.
107. W. Hertl, M. L. Hair, J. Phys. Chem., 75 (1971) 2181.
108. G. Ya. Guba, V. I. Bogillo and A. A. Chuiko, Teoret. i Eksperim. Khimiya, 28 (1992) 167.
109. V. V. Pavlov, G. Ya. Guba and A. A. Chuiko, Adsorbtsiya i Adsorbenty, No. 8 (1980) 35.
110. P. J. Crickmore and B. W. Wojciechowski, J. Chem. Soc., Faraday Trans. I, 73 (1977) 1216.
111. R.R.D.Kemp and B.W.Wojciechowski, Ind. Eng. Chem. Fund., 13 (1974) 332.
112. A. G. Ritchie, J. Chem. Soc., Faraday Trans. I, 73 (1977) 1650.

113. E. M. Pakhlov, Yu. V. Plyuto, E. F. Voronin and A. A. Chuiko, Teoret. i Eksperim. Khimiya, 23 (1987) 252.
114. E. M. Pakhlov, E. F. Voronin, V. I. Bogillo and A. A. Chuiko, Dopov. AN USSR, Ser.B (1989) 50.
115. M. I. Temkin, Zhurn. Fiz. Khimii, 11 (1938) 169.
116. M. I. D. Low, Chem. Rev., 60 (1960) 267.
117. E. T. Valtcheva, React. Kinet. Catal. Lett., 29 (1985) 137.
118. V. I. Levin, Uspekhi Khimii, 17 (1948) 174.
119. S. V. Roginskij, Adsorption and Catalysis on Heterogeneous Surfaces, Acad. Sci.USSR, Moscow, 1948.
120. A. N. Tihonov, Sov. Math. (Providence), 4 (1963) 1624.
121. A. B. Vasilieva and V. A. Tihonov, Integral Equations, Moscow State University, Moscow, 1989 (in Russian).
122. W. A. House, J. Colloid Interface Sci., 67 (1978) 166.
123. P. H. Merz, J. Comput. Phys., 38 (1980) 64.
124. M.Szombathely, P.Brauer and M.Jaroniec, J.Comput.Chem., 13 (1992) 17.
125. E.I.Benegas, V.D.Pereyra and G.Zgrablich, Surf. Sci., 187 (1987) L647.
126. W. A Steele, J.Phys.Chem., 67 (1963) 2016.
127. W. Rudzinski and D. H. Everett, Adsorption of Gases on Heterogeneous Surfaces, Academic Press, New York, 1992.
128. V. P. Zdanov, Surf. Sci. Rept., 12 (1991) 183.
129. A. K. Galley, Adv. Catal., 26 (1977) 247.
130. V.I.Bogillo and V.P.Shkilev, Kinetika i Kataliz, (in press).
131. V. I. Bogillo and V. P. Shkilev, Abstr. XIII Europ. Conf. on Chemistry at Interfaces, Kiev, Ukraine, 1994.
132. V. P. Shkilev and V. I. Bogillo, React. Kinet. Catal. Lett., 50 (1993) 355.
133. A. A. Chuiko, Ph.D. Thesis, Institute of Physical Chemistry, Kiev, Ukraine, 1971.
134. V. I. Bogillo, E. F. Voronin, V. I. Doroshenko and A. A. Chuiko, Ukr. Khim. Zhurn., (in press).
135. M. W Cole, N. S. Holter and P. Pfeifer, Phys. Rev.B, 33 (1986) 8806.
136. V. V. Turov and V. I. Bogillo, Abstr. XVI Ukr. Conf. on Organic Chemistry, Ternopol, Ukraine, 1992.
137. V. I. Bogillo, Extended Abstr. Int. Conf. Oxide Surface Chemistry and Reaction Mechanisms, Kiev, Ukraine, 1992.
138. V.I.Bogillo and V.P.Shkilev, Ukr.Khim.Zhurn. (in press).
139. G. A. Korn and T. M. Korn, Mathematical Handbook for Scientists and Engineers, Nauka, Moscow, 1968 (in Russian).
140. V.A.Tertykh, V.V.Pavlov, K.I.Tkachenko and A.A.Chuiko, Teoret. i Eksperim. Khimiya, 11 (1975) 174.
141. R. T. Sanderson, J. Phys. Chem., 105 (1983) 2259.
142. A. N. Vereshchagin, Inductive Effect. Constants of Substituents for Correlation Analysis., Nauka, Moscow, 1988 (in Russian).
143. V. N. Kondratev, (ed.), Dissociation Energy of Chemical Bonds. Ionization Potentials and Electron Affinities, Nauka, Moscow, 1974 (in Russian).
144. J. R. Luo and S. W. Benson, J. Phys. Chem., 92 (1989) 4643.
145. T. Koopmans, Physica, 1 (1934) 104.

146. V. I. Bogillo, Proc. Int. Symp. Effects of Surface Heterogeneity in Adsorption and Catalysis on Solids, Lublin, Poland, 1992.
147. V.I.Bogillo and A.A.Chuiko, Dopov. AN Ukraine, Ser.B, No. 4, (1993) 121.
148. V.I. Bogillo, A.S.Semenyuk and E.V.Utlenko, Ukr.Khim.Zhurn. 60 (1994) 326.
149. V.I.Bogillo, V.P.Shkilev and A.Voelkel, Ads. Sci. & Techn. (submitted for publication).

A. Dąbrowski and V.A. Tertykh (Editors)
Adsorption on New and Modified Inorganic Sorbents
Studies in Surface Science and Catalysis, Vol. 99

Chapter 1.10
Functionalized polysiloxane sorbents: preparation, structure, properties and use

Yu. L. Zub[a] and R. V. Parish[b]

[a]University of Kiev—-Mohyla Academy, 254070 Kiev, Ukraine

[b]University of Manchester, Institute of Science and Technology, Department of Chemistry, Manchester M60 1QD, United Kingdom

Frequently Used Abbreviations:

acac – Acetyl acetone, $[(CH_3)CO]_2CH_2$
APTES – 3-Aminopropyltriethoxysilane, $(C_2H_5O)_3Si(CH_2)_3NH_2$
CPTMS – 3-Chloropropyltrimethoxysilane, $(CH_3O)_3Si(CH_2)_3Cl$
dien – bis(2-aminoethyl)amine, $NH(CH_2CH_2NH_2)_2$
Et – Ethyl, C_2H_5
DMF – N,N′- Dimethylformamide
en – 1,2 - Diaminoethane, $H_2N(CH_2)_2NH_2$
ES – Electronic Spectra
FPS – Functionalized Polysiloxane Sorbent(s)
M^{+n} – Metal ion
Me – Methyl, CH_3
PAPS – Poly(3-aminopropyl)siloxane
PCMS – Poly(chloromethyl)siloxane
PCPS – Poly(3-chloropropyl)siloxane
PHS – Polyhydrosiloxane
PMS – Polymethylsiloxane
PMMS – Poly(mercaptomethyl)siloxane
PMPS – Poly(3-mercaptopropyl)siloxane
PPhS – Polyphenylsiloxane
PPS – Polyphosphinosiloxane
PVS – Polyvinylsiloxane
py – Pyridine, C_5H_5N
$r_{eff.}$ – effective pore radius
$S_{sp.}$ – specific surface area
TEOS – Tetraethoxysilane, $Si(OC_2H_5)_4$
TMS – Tetramethylsilane
V_{macro} – sorption volume of macropores
V_s – maximal sorption volume of pores
$V_{tot.}$ – total sorption volume of pores

1. INTRODUCTION

Functionalized polysiloxane sorbents (FPS) are spatially cross-linked organosilicon polymers with a controllable porous structure, which are not soluble, and do not swell in known common solvents. Their intermediate position among typical inorganic materials (silicas, silicates, quartz, etc.) and organic polymers results from their chemical compo-

sition and properties, since they contain both a silicon–oxygen framework and organic radicals (functional groups) attached to silicon atoms.

FPS are usually prepared by hydrolytic polycondensation of a mixture of tri– and tetra–functional organosilicon monomers, i.e., $R'Si(OR)_3$ and $Si(OR)_4$, respectively. The whole volume of the reaction mixture forms a hydrogel, which allows for the use of systems containing one, two or more components. After the hydrogel is aged, washed and dried, porous solids, xerogels are formed.

The surface of FPS is characterized by the presence of at least three dominant types of groups: hydrophobic hydrocarbon radicals R′ bonded to silicon atoms, often containing electron–donating or electron–accepting groups; residual silanol groups, ≡Si–OH, where the polymer chain terminates; oxygen atoms of siloxane bonds, ≡Si–O–Si≡. Such a variety of the surface character allows for interactions with different sorbates:

1. coordination interaction e.g., metal or hydrogen ions with donor and/or acceptor groups of the R′ radical,
2. molecular sorbent–sorbate interaction which may involve orientation, induction and dispersion effects,
3. hydrophobic interaction between hydrocarbon groups of sorbed substances and hydrophobic groups of the R′ group in the sorbent,
4. proton donation or cation exchange by residual silanol groups,
5. interaction of the oxygen atoms of siloxane chains with molecules which contain proton– donor groups.

By varying the conditions of gelation i.e. pH of the medium, sol concentration, duration of ageing, nature of the original reactants, presence of an intermicellar liquid, control of temperature during gel sedimentation and drying, conditions of hydrothermal treatment, etc., it is possible to devise syntheses of FPS with porous structures and a range of desired parameters. The sorption properties of such materials are determined essentially by the nature, sizes and geometry of the organic substituents on the silicon atoms.

Classification of FPS can be made on the basis of different features, for example:
– nature of the functional group,
– composition of the siloxane chain.
The former can be divided into two types: type A – sorbents containing saturated organic radicals on their surface (methyl, phenyl, etc.); type B – sorbents containing electron–accepting (vinyl, etc.) or electron–donor (amine, thiol, etc.) groups. Type A and B are thus clearly differentiated. However, in principle, functional groups of both types may be present simultaneously on the surface of sorbents.

Modification of organosilicon sorbents by metallic complexes in the gelation stage leads to the formation of a separate group of metal–containing FPS. Depending on the nature of the complex and a number of other factors the central metal atoms may or not become incorporated in the siloxane chain. In the first case a siloxane chain will contain chemically bonded heteroatoms, and the sorbents themselves can be of types A and B. In the second case, the nature of binding of the complex in a sorbent body may be quite different.
A monograph by Slinyakova and Denisova [1] published in 1988 generalized the results of the experimental investigations of FPS carried out for many years. They synthesized and studied mainly sorbents of type A, e.g. PMS, PPhS. In addition, the attention was also paid to same type B sorbents: PVS, PHS as well as sorbents containing various

heteroatoms e.g. Al, Ti, Zr in the siloxane chain. The present review presents the recent studies of FPS of type B and FPS containing the inserted transition–metals complexes.

2. METHODS OF PREPARATION AND STRUCTURES OF FPS

To prepare FPS containing surface groups such as amine, substituted phosphine, thiol, or halide, bonded to silicon by alkyl or similar chains, two–component systems are usually used (see Scheme 1):

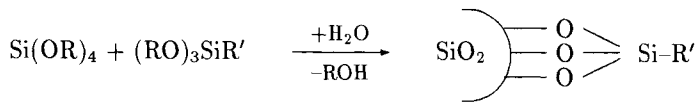

(1)

where R = Me, Et; R′ = $-(CH_2)_3NH_2$, $-(CH_2)_2PPh_2$, $-(CH_2)_3SH$, $-(CH_2)_3Cl$, etc.

The hydrolysis of $Si(OR)_4$ during polymer formation provides a cross–linking element, and is a structure – forming component [2]. However, PHS [1] as well as a number of other FPS can be also obtained by using a single–component system (see below).

The preparation of FPS containing amines as functional groups (PAPS) is one of the simplest. One of the first such studies is that by Neimark and coworkers [3], which is based on the hydrolysis of TEOS and APTES dissolved in methanol in an alkaline medium. A more detailed description of the preparation of both PAPS and a sorbent with a diaminoethane group has been given by Khatib and Parish [2], Scheme 1, R′= $-(CH_2)_3NH_2$ or $-(CH_2)_3NH(CH_2)_3NH_2$. In these cases the base necessary to catalyse, the hydrolysis and condensation was provided by one of the reagents. The hydrolysis of APTES alone (under these conditions) results in the formation of a mixture of oligomers which is completely soluble in water [2]. The optimum ratio for obtaining solid polymers was 1:2 (APTES/TEOS). There occurs formation of amine–containing oligomers which are removed from the xerogel during washing. Below this ratio, although loss of reactants is decreased, the number of nitrogen–containing groups also decreases. At the optimum ratio of reactants the NH_2 –content is $[NH_2]$ ~3.0 mmol/g.

From the stoichiometry of the initial reaction mixture, the simplest structure for these FPS would be a two–dimensional ladder matrix (see Scheme 2):

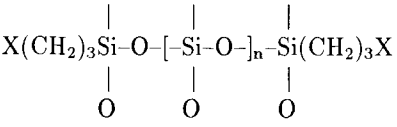

(2)

where X = $-NH_2$; $-NH(CH_2)_2NH_2$, etc.; n = 4.

The molar ratio of C/N is consistent with the suggested structure. However, the absolute quantities of these elements are smaller than those calculated for n = 4, but they are close to the compositions with n=6.5 for X= $-NH_2$ or n=8.4 for X = $-NH(CH_2)_2NH_2$. These average values show that in the condensation process there is partial oligomerisation of the aminosilanes. These oligomers are lost during washing of the xerogels which leads to an increase in the proportion of the number of "skeletal" SiO_4 groups.

Of course, the nature of the organic functional group exerts an influence on the structure and, as a consequence, on the stoichiometry of the eventual polymer. The real structure

of PAPS is undoubtedly more complex than that shown in Scheme 2. This was confirmed by the studies of Zub et al. in which water was added only after mixing the TEOS and APTES [4,5]. The IR spectra of these samples showed absorption bands of NH_2 groups at 3300 and 3365 cm^{-1}; this range indicates participation of these groups in hydrogen bonds. A strong absorption due to the vibrations of Si–O bonds was found in the range of 900–1200 cm^{-1}, which consisted of two components; 1060 and 1160 cm^{-1}. According to Finn and Slinyakova [6], this points to the formation of a three–dimensional framework of siloxane bonds.

The hydrolytic condensation of TEOS with CPTMS gives an FPS with surface chloropropyl groups. Catalysis of the condensation by both $Bu_2Sn(OAc)_2$ and HCl was used [2,7]. The former leads to the incorporation of tetrahedral Bu_2SnO_2 groups into the polymer (Sn–119 Moessbauer evidence [8]); the latter gives clean polymers and allows for wider TEOS : CPTMS ratios down to 1:1. The chloropropyl groups have been functionalized with many ligand groups: simple amines, chelating amines such as dien, Schiff bases, aminoacids [$-NHCH_2CO_2H$, $-N(CH_2CO_2H)_2$] and macrocycles [7,9], see Scheme 3. The functionalization reaction is sometimes restricted by narrow pores; $r_{eff.}$ for 3–aminopropyl– and 3–chloropropyl–functioanlized polymers is 44 and 33 Å, respectively [5,7]. For instance, 75% replacement of chlorine is achieved by the reaction with aniline, but only about 5% with diphenylamine [8]. Surprisingly, the macrocycle shown in Scheme 3 gave about 30% reaction [7]; however, in this case the starting material was 3–iodopropyl–functionalized, which gives greater reactivity.

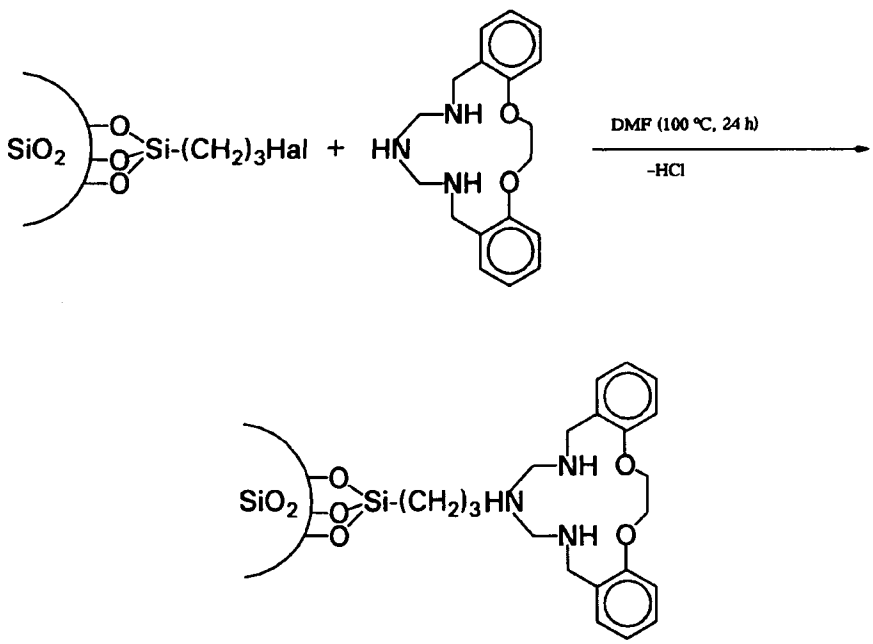

(3)

The synthesis of FPS containing en as a functional group was also carried out using a three -component system – a vinyl group acting as a "spacer" [10] obtained by taking $(MeO)_3Si-CH=CH_2$ as one of three initial reagents.

The hydrolytic polycondensation of P– and S–containing organotrialkoxysilanes with TEOS (1:2) was carried out (see Scheme 1, R'= $-(CH_2)_nPPh_2$, n = 2 and 3 [8]; R'= $-(CH_2)_3SH$ [2]). Non–aqueous solvents such as toluene or ethanol were used in the preparation of PPS with $(n-Bu)_2Sn(CH_3COO)_2$ as a catalyst. A disadvantage of this system is the incorporation of the catalyst into the polymer [8]. An attempt at the hydrolytic polycondensation of the phosphorus containing silanes again led to oils soluble in, for example, $CHCl_3$ [8]. Possibly, oligomeric siloxanes similar to those described by Brisdon and Watts [11] are formed. It should be also noted that the first reported synthesis of PPS [12] used a two–component system. Two other methods where employed in PPS preparation [8]:

a) solid PVS, obtained from the reaction of TEOS with $(EtO)_3SiCH=CH_2$, was treated with PPh_2H under an UV irradiation,
b) FPS derived from TEOS/CPTMS was treated with diphenylphosphine.

In the former case, only 10 % of vinyl groups took part in the interaction after 100 h but in the latter, 25 % reaction was obtained during 24 h. The first result is probably due to the opacity of the polymer, excluding the UV from the centre of the particles. Another observation suggests that fraction of the functional groups may be inaccessible to voluminous reactants.

Solid–state ^{29}Si NMR spectra were obtained for phosphine–containing polymers [8]. Two major signals were found with the centers at 105 and 60 ppm in relation to TMS which corresponds to silicon in $Si(O)_4$ and $(O_3)SiR'$ groups [R' = $-(CH_2)_nPPh_2$ (n = 2 or 3)]. The signals were wide and consisted of at least two peaks, possibly indicative of the existence of chains with different sets of neighbouring groups, for example, $Si(OSiO_3)_4$, $Si(OSiO_2R')(OSiO_3)_3$ etc. ^{13}C NMR spectra exhibit signals typical for such groups as $-C_6H_5$; $-OCH_2-$; $-CH_2-$; CH_3COO. Strong signals were found in ^{31}P NMR spectra at 9 and 17 ppm corresponding to $(CH_2)_nPPh_2$ groups. There was no evidence for the presence of phosphine– oxide groups. These data confirm the formation of rigid three–dimensional siloxane matrices in which 15–25 % of silicon atoms bear ligand groups [8].

In contrast to the 3–chloropropyl system, it is possible to prepare pure PCMS from the one–component system – $ClCH_2Si(OEt)_3$ [13,14]. Ethanol, DMF, diethyl ether, acetone and dioxane were used as solvents. The xerogel of PCMS was obtained as a porous white solid of the composition $(ClCH_2SiO_{3/2})_n$, insoluble in organic solvents and water. The porous structure of PCMS depends markedly on the nature of the organic medium used during sedimentation of the gel. An alcoholic medium gave a wide–pore adsorbent with a high content of mesopores. Pore volumes towards the benzene are following: V_s = 1.28 cm^3/g, $V_{tot.}$ = 1.37 cm^3/g, V_{macro} = 0.09 cm^3/g and S_{sp} =155 m^2/g). Adsorbents prepared in acetone, DMF or dioxane possess a macroporous structure with a low content of sorption pores, e.g. the pore volume (cm^3/g, C_6H_6) for PCMS prepared from dioxane is: V_s = 0.52, $V_{tot.}$ = 1.96, V_{macro} = 1.44, S_{sp} = 196 m^2/g. For a sorbent prepared from DMF: V_s = 0.39, $V_{tot.}$= 1.82, V_{macro} = 1.43, S_{sp} = 137 m^2/g. The use of diethyl ester favours the formation of PCMS with a high surface area (S_{sp} (C_6H_6) = 259 m^2/g), twice as great as that upon sedimentation in an alcoholic medium. Removal of the lyogel by washing this sorbent with ethanol leads to an increase in a sorption volume of pores and S_{sp} as compared

to the samples washed out with water [14]. Change in the concentration of $ClCH_2Si(OEt)_3$ in the reactant mixture influences slightly the porous structure of the PCMS xerogel. Calculation of the effective pore radius from the isotherm adsorption curves shows that the pore volume distributions for all PCMS samples do not have a maximum at any given radius, but give a wide distribution. This shows that the synthesized adsorbents are of various structures, and pores of a dominating size are not found.

The synthesis of FPS containing sulphhydryl functional groups also using a single- component system was reported[15–17]. Mercaptomethyltrimethoxysilane $(CH_3O)_3SiCH_2SH$ was first hydrolysed in alcohol–dioxane with an acid catalyst followed by condensation of the hydrolysis product in an alkaline medium, pH 7.8 – 8.2. The final product was a solid, porous, chalk-like, elastic sorbent, of composition corresponding to $HSCH_2SiO_{3/2}$. The existence of SH group is confirmed by an intense band in the IR spectrum of the xerogel near 2560 cm^{-1}. In the region of vibrations of the silicon–oxygen skeleton there were observed vibrational bands of a Si–O bond at 1140 and 1055 cm^{-1}, typical for spatially cross-linked FPS. The suggestion that this xerogel is spatially cross-linked into a three-dimensional polymeric skeleton is confirmed by its insolubility, its non-swelling in such organic solvents as benzene, hexane, alcohol, acetone, dioxane, etc. and its infusibility.

Poly[bis(2-silsesquioxanylethyl)sulphide] was synthesized by a hydrolytic polycondensation of bis(2-triethoxysilylethyl)sulphide [18] (Scheme 4):

$$[(EtO)_3Si(CH_2)_2]_2S \xrightarrow[-\ EtOH]{+\ H_2O} [-O_{3/2}Si(CH_2)_2S(CH_2)_2SiO_{3/2}-]_m \qquad (4)$$

It is a white powder, non-melting, insoluble in water and organic solvents with a bulk density of 0.5 g/cm^3 and a real density of 0.71 g/cm^3.

In a similar way, using bis-N,N′-(3-triethoxysilylpropyl)thiourea [19], a spatially cross-linked polymer was thiourea groups was prepared [20] (Scheme 5):

$$[(EtO)_3Si(CH_2)_3NH]_2C=S \xrightarrow[t,\ pH\ 8-9]{+\ H_2O,\ -EtOH} [O_{3/2}Si(CH_2)_3NH]_2C=S \qquad (5)$$

This sorbent has granules of a spherical form with particle sizes of 0.7–1.5 mm; it is white, insoluble and non-swelling in water and organic solvents. It is inflammable and not toxic (LD_{50} > 5000 mg/kg). A distinguishing feature of this polymer is its high chemical and thermal stability. Thus, the temperature at which oxidative thermodestruction commences for this sorbent is 240–280°C that is 70–100°C higher than that for organic sorbents. In addition, practically no loss of mass or sorbent capacity occurs after treatment in 5N acid solutions (HNO_3, HCl, H_2SO_4) and NH_4OH.

The synthesis of organosilicon polymers with highly acidic groups involves a number of difficulties. An attempt to carry out the hydrolysis of trimethyl(chlorosulfonylmethyl)silane was not successful since the existence of an electron-acceptor group at C atom linked to Si atom makes the Si–C bond susceptible to rupture, especially in the presence of bases [21]. A similar effect was also observed for a hydrolysis of methyl(chlorosulphonylmethyl)dichlorosilane [22]. Nevertheless, in the latter case such conditions were found under which this effect could be reduced to a minimum, and poly(methylsulphonatomethyl)siloxane was successfully prepared. Hydrolysis was carried out by gradual addition of water to a

solution of the monomer in a considerable excess of dioxane at 5–10°C. Scheme 6 was proposed to describe the formation of this polymer [22].

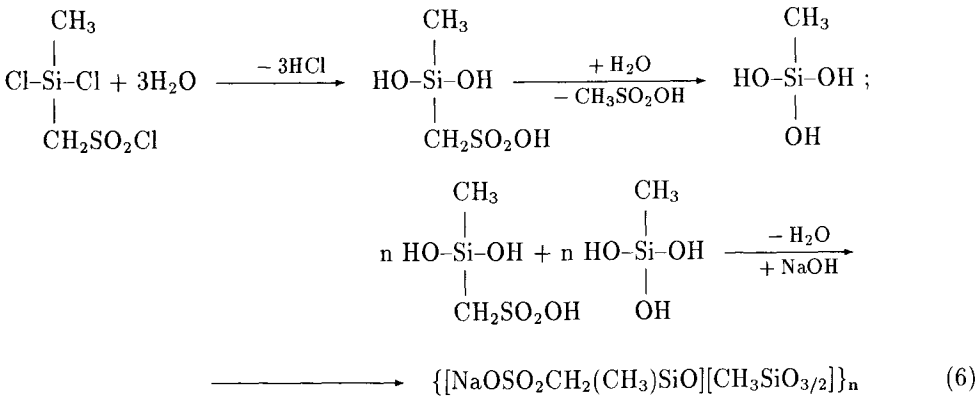

(6)

The resulting polymer was isolated in the form of the sodium salt, as a white powdery substance corresponding to the above composition. Absorption bands at 1200–1210 cm^{-1} typical for ν_{asym} (SO_2) in alkanesulphonic acids were found in the IR spectra. An absorption band at 1070 cm^{-1} seems to correspond to both stretching vibrations of a Si–O–Si bond and $\nu_{sym}(SO_2)$.

A method for the preparation of organosilicon sulphoacids without the necessity for synthesis of a monomer with HSO_3 groups was also described [23–25]. It consisted of oxidation of pre–synthesized PMPS by potassium permanganate or the treatment of poly(phenyl–benzyl–2– phenylethyl)siloxanes by chlorosulfonic acid with – $CHCl_3$ as a solvent.

Unger and coworkers [26] described the synthesis of FPS containing 1,2–epoxy–3– propoxypropyl groups. Initially, polyethoxysiloxane (MW = 800) was prepared from TEOS by acid hydrolysis, which was further used in hydrolytic polycondensation with 1,2–epoxy–3–propoxypropyltriethoxysilane. Homogeneity of the reaction medium in the second stage was maintained by addition of sodium or ammonium hydroxide, so that the final product contained either 1,2–dihydroxyl–3–propoxypropyl or hydroxylamine functional groups.

Over 30 years ago Chuiko, Pavlik and Neimark [27] described briefly preparation by the sol–gel method of FPS which contained $-(CH_2)_2COOH$ groups. The essence of the method consisted in an acidic hydrolysis (HCl) of 2–cyanoethyltriethoxysilane in the presence of TEOS. The resulting white product showed good sorbtion of $NHEt_2$ and py.

3. PROPERTIES

The sorption activity of polyaminosiloxane sorbents prepared by Parish and coworkers was demonstrated by the absorption of protons [2]. It was found that the majority (over 90 %) of the amino groups were accessible, provided that the contact with acid was maintained not shorter than 15 h. The content of amino groups (~3.0 mmol/g) on the surface of such sorbents was 3–5 times as much as that, for example, on aminosilicas prepared according to standard procedures [2,28,29]. Saturation with salts of 3d–metals

with pH optimum values of pH was also achieved after 15 hr. The greatest uptake shown by polyaminosiloxanes was for copper(II) (~1.5 mmol/g). Other metals (Co^{2+}, Ni^{2+}, Zn^{2+}) were absorbed to considerably lesser extents even at the optimum pH. This fact is connected, firstly, with the stereochemical requirements of the cations. Secondly, it is due to irregular distribution of amino groups in the polymer matrix, so that sufficient number of ligand groups is not available in all sites. Thirdly, the initial binding of a metal ion may block access to deeper sites in pores. However, the latter two factors refer to the case of Cu^{2+}. Absorption of Cu^{2+}, irrespective of the nature of the polyaminosiloxane ligand, leads to formation of the sorbents of complexes with a stoichiometry (Cu/N) close to 1:2 on the surface. Formation of square–planar complexes $[CuN_2]^{2+}$ was confirmed by ES and ESR data where four–coordination is presumably completed by water or anionic ligands.

A similar situation was observed for FPS with en functional groups [10]: 1) a minimum of 24 h is required for a saturation of the polymer with a metal ion, 2) not all functional groups are accessible, 3) known complexes are formed on the polymer surface with a maximum saturation by a metal: for copper – $[CuN_4]^{2+}$, for nickel – $[NiN_2(H_2O)_4]^{2+}$ or $[NiN_4(H_2O)_2]^{2+}$ depending on a composition of FPS used. There is a high content of amino groups on the surface of these sorbents, from 3.6 to 7.0 mmol/g by H^+ absorption.

In the case of other functionalized FPS, the content of surface groups may be markedly lower [7]. These sorbents were prepared by the reaction of PCPS with rather bulky ligands which could not penetrate the smaller pores: dien and the Schiff–base and macrocyclic derivatives. These materials also absorb Co^{2+}, Ni^{2+}, and Cu^{2+} from aqueous solutions, forming complexes on the surface the composition of which is determined by a nature of a functional group and the cation. In the case of the dien functionality, virtually all the ligand groups were bound to metal ions. Copper(II) binds only one dien, but nickel(II) binds both which is consistent with the six– coordination normally shown in Ni^{2+}. The glycinate and iminodiacetate functionalized polymers also bind metals well. Moreover, they may be used for chromatographic separation of Co^{2+}, Ni^{2+} and Cu^{2+} [9].

The hydrolytic stability of FPS containing amino groups was also briefly discussed [7]. A decrease in a ratio of $Si(OR)_4/(RO)_3SiR'$ to 1:1 leads to the appearance of oligomers which are leached into the solution and readily observed in Cu^{2+} complexes formation. This is thought to be due to hydrolysis of the FPS during storage, catalyzed by the amine groups. Functionalization of the amine group with HCl or a ketone gave stable polymers.

Slow absorption of Co^{2+} and Ni^{2+} ions from the ethanolic solutions when saturation was achieved after 24–48 h was observed for PPS [8]. The slow absorption indicates that many diphenylphosphine groups are located in narrow pores, access to which is limited by the slow diffusion of cations. In the majority of cases many sites are completely inaccessible or possibly blocked by previously bonded metal ions. A ratio of P/M close to 2 was obtained only in the case of two samples. The colour of polymers treated with metal salts, blue and dark–red, suggested that the resulting complexes are tetrahedral (CoP_2Cl_2) or square–planar (NiP_2Cl_2). This conclusion was confirmed also by ES studies. The spectra proved to be identical to those of the complexes $MCl_2(PPhPr^n_2)_2$ "diluted" with polymers not containing metals.

It should be noted that mechanical stirring of solutions during sorption of metals results in greater absorption than while shaking. This seems to be due to the fact that a prolonged stirring decreases the particle size of the sorbents, increasing the accessibility of ligand sites in small pores [8].

PCMS reveals interesting properties [14]. It is characterized by hydrophobicity expressed in insignificant adsorption of water vapour. The maximal sorption volume of pores by water is 0.05 cm^3/g, in a high adsorption capacity for hydrocarbon vapours: for C_6H_6 V_s = 1.12 cm^3/g; and for hexane V_s = 1.07 cm^3/g. A big hysteresis loop is observed in the adsorption isotherms of hydrocarbons as a result of capillary condensation of the vapour in large pores of the adsorbent. Similar adsorption data show a great organophilicity of the synthesized adsorbent and its high area porous structure with a great number of mesopores of a radius of over 100 Å. A study of py adsorption on a PCMS xerogel showed considerable chemisorption at a low relative pressure (2.0 mmol/g) [14].

The properties of PMMS are discussed in detail in [15,16]. This xerogel is organophylic with limited hydrophilicity. Its structural–sorption characteristics as are follows: real density = 1.65 g/cm^3, total volume of pores = 2.4 cm^3/g, maximum sorption volume of pores by benzene = 0.31, by hexane = 0.13, by methanol = 0.20, by pyridine = 0.19 and by water = 0.12 cm^3/g; volume of macropores = 2.1 cm^3/g, surface area by hexane isotherms = 80 m^2/g, by methanol = 84 m^2/g and by a low–temperature argon desorption = 162 m^2/g; calculated reducing capacity = 8.7 meq/g, found = 7.6 – 8.0 meq/g. A depth of oxidation depends on a particle size of xerogel. Only 1/3 of the total capacity is found for granules, but the powdered xerogel displays the full reduction capacity after 24 h as mentioned above. Ion–exchange properties of this xerogel were studied for a wide group of cations: Ag^+, Hg^{2+} , Pb^{2+} , Cu^{2+} , Zn^{2+} , Mn^{2+} , Co^{2+} , Ni^{2+} and Fe^{3+} at pH 1 and 4 and a contact time 15 min. It was shown that silver and mercury ions were extracted well at both pH values, the adsorption of Fe^{3+} and Co^{2+} ions is reduced sharply upon lowering pH to 1 and Ni^{2+} and Mn^{2+} are poorly sorbed at any value of pH. Thus, this xerogel in the range of pH 0.3 – 3 absorbs only silver and mercury ions. This gave a basis for development of procedures for the concentration of microquantities of silver from the samples of complex composition [30,31] and for treatment of mercury waste [32]. In addition, this sorbent is 50–60°C more thermostable (stable up to 230°C) than the known ionites and possesses high chemical stability. The sorption properties are not changed after treatment at room temperature with the concentrated solutions of such acids as H_2SO_4, HCl and HNO_3. Additionally, such sorbents extract efficiently also microquantities of Te^{4+} and in a lesser degree Se^{4+} [33, 34].

FPS with a sulphide functional gropup [18] extracts metals of the platinum group (Pd(II), Pt(IV) and Os(IV)) from hydrochloric or sulphuric acid solutions, the degree of metal extraction being increased significantly when the temperature of the solutions rises to 100°C. At this temperature a sorption equilibrium, for example, for Pt is maintained for 3 h that is much more less than that of an organic polythioether. Under certain conditions this sorbent is suitable for separation of Pt and Pd from Os. A systematic investigation of complex formation of Au(III) and Ag(I) with this polymer [35–37] showed that it possesses a high sorption capacity relative to these metals, and sometimes surpasses known organic analogues. High coefficients of interphase distribution show the possibility of using this polymer to separate and concentrate microquantities of Au(III) and Ag(I) from their solutions. A 10^5–fold excess of such elements as Cu(II), Fe(III), Co(II), Ni(II), Zn(II), Pb(II) does not prevent a quantitative sorption of these metals on the sorbent. It is believed [20,35,37] that the sorption mechanism includes complexation processes, oxidation–reduction due to the possibility of thiourea group existence in the polymer in the thiol form and ion–exchange due to thiuronium salts formation in the acidic media.

FPS containing HSO_3-groups [22] proved to be an efficient ion-exchanging sorbent for lanthanids. A study was carried out with Pr^{3+} and Tb^{3+}. It is promising for isolation of microquantities from solutions and for the separation of cerium from other Ln^{3+}. Sorbents of this type, including for example $[HSO_3(CH_2)_nSiO_{3/2}]_n$, show a sorption activity for Se(IV) and Te(IV) which rises with an increase in a number of methylene groups in the chain n=3 > n=2 > n=1 [33,34].

Some physicochemical properties of sulphocationites prepared by the method of functionalization of FPS have been described [24]. Oxidation of thiol groups gives polymers with a content of surface sulpho groups equal to 0.8 mmol/g but, by using the sulphonation method, 2.3 - 3.2 mmol/g can be achieved. The surface area for such sorbents is in the range of 121–525 m^2/g. The sulphonated PPhS has a wide pore distribution: the average radius 28 Å, and the total volume 0.40 cm^3/g. It was concluded that sulphonation is accompanied by destruction of the polymer. The parameters for the initial PPhS are respectively: 30 Å and 0.59 cm^3/g. Using solid-state ^{29}Si, ^{13}C NMR spectroscopy, the thermal and hydrothermal stability of functionalized PPhS was studied [25]. The polymer with $-C_6H_4SO_3H$ groups was found to be more stable than that with $-(CH_2)_3SO_3H$ during heating in a current of N_2 in the absence of H_2O vapours. The temperature of thermodestruction commencement is 300 and 270°C, respectively. In the presence of water vapour, the temperature of thermodestruction of the $-(CH_2)_3SO_3H$ sorbent is not changed while for the $-C_6H_4SO_3H$ sorbent it falls to 195°C. It should be noted that high thermal stability is a general characteristic feature of FPS.

4. FPS WITH INSERTED METALLOCOMPLEXES

The presence of metal atoms in porous organosilicon polymers gives rise to active sites necessary for specific adsorption interactions. The use of various types reactants as well as variation of reactant ratios and synthesis conditions allows for the production of new adsorbents with controllable porous structures and selective adsorption properties.

This method was first examined in a study by Samodumova [38] who used aquo-complexes of Co(II), Ni(II) and Cu(II) for a synthesis of polymetalmethylsiloxane adsorbents. Sodium methylsiliconate was hydrolytically polycondensed in the presence of $[M(H_2O)_n]^{2+}$, in an aqueous medium, pH=10, at room temperature, resulting in lyogel occupying the whole volume of the reacting mixture. After ageing for 24 h, the lyogels were washed and dried at 120°C for 8 hr. The general composition of these xerogels corresponded to the formula $(CH_3SiO_{3/2})_nM_x$. The synthesized adsorbents do not dissolve in organic solvents or swell. From n-hexane vapour adsorption isotherms, the parameters of the porous structure shown in Table 1 were calculated [38].

As can be seen in Table 1 the porous structure of these sorbents depends on both the nature of the metal and its amount: polymetalmethylsiloxanes are characterized by a higher surface areas and a smaller sorption pores, compared to PMS. The nature of a metal inserted into an organosilicon matrix has a significant influence on adsorption properties. Thus, the greatest value for adsorption of amines is shown by a copper-containing PMS ($0.07 \cdot 10^{-2}$ cm^3/m^2 for $p/p_s = 0.2$) which is 4–5 times as great as the adsorption of a non-specific adsorbate (hexane). Considerable adsorption of acac was found on Co-PMS (almost 6 times as much as adsorption for hexane); during absorption the solid acquires

Table 1
Composition and parameters of a porous structure of some polymetalmethylsiloxanes [38]

Sorbent	Si/M	V_{pores}, cm^3/g			S_{sp},	r_{eff},
		$V_{tot.}$	V_s	V_{macro}	m^2/g	Å
PMS		2.7	1.5	1.2	50	1000
Co–PMS	6:1	0.85	0.75	0.1	70	90
Ni–PMS	8:1	0.4	0.3	0.1	100	60
Cu–PMS1	15:1	1.3	1.2	0.1	60	80
Cu–PMS2	8:1	0.95	0.9	0.05	70	70

an intense pinky colour that can be explained by chemisorption of the β–diketone forming a surface acetylacetonate complex of cobalt.

Methods to control the porosity of Cu–PMS were developed [39]. It was shown that:
1) an increase in copper–content from 0.3 to 5.2 % causes a diminution in a pore size: $r_{ef.}$ from 820 Å to 47 Å, respectively and S_{sp} increases from 65 to 160 m^2/g by hexane adsorption,
2) an increase in pH of the sedimentation medium, even in the narrow interval in which gelation of PMS takes place, pH 8–12, also leads to a decrease in a pore size and increase in S_{sp},
3) the presence of copper ions in PMS hydrogels ensures a high hydrophilicity of the system and changes the character of the dependence of porosity parameters, such as S_{sp} and $r_{ef.}$, on the duration of hydrogel ageing, as compared with PMS. These parameters did not change much during the ageing period up to 24 h.

The possibility of insertion of aquo– and amine–copper(II) complexes or chromium(III) complexes into a PMS matrix during the synthesis was discussed [40,41]. Tetraamino complexes of copper such as $[Cuen_2(H_2O)_2]^{2+}$ and hexa– and penta–amino complexes of chromium: $[Cren_3]^{3+}$ and $[Cr(NEt_3)_5Cl]^{2+}$ were used. The synthesis of the adsorbents was performed in aqueous solutions at pH 9–10, in which amino complexes of transition metals undergo alkaline hydrolysis forming hydroxo–complexes. The presence of hydroxyl groups in the coordination sphere of the metal allowed a polycondensation reaction between the complex and hydrolysis products of sodium methylsiliconate (see Scheme 7).

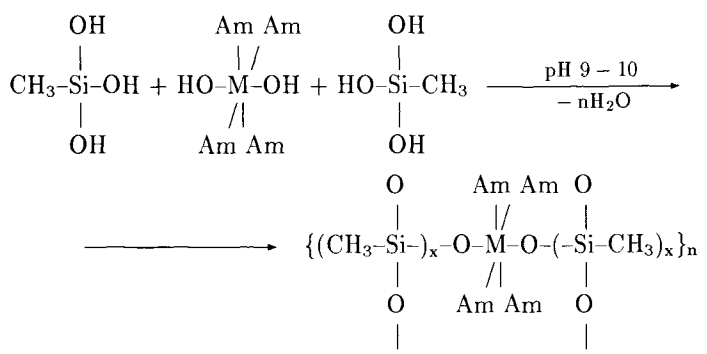

(7)

The insertion of amine complexes into the framework of a sorbent leads to substitution of some of the nitrogen-containing ligands by oxygen atoms of the organosiloxane matrix. On the other hand, coordinated water molecules in the coordination sphere of a complex inserted in a matrix are readily substituted by other ligands, e.g., ammonia in $[Cr(H_2O)_3(OSi\equiv)_3]$ or en in $[Cu(H_2O)_6]^{2+}$. The dependence of the quantity of a transition metal complex inserted in an adsorbent on its nature and on the ratio to sodium methylsiliconate in the reacting mixture is interesting. Thus, the amount of $[Cren_3]^{3+}$ inserted in the matrix increases linearly and reaches 0.5 % when the concentration of methylsiliconate is 5 times that of the concentration of the initial complex. Further increase in the concentration of the initial salt does not increase the amount of the complex inserted in the matrix. With Cr(III) complexes with monodentate ligands, saturation was observed already for a concentration ratio of 2:1, and approached a value of 1.0 – 1.1 % on the basis of the mass of chromium(III) ion contained in the adsorbent. In the case of copper (II) complexes, insertion into the matrix is practically twice as much as for the Cr(III) complexes with the same concentrations and saturation is not observed up to 5 %. This was accounted for [41] on the basis that octahedral complexes of Cr(III) have much stricter requiments for the disposition of oxygen atoms in the matrix cavities. In this case, it is not possible to reach a larger content of a complex. Copper(II) ions form tetragonally distorted complexes which adapt more easily to the possibilities of the matrix. Considerably higher copper(II) -contents in the adsorbent can be achieved in the polycondensation process.

An increase in the complex salt content in adsorbents to be described ensures preparation of more porous structures with a high area surface [40]. For these sorbents , as it was suggested, a specific adsorption of py and NEt_3 vapours is typical.

5. CONCLUSION

FPS of type B and FPS with inserted metalocomplexes are, undoubtedly, an interesting and prospective class of specific sorbents from a practical point of view. Thus, a high efficiency of FPS containing surface thiourea functional groups [20] upon a determination of gold and silver was confirmed by the example of natural gold-bearing sands, polymetallic and copper-molibdenium ores in Mongolia and technological copper concentrates. These metals are determined quantitatively by means of a sorbent in the range of their concentrations from $3.7\cdot10^{-5}$ – $22.7\cdot10^{-3}$ % – for Au(III); $6\cdot10^{-5}$ – $7\cdot10^{-3}$ % – for Ag(I) and practically to the Clark contents: $5\cdot10^{-7}$ % –Au; $1\cdot10^{-5}$ % – Ag from a dominating quantity of accompanying elements, first of all Cu as well as Bi, Sb, Fe, Ni, Co, As, Zn, etc.[20]. The presence of a specific adsorption in copper-containing PMS [38–41] was used in [42,43] for a sorption of N-(2,3-dimethylphenyl)anthranyl (mepheneamine) acid aiming at preparing anti-inflammatory drugs with a prolonged action. A sorption activity of the same sorbent in the aqueous solutions was also studied regarding the antibiotic of amine-glucoside row – gentamycin sulphate which is characterized by a high activity towards the most resistant gram-negative microorganisms [44]. Unger and coworkers [26] showed the possibility of using FPS of type B in a liquid chromatography.

The use of a "sol-gel" technology presents opportunities for development of scientific foundations for preparation of FPS with pre-selected and controllable properties of a di-

rected action. On one hand, formation of a porous structure of FPS is obtained according to general principles of structure formation of mineral adsorbents [1]. On the other hand, a great influence on a structure and sorption properties of FPS is exerted by the organic R′ radicals at a silicon atom. It is known that an increase in a size of an organic group leads to preparation of large–pore samples of sorbents. Thus, the total pore volume for PVS reaches 6 cm^3/g whereas a volume of sorption pores is only 10–15 % of the total. Introduction of atoms or atom groups of electron–donating or –accepting properties into R′ radicals allows to control sorption properties. The use of three– and more component systems gives still more possibilities of an influence on physicochemical and structural–adsorption properties of FPS, as already mentioned in literature [1,10,17,45–47]. Appearance of a synergistic effect peculiar for multi–component systems [48] is especially important in practice. Such copolymers have a great significance also for the theory of adsorption while studying intermolecular interactions of adsorbent–adsorbate. Introduction of transition metal complexes into a composition of FPS as expected [41] would lead to a specific character of adsorption of individual molecules and ions at the expense of both strengthening of acid–base properties upon complexation of coordinated ligands and a matrix itself, and substitution processes of ligands in a coordination sphere of the complex inserted into an organosiloxane matrix, or an additional coordination to a central ion of this complex. Studies [49–51] in which complexes of Co(II) with Schiff bases were inserted as the centres of fixation of a molecular oxygen may serve as an example.

ACKNOWLEDGMENT

Financial support from the INTAS (EC) Office, project No. 94 – 4612, is gratefully acknowledged.

REFERENCES

1. I.B.Slinyakova and T.I.Denisova, Organosilicon Adsorbents: Preparation, Properties, Application, Naukova Dumka, Kiev, 1988 (in Russian).
2. I.S.Khatib and R.V.Parish, J. Organomet. Chem., 369 (1989) 9.
3. A.A.Chuiko, G.E.Pavlik, G.B.Budkevich and I.E.Neimark, A Method of Preparation of Silica Gels Containing Aminoalkyl Group, USSR Patent No. 182 719 (1966).
4. Yu.L.Zub, L.S.Kovaleva, B.V.Zhmud, S.N.Orlik, Proc. 7th Int. Symp. Heterog. Catal., Bourgas, Part 1 (1991) 557.
5. Yu.L.Zub, Abstr. Annual Scientific Conf., Univ. Kiev–Mohyla Academy, Kiev, (1995) 42.
6. L.P.Finn and I.B.Slinyakova, Kolloid. Zhurn., 37 (1975) 723.
7. I.Ahmed and R.V.Parish, J. Organomet. Chem., 452 (1993) 23.
8. R.V.Parish, D.Habibi and V.Mohammadi, J. Organomet. Chem., 369 (1989) 17.
9. A.A.El–Nasser and R.V.Parish, to be published.
10. M.El–Nahhal and R.V.Parish, L. Organomet. Chem., 452 (1993) 19.
11. B.J.Brisdon and A.M.Watts, J. Chem. Soc., Dalton Trans., (1985) 2191.

12. F.G.Young, Nonlinear Polymer as Catalyst Precursor and Its Use in a Catalyst Preparation, Ger. Patent No. 2 330 308 (1974).
13. I.B.Slinyakova, M.G.Voronkov and E.Ya.Lukevits, A Method for Preparation of Organosilica Gel, USSR Patent No. 245 364 (1969).
14. I.B.Slinyakova, M.G.Voronkov and I.E.Krot, Kolloid. Zhurn., 35 (1973) 480.
15. L.P.Finn, I.B.Slinyakova, M.G.Voronkov, N.N.Vlasova and F.P.Kletsko, A Spatially Cross-linked Polymer for Cationexchangers and Redoxites and Method for Making the Same, USSR Patent No. 585 187 (1977).
16. L.P.Finn, I.B.Slinyakova, M.G.Voronkov, N.N.Vlasova, F.P.Kletsko, A.I.Kirillov and T.V.Shklyar, Dokl. AN SSSR, 236 (1977) 1426.
17. L.P.Finn, I.B.Slinyakova, M.G.Voronkov and N.N.Vlasova, Adsorbtsiya i Adsorbenty, No. 8 (1980) 98.
18. M.G.Voronkov, N.N.Vlasova, M.Yu.Adamovich, Yu.N.Pozhidaev and A.I.Kirillov, Zhurn. Obshch. Khimii, 54 (1984) 865.
19. M.G.Voronkov, N.N.Vlasova and A.E.Pestunovich, A Method for Preparation of N,N′-bis[3′-trialkyl(alkoxy)silylpropyl]thiourea, USSR Patent No. 643, 507 (1979).
20. G.Burmaa, Ph.D. Thesis, Russia, Irkutsk, Inst. Organic Chemistry, 1992.
21. G.D.Cooper, J. Org. Chem., 21 (1956) 1214.
22. N.N.Vlasova, M.G.Voronkov, S.A.Bolshakova, Yu.N.Pozhidaev and A.I.Kirillov, Zhurn. Obshch. Khimii, 54 (1984) 2306.
23. S.Suzuki, K.Tohmori and Y.Ono, Chem. Lett., (1986) 747.
24. S.Suzuki, K.Tohmori and Y.Ono, J. Mol. Catal., 43 (1987) 41.
25. S.Suzuki, Y.Ono, S.Nakata and S.Asaoka, J. Phys. Chem., 91 (1987) 1659.
26. K.K.Unger, N.Becker and P.Roumeliotis, J. Chromatogr., 125 (1976) 115.
27. A.A.Chuiko, G.E.Pavlik and I.E.Neimark, A Method of Preparation of Organosilica Gel, USSR Patent No. 164 680 (1964).
28. A.A.Chuiko, V.A.Tertykh, G.E.Pavlik and I.E.Neimark, Kolloid. Zhurn., 27 (1965) 903.
29. V.A.Tertykh and L.A.Belyakova, Chemical Reactions with Participation of Silica Surface, Naukova Dumka, Kiev, 1991 (in Russian).
30. O.V.Zemlyanushnova, A.I.Kirillov, I.P.Golentovskaya and N.N.Vlasova, Izv. Vysshykh Ucheb. Zaved., 25 (1982) 568.
31. M.G.Voronkov, N.N.Vlasova, A.I.Kirillov, O.V.Zemlyanushnova, M.M.Rybakova, F.P.Kletsko and Yu.N.Pozhidaev, Dokl. AN SSSR, 275 (1984) 1095.
32. A.I.Kirillov,O.N.Zemlyanushnova, N.N.Vlasova, M.G.Voronkov, I.B.Slinyakova and L.P.Finn, Zhurn. Anal. Khimii, 37 (1982) 1201.
33. N.N.Vlasova, L.M.Stanevich, S.A.Bolshakova and M.G.Voronkov, Zhurn. Prikl. Khimii, 60 (1987) 1479.
34. N.N.Vlasova, L.M.Stanevich, S.A.Bolshakova and M.G.Voronkov, Zhurn. Prikl. Khimii, 61 (1988) 2318.
35. G.Burmaa, A.E.Pestunovich, N.N.Vlasova and M.G.Voronkov, Izv. SO AN SSSR, Ser. Khim. Nauk, No. 5 (1990) 66.
36. N.N.Vlasova, A.E.Pestunovich, M.G.Voronkov, G.Burmaa and Sh.Luvsandorzh, A Method of Gold Extraction, Mongolian Patent No. 670 (1992).
37. G.Burmaa, N.N.Vlasova, A.E.Pestunovich, Yu.N.Pozhidaev,M.G.Voronkov, Izv. SO AN SSSR, Ser. Khim. Nauk, No. 4 (1992) 89.
38. I.M.Samodumova, Teoret. i Experim. Khimiya, 19 (1983) 748.

39. L.I.Kiseleva, I.M.Samodumova, L.N.Prikhodko and Yu.N.Shevchenko, Ukr. Khim. Zhurn., 55 (1989) 366.
40. I.M.Samodumova, K.B.Yatsimirskii, L.I.Kiseleva, Yu.N.Shevchenko and N.I.Yashina, Adsorbtsiya i Adsorbenty, No. 12 (1984) 60.
41. Yu.N.Shevchenko, N.I.Yashina, I.M.Samodumova and L.I.Kiseleva, Zhurn. Obshch. Khimii, 54 (1984) 1699.
42. E.E.Kriss, I.M.Samodumova, O.V.Krichfalushchii, G.T.Kurbatova, L.I.Kiseleva and L.I.Budarin, Zhurn. Neorgan. Khimii, 29 (1984) 2277.
43. E.E.Kriss, I.M.Samodumova, G.T.Kurbatova, L.I.Kiseleva and L.I.Budarin, Koord. Khimiya, 14 (1988) 1613.
44. K.B.Yatsimirskii, V.A.Znamenskii, L.V.Kejsevich, I.M.Samodumova, L.I.Kiseleva and A.P.Kaban, Vestnik AN USSR, (1986) 33.
45. L.P.Finn and L.N.Khokhlova, Abstr. 6th All–Union Conf. on Chemistry and Use of Organosilicon Compounds, Riga, (1986) 142.
46. Yu.L.Zub, L.S.Drozd and A.A.Chuiko, Book of Abstr.,IUPAC Symp. on the Characterization of Porous Solids, Marseille, (1993) 95.
47. Yu.L.Zub, M.Ya.Gorokhovatskaya, A.A.Chuiko and A.M.Nesterenko, Ext. Abstr. Fourth Int. Conf. on Fundamentals of Adsorption, Kyoto, (1992) 461.
48. I.E.Neimark, Adsorbents, their Preparation, Properties and Use, Nauka, Leningrad, (1978) 16 (in Russian).
49. T.N.Yakubovich and Yu.L.Zub, Book of Abstr. III Inter–State Workshop, Ukraine, Donetsk, (1993) 26.
50. T.N.Yakubovich, V.V.Teslenko, K.A.Kolesnikova, Yu.L.Zub and R.Leboda, in: G.Poncelet (ed.), Preparation of Catalysts VI , Elsevier, Amsterdam, 1995, p. 597.
51. T.N.Yakubovich, V.V.Teslenko, K.A.Kolesnikova and Yu.L.Zub, J. Inorg. and Organomet. Polymers, in press.

This Page Intentionally Left Blank

A. Dąbrowski and V.A. Tertykh (Editors)
Adsorption on New and Modified Inorganic Sorbents
Studies in Surface Science and Catalysis, Vol. 99

Chapter 1.11
Surface structure and molecular adsorption of apatites

T. Ishikawa

School of Chemistry, Osaka University of Education, 4–698–1 Asahigaoka, Kashiwara–shi, Osaka–fu 582, Japan

1. INTRODUCTION

Calcium hydroxyapatite $Ca_{10}(PO_4)_6(OH)_2$ (abbreviated CaHAP) is not only biological hard tissue but also an adsorbent for separating biomaterials such as proteins and a catalyst for dehydration and dehydrogenation of alcohols [1]. Understanding of the surface structure and properties of CaHAP are fundamentally important in the science and technology of this material. There are numerous studies on the surface properties of these materials in liquid phase such as the adsorption of biomolecules and ions. On the contrary a few studies on the surface of this material in the gas phase have be done by IR [2, 3], NMR [4], TPD [5] and XPS [6]. To our knowledge, the gas adsorption on CaHAP has not been investigated except the adsorption of CH_3OH and H_2O by Dry and Beebe [7]. The surface structure and properties of this material in the gaseous phase are important to explore the mechanism of catalysis in detail.

The nonstoichiometry of CaHAP has received extensive attention in medical and solid–state science, because the CaHAP formed in the calcified tissues or synthesized is mostly non– stoichiometric. Bett et al.[8] have reported that the catalytic activity of Ca–deficient CaHAP for the dehydration of butanol can be related to the surface acidic hydrogens of HPO_4^{2-} produced to maintain the electrical neutrality. Joris and Amberg [9, 10] have pointed out that the catalytic activity of cation–deficient CaHAP and strontium hydroxyapatite (abbreviated SrHAP) for the similar dehydration reaction is due to the acidic hydrogens of the H_2O molecules located in OH^-–defects caused by the deficiency of Ca^{2+} or Sr^{2+} ions rather than those of the surface HPO_4^{2-} ions.

Solid solutions (abbreviated SrCaHAP) of SrHAP and CaHAP can be rather easily prepared because of the similar ionic radii of Sr^{2+} (0.11 nm) and Ca^{2+} (0.10 nm) [11]. It is of interest to know the structure of SrCaHAP since Sr is a long–lifetime radioactive waste material having a high fission yield, which is liable to incorporate into the bone structure of the body. The interaction of CO_2 with HAP is important for the denaturation of human bone and tooth by CO_3^{2-} [12, 13] and the formation of long–lifetime radicals such as CO^-, CO_2^- and CO^{3-} on the calcified tissue [14, 15].

The Ca^{2+} ions of CaHAP can be rather readily replaced by other metal ions, so that there have been many studies on the ion–exchange behaviour of CaHAP [16–22]. However, to our knowledge, there seem to be few investigations on the surface structure and nature

of CaHAP doped with metal ions except some studies. Misono and Hall [23] studied the oxidation–reduction properties of Cu^{2+}– and Ni^{2+}–substituted CaHAP by EPR spectroscopy and suggested that the surface Cu^{+} ions produced by the reduction of the surface Cu^{2+} ions are the active sites for the H_2–D_2 exchange reaction. Recently, Matsumura et al. [24] reported that the oxidative coupling of methane to ethane and ethene can be effectively catalyzed over Pb^{2+}–substituted CaHAP and the surface Pb^{2+} ions activate methane and stabilize methyl radicals. However, details of the surface structures of CaHAP doped with these metal ions remain still unclear.

In this chapter, the surface structures of different kinds of HAPs and the adsorption of various molecules on the HAPs are described in detail, which may afford fundamental information for the usage of this material as adsorbent, catalyst, bioceramic and so on.

2. EXPERIMENTAL SECTION

2.1. Preparation of materials

Colloidal CaHAP and SrHAP particles were prepared by the method described in papers [3, 25]. $Ca(OH)_2$ (3.00 g) or $Sr(OH)_2$ (4.39 g) was dissolved in 20 dm^3 of deionized and distilled water free from CO_2 in an N_2 atmosphere by stirring overnight at room temperature. Various amounts (75 – 85 cm^3) of 10 % mass H_3PO_4 were added to the $Ca(OH)_2$ or $Sr(OH)_2$ solutions to prepare the samples with different Ca/P or Sr/P molar ratios. The resulting suspensions were stirred for 24 h at room temperature and then aged at 100°C for 48 h in a capped Teflon vessel. The white precipitates formed were filtered off, washed with deionized and distilled water and finally dried in an air oven at 70°C for 24 h.

The SrCaHAP particles of different compositions were prepared following the recipe reported previously [26]. To obtain the samples with different molar ratios Sr/(Ca + Sr) from 0 to 1, various amounts of $Ca(OH)_2$ and $Sr(OH)_2$ were dissolved in 20 dm^3 of deionized and distilled water free from CO_2. To these hydroxide solutions different amounts of 10 % H_3PO_4 were added, and the resulting white suspensions were aged under the same condition as for the preparation of CaHAP. The washing and drying of the formed precipitates were the same as for CaHAP and SrHAP.

The CaHAP particles doped with Fe^{3+} ions at different molar ratios Fe/(Ca+Fe) from 0 to 0.2 were synthesized by the similar method to the case of CaHAP. The reagents of 0.36 – 0.40 mol $Ca(OH)_2$ and 0 – 0.04 mol $FePO_4$, of which the total mole number was 0.4, were dissolved into 20 dm^3 of deionized and distilled water free from CO_2 in a capped Teflon container by stirring for 1 day at room temperature. H_3PO_4 (0.166 mol) were instantly added to the suspension while stirring. The resulting precipitates were aged, washed and dried under the same condition as for the preparation of CaHAP.

2.2. Characterization methods

The Ca, Sr and Fe contents were determined with a Seiko induced coupled plasma (ICP) spectrometer by first dissolving in HCl and PO_4^{3-} was assayed by molybdenum blue method. The morphology of the particles was observed using a Joel electron microscope. X– ray powder diffraction (XRD) was done with a Rigaku high–intensity diffractometer using nickel–filtered Cu–Kα radiation (60 kV, 125 mV). X–ray photoelectron spectroscopy

(XPS) was carried out using a Shimazu XPS apparatus. Transmission IR spectra were taken with a Digilab Fourier transform near-infrared (FTNIR) spectrophotometer using a PbSe sensor having high sensitivity in the wave number region above 2000 cm^{-1} with 2 cm^{-1} resolution. The vacuum cell is capable of heat treatment and gas adsorption *in situ*. The sample disks of 10 mm diameter for IR measurement were made by pressing powder of 15 - 100 mg at 50 $kg \cdot cm^{-2}$. The sample was pretreated at different temperatures from under 10^{-4} Torr for 2 h. The protons of surface OH groups of these samples were deuteriated by repeating adsorption-desorption cycles of D_2O.

2.3. Measurement of adsorption isotherms

The adsorption isotherms of N_2 and CO_2 were measured using a computer-aided volumetric apparatus designed in our laboratory at the boiling point of nitrogen and 25°C, respectively. The isotherms of H_2O, CH_3OH and CH_3I were determined at 25°C using an automatic gravimetric apparatus designed in our laboratory. The samples were pretreated under 10^{-4} Torr at different temperatures for 2 h.

3. RESULTS AND DISCUSSION

3.1. Surface structure of HAP

3.1.1. CaHAP

Figure 1 (a) shows the IR spectra of CaHAP with the Ca/P molar ratio of 1.64 pretreated at different temperatures in vacuo. All the spectra have a strong and sharp band at 3570 cm^{-1} which was assigned to OH^- ions on lattice sites of the CaHAP crystals [10]. Spectrum 1 of the sample treated at 150°C has a very broad absorption band at about 3300 cm^{-1}. This band almost disappeared spectrum 3 of the sample outgassed at 500°C. Accompanied by this change, the thermogravimetric (TG) curve of this material exhibited a steep weight decrease from room temperature to about 500°C together with an endothermic heat of desorption in the DTA curve. Furedi-Milhofer and co-workers [27] attributed this weight loss to the desorption of H_2O adsorbed inside micropores with a high energy adsorption. However, the t-curve [28] obtained from the nitrogen adsorption isotherm showed that this material exhibits no microporosity. Therefore, the weight loss by heating mentioned above might be caused by the dehydration of chemically adsorbed H_2O. Weak absorption bands appeared at about 3700 cm^{-1} simultaneously with a decrease of the 3300 cm^{-1} band in Fig. 1(a). These weak bands are shown in detail in spectra 1, 2, 3, 4, and 5 of CaHAP outgassed at 100, 200, 300, 400, and 500°C, respectively, Fig. 1(b). When evacuated at 100°C, a broad band appeared from 3650 to 3700 cm^{-1}, but three bands at 3682, 3673, and 3659 cm^{-1} became obvious by outgassing at 300°C. Cant et al. [29], Joris and Amberg [10] found an absorption band at about 3660 cm^{-1} which may be the same as the 3659 cm^{-1} band in this spectrum. The former two bands are newly found in this work. On elevating the outgassing temperature the 3682, 3673, and 3659 cm^{-1} bands became gradually weaker. H-D isotope exchange of this material resulted in the disappearance of 3682, 3673, and 3659 cm^{-1} bands, and the respective OD bands appeared at 2721, 2712, and 2705 cm^{-1}. Only a very small portion of the 3570 cm^{-1} band showed an isotope shift with the isotope wave number ratios of the original bands

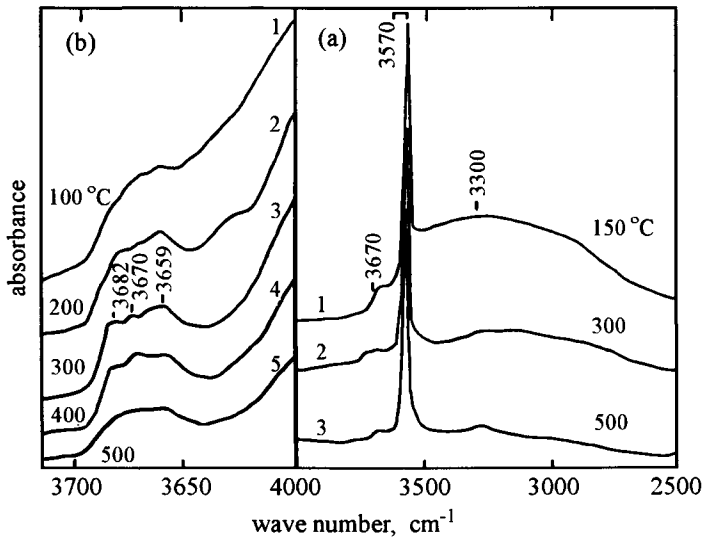

Figure 1. IR spectra of CaHAP (Ca/P=1.64) outgassed at different temperatures.

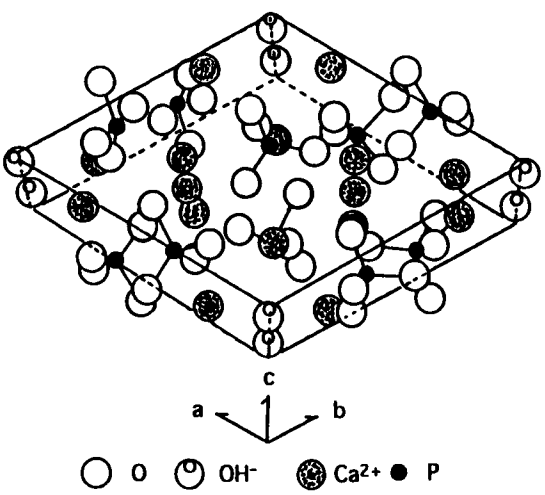

Figure 2. Crystal structure of CaHAP which is monolinic with lattice parameters with a = 0.9429 nm, b = 2a, c = 0.6883 nm and $\gamma = 120°$.

and OD bands of 1.375. The isotope ratios of the three bands mentioned above were 1.353, 1.354, and 1.352, respectively, which are almost equal to each other. This probably means that the bond nature of these OH groups is almost identical with each other. These bands can be assigned to P–OH groups, since the wave numbers of these bands are close to the 3666 cm^{-1} band assigned to P–OH groups of phosphoric acid supported on

silica gels [30]. These P–OH groups may constitute surface acidic phosphate ions, HPO_4^{2-} and/or $H_2PO_4^-$. The scheme of the crystal structure of CaHAP is shown in Figure 2. The CaHAP particles were rod–shape and their mean sizes were 70 nm (length) and 20 nm (width) by TEM observation. The predominant crystal face of the particles is **ac** or **bc** face [32, 33]. As seen in Figure 2 the ions on the particle surface are PO_4^{3-}, Ca^{2+} and OH^- ions. These ions would be hydrated because this CaHAP was prepared in the aqueous solution. Outgassing at high temperature removed the H_2O molecules bounded to these ions as confirmed by TG. The surface HPO_4^{2-} and $H_2PO_4^-$ ions would have been converted from the surface PO_4^{3-} ions by protonation to maintain the overall charge balance of Ca–deficient CaHAP [9, 34]. However, stoichiometric or Ca–rich CaHAP, of which Ca/P is larger than the stoichiometric ratio of 1.67, show the surface P–OH bands, indicating that compensating of the surface charge also causes the protonation of the surface phosphate ions. Therefore, we can consider that the protonation of these surface phosphate ions takes place to maintain the balance of not only the total charge but also the surface one. It is difficult to assign the 3682, 3670 and 3659 cm^{-1} bands to only one kind or a number of different kinds of P–OH groups. However, it should be mentioned that these groups may be free or isolated OH groups of similar bond nature, looking at the almost identical H–D isotope ratios, ion–exchange properties, and quite high wave numbers, of these bands [3]. The above discussion can be summarized as Table 1.

Table 1
Assignment of the IR bands of CaHAP (Ca/P=1.64)

cm^{-1}	assignment
3682	surface P–OH
3670 (vw)	surface P–OH
3659	surface P–OH
3570 (s)	bulk OH^-
3300 (b)	adsorbed and bound H_2O

(b) broad, (vw) very weak, (s) strong.

3.1.2. SrHAP

Figure 3 shows IR spectra of SrHAPs with different Sr/P ratios outgassed at 300°C for 2 h. The Sr–rich SrHAP (Sr/P >1.67) shows the four bands at 3710, 3684, 3674 and 3662 cm^{-1}.

With H–D exchange all these bands became weak and respective OD bands appeared 2742, 2730, 2717 and 2700 cm^{-1}, of which the wave number ratios are 3710 : 2742 = 1.353, 3684 : 2730 = 1.349, 3674 : 2717 = 1.352 and 3662 : 2700 = 1.356, close to the theoretical isotope ratio (OH : OD) of 1.374. Thus the 3710, 3684, 3674 and 3662 cm^{-1} bands are assigned to the stretching vibrations of OH groups. As mentioned in the above section, the 3682, 3673 and 3659 cm^{-1} bands observed for the Ca–deficient CaHAP (Ca/P<1.67) were assigned to the surface P–OH groups. The 3684, 3674 and 3662 cm^{-1} bands detected for the Sr–rich SrHAP are compatible with the surface P–OH bands of the Ca– deficient CaHAP. Hence, these three bands are assigned to the surface P–OH groups. The broad

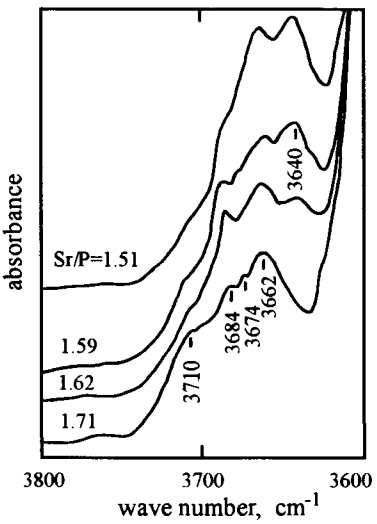

Figure 3. IR spectra of SrHAPs with various Sr/P ratios.

3710 cm^{-1} band did not appear in the case of the Sr-deficient SrHAP (Sr/P<1.67). The Sr-rich SrHAP contains a small amount of CO_3^{2-} ions and this band disappeared during the H-D exchange. Moreover, the 3710 cm^{-1} band of the Sr-rich SrHAP disappeared with the ion-exchange adsorption of the cations such as Ca^{2+} and Na^+, and a carbonated CaHAP showed a broad band around 3710 cm^{-1}. It seems most likely, therefore, that the 3710 cm^{-1} band can be ascribed not to the surface OH^- ions but to the surface C-OH groups.

Table 2
Assignment of the IR bands of Sr-deficient (A) and Sr-rich (B) SrAHP

A (Sr/P=1.59) cm^{-1}	B (Sr/P=1.71) cm^{-1}	assignment
—	3710 (b)	surface C-OH
3684	3684	surface P-OH
3674 (vw)	3674 (vw)	surface P-OH
3662	3662	surface P-OH
3640	—	surface P-OH
3595 (s)	3595 (s)	bulk OH^-
3000 (b)	3100 (b)	adsorbed and bound H_2O
—	2460	bulk CO_3^{2-}

(b) broad, (vw) very week, (s) strong.

The Sr-deficient SrHAP gave rise to a spectrum different from that of the Sr-rich sample; these SrHAPs did not show the 3710 cm^{-1} band besides the 3684, 3674 and 3662 cm^{-1} bands detected for the Sr-rich SrHAP, although the 3684 and 3674 cm^{-1} bands of the sample with Sr/P = 1.51 were hardly detectable. The 3640 cm^{-1} band observed for the Sr-deficient samples more slowly diminished during H-D exchange than those of the other three bands, accompanying the appearance of a new 2685 cm^{-1} band. The isotope ratio (3640 : 2685 = 1.356) of this band was close to those of the other bands, implying that the 3640 cm^{-1} band is also due to OH groups. Furthermore, the 3640 cm^{-1} band disappeared during the ion-exchange adsorption of metal ions. It seems reasonable, therefore, that this band should be assigned to the surface P-OH groups that are less acidic compared to the other three surface P-OH groups. Table 2 lists the assignment of all the bands of SrHAP, as a summary of the above discussion.

3.1.3. Fe(III)-substituted CaHAP

Figure 4 shows IR spectra of the samples with different molar ratios Fe/(Ca+Fe) (abbreviated X_{Fe}) treated in vacuo at 300°C. In the case of pure CaHAP (X_{Fe}=0), the

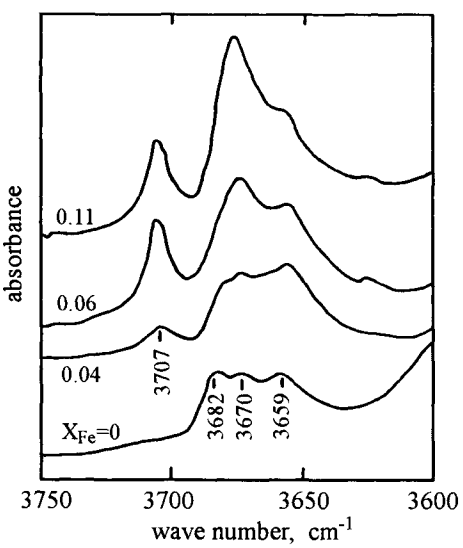

Figure 4. IR spectra of CaHAPs substituted with different amounts of Fe^{3+} ions.

3688, 3677 and 3658 cm^{-1} appeared and these bands have been assigned to the O-H stretching vibration of surface P-OH groups [3]. Note that the spectra markedly changed with Fe^{3+}-substitution and a new band appeared at 3707 cm^{-1} for Fe^{3+}-substituted CaHAP. This new band completely disappeared upon outgassing above 300°C while the other bands still appeared. The 3707 cm^{-1} band disappeared and a band appeared at 2733 cm^{-1} by H-D exchange. The ratio of the wave numbers of these two bands allows us to assign the 3707 cm^{-1} band to the surface OH groups. With increasing X_{Fe} the 3677 cm^{-1} band grew and the 3688 cm^{-1} band diminished, indicating that the state of surface P-OH

groups varies with Fe(III)-substitution.

It is well known that there are two kinds of Ca-sites in the CaHAP crystal; Ca^{2+} ion in one site is coordinated by 9 oxygen atoms from PO_4^{3-} ions (called site **I**) and Ca^{2+} ion in another site is coordinated by 6 oxygen atoms of PO_4^{3-} ions and one oxygen atom of OH^- ion (called site **II**) [35]. As mentioned in Section 3.1.1. the CaHAP particles used in this study were rod-shaped and elongated along the **c**-axis. The predominant crystal faces exposed on the surface of CaHAP particles are regarded as **ac** and **bc** faces that have the same structure. The structure of **ac** and **bc** faces was illustrated in Figure 2. The P-O groups of surface PO_4^{3-} ions turned into P- OH groups by protonation to balance the surface charge as already described. Since the Ca^{2+} ions of the predominant **ac** and **bc** faces belong to site **II**, the most of the surface Ca^{2+} ions belong to Ca^{2+} ions in site **II**. The Fe^{3+}- substitution of the surface Ca^{2+} ions in site **II**, bonding to OH^- ions, leads to the formation of surface Fe-OH groups. It seems reasonable therefore that the 3707 cm^{-1} band is assigned to the O-H stretching vibration of the surface Fe-OH groups. This band is close to the surface free Fe-OH bands from 3773 to 3659 cm^{-1} observed for a series of FeOOH [36]. This fact also supports the assignment of the 3707 cm^{-1} band described above.

3.2. Adsorption of molecules on HAP

3.2.1. Adsorption of H_2O on CaHAP

The adsorption isotherm of H_2O on CaHAP (Ca/P = 1.59) outgassed at 300°C for 2 h is shown in Figure 5. This isotherm belongs to the type-II in the BET classification. Figure 6 shows the change of IR spectra with H_2O adsorption on the same CaHAP as for Figure 5 . The spectrum 1 before the adsorption has a band at 4675 cm^{-1} that becomes small with the increase of the amount of adsorbed H_2O. A broad band appears around 5250 cm^{-1}. This band grows stronger proportionally to the amount of adsorbed H_2O from 0.34 $mmol \cdot g^{-1}$ and splits into 5205 and 5308 cm^{-1} bands. These bands can be assigned to the combination bands of H_2O [37]. The reason for this splitting will be discussed below. Parallel to this growth of the water combination band, the absorbances of the P-OH fundamental stretching bands at 3682, 3673 and 3659 cm^{-1} decreased. The same absorbance change was observed for the 4675 cm^{-1} band (Figure 6). Since this 4675 cm^{-1} band disappeared completely after H-D exchange, the functional group showing this band locates on the surface. Therefore, this band might be assigned to a combination of a vibration band of the fundamental stretching vibration of surface P-OH groups (ca. 3670 cm^{-1}) and its deformation vibration (ca. 1000 cm^{-1}). Figure 7 shows the absorbance of the 4675 cm^{-1} band as a function of amount of adsorbed H_2O. The absorbance decrease of the P-OH band at 4675 cm^{-1} with H_2O adsorption was observed but it was negligibly small from 0 to 0.34 $mmol \cdot g^{-1}$. As can be seen in Figure 7, the absorbance of the surface P-OH band at 4675 cm^{-1} decreased to about one-third of the total absorbance with increasing the adsorbed amount from 0.43 to 1.1 $mmol \cdot g^{-1}$, corresponding to the increase of about 5 H_2O molecules per nm^2. Therefore, two-thirds of the total P-OH groups interact with these H_2O molecules. The population of P-OH on the CaHAP surface can be estimated as mentioned below. The most developed crystalline surface of CaHAP is **ac** or **bc** plane as mentioned before, and there seem to be two PO_4^{3-} ions in this plane of a unit cell of area $\mathbf{a} = 0.943 \times \mathbf{c} = 0.688 nm^2$ [20], as can be seen from the crystal structure of CaHAP in Figure 3.

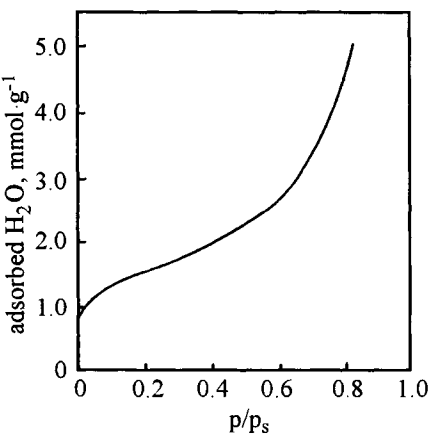

Figure 5. Adsorption isotherm of H_2O on CaHAP (Ca/P=1.59) at 25°C.

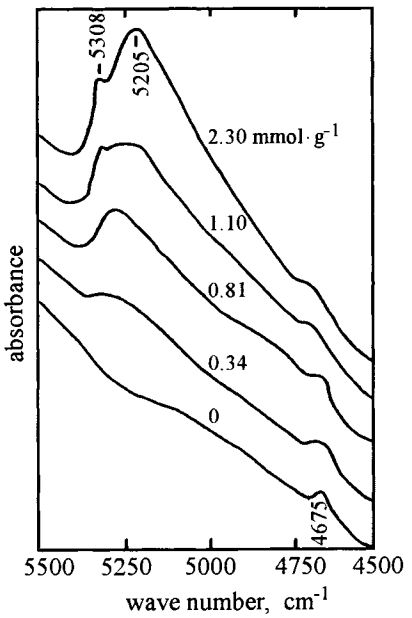

Figure 6. IR spectra of CaHAP (Ca/P=1.59) adsorbing various amounts of H_2O.

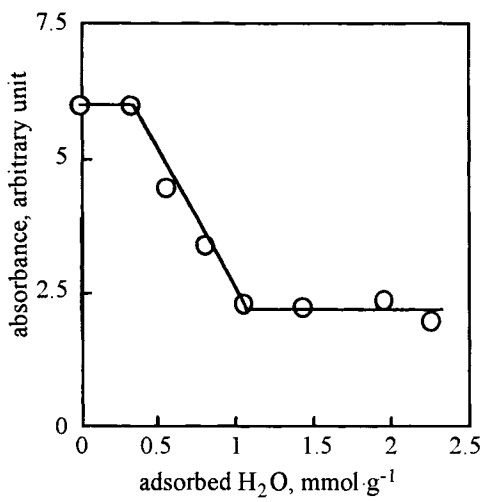

Figure 7. Relation between the absorbance of the 4675 cm^{-1} band and the amount of adsorbed H_2O for CaHAP (Ca/P=1.59).

To balance the surface charge, one of the surface PO_4^{3-} ions in this plane may be protonated to be HPO_4^{2-} ions having one OH group and the other may be protonated to be $H_2PO_4^{3-}$ ions having two OH groups. Therefore, the resulting surface population of P–OH groups per nm^2 is $3/0.688 = 4.4$ on the average. Therefore, from the result in Figure 7, two-thirds of the total of 4.4 P–OH or ca. 3 P–OH groups·nm^{-2} would be available for the adsorption of 5 H_2O molecules. Above 1.1 mmol·g^{-1} of BET monolayer capacity of H_2O adsorption, the absorbance of the P–OH band remained constant (Figure 7). This suggests that there would still be P–OH groups not interacting with H_2O molecules even after the multilayer adsorption of H_2O. Consequently, the absorbance change of P–OH bands on H_2O adsorption suggests that there seem to be at least three energetic steps of H_2O adsorption: (1) decomposed, hydrated, or strongly adsorbed H_2O: (2) H_2O adsorbed by hydrogen bonding with P– OH groups; and (3) H_2O adsorbed by hydrogen bonding and an adsorption interaction such as dipolar and dispersive interactions with the CaHAP surface and/or the adsorbed H_2O in the first step.

The configuration of adsorbed H_2O in the second and third steps may be inferred from the analysis of two separated combination bands of adsorbed H_2O at 5308 and 5205 cm^{-1} in spectra 4 and 5 in Figure 6. The wave number of the 5308 cm^{-1} band is close to that of H_2O vapour (5332 cm^{-1}) [37]. This suggests that the perturbation of the OH bond of OH groups of adsorbed H_2O showing the 5308 cm^{-1} band is much weaker than that of the OH bond showing the 5205 cm^{-1} band. The adsorbed H_2O having the 5205 cm^{-1} band may have the protons of adsorbed H_2O molecules forming a first layer by hydrogen bonding with the oxygen lone pairs of surface P–OH groups and/or of water molecules already adsorbed. Above the BET monolayer adsorption capacity (1.1 mmol·g^{-1}), the absorbance of the 5205 cm^{-1} band increased with the increase in the adsorbed amount of H_2O. The 5308 cm^{-1} band can be assigned to one or two free OH groups of adsorbed H_2O molecules, with one free and the other hydrogen bonded to the functional groups, in the former case, or less probably with both free and lone-pair electrons of its oxygen atom attached to the various sites in the latter case. The absorbance of the 5308 cm^{-1} band increased until the BET monolayer capacity (1.1 mmol·g^{-1}) was reached but stayed constant over this H_2O amount. The reason for this could be the fact that these free OH groups exist only on the surface of adsorbed layers or may remain inside the layer without hydrogen bonding. A model of the configuration of the surface P–OH groups and adsorbed H_2O is postulated in Figure 8, as a summary of the discussion described above.

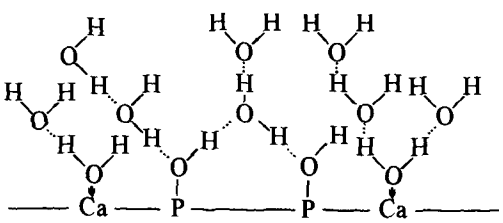

Figure 8. A model of the adsorption of H_2O on CaHAP.

3.2.2. Adsorption of CH_3OH on CaHAP

Figure 9 shows the adsorption isotherms of CH_3OH on CaHAP (Ca/P = 1.64) pretreated in vacuo at 300°C for 2 h. The adsorbed amount of CH_3OH increased very steeply at

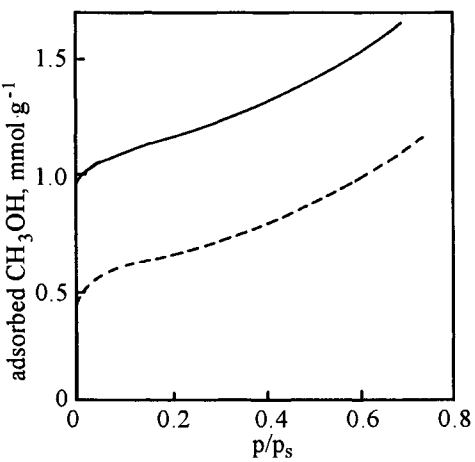

Figure 9. Adsorption isotherms of CH_3OH on CaHAP (Ca/P=1.64) at 25°C. The solid and dashed lines represent the first and second isotherms, respectively.

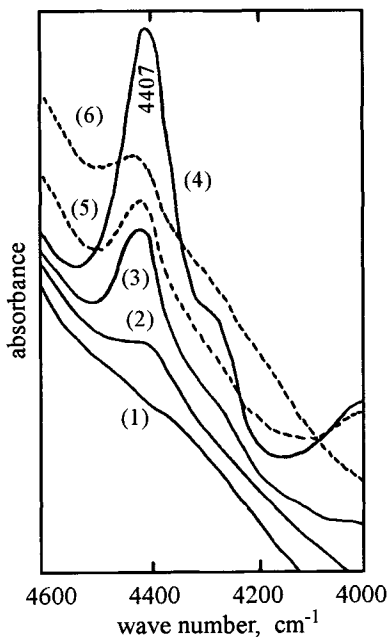

Figure 10. IR spectra of CaHAP (Ca/P=1.64) adsorbing various amounts of CH_3OH: (1) before adsorption, (2) 0.2 mmol·g^{-1}, (3) 0.5 mmol·g^{-1}, (4) 1.3 mmol·g^{-1}, (5) outgassed at 25°C after taking spectrum 4, (6) outgassed at 300°C after taking spectrum 5.

low relative pressure, indicating the strong interaction between CH_3OH and the surface CaHAP. The second adsorption isotherm shown by the dashed line was measured on the sample outgassed at 25°C after measurement of the first isotherm. The adsorbed amount of the first isotherm is larger than that of the second one and these isotherms are parallel to each other, implying that a part of CH_3OH adsorbed during the first isotherm is irreversibly adsorbed. The amount of irreversible adsorption of CH_3OH, evaluated from the adsorbed amount after outgassing at 25°C for 2 h after taking the isotherm, was 2.5 molecule·nm^{-2} based on the BET-N_2 specific surface area (94 $m^2 \cdot g^{-1}$).

To know the adsorption sites for CH_3OH, the *in situ* IR spectra were taken for the same sample as in Figure 9. The absorbances of the bands at 3683, 3670 and 3659 cm^{-1} due to the surface P–OH groups were decreased by CH_3OH adsorption and the C–H fundamental stretching bands appeared at 2845 and 2950 cm^{-1}. Figure 10 shows the change of IR spectra of CaHAP by CH_3OH adsorption. The spectra of CaHAP adsorbing CH_3OH show a band at 4407 cm^{-1} of which the intensities increase with increasing the amount of adsorbed CH_3OH. This band can be assigned to the combination vibration of

CH_3 groups of CH_3OH, because the spectrum in this range on CH_3OD adsorption had the same band as that of CH_3OH, whereas no band was observed in this wave number range on CD_3OD adsorption while a C–D combination band appeared at 3350 cm^{-1}. Since the quantitative estimate of the absorbances of two C–H bands at 2845 and 2950 cm^{-1} was difficult because of overlapping with O–H bands, the 4407 cm^{-1} band can be used for the quantitative discussion. Figure 11 shows the absorbances of surface P–OH band and the C–H combination band of adsorbed CH_3OH as a function of the amount of adsorbed CH_3OH. Below 1.1 molecule·nm^{-2} of adsorbed CH_3OH, the intensitiy of the surface P–OH

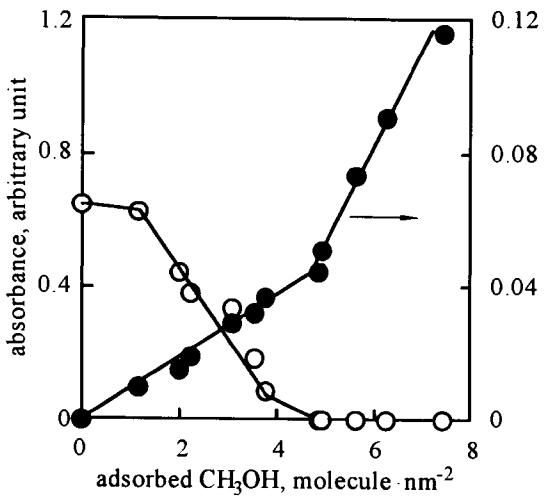

Figure 11. Adsorbance change of P–OH band at 3682 cm^{-1} (○) and C–H band at 4407 cm^{-1} (●) with CH_3OH adsorption for CaHAP (Ca/P=1.64).

bands mentioned above did not change appreciably in the site of the sharp rise of the corresponding isotherm, which indicates that CH_3OH molecules are adsorbed strongly on the sites other than P–OH groups in the initial stage. This behaviour is similar to that of the H_2O strongly adsorbed on CaHAP. Over 1.1 molecule·nm^{-2} of adsorbed CH_3OH, the surface P–OH band decreased proportionally to the adsorbed amount of CH_3OH and disappears at 5.0 molecule·nm^{-2} that is equal to the monolayer capacity obtained from the isotherm. These results indicate that 3.9 CH_3OH molecules interact with P–OH groups. Since the population of surface P–OH groups is 4.4 groups per nm^2 of the surface as described in Section 3.2.1., the surface P–OH groups bond with CH_3OH molecules with almost one to one correspondence. As can be seen in Figure 11, the absorbance of the combination band at 4407 cm^{-1} of adsorbed CH_3OH increased proportionally with the amount of adsorbed CH_3OH up to the monolayer capacity of 5.0 molecule·nm^{-2} (Figure 10). The 4407 cm^{-1} band becomes smaller when evacuating the sample adsorbing CH_3OH. The amount of irreversibly adsorbed CH_3OH, estimated as CH_3 groups from the absorbance of the 4407 cm^{-1} band, was 2.9 molecule·nm^{-2} that is roughly equal to n_i of 2.5 molecule·nm^{-2} obtained from the adsorption isotherms. As can be seen from

spectrum 6 of Figure 10, the absorbance of 4407 cm^{-1} band did not decrease any more over 300°C, which suggests that CH_3OH molecules adsorbed strongly attach to P–OH groups as CH_3O groups.

3.2.3. Adsorption of CH_3I on CaHAP

Figure 12 shows the adsorption isotherms at 25°C of CH_3I on CaHAP (Ca/P = 1.64) outgassed at 300°C for 2 h. The rise of the adsorbed amount of CH_3I in the low pressure range was not so steep as in the case of CH_3OH (Figure 9). The second isotherm was

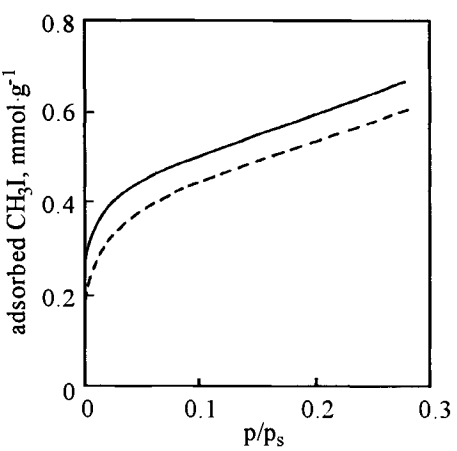

Figure 12. Adsorption isotherms of CH_3I on CaHAP (Ca/P=1.64) at 25°C. The solid and dashed lines represent the first and second isotherms, respectively.

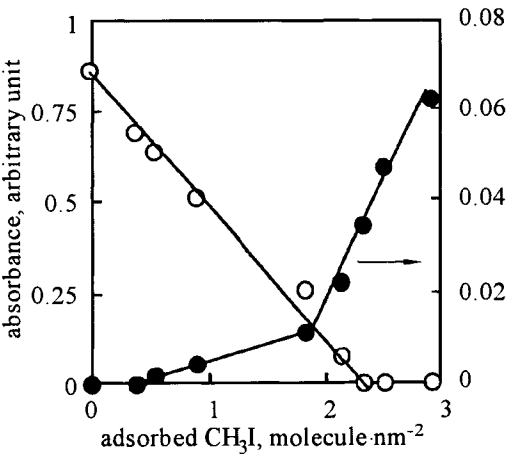

Figure 13. Adsorbance change of P–OH band at 3682 cm^{-1} (○) and C–H band at 4470 cm^{-1} (●) with CH_3I adsorption for CaHAP (Ca/P=1.64).

measured in the same manner as for CH_3OH adsorption. The amount of irreversible adsorption of CH_3I was 0.4 molecule·nm^{-2} less than that of CH_3OH. The IR spectra of CaHAP of the sample adsorbing CH_3I showed two C–H combination bands at 4470 and 4305 cm^{-1}. Figure 13 shows the absorbances of the surface P–OH band (3682 cm^{-1}) and the 4470 cm^{-1} band as a function of the adsorbed amount of CH_3I. The absorbance of the 3682 cm^{-1} band decreased linearly with the increase of adsorbed amount and this band disappeared above the monolayer adsorption capacity. On the other hand the 4470 cm^{-1} band grew with the increase of adsorbed amount except a low coverage region. The degree of the absorbance increase of this C–H band up to 2 molecule·nm^{-2} was smaller than that over this adsorbed amount. This fact suggests that CH_3I decomposed on adsorption to CH_3 radicals and escaped from the surface, leaving I atoms on the surface to some extent. This interpretation is supported by the XPS peaks appearing at 623 and 633 eV assigned to $I(3d_{3/2})$ and $I(3d_{5/2})$ states, respectively, after evacuating this sample, but the height of C(1s) peak at 287 eV was equal to that before adsorption. The irreversibly adsorbed I atoms cannot be removed by outgassing even at 300°C. One possible reaction of CH_3I

with the surface during the adsorption would be a kind of Grignard reaction as follows:

$$Ca(s) + CH_3I(a) = CaICH_3(s) \quad (1)$$

$$CaICH_3(s) + P - OH(s) = P - OCaI(s) + CH_4(g) \quad (2)$$

where (s), (a) and (g) represent the surface, adsorbed and gaseous species, respectively.

3.2.4. Adsorption of CO_2 on CaHAP, SrHAP and SrCaHAP

Figure 14 displays typical adsorption isotherms of CO_2 on CaHAPs with various Ca/P ratios outgassed at 300°C for 2 h. The second isotherms represented by the open marks were determined on the samples outgassed at 25°C for 2 h after taking the first isotherms.

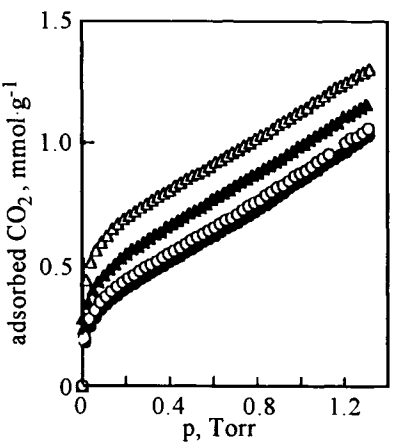

Figure 14. Adsorption isotherms of CO_2 on CaHAPs with different Ca/P ratios. The open and filled marks represent the first and second isotherms, respectively. ○, ●, Ca/P=1.62; △, ▲, Ca/P=1.55.

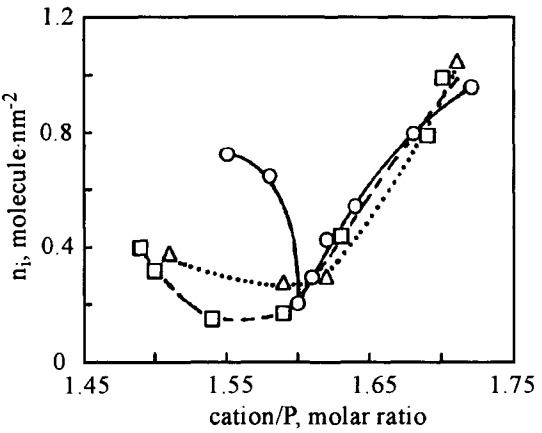

Figure 15. Relation between irreversible adsorption of CO_2 (n_i) and cation/P molar ratio for CaHAP (○), SrHAP (△) and SrCaHAP (□).

The adsorbed amount of the first isotherms shown by the solid marks was larger than that of the second isotherms, which suggests that a part of CO_2 molecules adsorbed during the first isotherm was irreversibly adsorbed, because CO_2 molecules reversibly adsorbed are considered to be desorbed by outgassing the sample before measurement of the second isotherm. Since the first and second isotherms over ca 200 Torr are parallel with each other, the amount of irreversible adsorption (noted n_i) can be evaluated from the average difference in the adsorbed amounts of the first and second isotherms over 200 Torr. Figure 15 shows the n_i values as a function of Ca/P molar ratios. It is of interest that n_i exhibits a minimum at Ca/P of 1.60. The interpretation for this fact will be given later. The *in situ* FTIR indicated that the surface P-OH groups are not the irreversible adsorption sites of CO_2 but the reversible ones, different from the adsorption of H_2O and CH_3OH. The adsorption isotherms of CO_2 on the SrHAP showed the difference between the adsorbed

amounts of the second and first isotherms as in the case of CaHAP. The n_i values obtained from the difference of adsorbed amounts are plotted against Sr/P ratios in Figure 15. The n_i values slightly decrease with increasing Sr/P and then increase, exhibiting a minimum around Sr/P = 1.6 while less clearly than n_i of CaHAP.

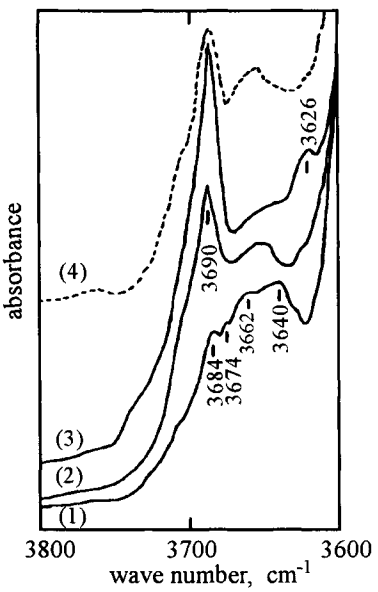

Figure 16. IR spectra of SrHAP (Sr/P=1.59) adsorbing various amounts of CO_2: (1)before adsorption, (2) 0.22 mmol·g^{-1}, (3) 1.02 mmol·g^{-1}, (4) evacuated at 25°C after recording spectrum 3.

Figure 16 compares the *in situ* IR spectra of the Sr-deficient SrHAP (Sr/P = 1.59) with various amounts of adsorbed CO_2. The 3640 cm^{-1} bands due to the surface P–OH groups gradually become smaller and a new strong band appeared at 3690 cm^{-1}. The 3690 cm^{-1} band shifted slightly to 3694 cm^{-1} and grew with increasing amounts of adsorbed CO_2. As can be seen in Figure 16, the surface P–OH bands of Sr-deficient SrHAP except the 3640 cm^{-1} band almost recovered when the samples were outgassed at 25°C. On the contrary, the 3640 cm^{-1} band did not recover after outgassing the sample, indicating that the surface P–OH groups showing this band are the irreversible adsorption sites for CO_2. To gain further insight into the irreversible adsorption mechanism of CO_2, the character of the 3690 cm^{-1} band due to CO_2 adsorption was examined by thermal treatment, H–D exchange and H_2O adsorption. On outgassing the sample at 100 – 200°C, the 3690 cm^{-1} band disappeared and the 3640 cm^{-1} band reappeared. H–D exchange reduced the 3690 cm^{-1} band, leading to a new band at 2725 cm^{-1} that is regarded as the OD band of the 3690 cm^{-1} band, taking into account the wave number ratio (OH/OD = 3690 / 2725 = 1.354). The adsorption of H_2O also reduced the 3690 cm^{-1} band. Furthermore, the Sr-deficient SrHAP impregnated with $NaHCO_3$ showed a band at 3688 cm^{-1} which disappeared as well as the 3690 cm^{-1} band when the sample was outgassed over

100°C. The 3690 cm^{-1} band can be assigned to the surface C–OH groups produced by the irreversible adsorption of CO_2 on the less-acidic surface P–OH groups inducing the 3640 cm^{-1} band through the following reaction:

$$P - OH(surface) + CO_2 \longrightarrow P - OCO(OH)(surface).$$

This surface species seems to be thermally unstable as it decomposes to CO_2 and P–OH during heating, because the 3640 cm^{-1} band reappeared when the sample was outgassed over 100 °C.

For the Sr-rich SrHAP (Sr/P = 1.71), the surface P–OH bands at 3684, 3674 and 3662 cm^{-1} and the surface C–OH groups at 3710 cm^{-1} diminished by CO_2 adsorption, but the 3694 cm^{-1} band appeared. Since all the surface OH bands reappeared on outgassing the sample at 25°C, these surface OH groups are the reversible adsorption sites of CO_2. However, the irreversible adsorption took place on the Sr-rich sample as stated above. As distinct from the Sr-deficient SrHAP (Sr/P = 1.59), the Sr-rich SrHAP has no less-acidic surface P–OH groups to give the 3640 cm^{-1} band and form the irreversible adsorption sites of CO_2. So we must find other irreversible adsorption sites of CO_2 than the less acidic surface P–OH groups. It is well known that the PO_4^{3-} defects of CaHAP are compensated by CO_3^{2-} and/or OH^- ions [38]. It seems most likely, therefore, that the OH^- ions that exist on the surface function as the irreversible adsorption sites of CO_2 on the Sr-rich SrHAP, because the OH^- ions are generally reactive to CO_2 as follows;

$$OH^-(surface) + CO_2 \longrightarrow HCO^{3-}(surface).$$

The 3694 cm^{-1} band observed for the Sr-rich SrHAP is assigned to the C–OH groups of the surface HCO^{3-} ions yielded by the irreversible adsorption of CO_2. Consequently, the surface P–OH groups of SrHAP function as the reversible adsorption sites of CO_2. The irreversible adsorption sites are the less acidic surface P–OH groups of the Sr-deficient SrHAP and the surface OH^- ions of the Sr-rich SrHAP. The irreversible adsorption of CO_2 yields the surface C–OH groups.

The amount of irreversible adsorption (n_i) of the solid solution (SrCaHAP) of CaHAP and SrHAP is shown in Figure 15. The n_i value can be fitted on a curve showing a minimum around a cation /P of 1.56. This result is in accordance with the cases of CaHAP and SrHAP. Thus, we can consider that the irreversible adsorption of CO_2 on HAPs generally depends on its non-stoichiometry. The n_i values of CaHAP and SrHAP are a minimum at Ca/P = 1.60 larger than ca. 1.55 for SrCaHAP and the curve for SrCaHAP is close to that for SrHAP. The n_i values of CaHAP are larger than those of SrHAP and SrCaHAP below cation/P = 1.60. These results are in good agreement with the result reported by Joris and Amerg [9]: the rate of dehydration of butanol over CaHAP or SrHAP decreases with the increase in Ca/P ratio up to ca. 1.60 and the rate over CaHAP is faster than that over SrHAP. However, since they did not use samples with Ca/P > 1.60, the minimum found in this study was not observed. They explained the higher catalytic activity of CaHAP crystals and the lower basicity of the Ca^{2+} ions. However, the larger n_i values of CaHAP cannot be satisfactorily accounted for by these two factors. Note that the minimum n_i values of each series are not zero, showing that the stoichiometric HAP adsorbs CO_2 irreversibly. These findings can be explained by considering that there are two kinds of irreversible adsorption sites for CO_2 on these HAPs, caused by the deficiency of cations like Ca^{2+} or Sr^{2+} and anions like PO_4^{3-}. With increasing cation/P ratio, the number of

adsorption sites resulting from the cation deficiency decreases, whereas that from the anion deficiency increases. Thus the curves for each sample possess a minimum. However, the kinds of site coexist at the minimum n_i value. The cation/P ratio showing a minimum n_i is less than the stoichiometric ratio of 1.67. This would be because the surface chemical composition differs from that of the bulk. It is feasible that the surface PO_4^{3-} ions are more easily exchanged by other anions, such as CO_3^{2-}, HCO^{3-} and OH^-, than the bulk PO_4^{3-} ions, to give a lower cation/P ratio.

4. SUMMARY

Various kinds of surface P–OH groups were found for CaHAP, SrHAP and SrCaHAP. The Fe^{3+}-substituted CaHAP possesses the surface Fe–OH groups besides the surface P–OH groups. These surface OH groups function as the adsorption sites for H_2O, CH_3OH, CH_3I and CO_2. The irreversible adsorption of these molecules depends on the kind of cations and non-stoichiometry of HAP.

ACKNOWLEDGMENTS

The author gratefully acknowledges the collaboration of Dr. K. Kandori, Mrs. A. Yasukawa, Mr. M. Wakamura and Mr. H. Saito. This work was supported in part by the Scientific Research Fund of the Ministry of Education of the Japanese Government and the Nippon Sheet Glass Fund for Materials Science and Technology.

REFERENCES

1. J. C. Elliott, Structure and Chemistry of the Apatites and Other Calcium Orthophosphates, Elsevier, Amsterdam, 1994.
2. S. Joris and C. Amberg, J. Phys, Chem., 20 (1971) 3172.
3. T. Ishikawa, M. Wakamura and S. Kondo, Langmuir, 5 (1989) 140.
4. J. P. Yesinowski, R. A. Wolfgang and M. Mobley, in: Adsorption on and Surface Chemistry of Hydroxyapatite, D. N. Misra, (ed.), Plenum, New York, 1984, p. 151.
5. P. Somasundaran and G. E. Agar, J. Colloid Interface Sci., 24 (1967) 433.
6. K. Konishi, M. Kambara, M., H. Noshi and M. Uemura, J. Osaka Dent. Univ., 21 (1987) 1.
7. M. E. Dry and R. A. Beebe, J. Phys. Chem., 64 (1960) 1300.
8. J. A. S. Bett, L. G. Christner and W. K. Hall, J. Am. Chem. Soc., 89 (1967) 5535.
9. S. J. Joris and C. H. Amberg, J. Phys. Chem., 75 (1971) 3167.
10. S. J. Joris and C. H. Amberg, J. Phys. Chem., 75 (1971) 3172.
11. R. L. Collin, J. Am. Chem. Soc., 81 (1959) 5275.
12. R. Z. Legelos, Nature (London), 206 (1965) 403.
13. J. C. Elliott, Calcif. Tissue Res., 3 (1969) 293.
14. P. Cevc, M. Schara and C. Ravnik, Radiat. Res., 51 (1972) 581.
15. P. Monens, F. Callens, P. Matthys, F. Maes, R. Verbeeck and D. Naessens, J. Chem. Soc., Faraday Trans., 87 (1991) 3137.

16. Y. Tanizawa, K. Sawamura and T. Suzuki, J. Chem. Soc., Faraday Trans., 86 (1990) 4025.
17. Y. Tanizawa, K. Sawamura and T. Suzuki, J. Chem. Soc., Faraday Trans., 86 (1990) 1071.
18. T. Suzuki, K. Ishigaki and M. Miyake, J. Chem. Soc., Faraday Trans. I, 80 (1984) 3157.
19. T. Suzuki, T. Hatsushika and M. Miyake, J. Chem. Soc., Faraday Trans. I, 78 (1982) 3605.
20. T. Suzuki, T. Hatsushika and Y. Hayakawa, J. Chem. Soc., Faraday Trans. I, 77 (1981) 1059.
21. R. M. H. Verbeeck, C. J. Lassuyt, H. J. M. Heijligers, F. C. M. Driessens and J. W. G. A. Vralijk, Calcif. Tiss. Int., 33 (1981) 243.
22. H. J. M. Heijligers, F. C. M. Driessens and R. M. H. Verbeeck, Calcif. Tiss. Int., 29 (1979) 127.
23. M. Misono and W. K. Hall, J. Phys. Chem., 77 (1973) 791.
24. Y. Matsumura, J. B. Moffat, S. Sugiyama, H. Hayashi, N. Shigemoto and K. Saitoh, J. Chem. Soc., Faraday Trans., 90 (1994) 2133.
25. T. Ishikawa, H. Saito and K. Kandori, J. Chem. Soc., Faraday Trans., 88 (1992) 2937.
26. T. Ishikawa, H. Saito, A. Yasukawa and K. Kandori, J. Chem. Soc., Faraday Trans., 89 (1993) 3821.
27. H. Furedi-Milhofer, V. Hlady, F. S. Baker, R. A. Beebe, N. W. Wikholm and J. S. Kittelberger, J. Colloid Interface Sci., 10 (1979) 1.
28. B. C. Lippens and J. H. de Boer, J. Catal., 4 (1965) 319.
29. N. W. Cant, J. A. S. Bett, G. R. Wilson and W. K. Hall, Spectrochim. Acta, 27A (1971) 425.
30. M. J. D. Low and P. Ramamurthy, J. Phys. Chem., 72 (1968) 3161.
31. K. I. Kay and R. A. Young, Nature, 204 (1964) 1050.
32. J. Arends, J. Schuthof, W. H. van der Linden, P. Bennema and P. J. van den Berg, J. Crystal Growth, 46 (1979) 213.
33. M. Kukura, L. C. Bell, A. M. Posner and J. P. Qurk, J. Phys. Chem., 76 (1972) 900.
34. E. E. Berry, J. Inorg. Nucl. Chem., 29 (1967) 317.
35. K. Sudarsanan and R. A. Young, Acta Crystallogr., B25 (1969) 1534.
36. T. Ishikawa, S. Nitta and S. Kondo, J. Chem. Soc., Faraday Trans. I, 82 (1986) 2401.
37. H. Yamatera, B. Fitpatrick and G. Gordon, J. Mol. Spectrosc., 14 (1964) 268.
38. G. Ronel and G. Montel, Compt. Rend. Acad. Sci., Paris Ser. C, 258 (1964) 923.

A. Dąbrowski and V.A. Tertykh (Editors)
Adsorption on New and Modified Inorganic Sorbents
Studies in Surface Science and Catalysis, Vol. 99

Chapter 1.12
Surface chemistry and adsorption properties of Al_{13} colloids

J.Y. Bottero[a] and J.M. Cases[b]

[a]Laboratoire des Géosciences de l'Environnement, URA 132 CNRS, CEREGE, Europole Méditerannéen de l'Arbois, BP 80, 13545 Aix-en-Provence Cedex 04, France

[b]Laboratoire Environnement Minéralurgie, URA 235 CNRS, ENSG, INPL, BP 40, 54501 Vandoeuvre Cedex, France

The surface chemistry of very small Al_{13} colloids precipitated at pH 6.5 or 7.5 from two acidic concentrate sols of isolated Al_{13} (r=[NaOH]/[Al]=2) and aggregated Al_{13} (r=[NaOH]/[Al]=2.5) has been determined by using the potentiometric titration and zeta potential in the NaCl electrolyte. The ZPC 8.2 is close to the IEP. In parallel adsorption of long chain alkylsulfonates on these particulates has been interpret by using two dimensional condensation on the heterogeneous surfaces. The interpretation of the isotherms coupled with the zeta potential versus equilibrium concentration showed that the nature of a normal bond between the adsorbate–adsorbent is mainly electrostatic. The specific surface area of particulates varies with pH from 540 m^2/g (pH 7.5) to 774 m^2/g (pH 6.5).

The site density number determined from the titration is ~1.1–1.2 / nm^2. This parameter is used to fit the titration and zeta curves of particulates in NaCl by using a non–linear programmation. Four main surface reactions were determined: two in relation to the amphoteric dissociation of =Al–OH surface groups (pK_1=6.4 and pK_2=10) and two with complexation of Cl^- on =Al–OH_2^+ site and Na^+ on =Al–O– site (pK_3=3.4 and pK_4=3.5).

1. INTRODUCTION

The hydrolysis of $AlCl_3 \cdot 6H_2O$ leads to Al_{13} polycation species which is the major component from acidic pH to neutral pH [1–5]. The aggregation of Al_{13} from pH=5 to pH=8 by decreasing the repulsions leads to the formation of large aggregates whose structure is fractal. The fractal dimension increases from 1.4 up to 1.8 with the pH increase [6]. These precipitates are formed by diluting the concentrate Al_{13} solution in water. They contribute to the removal of inorganic colloids and organics from water in drinking water treatment industry.

The role in adsorbing organics has been studied in the case of micropollutants [7]. These very divided solids remove only 30% of dibuthylphtalate molecules present in the surface water.

This paper deals with the surface chemistry and the surface heterogeneity of Al_{13} aggregates vs. pH.

2. MATERIALS AND EXPERIMENTAL METHODS

The Al_{13} precipitates are obtained by diluting concentrate Al_{13} sols prepared by hydrolyzing $AlCl_3 \cdot 6H_2O$ with NaOH. The concentrates Al_{13} solutions have an Al concentration of 0.1M and an hydrolysis ratio r=(NaOH)/(Al)=2 and 2.5. In r=2, Al_{13} polycations are not aggregated. In r=2.5, 70% of Al_{13} formed small aggregates.

Dilution at neutral pH=6.5 and 7.5 of r=2 and r=2.5 leads to the precipitates formed by the aggregation of isolated Al_{13} or small Al_{13} aggregates. These precipitates are denoted AH_2 and $AH_{2.5}$. A schematic view of these aggregates is shown in Figure 1.

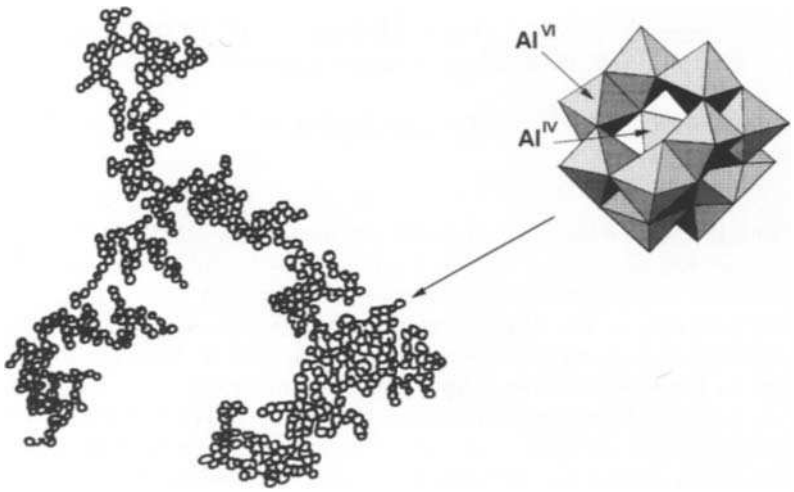

Figure 1. Schematic view of Al_{13} aggregates formed at neutral pH [5].

Surfactants used to characterize the main properties of the precipitate surface i.e. the specific surface area and heterogeneity are 1 sodium dodecane sulfonate–SDS (ref. Merck 12146) with a Krafft point of 31°C and solubility of $6.5 \cdot 10^{-3}$M [8] in water at 25°C and 1 sodium tetradecane sulfonate –STS (ref. Merck 12362) with a Krafft point of 46°C and solubility of $1.36 \cdot 10^{-3}$ M [8] in water at 25°C.

2.1. Experimental methods

Surface electrochemistry of AH_2 and $AH_{2.5}$

2.1.1. Potentiometric titration

Experiments were carried out on new precipitates in the NaCl electrolyte. All solutions were of analytic grade, prepared with milliQ water quality and bubbled by N_2 during one night before and during the experiment.

The total Al concentration after diluting is $2 \cdot 10^{-3}$M. The pH of the suspension is maintained at 7.5±0.1 and stabilized for 3 min. Then the precipitates are titrated by NaOH or HCl using a Titrimax–tacussel apparatus.

The supernatant of each suspension is titrated under the same conditions.

The balance of protons and hydroxyls at the surface ($Q_0 = \Gamma H^+ - \Gamma OH^-$) is calculated by the difference between the base or acid volumes required to bring suspension and blank to the same pH. The added NaCl electrolyte concentrations are 10^{-1}M and 1M.

2.1.2. Electrokinetic potential

Electrophoresis measurements were carried out using a laser Zee Meter Pen-Kem (Model 501).

Adsorption of surfactants.

The adsorption of SDS and STS at 25°C is carried out on Al_{13} precipitates at pH=6.5 and 7.5 in mineralized water with 0.125g NaCl and 0.025g $NaHCO_3$ in order to buffer the liquid bulk. In each beaker 1l of AH_2 or $AH_{2.5}$ suspension, stirred at 200 rpm, adequate concentration of SDS or STS is added. The pH is quickly stabilized at pH=6.5 or 7.5 by NaOH 0.1M. After 3 min; the suspension is stirred at 40 rpm for 30 min in order to obtain equilibrium attained after a few minutes (Figure 2).

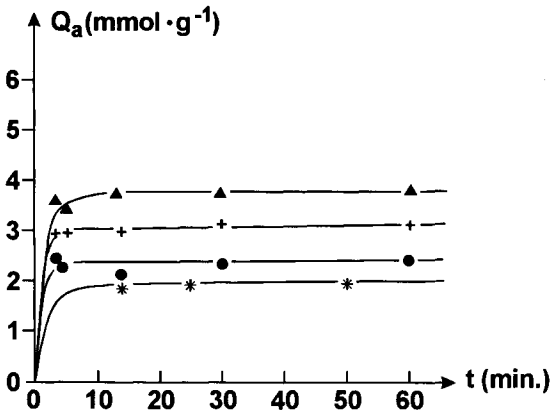

Figure 2. Kinetics of adsorption of sodium tetradecane sulfonate STS ($C_i=10^{-4}$ M)(▲,●) and sodium dodecane sulfonate SDS ($C_i=4{\cdot}10^{-5}$ M)(+,*) on AH_2 (▲,+) and $AH_{2.5}$ (●, *).

After the equilibrium is reached 20 ml is centrifuged at 15000 rpm for 20 min at 25°C. The equilibrium concentration $C_{eq.}$ is determined by colorimetry at 635 nm [9]. 500 ml is filtered on 2μm Millipore filters. The electrokinetic measurements are made on flocs smaller than 2μm.

3. THERMODYNAMICS OF SURFACTANT ADSORPTION ON SOLIDS

The adsorption of long chain ionic amphiphiles can be described by a model which accounts for potential energies, entropic terms in the adsorbed layer and surface energy heterogeneity of the adsorbent in the case of localized adsorption [10–12]. This is limited to the case where the adsorbate can form precipitates with the ions in equilibrium with

the solid. This new phase appears on the experimental isotherm as a vertical step at a saturation concentration $C_{sat.}$. The monolayer may not be reached.
Two cases may be considered:
a) Homogeneous surface
In the case of surfactants with more than 8 CH_2 groups in the alkyl chain and for a particular equilibrium concentration $C^*_{eq.}$, the filling of the surface abruptly increases from $\Theta \sim 0$ up to $\Theta = 1$. This vertical step corresponds to a two dimensional condensation for an undersaturation $\Delta\mu$ with respect to the precipitate phase obtained at $C_{sat.}$:

$$\Delta\mu = B - \Phi^0_a = kT \ln [C^*_{eq.}/C_{sat.}] \tag{1}$$

where Φ^0_a is the work to break the normal adsorbate–adsorbent bond, B is the constant for homologous surfactants (i.e. only the chain length is changed) which characterizes the interactions between surfactants in the adsorbed phase or in a precipitate phase.

Equation (1) implies that the adsorbed layer is in the same condensation state as a reticular plane of the precipitate considered as a reference phase. This assumes that lateral energies and entropic terms are constant for any solid. So the experimental isotherms built as the example with SDS and STS are superimposed in $(Q_a a, \Delta\mu)$ plane. Φ^0_a terms depend on the nature of the interaction between the solid sites and the surfactant head only.
b) Heterogeneous surface
Heterogenous surface can be considered as a homogeneous domain i of the surface area S_i and the normal adsorbate/adsorbent energy Φ^0_{ai}. The surface coverage Θ_a is:

$$\Theta = \sum_i S_i \Theta_i / S \tag{2}$$

where Θ_i is the surface coverage of homogeneous domain i which in the two-dimensional condensation hypothesis is empty or full. So Eq. (2) becomes:

$$\Theta = \sum S_i / S \tag{3}$$

On one homogeneous domain Eq.(1) can be used:

$$\Delta\mu^* = B - \Phi^0_{ai} \tag{4}$$

Equation 4 shows that the surface fills as Φ^0_{ai} decreases. If the solid does not modify the organization of the adsorbed layer as it is to do, Eq.(1) is unic.
The shape of the experimental isotherm in the $\Theta - \Delta\mu$ plane depends only on the distribution of Φ^0_{ai} on the $\Delta\mu$-axis and the extension of S_i on Θ-axis. The shape of the isotherm depends only on the distribution of heterogeneity.

In the case of two experimental isotherms, with for example SDS and STS, built on heterogeneous solid characterized by seven homogeneous domains i (Fig.2) the following expression:

$$[kT \ln C^*_{eq.i,n}]\Theta = -n\Delta G/2 + E \tag{5}$$

where $C^*_{eq.i,n}$, is the equilibrium concentration corresponding to the condensation on a domain i for a surfactant containing n CH_2 groups, ΔG is the Gibbs energy on transfer of one CH_2 group from the adsorbed layer to the solution and E is:

$$E = \Phi^0_{ai} + \omega_0/2 - kT \ln (v_a \cdot N_A)$$

where N_A is the Avogadro number, ω_0 is the repulsive head–head bond, and v_a is the average vibration volume of the surfactant head in the condensed layer. This last term is slightly dependent on the molecular mass for $10 \leq n \leq 18$ [13]. If on each domain i the condensed state is the same, the slope of the $\ln C_{eq.}$ vs. n curves is $-\Delta G$ whatever Q_a value.

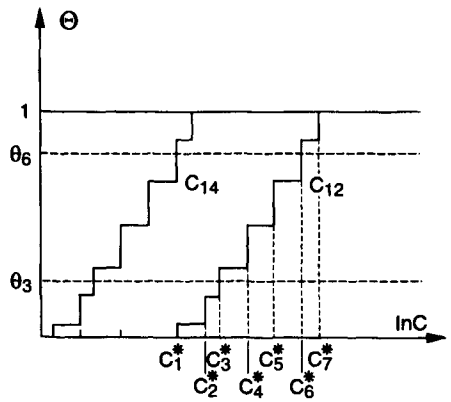

Figure 3. Schematic representation of the experimental isotherms on solids with seven homogeneous domains and surfactants with n=12 and 14.

4. ELECTROCHEMICAL INTERFACE MODEL OF Al_{13} PRECIPITATES

Al_{13} colloids are constituted by Ns amphoteric = $AlOH_i$ sites which may ionize as follows:

$$=AlOH_2^+ \rightleftharpoons =AlOH + H^+ \quad (6)$$

$$=AlOH \rightleftharpoons =AlO^- + H^+ \quad (7)$$

$=AlOH^+$ and $=AlO^-$ interact with the electrolyte ions e.g.:

$$=AlOH_2^+ + Cl^- \rightleftharpoons =AlOH_2Cl \quad (8)$$

$$=AlO^- + Na^+ \rightleftharpoons =AlONa \quad (9)$$

the uncharged sites =AlOH can react with Na^+ or Cl^- as follows:

$$=AlOH + Na^+ \rightleftharpoons =AlOHNa^+ \quad (10)$$

$$=AlOH + Cl^- \rightleftharpoons =AlOHCl^- \quad (11)$$

The latter reactions are possible if Na^+ and Cl^- are hydrated. In this way hydrogen bonds can explain the reactions with OH surface groups.
Reactions (6–12) are responsible for the development of an electrical double layer at the

interface, e.g.:
a) an internal layer of global charge σ_s:

$$\sigma_s = F/N_A \left\{ N[=AlOH^+] + N[=AlOHNa^+] - N[=AlO^-] - N[=AlOHCl^-] \right\} \quad (12)$$

where F and N_A are the Faraday and Avogadro numbers respectively, N[j] is the site density number of surface site j.
b) an external diffuse layer made of H^+, OH^-, Na^+, Cl^- with a charge σ_d:

$$\sigma_d = -11.74 \cdot 10^{-2} c^{1/2} \sinh(0.0194\zeta) \qquad C \cdot m^{-2} (\text{at } 25°C). \quad (13)$$

where ζ is the electrokinetic potential and $c = [Na^+] + [H^+] = [Cl^-] + [OH^-]$.
Equilibrium of the double layer requires:

$$\sigma_s + \sigma_d = 0 \quad (14)$$

Interfacial ionic activity and interfacial equilibrium constants

The Boltzman equation expresses the concentration of ion i belonging to the diffuse layer {i}d vs. its bulk concentration {i}b. As an example:

$$\{H^+\}_d = \{H^+\}_b \exp(-38.9 \cdot 10^{-3} \zeta)$$

and

$$(H^+)_d = \gamma_{d,H} \cdot \{H^+\}_d$$

where () indicate the activity , {} the concentration and γ the coefficient activity. Let $EY = \exp(+38.9 \cdot 10^{-3} \zeta)$, so the equilibrium constant corresponding to Eq.(6) is:

$$K_1 = N[=AlOH][H^+]_d / N[=AlOH_2^+] \quad (15)$$

and then:

$$K_1 = N[=AlOH][H^+] / N[=AlOH_2^+] EY \quad (16)$$

Similarly it is possible to derive from reactions (7–11) the same equations (Table 1).

Table 1
Surface reactions on Al_{13} colloids

Reactions	Equilibrium constants	Description
(1) $=AlOH_2 \rightleftharpoons =AlOH + H^+$	K_1EY	H^+ "desorption"
(2) $=AlOH \rightleftharpoons =AlO^- + H^+$	K_2EY	H^+ "desorption"
(3) $=AlOH_2^+ + Cl^- \rightleftharpoons =AlOH_2Cl$	K_3/EY	adsorption on
(4) $=AlONa \rightleftharpoons =AlO^- + Na^+$	K_4/EY	charged sites
(5) $=AlOH + Na^+ \rightleftharpoons =AlOHNa^+$	K_5EY	adsorption on
(6) $=AlOHCl \rightleftharpoons =AlOH + Cl^-$	K_6/EY	"neutral" sites

The defined K_j (j=1–6) are reported in Eq. (12) and give:

$$\sigma_s = F/N_A\, N[=AlOH]\left\{[H^+]/(K_1EY) + [Na^+]/(K_5EY) - K_2EY/[H^+] - [Cl^-]EY/K_6\right\} \quad (17)$$

with $N[=AlOH] = NS/(1+X)$
in which:

$$X = K_2EY/[H^+] + [H^+]/(K_1EY) + [H^+][Cl^-]/(K_1K_3) + K_2[Na^+]/(K_4[H^+]) + \\ + [Na^+]/(K_5EY) + [Cl^-]/K_6 \quad (18)$$

Point of zero charge
Using reactions 1 and 2 in Table 1:

$$N[=Al-O^-][H^+]2/N[=Al-OH_2^+] = K_1K_2 \exp(77.8 \cdot 10^{-3}\zeta) \quad (19)$$

Using the conventional definition of ZPC and IEP the relative amount of proton/hydroxyls consumed by the surface $Q_0 = \Gamma H^+ - \Gamma OH^-$ (mmol/m^2) can be analytically derived:

$$Q_0 = 10^2/N_A\left\{N[=Al-OH_2^+] + N[=Al-OH_2Cl] - N[=Al-O^-] - N[=Al-ONa]\right\} \quad (20)$$

5. RESULTS

5.1. Potentiometric titration

The evolution of Q_0 vs. $\Gamma H^+ - \Gamma OH^-$ (mmol·g^{-1}) is shown in Figures 4 and 5 for AH_2 and $AH_{2.5}$. In NaCl the ZPC of both precipitates is very close to 8.4 and 8.2 respectively.

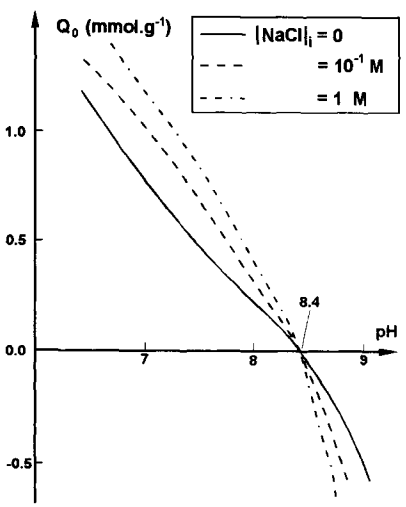

Figure 4. Potentiometric titration of AH_2.

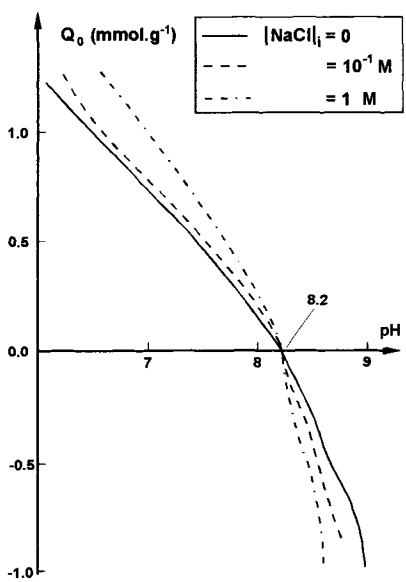

Figure 5. Potentiometric titration of $AH_{2.5}$.

Electrophoretic mobility.

Figure 6 is presents electrophoretic mobility of AH_2 and $AH_{2.5}$. The IEP of each precipitate is very close to their ZPC.

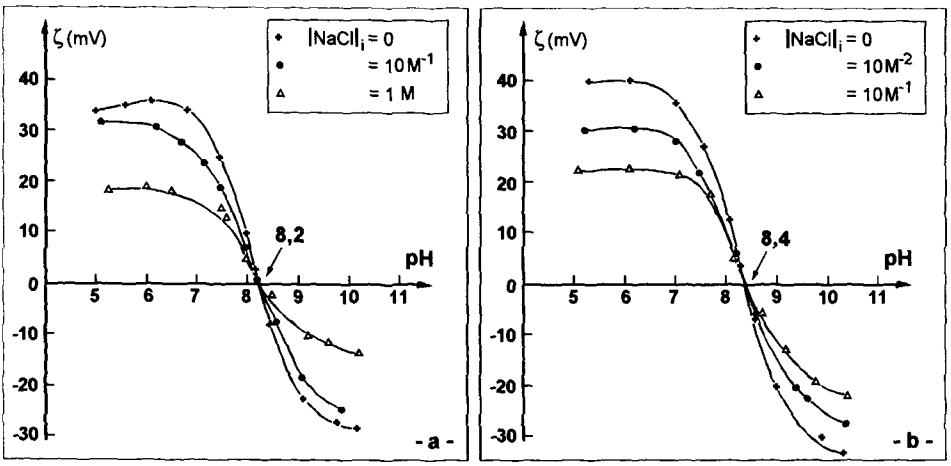

Figure 6. Electrophoretic mobility of AH_2 (b) and $AH_{2.5}$ (a) in the NaCl electrolyte.

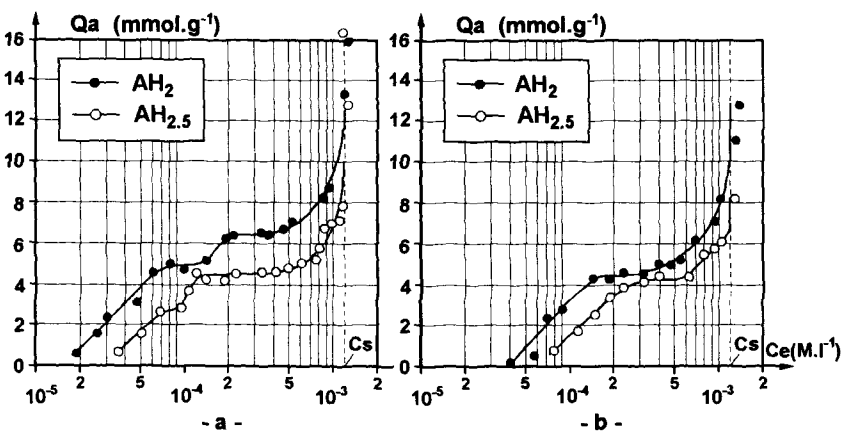

Figure 7. Adsorption isotherms of SDS on AH_2 (●) and $AH_{2.5}$ (○) at pH= 6.5 (a) and 7.5 (b).

Adsorption of SDS on AH_2 and $AH_{2.5}$

The adsorption isotherms of SDS onto both solids at pH 6.5 and 7.5 are shown in Figures 6a and 6b.

In the same manner the experimental isotherms curves obtained at pH 6.5 and 7.5 of STS on AH_2 and $AH_{2.5}$ are shown in Figures 8a and 8b.

All isotherms show at high $C_{eq.}$ values a vertical step characteristic of the formation of mixed SDS or STS/Al_{13} precipitates. The equilibrium concentration $C_{sat.}$ for which the

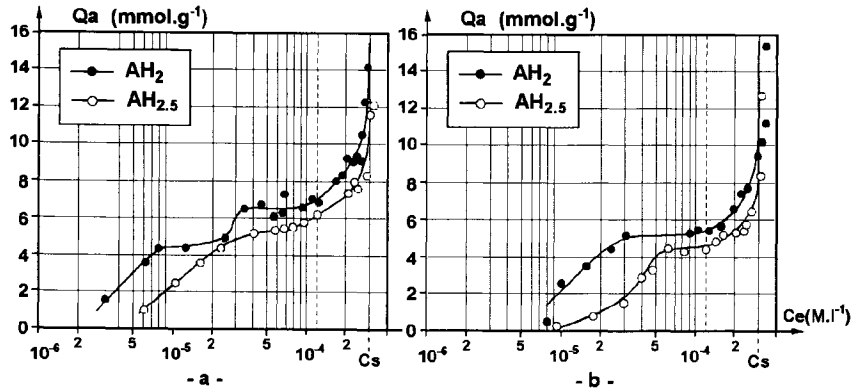

Figure 8. Adsorption isotherms of STS on AH_2 (●) and $AH_{2.5}$ (○) at pH= 6.5 (a) and 7.5 (b).

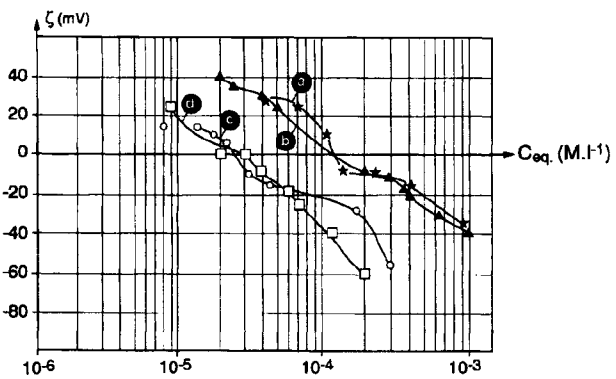

Figure 9. Zeta potential of AH_2 versus SDS (a,b) and STS (c,d) equilibrium concentration $C_{eq.}(mol{\cdot}l^{-1})$ at pH 6.5 (a,c) and pH 7.5 (b,d).

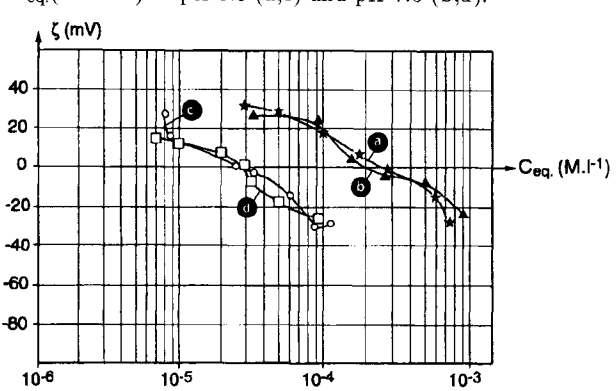

Figure 10. Zeta potential of $AH_{2.5}$ versus SDS (a,b) and STS (c,d) equilibrium concentration $C_{eq.}(mol{\cdot}l^{-1})$ at pH 6.5 (a,c) and pH 7.5 (b,d).

precipitates are formed are $1.3 \cdot 10^{-3}$ M and $3 \cdot 10^{-4}$ M for SDS and STS respectively whatever the pH 6.5 or 7.5. Correspondingly, the zeta potential of the particles of precipitates along the isotherm curves is shown in Figures 9 and 10.

6. DISCUSSION

Because the ZPC $\sim$ 8.2 values of AH_2 and $AH_{2.5}$, the surfaces are globally positive at pH= 6.5 and 7.5. The zeta potentials are positive in the absence of adsorbates. In the range of the $C_{eq.}$ values the zeta potential values vary from +40 mV ($C_{eq.} = 0$) to -60mV ($C_{sat.}$ values).

The zeta potential decreases as Q_a increases. The values of $C_{eq.}$ which corresponds to $\zeta = 0$, highest plateau of the isotherm curves (Figures 7 and 8). Beyond this plateau ζ is negative. If one considers that the normal adsorbate-adsorbent bond is mainly of electrostatic type, the $C_{eq.}$ values corresponding to $\zeta = 0$ coincide with the monolayer. In this case it is possible to normalize the isotherm curves by dividing Q_a by Q_0 which is the value of Q_a corresponding to the monolayer:

$$\Theta = Q_a/Q_0 \tag{21}$$

In the same way the $C_{eq.}$ values of each isotherm may be normalized by dividing them by $C_{sat.}$:

$$\Delta\mu = kT \ln C_{eq.}/C_{sat.} \tag{22}$$

In this case the experimental isotherms for SDS and STS on the same solid and pH are superimposed as shown in Figure 11.

The physical meaning of this normalization (see Eq. (1)) is that the surface field does not influence the organization of the adsorbed layer which is in the same condensation state as a reticular plane of the precipitate considered as a reference phase.

The lateral energy in the adsorbed layer calculated from Eq.(5) experimentally varies from 1.36±0.03 kT to 1.93±0.1 kT. It corresponds to an adsorbed layer in which the aliphatic chains are parallel and stretched towards the solvent. The free energy on transfer between CH_2 is not constant. It is not the case for smooth or plane surface. In the present case the adsorbed phase is in a very condensed state. In this case the molecular area of the surfactants in the adsorbed layer is minimal 20.8Å^2 [14]. Therefore the specific surface area of each solid precipitated at pH 6.5 and 7.5 may be calculated. At the monolayer the adsorbed amount Q_0 is:

$$Q_0 = (1/A) \cdot (1/N_A) \cdot S \tag{23}$$

where A is the molecular area when Q=1, N_A is the Avogadro's number and S is the specific surface area. Table 2 shows the values of S for different systems.

The specific surface areas depend on the pH (surface charge) and on the nature of the initial Al_{13} sol (r=2.0 or r=2.5). In the case of pure electrostatic mechanism it should depend on the adsorbate-adsorbent affinities.

The S values (Table 2) can be used to calculate the density site number from Figures 3 and 4 at pH=6.5 and 7.5. The site density number Ns $\sim$1.1/ nm^2. This value

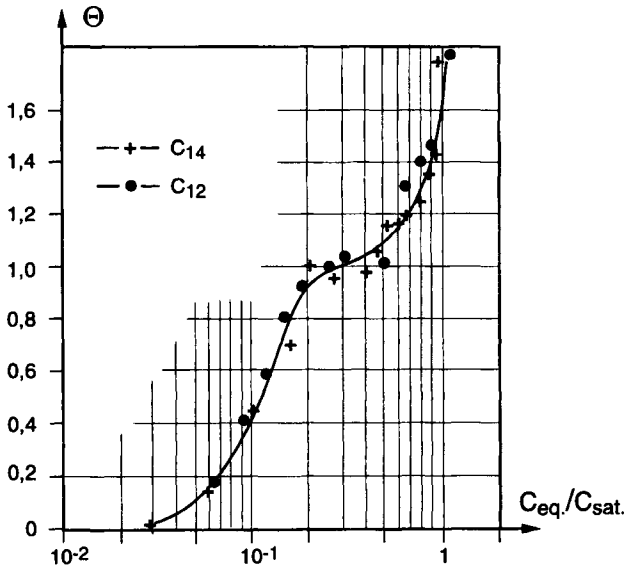

Figure 11. Superimposition of the experimental isotherms (Q, $\Delta\mu$) for SDS and STS on $AH_{2.5}$ at pH 7.5.

Table 2
Calculated values of the specific surface areas ($m^2 \cdot g^{-1}$) of AH_2 and $AH_{2.5}$ at pH 6.5 and 7.5

pH	SDS		STS		mean values	
	AH_2	$AH_{2.5}$	AH_2	$AH_{2.5}$	AH_2	$AH_{2.5}$
6.5	790	563	800	638	795±5	600±38
7.5	563	526	626	551	595±31	539±12

was chosen to calculate the K_j surface hydrolysis reaction constants as defined in Table 1. The mathematical method used is the gradient method. The optimization criterium is defined as follows:

$$\text{Crit} = 1/N \sum \{(\sigma_s + \sigma_d)/\sigma_d\}^2 \tag{24}$$

where N is the number of experimental points.
The gradient method enables estimation of K_j by searching the minimum of Crit value. The calculated values of pK_j for AH_2 and $AH_{2.5}$ are shown Table 3. These values allow to fit very well the z–pH curves (full lines in figure 6). The calculated distribution of surface sites is shown in figure 12.

The surface of AH_2 and $AH_{2.5}$ in NaCl is essentially formed of complexed sites. The adsorption of sulfonates is mainly due to an exchange with Cl^- ions.

Table 3
Calculated surface constants pK_j at three NaCl electrolyte concentrations and for Ns= 1.1 site/nm^2

NaCl		pK_1	pK_2	pK_3	pK_4	pK_5	pK_6
	0	6.65	10.15	3.18	3.38	-0.04	-1.2
AH_2	10^{-2}	6.65	10.15	3.16	3.35	0.04	-0.4
	10^{-1}	6.77	10.02	3.19	3.38	0.15	-0.3
	0	6.58	9.82	3.40	3.40	0.37	-1.6
$AH_{2.5}$	10^{-2}	6.20	10.20	3.49	3.69	-0.04	0.5
	10^{-1}	6.30	10.10	3.30	3.62	-0.04	-0.5

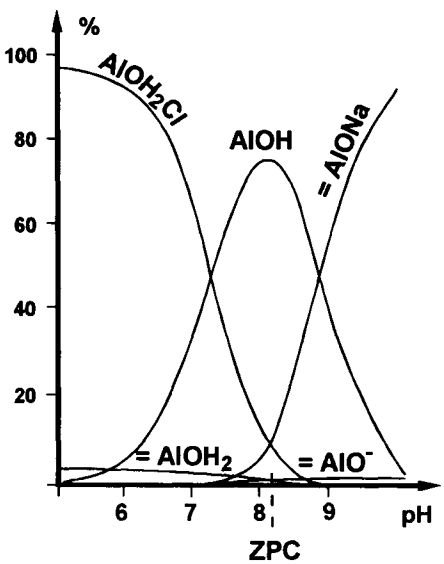

Figure 12. Surface sites distribution obtained from the calculation of pK_j.

6. CONCLUSION

The long chain alkylsulfonates are adsorbed on Al_{13} colloids through the anionic exchange. The Cl^- ions are displaced for sulfonate molecules. This exchange does not occur on the homogeneous surface. The experimental adsorption isotherms show that the Al_{13} colloid surface is heterogeneous. Nevertheless, the free energy on transfer between CH_2 is not constant and varies from 1.3 kT up to 1.9 kT. It is very high indicating a very important condensed state of alkyl chains in the adsorbed layer. The specific surface areas of AH_2 and $AH_{2.5}$ are very high and vary from ~500 m^2/g up to ~800 m^2/g. These large values allow to understand the extent of the removal and transport of organics or

inorganics through adsorption–complexation onto amorphous Al hydroxides particles in the natural media. Due to their reactivity, very large specific surface area, very small colloids are in aquatic and terrestrial media the major supporting phase favouring the transfer of matter and pollutants.

REFERENCES

1. J.Y. Bottero, J.M. Cases, F. Fiessinger, J.E. Poirier, J. Phys. Chem., 84 (1980) 2933.
2. J.Y. Bottero, J.P. Marchal, J.M. Cases, F. Fiessinger, Bull. Soc. Chim. Fr., 11 (1982) 439.
3. N. Parthasarathy, J. Buffle, Wat. Res., 19 (1985) 25.
4. P.M. Bertsh, G.W. Thomas, R.I. Barnishel, Soil. Sci. Am. J., 50 (1986) 825.
5. J.Y. Bottero, J.L. Bersillon, in: I.H. Suffet and P. Mac Carthy (eds.) Aquatic Humic Substances, ACS Book, Washington, DC, 1989, p.219.
6. J.Y. Bottero, M.A.V. Axelos, D. Tchoubar, J.M. Cases, J.J. Fripiat, F. Fiessinger, J. Colloid Interface Sci., 117 (1987) 47.
7. P. Thebault, J.M. Cases, F. Fiessinger, Wat. Res., 15 (1981) 183.
8. H.V. Tartar and K.A. Wright, J. Am. Chem. Soc., 61 (1939) 539.
9. M.J. Rosen and H.A Goldsmith, in: P.J. Eving and I.M. Kolthoff (eds.), Chemical Analysis, Publ. vol. 12, (1972) p.161.
10. E. Rakotonarivo, J.Y. Bottero, J.M. Cases, F. Fiessinger, Colloids Surf., 9 (1984) 273.
11. E. Rakotonarivo, J.Y. Bottero, J.M. Cases, F. Fiessinger, Colloids Surf., 16 (1985) 153.
12. J.M. Cases and F. Villieras, Langmuir, 8 (1992) 125.
13. J.M. Cases, D. Canet, N. Doerler, J.E. Poirier, in: J. Rouquerol and K.S.W. Sing (eds.), Adsorption at the Gas–Liquid and Liquid–Solid Interface, Elsevier, Amsterdam 1982, p.241.
14. B. Lemaire and P. Bothorel, Macromolecules, 13 (1980) 318.

This Page Intentionally Left Blank

Section 2

ADSORPTION FROM GASEOUS PHASE

This Page Intentionally Left Blank

A. Dąbrowski and V.A. Tertykh (Editors)
Adsorption on New and Modified Inorganic Sorbents
Studies in Surface Science and Catalysis, Vol. 99

Chapter 2.1
Computer simulation of adsorption on amorphous oxide surfaces

V. Bakaev and W. Steele

Department of Chemistry, 152 Davey Laboratory,
Penn State University, University Park, PA 16802, USA

1. INTRODUCTION

The understanding of adsorption on amorphous oxide surfaces is important first because the surfaces of almost all high specific surface area adsorbents are strongly heterogeneous. This means that isotherms, heats, and other characteristics of adsorption on those surfaces deviate considerably from what is expected on theoretical grounds for homogeneous surfaces which can be either single faces of ideal crystals or more idealized, absolutely smooth surfaces. Evidently, the degree of adsorption heterogeneity in a given system depends upon both the adsorbent and the adsorbate. For the simplest molecules like argon, it is generally believed that the adsorption heterogeneity is often just a manifestation of the irregularity of the surface atomic structure [1].

In some oxide adsorbents such as silica gel (SiO_2), the surface atomic structure is irregular (amorphous) because the adsorbent as a whole is amorphous. Other oxide adsorbents like rutile (TiO_2) are crystalline. However, the adsorption properties of argon on rutile are very close to those on silica gel. Since the interactions of argon with an oxide surface depend mainly upon the atomic arrangement of the surface oxide ions, one may conclude that the atomic arrangement of these ions at the surface of highly dispersed rutile must be rather similar to that for amorphous silica or in other words, the surface of a tiny crystal of rutile must be covered by an amorphous layer. This and other experimental evidence suggests that one treat the irregular, amorphous surface not only as an appropriate model for the surface of silica gel or other truly amorphous oxides, but also as a model for all heterogeneous oxide (and possibly not only oxide) surfaces as well [2, 3].

To carry out computer simulations of physical adsorption on an amorphous oxide, one has first of all to simulate the irregular (amorphous) atomic structure at its surface. This may be done in several ways. One of these directly models the formation of vitreous silica from the liquid. The first stage of this procedure is a molecular dynamics computer simulation of liquid SiO_2, which presupposes an adequate modeling of the essentially covalent forces between constituent atoms. Thus, we first review the modeling of these interatomic forces in Subsection 2.1. The next stage can consist of the simulation of rapid cooling (quenching) of this liquid. This, as well as other methods of computer simulation of amorphous oxide surfaces, is discussed in Subsections 2.2 and 2.3.

When the coordinates of the atoms of a solid adsorbent are in the computer's memory, one may proceed to simulate the adsorption of a simple gas on this model surface. Again the first stage of this simulation is the modeling of the interaction between an adsorbed molecule and the adsorbent. The difficult and yet unresolved problem at this stage is the modeling of the electrostatic and the induction energies of a polarizable and possibly polar adsorbate molecule in the very inhomogeneous electrostatic field at the surfaces of amorphous oxides. This problem is discussed in Subsection 3.1. Finally, in Subsections 3.2 and 3.3, we discuss the main results obtained in computer simulations of simple molecules like Ar or the spherically symmetric models of CH_4 or SF_6 on amorphous oxide adsorbents, both in the Henry's Law region and at higher coverages.

2. COMPUTER SIMULATION OF THE ATOMIC STRUCTURES OF AMORPHOUS OXIDES

We consider first the simulation of the atomic structure of vitreous silica because the majority of the simulations of amorphous oxides were done for this material. Some of these have simulated the formation of the vitreous silica surface in a very detailed fashion. Furthermore, the methods developed for the simulation of vitreous silica and its surface may be used with some modifications for other amorphous oxides. Subsequently, we consider less detailed methods of simulation of amorphous oxide surfaces which are not limited to SiO_2 but can be applied to various oxides. Finally the least detailed but the most general model - the Bernal surface (BS) - represents the atomic arrangement at the surface of any amorphous oxide (most important for physical adsorption) by the dense random packing of hard spheres.

2.1. Interatomic potentials

The construction of practical interatomic potential models for silica has a long history (see Refs. [5, 6] and references therein). Initially, two-body potentials were used for the interaction between ions i and j separated by a distance r:

$$u_{ij}(r) = q_i q_j / r + A_{ij} \exp(-b_{ij} r) - c_{ij}/r^6 \tag{1}$$

Here q_i is the effective charge of an atom; c_{ij} is a dispersion interaction constant; and A_{ij} and b_{ij} are parameters of the Born - Mayer atom-atom repulsion potential. To calculate the long range Coulomb term in Eq. (1) one generally has to employ the Ewald summation technique. To obviate this inconvenience, the Coulomb term has been multiplied by the screening factor (and the dispersion term has been neglected):

$$u_{ij}(r) = (q_i q_j / r) erfc(r/\beta_{ij}) + A_{ij} \exp(-b_{ij} r) \tag{2}$$

where β is an adjustable constant. It was assumed that this two-body potential is suitable for modeling the important features of the vitreous state but is not expected to work well for the various crystal structures where long range interactions play an important role [7]. The two-body potential of Eq. (2) was augmented in Ref. [7] by the three-body Stillinger - Weber [8] potential. This three-body potential was introduced because simulations of vitreous silica with the two-body potential of Eq. (2) gives a large number of bond defects

(ca. 6 - 8% of odd-coordinated Si and O), too broad a distribution of O-Si-O bond angles, and too large a Si-O-Si bond angle [7]. The three-body potential produces a decrease in the total binding energy of the system whenever the bond angle differs from the preferred tetrahedral value and thus corrects for these defects [7].

It has been argued, however, that the distorted bond angle distributions and incorrect numbers of odd-coordinated atoms are not a consequence of using a two-body potential but of improper treatment of the Coulomb term in Eq. (1) (e.g., using the approximation of Eq. (2)) [9]. The two-body potential of Eq. (1) can reproduce the structure of both crystalline and amorphous silica, provided that Ewald's method is used to ensure a proper description of the Coulombic energy (see below). Initially, parameters of these empirical potentials were fitted to match macroscopic properties simulated with their help. In particular, the parameters in Eq. (2), augmented by the three-body potential, were adjusted to match the radial pair correlation function of vitreous silica in Ref. [7]. A new stage in the development of a nonempirical two-body potential for silica began when the parameters in Eq. (1) were derived from fitting to the *ab initio* potential energy surface of a small cluster. This has been done for SiO_4^{4-} in Ref. [10] and for H_4SiO_4 in Ref. [11]. Parameters obtained in Ref. [11] were also optimized by comparison of the predicted elastic constants and unit-cell dimensions for quartz with experiment. Thus, if the potential obtained in Ref. [10] may be called *ab initio*, that obtained in Ref. [11] should be called mixed *ab initio*/empirical. Parameters of Eq. (1) from Ref. [11] which were obtained not only for silica but also for some other oxides are presented in Table 1.

Table 1
Force-field parameters of Eq.(1) for silica and other oxides [11]

i-j	A_{ij} (eV)	b_{ij} ($Å^{-1}$)	c_{ij} ($eVÅ^{-6}$)	q_i (electron charge)
O-O	1388.7730	2.76000	175.0000	$q_O = -1.2$
Si-O	18003.7572	4.87318	133.5381	$q_{Si} = 2.4$
Al-O	16008.5345	4.79667	130.5659	$q_{Al} = 1.4$
P-O	9034.2080	5.19098	19.8793	$q_P = 3.4$

The potential of Eq. (1) with parameters determined in Refs. [10, 11] was thoroughly tested in computer simulations of silica polymorphs. In Ref. [10], the structural parameters and bulk modulus of α-quartz, α-cristobalite, coesite, and stishovite obtained from molecular dynamics computer simulations were found to be in good agreement with the experimental data. The α to β structural phase transition of quartz at 850 K has also been successfully reproduced [12]. The vibrational properties computed with the same potential for these four polymorphs of crystalline silica only approximately reproduce the experimental data [9]. Even better results were reported in Ref. [5] where parameters of the two-body potential Eq. (1) were taken from Ref. [11]. It was found that the calculated static structures of silica polymorphs are in excellent agreement with experiments. In particular, with the pressure - volume equation of state for α -quartz, cristobalite, and stishovite, the pressure-induced amorphization transformation in α -quartz and the thermally induced $\alpha - \beta$ transformation in cristobalite are well reproduced by the model. However, the calculated vibrational spectra were only in fair agreement with experiments.

An important advantage of the use of the parameters of Eq. (1) reported in Ref. [11] is that they may be extended to cations other than Si.

The two-body potential of Eq. (1) with parameters from Ref. [10] was also employed in molecular dynamics simulations of equilibrium [6] and vibrational [13] properties of silica glass. We defer the discussion of the quenching procedure in simulations of silica glass until the next subsection and mention here only the final results. The simulated glass at 300 K has a structure that is close to that obtained from experimental neutron scattering measurements. Its bulk modulus, density, and internal energy are in reasonable agreement with experiment. The level of agreement is 1 - 3% for linear dimensions, 10% for the bulk module, and a few kcal/mol (0.5%) for the energies. These numbers are of the same order as those obtained for the crystalline polymorphs. A defect-free random tetrahedral network was obtained and this was taken as a proof that a properly chosen two-body potential model can reproduce the tetrahedral coordination of SiO_2 and that an accurate description of the directional bonding in this material may be obtained without recourse to three body interactions [6]. However, the glass transition temperature (2200 K) was considerably higher than experimental (1446 K) and the activation energy for diffusion (36700 K) was much lower than experimental (63 000 K). Finally, the vibrational density of states and the dynamic structure factor compared favourably with those obtained from the inelastic neutron scattering experiments [13].

The final conclusion is that the potential of Eq. (1) constitutes a good, although not perfect, model for all the condensed phases of silica [13].

Finally, we refer to a quite recent paper where a first- principles molecular dynamics simulation of amorphous and liquid SiO_2 was performed [14]. This work confirmed that computer simulation based on the quantum-mechanical calculation of interatomic energy gives basically the same atomic structure of amorphous SiO_2 as mentioned above simulations based on semiempirical potential of Eq. (1).

2.2. Simulation of vitreous silica

Now we consider simulations of the atomic structure of amorphous oxides especially at their surfaces. We begin with the best studied structure of amorphous silica. The structure of the bulk amorphous silica is generally obtained in computer simulation by first simulating liquid silica at a high temperature of about 4000 K [6] or even 6000 K [7]. This stage is followed by the simulation of quenching when the temperature steadily decreases at the rate of 10^{13} - 10^{14} K/s. This rate of cooling is the lowest practically achievable in computer simulations (cf., e.g., Refs. [6, 7]) but it is obviously many orders higher than the fastest rate achievable in real experiments. For example, to obtain amorphous metals by quenching the liquids, one needs an especially fast rate of cooling which is usually 10^5-10^6 K/s but can be as high as 10^8 K/s (see, e.g. Ref. [15], p. 27), which is still at least five orders of magnitude lower then the values given above.

Thus the simulation of quenching may not necessarily be an adequate model of the real process. This is an important fact if we take into consideration the fact that an amorphous state is generally metastable so that its structural characteristics depend upon the history of its formation. This distinguishs the amorphous state from the stable crystalline state whose structure is in principle determined by the thermodynamic parameters, e.g., pressure and temperature, and not upon the history of its formation. To be more specific, let us consider the simple case when a crystalline structure of a solid may be determined

as the lowest minimum of its cohesive energy, taken as a function of the position of all its particles. Such a function of very many variables usually has a huge number of local minima in addition to one global minimum. It is generally believed that those local minima determine various amorphous structures. These can even be determined in computer simulation as the so called "inherent structures" (cf., e.g., Ref. [6]). It was argued that in the course of the computer simulation of quenching from a temperature well above that of the glass transition, the system succeeds in hopping from one local minimum to another but ends up arrested in one local minimum as the temperature falls below the glass transition point [6]. Now it is in line with this viewpoint to suggest that it is the peculiarities of the process of quenching (initial state, rate of cooling etc.) which determine the final local minimum where the system will find itself at the end of quenching. The atomic structure which corresponds to that minimum (inherent structure) determines the atomic structure of the amorphous state obtained in a computer simulation. This arguement shows that amorphous atomic structures *may* not depend only upon the interatomic interactions and that the simulated amorphous structures may differ from the real ones even if the potential model is adequate. This is *a fortiori* true for the amorphous atomic structures of silica gel which are obtained not by the quenching of silica liquid to an ordinary glass but by coagulation in solution at room temperature.

However, we do not know exactly to what extent simulated amorphous atomic structures depend upon the rate of quenching. It is known, for example, that in the ion implantation technique for the preparation of amorphous metals, one can achieve effective rates of cooling of 10^{14} K/s (see, e.g. Ref. [15], p. 27) which is already close to that achievable in computer simulations. The resulting atomic structures are basically the same as those obtained by quenching techniques with six orders of magnitude smaller rates of cooling.

A computer simulation of the surface of the amorphous SiO_2 has been reported in Ref. [16]. It was accomplished in two steps. First, the bulk amorphous atomic structure was simulated by the usual MD melt-quench technique described above. Then a free surface was created by removing the periodic boundary condition in one dimension (Z) and freezing the bottom layer of atoms. After that the system was annealed at 1000 K and then cooled gradually to 300 K.

The main structural details of the simulated silica surface were: (i) The predominance of oxygen at the outer surface - this consists of bridging (siloxane) oxygens bonded to two silicon atoms, and nonbridging oxygen (NBO) bonded to one silicon atom (in agreement with experiment); (ii) strained siloxane bonds; and (iii) the presence of two-membered rings formed by edge-sharing tetrahedra that do not exist in the bulk. In addition to NBOs and two-membered rings, several other topological and bonding defects were identified in the surface region, e.g. three- and four-membered rings, over-coordinated oxygens and under-coordinated silicons. It was assumed that NBOs, three-coordinated silicons, edge-sharing tetrahedra, and three-membered rings are chemically reactive sites which might be associated with hydroxyls on the silica surface. Under this assumption, the concentration of surface hydroxyls (6.4/100 $Å^2$) was in good agreement with experimental estimates. However, this was actually the only value that was compared with experiment in Ref. [16].

The reliability of other statements concerning the structure of the glassy silica surface depends on the reliability of the interatomic potential model and the adequacy of the simulation procedure. We have already mentioned that if the two-body potential of Eq. (2)

used in Refs. [7, 16] is taken alone, it distorts the atomic structure of amorphous silica in comparison to that obtained using the potential of Eq. (1) with proper treatment of the Coulomb term. However, this deficiency of the two-body potential was corrected in Refs. [7, 16] by inclusion of the Stillinger-Weber three-body potential so that the total potential model appeared to be good enough to yield basic structural characteristics of bulk vitreous silica that reasonably reproduce the experimental data [7]. Besides, the previous simulation of the glassy silica surface mentioned in Ref. [16] was based on an approximate two-body potential that gave basically the same structural characteristics of the surface as those generated by the refined potential. As to the adequacy of the melt-quench technique used for the simulation of the glassy surface, the only thing to be said is that despite its unrealistic character, it does not drastically distort the atomic structure of glassy silica in the bulk. What influence an unrealistically fast quenching may have on the surface atomic structure is an open question at present.

The surface atomic structure of silica gel was also simulated in Refs. [17, 18]. Silica gel is another form of amorphous silica which is formed not in the process of cooling of the liquid but as a result of coagulation at room temperature. Its surface is the surface of small microspheres which together form an irregular porous structure. We consider here only the simulation of the surface atomic structure presented in Refs. [17, 18]. The pore structure of such a material clearly depends on the arrangement of the microspheres in space. Together with the surface atomic structure, the pore structure determines the adsorption properties of silica gel and we consider it in this context in the next section.

The simulation of the surface of silica gel in Ref. [17] is somewhat similar to the simulation of the glassy surface in Ref. [16]. The same potential was used and the simulation is accomplished in two stages. As in Ref. [16], the the first step involves a simulation of the atomic structure of the bulk vitreous SiO_2. This was a usual Monte Carlo simulation of a SiO_2 liquid followed by the quenching procedure as discussed above. A simulation box containing 512 silicon atoms and 1024 oxygen atoms at a density of 2.2 g/cc was used, together with periodic boundary conditions. In the second step, a point was chosen at random in the simulation box and a sphere of radius about 1.2 – 1.4 nm was inscribed around it. All of the silicon atoms within the sphere or its periodic images were then analyzed with respect to their nearest neighbour oxygen atoms. If the distance between an oxygen atom and the silicon atom was less than 0.202 nm (1.25 times the position of the first peak in the Si-O radial distribution function) the oxygen atom was considered to be bonded to the silicon atom. Silicon atoms which had abnormal coordination (three nonbridging oxygens [17] or only one siloxane oxygen atom [18]) were discarded along with their associated nearest-neighbour oxygens. As a result, a surface covered by oxygen atoms was obtained. It was assumed that NBOs represented hydroxyl groups on the surface of silica gel. This assumption was supported by the fact that the density of the NBO was 6.3 oxygens/nm^2 and the concentration of hydroxyl groups on the surface of fully hydroxylated silica has been reported to lie in the range 4.6 OH/nm^2 to 6.2 OH/nm^2 , the larger value corresponding to untreated or virgin silica [17]. This somewhat differs from that of Ref. [16] where the same concentration of hydroxyl groups was obtained when not only NBOs but also edge-sharing tetrahedra and three-membered rings were associated with hydroxyls (see above). Besides, one should have in mind that cutting out a microsphere from the bulk matter is an artificial procedure which does not correspond (even approximately) to quenching or annealing.

A similar simulation technique was used in Ref. [19] to obtain a model cylindrical pore in porous silica. Again a bulk silica atomic structure was simulated and the surface of a pore was created by removing silicon and oxygen atoms from the interior of a cylinder inscribed around a fixed axes. The simulation technique was essentially the same as in Refs. [17, 18], the only difference being that in the former case a silica surface was created by "boring" a pore from bulk silica while in the latter case it was created by "cutting out" a sphere from the bulk.

2.3. Simulation of other amorphous oxide structures

The reason why a central, long-ranged ionic potential can successfully model directional and short-ranged covalent forces in silica is attributed to the fact that Si-O bonds are so rigid that the Si-Si (or O-O) distances and Si-O-Si (or O-Si-O) angles are almost perfectly correlated [9]. This explanation suggests that one try even simpler central force potentials in molecular simulations of partially covalent structures. In Ref. [20] Mie's potential

$$u(r) = \frac{B}{r^m} - \frac{C}{r^n} \tag{3}$$

was used to simulate the surface structure of amorphous TiO_2 by melting the surface layer of a (100) face of rutile. The main problem which arises in this respect is to find coefficients B and C for the Ti-Ti, Ti-O, and O-O interactions which provide stability of the rutile structure at low temperature. That is to say, to find coefficients in Eq. (3) which make the forces at each atom in the elementary cell of rutile so low that its structure does not decay spontaneously during a MD run. It was shown in Ref. [20] that at least for rutile it is possible. Then the temperature may be increased until the structure melts. The next step may be the quenching of the liquid which was used to simulate amorphous SiO_2. However, it was mentioned in Ref. [6] that differences between the structural characteristics of liquid SiO_2 and those obtained after quenching are negligible. Generally this is not the case and there are appreciable differences in the radial correlation functions of amorphous and liquid metals, for example [15]. This does not mean, however, that this structural difference must necessarily be taken into account. It seems that its influence on adsorption characteristics is negligible in comparison with other factors discussed below. So the quenching was skipped in Ref. [20]. Thus the model used in Ref. [20] is less detailed than that used in Ref. [16] but, probably, more general because it can be applied to a variety of oxides.

An even more general and correspondingly less detailed atomic model of amorphous oxide surfaces has been called the Bernal surface (BS)[3, 21]. It is based upon the fact that many oxides and halides can be regarded as close-packed arrays of large anions with much smaller cations occupying interstitial (usually tetrahedral or octahedral) positions (see., e.g. Ref. [4]). In line with this point of view, the BS is a surface of a collection of dense randomly packed hard spheres, a sphere representing an oxide anion. The cations in interstitial positions between hard spheres are excluded from the simulation since they do not attract adsorbed molecules due to their small polarizability. Thus only the atomic structure of the oxide ions is considered. This is called the Bernal structure and has been used for modelling simple liquids and amorphous metals [15].

The computer simulation of the Bernal atomic structure with a flat (on average) surface was carried out with the help of algorithm described in Refs. [3, 22]. The coordination number of hard spheres in this structure is about 8 which may be compared with the O-O

coordination number in amorphous SiO_2 that is 6 [6]. The numbers differ, of course, but the difference is not that big in comparison with, e.g., the C-C coordination number in amorphous carbon which is about three. In Fig. 1 the BS is compared with the surface of a model amorphous carbon. The surface atomic structure of this amorphous carbon

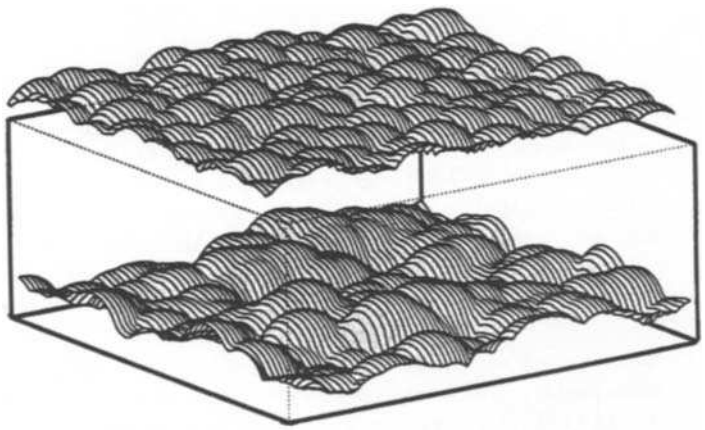

Figure 1. The surface of an amorphous oxide (upper panel) and an amorphous carbon (lower panel). The dimensions of surfaces are 3.6x3.6 nm and the two surfaces shown are (arbitrarily) separated by 1.5 nm.

was obtained by MD simulation of liquid carbon at 7000 K with the Tersoff interatomic potential [23]. The Tersoff potential is an empirical interatomic potential which stabilizes the atomic structures of graphite, diamond and several other hypothetical polymorphs of carbon that were calculated by quantum-chemistry methods [24, 25]. Implicitly introducing the many-body interactions, it takes account of the directional character of the covalent bonds in amorphous carbon.

The surfaces in Fig. 1 are obtained from arbitrarily selected computer-generated instantaneous configurations of an (oxide) BS and amorphous (liquid) carbon with the help of a probe hard sphere with a diameter close to that of an argon atom (0.33 nm). The upper of these surfaces is generated by the center of the probe sphere which rolls over the BS structure of hard spheres with diameter of a typical oxide ion (0.28 nm). In the case of amorphous carbon, a hard sphere with the van der Waals diameter of carbon (0.33 nm) is described around each carbon atom. These spheres overlap because the distances between carbon atoms are about 0.14 nm. The surface of amorphous carbon in Fig. 1 is generated by the center of the probe sphere that rolls over those overlapping hard spheres.

The surface number density of oxide ions in the BS model is about 2.1 times less than that for the carbon surface in Fig. 1 . However, the diameters of the overlapping spheres over which the probe sphere rolls are larger for the carbon surface in Fig. 1 than for the oxide surface. Thus one expects that the lower of the surfaces in Fig. 1 should be smoother than the upper one. However, this is not the case. The reason why the amorphous carbon surface seems to be rougher than the amorphous oxide surface lies

with the above mentioned difference of coordination numbers of hard spheres in the BS model and carbon atoms. The arrangement of carbon atoms is more open (coordination of atoms is lower) than the arrangement of oxide ions. Due to that, its surface is rougher in spite of the considerably higher number density of the former arrangement.

Thus, the surface of this amorphous carbon (which is a model of the surfaces of non-graphitized carbon blacks [23]) differs considerably from the surface of amorphous oxide and the main structural characteristics such as the C-C and O-O coordination numbers are also drastically different. Nevertheless, the adsorption properties of heterogeneous surfaces of various nongraphitized carbon blacks with respect to an inert adsorbate such as argon are not that drastically different and actually have many common features. We discuss these properties in the next section. Here we only use this fact to show that subtle structural differences of various models of amorphous oxide surfaces discussed above may be not that important for their adsorption properties in comparison to other factors such as indefiniteness of adsorption potential on oxide surfaces (see below). Because of its generality and in spite of its approximate character, the BS appears to be a convenient model for the computer simulation of adsorption on amorphous, and even more general (see Introduction) heterogeneous oxide surfaces.

3. ADSORPTION ON AMORPHOUS OXIDES

3.1. Adsorption potential

There is a long history of calculations of adsorption potentials for simple gases adsorbed on the exposed low index Miller planes of ionic crystals, especially alkali halides (see the review [26] and references therein). The total interaction potential energy between an adsorbed molecule and the surface of a solid is generally expressed as a sum of dispersion, repulsion, induction, and electrostatic contributions (see, e.g., Ref. [27]):

$$V = V_D + V_R + V_I + V_E \tag{4}$$

The first two terms in Eq. (4) represent the dispersion and repulsion contribution to the van der Waals energy and are generally described in computer simulations by a semi-empirical Lennard-Jones (LJ) potential which is, in fact, a form of Mie's potential of Eq. (3) where m=12, n=6, B=$4\epsilon\sigma^{12}$,and C=$4\epsilon\sigma^{6}$. Even if an expression for the van der Waals energy is different from LJ it is convenient to approximate it by a 12-6 function [28] for computational convenience.

The largest contribution to this gas-solid interaction for oxide surfaces comes from the oxide anions (the BS neglects all other contributions). Thus, the parameters of the LJ σ and ϵ for, e.g., the Ar-O interaction of some model amorphous oxide may be as a first approximation transferred from those for a different oxide with a well known regular atomic structure at the surface. An example is the (100) surface of MgO where the energy was evaluated and compared with reliable experimental data for a number of simple gases (for a discussion of such calculations see, e.g., Refs. [26, 27]). Such transferability seems reasonable if one studies physical adsorption on a heterogeneous surface of MgO which (cf. Introduction) may be modelled as an amorphous MgO surface. Unfortunately, the transferability of LJ parameters is not generally possible. For example, ϵ for Ar-O interaction determined from the temperature dependence of the Henry's Law constants

in zeolites has proved to be too large (1.5 times higher) than that for TiO_2 [28]. As a last resort in the determination of LJ parameters (when one cannot transfer them or calculate by some semi-empirical expression), one may fit them to match one point in the isotherm of adsorption. One obtains in such a way the lump parameters ϵ and σ which implicitly include many body interactions not accounted for by the LJ-potential as well as other terms like V_I (see below) in Eq. (4). The goal of the simulation is to determine the shape of the isotherm as well as other thermodynamic and transport properties. This is what, in fact, has been done in Refs. [17, 18, 21, 28, 29].

To calculate the induction and electrostatic contributions to the adsorption energy (V_I and V_E in Eq. (4)) one should first evaluate the electrostatic field at the surface of the crystal. Calculations of electrostatic fields near surfaces of ionic crystals have been done since 1930 (see references in [26]). In the case of amorphous silicates, one may do such an evaluation using effective charges for the anions and cations, as in the interatomic potentials of Eq. (1) and as set out in Refs. [10, 11]. Unfortunately this is not applicable to the BS model which excludes cations from consideration.

The usual way of evaluating the induction (polarization) energy is the well known formula:

$$V_I = \alpha E^2/2 \tag{5}$$

where α is the polarizability of an adsorbed molecule and E is the strength of electrostatic field at its center. However, it has been shown in Ref. [30] that Eq. (5) is a very poor and even misleading approximation to the induction energy of Ar at the surface of LiF, NaCl, and KCl. The reason for that is that the electrostatic field is very inhomogeneous near the surface of an ionic crystal and can change by orders of magnitude over an atomic length. Eq. (5) was derived for a homogeneous field where E is constant. To take account of weak inhomogeneity one may add to induction energy in Eq. (5) a term that includes the quadrupole polarizability [30]. It turns out that the quadrupole polarization makes about the same and sometimes even larger contribution to the induction energy as the dipole polarization. This does not mean that one may improve the evaluation of the induction energy merely by accounting for the quadrupole polarizability term but rather that the induction energy may not be calculatable from the multipole expansion. This is because one may not exclude similar or even greater contributions from higher multipole polarizabilities which are unknown at present. Thus, the main contribution to the induction energy can come from the unknown higher-order polarizabilities or it may be that even the whole expression diverges.

This point of view was set forth in Ref. [31] and is similar to that in Ref. [30]. However, when the contribution from the hyperpolarizability of Ar in zeolite was evaluated in Ref. [31], it proved to be less than that from quadrupole polarizability. This means that it is not the strength of the electrostatic field in the adsorption space that makes Eq. (5) a poor approximation for the induction energy but the inhomogeneity of that field. Eq. (5) is the second order perturbation of an atom in an external field which assumes that the field is relatively weak and homogeneous. Evaluation of the hyperpolarizability contribution shows that the assumption of weakness is probably valid for electrostatic fields typical in physical adsorption. Also, the induction energy may be evaluated as a second order perturbation of the neutral atom by the electrostatic field. When the field changes rapidly over the volume occupied by the adsorbed atom or molecule, Eq. (5) should be replaced

by another expression. One such has been used in the first calculations of the energy of physical adsorption on the surfaces of ionic crystals (see, e.g. Ref. [32], p. 37) but unfortunately was substituted by Eq. (5) in later works.

Conventionally, people realize that Eq. (5) gives a poor value of the induction energy and justify its use by the fact that the induction energy is only a small part (ca. 10%) of the total energy of physical adsorption (see., e.g., Ref. [27]). This argument would have been acceptable, if Eq. (5) were a rough but still reasonable expression for the induction component of the total energy of physical adsorption. It was shown above that this well may be not the case. In this situation, it seems more reasonable to omit the calculation of the induction component of the adsorption energy by Eq. (5). Its magnitude is about the same order of magnitude as the many-body dispersion contribution to the adsorption energy and the latter as a rule is not calculated in conventional computer simulations of physical adsorption. In fact, the many-body as well as induction contribution are implicitly included in computer simulations through the rescaling of parameters of the LJ-potential which have been fitted to match some part of the experimental data such as the Henry's Law constant.

When an adsorbed molecule has a dipole or quadrupole moment, the electrostatic energy should be taken into account. Here one encounters the same problem connected with the inhomogeneity of the electrostatic field near the surface of ionic crystals as was discussed above in connection with the calculation of induction energy. However, in this case the solution seems simpler, at least formally. Take, for example, a nitrogen molecule which has a considerable quadrupole moment. Usually the Coulomb interactions of such molecules are calculated in computer simulations with the help of a point charge model for the molecule (see, e.g., Ref. [40]). The values of the point charges and their position with respect to the center of a molecule are chosen to fit its quadrupole moment. However, in doing so one also generates all the higher multipole moments. In this way this model may be used (at least formally) for evaluation of the Coulomb interaction of a molecule with the highly inhomogeneous electrostatic field at the surface of an amorphous oxide.

As soon as the expressions and constants in Eq. (4) are fixed one may proceed with calculation of the adsorption energy at a given point of adsorption space. However, to make such a calculation possible one has to know the positions of all the atoms of adsorbent relative to the given point. In other words, one has to know exactly the atomic structure of the adsorbent. This is what is in fact unknown for amorphous oxides. Although one can simulate the atomic structure at the surface of an amorphous oxide as described above, the reliability of the result can at present only be checked by comparison of prediction of adsorption properties with experimental data. But the calculation of adsorption properties (described below) includes, generally speaking, two unknowns: the atomic structure of an adsorbent and the adsorption potential. This is the reason why the computer simulation of physical adsorption on amorphous oxides should be preceded by similar simulations on oxides with well defined crystalline structures.

Some zeolites provide such an opportunity. Computer simulations of simple molecules in zeolites have been carried out already for more than two decades. The goal of those works was in considerable degree motivated by an attempt to find and test proper relations for various terms of Eq. (4). We do not discuss these works in the present paper and refer an interested reader to a recent article concerning the computer simulation of the adsorption of rare gases in silicalite [41]. A silicalite is a form of porous crystalline SiO_2

with a well defined atomic structure. Thus, computer simulations of physical adsorption of simple molecules in silicalite and amorphous SiO_2 should include the same methods of calculation of various contributions to Eq. (4).

Physical adsorption on the (001) face of MgO also attracted considerable attention in recent years (see short review and references in Ref. [26]). It provides another opportunity to test methods of adsorption potential calculation which can be used later to simulate adsorption on adsorbents with less reliable atomic structure of surfaces like amorphous oxide. There is a large and rapidly changing electric field near the surface of MgO which should be much stronger than in silicalite due to small cations of Mg^{2+} and larger ionicity of MgO in comparison to SiO_2. Thus calculations with polar and quadrupole molecules which were carried out on that surface (see Ref. [26] and references therein) necessarily employ methods which may useful for computer simulations on amorphous oxides.

3.2. Infinitely small coverage (Henry's Law region)

When one can evaluate the energy of an adsorbed molecule in an arbitrary position near the surface of amorphous oxide, one may begin to calculate the adsorption characteristics of that surface. It is simpler to do that when the concentration of adsorbed molecules at the surface is infinitely small, i.e., in the Henry's Law region. Even in this case, calculations are usually carried out only for spherically symmetric molecules like rare gases or spherical models of more complex molecules like CH_4 and SF_6, the only exception being Ref. [19] where SF_6 was represented by a six-center model. In all cases the interaction of an adsorbed molecule with the oxide was modeled by LJ-potentials, the induction interaction being implicitly taken into account by the values of the parameters of the potential.

Henry's Law constants for Ar on the surface of amorphous oxide modeled as a Bernal surface (cf. Fig.1) have been considered in Ref. [39]. The Henry's Law constant may be calculated as

$$K_H = \int_0^L \int_0^L k(x,y)dxdy$$

where

$$k(x,y) = \int_{z_G}^{\infty} [exp(-U(x,y,z)/kT) - 1]dz \qquad (6)$$

Here $U(x,y,z)$ is the energy of an atom at an arbitrary point (x,y,z) over the surface; $z_G(x,y)$ is the Gibbs dividing surface with respect to which the adsorption is determined. (This surface is implicitly determined in experiments by helium calibration.) K_H is connected with the Gibbs adsorption N_a on area L^2 by the relation: $K_H = N_a kT/p$. Finally, $k(x,y)$ in Eq. (6) may be called the two-dimensional density of the Henry's Law constant. This function is shown in Fig. 2, which was taken from Ref. [39].

The picture in Fig. 2 may be considered as the distribution of adsorption activity over the surface of an amorphous oxide. It shows that the contribution to the Henry's Law constant K_H (which is a measure of adsorption activity for the entire surface) comes not from all parts of the surface as would be the case for a homogeneous surface such as the graphite basal plane but from special places corresponding to the sharp peaks in Fig. 2 which well may be called "adsorption sites". The concept of adsorption sites

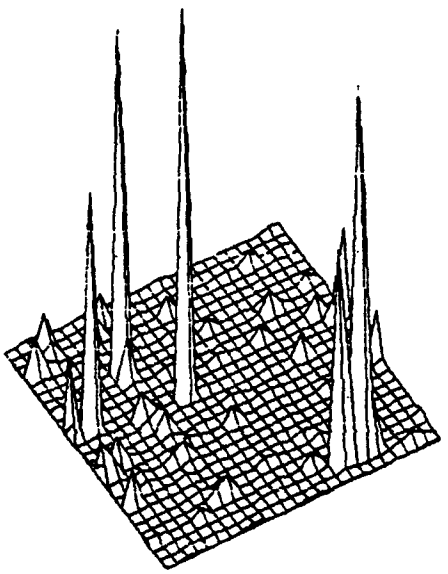

Figure 2. The density of the Henry's Law constant (k(x,y)) for Ar on a model amorphous oxide (BS) at 150 K.

was introduced in the theory of adsorption by Langmuir and is the basic notion for the theory of adsorption on heterogeneous surfaces [1]. However, it is not generally specified in this theory what an adsorption site actually is and Fig. 2 affords a rare case when this important concept of the theory of adsorption can be presented as a graphic image.

Another result obtained in Ref. [39] was that the dependence of $\ln K_H$ vs $1/T$ is not linear for a BS. At high temperature where the Boltzman factor in Eq. (6) tends to unity, the sharp peaks in Fig. 2 flatten and the difference between the adsorption sites and the other parts of the surface becomes less pronounced. This means that our model heterogeneous surface behaves in an adsorption sense as homogeneous at sufficiently high temperature. In particular the high temperature behaviour of $\ln K_H$ vs. $1/T$ approaches that of homogeneous surface, i.e., is almost linear at not too high a temperature. When temperature decreases the slope of that plot changes. However, when $T \rightarrow 0$ the dependence of $\ln K_H$ vs $1/T$ again asymptotically approaches a straight line which is steeper than the high temperature straight line. The low temperature asymptote corresponds to adsorption on the strongest adsorption site of the surface and this is the reason why it is so difficult to measure the low temperature Henry's Law constants for strongly heterogeneous surfaces like amorphous oxides [39]. To do that one has to reach such a small coverage on a heterogeneous surface that the probability of occupation of the strongest adsorption site is well below unity so that even for those few sites the Henry's Law holds true.

The purpose of calculating Henry's Law constants is usually to determine the parameters of the adsorption potential. This was the approach in Ref. [17], where the Henry's Law constant was calculated for a spherically symmetric model of CH_4 molecules in a model microporous (specific surface area ca. 800 m^2/g) silica gel. The porous structure of this silica was taken to be the interstitial space between spherical particles (diameter ca. 2.7 nm) arranged in two different ways: as an equilibrium system that had the structure of a hard sphere fluid, and as a cluster consisting of spheres in contact. The atomic structure of the silica spheres was also modeled in two ways: as a continuous medium (CM) and as an amorphous oxide (AO). The CM model considered each microsphere of silica gel to be a continuous density of oxide ions. The interaction of an adsorbed atom with such a sphere was then calculated by integration over the volume of the sphere. The CM model was also employed in Refs. [36] where an analytic expression for the atom – microsphere potential was obtained. In Ref. [37], the Henry's Law constants for spherically symmetric atoms in the CM model of silica gel were calculated for different temperatures and compared with the experimental data for Ar and CH_4. This made it possible to determine the well-depth parameter of the LJ-potential ϵ for the adsorbed atom – oxygen ion. This proved to be 339 K for CH_4 and 305 K for Ar [37]. On the other hand, the summation over ions in the more realistic AO model yielded $\epsilon/k = 184K$ for the CH_4 – oxide ion LJ-potential [17]. Thus, the value of ϵ for the CH_4 – oxide ion interaction for a continuous model of the adsorbent is 1.8 times larger than for the atomic model.

It is well known that the energy of interaction of an atom with the continuous solid is 2–3 times less than with the discrete (atomic) model (cf., e.g., Ref. [38], Figs. 2.2-2.4). Thus, to obtain the same Henry's Law constants with the two models, one has to increase ϵ for the continuous model. This, however, does not discredit the continuous model which is frequently used in adsorption calculations. In particular, we can use the above mentioned results of Ref. [37] to predict the value of ϵ for Ar which would have been obtained if one had carried out Henry's Law constant calculations for Ar in the AO model of Ref. [17] and compared them with experiment. One can multiply the value of ϵ for CH_4 obtained from AO model by the ratio of ϵ values for Ar and CH_4 in the CM model [36] to obtain $\epsilon/k = 165K$ for Ar in the AO model. This is very close to the value of 160 K obtained in Ref. [21, 28] by an independent method in which the value of the LJ parameter ϵ for the Ar – oxide ion interaction was chosen to match the results of computer simulation of the adsorption isotherm on the nonporous heterogeneous surface of TiO_2. Considering the independence of the calculations and the different character of the adsorbents (porous and nonporous), the closeness of the values of ϵ is remarkable (if it is not accidental). The result seems even more remarkable in the light of discussion presented in Ref. [28]. Another line of research has dealt with the influence of porous structure of the silica gel upon the temperature dependence of the Henry constants [36].

It was noted [21, 28] that the value of ϵ for the Ar – oxide ion interaction obtained earlier from analysis of the Henry's Law constants for various zeolites is 226 K. This value was confirmed by independent calculations of different authors (but on essentially the same zeolites). Thus it was concluded that the most important parameter for computer simulation of physical adsorption on oxides – the energy minimum of the atom/oxide ion interaction – is untransferrable from one adsorption system to another. The comparison of the results presented above suggest that this might not be the case – the parameter determined from amorphous oxides of different chemical natures (SiO_2 and TiO_2) and

of different structures (porous and nonporous) are reasonably close to each other. The reason why most zeolites drop out of this (would be) rule is unclear. One might think, for example, that atoms in zeolites should have larger induction energy than in amorphous oxides in the overall potential of Eq. (4) due to the strong electrostatic field produced by the cations present in most zeolite pores. As discussed above, this is often implicitly included in the dispersion – repulsion energy. Another possible reason which is valid also for silicalite with essencially the same chemical composition as amorphous SiO_2 (but different atomic structure) might be the many-body contribution to V_D in Eq. (4) that is also implicitly included in parameters of the two-body potential but should be different for adsorbents with different atomic arrangement.

With the value of ϵ obtained from the analysis of isotherm data, it was possible to obtain temperature dependent diffusion coefficients in the Henry's Law region for CH_4 in silica gel that are in fair agreement with experiment [17].

3.3. Coverages above the Henry region

Computer simulation of physical adsorption at finite coverages differs from that at infinitely small coverage in that the thermodynamic properties of the adsorbed film depend upon the interactions between adsorbed molecules as well as the interactions with the surface. The conventional assumption about this adsorbate-adsorbate interaction is that it is about the same as in bulk liquid, so that one can transfer the interatomic potentials used in the theory of liquids to problems in physical adsorption. It is well known from computer simulation of homogeneous liquids that many-body interactions constitute 10–20% of the total energy. The main term in the many-body energy is the three-body interaction which can be evaluated by the Axilrod-Teller formula [38]. Usually these are not calculated directly – that would take too much computer time. Rather, they are taken into account by renormalizing the parameters of two-body interaction potentials (usually LJ-functions). The same is true for physical adsorption, though in the latter case the third body in the three-body potential may be not only an adsorbed molecule but also an atom (ion) of the solid adsorbent. In this case, the effective pair-wise energy in an adsorbed layer depends upon the distance and orientations of the pairs relative to the solid surface. Thus the many-body contribution to the adsorbate/adsorbate intermolecular energy may be different from that in the bulk liquid but this difference is often neglected.

Computer simulations of the isotherm of adsorption are frequently based on the grand canonical Monte Carlo method [40]. If the atomic structure of the solid adsorbent is known and if the adsorbate/solid and adsorbate/adsorbate energies can be computed, this algorithm makes it possible to calculate isotherms of adsorption directly.

Here, we first consider the multilayer region of the simulated isotherms obtained for argon at 85 K on amorphous oxides, since it turns out that the curves in this region of coverage are sensitive to some of the characteristic features of the heterogeneity of the model surfaces. The simulated isotherm of Ar on the BS of the generalized model oxide was compared with the standard isotherm of Ar on nonporous amorphous SiO_2 in Ref. [33]. The simulated isotherm reproduced experimental data very well, apart from some small undulations which occurred near the inflection point of the simulated S-shaped isotherm (Type II [42]) where real isotherm has a long linear portion.

The statistical analysis of the isotherm in the BET region ($0.05 < P/P_0 < 0.35$) is presented in Table 2 [21]. In this table RS represent the real adsorption isotherm for Ar

on the surface of a heterogeneous rutile sample [43]. N_m is the monolayer capacity as determined from the BET equation referred to the whole sample (in the case of RS, this amounted to 39 g of rutile powder); C is a constant of the BET equation; χ^2 is a measure of the deviation of either the experimental or the simulated points of the isotherm from the BET model, and Q is the probability that this deviation is accidental. One sees that the deviation of experimental isotherm from the BET model is almost certainly accidental. In other words, the experimental isotherm complies well with the BET model. The BS in the first column of Table 2 designates a Bernal surface for the model amorphous oxide. In this case, the probability Q that the deviation of the isotherm simulated on this surface from the BET model is accidental is very low. This means that the simulated isotherm does not comply with the BET model. It is not that the BET equation cannot be applied to this case at all – one may see from Table 2 that the monolayer capacity and the C-constant are determined with reasonable accuracy for a BS where Q is very small. It simply means that the statistical analysis detects with certainty some systematic deviation of the the simulated isotherm from the BET model which in graphical presentation (cf. Ref. [33]) appear to be small and insignificant undulations of simulated isotherm. However small those undulations, they are absent in the experimental as well as the BET isotherm. It is concluded that the atomic structure of this model amorphous oxide deviates in some systematic way from the atomic structures of real amorphous oxides.

Table 2
Approximation of the isotherm of adsorption of Ar on the model amorphous oxide by the BET equation in the BET region

surface	N_m	C	χ^2	Q
RS	766±3 cm^3 at STP	88±5	0.681	0.88
BS	87.2±0.5	140±11	16.8	$2 \cdot 10^{-3}$
CBS	90.6±0.6	92±6	6.0	0.2

It was discovered in Ref. [21] that one may eliminate the undulations in a simulated isotherm if one make the amorphous oxide surface even rougher than the BS surface. This was achieved by randomly deleting oxide ions from the surface of the amorphous oxide. The resulting surface is called the corrugated Bernal surface (CBS). One may see from Table 2 that the Q value for the isotherm simulated on the CBS is considerably higher than for the BS, which means that this simulated isotherm complies with the BET equation considerably better than that on the BS. Besides, the C-constant that is the primary parameter in determining the shape of the BET isotherm is closer to the experimental value for the CBS than for the BS. It was argued in Ref. [21] that the reason for the improvement of the shape of simulated isotherm is appearance of a second type of heterogeneity on CBS which is absent on BS. In Ref. [44] this was called secondary surface heterogeneity (SSH) in contrast to the primary surface heterogeneity (PSH) illustrated in Fig. 1. Although the surfaces presented in Fig. 1 are rough, this roughness is short range. That is to say, the surface is planar on average and the ripples seen in Fig. 1 have wave lengths of about one atomic diameter. If the surface displays irregular undulations with wave lengths which are several times larger than an atomic diameter, one may speak

of SSH. A picture of CBS presented in Ref. [21] together with that of BS reveals that the former is rougher than the latter. The difference between them consists not only in the fact that CBS posesses some strong adsorption sites that are missing from the BS but also in that the CBS has some degree of SSH along with PSH. This secondary heterogeneity is also displayed, for example, by the rumpled graphite basal plane of Ref. [44]. Comparison of the isotherms of adsorption of Ar simulated on the rumpled graphite basal plane [44] and on amorphous carbon shows the same trend as those for the CBS and the BS. On the rumpled graphite basal plane (which has considerable SSH), the simulated isotherm of N_2 complies with the BET model and the value of C=194±17 is typical for real adsorption isotherms on industrial (nongraphitized) carbon blacks (C≈ 190) [44]. On the model amorphous carbon (with small SSH – cf. Fig. 1), the simulated isotherm of Ar can be described by the BET equation in the BET region but the value C=90±5 is s considerably smaller than that for the experimental isotherms (C≈150) [23].

Finally, we consider adsorption in the submonolayer region where the primary heterogeneity of the amorphous oxide surface and the adsorbate/adsorbent interactions both play an important role. A comparison of the experimental data for Ar at 85 K on a high specific surface area (85 m^2/g) rutile powder [43] with simulated isotherms on the (100) and (110) faces of a crystalline rutile [28] and on a BS [21] showed that the isotherms simulated on the ideal crystalline faces of rutile deviate drastically from the experimental results for all reasonable values of the parameters of the LJ potential for the argon/oxide interaction. This means that the surface of the highly dispersed rutile sample could not be an ideal crystalline surface. In fact, Drain and Morrison recognized in Ref. [43] that the surface of their rutile specimen was strongly heterogeneous. They determined the energetic distribution of adsorption sites and discussed the influence of that heterogeneity on the thermodynamics of adsorption. However, Drain and Morrison did not discuss the fundamental question: which kind of atomic disorder at the rutile surface gives rise to its heterogeneity?

In Ref. [21], it was shown that an amorphous oxide surface as represented by the BS model makes it possible to simulate isotherms that are close to the experimental one provided the energetic parameter ϵ of the argon/oxygen LJ potential is properly chosen. The value of ϵ turned out to be about 40% less than that obtained earlier for the same constant in zeolites. However, as shown above, the value of LJ-parameter ϵ obtained in Refs. [21, 28] is very close to the value deduced from calculations of the Henry's Law constant for silica gel in Refs. [17, 37]. Thus, one may conclude that the amorphous BS model is capable of reproducing the adsorption properties of the strongly heterogeneous surface of a highly dispersed rutile. This high specific surface area adsorbent is an example of a crystalline oxide whose surface layer is either amorphous or so irregular that it may be properly modelled as an amorphous surface.

Another general conclusion that may be drawn from the study of the BS model is that adsorption site model (cf. Fig. 2) which is conventionally considered to be the basis for the theory of adsorption on heterogeneous surfaces [1] has its important limitations. It was shown in Ref. [28] that new adsorption sites may be created in the course of adsorption. These are not the minima of adsorption potential as the normal adsorption sites on a free surface but the minima of the total potential energy of an adsorbed molecule including the energy of interaction with neighbouring adsorbed molecules. In fact, the available results for BS appear to give monolayers that are nearly close packed (in two dimensions)

regardless of the number and distribution of the sites. Thus the monolayer capacity of a heterogeneous surface is not equal to the number of adsorption sites on a free surface but may be larger. This partly removes the contradiction between the generally accepted point of view that the monolayer capacity depends upon the size of an adsorbed molecule and the adsorption site model which requires it to be equal to the number of adsorption sites on a free surface independently of the size of an adsorbed molecule.

Computer simulations of adsorption on silica gels reported in Refs. [17–19, 29, 36, 37] provide other examples of adsorption studies on amorphous oxides. In this case, adsorption on these solids depends not only upon the atomic structure of its surface but also on the peculiarities of its pore structure. In fact, only the globular porous structure of silica gel was properly modelled in Refs. [36, 37]. The atomic structure of the silica globules was approximated by a continuous density of oxides so that the surface of the silica gel was smooth (homogeneous) in this model. However, the adsorbent as a whole was heterogeneous due to its irregular porous structure. Despite the fact that such a model can give useful insights into the influence of packing of silica gel globules on the Henry's Law constants [36] or can be used for simulation of adsorption of mixtures [37], the overall agreement between the simulation and experimental data is only fair [37]. The reason for that is undoubtedly the inadequate modelling of the surface atomic structure of silica.

However, heterogeneity of silica surfaces was taken into account in Refs. [17, 18, 29]. These workers considered an amorphous arrangement of oxide ions which was simulated as described in Subsection 2.2, the model of the porous silica gel being similar to that in Refs. [36, 37]. At low coverages the simulated isotherm obeyed the Freundlich equation very accurately [18]. This is typical behaviour for adsorption on strongly heterogeneous surfaces (cf., e.g., Ref. [1]) and means the the limiting Henry's Law region had not been reached in the simulation study. Adsorption at higher coverages was analyzed in the spirit of a modern version of the Polanyi-type approach. The entire adsorption space was divided into small cells, each of which is characterized by the value of adsorption potential ϵ^* at its center [29]. The density of adsorbate in each cell was determined by computer simulation. The variation of this density with pressure is similar to the local isotherm of the theory of adsorption on heterogeneous surfaces [1]. Local values of the adsorption virial coefficients were determined by expanding this local isotherms as power series in pressure [29].

Finally, diffusion of SF_6 in the globular [18] and cylindrical pore[19] models of the silica gel was studied by the molecular dynamics technique as a function of coverage.

4. CONCLUSIONS

The technique of computer simulation makes it possible to realistically model the physical adsorption on amorphous solids. Such simulations consist of two stages: (i) the simulation of the atomic structure of the surface of the solid and (ii) the simulation of adsorption on that model surface.

The most detailed studies of the first stage have been done for amorphous silica. It was shown that effective charges in a two-body interatomic potential of Eq. (1) may be chosen in such a way that this potential which is used in ionic crystals can also be used in crystalline and amorphous SiO_2 where interatomic bonds are partially covalent. This conclusion can be possibly extended to other oxides. It was also shown that one

may fit parameters of the potential of Eq. (3) to give a stable TiO_2 (rutile) crystal. This means that one might possibly use also this potential to realistically simulate the atomic structures of other amorphous oxides.

Successful simulations of amorphous oxide adsorbents consist in first simulating the melting of the crystal. This may be final or it may be followed by simulation of quenching and annealing. The irregular atomic structures obtained in this manner contain anions and cations. Since cations play relatively minor role in physical adsorption, one may simulate a general (and, naturally, less detailed) model of the amorphous oxide surface as a dense random hard-sphere packing of anions. Surfaces generated by this model were called Bernal surfaces.

These are methods for the simulation of a flat amorphous surface. To simulate the atomic structure of a porous oxide adsorbent like silica gel, one may first simulate the bulk amorphous silica. Then cut out of it globules and arrange them in space to model the pore structure of silica gel. Other applications of this idea include the creation of pores such as those found in porous glass by deleting atoms from a simulated block of solid in such a way as to leave a cylindrical pore.

Once the model atomic structure of an amorphous oxide adsorbent is created, one may proceed to simulate physical adsorption on (or in) this material. The peculiarity of oxide adsorbents (compared to carbon adsorbents for example) is that one has to take account of the highly inhomogeneous electrostatic field at their surfaces. The problem of the reliable calculation of the effect this field upon the adsorption energy is not yet totally resolved. However, an effective adsorption potential is typically used in such situations, with parameters that are adjusted by, for example, fitting the calculations to the temperature dependence of the experimental Henry's Law constants. Such potentials generally give reasonable values for other simulated equilibrium and kinetic adsorption properties. There is even an indication that the effective parameters of the gas-solid adsorption potential are sometimes transferrable from one (oxide) adsorption system to another.

Some systematic deviations of simulated isotherms from experiment in the BET-region may be explained on assumption that real surfaces of amorphous oxide are characterized not just by the atomic roughness of the irregular amorphous atomic structure, but may also have another kind of roughness with a much larger scale of length.

Finally we would like to mention some problems which, in our opinion, should be addressed in connection with the problem of computer simulation of physical adsorption on amorphous oxides. First, there is the problem of transferability of the parameters of the dispersion potential atom/oxygen interaction from one oxide system to another. For instance, one may fit these parameters to describe adsorption of argon in silicalite and in another form of SiO_2, e.g. amorphous silica. The question is how much will these parameters differ. This problem has already been addressed in the adsorption literature and was partially discussed above but still has no clear cut answer. Second, there is a number of problems connected with the influence of strongly inhomogeneous electrostatic field at the surface of oxides upon adsorption properties. These have not yet been properly dealt with in computer simulations. For example, it is not *a priory* clear if the models of amorphous oxides described above are hydrophobic or not. On one hand, one may expect hydrophilic behaviour because oxide ions are given a considerable electric charge (cf. Table 1). On the other hand, the hydrophilicity of silica is conventionally connected with hydroxides on its surface so that the above models which does not consider hydroxides

explicitly may be expected to be hydrophobic. A direct computer simulation is necessary to solve this problem.

REFERENCES

1. W. Rudzinski and D.H. Everett, Adsorption of Gases on Heterogeneous Surfaces, Academic Press, London, 1992.
2. V.A. Bakaev, Dokl. AN SSSR, 279 (1984) 115; Doklady Phys. Chem. (Engl. transl.) 279 (1985) 983.
3. V.A. Bakaev, Surf. Sci., 198 (1988) 571.
4. F. A. Cotton and G. Wilkinson, Advanced Inorganic Chemistry. A Comprehensive Text, J. Wiley & Sons, New York, 1980, p. 16.
5. J.S. Tse and D.D. Klug, J. Chem. Phys., 95 (1991) 9176.
6. R.G. Della Valle and H.C. Andersen, J. Chem. Phys., 97 (1992) 2682.
7. B.P. Feuston and S.H. Garofalini, J. Chem. Phys., 89 (1988) 5818.
8. F.H. Stillinger and T.A. Weber, Phys. Rev., B31 (1985) 5262.
9. R.G. Della Valle and H.C. Andersen, J. Chem. Phys., 94 (1991) 5056.
10. S. Tsuneyuki, M. Tsukada, H. Aoki and Y. Matsui, Phys. Rev. Lett., 61 (1988) 869.
11. B.W.H. van Beest, G.J. Kramer and R.A. van Santen, Phys. Rev. Lett., 64 (1990) 1955.
12. S. Tsuneyuki, H. Aoki, M. Tsukada and Y. Matsui, Phys. Rev. Lett., 64 (1990) 776.
13. R.G. Della Valle and E. Venuti, Chem. Phys., 179 (1994) 411.
14. J. Sarnthein, A. Pasquarello and R. Car, Phys. Rev. Lett., 74 (1995) 4682.
15. F.E. Luborsky (Ed.), Amorphous Metallic Alloys, Butterworths, London, 1983.
16. B.P. Feuston and S.H. Garofalini, J. Chem. Phys., 91 (1989) 564.
17. J.M.D. MacElroy and K. Raghavan, J. Chem. Phys., 93 (1990) 2068.
18. J.M.D. MacElroy and K. Raghavan, J. Chem. Soc. Faraday Trans., 87 (1991) 1971; 89 (1993) 1151.
19. A. Brodka and T.W. Zerda, J. Chem. Phys., 95 (1991) 3710.
20. V.A. Bakaev, Surface Sci. Lett., 264 (1992) L218.
21. V.A. Bakaev and W. A. Steele, Langmuir, 8 (1992) 1379.
22. A. Bonissent and B. Mustaftschiev, Phil. Mag., 35 (1977) 65.
23. V.A. Bakaev and W.A. Steele, Adsorp. Sci. & Technol., 10 (1993) 123.
24. J. Tersoff, Phys. Rev., B37 (1988) 6991.
25. J. Tersoff, Phys. Rev. Lett., 61 (1988) 2879.
26. W.A. Steele, Chem. Rev., 93 (1993) 2355.
27. A. Lakhlifi, Mol. Phys., 78 (1993) 659.
28. V.A. Bakaev and W.A. Steele, Langmuir, 8 (1992) 1372.
29. J.M.D. MacElroy, Langmuir, 9 (1993) 2682.
30. H. Tatewaki and T. Nakamura, Surf. Sci., 108 (1981) L447.
31. V.A. Bakaev and L.F. Smirnova, Izv. AN SSSR, Ser. khim., No.2 (1978) 284. Bull. Acad. Sci. USSR, Div. Chem. Sci. (Engl. transl.) 27 (1978) 244.
32. D.M. Young and A.D. Crowell, Physical Adsorption of Gases, Butterworths, London, 1962.

33. V.A. Bakaev and A.V. Voit, Izv. AN SSSR, Ser. khim., No. 9 (1990) 2007; Bull. Acad. Sci. USSR, Div. Chem. Sci. (Engl. transl.), 39 (1991) 1822.
34. V.A. Bakaev and W.A. Steele, Langmuir, 8 (1992) 148.
35. V.A. Bakaev and W. A. Steele, J. Chem. Phys., 98 (1993) 9922.
36. R.D. Kaminsky and P.A. Monson, J. Chem. Phys., 95 (1991) 2936.
37. R.D. Kaminsky and P.A. Monson, Langmuir, 10 (1994) 530.
38. W.A. Steele, The Interaction of Gases with Solid Surfaces, Pergamon Press, Oxford, 1974.
39. V.A. Bakaev and O.V. Chelnokova, Surf. Sci., 215 (1989) 521.
40. M.P. Allen and D.J. Tildesley, Computer Simulation of Liquids, Clarendon Press, Oxford, 1987.
41. R.J.-M. Pellenq and D. Nicholson, Langmuir, 11 (1995) 1626.
42. S.J. Gregg and K.S.W. Sing, Adsorption, Surface Area and Porosity, 2'nd ed., Academic Press, London, 1982.
43. L.E. Drain and J.A. Morrison, Trans. Faraday Soc., 48 (1952) 840.
44. V.A. Bakaev, J. Chem. Phys., 102 (1995) 1398.

This Page Intentionally Left Blank

A. Dąbrowski and V.A. Tertykh (Editors)
Adsorption on New and Modified Inorganic Sorbents
Studies in Surface Science and Catalysis, Vol. 99

Chapter 2.2
On the nature of the energetic heterogeneity of water/oxide interface in adsorption phenomena occurring at oxide surfaces

W. Rudziński[a], R. Charmas[a] and T. Borowiecki[b]

[a]Department of Theoretical Chemistry, Faculty of Chemistry,
Maria Curie-Skłodowska University, 20-031 Lublin, Poland

[b]Department of Chemical Technology, Faculty of Chemistry,
Maria Curie-Skłodowska University, 20-031 Lublin, Poland

1. INTRODUCTION

It is now generally recognized that the surfaces of oxides are geometrically distorted and therefore energetically heterogeneous for adsorption. It has been realized by the scientists investigating adsorption from the gas phase for a long time. A variety of experimental techniques has been used to study the nature of these surface imperfections, and dozens of papers have been published on this subject. The reported results have already been a subject of a number of reviews [1]. Dozens of papers were published showing that successful correlations of the experimental data for gas adsorption onto oxides can be done only by using equations corresponding to a heterogeneous surface model [2,3]. The experimental studies were stimulated strongly by the widely spread view that these are the surface imperfections creating catalytic centres for many important catalytic reactions.

Bakaev's computer simulations [4-7] of oxide surfaces suggest that even in the case of oxides having a well defined bulk crystal structure, the degree of the surface disorder may be larger than it is generally believed.

Our attention here will be focused on the extremely important class of adsorption systems, composed of water being in contact with oxide surfaces. The reasons, why the behaviour of water/oxide interfaces is so important for various areas of science, life and industry, are well-known.

The calorimetric studies of the surface heterogeneity of oxides were initiated half a century ago, and experimental findings as well as their theoretical interpretation have been recently reviewed by Rudziński and Everett [2]. The last two decades have brought a true Renaissance of adsorption calorimetry. A new generation of fully automatized and computerized microcalorimeters has been developed, far more accurate and easy to manipulate. This was stimulated by the still better recognized fact that calorimetric data are much more sensitive to the nature of an adsorption system than adsorption isotherm for instance. It is related to the fact that calorimetric effects are related to temperature derivatives of appropriate thermodynamic functions, and tempearture appears generally

in exponential terms.

However, that recent impressive progress on experimental side was not accompanied by a sufficient progress in the interpretation of the obtained experimental data. As far as water/oxide interface is concerned the following problems deserve more theoretical and experimental studies.

(1) Which is the combined effect of the multilayer adsorption phenomena and the surface energetic heterogeneity on the heats of adsorption? There have been published some papers showing that combined effect on the behaviour of adsorption isotherms. To our knowledge not much has been published on the theoretical studies of the combined effect in the case of heats of adsorption yet. Meanwhile, because of the strong surface heterogeneity of oxides, the water adsorption has a highly mixed monolayer – multilayer character even at low relative pressures (p/p_0) in the equilibrium gas phase.

(2) There have been published numerous papers reporting the measurements of the heat capacity of water adsorbed on oxide surfaces. The likely important effect of the surface heterogeneity on the behaviour of heat capacity data has never been considered yet in the accompanying theoretical interpretations. It may only surprise us, because in the case of other adsorption systems such studies have already been published, demonstrating the crucial role of surface heterogeneity.

(3) There have been published experimental studies of phase transitions in the water adsorbed on solid surface, but their interpretation usually ignored the role of surface energetic heterogeneity. Meanwhile, it is now well-known, that the surface heterogeneity affects extremely strongly the phase transition in adsorbed films. In a regime of phase transition, even weak, non-uniform external fields affect strongly the behaviour of every physical system.

The adsorption of ions and the formation of the electric double layer at water/oxide interface are the physical phenomena the importance of which in life and technology can hardly be overestimated. So, no surprise that the mechanism of the formation of the electric double layer at water/oxide interfaces has been studied thoroughly in hundreds of papers and it would take far too long to review even the most fundamental of them. Various techniques have been used to measure proton and accompanying ion adsorption on the outermost surface oxygens of oxides. The most popular of these techniques are potentiometric titration and ζ-potential measurements. Then, radiometric methods allow the adsorption of individual ions to be monitored.

The interpretation of electrokinetic data is accompanied by some assumptions which introduce a certain degree of uncertainty. On the contrary, the potentiometric titration and the radiometric methods are directly related to the adsorption isotherms of ions. Thus, the most fundamental conclusions have been drawn from a suitable theoretical analysis of these adsorption isotherms being mainly based on a model of a homogeneous oxide surface.

As the accuracy of the adsorption isotherm measurements increased, the necessity to fit the experimental data quantitatively led to more and more refined theories of the electric double layer. However, these more refined and complicated theories failed to correlate experimental adsorption isotherms in some systems. The general feeling started to grow that the model of a homogeneous surface is too crude to explain well these adsorption phenomena.

Thus, in view of this large body of experimental and theoretical evidence of the surface

heterogeneity of the actual oxides, it may only surprise us, that this important physical factor received so little attention from the scientists investigating ion adsorption at electrolyte/oxide interfaces.

At the early stage of the theories of adsorption onto oxide surfaces, the emphasis was given to electrostatic interactions. The fact that adsorption frequently involves chemical bonding as well was not so commonly recognized until recently. This implies a dispersion of chemical bonding energies to be possible, arising form the different local status of the outermost surface oxygens.

At the end of the seventies Garcia-Miragaya and Page [8,9] and Street et al. [10] reported a successful correlation by Freundlich equation of the data of trace Cd^{2+} adsorption by both clay minerals and soils. Benjamin and Leckie [11] found the same for the trace adsorption of Cu^{2+}, Zn^{2+}, Cd^{2+} and Pb^{2+} onto amorphous iron oxyhydroxide. The use of Freundlich equation was also suggested in the works by Sposito [12,13].

In the theories of gas adsorption the applicability of Freundlich equation was long ago associated with the energetic heterogeneity of the adsorption sites on the actual solid surfaces. It was also known, that Freundlich equation is a simplified form of a more general isotherm equation which is now commonly called Langmuir–Freundlich isotherm. Thus, in 1980 Sposito [13] suggested that it was high time it were used also in the case of ion adsorption at water/oxide interfaces.

Benjamin and Leckie [11] were among the first who initiated the studies of the surface heterogeneity effects in 1981. They reported that the adsorption of Me^{2+} metal ions onto oxyferrihydride could be described only by assuming a large dispersion of adsorption site affinities. Two years later Kinniburgh et al. [14] tried to correlate such adsorption isotherms by using other empirical equations employed earlier to correlate experimental adsorption isotherms for single gas adsorption onto heterogeneous solid surfaces.

Theoretical studies of surface heterogeneity effects on ion adsorption within the electrical double layer were much advanced by Koopal, Van Riemsdijk and co-workers [15-19]. Rudziński and co-workers [20] have subjected calorimetric effects accompanying ion adsorption to their theoretical analyses. They showed that surface heterogeneity of oxides affected enthalpies of ion adsorption. A similar effect has been known for a long time in gas adsorption onto solid surfaces. In another paper, Rudziński et al. [21] showed that titration curves were much less sensitive to the surface heterogeneity than individual adsorption isotherms of ions measured by using radiometric methods. Titration curves probably involve a certain mutual cancellation of heterogeneity effects. This deserves some further experimental and theoretical studies. Rudziński et al. [22] developed the theory reproducing the behaviour of the log-log plots of the experimental adsorption isotherms of bivalent ions on oxides at low surface concentrations. These experimental adsorption isotherms show a transition from a linear log-log (Henry's) plot with a tangent equal to unity to a Freundlich log-log plot with tangent smaller than unity.

2. WATER (VAPOUR)/OXIDE INTERFACE

Several dozens of papers have already been published on the heat of immersion of various outgased solids into water. These were mainly silica, alumina, titania, ferrum, zinc and manganese oxides. Here, it would be far too long to quote even the most interesting

papers. So, let us quote at least some names of the authors like Zettlemoyer, Morimoto, Chessick, Rouqueroll, Della Gatta, Kondo, Wightman, but there should be listed also many others.

The reasons for which the mechanism of the oxide hydroxyl surface formation is so much important are well known. So only the discussion concerning the nature of hydrated oxides will be given. It can be obtained from the experimental data on heats of immersion in various types of immersion experiments. The direct measurements of the heats of adsorption of water from its vapour phase onto oxides were rarely reported. On the contrary, several dozens of papers have already been published on the heat of immersion of various outgassed oxides into water. The following types of immersion experiments have been carried out so far:

(1) The first, most popular is that in which measurements of the heat of immersion were considered as a function of the outgassing temperature of an oxide sample. The outgassing was carried out usually at high temperatures of several hundred of Celsius degrees, so, the measured effects concern the reconstruction of the hydroxylated surface.

(2) As the second type we consider the measurements in which a sample outgassed at room temperatures was pre-covered by a certain amount of the immersional liquid adsorbed from its gaseous phase, prior to immersion. In other words, the heats of immersion are considered as a function of the amount pre-adsorbed on a hydroxylated surface.

(3) The third type of the immersional experiments is quite new. These are the heats of immersion of an outgassed sample into aqueous solutions of varying pH. In other words, the heats of immersion are considered as a function of proton concentration in the immersional liquid. Until very recently, only three experiments of such a kind have been reported in literature. These were the heats of immersion of $\alpha-Al_2O_3$ reported by Roy and Fuerstenau [23], and next by Griffiths and Fuerstenau [24], and the heats of immersion of titanium dioxide reported by Foissy [25]. Quite recently, an extensive experimental study including various metal oxides has been published by Wierer [26], Machesky and Anderson [27], De Keizer et al. [28], and Machesky and Jacobs [29,30].

To understand the information resulting from these experiments, it is necessary to know the phenomena occurring during the immersion of an outgassed sample of metal oxide into water. Not getting into details which are still controversial, let us recall what has been known for a long time and generally accepted.

2.1. The mechanism of the formation of hydroxylated oxide surfaces by water adsorption from its vapour phase

It is well-known that the surface hydroxyl groups on such metal oxides as SiO_2,TiO_2, or Al_2O_3 are removed by thermal treatment in vacuum, resulting into the formation of an activated oxide structure $-Me < \overset{O}{O} > Me-$, as a result of the condensation of the adjacent hydroxyl groups, according to the following scheme:

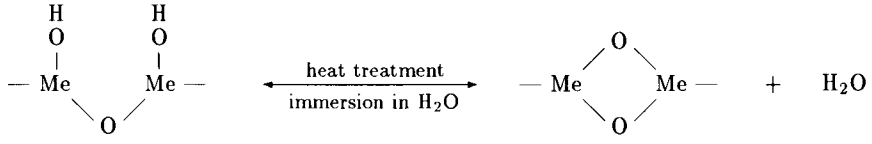

The activated site may be easily rehydrated by the adsorption of water. That scheme, still

coming from the works published by Morimoto and co-workers [31,32] is, in fact, more complicated. First of all, farther water molecules are adsorbed secondarily on the top of the already formed hydroxyls. The mechanism of that secondary adsorption is not quite clear yet.

Kiselev and Lygin [33] who studied the adsorbed state of water molecules on silica by means of IR spectroscopy concluded, that a water molecule was adsorbed on two surface hydroxyl groups through the formation of a hydrogen bond between the oxygen atom of the water molecule and two hydrogen atoms of the neighbouring hydroxyl groups. However, a quantitative demonstration for their conclusion was not given.

Hallabaugh and Chessick [34] drew a similar conclusion from the fact that the cross-sectional area of the water molecule in the monolayer on TiO_2 (rutile) was extremely large, i.e. 23.5Å^2. Also Morimoto et al. [35] arrived at a similar conclusion in their analysis of water adsorption isotherms on rutile. They proposed the following scheme for the secondary adsorption:

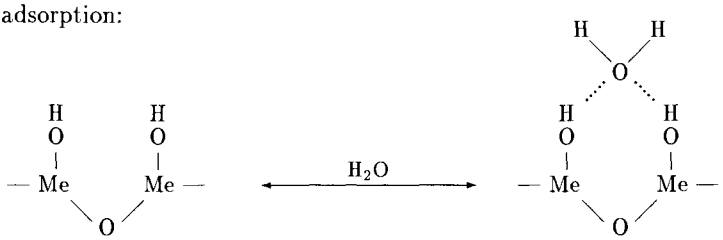

Exactly the same picture can be found in the work by McCafferty and Zettlemoyer [36] on water adsorption on $\alpha - Fe_2O_3$.

On the contrary, an IR study of water adsorbed on titanium oxides has brought Primet [37] to the conclusion that the secondary adsorption of water should be represented by the following scheme:

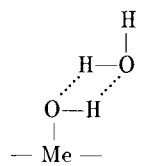

Griffiths and Fuerstenau [24] argued that the formation of the secondarily adsorbed molecules proceeded as follows:

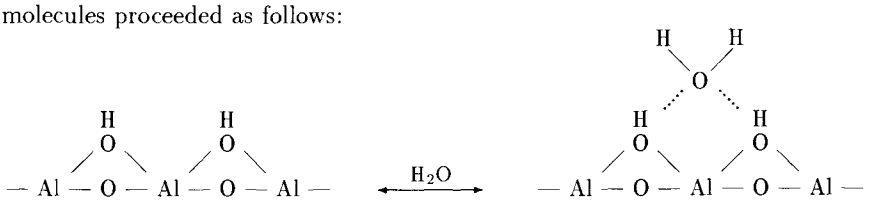

and led finally to an "iceberg" structure near a solid surface.

Doremieux-Morin et al. [38] carried a NMR study of water adsorbed onto rutile, anatase and an amorphous titanium oxide. On that basis they postulated that, in addition

to the Primet's mechanism, farther water molecules could be adsorbed also in three different ways:

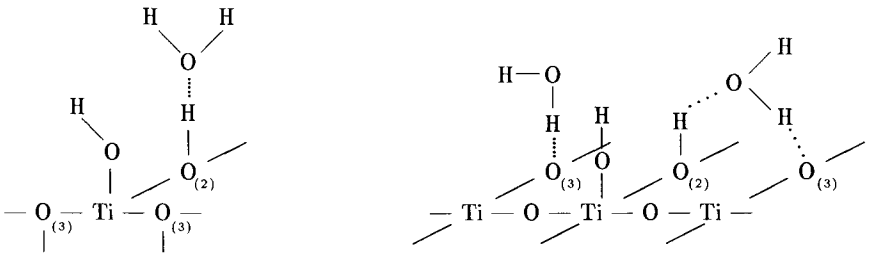

where (2) and (3) denote the co-ordination number of oxygen atoms. The situation when water molecule is bonded simultaneously to surface hydroxyl and a surface oxygen should be typical for amorphous surfaces possessing low-density planes.

The ways of secondary water adsorption on various metal oxides based on calorimetric investigations and IR spectroscopy were studied by Fubini et al. [39].

Thus, the later experiments would suggest that the first secondarily adsorbed water molecules are associated rather with only one hydroxyl. This statement is essential for developing isotherm equations for water adsorbed from vapour phase onto metal oxides.

2.2. The nature of the energetic heterogeneity of the actual water/oxide interfaces

So far, we have considered idealized surface structures of oxides. It is now commonly realized that the crystalography and chemical composition of the actual solid surfaces do not represent an extrapolation of appropriate bulk crystal properties. The actual (really existing) solid surfaces are characterized by a more or less decreased crystallographic order, leading also to variations in the local chemical composition. This, in turn, causes variations in adsorptive properties of adsorption sites, across the surface.

That phenomenon known as the "energetic heterogenity" of the real solid surfaces is believed now to be one of the fundamental, common features of the actual solid surfaces [2,3].

In our case, the energetic surface heterogenity means, first of all, the variations in the chemical status and the adsorptive features of the outermost surface oxygen atoms with respect to hydrogen bonding. The existence of the surface energetic heterogenity of oxides, with respect to water adsorption has been known for a long time. The most spectacular evidence came from calorimetric measurements.

Zettlemoyer and his co-workers [40,41] were among the first who demonstrated strong evidence for a great role of the surface energetic heterogeneity of oxides in their immersional experiments. Morimoto and co-workers [42] wrote that "the differential heat on TiO_2 decreased with increasing amount of chemisorbed water, suggesting an ordinary type of surface heterogeneity". In their studies of water adsorbed onto alumina Della Gatta et al. [43] concluded that "surface rehydroxylation involves rather high differential heat values (initial heat of about 40 kcal/mol), and the heat evolution is typical for a heterogeneous surface". Wightman et al. [44] reported that in their studies of water adsorption onto titanium dioxide, "the isosteric heat of adsorption decreased with increasing coverage indicating the heterogeneous nature of the titanium dioxide samples". The first quanti-

tative fit of the experimental heats of immersion in pure water [45] and in solutions of varying pH [20] was done by Rudziński et al., who assumed that the surfaces of oxides were energetically heterogeneous.

Although, the view about the energetic heterogeneity of oxide surfaces is now commonly accepted, the nature of that phenomenon and its role in adsorption is not well understood yet. The structure of oxide surfaces is still often assumed to be corresponding to their ideal crystallographic structure.

Meanwhile, as long ago as at the beginning of the sixties Peri [46-48] argued that after strong dehydratation the structure of aluminium oxides was very irregular, as shown in Fig. 1. Flockhardt et al. [49,50] assumed a lesser distorted structure of aluminium oxides, as shown in Fig. 2.

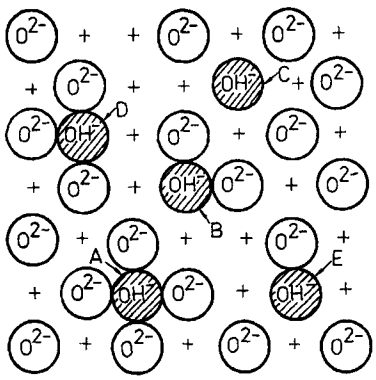

Figure 1. Peri's model of aluminium oxide surface after strong dehydration.

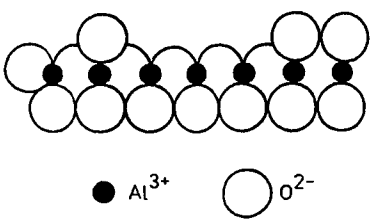

Figure 2. Flockhardt's model of aluminium oxide surface.

Hiemstra et al. [51-53] assumed that the surface heterogeneity of aluminium oxides arose solely from a different status of various surface oxygens, as shown in Figure 3.

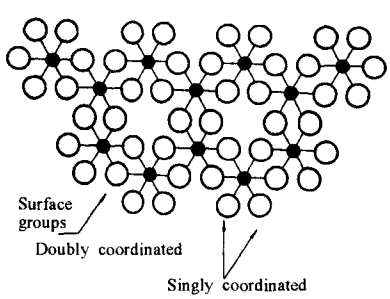

Figure 3. Hiemstra's model of aluminium oxide surface.

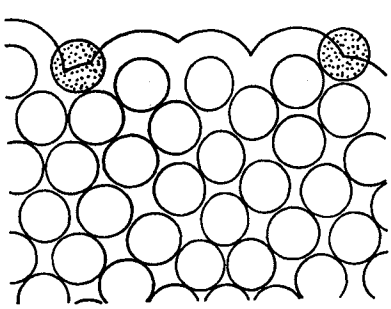

Figure 4. Bakaev's picture of an oxide surface.

Bakaev [4,54,55], on the contrary, believes that for the majority of the actual, i.e, really existing, oxide surfaces, the picture of an amorphous surface phase should be more realistic than that of a crystalline surface with defects. It means, Bakaev's model is similar to that assumed by Peri.

Bakaev pays the attention to an interesting piece of experimental evidence supporting his view, coming from the calorimetric experiments by Rouqueroll and co-workers [56,57]. They investigated the enthalpy of adsorption of nitrogen and argon on a crystalline rutile, and a rutile partially coated by amorphous silica. The enthalpies of adsorption of nitrogen were different, due to the particular electric field pattern near the rutile surface, "felt" by a nitrogen molecule. Argon atoms, on the contrary, are insensitive to the difference in electric fields, so, the close similarity of its enthalpy of adsorption on pure and coated rutile must testify to similarities in their surface structure. As the silica – coated rutile is, presumably, an amorphous surface, the similarity of the enthalpies of adsorption of argon indicates the amorphous structure of pure rutile too. The adsorption potential of argon is mainly determined by the interaction with large oxygen ions, since their polarizability is much larger than that of cations. So, the physical adsorption of argon on oxides is mainly determined by the amorphous structure of the oxygen atoms near the surface. Thus, for argon adsorption on oxides a representative model of surface phase could be the Bernal model [58], i.e., a dense random packing of hard balls. The surface of such a model amorphous solid may be visualized as the surface of a heap of ball bearings on a plate. The schematic visualization of such an atomic arrangement is presented in Fig. 4.

The white circles in Fig. 4 represent the oxygen atoms (ions) of adsorbent and the shadowed circle an adatom which "rolls" over the heterogeneous surface. (The presence of small cations is neglected here). The main objective of Bakaev's earlier works [5-7,59] was to calculate the 3-dimensional adsorption potential U(x,y,z) of such an adatom. It was done practically in the following way: A set of vectors $\{r_i\}$ was created in the computer memory representing a dense random packing of 2500 hard balls. The balls were contained in a square box of an area $(20 \times 20)D^2$, where D is the ball diameter. Periodic boundary contributions were imposed in the x- and y-directions, but no restrictions were imposed in the z-direction, perpendicular to the surface. Each ball represented an oxygen anion with a diameter D = 0.28 nm. Argon adatoms were assumed to interact with oxygen balls via a Lennard-Jones potential.

The next crucial mathematical operation in Bakaev's computations was finding the minima of the potential function U(x,y,z). Thus, an average number of 226 local minima has been found by Bakaev in his unit cell. That means, that the area associated with one local minimum is about 0.14 nm, compared to a value 0.15 nm accepted in BET method utilizing argon adsorption data to determine the area of TiO_2 [60]. The calculated distribution of the number of adsorption sites (local minima) among the values of these minima was compared next with Drain and Morrison's adsorption energy distribution for argon adsorbed on rutile [61]. The range of adsorption energies was similar, except that Drain and Morrison's energy distribution suggested a larger contribution from less active sites. This may be the contribution from cations, neglected in Bakaev's computer simulation. If we realize, however, that this is a purely *ab initio* result, one must be impressed by the success of Bakaev's research.

Bakaev's computer simulation provides an impressive support for random topography of oxide surfaces. Of course, some degree of surface organization should exist, and it will

increase when going more and more deeply into the solid bulk phase. The outermost layers of surface atoms (ions) may be amorphous, but the interior may have a well-defined structure.

The fact that the surfaces of the actual oxides are geometrically distorted and energetically heterogeneous is crucial for almost all catalytic reactions running on oxide surfaces as demonstrated by the numerous works published by Samorjai's school. Still new papers are published showing the importance of the geometric nonuniformity and energetic heterogeneity in various adsorption and catalytic systems. So, various experimental techniques have been used to study that important phenomenon. These findings were reported by Samorjai [62] and more recently by Hirschwald [63]. This latter review includes the impressive images of the surfaces of the actual oxides obtained by STM (Scanning Tunneling Microscopy) [64] (see Fig. 5).

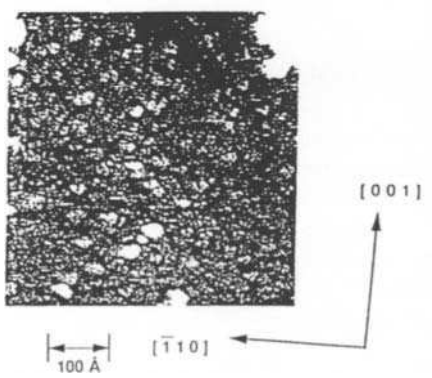

Figure 5. The picture 492 × 492 Å^2 obtained by STM [65] for TiO_2 (110) surface.

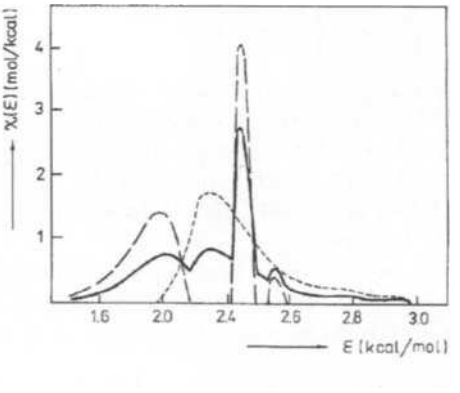

Figure 6. The energy distribution functions $\chi(\epsilon)$ for the system Ar-rutile studied experimentally by Drain and Morrison [61]. The slightly broken line (– – –) is the function evaluated by Rudziński and Jaroniec [66]; the strongly broken one (- - - - -) is the function determined by Dormant and Adamson [67]. The solid line is the average of these two functions.

The quantitative measure of the degree of surface heterogeneity in the model of the one-site-occupancy adsorption is the differential distribution of the fraction of surface sites among corresponding values of adsorption energy ϵ, $\chi(\epsilon)$, such that

$$\int_{\Delta\epsilon} \chi(\epsilon)\mathrm{d}\epsilon = 1 \tag{1}$$

where $\Delta\epsilon$ is the physical domain of ϵ.

Very often $\chi(\epsilon)$ is approximated by a simple analytical function and $\Delta\epsilon$ is assumed to be either $(0, +\infty)$ or $(-\infty, +\infty)$ interval for the purpose of mathematical convenience. Such simplifications do not usually introduce a significant error in the latter theoretical calculations, except for some extreme physical regimes [2]. The exact function $\chi(\epsilon)$ for

a real physical surface is expected to have a complicated shape in general. However, to a first crude approximation, it may be approximated by a simple smooth, gaussian–like function. This is demonstrated in Fig. 6.

The solid line in Fig. 6 is the function $\chi(\epsilon)$ for argon adsorbed onto rutile, obtained by averaging $\chi(\epsilon)$ calculated by two different methods. Thus, it can be clearly seen that $\chi(\epsilon)$ should, in this case, be well "smoothed" by a gaussian–like function. This statement should be true for both argon and water adsorption, because the interaction with surafce oxygens is the key factor in both cases.

Thus, we will represent $\chi(\epsilon)$ by the following gaussian–like function [68,69]

$$\chi(\epsilon) = \frac{\frac{1}{c}\exp\left\{\frac{\epsilon - \epsilon^0}{c}\right\}}{\left[1 + \exp\left\{\frac{\epsilon - \epsilon^0}{c}\right\}\right]^2} \tag{2}$$

centered at $\epsilon = \epsilon^0$, the spread (variance) of which is described by the heterogeneity parameter c. (The variance σ is equal to $\pi c/\sqrt{3}$).

In the case of monolayer adsorption the use of this function leads to the Langmuir–Freundlich isotherm which is probably the most commonly applied to correlate the experimental data at not very high surface coverages when the effects of multilayer adsorption can still be neglected.

Using such a simple function $\chi(\epsilon)$ is necessary in practical calculations, to avoid introducing many unknown parameters. That procedure is common for the majority of theoretical works on adsorption on heterogeneous solid surfaces.

2.3. Principles of the adsorption model

Although the model of adsorption from vapour phase will, to a large extent, depend upon the particular oxide sample under investigation the most probable adsorption mechanism should be following:

(1) First adsorbed molecules are used to rehydroxylate the following activated complex $-\mathrm{Me} <^{\mathrm{O}}_{\mathrm{O}}> \mathrm{Me}-$ to give surface hydroxyls.

(2) The most probable mode for the secondary adsorption, established in recent experiments is, when one water molecule is attached to one surface hydroxyl. Therefore, we consider the secondarily adsorbed molecules as occupying one adsorption site. The classical BET model is useful here for another reason as it considers both the primarily and secondarily adsorbed molecules to be localized.

The classical BET model does not consider the lateral interactions between the adsorbed molecules which may be important in our systems. However, one can generalize that model to take these interactions into account as demonstrated by De Oliveira and Griffiths [70] and by Asada and Sekito [71]. Here, another generalization which preserves the simplicity of the classical BET model is proposed [72].

We start by writing the expression for the grand partition function [73] Ξ^* for the classical BET model:

$$\Xi^* = (1 + \mathrm{y})^{\mathrm{M}}\,, \qquad \mathrm{y} = \frac{\mathrm{j}_1 \exp\left\{\frac{\mu}{\mathrm{kT}}\right\}}{1 - \mathrm{j}_\infty \exp\left\{\frac{\mu}{\mathrm{kT}}\right\}} \tag{3}$$

where j_1 and j_∞ are the molecular partition functions for the primarily and secondarily adsorbed molecules, M is the number of adsorption sites, k is the Boltzman constant, and T is the absolute temperature.

The adsorption isotherm $\overline{N}$, (the average number of particles in our adsorption system) is given by

$$\overline{N} = kT\left(\frac{\partial \ln \Xi^*}{\partial \mu}\right)_{T,M} = \frac{Mj_1 \exp\left\{\frac{\mu}{kT}\right\}}{\left[1 - j_\infty \exp\left\{\frac{\mu}{kT}\right\}\right]\left[1 - j_\infty \exp\left\{\frac{\mu}{kT}\right\} + j_1 \exp\left\{\frac{\mu}{kT}\right\}\right]} \tag{4}$$

Then, we assume the ideal gas approximation

$$\mu = \mu_0 + kT \ln p \tag{5}$$

and write j_1 in a form showing its dependence on the adsorption energy ϵ:

$$j_1 = j_1^0 \exp\{\epsilon/kT\} \tag{6}$$

With this notation we can write Eq. (4) in the following form:

$$\theta = \frac{\overline{N}}{M} = (1 + P)\frac{KP \exp\left\{\frac{\epsilon}{kT}\right\}}{1 + KP \exp\left\{\frac{\epsilon}{kT}\right\}} \tag{7}$$

where

$$K = \frac{j_1^0}{j_\infty}, \qquad P = \frac{k'\frac{p}{p_0}}{1 - k'\frac{p}{p_0}}, \qquad k' = j_\infty p_0 \exp\{\mu_0/kT\}, \qquad 0 \leq k' \leq 1 \tag{8}$$

and where p_0 is the saturated vapour pressure at the temperature T.

Equation (7) can then be rewritten to the following linear form:

$$F'(P) = \frac{k'\frac{p}{p_0}}{\overline{N}\left[1 - k'\frac{p}{p_0}\right]} = \frac{1}{MC} + \frac{C - 1}{MC}k'\frac{p}{p_0} \tag{9a}$$

where

$$C = K \exp\{\epsilon/kT\} \tag{9b}$$

convenient for appropriate best-fit numerical exercises. Choosing properly a value of the parameter k' [74,75], one should get a linear plot of F'(P) vs $k'(p/p_0)$ and the two other parameters, the value of the monolayer capacity M and parameter C, should be easily calculated from the parameters of this linear plot.

The features of the theoretical BET isotherm are well-known, but the related features of other thermodynamic functions have been rarely discussed, for instance, the corresponding expression for the isosteric heat of adsorption Q_{st}:

$$Q_{st} = k\frac{(\partial\theta/\partial\frac{1}{T})_p}{(\partial\theta/\partial \ln p)_T} \tag{10}$$

After performing appropriate differentiations, one obtains

$$Q_{st} = Q_0 - Q_1' \frac{\left[1 - k' \frac{p}{p_0}\right]^2}{1 + (C-1)\left[k' \frac{p}{p_0}\right]^2} \tag{11a}$$

where the parameters Q_0 and Q_1' are defined as follows:

$$Q_0 = -kT^2 \frac{\partial \ln(\frac{k'}{p_0})}{\partial T} \tag{11b}$$

$$Q_1' = kT^2 \frac{\partial \ln C}{\partial T} \tag{11c}$$

When the state of the molecules adsorbed in the second and higher layers is the same as the state of molecules in the saturated vapour, then k'=1, and

$$\lim_{p/p_0 \to 1} Q_{st} = Q_0 = \text{heat of liquefaction} \tag{12}$$

However, in the systems where k' is smaller than unity, Q_{st} cannot be interpreted as the heat of liquefaction, even at p/p_0 close to unity. And this will be the case of water adsorbed on a non-porous silica, investigated experimentally by Partyka et al. [76,77]. For this particular adsorption system, the estimated value of k' lies below 0.7.

Now let us consider an opposite extreme situation, i.e. when the state of the molecules in the second and higher layers is the same as the state of the primarily adsorbed molecules. Then, $j_1^0 = j_\infty$ and $Q_1' = -\epsilon$. This means that Q_1' will, in general, have negative values. Thus, it is to be expected that when k' is much smaller than unity, one will find high negative values of Q_1'. This will also be true in the case of water adsorbed on the non-porous silica investigated experimentally by Partyka and co-workers [76,77].

This fact has to be strongly emphasized in view of the general belief, that at p/p_0 close to unity, Q_{st} should approach the value of the heat of liquefaction. This will not be true in the systems where k' is much smaller than unity.

Equation (11a) offers an interesting way of checking the applicability of the classical BET model to represent the multilayer adsorption in real systems. For that purpose, let us remark that the shape of Q_{st} is governed by the function Q_s:

$$Q_s = \frac{[1 - k' \frac{p}{p_0}]^2}{1 + (C-1)[k' \frac{p}{p_0}]^2} \tag{13}$$

Having measured for a certain system the experimental adsorption isotherm $\theta(\frac{p}{p_0})$, one may draw Q_s as the function of θ, assuming various values of $k' \in \langle 0, 1 \rangle$ and C. In this way, one obtains a family of exponentially decreasing curves, the shape of which is similar to that of the experimentally observed heats of adsorption curves.

This, and the fact that BET equation fits usually well the data in the pressure region around $p/p_0 \approx 0.3$, supported the view of the wide applicability of BET model. This was indeed so until the experimental data were carefully measured and quantitatively analyzed over wider pressure regions (extending over two or three orders of magnitude of p/p_0).

It has also been demonstrated by several authors [2] that a successful fit of the experimental data requires not only the assumption that $k' < 1$, but also considering another important physical factor. This is the energetic surface heterogeneity of the actual gas/solid interfaces. In terms of localized adsorption, this means a variation in the value of ϵ on various surface sites. The accompanying variations in the molecular partition function j_1 are of lesser importance and are usually neglected.

The quantitative measure of the degree of surface heterogeneity in the model of the one-site-occupancy adsorption assumed here is the differential distribution of the fraction of surface sites among corresponding values of adsorption energy ϵ, $\chi(\epsilon)$, given by Eq. (1). This function is represented here by the gausian-like function (2).

2.4. Equations for adsorption isotherms and for the heats of adsorption from gas phase

In the case of a heterogeneous solid surface, the experimentally measured adsorption isotherm $N_t = \theta_t M$ is to be expressed by the following average:

$$\theta_t = (1 + P) \int_{\Delta\epsilon} \theta_1(\epsilon)\chi(\epsilon)d\epsilon \tag{14}$$

where

$$\theta_1(\epsilon) = \frac{KP \exp\{\frac{\epsilon}{kT}\}}{1 + KP \exp\{\frac{\epsilon}{kT}\}} \tag{15}$$

and represents the fraction of the surface sites of energy ϵ, covered by the primarily adsorbed molecules.

Using the Rudziński–Jagiełło method [78,79] to calculate the integral on the right hand side of Eq. (14), for the gaussian-like adsorption energy distribution defined in Eq. (2), we obtain:

$$\theta_t = \frac{N_t}{M} = -(1 + P)\mathcal{X}(\epsilon_c) = (1 + P)\frac{(K^0P)^{kT/c}}{1 + (K^0P)^{kT/c}} \tag{16}$$

where

$$\mathcal{X}(\epsilon_c) = \int \chi(\epsilon)\, d\epsilon \qquad \text{and} \qquad K^0 = K \exp\{\epsilon^0/kT\} \tag{17}$$

and the function ϵ_c found from the condition $(\partial^2\theta_1/\partial\epsilon^2)_{\epsilon=\epsilon_c} = 0$ has the following form:

$$\epsilon_c = -kT \ln(KP) \tag{18}$$

In the limit of monolayer adsorption model Eq. (16) reduces to the Langmuir-Freundlich isotherm which, nowadays, seems to be the most widely used expression to correlate experimental adsorption isotherms in the submonolayer coverage region.

A convenient way to correlate experimental data is offered by the following linear form of Eq. (16):

$$F(P) = \ln \frac{\frac{N_t}{M(1 + P)}}{1 - \frac{N_t}{M(1 + P)}} = \frac{kT}{c} \ln P + \frac{kT}{c} \ln K^0 \tag{19}$$

By choosing a proper value of the monolayer capacity M, (expressed in the same units as the experimantally determined adsorbed amount N_t) and the value of the parameter k', one should obtain a linear plot of F(P) vs ln P. This way of reducing experimental adsorption isotherms should be convenient for the following reasons. The starting value of M can be easily estimated by using the standard BET method, and the value of k' varies usually around 0.6–0.8. Then the values of the heterogeneity parameter $\frac{kT}{c}$ and K^0 are obtained as the result of the linear regression described above. Good linearity of the plot F(P) vs ln P will also be a check on a proper choice of the function $\chi(\epsilon)$ to represent the adsorption energy dispersion. Provided that our solid surface is homogeneous, such a linear regression should yield $\frac{kT}{c} = 1$.

Now, we consider the behaviour of the isosteric heat of adsorption of water, Q_{st}, as predicted by the model of a heterogeneous oxide surface. After certain rearrangements for the heterogeneous surface, Eqn (10) can be written as follows:

$$Q_{st} = k\frac{\frac{\partial \epsilon_c}{\partial \frac{1}{T}} - \frac{c}{1+P-\theta_t}\frac{\partial P}{\partial \frac{1}{T}}}{\frac{\partial \epsilon_c}{\partial \ln p} - \frac{c}{1+P-\theta_t}\frac{\partial P}{\partial \ln p}} \tag{20}$$

For ϵ_c given by Eq. (18), we can evaluate the derivatives appearing in Eq. (20):

$$\left(\frac{\partial \epsilon_c}{\partial \frac{1}{T}}\right)_p = kT^2 \ln P + TQ_1 - T(P+1)Q_0 \tag{21a}$$

$$\left(\frac{\partial \epsilon_c}{\partial \ln p}\right)_T = -kT(P+1) \tag{21b}$$

$$\left(\frac{\partial P}{\partial \frac{1}{T}}\right)_p = \frac{P(P+1)}{k}Q_0 \tag{21c}$$

$$\left(\frac{\partial P}{\partial \ln p}\right)_T = P(P+1) \tag{21d}$$

where the parameter Q_0 is given by Eq. (11b) and Q_1 is defined as

$$Q_1 = kT^2\frac{\partial \ln K}{\partial T} + kT \ln K \tag{21e}$$

Finally we comment on the possible effect of the interactions between adsorbed molecules. As already mentioned, theoretical studies of multilayer collective adsorption have been published by De Oliveira and Griffiths [70], Asada and Sekito [71] and Nicholson and Silvester [80]. De Oliveira and Griffiths used a mean field approximation (MFA) to account for the effect of the interactions between the adsorbed molecules. MFA was also used by Nicholson and Silvester who took into account the energetic surface heterogeneity by assumnig a gaussian distribution of adsorption energies and random surface topography. Asada and Sekito used the quasi-chemical (QA) approach, but did not extend their treatment to the case of a heterogeneous solid surface.

In all these cases a system of non-linear equations is obtained, the numerical solution of which yields the concentration profile near a solid surface. From that concentration profile the (excess) adsorption isotherm is calculated next. Thus, although more accurate, this theoretical treatment does not lead to simple compact expressions which are so much preferred in practical interpretation of experimental data.

Rudziński and Everett [2] have suggested recently that the popular simple BET model could be improved substantially, without losing its basic value of simplicity. They argue that because the fractional coverage in the first layer is usually much higher than in the second and higher layers the most substantial improvement will come from considering the lateral interactions in the first layer.

While accepting MFA, the constant K has to be multiplied by $\exp(\omega_1\theta_{1t}/kT)$, where θ_{1t} represents the fractional coverage in the first layer, and $\omega_1 w$ is the product of the number of the nearest sites (coordination number) multiplied by the interaction energy of two neighbouring molecules in the same plane. (We accept here the Bakaev's model [4] of surface topography of oxide surfaces).

In such a case, taking the lateral interactions into account means, again, multiplying K by $\exp(\omega_1\theta_{1t}/kT)$, so the function ϵ_c defined in Eq. (18) now takes the more general form

$$\epsilon_c = -kT\ln(KP) - \omega_1\theta_{1t} \tag{22}$$

The derivatives (21a) and (21b) appearing in the expression for the heat of adsorption (20) take the form

$$\left(\frac{\partial\epsilon_c}{\partial\frac{1}{T}}\right)_p = \frac{kT^2\ln P + TQ_1 - T(P+1)Q_0}{1-\omega_1\chi(\epsilon_c)} \tag{23a}$$

$$\left(\frac{\partial\epsilon_c}{\partial\ln p}\right)_T = \frac{-kT(P+1)}{1-\omega_1\chi(\epsilon_c)} \tag{23b}$$

$$\chi(\epsilon_c) = \theta_t\frac{1+P-\theta_t}{c(1+P)^2} \tag{23c}$$

By inserting Eqs. (23) into Eq. (20), we obtain

$$Q_{st} = Q_0 - \frac{Q_1 + kT\ln P}{(P+1)\left(1+\frac{c}{kT}\cdot\frac{1-\omega_1\chi(\epsilon_c)}{1+P-\theta_t}P\right)} \tag{24}$$

The adsorption isotherm has the following form:

$$\theta_t = (1+P)\frac{\left[K^0P\exp\left\{\frac{\omega_1\theta_{1t}}{kT}\right\}\right]^{kT/c}}{1+\left[K^0P\exp\left\{\frac{\omega_1\theta_{1t}}{kT}\right\}\right]^{kT/c}} \tag{25a}$$

where

$$\theta_{1t} = \frac{\theta_t}{(1+P)} \tag{25b}$$

Accordingly, the linearized Eq. (19) now takes a somewhat more general form:

$$F(P) = \ln \frac{\frac{N_t}{M(1+P)}}{1 - \frac{N_t}{M(1+P)}} = \frac{kT}{c}\left[\ln P + \frac{\omega_1}{kT} \cdot \frac{N_t}{M(1+P)}\right] + \frac{kT}{c} \ln K^0 \tag{26}$$

Our present model of collective multilayer adsorption also predicts critical phenomena existing in the adsorbed phase. And, because the surface coverage in the first adsorbed layer is likely to be much higher than in the next layers, the phase transition of lattice gas to the dense ordered phase will occur initially in the first layer. The critical parameters are found by solving the system of equations

$$\frac{\partial \ln p}{\partial \theta_{1t}} = 0 \qquad \text{and} \qquad \frac{\partial^2 \ln p}{\partial (\theta_{1t})^2} = 0 \tag{27}$$

The critical surface coverage (for the heterogeneous surface model with interactions) $\theta_{1t} = \theta_{1t}^c$ which solves this equation system [72] is equal to 0.5, i.e. is the same as for a homogeneous solid surafce. Putting $\theta_{1t} = 0.5$ in Eq. (27) [72] leads to the interrelation

$$\omega_1 = \frac{c}{4} \tag{28}$$

which needs some additional comments. It was demonstrated first by Hill [81] that in the systems characterized by a symmetric adsorption energy distribution, critical phenomena exhibit some striking features. A further evidence for this was reported recently by Rudziński and Everett [2].

Equation (28) is to be understood as the condition for the critical point to exist in the systems with a broad symmetrical adsorption energy distribution, characterized by the function (2). When $\omega_1 < \frac{c}{4}$, the phase transition will never occur, even at very low temperatures. (This is contrary to what would happen on a homogeneous surface, characterized by the same value of ω_1). When, on the contrary, $\omega_1 > \frac{c}{4}$, one will always have a finite region of surface coverages with two coexisting phases. This means that some special features related to the existence of the critical point will never be observed. Perhaps the most striking of them is the so-called *logarithmic discontinuity* on the heat capacity curve considered as a function of temperature.

For a purely monolayer model, the exact Onsager [82] solution for the two-dimensional lattice problem, predicts the so-called *logarithmic discontinuity* on the heat capacity curve at the critical temperature T_c. The deviations of the actual adsorption systems from the ideal Onsager model mean that, instead of a logarithmic discontinuity, more or less rounded peaks are observed, centered at $T = T_c$. The surface energetic heterogeneity is believed to be the main source of that rounding.

There is a large body of experimental data showing these rounded peaks. As far as water adsorption is concerned, the data published by Plooster and Gitlin [83] 25 years ago seem still to be the most informative. They are of a particular importance for us because the silica used in their experiments was non-porous. (Additional calorimetric studies have been carried out on porous oxides [84,85]).

This, surprisingly, would mean that in the case of water adsorption on non-porous silica the relation between the surface heterogeneity and the interactions between adsorbed

molecules is roughly like that in Eq. (28). This seems to be a quite exciting discovery for the following reason.

By comparing almost 100 different silicas, Zhuravlev [86] has shown that the surface density of hydroxyl groups is a physicochemical constant for a fully hydroxylated surface (5.0 -OH per nm^2). As the parameter ω_1 is related mainly to this surface density, this means that the dispersion of water–surface interactions is also a constant value to a greater or smaller extent. Only in such a case peaks on the heat capacity curves of water adsorption on various silicas should be generally observed, as, in fact, the case is.

Equation (28) provides us with the value of the critical temperature T_c when these critical conditions are put into the isotherm equation. Then

$$\frac{\left[K^0P \exp\left\{\frac{\omega_1\theta_{1t}}{2kT_c}\right\}\right]^{kT_c/c}}{1+\left[K^0P \exp\left\{\frac{\omega_1\theta_{1t}}{2kT_c}\right\}\right]^{kT_c/c}} = \frac{1}{2} \tag{29}$$

or, in another form,

$$\exp\{\omega_1/2kT_c\} = \frac{1}{K^0P} \tag{30}$$

As the pressures increase, and consequently the adsorbed amount, T_c will also increase, and this is what has been observed in the experiment. Looking at the Plooster and Gitlin [83] data, one can see that according to our theoretical predictions, the critical temperature goes down as the adsorbed amount increases. A similar behaviour has been reported recently by Tsugita et al. [87] who studied water adsorption on a non-porous α-ferric oxide.

At sufficiently high total surface coverages, θ_t, the density in the higher layers may also reach critical values, and then a second phase transition in the surface phase may take place. This would be demonstrated by appearance of a second peak on the heat capacity curve, considered as a function of temperature. The appearance of such a peak can be seen in the data of Plooster and Gitlin [83] at the statistical surface coverages higher than four. Tsugita et al. [87] also reported a second transition in the adsorbed phase at the statistical surface coverages higher than three.

The Monte Carlo computer simulations by Kim and Landau [88] prove that also in the second and higher adsorbed layers the critical surface coverage is equal to one half. This means that in water adsorption on oxides, the density of the slab-like multilayer phase is below one half at a statistical coverage of three adsorbed layers.

2.5. Theoretical interpretation of the heat of immersion

Now we consider one of the most popular calorimetric experiments and its relation to those considered previously. This is the measurement of the heat of immersion of an outgassed sample into water. The knowledge of the mechanism of water adsorption from its vapour phase is also essential to understand what happens during the immersional process.

In addition to the primary formation of a hydroxyl layer, and the secondary physical adsorption of water, metal oxides also develop a region of electrical inhomogeneity when

the solid is placed into the liquid water. Here, there is an excess of positive or negative charge fixed at the solid surface, exactly balanced by a diffuse region of an equal but opposite charge. This is known as the electrical double layer formed at water/oxide interfaces. The surface charge is due to the additional adsorption/dissociation of H^+ or OH^-, which runs according to the following scheme:

$$MeOH^0 + H^+ \longleftrightarrow MeOH_2^+ \tag{31a}$$

$$MeOH^0 \ (+ \ OH^-) \longleftrightarrow MeO^- + H^+ \ (+ \ H_2O) \tag{31b}$$

The MeO^-, $MeOH^0$ and $MeOH_2^+$ above denote the surface structures

$$\begin{array}{ccccccc} O^- & & OH^0 & & OH_2^+ & & \\ | & & | & & | & & \\ -Me- & O & -Me- & O & -Me- & & \end{array}$$

which are assumed to be either negative (MeO^-), neutral ($MeOH^0$) or positively charged ($MeOH_2^+$) surface complexes. The concentration of MeO^- sites and of the hydroxylated ones, $MeOH^0$ and $MeOH_2^+$, depends obviously on the pH of the aqueous solution in contact with the oxide.

The above picture of water/oxide interface does not obviously show the simultaneous, primary and secondary adsorption on non-dissociated water molecules. In their review, Etzler and Drost-Hausen wrote [89] "Furthermore, as mentioned elsewhere in this paper (and other papers by the present author and associates), it is obvious that vicinal water is essentially unaffected by electrical double layers". Several properties of the vicinal water appear to be similar for various solid surfaces characterized by various point of zero charge (PZC) values (the "paradoxical effect"). It is therefore to be expected that the contribution to the changes of the heat of immersion with changing pH, produced by the secondarily adsorbed vicinal water, is negligible.

Thus we ascribe the changes in the heat of immersion caused by changing the pH of the contacting solution as due to the changing concentrations of the surface complexes $MeOH^0$ and $MeOH_2^+$ which form at the expense of the removed water molecules. (For the purpose of clarity we do not discuss here the co-adsorption of accompanying ions, which are introduced when pH of the solution is changed). Thus, investigating the variation in the heat of immersion with changing pH should be a source of important information about the mechanism of proton adsorption at the water/oxide interface.

At very high pH, (pH $\approx$ 14), only the "empty" sites MeO^-, i.e. surface oxygens atoms with a bonded water molecule, in practice will be present at an oxide /water interface. On decreasing pH, these sites will be covered gradually by either one or two protons. The process of immersion of an outgassed oxide sample into an aqueous solution at certain pH can be carried out in two steps. In the first step, the sample is immersed into a solution the pH of which is equal to infinity (in practice, close to 14). Then, in the second step, the pH of the basic solution contacted with the solid sample is brought to the value at which the direct immersional experiment was carried out.

Let Q_{im}^{in} denote the heat evolved in the first immersional step. This is an interesting quantity for the following reason. At very high pH values, the protonized complexes $MeOH^0$ and $MeOH_2^+$ will not actually be present. This means that only non-dissociating water

molecules will be attached to the surface oxygen atoms. Thus, Q_{im}^{in} is the heat of formation of a water/vapour interface. On decreasing the pH, one or two protons will remove the non-dissociated water molecules. Thus the heat evolved during the second immersion step, $Q_{im}^{el}(pH)$, is expressed as follows [20]:

$$Q_{im}^{el} = M \int_{\infty}^{pH7} \left[Q_0 \left(\frac{\partial \theta_0}{\partial pH} \right) + Q_+ \left(\frac{\partial \theta_+}{\partial pH} \right) \right] dpH \tag{32}$$

where Q_0 and Q_+ are the molar differential heats associated with the formation of the protonized complexes $MeOH^0$ and $MeOH_2^+$; θ_0 and θ_+ are their surface fractions (individual adsorption isotherms), and M is the total number of moles of the surface oxygen atoms on which the surface complexes can be formed. The lower integration limit $+\infty$ has here a symbolic meaning; in practical calculations one has to put 14 as the lower integration limit.

Thus the heat of immersion Q_{im}, considered as a function of the preadsorption pressure p, is to be expressed as follows [90]:

$$Q_{im} = Q_{im}^{in} + Q_{im}^{el} + \int_{p/p_0}^{1} Q_{st}\, dp \tag{33}$$

where Q_{im}^{in} is the heat accompanying the formation of the water/vapour slab interface. Assumnig that its area is equal to the area of the investigated solid sample S, we have

$$Q_{im}^{in} = S \left(\gamma^g - T \frac{\partial \gamma^g}{\partial T} \right) \tag{34}$$

γ^g being the surface tension of the water/vapour interface.

We do not question the validity of this procedure but argue that one should also calculate the correction arising from the term Q_{im}^{el}. This means that Q_{im}^{in} cannot be identified with $Q_{im}(p/p_0 = 1)$ as it is commonly done.

For that purpose one has to measure the heats of immersion into solutions of varying pH and next to analyse these data using the equations developed in our earlier publications [20,91]. Unfortunately such additional experiments were not carried out in the case of the quartz sample investigated by Trolard et al. [77]. However, as the calorimetric Harkins-Jura method is very fast and elegant, calculating the term Q_{im}^{el} deserves further extensive study. It might be hoped that a simple theoretical evaluation of this term might be possible. The linear dependence of the molar heat of immersion of oxides upon their PZC value [92,93] suggests that some physical rules might exist which would be useful in calculating Q_{im}^{el} entirely theoretically.

Equations (33) and (34) form the theoretical basis for the "absolute" Harkins-Jura (HJ) method [76,94] to estimate the solid surface area. However, in the earlier calorimetric experiments applying the Harkins-Jura principle, the term Q_{im}^{in} was always neglected. Neglecting it may lead to certain discrepancies between the surface areas determined by the Harkins-Jura and BET methods in the case of water adsorbed on oxides.

This, in fact, has been observed for a long time, but so far ascribed to various porosity and capillary phenomena. Although it may be true in some cases, visible discrepancies

between HJ and BET surface areas were also observed in the case of non-porous oxide samples. This can be seen in Table 2 in the work by Partyka et al. [76].

Now let us consider the reverse problem of calculating Q_{st} from $Q_{im}(p/p_0)$ data, reported usually as the heat of immersion per weight of a solid sample. Then

$$Q_{st} = -\frac{\partial Q_{im}/\partial \frac{p}{p_0}}{\partial N_t/\partial \frac{p}{p_0}} \tag{35}$$

From the above relation, it follows that whenever

$$\lim_{p/p_0 \to 1} \frac{\partial Q_{im}}{\partial \frac{p}{p_0}} = 0 \qquad \text{for} \qquad k' < 1 \tag{36}$$

the following condition must hold

$$\lim_{p/p_0 \to 1} Q_{st} = 0 \tag{37}$$

because for $k' < 1$, the derivative $\partial N_t/\partial \frac{p}{p_0}$ has finite values in the limit $p/p_0 \to 1$.

This is the case for water adsorbed on the silica (ground quartz). The corresponding experimental heats of immersion curve were reported by Partyka et al. [76,77] and are redrawn here by us in Fig. 7(A). Also in this figure the heat of immersion of kaolinite in water is shown for comparison, redrawn from the work of Fripiat et al. [95]. Figure 7(B) shows the comparison of the isosteric heats of adsorption Q_{st} calculated from these immersion curves according to Eq. (35). Note that also in the case of water adsorption on kaolinite, Q_{st} does not reach the value of the heat of liquefaction, equal to 40.7 kJ mol^{-1}.

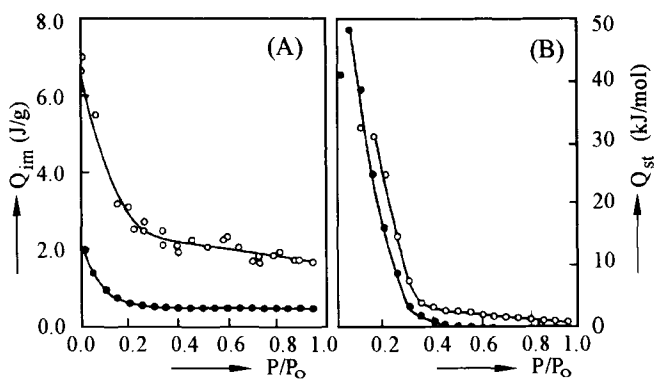

Figure 7. (A) The experimental heats of immersion $Q_{im}(p/p_0)$ into water for silica at 31^{0}C (●) and for kaolinite at 30^{0}C (○). The solid lines represent a numerical "smoothing" of the experimental points. (B) The isosteric heats of adsorption $Q_{st}(p/p_0)$ of water onto silica (●) and onto kaolinite (○) calculated from the smoothed heats of immersion.

This fact should be emphasized in view of the frequently expressed opinion that in the limit $p/p_0 \to 1$ the isosteric heat of adsorption should tend to the heat of liquefaction. We have already pointed out theretically, that this will never be true if $k' < 1$ and this seems

to be a typical situation in the case of water adsorption. Consider, for instance, the case of water adsorption on the hydrophobic surface of molybdenium disulfide investigated calorimetrically by Ballou and Ross [96], or water adsorption on Graphon, studied experimentally by Zettlemoyer et al. [97]. In both these cases, Q_{st} tends to $25 - 30$ kJ mol^{-1} when $p/p_0 \rightarrow 1$.

2.6. Comparison with experiment

In attempts to carry out a thermodynamic analysis of water adsorption onto oxides, one faces the following situations.

(1) The most frequently carried out measurements are those of adsorption isotherm but they are rarely accompanied by direct measurements of accompanying calorimetric effects.

(2) Heats of immersion are very often measured as a function of the heat–pretreatment temperature of the oxide sample. However, among the reported data, there are only a few cases where the loss of water (adsorption isotherm) was simultaneously monitored as a function of this heat–pretreatment temperature.

(3) Also, heats of immersion are frequently measured as a function of the preadsorption pressure. At the same time, these popular experiments are rarely accompanied by the measurements of adsorption isotherm.

(4) Recently, the measurements of the heat capacity of the adsorbed water have become very popular, but again, as a rule, they are rarely accompanied by adsorption isotherm measurements.

Thus, in spite of the large body of calorimetric data which have already been published, a quantitative thermodynamic analysis of water adsorption onto oxide surfaces is difficult. Among the cases where both adsorption isotherms and the accompanying heats of adsorption were monitored, the data on water adsorption on quartz published by Partyka et al. [76,77] are probably the most accurate. Therefore we have used these data in our quantitative thermodynamic analysis. The details of the experiment have been described [76,77] and an attempt at their thermodynamic analysis presented, but based on a less realistic model of a homogeneous silica surface. These theoretical efforts were stimulated by the well-known difficulty of describing the region of surface coverages within which the transition takes place between monolayer and multilayer characters of adsorption.

The shortcomings of the BET model in describing the adsorption in the multilayer region are well known. It is also known that for high multilayer coverages the FHH (Frankel-Hasley-Hill) slab theory [2] offers a more realistic approach. Thus, as the first theoretical exploration here, we tried to draw our experimantal adsorption isotherms in $\ln N_t$ vs $-\ln[\ln(p_0/p)]$ coordinates. According to the FHH approach, this should produce a straight line, provided that the adsorption phase is thick enough to behave like a "slab".

Figure 8 shows that the last ten points of our experimental isotherm, corresponding to the pressure range $\frac{p}{p_0} \geq 0.5$ yield a fairly linear plot, the tangent of which is equal to 0.323 (computer linear regression for the last ten points). This means that the fractal dimension D of our silica sample is about 2, i.e. we may safely neglect the fractal phenomena in water adsorption on that silica sample. This greatly simplifies our theoretical analysis, but it should be emphasized that adsorption on more porous surfaces $2 < D \leq 3$, can also be analyzed in terms of a suitably modified BET model [98-100].

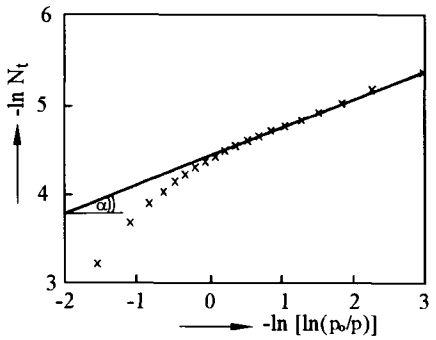

Figure 8. The linear regression of the last ten points of the experimental isotherm according to FHH (slab) theory.

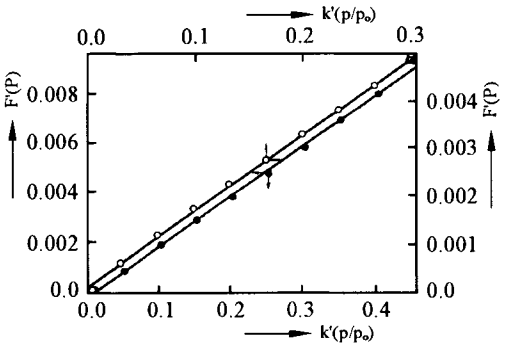

Figure 9. Comparison between the traditional BET linear regression of the first ten points when assuming k' = 1 (●) and the BET linear regression assuming k' as an additional best-fit parameter (○). The values of the parameters are collected in Table 1 in the first and second rows for the homogeneous surface model.

Table 1
The set of parameters collected from the linear regressions for the homogeneous surface model and from the linear regression and best fit for the molar differential heats of adsorption for heterogeneous surface model, taking into account the interactions between molecules

k'	M (μmol · g^{-1})	C	K^0	$\frac{\omega_1}{kT}$	$\frac{kT}{c}$	Q_0 (kJ · mol^{-1})	Q_1 (kJ · mol^{-1})
Homogeneous surface model							
1.00	50.0	111.6	—	—	—	—	—
0.68	62.5	46.5	—	—	—	—	—
Heterogeneous surface model							
0.68	73.0	—	31.2	0.60	0.51	0.5	-55.0

As the values of $\ln N_t$ for the first ten points of our experimental isotherm deviate clearly from the FHH plot, this suggests that they should rather be analyzed in terms of the BET model. Thus, Fig. 9 shows the traditional BET linear regression (Eq. (9a)) made by assuming k' = 1, and next adjusting that parameter to get the best possible regression for the first ten points. These linear regressions are shown in Fig. 9 and the corresponding best-fit parameters are collected in Table 1. Having estimated the BET parameters in such a way, we compared the two versions of the theoretical BET isotherm, corresponding to k' = 1 and k' $\neq$ 1, with the experimental data over the whole coverage region. This comparison is shown in Figs 10(A) and 10(B) and proves the necessity of introducing the variable parameter k' < 1, even in the case of the ordinary BET isotherm.

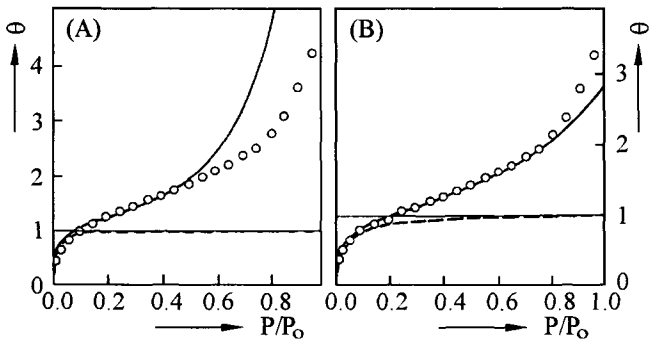

Figure 10. (A) Comparison between the experimental isotherm (o) and the theoretical curve calculated from the BET equation with k′ = 1, using the values of the parameters collected in the first row of Table 1, corresponding to the homogeneous surface model. (B) Comparison between the experimental isotherm (o) and the theoretical curve, assuming k′ as an additional best-fit parameter for linear regression. The corresponding values of the parameters are collected in Table 1 in the second row for the homogeneous surface model. The dotted lines are the isotherms of adsorption in the first layer, closest to the surface.

In the next step we proved to which extent our silica surface may be considered a homogeneous one. To that end we performed the computer linear regression, as indicated in Eq. (26), for the first ten experimental points. The result is shown in Fig. 11 and the corresponding best-fit parameters are collected in Table 1. Introducing the concept of ad-molecule interactions, i.e. multiplying K^0 by $\exp(\omega_1\theta_{1t}/c)$ and introducing the additional best-fit parameter ω_1, leads to a ceratin improvement in that linear regression. Therefore, we assumed $\omega_1 \neq 0$ in our further analysis.

The tangent of the theoretical line in Fig. 11 is equal to 0.51, indicating that our

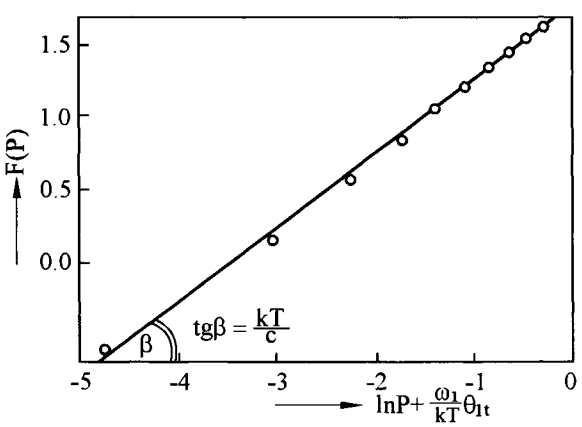

Figure 11. The linear regression of the first ten points in term of the heterogeneous surface model, taking into account the interactions between adsorbed molecules (Eq. (26)). The best fit prameters used in this calculation are collected in Table 1 for this model.

oxide surface is one of those most heterogeneous ever found in nature [2]. Therefore, our further theoretical analysis was carried out solely in terms of the generalized BET model, as applied to a heterogeneous solid surface. What is really exciting is the fact that the best-fit value of ω_1/c found in this linear regression, i.e. 0.3, is close to $\frac{1}{4}$, as required by Eq. (28) for the peaks on the heat capacity curves to exist. (Such distinct peaks are characteristic for physical regimes close to the critical point [2].)

In Fig. 12(A) the theoretical isotherm corresponding to the model of a heterogeneous oxide surface, calculated by assuming the parameters collected in Table 1, is compared with the experimental isotherm over the whole pressure region $0 < \frac{P}{P_0} \leq 0.95$. Let us compare this picture with that in Fig. 10(B).

The most interesting, of course, is the comparison of the theoretically calculated isotherms θ_1 and θ_{1t}. Accepting the more realistic model of an energetically heterogeneous oxide surface and interacting adsorbed molecules leads us to the conclusion that the true contribution to adsorption from the second and higher layers is, in fact, larger than that predicted by the ordinary BET model.

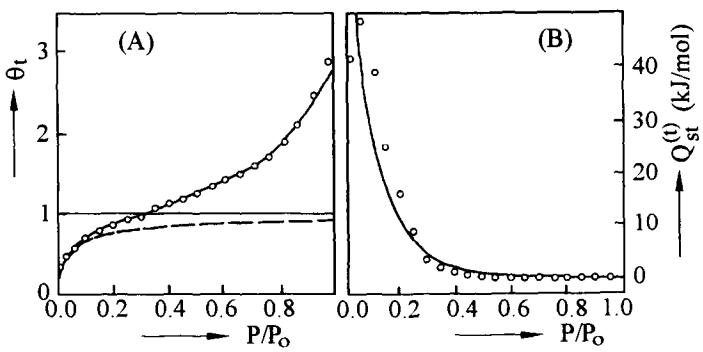

Figure 12. (A) Comparison between the experimental isotherm (o) and the theoretical curve corresponding to the heterogeneous surface model, taking into account the interactions between adsorbed molecules. The values of the parameters are collected in Table 1, in the row corresponding to the heterogeneous surface model. The dotted line is the isotherm of adsorption in the first layer, closest to the surface. (B) Comparison between the experimental molar differential heat of adsorption (o) and the theoretical one (—) for the parameters collected in Table 1 in the row corresponding to the heterogeneous surface model, taking into account the interactions between adsorbed molecules.

While considering the fit of the experimental heats of adsorption, one has two new best-fit parameters Q_0 and Q_1. The other parameters M, k', $\frac{kT}{c}$ and $\frac{\omega_1}{kT}$ are already known from the linear regression of the experimental adsorption isotherm according to Eq. (26) (see Fig. 11). In the determination of Q_1 and Q_0 by fitting the experimental heats of adsorption, one must remember that only the first ten points corresponding to $\frac{P}{P_0} < 0.5$ can be taken into consideration (the range of validity of the BET model). Therefore we decided to fit the heat of adsorption curve Q_{st} over the whole pressure range using the following concept.

Let dN_{mon} and dN_{pol} denote the increase in the number of the moles adsorbed in the first and higher layers respectively, when pressure is increased by dP. Further, let

Q_{mon} and Q_{pol} denote the molar differential heats of adsorption of the molecules adsorbed respectively in the first and higher layers. The experimentally observed molar differential heats of adsorption $Q_{st}^{(t)}$ will thus be given by the formula

$$Q_{st}^{(t)}(P) = \frac{\frac{\partial N_{mon}}{\partial P} Q_{mon} + \frac{\partial N_{pol}}{\partial P} Q_{pol}}{\frac{\partial N_t}{\partial P}} \tag{38}$$

As a good approximation for $\partial N_{mon}/\partial P$ we can take the derivative $M(\partial\theta_{1t}/\partial P)$ of θ_{1t} shown in Fig. 12(B). Further, as Q_{st} has significant values only in the region $\frac{p}{p_0} \leq 0.5$, we took $Q_{mon} = Q_{st}$ as the next good approximation (Eq. (24) for Q_{st}). From Fig. 12(A), one can see that for high $\frac{p}{p_0}$ values, the derivative $\partial N_{mon}/\partial P$ has small values compared with $\partial N_{pol}/\partial P$. This means that the condition for Q_{st} to be zero for high $\frac{p}{p_0}$ values is that Q_{pol} must be zero. In this way, we reduced a number of best-fit parameters to two: Q_0 and Q_1. Further, from Eq. (11b) it follows that Q_0 is related mainly to multilayer formation, i.e. it should not be much different from Q_{pol}. This was confirmed by our best-fit exercises showing that the best fit to the experimental curve $Q_{st}(p/p_0)$ is obtained by taking small values of Q_0 (see Table 1). Figure 12(B) shows the result of fitting the experimental heat of adsorption curve by Eq. (38). As the heat of liquefaction of bulk water is about 40.7 kJ mol^{-1}, the non-existing enthalpic effect accompanying the vapour phase–surface slab transition must suggest that the state of the water molecules in the slab formed on our silica is, in fact, not much different from that in the equilibrium bulk phase.

Concluding, the relations were developed by adopting a realistic model of adsorption, taking into account the surface energetic heterogeneity, the interactions between adsorbed molecules, and effects of polymolecular adsorption. The obtained expressions were next used in a quantitative analysis of calorimetric effects accompanying the adsorption of water on oxide surfaces. This analysis showed that properly designed calorimetric experiments, and their subsequent theoretical analysis, might be one of the most powerful tools to study the nature of water/oxide interface and other adsorption systems.

3. WATER (ELECTROLYTE)/OXIDE INTERFACE

It is generally known that metal oxide surface is covered with hydroxyl groups when oxide is placed in water. The presence of two free electron pairs of oxygen atom and possibility of hydrogen ion dissociation is the evidence of amphoteric character of these groups. On account of this, the most useful parameter in description of the water/metal oxide interface is pH of the solution being in contact with the surface. Adsorption of H^+ or OH^- ions causes protonization or deprotonization of the surface according to the Eqs. (31a) and (31b).

To describe in detail such a specific system as the metal oxide/solution interface, it is necessary to prepare a model describing dependences between potential and surface charge and draw up reactions, the occurrence of which leads to the changes of surface charge δ_0. The reaction equations describing an equilibrium state between the surface and solution as well as values of equilibrium constants of these reactions provide detailed information

about stoichiometry of the reaction enabling theoretical calculations of surface charge and individual adsorption isotherms of each surface complex.

Two parameters were introduced into the description of double electrical layer. One of them is the point of zero charge (PZC) which according to IUPAC definition [101] can be expressed as concentration of potential–determining ions PDI at which the surface charge is equal to zero ($\delta_0 = 0$), as well as the surface potential ($\psi_0 = 0$). Another parameter is isoelectric point (IEP) defined [101] as concentration of PDI at which the electrokinetic potential is equal to zero ($\zeta = 0$).

The models describing hydrolysis and adsorption on oxide surfaces are called surface complexation models in literature. They differ in the assumptions concerning the structure of the double electrical layer, i.e. in the definition of planes situation, where adsorbed ions are located and equations asociating the surface potential with surface charge ($\psi = f(\delta)$). The most important models are presented in the papers by Westall and Hohl [102]. The most commonly used is the triple layer model proposed by Davis et al. [103-105] from conceptualization of the electrical double layer discussed by Yates et al. [106] and by Chan et al. [107]. Reviews and representative applications of this model have been given by Davis and Leckie [108] and by Morel et al. [109]. We will base our consideration on this model.

3.1. Triple layer complexation model

The schematic picture of the triple layer model is shown in Fig. 13. According to the

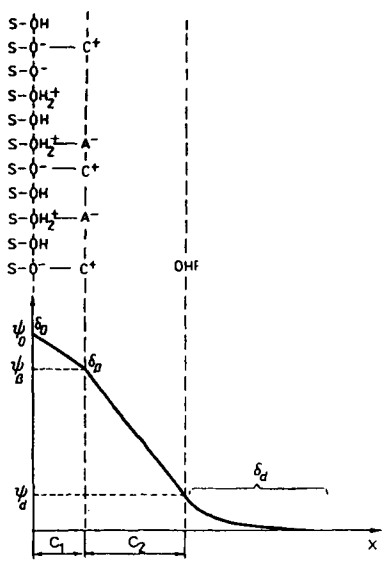

Figure 13. Scheme of the triple layer formed at metal oxide/electrolyte interface.

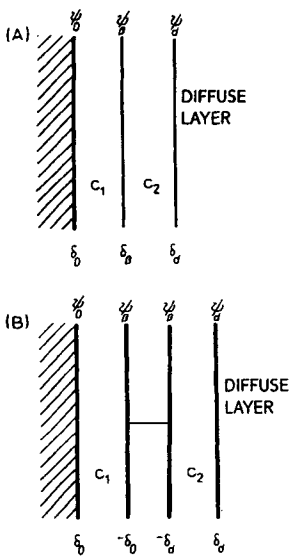

Figure 14. (A) Diagram of the charge distribution in the triple layer model. (B) Flat capacitors connected in series as equivalent of a triple layer model at the aqueous solution/metal oxide interface. Charge distribution on capacitor plates is obtained from the electroneutrality condition written in the form: $\delta_\beta = (-\delta_0) + (-\delta_d)$.

mass action law, the equations and intrinsic equilibrum constants for the reactions taking place on the surface are the following ones:

$$SOH_2^+ \overset{K_{a1}^{int}}{\longleftrightarrow} SOH^0 + H^+$$

$$K_{a1}^{int} = \frac{[H_{ads}^+][SOH^0]}{[SOH_2^+]} = \frac{(a_H)[SOH^0]}{[SOH_2^+]} \cdot \exp\left\{-\frac{e\psi_0}{kT}\right\} \tag{39a}$$

$$SOH^0 \overset{K_{a2}^{int}}{\longleftrightarrow} SO^- + H^+$$

$$K_{a2}^{int} = \frac{[H_{ads}^+][SO^-]}{[SOH^0]} = \frac{(a_H)[SO^-]}{[SOH^0]} \cdot \exp\left\{-\frac{e\psi_0}{kT}\right\} \tag{39b}$$

where S is the surface metal atom, $[SOH^0]$ and $[SOH_2^+]$ are the concentrations of the surface complexes of singly and doubly protonated surface oxygens respectively, $[SO^-]$ is the surface concentration of the free sites (unoccupied surface oxygens) and $[H_{ads}^+]$ is the concentration of protons at the surface. According to the Boltzman's statistics, probability of finding an ion at the surface is proportional to $\exp\{-\frac{e\psi}{kT}\}$, so, in the case of H^+ ions which are located in the layer of the potential ψ_0, $[H_{ads}^+] = (a_H)\exp\{-\frac{e\psi_0}{kT}\}$, where a_H is the activity of protons in the equilibrium bulk solution.

While changing pH of the solution being in contact with oxide surface by bringing in acid or base, acid radical ions (most frequently oxygen-free or monovalent) or alkaline metal ions are being introduced. As a result, besides potential determining ions H^+ responsible for pH of the solution, there are cations C^+ and anions A^- (e.g. K^+, Na^+, Cl^-, Br^-, NO_3^-, e.t.c.) which according to this theory are found not only in the counterion (diffuse) layer but also in the compact one. To avoid complications caused by the increase of the concentration of anions A^- or cations C^+ while adding acid or base (when pH is changed), the electrolyte solution being in contact with the oxide surface already at the beginning of the experiment contains added salt CA as a basic electrolyte so that C^+ or A^- addition accompanying pH change will not change much the concentration of C^+ and A^-. Thus, it can be assumed that activities (concentrations) of cations a_C and of anions a_A are constant throughout the experiment, and equal to $a_C = a_A = a$.

So, besides the surface reactions (39a) and (39b) there are also reactions leading to formation of the surface complexes SO^-C^+ and $SOH_2^+A^-$, which have the character of ion pairing. The two other equilibrium constants of these reactions are fundamental ones in the description of the adsorption of cations and anions of the basic electrolyte:

$$SOH^0 + C^+ \overset{{}^*K_C^{int}}{\longleftrightarrow} SO^-C^+ + H^+$$

$${}^*K_C^{int} \exp\left\{\frac{e(\psi_0 - \psi_\beta)}{kT}\right\} = \frac{[SO^-C^+](a_H)}{[SOH^0](a_C)} \tag{40a}$$

$$SOH_2^+A^- \overset{{}^*K_A^{int}}{\longleftrightarrow} SOH^0 + H^+ + A^-$$

$${}^*K_A^{int} \exp\left\{\frac{e(\psi_0 - \psi_\beta)}{kT}\right\} = \frac{[SOH^0](a_H)(a_A)}{[SOH_2^+A^-]} \tag{40b}$$

where $[SOC^+]$ and $[SOH_2^+A^-]$ are the concentrations of the surface complexes of adsorbed cations or anions. It follows from Fig. 13 that the adsorbed cations and anions are placed in the the β layer in which the potential has the value ψ_β.

Besides the above mentioned surface complexes there can also be formed $SOHC^+$, $SOHA^-$ as well as SOHCA [110] complexes, but their concentrations on the surface are so small that their presence is usually neglected.

According to Fig. 13, the surface charge density, δ_0, must be proportional to the sum of the concentrations of the following surface complexes:

$$\delta_0 = \frac{eN_A}{N_x}\left([SOH_2^+] + [SOH_2^+A^-] - [SO^-] - [SO^-C^+]\right) \tag{41}$$

and the charge coming from the specifically adsorbed ions of the basic electrolyte in the β plane, δ_β, is given by

$$\delta_\beta = \frac{eN_A}{N_x}\left([SO^-C^+] - [SOH_2^+A^-]\right) \tag{42}$$

where e is the elementary charge, N_A is the Avogadro number and N_x is the factor combining the surface with the solution volume in [m^2 of surface/dm^3 of solution].

Eqs. (41) and (42) neglect shares of free ions H^+ in the plane of charge δ_0 as well as of ions C^+ and A^- in the plane β. Eqs. (39) and (40) point to the presence of such ions at the surface in the compact area of the electric double layer. Appropriate calculations show, that the charge coming from the free ions is so small compared with that coming from the localized charges, that it can be neglected.

The triple layer model can also be presented by using the capacitors scheme shown in Fig. 14. As within the compact layer, there must be fulfilled the electroneutrality condition:

$$\delta_0 + \delta_\beta + \delta_d = 0 \tag{43}$$

The value of the diffuse layer charge can be obtained from Eqs. (41-42):

$$\delta_d = \frac{eN_A}{N_x}\left([SO^-] - [SOH_2^+]\right) \tag{44}$$

A total number of the sites capable of forming the surface complexes on the surface N_s (here surface density in [sites/m^2]) from the mass conservation law, is equal to:

$$N_s = \frac{N_A}{N_x}\left([SO^-] + [SOH^0] + [SOH_2^+] + [SOH_2^+A^-] + [SO^-C^+]\right) \tag{45}$$

In Fig. 14 the quantities c_1 and c_2 are the electrical capacitances for capacitors connected in series, assuming that the capacitances are constant in the regions between planes. As it can be deduced from that figure, there are the following relations between the charge and potential differences in the compact layer area

$$\psi_0 - \psi_\beta = \frac{\delta_0}{c_1} \tag{46}$$

and

$$\psi_\beta - \psi_d = \frac{-\delta_d}{c_2} \tag{47}$$

For further purposes we shall consider the following equivalent description of the reactions leading to the formation of free sites $[SO^-]$:

$$SOH^0 \longleftrightarrow SO^- + H^+ \tag{48a}$$

$$SOH_2^+ \longleftrightarrow SO^- + 2H^+ \tag{48b}$$

$$SO^-C^+ \longleftrightarrow SO^- + C^+ \tag{48c}$$

$$SOH_2^+A^- \longleftrightarrow SO^- + 2H^+ + A^- \tag{48d}$$

Introducing surface coverages θ_i's by the individual surface complexes ($i = 0, +, C, A$) and free sites ($i = -$):

$$\tilde{N}_s = [SOH^0] + [SOH_2^+] + [SOH_2^+A^-] + [SO^-C^+] + [SO^-]$$

$$[SOH_2^+]/\tilde{N}_s = \theta_+ \qquad [SOH^0]/\tilde{N}_s = \theta_0 \qquad [SO^-C^+]/\tilde{N}_s = \theta_C \tag{49}$$

we obtain the following set of equations corresponding to reactions (48):

$$K_{a2}^{int}\exp\left\{\frac{e\psi_0}{kT}\right\} = \frac{(a_H)\theta_-}{\theta_0} \tag{50a}$$

$$K_{a1}^{int} \cdot K_{a2}^{int}\exp\left\{\frac{2e\psi_0}{kT}\right\} = \frac{(a_H)^2\theta_-}{\theta_+} \tag{50b}$$

$$K_{a2}^{int}/{}^*K_C^{int}\exp\left\{\frac{e\psi_\beta}{kT}\right\} = \frac{(a_C)\theta_-}{\theta_C} \tag{50c}$$

$$K_{a2}^{int} \cdot {}^*K_A^{int}\exp\left\{\frac{e(2\psi_0 - \psi_\beta)}{kT}\right\} = \frac{(a_H)^2(a_A)\theta_-}{\theta_A} \tag{50d}$$

According to Eq. (41) the surface charge density, δ_0, can be expressed as follows:

$$\delta_0 = B[\theta_+ + \theta_A - \theta_- - \theta_C] \qquad \text{where} \qquad B = N_s \cdot e \tag{51}$$

and N_s in Eq. (51) is the density of surface sites, [sites/m^2].

A set of nonlinear equations (50) can be numerically solved to calculate next the individual isotherms of adsorption of ions θ_i's ($i = 0, +, A, C$). For that purpose the set of equations (13) is transformed to the form:

$$\theta_i = \frac{K_i f_i}{1 + \sum_i K_i f_i}, \qquad i = 0, +, A, C \tag{52}$$

where

$$K_0 = \frac{1}{K_{a2}^{int}} \qquad K_+ = \frac{1}{K_{a1}^{int} \cdot K_{a2}^{int}} \qquad K_C = \frac{{}^*K_C^{int}}{K_{a2}^{int}} \qquad K_A = \frac{1}{K_{a2}^{int} \cdot {}^*K_A^{int}} \tag{53}$$

As follows from Eq. (46), f_i's, $(i = 0, +, A, C)$, are the following functions of activity of protons and salt ions:

$$f_0 = \exp\left\{-\frac{e\psi_0}{kT} - 2.3pH\right\}, \qquad f_+ = f_0^2 \tag{54ab}$$

$$f_C = a_C \exp\left\{-\frac{e\psi_0}{kT} + \frac{e\delta_0}{kTc_1}\right\} \tag{54c}$$

$$f_A = a_A \exp\left\{-\frac{e\psi_0}{kT} - \frac{e\delta_0}{kTc_1} - 4.6pH\right\} \tag{54d}$$

Then, from the nonlinear set of Eqs. (52) and Eq. (51), the following equation is obtained:

$$\delta_0 = B\,\frac{K_+f_+ + K_Af_A - K_Cf_C - 1}{1 + \sum_i K_if_i}, \qquad i = 0, +, A, C \tag{55}$$

the solution of which allows to calculate δ_0 for each value of pH. Equation (55) which is nonlinear with respect to δ_0 can be easily solved by an iteration method. Having calculated δ_0 values, one can calculate the individual isotherms of ions from Eq. (52).

The triple layer model assumes two values of the parameter c_1 to exist, depending on the sign of the charge of the surface [111]:

$$c_1 = c_{1(1)} \quad \text{for} \quad pH < PZC \qquad \text{and} \qquad c_1 = c_{1(2)} \quad \text{for} \quad pH > PZC \tag{56}$$

The parameter c_1 is connected with the distance between the surface layer "0" and the layer "β" where cations and anions of basic electrolyte are located. For pH < PZC, i.e. in the acidic medium, there is much more of $SOH_2^+A^-$ complexes formed by anion adsorption, but when pH > PZC, SO^-C^+ complex is strongly predominant. Two different values of parameter c_1 suggest that the adsorbed anion and adsorbed cation are situated at different distances from the surface.

Except for a few rare cases, the experimental titration curves corresponding to different concentrations of basic electrolyte have a common intersection point (CIP) in PZC. That intriguing feature made us study consequences of treating it in a fully rigorous way. For the triple layer model, that way has been outlined in the works by Rudziński et al. [21,91]. A point of zero charge is determined by the condition $\delta_0(pH = PZC) = 0$. Taking equations (52-54) into account, for pH=PZC, Eq. (52) can be transformed as follows:

$$U = \frac{H^2}{K_{a1}^{int}K_{a2}^{int}} + \frac{H^2a_A}{K_{a2}^{int}{}^*K_A^{int}} - \frac{{}^*K_C^{int}a_C}{K_{a2}^{int}} - 1 = 0 \tag{57}$$

where

$$H = 10^{-PZC} \tag{58}$$

Then, Eq. (57) can be rewritten to another form

$$PZC = -\frac{1}{2}(\log K_{a1}^{int} + \log K_{a2}^{int}) - \frac{1}{2}\log\frac{1 + ({}^*K_C^{int}/K_{a2}^{int})a_C}{1 + (K_{a1}^{int}/{}^*K_A^{int})a_A} \tag{59}$$

The knowledge of PZC experimental value makes it possible to eliminate one of the four parameters of surface reaction equilibrium constants, even for those few reported cases where CIP was not observed in the system [112]. However, the reported experimental studies show that in most systems the PZC value does not practically depend on salt concentration in the bulk solution, (i.e. a common intersection point (CIP) occurs at pH = PZC) [104,112,113]. Except for the region of very low salt concentrations, one can assume that $a_C = a_A = a$. Thus, the independence of PZC of salt concentration can be formally expressed as:

$$\frac{\partial PZC}{\partial a} = -\frac{\partial U/\partial a}{\partial U/\partial PZC} = 0 \tag{60}$$

So, knowing that $\partial U/\partial PZC \neq 0$, we have

$$\frac{\partial U}{\partial a} = \frac{H^2}{K_{a2}^{int} {}^*K_A^{int}} - \frac{{}^*K_C^{int}}{K_{a2}^{int}} = 0 \tag{61}$$

After solving the set of Eqs. (57) and (61), the following relations are obtained:

$${}^*K_A^{int} = \frac{H^2}{{}^*K_C^{int}} \qquad \text{and} \qquad K_{a1}^{int} = \frac{H^2}{K_{a2}^{int}} \tag{62}$$

Equations (62) relating the parameters K_{a1}^{int} and K_{a2}^{int}, and ${}^*K_C^{int}$ and ${}^*K_A^{int}$ reduce the number of the unknown equilibrium constants determined from fitting suitable experimental data from four to two.
From relations (62), the following expression for PZC value is obtained:

$$PZC = \frac{1}{2}(pK_{a1}^{int} + pK_{a2}^{int}) \qquad \text{and} \qquad PZC = \frac{1}{2}(p^*K_C^{int} + p^*K_A^{int}) \tag{63}$$

where $pK_{ai}^{int} = -\log K_{ai}^{int}$, $i = 1, 2$ and $p^*K_i^{int} = -\log^* K_i^{int}$, $i = C, A$.

3.2. Determination of the surface potential ψ_0

Bousse, De Rooij and Bergveld [115-121] elaborated a method of an experimental determination for the surface potential ψ_0 of metal oxide surfaces using in their experiments the so called chemically sensitive electronic device CSED operating on the field-effect principle. The change of the semi-conductor surface potential is modulated by potential changes somewhere inside the structure, usually at the insulator (e.g. metal oxide)/electrolyte interface. The measurements of pH which can be made by employing insulators made of commonly used semi-conductors such as SiO_2, Si_3N_4 or Al_2O_3 are of a great interest in technology. The whole class of devices was called ion-sensitive (or unipolar) field-effect transistors ISFET's. They were described by Bergveld [121] and are the most frequently used devices in this field.

The theoretical model for determining the surface potential ψ_0 elaborated by Bousse et al. was found to be in a good agreement with experiment [117,118]. It was stated that the PZC value and the difference between pK_{a2}^{int} and pK_{a1}^{int} determined from ψ_0(pH) measurements were in good agreement with the results of surface charge measurements for colloidal suspensions. Another important finding was that the surface potential ψ_0 is much less sensitive to surface complexation with counter-ions than the surface charge δ_0 [120].

The theoretical approach to this problem was first limited to the application of the Nernst equation which predicts potential charge equal to 2.3 $\frac{kT}{e}$ Volts for a pH unit. This equation is satisfied by a glass electrode as the most popular device for pH measurements in electrochemistry. In turn, in the case of ISFET's device, the potential change value was much below the Nernst value. Therefore, the Nernst equation cannot be applied for the insulator such as a metal oxide which is neither an electric nor ionic conductor [118].

The paper by Van den Vlekkert et al. [120] presented the measurements of temperature dependence of the surface potential ψ_0 at the γ–Al_2O_3 electrolyte interface. According to these authors, such investigations are of a double significance. Firstly, because this device can be used as miniature sensors of pH measurements, e.g. in the clinical measurement of blood acidity. Secondly, the function $\frac{d\psi_0}{dT}$ has some relations to the thermal effects accompanying adsorption of one proton or two protons on the oxide surface. Knowing these values, one can determine indirectly the values of these heats. The heat values obtained in this way can be compared with those determined from suitable analysis of calorimetric experimental data.

The surface potential defined in the equations for the equilibrium constants (39) can be theoretically calculated as ψ_0(pH) from the equation developed by Bousse et al. [118,119]:

$$2.303(PZC - pH) = \frac{e\psi_0}{kT} + \sinh^{-1}\left(\frac{e\psi_0}{\beta kT}\right) \tag{64}$$

where the nondimensional quantity β has the form [120]

$$\beta = \frac{2e^2 N_s}{c_t kT}\left(\frac{K_{a2}^{int}}{K_{a1}^{int}}\right)^{1/2} \tag{65}$$

In Eq. (65) c_t is the linear capacitance of the double electrical layer and can be assumed equal to 0.2 F/m^2 [120]. The quantity β becomes dependent only on the kind of the oxide under investigation.

In the vicinity of PZC, Eq. (64) reduces to the following linear one:

$$\psi_0 = \frac{\beta}{\beta + 1}\frac{2.3kT}{e}(PZC - pH) \tag{66}$$

This approximation is valid around PZC for $|\ \frac{e\psi_0}{kT}\ | < \beta$. Looking at Eq. (66) one can deduce that for relatively large values β, $\frac{\beta}{\beta+1} \cong 1$ and the potential change corresponding to one pH unit becomes equal to that predicted by the Nernst equation. According to Van den Vlekkert [120], for the oxide γ - Al_2O_3 having PZC=8, β = 5. For such an oxide, Eq. (66) is satisfied within the range of pH=6 to pH=10, with some more serious deviations outside this range. The comparisons between the functions ψ_0(pH) calculated by accepting its simplified form Eq. (66), and its rigorous form given by Eqn (64) was shown by Rudziński et al. [91].

3.3. Equations describing ζ–potential effects

The next experimental source of information which is also going to be explored are the electrokinetic effects accompanying the formation of the elecric double layer. The ζ–potential measurements are carried out very frequently and their theoretical interpretation is apparently simple, but often leads to a poor agreement between theory and experiment.

A common feature of electrokinetic phenomena is a relative motion of the charged surface and the volumetric phase of the solution. The charged surface is affected by the electric field forces, and the movement of such surfaces toward each other induces the electrical field. That is a question of slip plane between the double layer and a medium. The layer bounded by the plane at the distance d from surface (OHP) can be treated as immobile in the direction perpendicular to the surface, because the time of ion residence in the layer is relatively long. Mobilty of ions in the parallel direction to the interfacial surface should also be taken into account. However, it seems that the ions in the double layer and in the medium surrounding it constitute a rigid whole and that the layer from x = 0 to x = d is immobile also in the sense of resistance to the tangent force action. There is no reason why the boundary plane of the solution immobile layer should overlap accurately with the OHP plane. It can be as well placed deeply in the solution. The potential in the boundary plane of the solution immobile layer is called potential ζ. Strictly speaking it is not a potential of interface because it is created in the liquid phase. It can be considered as the difference of potentials between a point far from the surface (in the bulk solution) and that in the slip plane.

However, many authors [122-124] assume equality of potentials $\zeta = \psi_d$ at least for low values of surface potentials and low concentrations of electrolyte in the bulk phase. At higher values of the potential and higher concentrations, viscosity close to the surface increases due to the increase of surface concentration. Then, the boundary plane of the mobile layer moves deep into the solution and the anticipated value $|\zeta|$ is lower than the value $|\psi_d|$. Both potentials ζ and ψ_d are diffuse ones and therefore must be of the same sign and must behave in the same way with the change of electrolyte concentration.

Despite the difficulties with accurate location of the plane with potential ζ, one value of potential ζ can be determined from the double layer theory,i.e. it is certain that $\zeta = 0$ when $\psi_d = 0$. Moreover, if the adsorption is not specific (i.e. $\delta_0 = -\delta_d = 0$) it can be also stated for sure that $\zeta = 0$ when $\psi_0 = 0$, i.e. PZC = IEP.

If one assumes that the relation $\zeta = \psi_d$ is valid for low concentrations [113,125-127], ζ can be theoretically calculated from equation obtained from the solution of the Poisson equation for the Stern model for 1:1 electrolyte:

$$\psi_d = \frac{2kT}{e} \ln \left[\frac{-\delta_d}{\sqrt{8\epsilon_0 \epsilon_r kTI}} + \sqrt{\frac{\delta_d^2}{8\epsilon_0 \epsilon_r kTI} + 1} \right] \tag{67}$$

where ψ_d and δ_d are the potentials and the charge density respectively in the d plane which means the onset of the diffuse layer, ϵ_r is the relative permittivity of solvent, (for water at T = 25°C ϵ_r = 78.25), $\epsilon_0 = 8.854 \cdot 10^{-12}$ F/m is the permittivity of free space and I is the ionic strength of the suspension (ions/m^3). The charge density in the d-plane, δ_d, reads

$$\delta_d = B[\theta_- - \theta_+] \tag{68}$$

The values of θ_- and θ_+ are calculated in the way described in section 3.1 for which the value of potential ζ is calculated.

If it is assumed that the slip plane of potential ζ lies at the distance Z from the plane of potential ψ_d [111,112,128-130], then employing the accurate solution of the Poisson

equation [131] leads to the equation,

$$\psi_d(Z) = \frac{2kT}{e} \ln \frac{1 + g_d \exp\{-\kappa Z\}}{1 - g_d \exp\{-\kappa Z\}} \qquad \text{where} \qquad g_d = \frac{\exp\left\{\frac{e\psi_d}{2kT}\right\} - 1}{\exp\left\{\frac{e\psi_d}{2kT}\right\} + 1} \tag{69a}$$

κ is the Debye–Hückel's reciprocal thickness of the double layer,

$$\kappa = \left(\frac{2e^2 I}{\epsilon_r \epsilon_0 kT}\right)^{1/2} \tag{69b}$$

and $\psi_d(Z)$ in Eq. (69a) is the potential at the distance Z from the diffuse layer. Accordingly, $\zeta = \psi_d(Z)$, and the value Z is usually a parameter in theoretical calculations. The value of the parameter Z affects the positions of the acidic and basic branches of the ζ-potential curve, but it does not affect the position of IEP. The influence of parameter Z on the electrokinetic curves was shown by Rudziński et al. [91].

3.4. Adsorption of simple ions and the heterogeneous surface model

As it was discussed by Rudziński et al. [20] the intrinsic constants K_i's can be written as follows

$$K_i = K_i' \exp\left\{\frac{\epsilon_i}{kT}\right\}, \qquad i = 0, +, A, C \tag{70}$$

where ϵ_i is the adsorption (binding) energy of the ith surface complex, and K_i' is related to its molecular partition function.

The experimentally measured adsorption isotherms have to be related to the following averages, θ_{it},

$$\theta_{it}(\{a\}, T) = \int_{\Delta\epsilon} \cdots \int \theta_i(\{\epsilon\}\{a\}, T)\chi(\{\epsilon\})\, d\epsilon_0\, d\epsilon_+\, d\epsilon_A\, d\epsilon_C \tag{71}$$

where $\{a\}$ is the set of the bulk concentrations $\{a_H, a_C, a_A\}$, $\{\epsilon\}$ is the set of the adsorption energies $\{\epsilon_0, \epsilon_+, \epsilon_A, \epsilon_C\}$, $\Delta\epsilon$ is the physical domain of $\{\epsilon\}$, and $\chi(\{\epsilon\})$ is the multidimentional differential distribution of the number of adsorption sites among various sets $\{\epsilon\}$, normalized to unity

$$\int_{\Delta\epsilon} \cdots \int \chi(\{\epsilon\})\, d\epsilon_0\, d\epsilon_+\, d\epsilon_A\, d\epsilon_C = 1 \tag{72}$$

In the case of a heterogeneous surface ϵ_i has different values on different SO^- sites of oxide surface. This is accompanied by the changes of K_i', constant but it is generally believed that these changes are of a secondary importance compared with the changes of chemical bond energy ϵ_i.

The integration result in Eq. (71) depends on two important factors characterizing properties of a heterogeneous surface: oxide surface topography and correlation degree of adsorption energies of various complexes.

In the hitherto existing studies of adsorption on heterogeneous surfaces two extreme models of surface topography were taken into account:

(1) Patchwise type surface, where adsorption centres having the same properties assembled in large patches on the surface. These patches are assumed to be so large that in reality they constitute independent adsorption (thermodynamic) subsystems being only in thermal and material contact (the exchange of adsorbate molecules between these subsystems is possible). Then it is still assumed, that the states in which two interacting molecules are adsorbed on two different patches make a neglectable contribution to the thermodynamic properties of the system. In the case of such a surface, the functions $\theta_i(\{\epsilon\}, \{a\}, T)$ in equation system (71) have the same analytical form as the functions θ_i considered so far for the homogeneous surface model. It is also possible that various patches have not only different adsorption energy sets $\{\epsilon\}$ but also different electrostatic capacities. Figure 15(A) presents a diagram of patchwise type surface.

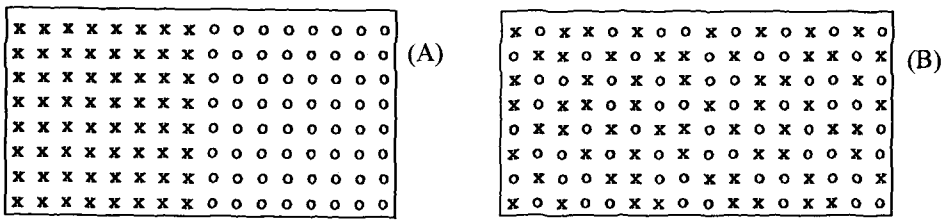

Figure 15. (A) Diagram of patchwise type surface. (B) Diagram of random type surface. Two types of adsorption centres are denoted by crosses and circles.

(2) Random type surfaces where centres corresponding to various sets $\{\epsilon\}$ are randomly scattered on a solid surface. This type of surface topography is shown in Fig. 15(B). Such random centre distribution causes that the probability of finding any other centre close to an adsorption centre is the same. As a result a microscopic composition of the adsorbed phase close to any centre is the same and it is identical with a mean composition of the phase on the whole surface $\{\theta_{it}\}$. It means that all interaction potentials are a function of the averaged concentration of surface complexes $\{\theta_{it}\}$. In Eqs. (71) functions θ_i's have the same form as for homogeneous surface model except for the fact that sets $\{\theta_i\}$ should be replaced by sets $\{\theta_{it}\}$. The adsorption system constitutes a thermodynamic entity characterized by one electrostatic capacity.

Another factor characterizing the properties of a heterogeneous surface is the degree of correlation between adsorption energies of various complexes on various centres.

(1) The case of high correlations between adsorption energies; though energies ϵ_i and $\epsilon_{j\neq i}$ change on passing from one to another centre, their difference $\Delta_{ji} = \epsilon_j - \epsilon_i$ remains unchanged. Therefore the function $\chi(\{\epsilon\})$ in Eq. (71) reduces to one-dimensional differential distribution $\chi_i(\epsilon_i)$.

(2) The case of lack of correlations between adsorption energies on various centres. Then the function $\chi(\{\epsilon\})$ in Eq. (72) becomes a product of one-dimensional distribution functions.

So far, mainly extreme physical situations have been taken into account. The reason for that was of a mathematical nature. Only for such extreme situations it was possible to

reduce the integral equation set (72) to the set of integral equations with single integrals. Actually existing systems show intermediate properties between those extreme physical situations. It can be assumed that in the case of well shaped crystals with a few crystallographic planes a patchwise model is more suitable. Amorphous samples will be more suited for the random model. However, the problem is not completely explicit. Even in the case of well shaped crystals, i.e. samples of a very high degree of arrangement of oxide bulk, the surface may have a low degree of surface atom arrangement. Further, a priori assumptions are even more difficult to be made for the correlations between adsorption energies of various complexes. At present stage the research is focused on the analysis of system properties corresponding to various extreme models, and on observation which of them reproduce experimental behaviour best.

Then, for the reasons explained in the paper by Rudziński et al. [21] we accept the random model of surface topography considering the fundamental physical question of whether the variables ϵ_i are totally independent. In other words, whether the value of ϵ_i is correlated in a way with $\epsilon_{j\neq i}$ (i,j=0.+,A,C) on passing from one to another site. These two models represent somewhat extreme views, and the truth probably lies somewhere in between. It is still too early to provide a definite answer for the fundamental question of which one of these two models is closer to reality.

The physical situation of very high correlations between the adsorption energies of various surface complexes was considered by Koopal and co-workers [132]. They assumed that no matter which is the adsorption site, the difference between the adsorption energies ϵ_i and ϵ_j is still the same and equal to Δ_{ij}. So, the one-dimensional distributions of the number of adsorption sites among ϵ_i, $\chi_i(\epsilon_i)$ look like those in Fig. 16. Of course, the sequence of the most probable adsorption energies ϵ_i^0 can change from one to another oxide. Thus, the intrinsic equilibrium constant K_j can be written as follows,

$$K_j = \tilde{K}_j \exp\left\{\frac{\epsilon_i}{kT}\right\} \tag{73}$$

where

$$\tilde{K}_j = K_j' \exp\left\{\frac{\Delta_{ji}}{kT}\right\} \tag{74}$$

Assuming also that $\chi_i(\epsilon_i)$ is the gaussian-like function (2), one obtains the adsorption isotherm equations for different surface complexes [21]:

$$\theta_{jt} = \frac{K_j^0 f_j}{\sum_j K_j^0 f_j} \frac{[\sum_j K_j^0 f_j]^{kT/c}}{1 + [\sum_j K_j^0 f_j]^{kT/c}}, \qquad j = 0, +, A, C \tag{75}$$

where

$$K_j^0 = \tilde{K}_j \exp\left\{\frac{\epsilon_i^0}{kT}\right\} \tag{76}$$

and where c is the heterogeneity parameter.

To evaluate the surface charge, one must transform the nonlinear equation system (75) taking into account Eq. (51):

$$\delta_0 = B \left(\frac{K_+^0 f_+ + K_A^0 f_A - K_C^0 f_C}{\sum_i K_i^0 f_i} \frac{[\sum_i K_i^0 f_i]^{kT/c}}{1 + [\sum_i K_i^0 f_i]^{kT/c}} - \frac{1}{1 + [\sum_i K_i^0 f_i]^{kT/c}} \right) \tag{77}$$

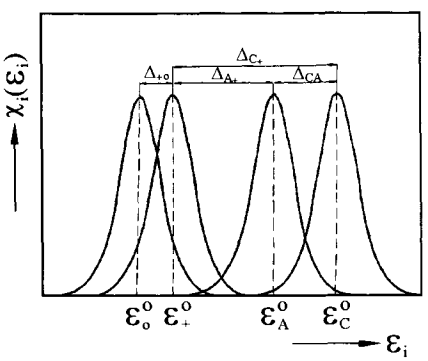

Figure 16. Schematic visualization of the adsorption energy distributions $\chi_i(\epsilon_i)$, (i= 0,+,A,C) for the model assuming high correlations to exist between the adsorption energies of various surface complexes.

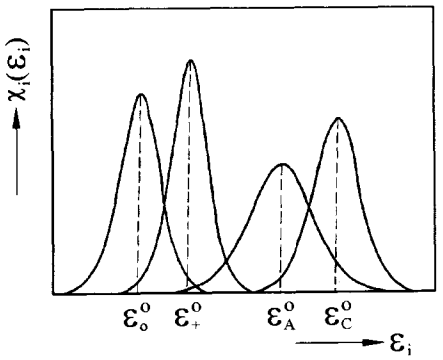

Figure 17. Schematic visualization of the adsorption energy distributions $\chi_i(\epsilon_i)$, (i= 0,+,A,C) for the model assuming a lack of correlations between the adsorption energies of various surface complexes.

This equation can be solved in the same way as Eq. (55).

Now we are going to establish the correlations between the intrinsic equilibrium constants in a similar way as in the case of the homogeneous surface model, considered in the previous section. The condition (61) for CIP to exist leads now to the following interrelations [21]:

$$K_{a2}^{int} = \frac{H^2}{K_{a1}^{int}} \cdot \left(\frac{H}{K_{a2}^{int}} + \frac{H^2}{K_{a1}^{int} \cdot K_{a2}^{int}} \right)^{kT/c-1} \qquad \text{and} \qquad {}^*K_A^{int} = \frac{H^2}{{}^*K_C^{int}} \tag{78}$$

The two above equations are independent. The first one (78a) is a nonlinear equation with regard to K_{a2}^{int} and can be solved by means of an iteration method. The other Eq. (78b) is linear with regard to ${}^*K_A^{int}$. Thus, in a similar way as in the case of the homogeneous surface model, we managed to reduce the number of the independent intrinsic equilibrium constants from four to two.

Now, we are going to consider another extreme model of surface heterogeneity, when Δ_{ij}'s are not correlated at all. That model has already been elaborated by Rudziński and co-workers [133,134], for the case of adsorption of liquid mixtures of non-electrolytes on heterogeneous solid surfaces. The relation between the one-dimensional adsorption energy distributions $\chi_i(\epsilon_i)$ are, for instance such, as shown in Fig. 17.

Appropriate considerations [21] lead now to the following adsorption isotherm equations for different surface complexes:

$$\theta_{it} = \frac{[K_i^0 f_i]^{kT/c_i}}{1 + \sum_i [K_i^0 f_i]^{kT/c_i}}, \qquad i = 0, +, A, C \tag{79}$$

where

$$K_i^0 = K_i' \exp\left\{ \frac{\epsilon_i^0}{kT} \right\} \tag{80}$$

and where c_i's are the heterogeneity parameters for different surface complexes, i=0,+,A,C. To evaluate the surface charge, one must transform the nonlinear equation system (79) by taking into account Eq. (51):

$$\delta_0 = B\,\frac{\left[K_+^0 f_+\right]^{kT/c_+} + [K_A^0 f_A]^{kT/c_A} - [K_C^0 f_C]^{kT/c_C} - 1}{1 + \sum_i [K_i^0 f_i]^{kT/c_i}} \tag{81}$$

This equation can be solved in the same way as Eq. (55).

Condition (61) for CIP to exist, leads now to the following interrelations [21]:

$$\left(\frac{H^2}{K_{a1}^{int} K_{a2}^{int}}\right)^{kT/c_+} + \left(\frac{\frac{kT}{c_C}}{\frac{kT}{c_A}} - 1\right)\left(\frac{{}^*K_C^{int} a}{K_{a2}^{int}}\right)^{kT/c_C} - 1 = 0 \tag{81a}$$

$$\frac{kT}{c_A}\left(\frac{H^2 a}{K_{a2}^{int} {}^*K_A^{int}}\right)^{kT/c_A} - \frac{kT}{c_C}\left(\frac{{}^*K_C^{int} a}{K_{a2}^{int}}\right)^{kT/c_C} = 0 \tag{81b}$$

Now we solve first the non-linear Eq. (81a) using, for example, the iteration method to obtain the value of K_{a2}^{int} for the assumed values of the parameters K_{a1}^{int} and ${}^*K_C^{int}$ as well as of the heterogeneity parameters . Next, we solve the second non-linear equation (81b) for the same parameters K_{a1}^{int}, ${}^*K_C^{int}$, kT/c_i, (i=A,C), and for the new calculated value of K_{a2}^{int}. In the same way as before, we reduce the number of the intrinsic equilibrium constants from four to two.

For the purpose of a theoretical analysis we took the experimental data from the Ph.D. Thesis by Thomas [135], which were also published in part [136]. Here we repeat only that part of information which is related closely to further discussion of our theoretical results. Thus, KCl was used as the basic electrolyte, and the experiments were carried out at 25°C. The titration and electrokinetic curves were monitored for three electrolyte concentrations, 0.1, 0.01, and 0.001 M, but the radiometric measurements were made only for the salt concentration 0.01 M. The BET area of the Alumina Ma sample was 117 m^2/g, whereas that obtained by the Harkins-Jura method was $84 m^2/g$. We took BET value for our numerical calculations.

A successful theory should, for a certain set of parameters, fit simultaneously experimental titration curves, electrokinetic curves, and the individual adsorption isotherms of K^+ and Cl^- measured radiometrically. Thus, to follow this investigation strategy, we took into consideration only the experimental data, measured at the salt concentration 0.01 M. For this electrolyte concentration the calculated activity coefficients of the cation and anion are equal to 0.902.

Four various alumina samples were investigated experimentally by Thomas [135,136], but we selected Alumina Ma for our theoretical-numerical analysis. The reason for that was following: while the quality of the experimental titration and electrokinetic curves was similar for all of them, the experimental radiometric individual isotherms of K^+ and Cl^- adsorption on Alumina Ma covered the widest range of pH values, and the experimental points seemed to exhibit the smallest experimental scatter.

The experimental titration curves had a common CIP, so they could be analyzed in terms of our theory. The CIP is located at 8.5 on pH scale, so, we accepted PZC=8.5 in

our theoretical analysis. The experimental IEP point was located at a different pH value equal to about 8.2. For all the alumina samples, the exprimentally determined PZC and IEP values were different.

Table 2
The values of the parameters obtained by fitting best experimental data by the equations developed for the three models of oxide surface. The last three columns are the values calculated from the best fit parameters. $c_{1(1)}$ and $c_{1(2)}$ are the two values of c_1: the former one for the acidic and the latter for the alkaline branch of the titration curve. The units for both c_1's are F/m^2 and for Z is Å

parameters											calculated values		
pK_{a1}^{int}	$p^*K_C^{int}$	N_s	$c_{1(1)}$	$c_{1(2)}$	Z	$\frac{kT}{c}$	$\frac{kT}{c_0}$	$\frac{kT}{c_+}$	$\frac{kT}{c_C}$	$\frac{kT}{c_A}$	pK_{a2}^{int}	$p^*K_A^{int}$	β
Homogeneous surface model													
6.0	8.7	12.	0.80	1.20	10.	-	-	-	-	-	11.00	8.30	4.4
Heterogeneous surface model (high correlation between adsorption energies)													
6.2	8.6	12.	0.85	1.50	20.	0.8	-	-	-	-	11.38	8.40	3.6
Heterogeneous surface model (lack of correlations between adsorption energies)													
5.9	8.7	12.	0.70	1.20	25.	-	.83	.93	.90	.86	11.05	8.34	3.7

Table 2 collects the values of the parameters found by fitting best simultaneously the data obtained independently from these three experimental sources (titration curves, electrokinetic curves and radiometric isotherms). The Minuit [137] subroutine was applied in our numerical calculations. The details of the calculations were discussed in the paper by Rudziński et al. [21].

Figure 18 shows the comparison between the experimentally measured and theoretically calculated surface charge δ_0. The solid line is common for all the three sets of the parameters collected in Table 2. It means, titration curves are practically insensitive to the heterogeneity effects. Some authors argue that they are practically insensitive to the accepted physical models [110,138,139].

On the contrary, the ζ-potential curve (Fig. 19) and the radiometrically measured individual adsorption isotherms of K^+ and Cl^- (Fig. 20) appear to be sensitive to the surface energetic heterogeneity of oxides. One can see in Fig. 20, that the model of surface heterogeneity assuming lack of correlations between different surface complexes leads to fit of the experimental data. Neglecting the surface heterogeneity leads to a serious under estimation of the concentration of SO^-C^+ complexes at low pH values and of $SOH_2^+A^-$ complexes at high pH values. Accepting the same model of surface heterogeneity is very essential for a proper fit of our experimental ζ-pH curves (Fig. 19). This is because only that model can show the difference between the PZC and IEP values.

Figure 21 explains the reason for that. This is caused by the fact that the crossing point of the curves θ_+ and θ_- is not located at PZC. Although they have very small values, they determine ζ potential, as it can be deduced from Eqs. (67-69). Figure 22 shows the theoretical curves θ_0, θ_C and θ_A for comparison.

As we have already emphasized, titration curves are much less sensitive to the surface

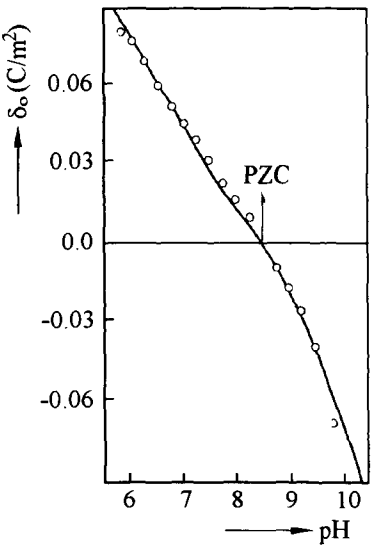

Figure 18. Comparison between the experimentally determined values of the surface charge δ_0 (○) of the Alumina Ma and the theoretically calculated ones (——) for the salt concentration 0.01 M for the three models of oxide surface (the three sets of parameters are collected in Table 2). The differences between three corresponding lines cannot be practically visible, so they are represented by the same solid line.

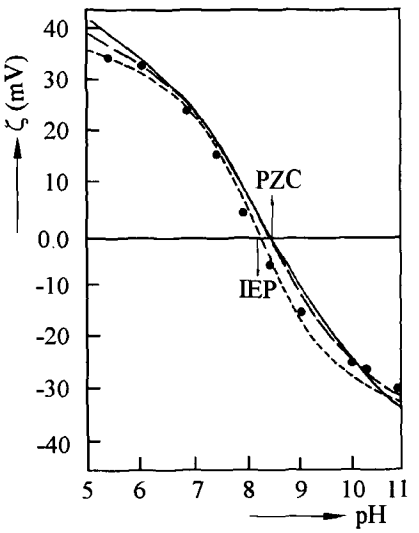

Figure 19. Comparison between experimentally determined values of ζ-potential (●) and those theoretically calculated for a homogeneous surface model (——), the model of surface heterogeneity assuming high correlation between adsorption energies (— — —), and the model neglecting the correlations between adsorption energies (- - - - - -). The calculations were performed by using the parameters collected in Table 2.

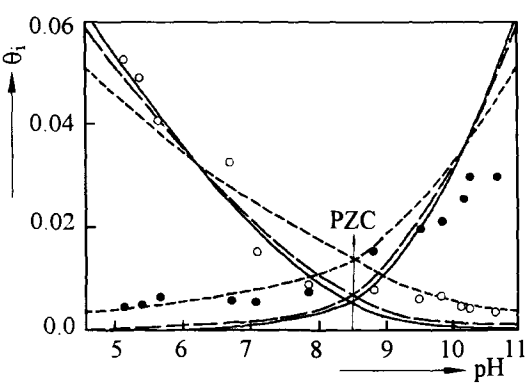

Figure 20. Comparison between the radiometrically measured, individual adsorption iostherms of SO^-C^+ (●) and $SOH_2^+A^-$ (○) and the theoretical ones, corresponding to the model of a homogeneous solid surface (——), the model of surface heterogeneity assuming high correlation between adsorption energies (— — —), and the model neglecting the correlations between adsorption energies (- - - - - -). The calculations were performed by using the parameters collected in Table 2.

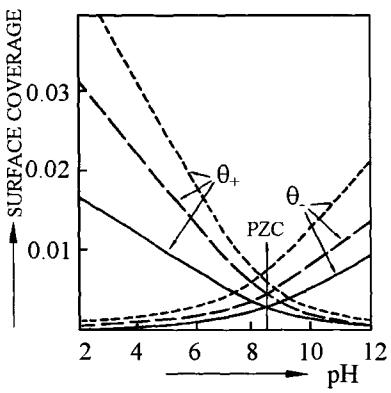

Figure 21. The theoretical values of θ_+ and θ_- calculated for the homogeneous surface model (——), the model of surface heterogeneity assuming high correlation between adsorption energies (— — —), and the model neglecting the correlations between adsorption energies (- - - - -) by using the parameters collected in Table 2.

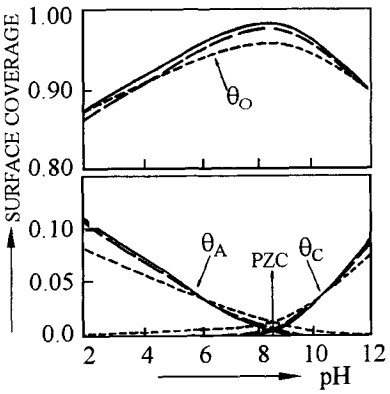

Figure 22. Comparison between the theoretical isotherms θ_A, θ_C and θ_0 for the model of homogeneous solid surface (——), the model of surface heterogeneity assuming high correlation between adsorption energies (— — —), and the model neglecting the correlations between adsorption energies (- - - - -) by using the parameters collected in Table 2.

energetic heterogeneity than individual adsorption isotherms of ions measured by using radiometric methods. Titration curves probably involve a certain mutual cancellation of heterogeneity effects. On the contrary, the electrokinetic curves appear to be quite sensitive.

3.5. Adsorption of bivalent cations at low concentrations

The adsorption of Me^{2+} metal ions at water/oxide interfaces at low ion concentration is a subject of a continuously growing interest. There are three problems of a great practical importance which stimulate that growing interest: (1) the adsorption in soil of highly poisoning cations of some heavy elements like Cd^{2+} or Pb^{2+}; (2) the adsorption in soil of radioactive ions in the areas where nuclear plants are located; (3) the adsorption of radioactive ions on corroded parts of nuclear plant installations.

In all these systems, concentrations of the ions are low, and their adsorption characteristics are strongly affected by heterogeneity. The logarithm of the adsorbed amount, plotted vs the logarithm of the ion concentration in solution is always a Freundlich linear plot with a tangent much smaller than unity. The experimental data reported by Kurdi et al. [140] presented in Fig. 23 can serve as an example.

However, at a sufficiently low ion concentration, a transition occurs into a Henry's plot, typical for a homogeneous solid surface, with the tangent equal to unity. Figures 24 and 25 present adsorption isotherms of bivalent metal ions to illustrate the above mentioned behaviour.

This special behaviour cannot be deduced from the adsorption equations developed in the publications [15-21], except the paper by Kinninburgh et al. [14]. They used an

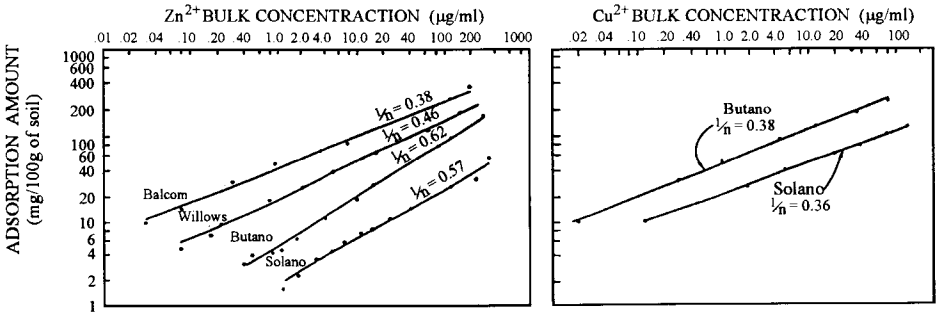

Figure 23. Experimental adsorption isotherms of zinc and copper ions adsorbed on different soils, reported by Kurdi and coworkers. (Figures 1 and 3 in ref [140].)

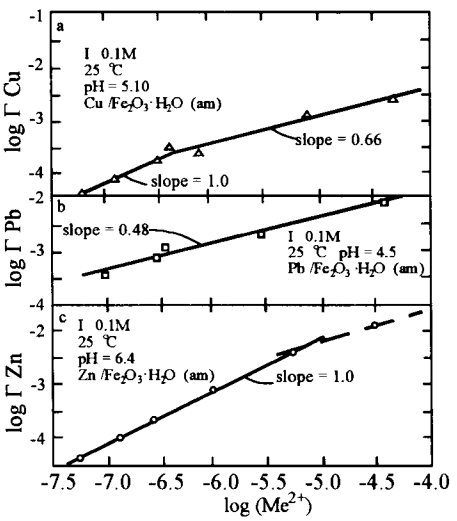

Figure 24. Experimental adsorption isotherms of the bivalent ions Cu^{2+}, Pb^{2+}, and Zn^{2+} adsorbed on the amorphous iron oxyhydroxide, reported by Benjamin and Leckie. (Figure 7 in Ref. [11]).

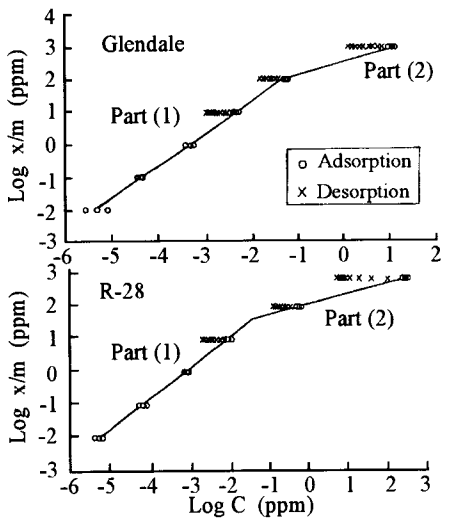

Figure 25. Experimental adsorption isotherms of zinc ion adsorbed on soils Glendale and R-28, reported by Elrashidi and O'Connor. (Figure 1 in Ref. [141].)

equation obtained by replacing bulk gas pressure by bulk ion concentration in the Toth empirical equation used to correlate experimental isotherms for single gas adsorption on solid surfaces. Van Riemsdijk et al.[15,16] criticized Kinniburgh et al. [14] for ignoring the electrical properties of the interface. As the Toth equation is an empirical one, its rigorous extension for a simultaneous, multicomponent, competitive adsorption is known. This means, the Toth equation cannot be used to describe the competition of metal ions with other surface complexes. Thus, the effect of pH or electrolyte concentration on metal

adsorption cannot be studied.

There was a need to construct a theoretical description of the adsorption of ions within the electrical double layer, which could explain the special features of ion adsorption at low ion concentrations. This has been done in the paper by Rudziński et al. [22].

If a strongly adsorbing bivalent metal ion M^{2+} is added to the system described by Eqs. (39) and (40), in which competitive adsorption of protons and ions of basic electrolyte occurs, then according to the triple layer model [103-105] its addition can cause the formation of two kinds of surface complexes: inner-sphere complexes SOM^+ formed at the 0-plain of the triple layer and outer-sphere complexes SO^-M^{2+} formed at the β-plain. Some recent studies by Hayes and Leckie [142-145] suggest that the formation of the inner-sphere complexes is more probable for divalent cations like Cu^{+2}, Pb^{+2}, Cd^{+2}, etc. than the formation of outer-sphere surface complexes. So, in general [142,143]:

$$SOH^0 + M^{2+} \overset{K_M^{int}}{\longleftrightarrow} SOM^+ + H^+$$

$$K_M^{int} \exp\left\{-\frac{e\psi_0}{kT}\right\} = \frac{(a_H)[SOM^+]}{(a_M)[SOH^0]} \tag{82}$$

Formation of other possible surface complexes SOM^+A^- and SOMA connected with the formation of the surface complex SOM^+ is not considered here, for the reasons explained by Hayes and Leckie [142-145].

Reaction (82) can also be written in the form corresponding to desorption reaction of bivalent metal ion:

$$SOM^+ \longleftrightarrow SO^- + M^{2+}$$

$$K_{a2}^{int}/K_M^{int} \exp\left\{\frac{2e\psi_0}{kT}\right\} = \frac{(a_M)\theta_-}{\theta_M} \tag{83}$$

where a_M is the bulk activity of the bivalent ion and $\theta_M = [SOM^+]/\tilde{N}_s$.

Due to the additional adsorption of bivalent metal ion, the value of the surface charge, δ_0, is increased by the charge contributed by this ion. Thus, the surface charge δ_0 is defined now as follows

$$\delta_0 = B[\theta_+ + \theta_M + \theta_A - \theta_- - \theta_C] \tag{84}$$

Individual adsorption isotherms of ions θ_i are defined through a set of Eqs. (52)-like but it is now a set of five equations (i=0,+,A,C,M), where besides the constants K_i's and functions f_i's given by Eqs. (53) and (54), there is a new constant K_M and a function f_M defined as follows:

$$K_M = \frac{K_M^{int}}{K_{a2}^{int}} \qquad \text{and} \qquad f_M = a_M \exp\left\{-\frac{2e\psi_0}{kT}\right\} \tag{85}$$

The above consideration can be extended for the model of heterogeneous surface by taking into account two extreme cases of random surface topography: one with high correlations between adsorption energies and another one assuming lack of correlations between adsorption energies of different surface complexes formed on different adsorption sites. To simplify mathematical calculations it will be assumed that $\Delta\epsilon$ is the interval $(-\infty, +\infty)$. Assuming such integration limits leads to an isotherm equation which does

not reduce to Henry's equation for very low coverages. However, this equation works well for higher surface coverages.

In the studies on monolayer adsorption of gases Rudziński and Everett [2] showed that a correction for physically reasonable limited domain $\Delta\epsilon$, i.e existence of minimum and maximum values ϵ_i^l and ϵ_i^m should be made to arrive at an isotherm equation reducing correctly to Henry's region.

Assuming the finite integration limits for the two different models of random surface we obtained [22] two different sets of equations for θ_{it}, corresponding to two different correlation models. These sets were used to calculate the surface coverage by bivalent metal ions which are found at a small ion concentration. The surface coverages for other ions have higher values, therefore Eqs. (75) and (79) obtained assuming infinite integration limits can be used. Then besides the parameters K_i^0 (i=0,+,A,C,M) important for both extreme models, the parameters $\frac{kT}{c_i}$, (i=0,+,A,C,M) and ϵ_i^m, ϵ_i^l, ϵ_i^0 are found in the model assuming lack of correlations between adsorption energies, and $\frac{kT}{c}$, ϵ^m, ϵ^l, ϵ^0 in the model with correlations.

Then, because the surface coverage by the bivalent metal ions is small compared to all others, we neglected its effects on the PZC value. Thus, the problem of establishing the relations between the intrinsic constants K_{a1}^{int}, K_{a2}^{int}, $^*K_C^{int}$ and $^*K_A^{int}$ from the condition CIP to exist remain unchanged. It should be noted, that in the case of a heterogeneous surface the solution of Eqs. (78) and (79) yields corresponding dependences on K_i^0 but not on K_i. These expressions are dependencies between intrinsic constants for the most probable energies ϵ_i^0.

Thus, all the other adsorption parameters necessary to describe the adsorption of bivalent ions can be found by an appropriate analysis of titration data, radiometric measurements and other independent experimental measurements. It is, therefore, recommended that fundamental studies of bivalent metal ion adsorption be accompanied by suitable additional experiments. Such a fortunate situation can be found in the case of the data published by Benjamin and Leckie (Fig. 24) on Cu^{2+}, Pb^{2+}, Zn^{2+}, and Cd^{2+} adsorption on an amorphous iron oxyhydroxide [11]. The corresponding titration data were analyzed by Davis and Leckie [104] in terms of the homogeneous surface model, and the estimated intrinsic equilibrium constants and other parameters were collected in Table 3. Although the tabulated values are expected to differ to some extent from appropriate values which would be found by applying a more realistic model of a heterogeneous oxide surface, we treated them as a good starting point in a certain model investigation. Thus, we took these values and then tried to find such values of the bivalent ion parameters that they could fit the data presented in Fig. 24(A) and 24(C).

Table 3
Values of the parameters obtained by Davies and Leckie [104], who analyzed their titration data for the amorphous iron oxyhydroxide in terms of the homogeneous surface model

$T = 25^0C$	PZC = 7.90	I = 0.1 M	
$pK_{a1}^{int} = 5.10$	$p^*K_C^{int} = 9.00$	$pK_{a2}^{int} = 10.70$	$p^*K_A^{int} = 6.90$
$N_s = 10$ sites/nm^2	$c_1 = 1.4$ F/m^2		

After numerous calculations it proved unattainable. The model assuming high correlations between energies of ion adsorption did not reflect existence of two different linear areas in the coordinate system log-log and predicts existence of Henry's region up to high coverages [22]. The results of calculations based on the model assuming lack of correlation between energies of various complexes predict a transition from Henry's region (the tangent of log-log plot is equal to one) to Freundlich's region (the tangent smaller than one). The problem is that the tangent in this transition region reaches values larger than unity [22]. Such behaviour has never been observed in the experiment. However, the different behaviour of the log-log plots suggest, that the degree of the correlations between the adsorption energies of ions may affect strongly the behaviour of these adsorption systems at low ion concentrations. This seems to create hope that the studies of the adsorption at low ion concentrations may provide the answer to the fundamental question, which correlation model is to be accepted.

Therefore we have decided that the equation describing a real adsorption isotherm θ_{jt} of the heavy metal ions, (Cu^{2+}, Pb^{2+}, Zn^{2+}, Cd^{2+} ...), will be represented by an analytical formula. Such possiblity is offered by the assumption that $\chi_j(\epsilon_j)$ is the rectangular energy distribution

$$\chi_j(\epsilon_j) = \begin{cases} \dfrac{1}{\epsilon_j^m - \epsilon_j^l} & \text{dla } \epsilon_j \in < \epsilon_j^l, \epsilon_j^m > \\ 0 & \text{elsewhere} \end{cases} \tag{86}$$

The rectangular distribution is a good approximation in the case of strongly heterogeneous surfaces [2]. And this is just the case of the bivalent metal ion adsorption (Freundlich's plots with $\frac{kT}{c_j} \ll 0.9$).

Then, the adsorption isotherm equation for the random model without correlation takes the form

$$\theta_{jt} = \frac{1 + \left(K_j^0 f_j\right)^{kT/c_j}}{1 + \sum_j \left(K_j^0 f_j\right)^{kT/c_j}} \cdot \frac{kT}{\epsilon_j^m - \epsilon_j^l} \ln \frac{1 + \exp\left\{\dfrac{\epsilon_j^m - \epsilon_{jc}}{kT}\right\}}{1 + \exp\left\{\dfrac{\epsilon_j^l - \epsilon_{jc}}{kT}\right\}}, \qquad j = M \tag{87}$$

The others θ_{jt}, (j=0,+,A,C) are calculated form Eq. (79) as their coverages reach higher values.

Now we face the situation that the same physical function $\chi_j(\epsilon_j)$ is represented by two analytical functions (1) and (86). However, we have already known, that in the case of a strongly heterogeneous surface, these functions should affect θ_{jt} in a similar way, if the parameters c_j, ϵ_j^l and ϵ_j^m are suitably chosen. So, we took the integration limits ϵ_j^l and ϵ_j^m as the best-fit parameters and adjusted c_j in Eq. (87) in such a way that at higher surface concentrations θ_{jt}, the tangent of the Freundlich log-log plot for θ_{jt} is equal to $\frac{kT}{c_j}$.

The corresponding isotherm equation for the model assuming high correlations between the adsorption energies of different surface complexes, reads

$$\theta_{jt} = \frac{K_j^0 f_j}{\sum_j K_j^0 f_j} \cdot \frac{kT}{\epsilon_j^m - \epsilon_j^l} \ln \frac{1 + \exp\left\{\dfrac{\epsilon_j^m - \epsilon_{jc}}{kT}\right\}}{1 + \exp\left\{\dfrac{\epsilon_j^l - \epsilon_{jc}}{kT}\right\}}, \qquad j = M \tag{88}$$

Other θ_{jt} (j=0,+,A,C), functions for this model are still calculated as in Eq. (75), because other ions appear at moderate concentrations. So, the contribution from the non-physical intervals $(-\infty, \epsilon_j^l)$ and $(\epsilon_j^m, +\infty)$ does not affect much the calculated θ_{jt} (j=0,+,A,C) functions.

Let us consider now behaviour of the function θ_{jt} described by Eqs. (87) and (88). Our model investigation showed, that θ_{jt} functions calculated by using Eq. (88) never exhibited the required transition from Henry's to Freundlich's plot. They exhibit Henry's behaviour up to quite high surface coverages.

The assumption of the high correlations between the adsorption energies of different surface complexes is responsible for this non-physical behaviour. As the transition from Henry's to Freundlich's plot has been observed in adsorption on so different materials, we arrive at the following important conclusion. The model assuming high correlations between the adsorption energies of various surface complexes is to be abandoned in the studies of ion adsorption within the electrical double layer formed at water/oxide interfaces.

On the contrary, our model calculations showed, that Eq. (87) corresponding to the assumption that no correlations exist between the adsorption energies of different surface complexes, could reproduce very well the behaviour observed in Fig. 24(A) and 24(B).

Thus, an extensive model investigation based on Eq. (87), was carried out to demonstrate its utility to fit the experimental data. We took the parameters obtained by Davis and Leckie [104] analyzing their titration curves (Table 3), calculated the corresponding pK_{a2}^{int} and $p^*K_A^{int}$ values from relation (81), and then adjusted the three other parameters pK_M^{int}, ϵ_M^l and ϵ_M^m to fit the experimental isotherms of Cu^{2+} and Zn^{2+} ions shown in Fig. 24. The results of these numerical exercises are shown in Fig. 26, and the obtained best-fit parameters are collected in Table 4.

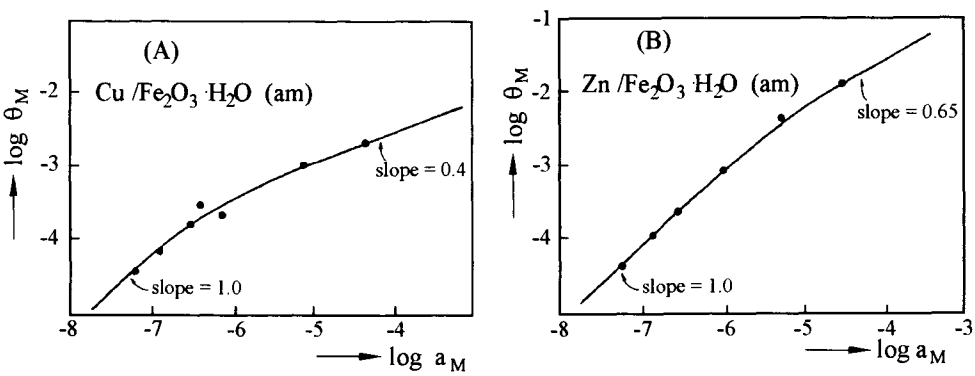

Figure 26. The results of our best-fit exercises based on Eq. (87). (A) The comparison of the experimental adsorption isotherm of Cu^{2+} ions adsorbed at pH=5.1, reported by Benjamin and Leckie [11], with our theoretical curves calculated by using Eq. (87) and the parameters collected in Tables 3 and 4. (B) The comparison of the experimental adsorption isotherm of Zn^{2+} ions adsorbed at pH=6.4, reported by Benjamin and Leckie [11], with our theoretical curves calculated by using Eq. (87) and the parameters collected in Tables 3 and 4.

Table 4
The sets of the parameters used by us in our model investigation shown in Fig. 27. Other parameters are those collected in Table 3, except that pK_{a2}^{int} and $p^*K_A^{int}$ are now equal to 10.70 and 6.80 respectively. These new values were calculated from the values of pK_{a1}^{int}, $p^*K_C^{int}$ and PZC as reported in Table 3 using relation 81 and the values of $\frac{kT}{c_i} = 0.7$

(A) $Cu/Fe_2O_3 \cdot H_2O$ (am)		
$pK_M^{int} = 2.40$	$\epsilon_M^l = -16$ kJ	$\epsilon_M^m = 12$ kJ
With these parameters the slope of the Freundlich log-log plot is 0.40 so, we took $\frac{kT}{c_M} = 0.40$ to calculate the isotherm in the Henry's and transition regions.		
(B) $Zn/Fe_2O_3 \cdot H_2O$ (am)		
$pK_M^{int} = 3.60$	$\epsilon_M^l = -2.0$ kJ	$\epsilon_M^m = 2.5$ kJ
With these parameters the slope of the Freundlich log-log plot is 0.65 so, we took $\frac{kT}{c_M} = 0.65$ to calculate the isotherm in the Henry's and transition regions.		

This is a pretty raw fit, and we suppose that we could arrive at a similar agreement with slightly different values of these parameters. We must, however, realize that the values obtained by Davis and Leckie [104] and collected in Table 3 were obtained by them while accepting the rather raw assumption of a homogeneous oxide surface, and only the parameters pK_{a2}^{int} and $p^*K_A^{int}$ were calculated by us using the correct relation (81) corresponding to the assumption that the oxide surface is heterogeneous.

The philosophy lying behind that best-fit exercise arose from our earlier observation that surface heterogeneity does not affect much titration curves and the estimated surface complexation parameters [22]. As we have already argued, there must exist some compensation effects in these composite adsorption isotherms. On the contrary, we found that surface heterogeneity affects strongly the individual adsorption isotherms of the surface complexes, measured radiometrically or in another way. This, of course, is also true in the case of the individually measured isotherms of adsorption of the bivalent ions.

Figure 27 provides even more convincing evidence for accepting the model assuming lack of correlations between energies of adsorption of various surface complexes in the description of phenomena occurring in the double electrical layer. Using Eq. (79) we also fitted the isotherms of adsorption of cadmium ions reported by Benjamin and Leckie [11] for three different pH values. These isotherms are shown in Fig. 27 (original Fig. 3 in Ref. [11]). This time we required that with the same set of the best fit parameters the calculated isotherms matched the measured ones for all the three pH values. The reason why we used Eq. (79) instead of Eq. (87) was that the isotherms for cadmium adsorption were reported only for the coverage region corresponding to Feundlich behaviour. In this region simple Eq. (79) can safely be used. As the slope of all these isotherms can easily be determined to be equal to 0.66 ($\frac{kT}{c_M} = 0.66$) for all the investigated pH values, we have only one unknown parameter, pK_M^{int}. Then, with only one best fit parameter, $pK_M^{int} = 3.9$ we arrive at an excellent agreement with the experimental data. The calculated adsorption isotherms match ideally the solid lines in this figure, drawn by Benjamin and Leckie as the best linear regression for their experimental points.

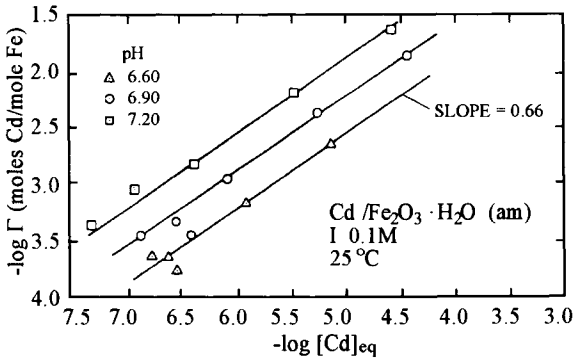

Figure 27. The effects of pH on the isotherms of cadmium ions, adsorbed on the amorphous iron oxyhydroxide investigated by Benjamin and Leckie [11]. The solid lines were drawn by Benjamin and Leckie [11] as the best linear regression for their experimental points. Our theoretical lines match exactly the Benjamin and Leckie solid lines if the best fit parameter $pK_M^{int} = 3.9$. Theoretical lines were calculated from Eq. (79) by using the parameters pK_{a1}^{int}, $p^*K_C^{int}$, PZC, N_s, c_1, I and T collected in Table 3, $kT/c_i = 0.7$ (i=0,+,A,C) and the parameters $pK_{a2}^{int} = 10.7$ and $p^*K_A^{int} = 6.8$ calculated by us from Eqs. (81).

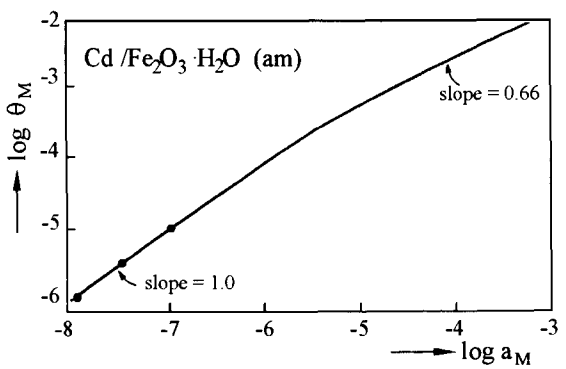

Figure 28. The comparison of our theoretical adsorption isotherm calculated by using Eq. (87) with the experimental data of Cd^{2+} adsorption measured by Benjamin and Leckie (data in Fig. 5 in Ref. [11].) The parameters are the same as those used to fit the data in Fig. 27 and the two additional parameters ϵ_M^l and ϵ_M^m appearing in Eq. (87) are equal to −8 kJ/mol and 8 kJ/mol respectively.

For pH=5.8 Benjamin and Leckie [11] measured the adsorption at much smaller concentrations of Cd^{2+} ions. For such small concentrations they observed the transition to Henry's log-log plot with tangent equal to unity. According to our theory the adsorption in that region is affected by the physical energy limits ϵ_M^l and ϵ_M^m. So, no surprise, that in order to fit these data we were forced to take into account that physical condition, i.e. to

use the more general Eq. (87).

While fitting these data we required that the theoretical log-log plot must have a tangent equal to 0.66 in the region where it becomes a Freundlich log-log plot (like in Fig. 27). Then we took the same parameters which were used to fit the data in Fig. 27, and adjusted only in addition ϵ_M^l and ϵ_M^m. Figure 28 shows the fit obtained when $\epsilon_M^l = -8$ kJ/mol and $\epsilon_M^m = 8$ kJ/mol.

4. CONCLUSIONS

We have analyzed here a variety of adsorption data obtained while investigating the adsorption at oxide/water vapour interface, and oxide/electrolyte interface. That analysis summarized our extensive research conducted during the past few years, and concerning the model of adsorption on oxide surfaces. Our analysis shows, that only the model of energetically heterogeneous surface can be a proper basis for a successful theoretical description of adsorption at water vapour/oxide, and oxide/electrolyte interfaces. It is also demonstrated, that a simultaneous analysis of adsorption isotherms and heats of adsorption may lead to a new level of understanding the mechanism of adsorption in those systems.

REFERENCES

1. See for instance: the Chapter I in the monograph by J.Nowotny and W.Wepper (eds.), Non-Stoichiometric Compounds: Surfaces, Grain Boundaries and Structural Defects, Kluwer, 1989.
2. W. Rudziński and D.H. Everett, Adsorption of Gases on Heterogeneous Surface, Academic Press, New York, 1992.
3. M. Jaroniec and R. Madey, Physical Adsorption on Heterogeneous Solids, Elsevier, Amsterdam, 1988.
4. V.A. Bakaev, Surface Sci., 196 (1988) 571.
5. V.A. Bakaev, Adsorption on Microporous Adsorbents, Proc. Int. Workshop, Berlin-Eberswalde, 2 (1987) 33.
6. V.A. Bakaev and M.M. Dubinin, Dokl. AN SSSR, 296 (1987) 369.
7. V.A. Bakaev and O.V. Chelnokova, Surf. Sci., 215 (1989) 521.
8. J. Garcia-Miragaya and A.L. Page, Soil Sci. Soc. Am. J., 40 (1976) 658.
9. J. Garcia-Miragaya and A.L. Page, Water, Air, Soil Pollut., 9 (1977) 289.
10. J.J. Street, W.L. Lindsay and B.R. Sabey, J. Environ. Qual., 6 (1977) 72.
11. M.M. Beniamin and J.O. Leckie, J. Colloid Interface Sci., 79 (1981) 209.
12. G. Sposito, Soil Sci. Soc. Am. J., 43 (1979) 197.
13. G. Sposito, in: R.H. Dowdy, D. Baker, V. Volk and J. Ryan (eds.), Chemistry in the Soil Environment, SSSA Spec. Pub., Soil Science Society of America, Madison, WI, 1980, p.45.
14. M.M. Kinniburgh, J.A. Barkes and M. Whitfield, J. Colloid Interface Sci., 95 (1983) 370.
15. W.H. Van Riemsdijk, G.H. Bolt, L.K. Koopal and J. Blaakmeer, J. Colloid Interface Sci., 109 (1986) 219.

16. W.H. Van Riemsdijk, J.C.M. De Wit, L.K. Koopal and G.H. Bolt, J. Colloid Interface Sci., 116 (1987) 511.
17. W.H. Van Riemsdijk, L.K. Koopal, and J.C.M. De Wit, J. Agric. Sci., 35 (1987) 241.
18. L.K. Koopal and W.H. Van Riemsdijk, J. Colloid Interface Sci., 128 (1989) 188.
19. A.W.M. Gibb and L.K. Koopal, J. Colloid Interface Sci., 134 (1990) 122.
20. W. Rudziński, R. Charmas and S. Partyka, Langmuir, 7 (1991) 354.
21. W. Rudziński, R. Charmas, S. Partyka, F. Thomas and J.Y. Bottero, Langmuir, 8 (1992) 1154.
22. W. Rudziński, R. Charmas, S. Partyka and J.Y. Bottero, Langmuir, 9 (1993) 2641.
23. P. Roy and D.W. Fuerstenau, J. Colloid Interface Sci., 26 (1960) 102.
24. D.A. Griffiths and D.W. Fuerstenau, J. Colloid Interface Sci., 80 (1981) 271.
25. A. Foissy, Ph.D. Thesis, University de Franche Comte, Besançon, 1985.
26. K. Wierer, Ph.D. Thesis, Facultät für Chemie und Pharmazie der Universität, Regensburgh, 1987.
27. M.L. Machesky and M.A. Anderson, Langmuir, 2 (1986) 582.
28. A. De Keizer, L.G.J. Fokkink and J. Lyklema, Colloids Surf., 49 (1990) 149.
29. M.L. Machesky and P.F. Jacobs, Colloids Surf., 53 (1991) 297.
30. M.L. Machesky and P.F. Jacobs, Colloids Surf., 53 (1991) 315.
31. T. Morimoto, N. Katayama, H. Naono and M. Nagao, Bull. Chem. Soc. Jap., 42 (1969) 1490.
32. T. Omori, J. Imai, M. Nagao and T. Morimoto, Bull. Chem. Soc. Jap., 42 (1969) 2198.
33. A.V. Kiselev, V.I. Lygin, Kolloid. Zhurn., 21 (1959) 561.
34. C.M. Hallabaugh, J.J. Chessick, J. Phys. Chem., 65 (1961) 109.
35. T. Morimoto, M. Nagao and F. Tokuda, J. Phys. Chem., 73 (1969) 243.
36. E. McCafferty and A.C. Zettlemoyer, J. Colloid Interface Sci., 34 (1970) 452.
37. M. Primet, Ph.D. Thesis, Lyon No. 640, 1970.
38. C. Dorémieux-Morin, M-A. Enriquez, J. Sanz and J. Fraissard, J. Colloid Interface Sci., 95 (1983) 502.
39. B. Fubini, V. Bolis, M. Bailes and F.S. Stone, Solid State Ionics, 32/33 (1989) 258.
40. J.J. Chessic and A.C. Zettlemoyer, J. Phys. Chem., 62 (1958) 1217.
41. A.C. Zettlemoyer and J.J. Chessic, J. Phys. Chem., 64 (1960) 1131.
42. M. Nagao, K. Yunoki, H. Muraishi and T. Morimoto, J. Phys. Chem., 82 (1978) 1032.
43. G. Della Gatta, B. Fubini and G. Venturello, J. Chim. Phys., 70 (1973) 64.
44. R.V. Siriwardane and J.P. Wightman, J. Colloid Interface Sci., 94 (1983) 502.
45. W. Rudziński and S.Partyka, J. Colloid Interface Sci., 89 (1982) 25.
46. J.B. Peri, J. Phys. Chem., 69 (1965) 211.
47. J.B. Peri and R.B. Hannan, J. Phys. Chem., 64 (1960) 1526.
48. J.B. Peri, J. Phys. Chem., 69 (1965) 220.
49. B.D. Flockhardt, J.A. Scott and R.C. Pinck, Trans. Faraday Soc., 62 (1966) 3.
50. B.D. Flockhardt, I.R. Leith and R.C. Pinck, Trans. Faraday Soc., 62 (1966) 542.
51. T. Hiemstra, W.H. Van Riemsdijk and G.H. Bolt, J. Colloid Interface Sci., 133 (1989) 91.
52. T. Hiemstra, J.C.M. De Wit and W.H. Van Riemsdijk, J. Colloid Interface Sci., 133 (1989) 105.

53. T. Hiemstra and W.H. Van Riemsdijk, J. Colloid Interface Sci., 136 (1990) 132.
54. V.A. Bakaev and W.A. Steele, Langmuir, 8 (1992) 1372.
55. V.A. Bakaev and W.A. Steele, Langmuir, 8 (1992) 1379.
56. D.N. Furlong, F. Rouquerol, J. Rouquerol and K.S.V. Sing, J. Colloid Interface Sci., 75 (1980) 68.
57. D.N. Furlong, F. Rouquerol, J. Rouquerol and K.S.V. Sing, J. Chem. Soc., Faraday Trans. 1, 76 (1980) 774.
58. J.L. Finney, in: F.E. Luborsky (ed.), Amorphous Metallic Alloys, Butterworts, London, 1983, p.42.
59. V.A. Bakaev, Izv. AN SSSR, Ser. Khim., No. 7 (1988) 1478.
60. S.J. Gregg and K.S.V. Sing, Adsorption, Surface Area and Porosity, Academic Press, New York, 1967, p.91.
61. L.E. Drain, J.A. Morrison, Trans. Faraday Soc., 48 (1952) 316.
62. G.A. Samorjai, Chemistry in Two Dimensions: Surfaces, Cornell University Press, Ithaca, New York, 1981.
63. W. Hirschwald, in: J. Nowotny and W.Wepper (eds.), Non-Stoichiometric Compounds, Surfaces, Grain Boundaries and Structural Defects, Kluwer, 1989, p.203.
64. A.L. De Lozanne, in: B.W. Rossiter and R.C. Baetzold (eds.), Investigations of Surfaces and Interfaces - Part A, Physical Methods of Chemistry Series, Willey, New York, 1993, p.112.
65. G.S. Roher, V.E. Henrich and D.A. Bonnell, Surf. Sci., 278 (1992) 146.
66. W. Rudziński and M. Jaroniec, Surf. Sci., 42 (1974) 552.
67. L.E. Dormant, A.W. Adamson, J. Colloid Interface Sci., 38 (1972) 285.
68. W. Rudziński, J. Michałek and J.A. Jonsson, Chromatographia, 22 (1986) 337.
69. W. Rudziński, J. Michałek, B. Brun, and S. Partyka, J. Chromatogr., 406 (1987) 295.
70. M.J. De Oliveira, R.B. Griffiths, Surf. Sci., 71 (1978) 687.
71. H. Asada, H. Sekito, Surface Sci. Lett., 258 (1991) L697.
72. W. Rudziński, R. Charmas and S. Partyka, Colloids Surf., 70 (1993) 111.
73. T.L. Hill, Statistical Mechanics, McGraw-Hill, New York, 1956.
74. R.B. Anderson, J. Am. Chem. Soc., 68 (1946) 686.
75. R.B. Anderson and W.K. Hall, J. Am. Chem. Soc., 70 (1948) 1727.
76. S. Partyka, F. Rouquerol, J. Rouquerol, J. Colloid Interface Sci., 68 (1979) 21.
77. F. Trolard, V. Valles, S. Partyka and Y. Tardy, Bull. Mineral., 109 (1986) 199.
78. W. Rudziński, L. Łajtar, J. Zając, E. Wolfram and J. Paszli, J. Colloid Interface Sci., 96 (1983) 339.
79. W. Rudziński, J. Zając and C.C. Hsu, J. Colloid Interface Sci., 103 (1985) 528.
80. D. Nicholson and R.G. Silvester, J. Colloid Interface Sci., 62 (1977) 447.
81. T.L. Hill, J. Chem. Phys., 17 (1949) 762.
82. L. Onsager, Phys. Rev., 65 (1944) 117.
83. M.N. Plooster and S.N. Gitlin, J. Phys. Chem., 75 (1971) 3322.
84. E.W. Berezin, A.V. Kiselev and A.A. Kozlow, J. Colloid Interface Sci., 45 (1973) 190.
85. E.W. Sidebottom and G.G. Litvan, Trans. Faraday Soc., 67 (1971) 2726.
86. L.T. Zhuravlev, Langmuir, 3 (1987) 316.

87. A. Tsugita, T. Takei, M. Chikazawa and T. Kanazawa, Langmuir, 6 (1990) 1461.
88. I.M. Kim and D.P. Landau, Surf. Sci., 110 (1981) 415.
89. F.M. Etzler and W. Drost-Hansen, Croat. Chem. Acta, 56 (1983) 563.
90. W. Rudziński and S. Partyka, J. Colloid Interface Sci., 89 (1982) 25.
91. W. Rudziński, R. Charmas, S. Partyka and A. Foissy, New J. Chem., 15 (1991) 327.
92. T.W. Hearly and W. Fuerstenau, J. Colloid Sci., 20 (1965) 376.
93. S.K. Miljonic and A.Lj. Ruvaroc, Thermochim. Acta, 11 (1975) 261.
94. W.D. Harkins and G. Jura, J. Phys. Chem., 66 (1944) 919.
95. J. Fripiat, J. Cases, M. François and M. Letellier, J. Colloid Interface Sci., 89 (1982) 378.
96. E.V. Ballou and S. Ross, J. Phys. Chem., 57 (1953) 653.
97. A.C. Zettlemoyer, G.J. Young, J.J. Chessick and F.H. Healey, J. Phys. Chem., 57 (1953) 649.
98. P. Pfeifer, Y.J. Wu, M.W. Cole and J. Krim, Phys. Rev. Lett., 62 (1989) 1997.
99. P.J. Lunde and F.L. Kester, Chem. Eng. Sci., 30 (1975) 1497.
100. J.J. Fripiat, in: D. Avnir (ed.), The Fractal Approach to Heterogeneous Chemistry, Willey, New York, 1989, p.331.
101. P. Somasundaran and E.D. Goddard, Modern Aspects of Electrochemistry, Plenum Press, New York, 1979, p.207.
102. J. Westall and H. Hohl, Adv. Colloid Interface Sci., 12 (1980) 265.
103. J.A. Davis, R.O. James and J.O. Leckie, J. Colloid Inteface Sci., 63 (1978) 480.
104. J.A. Davis and J.O. Leckie, J. Colloid Interface Sci., 67 (1978) 90.
105. J.A. Davis and J.O. Leckie, J. Colloid Interface Sci., 74 (1980) 32.
106. D.E. Yates, S. Levine and T.W. Hearly, J. Chem. Soc., Faraday Trans.1, 70 (1974) 1807.
107. D. Chan, J.W. Perram, L.R. White and T.W. Hearly, J. Chem. Soc., Faraday Trans.1, 71 (1975) 1046.
108. J.A. Davis, J.O. Leckie, in: E.A. Jenne (ed.), Chemical Modelling Aqueous Systems, American Chemical Society, Washington, DC, 1979, p.151.
109. F.M.M. Morel, J.G. Yested and J.C. Westall, in: M.A. Anderson and A.J. Rubin (eds.), Adsorption of Inorganics at Solid-Liquid Interfaces, Ann Arbor, MI, 1981, p.263.
110. R.E. Johnson Jr., J. Colloid Inteface Sci., 100 (1984) 540.
111. M.A. Blesa and N. Kallay, Adv. Colloid Interface Sci., 28 (1988) 111.
112. N. Kallay, R. Sprycha, M. Tonić, S. Žalec and Ž. Torbić, Croat. Chem. Acta, 63 (1990) 467.
113. R. Sprycha, J. Colloid Interface Sci., 102 (1984) 173.
114. N. Kallay, D. Babič and E. Matijevič, Colloids Surf., 19 (1986) 375.
115. L. Bousse, N.F. De Rooij and P. Bergveld, Surf. Sci., 135 (1983) 479.
116. L. Bousse, J. Chem. Phys., 76 (1982) 5128.
117. L. Bousse and P. Bergveld, J. Electroanal. Chem., 152 (1983) 25.
118. L. Bousse, N.F. De Rooij and P. Bergveld, IEEE Trans. Electron Devices, 30 (1983) 1263.
119. L. Bousse, J.D. Maindl, in: J.A. Davis and K.F. Hayes (eds.), Geochemical Processes at Mineral Surfaces, ACS Symposium Series, Am. Chem. Soc., Washington DC, 323 (1986) 79.

120. H. Van den Vlekkert, L. Bousse and N.F. De Rooij, J. Colloid Interface Sci., 122 (1988) 336.
121. P. Bergveld, IEEE Trans. Biomed. Eng., 17 (1970) 70.
122. J. Lyklema and J.Th.G. Overbeek, J. Colloid Sci., 16 (1961) 501.
123. R.J. Hunter, J. Colloid Interface Sci., 22 (1966) 231.
124. A.L. Smith, in: G.D.Parfitt (ed.), Dispersions of Powders and Liquids, Elsevier, London, 1969. p.32.
125. W. Smit and C.L.M. Holten, J. Colloid Interface Sci., 78 (1980) 1.
126. R. Sprycha and J. Szczypa, J. Colloid Interface Sci., 102 (1984) 288.
127. R. Sprycha and J. Szczypa, J. Colloid Interface Sci., 115 (1987) 590.
128. T.H. Harding and T.W. Hearly, J. Colloid Interface Sci., 107 (1985) 382.
129. N. Kallay and M. Tomić, Langmuir, 4 (1988) 559.
130. M. Tomić and N. Kallay, Langmuir, 4 (1988) 565.
131. A.W. Adamson, Physical Chemistry of Surfaces, Willey, New York, 1990.
132. L.K. Koopal, W.H. Van Riemsdijk and M.G. Roffey, J. Colloid Interface Sci., 118 (1987) 117.
133. W. Rudziński, J. Michałek, Z. Suprynowicz and K. Pilorz, J. Chem. Soc., Faraday Trans.2, 81 (1985) 553.
134. W. Rudziński, in: J.A. Jonsson (ed.), Chromatographic Theory and Basic Principles, Marcel Dekker, New York, 1988, p.52.
135. F. Thomas, Ph.D. Thesis, Universite de Nancy, 1987.
136. F. Thomas, J.Y. Bottero and J.M. Cases, Colloid Surf., 37 (1989) 281.
137. F. James and M. Roos, Comput. Phys. Commun., 10 (1975) 343.
138. G. Sposito, J. Colloid Interface Sci., 74 (1980) 32.
139. G. Sposito, J. Colloid Interface Sci., 91 (1983) 329.
140. F. Kurdi and H.E. Doner, Soil Sci. Soc. Am. J., 47 (1982) 1153.
141. M.A. Elarshidi and G.A. O'Connor, Soil Sci. Soc. Am. J., 46 (1982) 1153.
142. K.F. Hayes and J.O. Leckie, J. Colloid Interface Sci., 115 (1987) 564.
143. K.F. Hayes and J.O. Leckie, ACS Symp. Ser., Geochem. Process Miner. Surf., 323 (1986) 114.
144. C.J. Chisholm-Brause, G.E. Brown Jr. and G.A. Parks, Physica B, 158 (1989) 646.
145. C.J. Chisholm-Brause, A.L. Roe, K.F. Hayes, G.E. Brown Jr., G.A. Parks and J.O. Leckie, Physica B, 158 (1989) 674.

This Page Intentionally Left Blank

A. Dąbrowski and V.A. Tertykh (Editors)
Adsorption on New and Modified Inorganic Sorbents
Studies in Surface Science and Catalysis, Vol. 99

Chapter 2.3
Energetic heterogeneity of porous inorganic oxides: Adsorption and chromatographic studies

M. Jaroniec

Separation and Surface Science Center, Department of Chemistry, Kent State University, Kent, Ohio 44242, U.S.A.

Porous inorganic oxides are energetically heterogeneous due to various types of surface hydroxyls, impurities as well as surface and structural irregularities. There exist many methods to extract information about energetic heterogeneity of inorganic oxides from the low-pressure adsorption isotherms, gas chromatographic data as well as thermodesorption data. This heterogeneity is commonly characterized in terms of the adsorption energy distribution function. The current review presents a brief survey of the methods recommended especially to evaluate the adsorption energy distributions for porous inorganic oxides. A special emphasis is placed on the numerical procedures, which provide stable results. Some illustrations are given for porous silicas, which are the most popular inorganic oxides used as adsorbents, chromatographic packings and catalyst supports.

1. INTRODUCTION

Porous inorganic oxides have found wide applications in sorption-based separations, chromatography, catalysis and other areas of science and technology (see monographs [1–7] and references therein). The most popular oxides used as adsorbents, chromatographic packings and catalyst supports are silica [5,6,8,9] and alumina [7,10–12]. Also, porous oxides of other metals and semimetals (e.g., zirconia, titania, magnesia, ceria, thoria, urania, samaria, etc.), are of a great potential interest for adsorption, catalysis and chromatography [13–17]. According to the Kiselev's classification [18] inorganic porous oxides belong to the second class of adsorbents, which possess hydroxyl groups at their surface. The surface activity of these oxides depends strongly on the hydroxylation level [11]. They are able to interact specifically (e.g., via hydrogen bonding and/or acid-base interactions) with adsorbate molecules, which possess appropriate functional groups.

Among inorganic oxides silica is commonly used in chromatographic separations due to its high mechanical, chemical and thermal stability [4–6,11,19]. Synthesis of porous silica is well elaborated and allows preparation of small spherical particles of controlled size, porosity and specific surface area [8,20]. In addition to siloxane bridges the surface of silica particles contain different types of hydroxyl groups such as isolated (free), vicinal (bridged) and geminal silanols [6,8,11,19,20]. These groups control polarity of the silica surface and its reactivity [6,19,21]. The surface concentration of silanols in a hydrated

silica depends strongly on its thermal treatment [6,8,11,20,22]. For mesoporous silicas extensively degassed under vacuum conditions at 423– 473K the physically adsorbed water is removed and the surface concentration of silanols reaches a value about 4.6 groups per one nm^2 [6,8,11]. The fraction of different types of silanols depends on the preparation and thermal treatment of a given silica and its porous structure [6,8,11]. Thus, surface and sorption properties of silicas are strongly controlled by the presence of different silanols, adsorbed water molecules and metal impurities [6,8,23–28]. In addition, these properties can be drastically altered by chemical modification of the silica surface, which leads to the preparation of so–called chemically bonded phases used commonly in liquid chromatography [5,6,19]. For instance, a gradual replacement of silanols by various ligands allows preparation of chemically bonded phases of controlled polarity and surface heterogeneity. Again, the coverage density of these phases is controlled not only by chemical and geometrical properties of ligands but also by surface chemistry of the silica and its porous structure [29,30].

While porous unmodified and modified silicas are used commonly as adsorbents, chromatographic packings and catalyst supports, alumina is mostly used in adsorption and catalysis. In contrast to silica gels the chromatographic application of aluminum oxides is much smaller due to the less effective chemical modification of their surfaces [16]. Various forms of alumina have been found to possess differing number of hydroxyl groups and adsorbed water molecules depending on its thermal history [11]. The surface activity of alumina results from the defect structure produced during the amorphous to crystalline transition which occurs during the thermal dehydration process [31]. In the γ–form of alumina, which is most often studied [31– 33], only about 75% of the total number of aluminum sites are occupied, while the remaining sites exist as surface defects. At relatively low temperatures and in the presence of water vapor the –alumina strongly adsorbs water molecules. Its gradual dehydration under controlled thermal conditions causes the condensation of neighbouring hydroxyl groups, but only about 66% of these groups can be removed without affecting the solid's structure. Remaining groups in combination with neighbouring oxygen and aluminum atoms form the differing types of active sites, which control surface heterogeneity of this oxide [11]. Thus, alumina possess four most common active sites: aluminum–type acidic sites, oxygen–type basic sites, basic hydroxyls and proton defects acting as electron acceptors. The type of active sites and their distribution determine the surface, sorption and catalytic properties of a given porous alumina. Similarly as in the case of silica the surface properties of alumina can be strongly affected by metal impurities [34].

There is a growing interest in replacing silica and alumina in some chromatographic, sorption and catalytic applications by other porous oxides [13–17]. For instance, chromatographic applications of silica and silica–based bonded phases outside the range of pH = 2 to approximately 8 are seriously limited by destroying siloxane linkages (at low pH) and partial solubility of the silica matrix (at high pH) [19,20,22]. The dissolution of silica and removal of bonded ligands is accelerated at high temperatures. In contrast, porous oxides of transition metals, e.g., zirconia and titania, possess much better mechanical, chemical and thermal stability than silica (see review [15] and references therein). In addition to acidic and basic sites, which are present in alumina, zirconia possess oxidizing and reducing properties, which make this oxide unique and suitable for catalytic applications [35].

Inorganic oxides are usually prepared by precipitation from inorganic salts. A com-

mon procedure for preparing silica gels is based on the reaction of sodium silicate with hydrochloric acid but at higher concentrations so that a gel is directly formed [22]. Amorphous silica of high purity can be synthesized by hydrolysis of silicon tetrachloride with water and heating the resulting gel [36]. Hydrolysis of the silanes is usually employed to prepare silica aggregates of spherical shape. Similarly, other oxides can be prepared. For instance, porous tin oxide can be prepared from aqueous solutions of tin tetrachloride and precipitated by aqueous ammonia at pH = 11 [37,38]. Zirconia can be synthesized by precipitation of zirconium or zirconyl salts [15,39]. Hydrolysis of silicon and titanium tetrachlorides preadsorbed on various carbons was used to deposit silica and titania on the carbon surface [40–42].

High purity inorganic oxides can be obtained by thermal decomposition of various organometallic compounds, which is usually accompanied by the formation of a porous structure due to the elimination of gases during the calcination process. For instance, Ismail [17] studied thermal decomposition of samarium acetylacetonate, which led to formation of porous samaria. Acetoacetonate is capable to form organometallic compounds in media in which metal concentrations are low and this procedure is effective to isolate rare metals and prepare supported metal or metal oxide catalysts. Another examples of organometallic compounds used to prepare inorganic oxides are metal alcoholates, which can be applied as precursors for low– temperature synthesis of porous oxides [43–46].

An important step in the synthesis of inorganic oxides of chemical properties analogous to glasses and ceramics was the replacement of high–temperature heating procedures by polymerization and coagulation of inorganic hydroxides and organo–metallic compounds at the room temperature [47,48]. Extensive studies in this field carried out in the late seventies and eighties gave the birth of the sol–gel science [47]. Almost all of the important inorganic oxides can be prepared by the sol–gel process [47–60]. They can be synthesized from metal alkoxides, aryloxides, acyloxides and other organometallic compounds [58]. A typical illustration of a sol– gel process is preparation of porous silica by reacting silicon methoxide with water under controlled conditions. The resulting silica is a highly porous material with a well–developed porous structure and surface densely covered with various types of silanols. The surface and structural properties of this material are determined by many factors such as the water/silane ratio, temperature, pH, co–solvent, method and rate of drying, and so on [48]. A small change in conditions of the sol–gel process can affect significantly the surface and structural properties of the final product. Therefore, recent studies are focused on the preparation of inorganic oxides of controlled porosity [60].

A remarkable breakthrough in materials chemistry was the synthesis of novel mesoporous silicates and aluminosilicates (MCM–41 materials) by Mobil researchers [61,62]. Their synthesis initiated new era in the preparation of inorganic materials of well–defined structure and porosity. Again, this discovery was accomplished by merging inorganic and surfactant chemistries. The rod–like micelles of cationic surfactants were used as templates to form two or three monolayers of silica (or other inorganic particles) encapsulating the micelle external surface [63–65]. Subsequently, these composite species spontaneously assemble into a long–range ordered structure and then the silicate species in the interstitial spaces of the ordered organic–inorganic phase condense. By removing the organic species from the ordered organic–inorganic composite one can obtain an inorganic material with uniformly sized pores. For instance, MCM–41 molecular sieves have a regular, hexagonal array of uniform cylindrical channels [61,62]. By manipulating synthesis con-

ditions it is possible to control the size of these channels. There is a great interest in the synthesis, characterization and application of these inorganic solids, which are materials of 21st Century [66–75].

A further progress in the synthesis and applications of inorganic porous oxides can be accelerated by the development of characterization methods. Among various methods used to study the surface and structural properties of these materials, classical sorption–based techniques such as adsorption [11,76–79], chromatography [7] and thermal analysis [80] are still popular because they provide direct information about adsorbate–adsorbent interactions; for instance, the low–temperature nitrogen adsorption isotherm is recommended by the IUPAC to evaluate the BET specific surface area [81–86] and the mesopore–size distribution function [76,87], which are essential for characterizing the structural heterogeneity of large pores. These classical quantities are not sufficient to characterize the sorption properties of porous solids such as inorganic oxides, which are energetically and structurally heterogeneous materials [77,78,88–90]. On the other side, the energetic heterogeneity of inorganic oxides is an essential characteristics of these solids. In the current chapter, after a brief introduction of the concept of adsorbent heterogeneity, the selected sorption–based methods useful to estimate the energetic heterogeneity of inorganic oxides are reviewed with some experimental illustrations. This review is mainly focused on the low–pressure gas adsorption measurements and gas chromatographic measurements, which are essential for evaluation the energetic heterogeneity of inorganic porous oxides. The liquid/solid interface, which from the practical viewpoint is of great importance for understanding the surface chemistry of inorganic oxides is not the subject of the current review.

2. CONCEPT OF ADSORBENT HETEROGENEITY

Surface and structural heterogeneities of inorganic oxides can be studied directly by employing modern techniques such as atomic force microscopy (AFM), electron microscopy, X– ray analysis and various spectroscopic methods suitable for materials characterization and surface imaging (see monographs [91–94] and references therein). For instance, recent studies [95] in this field demonstrate a successful use of AFM to visualize, in situ, the formation and structure of adsorbed layers. Although these techniques are extremely useful for imaging solid surfaces, several research problems need to be solved before using them for a direct and quantitative characterization of the adsorbent heterogeneity. At present indirect methods such as sorption and chromatography are most often employed to evaluate various heterogeneities of porous solids (see books [76–79]. The quantities evaluated from sorption and chromatographic data provide information about the whole adsorbent–adsorbate system. Thus, these data can be used mainly to extract information about so–called "relative heterogeneity", i.e., heterogeneity of a solid seen by a given probe molecule [77].

The global heterogeneity of a solid adsorbent consists of both surface and structural heterogeneities [77]. The main source of the surface heterogeneity are different types of crystal planes, growth steps, crystal edges and corners, irregularities in the crystallographical structure of a surface such as cracks and flaws (geometrical roughness of the surface) as well as impurities strongly attached to the surface and various atoms and functional

groups exposed at that surface and available for adsorption (chemical nonuniformity of the surface). The structural heterogeneity, which is a volume property of a solid, is due to the existence of pores of different sizes and shapes. The chemical, geometrical and structural heterogeneities of a solid can be detected by different methods. For instance, analytical titration provides information about acidic and basic groups present on a solid surface. This method combined with spectroscopic techniques can be used successfully to evaluate chemical heterogeneity of a solid surface. Its geometrical and structural heterogeneities can be characterized respectively in terms of the fractal dimension [89] and the pore volume distribution [76,77].

Chemical, surface and structural heterogeneities of a solid can be probed by adsorbate molecules of different sizes, structures and polarity. Due to these heterogeneities the adsorption energy is a local quantity that depends on the (x,y)–position of a given adsorbate molecule on the solid surface. The differential distribution of the adsorption energy is a quantitative measure of the global energetic heterogeneity of a solid, i.e., it specifies the fractions of adsorbed molecules of a given adsorption energy but does not provide information about the source of this heterogeneity [77]. This distribution is a characteristic function for a given adsorbent–adsorbate system and it changes for adsorbates of different physicochemical properties because molecules of these adsorbates interact differently with adsorption sites. Therefore, adsorption and chromatographic data measured for different probe molecules, especially at low pressures, are useful for extracting information about energetic heterogeneity of solids.

Physical interpretation of the adsorption energy distribution is difficult and requires additional independent measurements if one wish to relate characteristic features of this distribution to definite types of adsorbent–adsorbate interactions. In case of inorganic oxides, which most often do not possess fine pores of molecular dimensions (i.e., micropores), the adsorption energy distribution characterizes surface heterogeneities generated by different hydroxyl groups and impurities present on the oxide surface. However, situation becomes more complex when micropores are present because the overlapping of adsorption forces from the opposite micropore walls is the source of a substantial energetic heterogeneity, which is difficult to separate from the surface heterogeneity.

3. INTEGRAL REPRESENTATION OF THE OVERALL ADSORPTION ISOTHERM

In most theoretical treatments of adsorption on heterogeneous solids the adsorbent surface is assumed to have a continuous distribution of adsorption sites with respect to the adsorption energy ε [77,78]. The resulting distribution function, denoted by $F(\varepsilon)$, is accepted as a quantitative characteristics of the energetic heterogeneity of a given solid and $F(\varepsilon)d\varepsilon$ is the fraction of the surface with adsorption energies between ε and $\varepsilon + d\varepsilon$. The relative surface coverage, $\Theta_t(p)$, for an energetically heterogeneous solid characterized by the energy distribution function $F(\varepsilon)$, is expressed by the well–known integral equation [77–79]:

$$\Theta_t(p) = \int_{\Delta} \Theta(p,\varepsilon)F(\varepsilon)d\varepsilon \qquad \text{for} \quad T = \text{const.} \tag{1}$$

where $\Theta_t(p)$ is the experimental adsorption isotherm. When measurements are made at a constant temperature T, the overall adsorption isotherm is obtained by assuming *a priori* a model for the local adsorption isotherm $\Theta(p, varepsilon)$. The integration region Δ in equation (1) is over all possible adsorption energies.

Since different models can be used to represent local adsorption on sites of the same adsorption energy, i.e., energetically homogeneous sites, the current review starts with the very popular and simplistic model formulated by Langmuir in 1918 [96]. This model describes localized monolayer adsorption by neglecting lateral attractive interactions in the surface phase and leads to the following expression for Θ:

$$\Theta(p, \varepsilon) = \frac{Kp}{1 + Kp} \tag{2}$$

In equation (2) K is the Langmuir's constant, which is defined as:

$$K = K_0(T) \exp\left(\frac{\varepsilon}{RT}\right) \tag{3}$$

where K_0 is the pre-exponential factor that contains the partition functions of an isolated molecule in the gas and surface phases with rotational, vibrational and transnational degrees of freedom. A detailed description of this factor is given in the monograph by Clark [97]. Adamson [98,99] has approximated the pre-exponential factor K_0 by the following equation:

$$K_0 = \frac{N_0 \sigma^0 \tau^0}{(2\pi M\ RT)^{1/2}} \tag{4}$$

where σ^0 denotes the actual area per molecule, τ^0 is Frenkel's characteristic adsorption time (i.e., which is assumed to be 10^{-13} seconds), N_0 is Avogadro's number, and M is the molecular mass of the adsorbate. For simple gases Hobson [100] found that equation (4) can be expressed as follows:

$$K_0(T) = 5.68 \cdot 10^{-5}(MT)^{-1/2} \qquad (1/\text{Torr}) \tag{5}$$

Equation (5) is often applied to estimate the pre-exponential constant [77,78]. Another useful approximation for K_0 was proposed by Adamson et al. [101], who expressed the pre-exponential constant in terms of the evaporation heat ε_v:

$$K_0(T) = p_s \exp\left(\frac{\varepsilon_v}{RT}\right) \tag{6}$$

where p_s is the saturation vapor pressure. It was shown that the value of the pre-exponential constant changes mainly the position of the energy distribution on the energy axis but its shape is almost not changed [102,103].

Inclusion of multilayer effects in Langmuir's original model leads to the BET adsorption model, which can be written in the following form [103]:

$$\Theta(p, \varepsilon) = \frac{Cx}{(1 - x)[1 + (C - 1)x]} \tag{7}$$

where $x = p/p_s$ is the relative pressure and $C = K \cdot p_s$. Although the BET model is a simplification of multilayer adsorption, it provides a relatively good description of the

initial stage of this process. Thus, it can be employed to make multilayer corrections of an experimental isotherm in order to evaluate energetic heterogeneity of a surface (i.e., only the initial submonolayer part is essential in this evaluation) [88].

The simplest model which extends Langmuir's localized monolayer approach for lateral interactions was proposed by Fowler and Guggenheim (FG) [104]. Accordingly, lateral interactions are described by the number of nearest neighbours, z, and by the interaction energy parameter, w. As has been shown elsewhere [77,78,88,90], inclusion of lateral interactions into local adsorption models requires that additional assumptions be made about the topography of adsorption sites. Two extreme models have been used to represent the topography of the sites on heterogeneous surfaces: the random distribution approximation (RDA) and the homotattic patch approximation (HPA).

For a random distribution of adsorption sites, statistical thermodynamics gives the following equation for the local isotherm [77,78]:

$$\Theta(\varepsilon, p, \Theta_t) = \frac{Kp \exp(zw\Theta_t)}{1 + Kp \exp(zw\Theta_t)} \tag{8}$$

The $zw\Theta_t$ term describes the average force field acting on an adsorbed molecule that arises from molecules located on the nearest-neighbour sites. In the HPA model, the average force field depends on the homotattic patch coverage $\Theta(\varepsilon)$ and the local isotherm is expressed as follows:

$$\Theta(\varepsilon, p) = \frac{Kp \exp(zw\Theta)}{1 + Kp \exp(zw\Theta)} \tag{9}$$

In contrast to localized adsorption, mobile adsorption models assume that molecules can diffuse freely on the surface. One of the most popular equations used to describe mobile adsorption is that proposed by Hill and de Boer [105] as an analogue of the FG isotherm. This equation can be obtained by combining the two-dimensional form of van der Waals equation with the Gibbs adsorption isotherm. Note that the pre-exponential factors for localized and mobile adsorption are different. In the case of localized adsorption, the pre-exponential factor K_0 takes into account the vibrations of adsorbing molecules in x, y and z direction, whereas the factor for the mobile adsorption contains only the partition functions for vibration in the z-direction and the transnational partition function describing mobility of adsorbing molecules in the (x,y)-plane.

The shape of the energy distribution depends on the assumed model for the local adsorption isotherm. This problem was discussed in Ref. [88], which contains some recommendations concerning the choice of the local adsorption model. It was pointed out that the concept of the energetic heterogeneity is clear for localized adsorption models. Assumption of the Langmuir model, which describes monolayer localized adsorption without lateral attractive interactions, does not require an additional assumption about topography of adsorption sites on the solid surface. It is not the case for mobile adsorption. For adsorption systems with significant effects of lateral interactions the FG equation can be used to represent the local adsorption. Since submonolayer data provide essential information about energetic heterogeneity of a solid surface, their correction for the multilayer effects is not necessary. In addition, the localized adsorption model works better at low temperatures, which are recommended to obtain argon and nitrogen adsorption

data for characterization of porous solids [81,82]. Some suggestions for selecting the local adsorption model were proposed by Merz [106], Brauer and Jaroniec [107].

There is an extensive literature dealing with inversion of the integral equation (1) with respect to the adsorption energy distribution (see books [77,78] and references therein). This inversion is not easy because of the numerical instability of solutions due to experimental errors of adsorption measurements [77,78,106,108,109]. The simplest way of inverting the integral equation (1) is based on the condensation approximation (CA) method [110,111]. According to this method the true local isotherm is replaced by the "condensation isotherm", which is a simple step function. In terms of this approximation a simple expression is obtained to calculate the energy distribution function, which is a negative derivative of the overall adsorption isotherm with respect to the adsorption energy. The key problem in the CA method is the relationship between the equilibrium pressure and the "condensation" adsorption energy because the above mentioned differentiation of the overall isotherm requires to express it in terms of this energy. There are many modifications of this method (see books [77,78] and references therein). Even recently [112] a simple extension of this method was proposed to evaluate the energetic heterogeneity of solids. In 1975 Jaroniec [113] combined and exponential adsorption isotherm with the CA method in order to get a simple and effective expression to evaluate the energy distribution from adsorption data. This method has been used to analyze many adsorption systems (see works [77,88] and references therein), and was found to agree with more advanced numerical methods [114,115]. Also, the CA function is used often as a first approximation of the energy distribution in iterative methods [90].

A numerous number of approaches has been proposed to solve the integral equation (1) analytically [77,78]. Although they have a great practical utility for characterizing heterogeneity effects in adsorption, their main disadvantage results from *a priori* assumption of a definite shape of the energy distribution. Among different types of local isotherms considered the Langmuirian isotherms have received the most attention. The resulting expressions for the overall adsorption isotherm contain adjustable parameters, which can be obtained by a numerical least square fit of the experimental adsorption data. The disadvantages of this procedure are the following: (i) it is unknown whether the assumed shape of $F(\varepsilon)$ is correct and (ii) often a variety of different analytical functions can be used to describe a given data set with about the same degree of accuracy. In contrast, the CA method and advanced numerical methods do not require this assumption [88]. In addition, numerical methods are much more suitable for dealing with ill-posed nature of the integral equation (1). At present, these methods are recommended to evaluate the energy distribution from experimental adsorption data [116].

4. NUMERICAL METHODS OF SOLVING THE INTEGRAL EQUATION OF ADSORPTION

From the mathematical point of view, equation (1) is a linear Fredholm integral equation of the first kind, which can be written in a more general form as follows:

$$g(y) = \int_a^b K(x,y)f(x)dx \tag{10}$$

The integral kernel K(x,y) represents the local isotherm in equation (1), i.e., the physicochemical model of adsorption on sites of the same energy, g(y) is the experimentally measurable adsorption isotherm $\Theta_t(p)$, and f(x) $\equiv$ F(ε) denotes the energy distribution function.

Many attempts have been undertaken to invert integral equation (9) with respect to f(x). The CA method and analytical solutions of the integral equation (1) were mentioned above. Also, it was noted that the calculation of F(ε) from equation (1) is a numerically ill–posed problem, i.e. small changes in $\Theta_t(p)$ caused by experimental errors can distort significantly the resulting F(ε). Additionally, this distortion is not only caused by experimental errors, but also by errors generated during the numerical calculations and errors arising from the quadrature of equation (1). The ill–posedness is mainly a mathematical numerical problem. Another difficulty in evaluating F(ε) on the basis of equation (1), which was addressed in the previous section, is associated with the selection of the integral kernel, used to model the local adsorption process. It is necessary to decide whether the assumptions of the local adsorption model are in accordance with the experimental data.

Theoretical foundations for solving numerically instable problems were developed by Tichonov [117,118], who introduced the regularization method. This method was first applied to gas adsorption by House [119] and Merz [106] and further developed by Papenhuijzen and Koopal [120], Brown et. al. [121,122], Jagiello [123] and Szombathely et al. [102]. The regularization method with singular value decomposition programmed by v. Szombathely [102] has been used extensively to study the energetic heterogeneity of several reference carbonaceous solids [116].

The first step in the regularization method is the discretization of the integral equation by a quadrature. Thus, integral equation (10) needs to be transformed into a system of the following linear equations:

$$\mathbf{g} = \mathbf{A}\mathbf{f} \tag{11}$$

where **g** and **f** are one–dimensional matrices representing respectively the functions g and f and **A** is a two–dimensional matrix representing the integral kernel K(x,y). The fundamental idea of numerical regularization is to replace the ill–posed problem of minimizing the function $\|\mathbf{Af} - \mathbf{g}\|^2$ by a well– posed one which smooth the calculated distribution function and distorts the origin problem insignificantly. This can be done by addition of a second minimizing term to $\|\mathbf{Af} - \mathbf{g}\|^2$:

$$\text{Min} \doteq \|\mathbf{Af} - \mathbf{g}\|^2 + \gamma\|\mathbf{W(f)}\|^2 \tag{12}$$

The regularization parameter γ is a measure of the weighing of both terms and $\|\mathbf{W(f)}\|^2$ is defined as follows:

$$\|\mathbf{W(f)}\|^2 \approx \int_a^b f^2(x)dx \tag{13}$$

By introducing this latter expression into equation (12) oscillations of the resulting distribution function may be suppressed.

The regularization method can be modified further through inclusion of additional restrictions on the function f, e.g. only allowing non–negative solutions (NNLS). Under these latter conditions, the regularization criterion given by equation (12) can be written as:

$$\text{Min} \doteq \|\mathbf{Af} - \mathbf{g}\|^2 + \gamma\|\mathbf{W(f)}\|^2 \quad \text{and} \quad f \succeq 0 \tag{14}$$

The regularization parameter γ is usually chosen through a series of trials by an interactive judgement about the solution. A detailed description of strategies for finding the optimal γ-value in adsorption applications is given in Ref. [102,123]. Usually as a starting point, a high regularization parameter is selected, e.g., $\gamma = 1$, which results in a strongly smoothed distribution function, with a residual, $\|\mathbf{Af} - \mathbf{g}\|^2$, generally higher than that associated with the experimental errors. Subsequently, γ is reduced in an iterative fashion until the experimental accuracy is reached. For instance, the program INTEG developed by v.Szombathely [102] is based on the singular value decomposition (SVD) of the matrix **A** that represents the discretized integral kernel K(x,y). A combination of regularization and SVD not only has computational advantages such as: the minimization of numerical errors and the fast optimization of the final solution by choosing different regularization parameters, but also provides a means of evaluating the validity of the physicochemical model selected to represent the local adsorption which is contained in **A**.

5. INTEGRAL REPRESENTATION OF THE RETENTION VOLUME

Gas–solid chromatography has been often used to measure various physicochemical quantities and to study the gas–solid adsorption systems. There is an extensive literature related to applications of this technique for characterizing adsorbents and catalysts [7]. Since gas chromatographic measurements are carried out at low partial pressures of the sample, the retention data are useful for estimating the energetic heterogeneity of solids. An advantage of gas chromatography is possibility of using various probe molecules and different temperatures. This technique is especially suitable for investigating inorganic oxides since they are most often nonporous or mesoporous solids and there is no additional complications related to diffusion in fine pores.

For an ideal gas phase the net specific retention volume $V_{N,t}$ and the specific adsorbed amount n_t are related as follows [124]:

$$V_{N,t} = jRT \left(\frac{\partial n_t}{\partial p} \right)_T \tag{15}$$

where p is the equilibrium pressure, j is the compressibility factor, T is the absolute temperature and R is the universal gas constant. There are two possible approaches for using retention data to evaluate the energetic heterogeneity of porous solids.

In the first approach, the retention measurements are initially used to calculate the adsorption isotherm by integrating equation (15) and subsequently the resulting isotherm is utilized to evaluate the energy distribution function by means of a method available in sorption literature (see monographs [77,78] and references therein). Recently, Roles and Guiochon [125–127] and Guan et al. [128] have reexamined the method of elution by characteristic points to calculate equilibrium adsorption isotherms and have discussed the precision and accuracy of this procedure. Also, Guiochon and co-workers [129–134] have employed this method to obtain adsorption isotherms for different adsorbates on inorganic porous oxides and used them to calculate the adsorption energy distributions. In contrast to the energy distributions obtained for these solids from conventional sorption measurements they reported relatively narrow energy distributions. Probably, it was caused by a narrow pressure range and high temperatures of chromatographic measurements as well

as by the employed method of calculations. Jagiello and co-workers [135–137] used also gas chromatography to evaluate adsorption isotherms and subsequently to calculate the energy distributions for modified silicas.

An alternative approach to that described above is a direct use of the retention data to calculate the adsorption energy distribution [138–146]. This approach was initiated in 1974 by Rudzinski et al. [138], who showed that the energy distribution function can be expressed as a series, which contains derivatives of the retention volume with respect to the equilibrium pressure. According to this formulation, the retention volume plotted as a function of the adsorption energy is the first–order approximation of the energy distribution. However, first derivative of the retention volume is the second–order approximation of this distribution. This approach was later refined and used to calculate energy distributions for different porous solids [143].

In 1976 Suprynowicz et al. [139] showed that differentiation of the integral equation (1) with respect to pressure gives a general integral representation of the overall retention volume:

$$V_{N,t}(p,T) = n_0 \int_{\Delta} V_{N,l}(p,T,\varepsilon)F(\varepsilon)d\varepsilon \tag{16}$$

where

$$V_{N,l} = jRT\left(\frac{\partial\Theta}{\partial p}\right)_T \tag{17}$$

Above $V_{N,t}$ is defined by equation (15) and n_0 is the monolayer capacity.

For an exponential representation of the local retention the integral equation (16) assumes the following form [142]:

$$V_{N,t}(p,T) = jRTn_0 \int_{K_m}^{\infty} K\exp(-Kp)F^*(K)\ dK \tag{18}$$

where $F^*(K)$ denotes the distribution of the Henry's constant expressed in an inverse unit of pressure and defined by equation (3) in terms of the adsorption energy ε and a temperature– dependent pre–exponential factor K_0. The parameter K_m is the Henry's constant related to the minimum adsorption energy.

Two types of retention data, i.e., (i) retention volumes measured at an infinite dilution of the solute as a function of temperature, and (ii) retention data recorded at different solute's concentrations and a constant temperature, can be used to characterize surface heterogeneity of porous solids in terms of the distribution function $F^*(K)$. This function, which is the result of inversion of the integral equation (18), can be easily converted to the adsorption energy distribution.

A simplified version of equation (18), which does not contain the pressure–dependent exponential term, can be used to describe the temperature–dependence of retention measurements. In this case retention volumes are measured at different temperatures and an infinite dilution of the sample. This simplified equation expressed in terms of the adsorption energy has the following form [144]:

$$V_{N,t} = jn_0K_0 \int_{\varepsilon_m}^{\infty} \exp\left(\frac{\varepsilon}{RT}\right)F(\varepsilon)d\varepsilon \tag{19}$$

Although the integral equation (19) can be inverted with respect to the energy distribution by using an advanced numerical algorithm, e.g., regularization method [102], this approach is not recommended because the number of experimental points measured at different temperatures is usually small. Therefore, analytical solutions of the integral equation (19) seem to be more useful for analyzing the temperature-dependent retention measurements. Gilpin et al. [144] solved equation (19) for a gamma-type energy distribution and obtained the following analytical equation for the overall retention volume:

$$V_{N,t} = jn_0K_0 \exp\left(\frac{\varepsilon_m}{RT}\right)\left(1 - \frac{1}{\rho RT}\right)^{-\gamma} \tag{20}$$

where ρ and γ are the parameters of the gamma distribution function and ε_m is the minimum adsorption energy. Equation (20) can be used to determine parameters of the gamma distribution of the adsorption energy and to predict the temperature-dependence of the solute's retention.

The full form of the integral equation (18) can be used to represent the pressure dependence of the retention volume. In addition to analytical methods of solving the integral equation (18), numerical methods may be also used to invert this integral with respect to the F*(K)-distribution function because the retention volume can be measured for a great number of pressure points. However, the pressure range available in retention measurements is relatively narrow and it transforms to a narrow energy region [129-131,146]. In this energy range the numerical stability of solution is poor. Thus, even in the case of the pressure dependence of the retention volume the analytical solutions of the integral equation (18) seem to be better than numerical ones.

It was shown in Ref. [142] that a gamma-type distribution of the variable K gives a simple analytical solution of equation (18):

$$V_{N,t} = jRTn_0 \exp(-K_m p)\left(\frac{q}{q+p}\right)^{m+1}\left[K_m + \frac{m+1}{q+p}\right] \tag{21}$$

where m and q are the parameters of the gamma-type F*(K)-distribution. Equation (21) fits very well experimental data [142].

Although retention volumes measured at different temperatures and pressures can be used to estimate the energetic heterogeneity of porous solids, the pressure-dependent data seem to be more suitable for this estimation because they can be collected for a greater number of experimental points. It appears that experimentally available ranges of temperatures and pressures are relatively narrow and the resulting retention data can be effectively described by analytical expressions such as equations (20) and (21) [147]. Application of advanced numerical methods for inverting the integral equation (18) is limited due to relatively narrow range of retention measurements.

6. ENERGETIC HETEROGENEITY OF SELECTED INORGANIC OXIDES

As it was mentioned earlier the surface heterogeneity of inorganic oxides, which consists of surface hydroxyls, attached impurities and surface roughness, is the main source of the energetic heterogeneity of these solids. Although the surface heterogeneity of oxides can

be investigated by various techniques, the goal of this section is to demonstrate the utility of low-pressure gas adsorption measurements and gas chromatographic measurements to characterize the energetic heterogeneity of these solids. There is a great number of papers dealing with the determination of the adsorption energy distributions from the gas/solid adsorption and gas/solid chromatographic data for various inorganic oxides, mostly for silica and alumina (see monographs [77,78,88] and references therein).

One of the most popular adsorption systems, which has been used to evaluate the energetic heterogeneity from low-pressure adsorption data, is the argon–rutile (titanium dioxide) system [88]. A main reason of its great popularity is the availability of accurate adsorption data measured by Drain et al. [148–150]. These authors [150] investigated in details the heat capacity, integral heat of adsorption and entropy of argon adsorbed on rutile. In addition, the measured argon adsorption data on rutile over a wide pressure range including low pressures and reported these data in a tabulated form [148]. Also, they determined the adsorption energy distributions from the low-temperature calorimetric measurements for argon, oxygen and nitrogen on rutile [149, 151]. Their experimental adsorption data for the argon–rutile system are unique in the sorption literature and therefore several authors used these data to test various methods of evaluating the energetic heterogeneity of solids [88]. Dormant and Adamson [152] were the first, who evaluated the adsorption energy distribution from the argon–rutile isotherm data by using an iterative method [99] and compared it with the distribution obtained from differential enthalpy data [149]. As can be seen in Figure 1 their method provides the energy distribution which

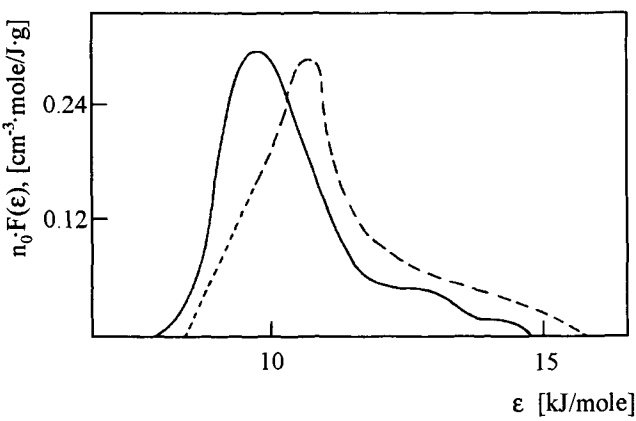

Figure 1. Comparison of the energy distributions for argon on rutile at 85 K evaluated from adsorption (solid line) [152] and calorimetric (dashed line) [149] data. Figure after modification taken from Ref. [152].

agrees well with that obtained by Drain and Morrison [149]. Analogous studies were carried out by Jaroniec et al. [153,154], who verified other numerical methods of evaluating the energy distribution on the basis of the argon–rutile adsorption isotherm. The energy distribution obtained by Dormant and Adamson [152] has a shape of one asymmetrical peak broadened in direction of high adsorption energies. This broadening shows two steps. The energy distributions shown in Figure 1 seem to provide a reasonable representation

of the surface heterogeneity of rutile with respect to argon because the accurate calorimetric data [149] were confirmed by adsorption studies [152–154]. A higher resolution of the adsorption energy spectrum was obtained by using more advanced numerical methods [155,156], which gave instead of these steps an energy distribution consisting of three peaks. This result seems to be supported by computer simulations of argon on the surface of titanium dioxide [157,158]. Other studies of the surface heterogeneity of titania involved nitrogen [159] and carbon monoxide [160,161] as probe molecules. It is noteworthy that in Ref. [160,161] adsorption studies of the heterogeneity effects of titania are supported by independent spectroscopic and calorimetric measurements.

The energetic heterogeneity of the gas/silica adsorption systems has been most often studied due to important applications of silica materials as adsorbents, chromatographic packings and catalyst supports. For instance, the adsorption data of nitrogen on maximally hydroxylated nonporous and wide-porous silica measured by Aristov and Kiselev [162] were often used to evaluate the energy distributions of these solids [113,114,163]. Shown is Figure 2 is the energy distribution for nitrogen on maximally hydroxylated silica at 78K evaluated by using the Jaroniec's method [113,163]. This distribution has two

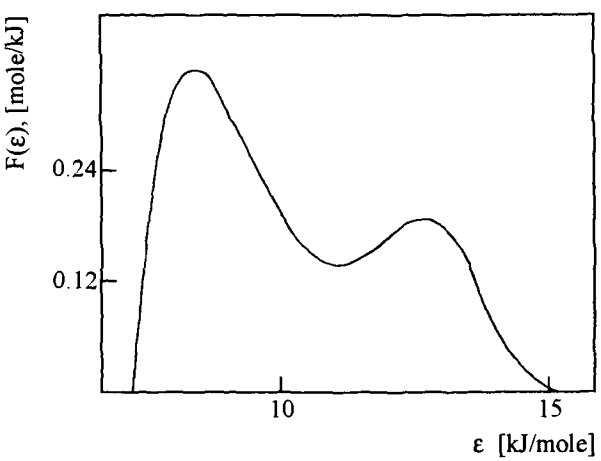

Figure 2. Adsorption energy distribution for nitrogen on maximally hydroxylated silica gel at 78 K. Figure taken from Ref. [113].

(weakly separated) peaks, which seem to correspond to distinct kinds of surface silanols. This shape of the energy distribution was confirmed by House [114], who used a regularization method. Recently, the Jaroniec's group [164,165] has been carried out systematic studies of the energetic heterogeneity of silica gels used in gas and liquid chromatography. For a series of chromatographic silicas the systematic and accurate low- temperature nitrogen adsorption measurements (including the range of very low pressures) have been carried out by using different conditions of the sample preparation. These adsorption studies have been supplemented by gas chromatographic, thermoanalytical and spectroscopic (NMR and IR) measurements. An illustration is shown in Figures 3 and 4, which present

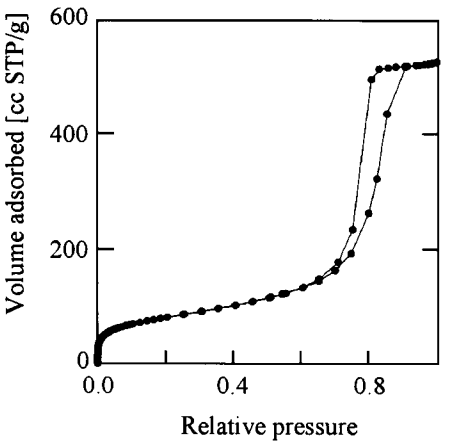

Figure 3. Complete nitrogen adsorption–desorption isotherm at 77.5 K on the Kromasil silica. Figure taken from ref. [165].

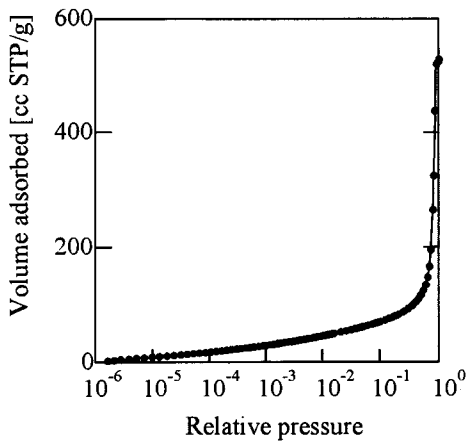

Figure 4. The semi–logarithmic plot of nitrogen adsorption isotherm shown in Figure 3.

respectively a complete nitrogen adsorption–desorption isotherm on Kromasil (spherical 5–mm silica from Eka Nobel, Bohus, Sweden) and a semi–logarithmic plot of the adsorption isotherm, which demonstrates clearly the low–pressure range of the data [165]. The pore–size distribution of this silica, calculated according to the DFT method [166], is shown in Figure 5. As can be seen from this figure there is no evidence for micropores in the silica sample studied. The energy distribution evaluated from the low–pressure adsorption data shown in Figure 4 by using the INTEG program [102] is presented in Figure 6. As can be seen this distribution can be considered as a combination of at least two peaks (two main types of adsorption sites) and resemblances the distribution shown in Figure 2. Also, the differential thermogravimetric (DTG) curve for thermodesorption of water molecules from the silica surface (see Figure 7) provides an additional confirmation for the calculated energy distribution. Analogous studies for other silica gels including a new family of uniformly mesoporous silicates (e.g., MCM–41) are in progress and will be discussed in near future in relation to thermogravimetric, chromatographic and spectroscopic investigations of these solids [21,167].

Although nitrogen has been most often used to study the energetic heterogeneity of silica [113,114,163,168–172], other adsorbates such as argon [169], benzene [113], cyclohexane and cyclohexene [138,141,142,146,173–175], n–hexane and n–hexene [135,137], n–heptane [134], chlorinated hydrocarbons [132,134,175,176], diethyl ether [132,134], methanol [132,134], ethanol [134] and pyridine [134] were used to probe various types of adsorption sites on the silica surface.

In the above mentioned papers the gas chromatographic data were mostly reported [132,134– 138,141,142,173–176]. The energy distributions obtained from the chromatographic data for hydrocarbons on the silicas studied are analogous more or less to the distribution shown in Figure 6 [135,137] or are the decreasing curves with [132,134] or without [141] small peak located at the range of high energies. Their shape is determined

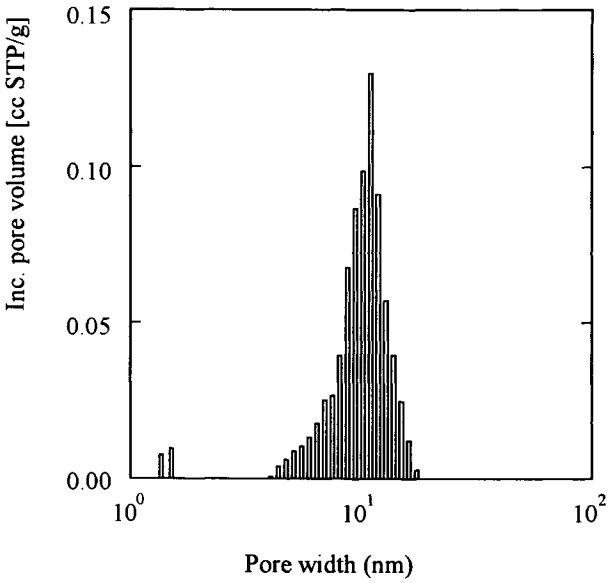

Figure 5. Incremental pore-size distribution for the Kromasil silica. Figure taken from Ref. [165].

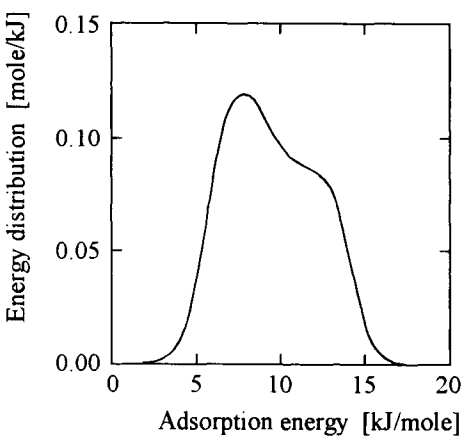

Figure 6. Adsorption energy distribution calculated from the low-pressure adsorption data for nitrogen on Kromasil. Figure taken from Ref. [165].

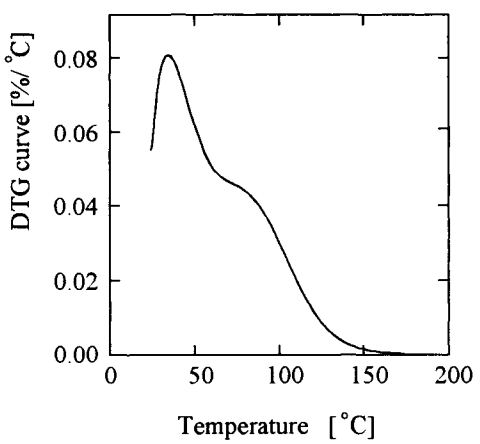

Figure 7. DTG thermogravimetric curve for thermodesorption of physically adsorbed water molecules from the Kromasil surface. Figure taken from Ref. [165].

not only by the origin of the silicas used but also by the properties of probe molecules. It appears often that the gas chromatographic measurements do not cover the entire range of adsorption energies and only the high–energy part of the distribution is available [134].

In comparison to silica the energetic heterogeneity of other inorganic oxides was studied to a less extent [130,131,160,177–179]. Roles et al. [130,131] studied the energetic heterogeneity of alumina by using gas chromatography. Although they reported the energy distributions consisting of separate sharp peaks, their result could be affected by the numerical method employed to calculate these distributions. An interesting work on the surface heterogeneity of alumina was published by Vasquez [177], who used a modified temperature–programmed desorption technique. The controlled thermo–desorption of various probe molecules from inorganic oxides appears to be extremely useful technique to study their surface heterogeneity [165,177,180].

7. CONCLUSIONS

Although the methodology of evaluating the energetic heterogeneity of inorganic porous oxides on the basis of low–pressure gas adsorption and chromatographic data contains a number of questions which need to be addressed in future studies, a significant progress has been done in this field in the last years. Recent developments in the sorption and chromatographic instrumentation allow accurate measurements at the low pressures for various probe molecules on inorganic oxides, which are essential for evaluating the adsorption energy distribution. In addition, the available numerical methods are suitable to calculate this distribution from the low– pressure gas adsorption and chromatographic data. The future studies in this field should focus on the improvement of the existing numerical methods (e.g., representation of the local adsorption by the density functional theory data and/or computer simulations data) and on the incorporation of other techniques such as calorimetry, spectroscopy, programmed thermodesorption, etc. to confirm the resulting energy distributions. In case of inorganic oxides the heterogeneity of proton binding sites, which can be estimated on the basis of liquid–solid adsorption data, is an important issue and deserves more attention in future studies [181–186].

Since in the last decade significant results have been achieved in the theory of adsorption from non–electrolytic liquid mixtures on heterogeneous solids (see reviews [187–189] and references therein), these results can be utilized in the study of heterogeneity of proton binding sites on inorganic oxides.

REFERENCES

1. R.T. Yang, Gas Separation by Adsorption Processes, Butterworths, Boston, 1987.
2. D.M. Ruthven, Principles of Adsorption and Adsorption Processes, Wiley, New York, 1984.
3. D.M. Ruthven, S. Farooq and K.S. Knaebel, Pressure Swing Adsorption, VCH Publishers, Inc., New York, 1993.
4. K.K. Unger (ed.), Packings and Stationary Phases in Chromatographic Techniques, Marcel Dekker, New York, 1990.

5. M.J.J. Hetem, Chemically Modified Silica Surfaces in Chromatography, Huthig, Heidelberg, 1993.
6. R.P.W. Scott, Silica Gel and Bonded Phases, Wiley, Chichester, 1993.
7. T. Paryjczak, Gas Chromatography in Adsorption and Catalysis, Harwood Ltd., Chichester, 1986.
8. H.E. Bergna (ed.), The Colloid Chemistry of Silica, Amer. Chem. Soc., Washington, D.C., 1994.
9. E.F. Vansant, P. Van der Voort and K.C. Vrancken (eds.), Characterization and Modification of the Silica Surface, Elsevier, Amsterdam, 1995.
10. H. Knozinger and P. Ratnasamy, Catalysis Rev. Sci. Eng., 17 (1978) 31.
11. J. Oscik, Adsorption, Harwood Ltd., Chichester, 1982.
12. H.L. Fleming, in: Fundamentals of Adsorption (A.I. Lapis, ed.), Amer. Inst. Chem. Eng., New York, 1987, p. 221.
13. K.K. Unger and U. Trudinger, Anal. Chem., 98 (1989) 145.
14. U. Trudinger, G. Muller and K.K. Unger, J. Chromatogr., 535 (1990) 111.
15. J. Nawrocki, M.P. Rigney and P.W. Carr, J. Chromatogr. A, 657 (1993) 229.
16. J.J. Pesek and V.H. Tang, Chromatographia, 39 (1994) 649.
17. H.M. Ismail, Colloids Surf. A, 97 (1995) 247.
18. A.V. Kiselev, Disc. Faraday Soc., 40 (1965) 205.
19. K.K. Unger, Porous Silica, its Properties and Use as Support in Column Liquid Chromatography, J. Chromatography Library, Elsevier, Amsterdam, vol. 16, 1979.
20. R.K. Iler, The Chemistry of Silica Solubility, Polymerisation, Colloid and Surface Properties and Biochemistry, Wiley, New York, 1979.
21. P. Van der Voort, I. Gillis-D'Hamers, K.C. Vrancken and E.F. Vansant, J. Chem. Soc., Faraday Trans., 87 (1991) 3899.
22. R.P.W. Scott, Adv. Chromatogr., 20 (1982) 167.
23. Z.E. Rassi, C. Gonnet and J.L. Rocca, J. Chromatogr., 125 (1976) 179.
24. J. Nawrocki, Chromatographia, 31 (1991) 177.
25. J. Nawrocki, Chromatographia, 31 (1991) 193.
26. J. Nawrocki, D.L. Moir and W. Szczepaniak, Chromatographia, 28 (1989) 143.
27. I. Novak and D. Berek, J. Chromatogr., 665 (1994) 33.
28. R. Leboda, Wiad. Chem. (Poland), 30 (1976) 677.
29. J. Nawrocki and B. Buszewski, J. Chromatogr., 449 (1988) 1.
30. B. Buszewski, J. Garaj, I. Novak and Z. Suprynowicz, J. Chromatogr., 446 (1988) 191.
31. R. Desai, M. Hussain and D.M. Ruthven, Can. J. Chem. Eng., 70 (1992) 699.
32. R. Desai, M. Hussain and D.M. Ruthven, Can. J. Chem. Eng., 70 (1992) 707.
33. P. Staszczuk, M. Jaroniec and R.K. Gilpin, Anal. Chim. Acta, 269 (1992) 157.
34. M. J. Jaycock and G.D. Parfitt, Chemistry of Interfaces, Harwood Ltd., Chichester, 1981.
35. J.A. Blackwell, Ph.D. Thesis, University of Minnesota, Minneapolis, 1991.
36. F.E. Bartell and Y. Fu, J. Phys. Chem., 33 (1929) 676.
37. R.S. Hiratsuka, S.H. Pulcinelli and C.V. Santilli, J. Non-Cryst. Solids, 121 (1990) 76.
38. G.E. de Souza Brito, C.V. Santilli and S.H. Pulcinelli, Colloids Surf. A, 97 (1995) 217.
39. K. Tanabe, Mater. Chem. Phys., 13 (1995) 347.

40. A. Matsumoto, K. Tsutsumi and K. Kaneko, Langmuir, 8 (1992) 2515.
41. A. Matsumoto, M. Ruike, T. Suzuki and K. Kaneko, Colloids Surf. A, 74 (1993) 15.
42. R.K. Gilpin, M.E. Gangoda, M. Jaroniec and X. Li, Ext. Abstracts of 21st Biennial Conf. on Carbon, Buffalo, New York, 1993, p. 444.
43. M.H. Chisholm, in: Inorganic Chemistry Towards the 21st Century, Amer. Chem. Soc., Washington, D.C., 1983, p. 243.
44. D.C. Bradley, Chem. Rev., 89 (1989) 1317.
45. D.C. Bradley, Adv. Chem. Radiochem., 15 (1972) 259.
46. H. Thoms, M. Epple, H. Viebrock and A. Reller, J. Mater. Chem., 5 (1995) 589.
47. C.J. Brinker and G.W. Scherer, Sol–Gel Science, Academic Press, New York, 1990.
48. D. Avnir, Mater. Chem., in press.
49. L.L. Hench and J.K. West, Chem. Rev., 90 (1990) 33.
50. J. Zarzycki, Heterogen. Chem. Rev., 1 (1994) 243.
51. H. Dislich, J. Non–Cryst. Solids, 73 (1985) 599.
52. H.P. Stephens, R.G. Dosh and F.V. Stohl, Ind. Eng. Chem. Prod. Res. Dev., 24 (1985) 19.
53. Z. Feng and L. Liu, J. Catal., 136 (1992) 423.
54. Z. Feng, W.S. Postula, A. Akgerman and R.C. Anthony, Ind. Eng. Chem. Res., 34 (1995) 78.
55. A.E. Stiegman, H. Eckert, G. Plett, S.S. Kim, M. Anderson and A. Yavronian, Chem. Mater., 5 (1993) 1591.
56. D. Avnir and V.R. Kaufman, J. Non–Cryst. Solids, 192 (1987) 181.
57. J. Samuel, Y. Polevaya, M. Ottolenghi and D. Avnir, Chem. Mater., 6 (1994) 1457.
58. R. Corriu, D. Leclercq, P. Lefevre, P.H. Mutin and A. Vioux, Chem. Mater., 4 (1992) 961.
59. P.M. Davis, C.J. Brinker and D.M. Smith, J. Non–Cryst. Solids, 142 (1992) 189.
60. C.J. Brinker, D.M. Smith, R. Deshpande, P.M. Davis, S. Hietala, G.C. Frye, C.S. Ashley and R.A. Assink, Catal. Today, 14 (1992) 155.
61. C.T. Kresge, M.E. Leonowicz, W.J. Ruth, J.C. Vartuli and J.S. Beck, Nature, 359 (1992) 710.
62. J.S. Beck, J.C. Vartuli, W.J. Roth, M.E. Leonowicz, C.T. Kresge, K.D. Schmitt, C.T.W. Chu, D.H. Olson, E.W. Sheppard, S.B. McCullen, J.B. Higgins and J.L. Schlenker, J. Am. Chem. Soc., 114 (1992) 10834.
63. J. Rathousky, A. Zukal, O. Franke and G. Schulz–Ekloff, J. Chem. Soc., Faraday Trans., 90 (1994) 2821.
64. C.Y. Chen, H.X. Li and M.E. Davis, Microporous Mater., 2 (1993) 17.
65. C.Y. Chen, S.L. Burkett, H.X. Li and M.E. Davis, Microporous Mater., 2 (1993) 27.
66. G.D. Stucky, Nature, 368 (1994) 317.
67. P.T. Tanev and T.J. Pinnavaia, Science, 267 (1995) 865.
68. A. Firouzi, D. Kumar, L.M. Bull, T. Besier, P. Sieger, Q. Huo, S.A. Walker, J.A. Zasadzinski, C. Glinka, J. Nicol, D. Margolese, G.D. Stucky and B.F. Chmelka, Science, 267 (1995) 1138.
69. P. Behrens, Adv. Mater., 5 (1993) 127.
70. P. Behrens and G.D. Stucky, Angew. Chem., 105 (1993) 729.
71. O. Franke, G. Schulz–Ekloff, J. Rathousky, J. Starek and A. Zukal, J. Chem. Soc. Chem. Commun., 93 (1993) 724.

72. J. Rathousky, A. Zukal, O. Franke and G. Schulz–Ekloff, J. Chem. Soc., Faraday Trans., 91 (1995) 937.
73. P.J. Branton, P.G. Hall and K.S.W. Sing, J. Chem. Soc. Chem. Commun., 93 (1993) 1257.
74. P.J. Branton, P.G. Hall and K.S.W. Sing, Adsorption, 1 (1995) 77.
75. P.L. Llewellyn, Y. Grillet, F. Schuth, H. Reichert and K.K. Unger, Microporous Mater., 3 (1994) 345.
76. S.J. Gregg and K.S.W. Sing, Adsorption, Surface Area and Porosity, 2nd ed., Academic Press, London, 1982.
77. M. Jaroniec and R. Madey, Physical Adsorption on Heterogeneous Solids, Elsevier, Amsterdam, 1988.
78. W. Rudzinski and D.H. Everett, Adsorption of Gases on Heterogeneous Solid Surfaces, Academic Press, London, 1992.
79. S. Ross and J.P. Olivier, On Physical Adsorption, Wiley, New York, 1964.
80. B. Wunderlich, Thermal Analysis, Academic Press, New York, 1990.
81. K.S.W. Sing, D.H. Everett, R.A.W. Haul, L. Moscou, R.A. Pierotti, J. Rouquerol and T. Siemieniewska, Pure Appl. Chem., 57 (1985) 603.
82. J. Rouquerol, D. Avnir, C.W. Fairbridge, D.H. Everett, J.H. Haynes, N. Pernicone, J.D.F. Ramsay, K.S.W. Sing and K.K. Unger, Pure Appl. Chem., 66 (1994) 1739.
83. D.M. Young and A.D. Crowell, Physical Adsorption of Gases, Butterworths, London, 1962.
84. D. Dollimore, Surface Technol., 4 (1976) 121.
85. D.H. Everett, G.D. Parfit, K.S.W. Sing and R.J. Wilson, J. Appl. Chem. Biotechnol., 24 (1974) 199.
86. J. Cortes, Advan. Colloid Interface Sci., 22 (1985) 151.
87. D.C. Havard and R.J. Wilson, J. Colloid Interface Sci., 57 (1976) 276.
88. M. Jaroniec and P. Brauer, Surf. Sci. Reports, 6 (1986) 65.
89. D. Avnir (ed.) The Fractal Approach to Heterogeneous Chemistry, Wiley, 1989.
90. M. Jaroniec, Adv. Colloid Interface Sci., 18 (1983) 149.
91. G.E. McGuire, L.M. Swanson, N.R. Parikh, S. Simko, P.S. Weiss, J.H. Ferris, R.J. Namanich, D.R. Chopra and A.R. Chourasia, Anal. Chem., 67 (1995) 199R.
92. J.P. Sibilis, A Guide to Materials Characterization and Chemical Analysis, VCH Publishers, New York, 1988.
93. R. Wiesendanger, Scanning Probe Microscopy and Spectroscopy Methods and Applications, University Press, New York, 1994.
94. J. DiNardo, Nanoscale Characterization of Surfaces and Interfaces, VCH Publishers, New York, 1994.
95. H. Cai, A.C. Hillier, K.R. Franklin, C.C. Nunn and M.D. Ward, Science, 266 (1994) 1551.
96. I. Langmuir, J. Am. Chem. Soc., 40 (1918) 1361.
97. A. Clark, The Theory of Adsorption and Catalysis, Academic Press, New York, 1970.
98. A.W. Adamson, Physical Chemistry of Surfaces, Wiley, New York, 1990.
99. A.W. Adamson and I. Ling, Advan. Chem. Ser., 33 (1961) 51.
100. J.P. Hobson, Can. J. Phys., 43 (1965) 1934.
101. A.W. Adamson, I. Ling, L. Dormant and M. Orem, J. Colloid Interface Sci., 21 (1966) 445.

102. M. v.Szombathely, P. Brauer and M. Jaroniec, J. Comput. Chem., 13 (1992) 17.
103. S. Brunauer, P.H. Emmett and E. Teller, J. Am. Chem. Soc., 60 (1938) 309.
104. R.H. Fowler and E.A. Guggenheim, Statistical Thermodynamics, Cambridge University Press, London, 1949.
105. J.H. de Boer, The Dynamical Character of Adsorption, Oxford University Press, Oxford, 1953.
106. P.H. Merz, J. Comput. Phys., 38 (1980) 64.
107. P. Brauer and M. Jaroniec, J. Colloid Interface Sci., 108 (1985) 50.
108. W.A. House, Colloid Sci., 4 (1982) 1.
109. C.F. Cerofolini and N. Re, La Rev. del Nuovo Cim., 16 (1993) 1.
110. S.S. Roginsky, Adsorption and Catalysis on Heterogeneous Surfaces, Acad. Sci. USSR, Moscow, 1948.
111. G.F. Cerofolini, Colloid Sci., 4 (1982) ch. 2.
112. M.M. Nederlof, W.H. van Riemsdijk and L.K. Koopal, Environ. Sci. Technol., 26 (1992) 763.
113. M. Jaroniec, Surf. Sci., 50 (1975) 553.
114. W.A. House, J. Chem. Soc. Faraday Trans. I, 74 (1978) 1045.
115. W.A. House, M. Jaroniec, P. Brauer and P. Fink, Thin Solid Films, 85 (1981) 87.
116. M. Heuchel, M. Jaroniec, R.K. Gilpin, P. Brauer and M. v.Szombathely, Langmuir, 9 (1993) 2537.
117. A.N. Tichonov, Dokl. AN SSSR, 39 (1943) 195; 153 (1963) 49.
118. A.N. Tichonov and V. Arsenin, Methods of Solution of Incorrect Tasks, Nauka, Moscow, 1979 (in Russian).
119. W.A. House, J. Colloid Interface Sci., 67 (1978) 166.
120. J. Papenhuijzen and L.K. Koopal, in: Adsorption from Solutions, R.H. Ottewill, C.H. Rochester and A.L. Smith (eds.), Academic Press, London, 1983, p. 211.
121. L.E. Brown and B.J. Travis, in: Fundamentals of Adsorption, A.L. Myers and G. Belfort (eds.), Amer. Inst. Chem. Eng., New York, 1984, p. 125.
122. J.A. Britten, B.J. Travis and L.E. Brown, AlChE Symp. Ser., 79 (1983) 1.
123. J. Jagiello, Langmuir, 10 (1994) 2785.
124. J.R. Conder and C.L. Young, Physicochemical Measurement by Gas Chromatography, Wiley, Chichester, 1979.
125. J. Roles and G. Guiochon, J. Chromatogr., 591 (1992) 233.
126. J. Roles and G. Guiochon, J. Chromatogr., 591 (1992) 245.
127. J. Roles and G. Guiochon, J. Chromatogr., 591 (1992) 267.
128. H. Guan, B.J. Stanley and G. Guiochon, J. Chromatogr., 659 (1994) 27.
129. J. Roles and G. Guiochon, J. Phys. Chem., 95 (1991) 4098.
130. J. Roles, K. McNerney and G. Guiochon, Anal. Chem., 64 (1992) 25.
131. J. Roles and G. Guiochon, Anal. Chem., 64 (1992) 32.
132. M. Pyda, B.J. Stanley, M. Xie and G. Guiochon, Langmuir, 10 (1994) 1573.
133. B.J. Stanley and G. Guiochon, J. Phys. Chem., 97 (1993) 8098.
134. B.J. Stanley and G. Guiochon, Langmuir, 11 (1995) 1735.
135. J. Jagiello, G. Ligner and E. Papirer, J. Colloid Interface Sci., 137 (1990) 128.
136. E. Papirer, S. Li, H. Balard and J. Jagiello, Carbon, 8 (1991) 1135.
137. I. Tijburg, J. Jagiello, A. Vidal and E. Papirer, Langmuir, 7 (1991) 2243.
138. W. Rudzinski, A. Waksmundzki, R. Leboda and Z. Suprynowicz, J. Chromatogr., 92 (1974) 25.

139. Z. Suprynowicz, M. Jaroniec and J. Gawdzik, Chromatographia, 9 (1976) 161.
140. J. Gawdzik, Z. Suprynowicz and M. Jaroniec, J. Chromatogr., 7 (1977) 131.
141. R. Leboda and S. Sokolowski, J. Colloid Interface Sci., 61 (1977) 365.
142. M. Jaroniec, X. Lu and R. Madey, J. Phys. Chem., 94 (1990) 5917.
143. S.P. Boudreau and W.T. Cooper, Anal. Chem., 59 (1987) 353.
144. R.K. Gilpin, M. Jaroniec and M.B. Martin–Hopkins, J. Chromatogr., 513 (1990) 1.
145. M.B. Martin–Hopkins, R.K. Gilpin and M. Jaroniec, J. Chromatogr. Sci., 29 (1991) 147.
146. M. Heuchel, M. Jaroniec and R.K. Gilpin, J. Chromatogr., 628 (1993) 59.
147. M. Jaroniec and J. Choma, Proc. of 5th Int. Conf. Fundamentals of Adsorption, Asilomar, CA, 1995.
148. L.E. Drain and J.A. Morrison, Trans. Faraday Soc., 49 (1953) 840.
149. L.E. Drain and J.A. Morrison, Trans. Faraday Soc., 48 (1952) 316.
150. J.A. Morrison, J.M. Los and L.E. Drain, Trans. Farady Soc., 47 (1951) 1023.
151. L.E. Drain and J.A. Morrison, Trans. Faraday Soc., 49 (1953) 654.
152. L.M. Dormant and A.W. Adamson, J. Colloid Interface Sci., 38 (1972) 285.
153. M. Jaroniec and W. Rudzinski, Colloid Polymer Sci., 253 (1975) 683.
154. W. Rudzinski, M. Jaroniec, S. Sokolowski and G.F. Cerofolini, J. Czech. Phys., B25 (1975) 891.
155. W. Rudzinski and M. Jaroniec, Surf. Sci., 42 (1974) 552.
156. B.K. Oh and S.K. Kim, J. Chem. Phys., 67 (1977) 3416.
157. V.A. Bakaev and W.A. Steele, Langmuir, 8 (1992) 1372.
158. V.A. Bakaev and W.A. Steele, Langmuir, 8 (1992) 1379.
159. J.A. Lum Wam and L.R. White, J. Chem. Soc. Faraday Trans., 87 (1991) 3051.
160. V. Bolis, B. Fubini, E. Garrone, C. Morterra and P. Ugliengo, J. Chem. Soc. Faraday Trans., 88 (1992) 391.
161. E. Garrone, V. Bolis, B. Fubini and C. Morterra, Langmuir, 5 (1989) 892.
162. B.G. Aristov and A.V. Kiselev, Kolloid. Zh., 27 (1965) 246.
163. M. Jaroniec, W. Rudzinski, S. Sokolowski and R. Smarzewski, Colloid Polymer Sci., 253 (1975) 164.
164. Y. Bereznitski, M. Jaroniec and M. Kruk, J. Chromatogr., to be published.
165. T. Czajkowska, M. Jaroniec and B. Buszewski, J. Chromatogr., submitted.
166. J.P. Olivier, W.B. Conklin and M. v. Szombathely, Stud. Surface Sci. Catal., 87 (1994) 81.
167. O. Sneh and S.M. George, J. Phys. Chem., 99 (1995) 4639.
168. A. Waksmundzki, M. Jaroniec and L. Lajtar, Ann. Soc. Chim. Polon., 49 (1975) 1197.
169. R.H. van Dongen, Surf. Sci., 39 (1973) 341.
170. J. Whalen, J. Phys. Chem., 71 (1967) 1557.
171. J.B. Sorrell and R. Rowan, Anal. Chem., 42 (1970) 1712.
172. A. Waksmundzki, J. Toth, M. Jaroniec and W. Rudzinski, Ann. Soc. Chim. Polon., 49 (1975) 1003.
173. R. Leboda, A. Waksmundzki and S. Sokolowski, Ann. Soc. Chim. Polon., 50 (1976) 1716.
174. R. Leboda, A. Waksmundzki and S. Sokolowski, Chem. Anal., 22 (1977) 42.
175. R. Leboda, S. Sokolowski and J. Rynkowski, Chem. Anal., 22 (1977) 55.
176. S.L. Kuo, A.L. Hines and N. Dural, Sep. Sci. Technol., 26 (1991) 1077.

177. S. Vasquez, J. Chem. Soc. Faraday Trans., 88 (1992) 2051.
178. D. Hinman and G.D. Halsey, J. Phys. Chem., 81 (1977) 739.
179. P. Staszczuk, M. Jaroniec and R.K. Gilpin, in: Microbalance Techniques, J. Keller and E. Robens (eds.), Multi–Science Publ., Brentwood, 1994, 101.
180. P. Carniti, A. Gervasini and A.K. Aurox, J. Catal., 150 (1994) 274.
181. W.H. van Riemsdijk, G.H. Bolt, L.K. Koopal and L.K. Blaakmeer, J. Colloid Interface Sci., 109 (1986) 210.
182. W.H. van Riemsdijk, J.C. De Witt, L.K. Koopal and G.H. Bolt, J. Colloid Interface Sci., 116 (1987) 511.
183. L.K. Koopal and W.H. van Riemsdijk, J. Colloid Interface Sci., 128 (1989) 188.
184. W. Rudzinski, R. Charmas and S. Partyka, Langmuir, 7 (1991) 354.
185. W. Rudzinski, R. Charmas, S. Partyka, F. Thomas and J. Bottero, Langmuir, 8 (1992) 1154.
186. C. Contescu, J. Jagiello and J.A. Schwarz, Langmuir, 9 (1993) 1754.
187. A. Dąbrowski, M. Jaroniec and J. Ościk, in: E. Matijevic (ed.), Surface and Colloid Science, vol.14, Plenum Press, New York, 1987, p. 83.
188. A. Dąbrowski and M. Jaroniec, Adv. Colloid Interface Sci., 27 (1987) 211.
189. A. Dąbrowski and M. Jaroniec, Adv. Colloid Interface Sci., 31 (1990) 155.

This Page Intentionally Left Blank

A. Dąbrowski and V.A. Tertykh (Editors)
Adsorption on New and Modified Inorganic Sorbents
Studies in Surface Science and Catalysis, Vol. 99

Chapter 2.4
Adsorption kinetics on real surfaces

G.F. Cerofolini

EniChem - Istituto Guido Donegani, 28100 Novara, Italy

1. THE INTRINSICALLY HETEROGENEOUS NATURE OF SURFACES OF CATALYTIC INTEREST

In *homogeneous catalysis* reactants and catalyst belong to the same (liquid or gas) phase. If products too are in the same phase (that happens in many situations), they must be separated from the catalyst at the end of reaction, that may render the overall process quite expensive.

A way to overcome this difficulty is *catalyst heterogenization.* With this technique the catalyst, whose activity has been identified in a homogeneous phase, is distributed onto a relatively inert, highly dispersed, solid support, thus originating the catalytic system:

$$\text{catalytic system} = \{\text{catalyst}, \text{support}\}$$

Catalyst heterogenization, however, requires in most cases a certain degree of manipulation of both the catalyst and the support (for instance, to allow for grafting), that can modify the catalytic activity of the unsupported catalyst. Moreover, a truly inert support (like SiO_2 seems to be) is an ideal concept because the unavoidable chemical defects (hydroxyl groups in the above example), stoichiometric defects (e.g., oxygen vacancies) or, in the case of crystalline supports, crystalline defects (e.g., grain borders) unavoidably flaw the inertness of the substrate and interfere with the catalytic activity. Even though the heterogenization process is introduced with the aim of minimizing the chemical role of the support, it may however have an antagonistic or synergic catalytic activity:

$$\text{activity (catalytic system)} \neq \text{activity (catalyst)} + \text{activity (support)}$$

A spectacular role of the substrate on the catalytic activity is displayed by the stereospecific character imparted to polypropylene by the $MgCl_2$ substrate in Ziegler–Natta catalysis.

Heterogeneous catalysis is essentially based on the special reactivity of surface sites, due either to crystalline or stoichiometric defects. Due to the need of achieving a very high surface area and to have unsaturated surface sites with strong chemical reactivity, the preparation of highly dispersed solids is often based on processes (like milling) responsible for phenomena (fracture, plastic deformation, etc.) where a macroscopic energy is imparted to few degrees of freedom. The concentration of a large energy on few degrees of freedom,

with the consequent creation of highly defective sites, is unavoidable during the preparation of highly dispersed solids even when the process is formed by close-to-equilibrium steps.

Consider, for instance, a silica aerogel prepared via the sol-gel technique with solvent supercritical extraction [1]. Due to the steric constraints of the embedded solvent during gelling, the silica polymer does not attain the proper configuration of the condensed phase. Supercritical extraction concentrates the extra energy of this configuration on the skeleton which does not undergo a structural collapse only thanks to the partially covalent nature of the Si – O bond. This extra energy will however result in highly strained or deformed bonds which are therefore expected to have some chemical reactivity.

It is therefore not surprising that silica aerogels prepared from organometallic precursors manifest a catalytic activity for the CO oxidation to CO_2 with molecular O_2 at 850 K or above, while a similar activity is not found for silica obtained from inorganic reagents [2]. A plausible pathway is sketched in Fig. 1, and assumes that the centre (**1**), formed by highly strained Si···O bonds produced in the gel by the steric constraints of the embedded alcohol and remaining after the relatively soft heat treatment of supercritical drying, reacts with atmospheric oxygen to form the double-peroxidic centre (**2**); the reaction of (**2**) with CO produces the peroxidic centre (**3**), which eventually reacts with CO thus restoring the original strained siloxanic centre (**1**):

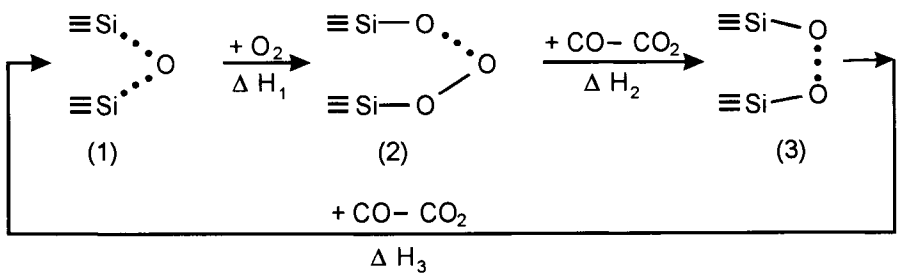

$$-\triangle H_1 = 2E_b(\mathrm{Si-O}) + E_b(\mathrm{O-O}) + E_b(\mathrm{O\cdots O}) - 2E_b(\mathrm{Si\cdots O}) - E_b(\mathrm{O=O})$$
$$-\triangle H_2 = E_b(\mathrm{C=O}) - E_b(\mathrm{O-O})$$
$$-\triangle H_3 = E_b(\mathrm{C=O}) + 2E_b(\mathrm{Si\cdots O}) - 2E_b(\mathrm{Si-O}) + E_b(\mathrm{O\cdots O})$$

Figure 1. The hypothesized cycle for CO conversion to CO_2 on silica aerogel, and the associate enthalpy changes.

The overall pathway is possible only when each step is energetically favoured; assuming the bond energies E_b as given in Ref. [3], the first step is possible only when

$$E_b(\mathrm{Si\cdots O}) - \tfrac{1}{2}E_b(\mathrm{O\cdots O}) < 3.0 \text{ eV}$$

while the third step is possible only for

$$E_b(\mathrm{Si\cdots O}) - \tfrac{1}{2}E_b(\mathrm{O\cdots O}) > 2.1 \text{ eV}$$

The above conditions are simultaneously satisfied, and the cycle is therefore possible, only for those sites with

$$2.1 \text{ eV} < E_b(\text{Si}\cdots\text{O}) - \tfrac{1}{2}E_b(\text{O}\cdots\text{O}) < 3.0 \text{ eV}$$

If, as expected, $E_b(\text{O}\cdots\text{O})$ is low (say, $E_b(\text{O}\cdots\text{O}) < 1$ eV), the catalytic centre for CO oxidation is formed by disiloxanic sites with $E_b(\text{Si}\cdots\text{O})$ around 3 eV (± 0.5 eV), vs. an unstrained bond energy of 4.8 eV.

The non-ideality of catalyst surfaces has ever been one the major difficulties in understanding the detailed mechanisms of contact catalysis. The *Advances in Catalysis* were opened in 1948 by an article of Taylor on *the heterogeneity of catalyst surfaces for chemisorption* [4]; that the matter was not easy to model is understood by observing that 41 years later *the role of particle size on the catalytic activity of supported metals* was the subject of of another review in the same series [5]; moreover, the family of solids of catalytic interest has since Taylor's review been increased by the availability of new techniques for the preparation of highly dispersed solids, like crystalline zeolites and amorphous aerogels.

In view of the above considerations, it is therefore not surprising that, with practically no exception, heterogeneous catalysts are characterized by a distribution of sites with a wide adsorption energy dispersion with respect to any given test gas; *the role of surface heterogeneity in adsorption* [6] is therefore one of the key factors which must taken into account for understanding the behaviour of highly dispersed solids.

Since the *adsorption* of reactants and *desorption* of products are unavoidable and fundamental steps of heterogeneous catalysis, there is a need of understanding the kinetics of adsorption-desorption phenomena on heterogeneous surfaces. In practically all situations the reaction involves two or more reactants, so that chemically interesting kinetics are multicomponent. This is immediately understood either considering the Rideal mechanism:

$$\begin{array}{rcl} \text{ss}^* + \text{A} & \rightarrow & \text{ss} - \text{A}^* \\ \text{ss} - \text{A}^* + \text{B} & \rightarrow & \text{ss}^* + \text{AB} \\ \hline \text{A} + \text{B} & \xrightarrow{\text{ss}^*} & \text{AB} \end{array}$$

in which the reaction occurs via the collision of an activated species A*, formed after the adsorption of A on the active surface site ss*, with a physisorbed or gas-phase molecule B (the star denotes a reactive configuration), or considering the Langmuir–Hinshelwood mechanism:

$$\begin{array}{rcl} \text{ss}^* + \text{A} & \rightarrow & \text{ss} - \text{A}^* \\ \text{ss}^* + \text{B} & \rightarrow & \text{ss} - \text{B}^* \\ \text{ss} - \text{A}^* + \text{ss} - \text{B}^* & \rightarrow & 2\text{ss}^* + \text{AB} \\ \hline \text{A} + \text{B} & \xrightarrow{\text{ss}^*} & \text{AB} \end{array}$$

in which the reaction occurs between two adsorbed species.

Though there is an appreciable amount of work devoted to multicomponent adsorption on heterogeneous surfaces (mainly due to Jaroniec and coworkers, reviewed in Ref. [7]),

this work will be concentrated on the simpler problem of single-component adsorption-desorption kinetics on heterogeneous surfaces, the aim being that of producing a rigorous and comprehensive extension of the theory of adsorption equilibrium on heterogeneous surfaces. In fact, a theory of adsorption-desorption kinetics on heterogeneous surfaces as general as that developed for equilibrium adsorption is still missing, and only limited attempts to take into account the role of surface non-idealities on adsorption-desorption kinetics have been contributed.

This fact is especially disappointing because heterogeneity is expected to play in kinetics a role as important as, or even more important than, in equilibrium. Moreover the theory of equilibrium adsorption on heterogeneous surfaces is limited to physisorption, while the theory of adsorption-desorption kinetics on heterogeneous surfaces includes physisorption and chemisorption and extends up to heterogeneous catalysis.

Rather than trying to describe the sparse and occasional results hitherto reported, this work is devoted to the foundation of a general and comprehensive theory of adsorption-desorption kinetics. The emphasis, however, will not be concentrated on the formal mathematical aspects of the theory, but rather on its physical bases; in particular, the validity of the methods developed will be checked by verifying how they are able to explain the observed experimental behaviours. Among them one plays a special role — the time-logarithm law known as Elovich equation.

2. A RATE EQUATION NAMED "ELOVICH"

Of the many isothermal kinetics observed on real surfaces for different processes like oxidation, chemisorption and desorption, only one has deserved a special attention — the time-logarithm law

$$\delta(t) = r_E \ln(t/t_m) \tag{1}$$

where $\delta(t)$ is the amount of matter involved in the kinetics at time t, and r_E and t_m are two characteristic parameters.

Though Eq. (1) is usually referred to as "Elovich equation", its observation was first reported by other authors. In fact, a time-logarithm law was first observed by Tamman and coworkers in 1922 for the *oxidation* of metals [8]. Tamman work was rediscovered much later by Vernon [9], who observed that the low temperature oxidation of iron obeys Eq. (1). The oxidation of a number of metals and semiconductors has since then been reported to be described by Eq. (1); among them Cr, Mn, Fe, Co, Ni, Cu, Zn, Cd, Si, Sn, Pb, Sb and Bi can be mentioned. The first observation of a *chemisorption* process obeying Eq. (1) was probably reported by Zeldowitch in 1934 [10], but it was only after its rediscovery by Elovich and coworkers [11, 12] that this equation became of wide use. It is on the basis of Ref. [12] that the time-logarithm law (1) took the name of "Elovich equation", though in view of Ref. [10] it could be more appropriately called "Zeldowitch equation"; it is also noted that in the German papers the person now commonly known as Elovich transliterated his name "Elowitz" [11] (this short historical note is taken from Landsberg [13] and reproduced here for completeness). A list of chemisorption systems obeying the Elovich equation is given in Ref. [14]. More recent, and not equally widespread, is the observation that *desorption* isotherms are often described by the Elovich equation [14].

Even though formula (1) gives an adequate rationalization of numerous kinetics over several orders of magnitude of time, it however fails at short times because for $t \leq t_m$ it gives $\delta(t) \leq 0$. A convenient way to circumvent this difficulty is to describe the kinetics with the following relationship:

$$\delta^m(t) = r_E \ln(1 + t/t_m) \tag{2}$$

which makes up for inability of Eq. (1) to describe the early stages of the kinetics.

If one wants that the total chemisorbed, desorbed or oxidized amount maintains finite even in the limit $t \to +\infty$, the long-time behaviour of Eq. (2) must also be modified since $t \to +\infty \Rightarrow \delta^m(t) \to +\infty$. The simplest change which can be brought is a cut-off:

$$\delta^{mM}(t) = \begin{cases} r_E \ln(1 + t/t_m) & \text{for } 0 \leq t < t_M \\ \delta_M & \text{for } t_M \leq t \end{cases} \tag{3}$$

where δ_M is the maximum amount of matter involved in the kinetics, and

$$t_M = t_m[\exp(\delta_M/r_E) - 1] \tag{4}$$

It is immediately verified that Eqs. (1) and (2) (and hence Eq. (3) for $t \leq t_M$) satisfy the following differential equation:

$$\frac{d\delta}{dt} = \frac{r_E}{t_m} \exp\left(-\frac{\delta}{r_E}\right) \tag{5}$$

which will be proved useful in suggesting possible underlying physical mechanisms.

The *macroscopic* meaning of the Elovich parameters is straightforward: t_m is a characteristic time below which the logarithmic behaviour is no longer observed, t_M is the time required to complete the process, while r_E/t_m is the initial desorption rate.

The *kinetics of adsorption and desorption and the Elovich equation* have been the matter of a comprehensive review by Aharoni and Tompkins in 1970 [14]. At that time, however, concepts now pervasive in physical chemistry of surfaces like fractality were not known, the mathematical theory of adsorption equilibrium on heterogeneous surfaces was at its beginning, and the notion of equilibrium surfaces had not demonstrated yet its usefulness in the understanding of adsorption phenomena on real surfaces. In view of these facts there is a space for another work, which however does not intend to be as comprehensive as that of Aharoni and Tompkins, but rather aims: to study the Elovich behaviour met in new situations, to elucidate the theoretical origin of Eq. (3), and to relate the macroscopic empiric parameters r_E, and t_m and t_M to *microscopic* quantities.

Reversing the historical order, this work will deal first with desorption and then with chemisorption.

3. ADSORPTION EQUILIBRIUM

A theory as rigorous and comprehensive as the theory of adsorption equilibrium on heterogeneous surfaces has not been developed yet for the description of adsorption [desorption] kinetics on [from] heterogeneous surfaces. This work aims to fill, at least partially, this gap and new methods are developed for kinetics in strict analogy to what was done

for equilibrium, in this way extending the pioneering work of Jaroniec and Madey [7]. The methods developed are applied to a special case, the Elovich desorption isotherm, which plays in kinetics a similar role to that played by the Freundlich or Temkin isotherms in adsorption equilibrium.

3.1. Adsorption isotherms on homogeneous surfaces

The theory of adsorption equilibrium on homogeneous surfaces is so formalized as to be considered a set of statistico-mechanical exercises [15]. When the adsorbed molecules can be considered as structureless particles, practically all models consider the adsorbed phase as a sequence of layers, each stabilized by the adsorption field generated by the underlying one and described either as a two-dimensional (2D) lattice or as a 2D van der Waals gas.

The following classification summarizes the most frequently considered adsorption models:

- submonolayer adsorption
  - localized
    - without lateral interactions (Langmuir)
    - with lateral interactions (Fowler–Guggenheim)
  - mobile
    - without lateral interactions (Volmer)
    - with lateral interactions (Hill–de Boer)

- multilayer adsorption
  - all layers localized
  - first n layers localized, top layers mobile (Broekhoff–van Dongen)
  - all layers mobile

An exception is represented by the Frenkel–Halsey–Hill theory, which describes the multilayer adsorbed film as a liquid perturbed by the presence of a surface.

The complexity of the description increases when the admolecule holds at the surface two or more sites or when the admolecule internal configuration may change after adsorption. For simplicity these situations will not be considered; Ref. [16] can be consulted for a survey of the mathematical methods required in these cases.

The Langmuir and Volmer equations are special cases of the Fowler–Guggenheim and Hill–de Boer equations, respectively, in which lateral interactions are allowed to vanish; the Brunauer–Emmett–Teller equation is a special case of the Broekhoff–van Dongen equation with $n = \infty$ and null lateral interactions; the model in which all layers are mobile is a special case of Broekhoff–van Dongen model with $n = 0$.

The Broekhoff–van Dongen isotherm allows for multilayer adsorption with lateral interactions and predicts the possibility of 2D phase transitions in each layer [17]. The most spectacular evidence for 2D phase transitions concerns the adsorption of heavy noble gases on highly homogeneous non-polar surfaces of low atomic weight (typically, exfoliated graphite obtained by thermal dissociation of its intercalation compound with $FeCl_3$). This situation guarantees that the adsorbate-adsorbate interaction prevails on adsorbent-adsorbate interaction and makes it possible the observation of phase transitions in each layer. See Ref. [18] for a short overview of this subject.

3.2. Adsorption isotherms on heterogeneous surfaces

Excepting these really few ideal cases and regardless of the fact that the BET method is routinely used for the determination of the monolayer volume even for systems which are poorly described by the BET equation, the above equations are not found to describe accurately adsorption equilibrium on most adsorbents of chemical interest.

These adsorbents are characterized by high dispersion and energy heterogeneity, typical examples being zeolites (with *queer shape*) and aerogels (which at certain scale lengths can be viewed as *fractals*). The concept of queer shape was introduced by Cerofolini to denote systems whose surface area increases in proportion to the volume, so that the surface contribution to the chemical potential does not disappear even in the thermodynamic limit [19]; the concept of fractal has become of widespread use in physical chemistry since the observation of Pfeifer, Avnir and Farin that the surface area of many adsorbents diverges in the limit of vanishing area of the adsorbate molecule [20, 21].

Of the equilibrium adsorption isotherms observed on real surfaces, three hold particular positions. They are: the Temkin isotherm, the Freundlich isotherm, and the Dubinin–Radushkevich isotherm, and are reviewed in Refs. [22, 23]. The analysis carried out in Ref. [24] of several previously reported, often quoted, adsorption systems has shown that the Freundlich and the Dubinin–Radushkevich isotherms are the high-pressure and low-pressure limits, respectively, of a unique isotherm referred to as FDR. In turn, the FDR isotherm is a special case of a more general isotherm proposed by Jaroniec [25] on the basis of a previous idea of Heer [26].

The FDR isotherm, improved for describing multilayer formation, is perhaps the function with the minimum number of parameters able to represent the most often quoted experimental isotherms (namely: N_2, O_2 or Ar on TiO_2 (rutile); N_2 or Ar on MgO; N_2 or Ar on hydroxylated SiO_2; N_2 or Ar on non-porous Al_2O_3 (γ or δ aluminas); N_2, C_6H_6 or n-C_6H_{14} on graphitized carbon blacks; and Ar, Kr or Xe on porous Ag); to give an idea of the quality of the FDR description of real adsorption systems, it may be mentioned that it describes accurately the adsorption of argon on porous silver over 10 orders of magnitude of pressure and 7 orders of coverage [24]. That the FDR isotherm is not simply a fitting scheme for all smooth isotherms (as the BET isotherm manifestly is in the neighborhood of the B point) is demonstrated by the following arguments [24]:

- for any given surface a unique energy distribution function explains the observed FDR behaviours for different gases provided that the adsorption energies are scaled by a factor which depends on the adsorbent-adsorbate pair; and
- the "frozen temperature" T_F (defined later, in Eq. (9)) determined for different surfaces using the same probe gas varies from one surface to another in relation to the preparation temperature just as expected.

Adsorption on heterogeneous surfaces is conveniently described in terms of ideal adsorption (*i.e.*, a process described by one or the other model described in the scheme of section 3.1.) on a surface characterized by an adsorption-energy distribution function $\varphi(q)$, where $\varphi(q)\mathrm{d}q$ respresents the fraction of surface with adsorption energy between q and $q + \mathrm{d}q$. This picture is usually referred to as *homotattic patch approximation.*

In this approximation the overall isotherm (*i.e.*, the functional relationship $\theta(p)$ giving the mean surface coverage θ as a function of the equilibrium pressure p at constant temperature T) is the local isotherm (*i.e.*, the functional relationship $\Theta(p, q)$ giving the

coverage Θ of each homotattic patch with adsorption energy q as a function of p at constant T) averaged over all the surface:

$$\theta(p) = \int_{\mathcal{D}_q} \Theta(p,q)\varphi(q)\mathrm{d}q \tag{6}$$

where $\mathcal{D}_q$ is the set of allowed values of q. The usual choices for $\Theta(p,q)$ are the Langmuir isotherm:

$$\Theta(p,q) = \frac{p}{p + p_{\mathrm{L}} \exp(-q/k_{\mathrm{B}}T)} \tag{7}$$

or the Jovanovic isotherm:

$$\Theta(p,q) = 1 - \exp\left(-\frac{p}{p_{\mathrm{J}}} \exp\left(\frac{q}{k_{\mathrm{B}}T}\right)\right) \tag{8}$$

where p_{L} and p_{J} are two characteristic pressures whose meaning is not of interest here. The above choices are mainly related to a criterion of simplicity. It is however noted that though the Langmuir model is a highly simplified description of adsorption on homogeneous surfaces, its theoretical bases are well ascertained (see however the recent criticism of Ref. [27]) and can be extended to the description of multilayer adsorption on heterogeneous surfaces in the BET region by a simple formal change [28]. By contrast, the validity of the Jovanovic isotherm (an adsorption isotherm proposed by Jovanovic in 1969 to consider the desorption-hindering collision of a desorbing molecule against gas-phase molecules; it was first derived with kinetic arguments [29], but a statistico-mechanical derivation is also known [30]) is still controversial, though the mathematical methods for the solution of the integral adsorption equation whose kernel is the Jovanovic isotherm are well established [7, 23, 31]. Though there is some arbitrariness in the choice of the local isotherm, it has been shown that, quite irrespective of the assumed theoretical adsorption model [32], the Temkin isotherm is related in this scheme to a uniform energy distribution fuction, while the FDR isotherm is related to an exponential distribution function with Gaussian cut-off [33]. These distributions are special cases of the distribution function of any equilibrium surface.

Though this interpretation is now commonly accepted in the interpretation of the classic empirical isotherms (Eq. (23), Chapter 6), it must be mentioned that other approaches have been proven to account for them [34].

3.3. Adsorption isotherms on equilibrium surfaces

The reasons why the FDR and Temkin are so frequently observed on real adsorbents is that the uniform and exponential distributions are the energy distribution functions of *equilibrium surfaces*, *i.e.* of heterogeneous surfaces grown in equilibrium conditions at high temperature and quenched in that configuration. The concept of equilibrium surface was demonstrated useful to explain the most common adsorption equilibrium isotherms by Cerofolini. In particular, the classic istherms proposed by Freundlich, Dubinin and Radushkevich, and Temkin have found a natural explanation in the frame of this theory: the FDR isotherm corresponds to the weak heterogeneity limit [35], while the Temkin isotherm corresponds to the limit of strong heterogeneity [36].

In its most elementary formulation, in which lateral interactions are ignored and the Dubinin–Radushkevich behaviour is consequently lost, the equilibrium surface is characterized by an adsorption energy distribution $\varphi_{eq}(q)$ given by

$$\varphi_{eq}(q) = \begin{cases} 0 & \text{for } 0 \leq q < q_m \\ r_F \exp\left(-\dfrac{q - q_m}{k_B T_F}\right) & \text{for } q_m \leq q < q_M \\ 0 & \text{for } q_M \leq q < +\infty \end{cases} \tag{9}$$

where T_F is a frozen temperature related to the temperature at which the surface was grown in equilibrium conditions, and r_F is a normalization factor such that

$$\int_{q_m}^{q_M} \varphi_{eq}(q) dq = 1$$

This condition gives:

$$r_F = \frac{1}{1 - \exp\left(-\dfrac{q_M - q_m}{k_B T_F}\right)}$$

According to the analysis of Cerofolini [33], in the weak heterogeneity limit, *i.e.* for $q_M - q_m \gg k_B T_F$, the adsorption isotherm behaves in the high pressure region as

$$\theta(p) \simeq \theta_F(p) := \begin{cases} (p/p_m)^s & \text{for } p \leq p_m \\ 1 & \text{for } p_m < p \end{cases} \tag{10}$$

where $p_m = p_L \exp(-q_m/k_B T)$ and $s = T/T_F$; while in the strong heterogeneity limit, *i.e.* for $q_M - q_m \lesssim k_B T_F$ but appreciably higher than $k_B T$, the distribution function is approximately uniform over $\mathcal{D}_q$ and the overall adsorption isotherm behaves in the high pressure region as

$$\theta(p) \simeq \theta_T(p) := \begin{cases} 0 & \text{for } 0 \leq p < \exp\left(-\dfrac{q_M - q_m}{k_B T}\right) \\ 1 + \dfrac{k_B T}{q_M - q_m} \ln\left(\dfrac{p}{p_m}\right) & \text{for } p_m \exp\left(-\dfrac{q_M - q_m}{k_B T}\right) < p \leq p_m \\ 1 & \text{for } p_m < p \end{cases} \tag{11}$$

Equations (10) and (11) are just the Freundlich and Temkin isotherms, respectively.

To a certain extent the theory of adorption equilibrium on real surfaces is well established: there are several reviews (see, for instance, Refs. [28, 31, 37]) and two extended monographs covering this subject [7, 23]; moreover, several simulation codes are available for the extraction of the energy distribution function from the observed adsorption isotherm.

Trying to extend the description from equilibrium to kinetics, similarities and differences are observed. The similarities concern the different theoretical descriptions which are possible even for ideal surfaces (essentially related to the possible kinetic order) but do not describe the kinetics observed in practical cases; the differences concern the fact that a theory of adsorption-desorption kinetics as general and comprehensive as the theory of

adsorption equilibrium does not exist yet for real surfaces. This work is devoted to make up for this lack.

Though this approach seems the most economic one, it is worthwhile noticing that an inverse approach can also be used. For instance, Crickmore and Wojciechoski proposed a description of adsorption equilibrium on heterogeneous surfaces in terms of rate processes [38].

4. DESORPTION KINETICS FROM HOMOGENEOUS SURFACES

The rate equations, giving the time derivative $d\Theta/dt$ of the coverage Θ of each homogeneous zone forming the surface, are assumed to be of the form

$$-\frac{d\Theta}{dt} = \frac{1}{\tau}\Theta^{\nu} \tag{12}$$

where τ is a characteristic desorption time in principle variable along the surface and ν is the reaction order. The analysis will be limited to kinetics of the first order ($\nu = 1$) and second order ($\nu = 2$), and to desorption time τ independent of Θ.

If $\Theta_0(\tau)$ is the local coverage at time $t = 0$, the rate equation (12) can be solved for all ν by separation of variables:

$$-\int_{\Theta_0(\tau)}^{\Theta} \frac{d\Theta}{\Theta^{\nu}} = \frac{t}{\tau} \tag{13}$$

thus giving a function $\Theta = \Theta_\nu(t, \tau)$.

Equation (13) can be solved in closed form both for first- and second-order kinetics. In fact, defining the coverage variation

$$\Delta_\nu(t, \tau) = \Theta_0(\tau) - \Theta_\nu(t, \tau)$$

one has

$$\Delta_1(t, \tau) = \Theta_0(\tau)[1 - \exp(-t/\tau)] \tag{14}$$

for first order kinetics, and

$$\Delta_2(t, \tau) = \frac{\Theta_0^2(\tau)t}{\Theta_0(\tau)t + \tau} \tag{15}$$

for second order kinetics.

The characteristic desorption time τ is easily related to energetic properties of the surface. In fact, elementary kinetic considerations give

$$\tau = \tau_0 \exp\left(\frac{E}{k_B T}\right) \tag{16}$$

where τ_0 is a characteristic time, E is the activation energy for desorption, k_B is the Boltzmann constant, and T is the surface temperature. In most cases one may assume $\tau_0 \approx 10^{-13}$ s.

5. DESORPTION KINETICS FROM HETEROGENEOUS SURFACES

In general the desorption kinetics from patchwise heterogeneous surfaces are given by:

$$\delta_\nu(t) = \int_{\mathcal{D}_\tau} \Delta_\nu(t,\tau)\phi(\tau)\mathrm{d}\tau \tag{17}$$

where $\phi(\tau)\mathrm{d}\tau$ is the fraction of surface with desorption time between τ and $\tau + \mathrm{d}\tau$ and $\mathcal{D}_\tau$ is the support of $\phi(\tau)$.

Equation (17) originates two problems:

- the *inverse problem*, related to the extraction of the distribution function $\phi(\tau)$ when the overall kinetics $\delta_\nu(t)$ are experimentally known; and
- the *direct problem*, related to the calculation of the overall kinetics $\delta_\nu(t)$ which are expected for a class of surfaces for which the distribution function $\phi(\tau)$ can be assumed as given.

The direct problem is not simply the calculation of the integral (17) for given $\phi(\tau)$, but also requires the specification of this function for the assigned surface preparation conditions.

The overall amount $\delta_\nu(t)$ desorbed at time t depends on the desorption-time distribution function $\phi(\tau)$ and on the set of initial conditions $\Theta_0(\tau)$. Clearly enough, if one wants to extract from the experimental function $\delta_\nu(t)$ the distribution function $\phi(\tau)$, one must operate in conditions for which $\Theta_0(\tau)$ is known. In the sequel the attention will therefore be limited to the case of Θ_0 constant with τ. If $\Theta_0(\tau)$ does not depend on τ, one may, without loss of generality, take $\Theta_0 = 1$, so that Eqs. (14) and (15) become

$$\Delta_1(t,\tau) = 1 - \exp(-t/\tau) \tag{18}$$

and

$$\Delta_2(t,\tau) = \frac{t}{t+\tau} \tag{19}$$

respectively.

At this stage of development the theory is already mature to allow the extraction of $\phi(\tau)$ from $\delta_\nu(t)$. In fact, since both kernels (14) and (15) do not depend on t and τ separately, but only on the ratio t/τ, the integral (17) can be reduced to a convolution integral which can be solved for $\phi(\tau)$ by standard techniques taken from the theory of Fourier transform. These rigorous methods, however, are not flexible and do not allow people to understand the physical meaning of the parameters contained in the experimental datum.

The theory proceeds more easily specifying the desorption time τ as in Eq. (16). Since in most cases τ_0 may be assumed to be a constant, $\tau_0 \approx 10^{-13}$ s, the unique random variable characterizing the surface in desorption experiments is E. Rather than describing the surface with the distribution function $\phi(\tau)$, it is convenient to describe the surface with the distribution function $\varphi(E)$, where $\varphi(E)\mathrm{d}E$ is the fraction of surface with desorption energy between E and $E + \mathrm{d}E$. Since in the desorption kinetics of physisorbed molecules one may reasonably assume that E coincides with the adsorption energy q, and since $\varphi(q)$ can be determined from adsorption equlibrium isotherms, the above choice of the independent variable gives the possibility to compare the results of the theory under development with those of a well established theory.

Defining

$$\hat{\Delta}_\nu(t, E) = \Delta_\nu(t, \tau(E))$$

where $\tau(E)$ is given by Eq. (16), Eq. (17) becomes

$$\delta_\nu(t) = \int_0^{+\infty} \hat{\Delta}_\nu(t, E)\varphi(E)\mathrm{d}E \tag{20}$$

Equation (20) is specialized to the form

$$\delta_1(t) = \int_0^{+\infty} \left[1 - \exp\left(-\frac{t}{\tau_0}\exp\left(-\frac{E}{k_\mathrm{B}T}\right)\right)\right]\varphi(E)\mathrm{d}E \tag{21}$$

for first order kinetics, and

$$\delta_2(t) = \int_0^{+\infty} \frac{t}{t + \tau_0 \exp\left(\frac{E}{k_\mathrm{B}T}\right)}\varphi(E)\mathrm{d}E \tag{22}$$

for second order kinetics. It is noted that, though the integration interval has been taken $(0, +\infty)$, in practice the support $\mathcal{D}_E$ of $\varphi(E)$ is contained in a finite interval $(E_\mathrm{m}, E_\mathrm{M})$. These integral representations of the time variation of the average surface coverage are the basic equations of the model.

The following three sections (from 6 to 8) are taken from the comprehensive theory of desorption kinetics developed by Cerofolini and Re [39].

6. THE INVERSE PROBLEM FOR DESORPTION KINETICS

A close inspection of kernels (18) and (19) with τ given by Eq. (16) shows that they resemble strictly the Langmuir isotherm (7) and the Jovanovic isotherm (8), respectively, of equilibrium adsorption on homogeneous surfaces. Though the analogy is not complete (in fact, assuming the one-to-one correspondences $p \leftrightarrow t$ and $q \leftrightarrow E$, the equilibrium equations do not depend on p and q separately but rather on the function $p\exp(q/k_\mathrm{B}T)$, while the desorption kinetics do not depend on t and E separately but rather on the function $t\exp(-E/k_\mathrm{B}T)$ (note the different signs of the exponents), many of the mathematical methods developed for the theory of adsorption equilibrium on heterogeneous surfaces can be extended to desorption kinetics from heterogeneous surfaces.

For both the Langmuir and Jovanovic isotherms several exact methods exist for the determination of the energy distribution function $\varphi(q)$ when the overall adsorption isotherm is precisely known. Rather than trying to modify these exact methods for desorption kinetics, this work will use two approximate methods which give simple analytical expressions for the distribution function in terms of derivatives of the overall isotherm, and which allow a better and more friendly analysis of results.

6.1. Condensation approximation

The condensation approximation (CA) was introduced in the study of equilibrium adsorption on heterogeneous surfaces by Roginsky in the forties [40, 41]. However, it was only after Harris's rediscovery [42] and Cerofolini's systematic application to realistic model isotherms [43] that this method has become of wide use in the analysis of real adsorption systems.

The CA consists in replacing the kernel $\hat{\Delta}_\nu(t, E)$ by the step function

$$\Delta_\nu^{\mathrm{c}}(t, E) = \begin{cases} 1 & \text{for} \quad t \geq t_\nu^{\mathrm{c}}(E) \\ 0 & \text{for} \quad t < t_\nu^{\mathrm{c}}(E) \end{cases} \tag{23}$$

where the function $t_\nu^{\mathrm{c}}(E)$ is determined by minimizing the distance d between the local kinetics $\hat{\Delta}_\nu(t, E)$ and their approximant (23):

$$d\left[\hat{\Delta}_\nu(t, E), \Delta_\nu^{\mathrm{c}}(t, E)\right] = \min. \tag{24}$$

It is immediately verified that condition (24) is satisfied for the Lagrangian distance and L^2 distance by taking

$$t_\nu^{\mathrm{c}}(E) = [\nu - 1 + \ln(3 - \nu)]\tau_0 \exp(E/k_{\mathrm{B}}T). \tag{25}$$

which applies to first order and second order kinetics.

Defining the inverse function of (25)

$$\mathcal{E}_\nu = k_{\mathrm{B}}T \ln\left(\frac{t}{[\nu - 1 + \ln(3 - \nu)]\tau_0}\right)$$

and putting

$$\hat{\delta}_\nu(\mathcal{E}_\nu) = \delta_\nu(t(\mathcal{E}_\nu))$$

one has

$$\hat{\delta}_\nu(\mathcal{E}_\nu) = \int_{-\infty}^{\mathcal{E}_\nu} \varphi_{\nu\mathrm{c}}(E)\mathrm{d}E \tag{26}$$

Of course, the solution of Eq. (26) will in general differ from the solutions of Eqs. (21) or (22); for this reason the distribution function $\varphi_{\nu\mathrm{c}}(E)$ in Eq. (26) has been denoted with the index "c". Equation (26) is immediately solved by a differentiation with respect to $\mathcal{E}_\nu$:

$$\varphi_{\nu\mathrm{c}}(\mathcal{E}_\nu) = \frac{\partial\hat{\delta}_\nu(\mathcal{E}_\nu)}{\partial\mathcal{E}_\nu} \tag{27}$$

Since $\mathcal{E}_2 = \mathcal{E}_1 + k_{\mathrm{B}}T\ln(\ln 2)$ and $\mathrm{d}\mathcal{E}_2 = \mathrm{d}\mathcal{E}_1$ the distribution function calculated in the hypothesis of first order kinetics coincides with that calculated in the assumption of second order kinetics provided that the energy axis is shifted by an amount $-k_{\mathrm{B}}T\ln(\ln 2) = 0.367k_{\mathrm{B}}T$

The approximation involved in this method can be evaluated with the methods developed by Harris [42] and Cerofolini [43]; it is mentioned without further discussion that Eq. (27) gives an adequate description of the distribution function $\varphi(E)$ provided that

the energy spectrum $\mathcal{D}_E$ is much wider than k_BT, $E_M - E_m \gg k_BT$, and $\varphi(E)$ varies smoothly with E

$$\varphi'(E)/\varphi(E) \ll 1/k_BT \tag{28}$$

6.2. Asymptotically correct approximation

The asymptotically correct approximation (ACA) was first introduced by Hobson [44] for the description of adsorption equilibrium on heterogeneous surfaces; it has however become of wide use in the analysis of adsorption isotherms only after Cerofolini's investigation of the involved errors (which are of the same order as in the CA) and demonstration of its usefulness in determining the maximum adsorption energy [28]. The ACA can be extended to desorption kinetics by replacing the supposedly true desorption isotherm kinetics $\hat{\Delta}_\nu(t, E)$ with their asymptotic limits. Since

$$t \to 0 \Rightarrow \forall \nu : \hat{\Delta}_\nu(t, E) \sim \frac{t}{\tau_0} \exp\left(-\frac{E}{k_BT}\right)$$

and

$$t \to 0 \Rightarrow \forall \nu : \hat{\Delta}_\nu(t, E) \to 1$$

the following asymptotically correct kinetics $\Delta^a_\nu(t, E)$ seem to be reasonable approximations of the supposedly true kinetics $\hat{\Delta}_\nu(t, E)$:

$$\Delta^a_\nu(t, E) = \begin{cases} 1 & \text{for} \quad t \geq t^a_\nu(E) \\ (t/\tau_0)\exp(-E/k_BT) & \text{for} \quad t < t^a_\nu(E) \end{cases} \tag{29}$$

where the function $t^a_\nu(E)$ is determined by minimizing the distance d between the local kinetics $\hat{\Delta}_\nu(t, E)$ and their approximants (29):

$$d\left[\hat{\Delta}_\nu(t, E), \Delta^a_\nu(t, E)\right] = \min. \tag{30}$$

It is immediately verified that condition (30) is satisfied for the Lagrangian distance and L^2 distance by taking

$$t^a(E) = \tau_0 \exp(E/k_BT) \tag{31}$$

irrespective of kinetics order.

Since $t^a(E) = t^c_2(E)$, the inverse function of $t^a(E)$ is the same as of $t^c_2(E)$. Defining the inverse function of (31), $\mathcal{E} = k_BT \ln(t/\tau_0)$, and putting $\hat{\delta}(\mathcal{E}) = \delta_\nu(t(\mathcal{E}))$ (where the index ν has disappeared in $\hat{\delta}(\mathcal{E})$ because the ACA approximation of the actual desorption kinetics does not depend on reaction order ν), one has

$$\hat{\delta}(\mathcal{E}) = \int_{-\infty}^{\mathcal{E}} \varphi_a(E)\mathrm{d}E - \exp\left(\frac{\mathcal{E}}{k_BT}\right) \int_{\mathcal{E}}^{+\infty} \exp\left(-\frac{E}{k_BT}\right) \varphi_a(E)\mathrm{d}E \tag{32}$$

Since the solution of Eq. (32) will in general differ from the solutions of Eqs. (21) or (22), the distribution function $\varphi_a(E)$ has been denoted with the index "a". Equation

(32) may be solved by differentiating with respect to $\mathcal{E}$, multiplying both members by $k_B T \exp(-\mathcal{E}/k_B T)$, and differentiating again with respect to $\mathcal{E}$; the result is

$$\varphi_a(\mathcal{E}) = \frac{\partial \hat{\delta}(\mathcal{E})}{\partial \mathcal{E}} - k_B T \frac{\partial^2 \hat{\delta}(\mathcal{E})}{\partial \mathcal{E}^2} \tag{33}$$

The degree of approximation involved in this method can be evaluated with the methods developed by Cerofolini [28]. Without discussing this matter in detail, it is immediately realized that CA and ACA give comparable results, at least for second order kinetics. In fact, combining Eqs. (27) and (33) one has

$$\varphi_a(\mathcal{E}) = \varphi_c(\mathcal{E}) - k_B T \varphi_c'(\mathcal{E}) = \varphi_c(\mathcal{E})[1 - k_B T \varphi_c'(\mathcal{E})/\varphi_c(\mathcal{E})]$$

so that if the condition (28) for the validity of the CA method is satisfied, one has

$$\varphi_a(\mathcal{E}) \simeq \varphi_c(\mathcal{E})$$

Appreciable differences may occur only in the regions where $\varphi_c(\mathcal{E}) \simeq 0$.

6.3. Beyond the second order approximation

Cerofolini and Re have extended the analysis of the overall desorption kinetics beyond the 2-nd order approximation by using the methods developed for equilibrium adsorption by Nederlof *et al.* (logarithmic symmetrical local isotherm approximation) [45], Rudziński and coworkers (3-rd order approximation) [46, 47, 48, 49], and Re (n-th order approximation) [50]. Details are given in Ref. [39].

7. EXPLAINING THE ELOVICH EQUATION IN TERMS OF SURFACE HETEROGENEITY

In this part we shall discuss Eq. (3) in the light of the CA method; the obtained results will later be adjusted to take into account the ACA correction to the distribution function.

7.1. The Elovich equation in the condensation approximation

Let us first consider second order kinetics. The Elovich equation (3), expressed in terms of $\mathcal{E}$, reads

$$\hat{\delta}_2^{mM}(\mathcal{E}_2) = \begin{cases} r_E \ln\left(1 + \dfrac{\tau_0}{t_m} \exp\left(\dfrac{\mathcal{E}_2}{k_B T}\right)\right) & \text{for} \quad -\infty < \mathcal{E}_2 \leq \mathcal{E}_{2M} \\ \delta_M & \text{for} \quad \mathcal{E}_{2M} < \mathcal{E}_2 < +\infty \end{cases} \tag{34}$$

where

$$\mathcal{E}_{2M} = \mathcal{E}_{2m} + k_B T \ln(\exp(\delta_M/r_E) - 1)$$

with

$$\mathcal{E}_{2m} = k_B T \ln(t_m/\tau_0)$$

In the sequel the index "2" to $\mathcal{E}$ and φ_c will be omitted to have more manageable expressions. The application of Eq. (27) to (34) gives:

$$\varphi_c(\mathcal{E}) = \begin{cases} \dfrac{r_E/\delta_M}{k_B T} \exp\left(\dfrac{\mathcal{E}-\mathcal{E}_m}{k_B T}\right) \Big/ \left[1+\exp\left(\dfrac{\mathcal{E}-\mathcal{E}_m}{k_B T}\right)\right] & \text{for } -\infty < \mathcal{E} \leq \mathcal{E}_M \\ 0 & \text{for } \mathcal{E}_M < \mathcal{E} < +\infty \end{cases} \tag{35}$$

whatever is the value of δ_M. A study of the distribution function (35) shows the following limiting behaviours:

$$\varphi_c(\mathcal{E}) \simeq \begin{cases} \dfrac{r_E/\delta_M}{k_B T} \exp\left(\dfrac{\mathcal{E}-\mathcal{E}_m}{k_B T}\right) & \text{for } -\infty < \mathcal{E} \lesssim \mathcal{E}_m - k_B T \\ \dfrac{r_E/\delta_M}{k_B T} & \text{for } \mathcal{E}_m - k_B T \lesssim \mathcal{E} \leq \mathcal{E}_M \\ 0 & \text{for } \mathcal{E}_M < \mathcal{E} < +\infty \end{cases} \tag{36}$$

Of course, the calculated distribution function cannot be an arbitrary function of $\mathcal{E}$ and must satisfy the mathematical conditions of non-negativity and of normalization; physical conditions too have to be satisfied: for instance, $\varphi_c(\mathcal{E})$ must be identically null for $\mathcal{E} < 0$ and must be temperature independent. There is no choice of $\mathcal{E}_m$ and $\mathcal{E}_M$ for which function (35) is temperature-independent; however, the asymptotic expansion (36) shows that $\varphi_c(\mathcal{E})$ varies with T only in a region centred on $\mathcal{E}_m$ of width $O(k_B T)$, while the calculated distribution function is approximately constant in the whole interval $(\mathcal{E}_m, \mathcal{E}_M)$ provided that the extremes $\mathcal{E}_m$ and $\mathcal{E}_M$, and therefore the difference $\mathcal{E}_M - \mathcal{E}_m$, are constant with T.

Equation (36) states that $\mathcal{E}_M$ must therefore be interpreted as the maximum adsorption energy

$$\mathcal{E}_M = E_M$$

while the distribution function vanishes exponentially with $\mathcal{E} - \mathcal{E}_m$ for $\mathcal{E} \lesssim \mathcal{E}_m$; in a way, $\mathcal{E}_m$ must be interpreted as an estimate of the minimum adsorption energy

$$\mathcal{E}_m \simeq E_m$$

Since in general $\varphi(E) \neq \varphi_c(E)$, even the maximum desorption energy E_M^c determined within the CA is in principle different from the true desorption energy E_M. The normalization condition for $\varphi_c(\mathcal{E})$

$$\int_{-\infty}^{E_M^c} \varphi_c(\mathcal{E}) \mathrm{d}\mathcal{E} = 1$$

gives the following equation for E_M^c:

$$r_E \ln\left(1+\exp\left(\frac{E_M^c - \mathcal{E}_m}{k_B T}\right)\right) = \delta_M$$

whose solution is

$$E_{\mathrm{M}}^{\mathrm{c}} - \mathcal{E}_{\mathrm{m}} = k_{\mathrm{B}}T \ln\left(\exp\left(\frac{\delta_{\mathrm{M}}}{r_{\mathrm{E}}}\right) - 1\right) \simeq k_{\mathrm{B}}T\frac{\delta_{\mathrm{M}}}{r_{\mathrm{E}}} \tag{37}$$

Combining this relationship with the physical meaning of $\mathcal{E}_{\mathrm{m}}$ and $\mathcal{E}_{\mathrm{M}}$, one eventually gets the meaning and the temperature dependence of the parameters t_{m} and r_{E}:

$$t_{\mathrm{m}} \approx \tau_0 \exp(E_{\mathrm{m}}/k_{\mathrm{B}}T) \tag{38}$$

with $\mathcal{E}_{\mathrm{m}} \simeq E_{\mathrm{m}}$, and

$$r_{\mathrm{E}} \simeq \delta_{\mathrm{M}} k_{\mathrm{B}}T/\Omega \tag{39}$$

with $\Omega = E_{\mathrm{M}} - E_{\mathrm{m}} \simeq \mathcal{E}_{\mathrm{M}} - \mathcal{E}_{\mathrm{m}}$ being the width of the energy spectrum.

Figure 2 shows the distribution functions calculated for second-order kinetics in the frame of the condensation approximation for Elovich equations with different values of Ω — it is immediately seen that the larger is the ratio $\Omega/k_{\mathrm{B}}T$ (*i.e.*, the more accurate is the calculated distribution function) the more $\varphi_{\mathrm{c}}(\mathcal{E})$ resembles a uniform distribution.

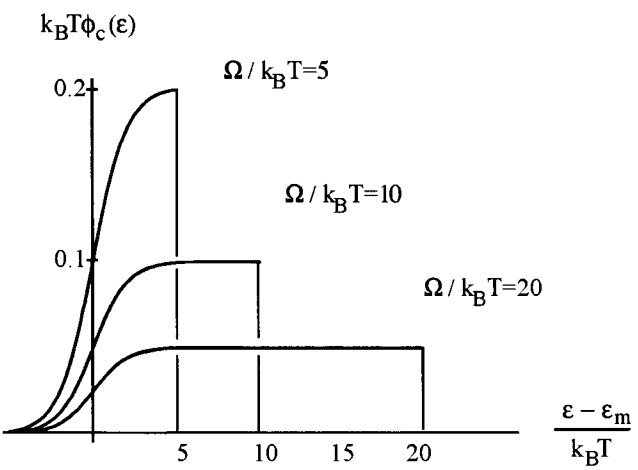

Figure 2. Distribution functions for Elovich equations with different values of Ω.

When first order kinetics are considered, the Elovich equation (3) reads

$$\hat{\delta}_1^{\mathrm{mM}}(\mathcal{E}_1) = \begin{cases} r_{\mathrm{E}} \ln\left(1 + \dfrac{\tau_0 \ln 2}{t_{\mathrm{m}}} \exp\left(\dfrac{\mathcal{E}_1}{k_{\mathrm{B}}T}\right)\right) & \text{for} \quad -\infty < \mathcal{E}_1 \leq \mathcal{E}_{1\mathrm{M}} \\ \delta_{\mathrm{M}} & \text{for} \quad \mathcal{E}_{1\mathrm{M}} < \mathcal{E}_1 < +\infty \end{cases} \tag{40}$$

where

$$\mathcal{E}_{1\mathrm{M}} = \mathcal{E}_{1\mathrm{m}} + k_{\mathrm{B}}T \ln(\exp(\delta_{\mathrm{M}}/r_{\mathrm{E}}) - 1) \tag{41}$$

with

$$\mathcal{E}_{1\mathrm{m}} = k_{\mathrm{B}}T \ln(t_{\mathrm{m}}/\tau_0) - k_{\mathrm{B}}T \ln(\ln 2) \tag{42}$$

The application of Eq. (27) to Eq. (40) gives a distribution function with the same shape as (35) in which $\mathcal{E}_2$, $\mathcal{E}_{2m}$ and $\mathcal{E}_{2M}$ are replaced by $\mathcal{E}_1$, $\mathcal{E}_{1m}$ and $\mathcal{E}_{1M}$, respectively. All the considerations on minimum and maximum adsorption energies made for second order kinetics therefore apply to first order kinetics provided that $\mathcal{E}_{2m}$ and $\mathcal{E}_{2M}$ are replaced by $\mathcal{E}_{1m}$ and $\mathcal{E}_{1M}$, respectively, as calculated from Eqs. (41) and (42).

It is noted that, irrespective of kinetic order, the condition of validity of the CA is that the dispersion of the energy spectrum is much wider that k_BT; this condition is satisfied only for $r_E/\delta_M \ll 1$, which is the condition for the validity of the above argument. Note that when this condition is satisfied, the difference between the calculated distribution functions for first- and second-order kinetics, consisting of a shift of the order of k_BT on the energy axis, is negligible.

7.2. The Elovich equation in the asymptotically correct approximation

A direct application of Eq. (33) to Eq. (34) gives:

$$\varphi_a(\mathcal{E}) = \begin{cases} \dfrac{r_E/\delta_M}{k_BT}\left[\dfrac{\exp\left(\dfrac{\mathcal{E}-\mathcal{E}_m}{k_BT}\right)}{1+\exp\left(\dfrac{\mathcal{E}-\mathcal{E}_m}{k_BT}\right)} - \dfrac{\exp\left(\dfrac{\mathcal{E}-\mathcal{E}_m}{k_BT}\right)}{\left[1+\exp\left(\dfrac{\mathcal{E}-\mathcal{E}_m}{k_BT}\right)\right]^2}\right] & \text{for } -\infty < \mathcal{E} \leq \mathcal{E}_M \\ 0 & \text{for } \mathcal{E}_M < \mathcal{E} < +\infty \end{cases} \tag{43}$$

The correction brought by the ACA to the CA

$$-\frac{r_E/\delta_M}{k_BT}\exp\left(\frac{\mathcal{E}-\mathcal{E}_m}{k_BT}\right)\Big/\left[1+\exp\left(\frac{\mathcal{E}-\mathcal{E}_m}{k_BT}\right)\right]^2$$

is non negligible only for $|\mathcal{E}-\mathcal{E}_m|/k_BT \lesssim 1$ (the above correction is rigorous only for second order kinetics; for first order kinetics the final considerations of the previous part apply); for large $|\mathcal{E}-\mathcal{E}_m|$ the correction vanishes exponentially irrespective of the sign of the difference $\mathcal{E}-\mathcal{E}_m$. Moreover, it is immediately seen that the asymptotic values of this correction for large negative values of $\mathcal{E}-\mathcal{E}_m$ is almost exactly equal, but of opposite sign, to the CA distribution function, so that these terms cancel each other. The disappearance in the ACA of the exponential tail calculated in the CA for $\mathcal{E} < \mathcal{E}_m$ strengthens the previous tentative interpretation of $\mathcal{E}_m$ as minimum desorption energy E_m.

The normalization condition for $\varphi_a(\mathcal{E})$

$$\int_{-\infty}^{E_M^a} \varphi_a(\mathcal{E})\mathrm{d}\mathcal{E} = 1$$

gives the following condition for the maximum desorption energy E_M^a consistent with ACA:

$$r_E \ln\left(1+\exp\left(\frac{E_M^a-\mathcal{E}_m}{k_BT}\right)\right) - r_E\frac{\exp\left(\dfrac{E_M^a-\mathcal{E}_m}{k_BT}\right)}{1+\exp\left(\dfrac{E_M^a-\mathcal{E}_m}{k_BT}\right)} = \delta_M$$

For $E_M^a - \mathcal{E}_m \gg k_B T$ this equation gives:

$$E_M^a - \mathcal{E}_m \simeq k_B T(1 + \delta_M/r_E) \tag{44}$$

which puts in one-to-one correspondence maximum desorption energy and kinetics completion. The comparison of Eqs. (37) and (44) shows that there is a small discrepancy between the estimates of E_M obtained in the frames of CA and ACA; this discrepancy is however of the order of $k_B T$ and becomes negligible in the range of validity of the CA and ACA — $k_B T/\Omega \ll 1$. More dangerous is the ACA internal consistency between the maximum desorption energies as follow from Eq. (43) and the normalization condition: the ACA distribution function should extend up to E_M^a to be normalized while it is identically null in the interval $(\mathcal{E}_M, E_M^a)$; this inconsistency is however of minor practical importance since the width of this interval is of the order of $k_B T$.

In conclusion, the explicit form of the Elovich equation as follows from the combined application of the CA and ACA is therefore

$$\delta^{mM}(t) = \begin{cases} \dfrac{k_B T}{\Omega} \ln\left(1 + \dfrac{t}{\tau_0} \exp\left(-\dfrac{E_m}{k_B T}\right)\right) & \text{for} \quad 0 \le t < \tau_0 \exp\left(\dfrac{E_m + \Omega}{k_B T}\right) \\ \delta_M & \text{for} \quad \tau_0 \exp\left(\dfrac{E_m + \Omega}{k_B T}\right) \le t \end{cases} \tag{45}$$

8. A DIRECT PROBLEM IN DESORPTION KINETICS — DESORPTION ISOTHERMS FROM EQUILIBRIUM SURFACES

This section is devoted to the calculation of the desorption kinetics from a heterogeneous surface characterized by a desorption energy distribution function $\varphi_{eq}(E)$ given by Eq. (9) with $E = q$, *i.e.* of the desorption kinetics from a surface which in equilibrium conditions obeys the Freundlich or Temkin isotherm. The local desorption kinetics will be assumed to be of the first order.

Inserting Eq. (9) in Eq. (21) one has

$$\delta_1(t) = \int_{E_m}^{E_M} \left[1 - \exp\left(-\frac{t}{\tau_0} \exp\left(-\frac{E}{k_B T}\right)\right)\right] \frac{r_F}{k_B T_F} \exp\left(-\frac{E - E_m}{k_B T_F}\right) dE \tag{46}$$

Putting

$$\begin{aligned} \tau_m &= \tau_0 \exp(E_m/k_B T) \\ \tau_M &= \tau_0 \exp(E_M/k_B T) \\ z &= (t/\tau_m) \exp(-(E - E_m)/k_B T) \end{aligned}$$

Eq. (46) becomes

$$\delta_1(t) = 1 + r_F s \left(\frac{\tau_m}{t}\right)^s \int_{t/\tau_m}^{t/\tau_M} z^{s-1} e^{-z} dz \tag{47}$$

with $s = T/T_F$ as in Eq. (10). This overall isotherm can be expressed in terms of higher transcendental functions:

$$\delta_1(t) = 1 + r_F s \left(\frac{\tau_m}{t}\right)^s [\Gamma(s, t/\tau_m) - \Gamma(s, t/\tau_M)] \tag{48}$$

where

$$\Gamma(s, z_0) = \int_{z_0}^{+\infty} z^{s-1} e^{-z} dz$$

is the incomplete gamma function (Ref.[51], Chapter 6).

It is difficult to recognize in which conditions the isotherm (48) is reduced to the Elovich behaviour. This goal is better accomplished by computing the integral (21) using a uniform distribution function, which is the strong-heterogeneity limit of the distribution function of equilibrium surfaces. In this case Eq. (21) becomes:

$$\delta_1(t) = \int_{E_m}^{E_M} \left[1 - \exp\left(-\frac{t}{\tau_0} \exp\left(-\frac{E}{k_B T}\right)\right)\right] \frac{1}{\Omega} dE \tag{49}$$

With the previous definitions, Eq. (49) becomes:

$$\delta_1(t) = 1 - \frac{k_B T}{\Omega} \int_{t/\tau_M}^{t/\tau_m} e^{-z} \frac{dz}{z} \tag{50}$$

which can be expressed in terms of higher transcendental functions:

$$\delta_1(t) = 1 - \frac{k_B T}{\Omega} [E_1(t/\tau_M) - E_1(t/\tau_m)] \tag{51}$$

where

$$E_1(z_0) := \int_{z_0}^{+\infty} e^{-z} \frac{dz}{z}$$

is the exponential integral (Ref.[51], Chapter 5). (To avoid confusion between the exponential integral $E_1(\cdots)$ and the desorption energy E, the roman has been used for the former and the italic for the latter; moreover, the index "1" in $E_1(\cdots)$ has a different meaning from the same index in $\delta_1(t)$.) For identifying the logarithmic behaviour it is then convenient to limit the attention to any time t in the interval (τ_m, τ_M) and divide the integration interval in two parts

$$\int_{t/\tau_M}^{t/\tau_m} e^{-z} \frac{dz}{z} = \int_{t/\tau_M}^{1} e^{-z} \frac{dz}{z} + \int_{1}^{t/\tau_m} e^{-z} \frac{dz}{z}$$

Since $e^{-z} = O(1)$ for $t/\tau_M < z \leq 1$, one has

$$\int_{t/\tau_M}^{1} e^{-z} \frac{dz}{z} \simeq -\ln(t/\tau_M)$$

this approximation being a good approximation for t close to τ_M; z^{-1} can in turn be assumed to be constant with respect to e^{-z} for $1 < z \leq t/\tau_m$, so that one has

$$\int_1^{t/\tau_m} e^{-z} \frac{dz}{z} = O(1)e^{-1}\left[1 - e^{-(t/\tau_m - 1)}\right]$$

Combining the above estimates, the isothermal kinetics (51) behave as

$$\begin{aligned}\delta_1(t) &\simeq 1 - (k_B T/\Omega)\left\{-\ln(t/\tau_M) + O(1)e^{-1}\left[1 - e^{-(t/\tau_m - 1)}\right]\right\} \\ &= 1 + (k_B T/\Omega)\left\{\ln(t/\tau_m) - \Omega/k_B T - O(1)e^{-1}\left[1 - e^{-(t/\tau_m - 1)}\right]\right\} \\ &= (k_B T/\Omega)\ln(t/\tau_m) - (k_B T/\Omega)O(1)e^{-1}\left[1 - e^{-(t/\tau_m - 1)}\right] \qquad (52)\end{aligned}$$

Since the factor $O(1)$ becomes $o(1)$ for t close to t_M and the correction to the logarithm behaviour vanishes as $O(1)t/\tau_m$ for t close to t_m, the approximate estimate (52) of (51) proves that *the Elovich desorption kinetics are expected to be observed on strongly heterogeneous surfaces which in equilibrium conditions obey the Temkin equation.* For a simplified demonstration that the Elovich equation is expected to be observed in the desorption from heterogeneous surfaces, see Refs. [22, 52].

9. CHEMISORPTION KINETICS ON HOMOGENEOUS SURFACES

The first observation of a chemisorption process obeying Eq. (1) was probably reported by Zeldowitch in 1934 for the catalytic oxidation of CO on MnO_2 [10]; a later study of the chemisorption of CO and CO_2 on MnO_2 demonstrated that Eq. (1) was satisfied [11]; but it was only after the discovery that Eq. (1) describes also the chemisorption of hydrogen and ethylene on a catalyst of reduced NiO [12] that this equation became of wide use. That Eq. (1) is indeed widely observed in chemisorption was confirmed by Taylor and Thon who analyzed previously published results for 10 systems and found that they were described by the time-logarithm law [53]. An extended list of adsorbent-adsorbate systems obeying the Elovich equation is given in Aharoni and Tompkins's review [14].

The chemisorption rate equations are

$$\frac{d\Theta}{dt} = \frac{1}{\tau}(1 - \Theta)^{\nu} \qquad (53)$$

where Θ is the coverage, ν is the reaction order and τ is a characteristic adsorption time, which in principle is a local property of the surface. Proceeding as for desorption kinetics, one has

$$\int_{\Theta_0(\tau)}^{\Theta} \frac{d\Theta}{(1 - \Theta)^{\nu}} = \frac{t}{\tau} \qquad (54)$$

Putting

$$\Delta_\nu(t, \tau) = \Theta_\nu(t, \tau) - \Theta_0(\tau)$$

the integration of Eq. (54) gives

$$\Delta_1(t,\tau) = [1 - \Theta_0(\tau)]\left[1 - \exp\left(-\frac{t}{\tau}\right)\right] \tag{55}$$

for first order kinetics, and

$$\Delta_2(t,\tau) = [1 - \Theta_0(\tau)]\frac{[1 - \Theta_0(\tau)]t}{[1 - \Theta_0(\tau)]t + \tau} \tag{56}$$

for second order kinetics.

The comparison of Eqs. (55) and (56) with Eqs. (14) and (15), respectively, shows that if $\Theta_0(\tau)$ is constant with τ (in particular, if $\forall\tau : \Theta_0(\tau) = 0$) the chemisorption kinetics have the same formal expressions as the desorption kinetics so that the considerations of Section 5 apply here.

The major differences between chemisorption and desorption are the dependences of the associated characteristic times τ on surface properties.

A time-logarithm behaviour can be recognized neither in Eq. (55) nor (56), so that the Elovich kinetics cannot be understood in terms of chemisorption kinetics on ideally homogeneous surfaces.

The first attempts for understanding the time-logarithm law started immediately after its experimental discovery [11]. However, the first systematic search of the reasons explaining the Elovich equation is probably due to Porter and Tompkins [54]. These authors assumed that the time-logarithm law (1) is observed during activated chemisorption and interpreted the resulting equation in terms either of pre-existing *surface heterogeneity* or of variation of the activation energy with coverage during the process (*induced heterogeneity*).

10. THE FIXED-HETEROGENEITY MODEL IN CHEMISORPTION

Dealing with non-equilibrium situations, it is not necessary for describing the adsorption kinetics to stipulate that the gas temperature T_g coincides with adsorbent temperature T. According to the kinetic theory of gases, the flux Φ of molecules impinging the unit area per unit time is given by:

$$\Phi = \frac{p}{\sqrt{2\pi m k_B T_g}}$$

where p is the gas pressure and m is the molecular mass. The characteristic time τ required to cover the surface with a fraction O(1) of monolayer is therefore given by:

$$\frac{1}{\tau} = \sigma\frac{p}{\sqrt{2\pi m k_B T_g}}\frac{1}{N_s a} \tag{57}$$

where $N_s a$ is the available area (N_s being the number of sites per unit area and a the cross section of each site) and σ is the sticking coefficient (*i.e.*, the probability that after the collision the molecule sticks at the surface). Of the quantities which define τ, only a, N_s and σ depend on the surface. Assuming the topographic equivalence of all zones of

the surface, σ alone can be considered as a local property. This quantity is expected to depend on T_g and T as well as on gas-to-adsorbent mass ratio, because the adsorption requires that most of the impinging kinetic energy is absorbed by the target during the impact, whose duration is in the time scale of 10^{-11} s. Direct experimental information on the sticking coefficient is poor, due to the difficulties of measuring this quantity in a high vacuum (anisotropic gas flows, pressure and temperature gas non-uniformities, etc.).

10.1. Physisorption

For physisorption more accurate information can be obtained by molecular dynamics simulations. These simulations, usually performed on model systems of spherical particles interacting via a Lennard-Jones potential to minimize computation time rather than to mimic any particular material, show that in this case condensation is a rapid and efficient phenomenon without significant hopping after condensation. In particular, considering the impact of projectiles with the same mass as the atoms forming the adsorbent (that allows an efficient energy transfer to the solid) and ignoring adsorbent temperature, recent simulations have shown that trajectories that arrive close to binding sites regain only a small fraction of the energy imparted to the solid and therefore have a chance of the order of unity to be trapped [55].

The condensation process in physisorption can therefore be regarded as a very efficient process with sticking coefficient close to unity quite irrespective of the considered adsorption site: $\sigma \simeq 1$. The constancy of σ implies the constancy of τ so that, quite irrespective of the homogeneous or heterogeneous structure of the surface, *no Elovich behaviour is expected for physisorption kinetics.*

10.2. Activated chemisorption

The above conclusion applies as well to non-activated chemisorption. In chemisorption, however, the chemical specificity of the reaction is such that factors like the crossing of electronic curves, the existence of steric constraints, and the coupling with the heat reservoir are expected to play a fundamental role, so that no general rule can be specified.

Considering that the Elovich behaviour usually describes the *chemisorption of molecules*, one may argue that in the situations where the Elovich equation is observed, chemisorption is an activated process.

During the last years significant information on chemisorption rates of translationally excited molecules has been obtained. This process is dominated by the normal component of the translational energy [56]. If one assumes that the sticking coefficient is 1 when this quantity is higher than the activation energy E of the process and 0 otherwise, one gets that, due to the Boltzmann distribution of energies, only a fraction $\exp(-E/k_BT)$ of the impinging flow $p/\sqrt{2\pi m k_B T}$ has a sufficient energy to penetrate the chemisorption valley and hence to react with surface atoms. Equation (57) is thus replaced by:

$$\frac{1}{\tau} = \sigma \frac{p}{\sqrt{2\pi m k_B T_g}} \frac{1}{N_s a} \exp\left(-\frac{E}{k_B T}\right)$$

so that, in view of the complete formal analogy discussed above between adsorption and desorption kinetics and of the conclusions of Section 7, the Elovich law observed in chemisorption kinetics is simply explained in terms of a surface characterized by a uniform distribution of activation energy E — *the Elovich chemisorption isotherm is expected to*

be the kinetics of activated chemisorption on energetically heterogeneous surfaces with a uniform distribution of activation energy.

11. THE INDUCED-HETEROGENEITY MODEL IN CHEMISORPTION

In the induced-heterogeneity model the chemisorption process is assumed to be an activated process and the clean surface is considered as homogeneous and characterized by chemisorption kinetics with activation energy E_0.

As the process progresses the chemisorption activation energy is then assumed to increase from E_0 to a value $E(\Theta)$ depending on the coverage Θ. If one stipulates that chemisorption kinetics are described by the rate equation:

$$\frac{d\Theta}{dt} = R_0 \exp\left(-\frac{E(\Theta)}{k_B T}\right) \tag{58}$$

(where R is suitable kinetic coefficient independent of Θ) and E depends linearly on Θ:

$$E(\Theta) = E_0 + w\Theta$$

(where w is a parameter giving the strength of lateral interactions), then one obtains a differential equation which coincides with Eq. (5) (and therefore can be integrated in closed form to give the Elovich behaviour) provided that

$$t_m = \frac{k_B T}{w R_0} \exp\left(\frac{E_0}{k_B T}\right) \tag{59}$$

and

$$r_E = k_B T / w \tag{60}$$

Irrespective of the assumed theoretical framework (fixed or induced heterogeneity), the parameters r_E and t_m have the same meaning: Eqs. (38) and (59) state that t_m is essentially related to the minimum activation energy for chemisorption, while Eqs. (39) and (60) state that r_E is the width of the domain of activation energy measured in units of $k_B T$.

Though the above derivation of the Elovich equation is very economic and succeeds in furnishing the empiric parameters r_E and t_m with precise microscopic meaning, Eqs. (39) and (38) respectively, one cannot be completely satisfied of it because of the following reasons:

- it is not clear why the r.h.s. of Eq. (58) does not contain a factor like $(1-\Theta)^\nu$ which limits the chemisorbed amount for long adsorption time — see Eq. (53);
- in many situations of practical interest the adsorbent is highly dispersed, that makes it difficult to accept that lateral interactions are responsible for the overall kinetics; and
- a linear dependence of E on Θ in the whole coverage range is undoubtfully a poor description of lateral interactions between chemisorbed molecules.

The last point deserves a special discussion. In fact, due to the short-range nature of the forces involved in chemisorption, $E(\Theta)$ is expected to depend on Θ only for $\Theta \gtrsim 1/c$, where c is the coordination number (*i.e.*, the number of nearest neighbours) of each adsorption site. Since the Elovich behaviour is associated with the final stages of the process, this is not a serious difficulty in activated chemisorption, where the appearance of the logarithmic kinetics is associated with high coverage.

The above chemisorption model can *formally* be extended to desorption kinetics. In fact, assuming the same rate equation as in Eq. (58)

$$-\frac{d\Theta}{dt} = R_0 \exp\left(-\frac{E(\Theta)}{k_B T}\right)$$

(except, of course, for the sign of the derivative) and a linear decrease of E with Θ,

$$E(\Theta) = E_0 - w\Theta$$

one gets a differential equation which coincides with Eq. (5) provided that the coefficients they contain satisfy certain conditions. This derivation, however, is only formal since the logarithmic behaviour is associated with the final stages of the desorption process where the coverage is negligible and E becomes independent of Θ. For this reason induced heterogeneity was not considered in the section devoted to desorption kinetics as a possible responsible for the Elovich behaviour.

12. THE SURFACE-RECONSTRUCTION MODEL IN CHEMISORPTION

While both the fixed-heterogeneity model and the induced-heterogeneity model ascribe the Elovich behaviour to (pre-existing or chemisorption-induced) energetic factors, the model proposed by Landsberg [13] ascribes it to topographic factors, related to surface reconstruction during chemisorption. The following description applies to chemisorption, but *mutatis mutandis* it can be extended to oxidation.

Landsberg postulated that:

(L1) chemisorption occurs via the collision of impinging gas-phase molecules on free surface sites;
(L2) chemisorption is responsible for surface reconstruction via generation of new sites at a rate proportional to the chemisorption rate; and
(L3) each newly exposed zone has the same topography as the surface from which it was generated.

12.1. Kinetics

The Landsberg model can be formalized as follows. Assumption (L1) reads

$$\frac{dN}{dt} = N_{s\star} a \sigma \frac{p}{\sqrt{2\pi m k_B T_g}} \tag{61}$$

where N and N_{s*} are the numbers of chemisorbed molecules and available chemisorption sites, respectively, both referred to the unit geometric area. The model described in Section 9 for first-order chemisorption on homogeneous surfaces is reproduced by taking

$$\begin{cases} N & = & N_s\Theta \\ N_{s*} & = & N_s(1-\Theta) \\ N_s & = & \text{constant.} \end{cases} \tag{62}$$

Landsberg, however, did not accept assumptions (62) and postulated (L2); in so doing he postulated that chemisorption has two contrasting effects: on one side the chemisorption of a molecule deactivates one site, but on another side it is also responsible for the creation of newly exposed area and hence of new adsorption sites. This can be restated by assuming that the active area lost per unit time and unit geometric area is $b\,\mathrm{d}N/\mathrm{d}t$, where b represents the net lost area per chemisorbed molecule. If the reconstruction mechanism is such that (L3) is satisfied, the number of available sites per unit geometric area evolves with time as

$$\begin{aligned} -\frac{\mathrm{d}N_{s*}}{\mathrm{d}t} &= b\frac{\mathrm{d}N}{\mathrm{d}t}N_{s*} \\ &= \frac{p}{\sqrt{2\pi m k_B T_g}}ab\sigma N_{s*}^2 \end{aligned} \tag{63}$$

Equation (63) can be integrated by variable separation and gives

$$\frac{N_{s*}(0)}{N_{s*}(t)} = 1 + \frac{p}{\sqrt{2\pi m k_B T_g}}N_{s*}(0)ab\sigma t \tag{64}$$

where $N_{s*}(0)$ is the density of surface sites at time $t = 0$. Inserting Eq. (64) into Eq. (61) one gets a differential equation which can be solved by variable separation:

$$N(t) = \frac{1}{b}\ln\left(1 + b\frac{t}{\alpha}\right) \tag{65}$$

with $\alpha = \sqrt{2\pi m k_B T_g}/pN_{s*}(0)a\sigma$. The comparison of Eq. (2) with Eq. (65) shows that they coincide for $r_E = 1/b$ and $t_m = \alpha/b$, and therefore provides the empirical parameters of the Elovich equation with a microscopic structural meaning.

In modern language assumption (L3) states that the surface reconstructs in a self-similar way. Though the exact mathematical specification of this self-similarity is an open problem, the appearance of the Elovich equation seems essentially related to a fractal nature of the reconstructed surface; this property is immediately understood by observing that the number of molecules accomodated on a given finite geometric surface area diverges as $t \to +\infty$.

The increase with time of the number of chemisorbed molecules is independent of b in the linear regime

$$t \to 0 \Rightarrow N \sim t/\alpha$$

and varies inversely with b in the long-time regime

$$t \to +\infty \Rightarrow N \sim \frac{1}{b}\ln\left(b\frac{t}{\alpha}\right) \sim \frac{1}{b}\ln t$$

Though Landsberg considered only the case $b > 0$, the case of negative b is interesting too and deserves an analysis. For $b < 0$ the solution of Eqs. (61) and (63) reads

$$N(t) = -\frac{1}{|b|} \ln \left(1 - |b| \frac{t}{\alpha}\right). \tag{66}$$

For $b > 0$ the surface reconstruction leads to a smooth increase with t of the chemisorbed amount, in such a way that the number of chemisorbed molecules diverges only for $t \to +\infty$; for $b < 0$ the surface reconstruction is sudden and leads to a divergence of N at a finite time t_∞, $t_\infty = \alpha/|b|$. Though the case $b < 0$ may appear quite formal, the fragmentation of the sphere-like support of Ziegler–Natta catalysts produced during olefin polymerization in industrial heterogeneous processes provides an example of Landsberg reconstruction with $b < 0$.

12.2. Structure

The study of adsorption on fractal surfaces has become in last years an extremely active field of research; Landsberg model may be considered as an early study in this field. The mechanism hypothesized by Landsberg has truly interesting properties:

- while adsorption on fractal surfaces is expected to produce surface defractalization [57], in the surface-reconstruction model adsorption is responsible for surface fractalization;
- in Landsberg model fractalization is described as a chain reaction; for $b > 0$ fractalization proceeds quietly and is completed only at $t = +\infty$, while for $b < 0$ fractalization occurs explosively and is completed at a finite time; and
- the fractal nature of the fully reconstructed surface is essentially different from the fractality of common adsorbents.

This last point deserves a special discussion. In fact, according to the seminal work of Pfeifer, Avnir and Farin [20, 21], highly dispersed adsorbents were found to have fractal surfaces; the fractal nature of the surface was established by measuring with the BET technique the surface area using adsorbents with scaled sizes and observing that the *extrapolation* to null size produced an infinite area. In Landsberg's model, by contrast, adsorption generates a surface whose area, measured with a molecular probe of assigned size, increases continuously as adsorption proceeds. The infinite surface area of a Landsberg-reconstructed surface is actual (*i.e.*, it can be measured with real molecular probes) though for $b > 0$ it is obtained only for $t \to +\infty$; the infinite surface area of a common fractal adsorbent is potential (*i.e.*, it results from an extrapolation process in the limit of null size of the adsorbed probe). In a way the complexity of a Landsberg-reconstructed surface is greater than that of highly dispersed fractal adsorbents.

Chemisorption is manifestly responsible for a swelling of the original surface that complicates the understanding of surface topography. Information on the topography of the reconstructed surface can be obtained by considering the region involved in chemisorption expressed in terms of original adsorbent. Fractalization proceeds via a progressive increase with time of N or of the thickness x of the adsorbent region involved in the fractalization process. There are two possibilities: either $N(t) + N_{s*}(t)$ increases with t faster than $x(t)$ or not. In the latter case the peak-to-peak roughness of the chemisorbed layer increases

with t and the layer does never revert to a continuous homogeneous phase; otherwise at a certain time $t_* - \mathrm{d}t$, with t_* such that

$$N(t) + N_{s*}(t) = \varrho x(t)$$

(where ϱ is the atomic density of the compound formed after chemisorption), the surface will attain its maximum fractal dimension, while at $t = t_*$ all the layer of thickness $x(t_*)$ will be constituted by the chemisorbed compound, thus producing a flat two-dimensional surface. This chemisorption-induced fractal-to-flat transformation can be viewed as a new kind of (inter)phase transition.

13. CONCLUSIONS

Surface heterogeneity has ever been considered to play a major role on adsorption [desorption] kinetics on [from] real surfaces and on heterogeneous catalytic processes. In fact, the most frequently observed kinetics which deviate from the theoretical first- or second-order ones, *i.e.* the time-logarithm law commonly known as Elovich equation, have in most cases been interpreted as due to surface heterogeneity.

Heterogeneity has been described in terms either of pre-existing differences in the activation energies of the adsorption-desorption process (intrinsic heterogeneity) or of variation of the activation energy with coverage during the process (induced heterogeneity).

Though both chemisorption and desorption kinetics can be explained by a model in which the surface is characterized by a fixed heterogeneity with a uniform energy distribution function, in chemisorption other explanations are possible, like induced heterogeneity or surface reconstruction.

It is therefore not unreasonable to ascribe the wide observation of the Elovich behaviour in chemisorption to the occurrence of one or the other of the considered models (surface heterogeneity, induced heterogeneity, or surface reconstruction), and to ascribe the smaller set of systems following the Elovich behaviour in desorption to a unique model — fixed surface heterogeneity.

REFERENCES

1. S.J. Teichner, G.A. Nicolaon, M.A. Vicarini and G.E.E. Gardes, Adv. Colloid Interface Sci., 5 (1976) 245.
2. Y. Matsumura, J.B. Moffat and K. Hashimoto, J. Chem. Soc., Faraday Trans., 90 (1994) 1177.
3. W.L. Jolly, Modern Inorganic Chemistry, McGraw Hill, New York, 1985.
4. H.S. Taylor, Adv. Catalysis, 1 (1948) 1.
5. M. Che and C.O. Bennett, Adv. Catalysis, 36 (1989) 55.
6. G.D. Halsey, Adv. Catalysis, 4 (1952) 259.
7. M. Jaroniec and R. Madey, Physical Adsorption on Heterogeneous Solids, Elsevier, Amsterdam, 1988.
8. G. Tamman and W. Köster, Z. Anorg. Allg. Chem., 123 (1922) 146.
9. W.H.J. Vernon, Trans. Faraday Soc., 31 (1935) 1668.

10. J. Zeldowitch, Acta Physicochim. URSS, 1 (1934–35) 449.
11. F. Characorin and S. Elowitz, Acta Physicochim. URSS, 5 (1936) 325.
12. S.Y. Elovich and G.M. Zhabrova, Zhurn. Fiz. Khimii, 13 (1939) 1761.
13. P.T. Landsberg, J. Chem. Phys., 23 (1955) 1079.
14. C. Aharoni and F.C. Tompkins, Adv. Catalysis, 21 (1970) 1.
15. T.L. Hill, An Introduction to Statistical Thermodynamics, Addison Wesley, Reading, MA, 1960.
16. J.W. Evans, Rev. Mod. Phys., 65 (1993) 1281.
17. J.C.P. Broekhoff and R.H. van Dongen, in: Physical and Chemical Aspects of Adsorbents and Catalysts, B.G. Linsen (ed.), Academic Press, London and New York, 1970, p. 63.
18. A. Thomy and X. Duval, Surf. Sci., 299/300 (1994) 415.
19. G.F. Cerofolini, Thin Solid Films, 55 (1978) 293; 79 (1981) 277.
20. P. Pfeifer and D. Avnir, J. Chem. Phys., 79 (1983) 3558.
21. D. Avnir, D. Farin and P. Pfeifer, J. Chem. Phys., 79 (1983) 3566; Nature 308 (1984) 261.
22. G.F. Cerofolini, in: Colloid Science, D.H. Everett (ed.), The Chemical Soc., London, 1983, vol. IV, p. 59.
23. W. Rudziński and D.H. Everett, Adsorption of Gases on Heterogeneous Surfaces, Academic Press, London, 1992.
24. P. Cavallotti, G.F. Cerofolini and A. Casarico, in: Principles and Applications of Pore Structural Characterization, J.M. Haynes and P. Rossi-Doria (Eds.), J.W. Arrowsmith, Bristol, 1985, p. 171.
25. M. Jaroniec, Surf. Sci., 50 (1975) 553.
26. C.V. Heer, J. Chem. Phys., 55 (1971) 4066.
27. J. Tóth, J. Colloid Interface Sci., 163 (1994) 299.
28. G.F. Cerofolini, Thin Solid Films, 23 (1974) 129.
29. D.S. Jovanovic, Kolloid Z. und Z. Polymere, 235 (1969) 1203, 1214.
30. G.F. Cerofolini, Z. Phys. Chem. (Leipzig), 259 (1978) 314.
31. G.F. Cerofolini and N. Re, Riv. Nuovo Cimento, 16 (1993) 1.
32. M. Jaroniec, S. Sokołowski and G.F. Cerofolini, Thin Solid Films, 31 (1976) 321.
33. G.F. Cerofolini, J. Colloid Interface Sci., 86 (1982) 204.
34. B. Kindl, R.A. Pachovsky, B.A. Spencer and B.W. Wojciechowski, J. Chem. Soc., Fraday Trans. I, 69 (1973) 1162.
35. G.F. Cerofolini, Surf. Sci., 51 (1975) 333; ibid. 61 (1976) 678; Vuoto, 8 (1975) 178; J. Low Temp. Phys., 23 (1976) 687.
36. N.I. Ionescu, Surf. Sci., 61 (1976) 294; Rev. Roum. Chim., 24 (1979) 83.
37. A.W. House, in: Colloid Science, vol.IV, D.H. Everett (ed.), The Chemical Soc., London, 1983, p. 1.
38. P.J. Crickmore and B.W. Wojciechowski, J. Chem. Soc., Fraday Trans. I, 73 (1977) 1216.
39. G.F. Cerofolini and N. Re, J. Colloid Interface Sci., in press.
40. S.Z. Roginsky, C. R. AN USSR, 45 (1944) 61, 194.
41. S.Z. Roginsky, Adsorption and Catalysis, on Heterogeneous Surfaces, AN USSR, Moscow, 1949 (in Russian).
42. L.B. Harris, Surf. Sci., 10 (1968) 129; ibid. 13 (1969) 377; ibid. 15 (1969) 182.
43. G.F. Cerofolini, Surf. Sci., 24 (1971) 391; J. Low Temp. Phys., 6 (1972) 473.

44. J.P. Hobson, Can. J. Phys., 43 (1965) 1934, 1941.
45. M.M. Nederlof, W.H. Van Riemsdijk and L.K. Koopal, J. Colloid Interface Sci., 135 (1990) 410.
46. C.C. Hsu, B.W. Wojciechowski, W. Rudziński and J. Narkiewicz, J. Colloid Interface Sci., 67 (1978) 292.
47. W. Rudziński, J. Narkiewicz and A. Patrykiejew, Z. Phys. Chem. (Leipzig), 260 (1979) 1097.
48. W. Rudziński and J. Jagiełło, J. Low Temp. Phys., 45 (1981) 1.
49. W. Rudziński, J. Jagiełło and Y. Grillet, J. Colloid Interface Sci., 87 (1982) 478.
50. N. Re, J. Colloid Interface Sci., 166 (1994) 191.
51. M. Abramowitz and I.A. Stegun, Handbook of Mathematical Functions, Dover, New York, 1972.
52. G.F. Cerofolini, Z. Phys. Chem. (Leipzig), 259 (1978) 1020.
53. H.A. Taylor and and N. Thon, J. Am. Chem. Soc., 74 (1952) 4169.
54. A.S. Porter and F.C. Tompkins, Proc. Roy. Soc. (London), A 217 (1953) 529.
55. G. De Lorenzi and G. Ehrlich, Surf. Sci. Lett., 293 (1993) L900.
56. M.U. Kislyuk, Surf. Sci., 302 (1994) 395.
57. E. Cheng, M.W. Cole and P. Pfeifer, Phys. Rev. B, 39 (1989) 12962.

A. Dąbrowski and V.A. Tertykh (Editors)
Adsorption on New and Modified Inorganic Sorbents
Studies in Surface Science and Catalysis, Vol. 99

Chapter 2.5
Inverse gas chromatography in the examination of acid–base and some other properties of solid materials

A. Voelkel

Poznań University of Technology, Institute of Chemical Technology and Engineering, 60–965 Poznań, Poland

1. INTRODUCTION: *IGC WHAT IS THIS ?*

In the last twenty years of the evolution of chromatographic techniques *Inverse Gas Chromatography* (IGC) has become widely accepted, accurate, reliable and relatively fast method for characterization of polymers and their blends, silicas, modified silicas and other minerals [1]. Inverse gas chromatography is an extension of the conventional gas chromatography in which a non–volatile material to be investigated is immobilized within a column. This stationary phase is then characterized by monitoring the passage of volatile probe molecules of known properties as they are carried through the column by an inert gas. The retention time and peak elution profiles of standard solutes, influenced by the interactions between the solute and stationary phase, are used in the respective relations leading to the quantitative measures of physicochemical properties of examined material. IGC is now used to study synthetic and biological polymers, copolymers, polymer blends, glass and carbon fibres, coal, solid food, modified silicas, surfactants, petroleum pitches, and heavy residues of oil distillation [1]. The basic tools for IGC are inexpensive, widely available and well suited for routine laboratory applications. IGC data may be collected quite rapidly over extended temperature ranges. A variety of probes may be used in the mobile phase to elucidate the characteristics of the stationary phase, characteristics that otherwise are only obtained at greater expenditure of time and money.

Actually, we should separate inverse gas chromatography into inverse gas–liquid chromatography and inverse gas–solid chromatography. The obvious basis of such discrimination is the state of the column content being examined. Polymers and their mixtures, commercial stationary phases, surfactants represent liquids (at the measurement temperature) involving a mixed mechanism of the retention of the test solutes. Modified silicas are examples of solids that have been studied, and, in this case, adsorption effects predominate, while solution partition in graft chains seems to be negligible. These problems will be discussed in details by Papirer and Balard in another chapter of this book.

Recently, much attention is being placed on fibres–reinforced/polymer systems as subjects of study. It was caused by increasing emphasis on high performance reinforced polymer composites. The concept of acid/base interactions across the fibre/polymer interface was noted particularly and the relevance of acid/base theories to the behaviour of po-

lymer surfaces and at interfaces were studied. Data acquisition via IGC appeared to be sufficiently rapid and accurate to have generated appreciable advances.

Dispersive and specific interactions are considered to contribute independently to the adsorption of probe molecules at the adsorbent surface. It was presented that the adhesion of the fibre–matrix interface depends clearly on the measured strength of acid/base interactions of both fibre and polymer–matrix. Fowkes [2,3] indicated also that the surface of fillers can be chemically modified to enhance acid–base interaction and increase adsorption.

Inverse gas chromatographic measurements may be carried out both at infinite dilution and at finite solute concentrations [1]. In the first case vapours of testing solutes are injected onto the column and their concentrations in the adsorbed layer proceed to zero. Testing substances interact with strong active sites on the examined surface. The retention data are then converted into, e.g. dispersive component of the surface free energy and specific component of free energy of adsorption. In the second case, i.e. at finite solute concentrations, the appropriate adsorption isotherms are used to describe the surface properties of polymer or filler. The differential isosteric heat of adsorption is also calculated under the assumption that the isotherms were obtained at small temperature intervals.

It has been known for many years that acid–base interactions are important component of polar forces and play the significant role in adhesion of organic substances to inorganic substrates [4–7]. However, the term "polar" has been used most often in the description of adsorption adhesion phenomena and the properties of solvents. The reason is that intermolecular forces were studied first in dense gases, where dispersion forces (d), dipole- dipole interactions (p), and dipole–induced dipole interactions (i) explain most of the intermolecular interactions between pairs of molecules. These forces were assumed to explain intermolecular interactions in solids and liquids, even after the discovery of hydrogen bonds. Although it was evidence that the strength of hydrogen–bonds is independent of the magnitude of dipole moments [8] the word "polar" is used to describe intermolecular interactions involving hydrogen bonds.

Acidic or basic solvents tend to compete for the surface active sites. Such competition of these solvents with polymers or fillers is a means of measuring the acidity or basicity of the materials.

2. ACIDITY AND BASICITY

2.1. Lewis acids and bases

The electronic or Lewis acid–base definitions may be summarized as follows [9]:

a) an acid is any species (molecule, ion, or non molecular solid) that can accept a share in a pair of electrons during the course of a chemical reaction;
b) a base is any species (molecule, ion, or non molecular solid) that can denote a share in a pair of electrons during the course of a chemical reaction;
c) neutralization is co–ordinate (heterogenic) bond formation between the acid and base:

$$A+ : B \rightleftharpoons A : B$$

The usage of the molecular orbital version of the Lewis definitions allows to discuss donor and acceptor interactions, involving delocalized electron systems and localized but multicentered bonds. Moreover, one can take into account all degrees of electron donation ranging from nearly zero in the case of weak intermolecular attractions and idealized ion association, to complete transfer of one or more electrons (redox).

The prediction and quantification of Lewis acid–base interactions may proceed in three main different ways [9]:

a) hard–soft acid–base (HSAB) principle of Pearson;

b) the E&C equation of Drago and Wayland;

c) the donor and acceptor numbers of Gutmann and co–workers with following modifications.

2.2. The HSAB principle

Parr and Pearson introduced the concept [10–13] of the absolute hardness (η) of a species defined as half the negative rate at which its electronegativity change with a change in its electron population at constant potential:

$$\eta = -(\delta\chi/\delta N)\,\nu/2 = \left(\delta^2 E/\delta N^2\right)/2 = (I - A)/2 \qquad (1)$$

where: χ is the electronegativity of a species, E – energy of a species changing with a change in its electron population (N) at constant potential ν; I is the ionization potential of the species and A is its electron affinity.

Pearson translated the above expressions into molecular orbital theory terms [14,15]. Later Lee [16] discussed the extension of this application to solids in terms of the energies of their valence and conduction bands.

2.3. Drago's four–parameter equation

A double–scale enthalpy equation proposed by Drago and Wayland to correlate (and predict) the enthalpy of adduct formation in gas–phase or poorly solvating media [17,18] is given by :

$$-\Delta H_{AB} = E_A E_B + C_A C_B \qquad (2)$$

Empirically determined parameters, E_A and C_A, are assigned to an acid while, E_B and C_B are assigned to a base. When substituted into equation (2), they give the enthalpy of adduct formation for the acid–base pair. E_A and E_B parameters supposedly represent the electrostatic contributions to adduct stability, while C_A and C_B parameters are the susceptibility of the acid and base, respectively, to form covalent bonds. With increasing amount of reliable enthalpy data, the E&C model was extended to many different acids and bases.

Jensen [9] indicated that there is no evidence that Drago's parameters reflect the relative electrostatic and covalent contributions to the bonding in resulting adducts. They were not correlated with either a physical property (dipole moment, ionization potential) or with a quantum–mechanically calculated index. Drago's approach is a purely empirical method of calculating enthalpy of formation for molecular adducts. Fowkes applied the Lewis E&C equation [19] and has attempted to determine E and C parameters for both polymers and surfaces. However, Jensen [9] indicated the potential problem connected

with such extension. E&C equation approach it is assumed that a molecule is either a Lewis acid or a a Lewis base, while most molecules have both donor and acceptor sites.

2.4. Donor and acceptor numbers

The donor number (DN) as the measure of Lewis basicity [20] was defined as the negative of the molar enthalpy of formation for the adduct formed between the base in question (donor D) and reference Lewis acid $SbCl_5$ (acceptor) in a 10^{-3}M solution of dichloroethane:

$$B + SbCl_5 \rightleftharpoons B * SbCl_5 \qquad (-\Delta H_{B*SbCl_5} \equiv DN)$$

The acceptor number (AN) was defined as dimensionless number related to the relative chemical ^{31}P-NMR shift in triethylphosphine oxide $(C_2H_5)_3PO$ in the particular acceptor solvent:

$$(C_2H_5)_3\,P = O \longrightarrow \text{Acceptor}$$

This was further scaled by assigning a value of 0 (zero) to the shift induced by hexane and a value of 100 to the shift produced by $SbCl_5$ upon interacting with $(C_2H_5)_3PO$ in a diluted 1,2 - dichloroethane solutions:

$$AN \equiv \frac{\delta_{corr.} \cdot 100}{\delta_{corr.[(C_2H_5)_3PO \cdot SbCl_5)]}} = 2.348 \cdot \delta_{corr.} \tag{3}$$

Gutmann further proposed [20] that the enthalpy of a given acid–base interaction could be approximated by a two parameter equation of the form:

$$-\Delta H_{AB} = \frac{AN \cdot DN}{100} \tag{4}$$

Where the factor of 100 converts the AN values from percentage to a decimal fraction.

Jensen [9] indicated that many reported values are only approximate, as determined indirectly from linear correlation with other measures of Lewis basicity, rather than being directly measured in the laboratory.

Riddle and Fowkes [21] have shown that dispersion–only liquids, such as hexane, produce a significant ^{31}P shift in $(C_2H_5)_3PO$. Hence, AN values should be corrected for this dispersion effect. In many cases, this correction is quite substantial. Thus, 13.7 of the original 14.2 AN units assigned to pyridine appear to be due to dispersion rather than to specific electron–pair donor–acceptor interactions, lowering its measure of "true" Lewis acidity from 14.2 to 0.5 . Riddle and Fowkes have found that these dispersion corrected AN values correlate well with the enthalpies of formation of the adducts formed between $(C_2H_5)_3PO$ and the examined acid. They proposed to use this enthalpy as the true measure of Lewis acidity for a species, which allows to express both the DN and AN* (modified AN parameter) numbers in the same units:

$$AN^* = -\Delta H\,[A \leftarrow (C_2H_5)_3PO] = 0.288(AN - AN^d) \tag{5}$$

where the AN values are the original values reported by Gutmann, AN^d are the dispersion contribution given by Riddle and Fowkes and A denotes acceptor.

3. SURFACE CHARACTERISTICS

3.1. Dispersive increment of surface free energy

Intermolecular interactions in adsorbent/adsorbate system may be dispersive and specific which corresponds to the dispersive (γ_s^d) and specific component (γ_s^s) of free surface energy (γ_s) of adsorbent:

$$\gamma_s = \gamma_s^d + \gamma_s^s \tag{6}$$

The standard free energy of transferring a mole of vapour from the gas phase to a standard state on the surface, i.e. adsorption energy, is given by:

$$\Delta G^0 = -RT \ln \frac{B \cdot V_N}{S \cdot g} \tag{7}$$

where: $B=2.99 \cdot 10^2$ (according to the deBoers definition of the surface pressure in the adsorbed state), S – is the specific area of adsorbent [m^2/g], g is the mass of the adsorbent in the column [g], and V_N is the net retention volume [m^3].
For a givens system B,S and g are constant and equation (7) changes into:

$$\Delta G^0 = -RT \cdot \ln V_N + \text{const.} \tag{8}$$

Please note that the value of constant in equation (8) depends on the arbitrary chosen reference state of adsorbed molecule.

For test substance free energy of adsorption (ΔG^0) is the sum of energies of adsorption attributed to dispersive and specific interactions. Adsorption of non–polar probes as n–alkanes is caused by dispersive interactions, whereas for polar probes both London and acid–base interactions contribute to ΔG^0:

$$\Delta G^0 = \Delta G^d + \Delta G^s \tag{9}$$

where ΔG^d, ΔG^s are the dispersive and specific component of the free energy of adsorption, respectively.

For n–alkanes $\Delta G^0 = \Delta G^d$ and changes with the number of carbon atoms in their molecules. The increment of adsorption energy corresponding to methylene group may be calculated from:

$$\Delta G_{CH_2} = -RT \ln (V_{N,n}/V_{N,n+1}) \tag{10}$$

where $V_{N,n}$ and $V_{N,n+1}$ denote the net retention volumes of two consecutive n–alkanes having n and (n+1) carbon atoms in their molecules.
This parameter is independent on the chosen reference state of the adsorbed molecule.

According to Dorris and Gray [22]:

$$\Delta G_{CH_2} = 6.023 \cdot 10^{23} \cdot a_{CH_2} \cdot 2 \left(\gamma_s^d \cdot \gamma_{CH_2}\right)^{1/2} \tag{11}$$

where a_{CH_2} denotes the surface covered by one methylene group (0.06 nm^2) and γ_{CH_2} is the free surface energy of polyethylene. Most often γ_{CH_2} is taken as 35.6 [mJ/m^2] or its variation with temperature is taken into account:

$$\gamma_{CH_2} = 35.6 + 0.058 \cdot (293 - T) \tag{12}$$

The dispersive component of surface free energy γ_s^d may be calculated from Eq.(11) with the use of experimentally determined ΔG_{CH_2}[23–47].

3.2. The specific component of free energy of adsorption

The specific component of free energy of adsorption is generally determined by the subtraction the dispersive component from the total free energy of adsorption. Several procedures of the calculation of the specific component have been presented in the literature. The differences between the respective procedures lie in the choose of the reference state of the adsorbed molecule.

Saint Flour and Papirer [48] proposed to determine the specific component of free energy of adsorption ΔG^s as the vertical distance between n–alkanes reference line and the point on diagram corresponding to the polar test probe. As the physicochemical property used for definition of the reference state they choose saturated vapour pressure $\log P_0$. Therefore, ΔG^s corresponds to the difference in free energies of adsorption between given test probe and hypothetical n–alkane having the same vapour pressure:

$$\Delta G_x^s = \Delta G_x^0 - \Delta G_x^d = -RT \cdot \ln (V_{N,x}/V_{N,ref}) \tag{13}$$

where: ΔG_x^0, ΔG_x^s, ΔG_x^d denote free energy of adsorption, and its specific and dispersive component, respectively, determined for the test solute x; $V_{N,x}$ and $V_{N,ref}$ refer to the net retention volumes of test substance and the reference hypothetical n–alkane.

Dong et al. [49] defined another reference state in terms of molecular polarizability of n–alkanes. In such a case the expression derived from equation (8) is as follows:

$$RT \ln V_N + C = C' \cdot P_{DS} \cdot P_{DP} - \Delta G^s \tag{14}$$

where C and C′ are two constants relating to the same reference state; P_D is the molar deformation polarization and indices S and P refer to solid (investigated substance) and the test probe, respectively.
In the case of adsorption of n–alkanes $\Delta G^s = 0$ and Eq.(14) becomes:

$$RT \ln V_N + C = C' \cdot P_{DS} \cdot P_{DP} \tag{15}$$

Authors of Ref. [49] proved that the variation of the term $RT \cdot \ln V_N$ as a function of the molar deformation polarization of n–alkanes P_{DP} is a straight line which slope equal to $C' \cdot P_{DS}$ is proportional to the surface ability for dispersive interactions. $\Delta G^s = 0$ is defined in the same way as in the case of Saint Flour–Papirer's method. However, in this procedure $\Delta G^s = 0$ values are always positive while in approach [48] the negative values of the specific component of the free energy of adsorption were observed. Later, Donnet et al. [29] observed that their earlier proposal (i.e. that from Ref.[49]) based on the fundamental London equation gives only a first approximation of the ionization energy of a molecule. They proposed to use Eq.(15) in the form:

$$RT \ln V_N + C = \theta_L = K \cdot (h\nu_s)^{1/2} \cdot \alpha_{0s} \cdot (h\nu_L)^{1/2} \cdot \alpha_{0L} \tag{16}$$

where $h\nu_i$ is the ionization potential of the i–th interacting material, α_0 the deformation polarizability and K a constant which takes into account the permittivity in the vacuum, the distance between interacting molecules and Avogadro number. S and L refer to solid

and liquid, respectively. The slope of Eq.(16) $\left[K \cdot (h\nu_s)^{1/2} \cdot \alpha_{0s}\right]$ is characteristic of a given solid surface and is related to the London dispersive component γ_s^d of this surface.

Chehimi and Pigois-Landureau [24] compared six methods of evaluating ΔG^s where RTln V_N values were related to the abscissa coordinates labelled as follows: I, ΔH^d_{vap}; II, ΔH_{vap}; III, T_b; IV, log P_0; V, $a(\gamma_L^d)^{1/2}$; VI, $(h\nu)^{1/2}\alpha_0 10^{49}$. Authors stated that the ΔH^d_{vap} approach is linked to those of authors of Refs. [48, 50] and, more importantly, takes into account the self-association character of the polar probes, as recommended by Fowkes [51].

3.3. Determination of acid–base interactions

Examination of the temperature dependence of gives the possibility of ΔG^s the determination of the enthalpy of specific interactions ΔH^s[28]:

$$\Delta H^s = -T^2 \frac{\delta}{\delta(T)} \left(\frac{\Delta G^s}{T}\right) \tag{17}$$

ΔH^s is given by the slope of the straight-line obtained by plotting $\Delta G^s/T$ against T^{-1}. Most often ΔH^s was determined according to the above equation. However, Kamdem et al. [31] proposed to determine ΔH^s by subtraction from ΔH^0_a value (enthalpy of adsorption) the increment corresponding to dispersive interaction proportional to the molecular mass of n- alkanes:

$$\Delta H^d_A \cong A \cdot M \tag{18}$$

where A is the proportional factor.
ΔH^0_A was determined directly from temperature dependence of the specific retention volume:

$$-\Delta H^0_A = R \frac{d(\ln V_g)}{d(1/T)} \tag{19}$$

Tiburcio and Manson's approach [52] was based mainly on the following assumption:

$$\Delta H^{ab} = \Delta H_A - \Delta H^d = \Delta H_A - \Delta H_{vap} \tag{20}$$

where ΔH_A, ΔH^d and ΔH_{vap} are the enthalpy of adsorption, its dispersive increment and the heat of vaporization of the injected probe. Authors have modified the method to evaluate ΔH^{ab} (equal to ΔH^s) from experimental values of enthalpy of adsorption:

$$\Delta H^{ab} = \left(\Delta H_{exp} - \Delta H^d\right)_{probe} - \left(\Delta H_{exp} - \Delta H^d\right)_{model} \tag{21}$$

where the model must be neutral and approximately similar in size to the adsorbate probe. Pigois-Landureau and Chehimi [23] have shown that the acid–base contribution to the enthalpy of adsorption (ΔH^{ab}) can be affected by the degree of self association of the polar probes and thus suggested to compare ΔH_A to ΔH^d_{vap}, the dispersive contribution to the heat of vaporization:

$$\Delta H^{ab} = \left(\Delta H_A - \Delta H^d\right)_{probe} - \left(\Delta H_A - \Delta H^d_{vap}\right)_{model} \tag{22}$$

Enthalpy of specific interactions between the examined surface and the test solute may be correlated to acid–base properties of both species by using Drago's equation [23,52] or, in author's opinion better (and often used), through the following equation:

$$-\Delta H^S = K_D \cdot AN + K_A \cdot DN \tag{23}$$

where: AN and DN are acceptor and donor number of test solute, respectively. Parameters K_A and K_D reflect the ability of the examined surface to act as electron acceptor and electron donor, respectively. AN denotes acceptor number in Gutmann [20] or Riddle–Fowkes scale [21]. However, the application of Gutmann's (AN) acceptor number cause significant problem with the expression of K_D units. As AN is unitless K_D should be expressed in energy units [kJ/mol] or [kcal/mol], while K_A must be unitless. Therefore, the comparison of electron donor and electron acceptor surfaces of examined surface are impossible. The expression of the test solute acceptor properties in Riddle/Fowkes scale (AN*) leads to both dimensionless K_A and K_D parameters and allows to determine their ratio, i.e. surface character $S_C = K_D/K_A$.

Procedure proposed by Papirer et al. [28,37–39,53] was used in characterization of silicas, modified silicas, oxides and minerals. Authors of refs. [23–28,30,54] used this method for characterization of carbon fibers, solid polymers, i.e. conducting polypyrroles, polycarbonates and poly(dimethacrylates), respectively. Voelkel and Krysztafkiewicz [55] characterized silicas modified by organic compounds.

Nardin et al. [28] studied the surface characteristics of carbonized and stabilized carbon fibers. They determined the dispersive component of the surface energy and the acid–base characteristics for both types of investigated surfaces. They found K_A parameter equal to 1.0 and 1.5, while K_D equal to 1.4 and 1.3, for carbonized and stabilized carbon fiber, respectively. Carbonized fibers presented an electron–donating character, suitable for strong interactions with an acidic resin. Stabilized fibers were more amphoteric. The surface character was quantitized by K_D/K_A parameter equal 1.4 and 0.9, respectively. However, as acceptor number of test solutes was expressed in Gutmann scale (without correction for dispersive interactions) one should take into account the limitations indicated above. Donnet and Park [30] examined the series of pitch–based carbon fibers. The free energies of adsorption corresponding to specific interactions were determined from Eq. (16). They explained the decrease of K_A from carbonization level (K_A=6.5) to graphitization level (K_A=3.6) by the decrease of the content of oxygen, while the increase of this parameter in the group of graphitized fibers may be related to the increase in active surface oxygen. As previously, uncorrected AN values were in calculation of K_D and K_A characteristics.

Kamdem et al. [31] have used the AN values of polar probes as suggested by Riddle and Fowkes in characterization of birch wood meal by IGC method. The reported values of K_D and K_A indicated that white birch wood surface has an amphoteric character and predominantly acidic sites are involved in the adsorption process.

Surface characteristics of the series of commercially available aluminas with the use of IGC were reported by Papirer et al. [34]. Values of the dispersive component of surface free energy γ_s^d varied from 65 to 100 mJ/m^2. Authors determined also K_D and K_A values. The variation of the electron donor parameter K_D was almost negligible (2.1–2.7), while K_A parameter increased from 5.6 to 9.9 units. The significant changes for acidity were related to the SiO_2 content. Acidity parameter, K_A, reached a constant value for a SiO_2 content of about 1000 ppm. However, AN and DN were taken from Gutmann's proposal

and authors didn't determined the units of K_D and K_A parameters. One may understand that K_D was expressed in [kcal/mol] and K_A was unitless.

The previous and other works were directed to the simplification of the procedure of determination of parameters reflecting acceptor and donor properties of surfaces. For instance, several authors used equation (23) in another form introducing at the left side ΔG^s instead of ΔH^s. Such treatment leads to the limitation of applicability and comparability of K_A and K_D to only one temperature. It means that K_A and K_D values will change with changing temperature of a measurement. Moreover, the from definition AN* and DN number express the enthalpy effects not free energy.

Papirer et al. [34] characterized the properties of aluminas parallely by K_D and K_A values and Ω parameter defined as:

$$\Omega = \frac{V_N(C_2H_5\text{–}O\text{–}C_2H_5)}{V_N(CH_2Cl_2)} \tag{24}$$

Authors suggested that whereas K_A describes the acidic character of Al_2O_3, the value of Ω gives more global information on the acid/base properties of the samples. The acid/base Ω parameter first increased with increasing amounts of SiO_2 and then decreases, indicating that the presence of other impurities (on the alumina surface) cannot be ignored.

Osmont and Schreiber introduced interaction parameter Ω as a measure of acidity and basicity of glass fibers [56]. This parameter was calculated by using specific retention volumes of the injected probes, i.e. n–butanol and butylamine. For acidic surfaces, where the specific retention volume for the base exceeds that for the acidic alcohol:

$$\Omega = 1 - \left(V_g^0\right)_b / \left(V_g^0\right)_a < 0 \tag{25}$$

where $(V_g^0)_b$ and $(V_g^0)_a$ denote specific retention volumes of the base and the acid, respectively.

For basic stationary phases the specific retention volume exceeds that for the butylamine and

$$\Omega = \left(V_g^0\right)_a / \left(V_g^0\right)_b - 1 > 0 \tag{26}$$

Schreiber et al. [57] proposed also another definition of acceptor and donor numbers (assigned here as AN_{Sch} and DN_{Sch}, respectively) not related to Gutmann's scale and defined as follows:

$$AN_{Sch} = V_{N,THF}/V_{N,ref} \tag{27}$$

$$DN_{Sch} = V_{N,CHCl_3}/V_{N,ref} \tag{28}$$

where $V_{N,THF}$, $V_{N,CHCl_3}$ denote the net retention volume of test probes – tetrahydrofurane and chloroform, respectively, while $V_{N,ref}$ has the same meaning as defined by Papirer, i.e. the net retention volume of the hypothetical n–alkane having the same vapour pressure as the polar test probe. Comparing the equation (13) one may conclude that acceptor and donor numbers defined by equations (27) and (28) are directly related to the specific component of free energy of adsorption.

Authors [57] used such defined AN_{Sch} and DN_{Sch} values to calculate new index of acid–base properties – K. It is defined as the difference between DN_{Sch} and AN_{Sch} numbers.

$K > 0$ for basic surfaces and $K < 0$ for acidic ones. K near zero determine the neutral and amphoteric surface.
Chehimi et al.[58] followed this idea and suggested the new index of acidity:

$$\Omega_A = V_N^{AB}(\text{base})/V_N^{AB}(\text{acid}) \tag{29}$$

and the new index of basicity:

$$\Omega_B = \Omega_A^{-1} = V_N^{AB}(\text{acid})/V_N^{AB}(\text{base}) \tag{30}$$

where V_N^{AB} denote the acid–base contribution to the net retention volume of the polar probe.
They proposed also two dimensionless hard (H) and soft (S) indices of basicity:

$$\Omega_{HB} = V_N^{AB}(CHCl_3)/V_N^{AB}(DXN) \tag{31}$$

$$\Omega_{SB} = V_N^{AB}(t-BuOH)/V_N^{AB}(THF) \tag{32}$$

where $CHCl_3$, DXN, t-BuOH and THF refer to chloroform, 1,4–dioxane, tert–butyl alcohol and tetrahydrofurane, respectively.
Here again the applicability of the described above indices is limited to only one temperature which strongly reduces their universality.

3.4. Specific interaction parameter $\mathcal{E}_\pi$

Alkanes have been used in conjunction with unsaturated and aromatic hydrocarbons to study specific interactions of different surfaces [59–61] in therms of the enthalpy of adsorption. Sidqi et al. [53] defined the specific interaction parameter $\mathcal{E}_\pi$:

$$\mathcal{E}_\pi = \Delta G^0_{\text{alkane}} - \Delta G^0_{\text{alkene}} \tag{33}$$

This quantity describes the π bond interactions with electron acceptor sites on the surface, i.e. is a measure of the specific interaction capacity of the surface. $\mathcal{E}_\pi$ may be easily determined from the retention data (net retention volume) of the n–alkane/n–alkene pair having the same number of carbon atoms in the molecules:

$$\mathcal{E}_\pi = RT \ln \frac{t_{N(n)}^{\text{alkene}}}{t_{N(n)}^{\text{alkane}}} \tag{34}$$

Jagiello et al. [62] indicated that the quantities ΔG_{CH_2} and $\mathcal{E}_\pi$ contain information about microstructure and surface chemical functionalities of the adsorbent. ΔG_{CH_2} is responsive to the changes in the microstructure as well as the addition (removal) of surface chemical groups. $\mathcal{E}_\pi$ is predominantly affected by changes in the electron acceptor ability of the adsorbent.

Specific interaction parameter $\mathcal{E}_\pi$ was used in the description of the surface properties of activated carbons [62] and pure and composite oxides [63].

3.5. The use of the solvation equation in inverse gas–solid chromatography

Abraham et al. [64] characterized fullerene as adsorbent in gas–solid chromatography experiment. From the adsorption isotherms, gas–solid partition coefficients defined by Eq.(35), were calculated:

$$K_c = (C_s/C_g); \quad C_g \rightarrow 0 \tag{35}$$

where C_s and C_g are the concentration of solute in the solid (g/g) and in the gas phase (g/dm^3). The K_c values were analysed through the solvation equation developed by Abraham [65]:

$$\log(SP) = c + rR_2 + s\pi_2^H + a\sum\alpha_2^H + b\sum\beta_2^H + l \cdot \log L^{16} \tag{36}$$

where SP is property of a series of solutes in a fixed phase; R_2 is an excess molar refraction, π_2^H is the solute dipolarity/polarisability, $\sum\alpha_2^H$ and $\sum\beta_2^H$ are the solute hydrogen–bond acidity and basicity, respectively, and log L^{16} is derived from the from the solute gas–hexadecane partition coefficient at 298K [65]. Here, log K_c where used as solute property, i.e. log (SP).

Authors indicated that as the descriptors in Eq.(36) refer to particular properties of the solutes, the coefficients in the equation will correspond to specific properties of the solid phase as follows: **r** – refers to the ability of the phase to interact with solute π– and n–electron pairs; **s** to the phase dipolarity/polarisability; **a** to the phase hydrogen–bond basicity; **b** to the phase acidity, and **l** to the phase lipophilicity. Analysis of these coefficients lead authors to the statement that solute dipolarity/polarisability, hydrogen–bond acidity, and general dispersion interactions influenced adsorption. The examined fullerene was weakly polarisable and had some hydrogen–bond basicity.

The same method was used in examination of carbonaceous adsorbents where log V_g was used as log (SP) in Eq.(36) [66].

REFERENCES

1. A.Voelkel, Crit.Rev.Anal.Chem., 22 (1991) 411.
2. F.M.Fowkes, in: Physicochemical Aspects of Polymer Interfaces, K. L. Mittal (ed.), vol. 2, Plenum Press, New York, 1983.
3. F.M.Fowkes and M.A.Mostafa, Ind.Eng.Chem.Prod.Res.Dev., 17 (1978) 3.
4. F.M.Fowkes, G.S.Ranay and M.J.Schrick, J.Phys.Chem., 63 (1959)1684.
5. J.C.Bolger and A.S.Michaels, in: Interface Conversion for Polymer Coatings, P.Weiss (ed.), Elsevier, New York, 1968.
6. Yu.S.Lipatov and L.M.Sergeeva, Adsorption of Polymers, Halsteol, New York, 1974.
7. P.Sprensen, J. Paint Technol., 47 (1975) 31.
8. G.C.Pimentel and A.L.McClellan, The Hydrogen Bond, Freeman, San Francisco, 1960.
9. W.B.Jensen, J. Adhesion Sci. Technol., 5 (1991) 1.
10. R.G.Parr and R.G.Pearson, J.Am.Chem.Soc., 105 (1983) 7512.
11. M.Berkowitz, S.K.Gosh and R.G.Parr, J.Am.Chem.Soc., 107 (1985) 6811.
12. W.Yang, and R.G.Parr, Proc.Natl.Acad.Sci., 82 (1985) 6723.

13. M.Berkowitz and R.G.Parr, J.Chem.Phys., 88 (1988) 2554.
14. R.G.Pearson, Proc.Natl.Acad.Sci., 83 (1986) 8440.
15. R.G.Pearson, Inorg.Chem., 27 (1988) 734.
16. L.H.Lee, J.Adhes., 36 (1991) 39.
17. R.S.Drago and B.Wayland, J. Am. Chem. Soc., 87 (1965) 3571.
18. R.S.Drago, G.C.Vogel and T.E.Needham, J. Am. Chem. Soc., 93 (1971) 6014.
19. F.M.Fowkes, in: Surface and Colloid Science in Computer Technology, K.L.Mittal (ed.), Plenum Press, New York, 1987.
20. V.Gutman, The Donor-Acceptor Approach to Molecular Interactions, Plenum Press, New York, 1978.
21. F.L.Riddle and F.M.Fowkes, J. Am. Chem. Soc., 112 (1990) 3259.
22. G.M.Dorris and D.G.Gray, J.Colloid Interface Sci., 71 (1979) 931.
23. E.Pigois-Landureau and M.M.Chehimi, J.Applied Polym.Sci., 49 (1993) 183.
24. M.M.Chehimi and E.Pigois-Landureau, J.Mater.Chem., 4 (1994) 741.
25. U.Panzer and H.P.Schreiber, Macromolecules, 25 (1992) 3633.
26. A.Voelkel, E.Andrzejewska, R.Maga and M.Andrzejewski, Polymer, 33 (1993) 3109.
27. A.Voelkel, E.Andrzejewska, R.Maga and M.Andrzejewski, Polymer, 35 (1994) 1789.
28. M.Nardin, H.Balard and E.Papirer, Carbon, 28 (1990) 43.
29. J.B.Donnet, S.J.Park and H.Balard, Chromatographia, 434 (1991) 434.
30. J.B.Donnet and S.J.Park, Carbon, 29 (1991) 955.
31. D.P.Kamdem, S.K.Bose and P.Luner, Langmuir, 9 (1993) 3039.
32. V.Bogillo and A.Voelkel, Polymer, in press.
33. E.Papirer, J.M.Perrin, B.Siffert, G.Philipponneau and J.M.Lamerant, J.Colloid Interface Sci., 156 (1993) 104.
34. E.Papirer, J.M.Perrin, B.Siffert and G.Philipponeau, J.Colloid Interface Sci., 144 (1991) 263.
35. E.Papirer, G.Ligner, H.Balard, A.Vidal and F.Mauss, in: Chemically Modified Oxide Surfaces, D.E.Leyden and W.T.Collins (eds.), Gordon and Branch Science Publishers, New York, 1989.
36. E.Papirer, P.Roland, M.Nardin and H.Balard, J.Colloid Interface Sci., 113 (1986) 62.
37. M.Sidqi, H.Balard, E.Papirer, A.Tuel, H.Hommel and A.P.Legrand, Chromatographia, 27 (1989) 311.
38. E.Papirer, H.Balard, Y.Rahmani,A.P.Legrand, L.Facchini and H.Hommel, Chromatographia, 23 (1987) 639.
39. H.Balard, M.Sidqi, E.Papirer, J.B.Donnet, A.Tuel, H.Hommel and A.P.Legrand, Chromatographia, 25 (1988) 712.
40. A.Vidal, E.Papirer, Wang Meng Jiao and J.B.Donnet, Chromatographia, 23 (1987) 121.
41. E.Papirer, A.Vidal and H.Balard, in: Inverse Gas Chromatography. Characterization of Polymers and Other Materials, D.R.Lloyd, T.C.Ward, H.P.Schreiber (eds.), ACS, Washington (1989).
42. E.Papirer, H.Balard and A.Vidal, Eur.Polym.J., 24 (1988) 783.
43. M.M.Chehimi, M.L.Abel, E.Pigois-Landureau and M.Delamar, Synthetic Metals, 60 (1993) 183.

44. K.Tsutsumi, T.Ohsga, Colloid Polymer Sci., 268 (1990) 38.
45. R.Zhang, J.Jagiello, J.F.Hu, Z.Q.Huang, J.A.Schwarz and A.Datye, Applied Catalysis A: General, 84 (1992) 123.
46. T.J.Bandosz, J.Jagiello, B.Andersen and J.A.Schwarz, Clays and Clay Minerals, 40 (1992) 306.
47. L.Lavielle and J.Schultz, Langmuir, 7 (1991) 978.
48. C.Saint Flour and E.Papirer, J.Colloid Interface Sci., 91 (1983) 69.
49. S.Dong, M.Brendle and J.B.Donnet, Chromatographia, 28 (1989) 469.
50. D.J.Brookman and D.T.Sawyer, Anal.Chem., 40 (1968) 106.
51. F.M.Fowkes, J.Adhesion Sci.Technol., 1 (1990) 7.
52. A.C.Tiburcio and J.A.Manson, J.Appl.Polym.Sci., 42 (1991) 427.
53. M.Sidqi, G.Ligner, J.Jagiello, H.Balard and E.Papirer, Chromatographia, 28 (1989) 588.
54. E.Andrzejewska, A.Voelkel, M.Andrzejewski and R.Maga, Polimery, 39 (1994) 464 (in Polish).
55. A.Voelkel and A.Krysztafkiewicz, Macromolecular Chemistry and Physics, submitted.
56. E.Osmont and H.P.Schreiber, in: Inverse Gas Chromatography. Characterization of Polymers and Other Materials, D.R.Lloyd, T.C.Ward and H.P.Schreiber (eds.), ACS Symposium Series No. 391, ACS, Washington,1989.
57. H.P.Schreiber, J.–M.Viau, A.Fetoui and Zhuo Deng, Polym.Eng.Sci., 30 (1990) 263.
58. M.M.Chehimi, M.–L.Abel, E.Pigois–Landureau and M.Delamar, Synthetic Metals, 60 (1993) 183.
59. T.Ahsan, B.A.Colenutt and K.S.W.Sing, J.Chromatogr., 464 (1989) 416.
60. T.Ahsan, B.A.Colenutt and K.S.W.Sing, J.Chromatogr., 479 (1989) 19.
61. S.K.Milonjic and M.M.Kopecni, Chromatographia, 19 (1984) 342.
62. J.Jagiello, T.J.Bandosz and J.A.Schwarz, J.Colloid Interface Sci., 151 (1992) 433.
63. Cr.Contescu, J.Jagiello and J.A.Schwarz, J.Catalysis, 131 (1991) 433.
64. M.H.Abraham, C.M.Du, J.W.Grate, R.A.McGill and W.J.Shuely, J.Chem.Soc., Chem. Commun., (1993) 1863.
65. M.H.Abraham, Chem.Soc.Rev., 22 (1993) 73.
66. M.H.Abraham and D.P.Walsh, J.Chromatogr., 627 (1992) 294.

This Page Intentionally Left Blank

A. Dąbrowski and V.A. Tertykh (Editors)
Adsorption on New and Modified Inorganic Sorbents
Studies in Surface Science and Catalysis, Vol. 99

Chapter 2.6
Chemical and morphological characteristics of inorganic sorbents with respect to gas adsorption

E. Papirer and H. Balard

Centre de Recherches sur la Physico–Chimie des Surfaces Solides, CNRS
F 68200 Mulhouse, France

1. INTRODUCTION

Knowledge of chemical, structural and morphological characteristics of solid surfaces greatly facilitates understanding of their behaviours when they are placed in gaseous, liquid or polymer environments, for instance. Whereas some "reference" materials such as graphite or muscovite have received much attention, common solids such as silicas, aluminas, talc, etc., have gained an interest only in recent years; the lack of adequate and convenient methods for the surface characterisation being one of the major reasons of the situation. In fact, only a very few methods may be considered as true surface examination methods: wettability procedures such as measurement of contact angles of liquid drops deposited on the surface of compressed powder disks [1] or capillary rise of liquid in a powder column [2], gas adsorption and interpretation of the value of the spreading pressure [3] and inverse gas chromatography [4]. The latter method has now become very familiar, but, as will be shown in this paper, the interpretation of the chromatographic data is all but not univocal.

The surface chemical and morphological characteristics of inorganic sorbents such as silicas, aluminas, talc, micas define both their chemical and physical adsorption potentials (surface energy). But the existence of mineral and organic surface pollutants will indeed strongly influence those properties.

2. RELATION BETWEEN SURFACE CHEMISTRY AND SURFACE ENERGY

There is very little information in the literature about a possible relation between surface chemistry and surface energy, even in general [5]. To our knowledge, most of the work on mineral oxides was made in our laboratory and will be reviewed in the following section.

2.1. Definition

Only a few definitions will be recalled in this instance. The surface energy of a solid (γ_s)

corresponds to its potential to exchange physical interactions. One usually distinguishes London (dispersive, universal, non-specific) interactions from specific interactions (polar, acid-base, H-bonding). γ_s^d encounters for London interactions whereas γ_s^{sp} encloses all the other types of interactions.

As stated above, IGC is possibly the most rapid method for the evaluation of γ_s^d and of a specific interaction parameter, Isp, that qualitatively describes the affinity of the solid surface for non specific interactions. London interactions between two partners are proportional to their polarisabilities, to their molecular ionisation potentials, and to the number of elemental volumes of the two phases in interaction. Hence, taking one partner as a molecular probe allows to detect changes that may occur when, for instance, submitting the other partner to heat treatments or chemical transformations.

2.2. Variation of surface properties by heat treatment of silicas and aluminas

Perhaps, the most easy and common way to change the surface properties of a solid is to submit it to a heat treatment. Silicas, for example, are heat treated so as to enhance their ability to adsorb water. Upon heat treatment, surface hydroxyls condense. The variation of the number and nature of surface hydroxyls or silanol groups may be evaluated using a series of techniques [6]. However, it is only recently that the concomitant variation of surface energy characteristics was evidenced by IGC [7].

The principles of IGC as well as experimental details have been reviewed elsewhere [8]. The attention of the reader is simply drawn to two possible ways to operate IGC: either under infinite dilution, or finite concentration conditions. For the determination of γ_s^d, exploiting IGC under infinite dilution conditions, minute amounts of a homologous series of n alkanes are injected in the GC and their retention volumes (Vn) are detected (volume of carrier gas necessary to push the solute through the column containing the solid to be examined). γ_s^d is then simply obtained by application of the following relationships:

$$\gamma_s^d = \frac{1}{\gamma_{CH_2}} \left[\frac{\Delta G_{CH_2}}{2 \cdot N_A \cdot a} \right]^2 \tag{1}$$

$$\Delta G_{CH_2} = RT \ln \frac{V_{n+1}}{V_n} \tag{2}$$

where γ_{CH_2} is the surface energy of a solid entirely made of CH_2 groups, i.e. poly(ethylene), N_A is the Avogadro's number and "a" is the cross-sectional area of a CH_2 group, ΔG_{CH_2} is the free energy of adsorption of a CH_2 group, V_{n+1} and V_n are the retention volumes of n alkanes having respectively (n+1) and n atoms of carbon. It should be stressed here that a few injected alkane molecules will be most strongly retained on the most active adsorption sites that may be of quite different natures: chemical groups, but also structural defects. In other terms, for a surface that is energetically very heterogeneous, the value of γ_s^d, determined by IGC, will essentially reflect the existence of those active sites and will, in no way, correspond to a mean value of the surface energy. In such cases, γ_s^d takes values too high to be consistent with a physical reality. Hence, much care should be taken to evaluate correctly the meaning of γ_s^d in such cases.

Fig. 1 shows the variation of γ_s^d measured at 100°C by IGC, when treating a pyrogenic or fumed silica (Aerosil from Degussa, Germany) at 100 - 700°C. The same figure presents

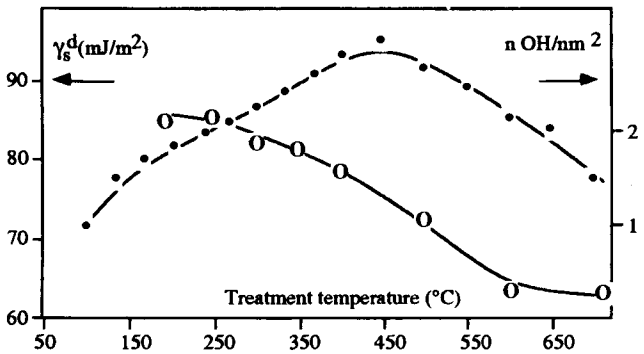

Figure 1. Variation of the London component (γ_s^d), measured at 80°C (o), and of the number of silanol groups (•) upon heat treatment temperarure (HTT) of a fumed silica sample.

also the evolution of the number of hydroxyl surface groups, measured radiochemically after esterification with ^{14}C labelled methanol.

Whereas the number of silanol groups diminishes monotonously upon increasing the heat treatment temperature, γ_s^d changes quite unexpectedly, going through a maximum. Comparing this observation with the results of Brinker et al. [9] who followed, by Raman spectroscopy, the formation of strained siloxane rings generated by the condensation of two adjacent silanol groups, suggests an explanation. These authors have shown that upon heating, three-member and highly polarisable siloxane rings are formed. Its concentration is optimum at about 500–600°C, and then decreases: three member siloxane rings transform into 4 membered, non polar, siloxane rings. Since γ_s^d is most sensitive to variation in polarisability, it is understandable that it will follow the trend of concentration evolution of 3 membered siloxane groups on the surface of silica.

Also very striking observations were made when examining, in a similar way, the variation of the γ_s^d of alumina (Aluminoxyd C, from Degussa) upon heating [10]. Such a sample is prepared using the same hydropyrogenation procedure as for the preparation of fumed silicas. Figure 2 exhibits the results which again reveal an augmentation of γ_s^d followed by a significant decrease after treatment of Al_2O_3 at 350°C.

At the first sight, the γ_s^d variation is surprising since Al_2O_3 was obtained at about 900°C and should therefore be stable below that temperature. In fact, after its preparation, the powder has been exposed to atmospheric conditions, i.e. to humidity. It is then that the surface may undergo an ageing process by fixation of water and transformation in an hydroxylated layer. However, no common analytical method (XR, IR, ESCA) is able to identify probably the molecularly thick surface layer. We undertook a series of experiments to verify this possibility. Firstly, we checked the irreversibility of the phenomena by examining the 600°C heat treated sample in the same way as the initial sample. No evolution of γ_s^d is recorded demonstrating that indeed the postulated hydroxylated layer has been entirely converted. Secondly, after "rehydration" of the 600°C treated sample, an operation which is simply performed by injecting water vapour, at 100°C, in the GC column containing the heat treated alumina, the Al_2O_3 surface shows again an evolution of γ_s^d very similar to the one observed with the "as received" sample. Finally, boehmite

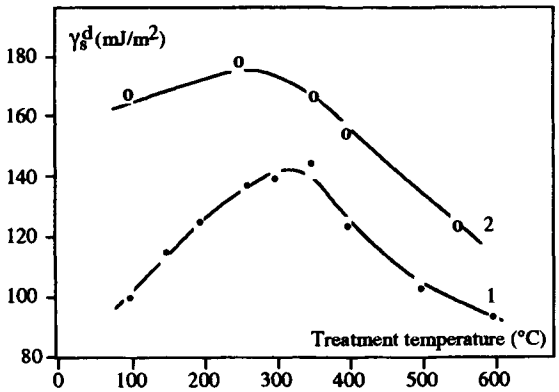

Figure 2. Variation of the London component (γ_s^d) of Al_2O_3 (1) and boehmite (2), measured at 60°C, after heat treatment at different temperatures.

was submitted to the IGC examination. The thermal decomposition of boehmite (Al_2O_3, H_2O) is well described in the literature [11]. It is known, in particular, that under controlled water pressure, boehmite transforms into γ-alumina precisely at 350°C. In our experimental conditions, the transformation was provoked under non-controlled water vapour pressure and hence, we are not expecting such a critical temperature of transformation, but rather a temperature range around 350°C. In Figure 2, it is apparent that γ_s^d of that treated boehmite samples also follows the same trends as the initial alumina sample. We may therefore conclude that, indeed, an ageing process causes the formation of a hydrated, but very thin, surface layer on particulate aluminas, which is of the boehmite type. The rather high values of γ_s^d detected on boehmite are possible to explain by nanorugosity effects as will be seen later.

Work to extend the approaches, using *IGC as a unique detector for surface events* is in progress. Clearly, IGC by itself will never be able, as chromatography in general, to deliver the whole message. Complementary methods must be applied as shown by the following example. Here, we [11] studied the surface characteristics of goethite, an iron oxide, by both IGC, and thermodesorption.

So far, to the best of our knowledge, the surface energy of goethite has never been investigated. Fig. 3 exhibits, on the one hand, the variation of γ_s^d (measured at 100°C) and the evolution of the water released during the thermal treatment, on the other hand.

One can make two remarks. Firstly, the γ_s^d value of initial goethite (FeOOH) is rather high, too high compared to the mean γ_s^d values of oxides. Secondly, the evolution of γ_s^d does not exactly correlate with the departure of water. Therefore, it seems reasonable to suspect that the change of γ_s^d is ascribable to chemical alteration of the surface upon heating, but also to some other factor, probably a change of nanostructure or nanomorphology as we shall discuss it afterwards.

2.3. Relation between surface contamination or modification and surface energy

The examples of surface properties determination presented so far, refer to almost pure oxides and a possible question could be: what is the influence on γ_s^d of surface contami-

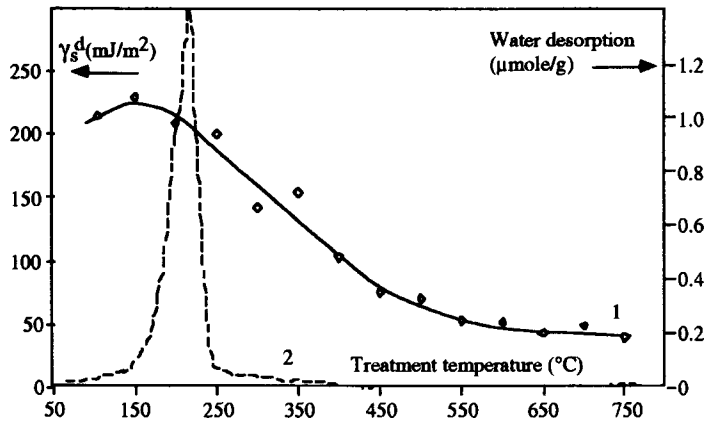

Figure 3. Effect of heat treatment of Goethite (95 m^2/g) on the γ_s^d values (1) and on the water release (2).

nants, either mineral or organic, either present as synthesis impurities or intentionally added so as to control the surface characteristics. Obviously, one would expect that the presence of contaminants or the treatment will have a definite influence. It remains to find a way to quantify this influence [13].

To test the role of impurities, a series of α aluminas, having different contents of mineral impurities, yet at ppm levels, was investigated (Table 1).

Table 1
Characteristics of α aluminas samples with different impurities contents (in ppm)

Alumina	A1	A2	A3	A4	A5	A6	A7	A8	A9
$S(m^2/g)$	10.6	6.0	9.3	11.7	10.8	0.8	1.5	0.8	0.6
CaO/Al_2O_3,	2	130	580	600	210	450	360	430	520
SiO_2/Al_2O_3,	45	290	630	990	620	1150	2050	700	1530
Na_2O/Al_2O_3,	<100	790	550	<150	710	<150	<150	<150	<150
MgO/Al_2O_3,	<10	330	730	890	800	–	–	–	–

The specific surface areas vary between 0.6 and 11.7 m^2/g. The main impurities of the Al_2O_3 samples are CaO, SiO_2, Na_2O and MgO. The eventual combination of these elements on the alumina surface is not known. The values of γ_s^d, determined at 100°C are in the 90–100 mJ/m^2 range and there is no evident correlation between γ_s^d whatever the impurities contents. However, it is known, particularly in catalysis, that the association of Al_2O_3 and SiO_2 leads to silico–aluminates of increased Lewis acidity. To check this, we evaluated an acid base parameter, which is simply the ratio of the retention volumes of a basic probe, i.e. diethyl ether, and of an acidic probe, i.e. dichloroethane:

$$\Omega = \frac{V_{C_2H_5-O-C_2H_5}}{V_{CH_2Cl_2}} \tag{3}$$

On an acidic surface, ether will be most efficiently retained whereas dichloroethane will be only weakly adsorbed. In other terms, Ω will take high values. The opposite would occur for a basic surface. The results recorded with aluminas are displayed in Fig. 4.

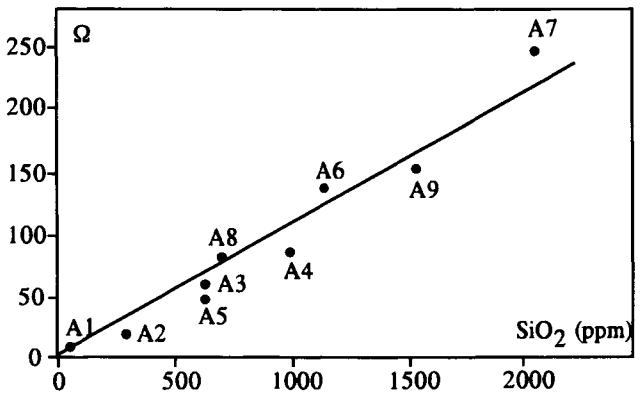

Figure 4. Variation of the surface acidity Ω (ratio of the tetention volumes of diethyl ether and dichloroethane) of aluminas containing increasing amounts of SiO_2 impurities.

As expected, a significant increase of Ω with augmenting amounts of SiO_2 impurities is observed. This has consequences on the polymer adsorption capacity (polymethylmethacrylate) as shown elsewhere [13].

Whereas impurities are often accidentally introduced on the surface of mineral oxides, during preparation there exists a most appropriate way to achieve "tailor-made" surfaces, essentially by well controlled chemical surface modification. In this instance, only two studies will serve as examples: the grafting of monoatomic alcohols, on the one hand, and the grafting of diols, on the other hand. The first example will allow to show how the grafted alkyl chains will arrange themselves on the surface of silicas whereas the second example will point to the influence of the surface nanomorphology on the reactivity and conformation of grafted diols. Both reactions respond to the following simplified esterification scheme:

$$\equiv Si - OH + ROH \longrightarrow \equiv Si - OR + H_2O \qquad (4)$$

Practically, the fixation of the mono- or diatomic alcohols or of the diol is achieved by heating silica with an excess of alcohol, either in an autoclave at 150°C, for low boiling point alcohols, or directly using alcohols having boiling points over 150°C [10].
Fig.5 shows the variation when the surface coverage with $-CH_2-$ groups increases.

It is interesting to note that this variation is far from being monotonous, since the reproducibility of the γ_s^d measurements is within ± 0.5 mJ/m^2. Two minima are observed corresponding to 15 and 23 CH_2/nm^2 respectively. Considering that the cross-sectional area of one CH_2 is equal to 0.06 nm^2 (hexagonal close packing) it becomes apparent that the minima are detected when one or two monolayers of $-CH_2-$ groups are formed on the surface of silica. Cross polarisation, magic angle spinning solid state ^{13}C NMR

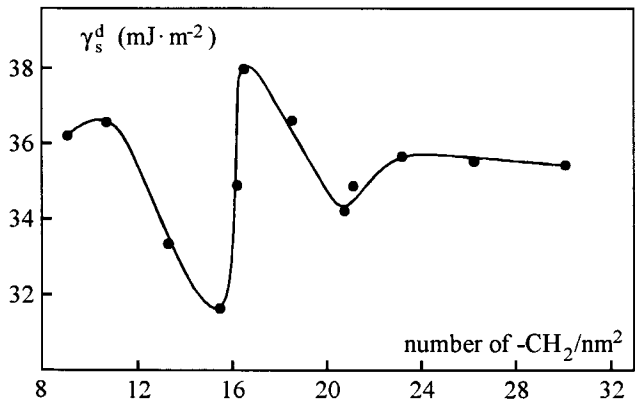

Figure 5. Variation of γ_s^d with the number of $-CH_2-$ groups grafted on the surface of a fumed silica (Aerosil 130, Degussa) using n-alcohols as reactants.

measurements, allowing to identify the mobility of the end methyl groups of the grafted alkyl chains, confirm the above description [14]. Indeed, the mobility of the CH_3 group is the lowest when a mono or double layer is achieved on the solid surface. All these results indicate that the alkyl chains form a dense and regular array (trans-trans configuration) of methylene groups disposed so as to favour optimum interactions with the silica surface, but also with neighbouring methylene groups. An optimal and more rigid organisation of the alkyl chains will also induce a limitation of interaction with the alkane probes, hence a reduction of γ_s^d.

In the following example, the morphology, at the molecular level, will play a special role. Using diols, instead of n alcohols opens the possibility of having these molecules tight on the surface by their both terminal hydroxyl groups:

$$\equiv Si-OH + HO-R-OH + HO-Si\equiv \longrightarrow \equiv Si-O-R-O-Si\equiv + 2H_2O \quad (5)$$

Depending on mono or diesterification, the modified silica surface will exhibit quite different surface properties. If the diol is fixed just by one of its reactive ends, then the modified silica will still exhibit polar (or hydrogen bonding) interaction capacity. Otherwise, when both reactive ends have been esterified, then the modified silica surface will have lost its H-bonding ability.

In order to test this opportunity, IGC was again applied but using as molecular probes, the alcohols capable of forming H-bonds with the grafted non esterified diol ends [15]. Figure 6 exhibits the results that appear to be astonishing at first sight.

The enthalpy of adsorption (ΔH) fluctuates according to the even or odd number of C atoms of the grafted diols. High values of ΔH point to strong H-bonding between the alcohol probes and the non-reacted hydroxyls of the diols fixed on the silica surface just by one extremity.

When increasing the chain length of the grafted diol, ΔH is even more important. The IGC results can be explained assuming differences in reactivity according to the parity of the diols, leading either to a mono or diesterification process.

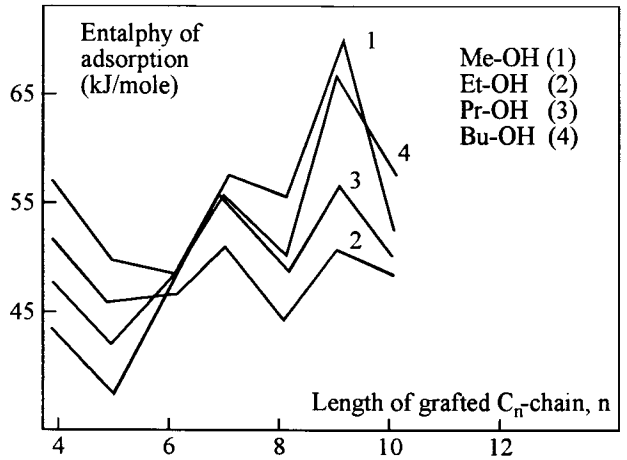

Figure 6. Variation of the enthalpy adsorption (ΔH) for alcohol probes on a fumed silica modified with diols of increasing numbers of carbon atoms.

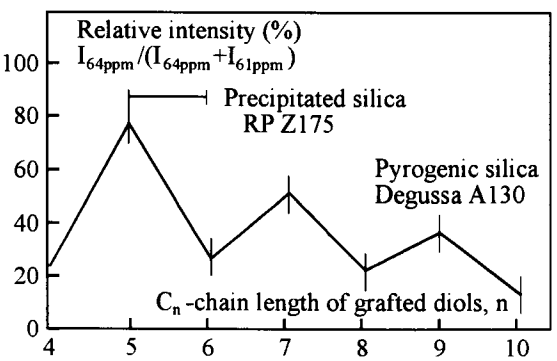

Figure 7. Variation of the ratio R (diesterification/monoesterification) determined by NMR as relative intensity $I_{64\ ppm}/(I_{64\ ppm}+I_{61\ ppm})$ on fumed and precipitated silicas modified with diols of increasing numbers of carbon atoms.

Indeed, solid state NMR confirms directly the hypothesis as can be seen in Fig. 7 which displays the ratio R, of diesterification/ monoesterification, oscillating as in the case of ΔHa. Comparing fumed and precipitated silicas gives a new insight in the fixation mechanism. With precipitated silica, diesterification is dominant and does not depend on the parity of grafted diols. In other terms, both ends of the reactive molecule find readily available silanol groups on the silica surface. Two facts can explain this observation. Firstly, precipitated silicas possess much higher surface silanol densities than fumed silicas: around 18 against 4 OH/nm^2 for fumed silicas. The very high silanol surface coverage of precipitated silicas is accounted for by non condensed silicic acid chains [6] which have some mobility. Hence, it is understandable that the free tangling end of the diol, initially

fixed by only one end, will find a partner silanol group to form a diester on the precipitated silica surface, whereas this is not true for fumed silica.

The oscillation phenomena of diols properties is also observed when plotting their fusion points vs. their number of carbon atoms. Uneven diols have lower fusion points than odd ones: an observation that is explained by the possibility even diols have, for evident steric reasons, to form "dimers", where odd diols may more easily form "polymers". Applying these arguments to the grafted chains, we arrive at the situation depicted in Fig. 8.

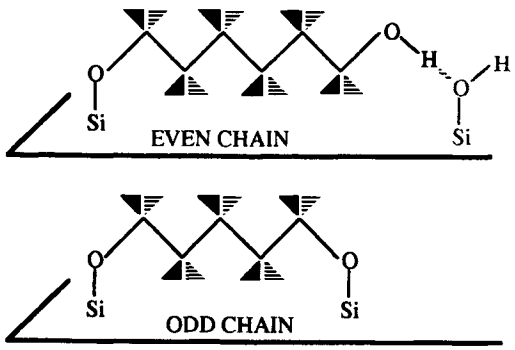

Figure 8. Schematic representation of the conformation of diols fixed on the quasi molecular planar surface of fumed silica.

Figure 8 describes the silica surface as planar on the molecular scale, at least on a scale comparable with the dimensions of the grafted molecules. If this is the case, then odd chain diols, when arranged in trans/trans configurations will have the optimal position to interact with both reactive ends of surface silanols: i.e., they will be able to form diesters.

On the other hand, even chain diols will be in a less favourable position, and for short chains, will give rise to monoesters. Obviously, the differences will vanish when comparing diols having relatively long chains since the greater mobility of the end links (non fixed part of the diol) will be comparable for both types of diols.

Of course, we do not expect to detect the same behaviours of diols on precipitated silicas that present rather rough surfaces as can be shown using a fractality approach [16] i.e., estimating the surface nanomorphology by the small angle X-ray diffraction or interpreting adsorption isotherms of a homologous series of adsorbents. The main conclusion of this part of our study is that:

- surface chemical reactions are locally sensitive to the nanorugosity of the solids surface,
- fumed silicas present a molecularly smooth surface that may be considered as *a model of a planar surface.*

3. INFLUENCE OF SURFACE NANORUGOSITY ON APPARENT SURFACE ENERGY

Since now we have evidence for the molecular flatness of the fumed silica surface, we may indeed use this silica for comparison with other silicas and then with other mineral oxide surfaces.

Definition of a morphology index

One possible way for the evaluation of the surface smoothness is the determination of fractality (D). Various approaches are described in the literature [6], based on the evaluation of the number (Nm) of molecules of a homologous (geometrical and energetical) series of molecules required to form a monolayer:

$$\log(\mathrm{Nm}) = -\mathrm{D}/2 \log \sigma + \mathrm{C} \tag{6}$$

where σ is the cross-sectional area of a given molecule. Other procedures are based on the interpretation of adsorption isotherms, or of small angle X-ray diffraction as already mentioned above. All these methods are rather time consuming whereas IGC apparently offers a more direct access to parent information we call nanorugosity: i.e. roughness at the molecular scale. The fundamental equation of IGC, at infinite dilution relates simply the net retention volume V_N to the effective area of adsorption: $V_N = K \cdot A$. Obviously, the area A will be influenced by both the existence of nanorugosity and the molecular size of the probe molecule eventually leading to the size exclusion effects. Thus, a method of detection of surface nanorugosity consists in a comparison of the retention volumes of linear n alkanes (V_N^L) and of branched (V_N^B) isomers:

$$\frac{V_N^B}{V_N^L} = \frac{K^B}{K^L} \frac{A^B}{A^L} \tag{7}$$

where K^B and K^L are the corresponding equilibrium constants (adsorption partition coefficients).

In the previous equation, there are two unknown quantities: the values of the equilibrium constants and the true values of the accessible areas. K^B and K^L are dependent on the polarisabilities of linear and branched alkanes that are not identical. But, their ratio can be measured on the reference silica, as well as the ratio of the actual contact areas. Consequently, the index of nanomorphology, I_m, will be defined by:

$$I_m = 100 \cdot \frac{V_N^B}{V_N^L} \frac{V_{N\ ref}^L}{V_{N\ ref}^B} \tag{8}$$

For a smooth surface, $I_m = 100$ % whereas I_m takes low values for rough surfaces.

Application to lamellar solids

Table 2 presents the specific surface areas, γ_s^d and I_m values of a variety of divided solids.

The I_m values were found using 2-methyl-heptane as the molecular probe. It is interesting to note that the very high values of γ_s^d are always associated with low values of Im. In other words, lamellar solids, such as clays, are typical for most heterogeneous surfaces.

Table 2
Specific surface area (S), dispersive component (γ_s^d) of the surface energy and nanomorphology index (I_m) of a variety of divided solids at 80°C

Samples	S(m^2/g)	γ_s^d (mJ/m^2)(at 80°C)	I_m (%)
Silica (fumed)	130	70	100
Silica (precipitated)	175	70	80
H-Magadiite	42	220	1
Talc	4	130	15
Kaolinite	20	210	50
Illite	30	170	60

Indeed, they present two totally different aspects : the basal and the lateral surfaces. Whereas the basal surface is rather flat, the peripheral surface is often the location of structural defects such as stacking faults, or partially missing atomic planes. The remaining sheet structure constitutes molecular size cavities in which the very flexible n-alkane chains will be able to enter, but not their branched isomers. When inserted between two sheets, the probe molecules will experience very high force fields and the information they will carry to the operator will concern essentially those very particular adsorption sites. It is then that the calculated γ_s^d value will be too large in comparison with a mean value of the surface energy of the entire solid. This, in turn, rises the question of the physical meaning of such a mean value! Before trying to find an answer to this question, the one that obviously cannot be simple, we shall describe a practical application of the I_m concept, the control of the surface modification of talc.

Talc is a layered magnesium silicate, the basal layer being exclusively made of siloxane bridges. These Si-O-Si bonds are chemically stable and practically apolar. In other terms, the surface of talc is rather inert offering a considerable resistance to surface treatment. Yet, such treatments are highly desirable, in particular, when talc is used as a filler for polymers like polyamides, for example. A typical treatment is the organosilane or coupling agent treatment. In that case, the coupling agent is supposed to make a link between the filler and the polymer chains. However, this is not possible with talc. Therefore, an attempt was made to coat talc with a thin layer of silica using a chemical vapour deposition procedure [17] starting with a SiH_4 - oxygen mix. The question that arises is to know where the silica will actually deposit: will it be on the entire surface of the talc or will it be preferentially on the lateral or peripheral faces of the talc crystals. The answer is given in Fig. 9 below which there is displayed the variation of γ_s^d and I_m of a series of talc samples modified under different conditions : treatment temperature, silane concentration, oxygen concentration, duration of treatment.

It can be seen that there exists a relationship between γ_s^d and I_m. The very high values of γ_s^d correspond to talc samples treated under moderate conditions. These values and the rather low morphology index clearly indicate, as we already know, that the talc is rather heterogeneous having lateral and base surfaces of totally different adsorption properties. As the treatment conditions become more severe, i. e. as the amount of deposited silica becomes more and more important, the γ_s^d decrease whereas the morphology indexes increase: the average talc surface becomes more and more smooth on the molecular level.

No other method than IGC is capable of delivering such conclusions showing clearly that chemical vapour deposition of silica on the talc surface starts, and is limited, on the lateral faces. Of course, this is not at all the wanted effect of the planned surface treatment.

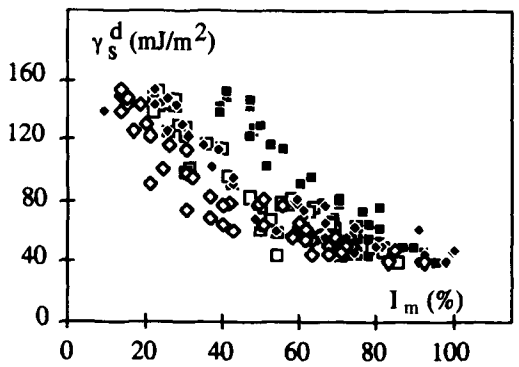

Figure 9. Variation of γ_s^d with respect to the nanomorphology index (I_m) of 2,5-dimethylhexane (◇), 2,2,4-trimethylpentane (◆), 2,3,4-trimethylpentane (□), 2,2,4,4-tetramethylbutane (■).

In the following section, we shall describe a different approach for the description of the surface properties of divided solids: the determination of the surface energetic heterogeneity starting with the gas adsorption isotherms.

4. INFLUENCE OF ENERGETIC SURFACE HETEROGENEITY ON GAS ADSORPTION

4.1. General considerations

The surface of a pure liquid, formed of identical molecular species, can be considered statistically as a perfect homogeneous surface and its surface energy can be easily defined and measured as the reversible work, per area unit, needed to extend its surface. On the contrary, atomic structures present on a solid surface are rigid. Consequently, the surface chemical composition and morphology, cracks, corners, steps, porous structures, can strongly change when moving from one surface point to another. As just stressed above, the surface of a mineral solid when examined on a molecular level is much complex and the surface energy concept, so far, holds only for perfectly homogeneous surfaces. Obviously, when considering solids behaving lamellar structure, such as talc, mica or clay minerals, one distinguishes two easily identifiable adsorption planes: the basal and the lateral surfaces possessing a quite different functionality and therefore showing different surface energy characteristics.

The problem becomes how to define the surface energy of such a material. In fact, already Langmuir when establishing his famous equation for the isotherm called by his name was well aware of the oversimplification he made when supposing that a solid surface is energetically homogeneous. Almost all real surfaces are heterogeneous. Moreover, as pointed out by Everett [18], "...the term heterogeneity should be applied to a specific

solid/adsorbate pair rather than to the solid itself. Thus a surface that is perceived as heterogeneous may, for many purposes, be seen as homogeneous by a large dye molecule". As a result of the heterogeneity of the solid surface, the force of interaction between an adsorbing molecule and the solid surface will vary depending on the adsorption site location. Upon collision with the substrate, gas molecules will tend to occupy the most energetical sites. When the vapour pressure increases, the highest-energy adsorption sites will be occupied whereas lower energy sites will remain available for supplementary adsorption. Of course, this process is not strictly sequential, only the probability of adsorption is closely related to the energy of the site. Moreover, the degree of mobility of the adsorbed molecule will depend on the magnitude of the potential pits and on the temperature. Hence, the first adsorbed molecules are less mobile than those that follow because of the high energy of interaction of the sites occupied preferentially at low surface coverage ratio, i.e. at low pressures. Therefore, adsorption on a solid surface is a very complex phenomenon that should be described not only in energy quantities, such as surface energy, or as dependant on nanomorphology, but also in terms of surface heterogeneity. On the other hand, the study of adsorption properties of a solid, i.e. determination of the adsorption isotherms of various probes will provide, in principle, a good way to obtain information on its surface heterogeneity.

An illustration of the surface heterogeneity of silica, deduced from isotherm measurements, is shown in Figure 10 which indicates the variation, with the coverage degree (θ), of the isosteric heat of adsorption Q_{st} of heptane and toluene, calculated from adsorption isotherms determined at 37° and 47°C, on a talc by Jagiello et al.[19].

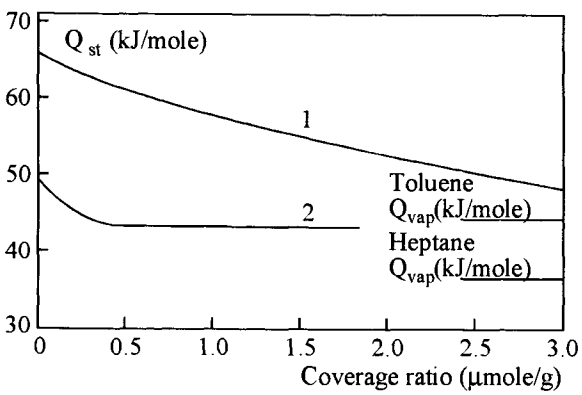

Figure 10. Variation of the isosteric heat of adsorption Q_{st} of toluene (1) and heptane (2) on a talc, with surface coverage.

ΔQ_{st} decrease most rapidly as the coverage ratio increases indicating the presence of active adsorption sites that are occupied by the first molecules admitted on the talc surface. A direct proof of surface heterogeneity is also given by the deviation observed, at low partial pressures, between the BET model and the actual isotherm.

Therefore, the surface heterogeneity of a solid may be obtained from the analysis of the adsorption isotherm profile and will be described in a form of an adsorption energy distribution function relating the number of adsorption sites having a given adsorption

energy to the adsorption energy of the molecule. Rudzinski and Everett [20], and Jaroniec and Madey [21] published extensive reviews on the adsorption of gases on heterogeneous surfaces.

Whatever the chosen calculation process, the isotherm analysis is based on a simple physical model describing, in the simplest way, the global experimental isotherm as a sum of partial isotherms corresponding to homogeneous adsorption patches. Hence, the amount of adsorbed molecules (probe) is given by the following Fredholm integral equation:

$$N(P_m, T_m) = N_0 \int_{\varepsilon^{min}}^{\varepsilon^{max}} \theta(\varepsilon, P_m, T_m)\chi(\varepsilon)d\varepsilon \tag{9}$$

where: $N(P_m, T_m)$ is the number of molecules adsorbed at the pressure P_m and at the temperature T_m of measurement (experimental isotherm), N_0 is the number of molecules corresponding to the formation of a monolayer, $\theta(\varepsilon, P_m, T_m)$ is the local isotherm corresponding to an adsorption energy ε, and $\chi(\varepsilon)$ is the function of distribution (DF) of the sites seen by the probe.

The solution of Eq. (9) is widely described in two monographs [20, 21] devoted to adsorption on heterogeneous surfaces.

In this equation, only the left term – the experimental isotherm – is known. The local isotherm, $\theta(\varepsilon, P_m, T_m)$, has to be selected according to the physical hypothesis describing the interaction of a molecule with an adsorption site and, eventually, with the neighbouring adsorbed molecules. Hence, the calculated distribution function $\chi(\varepsilon)$ is obviously dependent on the choice of the local isotherm. The most used local isotherm equations were reviewed by Wam and White [22].

The Langmuir local isotherm that supposes localised sites and no lateral interaction between adsorbed molecules, is the most widely used because of the impossibility of having access to the real values of the parameters used in other models such as the interaction energy between two adsorbed molecules.

Whatever the chosen local isotherm, the characteristic energy ε_j of an adsorption site of type j is related to the pressure P, for a coverage ratio θ_j equal to 1/2, by Equation (10):

$$\varepsilon_j = -RT \ln(P/K) \tag{10}$$

where K is a constant related to the type of the local isotherm.
For example, for the Langmuir local isotherm, K is related, according to Hobson [23], to the molar mass and the temperature of measurement by:

$$K = 1.76 \cdot 10^4 \cdot (M \cdot T)^{1/2} \tag{11}$$

Other equations are proposed in the literature that nevertheless lead to very close energy scales. Finally, assuming a local isotherm, one now has to find a suitable numerical resolution method for solving Equation (9).

4.2. Resolution methods of the Fredholm integral equation

From a mathematical point of view, inversion of Equation (9) is not a trivial task because it has no general solution [22]. It is an "ill posed" problem, i.e., a small variation in

the experimental data will cause a large variation in the site energy distribution function. Hence the existence, the uniqueness and the stability of the solution are not generally assured.

Different methods have been proposed to solve Equation (9). The first ascribes a given analytical form to the distribution function $\chi(\varepsilon)$ such as: a gaussian function [24,25], a gamma function [26] or a combination of two Langmuir isotherms discrete distributions [27] and try to reach the best fitting of the experimental isotherm, using a limited set of parameters.

According to these approaches, one assumes a given chemistry and/or morphology of the solid surface. Yet, the same function cannot simultaneously describe a macro-heterogeneous surface solid such as talc, clay minerals or crystalline silicas, having basal and lateral surfaces and a micro-heterogeneous one like the surface of an amorphous silica. Therefore many authors tried to develop resolution methods without making any assumption for the shape of the distribution function.

One of them uses a discrete distribution of monoenergetic sites [22] based on a discretization form of the equation (9) which can be rewritten in a form of limited development. At a given pressure of measurement, for n different discrete types of adsorption sites, Equation (9) can be rewritten as follows:

$$N(P_j) = \sum_{k=1}^{n} \theta(\varepsilon_k, P_j)\ c(\varepsilon_k) \tag{12}$$

Considering a number n of measurements, one ends up with a linear system of n equations. Solving it, one obtain the distribution function in form of a discrete series of $c(\varepsilon_k)$ coefficients. Despite the apparent simplicity of this method, the inversion of the characteristic matrix is not also a simple task. The instability of the solution increases quickly with increasing values of n and origins partially from the border effects so one has to call on a regularization parameter to control this natural instability [28]. The choice of the regularization parameter value entails a real subjective character to the method. To overcome these difficulties, methods based on the approximation of the local isotherm were proposed. The oldest and the simplest approximation of the local isotherm is the condensation approximation [29]. The condensation approximation assumes that the sites of adsorption of given energy are unoccupied below a characteristic pressure and entirely occupied over it. The distribution function for the condensation approximation (DFCA) is directly related to the first derivative of the isotherm according to Equation (13):

$$\chi_{CA}(\varepsilon) = \frac{p}{N_0}\left(\frac{\partial N(P,T)}{\partial P}\right) \tag{13}$$

This approximation gives an exact solution only at a measurement temperature near the absolute zero. At room temperature and over it, this approximation fails completely. To overcome this difficulty, a lot of other approximations were proposed and reviewed by Nederlof et al. [30]. Among them, for Langmuir local isotherm, the Rudzinski-Jagiello's method [31] allows, in principle, to compute the actual distribution function according to Equation (14):

$$\chi(\varepsilon) = \sum_{j=0}^{\infty} b_{2j} \cdot \chi_{CA}^{(2j)}(\varepsilon) \qquad \text{with} \quad b_0 = 1 \qquad \text{and} \quad b_{2j} = (-1)^{j+1} \cdot \frac{\Pi^{2j}}{(2j+1)!} \tag{14}$$

This assumes knowledge of the even derivatives of the DFCA which are obviously difficult to determine from the finite set of experimental points, without amplifying the experimental noise. Computer simulations, done for the bi-gaussian theoretical distributions, show that DFRJ provides a good approximation of the theoretical distribution, even for temperatures over the room temperature [32].

The main difficulty of this method stems from the necessity to perform multiderivation of the experimental DFCA. Its main advantage is to provide a fine control of the calculation process by the comparison of DFRJ of increasing order. To perform multiple derivations, Jagiello et al.[31] used a virial expansion in order to fit the experimental isotherms. More recently, Balard, Wang and Papirer [33] proposed to fit the DFCA, using the Fourier's series. Moreover, the corresponding Fourier's spectra provide a good way for the separation of the respective parts of the signal and of the experimental noise.

Finally, whatever the chosen method for the resolution of Equation (9) is, it is very important to emphasize that an efficient method has to:

- provide one or more criteria of quality, such as a parameter of regularization in order to control the calculation process,
- be validated by simulation, in order to be able to estimate its stability towards experimental noise and experimental conditions of acquisition.

Last but not the least, the correct acquisition of experimental data is essential, because calculation processes will amplify strongly the measurement errors.

4.3. Methods of acquisition

To acquire the desired experimental data, one may use classical volumetric or gravimetric methods that are generally employed and well appropriate for the experiments carried out at low temperature, using gaseous probes such as nitrogen, argon or krypton. However, for organic probes like alkanes or polar probes, one generally prefers chromatographic methods.

Using IGC, the first derivative of the adsorption isotherm can be easily calculated from the retention times and the signal heights of the points of the diffuse descending front of the chromatogram, according to the following equation given by Conder and Young [34]:

$$\left(\frac{\partial N}{\partial P}\right)_{L,t_r} = \frac{J \cdot D_s \cdot t_r'}{m \cdot R \cdot T} \tag{15}$$

where N is the number of absorbed molecules, L the column length, t_r the retention time of a characteristic point on the rear diffuse profile of the chromatogram, t_r' the corresponding reduced retention time, J the James–Martin coefficient, taking in account the compressibility of the gas due to the pressure drop inside the chromatographic column, D the output flow rate, m the mass of adsorbent, R the gas constant and T the absolute temperature at which the measurement is made.

This equation assumes that the contribution of the probe vapour to the gas flow rate across the column is negligible and can be considered as ideal, and that the contribution of the injection band and diffusion processes along the column play a minor role. One of the main advantages of the chromatographic method, especially when applying the Rudzinski–Jagiello's method, is the fact that this method provides directly the first derivative of the isotherm and therefore, in a very direct way the DFCA.

From the experimental data, applying the different methods of resolution described above, many authors tried to evidence the surface heterogeneity of solids surfaces using gaseous probes at low temperature or liquid organic probes over the room temperature.

4.4. Adsorption energy distribution functions measured at low temperature

Distribution functions of adsorption sites on silicas, for example, but also on titanium dioxide, silicates and so on [20, 21], have been established at low temperature, around 77 K, using gaseous probes. Figure 11 shows the distribution functions of the adsorption sites established using nitrogen or rare gases around 77 K.

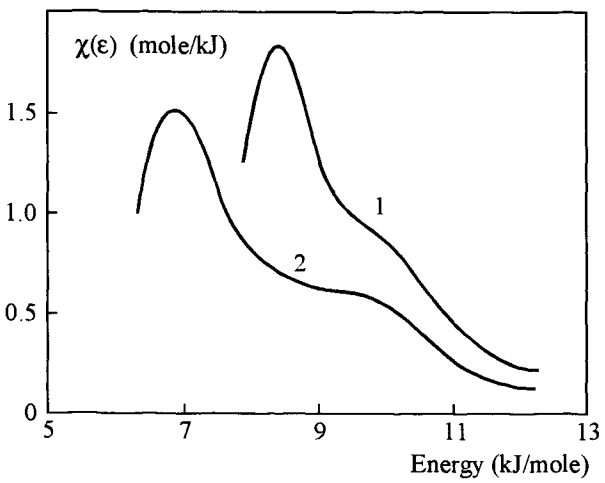

Figure 11. Distribution functions of the adsorption sites measured with krypton (1) and nitrogen (2) on Aerosil at 77 K (after van Dongen [35]).

Distribution functions exhibiting a shoulder in the energy region are generally observed for silicas. This fact underlines the real heterogeneous character of most mineral solids. Moreover, an important shift is observed towards higher energies, when going from nitrogen to krypton certainly due to the higher polarisability of the latter that changes the level of interaction of the probe with the functional groups. It would be interesting to verify if such observations could be supported using organic probes at higher temperature.

4.5. Adsorption energy distribution functions measured around the room temperature.

To our knowledge, only few studies were done on the determination of the surface heterogeneity of solids using IGC at finite concentration, if we exclude the works recently done in our group. In this instance, we first examine the case of solids that are heterogeneous on a quite macroscopic scale, originating generally from a lamellar structure like clays, micas or talcs.

The first application of our method was devoted to the monitoring of the grinding of a muscovite in the presence of different grinding additives that improve the efficiency and speed of grinding at very low concentration, i.e. smaller than 1%,. But, their presence

may also influence strongly the morphology and the surface energy of ground materials that play a major role for the final properties of the filled polymers.

Taking into account the complexity of the grinding process, an increase of the surface heterogeneity, by creation of crystal defects and major chemical modification of the surface, is expectable.Therefore, the knowledge of the adsorption energy distribution functions (DF), computed from the adsorption isotherm obtained by finite concentration chromatography, can provide more information on the grinding mechanism of a muscovite in water and in the presence of miscellaneous grinding agents.

Experimentally, the muscovite from Bihar (India), was coarsely broken and sieved. Particles, having sizes comprised between 50 and 125 μm, were submitted to grinding in an attritor comprizing a stirrer rotating at 290 rpm and filled with 500 stainless steel balls, 10g of mica and 200 cm^3 of a solution of the grinding additive in water.

Four grinding media were selected: pure water, an one molar solution of potassium chloride, a solution of pentanedioic acid (polyacrylic acid dimer) at 0.5% in water and a solution of a low molecular weight polyacrylic acid – PAA – 2500 (g/mole) at the same concentration. After filtration and washing, the ground mica was dried overnight in an oven at 50°C. The specific surface areas and the particle sizes of the ground solids were determined using the BET method and the Laser Coulter Sizer LS 130. Finite concentration chromatograms were acquired using stainless steel short columns.

The main consequence of grinding is a significant decrease of the particle diameter and consequently, an increase of the specific surface area. Looking at the evolutions of both particle size and specific surface area, it appears clearly that the nature of the additive influences significantly the kinetics of muscovite grinding. The most efficient is pentanedioic acid (PAA dimer), especially from the point of view of the particle size reduction. The less active is the PAA itself which is even less efficient than pure water.

Electron microscopy and IGC at infinite dilution [36] highlight the difference of the grinding processes using mineral (KCl) or organic additives and show that dimer is also the best additive for preserving the lamellarity of the ground solid and that KCl has the opposite effect. To confirm this assumption, it was of most importance to estimate the surface heterogeneity of the ground solids, using IGC at finite concentration and to evidence the relative contributions of both basal and lateral surfaces of the ground mica crystals.

Figure 12 shows the adsorption energy distribution functions of benzene for muscovites ground in the presence of the dimer of PAA and of 1M KCl.

If we exclude the case of the initial mica that exhibits a quite monomodal DF, all other DF are bimodal and the second peak at the higher adsorption energies appears with an increase of the grinding duration. It could be attributed to the lateral surfaces formed during the grinding process. It is also worth pointing out that the relative areas of the both peaks, centered around 22 kJ/mole and 27 kJ/mole, are dependent on the nature of the grinding additive. Dimer of PAA leads to a more intensive and continuously increasing peak, at high energy, for increasing durations of grinding whereas the area of the low energy peak becomes rapidly quite stable. The inverse evolution is observed in the case of the 1M KCl additive that favours the increase of the low energetical peak comparatively to the peak, at high energy.

These observations suggest that the dimer of PAA favours the breaking of muscovite crystals leading to the formation of numerous lateral surfaces whereas in the presence of

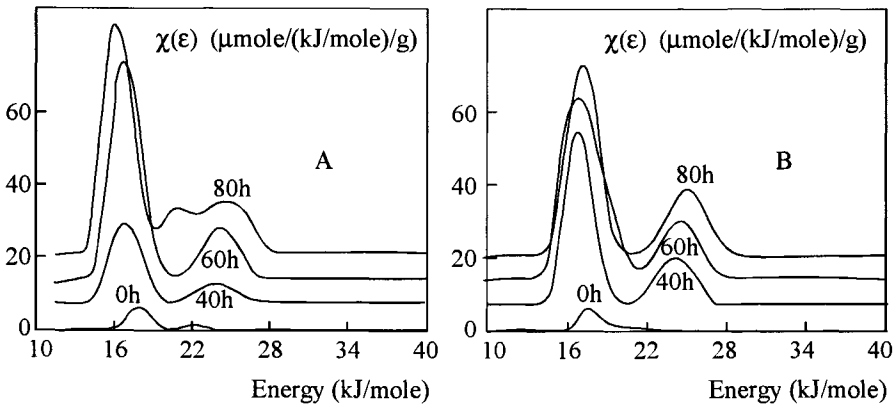

Figure 12. Adsorption energy DF of benzene at 30°C, on mica muscovite ground in the presence of 1M KCl (A) and of dimer of PAA (B).

1M KCl, preferential delamination of the muscovite crystal occurs. The same observations were done using other organic probes such as octane or isooctane, and this interpretation is supported by the measurement of the contribution of lateral surfaces to the total area using microcalorimetric monitoring of argon adsorption.

The second example concerns the surface heterogeneity of clay minerals. Important problems, such as limited yield of oil recovery arising during oil exploitation, involve interaction of pore filling fluids with the minerals that form the reservoir walls. The clay minerals, due to their relatively high specific surface area and electrical charge density, are the most active for the retention of oil. Illites and kaolinites are the clay minerals that are most frequently found and their wettability properties are believed to be in relation to the heavy oil ends retention process.

Surface heterogeneity of such minerals influences certainly their ability to retain petroleum in the reservoir. Therefore, we have examined by IGC at finite concentration, the surface properties of illites and kaolinites having a known genesis: heritage, transformation (degradation, agradation) or neoformation.

Adsorption energy distribution functions of apolar (hexane) or polar probes (propanol and pyridine) are depicted in Figure 13, for an heritated illite and an heritated kaolinite.

Three main remarks can be made about these distribution functions:

-firstly, these distribution functions evidence the strong heterogeneous character of these solids. Like for the ground micas, one can distinguish one or two main peaks at low energy related to the basal surfaces and less intensive peaks at high energy that originate certainly from the presence of lateral surfaces and other defects,

-secondly, distribution functions for hexane are relatively similar. It means that a probe that exchanges only non specific interactions, is not discriminating,

-thirdly, on the contrary, polar basic (pyridine) and polar acidic (propanol 2) probes lead to much more different distribution functions because of their ability to exchange specific interactions with the different functional groups present at the solid surface. They permit to distinguish clearly a kaolinite from an illite and show the highest surface energy and the highest surface heterogeneity of the latter whereas it was observed that genesis of the

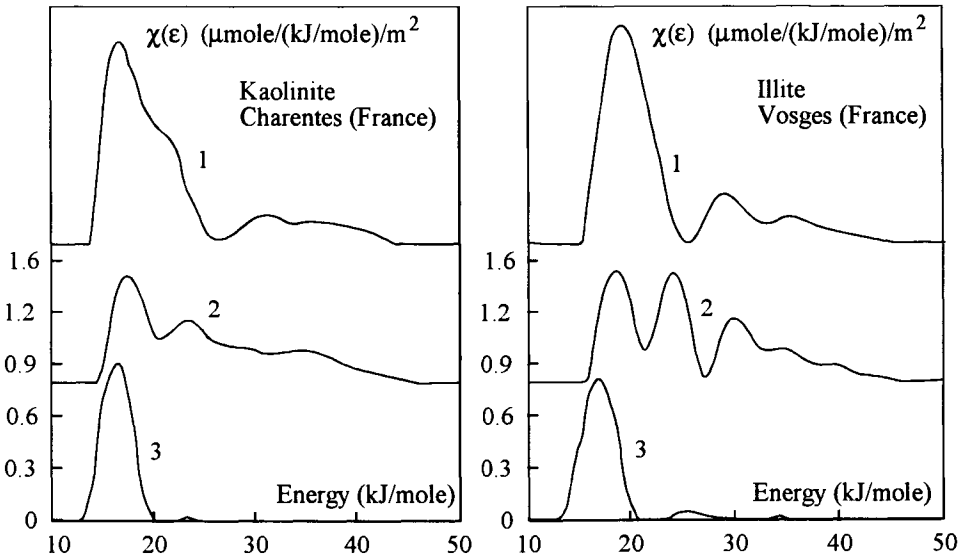

Figure 13. Adsorption energy DF of pyridine at 84°C (1), propanol-2 at 55°C (2) and hexane at 34°C (3), for heritated kaolinite and for heritated illite.

clay mineral does not influence strongly the shape of the distribution functions.

Therefore, distribution functions indicate that the surfaces of the illites, as indicated by more intensive peaks at high energy, are more heterogeneous than those of kaolinites. This difference will perhaps explain the highest hydrophilicity of illites, evidenced by the determination of water adsorption isotherms, comparing with that of kaolinites.

It suggests that water adsorption occurs mainly on structural defects of the clay mineral crystal rather than on the basal surfaces because, due to the presence of aluminol groups on one face of kaolinite, kaolinite would be, in principle, more hydrophylic than illite which exhibits only siloxane bridges on both faces of the crystal.

Coming back to oil adsorption, we have evidence that the asphaltenes adsorption dissolved in the water saturated toluene, is more strongly on kaolinite than on illites. It is obvious that the size of an asphaltene molecule does not permit its access to the sites of adsorption that are responsible for the water adsorption. In other words, only basal surfaces are accessible to the large and planar asphaltene molecules that interact preferentially with the aluminol groups of the kaolinite while water deactivates the more energetic and certainly less accessible sites of illites.

The last example of macroheterogeneous lamellar solids concerns talcs that are common fillers for polyolefinic matrices because their crystalline structure induces the crystallization of, say, the polypropylene matrix. Of course, talcs are natural products whose superficial properties depend on the location of the mine. Their characteristics are reported in Table 3.

To evidence this point, we have determined the distribution functions of some talcs extracted in different mines located in Europe and of a chlorite, a mineral frequently associated with talc. These distribution functions for benzene are depicted in Figure 14.

Table 3. Characteristics of some European talcs

Product	Origin	Form factor	Ar S (m^2/g)	N_2 S (m^2/g)
Chlorite	France	6.8	10.5	10.0
Talc 1	France	10.5	-	3.0
Talc 2	Spain	3.4	19.5	18.5
Talc 3	Italy	12.3	3.5	3.0
Talc 4	Austria	5.7	2.5	1.7

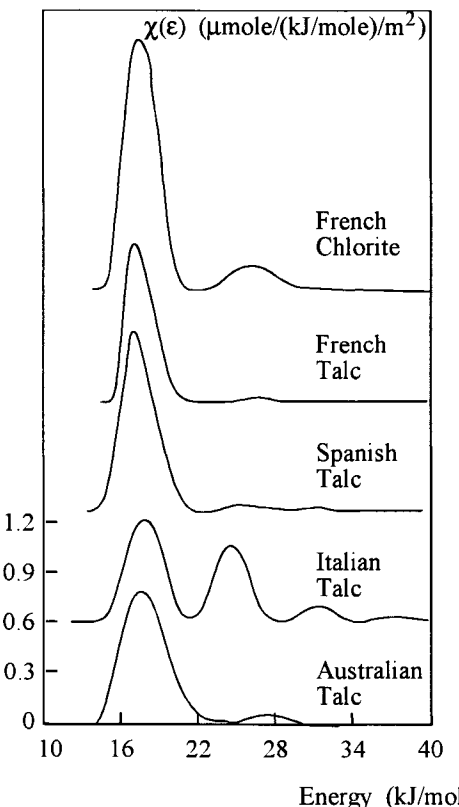

Figure 14. Adsorption sites distribution functions of talcs and chlorite using benzene as a probe, determined at 40°C.

If we exclude the case of the Italian talc, all the other distribution functions are bimodal and present a main peak at low energy around 17 kJ/mole characteristic for the basal surface and a very weak peak at the highest energy at 27 kJ/mole corresponding to lateral surfaces. It demonstrates that industrial talcs having low specific surface area exhibit mainly basal surfaces and that the difference in behaviour, as a specific filler for polyolefines origin certainly from other more macroscopic factors such as shape and size of

the crystallites. Chlorite exhibits a clearly higher surface heterogeneity than talcs. Finally, we may point out that the trimodality of the distribution function of the Italian talc is only observed with the benzene probe and not with octane and isooctane. Up to now, this phenomenon has not been explained but it may be due to the presence of silanol groups on the basal surface.

Finally, we studied the surface heterogeneity of three silicas using inverse gas chromatography and organic molecules as probes.One of them, the H–magadiite obtained by the acidic attack of a lamellar silicate is macroheterogeneous like the previously studied solids. For precipitated and pyrogenic silicas, which are amorphous solids, we cannot distinguish different types of surfaces such as lateral and basal surfaces, and the surface heterogeneity will be more localized and related to the local variability of both functionality and morphology. Figure 15 shows the distribution functions of these silicas.

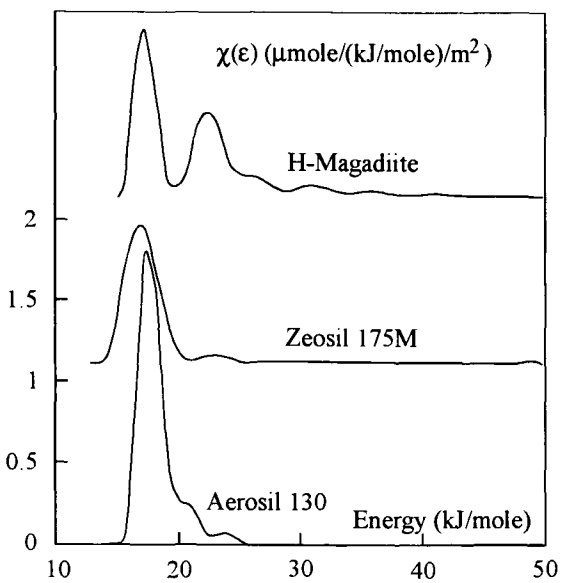

Figure 15. Distribution functions of the adsorption sites measured with octane on a lamellar silica (H–Magadiite), on a precipitated silica (Zeosil 175M) and on pyrogenic silica (Aerosil 130) at 40°C.

As expected, H–Magadiite, that is macroheterogeneous (basal and lateral surfaces) leads to a polymodal distribution function, whereas amorphous silicas lead to quite monomodal distribution functions since only very weak secondary peaks are observed.

Nevertheless, it is obvious that pyrogenic silica having the narrowest main peak, is representative of a quite homogeneous surface as already postulated when we examined the chemisorption of $\alpha - \omega$ diols. Precipitated silica exhibits a broader main peak and a more important secondary peak of higher energy, i; e; precipitated silica has a much more heterogeneous surface than the pyrogenic sample. Again, this is in agreement with our early finding: high capacity of methanol fixation, different behaviour towards diols.

5. CONCLUSION

The chemical and morphological surface properties of oxides (SiO_2, Al_2O_3) and of lamellar silicates (talc, muscovite, kaolinite, illite) have been examined using essentially inverse gas chromatography and hydrocarbons as molecular probes. IGC readily detects surface events that occur even after moderate thermal treatments. However, complementary methods are required to elucidate the nature of those events. We also showed that usual divided solids manifest most complex surface characteristics shedding some confusion on true surface energy determination. Actually, the surface properties cannot be described by a discrete value of the surface energy, but rather by a more appropriate but also more elaborated method such as energy site distribution curves.

REFERENCES

1. Z. Kessaissia, E. Papirer and J.B. Donnet, J. Colloid Interface Sci., 82 (1981) 526.
2. R.F. Giese, P. M. Costanzo and C. J. van Oss, Phys. Chem. Minerals, 17 (1991) 611.
3. P. Staszczuk, Chromatographia, 20 (1985) 724.
4. C. Saint Flour and E. Papirer, J. Colloid Interface Sci., 91 (1983) 69.
5. M.K. Chaudhury and G.M. Whitesides, Science, 255 (1992) 1230.
6. A.P. Legrand, H. Hommel, A. Tuel, A. Vidal, H. Balard, E. Papirer, P. Levitz, M. Czernichowski, R. Erre, H. van Damme, J.P. Gallas, J.F. Hemidy, J.C. Lavalley, O. Barres, A. Burneau and Y. Grillet, Adv. Colloid Interface Sci., 33 (1990) 91.
7. G. Ligner, A. Vidal, H. Balard and E. Papirer, J. Colloid Interface Sci., 133 (1989) 200.
8. H. Balard and E. Papirer, Progress Org. Coatings, 22 (1993) 1.
9. C.J. Brinker, R.K. Brow, D.R. Tallant and R.J. Kirkpatrick, J.Non–Cryst. Solids, 120 (1990) 26.
10. E. Papirer, A. Vidal and H. Balard, in: D.R. Lloyd, T.C. Ward and H.P. Schreiber (eds.), Inverse Gas Chromatography, ACS Symposium Series No. 391, Washington, 1989, p. 248.
11. E. Damingos and M.Soustelle, Ann. Chem., 13 (1988) 71.
12. E. Papirer, E. Brendl and H. Balard, unpublished results.
13. E. Papirer, J. M. Perrin, B. Siffert and G. Philipponneau, J. Colloid Interface Sci., 144 (1991) 263.
14. A. Tuel, H. Hommel, A. P. Legrand, H. Balard, M. Sidqi and E. Papirer, Colloids Surf., 58 (1991) 17.
15. E. Papirer and H. Balard, J. Adhesion Sci. Technol., 4 (1990) 357.
16. H. Barthel, F. Achenbach and H. Maginot, Proc. MOFFIS–93, Namur (B) (1991) 301.
17. H. Balard, D. Yeates, E. Papirer, M. Gastiger, P. Bouard, F. Clauss and R. Baeza, Proc. MOFFIS 93, Namur 1993, 217.
18. D.H. Everett, Langmuir, 9 (1993) 2586.
19. J. Jagiello J., Ligner G. and E. Papirer, J. Colloid Interface Sci., 137 (1) (1990) 128.

20. W. Rudzinski and D.H. Everett, Adsorption of Gases on Heterogeneous Surfaces, Academic Press, London, 1992.
21. M. Jaroniec and R. Madey, Physical Adsorption on Heterogeneous Solids, Elsevier, Amsterdam 1988.
22. J.A. Lum Wan and L.R. White, J.Chem. Soc. Faraday Trans.I, 87 (1991) 3051.
23. J.P. Hobson, Canad.J.Physics, 43 (1965) 1941.
24. S. Ross, Adsorption Technol., 67 (1971) 1.
25. W.A. House and M.J. Jaycock, J.Colloid. Polym Sci., 256 (1978) 52.
26. R.K. Gilpin, M. Jaroniec and M.B. Martin–Hopkins, J.Chromatogr., 513 (1990) 1.
27. J. Roles and G. Guiochon, J.Chromatogr., 591 (1992) 245.
28. M. Heuchel, M. Jaroniec and R.K. Gilpin, J. Chromatogr., 628 (1993) 59.
29. S.Z. Roginsky, Dokl. AN SSSR, 45 (1994) 194.
30. M.N. Nederlof, W.H. Riemsdjik and K. Koopal, J. Colloid Interface Sci., 135 (1990) 410.
31. W. Rudzinski, J. Jagiello and Y. Grillet, J. Colloid Interface Sci., 87 (1982) 478.
32. J. Jagiello and J.A. Schwarz, J.Colloid Interface Sci., 146 (1991) 415.
33. H. Balard, W.D. Wang and E. Papirer, Proceed. Am. Chem. Soc., Polymeric Materials–Science and Engineering, San Diego, USA, 70 (1994) 468.
34. J.R. Conder and C.L. Young, Physicochemical Measurements by Gas Chromatography, Wiley, New York, 1979.
35. R.H. van Dongen, Surf. Sci., 39 (1973) 341.
36. H. Balard, O. Aouadj and E. Papirer, Proceed. Am. Chem. Soc., Polymeric Materials– Science and Engineering, San Diego, USA, 70 (1994) 514.

A. Dąbrowski and V.A. Tertykh (Editors)
Adsorption on New and Modified Inorganic Sorbents
Studies in Surface Science and Catalysis, Vol. 99

Chapter 2.7
Structure and properties of the films formed by organic substances on silica gel surface. Investigations by inverse gas chromatography (IGC)

J. Rayss

Laboratory of Optical Fibers Technology, Faculty of Chemistry, Maria Curie–Sklodowska University, 20–031 Lublin, Poland

1. GAS CHROMATOGRAPHY

Gas chromatography has come into existence as an analytical method. The separation of analysed liquid or gaseous mixtures is the result of the difference in partition coefficients of their components between the gas (mobile) phase and liquid or solid surface (stationary phase). Depending on the kind of stationary phase the method is called "partition" or "adsorption" chromatography. The retention volume, defined as the volume of mobile phase causing the elution of the sample from the chromatographic column, is the value characterizing the interaction between the solute and stationary phase.

If the retention phenomenon in the chromatographic column is only the result of solute partition between the gas and liquid phase, then the retention volume is given by [1]

$$V_N = K_L \cdot V_L \tag{1}$$

where V_N is the net retention volume corrected for the gas phase compressibility, K_L is the Nernst partition coefficient and V_L is the volume of liquid (stationary) phase in the column. In the case of adsorption chromatography, for very low concentration of solute in the gas phase when the Henry's law region is reached, equation (1) can be written as

$$V_N = K_S \cdot A \tag{2}$$

where K_S is the surface partition coefficient equal to Henry's constant and A is the specific surface of adsorbent (stationary phase).

Because both K_L and K_S are the constants determining the thermodynamic equlibria at infinite dilution of solute in the gas phase the differential heat of sorption q_d^0 may be identified with differential enthalpy for isothermal transfer of 1 mole of solute from the reference standard gas phase to an adsorbed or diluted state, $-\Delta H$ [2,3]. Then

$$\frac{d(\ln V_N)}{d(1/T)} = \frac{-\Delta H}{RT} \tag{3}$$

1.1. Inverse gas chromatography

Equation (3) shows that the diagram of $\ln V_N$ vs $1/T$ relationship should be a straight line, if the mechanism of interaction between a solute and stationary phase (retention mechanism) does not change in the investigated temperature range. Every change of this mechanism results in a change of the slope of $\ln V_N = f(1/T)$ diagram or as a maximum in this diagram. Therefore, if there is chosen such a solute that its properties (e.g. vapour pressure) change continuously with the temperature increase, then the discontinuities in this diagram are the results of the change of stationary phase properties. The value of the retention volume is then a source of information about the physical state of the stationary phase. This kind of gas chromatography, due to a radical change of application of this method, is called *inverse gas chromatography*.

Inverse gas chromatography has been succesfully applied in various fields of research for many years. In 1962 Scott has showed its applicability in the investigation of melting of organic substances [4]. Next, Guillet [5] employed this method for researches of the phase transitions occuring in polymers, and Kelker and Schivitzhoffen [6] investigated the phase transitions in liquid crystals. Inverse gas chromatography was also used for phase transitions characterization in solids [7]. In the last years the properties of polymers were often investigated by inverse gas chromatography [8]. Also, the liquid stationary phases for gas chromatography were characterized and classified by IGC [9]. This chromatographic method is frequently used for determination of the solid surface properties, for example for estimation of dispersion and non-dispersion components of surface free energy [3,10,11].

It seems, however, that the most interesting results were achieved by inverse gas chromatography in the investigation of the properties of mono- and polymolecular films of organic substances on the surface of porous adsorbents.

1.2. Distribution of liquids on the surface of porous adsorbents

The knowledge of the physical state of the liquid stationary phase is of great importance for understanding the partition processes in liquid gas chromatography. There are many records of a fact that the properties, e.g. melting points, of a liquids deposited in a thin capillary or outspread on the solid surface are different from those in a bulk liquid. Giddings included this phenomenon in the model of liquid stationary phase distribution in the chromatographic column [12]. Giddings stated that liquid on solid support surface was divided into two forms: a thin surface film, the properties of which are different from those of bulk liquid, and an excess over this film capacity. This model was completed by Serpinet [13] by the finding that the surface film exists also under the bulk liquid and that the properties of the surface film strongly depend on the properties of solid surface. This is especially important if the interaction between the liquid molecules and solid surface leads to oriented mono- or polymolecular film creation. There many examples of such films formed on the surfaces of graphite or silica gel by hydrocarbons [14-16], long-chain amphiphilic substances as alcohols [17,18] and others [19,20].

2. MONOMOLECULAR FILMS OF LONG-CHAIN ALIPHATIC ALCOHOLS ON SILICA GEL SURFACE IN EQULIBRIUM WITH THE THREEDIMENSIONAL EXCESS OF AN ALCOHOL

The most widely studied system in which the monomolecular films are formed is the silica gel – long-chain aliphatic alcohol system. The reason may be similarity of the silica gel and water surfaces: the surface concentration of the silanol groups on the fully hydroxylated surface of silica gel is equal to 4.6 OH groups per 1 nm^2 [21]. The silanol groups are the adsorption centers for the alcohol molecules, anchoring them to the silica gel surface. In this way, the monolayer of alcohol molecules may be formed. If the amount of alcohol exceeds the monolayer capacity, then the excess forms, depending on the temperature, crystals or droplets on the monolayer surface, because the aliphatic alcohols belong to the autophobic substances [22]. The least possible surface occupied by one molecule in the monolayer is 0.21 nm^2, that is as much as in the monolayer in the solid-condensed (SC) state on the water surface [23]. Decrease of the surface concentration of alcohol molecules leads to the liquid-expanded (LE) monolayer and next to the monolayer in the gaseous state.

The methods of column packing preparation well known in gas chromatography practice [24] give the possibility to coat the silica gel surface with the monolayer of a given surface concentration or with the monolayer in SC state with a well-defined threedimensional excess if the specific surface area of adsorbent is known. On the other hand, inverse gas chromatography allows to determine the specific surface area of silica gel if aliphatic alcohol is used as a liquid stationary phase [25].

In Fig. 1 the diagrams of $\log V_S$ vs $1/T$ relationships for the column packings composed of n-octadecanol and silica gel (a specific surface area 27.3 m^2 and a mean pore diameter 125 nm) are presented. The retention volumes were determined with n-octane. According to Serpinet [26] V_S is the net retention volume related to 1 g of solid support in the column. V_S was chosen because the investigated column packings often contained a very small amount of stationary phase and because V_S is closely related to V_g, the retention volume generated by 1g of liquid stationary phase, due only to the partition of solute between the gas and liquid stationary phases

$$V_g = \Delta V_S / \Delta \tau \tag{4}$$

where ΔV_S is the specific retention volume V_S increase caused by the increase in loading ratio specified by $\Delta\tau$. $\Delta\tau$ may be, for example, a result of melting of the part of stationary phase (Fig. 1). The loading ratio τ is defined as the ratio of mass of stationary phase to the mass of solid support. According to Serpinet [26]

$$\tau = \tau_F + \tau_B \tag{5}$$

where τ_F corresponds to the part of stationary phase forming the surface film and τ_B is this part of stationary phase which is not influenced by the solid surface.

Curve A in Fig. 1 presents the $\log V_S = f(1/T)$ relationship for the column packing with the n-octadecanol amount considerably exceeding the monolayer capacity determined by τ_F. The first maximum in this diagram at 58°C, the melting point on n-octadecanol, is caused by melting of this part of n-octadecanol which is not bonded in the monolayer.

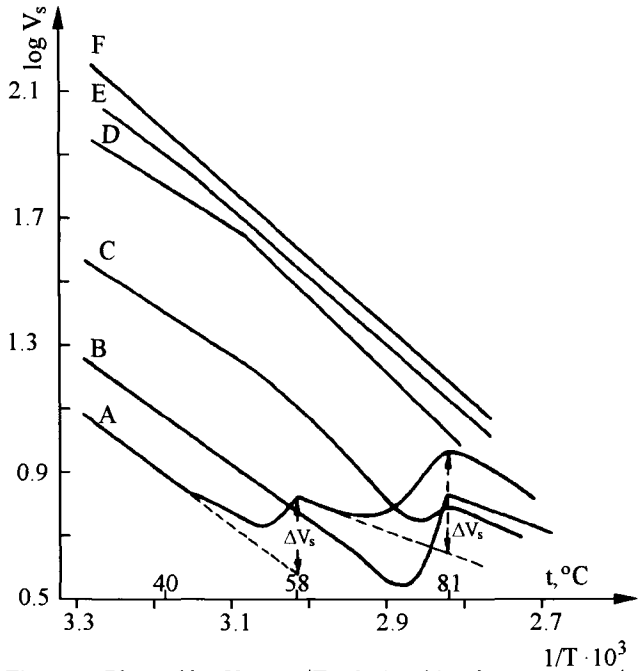

Figure 1. Plots of log V_S vs 1/T relationships for n-octane. A – 6.29%; B – 5.7%; C – 5.0%; D – 3.89%; E – 2.99% and F – 1.61% mass. of n-octadecanol deposited on silica gel.

Melting of the part of stationary phase changes the retention mechanism: the n-octane retention in the temperature range below 58°C is the result of adsorption on the surface of monolayer and crystals of solid n-octadecanol; above this temperature the main process responsible for the retention of n-octane becomes its dissolution in liquid n-octadecanol.

The value of the retention increase ΔV_S^{58} leads easily to the determination of the n-octadecanol monolayer capacity on the silica gel surface. If the specific retention volume V_g^{58} (retention volume generated by 1g of n-octadecanol at 58 °C) is known, then

$$V_S^{58} = \frac{\Delta V_g^{58}}{\tau_B} \tag{6}$$

and

$$\tau_F = \tau - \frac{\Delta V_S^{58}}{V_g^{58}} \tag{7}$$

Assuming, that the surface area occupied by one n-octadecanol molecule in monolayer is equal to 0.21 nm^2 [23] and knowing ΔV_g^{58} of solute determined in a separate experiment equation (7) gives a simple method of the adsorbent specific surface area determination, first described by Serpinet [25].

τ_F value may be also estimated in another way: by determination of ΔV_S^{58} vs τ relationship for a few column packings. The diagram of this relationship is a straight line and shows τ_F value in the abscissa. Also, the linear increase of ΔV_S^{58} for $\tau > \tau_F$ indicates that

the physical state of threedimensional droplets of n–octadecanol on its own monolayer is not influenced either by silica gel or monolayer surface.

It should be added that the non–linear shape of log V_S = f(1/T) diagram (curve A, Fig. 1) in the temperature region preceeding the melting point of n–octadecanol is the result of the $\gamma - \alpha$ polymorphic transition in the solid alcohol. Abrahamsson et al [27] and Tanaka et al [28] described precisely the γ and α structures.

The diagram presented in Fig. 1 (curve A) above 58°C is a straight line up to 71°C. The increase of retention volume beginning at this temperature may be only the effect of the phase transition occurring in the n–octadecanol monolayer. The result of this transition is that monolayer transforms from a SC to LE state and that the surface area occupied by a single molecule in the monolayer increases to 0.27 nm^2. It means that as much as 23% of alcohol molecules must be ejected from the monolayer to the threedimensional phase. Therefore, ΔV_S^{81} is the result of the increase of the liquid n–octadecanol amount in the column. The analysis of the Δ_S^{81} vs τ confirms that a single n–octadecanol molecule occupies 0.27 nm^2 in the expanded monolayer.

Curves B and C in Fig. 1 are plotted for the column packings composed of silica gel covered with monolayers characterised by the surface area per molecule 0.215 and 0.245 nm^2. Thus, the monolayer state is intermediate between SC and LE. Only one maximum, at 81°C, occurs in these diagrams and the value of this maximum decreases with the decrease of the surface concentration of n–octadecanol molecules. This fact confirms the origin of the maximum at 81°C as well as the mechanism of the SC – LE phase transition.

The results of the investigation of n–octadecanol monolayer with the threedimensional excess of this compound on the silica gel surface, obtained by inverse gas chromatography method, were verified by scanning differential calorimetry [29,30]. These experiments confirmed the SC – LE phase transition occurring in the monolayer at 81°C and brought additional, rather surprising, information concerning this phase transition. Namely, besides the endothermic peaks on the DTA curves accompanying the polymorphic $\gamma - \alpha$ transition in solid n–octadecanol, melting of the threedimensional excess of n–octadecanol and SC – LE transition in monolayer (81.5°C) an additional peak was registered at 76°C. It was stated that this peak was the result of SC – LE transition in part of monolayer covered by droplets of liquid n–octadecanol.

Therefore, the inverse gas chromatography method allows us to determine the model of long–chain aliphatic alcohol distribution on the surface of porous silica gel: if the amount of alcohol on adsorbent surface is equal or exceeds the monolayer capacity, then the monolayer is composed of alcohol molecules oriented their polar moieties to the adsorbent surface. The monolayer, in a solid–condensed state, is stable up to 81°C. At this temperature the monolayer transfers into a liquid–expanded state. The threedimensional excess of alcohol, because the autophobicity phenomenon, does not wet the monolayer surface.

3. LIQUID–EXPANDED AND GASEOUS MONOLAYERS OF LONG–CHAIN ALIPHATIC ALCOHOLS ON SILICA GEL SURFACE

The diagrams C, D, E and F in Fig. 1 present the log V_S vs 1/T relationships determined with n–octane on the column packings in which the surface area occupied by a

Table 1
The dependence of the phase transition temperature in n–octadecanol monolayer on its surface concentration, A is the surface area occupied by 1 molecule of n–octadecanol

τ,%	A, nm^2	Temperature of the phase transition, °C
0.095	11.203	—
0.500	2.453	—
1.18	1.039	—
1.61	0.764	—
2.16	0.570	—
2.53	0.484	43.9
2.99	0.411	45.5
3.53	0.349	47.6
3.89	0.315	50.8
5.00	0.246	52.2
5.70	0.215	81.0

single molecule of n–octadecanol is greater than 0.21 nm^2. If this surface area is within the range of 0.25 – 0.48 nm^2 one observes the inflection point in the diagram (curves C,D and E). For the area greater than 0.48 nm^2 the log V_S vs 1/T diagram is a straight line in all investigated temparature ranges, from –30 to 90°C. The change of slope of straight lines which are the components of the discussed diagrams suggests the change of the retention mechanism. The reason for this change must be the modification of the monolayer structure, because properties of either the solute (n–octane) or the silica gel do not change abruptly in the temperature range 40 – 52°C. The phase transitions, presented by the inflexions on log V_S vs 1/T diagrams, occur in monolayers characterized by the surface concentration of n–octadecanol molecules specific for the LE phase. The data from

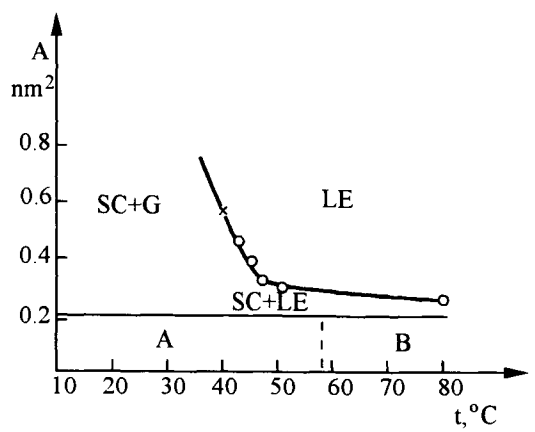

Figure 2. The phase diagram of n–octadecanol monolayer on silica gel surface.

Table 1 allow to construct the phase diagram of n-octadecanol monolayer on the silica gel surface (Fig. 2). This diagram, confronted to the analogous one for a monolayer on the water surface, is rather poor in details. One may suppose that, since the n-octadecanol molecules are "anchored" to the silica gel surface, only the phase transitions which give a relatively significant energetic effect or those leading to the well marked changes of monolayer structure are observed. Particularly, in Fig. 2 both the triple point of all three phases coexistence and the line representing the LE – G transition are not observed.

Some additional information about the structure of the n-octadecanol monolayer on the silica gel surface may be provided up by relationships between the retention volumes determined with the solutes differing in the molecule shape and their dimensions.

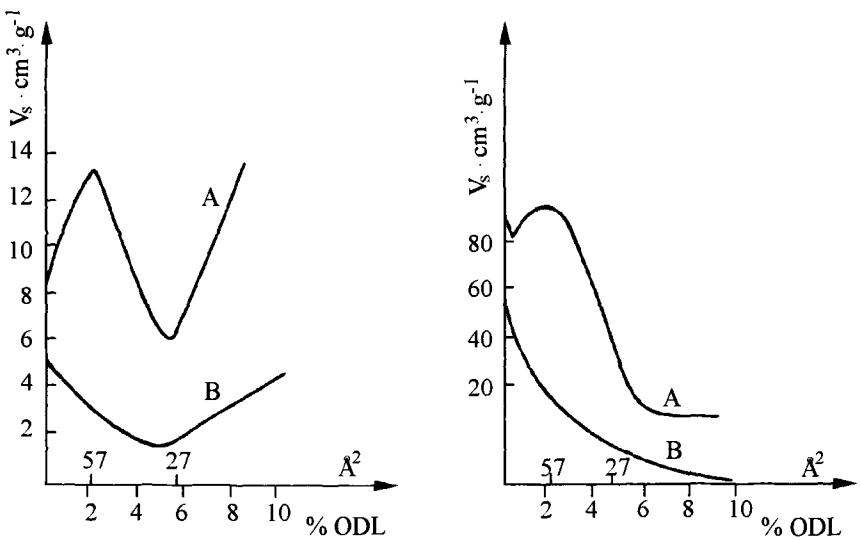

Figure 3. The diagrams of V_S vs τ relationships for n-octane (A) and chloroform (B) in 40°C (right) and 85°C (left). τ is expressed in % mass. of n-octadecanol.

In Fig. 3 such relationships for n-octane and chloroform are presented. The relationships were determined at 40°C, namely when the monolayer can exist in a SC or LE form or be composed of SC islands surrounded by two-dimensional gas. The shape of V_S vs τ relationship for n-octane may be interpreted as follows: the first alcohol molecules deposited on silica gel surface block the most active centers on solid surface. This fact manifests as the retention volume decrease. However, from the surface concentration 1 nm^2 up to 0.57 nm^2 per n-octadecanol molecule the retention volume increases. The reason for this increase is probably the penetration of n-octane molecules into the rising structure of n-octadecanol chains. Let us assume that the n-octadecanol molecules are uniformly distributed on the silica gel surface. Therefore, at a surface concentration 0.57 nm^2 per molecule the free spaces (0.38 nm^2 in their cross-section) between them are formed, which are compatible with the n-octane molecule diameter. Then the maximum of n-octane retention volume is the result of a kind of "molecular sieve" effect. If the surface concentration of n-octadecanol increases and exceeds 0.57 nm^2 per molecule, the

n–octane retention dramatically decreases, because its molecules do not penetrate into the structure formed by the hydrocarbons chains. The retention is then the result of n–octane adsorption on the terminal methyl groups of n–octadecanol molecules. As it is known [32], the interactions between methyl groups and hydrocarbon molecules are much weaker than with the $-CH_2-$ groups. This is confirmed by the fact that minimum of retention is observed for the column packing with the monolayer at the highest concentration (0.21 nm^2 per n–octadecanol molecule) while its surface is composed only of $-CH_3$ groups.

The shape of V_S vs τ relationship for chloroform is quite different. The retention volumes of this compound decrease monotonically with the τ increase. Therefore, one may suppose that the retention is rather the result of interaction between chloroform and silica gel surface than with the structure of the n–octadecanol chains on this surface.

A temperature 85°C is higher than the "critical crystallization temperature" [33] of n–octadecanol monolayer. This means that the highest surface concentration of the monolayer, irrespective of the amount of n–octadecanol deposited on silica gel, is equal to 0.27 nm^2 per molecule. The run of V_S vs τ diagram for n–octane is slightly different from that at 40°C. The retention volumes increase with τ up to a surface concentration 0.57 nm^2, but without a noticeable effect of silica gel surface deactivation, and next decrease to a minimum at τ corresponding to 0.27 nm^2 per n–octadecanol molecule, i.e. at the surface concentration characteristic for LE phase. The V_S increase beginning from this value is the result of n–octane dissolution in liquid threedimensional n–octadecanol.

The retention volumes of chloroform at 85°C (Fig. 3) decrease also to τ = 0.27 nm^2. The $CHCl_3$ also at 85°C does not "feel" the differences in the structure of n–octadecanol monolayers on the silica gel surface. Perhaps this is the result of the difference in the shape and dimensions of n–octane and chloroform molecules: a cross–section of n–octane molecule penetrating into the n–octadecanol monolayer is equal to 0.19 – 0.21 nm^2 while that of chloroform is 0.385 – 0.295 nm^2 [34], or, according to Van Voorhis et al, even 0.547 nm^2 [35].

4. THEORETICAL MODEL OF N–OCTADECANOL MONOLAYER ON SILICA GEL SURFACE

The previous part showed that inverse gas chromatography is a very useful tool in the investigation of long–chain aliphatic alcohol monolayers adsorbed on the surface of porous silica gel. Now a simple theoretical model of the adsorbed layer that can be used to analyse the experimental data obtained by inverse gas chromatography is considered. The model is based on the theory of adsorption of simple gases on solid surfaces and, initially restricted to fully localized adsorption [36–38], was extended to treat also long–chain molecules [39].

To describe the experimental observation [40] of the solid condensed – liquid expanded phase transitions in brush–like monolayers on silica gel a simple lattice model and the theory of orientational effects in adsorbed monolayers were used [36–38]. It was assumed that interaction between the n–octadecanol molecule and the solid could be presented as

$$E(\nu) = E_h + E_c(\nu) \tag{8}$$

where E_h is the energy of interaction between the hydroxyl group and the solid, $E_c(\nu)$ is the interaction between the hydrocarbon chain and the solid, ν is the angle between the

n- octadecanol molecule axis and the normal to the solid surface. The interaction between two adsorbed molecules i and j is assumed to be given by the sum

$$U(\omega_i, \omega_j, r_j) = U_{hh}(r_{ij}) + U_{hc}(\omega_i, r_{ij}) + U_{hc}(\omega_j, r_{ij}) + U_{cc}(\omega_i, \omega_j, r_{ij}) \tag{9}$$

where U_{hh} is the interaction energy between the hydroxyl groups of both molecules adsorbed on the sites separated by distance r, $U_{hc}(\omega_i, r_{ij})$ is the interaction energy between the hydroxyl groups belonging to the j-th molecule and the hydrocarbon chain belonging to the i-th molecule, $U_{cc}(\omega_i, \omega_j, r_{ij})$ is the interaction energy between hydrocarbon chains of both molecules and $\omega = (\nu, \varphi)$, where φ is the azimuthal angle defined in [39].

Besides, it was assumed that only half of the adsorption centers on silica gel surface can be occupied by n-octadecanol molecules and that all these centers are energetically equivalent. Thus, we can consider a surface lattice of sites be composed of two interpenetrating sublattices. At low surface concentration the adsorbed molecules are distributed randomly over the centers belonging to both sublattices. However, when the film density exceeds a certain value of A_o/A_d (A_d is the surface area occupied by a single molecule) a preferential adsorption on one of the sublattices must begin. This leads to the formation of a highly ordered structure, e.g. the monolayer in two-dimensional solid condensed state. If the interaction between only neighbouring hydrocarbon chains, perpendicularly oriented to the solid surface are taken into account, we can derive the equation of state for the adsorbed film [39]

$$\pi A_o/k_B T = \frac{1}{2}\ln\{1 - A_o/A\} + \Psi(A_o/A)^2 - \frac{1}{2}\Phi s^2 \tag{10}$$

where π - the spreading pressure, A_o - the minimal surface area occupied by a single molecule in the monolayer (e.g. 0.21 nm^2 for aliphatic alcohols on silica gel or water surface), A - the surface area occupied in the monolayer by one molecule, T - the temperature and s - the parameter which is a measure of the asymmetry of distribution of adsorbed molecules between two sublattices. Φ and Ψ are the adjustable parameters: Φ is determined by the difference between the interaction energies of adsorbed molecules on the same and the different sublattices - when the density of adsorbed film is lower than $A_o/A = 2\Phi$, then both sublattices are occupied uniformly by adsorbed molecules and $s = 0$. For higher densities of adsorbed monolayer the parameter s assumes non-zero value and

$$A_o/A = s\frac{\exp(\Phi s) + 1}{\exp(\Phi s) - 1} \tag{11}$$

The parameter Ψ determines first of all the critical temperature for the two-dimensional gas to expanded liquid transition and influences the temperature range where the expanded liquid and solid phase coexist. According to the presented model the values of Φ and Ψ and the temperature of transition from the expanded liquid to solid condensed phase can be either first-order or higher-order (continuous) transition. Therefore, the appearance of the tricritical point T_{tcr} is expected to be observed, where the regimes meet.

In Fig. 4 the phase diagram for n-octadecanol monolayer adsorbed on silica gel is presented. It can be seen that the fit of theoretical curve (full and broken lines) to the experimental points taken from Fig. 2 is satisfactory. The procedure of Ψ and Φ computing as well as the other procedures employed were described in Ref. [39].

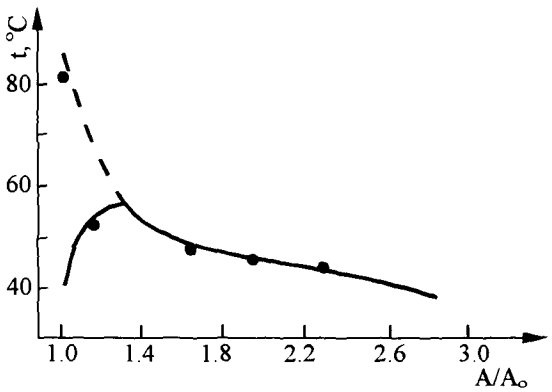

Figure 4. A comparison of the experimental (filled circles) and theoretical phase diagram of n-octadecanol monolayer on silica gel surface. A_0 is the minimal and A – the real surface area occupied by a single molecule in monolayer.

Of course, the model presented is rather simple and contains some unwarranted assumptions. The real situation of long-chain amphiphilic molecules on the silica gel surface must be more complex. Nevertheless, the model enables a qualitative interpretation to be made of the experimental findings. Moreover, the parameters Φ and Ψ can be also used for the approximate estimation of the energy of interaction between n-octadecanol molecules in the monolayer. It follows from the values $\Psi T = 1270K$ and $\Phi T = 830K$ that the energy of interaction between the neighbouring molecules adsorbed on the same sublattice is about 3.14 kJ mol^{-1} and the energy of interaction for a pair of molecules on different sublattices is 1.73 kJ mol^{-1} [39].

5. MIXED MONOLAYERS OF LONG-CHAIN ALIPHATIC COMPOUNDS ON SILICA GEL SURFACE

Serpinet, using the inverse gas chromatography method, demonstrated the existence of oriented monolayers of long-chain hydrocarbons on silica gel surface [13], on the other hand Untz [31] showed that hydrocarbons also form solid condensed and liquid expanded monolayers on glycerol but not on the water surface. However, the addition of some amount of amphiphilic molecules to the hydrocarbon provokes the mixed monolayer formation on the water surface. The phase transition in such a monolayer occurs at the temperature higher than the melting point of bulk hydrocarbon. It also appeared that the monolayers characterized by 1:1 ratio of hydrocarbon to alcohol molecules were particularly stable [41].

It can be predicted that the properties of mixed monolayers composed of hydrocarbon and alcohol molecules deposited on the water, glycerol and silica gel surfaces will be different despite a common feature of these surfaces which are the hydroxyl groups. The reason for these differences is the localized adsorption of alcohol molecules on silica gel and the heterogeneity of its surface. In Fig. 5 the results of investigation of mixed monolayers

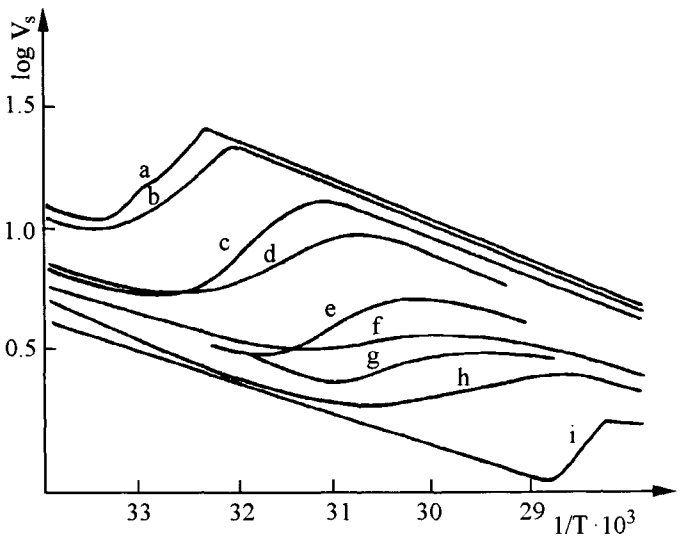

Figure 5. log V_S vs 1/T relationships for n-octane obtained on silica gel covered with mixed monolayers composed of n-nonadecane and n-octadecanol: a - 0%; b - 17.2%; c - 46.8%; d - 52.0%; e - 68%; f - 75%; g - 80%; h - 85.9% and i - 100% of n-octadecanol in monolayer.

(n- nonadecane and n-octadecanol) deposited on silica gel are presented [41]. The surface occupied by one molecule in the monolayers, independently of their composition, was equal to 0.21 nm^2. The shape of the curve a in Fig. 5 with the maximum above the melting point of pure n-nonadecane (32°C) shows that this compound forms the oriented monolayer on the silica gel surface. The monolayer is stable up to 36°C. It must be noted that not all n- nonadecane molecules deposited on silica gel are involved in monolayer, because one can also observe the V_S increase below 36°C. The inverse gas chromatography does not permit to evaluate the amount of n-nonadecane forming the oriented monolayer. The phase transition at 36°C leads to destruction of the oriented monolayer, because the specific retention volumes of the test substances measured experimentally and calculated on the basis of V_g values measured for n-nonadecane on the silanized support are in good agreement [41,42].

Addition of n-octadecanol to n-nonadecane (on condition that one molecule occupies 0.21 nm^2 in a monolayer) shifts the maximum on log V_S vs 1/T to higher temperature (curve b). The retention volumes of the test substances in pure n-nonadecane and for the column packing containing 17% mass. of n-octadecanol are almost equal. It means that the threedimensional phase above the phase transition temperature contains n-nonadecane only, thus first of all the n-octadecanol molecules remains in the oriented monolayer.

The temperature of the phase transition in mixed monolayers increases with the increase of n-octadecanol concentration, as in the monolayers on water or glycerol [31,41]. However, the maxima in log V_S vs 1/T plots are not so sharp as for liquid subphases, probably because the silica gel surface is not as homogeneous as that of liquid. At the higher concentration of n- octadecanol in a monolayer (curves f-h) two maxima appear

in the log V_S vs 1/T relationships. The first maximum corresponds probably to the phase transition in the part of monolayer poorer in n-octadecanol. The maximum of higher temperature is the result of SC – LE transition in this part of monolayer which is composed of almost pure n-octadecanol.

6. THE PROPERTIES OF LIQUID CRYSTAL LAYER ON THE SILICA GEL SURFACE

Liquid crystals are often used as the liquid stationary phases in gas chromatography. The first reports about their application in gas chromatography are dated from the sixties. At the beginnng of eighties more than two hundred liquid crystals were applied in gas chromatography [43,44]. The reason for this interest is a particular structure of the mesophase exhibiting a very high selectivity against the chromatographed mixtures. The temperature range of the mesophase existence is often too narrow for the analysts. Many methods were used in order to broaden this temperature range, for example the chromatographic columns are placed in the electric fields [45]. In some cases the solid surface which is the subphase of liquid crystal is the reason for the change of phase transition temperatures [46,47]. Of course, it is easy to expect that the utmost changes of liquid crystal properties should be observed in the film of liquid crystal molecules closest to the solid surface, but determination of the range of the surface influence is rather difficult. The inverse gas chromatography can help solve this problem.

p-butyl-p'-hexanoiloazobenzene (PBHB) deposited on silica gel characterized by the specific surface area 16.1 m^2/g was used in the investigations reported below. The nematic phase of this compound is stable between 58.5 and 65°C [48].

In Fig. 6 the log V_S vs 1/T relationships determined with n-octane and toluene are

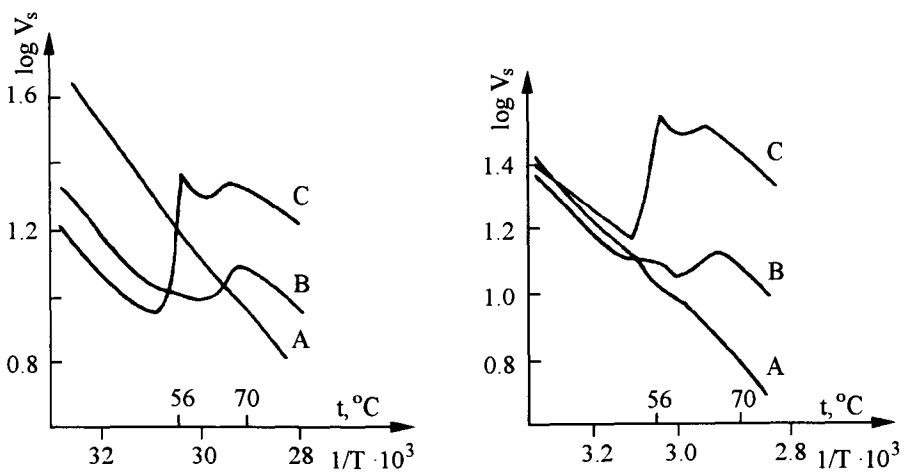

Figure 6. Log V_S vs 1/T relationships for n-octane (left) and toluene (right) obtained on silica gel covered with PBHB. A – 1.3%; B – 5% and C – 12.1% mass. PBHB.

presented. As previously, the maxima on the diagrams indicate the phase transitions in the liquid crystal film. The temperatures of the phase transition and the temperature ranges of the nematic phase stability, Δt_m, are collected in Table 2. These data show that the influence of silica gel surface on Δt_m is very clear especially for the thin PBHB layer. It is worth noting that the transition of the nematic phase into isotropic liquid clearly occurs at $\tau = 3\%$ mass. while the temperature of solid – mesophase transition can be determined for the column packing containing about 6% mass. of PBHB. The broadening of Δt_m of PBHB on silica gel is the result of decrease of solid – nematic transition temperature as well as the increase of the temperature of mesophase – isotropic liquid.

Table 2
τ_F values of PBHB on silica gel surface [48]

τ, % mass.	τ, g/m^2	ΔV_S^{72}, cm^3/g	τ_F, g/m^2
7.68	$4.74 \cdot 10^{-3}$	12.99	$3.23 \cdot 10^{-4}$
5.00	$3.09 \cdot 10^{-3}$	7.54	$3.06 \cdot 10^{-4}$
3.00	$1.86 \cdot 10^{-3}$	4.13	$3.39 \cdot 10^{-4}$

The plots of log $V_S = f(1/T)$ for n–octane and toluene at the temperature higher than 70°C are, of course, the straight lines, because the retention of this compounds is caused only by the solution in liquid (isotropic) PBHB. However, a certain part of PBHB deposited on silica gel does not transit into the isotropic liquid. This part of PBHB which does not melt even at 72°C was determined comparing, the ΔV_S and V_g values for n–octane using Eqs. 6 and 7. V_g for n–octane at 72°C was measured on column packing composed of silanized support Gas Chrom RZ and 5% mass. of PBHB. Liquid crystals do not form the oriented films on the silianized supports, also Δt_m is the same as for the bulk compounds [48].

The values of τ_F, independent of the total amount of PBHB deposited on silica gel τ, show that under the layer of isotropic liquid there exists the PBHB structure characterized by the properties different from those of bulk liquid. The surface occupied by a single PBHB molecule in this structure is equal to 1.92 nm^2. The cross–section of one molecule along its long axis, calculated according to McClellan and Harnsberger [34] is 1.7 – 2.0 nm^2. Therefore, it seems probable that at 72°C PBHB forms the monolayer composed of flat lying molecules on silica gel surface.

REFERENCES

1. J.R. Conder and C.L. Young, Physicochemical Measurements by Gas Chromatography, Wiley – Interscience, New York, 1979.
2. J.H. De Boer, The Dynamical Character of Adsorption, OUP, London, 1953.
3. G.M. Dorris and D.G. Gray, J. Colloid Interface Sci., 77 (1980) 353.
4. C.G. Scott, in: Gas Chromatography 1962, M. van Swaay (ed.), Butherworths, London, 1962, p.37.
5. J. Guillet, J. Macromol. Sci., A4 (1970) 669.

6. H. Kelker, E. van Schivitzhoffen, in: Advances in Chromatography, vol. 6, J.C. Giddings and R.A. Kelker (eds.), Marcel Dekker, New York, 1968, p.247.
7. B.T. Guran and L.B. Roberts, J. Gas. Chromatogr., 5 (1967) 574.
8. M.J. El-Hibri and P. Munk, Macromolecules, 21 (1988) 264.
9. A. Voelkel, J. Chromatogr., 435 (1988) 29.
10. E. Papirer, H. Balard and A. Vidal, Eur. Polym. J., 24 (1988) 783.
11. B. Biliński and W. Wójcik, Mater. Chem. Phys., 30 (1992) 209.
12. J. C. Giddings, Anal. Chem., 34 (1962) 458
13. J. Serpinet, J. Chromatogr., 68 (1972) 9.
14. M. Liphard, P. Glanz, H. Pilarski and G.H. Findenegg, Progr. Colloid Polym. Sci., 68 (1980) 131.
15. G.H. Findenegg, J. Chem. Soc., Faraday Trans. I, 69(1973) 1069.
16. J. Serpinet, J. Chromatogr., 77 (1973) 289.
17. A. DiCorcia, R. Samperi and C. Severini, J. Chromatogr., 198 (1980) 347.
18. J. Rayss, J. Colloid Interface Sci., 91 (1983) 376.
19. A.V. Kiselev, N.V. Kovaleva and Y.S. Nikitin, J. Chromatogr., 58 (1971) 19.
20. M.M. Kopecni and S.K. Miljonic, Anal. Chem., 52 (1980) 1032.
21. L.T. Zhuravlev, Colloids Surf. A, 74 (1993) 71
22. E.G. Shafrin and W.A. Zisman, J. Phys. Chem., 64 (1960) 519.
23. G.L. Gaines, Insoluble Monolayers at Liquid-Gas Interface, Interscience, New York, 1966.
24. W.R. Supina, The Packed Columns in Gas Chromatography, Supelco Inc., Bellefonte, 1974.
25. J. Serpinet, Wiadomości Chem., 30 (1976) 793.
26. J. Serpinet, Anal. Chem., 48 (1976) 2224.
27. S. Abrahamsson, G. Larsson and E. von Sydow, Acta Crystallogr., 13 (1960) 770.
28. K. Tanaka, T. Seto and T. Hayashida, Bull. Inst. Chem. Res. Kyoto Univ., 35 (1957) 123.
29. J. Rayss, J. Colloid Interface Sci., 81 (1981) 52.
30. J. Rayss, J. Colloid Interface Sci., 91 (1983) 376.
31. G. Untz, These, Universite Claude Bernard de Lyon, 1974.
32. F.M. Fowkes, J. Colloid Interface Sci., 5 (1968) 49.
33. D. Dervichian, J. Phys. Rad., 7 (1939) 333.
34. A.L. McClellan and H.F. Harnsberger, J. Colloid Interface Sci., 23 (1967) 577.
35. J.J. van Voorhis, R.G. Craig and F.E. Bartel, J. Phys. Chem., 61 (1957) 1513.
36. A. Patrykiejew, Thin Solid Films, 81 (1981) 89.
37. A. Patrykiejew, Thin Solid Films, 88 (1982) 359.
38. A. Patrykiejew, Thin Solid Films, 105 (1983) 259.
39. A. Patrykiejew, J. Rayss and J. Serpinet, Thin Solid Films, 173 (1989) 279.
40. J. Rayss, A. Patrykiejew and J. Serpinet, Thin Solid Films, 173 (1989) 13.
41. J. Rayss, M. Saint Pierre and J. Serpinet, J. Chim. Phys., 79 (1982) 233.
42. Z. Kessaisia, E. Papirer and J.-B. Donnet, J. Colloid Interface Sci., 82 (1981) 526.
43. H. Kelker, Advances in Liquid Crystals, vol. 3, Academic Press, New York, 1978.
44. Z. Witkiewicz, J. Chromatogr., 251 (1982) 311.
45. H. Watabe, T. Hobo and S. Suzuki, J. Chromatogr., 249 (1982) 209.
46. Z.P. Vetrova, N.T. Karabanov and Y. I. Yashin, Chromatographia, 10, (1977) 341.
47. W. Marciniak and Z. Witkiewicz, J. Chromatogr., 207 (1981) 333.
48. J. Rayss, Z. Witkiewicz, A. Waksmundzki and R. Dąbrowski, J. Chromatogr., 188 (1980) 107.

A. Dąbrowski and V.A. Tertykh (Editors)
Adsorption on New and Modified Inorganic Sorbents
Studies in Surface Science and Catalysis, Vol. 99

Chapter 2.8
The use of gas chromatography to study the adsorption from gaseous phase at the infinite dilution

F. J. López Garzón and M. Domingo Garcia

Departamento de Química Inorgánica, Facultad de Ciencias, Universidad de Granada, 18071 Granada, Spain

1. INTRODUCTION

The surface characteristics of inorganic solids are commonly measured by adsorption of gases and vapours which is normally carried out in a wide range of vapour pressures from low to high relative pressures (in many cases up to $P/P_0 = 1$). From these measurements average values of pore radius and surface energy are obtained. This is very useful for many purposes e.g. when solids are used as adsorbents in gas and liquid phases or as supports for catalysts. However, in several cases the concentration of substance to be adsorbed is very small and the adsorption process is not governed by the bulk textural properties of the solid. This occurs in the emission of fluent gases from car engines and industrial processes. For this reason it is not possible to explain the adsorption of one diluted adsorbate on the basis of the bulk surface properties of the adsorbent. This can be explained, however, by studying the surface characteristics on the basis of the adsorption at very low vapour pressure of the adsorbate at the so called zero surface coverage, where the amount adsorbed depends linearly on the vapour pressure (Henry's law region). For this purpose gas solid chromatography is a technique which is increasingly used.

Gas solid chromatography is an analytical technique used for many purposes. However, its use to obtain information about characteristics of the stationary phase is less common, and in this case is called inverse gas chromatography (IGC). One of the pioneer work on IGC was published by Greene and Pust [1] who used it to determine heats of adsorption. Additionally, a huge amount of research using IGC has been developed by Kiselev et al. [2]. They reported the adsorption of different adsorbates on several adsorbents measured by IGC, although they focused mainly on determination of the adsorption isotherms in the whole range of vapour pressures. Later on, Conder and Young [3] published a very interesting monograph dealing with different application of IGC: determination of adsorption isotherms, surface areas, thermodynamic and molecular parameters. Since then, many papers have been published on the use of IGC to characterize organic and inorganic solids.

2. THERMODYNAMIC PARAMETERS FROM INVERSE GAS CHROMATOGRAPHY (IGS)

The use of IGC to study adsorption processes is based on the assumption that the adsorption equilibrium is reached. This occurs at zero surface coverage when two experimental conditions are fulfilled. Firstly, the chromatograms have to be symmetric, and secondly, the maxima of the chromatographic peaks have to be independent of the amount of adsorbate injected. Moreover, as the amounts injected are very low, only very low concentrations of the adsorbate are in the gas and stationary phases and the adsorption process is only governed by adsorbate–adsorbent interactions. Therefore, under these conditions the adsorbate can be considered to behave as an ideal gas in the vapour phase and on the adsorbent surface, and the equilibrium constant of the adsorption can be expressed by [4]:

$$K = \frac{V_R}{SRT} \tag{1}$$

where K is the adsorption constant in the Henry's law region, V_R the net retention volume, S the surface area (normally obtained by CO_2 measurements), R the gas constant and T the temperature. Equation (1) is also written:

$$K = \frac{V_s}{RT} \tag{2}$$

where $V_s = V_R/S$ is the specific retention volume.
If the adsorbed gas behaves as an ideal gas, the following equation of state can be written:

$$\pi = \sigma RT \tag{3}$$

where π is the two-dimensional pressure and σ is the concentration of the adsorbate on the surface.
If the adsorption is produced in the Henry's law region, the relationship between σ and the pressure P of the reference state is:

$$\sigma = KP \tag{4}$$

The equation (3) is then:

$$\pi = KPRT \tag{5}$$

and taking into account equation (2):

$$\pi = V_s P \tag{6}$$

which provides a relationship between two and three dimensional pressures.
On the other hand if the standard pressure state is $P_{s,g}$, the change of the standard free energy of adsorption of 1 mol of adsorbate from this state to a standard adsorbed state is:

$$\Delta G_A^0 = -RT \ln \frac{P_{s,g}}{P} \tag{7}$$

which together with Equation (6) can be expressed as:

$$\Delta G_A^0 = -RT \ln \frac{V_s P_{s,g}}{\pi} \tag{8}$$

Following the De Boer's approach [5], $P_{s,g}$ is 1 atm (101 $kN \cdot m^{-2}$) and π can be taken as 0.338 $mN \cdot m^{-1}$, and hence:

$$\Delta G_A^0 = -RT \ln 2.99 \cdot 10^8 V_s \tag{9}$$

The standard enthalpy change ΔH_A^0 for the same process to which ΔG_A^0 refers, can be obtained as a consequence of the temperature dependence of V_s [4] obtained from the Gibbs–Helmholtz equation.

$$\ln V_s = -\frac{\Delta H_A^0}{RT} + C \tag{10}$$

3. POROUS CARBON MATERIALS

3.1. Specific retention volumes

The study of porous carbon materials using IGC is frequently carried out by adsorption of hydrocarbons at the zero surface coverage. This is doubly useful because it gives information on the textural characteristics of the carbon materials and also the adsorption capacity of these molecules is obtained. It should be pointed out that this adsorption capacity is obtained under dynamic conditions and frequently at relatively high temperatures, i.e. at the experimental conditions very close to the real situations at which the carbon materials are used (for instance to eliminate atmospheric pollutants)[6].

The reported results for the adsorption of linear hydrocarbons on activated carbons indicate a general relationship between the amount adsorbed, measured by the specific retention volumes, V_s, and a molecular parameter of the adsorbate related with its molecular weight (boiling point, polarizability or number of carbon atoms) [7–12]. In the case of linear polar molecules, V_s is related to the orientation polarization [13].

However, when hydrocarbons with different shape are adsorbed on activated carbons the values of V_s are not related to a property depending on the molecular weight [14]. This occurs with the adsorption of n–hexane (linear), benzene and cyclohexane (cyclic), and 2,2 dimethyl butane (2,2 DMB, branched) on activated carbons obtained from olive stones (Table 1). In order to explain these results we must consider the relationship between the molecular dimension of the adsorbates and the shape and size of the pores.

Constrictions at the entrance of pores are known to exist in activated carbons [15,16] in such a way that, depending on the pore size, these materials might exhibit a molecular sieve effect. This molecular sieve behaviour is apparent in the former carbons from the data in Table 2 which compiles the V_s/V_s' ratios (i.e. separation ratios) for these hydrocarbons. It is necessary to point out that carbons B and C were obtained by mild activation of sample A. Therefore, the former data suggest that carbon A has a constricted pore network which only permits adsorption of the smallest molecules (n–hexane and benzene)

Table 1
Surface areas and specific net retention volumes of hydrocarbons on activated carbons[a]

Sample	Carbon A		Carbon B		Carbon C	
Surface area(m^2/g)	522		613		746	
	V_s (cm^3/m^2)		V_s (cm^3/m^2)		V_s (cm^3/m^2)	
Temperature (K)	533	593	533	593	533	593
n-Hexane	0.23	0.03	12.59	2.74	6.81	1.34
Benzene	0.49	0.11	7.82	2.09	4.07	1.10
Cyclohexane	0.01	–	1.03	0.37	2.50	0.76
2,2 DMB	–	–	0.24	0.09	1.50	0.55

[a]Reprinted from: F. J. López-Garzón et al. [1]

Table 2
Separation ratios V_s/V_s' at 533 K for different hydrocarbons on activated carbons[a]

Sample	Carbon A	Carbon B	Carbon C
Benzene/Cyclohexane	49.0	7.6	1.6
n-Hexane/2,2 DMB	52.5	4.5	–
Benzene/2,2 DMB	32.7	2.7	–

[a] Reprinted from: F. J. López Garzón et al. [14]

and that the activation process progressively opens the micropores allowing the adsorption of the bigger adsorbates.

On the other hand, the data in Table 1 do not suggest any relationship between the total surface area of the adsorbent and the specific retention volume. To confirm this behaviour, two series of activated carbons (Table 3) obtained from almond shells (C-series) and olive stones (H-series) submitted to activation with CO_2 at different treatment periods (the number,hours, appended to C or H) were obtained [9] resulting in the samples with surface areas ranging from 840 to 1350 m^2/g.

Table 3
Surface areas of activated carbons obtained from almond shells (C-series) and olive stones (H-series) measured by CO_2 adsorption at 298 K[a]

Sample	Surface area (m^2/g)	Sample	Surface area (m^2/g)
C-2	840	H-2	1000
C-13	1080	H-13	1127
C-24	1284	H-24	1313
C-30	1308	H-30	1350

[a]Reprinted from: M. Domingo-Garcia et al. [9]

The specific retention volumes of these carbons for the adsorption of several organic molecules with different shapes and sizes are collected in Table 4.

Table 4
Specific retention volumes at 533 K[a]

Adsorbate	V_s (cm^3/g)							
	C-2	C-13	C-24	C-30	H-2	H-13	H-24	H-30
Cyclohexane	1.26	4.59	4.88	7.20	0.12	5.47	6.39	4.77
Benzene	3.88	9.04	7.08	8.73	4.07	8.80	7.24	5.73
2,2 DMB	0.43	0.48	5.71	6.54	0.04	2.76	5.52	3.91
n-Hexane	3.10	16.83	17.69	13.29	3.50	16.43	13.94	10.51
n-Pentane	2.25	1.41	2.40	2.30	0.54	2.98	2.47	2.03
n-Butane	0.35	0.25	0.54	0.56	0.17	0.72	0.49	0.40

[a]Reprinted from: M. Domingo-Garcia et al. [9]

Although differences in the adsorption capacities are apparent, no correlation between them and the surface areas of the carbons can be established. We can therefore conclude that the extent of the adsorption at the zero surface coverage should be more directly related to the adsorbate and pore size and shape than to the total surface area (or volume of pores) of the adsorbent. In connection with this, the adsorption of CO_2 on activated carbons from diluted ambient environments, measured in a conventional gravimetric system, has recently been shown to be more closely related with micropore size distribution rather than with the surface area or volume of micropores [17].

In addition, molecules with the same shape (linear hydrocarbons) show a direct relationship between V_s and its molecular characteristics (polarizability, molecular weight or boiling point) since, provided that they have the same minimum dimension, they have the same accesibility to the pores. In the case of differently shaped molecules, the differences in V_s suggest constrictions at the entrance of the pores that impede access of the largest molecules.

The existence of this kind of constrictions can be considered as disadvantage for the adsorption of several molecules, but in several circumstances it can be an advantage because the adsorbent can behave as a molecular sieve for molecules with similar size and shape [18,19]. In fact, the production of carbon materials with molecular sieve properties is in many cases a goal which can be achieved using different starting materials [15,20-27]. Among these, organic copolymers such as Saran (copolymer of vinylidene chloride and vinyl chloride) can be used to prepare carbon materials which have the advantage comparable to that obtained from the other row materials, of having a narrow micropore distribution.

Several activated carbons prepared by carbonization in N_2 at different temperatures (from 700 to 1300°C) have been used in a study on the adsorption of hydrocarbons by IGC [28]. For linear hydrocarbons the expected relationship between V_s and the number of carbon atoms is obtained.

However, V_s is affected by the size and shape of the adsorbates in such a way that the retention volume of 2,2 DMB in all the samples is negligible (very close to the gas hold-up time) which means that the limiting aperture size of the pores is 0.62 nm. Moreover, V_s for benzene and cyclohexane (Figure 1) being very similar are such that the separation ratio is close to 1 for the sample with a low degree of activation (700°C) and it increases slowly

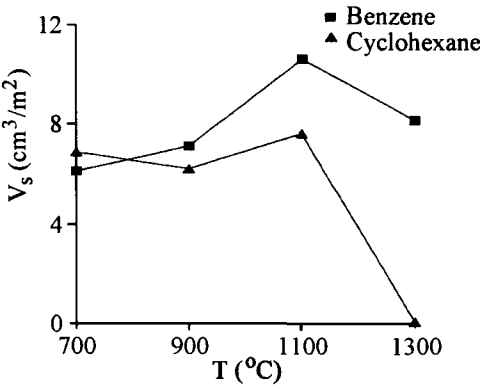

Figure 1. Specific retention volumes vs. the temperature of carbonization of Saran.

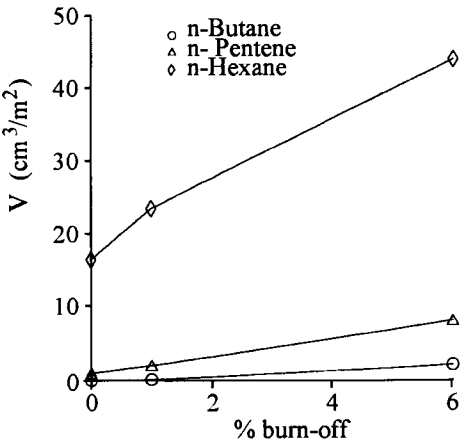

Figure 2. Variation of specific retention volumes with burn-off on S1300.

as the activation temperature increases, but at the highest treatment temperature this separation jumps dramatically up to 210. This is due to a shrinkage of the carbonaceous structure produced as a consequence of the treatment at 1300°C leading effectively to a molecular sieve carbon having a negligible uptake of cyclohexane and an important uptake of benzene.

This hypothesis is supported by additional experimental data. Therefore, when sample S1300 (obtained at 1300°C) is mildly gasified up to 1% burn-off the benzene/cyclohexane ratio clearly decreases (142.6). Moreover, when the gasification is increased up to a medium burn- off (6%) the molecular sieve effect disappears (benzene/cyclohexane ratio, 0.93), and V_s for 2,2 DMB is far from the gas hold-up time and can be measured (0.75 cm^3/m^2). This means that this treatment produced carbon removal which enlarged the pore constrictions. This fact is consistent with V_s values of linear hydrocarbons rising with increasing burn-off (Fig. 2).

In line with the former results a good way to obtain carbon materials with molecular sieve behaviour could be to introduce oxygen complexes at the entrance of the pores [28, 29]. For this purpose two of the former activated carbons (S900 and S1100, obtained at 900 and 1100°C respectively) were treated with HNO_3.

The behaviour of these samples measured by IGC shows a reduction of the adsorption capacity for both linear and cyclic hydrocarbons (Table 5). Moreover, V_s for the hydrocarbon 2,2 DMB on the oxidized carbons is quite close to the gas hold-up time, similar to that on the original samples, and the separation ratio for the couple benzene/cyclohexane is similar in both cases. These results show that the oxygen surface complexes fixed on the surface produce constrictions at the entrance of the pores, but do not result in the production of carbon materials with improved molecular sieve properties. One reason for this could be that the size of the oxygen complexes is not large enough. Therefore, if the size of the chemical complexes is increased the molecular sieve character for the couple benzene/cyclohexane would be expected to be developed. For this purpose, the S900 carbon was treated to introduce sulphur complexes on the surface [30]. Also a commercial acti-

Table 5
Comparison of V_s at 498 K, between the original (S900 and S1100) and the samples treated with HNO_3 (S900-ox and S1100-ox)[a]

Adsorbate	V_s(S900)/V_s(S900-ox)	V_s(1100)/V_s(1100-ox)
n-Butane	3.06	2.13
n-Pentane	4.56	3.06
n-Hexane	6.79	3.86
n-Heptane	10.60	4.75
Benzene	3.62	2.07
Cyclohexane	4.52	2.06

[a]Reprinted from: I. Fernández-Morales et al. [28]

vated carbon, A, with a wide distribution of micropores was treated to introduce sulphur surface complexes. Owing to higher thermal stability of carbon-sulphur surface complexes compared to those of carbon-oxygen [31,32] and the larger size of sulphur atoms these groups might be expected to reduce the aperture size of the pores more effectively. Two different treatments were used for S900. The first with CS_2 rendering samples S900-1 and S900-2, and the second one with sulphur rendering S900-3. The separation ratios obtained from IGC measurements for n-hexane, benzene and cyclohexane are shown in Table 6.

Table 6
Sulphur content and separation ratios at 498 K[a]

Sample	%S	V_s/V'_s (n-hexane/benzene)	V_s/V'_s (benzene/cyclohexane)	V_s/V'_s (n-hexane/cyclohexane)
S900	0	2.6	1.1	3.0
S900-1	3.14	2.6	20.7	54.0
S900-2	4.20	2.4	660.0	1575.0
S900-3	8.12	2.4	4.2	10.0
A	2.23	1.6	1.8	2.8
A-1	7.21	1.6	1.8	2.8

[a]Reprinted from: C. Moreno-Castilla et al. [30]

The data in Table 6 indicate that the fixation of sulphur does not cause molecular sieving of the n-hexane/benzene couple as can be clearly seen from the fairly constant separation ratio (2.6 for S900 series and 1.6 for A series). However, the use of CS_2 on S900 series produces separation ratios for the benzene/cyclohexane couple which increases with the sulphur content (up to S900-2). For the n-hexane/cyclohexane couple the separation ratio has the same trend as shown by benzene/cyclohexane, although with higher values since the difference between the mean sizes of n- hexane and cyclohexane is greater than between benzene and cyclohexane. Sample S900-3 (obtained using sulphur instead of CS_2) has smaller separation ratios showing that the treatment with CS_2 produces a more effective molecular sieve.

The adsorption of polar molecules at the zero surface coverage measured by IGC on porous carbon materials is reported [13] to be related with the dipolar moment of the molecule, although the lack of a relationship between both parameters has also been reported [33]. Similarly to the non-polar molecules, the extent of the adsorption at the zero surface coverage of a polar molecule such as methyl iodide, CH_3I, on activated carbons does not depend on the surface area of the adsorbents [34]. The introduction of oxygen surface complexes diminishes the extent of the adsorption because they hinder the access to the pores. When the oxygen surface complexes are eliminated the adsorption is clearly enhanced [35,36]. These results indicate that although methyl iodide has a dipolar moment and the activated carbons have surface chemical groups [37–39], the interaction with these chemical groups is negligible, and the adsorption is governed mainly by the molecular size and the dimension of the pores. Nevertheless if potassium iodide KI is added to the activated carbons there is an increase in the adsorbed amount (Table 7) [35,36], which supports the suggestion that adsorption of methyl iodide occurs by a mixed mechanism in pores and in KI [40]. In Table 7, C and H samples are the activated carbons already mentioned, Merck is a commercial activated carbon and carbons of P series are obtained [36] by carbonization of polyfurfuryl alcohol.

Table 7
Influence of KI on the surface area and specific net retention volume of CH_3I on activated carbons

Sample	Surface area[b] (m^2/g)		V_s (cm^3/m^2) (493 K)	
	Original	With KI	Original	With KI
C-13	1080	844	0.77	0.86
C-30	1308	1127	0.71	0.80
H-13	1127	1167	0.70	0.80
H-24	1313	1194	0.57	0.74
Merck	802	766	0.06	0.26
P1	408	405	0.35[c]	0.60[c]
P3	344	312	0.43[c]	0.81[c]
P4	468	474	0.30[c]	0.54[c]

[a]Reprinted from: M. Domingo-Garcia et al. [35,36]
[b]Measured by adsorption of CO_2 at 273 K.
[c]At 473 K.

3.2. Standard enthalpy of adsorption

For the determination of the standard enthalpy of adsorption at the zero surface coverage a linear dependence between ln V_s and $1/T$ is required (see Equation 10). In Fig. 3 typical plots showing this relationship for the activated carbon C-13 are shown. The standard enthalpy of adsorption is obtained from the slope of the plots. Fig. 4 shows the evolution of the standard enthalpy of adsorption of several hydrocarbons on the activated carbons obtained from the copolymer Saran.

From now on discussion of the standard thermodynamic parameters will be based on their absolute values. It is interesting to note the significant increase in the standard

enthalpy of adsorption of the linear hydrocarbons for sample S1300 (Figure 4) which means that the adsorption is produced onto pores reduced in size, which have been produced as a consequence of the temperature treatment.

Moreover, the standard enthalpy of adsorption for these hydrocarbons clearly decreases after gasification of the carbon (Figure 5). This is consistent with the idea stated before, that gasification of sample S1300 produced progressive opening of the pores to a small extent.

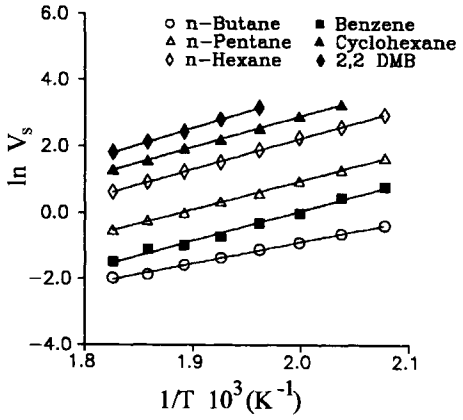

Figure 3. Plots of ln V_s vs. 1/T to obtain standard enthalpy of adsorption.

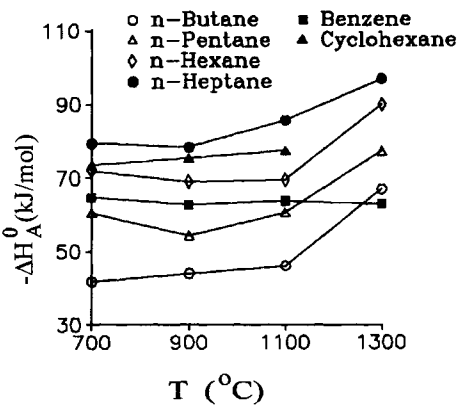

Figure 4. $-\Delta H_A^0$ of adsorption of hydrocarbons vs. the temperature of treatment of Saran.

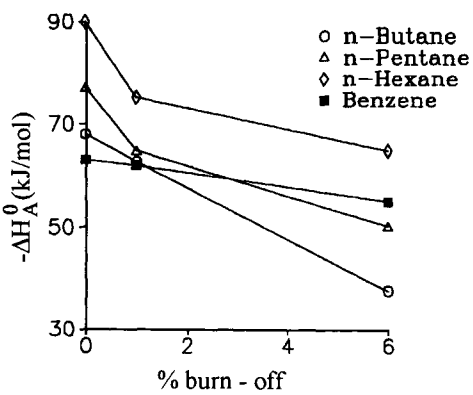

Figure 5. $-\Delta H_A^0$ vs. burn-off on S1300.

The effect on adsorption of the fixation of oxygen surface complexes is shown in Table 8. In addition to the decrease in V_s stated before, the adsorption is less energetic after the treatment [28-30] because partial blocking of the pores hinders the access of pores with similar dimension to the molecular size of the adsorbates. Moreover, it is interesting to point out that benzene is adsorbed more strongly on the original than on the oxidized

Table 8
$-\Delta H_A^0$ (kJ/mol) for original and oxidized Saran activated carbons[a]

Adsorbate	S900	S900-ox	S1100	S1100-ox
n-Butane	47.7	31.8	49.0	33.9
n-Pentane	53.6	47.7	59.8	47.7
n-Hexane	69.0	54.8	70.3	56.5
n-Heptane	76.6	64.4	83.7	66.9
Benzene	61.5	58.2	63.2	58.6
Cyclohexane	73.6	47.3	76.1	54.8

[a]Reprinted from: I. Fernández-Morales et al. [28]

samples, which means that no specific interaction is produced between benzene and the oxygen surface groups, or that if specific interaction is produced this is less energetic than the interaction between the molecule and the pore walls. This conclusion, although slightly surprising, is supported by a significant amount of data [9,14,28,30,41,42] like those in Table 9, in which the heat of liquefaction of (ΔH_L) the adsorbates is also included.

Values of ΔH_A^0 higher than ΔH_L are usually attributed [43–46] to adsorbate–adsorbent specific interactions, but the only molecule in Table 9 capable of these interactions with the surface chemical groups of the activated carbons is benzene, and in this case higher values of ΔH_A^0 for this molecule than for the other hydrocarbons would be expected. This is not the case in Table 9, where n-hexane has higher ΔH_A^0 than benzene in all cases. Moreover, the standard enthalpy of adsorption of all the adsorbates in Table 9 is much higher than the liquefaction heat of each molecule. All these data suggest that pores size has an influence on the enthalpy of adsorption. It has been suggested [47–50] that the high enthalpies of adsorption at the zero surface coverage rise rapidly when the molecule size becomes comparable to the pore size, i.e. the high values of ΔH_A^0 are produced as a consequence of a good fit of the adsorbates into the pores, in such a way that the higher the difference between the standard enthalpy of adsorption and the heat of liquefaction the closer the molecular and pore sizes are. From this point of view, [49] surface curvature effect (SCE) on the adsorption at zero surface coverage is possible.

In many cases, SCE occurs to a similar extent or even greater than the specific interac-

Table 9
$-\Delta H_A^0$ (kJ/mol) for the adsorption of hydrocarbons on activated carbons of C-series[a]

Adsorbate	C-2	C-13	C-24	C-30	ΔH_L
n-Butane	51.4	53.9	53.0	49.6	24.3
n-Pentane	71.8	71.8	69.9	68.5	27.6
n-Hexane	80.0	83.3	88.3	83.2	21.7
Benzene	66.0	77.4	76.8	72.4	34.1
Cyclohexane	66.0	76.7	73.6	75.3	32.8
2,2 DMB	58.4	75.0	71.0	71.6	30.4

[a]Reprinted from: M. Domingo-Garcia et al. [9]

tion. This occurs with the adsorption of methyl iodide on several carbon materials doped with KI. The interaction between methyl iodide and these carbons would be expected to be more energetic, in terms of the standard enthalpy of adsorption, than the interaction between the same molecule and the original activated carbons. This is due to the fact that in the former, the adsorption is controlled by specific and non-specific interactions [2], while in the latter the interaction is only non-specific. Nevertheless, the data collected in Table 10 show a stronger interaction on the original than on the activated carbons with KI, and in all the cases the standard enthalpy of adsorption is higher than the liquefaction heat of CH_3I (-27.6 kJ/mol).

Table 10
$-\Delta H_A^0$ of CH_3I on original activated carbons and on the same samples doped with KI[a]

Sample	Original	With KI	Sample	Original	With KI
P1	48.8	30.3	C-13	57.3	48.7
P2	39.5	26.2	C-30	53.3	48.3
P3	52.7	43.8	H-13	53.0	51.0
P4	64.9	49.6	H-24	49.8	47.0

[a]Reprinted from: M. Domingo-Garcia et al. [35]

These results clearly indicate the effect of SCE on the adsorption at the zero surface coverage, and also the inadvisability of using the traditional classification of adsorption on the basis of the type of interaction between the adsorbate and the adsorbent (specific or non-specific) to explain the results at this low coverage.

The standard adsorption enthalpy can also be used to gain information on changes in the surface characteristics of the carbon materials. For this purpose, molecular probes with different sizes and shapes can be used: n-hexane, benzene, cyclohexane and 2,2 DMB. All these molecules have six carbon atoms and are linear (n-hexane), cyclic (benzene and cyclohexane) and branched (2,2 DMB), and their mean molecular sizes range from 0.405nm (n-hexane) to 0.62nm (2,2 DMB).

The standard adsorption enthalpies of these molecules on the activated carbons of the C and H series are plotted in Figs. 6 and 7 against the mean molecular dimension of the adsorbate. In Fig. 6 an almost monotonic decrease of ΔH_A^0 is observed with the increase in the mean molecular dimension and a perceptible increase when the activation proceeds from C-2 to C-13 and only slight differences are observed between the remaining carbons. The explanation for this is that the activation of the raw material (almond shells) produces a polymodal distribution of micropores which are progressively opened during the subsequent activation. The trends of the plots in Fig. 7 are similar to those in Fig. 6 except for H-2, in which ΔH_A^0 decreases sharply when the molecular size increases from 0.52nm (benzene) to 0.62nm (2,2 DMB). This means that the least activated carbon of H-series has an important population of micropores with dimensions close to that of benzene or smaller, but the number of pores of dimension equal or higher than 0.60nm seems to be negligible. After treatment, these pores are opened and the final distribution of pores is polymodal in the dimension range under consideration.

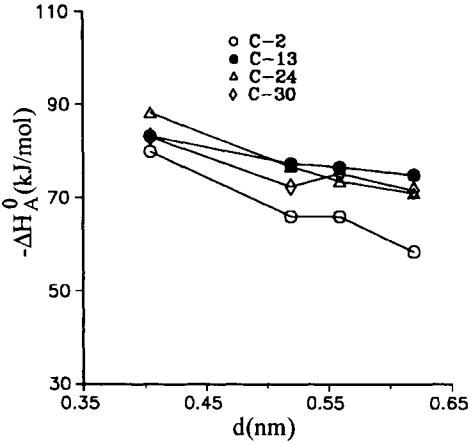

Figure 6. $-\Delta H_A^0$ vs. mean molecular dimension of the adsorbates on the activated carbons of the C-series.

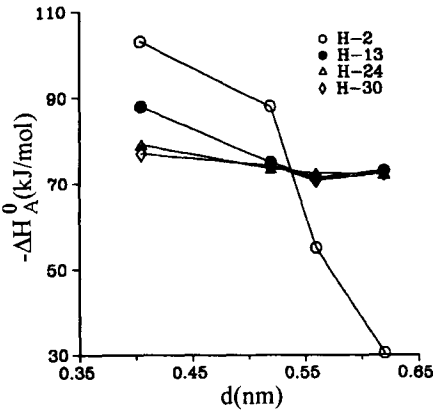

Figure 7. $-\Delta H_A^0$ vs. mean molecular dimension of the adsorbates on the activated carbons of the H-series.

3.3. The dispersive component of the surface free energy

In general, the physical interaction between an adsorbent and an adsorbate consists of two energetic factors: one produced by London dispersion forces (non-specific interaction) and the other produced by dipole-dipole interaction, dipole-induced dipole interaction, or hydrogen bonding (specific interactions). Specific interactions are generally accepted to be more energetic although, as discussed previously, it is inadvisable to use this classification in adsorption at the zero surface coverage. Nevertheless, the adsorption of a non-polar molecule on the surface of porous carbon materials is only controlled by dispersion forces, and therefore the standard free energy of adsorption has to be related to the dispersion forces between adsorbate and adsorbent. Following this argument, Dorris and Gray, in almost classical paper [51] proposed a method for the determination of the dispersion forces in terms of the dispersive component of the surface free energy γ_s^d. This is based on the equation proposed by Fowkes [52] relating the work of adhesion, W_A, between a non-polar adsorbate and the surface of an adsorbent:

$$W_A = \left[\gamma_s^d \gamma_L\right]^{1/2} \tag{11}$$

where γ_s^d is the dispersive (or London) component of the surface free energy and $\gamma_L = \gamma_L^d$ is the surface tension of the non-polar adsorbate. When the adsorbates are n-alkanes, Dorris and Gray assume that W_A is proportional to the incremental adsorption free energy per methylene group and they propose the following equation to estimate γ_s^d:

$$\gamma_s^d = \frac{1}{\gamma_{CH_2}} \left[\frac{-\Delta G_{CH_2}}{2N_A\, a_{CH_2}}\right]^2 \tag{12}$$

where γ_{CH_2} is the surface free energy of a polyethylene chain, ΔG_{CH_2} is the adsorption free energy of one methylene group, N_A is the Avogadro's number and a_{CH_2} is the area of the methylene group (0.06 nm^2). In order to use this equation it is necessary to determine

ΔG_A^0 of linear hydrocarbons by using Eq.(9). Gray et al. [51,53,54] reported values of γ_s^d obtained for cellulose materials, which are generally in good agreement with those expected for this type of materials. Chappell and Williams [55] also used Eq.(12) to estimate the cleanliness of organic fiber surfaces. These authors reported the Gray's method to be useful for determining the level of contamination of the surfaces. Nevertheless, they also concluded the method to yield values of γ_s^d higher than those expected for heterogeneous surfaces due to the adsorption at the zero surface coverage in most energetic adsorption sites.

Similarly, the use of this equation for different carbon materials renders unexpectedly high γ_s^d values compared with those obtained by other experimental techniques [9,41,46]. The reason for this, is reported to be [57], the effect of the SCE on the adsorption. This is expected because γ_s^d is a fuction of ΔG_A^0 in Eq.(12) and ΔG_A^0 is also related to ΔH_A^0. The SCE which produces very high values of ΔH_A^0 was also discussed. Therefore the ΔG_A^0 values are very high and consequently those of γ_s^d are larger than expected.

The effect of the SCE on the adsorbate–adsorbent interaction should be taken into account in order to improve γ_s^d determination. For this purpose it is necessary to replace the free energy of a methylene group adsorbed into a pore, ΔG_{CH_2}, by the free energy of the methylene group adsorbed in a flat surface $[\Delta G_{CH_2}(0)]$ in Eq.(12). Then this equation is written:

$$\gamma_s^d(0) = \frac{1}{\gamma_{CH_2}} \left[\frac{-\Delta G_{CH_2}(0)}{2N_A \, a_{CH_2}} \right]^2 \tag{13}$$

where $\gamma_s^d(0)$ is the dispersive component of the free energy of a flat surface. At this point the aim is to find a relationship between the experimental data of ΔG_{CH_2}, and the theoretical free energy per methylene group on a flat surface. For this purpose, the interaction model of a molecule with a curved surface proposed by Derouanne, Andre and Lucas [49] can be useful. According this approach the adsorbed molecule is the closest to the pore wall in such a way that the best fit between its size and the pore will be achieved. With this assumption, the general relationship between the van der Waals adsorption energies on a pore, W(d/a), and on a flat surface W(0) is given by:

$$\frac{W\left(\frac{d}{a}\right)}{W(0)} = \left(1 - \frac{d}{2a}\right)^{-3} \tag{14}$$

where d is the adsorption distance (equal to the radius of the adsorbed molecule) and a is the radius of the pore. Then if Eq.(14) is accepted, the relationship between the free energies per methylene group on a pore and on a flat surface is:

$$\Delta G_{CH_2}(0) = \Delta G_{CH_2} \left(1 - \frac{d}{2a}\right)^3 \tag{15}$$

Now a more general equation for γ_s^d is written:

$$\gamma_s^d(0) = \frac{1}{\gamma_{CH_2}} \left[\frac{\Delta G_{CH_2} \left(1 - \frac{d}{2a}\right)^3}{2N_A \, a_{CH_2}} \right]^2 \tag{16}$$

It is important to point out that for a flat surface (a = ∞, d = constant) Eq.(16) reduces to Eq.(12), the original Gray's equation. Moreover, for a fixed molecule size, d, γ_s^d increases as the pore size, a, decreases, and reaches a maximum when the radius of the adsorbate becomes equal to the pore radius (hypothetical case). Equation (16) is thus a more general equation than Eq.(12), and permits the dispersion component of the surface free energy for porous and non- porous materials to be determined.

To use Eq.(16) it is necessary to know the parameters a and d. Although the former is usually known, the latter is more difficult to determine, although the approximations [58,59] which relate the radius of the pore a and the size of the adsorbate d can be used.

Another possible approach is to obtain the d/2a ratio by applying equation (14) to the standard free energy of adsorption and to the free energy of liquefaction of the n-alkanes. In this case, the free energy of adsorption on a flat surface would be taken to be very similar to the free energy of liquefaction (or condensation). The latter can be calculated from the general relationship between ΔG_L, ΔH_L and $T\Delta S_L$. For this ΔS_L can be easily approximated from the change in entropy of an ideal gas passing from a three-dimensional to a two-dimensional state [5].

The data in Table 11 show the unrealistic values of γ_s^d which are normally determined on porous carbon materials by applying Eq.(12) which become more realistic and quite close to other values reported for coals and graphite (av. 39.5 $mJ \cdot m^{-2}$, obtained [60] from the contact angle measurements) when Eq. (16) is used.

Table 11
Dispersive component of the surface free energy for porous carbon materials P1-P4[a]

Sample	γ_s^d $(mJ \cdot m^{-2}4)^b$	$\gamma_s^d(0)^c$	$\gamma_s^d(0)^f$
P1	560.5	47.4	37.9
P2	448.7	37.9	30.3
P3	405.4	34.3	27.4
P4	419.5	35.5	28.4

[a]Reprinted from: López-Garzón et al. [57]. [b]Using equation (12). [c]Using equation (16). [f]Using equation (14) to obtain d/2a.

The data in the last column are obtained using Eq. (14) to calculate d/2a value, which then is substituted in Eq. (16) to determine γ_s^d. These data are also quite close to those from the contact angle measurements [60], showing that Eq. (14) is useful to determine d/2a.

4. NON-POROUS CARBON MATERIALS

These materials mainly include graphites, carbon blacks and graphitized carbon blacks, and are frequently used as standards in adsorption at high and low surface coverage due to the lack of porosity and their homogeneous surfaces [61-64]. For these reasons it is easy to find a relationship, for the adsorption of non-polar molecules (n-alkanes), between the specific retention volumes and a molecular property of the adsorbate such as the polarizability or the molecular volume, and the amount adsorbed, V_s, which is nor-

mally related to the specific surface area of the adsorbents [65–67]. Furthermore, for polar molecules as n–alcohols, there is also a relationship between the specific retention volume and a molecular property of the adsorbate. However, the trend for non–polar molecules is not coincident with that for polar molecules (Figure 8), so that two different trends are obtained: one for non–polar molecules (related to molecular properties: polarizability, molecular area or volume, boiling point) and the other for the polar adsorbates (related to the dipole moment, μ). Nevertheless it is interesting to point out that when the dipole moment of the n–alcohols decreases, the plot of the polar molecules tends to join that of the non–polar molecules, i.e. as the influence of m decreases, the behaviour of the n–alcohols approaches that of the n–alkanes.

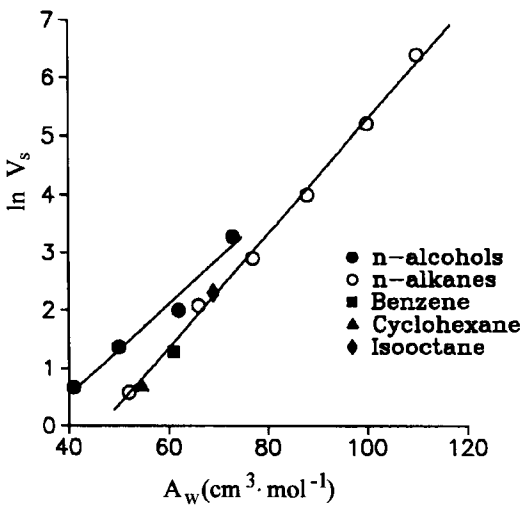

Figure 8. Variation of specific retention volumes for hydrocarbons and n–alcohols against the molecular area of the adsorbates.

Table 12
$-\Delta H_A^0$ (kJ/mol), for the adsorption on graphites and on a carbon black

Adsorbate	ΔH_L	Pyrolytic Graphite[a]	(V3G)[a]	Adsorbate	ΔH_L	Degussa Graphite[b]
n–Hexane	31.7	26.7	33.8	1–Propanol	43.4	29.7
n–Heptane	37.1	36.3	39.2	1–Butanol	45.7	33.1
n–Octane	42.9	42.5	44.2	1–Pentanol	52.1	35.1
n–Nonane	47.5	47.5	48.8	1–Hexanol	53.0	42.4

[a]Reprinted from: M. Domingo–Garcia et al. [65]
[b]Reprinted from: F. J. López–Garzón et al. [67]

As for the standard enthalpies of adsorption for alkanes, these are normally very close to those of liquefaction in the case of low surface area graphites, and for polar molecules

they are smaller than their liquefaction heats. Nevertheless, for carbon blacks (V3G) with the medium surface area (60–140 m^2/g) the standard enthalpies of adsorption for alkanes are higher than their liquefaction heats [58–61]. This indicates a low concentration of high energy sites on the graphite surface, whereas the average energy of the sites on the carbon black is higher.

These sites consist of irregularities on the surface such as cracks, pits or crystal defects on which the molecule interacts with more than one graphite layer. This latter assumption is supported by other experimental data collected in Table 13, which show the variation of the standard adsorption enthalpy with the degree of burn-off of a graphitized carbon black. It is apparent that as the gasification progresses the degree of surface heterogeneity increases and consequently the standard enthalpies of adsorption become higher and higher.

Table 13
Variation of $-\Delta H_A^0$ with burn-off on V3G[a]

Burn-off, %	n-Heptane	n-Octane	n-Nonane	n-Decane
0	39.4	44.2	48.0	
16.4	41.5	49.5	56.2	62.0
28.2	42.3	51.7	58.8	63.3
50.1	43.4	55.2	64.6	75.0
79.4	44.8	58.2	69.7	

[a]Reprinted from: F. J. López-Garzón et al. [66]

As regards the dispersive component of the surface free energy, if the adsorption at the zero surface coverage on these carbon materials were produced on the flat surface rather than onto the irregularities, Eq.(12) would be expected to render values of γ_s^d close to those obtained by direct determination from the contact angle measurements. Nevertheless, the data reported, obtained by adsorption of n-alkanes at the zero surface coverage, range for graphites between 78–80 $mJ \cdot m^{-2}$ [65–68] and 100 $mJ \cdot m^{-2}$, or even much higher than for carbon blacks [65,69,70]. Thus, irregularities on the surface of these carbon materials play an important role in the adsorption at the zero surface coverage in that the molecules are adsorbed mainly on these irregularities and consequently the values of γ_s^d obtained are higher than expected for a flat surface. It is noteworthy that the γ_s^d value obtained by applying Eq.(12) to the adsorption of n-alcohols on graphite [67] is 38 $mJ \cdot m^{-2}$ which is very close to those reported for graphite and coals [53]. Therefore it seems as if the adsorption of n-alcohols is produced by the interaction of the OH group with the chemical groups on the surface allowing for the interaction of the methylene groups of the chain with the flat surface of the adsorbent.

Finally, there are several approaches to determine the specific component of the surface free energy of carbon materials [71–73]. Among these, that proposed by Donnet et al [73] uses the standard adsorption free energy which is plotted against $(h\nu_L)^{1/2}\alpha \cdot 10^{-4}$, where h is the Planck constant, ν_L is the characteristic vibration frequency of the electron and α is the deformation polarizability. The method seems to provide reasonable results, although it does not take into account the effect of the surface irregularities.

5. SILICATES

One of the characteristics of these materials is that they have an important number of surface chemical groups (mainly silanol and siloxane groups) which can be modified by different treatments (eg. thermally, grafting, adsorption from solution) and poorly developed microporosity. Hence, the adsorption of molecules capable of specific interactions is mainly governed by the surface chemical groups, while that of the molecules which are adsorbed through non-specific interactions is mainly controlled by the porosity. This can be checked with the data in Table 14 [43]. These refer to the adsorption on an aluminosilicate, called Halloysite (H) thermally treated at temperatures ranging from 473 K (sample H-473) to 1273 K (sample H-1273). It is interesting to note that the specific retention volume is always much higher for benzene than for cyclohexane and n-hexane because bezene interacts with the surface chemical groups. Moreover, as the treatment temperature increases, V_s of benzene diminishes because the surface chemical groups decrease. The difference between n-hexane and cyclohexane is attributed to the small size of the former which has better access to the sample microporosity. It is therefore noteworthy that for the sample H-1273 for which the volume of pores smaller than 3.7 nm in radius is almost negligible, the specific retention volumes V_s for cyclohexane and n-hexane are almost coincident.

Table 14
Variation of textural characteristics of a halloisite with the heat treatment. Adsorption at the zero surface coverage of hydrocarbons[a]

Sample	S	V_1^b	$V_s(cm^3/m^2)$ (353K)		
	(m^2/g)	(cm^3/g)	Benzene	Cyclohexane	n-Hexane
H-473	93	0.106	17.04	3.56	8.41
H-673	96	0.089	8.94	0.81	1.24
H-873	81	0.076	3.22	0.40	0.60
H-1073	70	0.039	3.11	0.41	0.66
H-1273	29	0.004	0.80	0.15	0.18

[a]Reprinted from: F. Carrasco-Marín et al. [43]
[b]V_1 is the volume of pores with a radius $\leq$ 3.7nm

The standard enthalpies of adsorption (Table 15) of these molecules on the thermally treated aluminosilicate support the former explanation. So the adsorption of benzene on H-473 is the most exothermic due to the specific interaction with the silanol groups. When the thermal treatment progresses, the process becomes less and less exothermic due to: i) the partial dehydroxylation of the surface (H-673), ii) the change in the chemical surface groups (siloxane groups on H-873 and H-1073) and iii) the destruction of the chemical surface groups (H-1273). As a consequence of the latter process the standard enthalpy of adsorption of benzene on H-1273 is very similar to the heat of liquefaction.

For n-hexane and cyclohexane, similar trends in ΔH_A^0 are found as for benzene, due to the continuous destruction of the pores smaller than 3.7 nm in diameter so that when this pore volume is negligible, the standard enthalpy of adsorption is lower than the heat of liquefaction.

Table 15
Standard enthalpy of adsorption on thermally treated aluminosilicates[a]

Sample	$-\Delta H_A^0$ (kJ/mol)		
	Benzene	Cyclohexane	n-Hexane
H-473	68.6	45.4	59.9
H-673	55.8	41.0	46.7
H-873	44.1	33.3	40.7
H-1073	43.5	33.0	38.1
H-1273	32.9	24.0	26.0
$-\Delta H_L$	34.1	32.8	31.9

[a]Reprinted from: F. Carrasco-Marín et al. [43]

Because of the important role played by the surface chemical groups in several fields such as composite material, adhesion, catalysis, stationary phases for analysis, etc., attempts have been made to estimate and modify them [74–85]. Dorris and Gray [74] studied the adsorption of hydrocarbons on the silica-supported water surfaces and the change of the non-specific component of the surface free energy with water loading. Also, several estimations of the variation of surface free energy with a number of treatments, such as grinding or grafting with several organic molecules have been reported.

As expected, grinding produces an increase in γ_s^d as a consequenece of the increased irregularities on the surface. In addition grafting processes result in important changes in the dispersive and specific components of the surface free energy, and in many cases the surface coverage is the most important parameter related to these components. Also, the surface of silicas has been modified with several ions and the changes in the surface chemical characteristics have been established by the adsorption of organic molecules at the zero surface coverage [82,85].

ACKNOWLEDGMENT

The authors would like to thank the CICYT for their financial support under project AMB92-1032.

REFERENCES

1. S. A. Greene and A. Pust, J. Phys. Chem., 62 (1958) 55.
2. A. V. Kiselev and Y. I. Yashin, Gas-Adsorption Chromatography, Plenum Press, New York, 1969.
3. J. R. Conder and C. L. Young, Physicochemical Measurements by Gas Chromatography, John Willey & Sons, Chichester, 1979.
4. E. F. Meyer, J. Chem. Educ., 57 (1980) 120.
5. J. H. De Boer, The Dynamical Character of Adsorption, Oxford University Press, London, 1953.

6. H. Jüntgen and H. Kühl, in: P. A. Thrower (ed.), Chemistry and Physics of Carbon, vol. 22, New York, 1989, p. 145.
7. M. M. Selim and Th. A. El-Nabarawy, Carbon, 18 (1980) 287.
8. A. M. Youssef, Abstracts of 15th Carbon Conference, (1981), Philadelphia, p. 234.
9. M. Domingo-Garcia, I. Fernández-Morales, F. J. López-Garzón, C. Moreno-Castilla and M. J. Prados-Ramirez, J. Colloid Interface Sci., 136 (1990) 160.
10. J. Jagiełło, T. J. Bandosz and J. Schwarz, J. Colloid Interface Sci., 151 (1992) 433.
11. R-Y. Qin and J-B. Donnet, Carbon, 32 (1994) 165.
12. J. Jagiełło, T. J. Bandosz and J. Schwarz, Carbon, 32 (1994) 687.
13. M. M. Selim, Th. A. El-Nabarawy, T. H. Ghazy and T. Farid, Carbon 19 (1981) 161.
14. F. J. López-Garzón, C. Moreno-Castilla, A. Guerrero-Ruiz, F. Rodriguez-Reinoso and J. de D. López-Gonzalez, Adsorp. Sci. Technol., I (1984) 103.
15. M. Domingo-Garcia, I. Fernández-Morales, F. J. López-Garzón and C. Moreno-Castilla, Langmuir, 7 (1991) 339.
16. B. McEnaney, Carbon, 26 (1988) 267.
17. M. A. Salas-Peregrín, F. Carrasco-Marín, F. J. López-Garzón and C. Moreno-Castilla, Energy & Fuels, 8 (1994) 239.
18. S. K. Verma, Carbon, 29 (1991) 793.
19. A. L. LaCava, V. A. Ross and D. Wickens, Gas Sep. and Pur., 3 (1989) 180.
20. S. K. Verma and P. L. Walker, Jr., Carbon, 281 (1990) 175.
21. S. K. Verma and P. L. Walker, Jr., Carbon, 30 (1992) 829.
22. A. L. Cabrera, J. E. Zehner, C. G. Coe, T. R. Gaffney, T. S. Farris and J. N. Armor, Carbon, 31 (1993) 969.
23. S. N. Vyas and A. A. Lizzio, Abstracts of Carbon'94, Granada (Spain), 1994, p. 588.
24. J. L. Schmitt and P. L. Walker, Jr., Carbon, 9 (1971) 791.
25. J. L. Schmitt and P. L. Walker, Jr., Carbon, 10 (1972) 87.
26. C. Moreno-Castilla, O. P. Mahajan, P. L. Walker, Jr., H-J. Jung and M. A. Vannice, Carbon, 18 (1980) 271.
27. S. Yamada, Proc. of the 5 International Carbon Conference, Essen (Germany), 1992, p. 869.
28. I. Fernández-Morales, A. Guerrero-Ruiz, F. J. López-Garzón, I. Rodríguez-Ramos and C. Moreno-Castilla, Carbon, 22 (1984) 301.
29. A. A. Lizzio, S. N. Vyas and M. Rostane-Abadi, Abstracts of Carbon'94, Granada (Spain), 1994, p. 530.
30. C. Moreno-Castilla, I. Fernández-Morales, M. Domingo-Garcia and F. J. López-Garzón, Chromatographia, 20 (1985) 709.
31. B. R. Puri, in: P. L. Walker, Jr. (ed.), Chemistry and Physics of Carbon, vol. 6, Marcel Dekker, New York, 1970, p. 191.
32. C. H. Chang, Carbon, 19 (1981) 175.
33. S. K. Milonjić, Lj. L. Djurič, M. J. Polovina, Chromatographia, 29 (1990) 228.
34. F. Carrasco-Marín, M. Domingo-Garcia, I. Fernández-Morales and F. J. López-Garzón, Carbon, 29 (1991) 629.
35. M. Domingo-Garcia, I. Fernández-Morales, F. J. López-Garzón and M. Pyda, Chromatographia, 34 (1992) 568.

36. M. Domingo-Garcia, I. Fernández-Morales and F. J. López-Garzón, Carbon, 31 (1993) 75.
37. J. Rivera-Utrilla and M. A. Ferro-Garcia, Adsorp. Sci. Technol., 3 (1986) 293.
38. C. Moreno-Castilla, M. A. Ferro-Garcia, J. Rivera-Utrilla and J. P. Joly, Energy & Fuels, 8 (1994) 1233.
39. C. A. Leon y Leon and L. R. Radovic, in: P. A. Thrower (ed.), Chemistry and Physics of Carbon, vol. 24, Marcel Dekker, New York, 1994, p. 213.
40. V. R. Deitz, in: P. A. Thrower (ed.), Chemistry and Physics of Carbon, vol. 23, Marcel Dekker, New York, 1991, p. 233.
41. J. Jagiełło, T. J. Bandosz and J. Schwarz, Carbon, 30 (1992) 63.
42. X. L. Cao, B. A. Colenutt and K. S. W. Sing, J. Chromatogr., 555 (1991) 183.
43. F. Carrasco-Marín, M. Domingo-Garcia, I. Fernández-Morales and F. J. López-Garzón, J. Colloid Interface Sci., 126 (1988) 552.
44. S. K. Milonjić and M. M. Kopečni, Chromatographia, 19 (1984) 342.
45. J. Schultz, L. Lavielle and C. Martin, J. Chim. Phys., 84 (1987) 231.
46. M. M. Kopečni, S. K. Milonjić and R. J. Laub, Anal. Chem., 52 (1980) 1032.
47. E. G. Derouanne, J. Catal., 100 (1986) 541.
48. E. G. Derouanne, A. A. Lucas and J-M. Andr, Chem. Phys. Lett., 137 (1987) 336.
49. E. G. Derouanne, J-M. Andr and A. A. Lucas, J. Catal., 110 (1988) 58.
50. R. V. Jasra and S. G. T. Bhat, J. Catal., 115 (1989) 605.
51. G. M. Dorris and D. G. Gray, J. Colloid Interface Sci., 77 (1980) 353.
52. F. M. Fowkes, J. Colloid Interface Sci., 28 (1968) 493.
53. S. Katz and D. G. Gray, J. Colloid Interface Sci., 82 (1981) 318.
54. G. M. Dorris and D. G. Gray, J. Chem. Soc., Faraday Trans. I, 77 (1981) 725.
55. P. J. C. Chapell and D. R. Williams, J. Colloid Interface Sci, 128 (1989) 450.
56. A. J. Vukov and D. G. Gray, Langmuir, 4 (1988) 743.
57. F. J. López-Garzón, M. Pyda and M. Domingo-Garcia, Langmuir, 9 (1993) 531.
58. D. J. Everett and J. C. Powl, J. Chem. Soc., Faraday Trans. I, 72 (1976) 619.
59. P. L. Walker, Jr., L. G. Austin and S. P. Nandi, in: P. L. Walker, Jr.(ed.), Chemistry and Physics of Carbon, vol. 2, New York, Marcel Dekker, 1966, p. 257.
60. R. J. Good, N. R. Srivatsa, M. Islam, H. T. L. Huang, C. J. van Oss, J. Adh. Sci. Technol., 4 (1990) 607.
61. D. Atkinson and G. Curthoys, J. Chem. Educ., 55 (1978) 56.
62. A. J. Groumadas and D. P. Poshkus, J. Chem. Soc., Farady Trans. 2, 78 (1982) 2013.
63. E. Papirer, S. Li, H. Balard and J. Jagiełło, Carbon, 29 (1991) 1135.
64. J-B. Donnet, R-Y. Qin and M-J. Wang, Carbon, 153 (1992) 572.
65. M. Domingo-Garcia, I. Fernández-Morales, F. J. López-Garzón and C. Moreno-Castilla, J. Chromatogr., 294 (1984) 41.
66. F. J. López-Garzón and M. Domingo-Garcia, Chromatographia, 21 (1986) 447.
67. F. J. López-Garzón, I. Fernández-Morales and M. Domingo-Garcia, Chromatographia, 23 (1987) 97.
68. G. Crescentini, F. Mangani, A. R. Mastrogiacomo and P. Palma, J. Chromatogr., 392 (1987) 97.
69. M-J. Wang, S. Wolff and J-B. Donnet, Rubber Chem. Technol., 64 (1991) 714.
70. M-J. Wang and S. Wolff, in: J-B. Donnet, R. C. Bansal and M-J. Wang (eds.), Carbon Black, Second Edition, New York 1993, p. 229.

71. M–J. Wang, S. Wolff and J–B. Donnet, Rubber Chem. Technol., 64 (1991) 559.
72. S. Dong, M. Brendle and J–B. Donnet, Chromatographia, 28 (1989) 469.
73. J–B. Donnet and S. J. Park, Carbon, 29 (1991) 955.
74. F. J. López–Garzón, M. Pyda and M. Domingo–Garcia, Abstracts of Carbon'94, Granada 1994, p. 318.
75. G. M. Dorris and D. G. Gray, J. Phys. Chem., 85 (1981) 3624.
76. C. Saint Flour and E. Papirer, J. Colloid Interface Sci., 91 (1983) 69.
77. E. Papirer, P. Roland, M. Nardin and H. Balard, J. Colloid Interface Sci., 113 (1986) 62.
78. A. Vidal, E. Papirer, W. M. Jiao and J–B. Donnet, Chromatographia, 23 (1987) 121.
79. E. Papirer, H. Balard and Y. Rahmani, Chromatographia, 23 (1987) 639.
80. G. Ligner, M. Sidqi, J. Jagiełło, H. Balard and E. Papirer, Chromatographia, 29 (1990) 35.
81. I. Tijburg, J. Jagiełło, A. Vidal and E. Papirer, Langmuir, 7 (1991) 2243.
82. M. M. Kopečni, S. K. Milonjić and R. J. Laub, Anal. Chem., 52 (1980) 1032.
83. S. K. Miłonjić and M. M. Kopečni, Chromatographia, 19 (1984) 342.
84. M. M. Marcović, M. M. Kopečni, S. K. Miłonjić and T. S. Ceranić, Chromatographia, 26 (1988) 387.
85. M. M. Marcović, M. M. Kopečni, S. K. Milonjić, J. Chromatogr., 463 (1989) 281.
86. S. K. Milonjić, T. S. Ceranić and M. Dj. Petkovic, Chromatographia, 27 (1989) 306.

This Page Intentionally Left Blank

A. Dąbrowski and V.A. Tertykh (Editors)
Adsorption on New and Modified Inorganic Sorbents
Studies in Surface Science and Catalysis, Vol. 99

Chapter 2.9
Molecular statistic and gas chromatographic study of hydrocarbons adsorption on the modified layer silicates and silica in the Henry region

Yu.I.Tarasevich, E.V.Aksenenko and S.V.Bondarenko

Institute of Colloid Chemistry and Chemistry of Water,
National Academy of Sciences of the Ukraine,
252680 Kiev, Ukraine

1. INTRODUCTION

Modified layer silicates and silica are used extensively in various areas of science and technology [1,2], and in particular, in the gas chromatography - as adsorbents and supports. The first results concerning the application of organosubstituted layer silicates for the chromatographic separation of organic substances with near boiling points, in particular, the hydrocarbons, were published in [3-7]. The modified natural silica (diatomites) are commonly used as the supports in gas-liquid and gas-adsorption chromatography [8,9].

To improve the chromatographic characteristics of the organoderivatives of layer silicates and silica it is necessary to know their structure and the nature of adsorption centres, on which the chromatographic separation processes take place. These processes normally occur in the Henry region, i.e. at surface occupation values $\theta < 0.05$. It enables one to apply the molecular statistic methods to obtain the reliable estimates of thermodynamic characteristics of non-specific and weak specific adsorption of hydrocarbons on these solid surfaces. By comparing the results of such calculations for given geometric relief and surface chemistry of the solid, with the data obtained from gas chromatographic experiment, one can make definite conclusions concerning the nature of surface sites, on which the adsorption or separation processes take place.

The studies presented here are based essentially on the principle of comparison of the thermodynamic characteristics of adsorption measured on a number of organoderivatives of layer silicates and silica, with the data obtained from the molecular statistic calculations involving the portions of surface, which model the real surface of the materials studied. These surface portions were chosen on the basis of the adsorbent structure analysis and complex physico-chemical studies of the modifying layers structure.

When performing the studies summarized here, also the principle of structural chemical modelling [10] was extensively used, which imply the comparison of the results of chromatographic experiments on the adsorbents possessing predicted separation centres with those on the adsorbents which have only a small number of such centres, if any. The identification of the portions of chromatographic materials, on which the adsorption and separation processes take place, had formed a scientific background for the development

of new efficient adsorbents and supports for the chromatography.

The proposed review comprises the results of the studies outlined above.

2. GENERAL MOLECULAR STATISTIC APPROACH

In what follows, the physical adsorption of molecules on an adsorbent surface will be considered, thus restricting the discussion to the systems for which the two following assumptions are valid:

(i) The adsorbed molecules and the adsorbent surface are considered to be quasi-rigid. This means that the variation in the partition functions of the molecule and the adsorbent during the adsorption is negligibly small, so that the internal geometry of the adsorbed molecule and the surface, and also the relevant microscopic characteristics of the constituent atoms such as their polarizability, remain unchanged.

(ii) Closely associated with assumption (i) is the restriction on the interactions occurring within adsorption systems considered in this approximation. In particular, only weak interactions such as dispersion and polarization attractions and short-range atom-atom repulsions can be considered. No chemical bonding can be involved in this approximation.

The theory for this adsorption model has been treated extensively in the comprehensive study [11], to which we refer the reader for more detailed discussion. Only the essential expressions are presented here.

2.1. Thermodynamic quantities

The problem of estimating Henry's constant and related thermodynamic quantities can be reduced to the calculation of the integrals of the form (see [11]):

$$J_j = \frac{1}{8\pi^2 A} \iint_A dxdy \int_0^\infty dz \int_0^{2\pi} d\varphi \int_0^\pi \sin\theta d\theta \int_0^{2\pi} d\Psi G_j \tag{1}$$

where the integrands G_j can be expressed as

$$G_1 = \exp[-\Phi/kT] - 1$$
$$G_j = [-\Phi/kT]^{j-1} \exp[-\Phi/kT], \qquad \text{for } j = 2,3 \tag{2}$$

In these equations $\Phi = \Phi(x, y, z, \varphi, \theta, \Psi)$ is the energy of interaction of the molecule with the adsorbent surface, the integration extends over the spatial variables (x,y) which specify the point on the adsorbent surface above which the molecule is situated, the variable z which represents the distance between the molecule and the adsorbent surface, and the Eulerian angles (φ, θ, Ψ) describe the orientation of the molecule with respect to the surface; A is the surface area over which (x,y) integration is performed. Calculation of the integrals in equation (1) allows the thermodynamic quantities for the adsorption of a quasi-rigid molecule of the species i to be expressed as follows:

Henry's constant

$$K_{1,i} = J_{1,i} \tag{3}$$

and the differential heat of adsorption (equal but opposed in sign to the differential molar variation of the internal energy)

$$Q_{a,i} = -RT\,(J_{2,i}/J_{1,i}) \tag{4}$$

The differential molar variations of the entropy and heat capacity can also be expressed via the $J_{j,i}$ values. Clearly the expressions (3)–(4) are valid within the limit of negligible adsorption, i.e. the Henry region.

Next we list the expressions for the thermodynamic functions of adsorption for molecules possessing rotational isomerism, since this is the case in which we are mainly interested. In equations (3)–(4) above, and in what follows, the subscript i refers to the i-th isomer of the particular adsorbate which is considered to be an equilibrium mixture of isomers. For each isomer the following quantities may be defined: ν_i the *degeneracy* of the isomer, i.e. the number of geometrically distinct configurations of the isomer each possessing the same free energy, and ΔF_i the difference between the free energies of the i-th isomer and that with the lowest free energy value. For example, n-butane possesses one *trans* conformation and two *gauche* conformations, the corresponding values of ν_i being 1 and 2, and the ΔF_i values being 0 and 2.5 kJ/mol, respectively. In equations (5), (8) and (10) below the summation is performed over all the isomers of the adsorbate.

The molar portion of the i-th isomer in the gas phase can be calculated from the standard expression

$$\chi_i^{(g)} = \exp\,(-\Delta F_i/RT)\left[\sum_j \nu_j \exp\,(-\Delta F_j/RT)\right]^{-1} \tag{5}$$

Then the molar portion of the i-th isomer in the adsorbed state is:

$$\chi_i^{(a)} = \Gamma_i/\Gamma \tag{6}$$

with

$$\Gamma_i = K_{1,i}\chi_i^{(g)} \tag{7}$$

and

$$\Gamma = \sum_j \nu_j \Gamma_j \tag{8}$$

being the adsorption amount for the i-th isomer and the total adsorption for the adsorbate, respectively. Using Eqs. (4)–(8), one can express the thermodynamic quantities for the adsorbate as (for details refer to [11]):

$$K_1 = \Gamma \tag{9}$$

$$Q_a/RT = \sum_j \nu_j \chi_j^{(a)}\,(Q_{a,j}/RT) - T\sum_j \nu_j \chi_j^{(a)} d\left[\log\left(\chi_j^{(a)}\right)\right]/dT \tag{10}$$

2.2. Interaction energy and adsorption potential

We turn now to the question of the interactions involved in the interaction energy value Φ.

As a result of assumption (ii) above, it will be shown that the value of Φ can be expressed as the sum over the contributions of all the atoms present in the molecule, with these contributions being induced by the potential field of the surface. It should be noted here that although the interactions can be divided into two major classes, via pair or atom-atom interactions, such as dispersion and short-range repulsion forces, and an essentially non-pair interaction, that due to polarization, they can both be treated in a similar fashion within the framework of the proposed method.

Considering the pair interactions first, one can express the corresponding contribution to the value of Φ as:

$$\Phi_{pair} = \sum_m \sum_s f(r_{m,s}) \tag{11}$$

where the internal summation is performed over all the atoms of the adsorbent surface (s), while the external summation is that extending over all the atoms in the molecule (m). The s summation is, in fact, unrestricted; however, it can be shown that, to within an acceptable accuracy, the explicit summation can be performed over the limited number of surface atoms nearest to the adsorbed molecule, the remaining part of the sum being substituted by analytical integration over the remainder of the adsorbent assuming a homogeneous distribution for the atoms within the adsorbent bulk. Moreover, even this explicit summation can be further simplified for the case of the adsorbents possessing a layered atomic structure. This summation is performed over the limited number of atomic sheets nearest and parallel to the adsorbent surface, assuming that the atomic density is distributed homogeneously throughout the sheet. This summation can again be performed analytically.

A number of expressions exists for the atom-atom interactions, among which are the Buckingham–Corner or (6-8-exp) potential:

$$f^{(BC)}(r_{r,m}) = C^{(BC)}_{M,S} r^{-6}_{m,s} + B^{(BC)}_{M,S} \exp\left(-Q^{(BC)}_{M,S} r_{m,s}\right) \tag{12}$$

and the Lennard-Jones or (6-12) potential:

$$f^{(LJ)}(r_{m,s}) = C^{(LJ)}_{M,S} r^{-6}_{m,s} + B^{(LJ)}_{M,S} r^{-12}_{m,s} \tag{13}$$

Here the superscripts (BC) and (LJ) refer to the Buckingham-Corner and Lennard-Jones potentials, respectively; $r_{m,s}$ is the distance between the m-th atom of the molecule and the s-th atom of the surface. The coefficients C, D, B, Q depend on microscopic characteristics, such as static polarizability, ionization potential, etc. For a detailed discussion of atom-atom interaction potentials, the reader is referred to [12]. The subscripts M and S denote *atomic species* of the adsorbed molecule and the adsorbent surface; note that in summations like (11), it is implied that for any value of m (or s) there is the definite M (or S) value which corresponds to a particular atomic species. Therefore, the internal summation in equation (11) can be performed to give the sum of atomic contributions:

$$\Phi_{pair} = \sum_m h_M(r_m) \tag{14}$$

where

$$h_M(r_m) = \sum_s f(r_{m,s}) \tag{15}$$

Turning now to the non-pair polarization interaction, one can present it in a similar form:

$$\Phi_{ind} = \sum_m g_M(r_m) \tag{16}$$

where the m-th atom contribution, $g_M(r_m)$, may be expressed as:

$$g_M(r_m) = -(1/2)\alpha_M [E(r_m)]^2 = -(1/2)\alpha_M \left[\sum_s q_s r_{ms} r_{ms}^{-3}\right]^2 \tag{17}$$

Here, α_M is the polarizability of the M-th atomic species, and $E(r_m)$ is the electrostatic field created by the charges q_s of surface atoms at the point r_m where the m-th atom is situated. Calculation of $E(r_m)$ again involves an unrestricted summation over the adsorbent atoms; however, this can be simplified by noting that as the adsorbent bulk is electroneutral, the only contribution to the electrostatic field results from the portions of the adsorbent closest to the adsorbed molecule. For adsorbents possessing a layered structure, the calculation of the polarization energy contribution can be further simplified by introducing atomic sheets over which the charge is distributed homogeneously; summation over the atoms in the sheet then again reduces to the corresponding analytical integration.

It is now straightforward to introduce the concept of the adsorption potential of the adsorbent surface *with respect to a particular atomic species of the adsorbate molecule*. For any m-th atom of the M-th species of the adsorbed molecule, the potential value $V_M(r_m)$ can be calculated at the point r_m where this atom is situated. For example, for the BC and polarization potentials one can combine Eqs. (12), (15) and (17) to obtain:

$$V_M^{(BC+ind)}(r_m) = h_M^{(BC)}(r_m) + g_M(r_m) \tag{18}$$

while, for the combination of the LJ and polarization potential, a similar expression is valid:

$$V_M^{(LJ+ind)}(r_m) = h_M^{(LJ)}(r_m) + g_M(r_m) \tag{19}$$

For each position of the adsorbed molecule relative to the adsorbent surface, a set of the coordinates r_m for the atoms in the molecule exists which is completely determined by the coordinates (x,y,z) for the centre of inertia of the molecule with respect to the surface, the internal geometry of the molecule, and the Eulerian angles (φ, θ, Ψ) describing the orientation of the molecule with respect to the surface. Thus, by calculating the potential grid, i.e. the arrays of potential values $V_M(x_p, y_q, z_r)$ for each atomic species M with the spatial grid (x_p, y_q, z_r) extending over the relevant integration domain, it is possible to perform the integration in Eq. (1) numerically, calculating the potential values $V_M(r_m)$ by extrapolation over the grid.

However, in most cases of interest, the sixfold integration in (1) is incapable of numerical solution. Calculations performed so far for related models are those for the adsorption of the hydrocarbon molecules in zeolite cell voids, see, for example, [13]. In such cases, the spatial integration in equation (1) is restricted to a relatively small volume which is determined by the van der Waals' radii of the atoms which constitute the molecule and

the walls of the void. Furthermore, additional simplifications are brought up by the symmetry of the void. We have been interested mostly in calculations of the thermodynamic quantities for the systems in which adsorption takes place on porous adsorbent surfaces with pores open to the gaseous phase. For such cases, the integration volume in Eq. (1) is of the order of cubic nanometers, and with the computers available it has proved impossible to perform the relevant calculations within the accuracy needed. Fortunately, the symmetry properties of such systems can be exploited to solve this problem.

2.3. Calculation of thermodynamic functions for adsorption on homogeneous surface

Let us consider the case where the adsorption of the molecule occurs on a homogeneous surface, i.e. a surface whose adsorption potential exhibits negligible variations with the (x,y) coordinates. A good example of such an adsorbent is the basal plane of the graphite surface. It has been shown in [11] that, within 1% accuracy, the summation over the surface atoms in equation (15) can be replaced by a summation over a few atomic sheets nearest and parallel to the surface, the sum over the particular sheet being approximated by an integral:

$$\sum_{\{\text{sheet}\}} r^{-n} = \rho_S \int_{-\infty}^{\infty} dx \int_{-\infty}^{\infty} dy \left(Z^2 + x^2 + y^2\right)^{-n} = \frac{2\pi\rho_S Z^{-n+2}}{n-2} \tag{20}$$

$$\sum_{\{\text{sheet}\}} \exp(-Qr) = \rho_S \int_{-\infty}^{\infty} dx \int_{-\infty}^{\infty} dy \exp\left[-Q\left(Z^2 + x^2 + y^2\right)^{\frac{1}{2}}\right] = \frac{2\pi\rho_S(QZ-1)}{Q^2} \exp(-QZ) \tag{21}$$

with Z being the distance between the atomic sheet and the point in which the potential is calculated, and ρ_S the mean number atomic density of the S-th atomic species over the sheet. The summation over atoms located deeper in the adsorbent bulk may be replaced by an integration:

$$\sum_{\{\text{bulk}\}} r^{-n} = \mu_S \int_{-\infty}^{\infty} dx \int_{-\infty}^{\infty} dy \int_{-\infty}^{\infty} dz \left(z^2 + x^2 + y^2\right)^{-n} = \frac{2\pi\mu_S Z^{-n+3}}{(n-2)(n-3)} \tag{22}$$

with Z being the distance between the bulk boundary and the point at which the potential is calculated and μ_S the mean number atomic density of the S-th atomic species in the bulk. Note that the short-range repulsion which is represented by the exponential term for the BC potential is negligibly small for the bulk part of the potential and can therefore be omitted. It is to be noted also that in the case of a homogeneous surface the polarization interaction cannot be included into the calculations, as a matter of principle, since a system of infinite parallel homogeneously charged sheets produces no electrostatic field provided the whole set is electroneutral.

Now the adsorption potential is independent of the coordinates (x,y) parallel to the adsorbent surface, and one Eulerian angle (say, φ) can be chosen in such a way that the rotation of the molecule through it does not affect the z coordinates of the atoms of the molecule. Thus the integrations over (x,y,φ) can be performed analytically, and instead of equation (1) one obtains:

$$J_j = \frac{1}{4\pi} \int_0^{\infty} dz \int_0^{\pi} \sin\theta d\theta \int_0^{2\pi} d\Psi G_j \tag{23}$$

Moreover, for any given (θ, Ψ) value, the potential energy $\Phi(z, \theta, \Psi)$ can be expanded in the Taylor series near the equilibrium distance $z_0(\theta, \Psi)$:

$$\Phi(z, \theta, \Psi) = \Phi_0(\theta, \Psi) + \frac{1}{2}\Phi''_z(\theta, \Psi)(z - z_0)^2 + \ldots \tag{24}$$

In this *harmonic approximation*, with $\Phi_0(\theta, \Psi)$ and $\Phi''_z(\theta, \Psi)$ representing the values of Φ and its second derivative with respect to z at the point z_0, one can perform the steepest descent integration over z in equations (1) and (2) due to the exponential dependence of the integrands on z to obtain:

$$J_1 = I_1, \qquad J_2 = I_2 + I_1/2, \qquad J_3 = I_3 + I_2 + 3I_1/4 \tag{25}$$

where

$$I_j = \frac{1}{4\pi}\int_0^{\pi} \sin\theta d\theta \int_0^{2\pi} d\Psi \left[\frac{\Phi_0(\theta, \Psi)}{kT}\right]^{j-1} \frac{\sqrt{2\pi kT}}{\Phi''_0(\theta, \Psi)} \exp\left[\frac{-\Phi_0(\theta, \Psi)}{kT}\right] \tag{26}$$

We had implemented the formulae (3)-(13), (18)-(22), (25) and (26) into the computer program which performs the calculations along the following lines.

First, from the parameters of the BC or LJ potential, the one-dimensional potential grid $V^{(M)}(z_r)$ is built up covering a distance z which is of the order of the size of the molecule over the adsorbent surface. Then integration (26) is performed: for each (θ, Ψ) value the program searches for the minimum potential value $\Phi_0(\theta, \Psi)$ and, when the search is completed, the value of $\Phi''_z(\theta, \Psi)$ is calculated from the finite differences. It is seen from equation (26) that since the values of $\Phi_0(\theta, \Psi)$ and $\Phi''_z(\theta, \Psi)$ are independent of T, the calculations may be performed simultaneously for the set of temperature values.

Table 1
Values of the BC potential coefficients $C^{(BC)}$ [J/(mol·nm^6)], $D^{(BC)}$ [10^{-2}J/(mol·nm^8)], $B^{(BC)}$ [10^7J/mol] for the interaction of alkane atomic species with various surface atomic species[a]

Surface atomic species	H (alkane)			C (alkane)		
	C	D	B	C	D	B
H (modifier)[b]	0.168	0	11.90	0.463	0.884	3.35
C (modifier)	0.463	0.884	3.35	1.290	1.999	17.58
N (modifier)[b]	0.528	0	19.55	1.817	0	22.44
O (silicate)[b]	0.526	0	21.98	1.785	0	25.25
Si, Al (silicate)[b]	0.506	0	0	1.993	0	0
C (graphite)[c]	0.498	0.950	3.60	1.386	2.148	18.90
C (graphite real)[d]	0.574	1.090	4.20	1.590	2.470	21.80

[a]The $Q^{(BC)}$ parameter is equal to 35.7 nm^{-1} except for atomic pairs: H,H - 52.0 nm^{-1}; H,N - 45.6 nm^{-1}; C,N - 37.7 nm^{-1}; H,O - 47.3 nm^{-1}; C,O - 38.8 nm^{-1}

[b]The truncated atom-atom potential form was found to be relevant

[c]Parameters from [11]

[d]Parameters estimated for a real regularly inhomogeneous graphite surface

The Gaussian quadrature formula was used to perform the integration. The above procedure was repeated for each isomer in the set; finally, the mean thermodynamic quantities (5)-(10) were calculated.

The performance of the program was verified by reproducing the results presented in [11] for the thermodynamic properties associated with the adsorption of hydrocarbons on the homogeneous basal surface of graphite. The BC potential was used in the calculations, with the $C^{(BC)}$, $D^{(BC)}$, $B^{(BC)}$, $Q^{(BC)}$ coefficients listed in Table 1. For the reasons explained below, we have preferred to use the LJ potential in the calculations, and hence the next step was to estimate the coefficients $C^{(LJ)}$ and $B^{(LJ)}$ so as to obtain the best fit for the values obtained with the LJ potential to those obtained for the BC potential. The corresponding values of the standard LJ parameters from which the coefficients $C^{(LJ)}$ and $B^{(LJ)}$ may be readily calculated are summarized in Table 2.

Table 2
Values of the Lennard-Jones potential well depth F (J/mol) and characteristic radius R (nm) for calculating the Lennard-Jones potential coefficients $C^{(LJ)} = 2FR^6$ and $B^{(LJ)} = FR^{12}$ for the interaction of alkane atomic species with various surface atomic species

	H (alkane)		C (alkane)	
	F	R	F	R
H (modifier)	160.35	0.280	182.13	0.339
C (modifier)	182.13	0.339	283.87	0.383
N (modifier)	208.08	0.300	400.26	0.300
O (silicate)	195.10	0.300	377.65	0.300
Si, Al (silicate)	199.29	0.300	438.78	0.300
C (graphite)	178.78	0.339	275.49	0.383
C (graphite real)	203.00	0.339	314.00	0.383

2.4. Calculation of thermodynamic functions for adsorption on regularly inhomogeneous surface

We now proceed with the calculations of the thermodynamic adsorption quantities for a surface possessing a lower degree of symmetry, via a surface whose properties vary periodically along one dimension, say x, and do not depend on another lateral coordinate, y. For such a system, expression (1) becomes

$$J_j = \frac{1}{8\pi^2 X_0} \int_{X_0} dx \int_0^\infty dz \int_0^{2\pi} d\varphi \int_0^z \sin\theta d\theta \int_0^{2\pi} d\Psi G_j \qquad (27)$$

where X_0 is the period of the surface inhomogeneity; note that the analytical φ integration cannot now be performed since the equipotential surfaces are no longer planes parallel to the surface.

Another problem which arises with calculations involving inhomogeneous surfaces is that the summation over the adsorbent atoms (cf. equations (20)-(22)) can no longer be restricted to infinite atomic sheets, because the symmetry of the adsorbent implies the existence of less symmetric structural elements. This problem can be resolved if it is assumed that the adsorbent surface consists of *semi-infinite* atomic sheets and *solid quadrants*, representing the portions of the bulk adsorbent. To introduce these into the calculations of the adsorption potential, the following formulae were derived:
for the semi-infinite atomic sheet with the coordinates $0 < x < \infty$, $-\infty < y < \infty$, $z = 0$ the relevant averages of r^{-n} at the point $x = X$, $z = Z$ become:

$$\sum_{\left\{\begin{array}{c}\text{semi-}\\ \text{infinite}\\ \text{sheet}\end{array}\right\}} r^{-6} = \rho_S \int_0^\infty dx \int_{-\infty}^\infty dy \left[Z^2 + (x - X)^2 + y^2\right]^{-6}$$

$$= \frac{\pi \rho_S}{8} \frac{4Z^2 + 3X^2}{(Z^2 + X^2)^{3/2}[2(Z^2 + X^2)^{3/2} + X(3Z^2 + 2X^2)]} \tag{28}$$

$$\sum_{\left\{\begin{array}{c}\text{semi-}\\ \text{infinite}\\ \text{sheet}\end{array}\right\}} r^{-12} = \rho_S \int_0^\infty dx \int_{-\infty}^\infty dy \left[Z^2 + (x - X)^2 + y^2\right]^{-12} =$$

$$= \frac{\pi \rho_S}{1280} \frac{16384Z^8 + 48231Z^6X^2 + 60624Z^4X^4 + 35616Z^2X^6 + 8064X^8}{(Z^2 + X^2)^{9/2}}$$

$$\times \left[128(Z^2 + X^2)^{9/2} + X(315Z^8 + 840Z^6X^2 + 1008Z^4X^4 + 576Z^2X^6 + 128X^8)\right]^{-1} \tag{29}$$

and for the solid quadrant with the coordinates $0 < x < \infty$, $-\infty < y < \infty$, $0 < z < \infty$

$$\sum_{\left\{\begin{array}{c}\text{solid}\\ \text{quadrant}\end{array}\right\}} r^{-6} = \mu_S \int_0^\infty dx \int_{-\infty}^\infty dy \int_0^\infty dz \left[(Z - z)^2 + (x - X)^2 + y^2\right]^{-6} =$$

$$= \frac{\pi \mu_S}{6} \frac{Z^2 - 9XZ/8 + X^2}{(Z^2 + X^2)^{1/2}[(Z^2 + X^2)^{1/2}(Z^3X^3) + Z^4Z^2X^2/2 + X^4)]} \tag{30}$$

It should be noted that integration of the exponential term in equation (12) for the BC potential leads to a series of Bessel functions, an expression which is rather inconvenient for numerical calculation; that is why in a further development we have restricted ourselves to the Lennard- Jones dispersion and repulsion potential form. Also the repulsion (r^{-12}) component in the expression for interaction with the adsorbent bulk was found to be negligibly small and was therefore omitted from the calculations.

Finally the contribution of polarization interactions may be considered in the framework of the layered adsorbent model. Starting from the expression for the electrostatic field vector created by the line possessing a charge density τ:

$$E = 2(\tau/\varepsilon)(r/r^2) \tag{31}$$

with r being the shortest radius vector from the line to the point in which the field is calculated and e the dielectric permeability, it is possible to calculate the components of the field created by the portion of the charged sheet located at $A < x < B$, $-\infty < y < \infty$, $z = 0$ at the point X, Z:

$$E_x = \frac{2\sigma}{\varepsilon}\int_A^B dx \frac{(x - X)}{(x - X)^2 + Z^2} = \frac{\sigma}{\varepsilon}\log\left[\frac{(x - A)^2 + Z^2}{(x - B)^2 + Z^2}\right]$$

$$E_z = \frac{2\sigma}{\varepsilon}Z\int_A^B dx \frac{1}{(x - X)^2 + Z^2} = \frac{2\sigma}{\varepsilon}\left[\arctan\frac{X - A}{Z} - \arctan\frac{X - B}{Z}\right] \qquad (32)$$

where σ is the density of the charge which is distributed homogeneously over the sheet.

Generalizing the method described in the previous section, we have developed a computational program which performs the calculations for such systems. Again the potential grid is built for each atomic species; in this case the grid is two-dimensional, covering the relevant (x,z) integration domain. Moreover, since the adsorption surface is now inhomogeneous, the harmonic approximation (24) is no longer valid, as the z dependence of Φ need not be parabolic for the case of a molecule, say, near the wall of the pore. This implies that the five-fold integration in equation (27) must be performed numerically; again the Gaussian quadrature formulae were implemented into the program.

To check the performance characteristics of the program, we have performed a series of calculations for the thermodynamic adsorption properties of n-alkanes on a model microporous graphite surface.

The regularly inhomogeneous surface of the graphite was modelled by the layered adsorbent (interlayer distance 0.335 nm, the mean number atomic density of the carbon atoms in the layer $\rho_S = 38.2\ nm^{-2}$), with the surface micropores simulated by infinitely long parallel defects of the external atomic layer. In the calculations the width of the micropores and the interpore distance were varied. Clearly no polarization potential needs to be included in the calculations due to the nature of the interactions involved.

First, it was instructive to calculate the profiles of the 'local' (non-observable) quantity, representing the relative density of the molecules adsorbed in the vicinity of some point over the adsorbent surface. It was shown that near the pore edge this density decreases significantly, and the preferential adsorption takes place inside the pore near its wall, provided the pore is wide enough to accommodate the molecule.

Next we performed a series of calculations in which the width of the pore was varied. The results obtained in this case were rather predictable: preferential adsorption was observed for pores with a free section matching the van der Waals cross-section of the alkyl chain.

More interesting is, however, the question concerning the effect of the total surface inhomogeneity on the integral thermodynamic characteristics values. Here it should be noted that the calculations made in [11] for a homogeneous graphite surface were performed with the atom- atom potential well depth reduced by 13% with respect to the values estimated from the quantum mechanical expressions (compare last two entries in both Tables 1 and 2); this enabled a correspondence to be achieved between the calculated and experimental thermodynamic quantities. We believe however (see [14]) that this

discrepancy is due to the presence of surface micropores not accounted for in the calculations [11]. To support this point of view, we performed the calculations for a regularly inhomogeneous surface with narrow parallel micropores 2 to 3 nm apart which we believe simulates edge dislocations on the faces of the graphitized black microcrystallites having the same characteristic dimensions (see e.g. [15]). For non-reduced atom- atom interaction parameters marked as 'Graphite real' in the tables used in the calculations the results obtained were found to be closely similar to the experimental chromatographic data.

Thus, the proposed method of calculating the thermodynamic properties of molecules adsorbed on to regularly inhomogeneous surfaces in the Henry region can be considered adequate, enabling quite sensible results to be obtained concerning the degree of inhomogeneity of the graphitized blacks surface.

In section 5 the application of the above procedures for calculating the thermodynamic characteristics of the hydrocarbons adsorption on a number of model adsorbents will be given.

3. STRUCTURE AND ADSORPTION PROPERTIES OF MODIFIED LAYER SILICATES AND SILICA

In the studies, specially purified clay minerals, mainly from Ukrainian deposits, were used: montmorillonite (Pyzhev), hydromica and palygorskite (Cherkassy), kaolinite (Glukhov), vermiculite (Kovdor, Russia). The diatomite supports from Armenia and the Czech Republic (produced by Lachema), and macroporous silica (made in the experimental plant for production of adsorbents for petrochemical industry, Nizhnii Novgorod, Russia) were employed.

The specific surface values were calculated from BET equation, with the molecular areas taken as: N_2=0.162 nm^2; C_6H_{14}=0.50 nm^2; H_2O=0.108 nm^2.

3.1. Modified layer silicates

Natural layer silicates represent the mixed type porous adsorbents with structure consisting of mesopores, and micro- and macropores [16]. With respect to the character of their porous structure, the layer silicates can be divided into two classes: those with the expanding structural cell (montmorillonite, vermiculite), and with the rigid structural cell (kaolinite, hydromica, palygorskite).

The chemical modification of the adsorbent surfaces presents a lot of possibilities to change the structural-adsorption and separation characteristics of these adsorbents. Organic cations are adsorbed only on the external surfaces of layer silicates possessing the rigid structural cell. Therefore, the changes in the adsorption characteristics of the kaolinite, hydromica and palygorskite, caused by the substitution of organic cations for natural inorganic exchangeable cations, are similar to the changes in adsorption properties of silica due to its modification by organic substances: the deterioration of the adsorption ability of the minerals with respect to both polar and non-polar substances is observed. This is clearly seen in Table 3.

The nature of the changes in adsorption and separation properties of layer silicates with the expanding structural cell, caused by the modification, depends on the size of modifying organic cation.

Table 3
Amount of adsorbed cations a (meq/g), interplanar spacing d_{001} (nm) and specific surface area S (m^2/g) of modified layer silicates

Mineral	Cation	a	d_{001}	S (m^2/g)		
				N_2	C_6H_{14}	H_2O
Palygorskite	Ca^{2+}	0.23	1.04	224	153	302
	$[C_{16}H_{33}NH_3]^+$	0.26	1.04	-	161	210
	$[C_{16}H_{33}NH_3]^+$	0.47	1.04	-	147	131
Hydromica	K^+	0.26	1.02	120	120	150
	$[C_{16}H_{33}NC_5H_5]^+$	0.53	1.02	24	32	25
Kaolinite	Na^+	0.23	0.72	69	69	62
	$[C_{18}H_{37}NH_3]^+$	0.25	0.72	49	51	25
	$[C_{18}H_{37}NH_3]^+$	0.40	0.72	42	42	16
Montmorillonite	Ca^{2+}	1.00	1.00 [a]	15	32	481
	$[(CH_3)_4N]^+$	0.85	1.38	155	105	191
	$[C_{16}H_{33}NH_3]^+$	1.01	1.80	2.8	21	72
	$[C_{16}H_{33}NC_5H_5]^+$	0.75	1.77	2.8	27	91
Vermiculite	Na^+	1.50	1.25	-	9.1	169
	$[(CH_3)_4N]^+$	0.06	1.25	1.4	9.3	169
	$[C_{16}H_{33}NH_3]^+$	1.24	2.70 ; 1.35	3.6	-	113

[a] Dehydrated sample

Thus, the modification of the montmorillonite by short-chain cations (tetramethyl- and tetraethylammonium) leads to the penetration of organic cations into the interlayer spacing, which results in the moving the silicate layers apart from one another by 0.42-0.45 nm. The relatively small cations, $[(CH_3)_4N]^+$ and $[(C_2H_5)_4N]^+$ with areas of 0.26 nm^2 and 0.45 nm^2, respectively, occupy only a part of internal montmorillonite surface, providing a considerable free volume of micropores available for the molecules of inert gases, cyclic, aromatic and paraffin hydrocarbons [17,18]. In fact, for tetramethylammonium modified montmorillonite, a sharp increase in the specific surface area with respect to nitrogen and hexane, and a decrease in the specific surface area with respect to water, as compared to natural montmorillonite were observed, see Table 3. This can be attributed to the fact that some part of the natural mineral surface, accessible for H_2O molecules, is covered with organic cations during the modification process.

In the case of vermiculite, the short-chain organic cations do not penetrate into the interlayer space, and are adsorbed only on the external surface of the mineral. This is clearly seen from the analytical measurements, showing that only 0.06 meq/g of Na^+ ions is substituted when Na-vermiculite is treated with tetramethylammonium salt solution, the total exchange capacity being equal to 1.5 meq/g. Therefore, the values of specific surface area obtained from water and hexane adsorption isotherms for the initial and $[(CH_3)_4N]^+$ modified vermiculite are virtually the same (Table 3). Such a pronounced difference in the

accessibility of montmorillonite and vermiculite interlayer space to $[(CH_3)_4N]^+$ cation can be explained by different densities and distribution of the layer charge of the minerals.

Consider now the case of the modification of layer silicates, possessing an expanding structural cell, by long-chain organic cations. Here the spacing between the silicate layers depends on the amount of organic cations penetrated into the interlayer gaps, or, more specifically, on the relation between the values of S_0 - the area of the total silicate surface per one exchange center (0.57 nm^2 per unit charge for Pyzhev montmorillonite, 0.365 nm^2 per unit charge for Kovdor vermiculite), and S_c - the maximum area which can be occupied by an exchange organic cation (about 0.1 nm^2 per one $-CH_2-$ group of an alkyl chain). If $S_c < S_0$, then the exchange cations fit closely to the silicate layers which results in the formation of the monolayer of organic cations between the silicate layers. When $S_0 < S_c < 2S_0$, the flat organic bilayer is formed in the silicate interlayer gap. When the value of S_c exceeds $2S_0$, the organic cations form a layer with the individual cations oriented uniformly at some angle with respect to the silicate layer surface [19].

The way in which the exchange ions are distributed in the layer and in a crystal of a mineral is also important. It was shown in [20-25] that the substitution of inorganic or short-chain organic cation for the initial exchange complex of layer silicate in some cases involves the segregation of two sorts of ions between the layers. This segregation was observed using the X-ray method for residual inorganic and long-chain organic cations in the structure of the vermiculite [25-27]. It is to be noted that the vermiculite is characterized by a macroscopic level of the segregation in the sense that whole 'domains' of the mineral are saturated with the same cations. At the same time, the X-ray studies are incapable to provide any definite information concerning the distribution of long-chain organic cations in the montmorillonite structure because of random interstratification of packets containing initial and organic cations [28,29].

The combined studies of water and hexane adsorption were found to be most informative in this case. The molecules of hexane can be adsorbed only on external crystal surface of both initial and organosubstituted montmorillonite. On the contrary, water molecules can penetrate into those interlayer gaps of the montmorillonite, where the substitution of organic cations for non-organic ones had not occurred. Thus from the difference between the adsorption (or specific surface) values of water vapour and of hexane, the number of the silicate packets where no substitution had taken place, can be estimated [29].

Using this method it was shown that the modification of the mineral should be performed by the solutions containing as much organic substance as possible, with the excess of the modifier subsequently being washed out. It results in the reduction of the number of montmorillonite packets containing residual inorganic cations. In particular, the data for the adsorption of water and hexane on montmorillonite processed by the solutions containing an amount of the modifier equal to double and triple exchange capacity of the sample, had shown that the number of the packets containing residual inorganic cations was reduced by $\sim 30\%$ as compared to the case when the amount of modifier was equal to single exchange capacity of the sample.

Thus the combined use of X-ray and adsorption methods can be especially useful to determine the variation of the silicate sample structure resulting from the modification.

The studies summarized above had shown that the presorption of long-chain organic cations in the amount equal to the exchange capacity of the mineral with the rigid structural cell does not lead to the complete covering of the external surface by the modifying

layer. Instead, as the organic cations can associate into micromicelles, there can exist the portions of the surface free from organic cations. To achieve the maximal coverage of the surface, the superequivalent adsorption is to be performed. The excess of the modifier can be removed, if necessary, by washing [29].

If the organic cations occupy virtually the whole internal and external surface of the mineral, then the molecules of inert gases, saturated hydrocarbons and water are adsorbed mainly on their external surface [30-32]. In fact, Table 3 indicates a sharp decrease of specific surface values with respect to water for the organomodified montmorillonite and vermiculite as compared to the initial minerals. The specific surface area values of modified montmorillonite with respect to nitrogen and hexane are also smaller than those of natural mineral. This indicates the existence of an aggregating effect due to long-chain organic cations, which is especially evident in the case of the modified hydromica, see Table 3. The considerably higher values of the specific surface area of the adsorbents with respect to hexane as compared to those determined with respect to nitrogen are most likely due to the intercrystalline swelling of organosubstituted samples in hexane vapours.

The molecules of polar organic substances (normal alcohols, acetone, ethylacetate) and aromatic hydrocarbons are adsorbed not only on the external, but also on the internal surface of the montmorillonite modified by long-chain organic cations [33]. The penetration of the adsorbed molecules into the montmorillonite crystals is accompanied by the rearrangements in the interlayer space.

3.2. Modified silica

The adsorbents and supports based on silica materials, such as diatomites, wide-porous glasses and silica gels, are widely used in the gas chromatography. To suppress the adsorption activity of these materials, the chemisorption modification can be applied, resulting in the substitution of Si- O-C, Si-O-Si or Si-C groups for surface silanol groups. The alkylchlorosilanes, their derivatives and polymer molecules are most commonly used as the modifiers. The essence of the mechanism of the alkylchlorosilanes interaction with silicate material surface is that the individual modifier molecules are fixed to the surface by means of chemical bond, not interacting with one another. As the result, the modification decreases to a certain extent the chemical inhomogeneity, not excluding it completely [34].

In the case of polymer molecules, the silica surface can be regarded to be deactivated reliably enough only with respect to large polar molecules, whereas small polar molecules (like methyl and ethyl alcohols) can access the active sites of solid surface, in spite of the screening [34].

We have developed a more efficient method of the silica surface deactivation, based on the liquid phase modification by organosilicon olygomers [35]. The main advantage of this method is that a layer of chemisorbed and sewed together molecules of the hydrophobizer is formed on the surface. This layer not only neutralizes the active OH groups of silica surface, but also covers the surface with the continuous film, making other active adsorption-catalytic sites (like coordinately unsaturated Al^{3+} or Fe^{3+} ions) to be sterically inaccessible. The thickness of this layer on silica surface was estimated in [36] to be of about 2 nm.

Among other modifiers, the polyalkylhydrosiloxanes can be regarded to be the most promising ones, due to the presence of Si-H groups capable of chemical reacting. They can easily interact with surface hydroxyl groups with the isolation of the hydrogen:

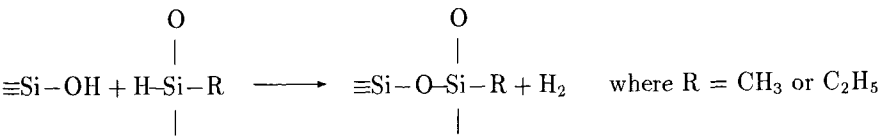

It is important that the topography of reaction capable organosilicon olygomeric modifiers is close to that of silica surface silanol groups. As the result, the 'geometric matching' occurs during the modification process, ensuring the most possible neutralizing of surface silanol groups [37].

Table 4 (reproduced from [38]) summarizes the adsorption characteristics of the initial and polymethylhydrosiloxane-modified macroporous silica with a pore radius r = 57.0 nm. Presented also are the adsorption characteristics of surface-porous adsorbent (see Section 4.2) prepared by the thermooxidation of modified silica in a narrow temperature range. The values of the water molecular area wH_2O and the heat of wetting q show that the modification results in the hydrophobization of the surface, while subsequent thermooxidation increases the adsorbent specific surface area.

Table 4
Amount of grafted modifier a (mg/m^2), specific surface area with respect to nitrogen S_{N_2} (m^2/g), BET adsorption monolayer values for various substances a_m (mmol/g), water molecular area w_{H_2O} (nm^2) and heat of wetting q (mJ/m^2) for the initial and modified silicas [38]

Silica	a (mg/m^2)	S_{N_2} (m^2/g)	a_m(mmol/g)			w_{H_2O} (nm^2)	q (mJ/m^2)
			C_6H_{14}	C_6H_6	H_2O		
Initial	-	44.0	0.133	0.185	0.350	0.208	250
Modified	2.0	31.0	0.101	0.104	0.017	3.04	36
Modified and Thermooxidized	2.0	120.0	0.126	0.140	0.022	9.90	22

4. GAS CHROMATOGRAPHIC STUDIES OF THE ADSORPTION OF HYDROCARBONS ON ORGANODERIVATIVES OF LAYER SILICATES AND SILICA

The substances used as the molecular probes in the gas chromatographic experiment consisted of molecules with no groups or bonds capable of specific interactions with the adsorbent surface [9]: saturated hydrocarbons with linear and branched structures, and cyclohexane and its methyl- and dimethyl-substituted homologues. Benzene and its derivatives were also used.

For gas chromatographic studies, a Chrom-5 chromatograph with a flame-ionization detector was used employing a sampling column of dimensions 100 cm × 0.3 cm and 250 cm × 0.3 cm. After filling with the respective adsorbents of 0.20-0.25 mm radius fraction, the columns were conditioned for 6 h at 70-170°C in a flow of the carrier gas (nitrogen). The liquid adsorbate samples (volume not exceeded 0.2 μl) were introduced

into the column via the carrier gas current, controlling the volume rate of the latter within the limits of 30-40 cm^3/min. This ensured that the relative vapour pressure of the adsorbate in the system was ca. $1 \cdot 10^{-3}$ to $1 \cdot 10^{-2}$ with an adsorbent monolayer capacity degree of occupation < 0.01. Adsorbate retention times could be reproduced experimentally to within 1% accuracy.

The differential (isosteric) adsorption heats Q_a for negligible adsorbent surface occupation were derived from the linear dependence of $\log(V_m/T)$ against 1/T slope, where V_m is the specific retention volume (cm^3/g) [9]. Direct evaluation of the V_m values over the temperature range 100-150°C and calculation of the isosteric adsorption heats were performed employing hexane as the reference substance. For other adsorbates, the relative retention volumes $V_{rel} = V_m^{adsorbate}/V_m^{hexane}$ were measured experimentally, allowing for the adsorption heat increments with respect to hexane to be estimated.

4.1. Natural and organosubstituted layer silicates

A sharp increase of the retention volumes V_m and heats of adsorption of saturated hydrocarbons on tetramethylammonium montmorillonite in the Henry region as compared with natural mineral (Table 5) shows that the adsorption and separation of these molecules take place in chink-like micropores having the width of ~ 0.45 nm on the (internal) surface of $(CH_3)_4N$ - montmorillonite [39].

Adsorption and separation processes involve also the active sites existing on the external surface of $(CH_3)_4N$ - montmorillonite, their role being more important in the case of adsorption of isoparaffins and cyclohexane molecules. This is indicated by a significantly smaller differences between the specific retention volumes of iso- and cycloparaffins on natural and tetramethylammonium samples than the difference in V_m values characteristic for n-paraffines on the same adsorbents. Thus, the tetramethylammonium montmorillonite adsorbs n-alkanes selectively from the mixtures containing iso- and cycloparaffines, which is confirmed by the values of relative retention volumes for such hydrocarbon pairs as, for instance, n-heptane / 2,4- dimethylpentane. These can be easily calculated from the data presented in Table 5.

Table 5
Specific retention volume V_m (cm^3/g) and differential heat of adsorption Q_a (kJ/mol) for hydrocarbons adsorption on natural palygorskite, and natural and tetramethylammonium - modified montmorillonite at 150°C

Adsorbates	Palygorskite		Montmorillonite		$(CH_3)_4N$ - montmorillonite	
	V_m	Q_a	V_m	Q_a	V_m	Q_a
Pentane	18.5	64.5	8.4	56.5	97.5	67.4
Hexane	67.1	75.6	35.1	64.0	369	76.2
Heptane	275	83.3	179	72.9	1368	84.2
2,4-Dimethylpentane	112	68.7	38.1	61.1	128	68.5
2,2,4-Trimethylpentane	252	81.2	85.8	72.0	166	81.0
Cyclohexane	32.7	59.5	11.4	53.6	71.4	62.4

It is interesting that the heats of adsorption of linear hydrocarbons on natural palygorskite are intermediate between the values characteristic for the adsorption on natural and tetramethyl- ammonium montmorillonite. This indicates the important role of the micropores of dimensions 0.37×0.64 nm, existing on ribbed surface of the palygorskite [40].

Under the conditions of gas-chromatographic experiment (at a surface coverage $\theta \sim 0.01$ and temperature range 100-150°C), the adsorption of aromatic hydrocarbons, as well as n– and isoparaffins, takes place on the external surface of layer silicates such as vermiculite and fluorohectorite, modified by long-chain organic cations. This is rather convincingly confirmed by a comparison of the specific retention volumes of n-hexane and benzene on initial and modified synthetic fluorohectorite. Table 6 (reproduced from [32]) shows a slight increase of the benzene retention volume on a cetylpyridinium-modified sample as compared to the initial one. However, the differences of V_m values for benzene (by a factor of 2.5) are not so high as, for instance, in the case of paraffins adsorption on natural and $[(CH_3)_4N]^+$ - modified montmorillonite (Table 5), but are in a good correspondence with the 1.9 fold increase of the V_m value determined for hexane.

Table 6
Specific retention volumes V_m (cm^3/g) of hydrocarbons on initial (Na^+) and $[C_{16}H_{33}NC_5H_5]^+$ - modified fluorohectorite at 150°C [32]

Adsorbate	Initial	Modified
Benzene	13.3	31.2
Hexane	1.47	2.76

The increase of the retention volume of benzene on a modified sample with respect to the initial sample, can be associated, similarly to the case of hexane adsorption, with intercrystalline swelling of the organic complex, when the molecules of aromatic hydrocarbons penetrate between the alkyl chains of the modifying cations adsorbed on the external surface of the mineral.

A rather different behaviour is observed [32] for modified montmorillonite, possessing more labile and disordered structure as compared with fluorohectorite and vermiculite.

When the amount of modifier on the montmorillonite surface increases, a regular decrease in differential heats of adsorption is observed, with the simultaneous increase of the specific retention volumes per unit area of external surface and Henry's constants for the hydrocarbons considered (Tables 7, 8). At the same time, an increase in the amount of long-chain cationic surfactants on the kaolinite surface leads to the decrease in both differential heat of adsorption and Henry's constant for benzene (Table 8), not surprisingly, because of a more complete covering of the kaolinite surface by the presorbed modifying layer and a decrease in the charge of the polar NH_3^+ groups of the modifier [41].

The anomalous changes in the adsorption and thermodynamic characteristics of hydrocarbons on montmorillonite indicates explicitly that, at low surface coverage, the adsorption and separation of hydrocarbons take place in the surface micropores on the lateral faces of the mineral. With the increase in the amount of adsorbed modifier, the processing degree of the mineral packets by the organic substance also increases, resulting in the increase of the retention volume of hydrocarbons, and corresponding increase of Henry's

constants. The adsorption of benzene in micropores is accompanied by an endothermic microswelling of the organophilized regions of the surface. As the result, the total heat of hydrocarbon adsorption on organomontmorillonite can even decrease with increasing amount of the presorbed modifier.

Table 7
Specific retention volumes V_s (cm^3/m^2) and differential heats Q_a (kJ/mol) of hydrocarbons adsorption on cetylammonium montmorillonite with different amounts of presorbed modifier a (meq/g) at 150°C

Adsorbate	a					
	1.01		1.35		1.60	
	V_m	Q_a	V_m	Q_a	V_m	Q_a
n-Hexane	0.53	36	0.75	31	1.20	26
n-Nonane	3.33	56	4.60	44	6.40	40
Ethylbenzene	7.71	50	9.20	38	-	-

Table 8
Specific retention volumes V_m (cm^3/g), Henry's constants K_1 (mm) and differential heats of adsorption Q_a (kJ/mol) of benzene on organo-substituted kaolinite and montmorillonite samples with different amounts of presorbed modifier a (meq/g) at 120°C

No.	Adsorbent	a	V_m	K_1	Q_a
1	Kaolinite	0.27	16.5	0.48	42
2	Kaolinite + octadecylammonium	0.50	14.3	0.46	38
3	Montmorillonite	1.01	13.8	3.44	31
4	Montmorillonite + cetylammonium	1.60	16.6	5.17	30
5	Li-montmorillonite (heated)	0.08	27.2	2.06	50
6	Li-montmorillonite (heated) + cetylpyridinium	0.22	7.3	0.96	39
7	Li-montmorillonite + cetylpyridinium	0.90	30.8	3.71	39

To confirm the validity of the conclusion made above concerning the fact that adsorption takes place in the micropores, we have estimated the thermodynamic characteristics of the adsorption of benzene on the crystallochemically identical samples with different degrees of processing of side surface, prepared on the basis of the Li-form of montmorillonite [42]. The thermal processing of the mineral Li-form can lead to the formation of pyrophillite analogue [16], in which an irreversible migration of Li^+ cations into vacant octahedral positions results in that the layers are mostly adjoined closely to one another, with their openings being inaccessible to the adsorption of hydrocarbon molecules. The modification of the Li-montmorillonite heated to 250-300°C with organic cations, similarly to the kaolinite modification, affects only the external surface of the mineral. The dependence of the adsorption thermodynamic characteristics for such samples on the amount of presorbed modifier is similar to that found for kaolinite, see Table 8, samples 1, 2 and 5, 6.

The decrease of V_m and K_1 values for the adsorption of benzene on the cetylpyridinium montmorillonite prepared from the heated Li-form (samples 5, 6) relative to the modified material based on initial Li-montmorillonite (sample 7) can be explained by the closing of the interlayer gaps of the thermoprocessed mineral. This prevents most active sites of the external surface, the micropores on side faces, from taking part in the adsorption-separation processes.

These experimental data show that the most selective chromatographic adsorbents can be prepared by the enhanced development of the pores on side faces of the crystals of swelling minerals. The number of surface micropores can be controlled by varying both the amount of the presorbed organic modifier and the composition of the inorganic exchange complex. In contrast to the lithium cations, fixed irreversibly in the structure of heated Li-montmorillonite promoting the formation of the 'compressed' structure of the mineral, the introduction of the univalent large-size Rb^+ or Cs^+ cations into the exchange complex of montmorillonite provides the significant increase of the contribution of crystal side faces into the total external surface due to the disordered relative displacement of neighbouring three-sheet layers [16,43].

The results presented below support the conclusions concerning the influence of the features, introduced to the mineral matrix by the exchange Cs^+ cation, on the chromatographic properties of organomontmorillonite. The samples of the cetylpyridinium montmorillonite prepared from Cs- and Ca-forms of the mineral, Cs-CPM and Ca-CPM respectively, contained 1.4 meq/g of the organic modifier. The glass columns were employed, filled with the adsorbents of 0.25-0.50 mm fraction, and conditioned for 6 h at 100-110°C in a flow of the carrier gas (nitrogen). The experiments were performed at 80°C with the volume rate of the carrier gas being within the limits of 30-40 cm^3/min.

Table 9
Selectivity values V_{rel} of the cetylpyridinium derivatives of montmorillonite

Adsorbent	ethylbenzene : p-xylene	m-xylene : p-xylene	o-xylene : m-xylene
Cs-CPM	1.19	1.37	1.10
Ca-CPM	1.15	1.25	1.03

From the experimental data [44], the selectivity of the adsorbents was calculated as the relative retention volume of the separated species. It can be seen in Table 9 that Cs-CPM adsorbent possesses better selectivity than the Ca-CPM one with respect to the separation of the isomers of xylene and ethylbenzene with like properties. The results enabled us to conclude that the separation of the isomers of m- and p-cresol up to the purity degree of 99% can be achieved using the columns with the theoretical plates number (TPN) not exceeding 200, and that for the o- and m-isomers - employing the packed intermediate efficiency columns with TPN of 2000-2500. To separate the same pairs of the species using the Ca-CPM, the capillary columns with the TPN of 20000 were required.

4.2. Organoderivatives of silica

The surface-porous adsorbent studied in this work was prepared from the non-porous diatomite support Chromaton N-AW (Lachema, Czech Republic) whose surface has been

modified with a polymethylhydrosiloxane of general composition $(CH_3SiHO)_n$, where n = 10-15, followed by subsequent thermo-oxidation of the modifying layer at 300°C. Macroporous silica with a pore radius of 57 nm [34], processed with the same organosilicon modifier under the conditions which excluded the development of surface micropores, was used as the reference sample. The amount of modifier deposited on the surface in each case was 0.3 g/g. The specific surface area of the samples as obtained from low-temperature argon desorption method was estimated to be as 100 and 60 m^2/g respectively. In what follows the first and second adsorbent mentioned above will be referred to as the thermo-oxidized and non-porous sample, respectively.

Figure 1 shows the dependency of the isosteric adsorption heats on the molecular mass of various substances employed, as determined using the method described above. Also shown are the Q_a values for the adsorption of the same gases on a homogeneous graphite surface, calculated according to the method described in Section 2.3, with the molecular geometry of the corresponding isomers obtained from the quantum MNDO / PM3 method.

We believe that a consistent interpretation of the results presented can be obtained based on the assumption that the microscopic structure of the adsorbent surfaces studied may be associated with two types or scales of surface porosity: (i) inhomogeneities with a characteristic size substantially smaller than that of the adsorbate molecule (surface inhomogeneity due to the atomic structure of the adsorbent), and (ii) inhomogeneities possessing a characteristic size comparable to that of the adsorbed molecule (surface microporosity arising from removal of fragments of the modifier layer during thermooxidation).

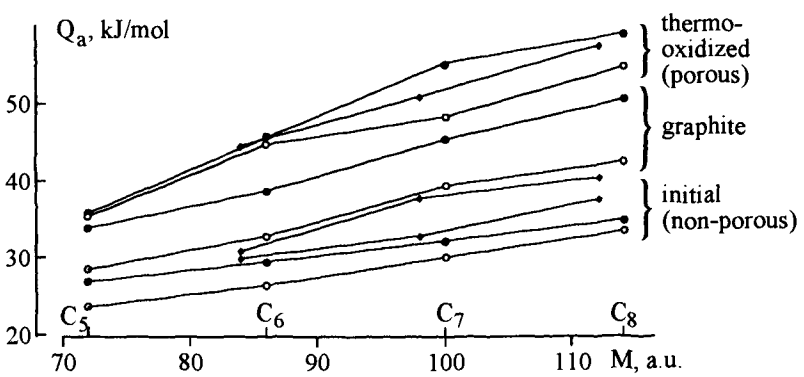

Figure 1. Isosteric heat Q_a for the adsorption of: ●, n-alkanes; ○, iso-alkanes; and ◆, cyclanes on various adsorbents plotted against their molecular mass M.

The similarity between the adsorption energies for the non-porous adsorbent studied and for the homogeneous graphite surface should be noted. This is revealed by the uniform linear increase in the Q_a values for the series of the normal alkanes, iso-alkanes and cyclanes with the increasing molecular mass, i.e. with an increase in the number of methylene or methyl groups interacting with the adsorbent surface. This similarity demonstrates the absence of microporosity on the surface of non-porous adsorbent. The fact that the Q_a values for molecules with near or equal molecular masses exhibit significantly less scattering for the non-porous adsorbent relative to the homogeneous graphite can also be

explained by the nature of the structural relief of the surface. This eliminates differences in the energetics of short range atom-atom interactions of the type which lead to more significant differences in the Q_a values characteristic for the adsorption of various isomers possessing near or equal molecular masses on a homogeneous basal graphite surface.

Somewhat different behaviour is observed for adsorption on the thermooxidized surface. Here a uniform increase in the isosteric heat of adsorption with a molecular mass was only observed for cyclanes, with Q_a value increments arising from the addition of methylene or methyl groups in the normal alkane and iso-alkane series being significantly less regular. An interpretation of these results may be proposed on the basis of the assumptions made above concerning the dimensions and topography of micropores formed on the adsorbent surface during thermoprocessing. If it is assumed that thermooxidizing results in the formation of long shallow defects in the surface layer, it is possible to estimate the size of these micropores from a comparison of the Q_a values obtained and the van der Waals dimensions of the adsorbing molecules. These dimensions may be calculated from the van der Waals atomic radii and the internal molecular geometry obtained from semi-empirical quantum chemical (MNDO/PM3) calculations; the resulting molecular sizes agree well with the kinetic molecular diameters listed in [45].

Let us first consider the normal alkanes series. It is seen from Figure 1 that the Q_a values increase linearly up to n-heptane, whereas for n-octane the increment in isosteric adsorption heat corresponding to the addition of one CH_2 group to the alkyl chain decreases considerably, being approximately equal to the value characteristic for the non-porous adsorbent. It is thus straightforward to conclude that adsorption takes place preferentially in long shallow micropores on the thermooxidized adsorbent surface, the mean width of these micropores slightly exceeding the van der Waals cross-section of the alkyl chain (0.42-0.46 nm) while their mean length lies between 1.17 and 1.22 nm, the values corresponding to the length of the n-heptane and n-octane molecules. It should be noted here that micropores resulting from the 'burning out' of elements of the modifier alkyl chain can hardly be regarded as rectilinear hollows in a perfect adsorbent surface; in contrast, what we have here are irregular convolutes. However, the account must be taken of the fact that the adsorbate represents a mixture of rotational isomers (three for n-pentane, seven for n-hexane, 11 for n-heptane and 27 for n-octane). As adsorption takes place dynamically, the particular microscopic configuration of a surface pore corresponds to preferential adsorption of the adsorbate molecule existing in that conformation which most closely matches the geometric shape of the pore. It will be shown in Section 5.2 below, that for adsorption of n-hexane on the side surface of organomodified montmorillonite, which corresponds to a set of long parallel micropores with a micropore width equal to the van der Waals cross-section of the alkyl chain, almost all the adsorbed molecules exist in the linear (*trans*) conformation. A similar effect could well occur in the case considered here; obviously the conformational distribution of the adsorbed molecules has to correspond to the shape distribution of the micropores.

Considering the iso-alkanes series next, here the Q_a values for iso-pentane and 2,2-dimethylbutane coincide well with those for n-pentane and n-hexane, while the values for 2,4-dimethylpentane and 2,2,4-trimethylpentane are considerably less than the corresponding values for n-heptane and n-octane. This effect can also be explained consistently using the concept of the adsorption in long surface micropores: the mean van der Waals cross-sections for the first two adsorbates (0.51 nm) differ only slightly from that

for the alkyl chain, while the cross-sections of more branched 2,4-dimethylpentane and 2,2,4-trimethylpentane molecules (0.67 nm) apparently exceed the width of the surface micropores, resulting in the significantly lower adsorption of these isomers relative to the n-alkanes.

These considerations can be used also to explain the linear increase in the Q_a values observed in the cyclanes series. In this case the molecular cross-section of cyclohexane in its most stable conformation is equal to 0.51 nm and does not increase significantly as methyl groups are added to the cyclic molecule.

To support our conclusions regarding the existence and approximate size of the micropores on the thermooxidized adsorbent surface, we had measured the adsorption isotherms for the hydrocarbons studied on both adsorbents at 130°C using the gas chromatographic method [9]. Adsorption increased for the non-porous adsorbent with increasing molecular mass of the adsorbent, with the adsorption isotherm for iso-octane lying between those for n-heptane and n- octane (Figure 2,a). In contrast, for adsorption on the microporous adsorbent the isotherm for iso- octane lies below that of n-heptane (Figure 2,b), indicating that the adsorbent micropores with the size of $\sim 0.51 \times 1.2$nm are inaccessible as far as branched adsorbate molecules are concerned.

It is to be noted that the considerations presented above demonstrate the application of the gas chromatographic version of the molecular probes method, proposed by authors in [46]. This method can be used to obtain reliable estimates of the size and shape of micropores on a chromatographic adsorbent surface. The fact that these estimates agree with the results of adsorption chromatographic measurements at non-zero coverage (Figure 2) supports the conclusion regarding the applicability of the method to the study of surface-porous adsorbents.

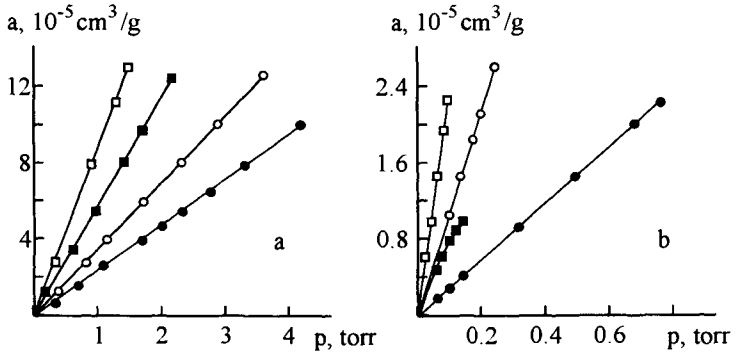

Figure 2. Adsorption isotherms for hydrocarbons on the non-porous adsorbent (a) and on the thermooxidized adsorbent (b): □, n-octane; ■, iso-octane; ○, n-heptane; and ●, n-hexane.

5. MOLECULAR STATISTIC CALCULATIONS OF THERMODYNAMIC FUNCTIONS OF HYDROCARBONS ADSORBED ON LAYER SILICATES

Theoretical molecular statistic calculations of adsorption thermodynamic properties for colloid systems are generally believed to be a quite cumbersome problem. This is mainly

because of an essential irregularity of the structure of such systems, preventing one from introducing a theoretical model, capable of mathematical consideration. In the present case, however, such models can be built and treated using the computational methods described in Section 2; some examples of this approach are presented below.

5.1. Homogeneous surface of modified kaolinite

We begin with a rather simple system and perform the calculations of the thermodynamic characteristics for the adsorption of hydrocarbons on the surface of a non-porous layer silicate, in particular, a structurally imperfect kaolinite modified with octadecylammonium chloride.

Using the value of the specific surface area of the kaolinite specimen prior to modification (70 m^2/g), the area occupied by each cation (1.2 nm^2) and the amount of adsorbed modifier, we have estimated the thickness of the modifying layer covering the surface of the silicate, assuming that no defects exist in this layer. The resulting values, together with the experimental data on the Henry's constants and the differential heats of adsorption obtained as reported in [47] are listed in Table 10 for the two specimens considered.

Table 10
Experimental and calculated values of the Henry's constants K_1 (μm) and differential heats of adsorption Q_a, (kJ/mol) of n-hexane on octadecylammonium-modified kaolinite possessing different amounts of presorbed modifier a (mmol/g), corresponding to different surface occupation coefficients n (layers) at 393 K [47]

Experimental values			Calculated values		
a	K_1	Q_a	n	K_1	Q_a
0.27	0.11	30	3	0.107	28.7
0.50	0.10	28	5	0.104	28.7

In the table, it can be seen that the adsorption characteristics remain virtually unchanged when the thickness of the layer of modifying cations is increased by a factor of almost two. Hence, since the adsorbed molecules are separated quite considerably from the surface of the original layer silicate, we conclude that it is interaction with the modifier which contributes mainly to the thermodynamic characteristics of adsorption, while details of the adsorbate - silicate interaction potential play only a marginal role.

We had taken this fact into account in performing the calculations for the thermodynamic quantities. The model adopted for this system was the basal plane of the kaolinite covered with three or five monolayers of octadecylammonium cations in their *trans* conformation closely packed with each other. This implies the existence of atomic sheets in the modifying layer as well as in the silicate layer nearest to the surface; the deeper silicate layers were included into the calculations in the bulk approximation. The data [11] were used for the BC potential coefficients employed for the interaction between the H and C atoms of the adsorbate molecule and H and C atoms of the modifier alkyl chain; for the coefficients describing the interaction between the alkane atomic species and the ions constituting the silicate lattice, we used the values reported in [13]. The coefficients for the interaction with the N atom in the modifying layer were estimated using the quantum-

mechanical relationships (see, for example, [12,48]).

The values of the coefficients used are summarized in Table 1 and the results obtained from the calculations for the model considered using the program described above are presented in Table 10, showing good agreement with the experimental chromatographic data. It should be noted that the contribution of the inorganic silicate matrix amounts to about 30% of the value of the total differential heat; at the same time, the 5% variations in the values of the alkane-silicate interaction coefficients $C^{(BC)}$, $D^{(BC)}$ and $B^{(BC)}$ do not affect the possibility of matching the resulting thermodynamic characteristics to those calculated, thus supporting the considerations discussed above. Again the values of the LJ potential coefficients (Table 2) were adjusted to match the results of the calculations using the BC potential.

5.2. Side surface of a swelling layer silicate

We now proceed to the subject of our main interest, the adsorption of hydrocarbons on the microporous surface of disperse silicates. A swelling silicate montmorillonite will be considered as an example of an adsorbent for which a significant increase in the retention volume and in the calculated Henry's constant occurs when the degree of modification increases, the heat of adsorption remaining virtually unchanged. It will be shown that this behaviour may be ascribed to preferential adsorption of hydrocarbon molecules in long micropores formed on the side surface of the mineral crystallites during the modification of swelling layer silicates.

The assumptions used in the model are as follows. It was shown in Section 3.1 that during the substitution of metal cations (which connects separate layers of the montmorillonite) with organic alkylammonia or alkylpyridinium cations, the separation between the aluminosilicate layers increases due to the formation of mono- or poly-layers of the modifier in the interlayer gaps. The amount of presorbed modifier for the adsorbent considered is sufficient for each successive block (i.e. the aluminosilicate layer covered with the modifier monolayer) of such 'multisandwich' structure to be separated from its neighbour by an extra monolayer of organic cations, i.e. the interlayer gap is three-times as wide as the alkyl chain width. From simple structural considerations it is clear enough that the intermediate submonolayer is more deficient than the monolayers adjacent to the silicate layers, with this monolayer defects being concentrated at their boundaries on the microcrystallite surface thus forming a system of long parallel micropores on this surface. The free cross-sectional width of the micropore openings is equal to the width of an alkyl chain (0.44-0.46 nm), the length of the micropores being limited by the characteristic microcrystallite size. The silicate layer thickness (0.94 nm) and triple the width of the alkyl chain constitute the total period (2.2 nm) of such a porous structure. This d_{001} value is characteristic for the cetylpyridinium montmorillonite, processed with the triple quantity of the modifier with respect to the exchange capacity. The excess of the modifier was then washed out, thus the final amount of the adsorbed modifier was a $\sim$ 1.1 mmol/g.

To support the considerations regarding the porous surface structure presented above, we have calculated a molecular-statistical estimate of the mean micropore depth using the model described above. The experimental results, theoretical results and the estimates are summarized in Table 11, reproduced from [49]. Note that in this case polarization interaction does not contribute significantly to the total energy since the mineral surface is covered by a layer of the modifier. The software package presented in section 2.3 was

Table 11
Experimental, calculated and estimated values of Henry's constant K_1 (μm) and differential heat of adsorption Q_a (kJ/mol) for n-hexane adsorbed on montmorillonite modified by cetylpyridinium (1.1 mol/kg) at 393 K

Evaluation method and conditions	K_1	Q_a
Experimental	0.60	36.4
Calculation for basal (non-porous) surface	0.12	29.7
Estimate for side surface	1.1	37.2
Calculation for side surface:		
pore depth = 0 nm	0.132	30.0
pore depth = 0.4 nm	0.027	29.5
pore depth = 0.55 nm	0.275	41.1
pore depth = 0.7 nm	5.053	75.1

used to calculate the thermodynamic characteristics of hexane adsorption on the basal homogeneous (non-porous) modified montmorillonite surface; then from the experimental chromatographic values, common thermodynamic relations, and the structural data [10] showing that the total basal surface is approximately equal to the total side surface, it was straightforward to estimate the thermodynamic functions characteristic for the side (microporous) adsorbent surface.

Next we performed a series of calculations of the thermodynamic functions associated with adsorption on a model microporous surface using different values of the mean pore depth; the software package described in section 2.4 was used. On comparing the calculated values with those estimated, it can be seen that the $K_1 \sim 1.1\mu$m value corresponds to a mean pore depth of the order of 0.6 nm, while the matching Q_a value requires a slightly smaller depth value of 0.5 nm. An independent estimation of the mean pore depth based on a comparison of the specific surface values with respect to hexane for non-modified and alkylpyridinium-modified montmorillonite [27] led to a pore depth value of the order of 1 nm, which is in good agreement with the molecular-statistical estimate given above.

The distribution of $\chi_i^{(a)}$ values over the conformations, calculated according to Eq. (6), had shown, rather predictable, that almost all adsorbed molecules exist in their *trans* conformation, matching the pore openings.

Thus the molecular-statistical calculations based on the microscopic model of the side surface of a swelling layer silicate with only one adjustable parameter, i.e. the mean pore depth, lead to a quite satisfactory agreement with the experimental data, supporting the reliability of the assumptions concerning the surface structure of modified layer silicates.

5.3. Ribbon-layered silicate: polarization interaction

A much wider class, however, is presented by adsorbents where the adsorbed molecules interact directly with the inorganic mineral surface. In this case, a simple account of dispersion attraction and short-range atom-atom repulsion forces would not suffice, for polarization interaction is expected to play a major role. The corresponding approach employed will be demonstrated using the molecular-statistical interpretation of the expe-

rimental data shown in Table 5 for the thermodynamic characteristics for the adsorption of n-hexane on the microporous surface of dehydrated palygorskite.

The structure of the ribbon-layer silicate, palygorskite, is built of staggered blocks. Such blocks are formed from two networks of silicon-oxygen tetrahedra connected by an octahedral network containing hydroxyl groups and coordinatively linked water molecules [1]. Thus the chessboard- like cross-section of the crystal contains blocks and channels, with the crystallographic channel dimensions for palygorskite dehydrated at 393 K being equal to 0.90 × 0.65 nm, corresponding to a free section of 0.64 × 0.37 nm dimensions. These channels are too small for linear hydrocarbon molecules to penetrate into them and adsorption thus takes place preferentially on the external mineral particle surface [16].

This external surface can be considered as being formed by the destruction of the crystal along the edges of the ribbons, i.e. breakage of weak edge Si-O-Si bonds with subsequent saturation of the released valence bonds by protons. The resulting surface possesses a repeating micropore relief, with the surface micropores characterized by a width of 0.70 nm (the crystallographic channel width minus the double OH bond length) and a depth of 0.65 nm. The adsorbate molecules are capable of direct contact with the silicate surface and for such a system the polarization contribution to the total potential energy value cannot be neglected. This contribution arises from the electrostatic field of the adsorbent surface associated with the distribution of charges, in particular, those of the polar SiOH groups located on the micropore edges and of water molecules linked with coordinatively unsaturated Mg^{2+} cations at the pore walls.

To determine the charges of lattice ions, quantum-chemical MNDO calculations were performed. Two cells were considered, one with and the other without isomorphic substitution of Al for Si in the basal tetrahedral layer, with a compensating Na^+ ion being introduced into the substituted cell. The average values of charges used for the molecular-statistical calculations were derived on the assumption that the relative percentage of both types of cell in the lattice is 1:7 [50]. The average charges were –0.61 e for the oxygen ions in the tetrahedra, +1.40 e for the Si and Al ions in the tetrahedral coordination, +0.25 e for the H ions compensating the broken bonds on the edges and –0.25 e for the intralayer hydroxyl groups. The compensating Na^+ ion charge was found to be +0.50 e; thus the average compensating ion charge per unit cell was taken to be equal to +0.06 e. The atomic charges of the bonded water molecule were put equal to those of the free water molecule, the average charge for the ions in the octahedral coordination being found from the requirement for electroneutrality.

Table 12 summarizes both the experimental data [16] and our theoretical estimates of the adsorption heat; here again the software package described in section 2.4 was used. It is seen that polarization interaction contributes significantly to the total value, substantially improving the agreement between the observed and calculated values. The two values listed in the table for the polarization interaction differ in that the more accurate one was obtained with the approximation in which the charge distribution in the immediate vicinity of the pore was accounted for by using homogeneously charged atomic *lines*, whereas that giving a slightly worse value employed an approximation involving homogeneously charged atomic *sheets*, cf. Eqs. (31,32). Thus, as the thermodynamic characteristics obtained depend significantly on the presence of the polarization interaction component, despite being insensitive to the detailed adsorption potential profile, it may be concluded that the good agreement observed between the calculated and measured

Table 12
Differential heat of adsorption Q_a (kJ/mol) of n-hexane on a palygorskite surface at 400 K

Evaluation conditions	Q_a
Polarization interaction excluded	48.0
Polarization interaction included:	
atomic sheets	88.3
atomic lines and sheets	83.6
Experimental	75.6

values is not accidental but presents strong evidence to support the correctness of the model employed.

Once more the molecular-statistical method based on a microscopic model of the microporous adsorbent leads to quite satisfactory agreement with the experimental data provided that the essential interactions of the adsorbed molecule with the adsorbent surface, including polarization and dispersion attraction, and short-range atom-atom repulsion, are taken into account.

6. NEW CHROMATOGRAPHIC ADSORBENTS AND SUPPORTS BASED ON LAYER SILICATES AND SILICA

We have developed the method [51,52] and technology [53] for the preparation of the chromatographic adsorbent Benton-80, based on the cetylpyridinium montmorillonite. It was shown [51-54] that this adsorbent possesses an enhanced separation characteristics with respect to the isomers of xylene in the mixtures with ethylbenzene, the isomers of cresol in the mixtures with phenol, α-olefins of the C_{14}-C_{18} series and other mixtures of substances with near boiling points, as compared with the organobentonite adsorbents Benton-18, Benton-34 and Benton-245.

New methods to improve the separation properties of the organomontmorillonites can also be proposed. For example, it was shown in Section 4 that the introduction of Cs^+ cations into the exchange complex of layer silicates, followed by the modification of the mineral by long-chain organic cations, results in the development of surface micropores on side faces of the adsorbent particles. This, in turn, leads to the increase of the adsorption sites, where the chromatographic separation of hydrocarbons takes place.

We had used this fact to develop a new efficient gas chromatographic adsorbent, the Cesium/cetylpyridinium montmorillonite (Cs-CPM), containing 0.15 meq/g of Cs^+ cations and 0.85 meq/g of cetylpyridinium cations in its exchange positions [55]. This adsorbent was imposed on an inert support together with the stationary liquid phase (SLP), namely, the polyphenylmethylsiloxane (PPMS) liquid, the dibutyltetrachloroterephtalate, 1,2,3-trans-(2cyanethoxy)propane in an amount of 3-15% mass. The Cs-CPM to SLP ratio was (2-3):1.

An efficient separation of the artificial and technical mixtures of the isomers of cresol, dichlorobenzene, mono-, di-, and trichlorotoluene demonstrates high chromatographic pro-

perties of the microporous Cs-CPM adsorbent. The data presented in Table 13, summarizing the results of [42,56], show that this adsorbent, used in combination with the PPMS SLP, is capable to separate completely the hardly separable isomers of trichlorotoluene, to achieve a high separation degree with respect to the isomers of monochlorotoluene and 3,5-/2,6-dichlorotoluene, and to separate partially the isomers of 2,6-/2,4-dichlorotoluene, all these being the mixtures unidentifiable on the chromatographic packings known. The separation criterion Ψ was calculated as in [57]. It is also seen in the table that the separation properties of the Cs-CPM adsorbent columns are considerably better than those of the Ca-CPM adsorbent columns.

An important advantage of the developed chromatographic adsorbent is that, in addition to satisfactory express-analytical characteristics, it possesses the 'general purpose' separation properties, while the SLPs traditionally used enable one to perform the separation of the isomers of one group of substances only, and with the larger retention time, see Table 13. The data presented in [38] show that this adsorbent possesses high selectivity with respect to the chromatographic separation of isomeric alkyl-, alkylchloro-, and chlorosubstituted benzenes (Fig. 3) and in the chromatographic analysis of the multicomponent mixture of the isomers of hydrocarbons and chlorated hydrocarbons present as the impurities in the technical 1,2-dichloroethane [58].

Table 13
Separation criterion Ψ and elution time t (min) for the isomers of mono-, di-, and trichlorotoluene

Packing composition	Monochlorotoluenes			Dichlorotoluenes			Trichlorotoluenes		
	m-: p-	o-: m-		3,5-: 2,6-	2,6-: 2,4-		2,3,6-: 2,3,5-	2,3,5-: 2,4,5-	
	Ψ		t	Ψ		t	Ψ		t
Cs-CPM + PPMS-4 + inert support	0.91	0.96	42.5	0.44	0.98	47.5	1	1	49.2
Ca-CPM + PPMS-4 + inert support	0.13	0	31.7	0	0.35	38.5	0	–	32.5
PPMS-4 + inert support	0	0	–	0	0	–	0.81	0	133

The method of liquid phase modification of silica by the solutions of organosilicon olygomers in toluene, followed by thermofixation of the modifier at 250-350°C was used in the preparation of inert thermostable chromatographic supports [35,59]. After the thermal, or acid and thermal pretreatment, the diatomite (Porochrom, Armenia, or Chromaton N-AW, Czech Republic) was subjected to the modification with the amount of polyethylhydrosiloxane (PEHS) or polymethylhydrosiloxane (PMHS) corresponding to 2.5 mg of organic substance per 1 m^2 of the surface.

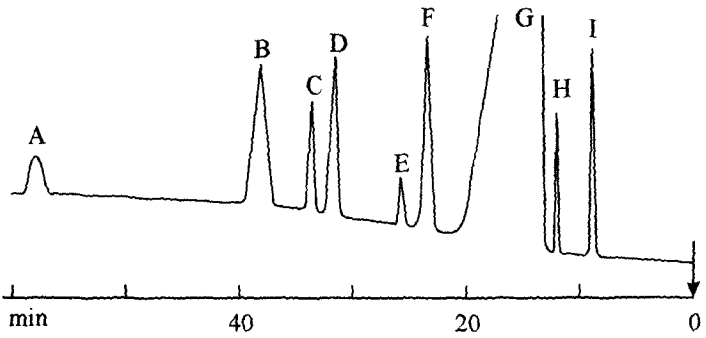

Figure 3. Chromatogram of technical 1,4-dichlorobenzene (G) and detected organic impurities: 1,2,3-trichlorobenzene (A), tetradecane (B), 1,2,4-trichlorobenzene (C), 1,2-dichlorobenzene (D), 1,3,5-trichlorobenzene (E), 1,3-dichlorobenzene (F), 4-chlorotoluene (H) and chlorobenzene (I) on the adsorbent containing 7% Cs-CPM, 3% dinonylphtalate; support - Chromaton N-AW-DMCS.

Table 14 summarizes the data obtained in [59,60]. Here the chromatographic characteristics of the supports modified using the liquid phase method, are compared with those of the Chromaton N-AW support modified with dimethylchlorosilane (DMCS) from the gas phase. The degree of surface deactivation was calculated from the peak asymmetry factor A_s measured at 0.1 peak height. The efficiency of the chromatographic column was estimated from the value of the equivalent theoretical plate height (ETPH). The supports were loaded into the columns without the stationary liquid phase.

Table 14
Chromatographic characteristics of initial and modified diatomite supports

Modifier	A_s		ETPH	
	Benzene	Ethanol	Benzene	Ethanol
		Porochrom		
None	11.0	58.1	2.9	84.1
PEHS	1.2	2.8	0.9	0.8
PMHS	1.1	1.8	0.8	0.9
		Chromaton N-AW		
None	2.9	41.6	1.7	45.6
PEHS	1.0	1.9	1.0	1.0
PMHS	1.1	1.7	0.9	0.9
DMCS	1.2	7.9	1.1	1.5

The advantages of the liquid phase modification method using the organosilicon oligomers as compared to the modification with Chromaton N-AW-DMCS are clearly seen from the table. Moreover, the modification of the low quality diatomite support (Armenia)

results in the material with the properties superior to the reference sample.

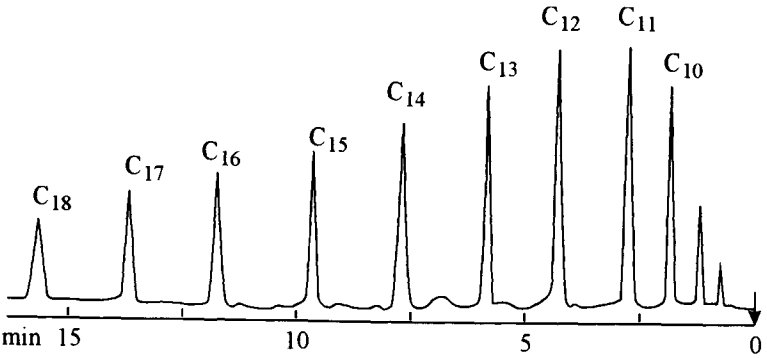

Figure 4. Chromatogram of mixture of alcohols on the column containing 5% silicone rubber and diatomite support modified by polyethylhydrosiloxane.

Fig. 4 illustrates the remarkable efficiency of the supports with respect to the separation of the mixtures of C_{10}-C_{18} alcohols [38].

An important performance characteristic of the supports, the thermal stability, was further improved using the thermooxidation of the modifying layer at 300-350°C [60]. The splitting out of the organic radicals made it possible to increase significantly the degree of 'sewing together' the chemisorbed olygomer molecules, leading to the decrease of the adsorption activity of the modified support, as the residual hydrophilic sites on its surface became virtually blocked off (the data presented in Table 4 show the decrease of the q and the increase of the w_{H_2O} values for the thermooxidized sample as compared to that modified without the thermooxidation). The thermooxidation of the modified layer provides also the sharp increase of the thermal stability of the product due to the bonding of the silicon atom with three oxygen atoms.

7. CONCLUSIONS

The comprehensive approach to the study of structural and adsorption-selective characteristics of surface-porous adsorbents is presented. This approach combines the gas chromatographic studies of the adsorption thermodynamics of various hydrocarbons on the organoderivatives of layer silicates and silica in the Henry region, and the molecular statistic methods of the calculations of thermodynamic characteristics of molecules adsorbed on these adsorbents, where the inhomogeneities of the surface are taken into account. It is shown that comparing the experimental data for real adsorbents with the results of calculations for the models of an adsorbent surface, it is possible to draw definite conclusions concerning the portions of surface where the adsorption and separation processes take place in the chromatographic regime.

These studies enabled us to develop new efficient adsorbents and supports based on layer silicates and silica. These materials are shown to be promising for the separation of mixtures of hydrocarbons and their chlorderivatives, alcohols and other substances, widely used in industry.

ACKNOWLEDGMENT

The research described in this publication was performed in part under Grant No. K 37 100 from the Joint Fund of the Government of Ukraine and International Science Foundation.

REFERENCES

1. R.E.Grim, Applied Clay Mineralogy, McGraw-Hill, New York, 1962.
2. R.K.Iler, The Chemistry of Silica, A Wiley - Intersci. Publ., New York, 1979.
3. R.M.Barrer and M.G.Hampton, Trans. Faraday Soc., 53 (1957) 1462.
4. C.T.Cowan and J.M.Hartwell, Nature, 190 (1961) 712.
5. J.V.Mortimer and P.L.Gent, Nature, 197 (1963) 789.
6. M.Taramasso and F.Veniale, Chromatographia, 2 (1969) 239.
7. P.Fuchs and M.Taramasso, Chromatographia, 2 (1969) 551.
8. S.D.Nogare and R.S.Juvet, Gas-liquid Chromatography, Intersci. Publ., New York, 1962.
9. A.V.Kiselev and Ya.I.Yashin, Gas-adsorption Chromatography, Plenum Press, New York, 1969.
10. Yu.I.Tarasevich, Structure and Surface Chemistry of Layer Silicates, Naukova Dumka, Kiev, 1988 (in Russian).
11. A.A.Avgul', A.V.Kiselev, and D.P.Poshkus, Adsorption of Gases and Vapours on Homogeneous Surfaces, Khimya, Moscow, 1975 (in Russian).
12. I.G.Kaplan, Introduction to the Theory of Intermolecular Interactions, Nauka, Moscow, 1982 (in Russian).
13. A.G.Bezus, A.V.Kiselev, A.A.Lopatkin and Pham Quang Du, J. Chem. Soc., Faraday Trans. 2, 74 (1978), 367.
14. Yu.I.Tarasevich, E.V.Aksenenko and S.V.Bondarenko, in: Proc. 5th Conf. Appl. Chem., 1, Hungarian Chemical Society, Budapest, 1989, p.135.
15. M.M.Dubinin, in: Main Problems of the Physical Adsorption Theory, Nauka, Moscow, 1970, 251 (in Russian).
16. Yu.I.Tarasevich and F.D.Ovcharenko, Adsorption sur des Mineraux Argileux, Institut Francais du Petrole, Rueil Malmaison, 1980.
17. R.M.Barrer and D.M.MacLeod, Trans. Faraday Soc., 51 (1955) 1290.
18. R.M.Barrer and K.E.Kelsey, Trans. Faraday Soc., 57 (1961) 452.
19. G.F.Walker, Clay Miner., 7 (1967) 129.
20. R.M.Barrer and K.Brummer, Trans. Faraday Soc., 59 (1963) 959.
21. B.K.G.Theng and D.J.Greenland, J.P.Quirk, Clay Miner., 7 (1967) 1.
22. T.F.Vansant and J.B.Uytterhoeven, Clays and Clay Miner., 20 (1972) 43.
23. M.B.McBride and M.M.Mortland, Clays and Clay Miner., 21 (1973) 323.
24. R.Levy and C.W.Transis, Clays and Clay Miner., 23 (1975) 475.
25. S.V.Bondarenko, Yu.I.Tarasevich and A.I.Zhukova, in: Adsorption and Adsorbents, 6, Naukova Dumka, Kiev, 1978, p.80 (in Russian).
26. F.D.Ovcharenko, N.S.Dyachenko, N.V.Vdovenko, A.B.Ostrovskaya and Yu.I.Tarasevich, Ukr. Khim. Zhurn., 33 (1967) 49.

27. A.I.Zhukova, S.V.Bondarenko, E.V.Sharkina, V.M.Rudenko and Yu.I.Tarasevich, in: Physico-Chemical Mechanics and Lyophility of Disperse Systems, 9, Naukova Dumka, Kiev, 1977, p. 9 (in Russian).
28. S.V.Bondarenko, A.I.Zhukova and Yu.I.Tarasevich, Ukr. Khim. Zhurn., 46 (1980) 370.
29. Yu.I.Tarasevich, S.V.Bondarenko and A.I.Zhukova, Kolloid. Zhurn., 42 (1980) 1128.
30. R.M.Barrer and K.E.Kelsey, Trans. Faraday Soc., 57 (1961) 625.
31. W.H.Slabaugh and G.H.Kennedy, J. Colloid Sci., 18 (1963) 337.
32. Yu.I.Tarasevich, S.V.Bondarenko and A.I.Zhukova, in: Adsorption of Hydrocarbons in Microporous Adsorbents - II, Preprints of the Workshop 22-16 November 1982, Ebersvalde, vol. 1, Acad. Sci. GDR, Berlin, 1982, p.100.
33. W.H.Slabaugh and P.A.Hiltner, J. Phys. Chem., 72 (1968) 4295.
34. G.V.Lisichkin (ed.), Modified Silica in Adsorption, Catalysis and Chromatography, Khimya, Moscow, 1986 (in Russian).
35. S.V.Bondarenko, A.V.Nazarenko and Yu.I.Tarasevich, Ukr. Khim. Zhurn., 52 (1986) 254.
36. M.Trau, B.S.Murray, K.Grant and F.Grieser, J. Colloid Interface Sci., 148 (1992) 182.
37. S.V.Bondarenko and Yu.I.Tarasevich, Kolloid. Zhurn., 50 (1988) 419.
38. Yu.I.Tarasevich, S.V.Bondarenko, A.I.Zhukova, A.V.Nazarenko and E.V.Aksenenko, Pure & Appl. Chem., 65 (1993) 2257.
39. S.V.Bondarenko, A.I.Zhukova, Yu.I.Tarasevich and F.D.Ovcharenko, Dokl. AN SSSR, 215 (1974) 891.
40. A.I.Zhukova, S.V.Bondarenko and Yu.I.Tarasevich, Ukr. Khim. Zhurn., 42 (1976) 708.
41. Yu.I.Tarasevich, G.V.Lantukh, A.I.Zhukova and S.V.Bondarenko, Teoret. i Eksperim. Khimiya, 18 (1982) 470.
42. Yu.I.Tarasevich, S.V.Bondarenko and A.I.Zhukova, in: Proc. 5th Conf. Appl. Chem., Budapest, 1989, vol. 1, p.188.
43. R.M.Barrer and J.S.S.Reay, J. Chem. Soc., No.11 (1958) 3824.
44. Yu.I.Tarasevich, A.I.Zhukova, S.V.Bondarenko and A.V.Nazarenko, Ukr. Khim. Zhurn., 55 (1989) 686.
45. D.W.Breck, Zeolite Molecular Sieves, Wiley. New York, 1974.
46. Yu.I.Tarasevich, A.I.Zhukova, E.V.Aksenenko, S.V.Bondarenko and A.V.Nazarenko, Adsorp. Sci. Technol., 10 (1993) 147.
47. Yu.I.Tarasevich, S.V.Bondarenko, Yu.V.Shulepov and E.V.Aksenenko, Adsorp. Sci. Technol., 6 (1989) 147.
48. I.Machanti and B.W.Ninham, Dispersion Forces, Academic Press, New York, London, 1976.
49. Yu.I.Tarasevich, E.V.Aksenenko and S.V.Bondarenko, Zhurn. Fiz. Khimii, 66 (1992) 712.
50. G.Brown (ed.), The X-ray Identification and Crystal Structure of Clay Minerals, Mineralogical Society, London, 1961.
51. A.I.Zhukova, S.V.Bondarenko and Yu.I.Tarasevich, Neftekhimiya, 21 (1981) 765.
52. N.S.Nikitina, Yu.I.Tarasevich, Yu.G.Nikulichev and A.E.Mysak, Neftekhimiya, 24 (1984) 700.

53. Yu.I.Tarasevich, Yu.G.Nikulichev, S.V.Bondarenko, N.S.Nikitina, A.E.Mysak and A.I.Zhukova, in: Petrochemistry and Petroleum Processing, 32, Naukova Dumka, Kiev, 1987, p.53 (in Russian).
54. S.V.Bondarenko, A.I.Zhukova and Yu.I.Tarasevich, J. Chromatogr., 241 (1982) 281.
55. Yu.I.Tarasevich, A.I.Zhukova, S.V.Bondarenko and A.V.Nazarenko, Ukr. Khim. Zhurn., 55 (1989) 686.
56. A.I.Zhukova, V.S.Kozlova, S.V.Bondarenko and Yu.I.Tarasevich, Zhurn. Prikl. Khimii, 62 (1989) 1311.
57. M.S.Wigderhouse, M.I.Afanasiev and K.A.Golbert, Uspekhi Khimii, 32 (1963) 754.
58. S.A.Arystanbekova, A.I.Zhukova, Yu.I.Tarasevich, S.V.Bondarenko, Z.M.Rivina and V.I.Rozhkov, Ukr. Khim. Zhurn., 57 (1991) 430.
59. S.V.Bondarenko, A.V.Nazarenko and Yu.I.Tarasevich, Zhurn. Prikl. Khimii, 62 (1989) 1259.
60. Yu.I.Tarasevich, A.V.Nazarenko, S.V.Bondarenko and I.Ya.Pishchaj, Ukr. Khim. Zhurn., 57 (1991) 723.

This Page Intentionally Left Blank

A. Dąbrowski and V.A. Tertykh (Editors)
Adsorption on New and Modified Inorganic Sorbents
Studies in Surface Science and Catalysis, Vol. 99

Chapter 2.10
Micropore filling mechanism in inorganic sorbents

K. Kaneko

Department of Chemistry, Faculty of Science, Chiba University,
1-33 Yayoi, Inage, Chiba 263, Japan

1. INTRODUCTION

There are two types of pores of intraparticle pores and interparticle ones[1]. The *intraparticle pores are in the primary particle itself, while the interparticle pores* originate from the interparticle void spaces. There are many minerals which have intrinsic intraparticle pores. Zeolites are the most representative porous solids whose pores come from the *structurally intrinsic intraparticle pores*. The pore geometry can be evaluated by their crystallographic data. The carbon nanotube of which pore wall is composed of graphitic sheets is also the *structurally intrinsic intraparticle pore* [2]. There are other types of pores in a single solid particle. Modification of intrinsic particle structures by specific evolution, leaching, and reaction procedures can create pores in solid particles. Porous metal oxides are produced by decomposition of their hydroxides. Acid treatment of sodium silicate glass creates pores due to leaching of sodium ions. Activated carbons of the most popular adsorbent are obtained by the activation reaction of carbonous materials using H_2O or CO_2. Thus, the modification also provides intrinsic intraparticle pores, although particles are not necessarily crystalline.

These modification methods can be widely applied to produce other types of porous solids. If we embed a foreign substance in the solid particle in advance, evolution or dissolution of the embeded substance leads to the pore. Also when pore-forming agents are introduced in the solid particle, pores are created. The intercalated graphites and pillared clays contain foreign substances in their structures, and then those pores should be designated *extrinsic intraparticle pores*. Primary particles stick together to form a secondary particle, depending on their chemical composition, shape, size, and their surrounding conditions. This secondary particles have interparticle pores. Silica gel is a representative of an interparticle porous material. Activated carbons having injected intrinsic-intraparticle pores are representative inorganic adsorbents[3-5]. They have been widely used in various technologies. Activated carbons are prepared from various precursors such as coconut shells, certain woods and coal. Granulated or formed activated carbons are produced from bituminous coals. The precursors are carbonized at about 800 K in an inert atmosphere, and then activated at about 1200 K in steam or CO_2 or mixtures of these. Carbonization and activation of the precursor materials develop the disordered micrographitic structure having slit-shaped pores. The principal pores in activated carbons are micropores whose

width is less than 2 nm, although activated carbons have not only micropores but mesopores (2nm < pore width < 50 nm) and macropores (pore width > 50 nm)[6,7]. As a micropore has a stronger adsorptive field than a flat or mesoporous surface, a marked enhanced adsorption proceeds even at a low relative pressure region. The adsorption by micropores is called micropore filling. The excellent adsorptive properties of activated carbons for a diluted system come from the enhanced adsorption field of micropores.

Recently activated carbons such as activated carbon fibers (ACFs) and superhigh surface area carbons have been developed. New activated carbons have more uniform micropore size distribution and greater surface area than traditional activated carbons. The carbon membranes for gas separation have been also developed lately[8]. The activation of the polyamide film leads to self-supported activated carbon film whose surface area is larger than 1100 m^2/g [9]. Thus various kinds of carbon adsorbents have been developed to find new applications. Scientific studies on activated carbon have been increasing according to development of these new carbon adsorbents with a special relevance to energy and environmental demands. In particular, controll of an adsorptive ability of activated carbon is requisite for new application. Consequently, basic principles for control of the micropore filling mechanism of activated carbons are shown here.

2. VAPOUR AND SUPERCRITICAL GAS IN MICROPORE FILLING

The van der Waals equation describes the critical phenomena of vapour to supercritical gas or fluid. Below critical temperature T_C gas which coexists with the liquid phase is called a vapour. Vapor has own saturated vapour pressure P_0. Then we can use the relative pressure P/P_0 for description of adsorption. Fundamentally, physical adsorption is valid for vapours [10]. As the molecule-surface interaction of physical adsorption is weak, a sufficient intermolecular interaction corresponding to heat of vapourization is necessary for predominant physical adsorption. Micropore filling is a physical adsorption enhanced by overlapping of the molecule-surface interaction potentials from opposite pore walls and the adsorptive force is the strongest in physical adsorption. Nevertheless, micropore filling is a predominant process only for vapour.

A gas above T_C is called a supercritical gas. As microporous materials are slightly effective for adsorption of a supercritical gas, there are great interests in adsorption of a supercritical gas by micropores. Not only pressure swing adsorption (PSA) technology for air, but also new technologies such as supercritical drying, supercritical extraction, and natural gas storage need further understanding of the supercritical gas adsorption by microporous solids. Although micropore filling cannot induce a predominant adsorption of the supercritical gas in almost cases, the supercritical gas can be adsorbed only by micropores enough narrow to have the strong molecule-surface interaction energy compared to the thermal energy. Basically, we cannot describe adsorption of the supercritical gas by microporous solids with the aid of a well- established adsorption equation such as the Dubinin-Radushkevich (DR) equation, because the saturated vapour pressure cannot be defined for the supercritical gas. The concept of the saturated vapour pressure is indispensable to thermodynamic description of gas adsorption, because bulk liquid is used as the standard state. Dubinin estimated the saturated vapour pressure of the supercritical gas as an adsorptive by extrapolation of the pressure vs. temperature relationship [11].

However, we need a more physical basis on the concept of the saturated vapour pressure for the adsorptive of the supercritical gas. When we use the molecular statistical approach to description of adsorption for the supercritical gas, the saturated vapour pressure is not necessarily indispensable. The distinction between vapour and supercritical gas can be taken into account through the intermolecular and molecule–surface interaction energies [12–15]. Nevertheless, it is better to discuss the micropore filling mechanisms for vapour and supercritical gas separately in order to obtain each physical picture.

3. STRONG ADSORPTION FIELD OF MICROPORES

The interaction between an admolecule and a surface atom as a function $\Phi(r)$ of the distance r between them can be expressed by the Lennard–Jones potential

$$\Phi(\mathrm{r}) = 4\varepsilon_{\mathrm{sf}} \left[(\sigma_{\mathrm{sf}}/\mathrm{r})^{12} - (\sigma_{\mathrm{sf}}/\mathrm{r})^{6}\right] \tag{1}$$

where $\varepsilon_{\mathrm{sf}}$ and σ_{sf} are the well depth and effective diameter for the admolecule–graphitic carbon atom. These cross parameters are calculated according to the Lorentz-Berthelot rules, $\varepsilon_{\mathrm{sf}} = (\varepsilon_{\mathrm{ss}}/\varepsilon_{\mathrm{ff}})^{1/2}$; $\sigma_{\mathrm{sf}} = (\sigma_{\mathrm{ss}}+\sigma_{\mathrm{ff}})/2$. Here, ($\sigma_{\mathrm{ss}}$, $\varepsilon_{\mathrm{ss}}$) and ($\sigma_{\mathrm{ff}}$, $\varepsilon_{\mathrm{ff}}$) are the Lennard-Jones parameters for a surface atom and a molecule, respectively. The interaction potential $\Phi(\mathrm{z})$ for an admolecule and a single graphite slab is given by the Steele 10–4–3 potential [16]

$$\Phi(\mathrm{z}) = 2\pi\rho_{\mathrm{C}}\varepsilon_{\mathrm{sf}}\sigma_{\mathrm{sf}}^{2}\Delta \left\{(2/5)(\sigma_{\mathrm{sf}}/\mathrm{z})^{10} - (\sigma_{\mathrm{sf}}/\mathrm{z})^{4} - \sigma_{\mathrm{sf}}^{4}/\left[3\Delta(0.61\Delta + \mathrm{z})^{3}\right]\right\} \tag{2}$$

where z is the vertical distance of the admolecule above the surface, $\Delta = 0.335$ nm is the separation between graphite layers, $\rho_{\mathrm{C}} = 114/\mathrm{nm}^2$ is the number of carbon atoms per unit area in a graphite layer. The exponent 10 and 4 terms denote the repulsive and attractive interactions of the molecule with the surface graphite plane, while the exponent 3 term results from the summation of the attractive part of the potential over the subsurface layers of the graphite. As the micropores of activated carbon can be approximated by the slit spaces between the predominant basal planes of micrographitic units, the whole interaction potential $\Phi(\mathrm{z})_{\mathrm{pore}}$ of a molecule with the micropore of an inter–graphite surface distance H can be given by Eq. (3):

$$\Phi(\mathrm{z})_{\mathrm{pore}} = \Phi(\mathrm{z}) + \Phi(\mathrm{H} - \mathrm{z}) \tag{3}$$

Consequently, we can evaluate the potential profile of the molecule adsorbed in the graphitic micropore. Here H is not the effective pore width w determined by the adsorption experiment. The relationship between H and w is expressed by Eq. (4) [15]:

$$\mathrm{H} = \mathrm{w} + 0.8506\sigma_{\mathrm{sf}} - \sigma_{\mathrm{ff}} \tag{4}$$

In the case of the N_2–graphitic slit pore system, w is equal to H – 0.24 nm. Fig. 1 shows potential profiles of a N_2 molecule in a slitlike graphite pore as a function of w using the one–center approximation. Here, the molecular position in Fig. 1 is expressed by a distance z from the central plane between two surfaces.

The solid line shows the potential profile for the single graphite surface. The potential becomes deeper with decrease in the w value. The potential profile has double minima for

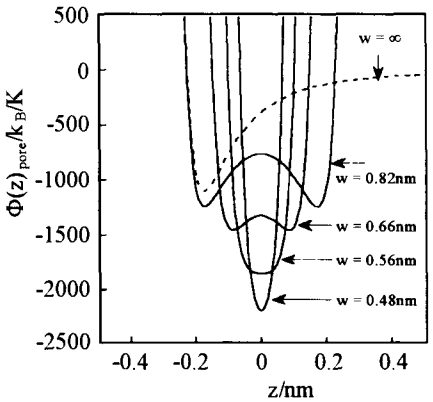

Figure 1. Potential profile of N_2 molecule adsorbed in a slitlike pore with different width as a function of vertical distance of adsorbate above the surface z.

w > 0.6 nm, but a narrower pore has a single potential minimum. Thus, micropores have stronger adsorption fields than flat or mesoporous surfaces, giving the type I adsorption isotherm, i.e. an enhanced adsorption at a low relative pressure range, which is called micropore filling. The micropore filling is distinguished from capillary condensation, that is, molecular adsorption by mesopores. As activated carbon has abundant micropores, it shows an excellent adsorption characteristics even for a diluted component gas.

We can estimate the effective pressure from the potential profile; molecules confined in the slitlike pore of 1 nm in width are presumed to be exposed to the high pressure of 100 MPa. Also application of the Laplace equation to estimate the pressure difference across the adsorbed liquid-gas interface gives 20 MPa for N_2 and 140 MPa for H_2O[17]. Therefore, the graphitic micropore can offer the high pressure field from the macroscopic view.

As the interaction potential at the mid-point of the slitlike pore is the deepest in the pore of w < 0.6 nm and it is not seriously different from the double minima even for w > 0.6 nm, molecular potential for a molecule in the micropore can be approximated by the potential at the mid-point of the slitlike pore. The molecular potential indicates the presence of the inherent micropore of the volume of W_L for each adsorptive. Here the inherent micropore must have sufficiently strong molecular field in comparison with the thermal energy at a measuring temperature. The inherent micropore volume W_L for vapour molecules is almost equal to the micropore volume W_0 obtained from N_2 adsorption at 77 K (Gurvitch rule); W_L for a supercritical gas which depends on the molecule-surface interaction can be evaluated as the saturated amount of adsorption from the Langmuir plot and W_L is less than W_0 in general.

If we control the micropore filling of activated carbon, we must change the factors relating to Lennard-Jones parameters of ε_{sf} and σ_{sf}. Hence control of both geometrical and chemical structures of the micropore sensitively affects the interaction potential. The chemical structure of the micropore wall can be modified by chemical reaction, thin film coating, and partial deposition of other substances. As adsorption by micropores is often

a diffusion–determining process and molecular association changes the gaseous state of supercritical gas to vapour, a chemical modification of not only micropore walls, but also the external surface can play an important role in the micropore filling control.

4. ANALYSIS AND CONTROL OF MICROPORE FILLING OF VAPOUR

4.1. Multi–stage micropore filling of N_2 vapour

The potential profile of N_2 in the graphitic slit pore of w > 0.6 nm has double minima, indicating the presence of monolayer adsorption on each micropore wall. As the barrier height between the double minima of the micropore of w > 0.7 nm is greater than 77 K, a distinct monolayer adsorption on each pore wall occurs in micropores of w > 0.7 nm. The predominant monolayer adsorption occurs at the low relative pressure region compared with the monolayer adsorption on the flat surface, because the N_2–graphitic surface interaction in micropores is greater than that on the flat surface. In the case of micropores having w > 1 nm, N_2 molecules should be adsorbed in the space between monolayers on both micropore walls after monolayer adsorption. Then, we can presume that in micropore filling of N_2 by micropores of w > 1 nm, there are two elementary processes monolayer adsorption on each micropore wall and filling in the residual space between the opposite monolayers on micropore walls. The separation of these elementary processes depends on the height of the potential barrier between double minima. In the micropores of w < 0.7 nm, which are called ultramicropores, a single layer or double layers can be formed between two graphitic walls. There should be a multi–stage micropore filling process on the real activated carbon having pore size distribution.

The recent Monte–Calro Grand Canonical Ensemble simulation studies support this two– stage model of micropore filling of N_2[13,18]. Fig. 2 shows the simulated N_2 adsorption isotherm of a graphitic slitlike pore of 1 nm in width at 77 K and the snapshots of the adsorbed system at different relative pressures. Simulations were performed using the Lennard–Jones parameters of ε_{ff}/k = 95.2 K and σ_{ff} = 0.375 nm for the a single center model of N_2 and the Steele 10–4–3 potential. There are two steps in the adsorption isotherm. The snapshots correspond to adsorption states below and above the adsorption step. These snapshots clearly show that the low and high pressure adsorption steps are due to monolayer adsorption on each micropore wall and filling adsorption in the residual space between the monolayers, respectively. If the micropore width is less than 0.7 nm, there is only a single adsorption step in the low pressure region. In the greater micropores of w > 1.3 nm, the low pressure step is less evident, while the high pressure one is greater.

Although the comparison of the simulated adsorption isotherm with the observed one is helpful to understand the micropore filling mechanism, we need a powerful experimental approach to analysis of micropore filling. The comparison plot is one of effective analyses. This is because activated carbon has the pore size distribution more or less, making the adsorption jump obscure. Sing, Atkinson and McLeod [19,20] proposed the two stage model of primary micropore filling and cooperative micropore filling for the micropore fillling mechanism with the aid of α_s– analysis. However, they did not sufficiently analyze the small α_s region. As the enhancement of adsorption by the micropore field is observed below an α_s value of 0.5, the micropore filling mechanism should be examined by the high resolution α_s–plot. Kaneko extended Sing's method and showed that there are two

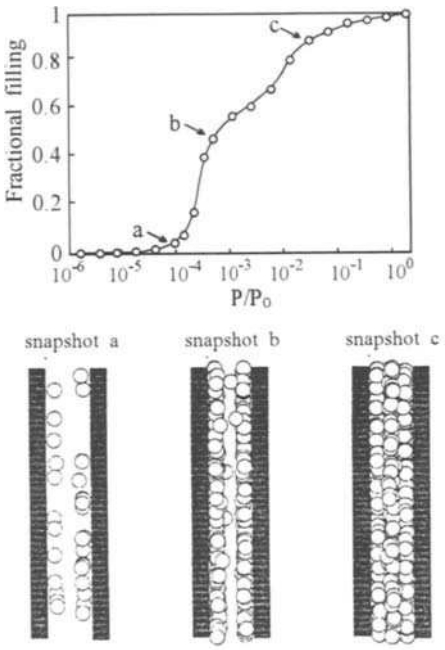

Figure 2. Simulated N_2 adsorption isotherm of a grafitic slitlike pore of 1 nm width at 77 K and snapshots of different stages.

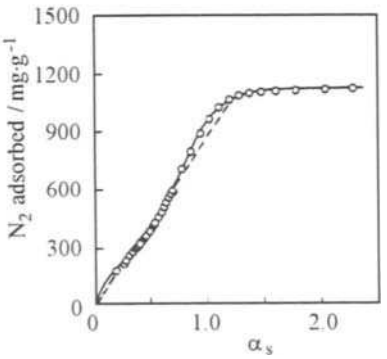

Figure 3. High resolution α_s–plot of activated carbon fiber (ACF).

upward swings from linearity of the α_s plot below saturation of micropores ($\alpha_s < 1$). The upward swing ("filling swing") in the lower region ($\alpha_s < 0.3$, here $\alpha_s = 0.3$ corresponds to $P/P_0 = 0.001$) originates from the monolayer adsorption enhanced by the micropore field, while another upward swing ("condensation swing") in the as region of 0.7 ($P/P_0 = 0.13$) to 1 comes from filling of molecules in the residual space between the monolayers on both micropore walls, which should be a kind of capillary condensation [21–23]. Probably the primary micropore filling and cooperative micropore filling correspond to the monolayer adsorption on each micropore wall and filling in the residual pore space. The latter filling process should be different from the representative capillary condensation, as suggested by Sing et al. [6]. It is preferable to use the term of cooperative filling proposed by Sing et al. [6] for the filling process in the residual space after monolayer completion.

The α_s–plot of the high resolution N_2 adsorption isotherm of ACF at 77 K is shown in Fig. 3. The α_s–plot was constructed on the basis of the standard N_2 adsorption isotherm of nonporous carbon black of type II. The N_2 adsorption isotherm is of type I, but there is a gradual increase in adsorption below $P/P_0 = 0.4$. The α_s–plot has two upward swings of "filling" and "condensation" swings. We can observe a linear region ($0.3 < \alpha_s < 0.7$) between two swings, which can be extrapolated to the origin. The measurement of the slope of the linear α_s–plot in $0.3 < \alpha_s < 0.7$ provides the definite surface area of microporous carbons without ambiguity. This method of surface area determination is designated

a subtracting pore effect (PSE) method, because monolayer adsorption occurs even in the micropore and this method removes enhanced effects by the strong micropore field.

4.2. Accelerated bilayer adsorption in micropore filling of He

There were active studies on He adsorption on the flat surface at 4.2 K about 40 years ago, showing the anomalous adsorption behaviour that the apparent BET monolayer capacity is two times of that expected from the real geometrical surface area. Steele took into account the fact that the energy of He atom in the second layer is appreciably larger than the energy of He atom in the liquid at 4. 2 K and proposed the modified BET equation including the first and second adsorbed layer binding strengths; the modified BET equation gave a reasonable monolayer capacity [24].

Kaneko et al. [25–28] have studied He adsorption of activated carbon at 4.2 K in order to develop a new characterization method for ultramicropores in stead of N_2 adsorption. He adsorption almost finishes within 5 min in activated carbon samples having micropores of $w > 0.7$ nm regardless of the low temperature conditions. The He adsorption isotherm has a sharper uptake below $P/P_0 = 0.02$, but the amount of He adsorption approaches to that of N_2 adsorption with the increase of P/P_0. The He adsorption isotherm has no hysteresis. Fig. 4 shows the wide pressure range adsorption isotherms of He at 4.2 K

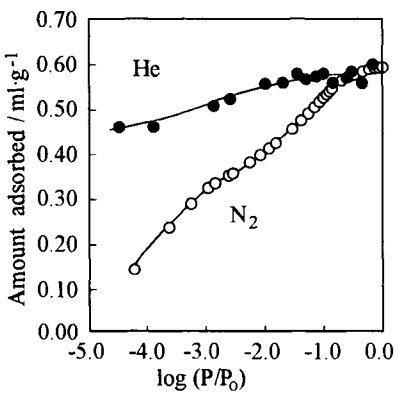

Figure 4. Wide pressure range adsorption isotherms of He at 4.2 K and N_2 at 77 K on ACF.

and N_2 at 77 K on ACF. Here, the amounts of adsorbed He and N_2 are expressed by their volumes using the density (0.205 g/ml) of He adsorbed in the micropore and the liquid density (0.807 g/ml), respectively. The abscissa is expressed by the logarithm of P/P_0. The adsorption amounts of He and N_2 increase with log (P/P_0). The amount of He adsorption becomes much greater than that of N_2 adsorption with the decrease of P/P_0. The significant adsorption difference between He and N_2 should originate from the accessibility of He molecule by an ultramicropore and the accelerated He bilayer adsorption which is observed in adsorption on the nonporous solid.

The He adsorption isotherm is described by the Dubinin–Radushkevich (DR) equation:

$$W/W_0 = \exp\left[-(A/E)^2\right], \quad A = RT\ln(P_0/P), \quad \text{and} \quad E = \beta E_0 \tag{5}$$

Here W is the amount of adsorption at P/P_0, W_0 the micropore volume, E_0 the characteristic energy, and β the affinity coefficient. βE_0 can be associated with the isosteric heat of adsorption, $q_{st,\phi=1/e}$, at the fractional filling ϕ of 1/e using the heat of vapourization, ΔH_v, at the boiling point:

$$q_{st,\phi=1/e} = \Delta H_v + \beta E_0 \tag{6}$$

The β for He was determined as 0.03. If we use the Dubinin–Stoeckli relation of E_0 and the mean half pore-width χ_0 ($\chi_0 E_0$ = constant) [29], the micropore size distribution from He adsorption isotherm can be determined. The micropore size distribution of ACF from He adsorption is often different from that from N_2. In the case of He adsorption, the second layer adsorption is accelerated even on the flat surface, as mentioned above. Consequently, the adsorption isotherm having a significant adsorption is observed even in an extremely low P/P_0 region, which is phenomenologically similar to micropore filling of ordinary vapour molecules. The potential profile change of He in the graphitic slit-pore with the pore width was examined; the enhanced potential effect for He due to overlapping is less important compared with that for N_2. Therefore, it was shown that even He adsorption in the slit-micropore at a low P/P_0 region is described by the modified BET equation proposed by Steele.

4.3. Pore entrance–enriched micropore filling of n–nonane

The surface of activated carbon is divided into the external surface and the pore surface (inner surface). The as plot for the N_2 adsorption isotherm can determine each surface area. It is possible that chemical structures of both surfaces are separately modified. Here it is described that even the control of only the external surface can change dramatically the adsorptive property of activated carbon. Micropore filling is quite effective for adsorption of vapours in general. Then activated carbon is an excellent adsorbent for ordinary organic vapours. However, the strong molecule–surface interaction often prevents completion of filling in whole of micropores. That is, strongly adsorbed molecules near the entrance of micropores block further adsorption. In such a case, it is extremely difficult to attain the adsorption equilibrium, and then only a quasi-equilibrium adsorption isotherm controlled by micropore diffusion is observed. Consequently, elimination of the diffusion limitation is necessary for improvement of adsorption characteristics of microporous solids even in the case of a strongly interacting vapour-solid surface system such as an organic vapour/activated carbon system.

As the micropore diffusion depends on the concentration of adsorptives near the entrance of the micropore, control of the chemical environment of the micropore entrance should be effective for removal of the diffusion limitation in the micropore filling process. n–nonane has been used for evaluation of smaller micropores with the aid of irreversible adsorption, because a n–nonane molecule interacts so strongly with the graphitic surface that n–nonane molecules near the micropore entrance do not diffuse into the interior[30]. This fact is supported by the calculation result that the one-center Lennard-Jones interaction energy of a n–nonane molecule with the graphitic micropore of 1 nm in width is quite large (3300K). Hence, it is difficult to attain the adsorption equilibrium in the n–nonane/activated carbon system at an ambient temperature. The external surface modification with long alkyl groups leads to the rapid adsorption equilibrium for the n–nonane/ACF system [31].

Dried ACF was immersed in a cyclohexane solution of titanium (isopropoxy)tristearate (TTS), $(CH_3)_2CHOTi\ R_3$ (here R = $OC(O)C_{17}H_{35}$) for 3 h at 333 K. TTS reacts with surface hydroxyls of ACF and $-TiR_3$ group replaces with the surface hydroxyl. As the TTS molecule cannot enter the micropore due to a steric restriction, the coverage of the external surface with TiR_3 is determined. As the micropores are partially blocked by TTS molecules, the total surface area decreased by about 30 % for the sample of the external surface coverage of 0.35. However, the micropore width did not change with the TTS-modification.

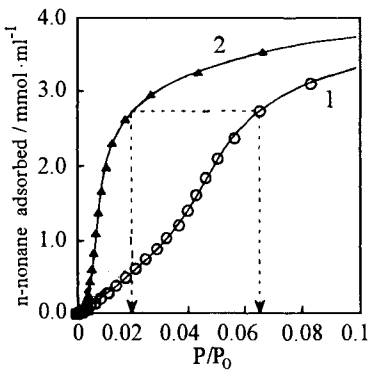

Figure 5. n-nonane adsorption isotherms on ACF (1) and TTS-modified ACF (2) at 303 K.

Fig. 5 shows the low pressure adsorption isotherms of n-nonane by the micropore entrance modified ACF and the pristine ACF. These adsorption isotherms were determined under the almost equilibrium conditions. A remarkable enhancement of n-nonane adsorption with the micropore entrance modification is observed in the low P/P_0 region, although the adsorption amounts at high P/P_0 region almost coincide with each other. The fractional filling of n-nonane at saturation is almost constant irrespective of the surface modification with TTS; the ratios of the saturation n-nonane adsorption W_0(nonane) to the saturation N_2 adsorption $W_0(N_2)$ for the modified ACF and ACF were 0.72 and 0.70, respectively. Thus, the low pressure uptake depends sensitively on the chemical state of the external surface, while the fractional filling at saturation does not change. Consequently, the slight uptake of the pristine ACF should be caused by the limitation of micropore diffusion. The diffusion limitation can be removed by application of n-nonane pressure of $P/P_0 > 0.1$ according to the result shown in Fig. 5. Accordingly, a marked enhancement of low pressure adsorption by the micropore-entrance modification is associated with enrichment of n-nonane molecules at the entrance of the micropore due to favourable interaction of n-nonane with hydrocarbon chains of TTS. The amount of the n-nonane enrichment can be estimated from the comparison of both adsorption isotherms in Fig. 5. With the adsorption amount indicated by the horizontal broken line, the equal amount of adsorption for both samples is obtained at different relative pressures of 0.065 (for ACF) and 0.02 (for TTS-modified ACF). That is, application of $P/P_0 = 0.065$ is necessary for the prescribed adsorption in the case of ACF, whereas the TTS-modified ACF does not need such a high P/P_0. Application of $P/P_0 = 0.02$ is sufficient for the adsorption by the TTS-modified ACF. Thus, the TTS-modification increases the concentration

of n-nonane molecules at the micropore entrance, inducing the micropore diffusion. This principle can be widely applied to other vapours.

4.4. Hydrophilicity or hydrophobicity controlled micropore filling

4.4.1. Hydrated silica-coated activated carbon fiber

The micropore of activated carbon is composed of micrographites, as mentioned before. Basically activated carbon has a hydrophobic nature. Although activated carbon is an excellent adsorbent for organic vapours, it is not effective for adsorption of hydrophilic molecules. Silica gel and zeolite are representative adsorbents for H_2O. Silica gel, however, is a mesoporous solid and it is not effective for adsorption of low concentrated H_2O. On the other hand, zeolite has micropores which can be used for adsorption of H_2O of very low concentration, but the adsorption capacity is not necessarily sufficient. The microporous adsorbent having the adsorption capacity greater than zeolite has been desired. The micropore walls coated with hydrated silica should provide modified activated carbon available for adsorption of H_2O. The example of ACF modified with hydrated silica having a great adsorption capacity for H_2O is given here [31].

The surface of ACF of w = 1.45 nm was modified with molecular adsorption-decomposition method using $SiCl_4$. $SiCl_4$ was adsorbed on the ACF and then hydrolyzed by introduction of H_2O vapour at 298 K. Afterwards, residual $SiCl_4$ and produced HCl vapours were removed, and then the treated ACF was heated at 573 K. The amount of the produced hydrated silica was determined by the measurement of the weight change. The micropore structure of the silica-coated ACF was examined by N_2 adsorption; the t-plot analysis of the N_2 adsorption isotherm showed that the micropore width decreases with the silica coating by 0.2 nm; the silica coating decreased the micropore volume and surface area from 1.49 ml/g and 2280 m^2/g to 0.68 ml/g and 1100 m^2/g, respectively. No spherical silica particles were observed on the external surface of the silica-coated ACF by scanning electron microscopy with a resolution of 10 nm. Therefore, hydrated silica should be deposited entirely on the micropore walls of the ACF.

The remarkable changes due to the silica coating of the micropore walls were observed in adsorptive properties for polar molecules such as H_2O and NH_3. Fig. 6 shows the adsorption isotherms of H_2O on the silica-coated ACF and pristine ACF at 303 K. The adsorption isotherm of H_2O on the pristine ACF shows typical type III character, which is characteristic of weak adsorbent-adsorbate interaction. The amount of H_2O adsorption increases steeply at $P/P_0 = 0.75$. On the contrary, the H_2O adsorption isotherm of the silica-coated ACF is of type IV. A marked enhancement of the H_2O uptake in the low P/P_0 region is observed, directly indicating that the surface of silica-coated ACF becomes hydrophilic. The adsorption isotherm of silica with the same surface area as the silica-coated ACF calculated using the adsorption data in the literature is also shown in Fig. 6 by a broken line. The calculated isotherm is similar to the observed one below $P/P_0 = 0.7$, although the amount of adsorption of the calculated isotherm is considerably lower than observed one by 50 mg/g. The discrepancy becomes significant above $P/P_0 = 0.8$; the calculated isotherm extends even above $P/P_0 = 0.8$, while the observed adsorption is saturated above $P/P_0 = 0.6$. Consequently hydrated silica is uniformly distributed on the ACF pore surface and the entire surface is available for H_2O adsorption and the observed saturation arises from the constraint due to micropore filling. The enhancement

of H_2O adsorptivity by the silica coating at the low pressure region compared with the calculated isotherm should be caused by the micropore filling effect.

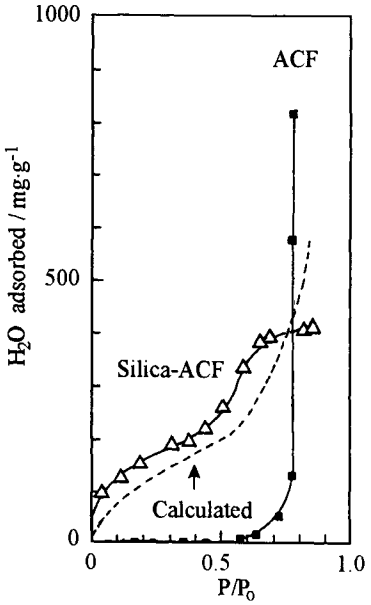

Figure 6. Adsorption isotherms of H_2O on silica-coated ACF and ACF at 303 K.

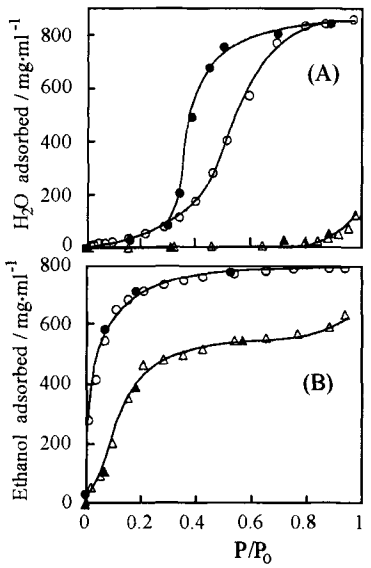

Figure 7. Adsorption isotherms of H_2O (A) and C_2H_5OH (B) on fluorinated ACF (△, ▲) and ACF (○, ●); open symbols–adsorption, solid symbols–desorption.

Thus, hydrated silica-coating leads to the hydrophilic ACF which is superior to the bulk hydrated silica for adsorption of H_2O at a low P/P_0 range.

4.4.2. Fluorinated activated carbon fiber

Fluorination is quite effective for introduction of hydrophobicity to the solid surface. Touhara et al. [33] reported that ACF can be fluorinated even below 473 K and the fluorine content can be controlled by the reaction temperature. ACF is composed of micrographites and the fluorination changes the unit structure of ACF from the micrographite to polycyclohexane frame. The predominant surface of ACF consists of the conjugated C=C bonds, whereas that of the fluorinated ACF is covered with the C–F bonds. Accordingly, the fluorinated ACF can offer the micropore having a perfect hydrophobicity.

The fluorinated ACF was prepared by reaction between a gaseous fluorine of 101.3 kPa and ACF at 373 K after drying the ACF sample. The chemical composition of the fluorinated ACF was $C_{1.4}F$ by the weight change. The α_s–plots of the N_2 adsorption isotherm indicated that the micropores are preserved after fluorination. Fig. 7(A) shows the adsorption isotherms of H_2O on the fluorinated ACF and pristine ACF at 303 K. The ordinate is expressed by the amount of adsorption per unit pore volume. The H_2O adsorption isotherm of ACF is of type V and has a marked hysteresis. This ACF, therefore, is hydro-

phobic. The H_2O adsorption isotherm of the fluorinated ACF is unusual; the adsorption is nil until $P/P_0 = 0.7$ and only 33.0 mg/ml even at $P/P_0 = 0.9$, which is negligibly small compared with that of ACF. The remarkable depression of H_2O adsorption is caused by the very weak interaction with H_2O molecules. Thus, fluorination can introduce a perfect hydrophobicity to ACF regardless of presence of micropores. The adsorption isotherms of C_2H_5OH on the fluorinated ACF and ACF at 301 K are shown in Fig. 7(B). The adsorption isotherm of C_2H_5OH on ACF is of typical type I, indicating a strong interaction of an ethanol molecule with the carbon surface. Nevertheless, the adsorption isotherm of C_2H_5OH on the fluorinated ACF is still close to type III in the low P/P_0 region, though the adsorption saturates at $P/P_0 = 0.2$. The bE_0 (4.85 kJ/mol) determined from the DR plot for is much smaller than that (10.62 kJ/mol) for ACF, suggesting the weak interaction of an ethanol molecule with the fluorinated microporous surface. Thus, the fluorination of the micropore walls enhances the hydrophobicity.

4.5. Cluster-mediated micropore filling

4.5.1. Organized molecular assembly formation upon H_2O adsorption

Even if the interaction of an admolecule with the micropore wall is too small to induce micropore filling, it is possible that the interaction energy of a cluster of admolecules with the micropore wall is sufficiently bigger than thermal energy. In such a case the cluster of admolecules can be adsorbed by micropores. This type of micropore filling should be called cluster-mediated micropore filling which can be valid for both vapours and supercritical gases. In particular, the concept of the cluster-mediated micropore filling is often helpful to enhance adsorption ability for a supercritical gas. The fact that a strong micropore filed leads to micropore filling of a supercritical gas through enhancement of an intermolecular interaction between admolecules will be described later. Here, it is shown that the cluster-mediated micropore filling is useful in controlling the adsorptivity even for vapour molecules. As this cluster-mediated micropore filling does not give a predominant adsorption at low pressure region, this is not a typical micropore filling.

The adsorption isotherm of H_2O on activated carbon is of type V due to a weak interaction of a H_2O molecule with the graphitic surface, as mentioned in subsection of 4.4. The reason why a remarkable adsorption begins at a medium relative pressure was explained by Dubinin, Zaverina and Serpinsky [34] using the assumption of cluster formation of H_2O molecules at a hydrophilic site without the direct evidence. They proposed an empirical adsorption equation which is helpful to analyze adsorption isotherms of H_2O on activated carbon. However, the study on the mechanism of H_2O adsorption is completely insufficient. The intermolecular interaction of H_2O is quite strong (20 kJ/mol) compared with other molecules. The main interaction is caused by the long-range Coulombic interaction and the contribution by the Lennard-Jones interaction is only 24 % [35]. We cannot approximate the interaction potential of a H_2O molecule with the graphitic micropore by the Lennard-Jones potential. It is assumed that H_2O molecules prefer the mutual cluster formation in the gas phase at a low P/P_0 region, and thereby H_2O molecules are not adsorbed in carbon micropores. When the cluster grows with the increase of the H_2O pressure and the interaction energy of the cluster with the micropore becomes enough great to be adsorbed compared with thermal energy, an observable H_2O adsorption in the micropore should begin. An in situ X-ray diffraction of H_2O adsorbed in carbonous

micropores can elucidate the adsorption mechanism clearly.

The H_2O adsorption on superhigh surface area carbon was studied by the in situ X-ray diffraction technique [36]. The surface area, micropore volume, and pore width of superhigh surface area carbon were 2670 m^2/g, 0.97 ml/g, and 1.3 nm, respectively. The H_2O adsorption isotherm determined at 303 K was of typical type V. The H_2O molecules were not adsorbed below $P/P_0 = 0.6$ and then they were abundantly adsorbed above $P/P_0 = 0.6$. Fig. 8 shows the X-ray diffraction patterns of adsorbed H_2O as a function of

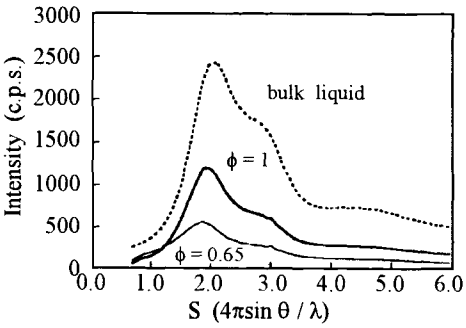

Figure 8. X-ray diffraction patterns of adsorbed H_2O (solid lines) and bulk liquid H_2O (dotted line) at 303 K.

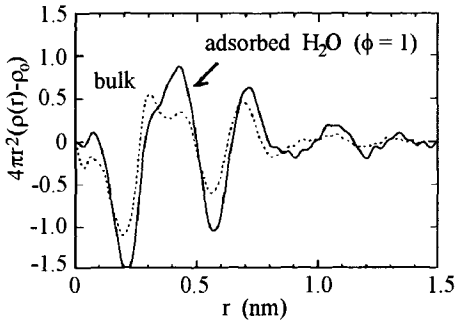

Figure 9. Radial distribution functions of adsorbed H_2O (ϕ = 1) and bulk liquid H_2O (solid and dotted lines, respectively).

ϕ. The X-ray diffraction pattern of bulk liquid H_2O at 303 K is also shown for comparison. Here the abscissa is expressed by the scattering parameter $S = 4\pi \sin\theta/\lambda$. Although the diffraction pattern of adsorbed H_2O has an apparent similarity with that of bulk liquid water, a significant low angle-shift of the highest peak is observed and the shift decreases with ϕ. The diffraction patterns were analyzed by the electron radial distribution, as shown in Fig. 9. A distinct difference between adsorbed H_2O and bulk liquid H_2O is observed in the peak structure of 0.3 – 0.5 nm. Although bulk water has the highest peak at 0.3 nm and another peak at 0.45 nm, the highest peak of the adsorbed H_2O is at 0.45 nm and the adsorbed H_2O has a shoulder around 0.35 nm. The shoulder position shifts to a greater value with ϕ. The structure such as peak or shoulder at 0.35–0.4 nm should be attributed to the nearest neighbour molecules, whereas the peak at 0.45 nm is due to the second neighbours. As bulk liquid water has interstitial molecules at the nearest neighbour positions due to the dynamic nature, the nearest neighbour peak is higher than the second neighbour peak[37]. Consequently, the information on the short range order in the 0.3–0.5 nm range directly supports formation of clusters or more ordered assembly of H_2O molecules in micropores. Furthermore, the distribution of adsorbed H_2O in the range above 0.6 nm is different from that of bulk liquid, suggesting the presence of long range order in the adsorbed H_2O.

Thus, in situ X-ray diffraction examination shows explicitly that H_2O adsorption in graphitic micropores is accompanied by formation of the ordered molecular assembly. The surface oxidation of activated carbon accelerates the cluster formation on the surface and thereby H_2O adsorption isotherm has an uptake in the low relative pressure.

4.5.2. Trimer–mediated micropore filling of acetaldehyde

There is no good carbonous adsorbent for aldehyde molecules. It is well–known that acetaldehyde molecules associate to form trimer (paraldehyde) in the presence of H_2SO_4:

$$3CH_3CHO \longrightarrow (CH_3CHO)_3$$

The boiling point of the monomer is 293.8 K, whereas paraldehyde has a cyclic structure and its boiling temperature is 397 K. As paraldehyde is more condensable, paraldehyde molecules can be adsorbed even on the surface where monomer cannot be adsorbed. Therefore, introduction of strong acid sites on the microporous carbon should enhance the amount of adsorption due to paraldehyde formation.

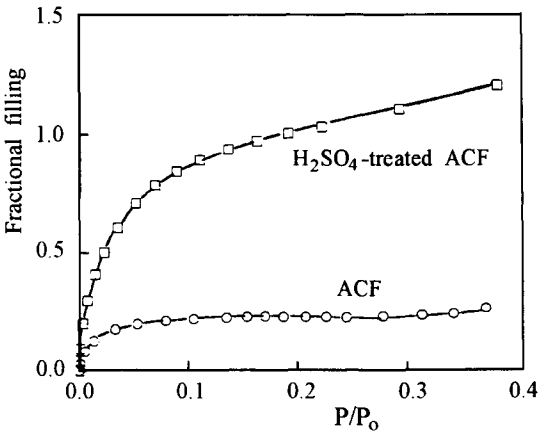

Figure 10. Adsorption isotherms of acetaldehyde by H_2SO_4–treated ACF and ACF at 303 K.

ACF was treated with a dilute H_2SO_4 solution. The microporosity change was examined by N_2 adsorption at 77 K. Fig. 10 shows adsorption isotherms of acetaldehyde on H_2SO_4–treated ACF and pristine ACF at 303 K. The adsorption at low pressure region increases markedly with the acid treatment. The amount of adsorption by H_2SO_4–treated ACF is more than five times of that of ACF. The fractional filling of H_2SO_4–treated ACF is more than 1 even at $P/P_0 = 0.4$. This remarkable enhancement should be ascribed to trimer formation at the acid site on the surface[38]. Thus, adsorption of acetaldehyde on H_2SO_4–treated ACF is a good example of the cluster–mediated micropore filling.

4.5.3. Permanent dipole–induced dipole interaction mediated micropore filling of SO_2

SO_2 has a great permanent dipole moment and the molecular diameter from the viscosity experiment is 0.54 nm. Micropore filling of polar molecules by carbonous micropores is not actively studied [39]. The interaction of SO_2 with the graphitic slit pore is described by the Lennard–Jones interaction and dipolar interaction. In particular, an organized structure due to a strong intermolecular interaction can be expected for a polar molecule such as SO_2 in the micropore.

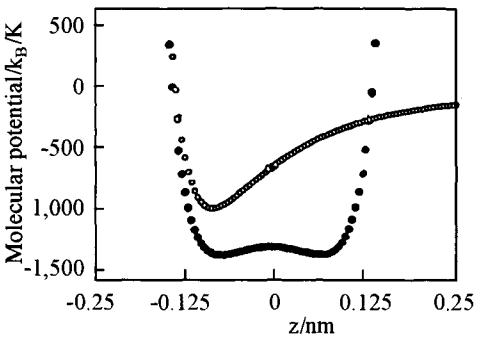

Figure 11. Potential profile of SO_2 with graphitic slitlike pore of 0.75 nm width (solid symbols). Open symbol denotes the flat surface.

The adsorption isotherm of SO_2 and the heat of SO_2 adsorption on ACF of the pore width of 0.75 nm were measured at 303 K as a function of the fractional filling ϕ. The SO_2 adsorption isotherm and heat of SO_2 adsorption of nonporous carbon black were also determined for comparison. The interaction potential of SO_2 with the graphitic slitlike pore is composed of nonpolar and polar terms. The nonpolar term is described by the Steele function and the polar interaction is approximated by the image potential. The Lennard-Jones parameters of $\sigma_{CM} = 0.385$ nm and $\varepsilon_{CM} = 84$ K from the Lorentz-Berthelot rules were used for calculation. Here the subscripts of C and M denotes the carbon atom and SO_2 molecule, respectively. Fig. 11 shows the potential profiles of SO_2 in the slitlike pore of 0.75 nm in width. The solid symbols denote the whole molecule-pore interaction potential profile including the interaction of the permanent dipole with the induced dipole in the graphitic micropore wall with the aid of the image potential [40]. The introduction of the image potential deepens the potential bottom and gives a significant contribution of 23 % to the whole molecule-pore interaction potential Ψ_S. This great permanent dipole-induced dipole interaction leads to the two-dimensional orientation of SO_2 molecules in the micropore. Furthermore, the lateral interaction of adsorbed SO_2 molecules becomes important at a higher ϕ. The lateral interaction Ψ_L of SO_2 is given by the Lennard-Jones interaction and the permanent dipole-permanent dipole interaction using the Sockmayer potential Ψ_{St}:

$$\Psi_{St} = 4\varepsilon_{SS}\left[(\sigma_{SS}/r)^{12} - (\sigma_{SS}/r)^{6}\right] - (\mu^2/r^3) \tag{7}$$

Here $\varepsilon_{SS} = 252$ K and $\sigma_{SS} = 0.429$ nm are the Lennard-Jones parameters for SO_2, $\mu = 1.61$ D is the permanent dipole moment, and $g(\theta_1, \theta_2, \phi_2 - \phi_1)$ is the angle-dependence of the dipole-dipole interaction. We presumed that the dipole moment is normal to the graphitic pore wall ($\theta_1 = \theta_2 = \pi/2$) and the mutual orientation is parallel ($\phi_2 - \phi_1 = 0$) or antiparallel ($\phi_2 - \phi_1 = \pi$). Total potential Ψ_{total} of an adsorbed SO_2 can be given by $\Psi_S + \Psi_L$. The calculated total potential as a function of the fractional filling is compared with the observed behaviour of heat of adsorption below.

The adsorption isotherm of SO_2 on nonporous carbon black was of type III. On the other hand, that on ACF was of type I, suggesting presence of the micropore filling

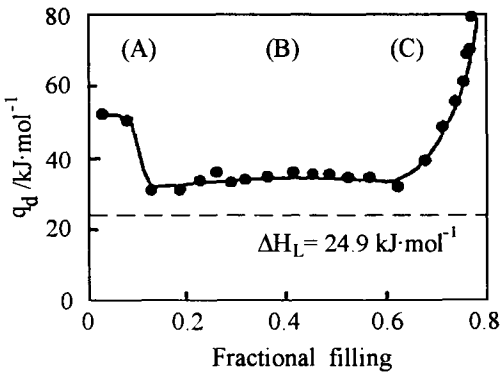

Figure 12. The change in the differential heat of SO_2 adsorption, q_d, for ACF.

process regardless of very weak interaction of SO_2 with a single graphitic surface. The SO_2 adsorption isotherm of ACF was well described by the DR equation. However, the DR plot bends downward at the fractional filling of 0.6 with increasing P/P_0, indicating some change in the adsorption process. Fig. 12 shows the change in the differential heat of SO_2 adsorption, q_d, on ACF. The abscissa ϕ is the fractional filling which is the ratio of the volume occupied by adsorbed SO_2 to the pore volume by N_2 adsorption at 77 K. The change is divided into three regions: stage A ($\phi < 0.2$), stage B ($0.2 < \phi < 0.6$), and stage C ($\phi > 0.6$). The high q_d value at the stage A is ascribed to the interaction of the SO_2 dipole with the local electric field due to the surface functional group. In the stage B, q_d is almost constant, being greater than the heat of condensation ΔH_v = 24.9 kJ/mol by about 10 kJ/mol. In the case of SO_2 adsorption on nonporous carbon black, the q_d value almost agreed with ΔH_v. Consequently, the great q_d value at the B stage comes from the strong SO_2 molecule–slitlike pore interaction. The ratio of q_d of the B stage for ACF to that for nonporous carbon black was 1.4, which equals to the theoretical ratio of the SO_2 molecule–pore interaction to the SO_2–single graphite surface interaction (1.40). Therefore, the stage B corresponds to the adsorption enhanced by the micropore field. As the parallel arrangement of SO_2 dipoles gives the excess stabilization due to the permanent dipole–induced dipole interaction, SO_2 molecules should form two-dimensional layer structure of the parallel dipoles in the micropore. Both of the great permanent dipole–induced dipole interaction and the permanent dipole–local electric field interaction are the cause for the observed predominant uptake of SO_2 at low pressure region(stage A). Further adsorption of SO_2 reduces the intermolecular distance, increasing the repulsive energy between the parallel dipoles. The calculated total molecular potential Ψ_{total} vs. ϕ curves for parallel and antiparallel dipole orientations intersected at $\phi = 0.6$. The parallel orientation is preferable below $\phi = 0.6$. According to the potential consideration, the antiparallel orientation becomes predominant above $\phi = 0.6$. The change of the stage B to C just corresponds to this prediction. Also the bending point of the DR plot of SO_2 adsorption isotherm agrees with $\phi = 0.6$. Therefore, micropore filling of polar SO_2 should accompany a two-dimensional phase transition of the parallel to antiparallel dipole orientation with the fractional filling. The dipole-oriented structure of SO_2 molecules can be regarded as a great ordered cluster. The formation of the ordered molecular structure

is mediated by the interaction of the permanent dipole with the induced dipole in the graphitic wall, inducing the marked uptake of SO_2 in the low pressure region [41].

5. ANALYSIS AND CONTROL OF MICROPORE FILLING OF A SUPERCRITICAL GAS

5.1. Quasivapour state of a supercritical gas confined in micropores

It is presumed that supercritical gaseous molecules are concentrated in the micropore space by affection of the strong molecule–pore interaction to induce an enhanced intermolecular interaction and the supercritical gas is transformed into a quasivapour. The quasivapour states depend strongly on the micropore width, because the micropore field strength is governed by the pore width. Each quasivapour has its inherent micropore volume W_L which is governed mainly by the molecule–pore interaction. Hence, the DR equation can be extended to the quasivapour of the supercritical gas, as follows[42,43]:

$$[\ln (W_L/W_0)]^{1/2} = (RT/\beta E_0)(\ln P_{0q} - \ln P) \tag{8}$$

Here, W_L is the inherent micropore volume and P_{0q} is the saturated vapour pressure of a quasivapourized supercritical gas. The plot of $[\ln(W_L/W_0)]^{1/2}$ vs. ln P leads to both values of P_{0q} of the supercritical gas in the quasivapour state under the micropore field and βE_0, that is, $q_{st,\phi=1/e}$. Thus, this extended DR plot is quite useful to obtain the important information on adsorption of a supercritical gas. This extended DR equation can describe the adsorption isotherm of the supercritical gas using the concepts of P_{0q} and W_L which are experimentally estimated by the Langmuir plot of the adsorption isotherm. P_{0q} and W_L can be related to the intermolecular interaction of supercritical gas in the quasivapourized state and the molecule–pore interaction, respectively. Then, we can define the quasirelative pressure of P/P_{0q} and express the adsorption isotherm of a supercritical gas, as if it was a vapour.

5.2. Intrapore field induced micropore filling of supercritical N_2 and CH_4

The thermodynamic description of the adsorption isotherm of a supercritical gas was shown in the above subsection. The thermodynamic approach cannot explain a more physical meaning of W_L. The molecular potential theory treats the interaction between an admolecule and the pore surface as a function of the distance, as mentioned before. If we use the model of the two parallel semi-infinite slabs of graphite as the micropore walls of activated carbon, the additive form $\Phi_{gr}(z)$ of the 9–3 potentials from both graphite slabs is obtained[43]:

$$\Phi_{gr}(z) = \left(3/10^{-1/2}\right)\varepsilon_{gr}\left\{(2/15)\left[(\sigma_{sf}/(d+z))^9 + (\sigma_{sf}/(d-z))^9\right] - \left[(\sigma_{sf}/(d+z))^3 + (\sigma_{sf}/(d--z))^3\right]\right\} \tag{9}$$

Here ε_{gr} is the minimum interaction energy between the graphite slab and a molecule, $2d = H$ is the internuclear distance of two parallel graphite surfaces, and z is a vertical distance from the central plane of two surfaces. The ratio of the energy minimum at the

midpoint between the two surfaces (at z = 0) to the energy minimum for a single surface can be approximated by Eq. (10):

$$\Phi_{gr}(0)/\varepsilon_{gr} = \left(6/10^{-1/2}\right)(\sigma_{sf}/d)^3 \tag{10}$$

Furthermore, d can be approximated by $w/2 + r_C$ (radius of a carbon atom). On the other hand, the adsorption potential of an adsorbed molecule was associated with the potential energy of an admolecule with the flat surface by Hill [45]. Horvath and Kawazoe [46] used this approximation and derived the following relationship between the adsorption potential and the molecular potential:

$$-A = RT\ln(P/P_0) = N_A\Phi_{gr}(z) + U^{CO} \tag{11}$$

Here U^{CO} is the additional potential energy due to molecules already adsorbed. For simplicity, we assume that only adsorptives with the strong potential $\Phi_{gr}(0)$ can be adsorbed in the micropore according to the Boltzmann distribution. The next intrapore-field dependent micropore filling equation can be obtained:

$$RT\ln(W_L/W_0) = \left(6/10^{-1/2}\right)N_A\varepsilon_{gr}[2\sigma_{sf}/(w + 2r_C)]^3 + U^{CO} \tag{12}$$

This equation correlates the inherent micropore volume for a supercritical gas with the micropore width. The linearity of intrapore-field dependent micropore filling (IFMF) plot can give the effectiveness of this analysis and both values of ε_{gr} and U^{CO} [47].

The adsorption isotherms of supercritical N_2 and CH_4 on ACFs were determined at 303 K over the pressure range up to 10MPa. Five kinds of ACFs of different micropore widths were used (P5 : 0.75 nm, P10: 0.79 nm, P15: 1.01 nm, P20: 1.13nm, and P25: 1.45 nm). The high pressure adsorption isotherms of N_2 on ACFs at 303 K are shown in Fig. 13. The ordinate in Fig. 13 is expressed by the ratio of the amount of high pressure adsorption in ml/g to the micropore volume W_0 determined by the low pressure N_2 adsorption at 77 K. Here the amount of the supercritical N_2 adsorption was obtained using the density of liquid N_2 (0.808 g/ml). The fractional filling of each ACF depends on the micropore width. The smaller the pore width, the greater the fractional filling. All adsorption isotherms can be approximated by the Langmuir equation. The inherent micropore volume W_L was determined by the Langmuir plot. The ratio of W_L to W_0 is 0.26 to 0.43; the ratio increases with the decrease of the average micropore width.

Each ACF sample has the different W_L value, indicating the presence of the micropores where supercritical N_2 can be transformed into quasivapour N_2. The quasivapour state can be supported by the extended DR plot. Fig. 14 shows the extended DR plots for the N_2 high pressure adsorption isotherms. All the plots are linear in the wide range, suggesting the basic idea given in the above subsection . The deviation from the linearity at the lower pressure region should come from the very low fractional filling of < 0.1 %, where the potential theory should be inappropriate. The intercept and slope of the linear plot provides the P_{0q} and βE_0 (or $q_{st,\phi=1/e}$). The P_{0q} and $q_{st,\phi=1/e}$ values are collected in Table 1. The P_{0q} for ACF samples is near 50 MPa and depends on the micropore width; the smaller the micropore width, the smaller the P_{0q}. The determined $q_{st,\phi=1/e}$ for supercritical N_2 at 303 K is compared with that for N_2 vapour at 77 K in Table 1. The important thing is that those values are close to each other. $q_{st,\phi=1/e}$ of supercritical N_2 is slightly greater than that of vapour N_2 by only 1–3 kJ/mol. Therefore, the adsorbed

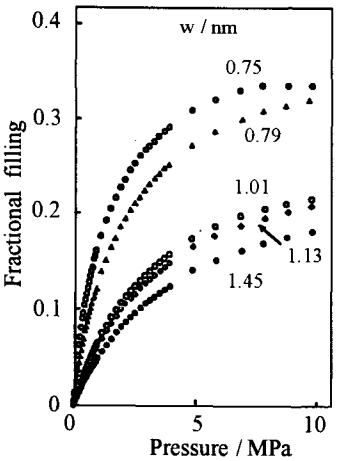

Figure 13. High pressure adsorption isotherms of supercritical N_2 at 303 K as a function of pore width w.

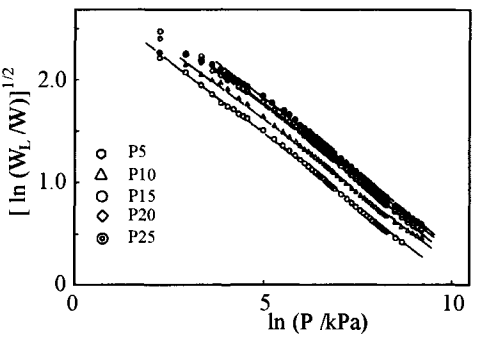

Figure 14. The extended DR plots of the high pressure adsorption isotherms of supercritical N_2 on ACF.

state of supercritical N_2 is essentially the same as that of the N_2 vapour in the micropore at 77 K. As only micropores having higher intrapore field can be available for inherent micropores for supercritical N_2, $q_{st,\phi=1/e}$ for supercritical N_2 is slightly greater than that for vapour N_2.

Table 1
Inherent micropore volume W_L, saturated vapour pressure P_{0q} and isosteric heat of adsorption $q_{st,\phi=1/e}$ for supercritical N_2 and isosteric heat of adsorption $q_{st,\phi=1/e}$ (77 K) for N_2 vapour

	W_L ($ml \cdot g^{-1}$)	P_{0q} (MPa)	$q_{st,\phi=1/e}$ ($kJ \cdot mol^{-1}$)	$q_{st,\phi=1/e}$ (77 K) ($kJ \cdot mol^{-1}$)
P5	0.14	23.4	14.2	12.8
P10	0.20	38.6	14.4	11.8
P15	0.23	50.7	14.2	12.3
P20	0.28	57.0	13.8	11.4
P25	0.35	63.6	14.1	10.8

The thermodynamic description of micropore filling of a supercritical gas introduces the difference in the micropore field strength into the W_L and P_{0q} values. Consequently, if we express the amount of high pressure adsorption per W_L and the equilibrium pressure per P_{0q}, the obtained adsorption isotherms must coincide with each other. Fig. 15 shows the reduced adsorption isotherm. Although the abscissa is 0.5 at best, the isotherm has the type I character. This reduced adsorption isotherm is described by the reduced DR equation:

$$W = W_L \exp\left[-(RT/\beta E_0)\ln(P_{0q}/P)\right]^2 \qquad (15)$$

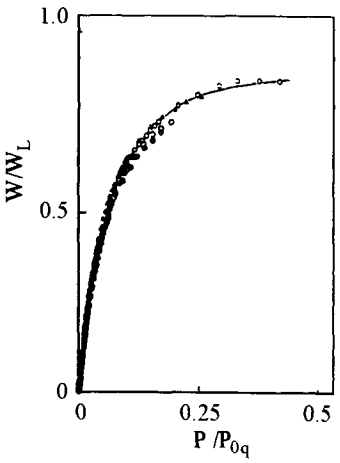

Figure 15. The reduced adsorption isotherm of supercritical N_2 on ACF.

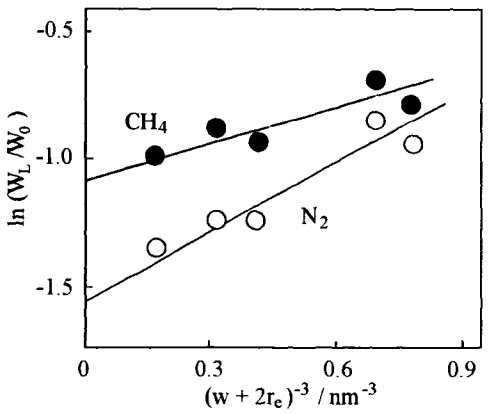

Figure 16. Intrapore field-induced micropore filling plots for supercritical N_2 and CH_4.

Here, βE_0 = 8.75 kJ/mol, which was obtained from the best fit conditions. This βE_0 agrees with that for micropore filling of vapour N_2 at 77 K (7.5–9.3 kJ/mol). This fact also indicates that high pressure adsorption process of supercritical N_2 is essentially identical to micropore filling of vapour N_2 at 77 K.

This idea was applied to high pressure CH_4 adsorption by ACF at 303 K. The high pressure CH_4 adsorption isotherms of five ACF samples (P5–P25) were measured. The adsorption tendency was similar to that of supercritical N_2; the smaller the micropore width, the greater the CH_4 adsorption. These high pressure CH_4 adsorption isotherms were also described by the reduced adsorption isotherm, although the deviation of the reduce adsorption data was greater compared with that for N_2. Hence, this quasivapour model should be widely applied to adsorption of other supercritical gases on activated carbon.

It will be shown that the concept of the inherent micropore volume W_L is associated with the intrapore field strength with the aid of Eq.(14). The IFMF plots for the supercritical N_2 and CH_4 are shown in Fig. 16. The plots are almost linear, which supports the intrapore-field induced micropore filling of the supercritical gas. The slope and intercept provide the interaction energy of an adsorbed molecule with the micrographitic surface and the cooperative adsorption energy. ε_{gr} and U^{CO} values for N_2 are 630 K and 4.0 kJ/mol, respectively; ε_{gr} and U^{CO} values for CH_4 are 315 K and 2.8 kJ/mol, respectively. Therefore, the interaction of CH_4 having no quadrupole moment is weaker than that of N_2 with the quadrupole moment. The interaction energy of an adsorbed N_2 with graphite is in the range of 880 to 1130 K[48,49]. The literature values were obtained as to the infinite graphite surface. The interaction energy with a micrographite surface should be less than that with the infinite graphite surface. In the gas phase at 77 K, stable N_2 dimers have been observed by IR spectroscopy and the quantum chemical calculation showed the stabilization of the N_2 dimer is 1.5 kJ/mol [50]. The obtained U^{CO} of 4 kJ/mol is close to the dimerization energy, suggesting that N_2 molecules are dimerized in the micropores even at

supercritical conditions. So far we have no spectroscopic evidences on the van der Waals molecules stabilized by the strong micropore field. The micropore filling of supercritical gas should be associated with the van der Waals formation.

5.3. Chemisorption-assisted micropore filling of supercritical NO and CH_4

As micropore filling is governed by both geometry of pores and chemical structure of the micropore wall, we can control it with chemical modification of the micropore walls. The chemical modification with substances having a chemisorptive activity for molecules is effective for enhancement of micropore filling of a supercritical gas, in particular. Here, an marked enhancement of micropore filling of supercritical NO and CH_4 with the chemical modification is described. As supercritical molecules are associated with each other through a chemisorptive affection of the surface, the chemisorption-assisted micropore filling is akin to the cluster- mediated micropore filling.

5.3.1. Iron oxide dispersion-induced micropore filling of supercritical NO

The critical temperature of NO is 180 K and NO is a supercritical gas at ambient conditions. Almost all microporous adsorbents cannot sufficiently adsorb supercritical NO, although NO of the representative atmospheric pollutant is desired to be removed with the good adsorbent. A NO molecule has an unpaired electron and gaseous NO shows paramagnetism. It is well- known that NO molecules are dimerized and show diamagnetism at the condensed phase[51].

Iron oxide dispersed-ACF (Fe-ACF) can adsorb great amount of NO (maximum: 320 mg/g adsorbent) in the dimer form at 303 K[17,42,43,52-55]. Figure 17 shows the ad-

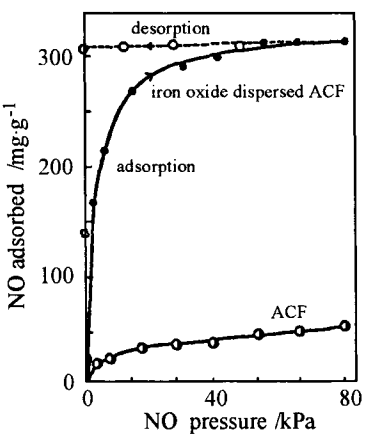

Figure 17. Adsorption isotherms of NO on iron oxide dispersed-ACF and ACF at 303 K.

sorption isotherm of NO on Fe-ACF at 303 K. Dispersion of ultrafine iron oxide particles enhances markedly NO adsorption. This isotherm indicates a remarkable hysteresis; the adsorbed NO cannot be removed by evacuation with a rotary pump at 303 K. This irreversibility arises from dimerization of NO in micropores through sharing the unpaired

electrons. The N_2 adsorption isotherm of the NO-preadsorbed ACF at 77 K showed micropore filling of NO explicitly. The NO adsorbed-ACF exhibits diamagnetism, although the calculated magnetic susceptibilities of ACF and NO gas corresponding to the adsorbed amount indicates paramagnetism. The diamagnetic susceptibility increased gradually with increasing temperature, which is caused by dissociation of the NO dimer. The fraction of the dimer was determined from the amount of NO adsorption and the magnetic susceptibility. The fraction of the dimer was 0.99 at 298 K, gradually decreasing to 0.95 at 373 K. The van't Hoff plot of the dissociation constant of the dimer gave the dissociation enthalpy of 22–24 kJ/mol, which is greater than that of the condensed phase by about 14 kJ/mol. Therefore, the micropore field enhances the inter-NO molecular interaction to produce the NO dimer and stabilize them by 14 kJ/mol. As NO dimer is vapour at an ambient temperature, supercritical NO can be adsorbed by micropores through the dimerization with the aid of the magnetic perturbation due to the high spin Fe^{3+} ions in the dispersed oxide. Not only the magnetic perturbation but also a weak chemisorptive mechanism should be associated with the enhancement of the NO micropore filling. The mixed valence formation in the dispersed iron oxides with doping of Ti^{4+} enhanced the micropore filling of NO and the adsorption isotherms were analyzed by the extended DR plot. The several NO adsorption isotherms can be expressed by a single reduced adsorption isotherm using P_{0q} and W_L [45]. Hence, even micropore filling by chemically modified micropores can be described by the quasi-vapour approach. The dispersion of the hydroxides of Cu or Mn was also effective for the enhancement of NO micropore filling in the oxides of Ti, V, Cr, Mn, Co, and Cu [56].

The micropore space can work as the high pressure field, as suggested in section 3. If this assumption is correct, we can observe a macroscopic high pressure effect in the micropore. The disproportionation reaction of $(NO)_2$ given by Eq. (16):

$$3(NO)_2 \longrightarrow (NO_2)_2 + 2N_2O \tag{16}$$

is known as the high pressure gas phase reaction above 20 MPa[57]. NO molecules dimerized in the micropore of ACF at a subatmospheric pressure of NO gives rise to the high pressure disproportionation reaction of the NO dimer in the micropores. Furthermore, the produced N_2O is reduced to N_2 at 423 K with the aid of dispersed transition metal oxides[58].

Thus, the enhancement effect for NO micropore filling is also associated with a special catalytic activity for NO.

5.3.2. Basic oxide–dispersion induced enhancement of micropore filling of CH_4

Methane is the main constituent of natural gas. Adsorption of methane at ambient temperature has been studied with a special relevance to methane storage. However, methane is a spherical molecule and the intermolecular interaction is quite weak. Furthermore, the bulk critical temperature is 191 K. It is quite difficult to adsorb methane sufficiently at ambient conditions. The adsorption conditions of CH_4 by activated carbon have been studied with molecular simulations[59,60]. The chemisorption-assisted micropore filling concept was applied to adsorption of supercritical CH_4. As the intermolecular interaction of CH_4 is quite weak compared with that of NO, CH_4 adsorption must be examined at high pressure region. As basic metal oxides such as MgO, CaO, Al_2O_3, NiO, and Cr_2O_3

have a catalytic effect on CH_4 at high temperature, they and their hydroxides were dispersed on ACF of 0.8 nm in the pore width in order to improve adsorptivity for supercritical CH_4. The microporosity of these oxide-dispersed ACFs was not seriously changed[61,62].

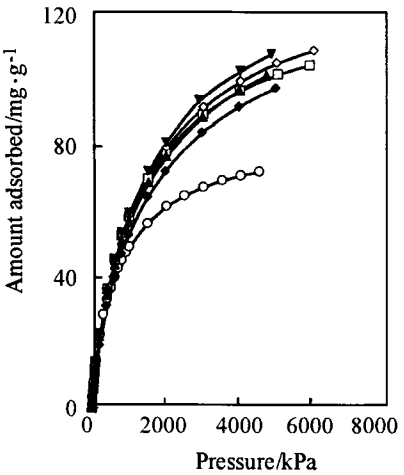

Figure 18. Adsorption isotherms of CH_4 on oxide dispersed-ACFs at 303 K.
○ ACF ◇ MgO-ACF □ CaO-ACF ◆ Al_2O_3-ACF ▲ Cr_2O_3-ACF ▽ NiO-ACF.

Fig. 18 shows high pressure CH_4 adsorption isotherms of metal oxide dispersed-ACF at 303 K. All the adsorption isotherms are Langmuirian, indicating the presence of micropores in which supercritical CH_4 can be filled. The oxide dispersion enhances remarkably the amount of CH_4 adsorption. The dispersion of NiO fine particles is the most effective for improvement of CH_4 adsorptivity. The W_L value of NiO-dispersed ACF is greater than that of ACF by 50 %. These high pressure adsorption isotherms were analyzed by the quasivapour theory using the extended DR equation: all extended DR plots showed a good linearity, providing P_{0q} and $q_{st,\phi=1/e}$ values with ΔH_v = 8.17 kJ/mol. The metal oxide dispersion increases P_{0q}, while $q_{st,\phi=1/e}$ is almost constant regardless of the dispersion. Although the enhancement effect is remarkable, the mechanism is not fully understood yet.

In this chapter good examples are shown that the adsorptivity of activated carbon for supercritical gas can be remarkably improved by the controlling of the pore geometry and chemical nature of the pore walls. Recently, clathrate formation of H_2O and NO in micropores of iron oxide dispersed-ACF without application of high pressure was reported [63]. This clathrate formation can be applied to induced micropore filling of a supercritical gas. The magnetic susceptibility measurement of O_2 molecules adsorbed in the carbon slit-shaped micropores was measured at the low temperature range of 1.7 to 60 K. The O_2 molecules in the micropore at low fractional filling are isolated each other and they become to form their cluster with the increase of the fractional filling [64,65] to exhibit random magnetism. The magnetic susceptibility measurement suggested that superhigh surface area carbon shows an unusual ferromagnetism [66]. An electronic interaction of a molecule with the carbon surface of activated carbon should be taken into account in

some physisorption aspects regardless of no predominant interaction [67–69]. The study on the physical properties both of molecules confined in the micropores and micropore walls should be helpful to elucidate the micropore filling mechanism.

REFERENCES

1. K. Kaneko, J. Membrane Sci., 96 (1994) 59.
2. S. Iijima, Nature, 354 (1991) 56.
3. R. C. Bansal, J.-B. Donnet and F. Stoeckli, Active Carbon, Marcel Dekker, New York, 1988.
4. H. Marsh, Introduction to Carbon Science, Butterworths, London,1989.
5. J. W. Patrick, Porosity in Carbons, Edward Arnold, London, 1995.
6. K.S.W. Sing, D.H. Everett, R.A. W. Haul, L. Moscou, R.A. Pierotti, J. Rouquerol, and T. Siemieniewska, Pure Appl. Chem., 57 (1985) 603.
7. J. Rouquerol, D. Avnir, C.W. Fairbridge, D.H. Everett, J.H. Haynes, N. Pernicone, Pure Appl. Chem., 66 (1954) 1739.
8. S. Sircar, in: Fundamentals of Adsorption, Kodsnsha, Tokyo, 1993, p.3.
9. M. Sato, H. Isobe, Yamamoto, K. Kaneko, Carbon, to be submitted.
10. A. W. Adamson, Physical Chemistry of Surfaces, Wiley, New York, 1990.
11. M.M. Dubinin, Chem. Rev., 60 (1960) 235.
12. D. Nicholson and N. G. Parsonage, Computer Simulation and the Statistical Mechanics of Adsorption, Academic Press, London, 1982.
13. N. A. Seaton, J. P. R. B. Walton and N. Quirke, Carbon, 27 (1991) 853.
14. P.B. Balbuena and K.E. Gubbins, Fluid Phase Equilibria, 76 (1992) 21.
15. K. Kaneko, R. Cracknell and D. Nicholson, Langmuir, 10 (1994) 4606.
16. W.A. Steele, Surf. Sci., 36 (1973) 317.
17. J. Imai M. Souma, S. Ozeki, T. Suzuki and K.Kaneko, J. Phys. Chem., 95 (1991) 9955.
18. T.Suzuki, K. Kaneko, M. Maddox and K.E. Gubbins, Langmuir, to be submitted.
19. D. Atkinson, A.I. McLeod and K.S.W. Sing, J. Chem. Phys., 81 (1984) 791.
20. K. S. W. Sing, Carbon, 27 (1989) 5.
21. K. Kakei, S. Ozeki, T. Suzuki and K. Kaneko, J. Chem. Soc., Faraday Trans., 86 (1991) 371.
22. K. Kaneko, C. Ishii, M. Ruike and H. Kuwabara, Carbon, 30 (1992) 1075.
23. K.Kaneko and C. Ishii, Colloids Surf., 67 (1992) 203.
24. W.A. Steele, J. Chem. Phys., 25 (1956) 819.
25. H. Kuwabara, T. Suzuki and K. Kaneko, J. Chem. Soc., Faraday Trans., 87 (1991) 1915.
26. N. Setoyama, M. Ruike, T. Kasu, T. Suzuki and K. Kaneko, Langmuir, 9 (1993) 2612.
27. K. Kaneko, N. Setoyama and T. Suzuki, in: Characterization of Porous Solids III, J. Rouguerol, F. Rodriguez-Reinoso, K.S.W. Sing and K.K. Unger (eds.), Elsevier, Amsterdam, 1994, p.593.
28. N. Setoyama and K. Kaneko, Adsorption, 1 (1995) 1.
29. M.M. Dubinin and H.F. Stoeckli, J. Colloid Interface Sci., 75 (1980) 34.
30. S.J. Gregg and M.M. Tayyab, J. Chem. Soc., Faraday Trans. 1, 74 (1978) 348.

31. Y. Hanzawa, T. Suzuki and K. Kaneko, Langmuir, 10 (1994) 2857.
32. A. Matsumoto, M. Ruike, T.Suzuki and K. Kaneko, Colloids Surf., 74 (1993) 15.
33. H. Touhara, K. Kadono, N. Watanabe, J.J. Braconnier, J. Electrochem. Soc., 134 (1987) 1071.
34. M.M. Dubinin, E. D. Zaverina and V.V. Serpinsky, J. Chem. Soc., (1955) 1760.
35. M. Rigby, E. B. Smith, W.A. Wakeham and G.C. Maitland, The Forces Between Molecules, Oxford Science Publisher, Oxford, 1986.
36. T. Iiyama, K. Nishikawa, T. Otowa and K. Kaneko, J. Phys. Chem., to be submitted.
37. K. Nishikawa and N. Kitagawa, Bull. Chem. Soc. Jpn, 53 (1980) 2804.
38. K. Kaneko and M. Sato, Chem. Phys. Lett., to be submitted.
39. F. Rodriguez–Reinoso, M. Molina–Sabio and M.A. Munecas, J. Phys. Chem., 96 2707 (1992).
40. A.D. Crowell, J. Phys. Chem., 49 (1968) 892.
41. Z. M. Wang and K.Kaneko, J. Phys. Chem. (in press.)
42. K. Kaneko, Langmuir, 3 (1987) 357.
43. K. Kaneko, Colloids Surf., 37 (1989) 115.
44. D.H. Everett and J.C. Powl, J. Chem. Soc., Faraday Trans. 1, 72 (1976) 619.
45. T.L. Hill, Adv. Catal., 4 (1952) 211.
46. G. Horvath and K. Kawazoe, J. Chem. Eng. Japan, 16 (1983) 470.
47. K. Kaneko, K. Shimizu and T. Suzuki, J. Chem. Phys., 97 (1992) 8705.
48. B. Kuchta and R. D. Etters, Phys. Rev., B36 (1987) 3400.
49. W.A. Steele, Chem. Rev., 93 (1993) 2355.
50. R.M. Berns and A. van Avoird, J. Chem. Phys., 72 (1980) 6107.
51. J. Billingsley and D.B. Callerar, J. Chem. Soc., 67 (1971) 589.
52. K. Kaneko, N. Fukuzaki and S. Ozeki, J. Chem. Phys., 87 (1987) 776.
53. K. Kaneko, A. Kobayashi, T.Suzuki, S. Ozeki, K. Kakei, N. Kosugi and H. Kuroda, J. Chem. Soc., Faraday Trans. I, 84 (1988) 1795.
54. K. Kaneko, in: Characterization of Porous Solids I, K.K. Unger, J. Rougerol, K.S.W. Sing and H. Kral (eds.) Elsevier, Amsterdam, 1988, p. 183.
55. Z.M. Wang, T.Suzuki, N. Uekawa, K. Asakura and K. Kaneko, J. Phys. Chem., 96 (1992) 10917.
56. K. Kaneko, H. Yamamoto, T. Suzuki and S. Ozeki, in: Fundamentals of Adsorption, Engineering Foundation, New York, 1989, p.355.
57. S.F. Agnew, B.I. Swanson, L.H. Jones and R.L. Milles, J. Phys. Chem., 89 (1985) 1678.
58. J. Imai and K. Kaneko, Cat. Lett., 20 (1993) 133.
59. K.R. Matranga, A.L. Myers, E.D.Glandt, Chem. Eng. Sci., 47 (1992) 1569.
60. Z.Tan, K. E. Gubbins, J. Phys. Chem., 96 (1992) 845.
61. K.Kaneko, K. Shimizu, K. Murata, S. Camara, T. Suzuki, Langmuir, 9 (1993) 1165.
62. K. Murata and K. Kaneko, J. Chem. Soc., Faraday Trans., to be submitted.
63. K. Fujie, T. Suzuki and K. Kaneko, Chem. Phys. Lett. (in press.)
64. H. Kanoh and K. Kaneko, J. Phys. Chem. (in press.)
65. H. Kanoh and K. Kaneko, Chem. Phys. Lett. (in press.)
66. C. Ishii and K. Kaneko, J. Phys. Chem. (in press.)
67. J. Imai and K. Kaneko, Langmuir, 8 (1992) 1695.

68. A. M. Rao, A.W.P. Fung, M.S.Dresselhaus and M. Endo, J. Mater. Res., 7 (1992) 1788.
69. T. Enoki, N. Kobayashi, A. Nakayama, K. Suzuki, C. Ishii, K. Kaneko, Y. Hosokoshi, M. Kinoshita, M. Endo and N. Shindo, Mat. Res. Soc. Symp., 349 (1994) 73.

A. Dąbrowski and V.A. Tertykh (Editors)
Adsorption on New and Modified Inorganic Sorbents
Studies in Surface Science and Catalysis, Vol. 99

Chapter 2.11
Phase transitions in adsorbed layers

A. Patrykiejew

Department of Chemical Physics, Faculty of Chemistry,
MCS University, 20031 Lublin, Poland

Results of recent theoretical and computer simulation studies of phase transitions in monolayer films of Lennard-Jones particles deposited on crystalline solids are discussed. Different approaches based on lattice gas and continuous space models of adsorbed films are considered. Some new results of Monte Carlo simulation study for melting and ordering in monolayer films formed on the (100) face of an fcc crystal are presented and confronted with theoretical predictions. In particular, it is demonstrated that the inner structure of solid films and the mechanism of melting transition depend strongly on the effects due to the periodic variation of the gas – solid potential.

1. INTRODUCTION

The study of phase transitions in adsorbed films has a rather short history but extremely abundant literature and quite impressing achievements. The first observations of phase transitions in adsorbed films were reported over 40 years ago [1 – 8]. Theoretical interpretation of those early findings was usually based on the predictions of either the two-dimensional version of the van der Waals equation of state [9] or on the mean-field solutions of the two-dimensional lattice gas model [10]. Until the late sixties, however, studies of phase transitions in adsorbed layers did not show any remarkable progress. A real breakthrough came when Tomy and Duval published a series of papers [11 –15] dealing with the volumetric measurements of adsorption of simple gases (argon, krypton, xenon and methane) on the exfoliated graphite surface. They showed that monolayer films may exhibit different phases, resembling the ordinary bulk gases, liquids and solids. The pioneering work of Tomy and Duval had a great impact and triggered intensive experimental studies of low temperature adsorption on highly uniform substrates. The field of research started to broaden rapidly due to the development of technologies for preparation of other substrates characterized by highly homogeneous surfaces [16 – 30]. Using different methods, such as classical volumetry [12 – 14], calorimetry [31 – 36], LEED [37 – 41], neutron diffraction and scattering [42 – 46], X-ray scattering [47 – 49] , Mössbauer spectroscopy [50 – 54], elipsometry [55,56] and NMR [57 – 60], experimentalists have collected a vast body of data. These results enabled to construct phase diagrams for a variety of systems and provided very precise information concerning the inner structure of different phases.

Experimental studies have been followed by intensive theoretical studies aiming at the development of models enabling better understanding of the observed phenomena and allowing to extract the most important factors determining the behaviour of real systems [61 - 70]. A remarkable progress has been also achieved due to the application of computer simulation methods [71 – 80]. These methods are particularly important for the problems of phase transitions in adsorbed films. The effects of statistical fluctuations in two-dimensional systems are much stronger than in the bulk three-dimensional systems and hence the predictions of simple closed-form approximate theories are bound to be incorrect. Computer simulations can provide exact solutions for any specified model of statistical mechanics, at least in principle. By confronting the results of simulations with the predictions of analytic theories one gets a unique opportunity to test the assumptions and approximations entering the latter. A direct comparison of simulation results with experimental data provides also a chance to verify the adequacy of the developed microscopic models. Finally, computer simulation gives insight into the system structure at a truly microscopic level, usually not accessible experimentally.

Phase transitions in monolayer films formed on single planes of crystalline solids have been attracting great interest for many years. Experimental studies have been carried out for adsorption of simple molecules on graphite [15], boron nitride [81,82], lamellar dihalides of the general formula MeX_2 [16 – 18], oxides [24,25], alkali halides [20 – 23] and metals [26 – 30,83 – 86]. A common feature of all those systems is the lateral periodicity of the gas – solid interaction potential [87,88]. In real systems, a competition between this periodic potential and lateral admolecule - admolecule interaction may lead to the formation of complex film structures as well as trigger various phase transitions. At sufficiently low temperatures, when the adsorbed film is a solid and thermal excitations as well as entropic effects do not play an important role, these energetic factors dominate the behaviour of adsorbed layers. Lateral interaction between adsorbed atoms favours the hexagonal close-packed structure, while the surface potential always favours the structure of the symmetry of the underlying adsorbing surface. Even in the case of triangular and honeycomb substrate lattices, density modulations due to substrate potential may lead to the appearance of complicated networks of misfit dislocations, separating regions of commensurate phase [89 – 91], orientational ordering of incommensurate phases [92,93] as well as to the formation of uniaxially registered phases [94]. The situation becomes still more complex in the case of adsorption on square and rectangular lattices [95 – 97].

In this chapter I do not attempt to give an exhaustive review of experimental and theoretical studies of phase transitions in adsorbed films, but rather focus on few selected topics. In particular, I concentrate on the problems of ordering in monolayer films formed on crystalline surfaces of different geometry and characterized by different relative size of adsorbed atoms and the unit cell of the surface lattice. The discussion concentrates on the results of computer simulation studies carried out for a special class of systems with the interaction between the adsorbed particles represented by the Lennard-Jones potential.

The organization of this chapter is as follows. The following Section 2 presents the discussion of some recent results concerning phase transitions in monolayer films described in the framework of lattice gas models. Then, the next section 3 is devoted to the problems of ordering in monolayer films formed on surfaces exhibiting finite lateral periodic variation of the gas – solid potential. Here, the conditions for the formation

of registered structures on crystals characterized by different symmetry of the surface, the commensurate-incommensurate phase transition and melting phenomena will be considered.

2. LATTICE GAS MODELS

When the modulation of the gas – solid potential is strong enough, the positions of adsorbed particles are confined to a close vicinity of the surface potential minima (adsorption sites) even at quite high temperatures. Under such conditions the ordered adsorbed phases are commensurate with the substrate surface lattice. These ordered phases may undergo various phase transitions when the density of the film or the temperature changes.

Theoretical modelling of such systems is usually based on various lattice gas models [75 – 77,98 – 104] and in many cases a remarkable agreement between theoretical predictions and experiment has been found. Wide popularity of lattice gas models results also from their flexibility and simplicity. By changing the parameters describing various interactions in the system, one can determine how they influence the structure of the ordered states, regions of their stability, and thermodynamic properties. In general, however, exact solutions of these models are not available and various approximations must be used. Apart from the mean-field type theories that can provide only very crude and often qualitatively incorrect results [99,105,106], the transfer matrix method [76,107 – 109], the renormalization group method [65,110 – 112] and the coherent anomaly method [113 – 117] have been applied. Particularly important results have been obtained with the help of computer simulation methods, however [76,77,105,106,118 – 120]. Lattice gas models are particularly well suited for the efficient use of Monte Carlo simulation method due to relatively streightforward vectorization or parallelization of the codes.

Here we concentrate on the results of studies carried out for two-dimensional lattice gas systems of particles interacting via the truncated Lennard - Jones (12,6) potential

$$u(r) = \begin{cases} 4\varepsilon[(\sigma/r)^{12} - (\sigma/r)^{6}], & \text{for } r \leq r_{max} \\ 0, & \text{for } r > r_{max} \end{cases} \tag{1}$$

where σ measures the size of adsorbed atoms, ε determines the strength of molecular interaction and r_{max} is the assumed cut-off distance.

In principle, the properties of such lattice gas systems can be derived from the grand canonical potential

$$\mathcal{H} = \frac{1}{2} \sum_{\substack{i,j \\ i \neq j}} u(r_{ij}) n_i n_j + (v - \mu) \sum_i n_i \tag{2}$$

where r_{ij} is the distance between the sites i and j, n_i is the occupation variable assigned to the ith site, $n_i = 0$ (1) when the site is empty (occupied), v is the gas – solid binding energy and μ is the chemical potential in the system. In general, the surface lattice unit cell is characterized by the vectors **a** and **b** of the length a and b, respectively. Denoting the angle between the vectors **a** and **b** by γ, the distances between different pairs of neighbours, r_{kl}, are given by

$$r_{kl} = \sqrt{[k^2a^2 + l^2b^2 + 2klab\cos\gamma]} \tag{3}$$

where k and l are integers. Depending on the assumed values of the ratio a/b and the angle γ, one can consider lattices of different symmetry. In particular, $a = b$ and $\gamma = \pi/2$ represents the square lattice, while $a = b$ and $\gamma = \pi/3$ corresponds to the triangular lattice. The possible ordered superstructures formed by the adsorbed particles depend on the symmetry of the surface lattice, the relative size of the lattice unit cell and the adsorbed particles (given by σ/a), the chemical potential and the temperature. It is convenient to introduce the reduced quantities and express all the distances in units of a (the length of the surface unit vector $\mathbf{a}$) and all the energy-like parameters and the temperature in units of ε. Besides, the gas - solid interaction energy v is irrelevant in the lattice gas models, since it does not influence the inner structure of the system, the regions of stability of different phases as well as the locations of possible phase transitions in the system. Therefore this quantity is absorbed into the definition of the reduced chemical potential

$$\mu^* = (\mu - v)/\varepsilon \tag{4}$$

It is of interest to consider the ground state (temperature $T = 0$) behaviour of this model [121] prior to the discussion of its properties at finite temperatures. The adsorbed layer unit cell, corresponding to the given superstructure, labelled by m, is characterized by the unit vectors $\mathbf{e}_1^m$ and $\mathbf{e}_2^m$ and

$$\mathbf{e}_k^m = m_{k,1}\mathbf{a} + m_{k,2}\mathbf{b} \tag{5}$$

where $m_{k,l}$ $(k, l = 1, 2)$ are integers.

At the ground state ($T^* = kT/\varepsilon = 0$) the stable states correspond to the minimum of the system energy, and the transition between different superstructures m (of lower density) and n (of higher density) occurs at the reduced chemical potential value given by:

$$\mu_{tr}^*(m, n) = \frac{\rho_n E_n^* - \rho_m E_m^*}{\rho_n - \rho_m} \tag{6}$$

where ρ_k is the density and E_k^* is the energy (per particle) resulting from the mutual interaction between adsorbed particles in the kth phase. The density, or the surface coverage, is defined by the ratio of the number of adsorbed particles to the total number of lattice sites and the energy is given by

$$E_k^* = \frac{1}{2} \sum_{\substack{j \\ (j \neq i)}} u(r_{ij}) \tag{7}$$

where the summation runs over all sites occupied by the adsorbed particles in the k-th ordered state. Apart from the different ordered states, the dilute (lattice) gas phase, with all sites empty ($\rho_G = 0$) in the ground state, and hence with the energy $E_G^* = 0$, must be also taken into account.

The results of systematic study of the ground state properties for systems characterized by different symmetry of the surface lattice and different size of the adsorbed particles have been presented in Ref. [121]. The obtained ground state phase diagrams have demonstrated that the structure of the ordered state is very sensitive to the system geometry as

well as to the external thermodynamic conditions (entirely determined by the chemical potential value μ^* at $T^* = 0$).

The finite temperature studies of Lennard-Jones lattice gas systems have been performed for the square [105,116], rectangular [106] and triangular [100,111,112] lattices using different approaches, including the simple mean-field theory, the renormalization group method, Monte Carlo simulation and Monte Carlo version of the coherent anomaly method.

In the case of a square lattice, the systems exhibiting the 1×1 and $\sqrt{2} \times \sqrt{2}$ ordered states have been considered. From the ground state calculations it follows that the systems characterized by $\sigma^* = \sigma/a \leq 1.0033$ exhibit only two different phases; the dilute gas phase and the dense 1×1 phase. The transition between these phases is of the first order and terminates at the critical point, T_c^*. For σ^* slightly exceeding this limiting value the situation becomes a little more complex. Apart from the dilute gas phase, the film may form two different ordered phases; the low density $\sqrt{2} \times \sqrt{2}$ phase and the high density 1×1 phase, depending on the magnitude of the chemical potential. Due to the symmetry properties of the hamiltonian for such systems, the transition between the gas phase and the $\sqrt{2} \times \sqrt{2}$ ordered phase appears to be exactly the same as the between the high density 1×1 phase and the low density $\sqrt{2} \times \sqrt{2}$ phase. The transition between these ordered phases may be discontinuous (first-order) or continuous (higher order) depending on the temperature. These two regimes meet at the tricritical point, T_{trc}^*. Thus, the first-order transition occurs at temperatures lower than T_{trc}^*, while the higher-order transition occurs at temperatures above T_{trc}^*. Figure 1 presents examples of phase diagrams for the systems with $\sigma^* = 1.0$ and 1.02, constructed from the Monte Carlo simulation data [105], and belonging to the aforementioned different regimes.

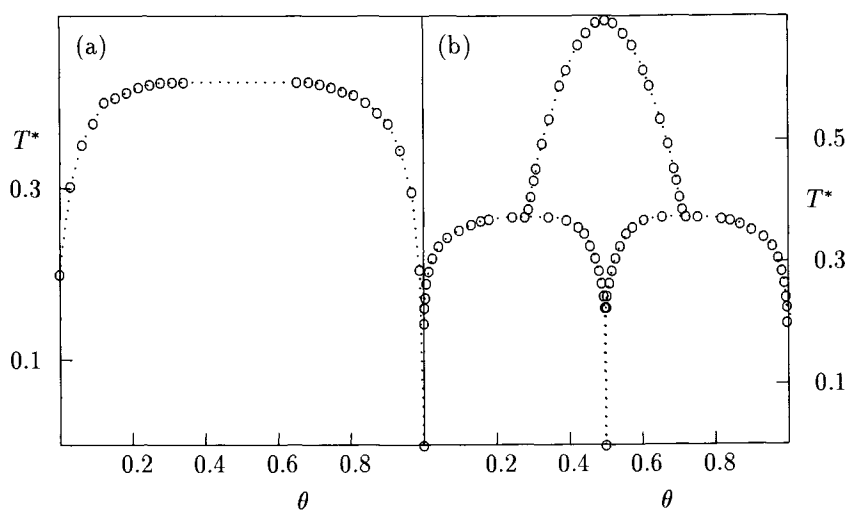

Figure 1. Examples of phase diagrams for the two-dimensional square lattice gas of Lennard-Jones particles of $\sigma^* = 1.0$ (part a) and 1.02 (part b) obtained from Monte Carlo simulation [105].

In the discussed here case of monolayer films formed on a square lattice, the observed phase transitions belong to the same universality class as the two-dimensional Ising model [122] and hence are characterized by the following values of the critical exponents:

$$\beta = 0.125 \quad \alpha = 0(\log), \quad \gamma = 1.75 \quad \text{and} \quad \nu = 1.0 \tag{8}$$

where β, α, γ and ν describe the behaviour of the order parameter, the heat capacity, the compressibility and the correlation length near the critical point, respectively.

Critical properties of the two-dimensional lattice gas of Lennard-Jones particles on a square lattice have been studied by Patrykiejew and Borowski [116] with the help of Monte Carlo version of the coherent anomaly method (CAM) developed by Suzuki and coworkers [115], as well as by the conventional Monte Carlo simulation [105]. The detailed presentation of the coherent anomaly method is well beyond the scope of this chapter. Therefore, here I confine myself to a brief description of its foundations and then present the results relevant to the considered problems.

The basic idea of the applied version of the coherent anomaly method is to consider a series of molecular clusters of increasing size. The properties of such finite clusters are then evaluated exactly, assuming that the particles located at the cluster boundary are subject to the local self-consistent fields (mean fields) exerted by outer particles (not belonging to the considered cluster), and then to extrapolate the results to the infinite cluster. In this way one hopes to extract information about the properties of macroscopic systems. The first step in CAM is to define a series of clusters, built around a chosen central particle n_o. This is done by defining a series of circles of different radius L_k. All sites of the lattice encompassed by a given circle form a cluster $\Omega(L_k)$. Next, the boundary region of the cluster $\partial\Omega(L_k)$ is defined. This is done by assigning any given particle to the region $\partial\Omega(L_k)$ if there is at least one site outside the cluster $\Omega(L_k)$ at the range of interaction, *i.e*, at the distance not exceeding the cut-off distance of the potential (1) given by r_{max}. Then, the hamiltonian for the cluster (which includes the effects due to local self-consistent fields located outside of the cluster) is splitted into two parts as follows:

$$\mathcal{H}(L_k) = \mathcal{H}_1(\Omega(L_k)) + \mathcal{H}_2(\partial\Omega(L_k)) \tag{9}$$

where the first term depends entirely on the mutual interaction between particles forming the cluster and is given by

$$\mathcal{H}_1(\Omega(L_k)) = \sum_{<ij>\in\Omega(L_k)} u^*(r_{ij}) n_i n_j \tag{10}$$

while the second term in the above equation (9), $\mathcal{H}_2(\partial\Omega(L_k))$, includes the chemical potential term as well as the terms representing the effects due to the local self-consistent fields and it has the following form:

$$\mathcal{H}_2(\partial\Omega(L_k)) = \sum_l u(r_l) \sum_{p\in\partial\Omega(L_k)} n_p z_p^l < n > -\mu^* \sum_{i\in\Omega(L_k)} n_i \tag{11}$$

In the above equation, the double subscripts ij at the distances r_{ij} have been replaced by a single subscript l, assuming that the sites i and j are the lth nearest neighbours, and z_l^p

is the number of l-type bonds connecting any given particle p belonging to $\partial\Omega(L_k)$ with the outer particles. The critical temperature of the finite cluster $T_c(L_k)$ is then defined in terms of the so-called "feedback" function:

$$\mathcal{F}(T, L_k) = \frac{1}{kT} \sum_{p \in \partial\Omega(L_k)} C_p < n_o n_p >_{T,\Omega(L_k)} \tag{12}$$

where

$$C_p = \sum_l z_p^l u(r_l) \tag{13}$$

and $< X >_{T,\Omega(L_k)}$ denotes the average value of the quantity X taken over the cluster, and defined by the following expression:

$$< X >_{T,\Omega(L_k)} = \frac{\mathrm{Tr} X \exp[\mathcal{H}_1(\Omega(L_k))/kT]}{\mathrm{Tr} \exp[\mathcal{H}_1(\Omega(L_k))/kT]} \tag{14}$$

The coherent anomaly method implies that the cluster critical temperature corresponds to the condition

$$\mathcal{F}(T_c(L_k), L_k) = 1.0 \tag{15}$$

and can be found from the temperature changes of the function $\mathcal{F}(T, L_k)$. Next, from CAM it also follows [115] that when the cluster size increases, the cluster critical temperature, $T_c(L_k)$, converges to the critical temperature of the macroscopic system, $T_c(\infty)$, *i.e.*, the following relation holds:

$$\lim_{L_k \to \infty} T_c(L_k) = T_c(\infty) \tag{16}$$

Besides, the following scaling relation should be satisfied:

$$T_c(L_k) \simeq T_c(\infty) + c L_k^{-1/\nu} \tag{17}$$

with ν being the usual critical exponent associated with the correlation length and c is a constant. The above relation can be used to estimate the value of the critical exponent ν. CAM allows also to derive equations describing the behaviour of various thermodynamic quantities at the cluster critical point, in terms of the multi-particle correlations $< n_o n_i \ldots n_j >$ [114-117], which can then be used to determine other critical exponents. For instance, the calculation of the compressibility requires the evaluation of the four-particle correlations, and this can be readily done with the help of Monte Carlo method. Studying the changes of such quantities with the cluster size one can estimate the values of other critical exponents.

In the case of simple lattice gas models with the interactions involving only the first nearest neighbours (*e.g.* in the case of the Ising model), it is possible to evaluate the appropriate averages for small clusters exactly, by a direct summation over all possible configurations of the system [115]. For systems involving long-ranged interactions it is necessary, however, to use larger clusters in order to obtain reliable results and the amount

of numerical calculations involved becomes prohibitely large. A possible way around those technical difficulties has been proposed by Katori and Suzuki [115] in the form of a Monte Carlo version of CAM (MCCAM). This method has been used by Patrykiejew and Borowski [116] to estimate critical properties of a series of systems with different size of adsorbed atoms (σ^*) ranging from 0.8 to 1.0.

Figure 2 presents a comparison of the critical temperatures for the square lattice gas model of Lennard-Jones particles obtained from MCCAM, with the results of the

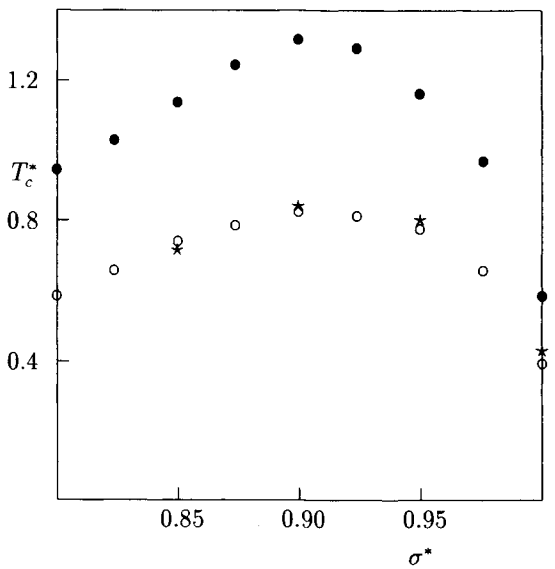

Figure 2. The critical temperatures *vs* σ^* for the two-dimensional Lennard-Jones systems on a square lattice obtained from MCCAM (○), mean-field (•) and conventional MC (⋆) calculations.

mean-field theory and with the results obtained from the conventional Monte Carlo simulation [105]. The obtained agreement between the MCCAM and MC results is quite good, while the results of mean-field calculations considerably overestimate the critical temperatures.

Attempts to estimate the values of the critical exponents γ and ν from the MCCAM calculations have not been very successful, however. In general, the values of γ has been found to exhibit systematic deviations towards the mean-field value ($\gamma_{MF} = 1.0$), while the exponent ν exhibited rather high positive deviations from the exact value. The applied version of CAM uses extremely simple mean-field theory (Bragg-Williams approximation) to calculate the self-consistent fields representing the effects of long range fluctuations, and requires considerably larger clusters for the successful application of the finite size scaling theory [123 - 126]. It is possible, that the application of other versions of CAM [117] would lead to a better estimation of the critical exponents. More convincing information concerning the values of critical exponents for the considered here systems have been obtained from the conventional Monte Carlo simulations [105]. The results confirmed the

expectation that all of them belong to the universality class of the two-dimensional Ising model.

From the scaling theory of critical phenomena for the macroscopic system it follows [122] that the behaviour of the density difference between the coexisting dense (l) and dilute (g) phases near the critical point is described by the following relationship

$$(\rho_l - \rho_g) \propto (|T - T_c|)^{\beta} \ , \ T < T_c \tag{18}$$

The value of the critical exponent β can be estimated from the slope of the log – log plot of $(\rho_l - \rho_g)$ *versus* $|T - T_c|$, providing that the value of the critical temperature is known and that the finite size effects can be neglected. Figure 3 shows that the above relation is quite nicely satisfied already for finite systems of the size (30×30) used in Monte Carlo simulation and the results are consistent with the known exact value of β equal to 0.125.

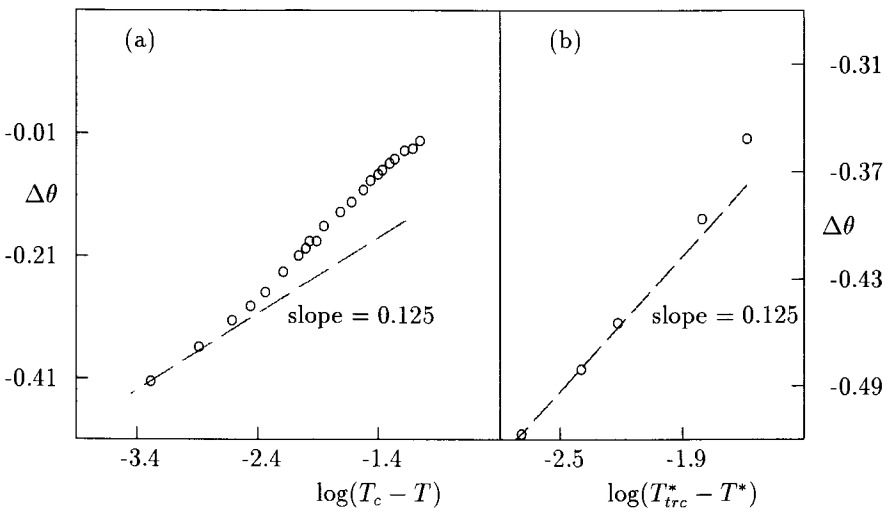

Figure 3. The dependences of $\rho_l - \rho_g$ *versus* $|T - T_c|$ for the two-dimensional Lennard-Jones lattice gas of $\sigma^* = 1.0$ and 1.01 on a square lattice.

The results for the film heat capacity and the compressibility have been also found to be consistent with the values of the critical exponents γ and α corresponding to the universality class of the two-dimensional Ising model (cf. eqn. (8)). It is noteworthy that the results presented in Fig. 2 are in a good qualitative agreement with experimentally observed dependences between the critical point temperatures for monolayer films and the dimensional incompatibility between adsorbent and adsorbate [17], defined by

$$I = \frac{(a - d_{(111)})}{d_{(111)}} \tag{19}$$

where a is the surface lattice constant and $d_{(111)}$ is the intermolecular spacing in the (111) plane of the adsorbate's bulk solid lattice and $d_{(111)} \propto \sigma$.

The extensive study of adsorption of various gases (argon, krypton, xenon and methane) on lamellar dihalides [127] have provided a rather unique opportunity to find correlations between the properties of the adsorbed films and the basic geometrical parameters characterizing the surface lattice.

Structure of the predominantly exposed crystal plane of lamellar dihalides is composed of halide ions only and these ions are arranged in such a way that the potential wells form a honeycomb lattice. Taking into account the results of theoretical calculations [88], which show that the effects of the gas – solid potential corrugation are mostly due to the uppermost layer of surface atoms (ions), we can expect that sorbents with the same halide ions should exhibit similar barriers for surface diffusion. Although no reliable estimations of these potential barriers for such systems are available, but the calculations based on the simple mean-field model of partially localized adsorption [130] have given the values of the order of 20 – 50 K for methane, argon and krypton adsorption. One should note that the magnitudes of these potential barriers are quite small as compared with the magnitudes of the gas – gas interaction energies. Nonetheless, even such a weak corrugation of the gas – solid interaction potential may be quite sufficient to stabilize the registered phase. One should note that in the considered here systems the symmetry of the self-organized close-packed phase is the same as that of the registered state. Thus, for small values of dimensional incompatibility even a weakly corrugated field may strongly stabilize the registered state. In general, one expects that the approaches based on lattice gas models are much better suited to describe the formation of adsorbed films on sorbents with surface lattices of hexagonal symmetry than on lattices of lower symmetry (e.g., on a square lattice).

Figure 4 presents a collection of experimentally determined critical temperatures for monolayer films formed on lamellar dihalides, plotted against the dimensional incompatibility between adsorbate and adsorbent. Comparing these results with the results for a square lattice (see Figure 2) we find that the qualitative picture is very similar. In both cases the critical temperature reaches maximum for the value of I close to zero.

The results shown in Figures 2 and 4 are intuitively obvious, and reflect the well known fact that the critical temperature in the system depends primarily on the strength of molecular interactions. In particular, in the lattice gas models the maximum of T_c is reached for the system of particles characterized by σ^* corresponding to the highest interaction between adsorbed particles. This can be readily demonstrated by considering the prediction of a very simple mean-field theory in the Bragg-Williams approximation.

In this case the critical temperature for a simple two-dimensional lattice gas with the first nearest neighbour interaction is given by:

$$T_c^{MF} = \frac{z u_{nn}}{4k} \tag{20}$$

where z is the number of nearest neighbours ($z = 4$ for the square lattice) and u_{nn} is the energy of interaction between a pair of neighbouring particles. Thus, the ratio T_c^{MF}/u_{nn} is constant for a given lattice and when u_{nn} increases the critical temperature must increase as well. In the case of lattice gas models involving long ranged lateral interactions between adsorbed particles one can define the following parameter U_{sum}

$$U_{sum} = -0.5 \sum_{j(j \neq i)} u(r_{ij}) \tag{21}$$

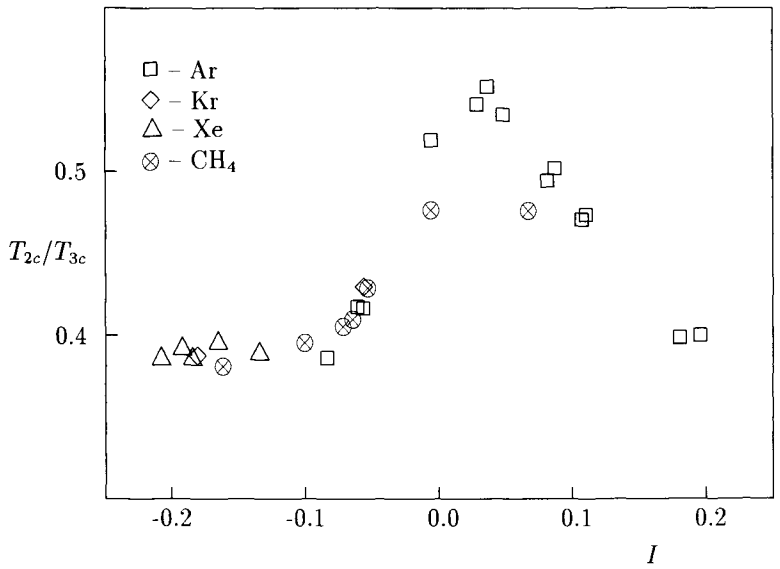

Figure 4. Ratio of two-dimensional critical temperature to its bulk (three-dimensional) value for various adsorbates on lamellar dihalides.

which measures the total energy of interaction between a given particle and all its neighbours found within the range of interaction (given by r_{max}).

In the case of a square lattice and for systems with the lateral interaction represented by the truncated Lennard-Jones pair potential with $r^*_{max} = 2.5\sigma^*$, the dependence of U_{sum} upon σ^* is represented by the following equation

$$U_{sum} = -8\varepsilon[C_{12}\sigma^{*12} - C_6\sigma^{*6}] \tag{22}$$

where

$$C_{12} = 1.015997141 \quad \text{and} \quad C_6 = 1.156625 \tag{23}$$

Therefore, we can expect that the critical temperature should be proportional to U_{sum}. The maximum of U_{sum} corresponds to $\sigma^* \approx 0.91$ and hence the critical temperature is also expected to reach maximum for this value of σ^*. Figure 5 shows the plots of the critical temperature against U_{sum} for a series of systems and determined with the help of Monte Carlo CAM method as well as resulting from the simple mean-field theory.

The observed changes in the experimentally determined critical temperatures with the dimensional incompatibility between adsorbate and adsorbent provide a direct evidence that the corrugation of the gas – solid interaction potential plays a very important role in determining the properties of adsorbed films. These findings support also the view that theoretical approaches based on the lattice gas models can appropriately represent adsorption of simple gases on crystals at low temperatures.

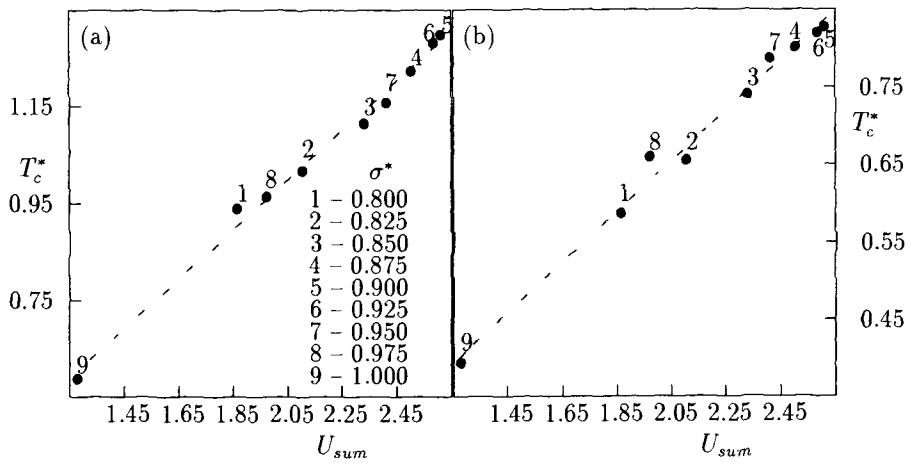

Figure 5. Critical temperatures for the two-dimensional Lennard-Jones lattice gas systems *versus* the parameter U_{sum}, for patricles of different size σ^*. Part (a) presents the mean-field results and part (b) the results of MCCAM.

In the case of rectangular lattices, the systems with different ratio of the lattice constants $b/a = 1.1$ and 1.2 and exhibiting different ordered states have been studied with the help of Monte Carlo simulation. From the ground state calculations it follows [121] that by changing the ratio b/a and the size of adsorbed particles σ^*, the systems with different ordered states are obtained. Besides, by changing the chemical potential in the system, various phase transitions between different ordered states may appear. For sufficiently small σ^* we find the 1×1 phase, while for σ^* slightly exceeding unity, we expect to find either the 1×2 or the $\sqrt{2} \times \sqrt{2}$ ordered state. These two phases are characterized by the same density and for a given σ^* the transition between them never occurs at $T^* = 0$. The situation changes at finite temperatures. Thermal excitations and entropic effects may considerably influence the structure of the ordered phase, leading to the development of domains corresponding to the 1×2 and to the $\sqrt{2} \times \sqrt{2}$ structures.

The systems exhibiting the 1×2 structure are then also expected to show commensurate and incommensurate phases, quite similar to those observed for the ANNNI model [75]. In the lattice gas systems the presence of incommensurate phases is restricted to the situations in which the substrate lattice can be divided into a certain number of equivalent interpenetrating sublattices and the ordered state corresponds to the preferential occupation of one of those sublattices. Incommensurability is manifested by the presence of regions with different occupied sublattices and the formation of walls between the domains of commensurate phase. In the case of the discussed here systems exhibiting 1×2 ordered phase we have two sublattices, since particles occupy alternate rows. Figure 6 shows examples of equilibrium configurations demonstrating the formation of incommensurate structure when the ordered 1×2 phase is heated up.

Another interesting prediction concerning the behaviour of lattice systems with anisotropic interactions in the x and y directions is that the transition between the 1×2 ordered phase and the disordered phase often shows nonuniversal behaviour [75,76,129,130]. This

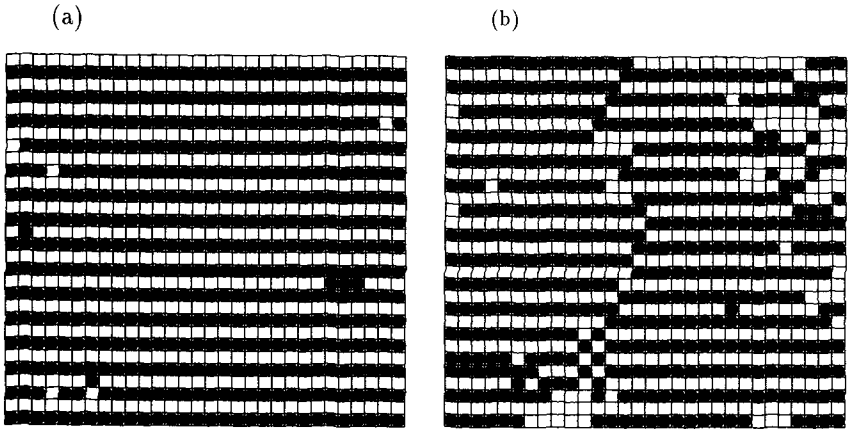

Figure 6. Equilibrium configurations for the two-dimensional Lennard-Jones lattice gas system with $b/a = 1.1$ and $\sigma^* = 1.03$ at $T^* = 0.20$ (part a) and 0.23 (part b).

implies that the values of critical exponents change with the magnitudes of interaction energies for different pairs of adsorbed particles. This was clearly demonstrated by Landau and Binder [130] for the Ising model with the antiferromagnetic nearest neighbour interaction and with added second- and third-nearest neighbour interactions, by the finite-size scaling calculations of Grynberg and Ceva [129] performed for the two-dimensional ANNNI model as well as by Dünweg *et al.* [76] for the centered rectangular lattice gas model applid to represent adsorption of atomic oxygen on the Mo(110) surface.

Determination of the critical exponents by Monte Carlo simulation is usually based on the aforementioned finite size scaling theory [123 - 126,131 - 134]. A detailed presentation of this theory is well beyond the scope of this chapter. Moreover, several excellent reviews concerning this theory are available [133,134]. Therefore, I confine the discussion to some basic facts showing that it is possible to obtain reliable information about the properties of macroscopic systems from the results obtained from computer simulations performed for finite systems. In a macroscopic system near the critical point the correlation length ξ diverges to infinity and the following relationship is satisfied:

$$\xi \propto |T - T_c|^{-\nu} \tag{24}$$

On the other hand, in a finite system of the size $L \times L$ the extent of correlations is limited and we have

$$\xi \propto L \tag{25}$$

In the consequence any continuous phase transition appears to be smeared over a certain temperature region $\Delta T(L)$ around a shifted transition temperature $T_c(L)$. Similar smearing occurs for the first-order phase transitions. A direct consequence of the system finitness is that the specific heat and the compressibility do not diverge at the critical temperature but exhibit finite maxima of the height depending on the system size L and

$$C_{max}(L) \propto L^{\alpha_m} \quad \text{and} \quad \chi_{max}(L) \propto L^{\gamma_m} \tag{26}$$

In general, the temperatures at which the heat capacity and the compressibility reach their respective maxima in finite systems are different. From the finite size scaling theory it follows that in the case of a second-order phase transition (e.g. at the critical point) $\alpha_m = \alpha/\nu$ and $\gamma_m = \gamma/\nu$, while for any first-order phase transition $\alpha_m = \gamma_m = d$, where d is the dimensionality of the system. The above predictions are often used to determine the nature of phase transitions studied by computer simulation methods [77]. The finite size scaling theory implies also that near the critical point the system free energy is given by

$$F(L,T) = L^{(\alpha-2)/\nu}\tilde{F}(\epsilon L^{1/\nu}) \tag{27}$$

where $\epsilon = (T - T_c)/T_c$ and $\tilde{F}(\epsilon L^{1/\nu})$ is a scaling function of the product $\epsilon L^{1/\nu}$ only. Now, it can be readily shown that the heat capacity and the compressibility for a finite system are given by

$$C(L,T) = L^{\alpha/\nu}\tilde{C}(\epsilon L^{1/\nu}) \tag{28}$$

and

$$kT\chi(L,T) = L^{\gamma/\nu}\tilde{\chi}(\epsilon L^{1/\nu}) \tag{29}$$

Thus, it is possible to estimate the value of the critical temperature and the values of critical exponents α, γ and ν by using the simulation results obtained for systems of different linear dimensions. Namely, if the values of T_c and the critical exponents are chosen properly, the plots of $CL^{-\alpha/\nu}$ and $\chi L^{-\gamma/\nu}$ against $\epsilon L^{1/\nu}$ for systems of different size should collapse onto a single curve, representing the appropriate scaling function.

The application of the finite size scaling analysis to the Monte Carlo simulation data for compressibility (performed for the two-dimensional Lennard-Lones lattice systems exhibiting the 1×2 ordered state) has shown [106] (see figure 7) that in the considered systems the order-disorder transition belongs to the universality class of two-dimensional Ising model with the critical exponents $\gamma = 1.75$ and $\nu = 1.0$.
It seems possible that the relative magnitudes of the interaction energies for different pairs, resulting from the assumed form of the pair potential (1), do not fall into the region in which the nonuniversal behaviour sets in.

The case of triangular lattice is particularly interesting since it corresponds to adsorption on graphite and on the (111) plane of several fcc metal crystals [15,102,103,135]. The distance between adjacent potential minima for the graphite basal plane is equal to 2.46Å and hence is too small to allow for their mutual occupation by even very small atoms of light noble gases. The same is true for adsorption on metals. Experimental studies have demonstrated that for rare gas atoms and simple molecules adsorbed on the graphite basal plane as well as on the (111) faces of fcc crystals the ordered state corresponds to either the $\sqrt{3} \times \sqrt{3}$ [102] or to the 2×2 phase [103,136,137] shown in Fig. 8.

The systems exhibiting the $\sqrt{3} \times \sqrt{3}$ ordered state are expected to belong to the universality class of the three-state Potts model, while those forming the 2×2 ordered state to the four-state Potts model [138 - 140]. These predictions have been confirmed by theoretical calculations as well as by experiment [103,136,137].

A series of model systems of Lennard-Jones particles adsorbed on triangular lattice have been studied by Berker and coworkers [111,112,141,142] with the help of renormalization group (RG) method and by Patrykiejew [100] with the help of Monte Carlo

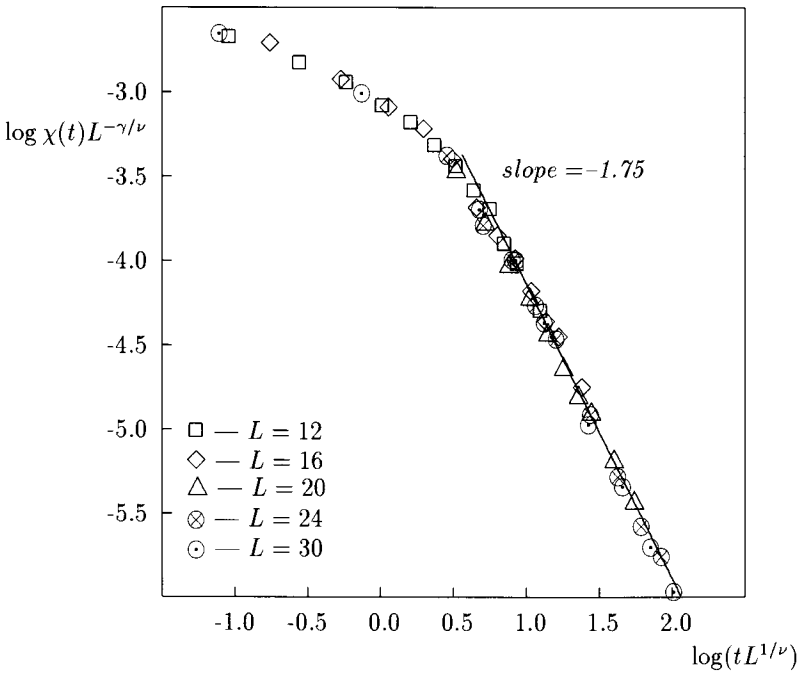

Figure 7. Finite size scaling of compressibility for the two-dimensional Lennard-Jones lattice gas on a rectangular lattice characterized by $b/a = 1.2$ and $\sigma^* = 1.07$.

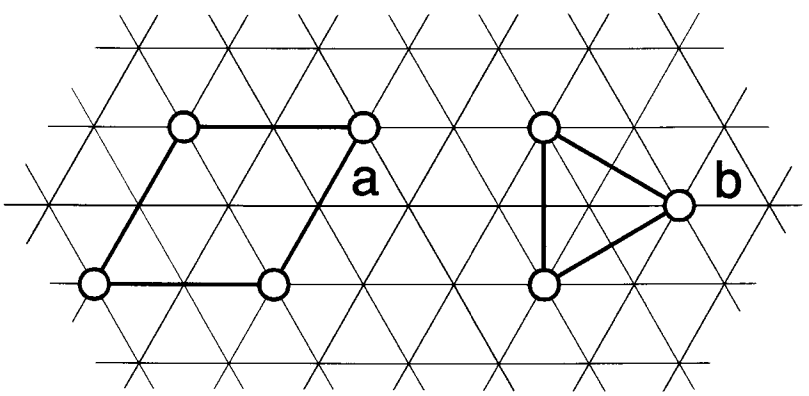

Figure 8. Unit cells of two stable solid phases formed on a triangular lattice: (a) 2×2 phase; (b) $\sqrt{3} \times \sqrt{3}$ phase.

simulation. The main goal of the RG calculations has been to determine how the size of adsorbed atoms determines the structure of the ordered states and influences the phase diagrams of monolayer films. In particular, in the considered range of σ^*, between 1.63 and 1.70, quite different types of ordering and phase transitions have been found. Thus, for $\sigma^* = 1.63$ and 1.6455 the systems exhibit only two different phases; the ordered $\sqrt{3} \times \sqrt{3}$ phase, belonging to the universality class of the 3-state Potts model, and the disordered fluid phase. The transition between these phases is of first-order at low temperatures and continuous (higher-order) at higher temperatures above the tricritical point. For slightly greater σ^* equal to 1.6460 a new liquid phase appears above the triple point temperature and its region of stability terminates at the critical temperature. Then, for systems with $\sigma^* \geq 1.6465$ the ordered 2×2 phase, which belongs to the universality class of the 4-state Potts model, is formed at low densities. Similar results have been obtained by Monte Carlo simulation [100], though a systematic shift of the phase boundaries towards higher temperatures was observed for all systems. This may be attributed to the approximate Migdal – Kadanoff renormalization method [143] used by Ostlund and Berker [112]. The same authors have then extended the renormalization group calculations, by taking into account the effects due to the finite size of crystallites and the temperature nonuniformities, that are present in real experimental situation [141]. They have obtained excellent quantitative agreement with experimental data for krypton and nitrogen adsorbed on graphite.

3. SURFACES WITH THE FINITE CORRUGATION OF SURFACE POTENTIAL

A serious drawback of lattice gas models is their inadequacy to describe properly the commensurate – incommensurate phase transitions, often observed in real systems [144 – 150]. The possibility of the formation of incommensurate phases results directly from the finitness of potential berriers between adjacent potential minima and from the off-lattice motion of adsorbed particles. Although attempts have been made to extend the lattice-gas models and include the possibility of the formation of incommensurate solid phases [151,152], but it is commonly accepted (and intuitively obvious) that the continuous-space theories are much better suited to describe behaviour of adsorbed films exhibiting incommensurate phases. Theoretical calculations of the gas – solid potential for a variety of systems [88] have shown that, in most cases, the lateral corrugation is rather low. Nevertheless, it appears to have a very big influence on the behaviour of adsorbed layers.

The problem of the gas – solid corrugation on the ordering and melting of dense monolayer films have been studied theoretically [153 – 157], and a remarkable progress has been also achieved owing to the availability of computer simulations. Large scale simulations for two-dimensional films on graphite have been performed by Abraham [158,159]. Kim and Steele [160] have used molecular dynamics to study melting of methane on graphite, assuming different corrugation of the methane – graphite potential. Since the properties of the adsorbed layers formed on the graphite basal plane have been intensively studied and there already exist excellent reviews in which various aspects of phase transitions in such systems are discussed in detail [15,33,73], we exclude them from the presentation.

Adsorption on substrates of different than hexagonal symmetry and assuming the finite corrugation of the gas – solid potential has been recently studied by many authors. Bruch and Venables [85] have considered the effects of the substrate surface lattice geometry and the corrugation of the gas – solid potential on the geometry of two-dimensional adsorbed films formed on the low index faces of fcc and bcc crystals. In particular, they have discussed the conditions for the formation of registered, uniaxially ordered and triangular adlayers on surfaces with rectangular ((110) fcc and bcc) and square ((100) fcc) symmetry. Bruch [96] has performed calculations of the ground state properties for two-dimensional Krypton and Xenon films on the (110) face of an fcc crystal.

The nature of melting transition in two-dimensional systems has been a matter of hot controversy for a long time. The theory of dislocation-mediated melting [153,154], based on the ideas of Kosterlitz and Thouless [161], predicts that the mechanism of this transition in two-dimensions may be quite different from that found in ordinary three-dimensional systems. In particular this theory predicts that the melting transition may be continuous and accompanied by the formation of the so called hexatic phase [154], bearing close resemblence to the nemetic liquid crystal, prior to the formation of ordinary liquid phase. The main difference between the solid, hexatic and liquid phases in two dimensional systems results from the properties of positional and orientational correlation functions. The solid phase is characterized by the quasi-long-range positional and the long range orientational correlations. In the hexatic phase, the positional correlations become short-ranged (exponential decay) while the orientational correlations exhibit slow algebraic decay (quasi-long-range order). In the fluid phase, both positional and orientational correlations are short-ranged. The relevance of this picture to monolayer films deposited on graphite has been reviewed by Strandburg [162]. Some of the presented examples seem to support the dislocation-mediated melting, but other clearly show that melting occurs via the first-order transition. The complexity of the behaviour of adsorbed layers formed on corrugated surfaces arizes also from the formation of incommensurate phases and the possibility of an "orientational epitaxy" in such phases, predicted by the theory of Novaco and McTague [92,93]. Depending on the system properties and the external conditions different incommensurate phases can appear. In many systems, the transitions between incommensurate and commensurate (IC transition) have been observed. Theoretical description of IC transitions is usually based on the concept of fluctuating domain walls [145,146,150]. Beautiful demonstration of the formation of domain walls has resulted from the computer simulation study of simple gases on graphite performed by Abraham [91].

Effects of the gas – solid potential corrugation on the behaviour of monolayers formed on the (100) face of an fcc crystal at finite temperatures have been recently studied by Patrykiejew *et al.* [163] with the help of Monte Carlo method. They have considered three-dimensional systems of constant volume and containing fixed number of particles interacting via the Lennard-Jones potential (1). The gas – solid interaction potential has been assumed to be represented by the two-fold Fourier series [88]

$$v(\mathbf{r}) = v_o(z) + V_b \sum_{\mathbf{g}} v_g(z) \exp(i\mathbf{g}\cdot\boldsymbol{\tau}) \tag{30}$$

where the summation runs over all non-zero two-dimensional reciprocal lattice vectors of the substrate surface lattice ($\mathbf{g}$), z is the distance from the surface, $\boldsymbol{\tau}$ is the two-dimensional

vector representing the position of an atom over the surface plane, relative to the surface lattice unit cell and V_b is the adjustable parameter which controls the effects of the gas – solid potential corrugation. The expression (15) (with $V_b = 1.0$) has been developed by Steele [88] who also demonstrated that in the case of (100) fcc surface it is sufficient to take into account only the first five non-zero reciprocal vectors **g** to obtain a good agreement with the summed potential.

The calculations have been carried out for a series of systems characterized by different size of adsorbed atoms (relative to the size of the surface lattice unit cell) and assuming different values of the parameter V_b, ranging from zero to unity. In the case of $V_b = 0$, one expects that at sufficiently low temperatures the properties of such systems should be essentially the same as the properties of strictly two-dimensional uniform systems. The behaviour of two-dimensional Lennard-Jones systems has been intensively studied [164 – 169] with the help of computer simulation methods and density functional theory. Although the mechanism of the melting transition is still not clear, but the phase diagram is now fairly well known. In particular, the triple point temperature is located at $T^*_{tr} = 0.40 \pm 0.01$ and the triple point density is equal to about $\rho^*_{tr} = \rho\sigma^{*2} \approx 0.79$ [167]. A little more controversial is the location of the critical point. Barker *et al.* [165] have obtained $T^*_c \approx 0.56$, while more recent Monte Carlo simulation [169] has given a somewhat lower value of 0.50 ± 0.02. The differences in the values of the critical point temperature obtained by different authors are not surprizing, however. The recent Monte Carlo simulations in the Gibbs ensemble [170,171] have clearly demonstrated that the way one cuts the interaction potential considerably influences the estimated critical temperature. It appears that the tail of the interaction potential (beyond the assumed cut-off distance) has a big influence on the obtained results.

Figure 9 presents the heat capacities *versus* temperature for the Lennard-Jones monolayers of different sigma and density adsorbed on the noncorrugated (flat) surface.

These results are in a good agreement with earlier findings. For the systems of the density lower then the triple point density ρ^*_{tr} we observe very sharp heat capacity maxima at the temperature of 0.38 ± 0.01. Although this value is slightly lower than the temperature of the triple point found in other works [160,166], but this can be attributed to the effects due to rather small cut-off distance of the potential (1) set at $r_{max} = 2.5\sigma^*$. Besides, finite size effects as well as the out-of-plane motion may contribute to the observed shift in the location of the melting point. The results obtained for the density exceeding the triple-point density do not show any trace of the melting transition. The heat capacity changes smoothly and exhibits only a broad maximum at high temperatures, similarly as in the case of films with lower density. These broad maxima are associated with desorption and transfer of adsorbed particles to the second layer as confirmed by the density profiles calculated at different temperatures. The desorption process starts at considerably lower temperatures for the system with the density exceeding ρ^*_{tr} than in other systems. Therefore, it is possible that the melting transition is accompanied by the transfer of adsorbed atoms to the second layer and hence no sharp heat capacity maximum is observed.

In the case when the gas – solid potential exhibits periodic variations, a competition between the surface potential corrugation and the gas – gas interaction becomes a major factor determining the structure of the film. From the calculations of the heat capacity for

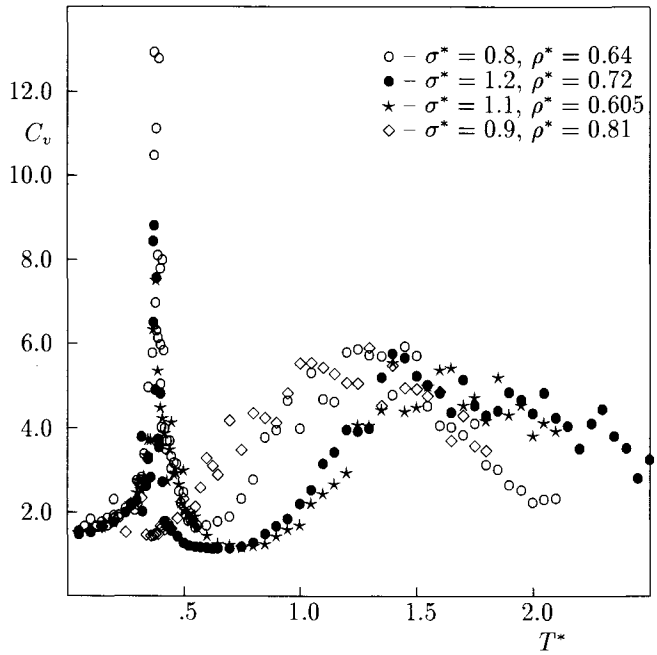

Figure 9. Heat capacities for the Lennard-Jones systems adsorbed on the planar surface obtained from the canonical ensemble Monte Carlo simulation [163].

isolated atoms adsorbed on lattices characterized by different symmetry and size [172,173] it follows that there is a gradual transition between localized and mobile states, leading to the appearance of broad peaks with the maximum located at the temperature $T^* = (0.21 \pm 0.01)V_t^*$, where V_t^* is the height of potential barrier for translation, defined as

$$V_t^* = V_{SP}^* - V_S^* \tag{31}$$

In the above, V_{SP}^* and V_S^* represent the minima of the gas – solid interaction potential corresponding to the saddle point and the center of the surface unit cell, respectively. Of course, one should not expect to observe such localized-to-mobile transition in dense films. An isolated atom adsorbed on a surface with non-zero corrugation effects always exhibits full localization in the ground state, while dense films may exhibit different structure depending on the height of the potential barrier between adjacent potential minima. In particular, in the case of adsorption on the (100) face of fcc crystal the film may form the hexagonal close-packed (incommensurate) phase, the uniaxially ordered phase or the registered phase of a square symmetry. Regions of stability of the hexagonal close packed (hcp) and the registered phases for monolayers formed on the (100) fcc surface at $T^* = 0.0$ are shown in Fig. 10. Although the results presented in figure 10 do not include uniaxally ordered states, but one can speculate that such structures are most likely to appear for the systems with the surface potential corrugation close to the values delimiting the regions of stability for the hexagonal close packed and the registered phases. Indeed, the results

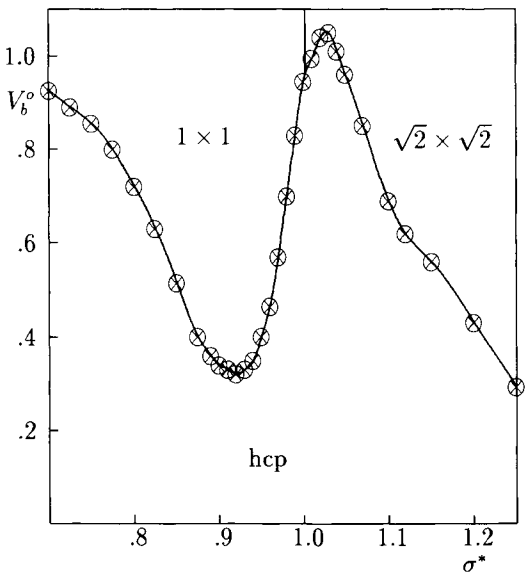

Figure 10. The regions of stability for the hexagonal close packed and the registered phases at $T^* = 0$ for monolayer films formed on the (100) face of an fcc crystal.

of Monte Carlo simulations have shown that uniaxial ordering develops in such systems at temperatures below the melting point. The transition between the low temperature ordinary hexagonal close packed phase and the uniaxially ordered phase appears to be smeared over a wide temperature range in the studied systems. Also, this transition appears to be reversible with respect to the direction of the temeprature changes. In order to detect the formation of the uniaxially ordered phase one can use the distribution function of particles over the surface $n_z(x, y)$, reduced to a single unit lattice cell and calculated at different distances from the surface as well as examine the snap-shots of equilibrium configurations generated during the simulation as shown in Figure 11.

Monte Carlo simulation performed for a series of systems characterized by different corrugation of the gas – solid potential and for particles of different size have shown that the mechanism of melting and disordering in monolayer films depends strongly on the gas – solid potential corrugation. In monolayers being a subject to only weakly corrugated potential and exhibiting the hexagonal close packed structure at the ground state, melting occurs at different temperatures depending on the gas – solid potential corrugation parameter V_b. Figure 12 shows the low temperature behaviour of the gas – gas and the gas – solid interaction energies for a series of systems with $\sigma^* = 0.8$ being a subject to the surface potential of different corrugation. In all cases we find clear indication of the phase transition. The location of this transition changes gradually towards lower temperatures with the corrugation of the gas – solid potential and seems to converge to zero for the corrugation at which the hexagonal close packed phase looses stability at the ground state (see Fig. 13). It should be noted that in the case of methane monolayer on graphite, studied by Kim and Steele [160], an opposite effect has been observed, *i.e.*, the increase in

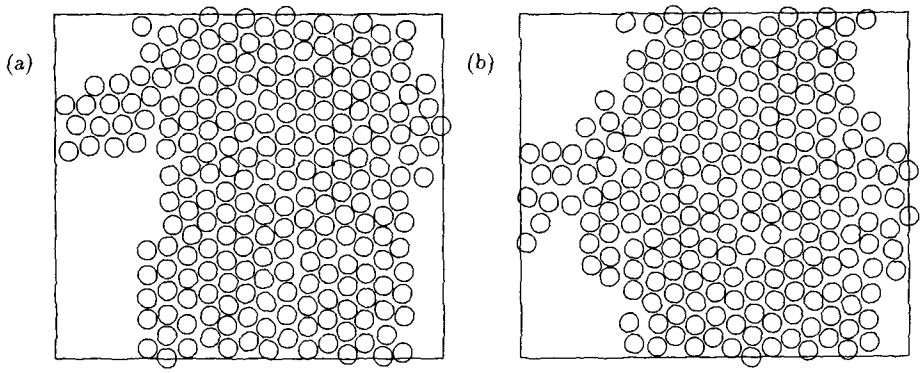

Figure 11. Equilibrium configuration for the system with $\sigma^* = 0.8$ and $V_b = 0.5$ at $T^* = 0.25$ and 0.30.

the gas – solid potential modulation has led to the increase of the melting temperature.

For the systems exhibiting the registered 1×1 ordered structure at low temperatures, the disordering is a continuous process occuring gradually over a wide temperature range. A quite different behaviour has been found for the registered films of larger particles ordering into the $\sqrt{2} \times \sqrt{2}$ structure. In this case the surface lattice can be considered as composed of two interpenetrating sublattices, and only one of them is occupied in the ordered phase. As the temperature increases this phase undergoes a transition into the disordered fluid characterized by more or less uniform occupation of both sublattices. This transition is expected to be similar to the order– disorder transition in the Ising model [77]. As the gas – solid potential corrugation becomes higher the order–disorder transition is shifted towards higher temperatures (see Fig 13.b). As the potential barriers between adjacent sites increase, the registered state retains stability over the wider temperature range. Similar situation occurs in the mentioned above study of methane films formed on graphite, and explains the observed increase of the transition temperature with V_b.

Although the observed changes in the thermodynamic properties of adsorption systems, such as the gas – gas and the gas – solid contributions to the total energy, the heat capacity and the compressibility, allow to estimate the melting temperature, but such quantities do not say much about the changes in the inner structure of the adsorbed film. To investigate subtle changes in the mutual arrangement of adsorbed particles and shifts of their positions relative to the surface lattice one needs to use appropriate tools. In numerous computer simulation studies of melting in two-dimensional systems [162,168,174,175] the local order has been measured using the bond-orientational order parameters [176]. For the considered here systems it has been found very useful to introduce three different bond-orientational order parameters, which are defined by the following equations:

$$\psi_l = \left| \frac{1}{N_b} \sum_m \sum_n \exp[il\phi_{mn}] \right| \quad , \quad l = 4, 6 \tag{32}$$

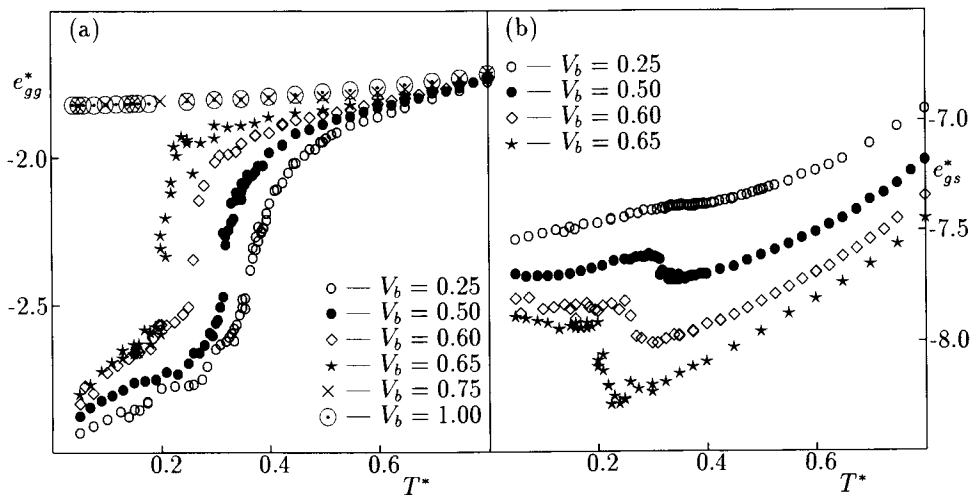

Figure 12. The gas - gas (part a) and the gas - solid (part b) components of the total energy for systems with $\sigma^* = 0.8$ and characterized by different corrugation of the gas - solid potential.

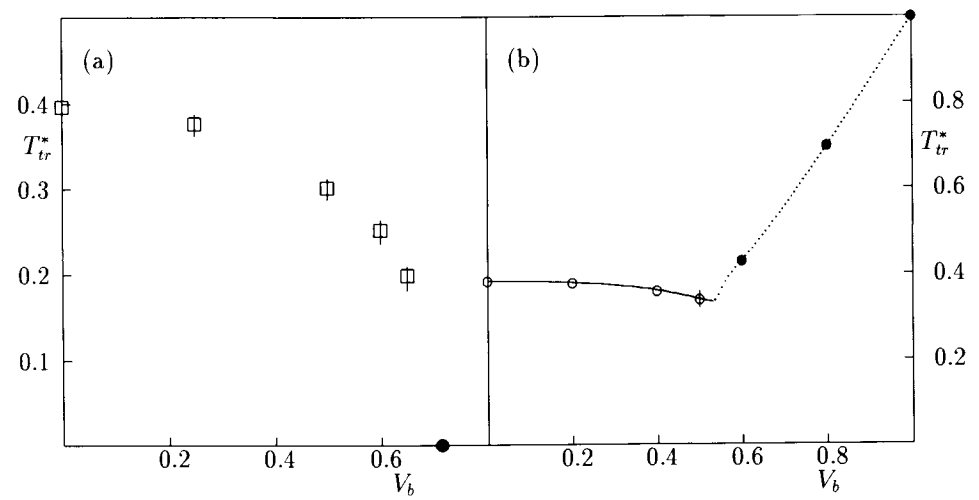

Figure 13. The dependence between the melting point and the parameter V_b. for systems with $\sigma^* = 0.8$ (part a) and 1.2 (part b). In Part a, the solid point marks the value of V_b delimiting the regions of hexagonal close packed and registered structures at $T^* = 0.0$. In part b, open circles mark the melting points for the hcp phase, and the filled points the order–disorder transition for the $\sqrt{2} \times \sqrt{2}$ phase.

and

$$\psi_6^e = \left| \frac{1}{N_b} \sum_m \sum_n \cos(6\phi_{mn}) \right| \tag{33}$$

In the above equations the first sums run over all particles in the system, the second sums are taken over all nearest neighbours of any particle m, ϕ_{mn} is the angle between the bond joining particles m and n and a chosen reference axis (taken to be one of the surface lattice axes) and N_b is the number of bonds in the system.

Basically, the bond-orientational order parameters defined by egn. (31) suffice to distinguish between the ordered and the disordered phases and to determine whether the film forms the registered or the hexagonal close packed structure. Namely, in the disordered, liquid or gas, phase the both bond-orientational order parameters ψ_4 and ψ_6 should be close to zero, since all possible mutual orientations of bonds appear with the same probability in the system. In the registered phases of square symmetry (1×1, $\sqrt{2} \times \sqrt{2}$ or 2×2) one expects that $\psi_4 \approx 1.0$ while $\psi_6 \approx 0.0$. On the contrary, when the solid phase has the hexagonal symmetry then $\psi_4 \approx 0.0$ and $\psi_6 \approx 1.0$. In the case of uniaxially ordered phase, we can expect nontrivial behaviour of the bond-orientational order parameters ψ_6^e, ψ_6 and ψ_4. The order parameter ψ_6^e, defined by egn. (32), has been primarily introduced in order to study orientational alignment in the hexagonal close packed incommensurate films, as predicted by the theory of McTague and Novaco [93]. Namely, one expects that $\psi_6^e = 1$ when one of the symmetry axes of the hexagonal solid phase coincides with the x or y axis of the surface lattice, *i.e.*, in the case of uniaxial epitaxy. When the orientation of the adsorbed film changes the bond-orientational parameter ψ_6^e decreases rapidly, while ψ_6 may remain nearly unchanged.

Apart from the defined above bond-orientational order parameters (see eqns. (31) and (32)) it is useful to define the corresponding susceptibilities

$$\chi_l(L,T) = \frac{1}{kT}[< \psi_l^2 > - < \psi_l >^2] \tag{34}$$

and

$$\chi_l^e(L,T) = \frac{1}{kT}[< \psi_l^{e2} > - < \psi_l^e >^2] \tag{35}$$

as well as the fourth-order cumulants

$$U_l(L,T) = 1 - \frac{< \psi_l^4 >}{3 < \psi_l^2 >^2} \tag{36}$$

and

$$U_l^e(L,T) = 1 - \frac{< \psi_l^{e4} >}{3 < \psi_l^{e2} >^2} \tag{37}$$

where $l = 4$ or 6. These quantities can be used to determine the location of the phase transition point as well as the order of the observed transition. In particular, the susceptibilities should behave in a similar way as the compressibility and obey appropriate

scaling laws. Thus, one can use the finite size scaling theory to distinguish between the first-order and the higher-order transitions and to determine the transition point as well as the critical exponents. The fourth-order cumulants have been studied extensively for various phase transitions [126,177 - 182]. In particular, the changes of the fourth-order cumulants with density for systems with different size have been recently used by Weber *et al.* [175] to determine the order of melting transition in the two-dimensional hard-disk system, while Marx *et al.* [182] have used the fourth-order cumulants to study orientation of nitrogen adsorbed on graphite.

Preliminary results of Monte Carlo simulation [183] have also demonstrated the usefulness of the bond - orientational order parameters in determining the inner structure of films adsorbed on the (100) face of an fcc crystal.

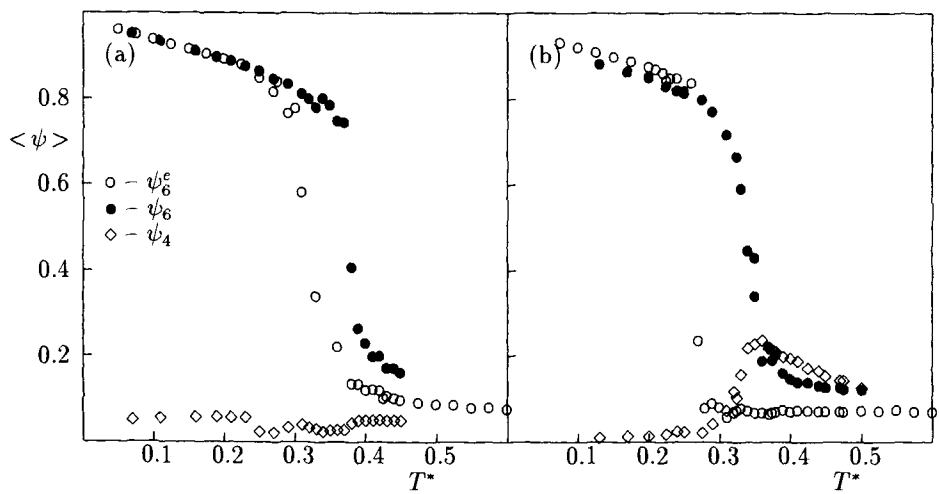

Figure 14. The bond-orientational order parameters for the two-dimensional films of particles with $\sigma^* = 1.2$ formed on the (100) fcc plane with characterized by different corrugation of the gas - solid potential (V_b=0.2 (a) and 0.4 (b)).

Figure 14 presents examples of the bond-orientational order parameter, plotted against temperature, which clearly indicate the existence of rotational alignment in the two-dimensional incommensurate solid phase formed on weakly corrugated surface. As is seen the bond-orientational order parameter ψ_6^e drops at considerably lower temperature then the order parameter ψ_6. This provides a direct indication that the incommensurate solid phase looses its parallel orientation relative to the x axis of the solid lattice but retains hexagonal symmetry over a certain temperature range. One should also note that the bond-orientational order parameter ψ_4 increases considerably near the melting point. This shows that the liquid phase exhibits partial positional ordering resulting from the effects due to the surface corrugation. In the system with higher corrugation of the gas - solid potential we find registered film at low temperatures (the bond-orientational order parameter ψ_4 approaches unity as the temperature goes to zero) while ψ_6 remains very low. In principle, the parameter ψ_6 should be equal to zero when the adsorbed film

forms a registered structure of a square symmetry. The observed deviations result from the finitness of the systems used in the simulation.

Similar approach can be used to study phase transitions in films formed on other crystals, e.g., on the (110) faces of fcc and bcc crystals of various metals. It is possible to define the appropriate bond-orientational order parameters suitable for determining the formation of registered and uniaxial structures. Such computer simulation studies can be very helpful in determining the role of the surface corrugation on the structure of adsorbed films and the nature of phase transitions between different adsorbed phases.

REFERENCES

1. G. Jura, W. D. Harkins, E. H. Loeser, J. Chem. Phys., 14 (1946) 244.
2. E. B. Rifkin, E. C. Kerr, H. L. Johnson, J. Am. Chem. Soc., 75 (1953) 785.
3. H. Clark, S. Ross, J. Am. Chem. Soc., 75 (1953) 6081.
4. S. Ross, W. Winkler, J. Am. Chem. Soc., 76 (1954) 2637.
5. S. Ross, H. Clark, J. Am. Chem. Soc., 76 (1954) 4281, 4297.
6. H. Clark, J. Phys. Chem., 59 (1955) 1068.
7. B. B. Fisher, W. G. McMillan, J. Am. Chem. Soc., 79 (1957) 2969.
8. D. M. Young, A. D. Crowell, Physical Adsorption of Gases, Butterworths, London, 1962.
9. J. W. Drenan, T. L. Hill, J. Phys. Coll. Chem., 54 (1950) 1132.
10. R. H. Fowler, Proc. Camb. Phil. Soc., 32 (1936) 144.
11. A. Thomy, X. Duval, Colloques Internationaux du CNRS, Nancy, 132 (1965) 81.
12. A. Thomy, X. Duval, J. Chim. Phys., 66 (1969) 1966.
13. A. Thomy, X. Duval, J. Chim. Phys., 67 (1970) 286, 1101.
14. M. Matecki, A. Tomy, X. Duval, J. Chim. Phys., 71 (1974), 1484.
15. A. Thomy, X. Duval, J. Regnier, Surface Sci. Rep., 1 (1981) 1.
16. A. Enault, Y. Larher, Phys. Lett., 48A (1974) 213.
17. Y. Nardon, Y. Larher, Surf. Sci., 42 (1974) 299.
18. A. Enault, Y. Larher, Surf. Sci., 62 (1977) 233.
19. Y. Larher, Molec. Phys., 38 (1979) 789.
20. D. Schmicker, J. P. Toennies, R. Vollmer, H. Weiss, J. Chem. Phys., 95 (1991) 9412.
21. D. Scarano, A. Zecchina, J. Chem. Soc., Faraday Trans. I, 82 (1986) 3611.
22. J. Heidberg, E. Kampshoff, R. Kühnemuth, O. Schönekäs, Surf. Sci., 269/270 (1992) 120.
23. J. Heidberg, E. Kampshoff, R. Kühnemuth, M. Suhren, H. Weiss, Surf. Sci., 269/270 (1992) 128.
24. J. P. Coulomb, T. S. Sullivan, O. E. Vilches, Phys. Rev., B 30 (1984) 4753.
25. M. Sidoumon,T. Angot, J. Suzanne, Surf. Sci., 272 (1992) 347.
26. J. M. Dickey, H. H. Farrell, M. Strongin, Surf. Sci., 23 (1970) 448.
27. M. A. Chesters, J. Pritchard, Surf. Sci., 28 (1971) 460.
28. H. Pfnür, D. Menzel, Surf. Sci., 148 (1984) 411.
29. E. R. Moog, M. B. Webb, Surf. Sci., 148 (1984) 338.
30. A. Glachant, M. Jaubert, M. Bienfait, G. Boato, Surf. Sci., 115 (1981) 219.

31. M. Bretz, J. G. Dash, D. C. Hickernell, E. O. McLean, O. E. Vilches, Phys. Rev., A 8 (1973) 1589.
32. T. T. Chung, J. G. Dash, Surf. Sci., 117 (1977) 559.
33. A. Marx, Phys. Rep., 125 (1985) 1.
34. A. Marx, E. F. Wassermann, Surf. Sci., 117 (1982) 267.
35. H. Wiechert, H. Freimuth, H.J. Lauter, Surf. Sci., 269/270 (1992) 452.
36. A. J. Jin, M. R. Bjurstrom, M. H. W. Chan, Prys. Rev. Lett., 62 (1989) 1372.
37. R. D. Diehl, S. C. Fain, Jr., Phys. Rev., B 26 (1982) 4785.
38. J. Suzanne, J. L. Sequin, H. Taub, J. P. Biberian, Surf. Sci., 125 (1983) 153.
39. H. You, S. C. Fain, Jr., Surf. Sci., 151 (1985) 361.
40. T. Meichel, J. Suzanne, C. Girard, C. Girardet, Phys. Rev., B 38 (1988) 3781.
41. M. Sidoumou, T. Angot, J. Suzanne, Surf. Sci., 272 (1992) 347.
42. J. K. Kjems, L. Passell, H. Taub, J. G. Dash, Phys. Rev. Lett., 32 (1974) 724.
43. J. P. Coulomb, R. Khan, M. Bienfait, Surf. Sci., 61 (1976) 291.
44. M. Monkenbusch, Ph. D. Thesis, Jülich, 1981.
45. G. J. Trott, H. Taub, F. Y. Hansen, H. R. Danner, Chem. Phys. Lett., 78 (1981) 504.
46. J. P. Coulomb, M. Bienfait, P. Thorel, Phys. Rev. Lett., 42 (1979) 733.
47. P. M. Horn, R. J. Birgenau, P. Heiney, E. M. Hammonds, Phys. Rev. Lett., 41 (1978) 961.
48. K. Kjaer, M. Nielsen, J. Bohr, H. J. Lauter, J. P. McTague, Phys. Rev., B 26 (1982) 5168.
49. K. Morishige, C. Mowforth, R. K. Thomas, Surf. Sci., 151 (1985) 289.
50. H. Shechter, J. Suzanne, J. G. Dash, Phys. Rev. Lett., 37 (1976) 706.
51. H. Shechter, J. Suzanne, J. G. Dash, J. Phys., (Paris), 40 (1979) 467.
52. H. Shechter, J. G. Dash, M. Mor, R. Ingalls, S. Bukshpan, Phys. Rev., B 14 (1976) 1876.
53. H. Shechter, R. Brenner, J. Suzanne, Surf. Sci., 114 (1982) L10.
54. H. Shechter, R. Brenner, J. Suzanne, S. Bukshpan, Phys. Rev., B 26 (1982) 5506.
55. J. W. O. Faul, U. G. Volkmann, K. Knorr, Surf. Sci., 227 (1990) 390.
56. H. S. Youn, X. F. Meng, G. B. Hess, Phys. Rev., B 48 (1993) 14556.
57. D. P. Grimmer, K. Lucszynski, in: Proc. Conference on Low Temperature Physics - LT13, W. J. O'Sullivan, K. D. Timmerhaus, E. F. Hammel, (eds.), Plenum, New York, 1973, p.376.
58. R. J. Rollefson, Phys. Rev. Lett., 29 (1972) 410.
59. J. W. Riehl, K. Koch, J. Chem. Phys., 57 (1972) 2199.
60. J. Tabony, G. Bomchil, N. M. Harris, M. Leslie, J. W. White, J. Chem. Soc. Faraday Trans. I, 75 (1979) 1570.
61. J. G. Dash, Films on Solid Surfaces, Academic Press, New York, 1975.
62. J. G. Dash, J. Ruvalds (eds.) Phase Transitions in Surface Films, Plenum, New York, 1979.
63. G. L. Price, J. A. Venables, Surf. Sci., 59 (1976) 509.
64. J. Villain, in: Oredering is Strongly Fluctuating Condensed Matter Systems, T. Riste, (ed.), Plenum, New York, 1980.
65. M. Schick, J. S. Walker, M. Wortis, Phys. Rev., B 16 (1977) 2205.
66. R. Pandit, M. Schick, M. Wortis, Phys. Rev., B 26 (1982) 5112.

67. D. E. Sullivan, M. M. Telo da Gama, in: Fluid Interfacial Phenomena, C. A. Ctoxton. (ed.), Wiley, Chichester, 1986.
68. A. Patrykiejew, M. Jaroniec, Adv. Colloid Interface Sci., 20 (1984) 273.
69. A. Patrykiejew, S. Sokołowski, Adv. Colloid Interface Sci., 30 (1989) 203.
70. D. K. Fairobent, F. W. Saam, L. M. Sander, Phys. Rev., B 26 (1982) 179.
71. D. Nicholson, N. G. Parsonage, Computer Simulation and the Statistical Mechanics of Adsorption, Academic Press, London, 1982.
72. F. F. Abraham, Rep. Progr. Phys., 45 (1982) 1113.
73. F. F. Abraham, Adv. Phys., 35 (1986) 1.
74. F. F. Abraham, Phys. Rep., 80 (1981) 339.
75. W. Selke, Phys. Rep., 170 (1988) 213.
76. B. Dünweg, A. Milchev, P. A. Rirvold, J. Chem. Phys., 94 (1991) 3958.
77. K. Binder, D. P. Landau, Advances in Chemical Physics, K. P. Lawley, (ed.), Wiley, New York, 1989.
78. A. Patrykiejew, D. P. Landau, K. Binder, Surf. Sci., 238 (1990) 317.
79. A. Patrykiejew, Langmuir, 9 (1993) 2562.
80. D. P. Landau, Phys. Rev., B 27 (1983) 5604.
81. J. Regnier, A. Thomy, X. Duval, J. Colloid Interface Sci., 70 (1979) 105.
82. C. Bockel, A. Thomy, X. Duval, Surf. Sci., 90 (1979) 109.
83. A. G. Naumovets, Surf. Sci., 299/300 (1994) 706.
84. M. Grunze, P. H. Kleban, W. N. Unertl, F. S. Rys, Phys. Rev. Lett., 51 (1983) 582.
85. J. Dericbourg, Surf. Sci., 310 (1994) L605.
86. L. D. Roelofs, A. R. Kortan, T. L. Einstein, R. L. Park, Phys. Rev. Lett., 46 (1981) 1465.
87. A. Clark, Theory of Adsorption and Catalysis, Academic Press, New York, 1972.
88. W. A. Steele, Surf. Sci., 36 (1973) 317.
89. S. Calisti, J. Suzanne, J. A. Venables, Surf. Sci., 115 (1982) 455.
90. J. Villain, M. B. Gordon, Surf. Sci., 125 (1983) 1.
91. F. F. Abraham, Phys. Rep., 80 (1981) 339.
92. A. D. Novaco, J. P. McTague, Phys. Rev. Lett., 38 (1977) 1286.
93. J. P. McTague, A. D. Novaco,Phys. Rev., B 19 (1979) 5299.
94. J. M. Gottlieb, L. W. Bruch, Phys. Rev., B 44 (1991) 5750, 5759.
95. L. W. Bruch, J. A. Venables, Surf. Sci., 148 (1984) 167.
96. L. W. Bruch, Surf. Sci., 150 (1985) 503.
97. A. Patrykiejew, S. Sokołowski, T. Zientarski, K. Binder, J. Chem. Phys., (in press).
98. D. P. Landau, in: Applications of the Monte Carlo Methods in Statistical Physics, Topics in Current Physics, vol. 36, K. Binder, (ed.), Springer, Berlin, 1984, p. 84.
99. K. Binder, D. P. Landau, Phys. Rev., B 21 (1980) 1941.
100. A. Patrykiejew, Thin Solid Films, 139 (1986) 209.
101. N. Georgiev, A. Milchev, M. Paunov, B. Dünweg, Surf. Sci., 264 (1992) 455.
102. S. N. Sun, M. Y. Chou, Surf. Sci., 280 (1993) 415.
103. N. C. Bartelt, T. L. Einstein, L. D. Roelofs, Phys. Rev., B 35 (1987) 1776.
104. K. Binder, D. P. Landau, Surf. Sci., 108 (1981) 503.
105. A. Patrykiejew, P. Borowski, Thin Solid Films, 195 (1991) 367.
106. A. Patrykiejew, S. Sokołowski, R. Zagórski, Thin Solid Films, 254 (1995) 116.
107. M. P. Nightingale, Physica, A 83 (1976) 561.
108. K. Kaski, W. Kinzel, J. D. Gunton, Phys. Rev., B 27 (1983) 6777.
109. F. Buda, G. M. Florio, P. V. Giaquinta, Phys. Rev., B 35 (1987) 2021.

110. M. N. Barrer, Phys. Rep., 59 (1980) 375.
111. A. N. Berker, S. Ostlund, F. A. Putnam, Phys. Rev., B 17 (1978) 3650.
112. S. Ostlund, A. N. Berker, Phys. Rev., B 21 (1980) 5410.
113. M. Suzuki, J. Phys. Soc. Japan, 55 (1986) 4205.
114. M. Suzuki, M. Katori, X. Hu, J. Phys. Soc. Japan, 56 (1987) 3092.
115. M. Katori, M. Suzuki, J. Phys. Soc. Japan, 56 (1987) 3113.
116. A. Patrykiejew, P. Borowski, Phys. Rev., B 42 (1990) 4670.
117. N. Ito, M. Suzuki, in: Computer Simulation Studies in Condensed Matter Physics, D. P. Landau, K. K. Mon, H.-B. Schütter, (eds.), Springer, Berlin, 1991, p.16.
118. W. Kinzel, W. Selke, K. Binder, Surf. Sci., 121 (1982) 13.
119. H. H. Lee, D. P. Landau, Phys. Rev., B 20 (1979) 2893.
120. J. Amar, S. Katz, J. D. Gunton, Surf. Sci., 155 (1985) 667.
121. P. Borowski, A. Patrykiejew, S. Sokołowski, Thin Solid Films, 177 (1989) 333.
122. H. E. Stanley, An Introduction to Phase Transitions and Critical Phenomena, Oxford University Press, Oxford, 1971.
123. Finite Size Scaling and Numerical Simulation of Statistical Systems, V. Privman, (ed.), World Scientific, Singapore, 1990.
124. M. E. Fisher, M. N. Barber, Phys. Rev. Lett., 28 (1972) 1516.
125. M. E. Fisher, in: Critical Phenomena, M. S. Green, (ed.), Academic Press, New York, 1971, p.1.
126. K. Binder, Z. Phys., B 43 (1981) 119.
127. F. Millot, Y. Larher, C. Tessier, J. Chem. Phys., 76 (1980) 3327.
128. A. Patrykiejew, Thin Solid Films, 88 (1982) 359.
129. M. D. Grynberg, H. Ceva, Phys. Rev., B 38 (1988) 9172.
130. D. P. Landau, K. Binder, Phys. Rev., B 31 (1985) 5946.
131. K. Binder, D. P. Landau, Phys. Rev., B 30 (1984) 1477.
132. K. Binder, Phys. Rev. Lett., 47 (1981) 693.
133. M. N. Barber, W. Selke, J. Phys., A 15 (1982) 617.
134. M. S. S. Challa, D. P. Landau, K. Binder, Phys. Rev., B 34 (1986) 1841.
135. J. Unguris, L. W. Bruch, M. B. Webb, J. M. Phillips, Surf. Sci., 114 (1982) 219.
136. L. D. Roelofs, A. R. Kortan, T. L. Einstein, R. L. Park, Phys. Rev. Lett., 46 (1981) 1465.
137. P. Piercy, H. Pfnür, Phys. Rev. Lett., 59 (1987) 1124.
138. S. Alexander, Phys. Lett., 54A (1975) 353.
139. M. Schick, Progr. Surf. Sci., 11 (1981) 245.
140. E. Domany, M. Schick, J. S. Walker, R. B. Griffiths, Phys. Rev., B 18 (1978) 2209.
141. S. Ostlund, A. N. Berker, Phys. Rev. Lett., 42 (1979) 843.
142. W. Kinzel, M, Schick, A. N. Berker, in: Ordering in Two Dimensions, S. K. Sinha, (ed.), North Holland, Amsterdam, 1980, p.381.
143. L. P. Kadanoff, Ann. Phys., New York, 100 (1976) 359.
144. J. P. McTague, J. Als-Nielsen, J. Bohr, M. Nielsen, Phys. Rev., B 25 (1982) 7765.
145. F. C. Motteler, J. G. Dash, Phys. Rev., B 31 (1985) 346.
146. M. den Nijs, in: Phase Transitions and Critical Phenomena, vol. 12, C. Domb, J. L. Lebowitz, (eds.), Academic Press, London, 1988.
147. J. M. Gottlieb, L. W. Bruch, Phys. Rev., B 44 (1991) 5750, 5759.
148. L. W. Bruch, Surf. Sci., 250 (1991) 267.
149. J. M. Gottlieb, Phys. Rev., B 42 (1990) 5377.

150. J. M. Houlrik, D. P. Landau, Phys. Rev., B 44 (1991) 8962.
151. D. A. Faux, G. Gaynor, C. L. Carson, C. K. Hall, J. Bernholc, Phys. Rev., B 42 (1990) 2914.
152. S. Ostlund, Phys. Rev., B 24 (1981) 398.
153. B. I. Halperin, D. R. Nelson, Phys. Rev. Lett., 41 (1978) 121.
154. D. R. Nelson, B. I. Halperin, Phys. Rev., B 19 (1979) 2457.
155. L. M. Sander, J. Hautman, Phys. Rev., B 29 (1984) 2171.
156. K. J. Niskanen, Phys. Rev., B 33 (1986) 1830.
157. N. D. Shripton, B. Joós, B. Bergersen, Phys. Rev., B 38 (1988) 2124.
158. F. F. Abraham, Phys. Rev. Lett., 50 (1983) 978.
159. F. F. Abraham, Phys. Rev., B 28 (1983) 7338.
160. H.-Y. Kim, W. A. Steele, Phys. Rev., B 45 (1992) 6226.
161. J. M. Kosterlitz, D. J. Thouless, J. Phys., C 6 (1973) 118.
162. K. J. Strandburg, Rev. Mod. Phys., 60 (1988) 161.
163. A. Patrykiejew, S. Sokołowski, T. Zientarski, K, Binder, J. Chem. Phys. (in press).
164. D. Henderson, Molec. Phys., 34 (1979) 301.
165. J. A. Barker, D. Henderson, F. F. Abraham, Physica A, 106 (1981) 226.
166. J. M. Phillips, L. W. Bruch, R. D. Murphy, J. Chem. Phys., 75 (1981) 5097.
167. J. Tabochnik, G. V. Chester, Phys. Rev., B 25 (1982) 6778.
168. C. Udink, D. Frenkel, Phys. Rev., B 35 (1987) 6933.
169. M. Rovere, D. W. Heermann, K. Binder, J. Phys. Condens. Matt., 2 (1990) 7009.
170. A. Z. Panagiotopoulos, Mol. Simul., 9 (1992) 1.
171. B. Smit, D. Frenkel, J. Chem. Phys., 94 (1991) 5663.
172. T. L. Hill, J. Chem. Phys., 14 (1946) 441.
173. J. J. Doll, W. A. Steele, Surf. Sci., 44 (1974) 449.
174. C. Udink, J. van der Elsken, Phys. Rev., B 35 (1987) 279.
175. H. Weber, D. Marx, K. Binder, Phys. Rev, B (preprint).
176. Bond-Orientational Order in Condensed Matter Systems, K. J. Strandburg, (ed.), Springer, New York, 1992.
177. K. Binder, Ferroelectics, 73 (1987) 43.
178. D. Marx, P. Nielaba, K. Binder, Phys. Rev., B 47 (1993) 7788.
179. K. Vollmayr, J. D. Reger, M. Scheucher, K. Binder, Z. Phys., B 91 (1993) 113.
180. D. Marx, S. Sengupta, O. Opitz, P. Nielaba, K. Binder, Molec. Phys., (in press).
181. M. S. S. Challa, D. P. Landau, Phys. Rev., B 33 (1986) 437.
182. D. Marx, S. Sengupta, P. Nielaba, K. Binder, Surf. Sci., 321 (1994) 195.
183. A. Patrykiejew, T. Zientarski, K. Binder (unpublished).

This Page Intentionally Left Blank

A. Dąbrowski and V.A. Tertykh (Editors)
Adsorption on New and Modified Inorganic Sorbents
Studies in Surface Science and Catalysis, Vol. 99

Chapter 2.12
Drying of gases and liquids by activated alumina

S. Sircar, M. B. Rao and T. C. Golden

Air Products and Chemicals, Inc., 7201 Hamilton Boulevard, Allentown, PA, 18195, USA

1. INTRODUCTION

Removal of trace and bulk water from a fluid (gas or liquid) stream is a major unit operation in the chemical and petrochemical industries [1–3]. The drying process is necessary to (a) prevent condensation and freeze-out of water in plant pipeline and equipment, (b) eliminate corrosion in process equipment, (c) protect against undesirable chemical reactions such as hydration, hydrolysis, etc., (d) prevent catalyst poisoning, and (e) meet product fluid composition specification. Selective adsorption of water on a solid desiccant such as zeolites, silica gels and activated aluminas is often used as the method of drying the fluid stream. Various forms of cyclic pressure swing adsorption (PSA) and thermal swing adsorption (TSA) concepts are generally used as the drying process. These processes utilize regenerative schemes consisting of adsorption and desorption steps so that the adsorbent can be repeatedly used for drying the fluid stream. The design and cost of operation of these processes demand certain properties for adsorption of water by the adsorbent which facilitate the adsorption and desorption steps. Activated aluminas often provide a large spectrum of desirable adsorptive properties for such drying applications. These properties include adsorption equilibria, adsorption kinetics, heats of adsorption, and adsorption and desorption column dynamics which govern the performance of the drying process. This chapter briefly describes these properties for adsorption of water on various forms of alumina and illustrates several conventional drying processes using alumina.

2. PHYSICOCHEMICAL STRUCTURE OF ALUMINA

Most aluminas are produced by precipitation from an aluminate solution using the well-known Bayer process [4]. Numerous stable and transitional forms of alumina can be formed. The thermodynamically stable forms such as alpha alumina are of little use for drying application because of their low surface areas and porosities. The transitional aluminas such as gamma and eta which are formed by thermal dehydration of aluminum hydroxides are mostly used as desiccants. They consist of Al^{+3} and O^{-2} ions bonded in either tetrahedral or octahedral coordination. The resulting crystal structure is cubic or hexagonal closed packed. Generally, the oxygen sublattice is fairly well organized and

the aluminum sublattice is more disordered which actually makes many commercially available aluminas (mainly gamma form) amorphous in nature. A random grouping of aluminum oxides and hydroxides form the structure of the commercial alumina. These can create a large spectrum of micro- and meso pores with surfaces containing both basic (hydroxyl and O^{-2} anion vacancies) and acidic (unsaturated Al^{+3} ions as Lewis and protonated hydroxyl as Brönsted) sites of various strengths and concentrations [4].

The chemical nature of the sites of alumina for water adsorption is not clearly understood. Chemisorption of water through dissociation into H^+ and OH^- ions which attach to the alumina surface, hydrogen bonding of water with surface oxygen and hydroxyl groups, van der Waals and pole-pole interactions between the water molecule and the alumina surface as well as condensation of water vapour in the mesopores of alumina are possible mechanisms [5].

Table 1 lists some of the physical properties of several commercially produced activated aluminas. It shows the available variety of structural properties. These values were obtained from the manufacturer's literature.

Table 1
Physical properties of activated aluminas

	F-1	H-151	AA-300	R-P Grade A	A-201	Actal
Manufacturer	Alcoa USA	Alcoa USA	Alcan Canada	Rhone-Poulenc France	Kaiser USA	Laporte UK
BET Area (m^2/g)	260	350	330	340	350	275
Pore Volume (cm^3/g)	0.40	0.43	0.44	0.40	0.46	0.50
Bulk Density (g/cm^3)	0.85	0.85	0.84	0.77	0.75	0.64
Particle Density (g/cm^3)	1.42	1.38	1.34	-	1.40	1.15
Mean Pore Diameter (Å)	26	43	65	20, 40	52	28

3. ADSORPTION OF WATER VAPOUR FROM GAS STREAMS ON ACTIVATED ALUMINAS

The difference in the pore structure and surface chemistry of different activated aluminas is manifested by significantly different characteristics for adsorption of water vapour as pure gas or from gas mixtures. These properties are illustrated below.

3.1. Equilibrium adsorption of pure water vapour

The isotherms for adsorption of pure water vapour on activated aluminas are typically Type I (microporous) or Type IV (mesoporous) in shape according to the Brunauer classification [6]. Figure 1 shows several examples. Alcoa F-1 alumina has a type I shape while Alcan AA-300 and Alcoa H-156 exhibit type IV shapes. The plots represent the specific amount of water vapour adsorbed (n, g/g) as functions of the relative vapour pressure of water ($x = P/P^s$) at 30°C. P(atm) is the water vapour pressure over the adsorbent

and Ps(atm) is the saturation vapour pressure of water at 30°C. These data were measured in Air Products laboratories. They demonstrate the substantially different adsorption characteristics of water vapour on different samples of alumina. The specific saturation adsorption capacities of water (m, g/g) by the alumina at the limit of $x \rightarrow 1$ is controlled by the pore volume of the adsorbent. The entire pore volume is filled with liquid water at that limit.

Empirical adsorption equilibrium models like Langmuir and Freundlich can generally be used to describe type I pure water vapour adsorption isotherms on aluminas [6]:

$$n = \frac{mbP}{1 + bP}; \quad b = b_0 e^{q_0/RT} \qquad \text{Langmuir:} \qquad (1)$$

$$n = CP^k; \quad C = C_0^{kq_0/RT} \qquad \text{Freundlich:} \qquad (2)$$

where $b(atm^{-1})$ and $C(atm^{-k})$ are the Langmuir and Freundlich gas-solid interaction parameters, respectively. They are exponential functions of temperature. q_0 (kJ/mole) is the isosteric heat of adsorption of water vapour on the alumina at the limit of zero water loading ($n \rightarrow 0$). b_0, C_0 and k are temperature independent constants. T is the temperature of adsorption, P is the equilibrium adsorption pressure and R is the gas constant.

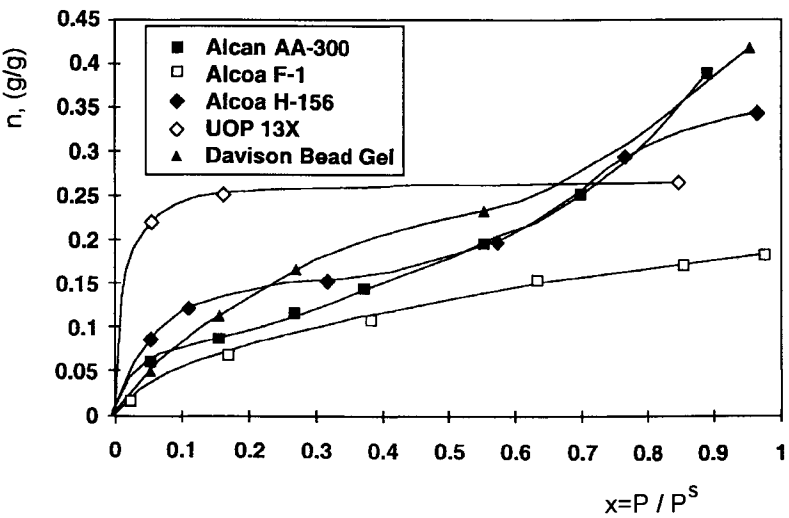

Figure 1. Water vapour isotherms on aluminas, 13X zeolite, and silica gel at 30°C.

Equations (1) and (2) are applicable when the alumina is energetically homogeneous (isosteric heat of adsorption, q, is independent of water loading, n). The Toth equation can be used when the alumina is energetically heterogeneous (q decreases with increasing n) and the isotherm shape is Type I [7]:

$$n = \frac{mbP}{[1 + (bP)^k]^{1/k}}; \quad b = b_0 e^{q_0/RT} \qquad \text{Toth:} \qquad (3)$$

$k(\leq 1)$ is a temperature dependent heterogeneity parameter.

Both types I and IV isotherms can be described in terms of adsorption (micro and meso pores) and condensation (mesopores only) of water vapour [8]:

$$n = \frac{(Vm/v_L)cx}{1+(c-1)x} + \frac{(S_M \cdot mb)x}{1+(b-1)x} \; ; \quad 0 \leq x \leq x_m \tag{4a}$$

$$n = \frac{(Vm/v_L)cx}{1+(c-1)x} + \frac{2\alpha}{p}\overline{V}\frac{\Gamma(p,\epsilon_x)}{\Gamma(p)} \cdot \frac{mbx}{1+(b-1)x} + \left(\frac{\overline{V}}{v_L}\right)\left[\frac{\Gamma(p+1,\epsilon_m)-\Gamma(p+1,\epsilon_x)}{\Gamma(p+1)}\right] \; ; \quad x_m \leq x \leq 1 \tag{4b}$$

where Vm (cc/g) and $\overline{V}$ (cc/g) are, respectively, the micro and total specific pore volumes of the alumina, S_M (cm^2/g) is mesopore BET surface area. m (mol/g) is the monolayer capacity for water adsorption on mesopore area and v_L (cc/mol) is the molar volume of liquid water. c and b are, respectively, gas–solid interaction parameters for the micro and meso pores. Parameters α and p describe the pore size distribution (gamma function) of the adsorbent. The condensation in the mesopores is described by the Kelvin model which begins when the water relative vapour pressure is x_m.

Figure 1 also shows the pure water vapour adsorption isotherms on UOP 13X zeolite and a sample of Davison silica gel at 30°C. These data were measured at Air Products' laboratories. They are, respectively, type I and IV in shape. The zeolite adsorbs water very strongly (very high capacity at low x). The water adsorption capacities of the silica gel is comparable to those of the aluminas at low x but it exhibits higher water adsorption capacities at higher values of x. The Henry's law constants [$K = \left(\frac{\partial n}{\partial x}\right)_T$ at $x \to 0$] for the isotherms of Figure 1 are given in Table 2. The moderate strength of adsorption of water by the aluminas and silica gels make them easier to desorb in a drying process cycle. The aluminas are, however, preferred over silica gels in most practical processes because of their mechanical integrity.

Table 2
Henry's law constants for pure water adsorption on various desiccants

Adsorbent	Henry's law constants (K) at 30°C (g/g)
Alcoa F1	1.1
Alcoa H-156	2.7
Alcan AA-300	2.4
13X Zeolite	140.0
Davison silica gel	1.2

3.2. Heterogeneity of adsorption of water vapour

As mentioned earlier, the alumina surface can be energetically homogeneous or heterogeneous for adsorption of water vapour. The variation in isosteric heat of adsorption (q) with water loading (n) provides a measure of the degree of heterogeneity of the alumina. Figure 2 shows plots of q vs n for three samples of alumina.

The isosteric heat of adsorption exhibits the highest value in the Henry's law region ($x \rightarrow 0$) and then gradually decreases to the heat of vapourization of water (42 KJ/mol) at condensation point ($x \rightarrow 1$). Figure 2 shows that Alcan PSA–I alumina shows a very small variation in q values (relatively homogeneous) over the entire water vapour pressure range while the other two aluminas (RP–Grade A and Alcan AA–300) exhibit large variations (highly heterogeneous) of q values [9]. The comparative isosteric heat of adsorption of water vapour on 13X zeolite is ~75 kJ/mol which remains practically constant over the entire range of the water adsorption isotherm. Thus, aluminas require much less energy for desorption.

The isosteric heat of adsorption at a given water loading (n) can be calculated by measuring isotherms at different temperatures [6]:

$$\frac{q(n)}{RT^2} = \left[\frac{\partial \ln P}{\partial T}\right]_n \tag{5}$$

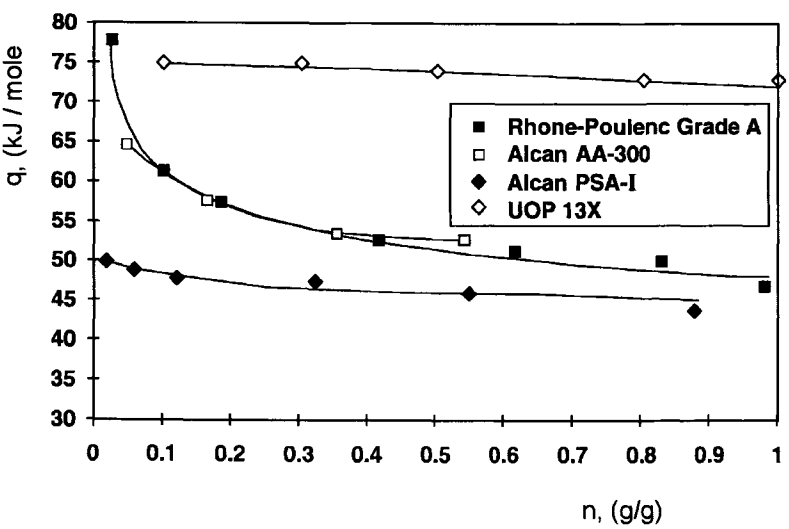

Figure 2. Isosteric heat of adsorption for water vapour on aluminas and 13X zeolite

For the heterogeneous Toth isotherm, q is given as a function of fractional coverage ($\theta = n/m$) by [17]:

$$q = q^0 + \left(\frac{RT^2}{k}\right) \cdot \left(\frac{d \ln k}{dT}\right) \left[\frac{\left(1-\theta^k\right) \ln\left(1-\theta^k\right) + \theta^k \ln \theta^k}{\left(1-\theta^k\right)}\right] \tag{6}$$

q_0 is the isosteric heat of adsorption of water at the limit of zero loading ($\theta \rightarrow 0$).

3.3. Temperature dependence of water adsorption isotherms

Figure 3 shows the isotherms for adsorption of water on Alcan AA-300 at 30 and 70°C.

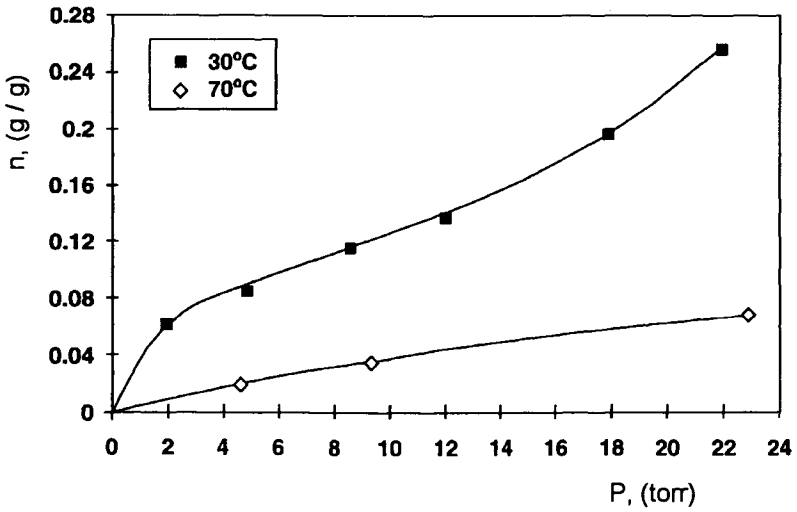

Figure 3. Water vapour isotherms on Alcan AA-300 alumina at 30 and 70°C.

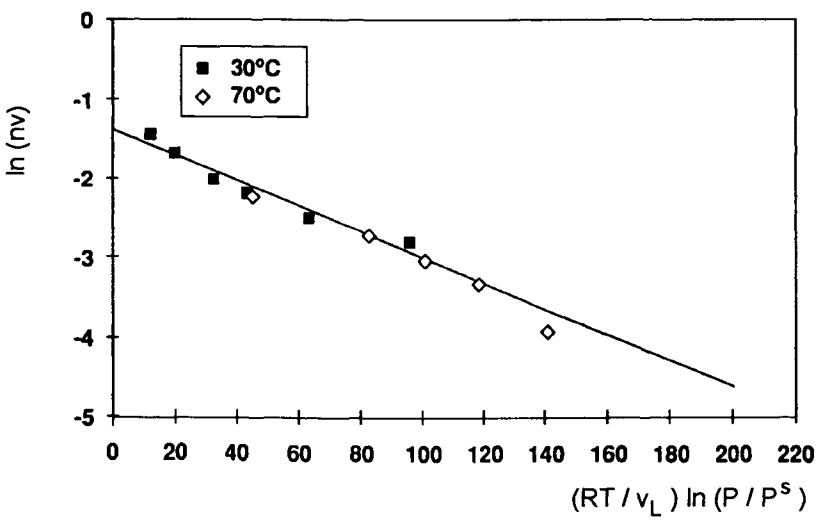

Figure 4. Polanyi potential plot for water vapour adsorption at 30 and 70°C on Alcan AA-300 alumina.

These data were also measured in the Air Products' laboratories. The Polanyi potential concept [6] can be used to coalesce these isotherms at different temperatures into a single

curve as shown by Figure 4. The ordinate of the plot represents the amount of water adsorbed expressed as liquid volume. The abcissa represents the Polanyi potential. The concept can be used to obtain a first pass estimation of temperature dependence of water vapour adsorption on aluminas.

3.4. Adsorption of water vapour from gas mixtures

The selectivity of adsorption ($S = n_1y_j/n_jy_1$) of water vapour (component 1, mole fraction y_1) on aluminas over component j (mole fraction y_j) of a gas mixture can be complex functions of adsorbate loadings (n_1,n_j), system temperature and pressure. There is a scarcity of published data on water adsorption from multicomponent gas mixtures on alumina. Typically, it is assumed that water is exclusively adsorbed on aluminas ($S \rightarrow \infty$,$n_j \rightarrow 0$) from non- polar gases such as air or natural gas. The assumption may not be valid when the gas mixture contains polar components. The mixed gas Langmuir or Toth models may be used to describe multicomponent Type I equilibria on aluminas [6,7]. No isotherm model is available to describe adsorption of water from gas mixtures when there is partial condensation of water in the mesopores of the alumina.

3.5. Kinetics of adsorption of water vapour

The kinetics of actual adsorption of water on the sites of alumina is very fast. However, a substantial resistance to mass transport can be exhibited by the finite diffusivity of water molecules from the external gas phase to the adsorption sites through the porous network of the adsorbent particle. Diffusion of water vapour (molecular and Knudsen) through the pores of the alumina particle as well as the surface diffusion of adsorbed water on the pore walls [11-13] can contribute to the overall transport process. The presence of other non-adsorbing or adsorbing components can significantly influence both pore and surface diffusivity values for water. Table 3 shows a family of water vapour diffusivity data on Rhone-Poulenc grade A alumina in presence of N_2 and He as carrier gases at a total gas pressure of 1.0 atmosphere. The water isotherm has a type IV shape [9,11]. Pore diffusion

Table 3
Pore (Dp) and surface diffusivities (Ds) of water vapour on Rhone-Poulenc alumina

Partial pressure of water vapour (Pa)	Carrier gas	Temperature (°C)	Dp (cm^2/s)	Ds (cm^2/s)
59	N_2	24.0	$4.7 \cdot 10^{-2}$	0
		100.0	$6.7 \cdot 10^{-2}$	0
709	N_2	24.0	$4.7 \cdot 10^{-2}$	0
2013	N_2	24.0	$4.7 \cdot 10^{-2}$	$2.9 \cdot 10^{-6}$
2733	N_2	24.0	$4.7 \cdot 10^{-2}$	$2.9 \cdot 10^{-6}$
709	He	24.0	$11.0 \cdot 10^{-2}$	0
		100.0	$13.7 \cdot 10^{-2}$	0
2013	He	24.0	$11.0 \cdot 10^{-2}$	$2.9 \cdot 10^{-6}$

of water dominates the overall transport into the Rhone–Poulenc alumina particles at low water loadings. Surface diffusion of water on pore walls, on the other hand, contribute substantially to overall transport process at high water loadings (x values above the point of inflection of type IV isotherm).

Fickian Diffusion and Linear Driving Force models are generally used to describe the transport of water vapour into the alumina particles. For isothermal adsorption of water vapour from a constant partial pressure (P^0) batch adsorption system on a spherical adsorbent particle of radius Rp, the uptake profiles are given by [13]:

Fickian Diffusion (FD):
$$\frac{m(t)}{m^0} = 1 - \frac{6}{\pi^2} \sum_{m=1}^{\infty} \frac{1}{n^2 \exp\left(-n^2\pi^2 Dt/R_p^2\right)} \tag{7}$$

Linear Driving Force (LDF):
$$\frac{m(t)}{m^0} = 1 - e^{-kt} \tag{8}$$

where m(t) is the amount of water adsorbed at time t on an initially clean adsorbent. m^0 is the equilibrium adsorption capacity of water at P^0 and T. D and k are the overall diffusivity or mass transfer coefficient for adsorption of water vapour into the particle. Isothermal uptake measurements, however, may not be feasible due to generation of heat of adsorption [14] and non-isothermal uptake models (FD and LDF) must be used [13,14].

3.6. Column dynamics for ad(de)sorption of water vapour

The dynamics of ad(de)sorption of water vapour from a carrier gas in a packed alumina column is governed by the adsorption equilibria and kinetics for the system. For the adsorption process, a mass transfer zone (MTZ) for water is formed within the column which propagates from the feed gas end to the column exit. The MTZ is generally constant

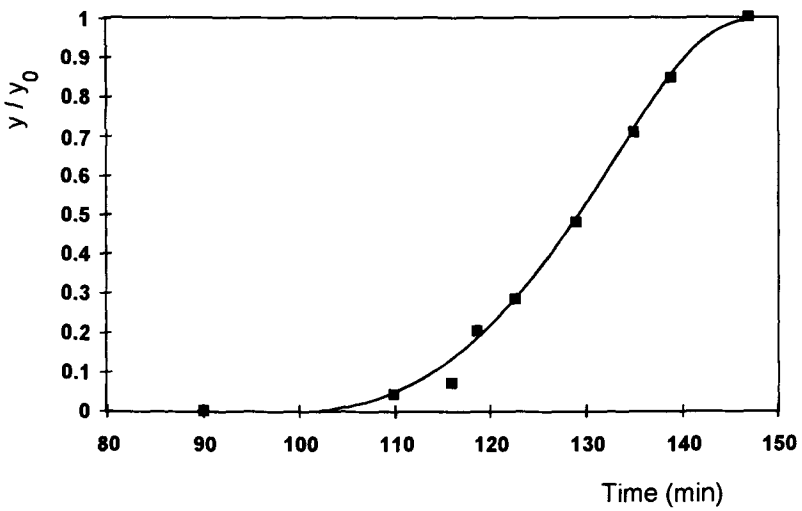

Figure 5. Water breakthrough curve on Alcan AA-300 alumina at 50°C. Feed: 3370 ppm water in N_2 at ambient pressure.

pattern in shape when the water adsorption isotherm is Type I or when the water partial pressure is below the inflection point of a type IV isotherm [13]. Otherwise a proportionate pattern MTZ is formed [13]. Figure 5 shows the constant pattern water breakthrough curve (exit gas water composition vs time) from an Alcan AA-300 column at 50°C where the feed gas contained 3370 ppm of water vapour in nitrogen at atmosphere pressure. These data were measured in Air Products' laboratory. The column remains essentially isothermal when the feed gas water concentration is very dilute. A non-isothermal type I or type II column dynamics is exhibited when the water concentration in feed is moderate [15,16]. Figure 6 shows an example of type II non-isothermal column breakthrough curve from a Laporte alumina at 26.6°C where the feed gas contained an air-water (37% RH) mixture [17].

There is no published data on desorption of water vapour from a column by purging the column with a water free gas. However, such a desorption process produces a proportionate pattern MTZ within the column for a type I adsorption isotherm. The zones are generally governed by local adsorption equilibria within the column [18,19].

The constant pattern water breakthrough curve for isothermal adsorption of trace moisture (Langmuir isotherm) from an inert carrier gas can be described by [15]:

$$(t_2 - t_1)\frac{(1+b)}{b}\cdot k = \frac{1}{\lambda^0}\ln\left[\frac{\phi_2(1-\phi_1)}{\phi_1(1-\phi_2)}\right] + \ln\frac{\phi_1}{\phi_2} \qquad (9)$$

where t_i is the time at which the exit gas water molar fraction is given by y_i. ϕ_i is the ratio of y_i to feed gas water molar fraction y_i^0. λ^0 ($= n^0/m$) is the fractional water loading at the feed gas conditions. b and m are Langmuir parameters. k is the LDF mass transfer coefficient for water.

Analytical equations to describe isothermal proportionate pattern water desorption

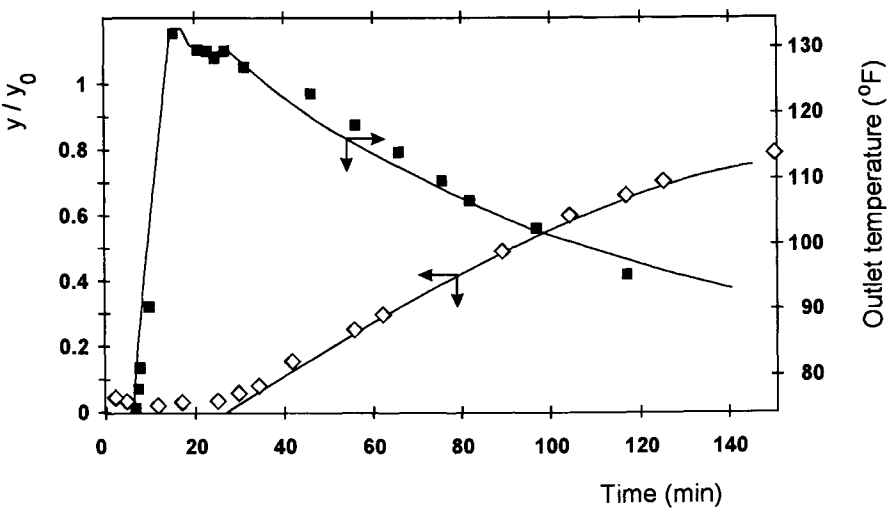

Figure 6. Nonisothermal column breakthrough curve for water (37 % R.H.) from air on Laporte alumina at 26°C.

characteristics (Langmuir isotherm) by purging the column with an inert carrier gas are also available [19]. They demonstrate that the efficiency of desorption of water by purge is facilitated when the Henry's law constant for water adsorption is low to moderate. Thus, activated aluminas fulfill that requirement.

4. ADSORPTION OF WATER FROM LIQUID STREAMS ON ACTIVATED ALUMINAS

The adsorption of water from a binary or multicomponent liquid mixtures is characteristically different from that from gaseous phase because the pore space within the alumina is always filled with a liquid mixture. Nevertheless, the key characteristics (equilibria, kinetics and ad(de)sorption column dynamics) for adsorption of trace and bulk water from a liquid mixture is very well studied.

4.1. Equilibrium adsorption of trace water from liquid mixtures

The pertinent experimental variable to describe equilibrium adsorption of water from a liquid mixture is the surface excess of water (n_1^e, moles/g):

$$n_1^e = n_1 - [\Sigma n_j]\, x_1 \tag{10}$$

where n_1 is the actual specific amount of water (component 1) adsorbed from the mixture (equilibrium bulk phase molar fraction of water = x_1). nj is the specific amount of component j adsorbed from the mixture [20]. n_1^e is a function of x_1 and the system temperature and it can be directly measured experimentally.

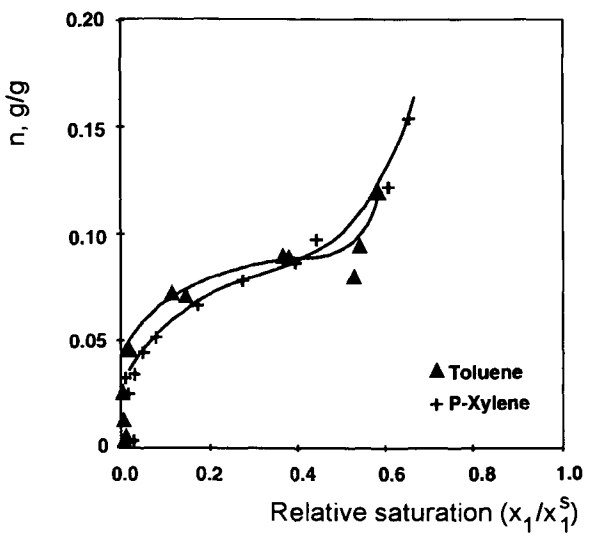

Figure 7. Trace water adsorption isotherms from toluene and p-xylene on Alcoa H-152 alumina at 22°C.

The surface excess isotherm $[n_1^e(x_1)]$ of trace water ($x_1 \ll 1$) from a mixture on activated alumina can have types I and IV shapes analogous to those for adsorption of pure water vapour [20,21].

Figure 7 shows an example of type IV isotherms for adsorption of trace water from toluene and p-xylene mixtures on Alcoa H-152 alumina at 22°C [22]. The abcissa of the plot represents relative saturation of water (x_1/x_1^s), where x_1^s is the molar fraction of water at the solubility limit in the hydrocarbon liquid. Equilibrium isotherm models analogous to those used for pure water vapour adsorption can be derived for describing trace water adsorption from liquid mixtures [20–22].

4.2. Equilibrium adsorption of bulk water from a binary liquid mixture

The surface excess isotherm for adsorption of bulk water ($0 \leq x_1 \leq 1$) from a binary liquid mixture can be 'U' (water selectively adsorbed at all values of x_1) or 'S' (water not selectively adsorbed at all values of x_1) shaped [20]. Figure 8 shows an example of 'U' shaped isotherm for adsorption of water–alcohol binary mixture on Alcoa H-152 alumina

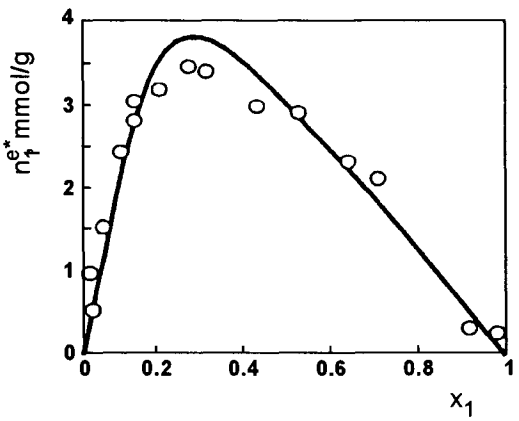

Figure 8. Water–ethanol binary adsorption isotherm on Alcoa H-152 alumina at 30°C.

at 30°C [23]. The monolayer–pore filling (MPF) models can be used to describe these binary isotherms [24,25]:

$$n_1^e = m_1 \frac{[Sa_1x_2 - a_2x_1]}{Sa_1 + \beta a_2} \tag{11}$$

$$S = S_0 [Sa_1 + a_2]^{(\beta-1)/\beta} \tag{12}$$

where m_i is the pore filling capacity of component i. S is the selectivity of adsorption $[S = n_1a_2/n_2a_1]$ of water (component 1) over component 2 of the mixture. ai is the liquid phase activity of component i. $\beta(=m_1/m_2)$ is the size ratio of the two components. S_0 is the selectivity of adsorption water at the limit of $x_1 \rightarrow 0$. Equations (11) and (12) describe

the surface excess isotherm for water on an energetically homogeneous adsorbent. Models are also available to account for energetic heterogeneities of the adsorbent [25].

The effect of temperature on the surface excess isotherms of water from liquid mixtures on the aluminas is generally much less pronounced than those for adsorption from vapours [26].

4.3. Kinetics of adsorption of water from liquid mixtures

The resistance to mass transport for adsorption of water into alumina particles can be governed by diffusion of water molecules through the liquid filled pores as well as by surface diffusion of adsorbed water molecules on the pore walls. A surface excess linear driving force model [SELDF] has been successfully used to describe the adsorption of water from liquid mixtures [27]. For isothermal adsorption of water from a bulk liquid mixture from a constant water composition (x_1^0) batch adsorption system, the uptake profile is given by:

$$\frac{n_1^e(t)}{n_1^{e0}} = 1 - e^{-kt} \tag{13}$$

where $n_1^e(t)$ is the surface excess of water adsorbed at time t on an initially clean adsorbent. n_1^{e0} is the equilibrium surface excess of water at x_1^0 and T. k is the overall mass transfer coefficient for adsorption of water into the adsorbent particle. The kinetics of adsorption of water from liquid mixtures on aluminas are generally orders of magnitude slower than that from gases. Therefore, smaller adsorbent particles are used for liquid drying in order to reduce the transport distance within the adsorbent [27–29].

4.4. Column dynamics for ad(de)sorption of water from liquid mixtures

The dynamics of ad(de)sorption of liquid water from a mixture in packed alumina columns is also governed by the adsorption equilibria and kinetics. For the adsorption process, a MTZ for water is formed within the column which propagates from the feed

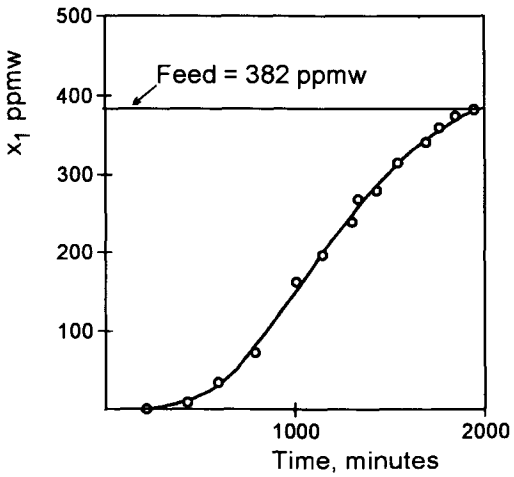

Figure 9. Breakthrough curve for water from p-xylene on Alcoa H-152 alumina at 22°C.

liquid end to the column exit. The MTZ is generally constant pattern [23, 27–29] for an 'U' shaped isotherm (bulk mixture) or for type I isotherm (trace mixture). The column remains nearly isothermal for adsorption from liquid mixtures. Figure 9 shows an example of the MTZ for adsorption of trace water (382 ppm in feed) from p-xylene on H–152 alumina at 22°C [22]. Figure 10 shows an example of the MTZ for adsorption of bulk water (20 molar % in feed = x_1^F) from alcohol on H–152 alumina at 25°C [23]. The ordinate of Figure 10 gives column effluent molar fraction of water (x_1) as a function of total specific quantity of column effluent (Q). The SELDF mass transfer coefficient for this liquid phase system (k=0.0125 seconds^{-1}) is much smaller than typical k values of 300 seconds^{-1} for a gas phase system using the same size adsorbent particles.

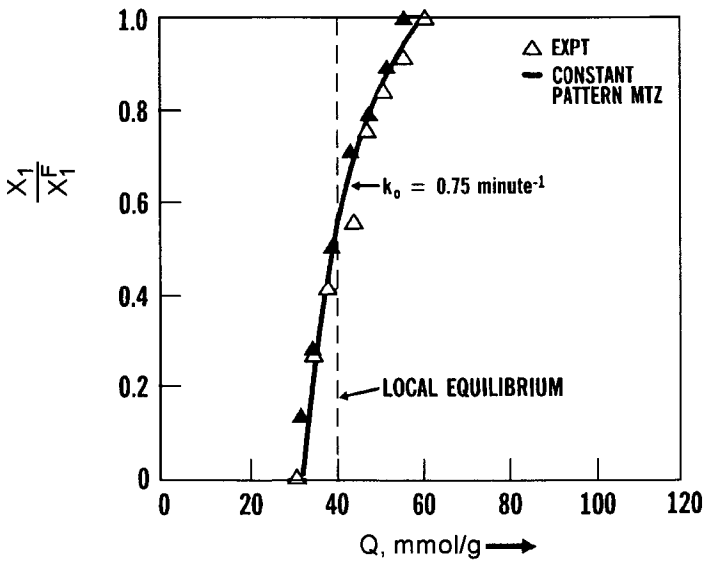

Figure 10. Breakthrough curve for 20 molar % water in ethanol binary liquid mixture on Alcoa H–152 alumina at 25°C.

Analytical mathematical models describing (a) the propagation of constant pattern MTZ and (b) the desorption profiles under local equilibrium conditions in packed columns for ad(de)sorption of bulk binary liquid mixtures having an 'U' shaped surface excess isotherm and obeying SELDF kinetic mechanism are available [27].

5. PROCESSES FOR DRYING OF GASEOUS AND LIQUID MIXTURES

Numerous commercial processes have been developed for dehydration of gaseous mixtures containing trace to dilute amounts of water and for removal of trace to bulk amounts of water from liquid mixtures using activated aluminas as adsorbents. The following sections outline a few of these processes.

5.1. Thermal swing adsorption (TSA) processes for removal of trace water from gases and liquids

The basic concept of a TSA drying process consists of (a) selective adsorption of trace or dilute water from the contaminated fluid mixture by flowing the fluid over a packed column of alumina particles while withdrawing a dry product stream until the water concentration at the column effluent rises to a predetermined value and then (b) thermal desorption of the adsorbed water by heating the column with a relatively dry fluid stream. The adsorbent is repeatedly used in a cyclic manner by carrying out steps (a) and (b). More than one adsorbent column is required for continuous processing of the wet feed fluid stream and production of a dry fluid stream.

The adsorbent column is generally regenerated immediately after the adsorption step when the feed stream is a gaseous mixture. In addition, the adsorbent column is usually drained to remove inter-particle liquids before regeneration begins, when the feed stream is a liquid mixture.

Many different regeneration options are practiced [30–34]. For example, a portion of the dry product gas can be used to provide for the regeneration gas. Figure 11 is a schematic flow diagram for a three column TSA gas drying system. The dry regenerated gas is passed through one column (which has completed heating step) in order to cool the column. The effluent from that column is heated and passed through another column (which has completed adsorption step) for desorption of water. The third column (which has completed cooling step) is used to remove water from fresh feed. Hot wet feed gas can also be used for regeneration [30]. The temperature range of regeneration for the activated aluminas is 200–300°C and the quantity of regenerating gas is 10–15% of feed gas processed. Higher regeneration temperatures are used when more stringent drying is required. For example, a 200°C regeneration is sufficient when the water concentration of effluent product gas is about 10 ppm. A 300°C regeneration reduces the product gas water concentration to below 1 ppm.

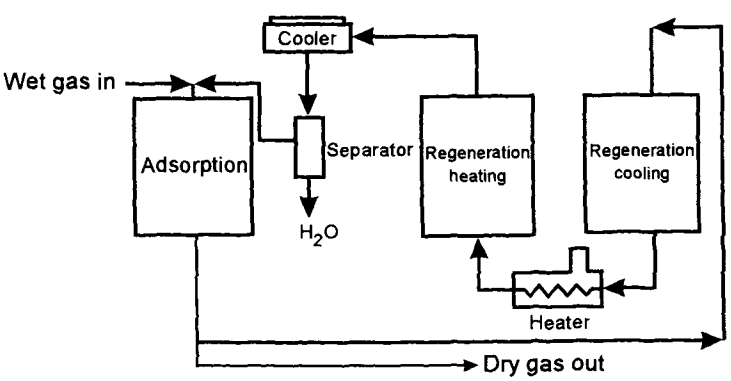

Figure 11. Schematic flow diagram for three column thermal swing adsorption system for gas drying.

Figure 12 is a schematic flow diagram for a two column liquid phase TSA drying system where trace water is removed from a hydrocarbon stream [31]. An external regeneration

gas is used in this scheme. The hot effluent gas during the regeneration step is cooled and condensed to form a two phase immiscible liquid mixture. The hydrocarbon–rich phase is recycled to the TSA system by mixing it with the fresh feed stream while the water– rich phase is rejected.

The dynamic desiccant capacity of the alumina in a TSA process depends on the type of alumina, nature and composition of the feed stream, regeneration temperature, etc. A typical water removal capacity for alumina is 5–15% by weight. The typical total cycle time for a TSA process is 2–8 hours.

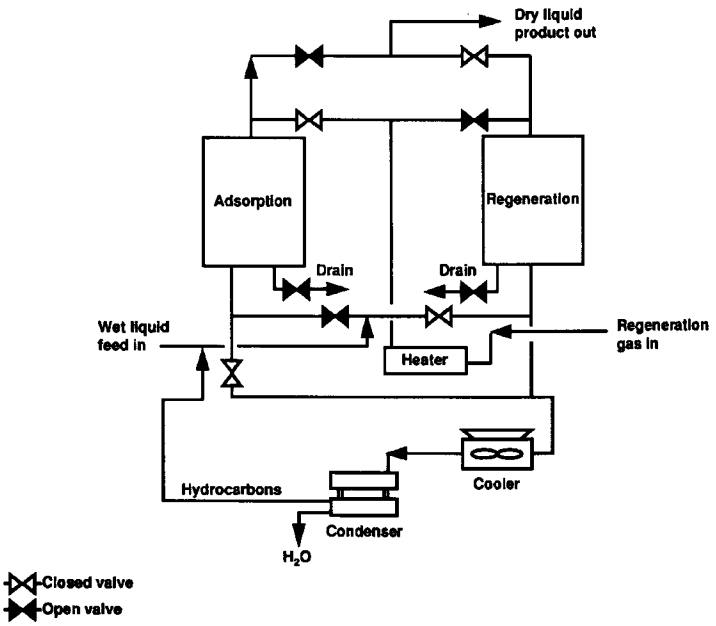

Figure 12. Schematic flow diagram for two column thermal swing adsorption system for liquid drying.

5.2. Pressure swing adsorption (PSA) process for removal of trace water from gases

The basic concept of a PSA drying process consists of (a) selective adsorption of trace or dilute water from the contaminated gas at a relatively high (50–100 psig) total gas pressure by flowing the gas over a packed bed of alumina particles while withdrawing a dry product gas stream until the water concentration at the column effluent rises to a predetermined level and then (b) desorption of the adsorbed water from the alumina by lowering the superincumbent partial pressure of the water in the column. Again the adsorbent is repeatedly used in a cyclic manner by carrying out steps (a) and (b). The desorption in a PSA process is achieved by (a) lowering the total gas pressure of the column to near ambient (depressurization) and by (b) flowing a portion of the dry product gas over the column at near ambient pressure (purge). Adsorption at a relatively low pressure (5–10 psig) and desorption under vacuum (both depressurization and purge) are also

possible options [33-36].

Figure 13 is a schematic flow diagram for a two column Skarstrom type [36] PSA drier. The process can be used to obtain very dry product gas (< −60°C dew point). The product purity depends on the type of alumina used, feed gas pressure and dry purge gas quantity. Typically a practical PSA drier uses 15–30% of product gas as purge. The typical total cycle time for a PSA process is 2-4 minutes.

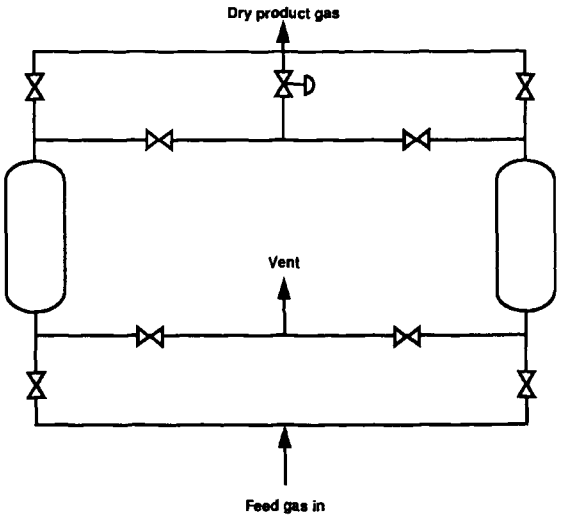

Figure 13. Schematic flow diagram for two column Skarstrom pressure swing adsorption cycle for gas drying.

5.3. Concentration swing adsorption (CSA) and concentration–thermal swing adsorption (CTSA) processes for drying bulk liquid mixtures

Removal of bulk water from liquid mixtures by adsorption require different processing concepts. Novel CSA and CTSA concepts are developed [23,28,29] where the adsorption step is carried out by flowing the wet bulk liquid mixture through a packed column of alumina in order to produce a dry product liquid stream. The less selectively adsorbed components of the liquid mixture are then removed from the column (from the intra- and inter-particle void space) by rinsing the column with pure water. The water saturated column is then subjected to the desorption step by flowing an extraneous non-adsorbing liquid stream or by thermally heating with a relatively dry extraneous gas stream. The column is drained to remove inter-particle water prior to thermal regeneration.

Figure 14 shows a schematic flow diagram of a CTSA drying process for bulk liquid mixture where dry air produced by a PSA drier is used to heat the liquid drying columns.

5.4. Design of TSA and PSA drying processes

The design of practical TSA and PSA processes often require bench or pilot scale operational data because of the lack of quantitative methods for estimation of multicomponent

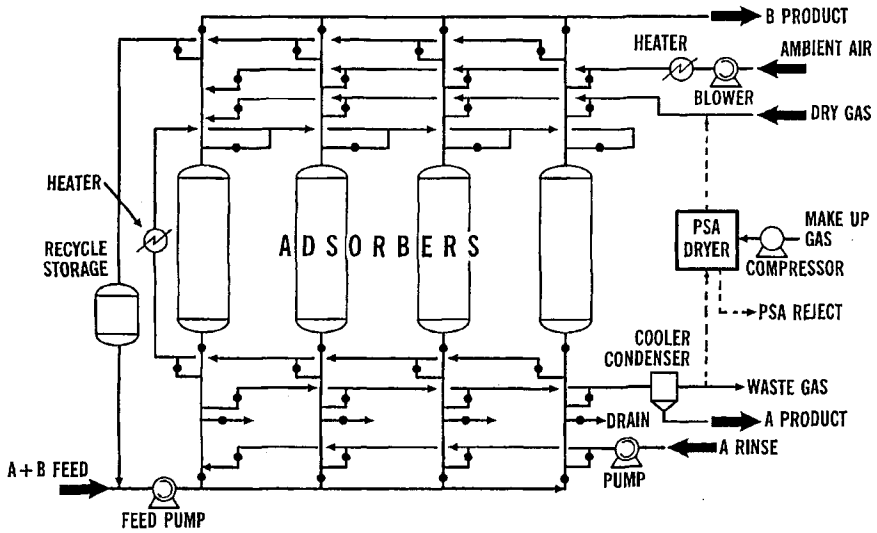

Figure 14. Schematic flow diagram for concentration–thermal swing adsorption system for bulk liquid drying.

gas and liquid adsorption equilibria, kinetics and column dynamics [37]. Mathematical models of these processes are often very useful for scale up and optimization. These models require simultaneous solutions of mass, heat and momentum balance equations (partial differential equations) describing the ad(de)sorption processes within the columns. The equations are solved using appropriate initial and boundary conditions for each step of the process. Multicomponent adsorption equilibria, heat and kinetics constitute the key input variables for the solutions of the models. Manufacturers of commercial drying (gas and liquid) process systems have developed several pratical short–cut design procedures [30–36].

6. CONCLUSION

Drying of gases and liquids by activated alumina is a very flexible and versatile process concept. A large variety of synthetic alumina structures having a range of properties for adsorption water from various gases and liquids is commercially available. Numerous PSA, TSA and CSA process concepts have been designed to remove trace or bulk water from gaseous and liquid streams.

REFERENCES

1. D. Basmadjian, The Adsorption Drying of Gases and Liquids, Chapter 8 (pp 307–357) in: Advances in Drying, vol. 3 (1984).
2. G. Keller, R. A. Anderson and C. M. Yon, Adsorption, Chapter 12 (pp 644–696)

in: Handbook of Separation Process and Technology, R. W. Rousseau (ed.), John Wiley and Sons, New York (1987).
3. A. L. Kohl and F. C. Riesenfeld, Gas Dehydration and Purification, Chapter 12 (pp 574–656), in: Gas Purification, Gulf Publishing Co., Houston (1979).
4. K. P. Goodboy and H. L. Fleming, Chem. Eng. Prog., (1984) 63.
5. H. Knozinger and P. Ratnasamy, Cat. Rev. Sci. Eng., 17 (1978) 31.
6. D. M. Young and A. D. Crowell, Physical Adsorption of Gases, Butterworths, London, 1962.
7. M. Jaroniec and J. Toth, J. Colloid Polym. Sci., 254 (1976) 643.
8. S. Sircar, Carbon, 25 (1987) 39.
9. R. Desai, M. Hussain and D. M. Ruthven, Can. J. Chem. Eng., 70 (1992) 699.
10. S. Sircar, Langmuir, 7 (1991) 3065.
11. R. Desai, M. Hussain and D. M. Ruthven, Can. J. Chem, Eng., 70 (1992) 707.
12. L. Marcussen, Chem. Eng. Sci., 29 (1974) 1061.
13. D. M. Ruthven, Principles of Adsorption and Adsorption Processes, John Wiley and Sons, New York, 1984.
14. S. Sircar, J. Chem. Soc. Faraday Trans. I., 79 (1983) 785.
15. S. Sircar and R. Kumar, I&EC Process Des. Dev., 22 (1983) 271.
16. C. L. Chou, Chem. Eng. Communications, 36 (1987) 211.
17. J. W. Carter and D. J. Barrett, Trans. Inst. Chem. Engrs., 51 (1973) 75.
18. S. Sircar and R. Kumar, I&EC Process Des. Dev., 24 (1985) 358.
19. S. Sircar and T. C. Golden, I&EC Research, in press.
20. J. J. Kipling, Adsorption from Solutions of Non–Electrolytes, Academic Press, New York, 1965.
21. S. Sircar, A. L. Myers and M. C. Molstad, Trans Faraday Soc., 66 (1970) 2354.
22. S. Joshi and J. R. Fair, Ind. Eng. Chem., 30 (1991) 177.
23. M. B. Rao and S. Sircar, Adsorption Sci. Tech., 10 (1993) 93.
24. S. Sircar, Surf. Sci., 148 (1984) 478.
25. S. Sircar, Surf. Sci., 148 (1984) 489.
26. S. Sircar, I&EC Research, 32 (1993) 2430.
27. S. Sircar and M. B. Rao, AIChE J., 38 (1992) 811.
28. M. B. Rao and S. Sircar, Sep. Sci. Tech., 27 (1992) 1875.
29. M. B. Rao and S. Sircar, Sep. Sci. Tech., 28 (1993) 1837.
30. Trade Publication (F35–14480), Choosing an Alcoa Activated Alumina Desiccant Basics of Dehydration Design, Alcoa, Pittsburgh, Pennsylvania, U.S.A., 15219.
31. Trade Publication (F35–14481), Dehydrating Liquids With Alcoa Activated Aluminas, Alcoa, Pittsburgh, Pennsylvania, U.S.A., 15219.
32. Trade Publication, Activated Alumina, Rhone–Poulenc, Paris, France.
33. Trade Publication (IC–117R 2500), Improve Your Gas Drying Operations, Kaiser Chemicals, Oakland, California, U.S.A. 94643.
34. D. H. White, Selecting the Right Desiccant Dryer, Machine Design, 2 (1985).
35. Trade Publication, Drying with Harshaw Activated Aluminas, Harshaw Chemical Company, Cleveland, Ohio, U.S.A. 44106.
36. C. W. Skarstrom, U. S. Patent 2,944,627 (1960).
37. S. Sircar, Proceedings of Third International Conference on Fundamentals of Adsorption, Sonthofen, Germany, pp 815–843 (1991).

Section 3

ADSORPTION FROM SOLUTION

This Page Intentionally Left Blank

A. Dąbrowski and V.A. Tertykh (Editors)
Adsorption on New and Modified Inorganic Sorbents
Studies in Surface Science and Catalysis, Vol. 99

Chapter 3.1
Characterization of inorganic sorbents by means of adsorption at the liquid – solid interface

A. Dąbrowski[a], R. Leboda[a], J. Goworek[a] and J.K. Garbacz[b]

[a]Faculty of Chemistry, M. Curie – Skłodowska University,
20–031 Lublin, Poland

[b]Institute of Chemical Technology and Engineering, Polytechnical and
Agricultural University, 85–326 Bydgoszcz, Poland

1. INTRODUCTION

Adsorption from liquid mixtures on solids underlies a number of extremely important processes and plays a significant role in many fields of the natural sciences. Studies of this phenomenon were reported in several monographies and reviews e.g. [1–3]. The formulation of a unified theory of adsorption from solutions is difficult because there are liquid mixtures with extremely different physicochemical properties. Usually, existing theoretical descriptions are limited to the following cases:

1. non–electrolytic miscible mixtures composed of molecules of comparable sizes,
2. non–electrolytic liquid mixtures of components of limited miscibility,
3. electrolytic liquid mixtures,
4. liquid mixtures composed of both small and large molecules.

Additional difficulties in formulating an adsorption theory for the liquid – solid interface result from a variety of interactions between components of a liquid mixture and from a complex structure of the adsorbent, which may possess different types of pores and strong surface heterogeneity. Our considerations will be limited to physical adsorption on heterogeneous solid surfaces of components of comparable molecular sizes from non–electrolytic (non–ideal or ideal) miscible binary liquid mixtures.

In terms of this adsorption, properties of various adsorbents, among them the inorganic sorbents can be determined. It must be emphasized that inorganic sorbents such as silica, alumina, titania, complex carbon – mineral sorbents, apatites, e.t.c., are both structurally and energetically heterogeneous. Their total heterogeneity may be described by the kinds of adsorption potential distribution function which is one of the most significant characteristics of the aforementioned solids.

Surface phase capacity, i.e., the total amount of substances in the adsorbed phase is the second factor determining the sorption properties of the solid sorbents. This quantity is useful for calculating thermodynamic functions which characterize competitive adsorption at the liquid – solid interface and for determining the specific surface area of the sorbents.

This paper presents the methods for determining the adsorption distribution functions as well as the surface phase capacity from the excess adsorption isotherms. These isotherms are usually measured to characterize adsorption at the liquid – solid interface. In the first part we will discuss the isotherm equations describing energetical heterogeneity of the solids . The methods utilizing these equations for determining the surface phase capacity of the solids will be considered in the second part. Succeeding part deals with the concept of the global activity coefficients which are evaluated from the excess adsorption data and characterize nonideality of the surface phase resulting from the differences in molecular interactions which are additionally perturbed by heterogeneity of the solid. A procedure for separating a nonideality of the adsorbed phase caused by intermolecular forces from that generated by surface heterogeneity is presented. The approach to the global surface activity coefficients is very efficient in correcting the surface phase capacity evaluated by classical methods.

We will dwell also on the description of the structural heterogeneity of the inorganic sorbents. It refers both to the characteristic energy of adsorption and the specific capacity of adsorption phase.

The other possibilities for characterizing structural properties of inorganic sorbents concern the thermogravimetric analysis. To this end the thermal desorption of pure liquids is investigated by using various heating programs. In terms of this approach the pore – size distribution curves may be obtained to investigate the porosity of adsorbents, among them inorganic ones.

Several experimental systems including inorganic sorbents are analyzed and their adsorption characteristics are estimated to illustrate the applicability of the presented theoretical relationships.

2. EQUATIONS FOR MONOLAYER ADSORPTION ON ENERGETICALLY HETEROGENEOUS SURFACES

Let us assume that adsorption from the solutions containing 1–st and 2–nd components of similar molecular sizes on a solid surface is determined by the difference between adsorption energies of both components, i.e., $E_{12} = E_1 - E_2$.The solid surface is energetically homogeneous when all adsorption sites have the same value of E_{12}. If not, the surface is energetically heterogeneous. When the adsorption process occurs on the surface showing a discrete distribution of E_{12} which can be replaced by a continuous distribution $F(E_{12})$, then the following integral expression is in force [1]:

$$x^s_{1,t}\left(x^l_1\right) = \int_{\Omega} x^s_1\left(x^l_1, E_{12}\right) F\left(E_{12}\right) dE_{12} \tag{1}$$

Here $x^s_{1,t}$ denotes the total mole fraction on the whole heterogeneous surface, but the kernel of Eq.(1) is given by the Everett isotherm [4]:

$$x^s_1\left(x^l_1, E_{12}\right) = \frac{K_{12}X_{12}}{1 + K_{12}X_{12}} \tag{2}$$

where K_{12} is the equilibrium constant and X_{12} represents a function which corresponds to

the model adsorption system assumed [2]. We can distinguish four models of adsorption systems:
1. The NBP-na model – both phases are nonideal but the surface phase is non –autonomous,
2. The NBP-a model – both phases are nonideal but the surface phase is autonomous,
3. The IAP model – the surface phase is ideal,
4. The IBP model – both phases are ideal.

The function $F(E_{12})$ appearing in Eq.(1) is normalized to unity over the integration region and deals with the energetically heterogeneous solids. This function gives no information about topography of adsorption sites on the surface. For IAP and IBP models the type of this topography is unimportant. The other models require assumptions concerning the distribution of adsorption sites on surfaces. Up to this point, two basic models are distinguished: the patchwise model and the random model [1]. Besides, the intermediate models are possible [5]. The random model of heterogeneous surfaces is more realistic than the patchwise one and is suitable for many inorganic sorbents such as silica, alumina, titania, apatites, etc. There are feasible theoretical approaches to investigate the influence of the choice of the topography on the adsorption isotherms and the functions $F(E_{12})$ [6]. For the random model, Eq.(1) may be solved by means of various methods leading to two groups of adsorption isotherms. The first group may be expressed in the following general form:

$$x^s_{1,t} = x^s_{1,t}\left(X_{12}; n^s_t, \lambda, \overline{K}_{12}\right) \tag{3}$$

where λ is the heterogeneity parameter, but $\overline{K}_{12}$ and n^s_t denote the mean value of K_{12} on the whole heterogeneous surface and the total surface capacity, respectively.
Eq. (3) corresponds to the following energy distribution function:

$$F = F\left(E_{12}; \lambda, E^0_{12}\right) \tag{4}$$

where E^0_{12} is the characteristic energy for a given adsorption system.
The second group of adsorption isotherms derived from Eq. (1) has the form:

$$x^s_{1,t} = x^s_{1,t}\left(X_{12}; n^s_t, B_j, X^0\right), \qquad j = 1, 2, 3, \ldots, J \tag{5}$$

where B_j are the heterogeneity parameters and X^0 is a constant characteristic for a given adsorption system. Eq. (5) corresponds to the following distribution function:

$$F = F\left(E_{12}; B_j, E^0_{12}\right), \qquad j = 1, 2, 3, \ldots, J \tag{6}$$

The analytical forms of the adsorption isotherms and energy distribution functions given by Eqs.(3–6) were presented in our review [1]. By means of these equations there can be obtained the energy distribution function and parameter n^s_t which are important characterizations for the experimental adsorption systems. Consequently, by means of the functions $F(E_{12})$ and the parameters n^s_t one can obtain quantitative characterization of the adsorbent heterogeneity, sorption properties of the solid, possibility to calculate the surface phase composition and potentiality for calculating the thermodynamic functions which characterize adsorption at the solid – liquid interface.

It should be emphasized that all interpretations and conclusions should be treated as a consequence of the assumed adsorption models. This choice towards a real adsorption system is difficult and even sometimes impossible.On the other hand, the physical interpretation of the distribution function $F(E_{12})$ is a basic problem in adsorption on heterogeneous solids from solutions. This distribution gives only a quantitative characterization of the energetic adsorbent heterogeneity with respect to the adsorbates. Comparative studies of the functions $F(E_{12})$ obtained from the data referring to the same adsorbent and different adsorbates or data dealing with the adsorption of one selected adsorbate on adsorbents of controlled heterogeneity can be useful in physical interpretation of the function $F(E_{12})$.

3. METHODS FOR DETERMINING THE SURFACE PHASE CAPACITY

The second basic problem in adsorption from solutions deals with the physical interpretation the parameter n_t^s which may be determined from the excess isotherms. The total excess isotherm is given by the expression:

$$n_{1,t}^{\sigma(n)}\left(x_1^l\right) = n_t^s\left(x_{1,t}^s - x_1^l\right) \tag{7}$$

but n_t^s can not be experimentally measured. The extensive quantities in Eq.(7) refer to the mass unit of the solid adsorbent. The methods for evaluating the parameter n_t^s can be divided into four groups:

1. the mass - balance equation,
2. the equations describing adsorption process on both homogeneous and heterogeneous surfaces,
3. the Williams algebraic equation used in terms of pure - gas adsorption data,
4. other relationships derived for liquid - solid adsorption.

In this work the independent method for determining the parameter n_t^s is presented. The main idea of this method is supported by a new form of the so - called exponential adsorption isotherm [2] and takes into account both heterogeneity of the solids and the nonideality of the liquid mixtures. One ought stress that this method in contrast to aforementioned is suitable for analyzing all types of the excess adsorption isotherms.

A general exponential adsorption isotherm for describing adsorption data on heterogeneous solid surfaces converges with Eq.(5) and has the following form [7]:

$$x_{1,t}^s = \frac{n_{1,t}^{\sigma(n)}}{n_t^s} + x_1^l = \exp\left\{\sum_{j=1}^{k} A_j \cdot \left[RT \ln\left(\frac{a_{12}^l}{X^0}\right)\right]^j\right\}, \quad \text{for } a_{12}^l \le X^0 \tag{8}$$

where: $a_{12}^l = a_1^l/a_2^l$ is the ratio of the activities of components 1 and 2, A_j denotes the heterogeneity parameters, $x_{1,t}^s$ is the total mole fraction of the 1-st component, but n_t^s deals with the surface phase capacity on the whole heterogeneous surface of the solid. After taking the logarithms, Eq. (8) becomes:

$$y = B_1 z + B_2 z^2 + \ldots + B_k z^k \tag{9}$$

where:

$$B_j = A_j\,(RT)^j$$

$$y = \ln\left(\frac{n_{1,t}^{\sigma(n)}}{n_t^s} + x_1^l\right)$$

$$z = \ln\left(\frac{a_{12}^l}{X^0}\right)$$

The parameters B_j, for j=1,2,...,k were evaluated numerically by approximating the adsorption data $n_{1,t}^{\sigma(n)}$ vs. x_1^l in terms of the non-linear regression model. Hypothetical model for this regression has the form:

$$y_i = B_1 z_i + B_2 z_i^2 + \ldots + B_k z_i^k + \varepsilon_i \quad , \qquad i = 1, \ldots, n \tag{10}$$

where n denotes the number of the points (z_i, y_i), but ε_i are the errors for the random variable E_i. We can suppose that E_i have the expected values $E_i = 0$ and the same variances σ^2. Moreover, the values E_i have the normal distribution $N(0, \sigma)$, for i=1,2,...,n. The parameters B_j are approximated by means of estimators b_j. These estimators we can obtain in terms of the least square method with due regard for B_j, j=1,2,...,k:

$$Q(B_1, B_2, \ldots, B_k) = \sum_{i=1}^{n} \varepsilon_i^2 = \sum_{i=1}^{n} \left[\sum_{j=1}^{k} y_i - B_j (z_i)^j\right]^2 \tag{11}$$

The parameter X^0 is evaluated as the minimal value X^0_{min} for which, from the physical point of view, the following conditions must be satisfied [1]:

$$\left.\begin{array}{l} 0 < x_{1,t}^s < 1 \\ \left(\dfrac{dx_{1,t}^s}{dx_1^l}\right) > 0 \end{array}\right\} \tag{12}$$

The choice of the optimal values of the parameter k we can do by means of statistical test of significance for regression coefficients in terms of Student's t-test.

Missing all mathematical and numerical details connected with our procedure we can state that the parameter n_t^s is evaluated as follows:

1. we settle k = 1 for the approximating polynomial and the value of n_t^s for which the sum of square deviations is minimal; significance level for the Student's t - test, $\alpha = 0.1$,
2. we suppose the significance of the estimator b_1,
3. we restart with calculations, but for k = 2 and examine the significance of the estimator b_2; if this estimator is equal zero, then we can take the n_t^s for k = 1,
4. if the value of estimator $b_2 \neq 0$, we restart with our calculations for k = 3, etc.

The numerical procedure as described above gives credible results with respect to the values of the surface phase capacity the systems studied. On the other hand, knowledge the heterogeneity parameters B_j and X^0 gives possibility for evaluating the energy distribution functions by means of the suitable equation corresponding with the expression (8) [1].

Figures 1 and 2 show the results of our analysis for the literature system [8]: butanol (1) + benzene (2) on silica gel at 298K. For illustrative purposes in Table 2 the results of analysis for experimental systems are presented. These systems were taken from the literature and investigated in terms of IAP adsorption model. Essential information about these systems is placed in Table 1.

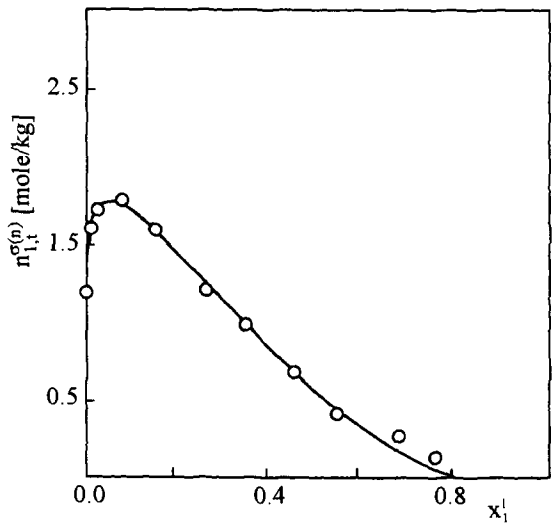

Figure 1. Excess adsorption isotherm $n_{1,t}^{\sigma(n)}$ vs. x_1^l of n-butanol (1) from benzene (2) on silica gel at 298 K: o-experimental points, — theoretical isotherm according to Eqs. (7) and (8).

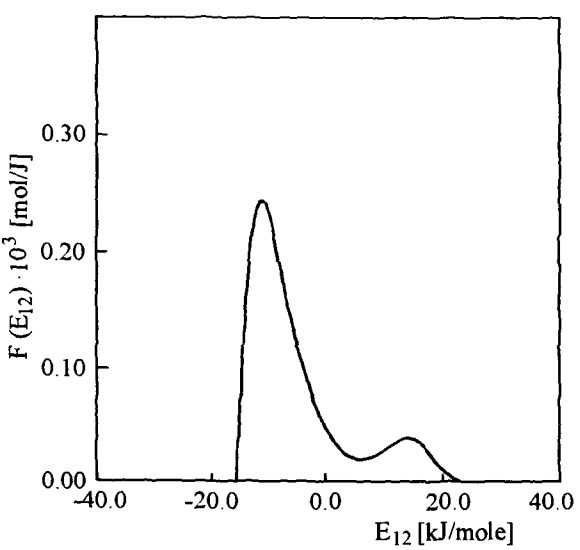

Figure 2. Adsorption energy distribution $F(E_{12})$ vs. E_{12} for the system n-butanol (1) from benzene (2) on silica gel at 298 K.

Table 1
Essential information about adsorption systems studied by means of Eqs. (7), (8) and (11). For all systems T=293 K, for system C, T=303 K

Code	Adsorbent	Solution		Ref. to exp. data	
		Component 1	Component 2	$n_{1,t}^{\sigma(n)}$	bulk act. coefficients
A	Boehmite	Benzene	Cyclohexane	[9]	[10]
B	Boehmite	Chloroform	Benzene	[9]	[9]
C	Silica gel	Benzene	Cyclohexane	[11]	[11]
D	Titania gel	Ethanol	Benzene	[10]	[10]
E	γ– alumina	1,2–dichloroethane	Benzene	[9]	ideal
F	Gibbsite	Methanol	Benzene	[9]	[12]
G	Boehmite	Methyl acetate	Benzene	[9]	[10]
H	Boehmite	1,2–dichloroethane	Benzene	[9]	ideal
I	Titania gel	1,2–dichloroethane	Benzene	[9]	ideal

It has to be stressed that the monolayer surface phase capacity is assumed to be constant over the whole bulk concentration region, i.e., $n_t^s = \text{const.}$, for $x_1^l \in (0,1)$. Under this assumption we can assess the specific surface areas of the solid adsorbents if the cross - sectional areas of adsorbed molecules are known. However, the following question arises here: what molar areas to assign to the different kinds of molecules? This problem is similar in the case of gas - solid adsorption and it may be sufficient to refer to the compilation by McLellan and Harnsberger [13]. It has been found that cross - sectional molar areas calculated by means of the molar volumes of the pure components are mostly in agreement with nitrogen surface area values [14].

Table 2
Adsorption characteristics obtained for the experimental systems from Table 1 studied by means of Eqs. (7), (8) and (11)

Code	n_t^s (mole/kg)	X^0	k	Q
A	1.14	6.61	4	0.0023
B	1.39	11.11	4	0.0005
C	2.24	5.96	4	0.0018
D	1.18	4.98	3	0.0016
E	0.76	6.23	3	0.0008
F	2.23	7.85	3	0.0020
G	1.27	6.29	4	0.0001
H	0.98	3.48	4	0.0011
I	0.68	9.00	4	0.0003

4. CONCEPT OF THE GLOBAL ACTIVITY COEFFICIENTS

For liquid – solid adsorption from binary mixtures consisting of molecules of equal sizes on a heterogeneous surface of a random distribution of adsorption sites the average equilibrium constant $\overline{K}_{12}$ referring to the whole surface has the following form [15]:

$$\overline{K}_{12} = \frac{a^s_{1,t} a^l_1}{a^l_1 a^s_{2,t}} \tag{13}$$

In Eq.(13) the symbol a^l_i denotes the bulk activity of the i–th component, but $a^s_{i,t}$ is the total (average) activity of this component in the surface phase. For these activities we can write:

$$\left.\begin{aligned} a^l_i &= x^l_i f^l_i \\ a^s_{i,t} &= x^s_{i,t} f^s_{i,t} \end{aligned}\right\} \qquad i = 1,2 \tag{14}$$

The total (global) activity coefficient $f^s_{i,t}$ (i=1,2) reflects the non–ideality of the surface phase caused by differences in molecular interactions and the non–ideality of this phase generated by the adsorbent heterogeneity. According to our earlier considerations [16,17] this coefficient is expressed as follows:

$$f^s_{i,t} = f^s_{i,int} f^s_{i,h} \qquad i = 1,2 \tag{15}$$

where $f^s_{i,int}$ denotes the activity coefficient describing the non–ideality of the surface phase due to differences in molecular interactions, but $f^s_{i,h}$ denotes the non–ideality of this phase arising from surface heterogeneity, respectively. On the other hand, combining Eq.(1) with the analytical forms of the distribution functions $F(E_{12})$ [1] and using Stieltje's transform method [18] the following equation describing liquid – solid adsorption on random heterogeneous surfaces we can obtain:

$$x^s_{1,t} = \left[\frac{\left(\overline{K}_{12} X_{12}\right)^n}{1 + \left(\overline{K}_{12} X_{12}\right)^n}\right]^{\frac{m}{n}} \tag{16}$$

This expression corresponds with the general equation (3). The average equilibrium constant $\overline{K}_{12}$ is connected with the characteristic energy E^0_{12} which determines the position of the function $F(E_{12})$ on the energy axis. Symbols n and m denote the heterogeneity parameters belonging to the interval $(0,1>$ which determine the width and assymetry of the one – peak distribution functions given by Eq.(4). Equation (16) reduces to the generalized Freundlich isotherm for n=1, the Langmuir – Freundlich isotherm for n=m and the Toth equation for m=1. The physical meaning of the heterogeneity parameters n and m refers to their influence on the shape of the functions $F(E_{12})$ [17]. Let us introduce the following notation: $f^q_{12} = f^q_1/f^q_2$, $f^q_{21} = (f^q_{12})^{-1}$, $x^q_{12} = x^q_1/x^q_2$ (q=l,s) and $\beta_{12} = f^l_{12}/f^s_{12,int}$. By means of Eqs. (13 – 16) we can prove that the function $\ln f^s_{12,h}$ vs. x^l_1 is dependent on the heterogeneity parameters n and m only. From Eqs. (13) and (14) we have:

$$f^s_{12,h} x^s_{12,t} = \overline{K}_{12} x^l_{12} \beta_{12} \tag{17}$$

By using Eq. (16) we can write:

$$\overline{K}_{12} x^{l}_{12} \beta_{12} = \left[\frac{\left(x^{s}_{1,t}\right)^{n/m}}{1 - \left(x^{s}_{1,t}\right)^{n/m}} \right] \tag{18}$$

By comparing Eqs. (17) and (18) and after taking the logarithms we obtain the following expression:

$$\ln f^{s}_{12,h} = \frac{1}{n} \ln \left[\frac{\left(x^{s}_{1,t}\right)^{n/m}}{1 - \left(x^{s}_{1,t}\right)^{n/m}} \right] - \ln x^{s}_{12,t} \tag{19}$$

The total mole fraction $x^{s}_{1,t}$ depends on the bulk concentration x^{l}_{1} only and we can state that $\ln f^{s}_{12,h}$ vs. x^{l}_{1} is the function of the heterogeneity parameters n and m. For this reason this function is helpful for characterizing the liquid – solid experimental systems. The general form of the dependence $\ln f^{s}_{12,h}$ vs. x^{l}_{1} obtained by means of Eqs. (13) and (14) has the following form (for the NBP–na model of adsorption system):

$$\ln f^{s}_{12,h} = \ln \overline{K}_{12} + \ln x^{l}_{12} + \ln \beta_{12} - \ln x^{s}_{12,t} \tag{20}$$

For the IBP model the term $\ln \beta_{12} = 0$ and Eq.(20) gives the simpler expression:

$$\ln f^{s}_{12,h} = \ln \overline{K}_{12} + \ln x^{l}_{12} - \ln x^{s}_{12,t} \tag{21}$$

We can assess the function $\ln f^{s}_{12,h}$ vs. x^{l}_{1} by means of independent thermodynamic data on the bulk activity coefficients. To this end the following procedure is proposed: by assuming that $f^{l}_{i,int}(x^{l}_{1}) = f^{s}_{i,int}(x^{s}_{1,t})$, calculation of the function $\ln f^{s}_{12,int}$ vs. x^{l}_{1}; this operation is connected with recalculation of the function $\ln f^{s}_{12,int}$ vs. x^{l}_{1} to the function $\ln f^{s}_{12,int}$ vs. x^{l}_{1} by means of the isotherm $x^{s}_{1,t}(x^{l}_{1}) = (n^{\sigma(n)}_{1,t}/n^{s}_{t}) + x^{l}_{1}$. In view of the dependence:

$$\ln f^{s}_{12,t} = \ln f^{s}_{12,h} + \ln f^{s}_{12,int} \tag{22}$$

the functions $\ln f^{s}_{12,h}$, $\ln f^{s}_{12,int}$, and $\ln f^{s}_{12,t}$ vs. x^{l}_{1} may be obtained from the experimental excess adsorption isotherms and used for characterizing the liquid – solid experimental systems.

Comparison of these functions with the suitable model studies carried out in terms of Eq.(16) [15–17] gives the simple method for obtaining the information about the heterogeneity of the solid adsorbents and the criterions for accepting the values of the surface phase capacity.

For the illustrative purposes Eqs.(20) and (22) were applied for analysis a few experimental systems. Information concerning these systems is included in Table 3.

Figure 3 shows the functions $\ln f^{s}_{12,h}$ vs. x^{l}_{1} calculated via Eq. (20) for the experimental system: benzene(1) + n-heptane(2) on silica gel with the changing parameter of surface phase capacity.

Table 3
Essential information about adsorption systems studied by means of Eqs. (20) and (22). Temperature: A – 297 K, B – 303 K, C – 273 K, D – 303 K, E – 333 K, F – 293K

Code	Adsorbent	Solution		Ref. to exp. data	
		Component 1	Component 2	$n_{1,t}^{\sigma(n)}$	bulk act. coefficients
A	Silica gel	Benzene	n – Heptane	[19]	[20]
B	Silica gel	Benzene	n – Heptane	[11]	[11]
C	Silica gel	Benzene	Cyclohexane	[21]	[20]
D	Silica gel	Benzene	Cyclohexane	[21]	[20]
E	Silica gel	Benzene	Cyclohexane	[21]	[20]
F	Boehmite	Methyl acetate	1,2 – dichloroethane	[9]	[10]

Table 4 contains the values $\overline{K}_{12}$ and n^s evaluated according to Everett method [4]. This method gives only approximate values of $\overline{K}_{12}$ for heterogeneous surfaces, but this accuracy is sufficient to evaluate $\ln f_{12,h}^s$ vs. x_1^l, since these values do not change the nature of this function, but only moves its position with respect to the x_1^l axis. All systems from Table 1 were analysed in terms of the IAP adsorption model (non-ideality of the bulk solution).

Table 4
Values of the average equilibrium constant and the surface phase capacity for experimental systems placed in Table 3

Code	Average equilibrium constant	Surface phase capacity according to Everett method	Surface phase capacity corrected by means of Eq.(20)
	$\overline{K}_{12}$	n^s (mole/kg)	n_t^s (mole/kg)
A	166.77	2.02	2.40
B	14.77	2.90	3.90
C	18.85	3.36	4.30
D	17.02	3.05	3.90
E	12.58	2.56	3.60
F	20.94	1.30	1.90

We can observe the influence of this parameter on the function in question. With regard to model calculations [17], the function $\ln f_{12,h}^s$ vs. x_1^l evaluated for the surface phase according to Everett method, i.e., for $n^s = 2.02$ mole/kg must be rejected. On the other hand, the value $n^s = n_t^s = 2.40$ mole/kg may be introduced as the corrected value of the surface phase capacity. It follows from Figure 3 that the distribution function characterizing the heterogeneity of silica gel with respect to the benzene(1) + n-heptane(2) liquid mixture

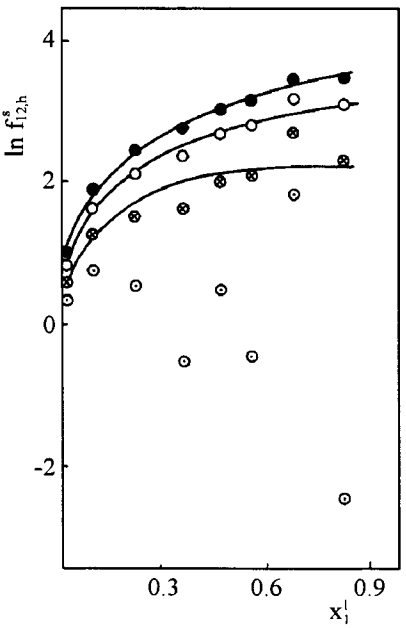

Figure 3. Functions $\ln f^s_{12,h}$ vs. x^l_1 for adsorption of benzene (1) + n–heptane (2) on silica gel at 297 K for $\overline{K}_{12}$ = 166.80 and various values of n^s: ●, n^s = 2.60 mole/kg; ○, n^s = 2.40 mole/kg; ⊗, n^s = 2.20 mole/kg; ⊙, n^s = 2.02 mole/kg. Figure taken from Ref. [17].

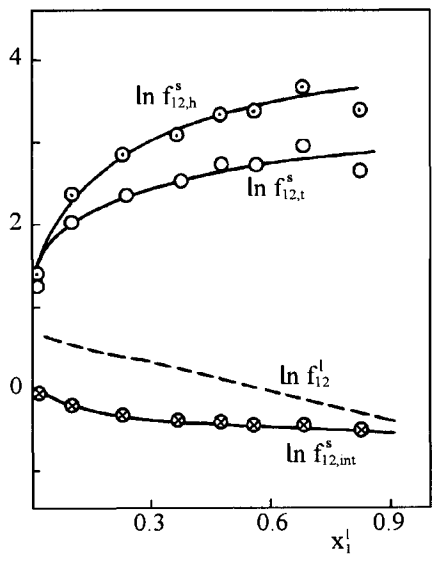

Figure 4. Functions $\ln f^s_{12,h}$, $\ln f^s_{12,t}$, $\ln f^s_{12,int}$, and $\ln f^l_{12}$ vs. x^l_1 for adsorption of benzene(1) + n–heptane(2) on silica gel at 297 K for $\overline{K}_{12}$ = 166.80 and n^s_t = 2.40 mole/kg. Figure taken from Ref. [17].

corresponds to Toth's equation [17]. The liquid mixture shows a certain bulk non–ideality [20] and Figure 4 display that the surface phase is slightly non–ideal in the whole concentration range. The curve $\ln f^s_{12,h}$ vs. x^l_1 has significant values, which is evidence for strong surface heterogeneity of silica gel. Due to the opposite signs of $\ln f^s_{12,h}$ vs. x^l_1 and $\ln f^s_{12,int}$ vs. x^l_1, the global surface non–ideality represented by the function $\ln f^s_{12,t}$ vs. x^l_1 is smaller than that arising from the surface heterogeneity of the solid. The non–ideality generated by molecular interactions in the bulk and surface phase is similar. This same conclusion deals also with the experimental system: methyl acetate(1) + 1,2–dichloroethane(2) on boehmite. The suitable functions for this system are displayed in Figure 5. Comparison of these functions with the model studies [17] shows that a symmetrical quasi – Gaussian distribution function represents the surface heterogeneity of the boehmite.

Concluding the above considerations we can state that the concept of global activity coefficients gives a simple method for assessing the adsorbent heterogeneity in the liquid – solid adsorption and can be useful for accepting the values of surface phase capacity.

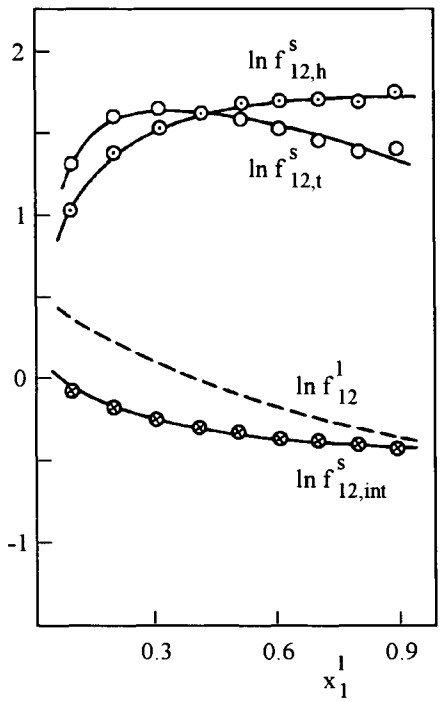

Figure 5. Functions $\ln f^s_{12,h}$, $\ln f^s_{12,t}$, $\ln f^s_{12,int}$, and $\ln f^l_{12}$ vs. x^l_1 for adsorption of methyl acetate(1) + 1,2-dichloroethane (2) on boehmite at 293 K for $\overline{K}_{12} = 20.94$ and $n^s_t = 1.90$ mole/kg. Figure taken from Ref. [17].

5. DESCRIPTION OF THE STRUCTURAL HETEROGENEITY OF SOLIDS

The present stage of development of the theory of micropore volume filling [22] as far as the gaseous adsorbate is concerned, is characterized, among others, by the introduction and discussion of the idea of the so–called structural heterogeneity of an adsorbent [23–26]. The differential distribution of the parameter connected with the characteristic energy of adsorption is assumed to be the measure of this quantity. The total adsorption is expressed by an integral from an appropriate local function (which is one of the mentioned theory's equations) in the interval of variation of this parameter. The abovementioned question - regarding a binary non–electrolyte liquid solution solid system is the subject of this part of our considerations. As it was shown [27–30], the isotherm of adsorption from binary liquid mixture of non– electrolytes on a homogeneous set of micropores takes the following form:

$$x^s_{1,1} = \exp(-By) \tag{23}$$

where y is one–to–one function of x_1^l, whereas the parameter B is given by the relation:

$$B = \left(\frac{RT}{E}\right)^n \tag{24}$$

where E denotes the characteristic energy of adsorption while n equals one or two.

If we assume that: (i) expression (23) defines the local function, $x_{1,l}^s(y, B)$ associated with the definite B value and (ii) B is a continuous variable, then the total adsorption isotherm takes a general form similar to that expressed by Eq. (1).
Namely:

$$x_{1,t}^s(y) = \int_{\Omega} x_{1,l}^s(y, B) \cdot F(B)\, dB \tag{25}$$

where F(B) stands for the differential distribution of B, and Ω is the interval of its variation. Accepting various normalized analytical forms for the function F(B), various total adsorption isotherms describing adsorption process on the whole microporous adsorbent can be obtained. As the examples, we will apply the well–known Gaussian and Rayleigh distribution functions [31,32]. The forms of these functions and the corresponding equations of a real adsorption are given below:
1. The Gaussian distribution

$$F(B) = 2\left[\Delta\sqrt{2\pi}\ \mathrm{erfc}\left(\frac{B_0}{\Delta\sqrt{2\pi}}\right)\right]^{-1} \exp\left[-\frac{(B - B_0)^2}{2\Delta^2}\right] \tag{26}$$

$$x_{1,t}^s(y) = \exp\left(\frac{y^2\Delta^2}{2} - B_0\right) \frac{\mathrm{erfc}\left(\frac{\Delta y}{\sqrt{2}} - \frac{B_0}{\Delta\sqrt{2}}\right)}{\mathrm{erfc}\left(\frac{-B_0}{\Delta\sqrt{2}}\right)} \tag{27}$$

2. The Rayleigh distribution

$$F(B) = \frac{B - B_0}{\Delta^2} \exp\left[-\frac{(B - B_0)^2}{2\Delta^2}\right] \tag{28}$$

$$x_{1,t}^s(y) = \exp(-B_0 y)\left[1 - \frac{\Delta y}{2}\sqrt{2\pi}\exp\left(\frac{y^2\Delta^2}{2}\right)\ \mathrm{erfc}\left(\frac{y\Delta}{\sqrt{2}}\right)\right] \tag{29}$$

where erfc is the error function compliment while B_0 and Δ denote the characteristic parameters of the particular distributions. In the limit of $\Delta \to 0$, each of the presented distributions becomes the delta function, $\delta(B - B_0)$, while the total isotherm becomes identical to the local one corresponding to an adsorbent which is structurally homogeneous. Regarding to the function $y(x_1^l)$, two solutions were obtained in two independent ways. The first one has the form [27, 31]:

$$y = \ln^n \frac{a_1^* \cdot a_2^{*(1 - x_1^*)/x_1^*}}{a_1^l \cdot a_2^{l(1 - x_1^l)/x_1^l}} \tag{30}$$

where the asterisk relates to the bulk mixture saturated with respect to the 1–st component. The second derivation gave the following result [29, 30, 32]:

$$y = \ln^n \left(1 + \kappa \frac{a_2^l - a_2^*}{a_1^l}\right) \tag{31}$$

where κ is a constant parameter.

Let us notice that the expressions (30) and (31) are useful for describing adsorption from binary liquid mixtures exhibiting both limited ($a_1^* < 1$ and $a_2^* > 0$) and unlimited ($a_1^* = x_1^* = 1$ and $a_2^* = x_2^* = 0$) miscibility of components. Additionally, a_2^l is, according to Gibbs – Duhem equation, one–to–one function of a_1^l, thus both these activities depend, at fixed p and T, on x_1^l only.

Computations may be carried out by optimizing the parameters of the applied equations as well as the specific capacity of adsorbed phase for obtaining the best fit of theoretical excess isotherms to the experimental data. Tables presented below contain the characteristics of the adsorption systems from Table 1 illustratively used for computations and the calculation results obtained for Eq.(7) combined with substitutions (27) or (29) under the assumption that n_t^s = const.

Table 5
Description of selected adsorption systems from Table 1 via Eq.(27) (Gaussian distribution) combined with Eq.(30) [31]

System	n = 1				n = 2			
	B_0	Δ	n_t^s (mole/kg)	$q^* \cdot 10$	B_0	Δ	n_t^s (mole/kg)	q·10
A	0.044	0.326	1.325	9.95	0.005	0.093	0.960	9.99
B	0.068	0.331	1.468	9.76	0.004	0.091	1.136	9.85
C	0.024	0.287	3.911	9.95	0.002	0.077	2.794	9.97
D	0.003	0.077	1.182	9.94	0.003	0.039	1.170	9.93
E	0.083	0.419	0.889	9.99	0.007	0.123	0.512	9.99
F	0.009	0.250	2.419	9.99	0.001	0.121	2.177	9.99
G	0.024	0.217	1.200	9.88	0.001	0.045	1.021	9.77
I	0.084	0.420	1.134	9.99	0.005	0.122	0.652	9.99

q^* is the non–linear correlation coefficient

Reprinted from: P. Cysewski, J.K. Garbacz, S. Biniak, A.Świątkowski and A. Dąbrowski, Ads. Sci. Tech., 5 (1988) 106.

The critical analysis of the numerical results placed in Tables 5–8 instructs that for a given adsorption system, one can obtain a comparably accurate descriptions (measured by the q values) of the experimental isotherms on the basis of different theoretical relationships. Since different adsorption equations relate to different paires of B_0 and Δ values, thus it must be emphazised that the adsorbent structural heterogeneity description based on the method presented above has a conventional character and is, similarly as an adsorbent specific surface area, connected with the applied theoretical model.

Table 6
Description of selected from Table 1 adsorption systems via Eq. (29) (Rayleigh distribution) combined with Eq.(30) [31]

System	n = 1				n = 2			
	B_0	$\Delta \cdot 10^3$	n_t^s (mole/kg)	q·10	$B_0 \cdot 10^3$	Δ	n_t^s (mole/kg)	q·10
A	0.206	0.795	1.207	9.62	99.90	0.002	1.132	9.98
B	0.198	0.010	1.168	8.87	14.90	0.100	1.721	9.98
C	0.150	0.358	3.224	9.55	78.20	0.002	3.085	9.97
D	0.038	1.000	1.195	9.93	22.10	0.006	1.177	9.93
E	0.134	0.023	0.342	9.88	142.10	0.013	0.758	9.99
F	0.117	0.452	2.308	9.98	0.01	0.091	2.224	9.99
G	0.178	0.274	1.334	9.54	0.01	0.045	1.115	9.81
I	0.125	0.447	0.421	9.79	29.10	0.126	1.095	9.99

Reprinted from: P. Cysewski, J.K. Garbacz, S. Biniak, A. Świątkowski and A. Dąbrowski, Ads. Sci. Tech., 5 (1988) 106.

Table 7
Description of selected from Table 1 adsorption systems via Eq.(27) (Gaussian distribution) combined with Eq. (31) [32]

System	n = 1					n = 2				
	$B_0 \cdot 10^2$	Δ	$\kappa \cdot 10$	n_t^s (mole/kg)	q·10	$B_0 \cdot 10^2$	Δ	κ	n_t^s (mole/kg)	q·10
A	11.40	1.202	1.544	0.963	9.98	77.1	0.149	1.566	9.454	9.98
B	2.79	0.417	8.862	1.237	9.79	78.1	0.137	1.566	9.513	9.99
E	4.88	0.663	7.066	0.647	9.99	22.9	4.760	3.713	5.716	9.99
H	3.54	0.601	6.090	1.184	9.99	26.0	0.105	2.603	9.980	9.99
I	5.03	0.577	9.949	0.887	9.99	29.9	6.105	2.604	7.972	9.99

Reprinted from: J.K. Garbacz, P. Cysewski and A. Świątkowski, Pol. J. Chem., 65(1991)479.

Table 8
Description of selected from Table 1 adsorption systems via Eq.(29) (Rayleigh distribution) combined with Eq. (31) [32]

System	n = 1					n = 2				
	$B_0 \cdot 10^3$	Δ	$\kappa \cdot 10$	n_t^s (mole/kg)	q·10	$B_0 \cdot 10^3$	$\Delta \cdot 10$	κ	n_t^s (mole/kg)	q·10
A	0.004	1.715	1.618	1.784	9.99	33.54	2.343	0.772	1.030	9.98
B	8.13	0.603	4.091	1.566	9.86	33.54	0.899	1.669	1.203	9.94
E	156	1.616	2.132	1.093	9.99	0.001	2.692	1.138	0.568	9.99
H	775	0.266	3.263	1.667	9.99	157.90	.005	1.714	1.088	9.99
I	3.85	1.596	2.949	1.987	9.99	0.003	1.928	1.839	0.835	9.99

Reprinted from: J.K. Garbacz, P. Cysewski and A. Świątkowski, Pol. J. Chem.,65(1991)479.

6. POROSITY OF SOLIDS BY THERMAL DESORPTION OF LIQUIDS

The other posibility for characterizing structural properties of inorganic sorbents deals with the thermogravimetric analysis. By means of this analysis the pore size distribution, pore volume and specific surface area of adsorbents and catalysts which are fundamental adsorption characteristics may be obtained.

Gas adsorption and mercury porosimetry are the standard techniques for studying the textural properties of porous solids [33]. Both these methods have well known more or less severe limitations. Thus, many afforts are made to apply a new experimental techniques in a complementary manner. In recent years numerous experimental methods for porous structure analysis have been developed [see Refs. 34, 35 and articles therein). Among others, we have proposed application of thermogravimetric (TG) technique for the characterization of the porosity of the adsorbents used in liquid and gas chromatography [36-38]. The measurements were performed by using Controlled Transformation Rate Thermogravimetry (CRTG) in the manner developed by Paulik and Paulik [39] and called by them as quasi-isothermal heating mode. The method makes possible to maintain as close as possible quasi-isothermal conditions and hence to increase the resolution of thermal analysis. Thermal analysis proved to be quite useful to characterize the porosity of solids within the mesopores. The advantages and restrictions of thermogravimetric method are presented below for silica gels and aluminium oxide. Textural parameters obtained from TG experiment are compared with those from nitrogen adsorption method.

6.1. Thermogravimetric method

The experiment consists of the measurements of mass loss of the liquid wetting the sorbent perfectly on temperature using quasi-isothermal program of heating. The main feature of this program is a constancy of temperature within the time when the transformations connected with distinct mass changes take place in the sample. Usually, this heating mode is used in the investigations of thermal decomposition or dehydration. (see e.g. Refs. 39, 40). Desorption of adsorbed species from porous material is a process of a different type and takes place within some temperature range. However, the desorption of liquid adsorbates from the pores of different dimensions may be assumed as a process which is the sum of several isothermic processes. During isothermal process the temperature of the sample spontaneously assumes a constant value, this proves that quasi-equilibrium exists between the wet solid and the gas atmosphere above the sample. Each isothermic process corresponds to desorption from a given group of pores of uniform dimensions. Thus, during the desorption experiment carried out by using quasi-isothermal program the temperature and the heating rate are not constant. If evapouration of liquid is slow the fixed mass loss level regulating the run of the program is not exceeded. As a result the linear increase of temperature is realized. At a certain temperature when intensive evapouration occurs, the abovementioned level is exceeded and quasi-isothermal conditions are established. The sharp evapouration of liquid takes place at the boiling point of the liquid out of pores or at temperature for which the pressure of the saturated vapours above the liquid meniscus in the pore becomes equal to atmospheric pressure. Figure 6 shows the typical desorption curve (solid line) for a liquid which wets the adsorbent perfectly and interacts with its surface only physically.

The results have been expressed as conventional TG curve, mass loss against tem-

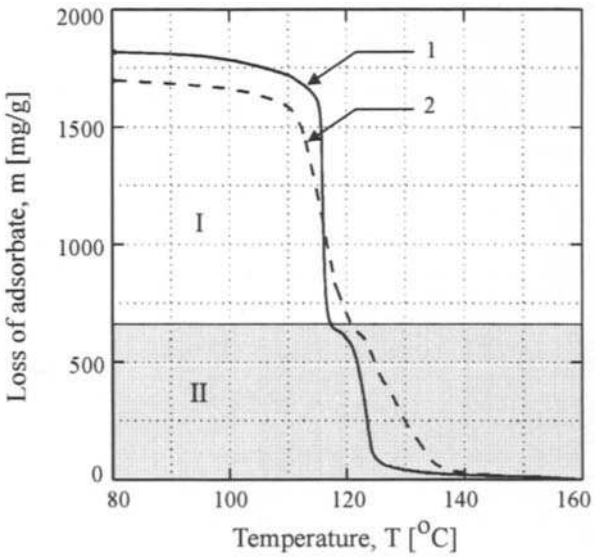

Figure 6. Thermal desorption of liquid from a mesoporous adsorbent: I – desorption of the bulk liquid out of pores, II – desorption of liquid from the pores. Solid line (1) – quasi-isothermal program, broken line (2) – linear program.

perature, $\Delta m=f(T)$. In Figure 7 the dependence of temperature vs. time for the same desorption process is also shown.

For illustrative purposes, the dotted curves represent the results obtained by applying dynamic heating program with continuously increasing temperature. In this last case the characteristic points on the desorption curve connected with the textural properties of solid disappear. Segment I of the TG curve represents the bulk liquid outside the pore structure of the adsorbent. Intensive evapouration at this stage of the process takes place at the boiling point of the liquid (perpendicular segment). When the first stage of desorption is completed the temperature increases and the desorption from pores starts. Segment II corresponds to desorption of adsorbate within the pores together with the adsorbed film on the walls of pores and is, therefore, a measure of the total pore volume. On the upper segment of the desorption curve one can observe the inflection point. The region in the immediate vicinity of this point corresponds to the desorption from pores which volume composes greatest part of the total pore volume.

The plot $\Delta m=f(T)$ may be converted into a plot volume liberated versus pore radius $\Delta V=f(r)$ using the Kelvin equation:

$$\ln \frac{p}{p_0} = -\frac{2\gamma}{r_k} \cdot \frac{V_M}{RT} \tag{32}$$

Eq.(32) gives the relationship between the saturated vapour pressure of liquid over the curved (inside the pores) and the flat liquid surface, p and p_0, respectively, r_k is the radius of the liquid meniscus, γ is the surface tension of liquid, V_M is the molar volume and T is absolute temperature. It follows from Eq.(32) that the sharp emptying of the pore

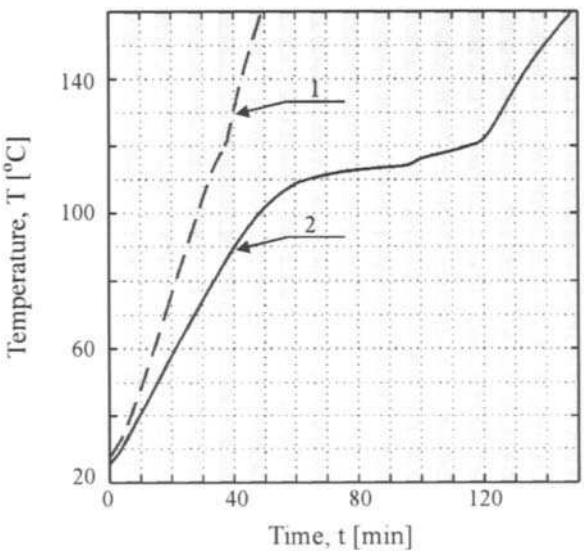

Figure 7. Temperature–time dependence for adsorption of liquid from mesoporous adsorbent. 1 – linear program, 2 – quasi-isothermal program.

of a given diameter occurs under the experimental conditions applied when the pressure of liquid vapour becomes equal to atmospheric pressure. For large pore dimensions the evacuation of liquid from the pores occurs at temperatures only a little higher than the boiling point of the bulk liquid. When the pore dimensions decrease the higher temperature is required for their emptying.

When evapouration from a pore occurs a strongly held monolayer or multilayer film of adsorbate molecules of thickness d, remains on the pore walls. With the usual assumptions that the pores are cylindrical and that the contact angle of liquid with the adsorbed film is zero, r_k becomes equal to the radius of the core. The radius of the pore is give by $r=r_k+d$. Differentiating the dependence $\Delta V=f(r)$ the pore size distribution $\Delta V/\Delta r = f(r)$ for a given sorbent may be derived. Unfortunately, standard values of d under the conditions of TG experiments are very difficult to establish unambiguously. Consequently, it is not possible to proceed directly from these data to a pore size distribution but only to a core size distribution. The thickness of the surface film depends on the heating program used in the experiment. However, as we have stated earlier, the effect of the surface film may be minimized by choosing an optimal heating program of TG experiment. The differences between the peak location of the pore size distributions from the nitrogen adsorption and TG methods were discussed in terms of the surface film effect in the paper [41]. The heating program must be neither too slow nor to fast.

In both cases the pore distributions are deformed and the location of the pore size distribution peaks differs considerably from those obtained from the nitrogen adsorption method. If is too slow, desorption will be too slow, so that air can mix with the vapour. When $p < 1$ atm the evapouration from the pores at each measuring temperature is possi-

ble. As the result mass loss at lower temperatures is increased by the mass of adsorbate evapourated from narrower pores as well as the thinning of the surface film at a given temperature. If heating program is too fast, the temperature of the sample lags behind the measured temperature. As the result the radius calculated from measured temperature by Kelvin equation is smaller than actual radius. Moreover, fast program leads to temperature instability of the sample. The heating mode influences substantially the time of the desorption process and consequently the shape of the pore/core size distribution curve.

All desorption curves described below were measured with Derivatograph 1500C (MOM, Hungary). The measurements were performed using quasi-isothermal program at a heating rate 3°/min within the linear heating range and fixed mass loss level regulating the program 0.5 mg/min. The samples, in the form of paste, were prepared by adding excess of liquid adsorbate to the dry adsorbent.

From our previous studies of TG method and its application to the characterization of mesorpores we may draw some general conclusions concerning this method. The following guidelines for obtaining meaningful results are suggested:

- liquid wetting the porous solid should interacts with the surface only physically,
- liquid should be dried before experiment and stored over 3A and 4A molecular sieves,
- high purity liquids should be used because impurities may substantially change the boiling point of a liquid and consequently causes errors in calculations of the pore radii from the Kelvin equation,
- physically adsorbed water should be removed from the hydroxylated silica surface. Oxide adsorbents are ussualy dried by prolonged heating at 180°C. These conditions are sufficient to remove the physically bonded water and temperature is low enough to avoid removing surface hydroxyl groups.
- the best equilibrium conditions are obtained by using a spiral or labyrinth type of crucible. This type of crucible makes it possible to keep over the sample a self-generated atmosphere of liquid vapours.
- The samples should be outgassed before experiment to facilitate the penetration of pores by the adsorbate.

6.2. Pore size distributions (PSD)

Figure 8 shows thermodesorption curves for a series of silica gels of different mesoporosity, Si-40, Si-60, Si-100 and Si-200 (Merck, Germany).

It can be seen that all curves present an inflection point above boiling point of liquid which progressively shifts from higher to lower temperatures as the mean pore diameter increases. From the shape of these curves it can be said that there exists close correlation between the porosity of solid and location of characteristic points of the curves which can be ascribed to appropriate stages of desorption process. The upper segments of the curves are depending uppon particular interactions between the liquid molecules and the adsorbent surface. Generally, one can say that the width of segment II of desorption curve is determined by the specific properties of liquid and characteristic for a given liquid adsorbate temperature – radius dependence. For ilustrative purposes Figure 9

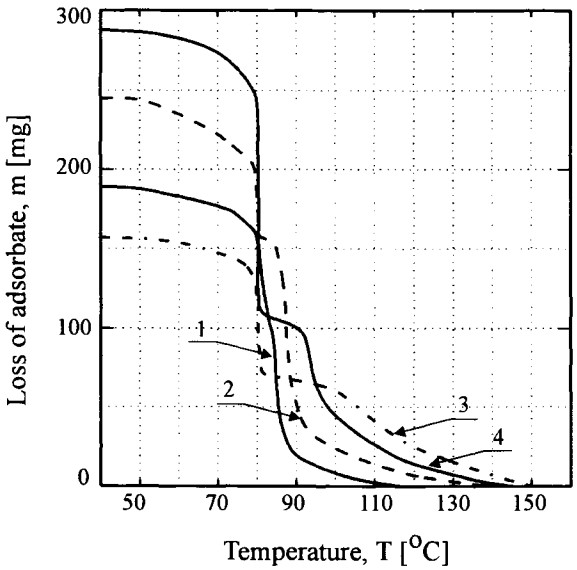

Figure 8. Desorption curves (mass loss against temperature) of benzene from various silica gels: 1 – Si-200, 2 – Si-100, Si-60, 4 – Si-40. Figure taken from Ref. [36].

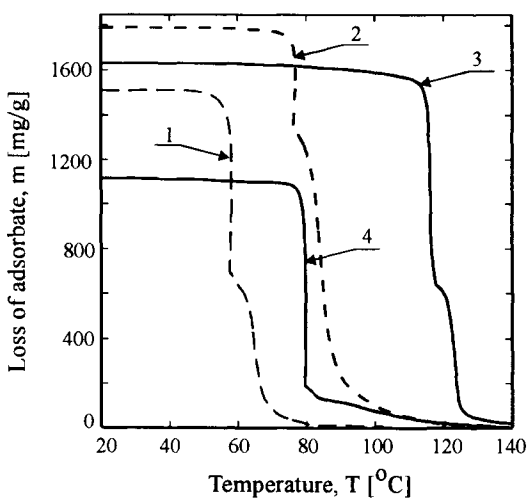

Figure 9. TG curves of desorption for silica gel (curves 1,2,3) and aluminium oxide (curve 4). 1 – acetone, 2 – carbon tetrachloride, 3 – n-butanol, 4 – benzene.

shows thermodesorption curves of various liquids for silica gel Si-100 (curves 1, 2, 3). Curve 4 represents desorption of benzene from aluminium oxide Al_2O_3 150T using the same quasi-isothermal program.

The shape of TG curves in the case of aluminium oxide is quite different in comparison to silica gel. Figure 10 shows adsorption/desorption isotherms of nitrogen at -195°C for the same adsorbents. Also in this case the shape of hysteresis loop is different for both types of oxide adsorbents.

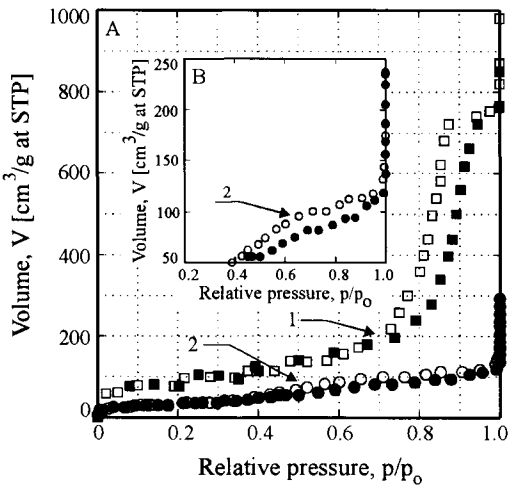

Figure 10. Part A – adsorption/desorption isotherms of nitrogen at -195°C for silica gel Si-100 (1) and aluminium oxide 150T (2). Part B – hysteresis loop for aluminium oxide 150T.

Applying the procedure of the calculations described earlier the appropriate pore/core size distribution (PSD) curves $\Delta V/\Delta r$ vs. r for adsorbents investigated may be calculated. From the heights of segments II of the TG curves the total pore volumes were estimated. In Figures 11 and 12 the pore/core size distributions derived from TG experiment are compared with those from nitrogen adsorption experiment.

The PSD curves in the case of nitrogen adsorption, were calculated by the BJH method [43] with corrections of the pore radii in respect of the surface film thickness d, where $d = 4.3 \cdot \sqrt[3]{5/(\ln p/p_0)}$. Points in Figures 11 and 12 represent the PSDs calculated from nitrogen adsorption data.

The pore radii at the peak of PSD, r_{peak} and total pore volumes V_p calculated on the basis of the experimental data obtained by using different techniques are collected in Table 9.

As shown, in the case of acetone, the location of the peak of PSD, r_{peak} is shifted toward smaller radii in comparison with the PSD calculated from nitrogen adsorption data. However, in the case of n-butanol and carbon tetrachloride the difference $r^{N_2}_{peek} - r^{TG}_{peek}$ is small. It should be noted that the total pore volumes calculated from TG curves for both adsorbents are very similar to those estimated from the nitrogen adsorption isotherms.

Pore size distributions for Al_2O_3 150T derived from different experimental data are close together. Points represent the PSD curves calculated from nitrogen adsorption data.

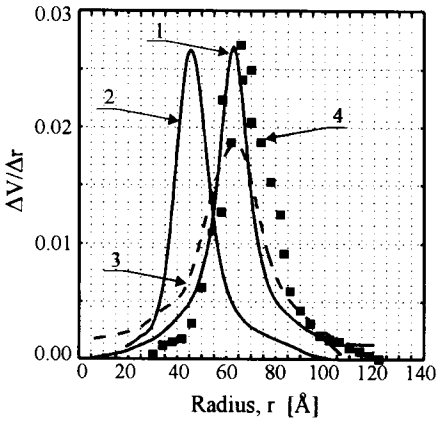

Figure 11. Pore/core size distribution curves for silica gel Si-100; 1 – carbon tetrachloride, 2 – acetone, 3 – n-butanol, 4 (points) – pore size distribution derived from nitrogen adsorption data.

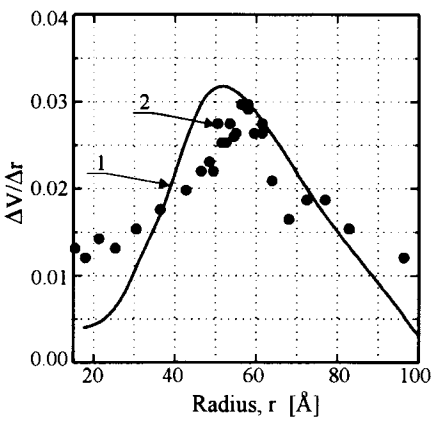

Figure 12. Pore/core size distribution curve for aluminium oxide 150T; 1 – benzene, 2 (points) – pore size distribution derived from nitrogen adsorption data.

Table 9
Parameters characterizing the porous structure of adsorbents obtained by using various methods

Method	Adsorption			Thermogravimetry	
	S_{BET}	V_p	$r_{peek}^{N_2}$	V_p	r_{peek}^{TG}
Adsorbent/adsorbate	[m^2/g]	[cm^3/g]	[Å]	[cm^3/g]	[Å]
Al_2O_3 150T/benzene	50	0.24	55	0.22	59
Si-100/acetone	320	1.10	66	0.96	44
Si-100/CCl_4	320	1.10	66	1.05	64
Si-100/n-butanol	320	1.10	66	0.92	63

As a conclusion, one can say that the thermogravimetric technique is a usefull method in the investigations of the porosity of solids. Our analysis, based on the Kelvin equation, of the thermogravimetric curves for silica gel wetted with liquid n-butanol and carbon tetrachloride leads to core/pore size distributions curves which are similar, but not identical in shape to the pore size distribution curves derived by standard procedure from low temperature nitrogen adsorption/desorption isotherms. The linear heating mode is

inadequate in the investigations of the porosity of solids. Mostly appropriate conditions of TG experiment are attained in the case of quasi-isothermal heating mode.

7. GENERAL TRENDS AND PERSPECTIVES

Alternative approaches to liquid adsorption based on Monte Carlo simulation and molecular dynamics methods, statistical thermodynamics as well as advanced experimental techniques can create new possibilities in the investigations of the solid adsorbents. The nearest perspectives referring to the liquid adsorption on solids will include the following:

1. making the thermodynamic description of adsorption both at the gas – solid and the liquid – solid interfaces uniform to predict adsorption isotherms from solutions based on single gas isotherms,
2. investigations into structural changes in the surface phases,
3. simultaneous studies on heats and adsorption isotherms determined at different temperatures,
4. preparation of a theoretical approach making it possible to predict adsorption isotherms at different temperatures from the isotherm determined at the given temperature.

8. CONCLUSIONS

The simple theoretical description of the adsorption from solutions on solids can be useful for characterizing sorption properties of inorganic sorbents. Such properties as the energetical and structural heterogeneities, surface phase capacity, specific surface area, pore size distribution curves and others are very important with regard to wide application of inorganic adsorbents on laboratory and industrial scales.

REFERENCES

1. A. Dąbrowski, M. Jaroniec and J. Ościk, in: E. Matijevic (ed.), Surface and Colloid Science, vol.14, Plenum Press, New York, 1987, pp. 83–213.
2. A. Dąbrowski and M. Jaroniec, Adv. Colloid Interface Sci., 27 (1987) 211.
3. A. Dąbrowski and M. Jaroniec, Adv. Colloid Interface Sci., 31 (1990) 155.
4. D.H. Everett, Trans. Faraday Soc., 60 (1964) 1803.
5. M. Jaroniec , Adv. Colloid Interface Sci. 18 (1983) 149.
6. M. Jaroniec and R. Madey, Physical Adsorption on Heterogeneous Solids, Elsevier, Amsterdam, 1988.
7. A. Dąbrowski and P. Podkościelny, in preparation.
8. J. Goworek, Colloids Surf.,47 (1990) 169.
9. J.J. Kipling and D.B. Peakall, J.Chem. Soc., (1956) 4828.
10. A. Blackburn, J.J. Kipling and D.A. Tester, J. Chem. Soc., (1957) 2373.
11. S. Sircar and A.L. Myers, J. Phys. Chem., 74 (1970) 2828.
12. S.C. Hwang and R.L. Robinson, J. Chem. Eng. Data, 22 (1977) 319.

13. A.L. McLellan and H.F. Harnsberger, J. Colloid Interface Sci., 23 (1967) 577.
14. G. Schay and L.G. Nagy, J. Colloid Interface Sci., 38 (1972) 302.
15. A. Dąbrowski and M. Jaroniec, Chem. Scripta, 29 (1989) 21.
16. A. Dąbrowski, Chem. Scripta, 25 (1985) 182.
17. A. Dąbrowski, P. Podkościelny, J. Goworek and J.K. Garbacz, Thermochimica Acta 1 (1995) 229.
18. A. Dąbrowski, J. Ościk, W. Rudziński and M. Jaroniec, J. Colloid Interface Sci., 69 (1979) 207.
19. G. Foti, L.G. Nagy and G. Schay, Acta Chim. Hung., 76 (1973) 269.
20. G. Scatchard, S.E. Wood and J.M. Mochel, J. Am. Chem. Soc., (1946) 1957.
21. S. Sircar, J. Novosad and A.L. Myers, Ind. Chem. Eng. Fundam.,11 (1972) 249.
22. M.M. Dubinin, Adsorption – Desorption Phenomena, F. Ricca (ed.), New York, 1972.
23. H.F. Stoeckli, J. Colloid Interface Sci., 59 (1977) 184.
24. H.F. Stoeckli and U. Huber, Agents and Action, 7 (1977) 411.
25. M. Rozwadowski and R. Wojsz, Carbon, 22 (1984) 363.
26. M. Rozwadowski and R. Wojsz, Carbon, 59 (1984) 837.
27. J.K. Garbacz, P. Cysewski, S. Biniak and A. Świątkowski, Ads. Sci. Tech., 3 (1986) 253.
28. J.K. Garbacz, S. Biniak and P. Cysewski, Ads. Sci. Tech., 4 (1987) 105.
29. J.K. Garbacz, P. Cysewski and S. Biniak, Polish J. Chem., 63 (1989) 205.
30. J.K. Garbacz, P. Cysewski, S. Biniak and A. Świątkowski, Polish J. Chem., 64 (1990) 267.
31. P. Cysewski, J.K. Garbacz, S. Biniak, A. Świątkowski and A. Dąbrowski, Ads. Sci. Tech., 5 (1988) 106.
32. J.K. Garbacz, P. Cysewski and A. Świątkowski, Polish J. Chem., 65 (1991) 479.
33. S.J. Gregg and K.S.W. Sing, Adsorption, Surface Area and Porosity, Academic Press Inc., London, 1982.
34. F. Rodriguez-Reinoso, J. Rouquerol, K.S.W. Sing and K.K Unger (eds.), Characterization of Porous Solids II, Elsevier, Amsterdam, 1991.
35. J. Rouquerol, F. Rodriguez-Reinoso, K.S.W. Sing and K.K. Unger (eds.), Characterization of Porous Solids III, Elsevier, Amsterdam, 1994.
36. J. Goworek and W. Stefaniak, Colloids Surf., 60 (1991) 341.
37. J. Goworek and W. Stefaniak, Colloids Surf., 69 (1992) 23.
38. J. Goworek and W. Stefaniak, Mat. Chem. Phys., 32 (1992) 244.
39. F. Paulik and J. Paulik, J. Thermal. Anal., 5 (1973) 253.
40. J. Rouquerol, J. Thermal Anal., 5 (1973) 203.
41. J. Goworek and W. Stefaniak, Colloids Surf., 62 (1992) 135.
42. J. Goworek and W. Stefaniak, in: J. Rouquerol, F. Rodriguez-Reinoso, K.S.W. Sing and K.K. Unger (eds.), Characterization of Porous Solids III, Elsevier, Amsterdam, 1994, p.401.
43. E.P. Barrett, L.G. Joyner and P.H. Halenda, J. Am. Chem. Soc., 73 (1951) 373.

A. Dąbrowski and V.A. Tertykh (Editors)
Adsorption on New and Modified Inorganic Sorbents
Studies in Surface Science and Catalysis, Vol. 99
1996 Elsevier Science B.V.

Chapter 3.2
Study of adsorption from solutions by chromatography

V.Ya.Davydov

Department of Chemistry, M.V.Lomonosov Moscow State University,
Moscow 119899,Russia

1. INTRODUCTION

The most studies of adsorption from solution have been concerned with the adsorption from two–component mixture, for example [1,2]. Practical use of adsorption however deals with the adsorption from multicomponent systems. In liquid chromatography in a many cases for the separation of mixture of solutes the multicomponent eluents are used. The most difficulties in the investigation of adsorption from multicomponent systems arise at the determination of some component concentration at once in equilibrium solution over the adsorbent. Moreover for the determination of adsorption isotherm in this case large experimental data are needed.

The chromatographic method of analysis makes it possible to investigate the adsorption from multicomponent systems. For study of adsorption from solutions of volatile compounds gas chromatography can be used and for the investigation of solid compound or non–volatile substances liquid chromatography is used. In this cases chromatography is applied as method of determination of components concentration in equilibrium solution over the adsorbent [3–5].

The isotherm of adsorption from solution may be determined by frontal chromatograms [6–8]. In [6] it was shown that if to take into consideration the broadening the band owing to diffusion, the adsorption isotherms determined by the column chromatography and in a batch process are coincided. This method can be used for the calculation of S–shape isotherm of adsorption. The isotherm of adsorption can be determined by frontal chromatography if the adsorbents have not fine pores [7].

2. ADSORPTION FROM MULTICOMPONENT SOLUTIONS

2.1. Adsorption of volatile compounds

Study of adsorption from multicomponent systems makes it possible to determine the mutual effect of component on adsorption of each other and to use the main relationships for the optimization of the separation in liquid chromatography.

The simplest case of adsorption from multicomponent solutions is the adsorption from ternary solutions. The isotherms of components adsorption in such systems are expressed

by surfaces the shapes of which are determined by the surface chemistry of adsorbent and the structure of compounds.

For the determination of component concentration in equilibrium solution the columns packed by adsorbent with some stationary phase is used for the complete separation of component. The adsorption of volatile compounds on hydroxylated silica from ternary solutions was investigated by gas chromatography [3 – 5].For all components the heats of adsorption on silica were known and it was possible to find the correlation between the heats of adsorption and the shape of isotherm of component adsorption.

The composite isotherms of hexane, benzene and dioxane adsorption from their mixture on silica are presented on Fig. 1. The isotherms of adsorption are expressed by projections of the same adsorption lines on concentration triangle.

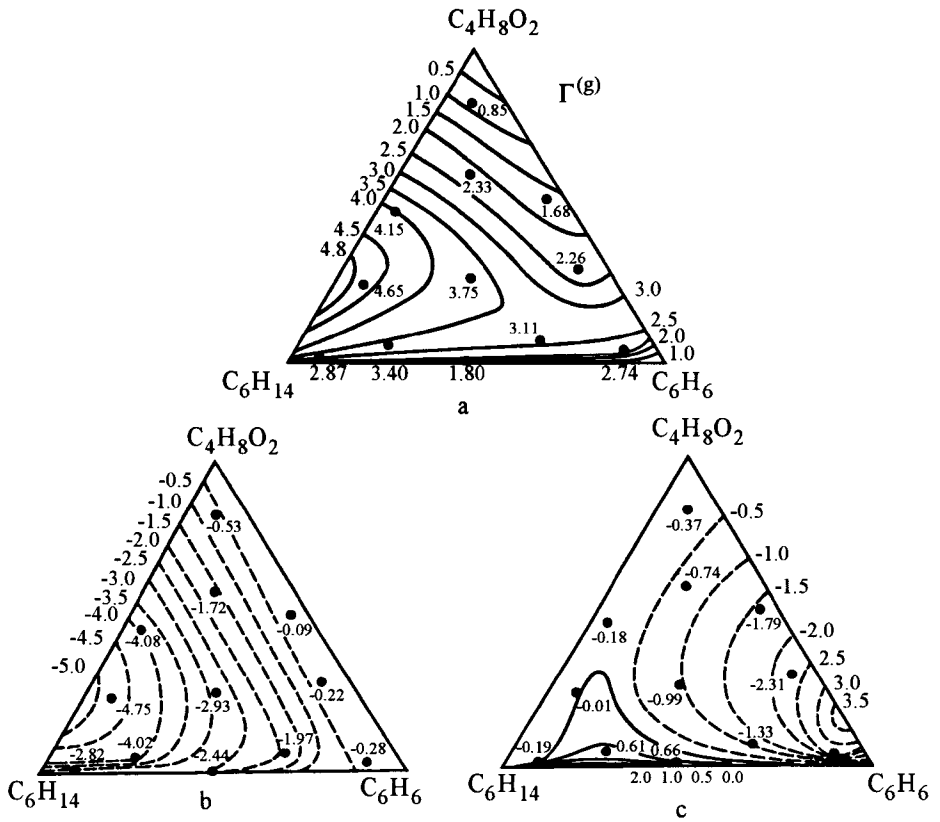

Figure 1. The isotherms of adsorption (projection of lines with equal adsorption on concentration triangle) of dioxane (a), n-hexane (b) and benzene (c) on silica gel from their mixtures. The numbers near the dots and lines are the values of excess adsorption $\Gamma^{(g)}$, μmol/m^2.

Fig. 2 shows the isotherms of n-hexane, benzene and carbon tetrachloride adsorption on silica from their mixtures and on Fig. 3 the isotherms of dioxane, acetone and water adsorption from their mixtures on hydroxylated silica are presented. Fig. 4. shows the

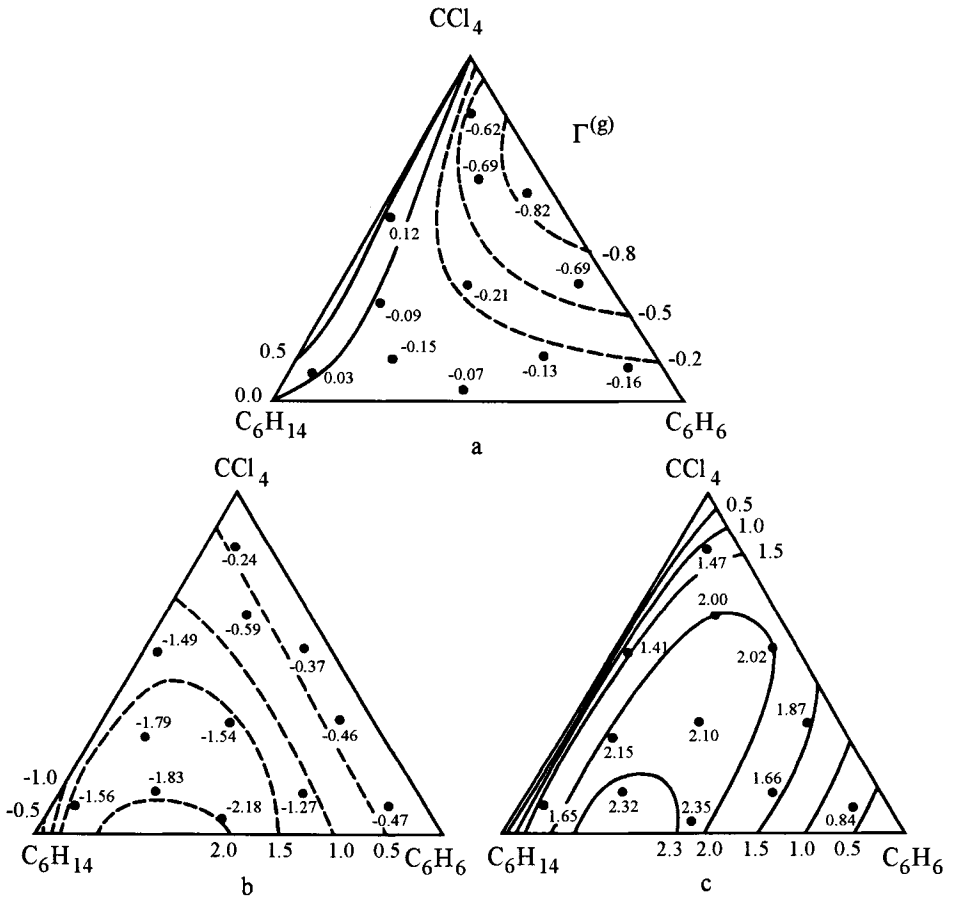

Figure 2. The isotherms of adsorption of carbon tetrachloride (a), n-hexane (b) and benzene (c) from their mixture on silica. The numbers near the dots and lines are the values of excess adsorption $\Gamma^{(g)}$, μmol/m^2.

isotherms of adsorption of acetone and dioxane from water and of dioxane from acetone on the same silica.

All systems include compounds which make it possible to determine the effect of different types of intermolecular interactions on the component adsorption. On adsorption in system benzene – n-hexane – carbon tetrachloride – hydroxylated silica, the hydrogen bond of dioxane with surface silanol groups is the most important. On adsorption from benzene – n-hexane – carbon tetrachloride on silica the only benzene can interact with silanol groups by weak hydrogen bonds and for n-hexane and carbon tetrachloride the dispersion interactions are realized. In the case of adsorption from dioxane – acetone – water mixture on silica all components are capable to form of hydrogen bonds with surface hydroxyl groups on silica moreover dioxane and acetone molecules form rather strong hydrogen bond with water as well as water molecules form hydrogen bonds with each other.

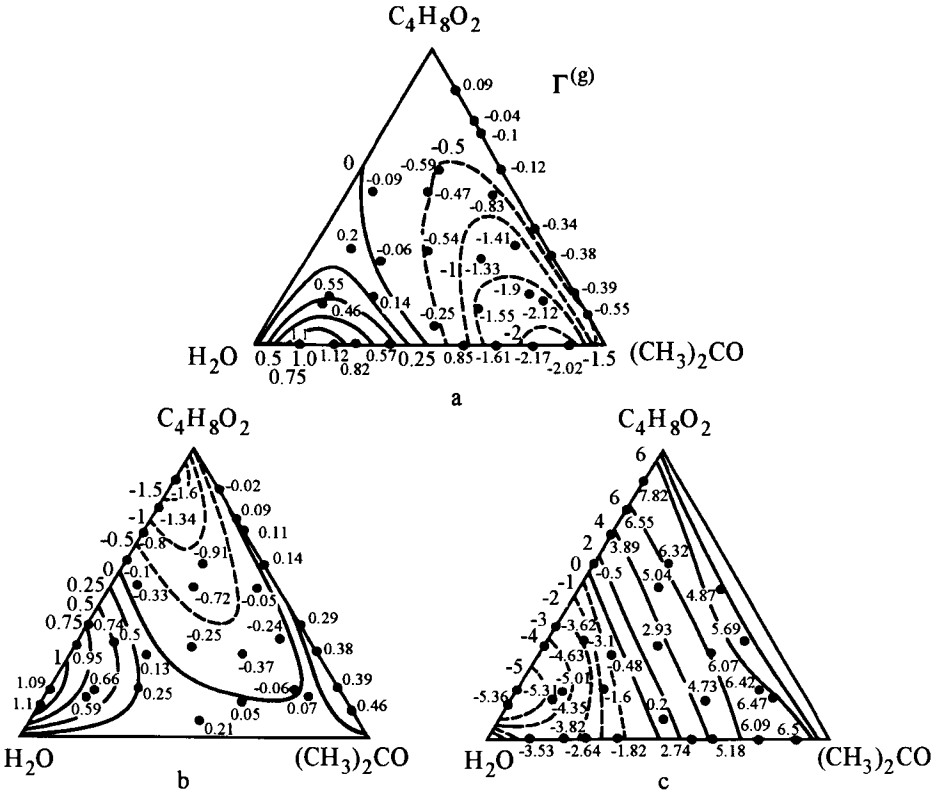

Figure 3. The isotherms of adsorption of acetone (a), dioxane (b) and water (c) from their mixture on silica gel. The numbers near the dots and lines are the values of excess adsorption $\Gamma^{(g)}$, μmol/m^2.

So this adsorption system is very complicate from the point of view the intermolecular interactions.

On adsorption of components from benzene, hexane and dioxane mixture on silica the composite isotherm of dioxane adsorption is positive in all region of equilibrium concentrations and of n–hexane is negative. The composite isotherm of benzene adsorption changes from positive to negative depending on the region equilibrium concentration in concentration triangle. At small dioxane concentration the benzene adsorption is positive but benzene excess adsorption becomes negative with the increasing of dioxane concentration in a mixture.

Such form of composite isotherm of components adsorption may be qualitatively explained by the heats of vapour adsorption of these components on silica. The heats of dioxane, benzene and n–hexane adsorption are 66.9, 42.7 and 36.8 kJ/ mol respectively at about half monolayer coverage [9]. In accordance with heats of adsorption dioxane strong adsorbs and n–hexane is displaced from the adsorbent surface. The heat of benzene adsorption is smaller than those of dioxane and is larger than those of n–hexane owing to these the

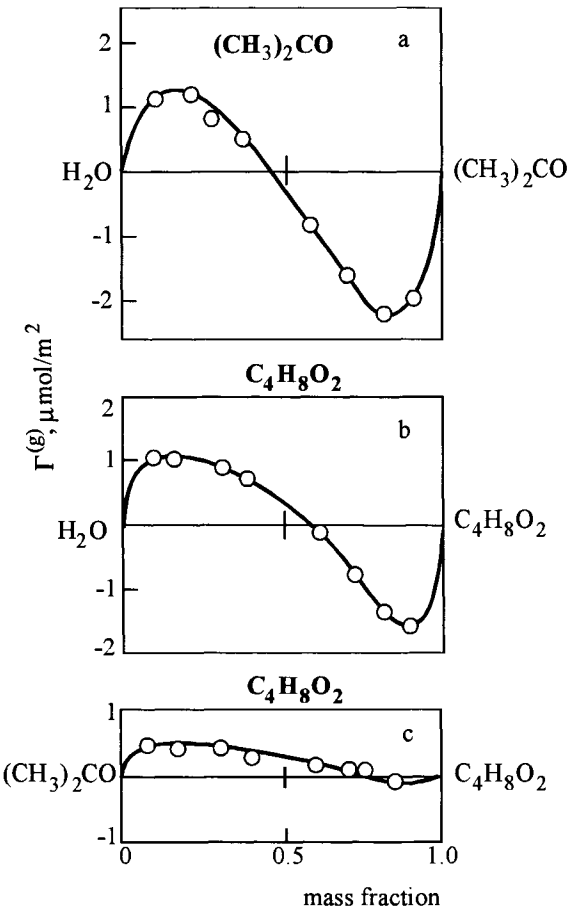

Figure 4. The isotherms of excess adsorption on silica gel of acetone from water (a), dioxane from water (b) and dioxane from acetone (c).

benzene excess adsorption may be both positive and negative depending on the composition of equilibrium solution. The difference in a heats of dioxane and benzene adsorption is determined by strength of hydrogen bonds of these compounds with silanol groups. The energy of dispersion interactions of all these molecules with silica surface are similar because of the heats of components adsorption on dehydroxylated silica surface are similar [9]. Thus the benzene, dioxane and n–hexane adsorption on hydroxylated silica surface from their mixture is determined by hydrogen bonds of the first two components. The other types intermolecular interactions are not so important. The adsorption of benzene becomes negative at about 2% concentration of dioxane in solution. Such effect of strong adsorbing component at small concentration on the adsorption of other compounds is used in liquid chromatography to reduce the retention volumes of separating components.

On adsorption of benzene, n–hexane and carbon tetrachloride from their mixture on hydroxylated silica the excess adsorption of benzene is positive in all concentration region with the accordance of the higher heats of benzene adsorption in compared with the heats of adsorption of other components. The heats of adsorption of n–hexane and carbon tetrachloride on silica are similar and small positive excess adsorption of carbon tetrachloride is determined by difference in molecular area of molecules on the silica surface which is large for n–hexane.

On adsorption of dioxane, acetone and water from their mixtures on hydroxylated silica the positive excess adsorption of dioxane and acetone are only at small concentrations of these compounds (Fig. 3 and 4). At mass fraction more than 0.5 the excess adsorption of dioxane as well as acetone are negative and water asdsorption is positive. Such type of excess isotherm of adsorption of dioxane and acetone from water is realized owing to the strong interactions of these components not only with silanol groups of silica surface but also with water molecules in solution and strong interaction of water with silica surface and interaction of water molecules with each other in a bulk and surface solutions. The shape of adsorption isotherms of these component can not be explained only in term of heats of adsorption on silica as it was possible to do for the system dioxane, benzene, n–hexane and silica. The excess adsorption of dioxane from acetone on silica is determined by differences in energy of hydrogen bonding of dioxane and acetone molecules with silanol groups. Since the heats of dioxane adsorption are a little higher than the heats of acetone adsorption [9], the excess of dioxane adsorption from acetone is small but positive in almost all region of dioxane concentration (up to mass fraction 0.8) (Fig. 4).

On adsorption of components: dioxane, acetone and water from their mixtures there are regions with positive and negative excess adsorption of both dioxane and acetone. The presence of dioxane for example results in the decreasing of acetone adsorption although this decreasing is not too large in compared with the decreasing of benzene adsorption (Fig. 1) owing to small difference in adsorption heats of dioxane and acetone on hydroxylated silica.

In studied systems all cases of mutual component influences on adsorption from multicomponent solutions are presented: the depressing of adsorption of one component by other stronger adsorbed component (sharp decreasing of benzene adsorption at addition of dioxane); the effect of addition of component with similar heat of adsorption on adsorption of other compound (small decreasing of dioxane adsorption from water with the increasing of acetone concentration) and the increasing of adsorption of one component at the addition of other component (the increasing of dioxane adsorption from benzene with the grow of n–hexane concentration).

2.2. Adsorption of non–volatile compounds

Liquid chromatography can be recommended as analytical method to determine the equilibrium concentration on study the adsorption of non–volatile and unstable substances from solutions under static condition [10]. Cymarin (one of cardiac glycosides) adsorption on silanized silica gel from water – ethanol solvent was investigated as the example.

Fig. 5a shows the adsorption isotherm of cymarin from water – ethanol solution determined under static conditions. One can see from this figure that this isotherm is convex towards the n^s axis although the equilibrium concentrations are rather low. Extrapolating the derivative of adsorption by concentration towards zero concentrations, the Henry con-

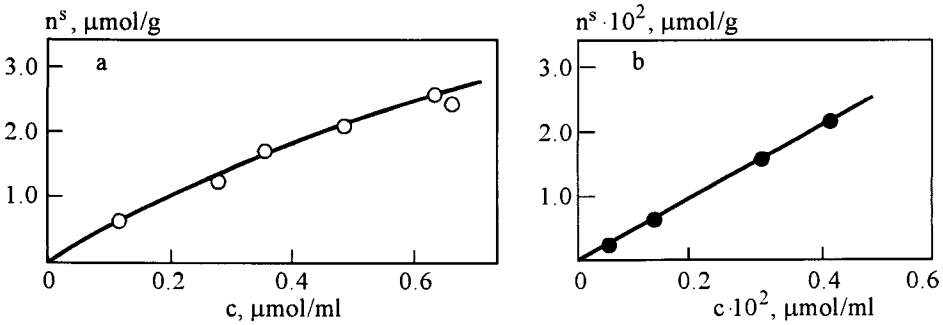

Figure 5. Adsorption isotherm of cymarin from water–ethanol (7:3) solution on LiCrosorb RP–2 at 20°C under static conditions (a) and under dynamic chromatographic conditions (b).

stant was found as $K_{n^s,c,1} = 5.0$ cm^3/g; here the n^s indicates that the adsorption value is in- μmol/g, c indicates that the equilibrium concentrations in μmol/cm^3 and 1 indicates a low (zero) concentration of the adsorbate.

Besides this method of extrapolation towards $c = 0$, $n^s = 0$ of the static isotherm, it is possible to determine the Henry constant directly from the specific retention volume for zero sample size V_m if the elution time of the substance from the column does not depend on the sample size at a constant flow rate. In this case $K_{n^s,c,1} = V_m$.

The possibility of studying the adsorption from solutions directly in the chromatographic columns that means under dynamic conditions using the values of the retention volumes is of great interest. However, it is more difficult to obtain an equilibrium by liquid chromatography because of the diffusion in liquids is much slower. One should take in account that there is no real equilibrium but that the center of mass of the band is considered to be the field of an almost equilibrated distribution. Consequently, in the case of equilibrium chromatography the velocity of transfer of the center of the band through the column is considered to be almost equal to the velocity of transfer of the whole band. Any variation of the equilibrium, the longitudinal diffusion and the heterogeneity in the eluent flow provoke the broadening of the band, but its center of mass moves as if the process in the column would have been equilibrated. If the bands are symmetrical it becomes possible to determine from the retention volumes the Henry constant for adsorption equilibrium from solution.

Fig. 5b shows the initial linear part of the isotherm of cymarin adsorption on silanized silica gel obtained from the chromatographic peaks. In this region of the isotherm the concentrations are 100 times lower than in the region of the isotherm measured under static conditions (Fig. 5a). The slope of the isotherm in Fig. 5b gives a Henry constant equal to 5.05±0.02 cm^3/g what coincides (within the limit of possible errors) with the extrapolated slope of the adsorption isotherm obtained under static conditions (Fig. 5a, $K_{n^s,c,1} = 5.00$ cm^3/g). For the given system (cymarin, water–ethanol eluent, LiChrosorb RP–2), the values of the Henry constants determined when studying the adsorption under both static and chromatographic (dynamic) conditions were almost equal, although the adsorbent particles were rather large (about 30 μm) and the pores were not very wide (about 6 nm). This proves that under the chromatographic conditions used all the surface

of the adsorbent was accessible even to the comparatively large cymarin molecules.

As it seems reversed- phase systems favour the use of the chromatographic method when determining the Henry constants. However, when polar adsorbents and nonpolar eluent are used while study the adsorption, there is always the danger that some moisture penetrates from the eluent on to the adsorbent resulting in a gradual decrease of the retention time of the compounds under investigation.

2.3. Determination of thermodynamic characteristics of adsorption from solutions

The thermodynamic characteristic of adsorption from solutions can be determined from the dependence of adsorption on temperature. But the determination of adsorption isotherms from solution at different temperatures is the rather complicate problems. Liquid chromatography may be very useful method for the determination of thermodynamic characteristics of adsorption at small coverage [11] because of the measurement of retention volume (the Henry constant) at different temperatures of the chromatographic columns makes it possible to calculate the heats of adsorption and the differential standard change entropy of adsorption from:

$$\ln V = -\Delta\overline{H}/RT + \Delta\overline{S}^0/R \qquad (1)$$

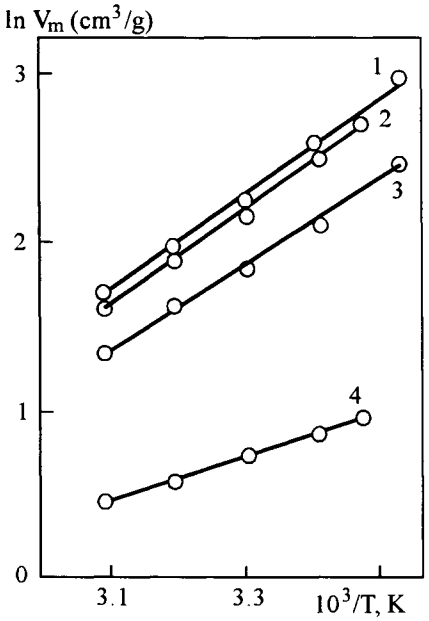

Figure 6. Dependence of the retention volume of K-strophanthin-β on temperature on silica gels modified with the following reagents: diphenyldichlorosilane (1), methyl-β-phenylethyldichlorosilane (2), methylphenyldichlorosilane (3), dimethyldichlorosilane (4). Mobile phase water–ethanol (7:3).

where V is the retention volume (the Henry constant) (V_m,cm^3/g or V_a,cm^3/m^2), $-\Delta\overline{H}$ is the change of adsorption enthalpy (differential heat of adsorption), $\Delta\overline{S}^0$ is the standard changes of differential entropy of adsorption, R and T are the gas constant and temperature respectively.

On Fig. 6 the dependencies of ln V_m on 1/T for the adsorption of K-strophanthin-β (the other cardiac glycoside) on four modified silica gels are presented. From this figure it can be seen that the smallest energy of interactions of the glycoside from water- ethanol solution expressed by $-\Delta\overline{H}$ is observed on the silica gel with bonded methyl groups while the highest interaction energy is observed on silica with bonded phenyl groups. This adsorbent has the largest concentration of carbon atom force centers. It is very easy also to investigate the effect of the eluent composition on adsorption equilibrium constant (the retention volume) by liquid column chromatography [12].

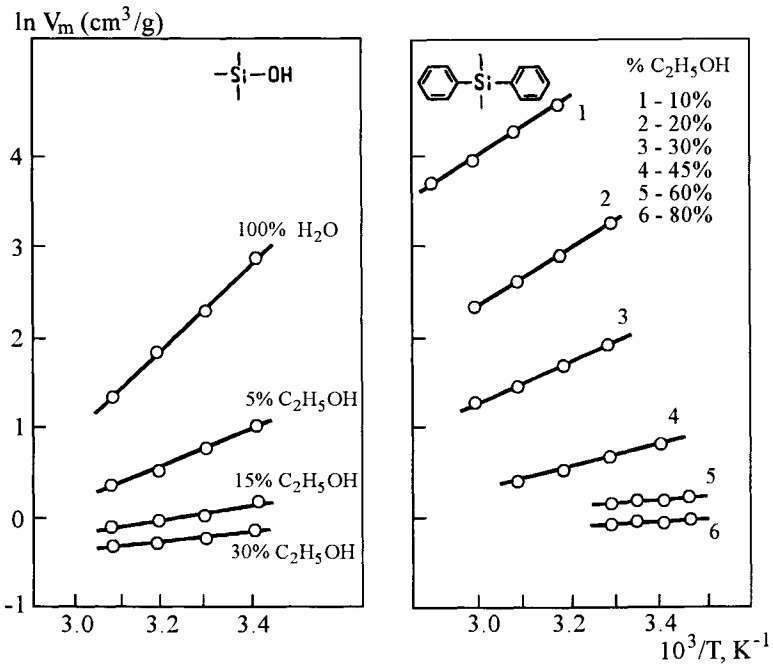

Figure 7. Dependence of the retention volume of cymarin on temperature for eluents with different ethanol concentrations on LiChrosorb SI-100 and on the same adsorbent with bonded diphenylsilyl groups.

Fig. 7 shows the ln V_m vs. 1/T plots for cymarin on silica gels with hydroxylated surface and silica gel with bonded diphenylsilyl groups. On both the hydroxylated silica surface and on the surface with bonded diphenylsilyl groups V_m of cymarin sharply decreases with the increase of the ethanol concentration in the eluent as usual in reversed-phase liquid chromatography. With the increase of the ethanol concentration in the eluent the

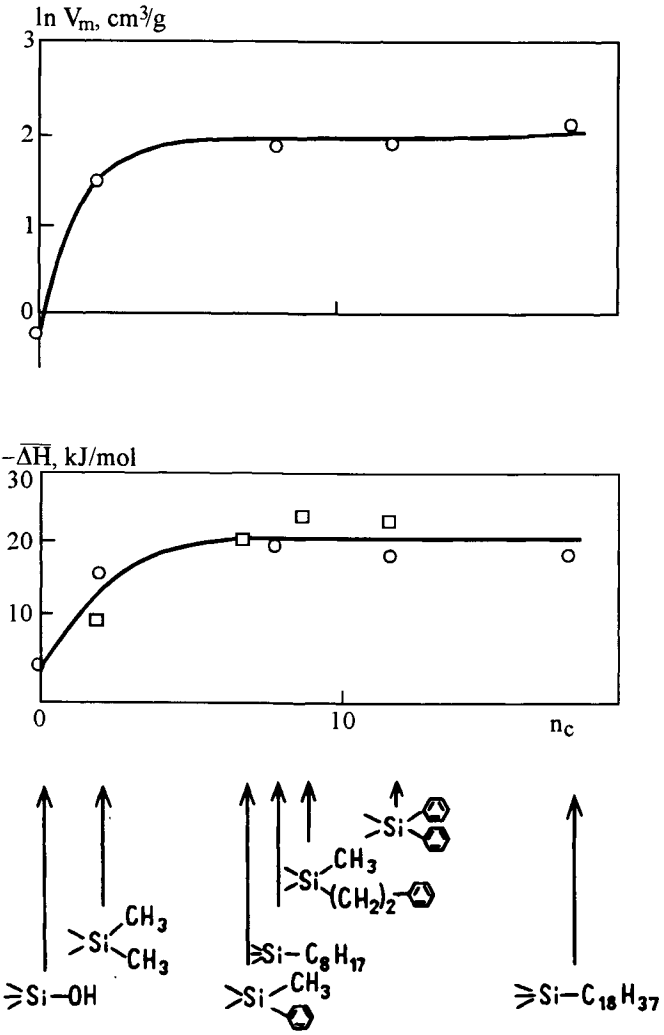

Figure 8. Dependence of ln V_m and $-\Delta\overline{H}$ values on the number of carbon atoms of the modifying group bonded to the silica gel surface for cymarin from water–ethanol (7:3) eluent.

differential enthalpy of adsorption from a water–ethanol mixture used as the eluent decreases but in a different manner on the two surfaces. By increasing the ethanol content up to 20%, the value of $-\Delta\overline{H}$ changes slowly on modified silica and very sharply on the silica gel with a hydroxylated surface [12].

By V_m values of cymarin on silica gels with bonded different groups at constant eluent composition, it is possible to evaluate qualitatively the influence of the intermolecular

interactions between cymarin and these functional groups.

Fig. 8 shows that the retention volume of cymarin increases rapidly with the chain length up to about C_8 and then varies relatively slowly when the chain length increases from C_8 to C_{18}. The $-\Delta\overline{H}$ values also increase with the increase in the carbon number of the bonded groups up to C_7 - C_8 and then remains practically constant. As can be seen from Fig. 8 the same relationship is observed for silica with phenylsilyl groups [12].

Thus liquid chromatography makes it possible to determine the equilibrium constant at small coverage (the retention volume or Henry constant) and to characterize the compounds adsorption from multicomponent solutions. From the dependence of retention volumes on temperature the changes of enthalpy and entropy of adsorption can be calculated.

On study of different structure compounds adsorption on adsorbents with different surface chemistry the thermodynamic characteristics of adsorption may be used to find the correlation between the structure of adsorbed molecules and these thermodynamic characteristics and to understand the role of different functional groups bonded to the surface.

2.4. Adsorption of compounds from water solution on hydroxylated silica

The study of compounds adsorption from water solutions on silica is very important because this process can be used for the purification of water from pollutants. The mechanism of different substances adsorption may be determined from the retention volumes in liquid chromatography [12]. The free hydroxyl groups are the most active among the hydroxyl groups on the silica surface capable of forming hydrogen bonds with the molecules in solution [13]. The mean surface concentration of these groups is about 2.6 OH/nm^2 [14]. For this reason those parts of the silica surface which do not participate in the formation of hydrogen bonds with the dissolved molecules, occupy a rather significant portion of

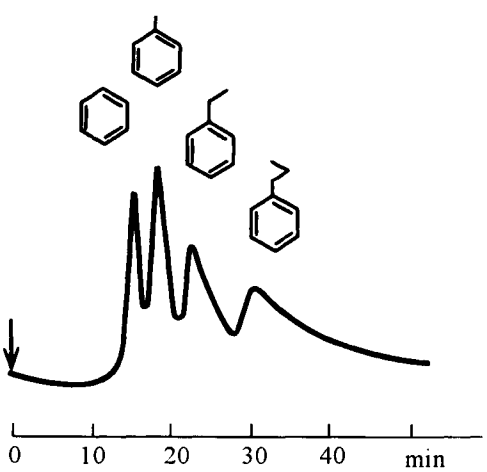

Figure 9. Separation of benzene, toluene, ethylbenzene and propylbenzene on silica gel LiChrosorb SI-100 from water at 20°C.

the total surface. In addition dispersion in interactions of any molecules are also occurring with the silica framework. Due to this, even hydrocarbons positively adsorb from water on the silica surface and the hydrocarbon mixture can be separated on a column packed by silica gel from water (Fig. 9).

With the increase of the alkyl chain length of some mono-n-alkyl benzene derivatives, the retention time increases as in the case of reversed-phase liquid chromatography.

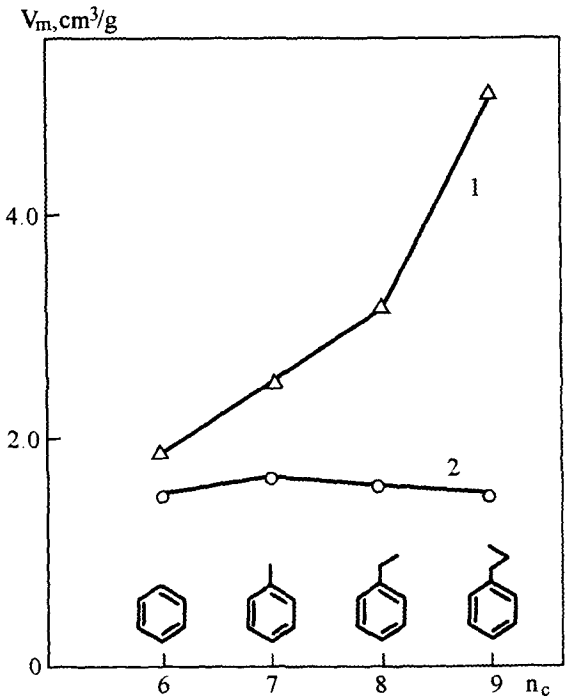

Figure 10. Dependence of retention volume of benzene and some of its derivatives on the number carbon atoms on silica gel from water (1) and from n-hexane (2).

Fig. 10 shows the dependence of V_m for benzene and its derivatives on the number of carbon atoms in their molecules for silica gel with hydroxylated surface when using water and n-hexane as the eluent. With hexane the retention volume rises starting at benzene up to toluene and then decreases with the increase of the alkyl chain due to the stronger interaction of the chain with a chemically similar eluent such as n-hexane. In the case of water as an eluent, benzene and its derivatives are retained stronger than from hexane, although the surface with silanol groups strongly adsorb water. The strong adsorption of hydrocarbons on the hydroxylated silica surface from aqueous solutions can be explained on the basis of the strong dispersion interactions with silica and the weak interactions with water.

The investigation of the dependence of the retention volume of benzene and its mono-n-alkyl derivatives on the temperature permits to evaluate some other thermodynamic characteristics of adsorption. Fig. 11 illustrates the relationships between ln V_m and 1/T for

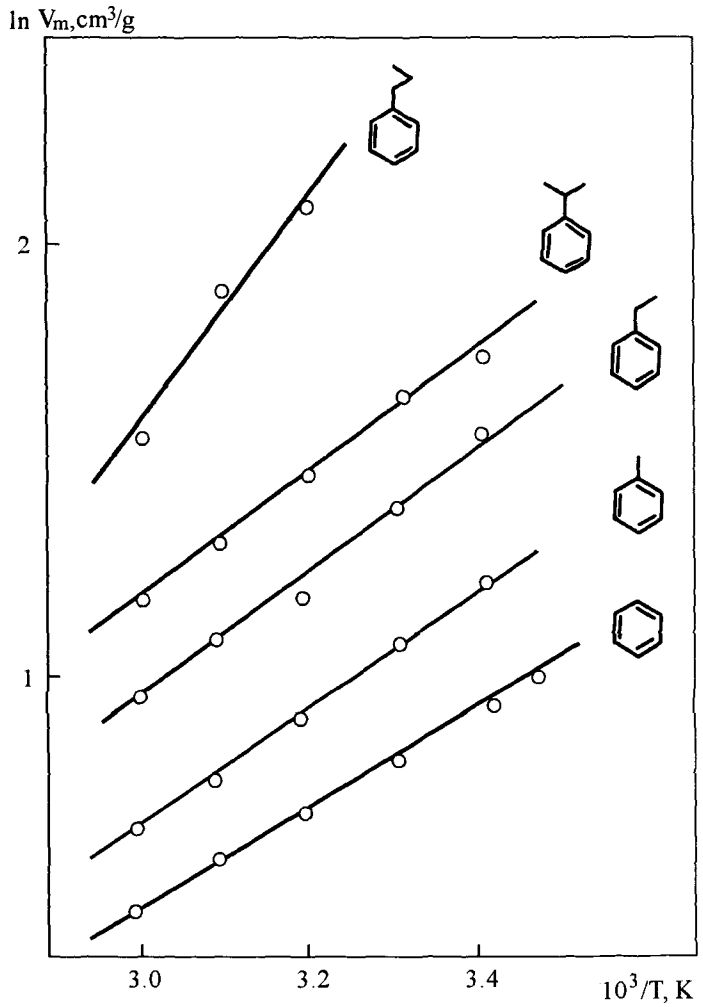

Figure 11. Dependence of ln V_m values for benzene and some of its alkyl derivatives on reciprocal temperature. Adsorbent–silica gel, eluent–water.

benzene, toluene, ethylbenzene, cumene and propylbenzene on the hydroxylated surface of silica gel from aqueous solution.

With the increase in the alkyl chain, the slope of the plots, i.e. the change in the differential adsorption enthalpy ($-\Delta\overline{H}$) increases. Fig. 11 also shows that branching of an alkyl chain with a given number of carbon atoms leads to a weakening in the retention and to a decrease in $-\Delta\overline{H}$.

In adsorption from solutions the contributions of the intermolecular interactions be-

tween the solute and the adsorbent and between the solute and the solvent (eluent) are important. Although the differential heat of adsorption of water vapour on silica gel with a hydroxylated surface is higher than for benzene, the weak intermolecular interaction of the hydrocarbons with water and their dispersion interaction with the silica framework forces their molecules to be ejected from the bulk aqueous solution to the hydroxylated silica gel surface. In this way the weak dispersion intermolecular interaction between the hydrocarbon and water and the dispersion but stronger interaction between the hydrocarbon and the silica determine the adsorption of hydrocarbons from aqueous solutions.

In order to explain the role of the hydrogen bonds which could be formed between the solute molecules dissolved in water and the silanol groups of the silica surface the retention volumes of a series of polar compounds such as pyridine, cyclohexanone, acetone, diethyl ether, ethyl acetate, dioxane and some polar benzene derivatives were determined [12]. For these compounds the hydrogen bonds with surface silanol groups at the adsorption from gas phase had already been investigated by spectral and calorimetric methods during gas-phase adsorption [9]. The greatest values of V_m and $-\Delta\overline{H}$ are observed for pyridine and the smallest for dioxane. In this series the strong base has the highest values of V_m and $-\Delta\overline{H}$ when the interaction with the surface silanol groups predominates.

2.5. Evaluation of molecular groups contributions to the adsorption equilibrium constant

The main problem in adsorption from solutions is to predict the isotherm of adsorption as well as in liquid chromatography the retention of compounds on the basis of molecular structure of solutes and surface chemistry of adsorbent. Unfortunately the geometry of adsorbent surface is unknown as well as the structure of the solution near the adsorbent surface. Owing to this the calculation of adsorption equilibrium constant for the adsorbents used for adsorption and liquid chromatography is very complicate and in many cases is practically impossible.

However the most general method of estimation of the retention volumes (the Henry adsorption constant or the equilibrium adsorption constant at small coverage) is based on linear free energy relationships [15–21]. Each molecular group or fragment can be assumed to make its own contribution to the retention of a molecule. The assumption that each group is independently adsorbed, i.e., additivity of interaction with the surface is fulfilled. This is a rough approximation because in large molecules such groups can be located at different distances from the surface and therefore the energy of their interaction with the surface will differ. During the adsorption from solutions when the interaction of an adsorbed molecules with the eluent is of great importance, the difference in adsorption energy of similar groups becomes smaller, although for some groups the energy of interaction is different from the average energy of interaction of similar groups with the adsorbent. If it is shown experimentally that one group differs greatly from other similar groups then it should be considered as a separate group with its own contribution to retention.
According to such assumption

$$\ln V_m = \sum a_i \cdot n_i \tag{2}$$

where V_m is the retention volume of compound, calculated from the column retention volume V'_R ($V_m = V'_R/m$), a_i is the logarithm of retention volume of i-th group

($a_i = \ln V_{mi}$), n_i is the number of functional groups of a one type in a molecule, m is the mass of adsorbent in a column. If the specific surface area of adsorbent, s, is known so V_a value can be calculated ($V_a = V_m/s$). The retention volumes V_m and V_a are equal to the Henry constant of adsorption equilibrium, K_1, corresponding to the initial linear part of the adsorption isotherm expressed in adsorption per g or m^2. However in a many cases both the mass of adsorbent in a column and the specific surface area of adsorbent are unknown. The capacity factor k′ (dimensionless value) which is proportional to the constant of adsorption equilibrium is usually used for the characterization of retention of compounds. In such cases

$$\ln k' = \sum a_i \cdot n_i \tag{3}$$

where a_i is the logarithm of capacity factor of the i-th group ($a_i = \ln k_i'$) at the phase ratio the stationary to the mobile phases equal to 1, and n_i is the number of the i-th groups in a molecule. It is probably possible to use this approach because in many cases for HPLC systems the phase ratio does not differ too much from 1.

The R_F values from thin layer chromatography also can be used for the calculation of the contributions of molecular groups to the retention of molecules. From the experimental R_F value the capacity factor k′ can be calculated [22] by the equation:

$$\ln k' = \ln(1 - R_F)/R_F = R_M \tag{4}$$

where k′ is the capacity factor, R_F is the retardation factor and R_M is the logarithm of capacity factor k′. In accordance with the equation (3)

$$R_M = \ln k' = \sum \Delta R_{Mi} \cdot n_i \tag{5}$$

where ΔR_{Mi} is the contribution of the i-group to the retention (to the ln k′) and n_i is the number of i-groups or fragments in a molecule.

To calculate the contributions of all molecular groups to retention (adsorption equilibrium constant) a_i, ΔR_{Mi} under some standard conditions, it is necessary to determine the retention volumes V_M (V_a) or capacity factor k′ or R_M values from R_F data for a number of compounds possessing different amounts of such groups and to solve the systems of linear equations (2 or 3 or 5) by the least -squares method.

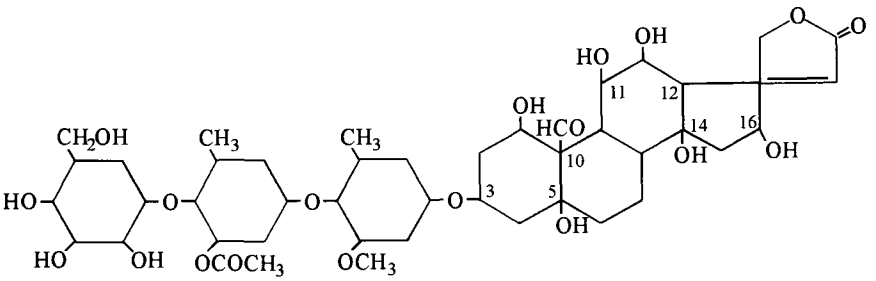

Figure 12. Formula of cardiac glycoside and its possible functional groups.

The molecules of cardiac glycosides and also steroid hormones can be assumed to consist of -OH (C_{12}), -OH (C_{16}), -OH, -O-, >C=O, -HC=O, $-CH_n$ (n = 0 - 3) groups (see formula of cardiac glycoside) [18,19].

From the experimental data on retention of cardiac glycosides [18,19] the contributions of these groups to the retention have been calculated the values of which are presented in Table 1.

Table 1
Value of $a_i = \ln V_{ai}$ for various functional groups of cardiac glycosides and steroid hormones. Adsorbent–silica with bonded diphenylsilyl groups; eluent – water-ethanol (65 : 35); temperature 50°C

Functional group	–OH (C_{12})	–OH (C_{16})	–OH	–O–	>C=O	–HC=O	$-CH_n$
a_i	–1.4603	– 0.8188	– 0.6055	– 0.2315	– 0.1598	– 0.7854	0.2444

As shown in Table 1 the retention of steroids is decreased by all hydrophilic groups to a certain extent whereas $-CH_n$ groups increases the retention. The contributions of hydroxyl groups at C_{12} and at C_{16} to retention of steroids are quite different from the contribution of other hydroxyl groups of glycone and aglycone.

Correlation of experimental ln V_a values with those calculated by the additive scheme ($\sum a_i n_i$) is shown in Fig. 13. The experimental and calculated values are shown to correlate well ($r = 0.964$) for such different and complicate molecules.

The molecules of cardiac glycosides can be presented by other number of different functional groups [20]. These molecules consist of a steroid part, the aglycone, and of the glycone, which is a mono–, di–, tri– or tetrasaccharide. Assuming that the >C<, >C=, >CH–, $-CH_2-$, $-CH_3$ and =CH– groups have similar contributions to retention [19], the cardiac glycoside molecules can be presented by the following functional groups: $-CH_n$ ($n = 0 - 3$), –O–, –HC=O, –COO– and –OH. However, not all hydroxyl groups are known to be equivalent. In a glycone the hydroxyl groups can form, due to their close arrangement, intramolecular hydrogen bonds, although a weak one, while in an aglycone the hydroxyl groups are isolated and their contribution to the interaction with the eluent molecules will be different. In addition it has also been observed that in position C_{12} the effect of the hydroxyl group on retention is more significant than, for example, in position C_{16} (see Table 1). Thus, the hydroxyl groups can be classified as glycone hydroxyl groups ($-OH_G$), and aglycone hydroxyl groups ($-OH_A$), and among the latter the hydroxyl groups –OH (C_{12}) and –OH (C_{16}) should be considered separately. In [20] considering steroid hormones, together with the cardiac glycosides, a few additional functional groups should also be specified such as >C=O, $-C\equiv C-$ and $-OH_{AR}$ the latter referring to an estrogen hydroxyl group in position C_3.

Obviously for steroids a greater number of functional groups present in different positions could be distinguished. However, excessive experimental data would be required such a case and, still, it would be impossible to determine the exact contribution of each group, due to the difference of these groups with regard to the adsorbent surface and interaction with the eluent molecules. Therefore it is necessary to select a minimum number of functional groups, which should, however, be sufficient to properly describe the experimental data.

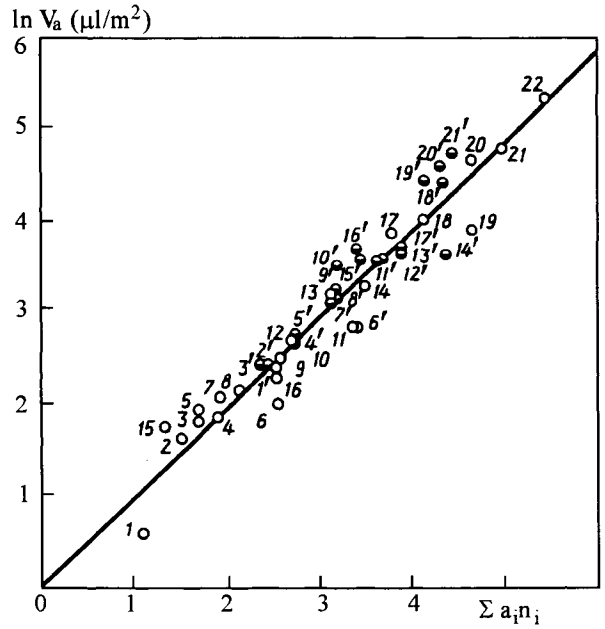

Figure 13. Correlation between the experimental values (ln V_a) of cardiac glycosides (open dots) and steroid hormones (semi-closed dots) and the calculated values ($\sum a_i n_i$) according Table 1. The numbers correspond to the compounds for cardiac glycosides: 1 = G-strophanthin, 2 = K-strophanthoside, 3 = corelborine-π, 4 = eryzimoside, 5 = convallatoxin, 6 = olitoriside, 7 = K-strophanthin-β, 8 = desglucocheirotoxin, 9 = strophanthidin, 10 = glucogitoroside, 11 = eryzimin, 12 = strophanthidin acetate, 13 = desacetyl lanatoside C, 14 = cymarin, 15 = lanatoside C, 16 = digoxin, 17 = lanatoside B, 18 = oleandrin, 19 = gitoxin, 20 = lanatoside A, 21 = digitoxin, 22 = acetyl digitoxin, and for steroid hormones: 1′ = prednisolone, 2′ = hydrocortisone, 3′ = estriol, 4′ = prednisone, 5′ = cortisone, 6′ = adrenosterone, 7′ = corticosterone, 8′ = prednisone acetate, 9′ = cortison acetate, 10′ = estradiol, 11′ = testosteron, 12′ = ethynylestradiol, 13′ = methanedrosteonolone, 14′ = pregnine, 15′ = methylestradiol, 16′ = estrone, 17′ = methyltestosterone, 18′ = progesterone, 19′ = desoxycorticosterone acetate, 20′ = mestranol, 21′ = megestrol acetate.

Using the equation (3) the contributions of individual groups to retention $A_I = \ln k'_i$ can be calculated from the experimental k′ values for some steroids. The calculated a_i values are presented in Table 2.

The data of Table 2 show that in the case of chromatography on hydrophobic adsorbent surface, using aqueous ethanol as the eluent, only $-CH_n$ and $-C{\equiv}C-$ groups increase the value ln k′ and accordingly, the retention of steroid molecules. All the hydrophilic groups reduce the ln k′ value and the retention. It is also clear from Table 2 that different type hydroxyl groups are not equivalent.

From data of Table 2 and structural formula of steroid molecules can be calculated the ln k′ by equation (3) and then k′ of steroids. The comparison of the experimental ln k′ values and calculated ones are presented on Fig. 14.

Table 2
Values of $a_i = \ln k'_i$ for various functional groups, on silica with the bonded octadecylsilyl groups at 50°C, using ethanol–water (35:65) eluent

Functional groups	$-CH_n$	$-O-$	$>C=O$	$-HC=O$	$-COO-$	$-OH_G$
a_i	0.198	− 0.269	− 0.031	− 1.718	− 0.136	− 0.432
Functional groups	$-OH_A$	$-OH_{AR}$	$-OH(C_{12})$	$-OH(C_{16})$	$-C\equiv C-$	
a_i	− 0.700	− 0.226	− 2.283	− 0.896	0.084	

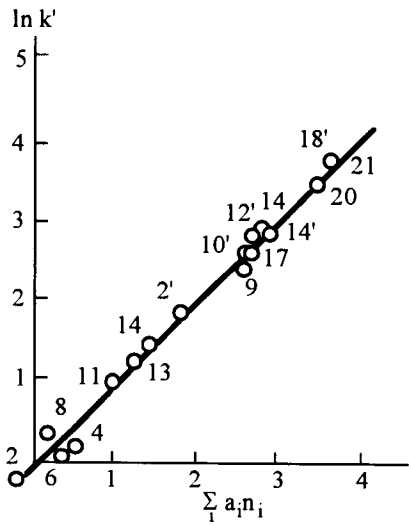

Figure 14. Correlation between the experimental and calculated values of ln k′ of cardiac glycosides and steroid hormones, at 50°C on silica gel with bonded octadecylsilyl groups from eluent: ethanol–water (35:65). The numbers correspond the compounds on Fig. 13.

From k′ values of steroids determined at different temperatures from eluent of various compositions the differential enthalpy of adsorption from solution ($-\Delta\overline{H}$) at small coverage for some eluent composition can be calculated from:

$$\ln k' = -\Delta\overline{H}/RT + \Delta\overline{S}^0/R + \ln\varphi \qquad (6)$$

where k′ is capacity factor of compound and φ is phase ratio. The values of $a_i = \ln k'_i$ can be calculated for the same eluent compositions and temperatures by equation (3). Then the contributions of individual groups of molecules to the differential enthalpy of adsorption ($-\Delta\overline{H}_i$) can be calculated by equation (7):

$$\ln k'_i = -\Delta\overline{H}_i/RT + \Delta\overline{S}^0/R + c \qquad (7)$$

where k_i' is the contribution of individual group of molecule to the capacity factor and $-\Delta\overline{H}_i$ is the contribution of individual groups to the differential enthalpy of adsorption and c is constant.

Table 3
Changes in the differential enthalpy of adsorption ($-\Delta\overline{H}$) of some cardiac glycosides and steroid hormones from aqueous ethanol used as the eluent, on silica gel with bonded octadecylsilyl groups

Substance	$-\Delta\overline{H}$, kJ / mol ethanol concentration in the eluent		
	30%	35%	45%
Cardiac glycosides:			
K-strophanthoside		11.3	5.9
K-strophaanthin-b	15.2	11.6	7.1
Convallatoxin	16.0	11.9	3.9
Strophanthidin		12.4	4.1
Cymarin	17.4	13.1	4.2
Lanatoside C	24.3	18.6	7.1
Digoxin	23.6	18.0	5.8
Lanatoside B	37.3	30.7	17.6
Gitixin		29.1	17.6
Lanatoside A	45.1	33.0	19.2
Digitoxin	40.2	32.5	18.6
Steroid hormones			
Hydrocortisone	26.3	23.0	12.0
19-nor-testosterone	28.8	25.1	14.4
Estradiol	32.9	31.1	19.5
Ethynylestradiol	35.7	31.6	18.5
Pregnine	31.6	26.8	14.5
Progesteron	36.3	32.5	20.6

On Table 3 the enthalpy of adsorption of some steroid compounds are presented for different eluent compositions and on Table 4 the contributions of individual groups to the enthalpy of adsorption from solution for the same eluent composition is presented [20].

It is clear from Table 3 that the increasing of ethanol concentration in the eluent result in the decreasing the enthalpy of adsorption of steroids from solutions.

While for hydrophobic groups the heats of adsorption are positive, for most of hydrophilic groups the heats of adsorption are negative and serves to measure the heat of desorption from the surface under a given eluent composition. With the increasing of ethanol concentration in eluent the heats of adsorption of hydrophobic groups decrease as well as for hydrophilic groups the heats of desorption. These results is particularly attractive because it is impossible to experimentally measure these values in adsorption from solutions.

Table 4
The contributions of steroids functional groups to the differential entropy of adsorption from ethanol–water eluents ($-\Delta\overline{H}$ i) on silica with bonded octadecylsilyl groups

Functional gruop	$-\Delta\overline{H}_i$, kJ / mol ethanol concentration in the eluent		
	30%	35%	45%
$-CH_n$	2.0	1.6	0.9
-O-	- 2.7	- 3.8	- 1.7
>C=O	0.8	0.9	1.4
-HC=O	- 13.2	- 11.2	- 5.8
-COO-	- 4.8	- 0.6	- 1.3
$-OH_G$	- 2.0	- 1.3	- 0.6
$-OH_A$	- 7.4	- 3.5	- 3.1
$-OH_{AR}$	4.2	5.8	7.6
-OH (C_{12})	- 18.7	- 14.4	- 12.4
-OH (C_{16})	- 6.8	- 2.9	- 1.3
-C≡C-	2.7	0.5	0.06

The data of Table 1 - 4 make it possible to understand the mechanism of adsorption of steroid compounds on hydrophobic surface of adsorbents from water- ethanol solutions and the role in adsorption of different functional groups of these substances.

The other mechanism of cardiac glycosides adsorption is realized on adsorption on hydroxylated silica gel. From R_F values [23] the $\ln k' = R_M$ of cardiac glycosides were calculated by the equation (5). From these data it was possible to evaluate the contribution of more polar groups to the retention because in Ref.[23] the cardiac glycosides with more different aglycones were used for thin layer separations. It was possible to consider as separate not only -OH (C_{12}) and -OH (C_{16}) but also -OH (C_{14}), -OH (C_5), -OH (C_3), -OH (C_{11}) and -OH (C_{10}). The hydroxyl groups at C_{14} and C_1 was considered as identical. Thus the cardiac glycoside molecules can be presented by the following functional groups: $-CH_n$ (n = 0, 1, 2, 3), -O-, -HC=O, -COO-, $-OH_G$, -OH (C_{12}), -OH (C_{16}), -OH (C_{14} and C_1), -OH (C_5), -OH (C_3), -OH (C_{11}) and -OH (C_{10}) (see formula of cardiac glycoside, Fig. 12).

The contributions of these groups to the retention ($\ln k'_i = \Delta R_{Mi}$) determined by solving of system of linear equations (5) are presented on Table 5.

It is clear from Table 5 that in reversed phase chromatography $-CH_n$ groups increase the retention ($\ln k'_i > 0$) and all hydrophilic groups decrease it ($\ln k'_i < 0$), but in normal phase chromatography the $-CH_n$ groups decrease the retention cardiac glycosides and hydrophilic groups increase the retention owing to the hydrogen bonds these groups with silanol groups on surface of silica gel. The mechanism of adsorption of cardiac glycosides is different in these cases.

The contributions of hydroxyl groups to the retention are quite different because of different geometric arrangement in a molecule and owing to this the forming of hydrogen bonds of different energy. The most strong interactions of hydroxyl groups of glycone

Table 5
The contributions of functional groups or fragments of cardiac glicosides to retention (ΔR_{Mi}) on silica gel from benzene–ethanol (3 : 1) mobile phase at room temperature and ln k'_i on silica with bonded diphenylsilyl groups from water–ethanol (65 : 35) at 50°C [24]

Functional gruop	ΔR_{Mi}	ln k'_i
$-CH_n$	– 0.096	0.193
–O–	0.052	– 0.136
-HC=O	0.115	– 0.659
–COO–	0.218	– 0.278
$-OH_G$	0.593	– 0.491
–OH (C_{12})	0.309	– 1.533
–OH (C_{16})	0.285	– 0.809
–OH (C_{14} and C_1)	0.762	
– OH (C_5)	0.600	
–OH (C_3)	0.612	– 0.720
–OH (C_{11})	0.343	
–OH (C_{10})	0.403	

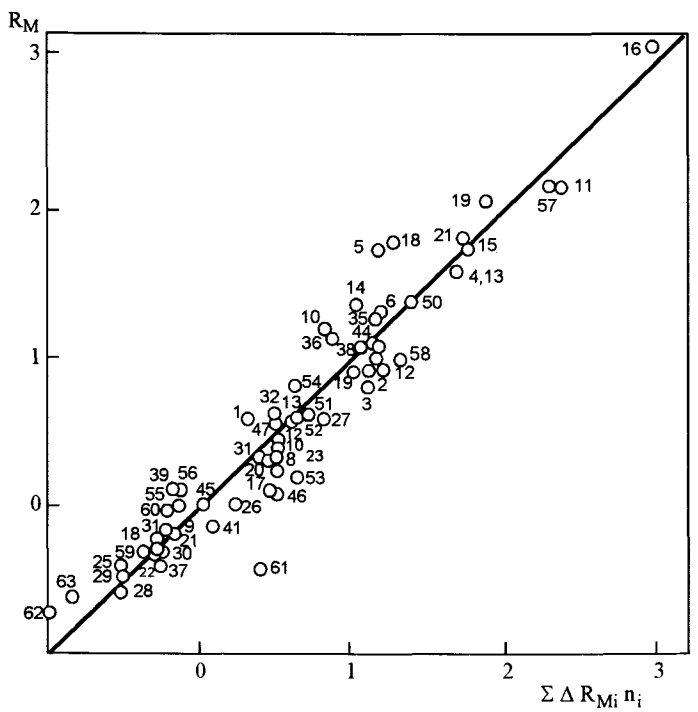

Figure 15. Correlation between the experimental and calculated values of R_M of cardiac glycosides on silica gel from benzene–ethanol (3 : 1) mobile phase. The names of 63 cardiac glycosides can be find in Ref.[23].

and of hydroxyl groups of aglycone in position of C_{14}, C_1, C_3 and C_5 is observed. The contributions of other polar groups to the adsorption of glycosides on silica are relatively small. The R_M values of cardiac glycosides calculated by using of ΔR_{Mi} from Table 5 and formula of glycosides are compared with the experimental values of R_M on Fig. 15. According to Fig. 15 generally there is a rather good agreement between these value if to take into consideration not very precise R_F values in thin layer chromatography.

The adsorption from solutions of polycyclic aromatic hydrocarbons, alkylbenzenes and benzene derivatives is of great interest from many points of view. To understand the mechanism of their adsorption and to predict the equilibrium adsorption constant also it is possible to use the contributions of functional groups of fragments of molecules to retention in reversed-phase and normal-phase liquid chromatography [21]. The contributions of different molecular groups as well as the dependence of these contributions on mobile phase composition have been evaluated from experimental data in work [25].

It is possible to propose that polycyclic aromatic hydrocarbons and some of their derivatives can be presented by $-HC=$, $>C=$, $-CH_2-$ and $-CH_3$ groups only (Fig. 16 a).

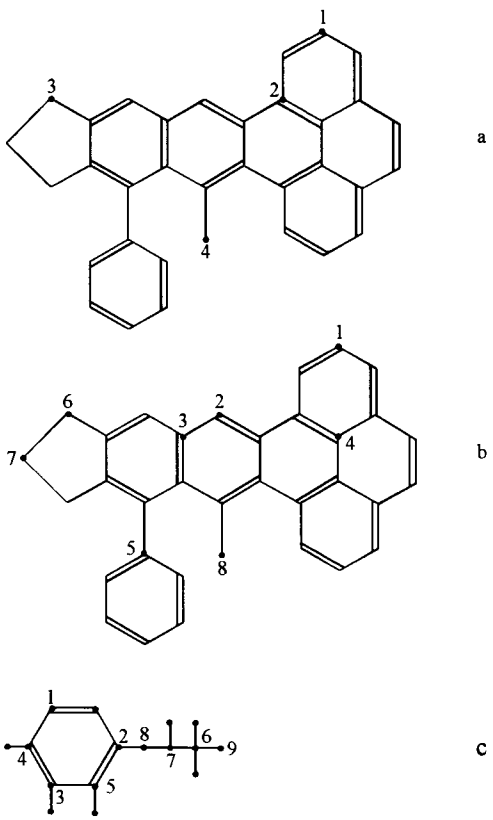

Figure 16. Molecular groups of hydrocarbons to be considered as different; (a and b) polycyclic aromatic hydrocarbons, (c) alkylbenzenes.

Table 6
The a_i values for various functional groups of polycyclic aromatic hydrocarbons. Adsorbent: μ-Bondapak C_{18}, methanol-water (65 : 35) eluent, ambient temperature

Functional group	(1) -HC=	(2) >C=	(3) $-CH_2-$	(4) $-CH_3$
a_i	0.124	0.224	0.238	0.306

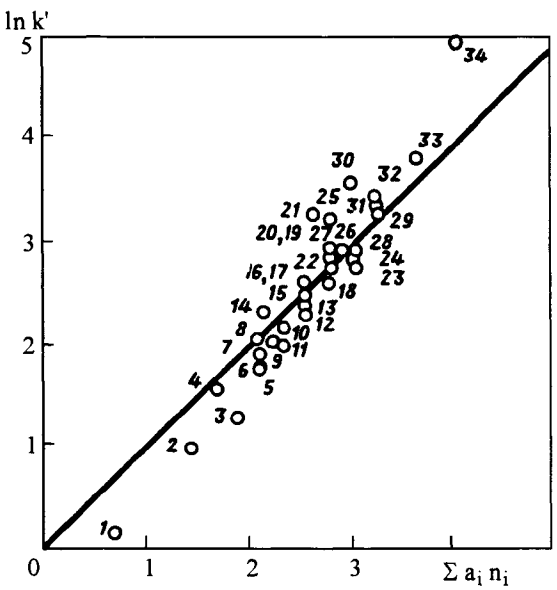

Figure 17. Correlation between the experimental ln k' and calculated $\sum a_i n_i$ according to the data of Table 6.
1= benzene, 2= naphthalene, 3= acenaphthylene, 4= biphenyl, 5= acenaphthene, 6= fluorene, 7= phenanthrene, 8= anthracene, 9= 2,3,-dimethylnaphthalene, 10= 9,10-dihydrophenanthrene, 11= 9,10,-dihydroanthracene, 12= fluoranthene, 13= pyrene, 14= bibenzyl, 15= 9-methylanthracene, 16= 2-methylphenanthrene, 17= 2-methylanthracene, 18= 1,2-dihydropyrene, 19= 1,2,-benzofluorene, 20= 2,3-benzofluorene, 21= p-terphenyl, 22= triphenylene, 23= 1,2,6,7,-tetrahydropyrene, 24= 1,2,3,4,-tetrahydrofluoranthene, 25= tetracene, 26= 9,10-dimethylanthracene, 27= chrysene, 28= 5,12-dihydrotetracene, 29= 1,2,3,6,7,8-hexahydropyrene, 30= 1,2,3,4,5,6,7,8- octahydroanthracene, 31= perylene, 32= 3,4-benzofluoranthene, 33= 7,12-dimethylbenz (α)-anthracene, 34= 9,10- diphenylanthracene.

The contributions of these groups to retention on adsorbent μ-Bondapak C_{18} from methanol-water (65:35) eluent at ambient temperature were calculated from the retention data of 34 polycyclic aromatic hydrocarbons [25]. It should be noted that, according to such proposition, the isomer molecules such as phenanthrene and anthracene as well as tetracene and chrysene respectively are to be considered as similar although the experimental values of their capacity factors are different.
In Table 6 the a_i values for some groups of polycyclic aromatic hydrocarbons are presented.

Table 7
The calculated a_i values for various functional groups of polycyclic aromatic hydrocarbons for the condition as in Table 6

Functional group	(1) –HC=	(2) –HC=	(3) >C=	(4) >C=
a_i	0.035	0.112	0.393	0.217
Functional group	(5) >C=	(6) $-CH_2-$	(7) $-CH_2-$	(8) $-CH_2-$
a_i	0.714	0.131	0.319	0.157

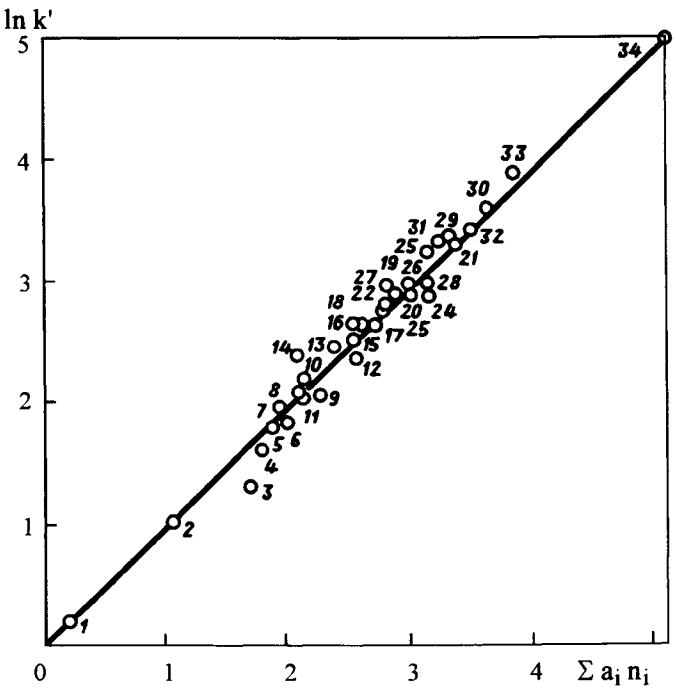

Figure 18. Correlation between the experimental ln k′ and calculated $\sum a_i n_i$ by using data of Table 7. The numbers correspond to the compounds on Fig. 17.

The comparison of the experimental and calculated from the data of Table 6 and formula of compounds the ln k′ is presented on Fig. 17. The correlation between these values is not quite good. The largest difference is observed for the smallest flat molecules such as benzene, naphtalene, acenaphthylene and for non–planar molecules such as p–terphenyl, 1,2,3,4,5,6,7,8–octahydroanthracene and 9,10–diphenylanthracene. The calculated ln k′ of phenanthrene and anthracene, tetracene and chrysene are the same respectively.

To take into account the differences in the retention of isomer polycyclic hydrocarbons and also non-planar arrangement of some groups of partly hydrogenated and phenylderivatives of polyaromatic molecules, the more number of groups should be considered as different (Fig. 16 b).

In Table 7 the calculated a_i values for various groups are presented.

On Fig. 18 the comparison of the experimental ln k′ and calculated S a_i n i values by the data of Table 7 are presented.

The correlation between the experimental and calculated ln k′ values is better for such approach by means of which the differences in the retention of the isomer polycyclic aromatic hydrocarbons molecules such as phenanthrene, anthracene and tetracene, chrysene respectively can be calculated. Since the a_i values of polycyclic aromatic hydrocarbons are positive in reversed-phase chromatography (Table 6 and 7), so for compounds with the larger number of groups the retention volume (equilibrium adsorption constant) will be

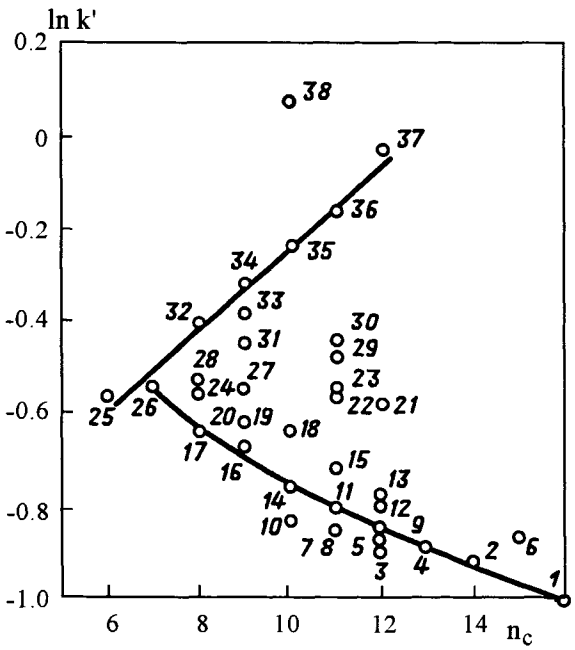

Figure 19. Dependence of ln k′ on the number of carbon atoms of alkylbenzenes according to the data of [26].

1= n-decylbenzene, 2= n-octylbenzene, 3= m-diisopropylbenzene, 4= n-heptylbenzene, 5= n-hexylbenzene, 6= 1-propyl-2,4,6.-triethylbenzene, 7= neopentylbenzene, 8= isopentylbenzene, 9= 1,3,5,-triethylbenzene, 10= isobutylbenzene, 11= n-amylbenzene, 12= p-diisopropylbenzene, 13= 1-ethyl-4-tert.-butylbenzene, 14= n-butylbenzene, 15= p-tert.-butyltoluene, 16= p-propylbenzene, 17= ethylbenzene, 18=tert.-butylbenzene, 19= m-ethyltoluene, 20= cumene, 21= 1-propyl-2,4,6,- trimethylbenzene, 22= cyclopentylbenzene, 23= 1-ethyl-4-isopropylbenzene, 24= m-xylene, 25= benzene, 26= toluene, 27= 1,3,5,-trimethylbenzene, 28= p-xylene, 29= 2-methyl-3-phenylbutane, 30= 1-ethyul-2,4,6,- trimethylbenzene, 31= o-ethyltoluene, 32= o-xylene, 33= 1,2,4-trimethylbenzene, 34= 1,2,3-trimethylbenzene, 35= 1,2,3,4-tetramethylbenzene, 36= pentamethylbenzene, 37= hexamethylbenzene, 38= naphthalene.

larger too, depending on the a_i values of cause. In this case the adsorption of such compounds is determined by mainly by dispersion interaction of each group with hydrophobic surface of adsorbent and by strong hydrogen bonds of eluent molecules.

In a case of adsorption of alkylbenzenes on hydroxylated silica gel from hydrocarbons the most important are hydrogen bond of aromatic ring with silanol groups of adsorbent surface and dispersion interaction of alkylbenzene molecules with hydrocarbon eluent molecules.

The correlation between the retention and number of carbon atoms in a molecules can not be found. On Fig. 19 the dependence of the alkylbenzenes retention on hydroxylated silica from n-pentane on the number of carbon atoms of these molecules is presented from data of [26].

It is possible to determine only qualitative regularity from such dependence for polymethylbenzenes and mono n-alkylbenzenes.

In [26] the difference in the retention of alkylbenzene derivatives having the same groups in various position (o-, m-, p-) was observed . So to take this experimental fact into account, it was suggested that the alkylbenzene molecules consist of groups: (1) -HC=, (2) >C=, (3) >C= (m), (4) >C= (p), (5) >C= (o), (6) >C<, (7) -HC<, (8) $-CH_2-$, (9) $-CH_3$ (see Fig .16 c).

The contributions of these groups to retention (a_i values) evaluated from the retention of 38 alkylbenzenes on hydroxylated silica from n-pentane at room temperature [26] are presented on Table 8.

Table 8
Values of a_i for various functional groups of alkylbenzenes. Adsorbent: Silasorb, eluent: n-pentane, ambient temperature

Functional group	(1) -HC=	(2) >C=	(3) >C= (m)	(4) >C= (p)	(5) >C= (o)
a_i	- 0.074	0.120	0.128	0.152	0.241
Functional group	(6) >C<	(7) - HC<	(8) - CH_2-	(9) $-CH_3$	
a_i	0.334	0.149	- 0.072	- 0.264	

It is clear from Table 8 that the increase of the number $-CH_2-$ and $-CH_3$ groups in a molecule results in the decreasing of the molecule retention on the whole. Whereas the introducing of $-CH_3$ groups in benzene ring in o-position as well as the branching of alkyl chain result in higher retention owing to the large contributions of >C= (o), >C<, or -HC< groups to retention.

The comparison of the experimental and the calculated ln k′ values obtained by using the contributions to retention of different groups (Table 8) and the number of groups in a molecule is presented on Fig. 20. The calculated and experimental ln k′ values are in a quite good agreement. Thus in the case of normal-phase chromatography it is possible to find the differences of contribution to the adsorption equilibrium constant of various functional groups of alkylbenzenes.

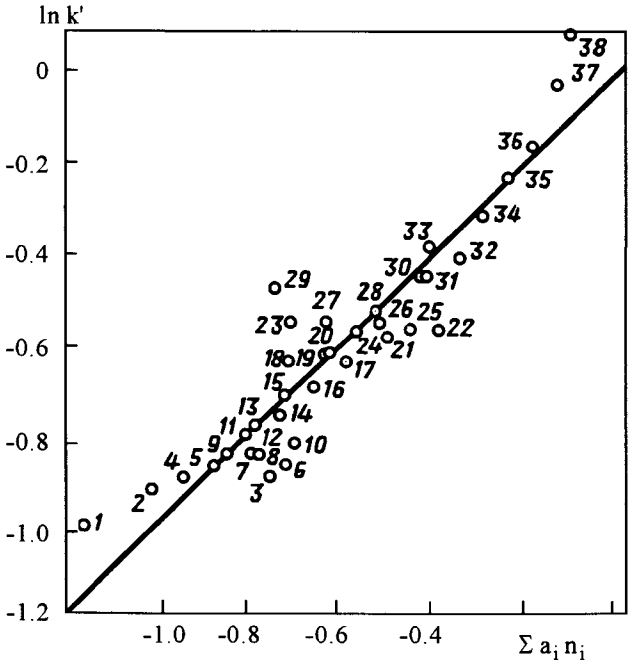

Figure 20. Comparison of the experimental ln k′ and calculated values of $\sum a_i n_i$ from the data of Table 8 for alkylbenzenes on silica gel from n–pentane.

Table 9
Values of a_i for various functional groups of benzene derivatives. Adsorbent: Nucleosil 10 RP 18, temperature 25°C, eluent: methanol (MeOH) – tetrahydrofurane (THF) – water (H_2O) of volume fraction (0.35 : 0.35 : 0.30)

Functional group	a_i	Functional group	a_i	Functional group	a_i
– HC =	0.026	> C=O	– 0.952	– OH (Ar)	– 1.205
> C =	0.159	– NH_2	– 0.991	– COO –	– 0.879
> C = (o)	0.328	– O –	– 0.221	– N <	0.556
> C = (m,p,)	0.472	– HC =O	– 1.259	– NH–	0.013
– CH_2–	0.299	– CN	– 1.286	– N =	– 1.513
– CH_3	– 0.182	– OH	– 2.167	– NO_2	– 0.704
– HC <	0.949	– Cl	– 0.093		

The contribution of functional groups to retention depends on the composition of eluent. To determine the dependence of the retention on eluent composition it is not simple problem especially for multicomponents eluents. If to determine the dependencies of contributions of functional groups to retention on eluent composition so it is possible to calculate the retention (ln k′) of many compounds on the whole for the different eluent

compositions. For this purpose the data for 32 compounds [27] were used. The calculated a_i values for some functional groups on adsorbent: Nucleosil 10 RP 18 from eluent containing water, methanol and tetrahydrofurane at 25°C are presented in Table 9.
Using a_i values it is possible to evaluate the retention of molecules for mobile phase MeOH–THF–H_2O (0.35:0.35:0.30). On Fig. 21 the comparison of calculated and experimental ln k′ values for 32 solutes is presented. The correlation between the calculated and experimental data is quite high.

The dependence of a_i values on mobile phase composition can be expressed by the projection of lines with the same meaning of a_i values on a concentration triangle. On Fig. 22 the dependence of a_i for – HC= and – Cl groups and on Fig. 23 for – OH and $-NH_2$ groups are presented.

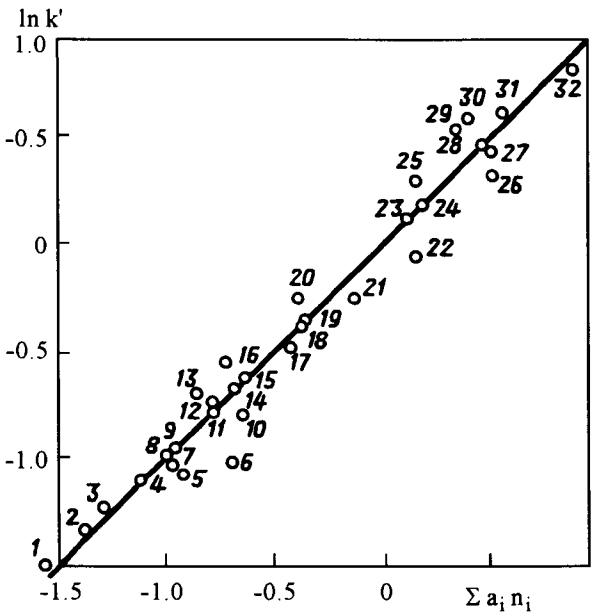

Figure 21. Correlation between the experimental ln k′ values [27] and calculated by using data of Table 9 for the mobile phase composition MeOH–THF–H_2O (0.35:0.35:0.30).
1= benzyl alcohol, 2= dimethyl phthalate, 3= 2–phenylethanol, 4= 1–phenylethanol, 5= phenol, 6= acetophenone, 7= 3–phenylpropanol, 8= benzonitrile, 9= benzaldehyde, 10= o–nitroaniline, 11= diethyl phthaiate, 12= p–nitroacetophenone, 13= m–nitrophenol, 14= quinoline, 15= o–cresol, 16= aniline, 17= nitrobenzene, 18= 2,4–dimethylphenol, 19= m–dinitrobenzene, 20= benzophenone, 21= anisole, 22= benzene, 23= N–methylaniline, 24= chlorobenzene, 25= toluene, 26= naphthalene, 27= anethole, 28= N,N–dimethylaniline, 29= diphenyl ether, 30= ethylbenzene, 31= biphenyl, 32= anthracene.

It is clear from Fig. 22 that the hydrophobic groups increase the adsorption of molecules in water rich solution but at higher concentrations of organic compounds in solution these groups decrease the adsorption of compounds owing to stronger interactions with eluent molecules. As for hydrophilic groups (hydroxyl and amino groups) so these groups in

all concentration region decrease the adsorption of molecules on the whole because of hydrogen bonding with all molecules of solution containing such compounds as water, methanol and tetrahydrofurane (Fig. 23).

Thus chromatography as analytical method of determination of equilibrium concentration can be used for the adsorption study from solutions both volatile and non-volatile compounds. Moreover the retention data and their dependence on temperature make it possible to determine very easily the adsorption equilibrium constants and thermodynamic

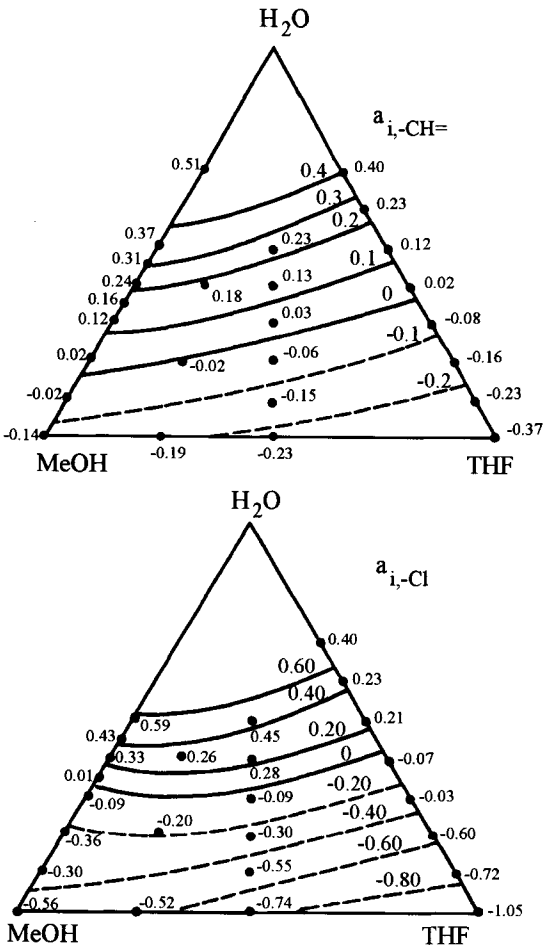

Figure 22. Dependencies of a_i values for – HC= and – Cl groups on mobile phase composition (MeOH–THF–H_2O). Adsorbent: Nucleosil 10 RP 18.

characteristics of adsorption from solutions at small coverages which is rather complicate under static conditions. The calculations of the contributions of functional groups to the equilibrium constant and to the heat of adsorption may be used for the understanding the mechanism of adsorption and are the quantitative characteristic of molecular interac-

tion on adsorption from solutions. The contributions of molecular groups to the retention volume can be used also for the prediction of the retention times and the optimization of the compounds separation by liquid chromatography.

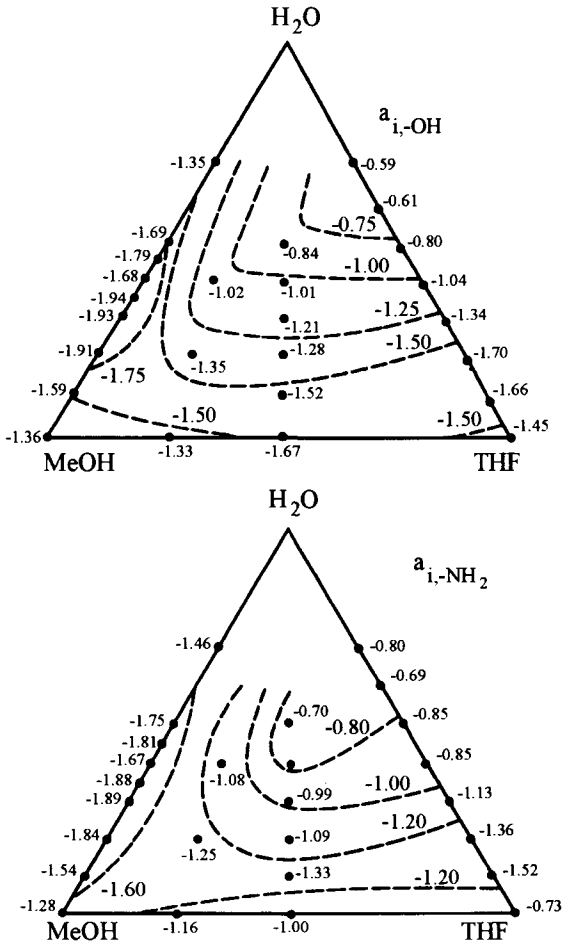

Figure 23. Dependence of a_i values for –OH and $-NH_2$ groups on mobile phase composition (MeOH–THF–H_2O). Adsorbent: Nucleosil 10 RP 18.

REFERENCES

1. J.J.Kipling, Adsorption from Solutions of Non-Electrolytes, Academic Press, London, New York, 1965.
2. G.D.Parfitt, C.H.Rochester, Adsorption from Solution at the Solid/Liquid Interface, Academic Press, London, New York, 1983.
3. V.S.Vasilieva, V.Ya.Davydov, A.V.Kiselev, Dokl. AN USSR, 192 (1970) 1299.
4. V.Ya.Davydov, A.V.Kiselev, D.Shtefens, Zhurn. Fiz. Khimii, 47 (1973) 2091.

5. V.Ya.Davydov, A.V.Kiselev, Yu.M.Sapojnikov, Kolloid. Zhurn., 41 (1979) 353.
6. S.I.Zverev, O.G.Larionov, K.V.Chmutov, Zhurn.Fiz.Khimii,48 (1974) 1556, 2126, 2350.
7. S.A. Busev, O.G.Larionov, Zhurn.Fiz.Khimii, 56 (1982) 1238.
8. F.Koster, G.H.Findenegg, Chromatographia, 15 (1982) 743.
9. G.Curthoys, V.Ya.Davydov,A.V.Kiselev, S.A.Kiselev, B.V.Kuznetsov, J.Colloid Interface Sci., 48 (1974) 58.
10. V.Ya.Davydov, A.V.Kiselev, Yu.M.Sapojnikov, Chromatographia, 13 (1980) 745.
11. V.Ya.Davydov, M.Elizalde Gonzalez, A.V.Kiselev, K.Lenda, Chromatographia, 14 (1981) 13.
12. M.Boumahraz, V.Ya.Davydov, M.Elizalde Gonzalez, A.V.Kiselev, Chromatographia, 17 (1983) 143.
13. V.Ya.Davydov, A.V.Kiselev, B.V.Kuznetsov, Zhurn. Fiz. Khimii, 39 (1965) 2058.
14. V.Ya.Davydov, A.V.Kiselev, L.T.Zhuravlev, Trans. Faraday Soc., 60 (1964) 2245.
15. R.Kaliszan, Quantitative Structure –Chromatographic Retention Relationships. Chemical Analysis, vol.93 . Wiley–Interscience, New York, 1987.
16. E.Tomlinson, J.Chromatogr., 113 (1975) 1.
17. B.K.Chen, Sc.Horvath, J.Chromatogr., 171 (1979) 15.
18. V.Ya.Davydov, in: Chromatography' 84, H. Kalasz and L.S.Ettre (eds.), Akademiai Kiado, Budapest, 1986, p. 351.
19. V.Ya.Davydov, J.Chromatogr., 356 (1986) 123.
20. V.Ya.Davydov, G.N.Filatova, E.Smolkova–Keulemansova, Yu.Zima, Chromatographia, 24 (1988) 1059.
21. V.Ya.Davydov, Wang Feng, Zhu Zhenghe, J.Chengdu Univ. Sci. and Tech., 41 (1988) 9.
22. A.Zlatkis and R.F.Kaizer, (eds.), HPTLC High Performance Thin–Layer Chromatography, Elsevier, Amsterdam, Oxford, New York etc., 1977.
23. E.P.Kemertelidze, V.P.Georgievskii, Physico–chemical Methods of Analysis of Some Biological Active Plant Compounds, Metzniereba, Tbilisi, 1975 (in Russian).
24. V.Ya.Davydov, Vestn. Mosk. Univ., seriya 2, Khimija, 30 (1989) 43.
25. R.J.Hurtubise, T.W.Allen, H.F.Silver, J.Chromatogr., 230 (1981) 117.
26. J.Kriz, L.Vodicka, J.Pancocharova, M.Kuras, J.Chromatogr. 219 (1981) 53.
27. P.J.Schoenmakers, H.A.H.Billet, L. de Galan, J.Chromatogr. 218 (1981) 261.

This Page Intentionally Left Blank

A. Dąbrowski and V.A. Tertykh (Editors)
Adsorption on New and Modified Inorganic Sorbents
Studies in Surface Science and Catalysis, Vol. 99

Chapter 3.3
Equilibria of adsorption from solutions on the silica surface

V. A.Tertykh and V. V.Yanishpolskii

Institute of Surface Chemistry, National Academy of Sciences of the Ukraine,
252022 Kiev, Ukraine

1. INTRODUCTION

Silicas with chemically modified surface are widely used in practice of high-performance and affinity chromatography, in catalysis by grafted enzymes and metal complexes, for concentrating ions and organic substances, for prolonged and controlled release of pharmaceutical and other active compounds. Depending on the problem to be solved, there are various requirements for the interaction of the surface sites with molecules or ions. For example, in high performance liquid chromatography the interactions should not be very strong, while for immobilized catalysts the bond to the surface must be particularly strong so as to ensure stability while working. Prediction of the behaviour of grafted compounds requires a quantitative description of such interactions and of the effect of various factors upon them.

The main problem of the quantitative description of equilibria involving a solid surface is to estimate the composition of one phase, e.g. an adsorbent, by the composition of the other phase. Mathematical description of equilibrium systems is based on equations resulting from the mass action law and from the material balance [1-4]. It should be noted that such approaches (being independent of each other) are used for a description of biological systems, adsorption, complex formation of metal ions with ligands, dissociation of acids and bases [5- 11]. They have identical mathematical and thermodynamical principles although some definitions differ slightly due to historical reasons. In particular, researchers use dissociation constants when describing biological systems and acid-base equilibria [8-13], and association constants (a stability constant) are usually applied when describing a complexation process [2,14]. All these research areas merge practically into one on studying surface equilibria that requires their simultaneous consideration.

Let us discuss a complex formation in the case of two interacting particles A and B according to the scheme

$$A + B \rightleftharpoons AB$$

where A may be an adsorption site of the starting or modified surface, an active enzyme centre, a binding site of antibody or receptor, an immobilized ligand of various structures, and B may correspondingly be the other particle forming a complex with A being an ion

of hydrogen or of metals, an inorganic ion, a substrate or inhibitor of enzymes, an antigen or hormone. One can also consider other corresponding combinations of interacting pairs of A and B. Such a complexation may result in an adsorption complex, enzyme-substrate complex, enzyme- inhibitor complex, antigen-antibody complex, donor-acceptor complexes, and surface chemical compounds. In the present paper a binding site is denoted by L, a sorbed particle by M, and if multistage surface reactions are concidered, during the first stage L-sites are sites of the initial complexing, M is a modifying molecule, during the second stage a grafted particle M is regarded as an L for the subsequent formation of adsorption complexes and surface compounds.

The present paper considers equilibria of adsorption on surface beginning from a simple case of uncompeting sorption on a monobasic site, sorption in the presence of competition, adsorption on dibasic sites, adsorption of polybasic organic molecules on monobasic cation and anion exchanger or dibasic ampholyte.

The equilibria of complexation of metals with ligands are classified as best studied. The results of their investigations are summarized in the well known reference books [14].

For ligands grafted to a solid matrix it is very expedient to employ experiments carried out for complex formation in solution in order to predict the properties and the stability constants of the grafted ligands with various metals. Almost all the methods for calculating constants in solutions, especially for the stepwise complexing, are based on considering the metal ion as a centre for binding various ligands. In the case of complex formation on a surface, when the potential ligands are held by chemical bonds with solid matrix, it is more convenient to consider the grafted ligand as a centre for metal ion binding. This does not change the essentials of the treatment, but helps to avoid the difficulty of defining the concentration of the grafted ligands. The well-known methods for determining the stability constants of complexes in solution depend on measurements of equilibrium concentrations of ligands [1,2,14]. In order to determine these stability constants for the complexing on a surface it is necessary to use equations based on equilibrium concentrations of metal ions. Only then one can realize all the advantages of transferring the ligands into a heterogeneous state, namely the simplicity of separating metal complexes from solution without changing the equilibrium concentration of metal ions in solution.

For a given sorbent the concentration of ligands on the surface is constant. The equilibrium concentration of the grafted ligands changes only when the initial concentration of metal ions is varied. Varying the ratio between the volume of the solution and the mass of sorbent changes merely the amount of ligands in the system. Their concentration on the surface, i.e. at the site of complex formation, does not change, and the composition of the complexes formed remains the same [15-17]. This makes it possible to speak of "complex formation sites" on the surface [16,17]. It should be emphasized that in the case of polydentate sorption site the experimental determination of stepwise complexation stability constants on a surface is very complex. The same situation arises in solution on going from monodentate to polydentate ligands. Thus, on going from ammonia to ethylenediamine or triethylenetetramine one considers not the stepwise constants for each donor nitrogen atom, but a single constant for ethylenediamine or triethylenetetramine molecules. On passing to macrocycles with fixed donor atoms one speaks of the binding of metal ions [18,19] by the macrocyclic molecule, which is considered as a site for bonding metal ions with a single stability constant. A similar situation is observed for ligands containing several carboxyl groups, such as citric acid and ethylenediaminetetraacetic acid, and also

for 8-hydroxyquinoline and other molecules including biomolecules whose binding sites have complex and unknown structures mostly [5,6,8-11]. Further in a similar manner we shall also consider adsorption sites on silica surface irrespective of their dentateness and structure.

2. EQUILIBRIA OF SILICA SURFACE SITES COMPLEXING WITH THE ONE–VALENCE CATIONS IN AQUEOUS SOLUTIONS (ACID–BASE PROPERTIES OF SURFACE ADSORPTION SITES)

2.1. Monobasic sites without competing adsorption

Let us consider the equilibrium reactions on surface sites, assuming that they obey the laws observed in solution. Such a consideration will allow us to see how the immobilized ligand will behave on condition that its properties are unchanged. Accordingly, experimental differences found will allow us to judge a change in ligand properties after immobilization.

On adding a sample of sorbent with grafted complex-forming sites$[L]_0$ to a solution containing metal ions at an initial concentration $[M]_0$, complex formation between them will reduce the concentration of metal ions to an equilibrium value [M], which can be determined experimentally by a lot of methods. The equilibrium concentration of the adsorption sites, [L], is difficult to determine experimentally. But, as it is known [3-10,20], the equilibrium constant in such cases can be determined also without using this value. This interaction can be represented in the form :

$$[L] + [M] \underset{k_{-1}}{\overset{k_1}{\rightleftharpoons}} [LM] \tag{1}$$

The association constant β or dissociation constant K_d for such process is usually expressed on the basis of the of mass action law [1-4,9,21] in the form:

$$\beta = \frac{1}{K_d} = \frac{[LM]}{[M][L]} = \frac{k_1}{k_{-1}} \tag{2}$$

by analogy with the description of this equilibrium in solution. Thus, if the value of β and the rate constants k_1 and k_{-1} for the forward and reverse reactions are known both the thermodynamic and the kinetic parameters of the equilibrium on the surface can be described. From Eq. (2) and the material balance condition for the binding site, $[L]_0 = [L] + [LM]$, we can obtain the following equation:

$$[LM] = \frac{\beta[L]_0[M]}{1 + \beta[M]} \tag{3}$$

for the isotherm of sorption of the metal ions or other species on the binding site in the absence of competing reactions (Fig.1). This equation is identical to the Langmuir equation, which was pointed by Hitchcock as early as 1926 [22], and, in principle, describes a complex formation irrespective of its occurrence, in a solution or on a surface. Formally it is thermodynamically all the same whether a binding site is soluble, fixed on the solid surface or is present in biological tissues. Differences are in that the total concentration

$[L]_0$ is known for solution studies, and as regards the surface the information on the amount and nature of adsorption sites is mostly absent. The methods for determining of their number by interaction with certain substances including a titration and evaluation of capacity by metal ion sorption are also based finally on surface equilibria and hence require account of equilibrium (1) and an equation of a type (3). For example, in the case of proton adsorption Eq. (3) has the following form:

$$[LH] = \frac{[L]_0[H]}{K_d + [H]} \tag{3a}$$

Usually, when determining the ionization constants of acid–base groups on surface a use is made of not this equation but of the Henderson–Hasselbalch equation:

$$pH = pK_d + \log \frac{\alpha}{1 - \alpha} = pK_d + \log \frac{[L]}{[LH]} \tag{3b}$$

However, there is no contradiction here since Eq. (3) and the Henderson–Hasselbalch equation (3b) are equivalent.

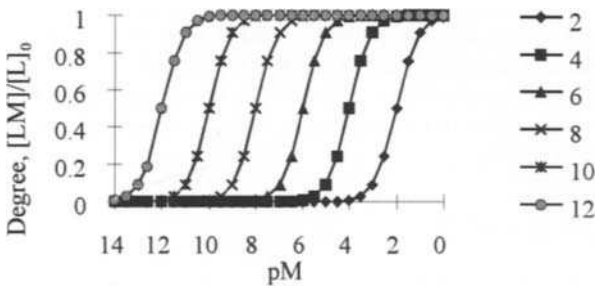

Figure 1. Adsorption isotherms without competition. $pM = -\log[M]$, numbers in the legend are values of $\log \beta$. The curves were calculated from Eq. (3).

Taking into account the material balance equation for the metal ions, $[M]_0 = [M]+[LM]$, we obtain from (2) the equation:

$$[LM] = \frac{\beta[M]_0[L]}{1 + \beta[L]} \tag{4}$$

analogous to that derived for the equilibrium in solution and its relationship to various complexing functions is shown in Ref. [23].

Since in aqueous solutions there is actually competition for the ligands between the metal ions [M] and protons [H], Eq. (3) applies only to the interaction of completely deprotonated surface sites with metal ions. In practice partially deprotonated ligands are usually involved.

2.2. Monobasic sites with competing adsorption

In this case, the equilibrium on the surface has the form:

$$[LH] \xrightleftharpoons{K_a} [H] + [L] + [M] \xrightleftharpoons{\beta} [LM]$$

$$\beta = \frac{[LM]}{[M][L]} = \frac{1}{K_d}, \qquad K_a = \frac{[L][H]}{[LH]} \tag{5}$$

where K_a is the dissociation constant of a sorption site. In this case the equation of a sorption isotherm of metal ions or other particles has the form:

$$[LM] = \frac{\beta[L]_0[M]}{1 + \frac{[H]}{K_a} + \beta[M]} = \frac{[L]_0[M]}{K_d\left(1 + \frac{[H]}{K_a}\right) + [M]} \tag{6}$$

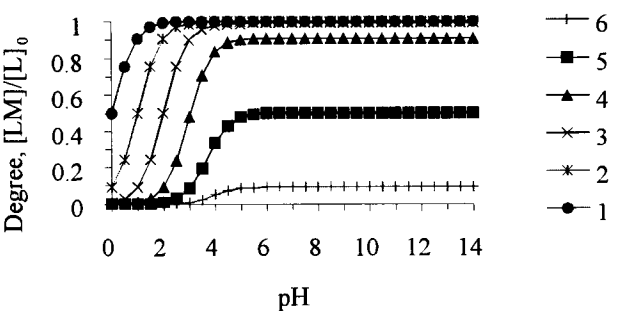

Figure 2. Degree of substitution of surface sites by metal ions versus pH. The curves were calculated from Eq. (6) using $\beta = 10^5$ l/mol, $K_a = 10^{-4}$ mol/l, numbers in the legend are equilibrium concentrations of metal ions $pM = -\log[M]_{eq}$.

As it is seen from Eq. (6) and Fig.2, at $\beta M \ll 1 + \frac{[H]}{K_a}$ to attain the complete substitution of adsorption sites is generally impossible. In particular, such an equilibrium takes place for titrating a silica by alkaline metal ions (for instance, Na^+):

$$\equiv SiOH \xrightleftharpoons{K_a} H^+ + \equiv SiO^- + Na^+ \xrightleftharpoons{\beta} \equiv SiO^-Na^+ \tag{7}$$

Equilibria (5) and (7) can be also represented in the form of the proton sorption isotherm (Fig.3):

$$[LH] = \frac{[L]_0[H]}{K_a(1 + \beta[M]) + [H]} \tag{8}$$

Equitions (6) and (8) are of a more general character than Eq. (3) is, as during adsorption from aqueous solutions there is always a competition of particles being adsorbed.
However, this circumstance is not always taken into consideration and dissociation constants of surface sites are determined by the Henderson–Hasselbalch equation, which does

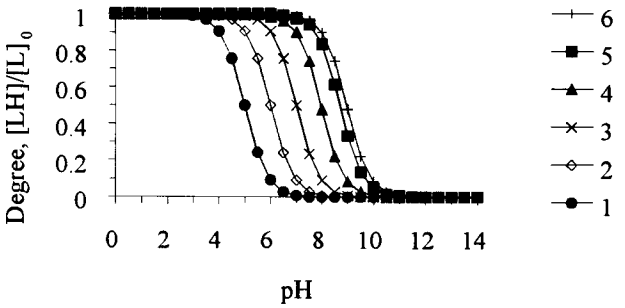

Figure 3. Isotherms of proton adsorption in the presence of competing metal ions. The curves were calculated from Eq. (8) using $\beta = 10^5$ l/mol, $K_a = 10^{-9}$ mol/l, numbers in the legend are equilibrium concentration of metal ions $pM = -\log [M]_{eq}$.

not take into account a competitive interaction with metal ions and can be valid only for $\beta M \ll 1$. In addition, within the scope of the theory explaining the influence of a surface electrostatic potential on titration curves of polyelectrolytes it is believed that silica particles assume a negative charge when ionizing silanol surface groups [24–26]. This must lead to overestimation in experimentally determined pK values. The real or intrinsic constant does not depend on the surface charge here. An influence of an electrostatic effect on a titration course and on a dissociation constants is taken into account when studying organic polymers including proteins [12,20,27] and modified silicas [28,29].

As is known [24,28] in most cases disperse silicas have globular structure. For rigid spheres of a b radius with an uniformly distributed charge the following equation is proposed:

$$pH = pk_{int} + \log \frac{\alpha}{1-\alpha} - 0.868\omega\overline{Z} \tag{9}$$

where

$$\omega = \frac{e^2}{2\varepsilon kT}\left(\frac{1}{b} - \frac{\chi}{1+\chi a}\right) = 3.57\left(\frac{1}{b} - \frac{\chi}{1+\chi a}\right)$$

Here e is the electron charge, ε is the dielectric constant of the medium, a is the distance of the maximum approach of a small ion and a spherical particle, often taken equal to (b+ 2.5Å), χ is the Debye–Hückel parameter, 3.57 is the constant coefficient for aqueous systems at 25°C on condition that distances are measured in angstroms), pk_{int} is the intrinsic ionization constant, $\overline{Z} = -\alpha n$ is the average value of the total charge of a particle (it is equal numerically to the number of protons having formed on dissociation), n is the number of dissociating groups in a particle.

It follows from Eq. (9) that when a macromolecule is in the shape of a globe, the intrinsic ionization constant for a definite type of ion-exchangeable sites is changed in the presence of a charge so that:

$$pk = pk_{int} - 0.868\omega\overline{Z} = pk_{int} - 0.868\omega\alpha n \tag{10}$$

or

$$k = k_{int}e^{2\omega\overline{Z}}$$

In aqueous solutions at 25°C χ is a function of only ionic strength, μ ($\chi = 0.33\mu^{\frac{1}{2}}$ Å^{-1}), and the above-mentioned expression for ω assumes the form:

$$\omega = 3.57\left(\frac{1}{b} - \frac{0.33\mu^{\frac{1}{2}}}{1 + 0.33a\mu^{\frac{1}{2}}}\right)$$

Taking into account that non-porous aerosil particles have a spherical structure, this theoretical treatment is applicable also in this case. A silica represents a heterochain inorganic polymer of silicic acid. However, most of its modifications are difficult to characterize in such terms as molecular mass and amount of functional groups per monomer unit and this question is still under discussion. However, such estimates can be made for aerosil, a highly disperse silica produced by combustion of silicon tetrachloride in the oxygen-hydrogen flame.

Depending on the specific surface area the aerosil particle diameter is 5-50 nm [30]. Thus, from the geometric dimensions of particles one can calculate the molecular mass, specific surface area of aerosil, and concentration of surface Si atoms in one particle. Let us use the notation given in [24]: $\mathbf{n_t}$ = full number of silicon atoms in a particle, $\mathbf{n_s}$ = number of silicon atoms on the particle surface, d = diameter of the particle, ρ = density of silica, 2.2 g/cm^3.

Thus, the number of residues of SiO_2 and hence of silicon atoms located in a particle is equal to:

$$n_t = \frac{\rho\pi d^3 N}{6M}$$

where M is the molecular mass of SiO_2 (60.1), N is the Avogadro number. From the n_t value we find n_s:

$$n_s = \pi\left(\frac{6n_t}{\pi}\right)^{\frac{2}{3}}$$

Using the value of aerosil surface area determined as:

$$S_{sp} = \frac{6}{\rho d}$$

one can calculate the number of silicon surface atoms and molecular mass for one particle of aerosil with a certain surface area (see Figs. 4 and 5). For example, for aerosil with a surface area of 182 m^2/g, a particle diameter of 15 nm, a molecular mass of $2.34 \cdot 10^6$, in a particle 38900 silicon atoms and 5500 out of them are on the particle surface. Here it is supposed that the particles are monodisperse, though, as known, there is a definite distribution of diameters of particles [30].

The application of this model (Figs. 6 and 7) shows that the degree of distortion of a titration curve decreases upon an increase in the ionic strength of a solution, and we must obtain an intrinsic constant of pk_{int} by extrapolating experimental values of pK_a to the zero degree of ionization.

However, it is found experimentally that not only a stretching of a titration curve occurs but also an increase in the intrinsic ionization constant of silanol groups (a decrease in pk_{int}) is observed with increasing the ionic strength (a shift of a titration curve into the

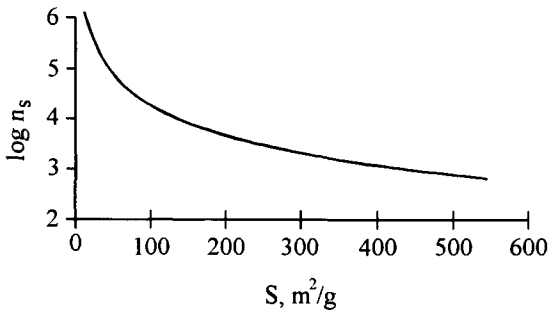

Figure 4. Dependence of quantity of surface silicon atoms of one particle on specific surface area of aerosils.

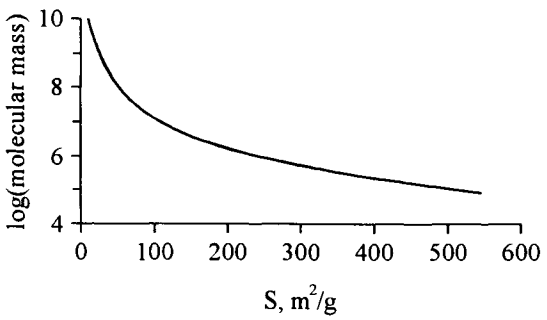

Figure 5. Dependence of molecular mass of one particle on specific surface area of aerosils.

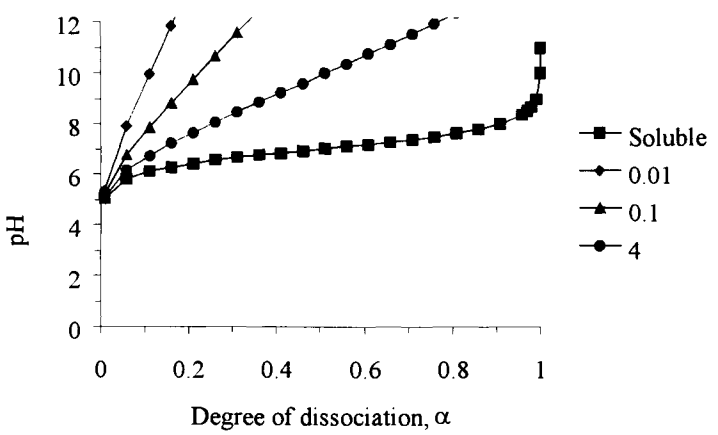

Figure 6. Effect of ionic strength (numbers in the legend are concentrations of NaCl in mol/l; *soluble*: is hypothetical curve without influence of electrostatic potential of surface, i.e. $\overline{Z} = 0$) on titration curves of silica with a particle diameter of 15 nm, $pK_a = 7$, a number of dissociating groups in a particle $n = n_s/2$. The curves were calculated from Eq. (9).

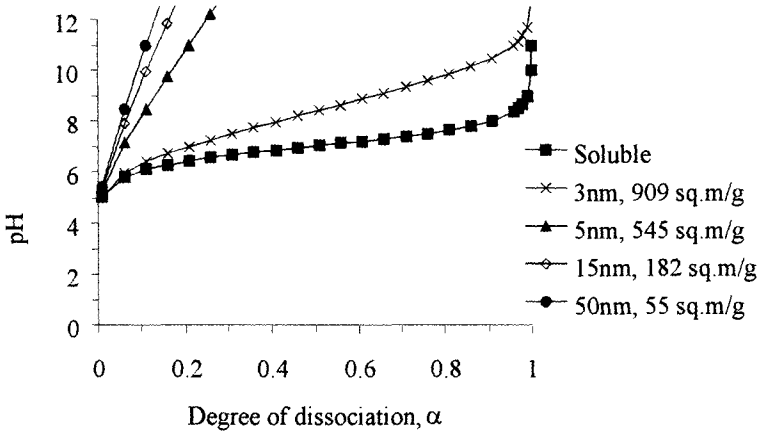

Figure 7. Effect of particle diameter on titration curves of silica ($pK_a = 7$, ionic strength 0.01). The curves were calculated from Eq. (9), $n = n_s/2$, *soluble* as in Fig.6.

acid range). In addition, the value of the slope of a plot on $pK_a - \alpha$ coordinates exceeds considerably the experimentally observed values. Thus, in Ref. [26] this slope is 2.5–2.9 and does not depend practically on the ion strength, while according to Eq. (9) it is equal to 16 for 0.1 M NaCl and 6 for 4 M NaCl.

This behaviour may be explained if equilibrium (5) and isotherms (6) and (8) are taken into account. Then an intrinsic ionization constant k_{int} is equal to $K_a(1 + \beta[M])$ and the

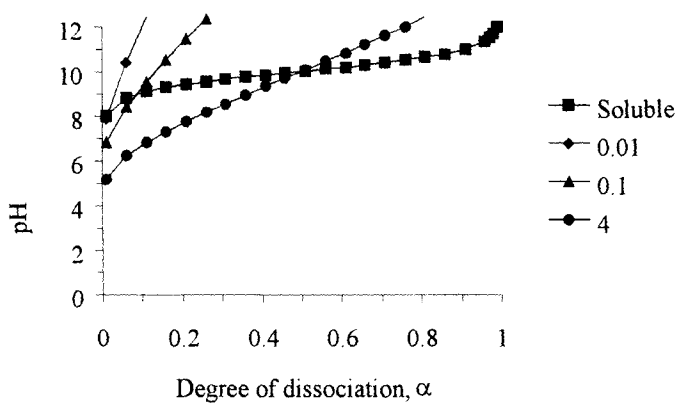

Figure 8. Effect of ionic strength on titration curve of silica with a particle diameter of 15 nm. Numbers in the legend are concentrations of NaCl in mol/l, *soluble* as in Fig.6. Curves were calculated from Eq. (11) using $pK_a = 10$, $\beta = 200$ l/mol.

Henderson–Hasselbalch equation assumes the form:

$$pH = pK_a - \log(1 + \beta M) + \log \frac{\alpha}{1 - \alpha} - 0.868\omega\overline{Z} \tag{11}$$

With allowance for the data of Ref. [26] Fig. 8. gives estimated curves for titration of silica with a particle size of 15 nm (182 m^2/g) and a dissociation constant of silanol groups $pK_a = 10$. As seen from the figure , the account of influence of an electrostatic field of the ionized surface and a competition of hydrogen ions and sodium ions allows us to explain partly all anomalies of titration curves of silica without introducing supplementary postulates.

Thus, if the stretching of titration curves is related to an electrostatic effect, then its influence is considerably less than that predicted by the theory [12,20]. The observed stretching of the titration curves may be also due to the presence of several types of acidic sites [31]. This result is very important as it raises a possibility to explain the considerable scattering of data on the dissociation constant for silanol groups of silica surface cited in literature [24,26,31,32]. Thus, it may be claimed that the acidity of silica silanol groups is close to that of orthosilicic acid and all the observed experimental variations are caused by geometrical characteristics of particles and experimental conditions, namely, by the value of ionic strength and nature of applied metal cation (the value of β). For example, for 4M NaCl the observed (apparent) increase in the acidity approaches 3 units of pK (a decrease of pK from 10 to 7,1) and with β for Na^+ being equal to 200 l/mol.

2.3. A dibasic surface site

It is known that surface silanol groups can act as ligands upon complex formation with bivalent metal ions [33]. In this case the adsorption site must be a divalent one and equilibria may be represented in the form as follows:

$$\begin{array}{ccccc} [LH_2] & \overset{K_1}{\rightleftharpoons} & [H] + [LH] & \overset{K_2}{\rightleftharpoons} & [L] + [H] \\ & & + & & + \\ & & [M] & & [M] \\ & & \beta_1 \uparrow\downarrow & & \beta \uparrow\downarrow \\ & & [LHM] & & [LM] \end{array} \tag{12}$$

The form of the sorption isotherm will obviously depend on the form of the deprotonated site which forms a complex with the metal. In calculating equilibrium constants in solution it is usual to consider only completely deprotonated ligands, and we shall also confine our analysis to this case, although both the forms [L] and [LH] may be important in complex formation.

The sorption isotherm for a completely deprotonated dibasic site is described by the relation:

$$[LM] = \frac{\beta[L]_0[M]}{1 + \dfrac{[H]}{K_1} + \dfrac{[H]^2}{K_1K_2} + \beta[M]} \tag{13}$$

If only a single deprotonated form [LH] were involved in complex formation, which is actually unreal, the sorption isotherm would have the form:

$$[LHM] = \frac{\beta_1[L]_0[M]}{\left(1 + \frac{[H]}{K_1} + \frac{K_2}{[H]}\right) + \beta_1[M]} \tag{14}$$

(14) Though, in fact, according to Eq. (12) there may be present both the forms [LHM] and [LM], it is also possible to infer that there exist such cases (e.g., intermediate stages during catalysis and chemisorption) when only one of them is of importance. As an example the relationships of the Eq. (14) type describe the dependence of the activity of enzymes (including immobilized ones) on pH [11,34]. Equations (13) can be written as:

$$[LM] = \frac{\beta[L]_0[M]}{F + \beta[M]} \tag{15}$$

(15) where F is the Michaelis pH–function [10,11] corresponding to the deprotonated form of the sorption site which is involved into complex formation. These functions express the fraction of any ionic form of the binding sites. This fraction is equal to their overall amount divided by the corresponding pH function of the n–basic site. The pH functions for the completely deprotonated site have been given in a general form in Ref. [15]. However, the authors [15] used not the dissociation constants K_d but the protonation constants K_p. This circumstance must be taken into account, because the first dissociation constant is equal to the reciprocal of the last protonation constant; for example, for a tribasic site $K_{d1} = 1/K_{p3}$. It should be noted that when $[H] \ll K_1$ and $[H] \ll K_2$ isotherms (6) and (13) assume the form of isotherm (3), i.e., they describe the interactions of completely deprotonated sites. However, it should be noted that modified silicas may rarely be obtained with the monofunctional surface and hence with the identical binding sites. In this case the sorption isotherm consists of a sum of several isotherms for each of the binding sites. For example, for two types of binding sites the experimental isotherms consist of a sum of two isotherms:

$$[LM] = \frac{\beta_1[L^I]_0[M]}{F^I + \beta_1[M]} + \frac{\beta_2[L^{II}]_0[M]}{F^{II} + \beta_2[M]} \tag{16}$$

where $[LM] = [L^IM] + [L^{II}M]$ is the total amount of molecules bound, $[L^I]_0$ is the overall concentration of binding sites of the first type, $[L^{II}]_0$ is that of another type, F^I and F^{II} and β_1 and β_2 are the corresponding acidity functions and association constants for sites of the first and second type. In fact, a set of equilibrium constants with different partition functions can be observed on a surface. [35–37]. However, this does not influence the general character of dependencies.

3. EQUILIBRIA OF THE SILICA SURFACE SITES COMPLEXING WITH THE ORGANIC MOLECULES (CATIONS, ANIONS, ZWITTER-IONS)

3.1. Binding of competing molecules with surface sites

Let us consider in which way the presence of interfering molecules or ions $[M_1]$ that also interact with grafted ligands [L] will affect the sorption of target molecules or ions [M]. Equilibria in this case can be represented by the scheme:

$$[LM] \overset{K_d}{\rightleftharpoons} [M] + [L] + [M_1] \overset{K_1}{\rightleftharpoons} [LM_1] \tag{17}$$

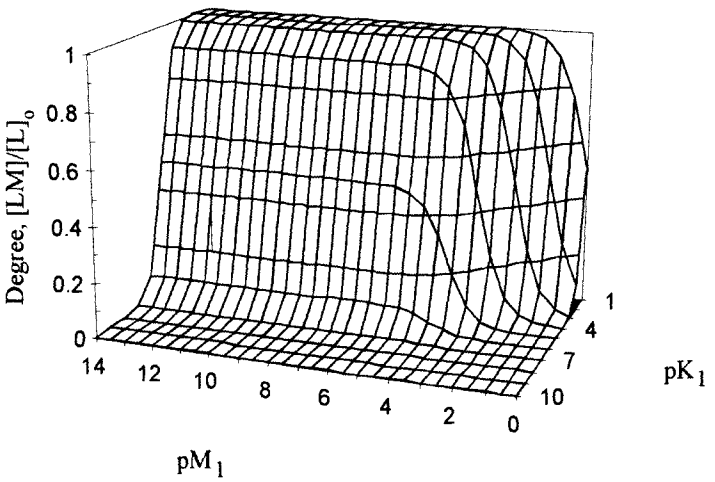

Figure 9. Dependence of sorption of molecules M on concentration ($pM_1 = -\log M_1$) and dissociation constants of competing molecules. Curves were calculated from Eq. (18) using $K_d = 10^{-5}$ mol/l, $[M] = 10^{-5}$ mol/l.

In this case the adsorption isotherm (Fig.9) has the following form:

$$[LM] = \frac{[L]_0[M]}{K_d\left(1 + \frac{[M_1]}{K_1}\right) + [M]} \tag{18}$$

As it is seen, equilibrium (17) and isotherm (18) are similar to those represented by Eqs. (5) and (6) respectively.

3.2. Binding of competing molecules with adsorbing molecules

When the soluble ligand (inhibitor) [I] competes for molecule [M] with the ligand grafted to the surface, equilibria can be written down as follows:

$$\begin{array}{lcl} [L] + [M] & \overset{K_d}{\rightleftharpoons} & [LM] \\ + & & \\ [I] & \overset{K_I}{\rightleftharpoons} & [MI] \end{array} \tag{19}$$

Since in this case free and inhibitor-coupled molecules ([M] + [MI]) will be in a solution, it is convenient to use the degree of binding of molecules is, i.e. the ratio of the amount of surface-bonded molecules to their total amount in the system. It should be noted that this value in Refs.[38,39] is called a distribution coefficient that does not correspond to the physical sense of this coefficient used commonly in chromatography:

$$\frac{[LM]}{[M]_0} = \frac{[L]}{K_d\left(1 + \frac{[I]}{K_I}\right) + [L]} \tag{20}$$

Equilibria (19) can also be described in terms of the total concentration ([M] + [MI]) = $[M]_{eq}$ in the solution:

$$[LM] = \frac{[L]_0[M]_{eq}}{K_d\left(1 + \frac{[I]}{K_I}\right) + [M]_{eq}} \tag{21}$$

From (21) the distribution coefficient may be expressed as:

$$D = \frac{[LM]}{[M]_{eq}} = \frac{[L]_0}{K_d\left(1 + \frac{[I]}{K_I}\right) + [M]_{eq}} \tag{22}$$

3.3. Deprotonated surface site and protonated molecules in solution

If a complex is formed by a deprotonated form of surface sites [L] (for example, -COO-, ≡SiO-) and a protonated form of the adsorbate [MH] (for example, $R\text{-}NH_3^+$) then the equilibria have the form:

$$[L] + [H] \overset{K_1}{\rightleftharpoons} [LH]$$

$$+$$

$$[MH] \overset{K_2}{\rightleftharpoons} [M] + [H]$$

$$K_d \uparrow\downarrow$$

$$[LMH] \tag{23}$$

The equation of the isotherm for such an equilibrium will be as follows:

$$[LMH] = \frac{[L]_0[M]_{eq}}{K_d\left(1 + \frac{[H]}{K_1}\right)\left(1 + \frac{K_2}{[H]}\right) + [M]_{eq}} \tag{24}$$

where $[M]_{eq} = [M] + [MH]$ is the total concentration of adsorbate molecules in solution (Figs.10,11).

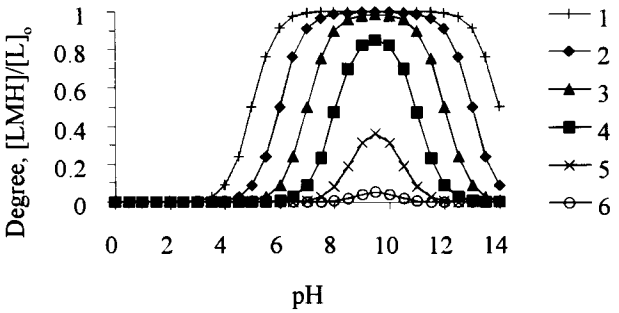

Figure 10. Competition of adsorption of protonated molecules and protons on deprotonated surface sites. Curves were calculated from Eq. (24) using $K_d = 10^{-5}$ mol/l, $K_1 = 10^{-5}$ mol/l, $K_2 = 10^{-10}$ mol/l, numbers in the legend are equilibrium concentrations of molecules $pM = -\log[M]_{eq}$.

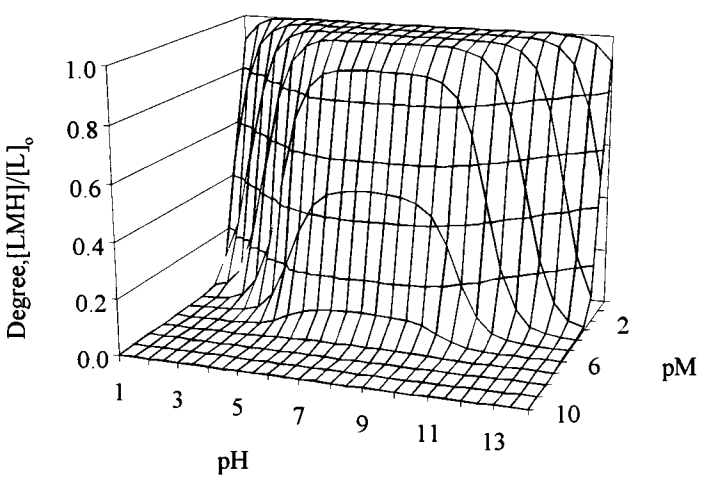

Figure 11. Competition of adsorption of protonated molecules and protons on deprotonated surface sites. Curves were calculated from Eq. (24) using $K_d = 10^{-10}$ mol/l, $K_1 = 10^{-5}$ mol/l, $K_2 = 10^{-10}$ mol/l, $pM = -\log[M]_{eq}$.

3.4. Protonated surface sites and deprotonated molecules in solution

When the complex is formed by a protonated form of surface sites and a deprotonated form of a molecule in solution (Fig.12), then equilibria and equations of the isotherm have the form:

$$\begin{array}{lll} [L] + [H] \overset{K_1}{\rightleftharpoons} & [LH] & \\ & + & \\ & [M] \quad +[H] \overset{K_2}{\rightleftharpoons} & [MH] \\ & K_d \uparrow\downarrow & \\ & [LHM] & \end{array} \tag{25}$$

$$[LMH] = \frac{[L]_0[M]_{eq}}{K_d\left(1 + \frac{K_1}{[H]}\right)\left(1 + \frac{[H]}{K_2}\right) + [M]_{eq}} \tag{26}$$

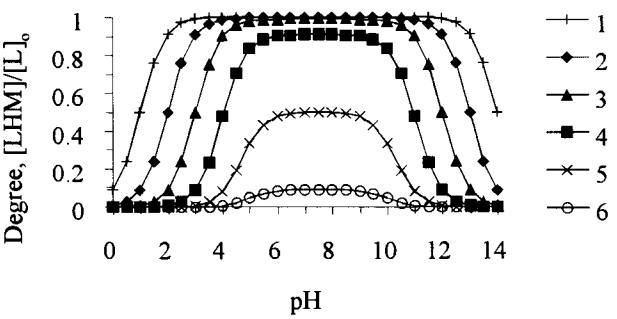

Figure 12. pH–dependence of adsorption of deprotonated monobasic molecules on protonated surface sites. Curves were calculated from Eq. (26) using $K_d = 10^{-5}$ mol/l, $K_1 = 10^{-10}$ mol/l, $K_2 = 10^{-5}$ mol/l, numbers in the legend are equilibrium concentration of molecules pM = $-\log[M]_{eq}$.

3.5. Monobasic surface site and polybasic molecules (polyelectrolytes) in solution

Let us consider a case of the interaction of polybasic molecules (which are all amino acids and proteins [39,40]), with adsorption surface sites. As an example, let us consider the dissociation of a tribasic molecule (lysine, arginine):

$$\begin{array}{lllll} [MH_3] & \overset{K_1}{\rightleftharpoons} & [MH_2] + [H] & \overset{K_2}{\rightleftharpoons} & [MH] + [H] \quad \overset{K_3}{\rightleftharpoons} \quad [M] + [H] \\ +2 & & +1 & & 0 \qquad\qquad -1 \end{array} \tag{27}$$

where the numerals designate charges of corresponding molecules. Adsorption sites on a surface can be cation–exchangeable, anion–exchangeable or possess amphoteric properties.

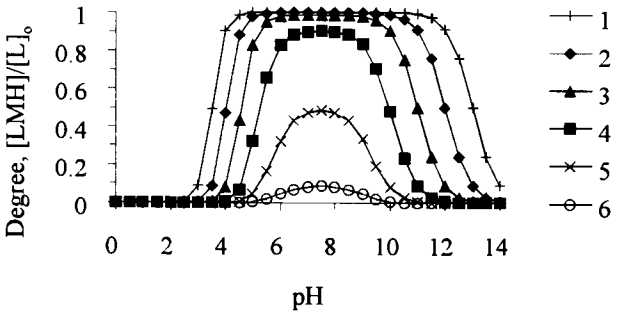

Figure 13. pH–dependence of adsorption of deprotonated dibasic molecules on protonated surface sites (anion exchanger). Curves were calculated from Eq. (30) using $K_d = 10^{-5}$ mol/l, $K = 10^{-9}$ mol/l, $K_1 = 10^{-5}$ mol/l, $K_2 = 10^{-6}$ mol/l, numbers in the legend are equilibrium concentrations of molecules $pM = -\log[M]_{eq}$.

Let us consider the case, when the adsorbate interacts with protonated or deprotonated surface sites. It follows from this that molecules can be bound when they have a charge at least +1 or –1. Evidently, this molecular state is described by two successive ionization constants which determine a transition between these molecular states.

It is seen from equilibrium (27) that only K_2 and K_3 determine a relationship between molecules with charges +1, 0, -1. It can be assumed for any protein that:

$$\begin{matrix}[MH_2] & \overset{K_1}{\rightleftharpoons} & [MH] + [H] & \overset{K_2}{\rightleftharpoons} & [M] + [H] \\ +1 & & 0 & & -1 \end{matrix} \tag{28}$$

where K_1 and K_2 are ionization constants of amino acid residues responsible for a change in the protein. Thus, a $[MH_2]$–form will be bound on a cation exchanger, and a [M]–form on an anion exchanger. As Scopes has shown [39], adsorption of proteins despite their complex structure can be however described practically quantitatively by one "apparent" dissociation constant. If one takes into account that adsorption sites dissociate also in the range of pH to be studied, then equilibria in a general form can be represented as follows:

$$\begin{matrix}[LH] & \overset{K}{\rightleftharpoons} & [L] + [H] \\ + & & + \\ [M] & & [MH_2] \\ K_d \uparrow\downarrow & & K_d \uparrow\downarrow \\ [LHM] & & [LMH_2] \end{matrix} \tag{29}$$

For an *anion exchanger* the isotherm (Fig.13) has the form:

$$[LMH] = \frac{[L]_0[M]_{eq}}{K_d\left(1 + \frac{K}{[H]}\right)\left(1 + \frac{[H]}{K_2} + \frac{[H]^2}{K_1K_2}\right) + [M]_{eq}} \tag{30}$$

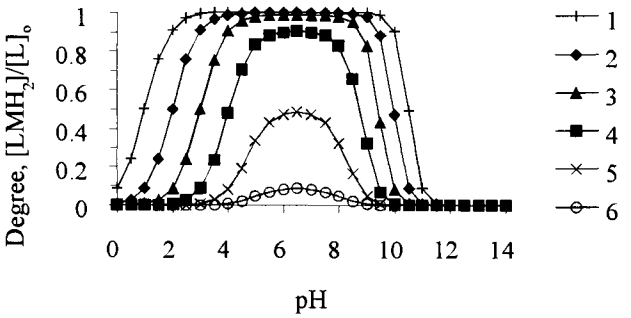

Figure 14. Adsorption of protonated dibasic molecules on deprotonated surface sites (cation exchanger). Curves were calculated from Eq. (31) using $K_d = 10^{-5}$ mol/l, $K = 10^{-5}$ mol/l, $K_1 = 10^{-8}$ mol/l, $K_2 = 10^{-9}$ mol/l; numbers in the legend are equilibrium concentrations of molecules $pM = -\log[M]_{eq}$.

but for a *cation exchanger* (Fig.14) it is

$$[LMH_2] = \frac{[L]_0[M]_{eq}}{K_d\left(1+\frac{[H]}{K}\right)\left(1+\frac{K_1}{[H]}+\frac{K_1K_2}{[H]^2}\right)+[M]_{eq}} \tag{31}$$

From equilibrium (28) it is seen that K_1 and K_2 constants determine the value of the isoelectric point of amphoteric molecules. In a general form the isoelectric point is equal to:

$$pI = \frac{(pK_1 + pK_2)}{2} \tag{32}$$

Thus, the equations of isotherms (30) and (31) can be used to determine the isoelectric points of proteins by the dependence of their sorption on pH. This approach is realized in Refs. [41,42]. However, it should be noted that this determination is only possible for a low affinity of protein molecules to surface sites. As Figs. 12 and 13 show, for a high affinity (a low K_d) a significant sorption is observed also at pH>pI for cation exchangers and at pH<pI for anion exchangers.

3.6. Dibasic surface sites and dibasic molecules (polyelectrolytes) in solution

Rather frequently the surface sites of modified silicas can also consist of two and more types of centres of diverse nature. For example, during modification of silica with γ-aminopropyl- triethoxysilane the surface practically always contains both ≡SiOH and $-CH_2CH_2CH_2NH_2$ groups. In this case the surface shows amphoteric properties and just as for polyelectrolytes we can write:

$$\underset{+1}{[LH_2]} \overset{K_1}{\rightleftharpoons} \underset{0}{[LH] + [H]} \overset{K_2}{\rightleftharpoons} \underset{-1}{[L] + [H]} \tag{33}$$

For convenience with regard to the notation for dissociation constants of surface sites and adsorbed molecules, Eq.(28) can be rewritten in the following form:

$$\underset{+1}{[MH_2]} \overset{K_3}{\rightleftharpoons} \underset{0}{[MH] + [H]} \overset{K_4}{\rightleftharpoons} \underset{-1}{[M] + [H]} \tag{28a}$$

As is seen from Eqs. (33) and (28a), in this case the consideration of equilibria becomes complicated, because the surface may interact both with the $[MH_2]$- and [M]- types of an adsorbate. Under the assumption that the interaction involves only oppositely charged surface sites and adsorbed particles, it is possible to write the following equilibria:

$$\begin{array}{ccc} [LH_2] & \overset{K_1}{\rightleftharpoons} [LH] + [H] & \overset{K_2}{\rightleftharpoons} [L] + [H] \\ + & & + \\ [M] & & [MH_2] \\ \uparrow\downarrow K_{d1} & & K_{d2} \uparrow\downarrow \\ [LH_2M] & & [LMH_2] \end{array} \tag{34}$$

If the sorption is observed only for the [M]-type ($K_{d1} \ll K_{d2}$), the isotherm equation takes the form

$$[LH_2M] = \frac{[L]_0[M]_{eq}}{K_{d1}\left(1 + \frac{K_1}{[H]} + \frac{K_1K_2}{[H]^2}\right)\left(1 + \frac{[H]}{K_4} + \frac{[H]^2}{K_3K_4}\right) + [M]_{eq}} \tag{35}$$

and when the adsorption involves only the $[MH_2]$-type ($K_{d1} \gg K_{d2}$), we get the following equation:

$$[LMH_2] = \frac{[L]_0[M]_{eq}}{K_{d2}\left(1 + \frac{[H]}{K_2} + \frac{[H]^2}{K_1K_2}\right)\left(1 + \frac{K_3}{[H]} + \frac{K_3K_4}{[H]^2}\right) + [M]_{eq}} \tag{36}$$

Fig. 15 displays the pH dependence of the degree of covering of the ampholyte surface with positively charged dibasic molecules. For negatively charged molecules (Eq. (35)), we can observe a nearly similar dependence. The only distinction is in the fact that for molecules with positive charges $[MH_2]$ the ascending curve sections are governed by the surface properties and the descending ones are determined by adsorbed molecule properties, while for negatively charged molecules [M] the situation is quite the reverse. As it is seen from Figs.13–15 when on the surface there are at the same time both acid and base sites (ampholyte), the ascending and descending curve sections are more steep than in the presence of only acid or only base sites (quadratic dependence on the concentration of hydrogen ions) respectively.

From the isotherms reported one can easily determine the distribution coefficient, i.e., the relation of concentrations of the sorbed and dissolved substance (equation (22)). In a general form, the distribution coefficient may be represented as follows:

$$D = \frac{[L]_0}{FK_d + [M]_{eq}} \tag{37}$$

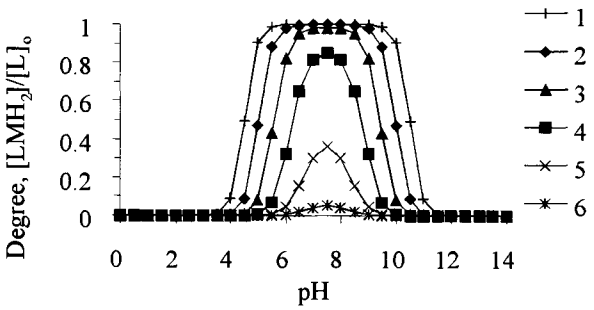

Figure 15. Adsorption of protonated dibasic molecules on deprotonated dibasic surface sites (ampholyte). Curves were calculated from Eq.(36) using $K_{d2} = 10^{-5}$ mol/l, $K_1 = 10^{-6}$ mol/l, $K_2 = 10^{-6}$ mol/l, $K_3 = 10^{-8}$ mol/l, $K_4 = 10^{-9}$ mol/l; numbers in the legend are equilibrium concentrations of molecules $pM = -\log[M]_{eq}$.

where $F = F_S F_M$ is the acidity function whose form is governed by the nature of the system studied, F_S is the acidity function of surface sites, F_M is the acidity function of adsorbed molecules (see, for example, above mentioned isotherms (24), (26), (30), (31), (35), (36) or the expression obtained for the case of a competition of soluble molecules for an adsorption site or a competition of soluble ligands for an adsorbing molecule (Eqs. (18), (21)).

4. RELATION OF THE SORPTION ISOTHERM TO THE PARAMETERS USED IN CHROMATOGRAPHY

A distribution coefficient is used widely in various areas involving two-phase systems [43,44] to describe behaviour of immobilized enzymes, electrode systems, different kinds of chromatographic separation and, in particular, makes it possible to correlate analytically parameters describing equilibria on a surface with parameters of column and thin-layer chromatography, whose success is determined mostly by extensive use of pristine and modified silicas as adsorbents and supports.

The principal equation of liquid chromatography has the form [45,46]:

$$V_R = V_M + DV_S \tag{38}$$

where V_R is the retention volume, V_M is the dead volume of the column, and V_S is the volume of the stationary phase (the volume of the liquid, the area of the surface, or the mass of the adsorbent), and D is the thermodynamic distribution coefficient, equal to the ratio between the concentrations of substance in the stationary and mobile phases.
In practice the capacity coefficient:

$$k^I = D\left(\frac{V_S}{V_M}\right) \tag{39}$$

is used more frequently.

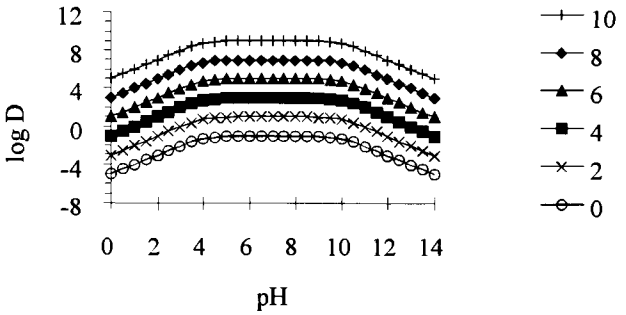

Figure 16. Dependence of distribution coefficient on pH. Curves were calculated from Eq. (33) using $[L]_0 = 10^{-4}$ mol/g, F from Eq. (24) with $K_1 = 10^{-4}$ mol/l, $K_2 = 10^{-10}$ mol/l, numbers in legend are $pK_d = \log K_d$, $[M]_{eq} \ll FK_d$.

By substituting (39) in (38) we obtain

$$V_R = V_M \left(1 + k^I\right) \tag{40}$$

Substituting Eq.(37) into Eq. (39) yields:

$$k^I = \frac{[L]_0}{FK_d + [M]_{eq}} \left(\frac{V_S}{V_M}\right) \tag{41}$$

Substituting (41) into (40) gives the relation between the parameters of the modified silica ($[L]_0$ and β), the retention volume, and the equlibrium concentration $[M]_{eq}$ of ions in solution, which makes it possible to obtain stability constants from chromatographic data. The value of k^I can also be determined by thin-layer chromatography [45]:

$$k^I = \frac{1}{R_f} - 1 \tag{42}$$

where R_f is the ratio between the rates of motion of the zone and of the solvent front.

As seen from equation (41) the k′ value can be varied by means of varying F that depends on pH and the nature of adsorption sites and adsorbate, and of varying K_d that is determined for a particular compound [M] only by properties of adsorption sites. Equations (40) and (41) can be used to estimate k′ and V_R. Thus, in liquid chromatography it is necessary that values of k′ should be between 1.5 and 4. In this case by varying the pH and consequently F, required values of the apparent constant $K_{app} = FK_d$ can be obtained. In concentrating ions and for using grafted metal complexes in catalysis the retention volume, and consequently also k′, should be very large. In affinity chromatography at first very large values of k′ are necessary to separate interfering proteins at first stages, following which they must be lowered by adding competing compounds[38,39,47,48]. As in the case of metal complexes, this can often be achieved by changing the pH of the medium.

5. CONCLUSIONS

Thus, the consideration of equilibria for the interaction of surface sorption sites with ions (or other species) in solution makes it possible to derive relations between many of the parameters used in various fields of application of pristine and modified silicas. Some of the results obtained are summerized in Table 1.

Table 1
Acidity function (pH-function) (See Eq. (37)) of various types of the sites (F_S) and of the adsorbed molecules (F_M)

Equilibria	Acidity function	
	F_S	F_M
Deprotonated monobasic sites and cations in solution	$\left(1+\frac{[H]}{K_a}\right)$	
Completely deprotonated dibasic sites and cations in solution	$1+\frac{[H]}{K_1}+\frac{[H]^2}{K_1K_2}$	
Single deprotonated dibasic sites and cations in solution	$1+\frac{[H]}{K_1}+\frac{K_2}{[H]}$	
Deprotonated surface sites and protonated molecules in solution	$1+\frac{[H]}{K_1}$	$1+\frac{K_2}{[H]}$
Protonated surface sites and deprotonated molecules in solution	$1+\frac{K_1}{[H]}$	$1+\frac{[H]}{K_2}$
Monobasic surface sites (anion exchanger) and dibasic molecules (polyelectrolytes) in solution	$1+\frac{K}{[H]}$	$1+\frac{[H]}{K_2}+\frac{[H]^2}{K_1K_2}$
Monobasic surface sites (cation exchanger) and dibasic molecules (polyelectrolytes) in solution	$1+\frac{[H]}{K}$	$1+\frac{K_1}{[H]}+\frac{K_1K_2}{[H]^2}$
Dibasic surface sites and dibasic molecules (polyelectrolytes) in solution (negatively charged molecules)	$1+\frac{K_1}{[H]}+\frac{K_1K_2}{[H]^2}$	$1+\frac{[H]}{K_4}+\frac{[H]^2}{K_3K_4}$
Dibasic surface site and dibasic molecules (polyelectrolytes) in solution (positively charged molecules)	$1+\frac{[H]}{K_2}+\frac{[H]^2}{K_1K_2}$	$1+\frac{K_3}{[H]}+\frac{K_3K_4}{[H]^2}$

It should be emphasized that although the isotherms presented apply only to the simple case of a single kind of sites on the surface, they reflect correctly behaviour of grafted ligands (surface chemical compounds).

ACKNOWLEDGEMENTS

The work was financially supported by the Foundation of Fundamental Investigations of the State Committee for Science and Technologies of Ukraine (Project No. 3.2/123).

REFERENCES

1. V.I. Belevantsev and B.I. Peshchevitskii, The Investigation of Complex Equilibria in Solution, Novosibirsk, 1978 (in Russian).
2. M. Beck, I. Nagypal, Chemistry of Complex Equilibria, Akademiai Kiado, Budapest, 1989.
3. D.A. Deranleau, J. Am. Chem. Soc., 91 (1969) 4044.
4. D.A. Deranleau, J. Am. Chem. Soc., 91 (1969) 4050.
5. W.E. Paul (ed.), Fundamental Immunology, Raven Press, New York,1984.
6. P.V. Sergeev and N.L. Shimanovskii, Receptors of Physiologically Active Substances Meditsina, Moscow, 1987 (in Russian).
7. V.D. Gorchakov,V.I. Serzhenko, and V.G. Vladimirov, Selective Hemosorbents, Meditsina, Moscow, 1989 (in Russian).
8. S.D. Varfolomeev (ed.), Modern Problems in Biokinetics, Moscow University, Moscow, 1987 (in Russian).
9. A.G. Marshall, Biophysical Chemistry, John Wiley and Sons, New York, Santa Barbara, Chichester, Brisbano, Toronto, 1978.
10. J.L. Webb, Enzyme and Metabolic Inhibitors, Academic Press, New York and London,1963.
11. M. Dixon and E.C. Webb, Enzymes, Longman Group Ltd., 1979.
12. R. B. Martin, Introduction to Biophysical Chemistry, McGraw-Hill Book Company, New York, San Francisco, Toronto, London, 1964.
13. R.G. Bates, Determination of pH. Theory and Practice, John Wiley and Sons Inc., New York, London, Sydney, 1964.
14. A.E. Martell and R.M. Smith (eds.), Critical Stability Constants, Plenum Press, New York, London, 1974.
15. G.V. Lisichkin (ed.), Modified Silicas in Sorption, Catalysis and Chromatography, Khimiya, Moscow, 1986 (in Russian).
16. A.P. Filippov, Teoret. Eksperim. Khimiya., 21 (1985) 693.
17. A.P. Filippov, Teoret. Eksperim. Khimiya., 19 (1983) 463.
18. K.B. Yatsimirskii, Teoret. Eksperim.Khimiya., 16 (1980) 34.
19. K.B. Yatsimirskii and Ya.D. Lampeka,Physical Chemistry of Complexes of Metals with Macrocyclic Ligands, Naukova Dumka, Kiev, 1985 (in Russian).
20. C. Tanford, Physical Chemistry of Macromolecules,Wiley and Sons , Inc., New York, 1961.
21. G.V.Kudryavtsev, Zhurn. Fiz. Khimii., 61 (1987) 468.
22. D.I. Hitchcock, J. Am. Chem. Soc., 48 (1926) 2870.
23. V.A. Tertykh,V.V. Yanishpolskii, Teoret. Eksperim. Khimiya, 27 (1991) 361.
24. R.K. Iler, The Chemistry of Silica, A Wiley-Interscience Publication , New York, Chichester, Brisbano, Toronto, 1979.
25. G.H.Bolt, J.Phys.Chem., 61 (1957) 1166.

26. V.A. Tertykh, V.V. Yanishpolskii , and S.S. Kotlyar, Kolloid. Zhurn., 44 (1982) 1114.
27. J.A. Marinsky, Coord.Chem.Rev.,19 (1976) 125.
28. B.V. Zhmud, A.A.Golub, Zhurn. Fiz. Khimii, 67 (1993) 734.
29. B.V. Zhmud, A.A.Golub, J. Colloid Interface Sci.,167 (1994) 186.
30. E. Wagner, H. Brunner, Angew.Chem., 72 (1960) 744.
31. L.H. Allen, E. Matijevic, L. Meites, J. Inorg. Nucl.Chem., 33 (1971) 1293.
32. A.N. Chebotarev, V.G. Markova, Ukr. Khim. Zhurn., 57 (1991) 1073.
33. P.W. Schindler , B. Wrst, R. Dick, P. Wolf, J. Colloid Interface Sci., 55 (1976) 469.
34. S.A. Ogii, V.V. Yanishpolskii, V.A. Tertykh, Ukr. Biokhim. Zhurn., 62 (1990) 48.
35. Yu.V. Kholin, S.A. Mernii, Zhurn. Fiz. Khimii, 67 (1993) 2229.
36. V.V. Skopenko, Yu.V. Kholin, V.N. Zaitsev, S.A. Mernii, D.S. Konyaev, Zhurn. Fiz. Khimii, 67 (1993) 728.
37. Yu.V. Kholin, V.N. Zaitsev, S.A. Mernii, N.D. Donskaya, L.N. Chistyakova, Ukr. Khim. Zhurn., 59 (1993) 910.
38. R.K. Scopes, Anal. Biochem.,114 (1981) 8.
39. R.K. Scopes, Protein Purification, Springer–Verlag, New York, Heidelberg, Berlin, 1982.
40. V.M. Kolikov, B.V. Mchedlishvili, Chromatography of Biopolymers on Macroporous Silicas, Nauka, Leningrad, 1986 (in Russian).
41. G.P. Lampson, A.A. Tytell, Anal. Biochem., 11 (1965) 374.
42. V.C. Yang, R. Langer, Anal. Biochem., 147 (1985) 148.
43. J.B. Taylor, H.E.Swaisgood, Biotechnol. and Bioeng., 23 (1981) 1349.
44. M. Jaroniec, J. Chromatogr., 656 (1993) 37.
45. H.Engelhardt, Hochdruck–Flussigkeits–Chromatographie, Springer – Verlag, Berlin, Heidelberg, New York, 1977.
46. P.J.Schoenmakers, Optimization of Chromatographic Selectivity, Elsevier, Amsterdam, Oxford, New York, Tokyo, 1986.
47. J.Turkova, Affinity Chromatography, Elsevier, Amsterdam, Oxford, New York, Tokyo, 1978.
48. P.D.G. Dean, W.S. Johnson, F.A. Middle (eds.), Affinity Chromatography, IRL Press, Oxford, Washington DC, 1985.

This Page Intentionally Left Blank

A. Dąbrowski and V.A. Tertykh (Editors)
Adsorption on New and Modified Inorganic Sorbents
Studies in Surface Science and Catalysis, Vol. 99

Chapter 3.4
Adsorption from dilute solutions – some novel aspects

P. Nikitas

Laboratory of Physical Chemistry, Department of Chemistry,
Aristotle University of Thessaloniki, 54006 Thessaloniki, Greece

1. INTRODUCTION

The conventional approach which is followed in the theoretical description of adsorption from solution is based on the solvent–replacement reaction [1–5]:

$$A_i^b + n_i S^s \rightleftharpoons A_i^s + n_i S^b \quad (1)$$

which describes the adsorption of the i–th solute (A_i) from the bulk (b) of a non electrolyte solution at the surface phase (s) via the replacement of n_i solvent molecules (S). The adsorption isotherms arise directly from this equation by applying the mass action law and they are usually expressed in terms of mole fractions and the corresponding activity coefficients of the constituents in the bulk solution and at the adsorbed layer. Problems appear in the calculation of the activity coefficients, which is strictly achieved on the basis of molecular theories, like the regular solution theory. A number of models based on this approach are presented and discussed in [5].

Recent studies [6–14] on adsorption from electrolyte solutions on energetically homogeneous electrode surfaces, like the surface of the Hg electrode, show that at least for aqueous solutions the above approach should be re–examined in two respects: first in what concerns the adsorption mechanism (1) and second the treatment of the intermolecular interactions at the surface solution. The adsorption mechanism (1) should be re–examined since, using a thermodynamic method proposed for the determination of the size ratio parameter n_i, the value $n_i = 1 \pm 0.2$ has been found for a variety of experimental systems, despite the fact that the adsorbate molecules can have dimensions considerably different from those of the solvent molecules [6–11]. In what concerns the intermolecular interactions, in the presence of polar molecules a significant contribution arises from the electric field across the surface solution, which is created by their dipoles [7,12–14]. Similarly, an electric field is established when ions, either from an electrolyte in the bulk solution or from impurities, penetrate the surface solution. In both cases this field is expected to have a dominant effect on the surface activities.

In this chapter the above phenomena are examined in detail. As a result new adsorption isotherms are developed, which can take into account changes in the surface layer dielectric constant, thickness and orientation of the adsorbed species during the adsorption process. The effect of ions adsorption is also examined. Finally, their extension to

include heterogeneity effects, which are frequently encountered during the adsorption on solid surfaces, is considered.

2. THE SIZE RATIO PARAMETER

2.1. Definition of the size ratio parameter

In adsorption studies the size ratio parameter, n, is defined as the number of solvent molecules replaced from the adsorbed layer by one molecule of the adsorbate. This is a definition at a molecular level. An alternative definition of n as a purely thermodynamic quantity is given by the ratio

$$n = A_A/A_S \tag{2}$$

where A_A and A_S are the partial surface areas of the adsorbate (A) and solvent (S) respectively at the adsorbed layer. The relationship between the molecular and the thermodynamic size ratio parameter can be established only if we assume a certain model for the adsorbed layer. This is attempted below.

2.2. A thermodynamic determination of n

Recently we have proposed a thermodynamic method, which allows the experimental evaluation of n [6–8]. The prerequisites needed for the application of the method are the following: the adsorbed layer should be composed of solvent and constant orientated adsorbate molecules and its thickness should be equal to one molecular diameter of adsorbate molecules. These conditions can be safely detected experimentally and if they are fulfilled, n may be obtained from surface pressure data by means of the following equation [8]:

$$n = \lim_{\theta \to 1} \frac{\theta(1 - B)}{B(1/x_S^b - \theta) - x_A^b/x_S^b} \tag{3}$$

where

$$B = \exp\left\{\ln a_A^b - \Pi A_S/RT + \lambda\right\} \tag{4}$$

and

$$\lambda = -\lim_{\theta \to 1} \left\{\ln a_A^b - \Pi A_A/RT\right\} \tag{5}$$

In these equations θ is the adsorbate surface coverage calculated from surface pressure data by means of the Gibbs adsorption equation, x_A^b, x_S^b are the mole fractions of the adsorbate and solvent respectively in the bulk solution, a_A^b is the activity of the adsorbate in the bulk solution, $\Pi(= \gamma^0 - \gamma)$ is the experimental surface pressure of the adsorbed film, γ is the surface tension of the test solution, γ^0 is the value of γ of the pure solvent, R is the gas constant and T is the temperature.

It is seen that n is derived by means of two extrapolations. Due to these extrapolations the method is extremely sensitive to experimental errors and for this reason it is applicable only to air / solution and liquid / liquid interfaces. Up to now the method has been applied to the air / aqueous, Hg / aqueous, and Hg / methanolic solution interfaces. In all cases

the value $n = 1 \pm 0.2$ was found, despite the considerable differences in the size of the adsorbates used [6,7,10].

2.3. Molecular significance of n

The molecular significance of n and particularly of the value $n = 1 \pm 0.2$ can be emerged only if we analyse it in terms of molecular models of the adsorbed layer. Thus, let us suppose that at an adsorbed layer with thickness of one diameter of the adsorbate molecules the solvent molecules do not associate on the adsorbing surface and form m layers on it. In this case, the area of the adsorbed layer A can be expressed as:

$$A = N_A S_A + N_S(S_S/m) \tag{6}$$

where S_A, S_S are the projected areas of the adsorbate and solvent molecules on the adsorbing surface and N_A, N_S are the number of molecules of the adsorbate and solvent at the surface solution. However, from Euler's theorem we have [15]:

$$A = N_A A_A + N_S A_S \tag{7}$$

and therefore

$$n = A_A/A_S = mS_A/S_S \tag{8}$$

where $m \geq 1$. Now if we take into account that in aqueous solutions $S_S \approx 0.1$ nm^2 and $S_A > 0.24$ nm^2, then the value $n \approx 1$ clearly indicates that the solvent cannot exist in the form of monomers.

The value $n \approx 1$ can be explained if we assume that clusters of solvent molecules with dimensions similar to the adsorbate molecules pre-exist on the electrode surface. In this case $A_A \approx A_S$ and therefore $n \approx 1$. However, it is rather improbable that the water molecules adjust themselves into displaceable clusters equivalent to the area of the adsorbate for various sizes of the latter [16].

A more reasonable explanation of the value $n \approx 1$ is given in [11]. Suppose that the solvent molecules associate at the surface solution to form clusters S_c with dimensions quite greater than those of the adsorbate molecules. Such clusters are not expected to behave like compact organic molecules and therefore they can break upon the adsorption of the adsorbate.

In particular, according to this adsorption mechanism, each adsorbate molecule A cuts from S_c a smaller cluster S_A of solvent molecules with equivalent to A dimensions and displaces it towards the bulk solution, where it is disintegrated into g monomeric solvent molecules. Thus, irrespective of the size of the original solvent clusters S_c the adsorbate molecules do not "see" either these clusters or the monomeric solvent molecules but only the clusters S_A, which have always dimensions equal to those of the adsorbate molecules. In this respect the adsorbed layer behaves as if it were composed of adsorbate A molecules and solvent clusters S_A with equal dimensions. For this reason, this adsorption mechanism is compatible with a value of n close to unity. Moreover, if it is analysed within the frames of classical thermodynamics, we obtain that the adsorption equilibrium may be described by the following equation [11]:

$$\overline{\mu}_A - \mu^s_{S_A} = \mu^b_A - g\mu^b_S = \mu^{0,b}_A - g\mu^{0,b}_S + kT \ln \left\{ a^b_A / \left(a^b_S \right)^g \right\} \tag{9}$$

where $\overline{\mu}_A$ denotes in general the adsorbate chemical (for neutral adsorbates) or electrochemical (for ionic species) potential at the surface solution, $\mu^s_{S_A}$ is the surface chemical potential of the clusters S_A and μ^b_i is the chemical potential of the i–th species in the bulk solution. If the adsorbate is a neutral compound, its surface chemical potential may be symbolised by μ^s_A instead of $\overline{\mu}_A$.

Equation (9) shows that, at least formally and despite the fact that the solvent clusters S_A pre–exist only potentially and appear just at the moment of the adsorption process, the equilibrium properties of this process can be described in terms of the chemical potentials of the clusters S_A.

At multicomponent surface solutions the existence of large solvent clusters S_c affects the mathematical formulation of the equilibrium equations as follows. Suppose that the adsorbed layer is composed of polar solvent molecules, which form clusters S_c bigger than the adsorbate molecules, and N monomeric adsorbate species, A_1, A_2, ... , A_N, which may be N distinct states of the same adsorbate or N different adsorbate molecules. According to the arguments presented in [17] and above, the adsorption process may be described by the following system of equilibrium equations:

$$\overline{\mu}_{A_i} - \mu^s_{S_i} = \mu^b_{A_i} - g_i\mu^b_S = \mu^{0,b}_{A_i} - g_i\mu^{0,b}_S + kT \ln\left\{a^b_{A_i} / \left(a^b_S\right)^{g_i}\right\} \quad (i = 1, 2, \ldots, N) \tag{10}$$

which show that the adsorbed layer behaves as a surface solution composed of 2N species: N adsorbate species A_1, A_2, ..., A_N and N kinds of solvent clusters S_1, S_2, ..., S_N, with dimensions equal to those of A_1, A_2, ..., A_N, respectively. Note again that these solvent clusters exist only potentially at the adsorbed layer and appear just at the moment when a bulk adsorbate molecule assails an original cluster S_c. It is evident that if the adsorbate species A_i have different dimensions, then the clusters S_i will also have different dimensions.

We should point out that in [17] the chemical potentials $\mu^s_{S_i}$ in Eq. (10) have been substituted by $r_i\mu^s_{S_1}$, where $r_i = g_i/g_1$, since [17]:

$$\mu^s_{S_i} = r_i\mu^s_{S_1} \tag{11}$$

However, this substitution must be avoided, because Eq. (11) in fact presumes the equilibrium among the solvent clusters S_1, S_2, ..., S_N. But such an equilibrium cannot be established, since these solvent clusters are not independent species and exist only potentially at the adsorbed layer.

If the solvent does not associate on the adsorbing surface, or its association does not affect the adsorption mechanism which takes place via the displacement of single solvent molecules, then the equilibrium is described from the well known system of equations:

$$\overline{\mu}_{A_i} - n_i\mu^s_S = \mu^b_{A_i} - n_i\mu^b_S = \mu^{0,b}_{A_i} - n_i\mu^{0,b}_S + kT \ln\left\{a^b_{A_i} / \left(a^b_S\right)^{n_i}\right\} \quad (i = 1, 2, \ldots, N) \tag{12}$$

where $n_i = g_i$.

To sum up the application of the thermodynamic method for the determination of n has given rather strong indications about the formation of large water clusters, which in aqueous solutions favour an adsorption mechanism like that described by Eqs. (9) and (10). There are also indications that the same behaviour is likely when adsorption takes place from non aqueous but polar solvents, like methanol. In contrast, the surface

behaviour of non polar solvents remains obscure. Thus, a lot of work on this topic is still to be carried out.

3. SURFACE CHEMICAL POTENTIALS FOR SPECIES ADSORBED ON HOMOGENEOUS SURFACES

3.1. Introduction

The equilibrium properties of an adsorbed layer can be examined based on the chemical or electrochemical potentials of the constituents of this layer and the equilibrium equations derived in the section above. This is the simplest approach, although problems might appear in the description of the adsorbed layer properties during a surface phase transition [18]. Alternatively, the chemical potentials may be used for the determination of the grand ensemble partition function of the adsorbed layer, which in turn is used for the derivation of the equilibrium equations. This approach is mathematically more complex, but it leads to a better description of an adsorbed layer when it undergoes a phase transformation [18]. The present analysis for simplicity is restricted to the first approach.

The chemical potential of an adsorbed species is affected by differences in size of the constituents of the adsorbed layer, the interactions of the adsorbed particles with the two bulk phases, and the particle–particle interactions within the adsorbed layer. The differences in size of the adsorbed particles may be taken into account by means of lattice statistics [13,19–22]. The interactions of an adsorbed particle with the two adjacent bulk phases are, to a good approximation, independent of the surface composition, provided that the adsorbing surface is energetically homogeneous. Therefore, in this case they can be taken into account by adding a constant to the chemical potentials. In contrast, when the adsorbing surface is energetically heterogeneous, a more precise treatment, which depends on the topography of the surface, is needed [4,5]. Finally, in what concerns the particle–particle interactions, the short–range London type interactions may be taken into account by means of lattice statistics. Such studies are already known in literature [4,19,23–29]. These interactions are expected to have a predominant contribution to the chemical potentials in case of adsorbed layers composed of non polar molecules. In contrast, in adsorbed layers composed of polar solvent or/and adsorbate molecules the main contribution to the chemical potentials should arise from the long–range dipole–dipole Coulombic forces.

Within the frames of the regular solution approach adopted in [4,19,23–29] the dipole–dipole interactions are treated similarly with the short–range ones and for this reason in many cases no distinction between these interactions is made. The dipole–dipole interactions arise from the electric field which is established due to the dipoles of the adsorbed particles. This feature is taken into account here to develop an alternative approach to treat these interactions. The treatment concerns adsorbed layers on energetically homogeneous surfaces. This is a necessary step in formulating an adsorption theory for heterogeneous surfaces, which is presented in section 5.

3.2. Analytical expressions for chemical / electrochemical potentials of adsorbed species

Consider an adsorbed layer with area A and thickness l composed of N species, which may be the solvent molecules, molecules of neutral organic adsorbates and ions of various types, which are denoted by 1, 2, ..., N_I. The ions may have differences in size. For this reason we further assume that the locus of the centres of ions 1, 2, ..., m_1 determines the plane 1 of Fig. 1, the locus of the centres of ions $m_1 + 1$, $m_1 + 2$, ..., m_2 determines the plane 2, etc. Thus, a general subdivision of the adsorbed layer into m sublayers with thickness l_1, l_2, ..., l_m is adopted.

If one or more species have polar molecules, then due to their dipole moment vectors an electric field may be established in the adsorbed layer. In particular, the normal to the adsorbing surface components of the dipoles leads to the development of a potential drop across the adsorbed layer. We denote the total potential difference across the entire adsorbed layer by $\Delta\varphi = \varphi^a - \varphi^m$, where φ^a, φ^m are the inner potentials at the adsorbing surface and at the plane m, respectively. Similarly, the in-plane components of the dipoles may establish a potential drop, $\Delta\psi$, along an arbitrary axis y parallel to the adsorbing surface (Fig. 2). The in-plane field appears only when configurations of rows of dipoles parallel to the adsorbing surface are formed. In contrast, if the dipole in-plane components are randomly oriented throughout the surface, then $\Delta\psi = 0$.

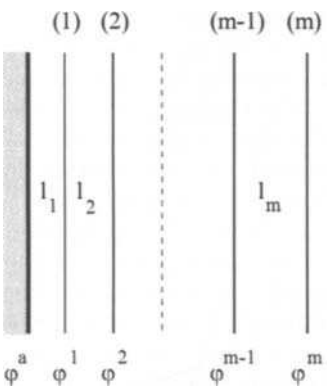

Figure 1. A schematic division of an adsorbed layer into m sublayers in the presence of ions with different radii.

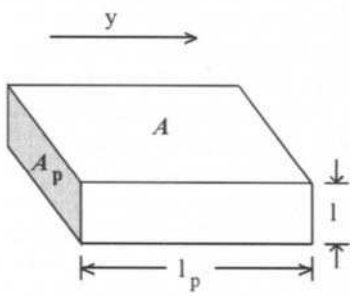

Figure 2. A schematic model of an adsorbed layer with thickness l and area A.

In order to examine the effect of the electric field of the dipoles to the chemical / electrochemical potentials, we define the new thermodynamic function

$$\Phi = U - TS + pV - Q_n\Delta\varphi - Q_p\Delta\psi \tag{13}$$

where U, S, V are the internal energy, entropy and volume of the adsorbed layer, respectively, p is the pressure, T is the temperature, Q_n is the induced charge on the surface of the adsorbed layer which is adjacent to the adsorbing surface and Q_p is the induced charge due to the potential drop $\Delta\psi$ at the lateral area A_p of the adsorbed layer depicted in Fig.2.

The total differential of the internal energy is given by [15,30,31]:

$$dU = TdS - pdV + \gamma dA + dU^{el} + \sum_{i=1}^{N} \mu_i dN_i \tag{14}$$

where the infinitesimal work due to the electric field dU^{el} may be expressed as [31]:

$$dU^{el} = \int_A \varphi d\sigma dA + \int_V \varphi d\sigma dV = \sum_{k=1}^{m} \varphi^k dQ^k \tag{15}$$

Here, σ denotes the charge density and φ the inner potential. Note that the adsorbed ions are located at the planes 1, 2, ..., m–1, whereas plane m determines the thickness of the adsorbed layer. The charge of these ions is counterbalanced by the charge of the "diffuse" layer, which extends from plane m up to the homogeneous electrolyte solution. Hence, from the electroneutrality condition of the whole interface we have:

$$Q^m = -Q^1 - Q^2 - \ldots - Q^{m-1} \tag{16}$$

and therefore

$$dU^{el} = \sum_{k=1}^{m} z_i e^0 \varphi^i dN_i - \sum_{k=1}^{m} z_i e^0 \varphi^m dN_i \tag{17}$$

where z_i is the charge number of the i–th ions, e^0 is the proton charge and φ^i is the inner potential of the plane where the centre of an i–th ion is located. That is, φ^i can take the values φ^1, φ^2, ..., φ^{m-1}. If this expression of dU^{el} is introduced into Eq. (14) and take into account: a) Euler's theorem expressed by Eq. (7) and b) the definition of the electrochemical potential of ions from

$$\overline{\mu}_i = \mu_i + z_i e^0 \varphi^i \tag{18}$$

then we obtain for the total differential of Φ the following expression:

$$d\Phi = -SdT + Vdp - Q_n d\Delta\varphi - \Delta\varphi dQ_n - Q_p d\Delta\psi - \Delta\psi dQ_p + \sum_{i=1}^{N} \left(\overline{\mu}_i - z_i e^0 \varphi^m + \gamma A_i\right) dN_i \tag{19}$$

We should point out that the sum in this equation includes charged ions as well as uncharged species. In the later case $z_i = 0$ and the electrochemical potentials $\overline{\mu}_i$ become chemical potentials μ_i^s.

The induced charge Q_n may be expressed in terms of $\Delta\varphi$ and N_i as follows. If P is the total polarization of the adsorbed layer due to the normal to the adsorbing surface components of the dipoles, then under the assumption that the induced polarization is proportional to the field $\Delta\varphi/l$ we have [14,32]:

$$P = VQ_n/A = Q_n l = P_\mu - P_\alpha = \sum_{i=1}^{N} P_{in} N_i - \sum_{i=1}^{N} \alpha_{in} N_i \Delta\varphi/l \tag{20}$$

Here, P_μ is the dipole polarization, due to orientation of the permanent dipoles normal to the adsorbing surface, P_α is the induced polarization, caused by translation effects, P_{in} is the average value of the permanent dipole vector normal to the adsorbing surface of the i–th species and α_{in} is its polarizability. From the electrostatic theory of dielectrics, as well as from simple molecular models, we know that P_{in} is constant and independent of the electric field when the adsorbed species retain a certain orientation on the adsorbing surface. When an adsorbed species reorientates, then we can examine this process by assuming the existence of q distinct polarization states of the adsorbed species on the adsorbing surface. These distinct states of an adsorbed molecule can be treated as q different adsorbed species, with different values of P_{in}. Therefore, a reorientation process on the adsorbing surface may be treated by increasing the number of the adsorbed species. Equation (20) yields:

$$Q_n = \sum_{i=1}^{N} \left(p_{in}/l - \alpha_{in}\Delta\varphi/l^2 \right) N_i \tag{21}$$

An alternative expression of Q_n may be derived if we assume that the electric field across the monolayer is homogeneous only across the subregions defined above. Then from the Gauss theorem of electrostatics we obtain:

$$\varepsilon_0 \left(\varphi^a - \varphi^1 \right) A/l_1 = Q_n \tag{22}$$

$$\varepsilon_0 \left(\varphi^1 - \varphi^2 \right) A/l_2 = Q_n + Q^1 \tag{23}$$

.....

$$\varepsilon_0 \left(\varphi^{m-1} - \varphi^m \right) A/l_m = Q_n + Q^1 + \ldots + Q^{m-1} \tag{24}$$

where ε_0 is the permitivity of a vacuum and Q^1, Q^2, ..., Q^{m-1} are the charges due to the adsorbed ions at the planes 1, 2, ..., m–1. The sum of these equations yields the following expression for the induced charge Q_n:

$$Q_n = \varepsilon_0 A\Delta\varphi/l - \sum_{i=1}^{N} z_i e^0 N_i (l - \rho_i)/l \tag{25}$$

where ρ_i is the radius of the i–th ions. We note again that the sum of Eq. (25) includes and uncharged species with $z_i = 0$.
Similar calculations yield the expressions:

$$Q_p = \sum_{i=1}^{N} \left(P_{ip}/l_p - \alpha_{ip}\Delta\psi/l_p^2 \right) N_i \tag{26}$$

and

$$Q_p = \varepsilon_0 A_p \Delta\psi/l_p \tag{27}$$

The physical meaning of A_p, l_p is given in Fig. 2, where for simplicity an adsorbed layer with the shape of a rectangular parallelepiped is shown.

Equations (21), (25) - (27), in combination with Eq. (19), yield:

$$d\Phi = -SdT + Vdp - \left\{\varepsilon_0\Delta\psi A_p/l_p - \sum_{i=1}^{N}\alpha_{ip}N_i\Delta\psi/l_p^2\right\}d\Delta\psi -$$
$$-\left\{\varepsilon_0\Delta\varphi A/l - \sum_{i=1}^{N}z_ie^0N_i(1-\rho_i)/l - \sum_{i=1}^{N}\alpha_{in}N_i\Delta\varphi/l^2\right\}d\Delta\varphi +$$
$$+\sum_{i=1}^{N}\left\{\overline{\mu}_i - z_ie^0\varphi^m + \gamma A_i - P_{in}\Delta\varphi/l + \alpha_{in}\Delta\varphi^2/l^2 - P_{ip}\Delta\psi/l_p + \alpha_{ip}\Delta\psi^2/l_p^2\right\}dN_i \quad (28)$$

At this point it is worth noting the following. The adsorbed layer is not an autonomous phase [15] and therefore the validity of Eq. (28) may be questioned. However, we have shown in [33,34] that the interactions of the adsorbed layer with the two phases which form it, i.e. the adsorbent and the solution, do not affect the form of this equation, since they may be included in the entropy S of the adsorbed layer.
Equation (28) by cross-differentiation gives:

$$\left(\frac{\partial\left(\overline{\mu}_i - z_ie^0\varphi^m + \gamma A_i - P_{in}\Delta\varphi/l + \alpha_{in}\Delta\varphi^2/l^2 - P_{ip}\Delta\psi/l_p + \alpha_{ip}\Delta\psi^2/l_p^2\right)}{\partial\Delta\varphi}\right)_{T,p,\Delta\psi,N_i} =$$
$$= -\left(\frac{\partial\left(\varepsilon_0\Delta\varphi A/l - \sum z_ie^0N_i(1-\rho_i)/l - \sum\alpha_{in}N_i\Delta\varphi/l^2\right)}{\partial N_i}\right)_{T,p,\Delta\varphi,\Delta\psi,N_{k\neq i}} =$$
$$= -\varepsilon_0\Delta\varphi A_i/l - z_ie^0(1-\rho_i)/l + \alpha_{in}\Delta\varphi/l^2 \quad (29)$$

which, after integration along a path of constant temperature, pressure, potential difference $\Delta\psi$ and composition, results in:

$$\overline{\mu}_i - z_ie^0\varphi^m + \gamma A_i - P_{in}\Delta\varphi/l + \alpha_{in}\Delta\varphi^2/l^2 - P_{ip}\Delta\psi/l_p + \alpha_{ip}\Delta\psi^2/l_p^2 =$$
$$\mu_i^*(T,p,\Delta\psi,N_1,N_2,\ldots) - \varepsilon_0\Delta\varphi^2A_i/2l - z_ie^0(1-\rho_i)\Delta\varphi/l - \alpha_{in}\Delta\varphi^2/2l^2 \quad (30)$$

The term $\mu_i^*(T,p,\Delta\psi,N_1,N_2,\ldots)$ can be expressed as a function of $\Delta\psi$ if Eq. (30) is differentiated with respect to $\Delta\psi$ assuming constant T, p,$\Delta\varphi$, N_i values and make use of the cross-differential result:

$$\left(\frac{\partial\left(\overline{\mu}_i - z_ie^0\varphi^m + \gamma A_i - P_{in}\Delta\varphi/l + \alpha_{in}\Delta\varphi^2/l^2 - P_{ip}\Delta\psi/l_p + \alpha_{ip}\Delta\psi^2/l_p^2\right)}{\partial\Delta\psi}\right)_{T,p,\Delta\varphi,N_i} =$$
$$= -\left(\frac{\partial\left(\varepsilon_0\Delta\psi A_p/l_p - \sum\alpha_{ip}N_i\Delta\psi/l_p^2\right)}{\partial N_i}\right)_{T,p,\Delta\varphi,\Delta\psi,N_{k\neq i}} =$$
$$= -\varepsilon_0\Delta\psi A_i l/l_p^2 + \alpha_{ip}\Delta\psi/l_p^2 \quad (31)$$

Then after integration we obtain:

$$\mu_i^*(T,p,\Delta\psi,N_1,N_2,\ldots) = \mu_i^*(T,p,N_1,N_2,\ldots) - \varepsilon_0\Delta\psi^2A_il/2l_p^2 + \alpha_{ip}\Delta\psi^2/2l_p^2 \quad (32)$$

which in combination with Eq. (30) results in:

$$\overline{\mu}_i = \mu_i^*(T, p, N_1, N_2, \ldots) + z_i e^0 \varphi^m + z_i e^0 \Delta\varphi(l - \rho_i)/l - \gamma A_i + P_{in}\Delta\varphi/l + P_{ip}\Delta\psi/l_p - \varepsilon_0\varepsilon_{in}(\Delta\varphi/l)^2 A_i l/2 - \varepsilon_0\varepsilon_{ip}(\Delta\psi/l_p)^2 A_i l/2 \quad (33)$$

Here, the quantities ε_{in} and ε_{ip} are defined from:

$$\varepsilon_{in} = 1 + \alpha_{in}\varepsilon_0 A_i l \qquad \varepsilon_{ip} = 1 + \alpha_{ip}/\varepsilon_0 A_i l \quad (34)$$

and, according to the usual Laplace–Debye equation [35], they express "distortional" dielectric constants of the monolayer when it consists exclusively of the i–th species.

It is seen that in order to compute an explicit dependence of the chemical potential $\overline{\mu}_i$ on the surface composition, the dependence of $\Delta\varphi$ and $\Delta\psi$ upon the composition of the adsorbed layer is needed. This interconnection arises directly from Eqs. (21), (25) - (27), which yield:

$$\Delta\varphi/l = \sum_{i=1}^{N} \left\{P_{in} + z_i e^0(l - \rho_i)\right\} \theta_i/\varepsilon_0\varepsilon_n l A_i \quad (35)$$

$$\Delta\psi/l_p = \sum_{i=1}^{N} P_{ip}\theta_i/\varepsilon_0\varepsilon_p l A_i \quad (36)$$

In these equations θ_i is the surface coverage of the i–th species defined from:

$$\theta_i = N_i A_i/A \quad (37)$$

and ε_n, ε_p are "distortional" dielectric constants of the adsorbed layer, since they are given by:

$$\varepsilon_n = \sum_{i=1}^{N} \varepsilon_{in}\theta_i \quad \text{and} \quad \varepsilon_p = \sum_{i=1}^{N} \varepsilon_{ip}\theta_i \quad (38)$$

Equation (33) expresses the electrochemical potential of every neutral or ionic species adsorbed at an uncharged interface. It can be simplified considerably when the adsorbed layer consists of only two components, neutral solvent (S) molecules and adsorbate (A) neutral or ionic species. Then Eq. (33) yields:

$$\{\overline{\mu}_A - \overline{\mu}_A(\theta = 1)\}/kT = \{\mu_A^* - \mu_A^*(\theta = 1)\}/kT - \left(\gamma - \gamma^{0*}\right) A_A/kT + z_A e^0 [\varphi^m - \varphi^m(\theta = 1)]/kT + nB_n(1 - \theta)^2/\varepsilon_{An}\varepsilon_n^2 + nB_p(1 - \theta)^2/\varepsilon_{Ap}\varepsilon_p^2 \quad (39)$$

$$\{\mu_S^s - \mu_S^s(\theta = 0)\}/kT = \{\mu_S^* - \mu_S^*(\theta = 0)\}/kT - (\gamma - \gamma^0)A_S/kT + B_n\theta^2/\varepsilon_{Sn}\varepsilon_n^2 + B_p\theta^2/\varepsilon_{Sp}\varepsilon_p^2 \quad (40)$$

In these equations γ^0 and γ^{0*} are the values of the surface tension γ in the limits $a_A^b \to 0$ and $a_A^b \to 1$, respectively, θ is the surface coverage of the adsorbate and the constants B_n, B_p are given by:

$$B_n = -\left(\varepsilon_{An}P_{Sn} - \varepsilon_{Sn}P_{An}A_S/A_A\right)^2/2A_S\varepsilon_0 lkT \quad (41)$$

$$B_p = -(\varepsilon_{Ap}P_{Sp} - \varepsilon_{Sp}P_{Ap})^2 / 2A_S\varepsilon_0 lkT \tag{42}$$

If there is no anisotropy of the polarizability, then $\varepsilon = \varepsilon_n = \varepsilon_p$ and Eqs. (39), (40) are further simplified to:

$$\{\overline{\mu}_A - \overline{\mu}_A(\theta = 1)\}/kT = \{\mu_A^* - \mu_A^*(\theta = 1)\}/kT - \left(\gamma - \gamma^{0^*}\right) A_A/kT + \\ + z_A e^0 [\varphi^m - \varphi^m(\theta = 1)]/kT + nB(1-\theta)^2/\varepsilon_A\varepsilon^2 \tag{43}$$

$$\{\mu_S^s - \mu_S^s(\theta = 0)\}/kT = \{\mu_S^* - \mu_S^*(\theta = 0)\}/kT - \left(\gamma - \gamma^0\right) A_S/kT + B\theta^2/\varepsilon_S\varepsilon^2 \tag{44}$$

where $B = B_n + B_p$.

In Appendix we show that the expression of chemical potentials given by Eq. (33) takes into account the long–range lateral interactions among the adsorbed particles due to the normal to the adsorbing surface components of their dipoles. Similarly it can be shown that the in– plane interactions of their dipoles contributes also to the expression of Eq. (33). In what concerns the short–range interactions and / or the repulsive long–range Coulombic interactions among adsorbed ions, they are implicitly included in the term $\mu_i^*(T, p, N_1, N_2, \ldots)$. Indeed this term is the chemical potential in the absence of the fields $\Delta\varphi$, $\Delta\psi$ and changes in the area A. That is, $\mu_i^*(T, p, N_1, N_2, \ldots)$ expresses the chemical potential of the i–th species when the adsorbed layer behaves like a bulk solution. Thus, we may write in general:

$$\mu_i^*(T, p, N_1, N_2, \ldots) = \mu_i^{*s}(\theta_i = 1) + kT \ln a_i^s = \\ \mu_i^{*x}(\theta_i = 1) + kT \ln f_i^x x_i = \mu_i^{*\theta}(\theta_i = 1) + kT \ln f_i^\theta \theta_i \tag{45}$$

where $\mu_i^*(\theta_i = 1)$ is the value of $\mu_i^*(T, p, N_1, N_2, \ldots)$ in its standard state, a_i^s is the activity of i, x_i is its surface mole fraction, f_i^x is the corresponding activity coefficient, θ_i is the surface coverage of the i–th species and f_i^θ is the corresponding to θ_i activity coefficient. Analytical expressions of these coefficients are discussed below.

Finally, we should make the following clarification in what concerns the surface chemical potential of the solvent clusters appearing in Eq. (10). The various solvent clusters do not have different surface coverages, since the following relationship is valid:

$$N_{S_1}A_{S_1}/A = N_{S_2}A_{S_2}/A = \ldots = N_{S_N}A_{S_N}/A = \theta_S \tag{46}$$

Therefore, the surface chemical potential of the i–th solvent cluster may be expressed as

$$\mu_{S_i}^s = \mu_{S_i}^{*s} + kT \ln f_{S_i}^\theta \theta_S - \gamma A_{S_i} + P_{S_i n}\Delta\varphi/l + P_{S_i p}\Delta\psi/l_p - \\ -\varepsilon_0\varepsilon_{S_i n}(\Delta\varphi/l)^2 A_{S_i} l/2 - \varepsilon_0\varepsilon_{S_i p}(\Delta\psi/l_p)^2 A_{S_i} l/2 \tag{47}$$

where, according to the arguments presented in the previous section, the partial area A_{S_i} is equal to that of the i–th adsorbate.

3.3. Changes in the adsorbed layer thickness

When the adsorbate molecules have dimensions considerably different from those of the solvent molecules, then changes in the adsorbed layer thickness cannot be ruled out.

In order to take into account this feature, we suppose that in general l is a function of N_i. In this case Eq. (28) extends to:

$$d\Phi = d\Phi(l = \text{constant}) - \Delta\varphi \sum_{i=1}^{N} \left(2\alpha_{in} N_i \Delta\varphi / l^3 - P_{in} N_i / l^2\right) dl \tag{48}$$

which eventually results in:

$$\overline{\mu}_i = \overline{\mu}_i(l = \text{constant}) - (\Delta\varphi/l) \left\{ \sum_{k=1}^{N} \left(z_k e^0 - \varepsilon_0 \Delta\varphi A_k / 2l\right) N_k \right\} \left(\frac{\partial l}{\partial N_i}\right) - \\ - \varepsilon_0 (\Delta\psi / l_p)^2 A \left(\frac{\partial l}{\partial N_i}\right) / 2 \tag{49}$$

where $d\Phi(l = \text{constant})$ and $\overline{\mu}_i(l = \text{constant})$ are given by Eqs. (28) and (33), respectively.

4. ADSORPTION ISOTHERMS FOR HOMOGENEOUS SURFACES

4.1. Multicomponent adsorption

Suppose an adsorbed layer composed of N+1 species, which may be molecules of different charged or uncharged species or some of them different states of certain adsorbates or solvent molecules. If we denote by S one of the solvent states on the adsorbing surface and by i (= 1, 2, ..., N) the adsorbate species, then use of Eqs. (10), (33), (47) and (49) yields the following system of adsorption isotherms:

$$\ln(\theta_i/\theta_S) + \ln\left(f_i^\theta / f_{S_i}^\theta\right) = \ln\left(\beta_i a_I^b\right) - z_i e^0 \varphi^m / kT - z_i e^0 \Delta\varphi (l - \rho_i)/lkT - \\ - (b_i - b_S)\Delta\varphi/l + (c_i - c_S)(\Delta\varphi/l)^2 - (d_i - d_S)\Delta\psi/l_p + (e_i - e_S)(\Delta\psi/l_p)^2 + \\ + (\Delta\varphi/l) \left\{ \sum_{k=1}^{N} N_k (z_k e^0 - \varepsilon_0 \Delta\varphi A_k / 2l) \right\} \{(\partial l/\partial N_i) - (\partial l/\partial N_{S_i})\} / kT + \\ + \varepsilon_0 (\Delta\psi/l_p)^2 A \{(\partial l/\partial N_i) - (\partial l/\partial N_{S_i})\} / 2kT , \quad (i = 1, 2, \ldots, N) \tag{50}$$

where

$$\ln \beta_i = \left\{\mu_i^{0,b} - g_i \mu_S^{0,b} - \overline{\mu}^* + \mu_{S_i}^{*s}\right\} / kT - g_i \ln a_S^b \tag{51}$$

$$b_i = P_{in}/kT, \qquad c_i = \varepsilon_0 \varepsilon_{in} A_i l / 2kT \tag{52}$$

$$d_i = P_{ip}/kT, \qquad e_i = \varepsilon_0 \varepsilon_{ip} A_i l / 2kT \tag{53}$$

Note that Eq. (50) holds for both neutral and ionic adsorbates provided that $z_i = 0$ must be used for uncharged species, whereas for small ions $b_i = d_i = 0$ is valid.

The term with the activity coefficients in Eq. (50), $\ln(f_i^\theta / f_{S_i}^\theta)$, may be calculated from the corresponding expressions presented in [23–29]. Moreover, the application of this isotherm necessarily requires a functional dependence of l upon N_i (i = 1,2,...,N). The simplest expression which may be adopted is the linear one:

$$l = \sum_{i=1}^{N} l_i \theta_i + l_S \theta_S \tag{54}$$

where l_i, l_S is the thickness of the inner layer composed exclusively of species i and solvent molecules (S), respectively.

4.2. Limiting cases

The generalised adsorption isotherms, Eqs. (50), can be used to generate simpler isotherms applicable to real systems. Here, for simplicity we examine the following adsorption processes at monolayers of constant thickness: a) the single adsorption of a neutral or ionic adsorbate which possess a constant orientation at the monolayer, (b) the reorientation from a flat position to a normal one of a neutral adsorbate, and c) the co–adsorption of two adsorbates.

4.2.1. Adsorption of a constant orientated adsorbate

The adsorption isotherm of a constant orientated adsorbate may be derived directly from Eq. (50) if we put i = A. However, a more compact expression of this isotherm is obtained if Eqs. (39), (40) are substituted in Eq. (12). Then it may be expressed as:

$$\ln \frac{\theta}{(1-\theta)^n} + \ln \left[f_i^\theta/(f_s^\theta)^n\right] = \ln\left(\beta a_A^b\right) - z_A e^0 \varphi^m/kT - \frac{nB_n}{\varepsilon_n^2}\left\{\frac{(1-\theta)^2}{\varepsilon_{An}} - \frac{\theta^2}{\varepsilon_{Sn}}\right\} - \frac{nB_p}{\varepsilon_p^2}\left\{\frac{(1-\theta)^2}{\varepsilon_{Ap}} - \frac{\theta^2}{\varepsilon_{Sp}}\right\} \tag{55}$$

where, according to the arguments presented in section 2, n is close to unity at polar and n = g at non polar solvents. The equilibrium constant β is here given by:

$$\ln \beta = \left\{\left(\gamma^0 - \gamma^{0^*}\right) A_A - \overline{\mu}_A(\theta = 1) + n\mu_S^s(\theta = 0) + \mu_A^{0,b} - g\mu_S^{0,b}\right\}/kT - g \ln a_S^b \tag{56}$$

When the adsorbed molecules have isotropic polarizabilities, Eq. (55) is further simplified to:

$$\ln \frac{\theta}{(1-\theta)^n} + \ln\left[f_A^\theta/\left(f_S^\theta\right)^n\right] = \ln\left(\beta a_A^b\right) - z_A e^0 \varphi^m/kT - \frac{nB}{\varepsilon_A^3}\frac{(1-\theta)^2 - \rho\theta^2}{\left[\theta + (1-\theta)/\rho\right]^2} \tag{57}$$

where

$$\rho = \varepsilon_A/\varepsilon_S \tag{58}$$

The activity coefficients are affected from differences in size, the short–range lateral interactions among the adsorbed particles and in the case of adsorbed ions from the repulsive Coulombic interactions among these ions. Analytical expressions for the activity coefficients may be obtained either from statistical mechanical models or experiment. Thus, an approximate expression, arising from monolayer models under mean field approximation, is the following [12,13,21]:

$$\ln\left[f_A^\theta/\left(f_S^\theta\right)^n\right] = (n-1)\ln(1 - \theta + \theta q/n) + A^{AS} q \frac{(1-\theta)^2 - \theta^2 q/n}{(1 - \theta + \theta q/n)^2} + \frac{zq}{2}\ln\frac{q}{n} \tag{59}$$

where

$$q = (zn - 2n + 2)/z \tag{60}$$

$$A^{AS} = z\{w_{AS} - (w_{AA} + w_{SS})/2\}/kT \qquad (61)$$

Here, z is the co-ordination number of the lattice and w_{kj} is the interaction energy between the species k (=A,S) and j (=A,S). In Eq. (59) the first term of the r.h.s. expresses the contribution due to the difference in the sizes of the adsorbed molecules if in non polar solvents the solvent molecules do not associate to form clusters.

A more general expression for the interaction term, when it is expressed as a function of mole fractions, can be obtained from the experimental properties of binary non electrolyte solutions. Such an expression arises when the excess free energy of the adsorbed layer expands to a power series and is discussed in [36,37].

The properties of the adsorption isotherm expressed by Eq. (57) depend upon the strength of both the dipole–dipole and the short-range particle–particle interactions. An ideal behaviour is predicted when the adsorbed particles are neutral organic molecules, the magnitude of the short-range interactions is such that $A^{AS} = 0$ and the dielectric properties of the adsorbed layer fulfil the condition $B = 0$.

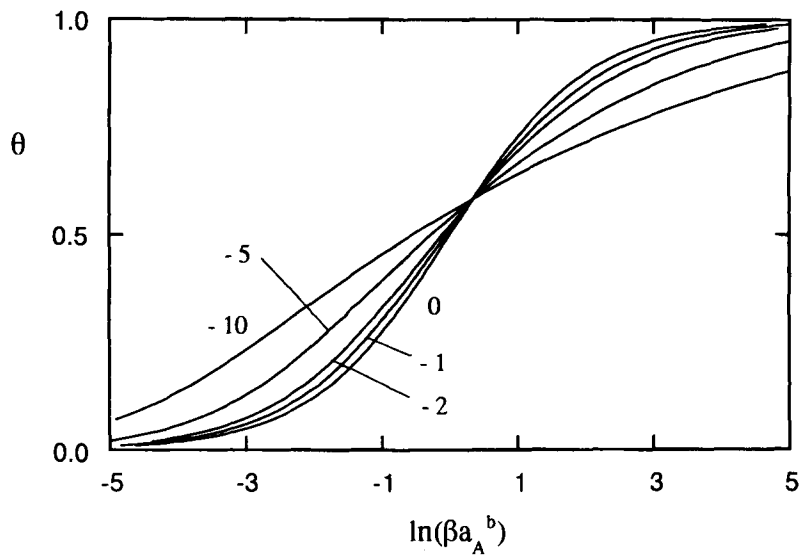

Figure 3. Adsorption isotherms calculated from Eqs. (57) – (59) using $n = 1$, $z_A = 0$, $A^{AS} = 0$, $\rho = 0.5$ and values of $B/(\varepsilon_A)^3$ indicated in the figure.

Deviations from the ideal behaviour affect the adsorption process in various ways. Thus, from the known properties of Eq. (57) when $B = 0, z_A = 0$ and $n = 1$, the following conclusions can be deduced [38,39]: the parameter A^{AS} may take negative as well as positive values. In the first case, the attractive London type forces among dissimilar molecules predominate over those among similar species. For this reason, the adsorbate molecules tend to smear almost uniformly among the solvent molecules leading to rather flat adsorption isotherms. In the second case the attractive forces among similar molecules prevail over those among dissimilar molecules. This favours a tendency of the similar

molecules to form clusters at the adsorbed layer, which eventually may lead to a phase transition. For this reason the adsorption isotherms acquire progressively a sigmoid shape.

In contrast to the interaction parameter A^{AS}, the parameter B of the dipole–dipole interactions is always lower or equal to zero. This means that the electric field established at the adsorbed layer from the dipoles of the adsorbed species does not favour the occurrence of surface phase transitions. Indeed, Fig. 3 shows that as B decreases the adsorption isotherms become progressively more flat. The inability of an adsorbed layer to undergo a phase transition when $A^{AS} = 0$ and $B \neq 0$ can be also shown from the absence in this case of critical properties. Indeed, if we differentiate Eq. (57) with respect to θ and take into account that at the critical point $\partial \ln(\beta a_A^b)/\partial\theta = 0$, we obtain

$$\frac{1-\theta+n\theta}{\theta(1-\theta)} - \frac{2nB}{\varepsilon^3} = 0 \tag{62}$$

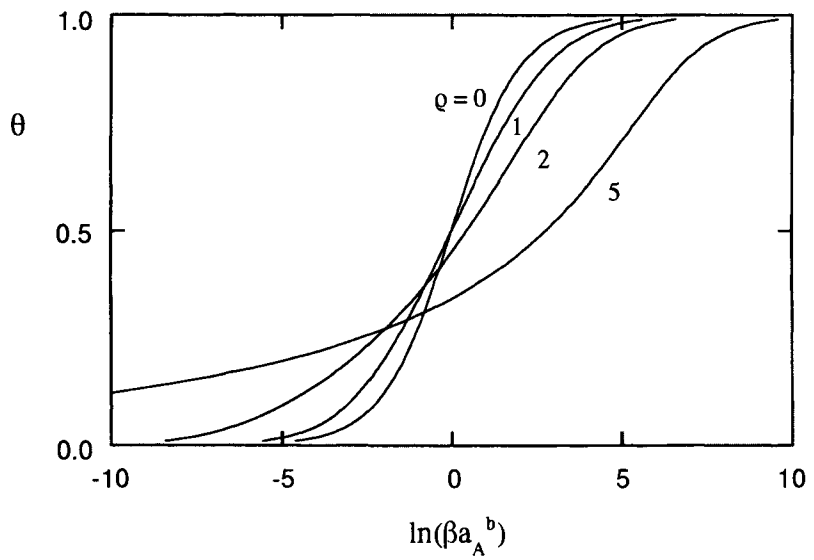

Figure 4. Adsorption isotherms calculated from Eqs. (57) – (59) using n = 1, $z_A = 0$, $A^{AS} = 0$, $P_{An} = 0$, $B/(\varepsilon_A)^3 = -1$ and values of ρ indicated in the figure.

However, this equality can never hold, since $n \geq 1$, $B \leq 0$ and $\varepsilon > 0$. Therefore, in contrast to the short-range interactions which may favour the formation of surface nuclei that lead to phase transition, the electric field of the adsorbed dipoles favours the opposite process, i.e. the smearing of the adsorbed solute molecules among the solvent molecules. That is, the electric field $\Delta\varphi/l$ in fact increases the adsorbate surface solubility.

The magnitude of the dipole–dipole interactions depend upon the "distortional" dielectric constants ε_A and ε_S. Their effect to the adsorption isotherms is rather complicated depending on whether they affect the value of B or not. Fig. 4 shows adsorption isotherms calculated from Eq. (57) with a constant value of $B/(\varepsilon_A)^3$ but various values of the ratio $\rho = \varepsilon_A/\varepsilon_S$. This condition can be achieved if we assume that a) the in-plane field is

negligible due to a random distribution of the adsorbed dipoles and b) $P_{An} = 0$. It is seen that the decrease of the solvent dielectric constant at the surface solution results in a small increase of adsorption at low surface coverages, which is followed by a decrease in adsorption at surface coverages higher than 0.4.

The surface pressure of the adsorbed film can be calculated from the solvent chemical potential, which, due to its uniformity, leads to:

$$\mu_S^s - \mu_S^s(\theta = 0) = \mu_S^b - \mu_S^{0,b} = kT \ln a_S^b \tag{63}$$

This equation in combination with Eq. (44) yields:

$$\Pi A_S/kT = -\left[\mu_S^* - \mu_S^*(\theta = 0)\right]/kT + \ln a_S^b - \frac{B}{\varepsilon_A^3} \frac{\rho\theta^2}{[\theta + (1-\theta)/\rho]^2} \tag{64}$$

where for the first term of the r.h.s. of the above equation the following expression, valid at monolayer models under mean field approximation [12,13,19], may be used:

$$\left[\mu_S^* - \mu_S^*(\theta = 0)\right]/kT = \ln(1-\theta) - \frac{z}{2}\ln(1 - \theta + \theta q/n) + A^{AS}\frac{\theta^2 q^2/n^2}{(1-\theta+\theta q/n)^2} \tag{65}$$

Using the above equations we have attempted to reproduce the experimental data of two series of adsorbates: one series of neutral organic adsorbates and a series of small ionic adsorbates both adsorbed on the energetically homogeneous surface of Hg. In particular, we have analysed the experimental data of tri-n-octylphosphine oxide (TOPO), dodecyldiphenyl-phosphine oxide (DDPO) and but-2-yne-1,4-diol (BD) adsorption on Hg, as an example of neutral organic adsorbates adsorption. Data were taken from [40–43]. The ionic adsorbates used were the inorganic ions Cl^-, Br^- and I^-, the adsorption of which has been studied in [44–46]. Note that all the above data concern adsorption on a charged Hg electrode. For this reason we have chosen only those data which correspond to the potential of zero charge, where the Hg surface is uncharged.

Comparison tests are shown in Figs. 5 and 6. In Fig. 5 the experimental surface pressure data of the adsorbed film of the neutral organic adsorbates are compared with calculated values from Eqs. (57) - (59), (64), (65) using n = 1. In Fig. 6 the comparison is carried out between experimental and calculated values of the charge σ of the specifically adsorbed anions. This charge is connected with the surface coverage via the following equation:

$$\sigma = -\theta(M/A)e^0 \tag{66}$$

where M/A is the number of adsorption sites per unit area. The surface coverage θ is calculated from Eqs. (57) and (59). It is seen that the theory describes almost quantitatively the adsorption features of both systems.

In order to choose the molecular parameters used in the various calculations, we have worked as follows: recent studies [47,48] on the ratio $\rho = \varepsilon_A/\varepsilon_S$ have shown that in the case of neutral organic compounds adsorbed at the solid / liquid or liquid / liquid interface its most probable value ranges from 0.3 to 0.5. In contrast, at the air / solution interface or in the case of small inorganic anions adsorption r may take values greater than 1. For this reason we have adopted the value $\rho = 0.4$ for all organic adsorbates used in the present publication. Then the two parameters, A^{AS} and $B/(\varepsilon_A)^3$, were obtained by a least squares procedure.

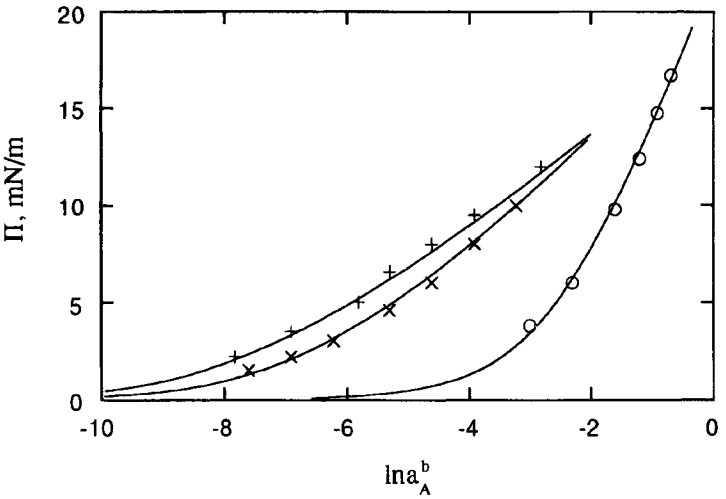

Figure 5. Comparison between experimental and calculated surface pressure data for TOPO (+ + +), DDPO (x x x) and BD (o o o) adsorption at the Hg/solution interface. Data were taken from Refs. [40–43]. Curves were calculated from Eqs. (57) – (59), (64) and (65) with n = 1, $z_A = 0$ and $\rho = 0.4$. Other parameters used: (TOPO) $A^{AS} = 0$, $\ln\beta = 7.3$, $B/(\varepsilon_A)^3 = -6.5$, $kT/A_S = 2.55 mN^{-1}m$; (DDPO) $A^{AS} = 0$, $\ln\beta = 6.0$, $B/(\varepsilon_A)^3 = -6.5$, $kT/A_S = 3.27 mN^{-1}m$; (BD) $A^{AS} = 1$, $\ln\beta = 2$, $B/(\varepsilon_A)^3 = -6.0$, $kT/A_S = 9.79 mN^{-1}$ m.

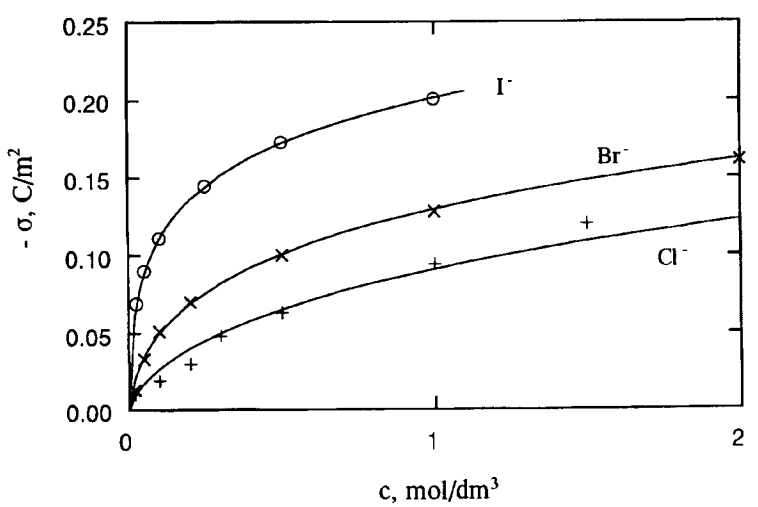

Figure 6. Adsorption isotherms for I^-, Br^- and Cl^- adsorption on Hg from aqueous solutions. Points are experimental data taken from Refs.[44–46]. Curves have been calculated from Eqs. (57) – (59), (66) – (68) with n = 1, $z_A = -1$, $\rho = 2.5$, $B/(\varepsilon_A)^3 = -0.01$. Other parameters used: (I^-) $\ln\beta = -5.1$, $A^{AS} = -12$, $M/A = 6 \cdot 10^{18}$ sites m^{-2}; (Br^-) $\ln\beta = -7.1$, $A^{AS} = -9.5$, $M/A = 7.5 \cdot 10^{18}$ sites m^{-2}; (Cl^-) $\ln\beta = -6.8$, $A^{AS} = -7$, $M/A = 8.8 \cdot 10^{18}$sites m^{-2}.

In what concerns the tests of the ionic isotherm, they can be carried out only if an analytic expression of φ^m is available. That is, the present theory must be necessarily combined with a diffuse layer theory. Therefore, the validity of these isotherms depends to a certain degree on the validity of theory of the diffuse layer adopted for the calculation of φ^m. For simplicity we used the Gouy–Chapman theory and the well known equation [49]:

$$\varphi^m \text{ (in V)} = 0.05141 \ln\left\{K + \sqrt{K^2 + 1}\right\} \tag{67}$$

where

$$K = -\frac{\theta(M/A)e^0}{7.67 \cdot 10^{-4}\sqrt{\varepsilon^d T c}} \tag{68}$$

Here, ε^d is the dielectric constant of the diffuse layer which is approximated to that of the bulk solution, and c is the bulk 1:1 electrolyte concentration in mol/l.

Since in all calculations the value n = 1 was chosen, the number of lattice sites per unit area M/A was calculated from the crystal radii of ions, assuming an hexagonal lattice structure. The bulk activity of the ions a_i^b was approximated by the mean activity of the salt calculated from the Debye–Huckel equation. Finally, an estimation of the magnitude of $B/(\varepsilon_A)^3$ shows that this parameter ranges from –3 to 0. Indeed if we assume that $P_S = 6 \cdot 10^{-30}$Cm, $l = 5 \cdot 10^{-10}$m, $M/A = 6 \cdot 10^{18}$ sites m^{-2} and $\varepsilon_A = 2$, then:

$$B/\varepsilon_A^3 = -P_S^2(M/A)/2l\varepsilon_0\varepsilon_A kT \approx -3 \tag{69}$$

This value tends to zero when P_S decreases and ε_A increases. In the present calculations we have chosen $\rho = 2.5$ and $B/(\varepsilon_A)^3 = -0.01$. The latter value arises from Eq. (69) if we use the molecular parameters adopted in [48]. However, we should point out that extensive tests using various values of $\rho = \varepsilon_A/\varepsilon_S$ and $B/(\varepsilon_A)^3$ ranging from –3 to 0 have shown that in all cases of ionic adsorption a great negative value of A^{AS} is necessary to achieve a good representation of the experimental data. But in this case, i.e. when a great negative value of A^{AS} is used, the shape of the adsorption isotherm is exclusively determined from A^{AS}. That is, the dipole–dipole interactions have a negligible effect on the specific adsorption of ions and therefore the corresponding term in the isotherm may be ignored in approximate calculations.

4.2.2. Adsorption of re–orientated species

Unsymmetrical solute molecules usually re–orientate on the adsorbing surface [38,50–58]. In addition, electrochemical studies on the properties of the inner part of the electrical double layer have shown that the solvent molecules are likely to re–orientate at the surface solution during an adsorption process [1,59,60]. Thus, the re–orientation of adsorbed species on the adsorbing surface is a feature which cannot be ignored, at least at certain cases. Here, for simplicity we restrict our study to the adsorption behaviour of a neutral solute, the molecules of which exhibit two distinct orientations at the adsorbed layer.

If we denote the two adsorbate states by 1 and 2, then the adsorption isotherms are given by Eq. (50) with i = 1. 2. Alternatively, we can take into account that the equilibrium in this system can be represented by:

$$\mu_1^s - \mu_{S_1}^s = \mu_A^b - g_1\mu_S^b \tag{70}$$

$$\mu_2^s - \mu_1^s - (r-1)\mu_{S_1}^s = (g_1 - g_2)\mu_S^b \tag{71}$$

where the second equation represents the surface equilibrium between the two states of the adsorbate A. Then the adsorption isotherms may be expressed as:

$$\ln(\theta_1/\theta_S) + \ln(f_1^\theta/f_S^\theta) = \ln(\beta_{1S}a_A^b) - (b_1 - b_S)\Delta\varphi/l + (c_1 - c_S)(\Delta\varphi/l)^2 - \\ -(d_1 - d_S)\Delta\psi/l_p + (e_1 - e_S)(\Delta\psi/l_p)^2 \tag{72}$$

$$\ln(\theta_2/\theta_S^r) + \ln\left[f_2^\theta/\left(f_S^\theta\right)^r\right] = \ln\left(\beta_{2S}a_A^b\right) - (b_2 - rb_S)\Delta\varphi/l + \\ +(c_2 - rc_S)(\Delta\varphi/l)^2 - (d_2 - rd_S)\Delta\psi/l_p + (e_2 - re_S)(\Delta\psi/l_p)^2 \tag{73}$$

where $r = A_2/A_1$ and the fields $\Delta\varphi/l$, $\Delta\psi/l_p$ are given by Eqs. (35) and (36).

These equilibrium equations were used to describe the adsorption properties of 4-methylpyridine on Hg at the potential of zero charge. For simplicity we have assumed a negligible effect from the short-range interactions and the in-plane field. That is, we have adopted the approximations:

$$\ln\left(f_1^\theta/f_S^\theta\right) = \ln\left(f_2^\theta/\left(f_S^\theta\right)^r\right) = 0 \quad \text{and} \quad \Delta\psi = 0 \tag{74}$$

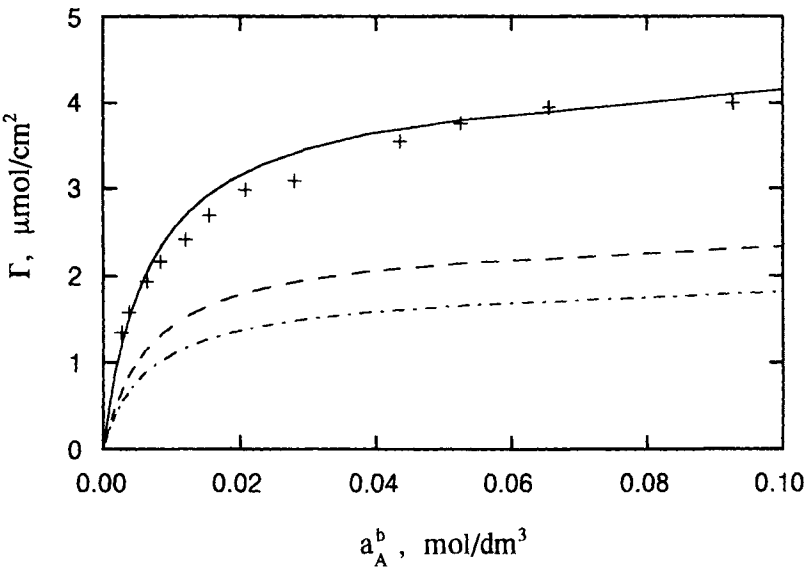

Figure 7. Adsorption isotherms for 4-methylpyridine adsorption on Hg from aqueous solutions. Points are experimental data taken from Refs. [57,58]. Curve (—) represents the total (Γ) adsorption isotherm, curve (– – –) represents the variation of Γ_1 and curve (– · – ·) the variation of Γ_2. They have been calculated from Eqs. (72) – (75) using $r = 1.4$; $l = 5 \cdot 10^{-10}$ m; $b_1 - b_S = 4.8\ lV^{-1}$; $b_2 - rb_S = -0.27\ lV^{-1}$; $c_1 - c_S = -10\ l^2V^{-2}$; $c_2 - rc_S = -13.5\ l^2V^{-2}$; $\ln\beta_{1s} = 3.9$; $\ln\beta_{2s} = 4.4$; $\varepsilon_1 = 2$; $P_S = -3 \cdot 10^{-30}$ C m; $M/A = 3.33 \cdot 10^{18}$ sites/m^2 and $T = 298$ K.

Fig. 7 shows experimental and calculated adsorption isotherms for 4–methylpyridine adsorption on Hg. Data were taken from [57,58]. The surface concentration of 4–methylpyridine was calculated from:

$$\Gamma = \Gamma_1 + \Gamma_2 = \theta_1/A_1 + \theta_2/A_2 \tag{75}$$

with $A_1 = 1.8 \cdot 10^9$ cm^{2}mol^{-1} and $A_2 = 2.53 \cdot 10^9$ cm^{2}mol^{-1} [57].

The molecular parameters used in the calculations are those obtained in [17] from the field dependence of the adsorption of 4–methylpyridine. It is seen that the theoretically calculated data are in good agreement with the corresponding experimental data, indicating the validity of the model under consideration. In this case we can use the model to obtain a more detailed picture of the structure of the adsorbed layer. For example, whereas the experimental data give no information about the two states of 4–methylpyridine on Hg [57], this information can be taken from the predictions of the model. This is done in Fig. 7, where the dependence of the partial surface concentration of the two adsorbate states upon the bulk activity of 4–methylpyridine is depicted.

4.2.3. Co–adsorption of two adsorbates

The co–adsorption of two adsorbates exhibits striking similarities with the re–orientation process examined above, since in both cases more than two species are present at the adsorbed layer. If we denote by r the ratio $r = A_B/A_A$, then the adsorption isotherms arise directly from Eq. (50) and may be expressed as:

$$\ln(\theta_A/\theta_S) + \ln\left(f_A^\theta/f_S^\theta\right) = \ln\left(\beta_{AS}a_A^b\right) - z_Ae^0\varphi^m/kT - z_Ae^0(1-\rho_A)/lkT - \\ -(b_A - b_S)\Delta\varphi/l + (c_A - c_S)(\Delta\varphi/l)^2 - (d_A - d_S)\Delta\psi/l_p + (e_A - e_S)(\Delta\psi/l_p)^2 \tag{76}$$

$$\ln(\theta_B/\theta_S) + \ln\left(f_B^\theta/f_S^\theta\right) = \ln\left(\beta_{BS}a_A^b\right) - z_Be^0\varphi^m/kT - z_Be^0(1-\rho_B)/lkT - \\ -(b_B - rb_S)\Delta\varphi/l + (c_B - rc_S)(\Delta\varphi/l)^2 - (d_B - rd_S)\Delta\psi/l_p + (e_B - re_S)(\Delta\psi/l_p)^2 \tag{77}$$

In case of neutral organic adsorbates ($z_A = z_B = 0$) we can approximately assume that the short–range interactions have a negligible contribution and delete the two terms with the activity coefficients in Eqs. (76) and (77). This approximation is not valid when one or both adsorbates are ionic species. In this case the activity coefficients should be expressed in terms of the surface composition. As we have already pointed out, the expressions for the activity coefficients developed in [23–29] may be used for this purpose. These expressions can be simplified considerably when only one of the co–adsorbates, say adsorbate A, is an ionic species. Then if we again assume that the short–range London type interactions have a negligible contribution, the activity coefficients may be expressed as:

$$\ln\left(f_A^\theta/f_S^\theta\right) = A^i(1 - 2\theta_A) \quad \text{and} \quad \ln\left(f_B^\theta/f_S^\theta\right) = 0 \tag{78}$$

where $A^i = -zw_{AA}/2kT$.

Fig. 8 shows typical adsorption isotherms of a neutral adsorbate in the presence of a second one. The model predicts the expected decrease in adsorption due to the co–adsorption of the second adsorbate. However, a more interesting case, not predicted by previous theories, is that depicted in Fig. 9. This figure shows the effect of specifically adsorbed

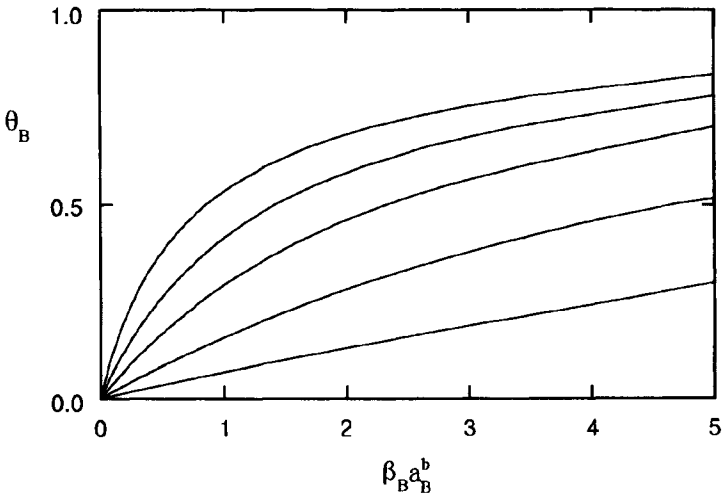

Figure 8. Adsorption isotherms of an adsorbate B in the presence of a co-adsorbate A in the following reduced concentrations: $\ln \beta a_A = -100, -1, 0, 1, 2$ (from top to bottom). They have been calculated from Eqs. (76) – (78) using the following parameters: $r = 4$; $z_A = z_B = 0$; $l = 6 \cdot 10^{-10}$m; $b_A - b_S = 3\ lV^{-1}$; $b_B - rb_S = 4\ lV^{-1}$; $c_A - c_S = -3\ l^2V^{-2}$; $c_B - rc_S = -3\ l^2V^{-2}$; $\varepsilon_A = 3$; $P_S = -2 \cdot 10^{-30}$Cm; $M/A = 4 \cdot 10^{18}$sitesm^{-2}; $A^i = 0$ and $T = 298$ K.

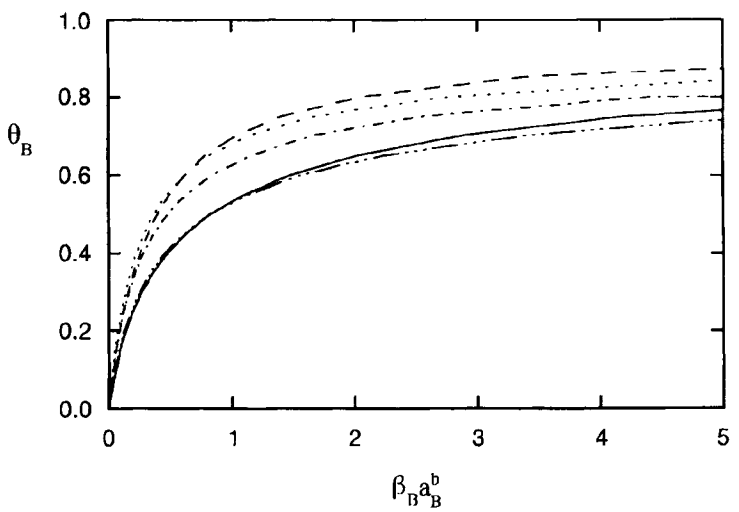

Figure 9. Adsorption isotherms of a neutral organic adsorbate B in the presence of specifically adsorbed inorganic anions A of an 1:1 electrolyte in the following concentrations: c (in mol·dm^{-3}) = 0 (—); 0.1 (– – –); 1 (···); 2 (– · –) and 5 (– ··· –). They have been calculated from Eqs. (76) – (78) using: $r = 3$; $z_A = -1$; $z_B = 0$; $l = 6 \cdot 10^{-10}$ m; $\rho_A = 2.5 \cdot 10^{-10}$ m; $\varepsilon_A = 25$; $\varepsilon_S = 9$; $\ln \beta = -3.5$; $b_B - rb_S = 4\ lV^{-1}$; $c_B - rc_S = -3\ l^2V^{-2}$; $P_S = -2 \cdot 10^{-30}$Cm; $M/A = 8.33 \cdot 10^{18}$ sites m^{-2}; $A_i = -9.5$ and $T = 298$ K.

anions on the adsorption of a neutral adsorbate. The molecular parameters were selected to approximate the adsorption of Br^- anions on the uncharged Hg surface. We note an unexpected behaviour; the presence of specifically adsorbed anions may increase the adsorption of a neutral adsorbate. This happens in our example at concentrations of electrolyte lower than 2M and it is due to changes in the field $\Delta\varphi/l$ caused by the adsorbed anions.

Indirect experimental evidence of this phenomenon can be found in [61], where it has been observed that the free energy of adsorption of ethylene glycol on Hg in the presence of specifically adsorbed Cl^-, Br^- and I^- ions is much higher than the expected value in the absence of these ions.

5. ADSORPTION ON HETEROGENEOUS SURFACES

5.1. Types of surfaces

The results presented above show that the adsorption characteristics on energetically homogeneous adsorbing surfaces are determined by three main factors. The short-range interactions expressed by the parameter A^{AS}, the dipole-dipole interactions, the contribution of which in the simple case of single adsorption is determined by the parameters $\rho = \varepsilon_A/\varepsilon_S$ and $B/(\varepsilon_A)^3$, and the co-adsorption of other adsorbates. On solid surfaces an additional factor should be taken into account. It is the heterogeneity of the adsorbing surface.

Previous studies [4,5,62] have shown that the heterogeneity of the adsorbing surface can be modelled by assuming two types of surfaces: surfaces with random and patchwise topography. In the first case the adsorption sites with different adsorption energy are randomly distributed over the adsorbing surface, whereas in the second case the adsorption sites with equal energy are present in groups or patches, where each patch is considered an autonomous phase. Surfaces with medial or regular distribution of the adsorption sites have been also considered in some adsorption studies [5,63,64].

5.2. Adsorption isotherms on random and patchwise surfaces

The work carried out in [5,62–66] allows the direct extension of the adsorption isotherms developed in the previous section to heterogeneous surfaces. Here, for simplicity, we restrict our study to extend only the adsorption isotherm (57) with $n = 1$ and $z_A = 0$ to random and patchwise surfaces.

If we denote by θ_i the partial surface coverage of the adsorbate A, i.e. the surface coverage on sites with adsorption energy U_i, then the partial adsorption isotherm valid for the adsorption on these sites may be written as:

$$\frac{\theta_i}{1-\theta_i} e^{-U_i/kT} = \beta a_A^b \exp\left\{-A^{AS}(1-2\theta)\right\} \exp\left\{\frac{-B}{\varepsilon_A^3} \frac{(1-\theta)^2 - \rho\theta^2}{[\theta + (1-\theta)/\rho]^2}\right\} \tag{79}$$

when the adsorbing surface have a random site distribution, and

$$\frac{\theta_i}{1-\theta_i} e^{-U_i/kT} = \beta a_A^b \exp\left\{-A^{AS}(1-2\theta_i)\right\} \exp\left\{\frac{-B}{\varepsilon_A^3} \frac{(1-\theta_i)^2 - \rho\theta_i^2}{[\theta_i + (1-\theta_i)/\rho]^2}\right\} \tag{80}$$

for surfaces with patchwise topography. In both cases the total adsorption isotherm may be calculated from:

$$\theta = \sum_i \theta_i M_i / M \approx \int_{-\infty}^{\infty} \theta_i \chi(U) dU \tag{81}$$

where M_i is the number of adsorption sites with energy U_i and $\chi(U)$ is the site energy distribution function. It is evident that the summation in Eq. (81) is replaced by integration only when θ_i is a continuous function of the adsorption energy U (= U_i).

The integral of Eq. (81) is usually calculated numerically. An analytical solution can be achieved on random surfaces when their heterogeneity is described by the uniform distribution [66]:

$$\chi(U) = \begin{cases} 0 & U < U_m - U_0, \quad U > U_m + U_0 \\ 1/2U_0 & U_m - U_0 < U_m + U_0 \end{cases} \tag{82}$$

Thus, if Eqs. (79) and (82) are substituted in Eq. (81), we obtain the adsorption isotherm

$$\theta = \frac{1}{2\lambda} \ln \frac{1 + Ke^{\lambda}}{1 - Ke^{-\lambda}} \tag{83}$$

Here, K denotes the r.h.s. of Eq. (79) and $\lambda = U_0/kT$ is an heterogeneity factor which increases with increasing heterogeneity of the adsorbing surface. Homogeneous surfaces correspond to $\lambda = 0$. At patchwise surfaces Eq. (80) should be solved numerically with respect to θ_i and the total adsorption isotherm is determined again numerically from Eqs. (81) and (82).

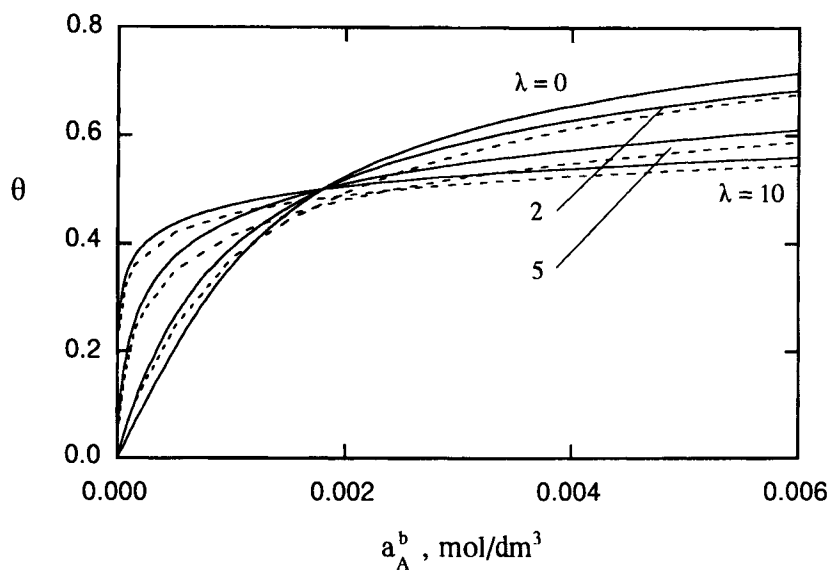

Figure 10. Adsorption isotherms on random (—) and patchwise (– – –) heterogeneous surfaces calculated from Eq. (83) and Eqs.(80) – (82), respectively, using the following parameters: $\rho = 0.4$; $A^{AS} = 1$; $\ln \beta = 6$; $B/(\varepsilon_A)^3 = -6.5$ and λ values indicated in the figure.

Fig. 10 shows that the type of the heterogeneity of the adsorbent does not play an important role in the adsorption process. At both models of surfaces, i.e. at random and patchwise surfaces, at low surface coverages the curves of the isotherms for heterogeneous adsorption lie above the corresponding isotherm for homogeneous adsorption, while the inverse holds at high θ values. This is a typical behaviour and it is attributed to the fact that at low coverages the adsorbate molecules are adsorbed preferentially on the most active sites, whereas the less active sites come into play at high coverages where all the active sites have been occupied [65]. The difference in the adsorption isotherms on random and patchwise surfaces are in general quite small and therefore as a first approximation Eq. (83) can be used to interpret adsorption data of single adsorption on heterogeneous surfaces.

6. CONCLUSIONS

The treatment presented above has shown that classical thermodynamics fed with a minimum of modelistic assumptions can be used for the determination of the explicit dependence of the electrochemical potentials of adsorbed species upon the dipole–dipole interactions among these species. The electrochemical potentials can be further used for the derivation of the adsorption isotherm and more general the equilibrium properties of adsorbed layers at uncharged interfaces.

It was found that the obtained isotherms are markedly different from those which take into account only short–range interactions, like the Flory–Guggenheim isotherm for local adsorption. The dipole–dipole interactions play an important role in the properties of adsorbed layers, since they smear the adsorbed solute molecules among the solvent molecules, increasing the adsorbate surface solubility. Another interesting implication caused by the electric field of the adsorbed dipoles is the increase in the adsorption of a neutral adsorbate in the presence of specifically adsorbed anions, a property which is not predicted by previous models although experimental evidence of this phenomenon does exist.

The proposed thermodynamic treatment has two main advantages. It keeps the modelistic assumptions to a minimum and it is relatively simple. The first advantage increases the applicability and reliability of the treatment, since there is no need for questionable structural assumptions and / or drastical approximations, like those involved in statistical mechanical treatments. The second advantage allows many interesting adsorption phenomena, like co–adsorption and re–orientation processes as well as the effect of the specific adsorption of ions and the heterogeneity of the adsorbing surface on the equilibrium properties of adsorbed layers, to be readily taken into account.

APPENDIX

In section 3 the contribution to the surface chemical potentials arising from the field of the potential drop $\Delta\varphi$ was derived from the combination of classical thermodynamics with the electrostatic theory of dielectrics. This contribution may be alternatively calculated as follows. Suppose that in general an adsorbed layer with M lattice sites, area A and thickness l consists of N_i neutral molecules of the i–th species, i = 1, 2, ..., N. If

these species behave like point dipoles situated in vacuo, then the contribution of the electrostatic interactions to the Helmholtz energy of the adsorbed layer, A^{el}, is given by [12, 67–70]:

$$A^{el} = U^{d-d} + \sum_{i=1}^{N} \alpha_i N_i \Delta\varphi^2 / 2l^2 \tag{A.1}$$

where the first term of the r.h.s. of Eq. (A.1) is the dipole–dipole interaction energy and the second one is the energy required to produce induced dipoles.

If we assume a random distribution of the adsorbed molecules over the lattice sites, then a mean electric field equal to $\Delta\varphi/l$ acts to each site. In this case the dipole–dipole interaction energy U^{d-d} may be expressed as [70,71]:

$$U^{d-d} = \frac{1}{2} (\Delta\varphi/l) \sum_{i=1}^{N} (P_{in} - \alpha_{in} \Delta\varphi/l) N_i \tag{A.2}$$

Therefore, A^{el} may be written as:

$$A^{el} = \frac{1}{2} \sum_{i=1}^{N} (P_{in} N_i) \Delta\varphi/l = \frac{1}{2\varepsilon_0 \varepsilon_n l A} \left(\sum_{i=1}^{N} P_{in} N_i \right)^2 \tag{A.3}$$

where we have taken into account Eq. (35) with $z_i = 0$. Now the contribution to the chemical potentials from the field $\Delta\varphi/l$ may be calculated from:

$$\mu_i^{el} = \partial A^{el} / \partial N_i = P_{in} \Delta\varphi/l - \varepsilon_0 \varepsilon_{in} (\Delta\varphi/l)^2 A_i l/2 \tag{A.4}$$

If this equation is compared with Eq. (33), we readily conclude that the more general quasi–thermodynamic treatment presented in section 3 takes into account the dipole–dipole interactions among the normal components of the dipole moment of the adsorbed species.

REFERENCES

1. J.O'M. Bockris, M. Devanathan and K. Müller, Proc. Roy. Soc. (London), A274 (1963) 55.
2. D.H. Everett, Trans. Faraday Soc., 60 (1964) 1803.
3. D.H. Everett, Trans. Faraday Soc., 61 (1965) 2478.
4. M. Borowko and M. Jaroniec, Adv. Colloid Interface Sci.,19 (1983) 137.
5. M. Jaroniec and R. Madey, Physical Adsorption on Heterogeneous Solids, Elsevier, 1988.
6. P. Nikitas, J. Electroanal. Chem., 263 (1988) 147.
7. P. Nikitas and A. Pappa–Louisi, J. Phys. Chem., 94 (1990) 361.
8. P. Nikitas and S. Sotiropoulos, J. Electroanal. Chem., 309 (1991) 1.
9. S. Trasatti, Chemtracts, 2 (1990) 80.
10. S Trasatti, Electrochim. Acta, 37 (1992) 2137.
11. P. Nikitas, Electrochim. Acta, 38 (1993) 2663.
12. P. Nikitas, J. Chem. Soc., Faraday Trans. 1, 82 (1986) 977.
13. P. Nikitas, J. Phys. Chem., 91 (1987) 101.

14. P. Nikitas, Electrochim. Acta, 39 (1994) 865.
15. R. Defay, I. Progogine and D.H. Everett, Surface Tension and Adsorption, Longmans, 1966.
16. H.P. Dhar, B.E. Conway and K.M. Joshi, Electrochim. Acta, 18 (1973) 789.
17. P. Nikitas, J. Electroanal. Chem., 375 (1994) 319.
18. P. Nikitas, Langmuir, 9, (1993) 2737.
19. E. Guggenheim, Mixtures, Oxford University Press, Oxford, 1952.
20. I. Prigogine, A. Bellemans and V. Mathot, Molecular Theory of Solutions, North–Holand, Amsterdam, 1957.
21. E.J. DiMarzio, J. Chem. Phys., 35 (1961) 658.
22. R.E. Boehm and D.E.J. Martire, J. Chem. Phys., 67 (1977) 1061.
23. P. Nikitas and A. Pappa–Louisi, Can. J. Chem., 64 (1986) 328.
24. W.A. Steele, J. Phys. Chem., 67 (1963) 2016.
25. R.E. Boehm and D.E. Martire, J. Phys. Chem., 84 (1980) 3620.
26. M. Borowko, J. Colloid Interface Sci., 85 (1982) 540.
27. S. Sircar, J. Chem. Soc., Faraday Trans. 1, 82 (1986) 843.
28. M. Borowko, J. Colloid Interface Sci., 102 (1984) 519.
29. M. Jaroniec and D.E. Martire, J. Chromatogr., 351 (1986) 1.
30. R. Aveyard and D. Haydon, An Introduction to the Principles of Surface Chemistry, Oxford University Press, 1973.
31. J.G. Kirkwood and I. Oppenheim, Chemical Thermodynamics, McGraw–Hill, N.Y., 1961.
32. C.J.F. Böttcher, Theory of Electric Polarization, Elsevier, London, 1973.
33. P. Nikitas, Electrochim. Acta, 37 (1992) 81.
34. P. Nikitas, S. Sotiropoulos and N. Papadopoulos, J. Phys. Chem., 96 (1992) 8453.
35. J.R. MacDonald and C.A. Barlow, J. Chem. Phys., 39 (1963) 412.
36. P. Nikitas, J Chem. Soc., Faraday Trans. 1, 80 (1984) 3315.
37. P. Nikitas, J Chem. Soc., Faraday Trans. 1, 81 (1985) 1767.
38. B.B.Damaskin, O.A.Petrii and V.V.Batrakov, Adsorption of Organic Compounds on Electrodes, Plenum Press, New York, 1971.
39. F. Pulidori, G. Borghesani, R. Pedriali, A. de Battisti and S. Trasatti, J. Chem. Soc., Faraday Trans. 1, 74 (1978) 79.
40. P. Nikitas, A. Pappa–Louisi and D. Jannakoudakis, J. Electroanal. Chem., 162 (1984) 175.
41. A. Pappa–Louisi, P. Nikitas and D. Jannakoudakis, Electrochim. Acta, 29 (1984) 515.
42. A. Pappa–Louisi and P. Nikitas, Can. J. Chem., 64 (1986) 333.
43. E. Dutkiewicz, J. D. Garnish and R. Parsons, J. Electroanal. Chem., 16 (1968) 505.
44. D.C. Grahame, J. Am. Chem. Soc., 80 (1958) 4201.
45. D.C. Grahame and R. Parsons, J. Am. Chem. Soc., 83 (1961) 1291.
46. J. Lawrence, R. Parsons and R. Payne, J. Electroanal. Chem., 16 (1968) 193.
47. P. Nikitas and A. Pappa–Louisi, J. Electroanal. Chem., in press.
48. P. Nikitas, J. Phys. Chem., 98 (1994) 6577.
49. D.C. Grahame, Chem. Rev., 41 (1947) 441.
50. B.B. Damaskin, J. Electroanal. Chem., 21 (1969) 149.
51. B.E. Conway and H.P. Dhar, Electrochim. Acta, 19 (1974) 445.
52. R.G. Barradas, P.G. Hamilton and B.E. Conway, Collect. Czechoslov. Chem. Commun., 32 (1967) 1791.

53. H.Nakadomari, D.M.Mohilner and P.R.Mohilner, J. Phys. Chem., 80(1976) 1761.
54. S. Trasatti and G. Olivieri, J. Electroanal. Chem., 27 (1970) Appendix 7.
55. D. Kozminska, Z. Borkowska and B. Behr, Can. J. Chem., 59 (1981) 2043.
56. T. Wandlowski and E. Kretschmer, J. Electroanal. Chem., 209 (1986) 203.
57. P. Nikitas and A. Pappa–Louisi, Electrochim. Acta, 38 (1993) 1573.
58. A. Pappa–Louisi, P. Nikitas and Ph. Andonoglou, Electrochim. Acta, 38 (1993) 1585.
59. W. Fawcett and R. deNobriga, J. Phys. Chem., 86 (1982) 371.
60. W. Fawcett, Israel J. Chem., 18 (1979) 3.
61. S. Trasatti, J. Electroanal. Chem., 28 (1970) 257.
62. W. Rudzinski and D. H. Everett, Adsorption of Gases on Heterogeneous Surfaces, Academic Press, London, 1992.
63. M. Jaroniec, A. Patrykiejew and M. Borowko, Progress in Surface and Membrane Sci., 14 (1981) 1.
64. M. Jaroniec, Adv. Colloid Interface Sci., 18 (1983) 149.
65. D. Young and A. Crowell, Physical Adsorption of Gases, Butterworths, London, 1962.
66. P. Nikitas, Electrochim. Acta, 33 (1988) 647.
67. M.V.Sangaranarayanan and S.K.Rangarajan, J. Electroanal.Chem.,176(1984)1.
68. S. Levine, G.M. Bell and A.L. Smith, J. Phys. Chem., 73 (1969) 3534.
69. S. Levine, K.Robinson, A.L. Smith and A.C. Brett, Discuss. Faraday Soc., 59 (1975) 133.
70. W. Fawcett, S. Levine, R. deNobriga and A. McDonald, J. Electroanal. Chem., 111 (1980) 163.
71. P. Nikitas, J. Electroanal. Chem., 227 (1987) 237.

This Page Intentionally Left Blank

A. Dąbrowski and V.A. Tertykh (Editors)
Adsorption on New and Modified Inorganic Sorbents
Studies in Surface Science and Catalysis, Vol. 99
1996 Elsevier Science B.V.

Chapter 3.5
Ion adsorption on mineral oxide surfaces

Luuk K. Koopal

Department of Physical and Colloid Chemistry, Wageningen Agricultural University, 6703 HB Wageningen, The Netherlands

1. INTRODUCTION

In aqueous solutions surfaces are often charged and the surface charge is an important parameter with respect to many properties of dispersed materials. The surface charge will, for example, affect the "reactivity" of the surface, adsorption of ionic species, wetting and adhesion characteristics of particles and their colloidal stability. There is an element of arbitrariness in deciding which charge we identify as the surface charge. For most mineral oxides it is generally accepted that at least part of the surface atoms combine with water to form surface oxygen groups. The surface charge may result from adsorption and/or desorption of protons on the oxygen groups.

Apart from the surface charge resulting from proton adsorption or desorption, particles may also become charged by other mechanisms. For instance, constituent ions of the crystalline solid may adsorb and contribute to the surface charge. For clay type minerals for which the surface is composed of edges and plates, the edge charge is due to dissociation of surface hydroxyls, but the plate charge is due to isomorphic substitution. Furthermore various ions may adsorb "specific" (i.e. through non-coulombic interaction forces) and also this adsorption contributes to the surface charge.

To distinguish between the charge contributions of the different ions we define the "primary surface charge density", σ_s, of a mineral surface as:

$$\sigma_s = F(\Gamma_H - \Gamma_{OH}) \tag{1}$$

where F is the Faraday and Γ_i the adsorbed amount of ion i (H^+, OH^-) in mol/m^2. Γ_{OH} is the amount of OH^- that associates with adsorbed protons under the formation of water. The definition of σ_s is chosen for two reasons: (1) protons and hydroxyl ions have an active role in the protonation of the surface oxygens of mineral oxides and (2) protons and hydroxyl ions are inevitably present in aqueous solutions. The advantage of this definition is that the primary surface charge can be obtained relatively easy through potentiometric proton titrations of mineral suspensions. With the present definition of σ_s we call protons and hydroxyl ions "primary charge determining ions" or briefly "charge determining" (c.d.) ions to distinguish them from the other ions.

For most oxides there is a pH at which the proton and hydroxyl ion adsorption just compensate each other, this pH is called the point of zero charge or pzc [1]. In general

for low pH σ_s will be positive, for high pH σ_s will be negative. The more acidic the oxide, the lower is the pzc. Note that the pzc is, in general, not equal to the isoelectric point, or iep, a surface property that can be measured by e.g. electrophoresis [2]. The pzc is strictly derived from Eq. (1): $\sigma_s = 0$, whereas the iep is a more general electrokinetic property related to overall charge neutrality of a particle (not only related to the proton or hydroxyl ion adsorption).

In general a mineral oxide surface in contact with an electrolyte solution of a given pH, outside the pzc, will develop a primary surface charge. In order to satisfy the requirements of electroneutrality the adsorption of primary c.d. ions is followed by a positive adsorption of counter–ions and negative adsorption of co– ions in the immediate vicinity of the surface. The charged interface plus the solution region in which the surface charge is counter balanced is called "the electric double layer". Due to the opposing actions of energy (coulombic) and entropy the counter–ions and co–ions are distributed in a diffuse layer. This situation is very similar to that around ions in electrolyte solutions as described in the Debye–Hückel theory [3]. The main difference is that near a surface the potentials can be much higher than around simple ions.

In this chapter the electrical double layer of mineral oxides will be described. Firstly the solution part of the double layer will be considered, secondly the surface charge part. For the latter a distinction will be made between homogeneous and heterogeneous surfaces. Considering the oxide surface as homogeneous leads to a relatively simple description of the double layer. This description is the starting point for the treatment heterogeneous double layers. Apart form the adsorption of primary c.d. ions to the surface specific or non– coulombic adsorption of ions will be considered. The often made distinction between "indifferent" electrolytes and ordinary electrolytes will be followed, unless stated otherwise. Ions of an indifferent electrolyte are assumed to adsorb through coulombic interactions only, they do not adsorb specifically. It is frequently assumed that most simple 1–1 electrolytes are indifferent when the electrolyte concentration is not too high.

2. DOUBLE LAYER MODELS FOR FLAT SURFACES

2.1. Diffuse double layer or Gouy–Chapman model

Before discussing the surface charge itself the solution side of the double layer will be considered. Following Gouy [4] and Chapman [5] a rigid impenetrable planar surface with a given charge density in contact with an indifferent electrolyte solution is analysed. The ions in solution respond to the force field of the surface and form a diffuse charge layer adjacent to the surface. For all ions i the distributions in the field of the surface can be described by the Boltzmann law. If it is assumed that the ions are point charges which only interact through coulombic forces this distribution can be expressed as:

$$c_i(z) = c_i(\infty) \exp\left\{\frac{-\tau_i F \psi(z)}{RT}\right\} \tag{2}$$

where $c_i(z)$ is the concentration of ions i at distance z from the surface, τ_i the charge number of the ions, including their sign, F the Faraday and $\psi(z)$ is the potential in the double layer. The reference point for the potentials is the bulk solution where $\psi(\infty) = 0$ and the concentration of each type of ion is its bulk concentration. The potential $\psi(z)$

is assumed to be a mean field electrostatic potential, for the subtleties of potentials in the double layer we refer to [6]. Equation (2) is in agreement with the statement that counter–ions are attracted and co–ions are repelled by the charged surface.

The space charge density $\rho(z)$ neutralizing the surface charge is related to the local electrolyte concentrations. For a symmetrical indifferent electrolyte $\rho(z)$ can be written as:

$$\rho(z) = \tau F \{c_+(z) - c_-(z)\} \tag{3}$$

where the local concentrations are given by Eq. (2) and $\tau = \tau_+ = \tau_-$. The additional relation between the potential ψ and the space charge density $\rho(z)$ is given by the Poisson equation that for a flat interface reads:

$$\frac{d^2\psi}{dz^2} = \frac{-\rho(z)}{\varepsilon_0 \varepsilon_r(z)} \tag{4}$$

where ε_0 is the permittivity of vacuum and $\varepsilon_r(z)$ the relative dielectric constant at distance z from the surface. In the Gouy–Chapman (GC) approximation $\varepsilon_r(z)$ set equal to its value in bulk solution. By combining Eqs. (2) to (4) a differential equation is obtained that describes the variation of ψ with location in the diffuse layer:

$$\frac{d^2\psi}{dz^2} = -\frac{\tau F c_s}{\varepsilon_0 \varepsilon_r}\left[\exp\left\{\frac{-\tau F \psi(z)}{RT}\right\} - \exp\left\{\frac{\tau F \psi(z)}{RT}\right\}\right] \tag{5}$$

where $c_s = c_+(\infty) = c_-(\infty)$. Equation (5) is the GC form of the Poisson–Boltzmann (PB) equation. Integration of Eq. (5) gives the field strength:

$$\frac{d\psi}{dz} = -\left(\frac{8RTc_s}{\varepsilon_0 \varepsilon_r}\right)^{0.5} \sinh\left\{\frac{\tau F \psi(z)}{2RT}\right\} \tag{6}$$

A second integration yields the potential distribution according to the GC theory:

$$\tanh\left\{\frac{\tau F \psi(z)}{4RT}\right\} = \tanh\left\{\frac{\tau F \psi_d}{4RT}\right\} \exp(-\kappa z) \tag{7}$$

where ψ_d is the potential at the onset of the diffuse layer and κ is defined by:

$$\kappa^2 = \left(\frac{F^2}{\varepsilon_0 \varepsilon_r RT}\right) \sum_i c_i \tau_i^2 \tag{8}$$

κ has the dimension of a reciprocal length and κ^{-1} is called the "Debye length". For aqueous solutions of symmetrical electrolytes Eq. (8) reduces to:

$$\kappa^2 = \frac{2F^2 c_s \tau^2}{RT \varepsilon_0 \varepsilon_r} \tag{9}$$

When the primary surface charge is compensated by ions in the diffuse layer only and the diffuse layer starts at the surface plane, ψ_d equals the average, smeared out, surface potential ψ_s and the electroneutrality condition requires that $\sigma_s = -\sigma_d$ with σ_d the diffuse layer charge.

The relation between the diffuse charge density σ_d and the diffuse layer potential ψ_d can be obtained from Eq. (6) and realising that according to Gauss law:

$$-\sigma_s(=\sigma_d) = \varepsilon_0\varepsilon_r\left(\frac{d\psi}{dz}\right)_{z=0} \tag{10}$$

$$-\sigma_d = (8RT\varepsilon_0\varepsilon_r c_s)^{0.5}\sinh\left(\frac{\tau F\psi_d}{2RT}\right) \tag{11}$$

The negative sign in Eq. (11) means that a negative value of ψ_d (or ψ_s) leads to a positive charge in the diffuse layer. Equation (11) can also be reversed to express ψ_s as a function of σ_d:

$$\psi_d = \frac{2RT}{\tau F}\,\text{arcsinh}\left\{\frac{-\sigma_d}{(8RT\varepsilon_0\varepsilon_r c_s)^{0.5}}\right\} \tag{12}$$

The GC theory also allows us to calculate the ionic components of charge of a diffuse layer, i.e. the charge densities due to the surface excess amounts of the cations and anions that compensate the surface charge [7, 8]:

$$\sigma_{+,d} = (2RT\varepsilon_0\varepsilon_r c_s)^{0.5}\left[\exp\left(\frac{-\tau F\psi_d}{2RT}\right) - 1\right] \tag{13}$$

and

$$\sigma_{-,d} = -(2RT\varepsilon_0\varepsilon_r c_s)^{0.5}\left[\exp\left(\frac{\tau F\psi_d}{2RT}\right) - 1\right] \tag{14}$$

For low potentials where the exponentials may be replaced by their linear terms these equations show that $\sigma_{+,d} = -\sigma_{-,d}$. For high potentials the counter ion charge increases exponentially and the co–ion charge approaches a limiting value:

$$\sigma_{co-ion}\,(\text{large}\,|\psi_s|) = \left|(2RT\varepsilon_0\varepsilon_r c_s)^{0.5}\right| \tag{15}$$

for room temperature this amounts to $59\sqrt{c_s}$ mC/m^2 when c_s is in mol/dm^3.

Differentiation of σ_s with respect to ψ_s provides the relation for the differential capacitance of the diffuse layer:

$$C_d = \varepsilon_0\varepsilon_r\kappa\cosh\left(\frac{\tau F\psi_d}{2RT}\right) \tag{16}$$

For small potentials cosh x goes to unity and Eq. (16) reduces to:

$$C_d = \varepsilon_0\varepsilon_r\kappa \tag{17}$$

Equation (17) shows that under these conditions the diffuse double layer can be seen as a the plate condenser with dielectric constant $\varepsilon_0\varepsilon_r$ and a plate distance κ^{-1}. Therefore κ^{-1} is also called the double layer thickness. Under the same conditions simplified expressions can be obtained for ψ_d and σ_d. For low potentials the approximations tanh x = x and sinh x = x can be used and Eqs. (7) and (11) reduce to respectively:

$$\psi(z) = \psi_d\exp(-\kappa z) \tag{18}$$

$$-\sigma_d = \varepsilon_0 \varepsilon_r \kappa \psi_d \tag{19}$$

The expressions for low potentials are the so called Debye–Huckel (DH) limits of the diffuse double layer model.

The implication of Eq. (11) or (19) is that if we assume ψ_d to be constant, σ_d becomes a function of the ionic strength. Conversely if σ_d is assumed to be constant, ψ_d is a function of κ. Both the constant charge and the constant potential case are idealisations, in practice neither σ_d nor ψ_d may stay constant, nevertheless keeping the salt concentration constant during an experiment simplifies the situation considerably.

The GC theory of the double layer has been useful in developing a good understanding of double layer behaviour. All equations shown apply to symmetrical electrolytes, for non-symmetrical and for mixed electrolytes the treatment is essentially the same [9, 10, 11]. For other geometries numerical solutions exist [12]. More rigorous treatments and discussions about the structure of the diffuse double layer can be found in Refs. [13,14]. A simple way to avoid, at least partly, the limitations of the GC theory is by taking into account the finite size of the ions in the first molecular layer near the surface as suggested by Stern [15]. Although also this approach has been criticised [16] experience has shown that the SGC models work very satisfactory in practice.

2.2. Stern–Gouy–Chapman double layer model and specific adsorption

In the Stern–Gouy–Chapman (SGC) theory the double layer is divided into a Stern layer, adjacent to the surface with a thickness d_1 and a diffuse (GC) layer of point charges. The diffuse layer starts at the Stern plane at distance d_1 from the surface. In the most simple case the Stern layer is free of, charges. The presence of a Stern layer has considerable consequences for the potential distribution: across the Stern layer the potential drops linearly from the surface potential ψ_s to the potential at the Stern plane, ψ_d. Often ψ_d is considerably lower than ψ_s, especially in the case of specific adsorption (s.a.).

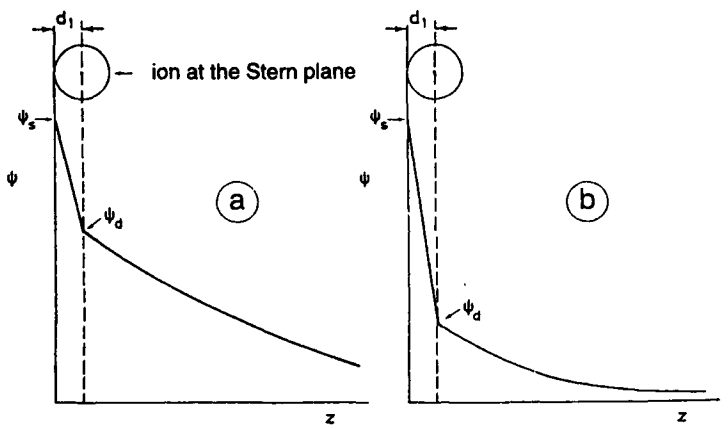

Figure 1. Potential decay for the SGC model. (a) In the absence of specific adsorption; (b) with weak specific adsorption of counterions.

The potential drop ($\psi_s - \psi_d$) is related to the Stern layer capacitance C_1:

$$\psi_s - \psi_d = \frac{\sigma_s^*}{C_1} \tag{20}$$

where σ_s^* is the net charge density at the surface plane and C_1 is a positive quantity defined as:

$$C_1 = \frac{\varepsilon_1 \varepsilon_0}{d_1} \tag{21}$$

with ε_1 the relative permittivity of the medium in the Stern layer and d_1 is of the order of the diameter of water molecules. Equation (21) can be compared to Eq. (17) expressing the diffuse layer capacitance for low potentials.

The values of both d_1 and ε_1 are affected by the type of surface and separation of the two quantities is not necessary if C_1 is considered as one (adjustable) parameter that accounts for differences in the solution part of the double layer for different surfaces. For mineral oxide/aqueous electrolyte solution interfaces C_1 has a high value (1 to 2 mF/m^2) [17], i.e. assuming that d_1 is of the order of a molecular diameter, ε_1 turns out to be of the same order of magnitude as ε_r of the bulk solution. The relatively large value of C_1 as compared to that for the AgI or Hg aqueous solution interface is due to the presence of the surface hydroxyls [18]. In principle C_1 is also a function of the charge density, but in practice C_1 is often considered to be constant.

The Stern layer concept can be used with or without specific adsorption of s.a. ions. Even in the absence of specific adsorption the first consequence of the SGC model as compared to the GC model is that the distinction between c.d. ions and other ions becomes more pronounced: ψ_s is the leading potential for the c.d. ions, ψ_d that of the other ions.

In the presence of s.a. ions one has to decide at which plane these ions adsorb. The most simple choice is that the s.a. ions are located at the Stern plane. This choice is appropriate for ions that form outer sphere complexes with the surface sites or for ions that have no affinity for the proton sites. Specifically adsorbing counterions that are forming inner sphere complexes with the surface groups screen the primary surface charge very effectively and the difference between primary and secondary surface charge becomes vague. In this case it is appropriate to place the s.a. charge at the surface plane, or partly at the surface plane and partly at the Stern plane.

When the s.a. charge is subdivided over two planes, the fraction of the charge brought to the surface plane can be determined using Paulings concept of bond valence [19]. In solution many s.a. ions are surrounded by a primary hydration shell or with oxygen groups. According to the bond valence principle the central ion in such a complex distributes its charge over the co-ordinated ligands and the bond valence, ν, is the charge of the central ion divided by its co-ordination number. When it is assumed that s.a. ion X^z binds with n_x of its ligands to the surface groups, it brings a charge fraction $n_x\nu_x$ to the surface plane and a fraction ($z_x - n_x\nu_x$) to the Stern plane. That is to say, the total s.a. charge of X, σ_x, is separated into two contributions: $(n_x\nu_x/z_x)\sigma_x$ is placed at the surface plane and $\{(z_x - n_x\nu_x)/z_x\}\sigma_x$ at the Stern plane. The s.a. charge, σ_0, at the surface plane is then:

$$\sigma_0 = \sum_x \frac{n_x \nu_x \sigma_x}{z_x} \tag{22}$$

where the summation covers the specific adsorption over all species X. The s.a. charge, σ_1, at the Stern plane becomes:

$$\sigma_1 = \sum_x \left(\frac{z_x - n_x \nu_x}{z_x} \right) \sigma_x \tag{23}$$

In the above equations the σ_i values include the charge sign and electroneutrality of the double layer requires that:

$$\sigma_s + \sigma_0 + \sigma_1 + \sigma_d - 0 \tag{24}$$

In practice one has to decide for each s.a. ion what type of complex it forms with the surface sites.

In order to calculate the surface potential it should be realised that ψ_s can be divided in two parts:

$$\psi_s = (\psi_s - \psi_d) + \psi_d \tag{25}$$

By combination of Eq. (25) with Eq. (20) and using $\sigma_s^* = \sigma_s + \sigma_0$ and $-\sigma_d = \sigma_s + \sigma_0 + \sigma_1$ one obtains:

$$\psi_s = \frac{\sigma_0 + \sigma_s}{C_1} + \frac{2RT}{\tau F} \operatorname{arcsinh} \left\{ \frac{-\sigma_d}{(8RT\varepsilon_0\varepsilon_r c_s)^{1/2}} \right\} \tag{26}$$

Note that ψ_s is the leading potential for the adsorption of c.d. ions, whereas both ψ_s and ψ_d determine the adsorption of s.a. ions that form inner sphere surface complexes (see Eq. (53)). Equation (26) is quite general. In the absence of s.a. both σ_0 and σ_1 are zero and $\sigma_s = -\sigma_d$. For s.a. ions that form outer sphere complexes $n_x = 0$, $\sigma_0 = 0$ and $\sigma_s + \sigma_1 = -\sigma_d$. For inner sphere complexes the full Eq. (26) holds and one has to decide whether a mono-dentate or a bi-dentate complex is formed. The advantage of the above way of modelling is that specificity is introduced by giving each type of ion its own "screening ability" without introducing adjustable parameters.

In general it is difficult, if not impossible, to measure ψ_s directly. At best one can measure changes in ψ_s as a function of the solution concentration of c.d. ions using the ISFET technique [20, 21]. However, in most cases ψ_s has to be calculated with Eq. (26) using measured values of σ_i. A way to derive ψ_d from experimental data is by equating ψ_d to the electrokinetic potential ζ [2]. For low values of the ionic strength this is a good approximation. Once ψ_d is known σ_d can be calculated with Eq. (12) and $\sigma_0 + \sigma_1$ can be calculated using Eq. (24) when σ_s is obtained from potentiometric titrations. For a given value of the Stern layer capacitance ψ_s can now be calculated using Eq. (26).

2.3. Triple layer model

In all situations discussed so far only one Stern layer capacitance is required. In literature it is however often assumed [7, 8, 22] that diffuse ions can approach the surface up to the Stern plane and that s.a. ions are located at a newly defined adsorption plane, the inner Helmholtz plane. The inner Helmholtz plane is located in between the surface plane and the Stern or outer Helmholtz plane. The double layer model composed of an inner and outer Helmholtz layer plus a diffuse layer is generally called the triple layer (TL) model.

The potential drop over the inner Helmholtz layer and the outer Helmholtz layer can be described by two capacitances: the inner and the outer Helmholtz layer capacitance.

Although for ideally flat interfaces it is physically elegant to make a distinction between an inner and an outer Helmholtz plane [7, 8], this distinction is hardly relevant for ordinary solids where the presence of surface irregularities makes it impossible to obtain unique values for the capacitances of both Helmholtz layers. Therefore rather arbitrary assumptions have to be made about at least one of the capacitances, whereafter the other capacitance value is used together with other model parameters as fitting parameter. The value of 0.2 F/m^2 often assumed for the outer Helmholtz layer capacitance is not realistic for oxide surfaces [18, 23] and may lead to obscurities with the other fitting parameters.

In authors opinion regulation of the screening of the surface charge by specific adsorption can adequately be incorporated by placing the s.a. ions at either the Stern plane (outer sphere complexes) or surface plane (inner sphere complexes). When a higher degree of sophistication is required Paulings bond valence principle [19] can be used to partition the valence of the s.a. ion over the surface plane and the Stern plane as indicated above. This also allows to discriminate between mono–dentate and bi–dentate binding. Therefore, and to avoid superfluous parameters that make the double layer model unnecessary complex the use of the Stern layer model in which the inner and outer Helmholtz plane coincide is strongly recommended. Especially when the surface is treated as pseudo homogeneous it overdone to introduce at the solution side of the double layer arbitrary details.

3. DOUBLE LAYER MODELS FOR PERMEABLE PARTICLES

3.1. Donnan model

The SGC model is developed for rigid particles. Treatment of particles that are highly porous or permeable for ions, as is e.g. the case for some silicas, can be done on the basis of a Donnan model [24, 25, 26]. In this case the particle charge is considered to be restrained in about the particle volume by a hypothetical membrane permeable to small ions only. The membrane separates two phases: the bulk solution and the Donnan phase. The Donnan phase volume or Donnan volume is the solution volume within the membrane. The Donnan volume contains the primary charge (fixed at the solid matrix), these charges lead to a potential distribution around the charged sites. With sufficient charges present the local double layers overlap strongly and result in approximately one electrostatic potential $\psi_{d,D}$ inside the entire Donnan phase. Similarly as in the GC theory $\psi_{d,D}$ is defined with respect to the bulk solution. At the surface of the membrane the electrostatic potential drops to zero in this simple model.

Due to the presence of $\psi_{d,D}$ counterions of the primary charges are accumulated in the Donnan phase and co–ions repelled. In equilibrium the electrochemical potentials of the small ions at each side of the membrane must be the same, this can be expressed as:

$$c_{i,D} = C_i \exp\left(\frac{-\tau_i F \psi_{d,D}}{RT}\right) \tag{27}$$

where $c_{i,D}$ is the ion concentration in the Donnan phase and c_i that in bulk solution. In deriving Eq. (27) it has been assumed that there are no specific effects, both the solution

and the Donnan phase are ideal. The primary charge density in the Donnan phase, $\rho_{s,D}$ is related to the proton and hydroxyl ion uptake:

$$\rho_{s,D} = \frac{F(X_H - X_{OH})}{V_D} \tag{28}$$

where X_i is the uptake of i in mol/kg, V_D is the specific volume of the Donnan phase in m^3/kg and $\rho_{s,D}$ is expressed in C/m^3. In the absence of s.a. $\rho_{s,D} = -\rho_{d,D}$ where $\rho_{d,D}$ is the "diffuse" Donnan charge.

The concentrations of small ions inside the Donnan phase can be obtained from the condition of electroneutrality in this phase. In the presence of a symmetrical indifferent electrolyte one obtains:

$$\rho_{d,D} = F\tau(c_{+,D} - c_{-,D}) \tag{29}$$

where it has been assumed that the contributions of the H^+ and OH^- ions to the charge neutralisation are small and can be neglected. Substitution of the expressions for $c_{i,D}$ in Eq. (29) leads to the expression for $\rho_{d,D}$ as a function of $\psi_{d,D}$:

$$-\rho_{d,D} = 2\tau c_s F \sinh\left(\frac{\tau F \psi_{d,D}}{RT}\right) \tag{30}$$

or of $\psi_{d,D}$ as a function of $\rho_{d,D}$

$$\psi_{d,D} = \frac{RT}{\tau F} \operatorname{arcsinh}\left(\frac{-\rho_{d,D}}{2\tau c_s F}\right) \tag{31}$$

For low potentials these expressions reduce to:

$$-\rho_{d,D} = \left(\frac{2\tau^2 c_s F^2}{RT}\right)\psi_{d,D} = \kappa^2 \varepsilon_0 \varepsilon_r \psi_{d,D} \tag{32}$$

The above equations can be compared with the GC equations (11), (12) and (19) for ψ_d and σ_d respectively. In the Donnan equations the salt concentration appears directly, whereas in the GC equations κ or $\sqrt{c_s}$ appears, this indicates that the salt effects are relatively large for the Donnan model.

The simple Donnan model has limitations that are comparable to those of the GC model. The assumption that $\psi_{d,D} = 0$ just outside the hypothetical membrane is reasonable as long as the particle size is much larger than κ^{-1}. For particle sizes that are of the order of κ^{-1} the hypothetical membrane can be thought at about a distance κ^{-1} from the particle surface to incorporate the diffuse layer ions in the Donnan phase [25]. Ultimately this leads to a value of V_D that is larger than the void volume inside the particles and an average Donnan potential that is somewhat lower than the potential without this correction. The magnitude of the differences will depend on κ^{-1}.

3.2. Stern–Donnan model and specific adsorption

A notable limitation of the simple Donnan model is that the potential may not be uniformly distributed through the Donnan phase: close to the charged sites the potential will be the highest and the fixed charges may be grouped together in small island like domains [24]. Potentials calculated with Eq. (31) therefore tend to be the average potentials inside

the Donnan phase and $c_{i,D}$ values are averages too. To some extent this weakness can be corrected by taking into account two potentials rather than one: $\psi_{s,D}$ at the location of the charged sites and starting at a molecular distance d_1 of the sites a lower potential $\psi_{d,D}$ in the remainder of the Donnan phase. The layer d_1 is assumed to be free of charges. Formally the potential $\psi_{s,D}$ can now be split in two contributions:

$$\psi_{s,D} = (\psi_{s,D} - \psi_{d,D}) + \psi_{d,D} \tag{33}$$

where $\psi_{d,D}$ is given by Eq. (31) and the potential drop $(\psi_{s,D} - \psi_{d,D})$ can be defined by introducing a proportionality factor, $C_{1,D}$, comparable to the Stern layer capacitance in the SGC model:

$$\psi_{s,D} - \psi_{d,D} = \frac{\rho_{s,D}}{C_{1,D}} \tag{34}$$

In order to keep the model simple $C_{1,D}$ is assumed to be independent of the salt concentration and $\rho_{s,D}$. $C_{1,D}$ is an adjustable parameter, expressed in F/m^3, that allows us to make a Donnan model of a similar complexity as the SGC model. The potential $\psi_{s,D}$ can now be written as:

$$\psi_{s,D} = \frac{\rho_{s,D}}{C_{1,D}} + \frac{RT}{\tau F} \operatorname{arcsinh} \left(\frac{-\rho_{d,D}}{2\tau c_s F}\right) \tag{35}$$

Similarly as with C_1 in the SGC model introduction of $C_{1,D}$ in the Donnan model allows incorporation of specific effects due the type of solid and distinguishes between c.d. ions and other ions. For c.d. ions $\psi_{s,D}$ is the leading potential and other ions are governed by $\psi_{d,D}$. For the c.d. ions $\psi_{d,D}$ in Eq. (27) has therefore to be replaced by $\psi_{s,D}$.

In the presence of s.a. ions the primary charge $\rho_{s,D}$ is partially compensated by the s.a. charge $\rho_{1,D}$, the remainder by the "diffuse" Donnan charge $\rho_{d,D}$. In the case of weak adsorption the s.a. ions are located at distance d_1 and Eq. (35) can be used with $-\rho_{d,D} = \rho_{s,D} + \rho_{1,D}$. In the case of strong ion complexation (inner sphere complexes formed) the complexing ions can be placed at the site of the primary charges and Eq. (35) has to be modified to:

$$\psi_{s,D} = \frac{\rho_{s,D} + \rho_{1,D}}{C_{1,D}} + \frac{RT}{\tau F} \operatorname{arcsinh} \left(\frac{-\rho_{d,D}}{2\tau c_s F}\right) \tag{36}$$

In this case both the adsorption of c.d. ions and that of s.a. ions is determined by $\psi_{s,D}$, so that for these ions $\psi_{d,D}$ in Eq. (27) should be replaced by $\psi_{s,1}$.

A discussion of the Donnan model, including its use in mixed electrolytes, has been given by Bolt [26]. Bolt applied these models for the description of the ion exchange properties of clay minerals. Ohshima and Kondo [27] give more elaborate expressions for the potential inside and outside the Donnan phase. Their results are based on a uniform density of the fixed sites and they show that $\psi_{d,D}$ decreases if the outer bound of the Donnan phase is reached.

Because of the similarity with the SGC model the modified Donnan model will be called the Stern-Donnan (SD) model. The SD model is newly derived and intended to be of use for a description of ion adsorption in porous or permeable particles without having to specify the permeability or porosity precisely. The SD model with small islands

of charge is a kind of hybride between the simple Donnan model and a simple constant capacitance double layer model for a rigid surface.

4. ADSORPTION OF SURFACE CHARGE DETERMINING IONS

4.1. Site binding

In the previous section the presence of a surface charge has been presumed and the solution side of the double layer was analysed. In this section the adsorption of c.d. ions will be discussed. Based on earlier work of the Australian group Healy and White [28] have formulated the statistical thermodynamic backgrounds for adsorption of c.d. ions on a homogeneous substrate. Essentially their treatment extends the Langmuir model for adsorption by considering not only "chemical" or "intrinsic" interactions with the surface, but also coulombic interactions. The chemical interactions are characterised by an intrinsic affinity constant, the coulombic interactions by taking into account the surface potential. The adsorption of c.d. ions to specific sites at the surface is briefly called site binding. Healy and White [28] mainly considered the adsorption of c.d. ions in the presence of an indifferent electrolyte. Other reviews [21, 29, 30] also discuss c.d. ion adsorption in the presence of specific adsorption.

In the next sections adsorption isotherm equations for primary c.d. ions will be discussed. The model will be illustrated for homogeneous surfaces with one type of surface group in contact with an electrolyte solution. This simple system serves as a starting point for a more detailed description in which surface heterogeneity is taken into account.

4.2. Origin of the surface charge

The surface charge description of amphoteric mineral oxides has been given considerable attention in literature [see e.g. 22, 28–30], but, to some extent, it is still controversial. The controversy essentially boils down to the representation of the surface group(s) that act as proton adsorption site(s). In the classical [22, 30] and most common approach the surface is assumed to be monofunctional with a postulated surface oxygen group that can undergo two protonation steps, each governed by its own pK_H value ("two-pK_H" model):

$$SO^- + H^+ \rightleftharpoons SOH \qquad K_{H,1} \tag{37a}$$

$$SOH + H^+ \rightleftharpoons SOH_2^+ \qquad K_{H,2} \tag{37b}$$

In 1982 Bolt and Van Riemsdijk [31, 32] proposed an alternative representation of the surface oxygen groups:

$$SOH^{1/2-} + H^+ \rightleftharpoons SOH_2^{1/2+} \qquad K_H \tag{38}$$

In this way only one protonation step and one pK_H value is required to be able to describe the amphoteric character of the mineral oxides ("one-pK_H" model). Fairly recently

Hiemstra et al. [18, 33, 34] have suggested an integrated approach that enables a critical examination of the older models. This model is the basis for the present treatment.

Premises of the treatment of Hiemstra et al. are: (a) the chemistry of the surface groups can be derived from the structure of the mineral oxides using Paulings concept of bond valence [19], (b) surface oxygens are the sites for proton adsorption, they can associate with one or two protons. This leads to the following protonation reactions of a surface oxygen:

$$Me_n - O^{(n\nu-2)} + H^+ \rightleftharpoons Me_n - OH^{(n\nu-1)} \qquad K_{n,1} \qquad (39a)$$

$$Me_n - OH^{(n\nu-1)} + H^+ \rightleftharpoons Me_n - OH_2^{(n\nu)} \qquad K_{n,2} \qquad (39b)$$

where ν is the bond valence (local neutralisation of charge) and n the number of metal ions that are co-ordinated to the oxygen group. Due to the introduction of the bond valence ν the formal charge per site is not necessarily an integer, common values of ν for metal ions in a hexa-co-ordination are 1/2 and 1/3. In metal (hydr)oxides different types of surface oxygens can be present: singly (n=1), doubly (n=2) and triply (n=3) co-ordinated with metal cations of the solid. Note that the classical representation with Eqs. (37a) and (37b) is a special case of Eqs. (39a) and (39b) for n=1 and ν=1, whereas the model suggested by Bolt and Van Riemsdijk (Eq. (38)) is equivalent to Eq. (39b) for n=1 and ν=1/2.

The equilibria (39a) and (39b) show that for a monocomponent surface with only one type of surface oxygen, in general, two protonation reactions are possible and two equilibrium protonation constants, $K_{n,1}$ and $K_{n,2}$, are required to describe the protonation. In principle, each monofunctional oxide surface therefore is a "two-pK_H" surface. In practice it is, however, quite well possible that, in the ordinary pH range, only one of the two reactions is "active" so that the monofunctional surface behaves as a "one-pK_H" surface. The "activity" of each of the two reactions depends on its $pK_{n,i}$ value. For the description of the charging of a metal oxide surface it is thus of importance to have *a priori* knowledge of the set of $pK_{n,i}$ values of the different surface oxygens. Whether a monofunctional metal oxide surface should be treated as a "two-pK_H" surface or as a "one-pK_H" surface is thus not a matter of principle, but of practice. In order to be able to judge what will happen in practice Hiemstra et al. have provided a method for the *a priori* calculation of the intrinsic protonation constants of the surface oxygens on the basis of the behaviour of metal (hydr)oxide complexes in solution.

Hiemstra also emphasises surfaces heterogeneity by noting that (a) the surface planes may contain more than one type of surface oxygens and (b) crystalline metal oxides expose different crystal planes to the solution and these planes will, in general, have different surface groups. For an appropriate description of the protonation of oxide surfaces the multi site type (multifunctional) nature is thus essential and the authors have called their model: MUSIC, an acronym for multi site complexation. For optimal use of MUSIC the intrinsic protonation constants have to be known *a priori*.

4.3. Log $K_{n,i}$ values for the protonation of the surface oxygens

The calculation of the log $K_{n,i}$ values by Hiemstra et al. [33] is based on Paulings idea of local charge neutralisation [19] in combination with the assumption that the standard Gibbs energy of adsorption of a proton according to Eq. (39a) or (39b) is depending on the local electrostatics. In principle this type of approach had been used before by Parks [35] and Yoon et al. [36] to study the pzc of oxides. Hiemstra derives the following simple expression for log $K_{n,i}$:

$$\log K_{n,i} = A - B(n\nu/L) \tag{40}$$

where A and B are constants, L is the distance between the metal ion and the adsorbed proton and n and ν are introduced with Eq. (39). Once A and B are known log $K_{n,i}$ can be calculated. In order to obtain A and B first the protonation reactions of metal (hydr)oxides in solution, for which the log $K_{1,i}$ values, ν, L and n (n=1) are known, are analysed using Eq. (40). A distinction has been made between oxo and hydroxo complexes and between two different electron configurations of the central metal ion. For each class of complexes log $K_{1,i}$ vs. $n\nu/L$ turns out to be a straight line with a slope B that is the same for all four classes. Based on this observation Hiemstra et al. assume that for oxygen groups on metal (hydr)oxide surfaces the value of B is the same as that observed for the solution complexes, i.e.

$$B(\text{surface complex}) = B(\text{solution complex}) \tag{41}$$

The value of A differs strongly for the comparable oxo and hydroxo complexes. The difference amounts to 14 log K units which is of the same order of magnitude as that between the log K values for the two protonation steps of a water oxygen (17 log K units). The value of A(surface complex) should in general be different from A(solution complex) because of the difference in spatial arrangement. To calibrate the shift of A(solution complex) to A(surface complex) Gibbsite is used as primary reference material. Gibbsite, $Al(OH)_3(s)$, is a well defined metal oxide that obtains its surface charge through protonation of the $Al\text{–}OH^{1/2-}$ group for which a log K_H value equal to 10 ± 0.5 has been established [34, 37] (see also sec. 4.7.). Comparison of this value with the log K of the corresponding solution complex $Al(OH)_3{\cdot}3H_2O$, shows that the proton affinity constant for the surface group of this crystalline oxide is 4 log K units higher. Next it is assumed that the same difference holds for the other crystalline oxides. For corresponding solution and surface complexes one thus finds

$$A(\text{surface complex, crystalline solid}) = A(\text{solution complex}) + 4 \tag{42a}$$

For silica, an amorphous oxide, with a less perfect structure A(surface complex) may be less different from A(solution complex). Silica is therefore used as second reference material. Silica obtains its charge by dissociation of the Si–OH group. By comparing experimental results with model calculations for silica Hiemstra [34] finds a log K_H value of 7.2 to 7.5 (see also sec. 4.6), which is very similar to the log K_H of Si–OH complexes in solution so that

$$A(\text{surface complex, silica}) \approx A(\text{solution complex}) \tag{42b}$$

With Eqs. (40) to (42) the proton association constants of surface groups can be calculated using n, ν and L derived from structure and/or crystallographic data of the oxides.

Table 1 shows the collection of proton association constants for a series of surface groups on various important metal (hydr)oxides calculated by Hiemstra et al. [33].

In judging these values it should be realised that for the solution complexes n=1, whereas for surface complexes n can be 1, 2 or 3. Although the effect of n is incorporated in the model it is to be expected that for the high the values of n the predictions are a first order approximation only. For oxides with partially disordered crystal faces or for oxide layers deposited on other surfaces, where the crystalline structure of the oxide layer may be less perfect than that of the pure crystalline oxide [38], the values quoted in Table 1 should be considered as upper limits. The lower limits are obtained by subtracting 4 log K units from the given value. For silica two limits are presented: the values in brackets are upper limits based on Eq. (42a), the lower, more realistic values are based on Eq. (42b). Hiemstra et al. [18, 33, 34] have been successful in describing both the pzc and the charge vs. pH curves of a number of crystalline metal oxides using the data of Table 1. A discussion of the method to obtain the log K values, including some suggestions to simplify the calculation of the constants, has been presented by Bleam [39].

Table 1
Calculated proton association constants for a series of surface groups

Surface group	Formal charge	log K_H
Al–OH	-1/ 2	10.0
Al_2–O	-1	12.3
Al_2–OH	0	-1.5
Al_3–O	-1/2	2.2
Fe–OH	-1/2	10.7
Fe_2–O	-1	13.7
Fe_2–OH	0	-0.1
Fe_3–O	-1/2	4.3
Ti–OH	-1/3	6.3
Ti_2–O	-2/3	5.3
Ti_3–O	0	-7.5
Si–O	-1	(11.9) 7.5
Si–OH	0	(-1.9) -5
Si_2–O	0	(-16.9) -20

4.4. One–pK_H or two–pK_H model

Tabulated log K values for the different surface oxygen groups can now be used to judge the practical reality of Eqs. (39a) and (39b). The conclusion is that the difference between $\log K_{n,1}$ and $\log K_{n,2}$ for the protonation of the corresponding oxo and hydroxo complex amounts to about 14 log K units. This implies that only one of the protonation reactions will be "active" in the normally accessible pH range. In practice, surface oxygens therefore behave as "one–pK_H" groups, or alternatively, monofunctional surfaces act as "one–pK_H" surfaces. The description of the amphoteric nature of a homogeneous oxide surface by Eqs. (37a) and (37b) is thus always an artefact. The two pK_H values, found by fitting the two–pK_H model to experimental data cannot belong to the same surface

oxygen unless $\Delta pK \approx 14$ and such large values are not found in practice. The one-pK_H model based on Eq. (38), provides the correct expression if the surface is homogeneous and the charges of the surface groups are $1/2^-$ and $1/2^+$ respectively.

For ordinary (heterogeneous) surfaces both older models are in principle incorrect. Treating heterogeneous surfaces as pseudo homogeneous using the one-pK_H model has the great advantage that it is a simple model that gives a fairly realistic description of the amphoteric nature of the oxides. The two-pK_H model complicates the situation by using two pK_H values to describe the amphoteric nature. In the model the two log K_H values belong to the same surface oxygen, but in practice they have to represent different groups. As compared to the one-pK_H model an additional and superfluous parameter is introduced that has no physical significance.

Before discussing heterogeneous oxides in detail, homogeneous (mono-functional) surfaces will be considered. Hiemstra et al. [34] have shown that to a good approximation Gibbsite, $Al(OH)_3(s)$, and silica, SiO_2, have only one active type of surface oxygen that reacts with a proton in the normal pH range. For these monofunctional surfaces the site binding treatment will be illustrated in some detail. The treatment of multifunctional surfaces is a logical extension of the monofunctional surfaces.

4.5. Surface charge of monofunctional surfaces

In Gibbsite, $Al(OH)_3(s)$, the structure is characterised by Al^{3+} in a hexa- co-ordination with OH^- [33, 34, 37]. For the neutralisation of each OH two Al ions participate, however, at the surface broken bonds occur that cause a lacking degree of neutralisation of the OH groups and this lack will lead to proton adsorption. The dominant planar 001 face of Gibbsite has doubly co-ordinated surface oxygens, whereas the edge face has doubly and singly co-ordinated oxygen groups. The doubly co-ordinated Al_2-OH^0 groups are inert in the normal pH range (see Table 1), so that the singly co-ordinated Al-$OH^{1/2-}$ groups at the edges are the active groups. For the protonation one can thus write:

$$Al - OH^{1/2-} + H + \rightleftharpoons Al - OH_2^{1/2+} \tag{43}$$

Equation (43) is a special case of the general reaction (39b) with n=1 and ν=+1/2 and it corresponds to the one-pK_H model represented by Eq. (38). In principle it is also possible to desorb a proton from the Al-$OH^{1/2-}$ group, but in the normal pH range this is not feasible.

An alternative and also quite simple situation occurs for silica [34]. The silica structure can be considered as the result of polymerisation of silica tetrahedra in which the charge of the Si^{4+} ion is distributed over four oxygens, which is equivalent to a bond valence $\nu = 1$, i.e. two Si ions can neutralise the negative charge of an oxygen. At the surface this leads to doubly co-ordinated Si_2-O^0 groups and singly co-ordinated Si-O^- groups. In the ordinary pH range the Si_2-O^0 group can be considered as inert (see Table 1), but the Si-O^- groups may react with a proton

$$Si - O^- + H^+ \rightleftharpoons Si - OH^0 \tag{44}$$

Equation (44) is an example of reaction (39a) with ν=1 and n=1. In principle this reaction can be followed by the adsorption of a second proton but in the normal pH range this is not likely (see Table 1).

Equations (43) and (44) are very useful as starting point for the site binding approach. In general both reactions can be written in a simplified form

$$S + H \rightleftharpoons SH \tag{45}$$

where S is the reference site (SiO^- or $Al\text{-}OH^{1/2-}$) that can accept a proton and SH is the protonated site. According to Healy and White [28] the adsorption of a proton according to Eq. (45) from an electrolyte solution containing an acid or base to site S can be described as:

$$K_H = \frac{\{SH\}}{\{S\}\{H_s\}} \tag{46}$$

where $\{H_s\}$ is defined as:

$$\{H_s\} = \{H\} \exp\left(-\frac{F\psi_s}{RT}\right) \tag{47}$$

and { } denotes a surface group activity (mol/m^2) or solution activity (mol/m^3) and K_H is the equilibrium constant for proton association with site S in the absence of the surface charge. $\{H_s\}$ is an expression for the proton activity in the solution at the location of the proton adsorption site. Due to the negative surface charge protons accumulate near the surface according to Eq. (2) and at the location of the surface sites the (smeared out) potential equals ψ_s. The proton activity in bulk solution, $\{H\}$, can be found from the pH or the proton concentration [H] and the bulk activity coefficient $\gamma_\pm$ [40, 41]. The equilibrium constant K_H is related to the standard Gibbs energy of adsorption Δg_H^0:

$$K_H = \frac{1}{55.5} \exp\left(-\frac{\Delta g_H^0}{RT}\right) \tag{48}$$

where 55.5 is the molar concentration of water. Discreteness of charge effects are assumed to be constant and included in K_H [23, 28, 33]. K_H is a measure of the proton affinity for site S at the point where $\psi_s = 0$. Some values of $\log K_H$ for different surface groups are shown in Table 1.

In the presence of s.a. sites S and SH may also form complexes with respectively a cation, C, or an anion, A, according to Eqs. (49) and (50):

$$S + C \rightleftharpoons S - C \qquad K_C \tag{49}$$

and

$$SH + A \rightleftharpoons SH - A \qquad K_A \tag{50}$$

The adsorption of cations and anions can be described with respectively Eqs. (51) and (52):

$$K_C = \frac{\{S - C\}}{\{S\}\{C_{sd}\}} \tag{51}$$

$$K_A = \frac{\{SH - A\}}{\{SH\}\{A_{sd}\}} \tag{52}$$

where K_C and K_A are the intrinsic equilibrium constants and $\{C_{sd}\}$ and $\{A_{sd}\}$ are the activities of C and A in solution at the location of the sites. For complexes of ions X with n_x valence bonds co-ordinated with the surface (see sec. 2.2.) these activities can be expressed by Eq. (53):

$$\{X_{sd}\} = \{X\} \exp\left[-\frac{n_x \nu_x F(\psi_s - \psi_d)}{RT} - \frac{z_x F \psi_d}{RT}\right] \tag{53}$$

For inner sphere complexes with the entire charge at the surface plane $n_x \nu_x = z_x$ and the Boltzmann factor becomes simply $\exp(-z_x F \psi_s / RT)$. For outer sphere complexes $n_x = 0$ and both activities are determined by ψ_d only. Assuming that, except for the electrostatic interactions, the surface phase behaves ideal, the ratios of the surface group activities in Eqs. (46), (51) and (52) can be replaced by ratios of site fractions, $\theta_X = SX/N_s$ where N_s is the total density of surface sites:

$$N_s = \{S\} + \{SH\} + \{S - C\} + \{SH - A\} \tag{54}$$

The adsorption isotherm equations become:

$$\frac{\theta_H}{\theta_R} = K_H\{H_s\} \tag{55}$$

for the protons,

$$\frac{\theta_C}{\theta_R} = K_C\{C_{sd}\} \tag{56}$$

for the cations, and

$$\frac{\theta_A}{\theta_H} = K_A\{A_{sd}\} \tag{57}$$

for the anions. The anion adsorption can also be expressed with respect to the reference site S by using Eq. (55):

$$\frac{\theta_A}{\theta_R} = K_H K_A\{H_s\}\{A_{sd}\} \tag{58}$$

In these equations $\theta_R = 1 - \Sigma_i \theta_i$ with i (H, C, A). The expression for θ_R emphasises the competitive (multicomponent) nature of the adsorption. θ_R equals in the present situation:

$$\theta_R = [1 + K_H\{H_s\} + K_C\{C_{sd}\} + K_H K_A\{H_s\}\{A_{sd}\}]^{-1} \tag{59}$$

In the absence of specific adsorption $\theta_R = (1 + K_H\{H_s\})^{-1}$ and Eq. (55) simplifies to:

$$\theta_H = \frac{K_H\{H_s\}}{1 + K_H\{H_s\}} \tag{60}$$

Equation (60) is formally equivalent to the Langmuir equation, but $\{H_s\}$ is not a bulk concentration.

So far the model is still quite general and the same for silica and gibbsite, the difference between the two surfaces appears upon introduction of the charge density. For silica the surface charge density equals:

$$\sigma_s = -F[\{S\} + \{S - C\}] = -FN_s(\theta_R + \theta_C) = -FN_s(1 - \theta_H - \theta_A) \tag{61}$$

whereas for gibbsite we have:

$$\begin{aligned}\sigma_s &= 0.5F[-\{S\} + \{SH\} - \{S - C\} + \{SH - A\}] = \\ &= 0.5FN_s(-\theta_R + \theta_H - \theta_C + \theta_A) = -0.5FN_s(1 - 2\theta_H - 2\theta_A)\end{aligned} \tag{62}$$

In the absence of s.a. the pzc of silica is obtained from Eq. (61) for $\theta_H = 1$ and $\theta_A = 0$. Under these conditions the pzc for gibbsite is obtained from Eq. (62) for $\theta_H = 0.5$ and $\theta_A = 0$. In order to illustrate the consequences of the difference in charging behaviour of silica and gibbsite $(1 - \theta_H)$ in the absence of s.a. (see Eq. (60)) is plotted in Fig. 2 as a function of $\log K_H\{H_s\}$.

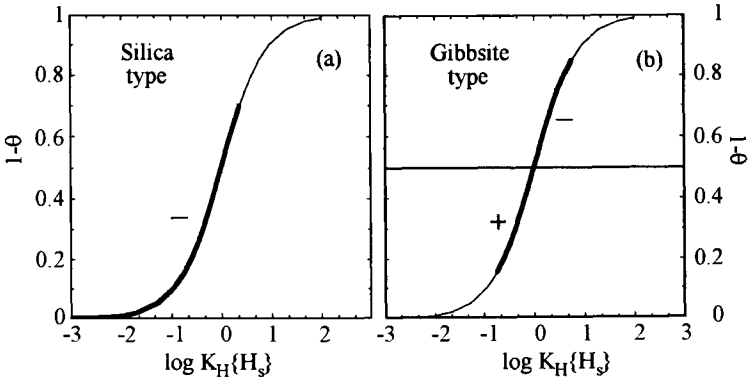

Figure 2. Charging behaviour of silica type (panel a) and gibbsite type (panel b) surfaces.

In these plots the electrostatic repulsion is masked (incorporated in $\{H_s\}$). Figure 2a clearly shows that for silica the pzc is reached asymptotically, $(1 - \theta_H) \rightarrow 0$ and that charging is relatively difficult. For gibbsite, Fig. 2b, the pzc occurs at $\theta_H = 0.5$ with a sharp intersection point with the zero charge axis and charging the surface (either positive or negative) is relatively easy. Replacing pH_s by pH does not affect this characteristic difference, it will only lower the slope of the curves. As will be shown below also the surface potential vs. pH relation differs for silica and gibbsite. In general, different types of silica follow the silica curve [42], see Fig. 3, whereas most of the other common metal (hydr)oxides [43] have σ_s vs. pH curves that resemble the gibbsite curve, see Fig. 4.

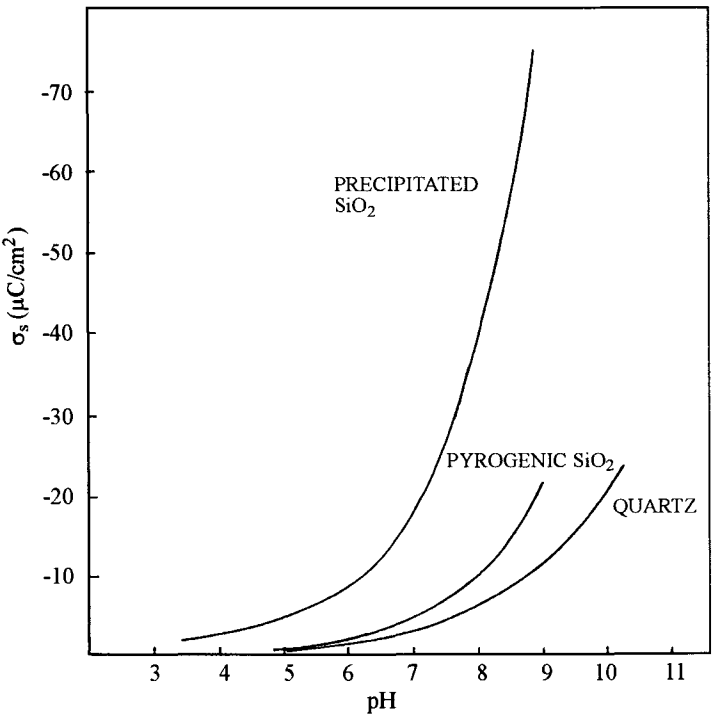

Figure 3. Surface charge-pH curves for different silicas [42b].

Based on this difference and as a first order approximation two classes of mineral oxides can be distinguished: silica type and gibbsite type. The special behaviour of silica type surfaces is due to the fact that near the pzc of silica a considerable number of uncharged surface groups is present, whereas for the gibbsite type oxides charge neutralisation is due to compensation of positive and negative groups.

In practice isotherm Eqs. (55) to (58) cannot be used directly. For instance, even when it is assumed that s.a. is absent and that N_s, K_H and $\{H\}$ are known, $\{H_s\}$ is not known as long as ψ_s is unknown. For the s.a. ions the same applies. As mentioned in sec. 2.2. it is difficult to measure ψ_s directly. The problem can be solved by combining the site binding model with one of the double layer models described in sects. 2 and 3. The double layer model provides the additional relation between σ_s and ψ_s. In principle the adequacy of the chosen double layer model can be verified, independent of the site binding model, by replotting the experimental σ_s vs. pH data at different salt concentrations as σ_s vs. pH_s curves. When the double layer model is appropriate the result is a "master curve" [44,45]. For a homogeneous one-pK_H surface the master curve should reflect Fig. 2 (Langmuir curve). For a heterogeneous surface the master curve reflects the chemical heterogeneity observed by the protons [44, 46-48].

The combination of site binding model and double layer model will be worked out in some more detail for silica and gibbsite type surfaces in the next two sections.

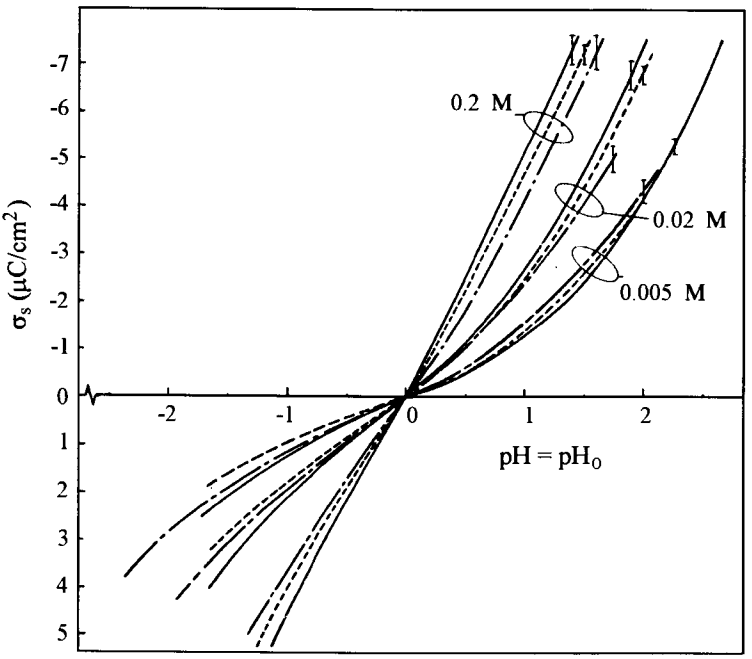

Figure 4. Surface charge-pH curves for rutile (—), rhutenium dioxide (– – –) and haematite (– · –) in KNO_3 [43].

4.6. Silica type surfaces

For silica type surfaces Eq. (44) gives the characteristic protonation reaction and Eq. (61) provides the relation for σ_s. In the presence of a simple 1-1 electrolyte of s.a. ions that weakly adsorb at the Stern plane Eqs. (61) and (55) to (59) can be combined to an implicit equation for σ_s as a function of pH:

$$\sigma_s = \frac{-FN_s(1 + K_C\{C_d\})}{1 + K_H\{H_s\} + K_C\{C_d\} + K_H K_A\{H_s\}\{A_d\}} \tag{63}$$

where $\{H_s\}$ has to be calculated with Eq. (47) using the basic SGC model, Eq. (26) with $\sigma_0 = 0$ and $\sigma_s = -\sigma_d$. $\{C_d\}$ and $\{A_d\}$ can be obtained from Eq. (53) for $n_x = 0$. For low potentials where ψ_d and σ_d are related by Eq. (19) (DH limit) the most simple expressions are found:

$$\{H_s\}_{DH} = \{H\} \exp\left\{-\frac{F}{RT}\left(\frac{\sigma_s}{C_1} + \frac{-\sigma_d}{\varepsilon_0 \varepsilon_r \kappa}\right)\right\} \tag{64}$$

$$\{C_d\}_{DH} = \{C\} \exp\left\{-\frac{F}{RT}\left(\frac{-\sigma_d}{\varepsilon_0 \varepsilon_r \kappa}\right)\right\} \tag{65}$$

$$\{A_d\}_{DH} = \{A\} \exp\left\{\frac{F}{RT}\left(\frac{-\sigma_d}{\varepsilon_0 \varepsilon_r \kappa}\right)\right\} \tag{66}$$

where σ_s, σ_1 and σ_d are related by the electroneutrality Eq. (24) with $\sigma_0 = 0$; σ_1 and σ_d are given by respectively Eqs. (67) and (68):

$$\sigma_1 = F(\{S - C\} - \{SH - A\}) = FN_s(\theta_C - \theta_A) \tag{67}$$

$$\sigma_d = F[\{S\} + \{SH - A\}] = FN_s(\theta_R + \theta_A) = FN_s(1 - \theta_H - \theta_C) \tag{68}$$

Equations (63) to (68) show that even in the DH limit σ_s cannot be written explicitly. In general σ_s is a function of N_s, C_1 and κ (or the salt concentration).

Some results for silica type surfaces in the absence of s.a. are shown in Fig. 5.

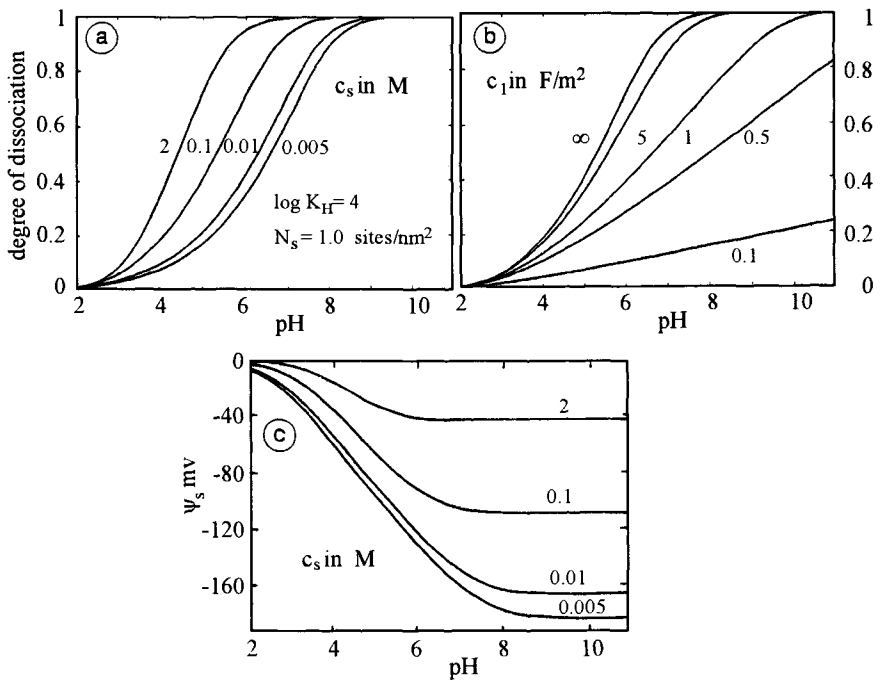

Figure 5. Surface electrostatics as a function of pH for silica type surfaces. (a) effect of the salt concentration, c_s, on the surface charge; (b) effect of C_1 for a given salt concentration; (c) salt effect on the surface potential ψ_s. N_s = 1 site/nm^2, $\log K_H = 4$ and there is no s.a, C_1=∞, for panel (a) and (c).

The screening effect of the indifferent electrolyte is shown in panel (a). For high salt concentration (2M) the electrostatic interaction is small and the $(1 - \theta_H)$ vs. pH curve resembles the $(1 - \theta_H)$ vs. pH_s curve shown in Fig. 2a. The lower the salt concentration, the larger become the deviations from the $(1 - \theta_H)$ vs. pH_s curve. The effect of C_1 on the charging behaviour is illustrated in panel (b). The curve for $C_1 = \infty$ corresponds with the curve at 0.1M salt in panel (a). For low Stern layer capacitances the screening of the surface charge by electrolyte is very poor and charging the surface becomes extremely difficult. Panel (c) shows a plot of ψ_s vs. pH at the same salt concentrations as shown in panel (a).

The ψ_s(pH) relation for silica type surfaces can be obtained by combining Eqs. (55) and (47):

$$\psi_s = \frac{2.3\ RT}{F}\left[\log K_H - pH - \log\left\{\frac{\theta_H}{\theta_R}\right\}\right] \tag{69}$$

where θ_R is given by Eq. (59). In the absence of s.a. $\theta_R = 1 - \theta_H$ and Eq. (69) can be written as:

$$\psi_s = \frac{2.3\ RT}{F}\left[\log K_H - pH - \log\left\{\frac{-FN_s - \sigma_s}{\sigma_s}\right\}\right] \tag{70}$$

where use has been made of Eq. (61) with $\theta_A = \theta_C = 0$. For low potentials and low absolute values of the surface charge Eq. (70) reduces to:

$$\psi_s = \frac{2.3\ RT}{F}\left[\log K_H - pH - \log\left\{\frac{-FN_s}{\sigma_s}\right\}\right] \tag{71}$$

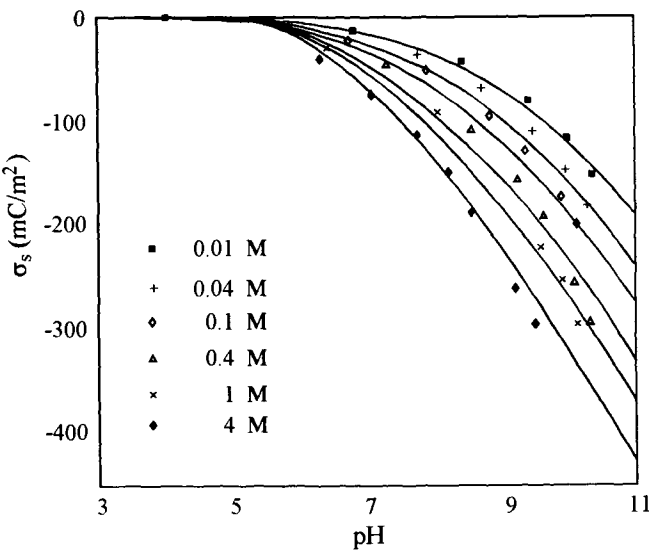

Figure 6. Calculated and experimental σ_s(pH) curves of heat treated silica [34]. The experimental data are taken from Bolt, G.H., *J. Phys. Chem.* **61** 166 (1957).

Equations (70) and (71) show that even in the absence of s.a. ψ_s is not only dependent on $\log K_H - pH$, but also on σ_s. This is clearly expressed in panel (c) of Fig. 5. The surface potential of silica type surfaces is, in general, strongly deviating from the Nernst equation according to which the potential is independent of c_s and linearly dependent on pH.

Hiemstra et al. [18, 34] have shown that the surface charge data of rigid, non porous silica can be described by the present model using $\log K_H = 7.5$, $N_s = 8$ sites/nm^2 and C_1=2.9 F/m^2, see Fig. 6 The value of $\log K_H$ is equal to the lower limit for the Si-O$^-$ group

given in Table 1. The value of 8 sites/nm^2 is suggested by Iler [49] for a fully hydroxylated silica. The value for the Stern layer capacitance is used as a fitting parameter. The high value of C_1 can be understood if it is assumed that the reactive groups protrude from the surface into the solution [18].

For gel type or precipitated silicas that may be (partially) penetrable for protons the shape of the σ_s(pH) curves is comparable, but the magnitude of the charge densities may be quite different [42]. Results obtained for Stöber silica in the presence of simple 1-1 electrolytes suggest that in this case a Donnan model (volume charge densities) is more appropriate as double layer model than a SGC model.

4.7. Gibbsite type of surfaces

For gibbsite type surfaces the characteristic protonation reaction is given by Eq. (43) and the surface charge by Eq. (62). In the presence of a simple 1-1 electrolyte of s.a. ions that weakly adsorb at the Stern plane Eqs. (62) and (55) to (59) can be combined to give σ_s:

$$\sigma_s = \frac{-0.5\ FN_s\,[1 - K_H\{H_s\} + K_C\{C_d\} - K_H K_A\{H_s\}\{A_d\}]}{1 + K_H\{H_s\} + K_C\{C_d\} + K_H K_A\{H_s\}\{A_d\}} \tag{72}$$

where $\{H_s\}$ has to be calculated with Eq. (47) using the basic SGC model, Eq. (26) with $\sigma_0 = 0$ and $\sigma_s = \sigma_d$. $\{C_d\}$ and $\{A_d\}$ are found by Eq. (53) for $n_x = 0$. An equation for σ_s that can be used for different values of ν is derived in [29]. For low potentials $\{H_s\}$, $\{C_d\}$ and $\{A_d\}$ are given by Eqs. (64) to (66). The expression for σ_1 is given by Eq. (61) and that for σ_d by Eq. (73):

$$\begin{aligned}\sigma_d &= 0.5F\,[\{S\} - \{SH\} - \{S-C\} + \{SH-A\}] = \\ &= 0.5FN_s(\theta_R - \theta_H - \theta_C + \theta_A) = 0.5FN_s(1 - 2\theta_H - 2\theta_A)\end{aligned} \tag{73}$$

Some results for gibbsite type of surfaces obtained with the SGC model in the absence of s.a. ($\theta_C = \theta_A = 0$) are shown in Fig. 7. In panel (a) σ_s is plotted versus pH as a function of the salt concentration. Two values of N_s (2 and 8 sites/nm^2) are chosen, the high value of N_s is most realistic for ordinary metal oxides. $C_1 = 2$ F / m^2, for smaller values of C_1 smaller values of σ_s would have been obtained. The curves at different ionic strength intersect each other at the pristine pzc, $\theta_H = 0.5$. At this point the surface potential ψ_s is zero, so that c_s is not affecting the proton adsorption. Moreover, at $\theta_H = 0.5$, $\{H_s\} = \{H\}_0$ the bulk proton activity at the pristine pzc and $\log K_H = -\log\{H\}_0 = pH_0$.
To obtain the expression for ψ_s Eqs. (55) and (47) have to be combined:

$$\psi_s = \frac{2.3\ F}{RT}\left[pH_0 - pH - \log\left\{\frac{\theta_H}{\theta_R}\right\}\right] \tag{74}$$

where use is made of the fact that $\log K_H = pH_0$ and θ_R is given by Eq. (59). In the absence of s.a. Eq. (74) can be combined with Eq. (62) for $\theta_C = \theta_A = 0$, the result is:

$$\psi_s = \frac{2.3\ F}{RT}\left[pH_0 - pH - \log\left\{\frac{FN_s + 2\sigma_s}{FN_s - 2\sigma_s}\right\}\right] \tag{75}$$

Equation (75) shows that at the pristine pzc ($d\psi_s/dpH$) follows the Nernst law for an electrode. Away from the pzc the second term on the r.h.s. also contributes and ψ_s(pH)

is non-Nernstian. The degree of non ideality depends strongly on N_s. For large values of N_s, $2\sigma_s/FN_s$ is small even a few pH units away from the pzc, so that the second term on the r.h.s. of Eq. (75) is small and ψ_s is pseudo Nernstian. An illustration of ψ_s(pH) curves for a gibbsite type oxide in the absence of s.a. as a function of c_s is shown in Fig. 7b for two values of N_s. The salt effect on ψ_s is hardly noticed for the high value of N_s.

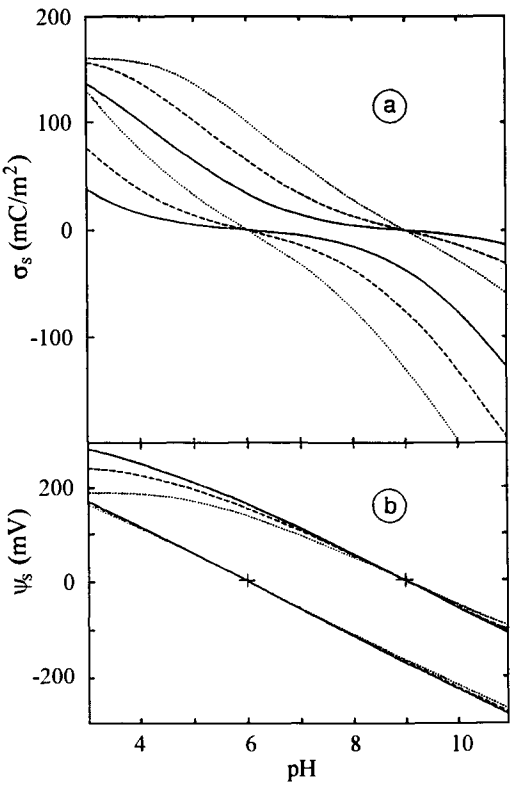

Figure 7. Surface electrostatics for gibbsite type surfaces. Panel (a) shows two sets of σ_s(pH) curves for three salt concentrations (— 10^{-3}, - - - 10^{-2}, ··· 10^{-1} M). For the two sets two values of N_s and two different values of $\log K_H$ are combined (N_s = 8 sites/nm^2 in combination with $\log K_H = 6$ and N_s = 2 sites/nm^2 in combination with $\log K_H = 9$). C_1 = 2 F/m^2 for both sets. Panel (b) shows the comparable ψ_s(pH) curves.

Experimentally the near Nernstian behaviour of ψ_s has been established for several gibbsite type oxides [21, 50, 51].

For the gibbsite surface Hiemstra et al. [34, 37] have shown that the experimental σ_s(pH) data can be described with the present model, see Fig. 8. The pristine pzc is found at $pH_0 = 10 \pm 0.5$ and the model immediately shows that $\log K_H = 10$. This value is used as reference in the calculation of the $\log K_H$ values shown in Table 1. In gibbsite only the edge plane Al–$OH^{1/2-}$ groups are active, σ_s and the parameters N_s and C_1 thus apply to

the edge face. $N_s \approx 10$ sites/nm^2 edge area has been derived from crystallographic data. The specific surface area of the edge face can be estimated with the help of electron micro graphs, and amounts to about 15 to 20 % of the total (BET) surface. With this estimate and using C_1 as fitting parameter the σ_s(pH) curves can only be described in a crude way (see the dashed curves in Fig. 8, $C_1 = 4$ F/m^2). Hiemstra et al. therefore conclude that specific adsorption of salt ions occurs. After incorporation of specific adsorption ($\log K_C = \log K_A = 0.1$) and using C_1=1.4 F/m^2 the solid curves of Fig. 8 are obtained.

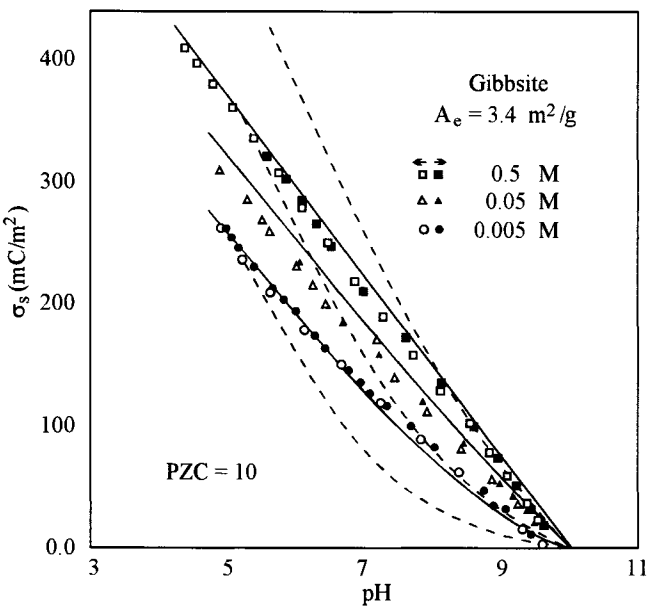

Figure 8. Series of σ_s(pH) curves at three NaCl concentrations. The markers indicate the experimental data. The dashed curves are calculated without taking into account specific adsorption. The solid curves are calculated using the one–pK_H SGC model with specific adsorption of NaCl [37].

The surface charge vs. pH curves of other well studied metal hydroxides can all be described fairly well with the gibbsite one–pK_H model [31, 34, 52–54]. The more complex reality that these surfaces are multifunctional does not affect the σ_s(pH) curves to such an extent that the one–pK_H model cannot be used. Gibb and Koopal [54] applied the one–pK_H SGC model to describe the surface charge of rutile and hematite. Results for rutile are plotted in Fig. 9; for a good fit s.a. of the K^+ and NO_3^- ions had to be incorporated. Besides the σ_s(pH) curves also, C*, the capacitance ($d\sigma_s$/dpH) is shown. Around the pzc the capacitance provides a good test for the model description [54]. Experimental capacitance values above pH=10 are unreliable.

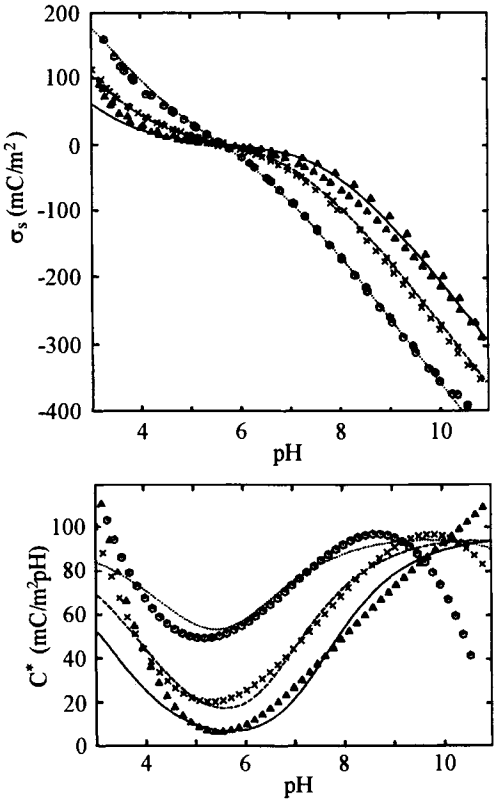

Figure 9. Surface charge and capacity ($d\sigma_s/dpH$) results for rutile at three concentrations of KNO_3. The markers denote the experimental results, the curves are calculated with the one-pK_H SGC model in the presence of specific adsorption [54].

4.8 The two-pK_H model

As an alternative for the one-pK_H model the classical two-pK_H model has been used in combination with several double layer models. Schindler and Stumm and co-workers [e.g., 55–59] mainly used a constant capacitance model. Huang [60–62] and Dzombak and Morel [63] have made tabulations based on the two-pK_H GC model. Both these models are relatively simple but the obtained log K_H values have no physical meaning at all.

Most frequently used is the two-pK_H TL model that has been reviewed by James and Parks [22]. Although the two-pK_H TL model can describe most σ_s(pH) results well, it is impossible to obtain a unique set of parameters on the basis of σ_s(pH) curves [23] so that a wealth of parameters is obtained without physical significance. Some authors [64, 65] have used the two-pK_H model in combination with different kinds of multi-layer models. Also with these more complicated models none of the fitted pK_H values has physical significance.

In general it may be concluded combination of the two-pK_H model with complicated double layer models lead to physically irrelevant parameters. Modelling implies simplifi-

cation of reality, in this respect the one-pK_H SGC model has far more to offer than the two-pK_H TL model. For an improvement of the description of well studied oxides one should have a closer look at the heterogeneity. This route has been followed successfully by Hiemstra et al. [33, 34].

5. SPECIFIC ADSORPTION

5.1. General aspects

So far the emphasis has been on adsorption of c.d. ions in the presence of weak or no specific adsorption of the background electrolyte. For most surfaces in contact with common 1–1 electrolytes this is a reasonable approximation. For high concentrations of 1–1 electrolytes or with divalent counterions substantial s.a. is however common. Direct studies of specific adsorption have been made using radio labelling techniques [66, 67]. Also many examples of electrokinetic measurements of specific adsorption can be found in the literature [e.g., 68–72].

In the presence of s.a., in principle, both the pzc and the iep shift if the ionic strength is increased or the type of electrolyte is changed. In general, the s.a. of cations and anions is different and this leads to a pzc, that is no longer equal to the iep. For instance, with s.a. of cations at the pristine pzc the pzc (non pristine) shifts to lower pH, whereas the iep shifts to higher pH [1]. A difference between the iep and the pzc is a clear indication of specific adsorption. Electrokinetic measurements are therefore very useful to obtain a qualitative insight into specific adsorption.

In general specific adsorption is pH dependent. For a given initial cation concentration a rapid increase in uptake of the multivalent cations usually occurs over a narrow pH range [59, 68, 73–75]. Affinity studies can be made by comparing the cation uptake as a function of pH at a given total cation concentration [see e.g., 76–79]. With oxyanions mostly a gradual decrease in adsorption with increasing pH is found [80–82].

5.2. Specific adsorption on proton sites versus adsorption on independent sites

With modelling attempts of specific adsorption it is important to distinguish between s.a. ions that adsorb at the same adsorption sites as the protons, and s.a. ions that adsorb on independent sites. The first type of specific adsorption has been assumed in sections 4.5. to 4.7. Spectroscopic studies on metal ion adsorption [83–85] support this view. The description presented in sections 4.5. to 4.7. is adequate for monovalent ions. However, modelling of complexation of multivalent ions with surface groups is faced with several complications.

(1) Speciation in bulk solution: multivalent anions may react with protons, and many multivalent cations hydrolyse at high pH values.

(2) Speciation at the surface: for one ionic species different surface complexes are formed at different pH values and/or different surface complexes are in equilibrium with each other at a given pH.

(3) The stoichiometry of the binding reaction is important; multivalent ions may form mono- or bi-dentate complexes.

(4) Due to complexation the double layer is affected and this change will affect both the s.a. ions and the protons. For instance, metal ion adsorption will enhance the desorption

of protons. The net effect is a proton/M exchange ratio that is only partly due to the stoichiometry of the reaction. The exchange ratio is thus not an immediate clue to the stoichiometry.

These complications make a unique description of surface complexation of multivalent ions rather difficult. *A priori* assumptions regarding the type(s) of adsorbing species and the type(s) of surface complexes formed cannot be avoided and different opinions will exist as to the most reasonable assumptions.

When only little information is available on both the surface structure and the type of complexes formed it is reasonable to investigate the adsorption with the simple one-pK_H model of a pseudo homogeneous surface and to describe the complexation with Eqs. (55) to (59). Review [29] and Refs. [52-54] can be consulted for details of this type of description. In review [29] also the bond valence concept is used to describe complexation. No attempts have been made to predict complexation constants so that these have to be treated as adjustable parameters.

Van Riemsdijk et al. [53] were the first to show that electrostatic effects could explain non-stoichiometric exchange ratios. Predictions with the one-pK_H SCG model and the two-pK_H SGC model were both in a good agreement with experimentally observed proton/M ratios and metal ion isotherms at a series of pH values for rutile, hematite and amorphous iron oxide. In contrast with Benjamin and Leckie [86], Van Riemsdijk et al. [53] concluded that incorporation of surface heterogeneity is not required to describe cadmium adsorption on amorphous iron oxide.

Most studies of metal ion complexation rely on the two-pKH model. Schindler and Stumm [59, 69, 78, 82, 87] combine the two-pKH constant capacitance model with stoichiometric reactions of the metal ions with surface hydroxyls. Huang et al. [62] and Dzombak and Morel [63] tabulate ion affinity constants on the basis of the two-pKH GC model. Leckie and co-workers [88-90] combine the model cation and anion adsorption with the two-pKH TL model. Hayes makes a distinction between strongly and weakly adsorbing ions [89, 90]. A series of reviews on s.a. using the two-pKH model can be found in [91].

Another simplification is to assume that the sites of the s.a. ions are entirely independent of the sites for c.d. ions. This is, for instance, a reasonable assumption when the s.a. ions are much larger than the surface sites. For ordinary inorganic ions this is not often the case, but for organic ions it may be a good option. Stern [15] has introduced this type of modelling. In this case the adsorption of s.a ions can be described with the monocomponent versions of Eqs. (55) to (59). The advantage of taking independent sites for the s.a. ions is that the precise nature of the ion-surface complex does not have to be specified and the proton/X ratio is completely determined by the electrostatics [72]. Problems with speciation in solution or at the surface and with surface heterogeneity still exist.

Cation adsorption on oxides has been analysed by several authors [72, 92-96] under the assumption that s.a. ions are not in competition with protons. Fokkink et al. [72, 94] also studied the temperature dependence of metal ion adsorption on hematite and rutile. Although they treat the metal ion sites as independent of the proton sites they state that their results form "a direct indication for the occurrence of surface complex formation".

6. SURFACE HETEROGENEITY

6.1. General remarks

The description of ion adsorption from aqueous electrolyte solutions to heterogeneous surfaces is based on the concepts developed for gas adsorption [97– 100]. Heterogeneity of mineral surfaces can be due to different oxygen groups on one crystal plane, different crystal planes, plane imperfections, multiple domains, disordered crystal lattices, surface impurities, etc. In general the adsorption on a heterogeneous surface can be treated as the summation of the adsorption that occurs on the different site types. The adsorption on each class of sites can be described by a *local* isotherm equation. The *overall* isotherm is found as the weighted summation or integration of the local contributions. The local isotherm equation is similar to the equations derived in sec. 4 and depends on the way the different classes of sites are distributed over the surface. Two limiting situations of heterogeneity can be considered: random and patchwise.

For random or regular heterogeneity the different site types are mixed in a random or regular way. With ion adsorption the lateral interactions are of coulombic nature and these interactions are long range. For random surfaces the (smeared out) electrostatic surface potential can therefore be considered to be the same over the entire surface. This will even be the case when the similar sites are grouped together in small clusters as long as these clusters are sufficiently smaller than the effective length scale, κ^{-1} of the interactions [101].

For patchwise heterogeneity the different classes of sites are grouped together in patches. Each patch itself may be homogeneous, or heterogeneous if the sites are mixed randomly or regularly. This situation may occur with crystalline metal oxides when the crystal planes are occupied with different types of surface groups. The lateral interactions over the patch boundaries can be neglected (non interacting patches) if the boundary region is small with respect to the patch size. In the case of ion adsorption non interacting patchwise surfaces have to be composed of rather large patches, the length scale of the patch should be considerably larger than κ^{-1}. With non interacting patches each patch develops its own (smeared out) electrostatic potential, this simplifies the situation considerably [32, 101, 102]. Treatments of patchwise heterogeneous surfaces that consider interactions over the patch boundaries are scarce [101,103]. Koopal and Dukhin [104] provide some arguments that surfaces with interacting patches can be treated as near homogeneous. Random heterogeneous patches can be treated as random heterogeneous surfaces, whereafter the patch contributions are added to obtain the adsorption on the entire surface.

The present treatment is restricted to non interacting patchwise heterogeneity and random heterogeneity. The first part of this section is concerned with the theory of monocomponent ion adsorption on heterogeneous surfaces, the second part with multicomponent ion adsorption.

6.2. Generalized equations for monocomponent adsorption

The overall proton adsorption from an indifferent electrolyte solution on a heterogeneous surface can simply be described as the sum of the local adsorption contributions. The effect of lateral interactions should be taken into account in the local isotherm. For a patchwise surface with a discrete distribution of intrinsic affinity constants the total

adsorption, $\Gamma_{H,t}$, is thus:

$$\Gamma_{H,t} = \overline{N}_s \theta_{H,t} = \sum_j \frac{A_j}{A_t} N_j \theta_{H,j}(K_H, \{H_s\}^*) \tag{76}$$

where $\overline{N}_s$ is the average site density, A_j is the area occupied by sites S_j, A_t the total area, N_j the site density of patch j and $\theta_{H,j}(K_H, \{H_s\}^*)$ is the local isotherm equation for proton adsorption on sites S_j. Instead of Eq. (76) one can also write:

$$\theta_{H,t} = \sum_j \left(\frac{A_j}{A_t}\right)\left(\frac{N_j}{\overline{N}_s}\right)\theta_{H,j}(K_H, \{H_s\}^*)$$

or

$$\theta_{H,t} = \sum_j f_j \theta_{H,j}(K_H, \{H_s\}^*) \tag{77}$$

where f_j is a weighted area fraction of sites S_j:

$$f_j = \left(\frac{A_j}{A_t}\right)\left(\frac{N_j}{\overline{N}_s}\right) = f_j^A \left(\frac{N_j}{\overline{N}_s}\right) \tag{78}$$

and f_j^A is the normal area fraction. For a continuous distribution of affinity constants summation (77) can be replaced by an integration:

$$\theta_{H,t} = \int_\Delta \theta_H(K_H, \{H_s\}^*) f(\log K_H) d \log K_H \tag{79}$$

where $f(\log K_H)$ is the differential distribution function of $\log K_H$, Δ the relevant range of integration and $\theta_H(K_H, \{H_s\}^*)$ the local isotherm function. The function $f(\log K_H)$ indicates the probability of finding sites with an affinity in the range $f(\log K_H) + d \log K_H$. The product $f(\log K_H) d \log K_H$ is equivalent to the fraction f_j in the discrete case. Equations (77) and (79) are generalized adsorption equations.

For a random heterogeneous surface Eqs. (77) and (79) also apply. However, area fractions or local site densities are not relevant and in this case f_j is simply the fraction of sites S_j.

The function $\theta_{H,j}$ depends on the type of surface oxygens. For gibbsite type (amphoteric) groups a combination of Eq. (60) and (62) with $\theta_A = \theta_C = 0$ can describe the local isotherm. In [29] a generalized gibbsite type one-pK_H model has been described that can be used for different values of n and ν. For silica type (acid) groups Eq. (60) in combination with (61) with $\theta_A = \theta_C = 0$ can be used to describe the local isotherm. For a discrete distribution a specific equation for $\theta_{H,j}$ can be used for each of the different groups to represent the surface groups as accurate as possible. In the case of a continuous distribution function with both gibbsite type and silica type oxygens the distribution function will become bimodal, one part for the gibbsite groups the other for the silica groups, each with its own local isotherm equation.

The distinction between patchwise and random heterogeneity can be expressed by the equation for $\{H_s\}^*$. For random heterogeneity where the local site density matches the

average site density and the potential is assumed to be uniform over the entire surface, $\{H_s\}^*$ can be written as:

$$\{H_s\}^* = \{H_s\}_t = \{H\} \exp\left(\frac{-F\psi_{s,t}}{RT}\right) \tag{80}$$

where $\psi_{s,t}$ is the (smeared out) surface potential. For a given value of $\sigma_{s,t}$ the potential $\psi_{s,t}$ can be calculated with, for instance, the SGC model assuming a reasonable value for $C_{1,t}$, see Eq. (26) with $\sigma_{0,t} = 0$ and $\sigma_{s,t} = -\sigma_{d,t}$. An advantage of the random heterogeneity model is that there is only one set of double layer parameters ($\sigma_{s,t}$; $\psi_{s,t}$; $C_{1,t}$) required for the entire surface. Analysis of $\sigma_{s,t}$(pH) curves of random heterogeneous surfaces is therefore relatively easy. A systematic way to study these surfaces is by using the "master curve" procedure suggested by the Wit et al. [44, 45] in combination with the heterogeneity analysis described by Nederlof et al. [46–48].

For patchwise heterogeneity with non–interacting patches, each patch has its own, smeared out, patch potential and $\{H_s\}^*$ becomes:

$$\{H_s\}^* = \{H_s\}_p = \{H\} \exp\left(\frac{-F\psi_{s,p}}{RT}\right) \tag{81}$$

where $\psi_{s,p}$ is the potential for patch p. In principle, the potentials $\psi_{s,p}$ can be calculated with the help of the SGC model, Eq. (26) with $\sigma_{0,p} = 0$ and $\sigma_{s,p} = -\sigma_{d,p}$. In practice however, this calculation is not easy, only when A_j and the parameters N_j, $K_{H,j}$ and $C_{1,j}$ of each patch are known a measured value of σ_s can be separated into the patch contributions. Analysis of experimental σ_s(pH) curves of patchwise heterogeneous surfaces can also be done by considering apparent affinities instead of intrinsic affinities. The apparent proton affinity for site S_j is defined as:

$$K_{H,app,j} = K_{H,j} \exp\left(\frac{F\psi_s^*}{RT}\right) \tag{82}$$

where ψ_s^* for a patchwise surface equals $\psi_{s,j}$. According to Eq. (82) the electrostatic interactions also contribute to the heterogeneity. In order to suppress the electrostatic effects the proton adsorption should be measured at relatively high (0.1 M) salt concentrations [48,102,105].

Prediction of σ_s(pH) curves of patchwise heterogeneous surfaces is possible when detailed information on the double layer parameters is available. Such calculations are very useful to obtain theoretical insight in he behaviour of patchwise heterogeneous surfaces. Some examples of this type of calculations can be found in refs. [32,101,102].

Specific ion adsorption on independent sites. By replacing H by X and the subscript s by d the equations shown above also apply to s.a. of ion X, provided the sites for adsorption are independent of those of the other ions. The effect of independent specific adsorption on, for instance, the proton adsorption is noticed in the double layer expression for the potential. For surface complexation the above equations are not appropriate because this is a form of multicomponent adsorption with s.a. and c.d. ions competing for the same sites. In this respect the description of specific adsorption on independent sites is far more simple than that of surface complexation.

6.3 The two–pK_H model as local isotherm.

Use of the classical two–pK_H model to describe the local isotherm for proton adsorption on an amphoteric oxide in the presence of an indifferent electrolyte complicates the situation considerably. The two pK values represent, in an artificial way, the amphoteric nature of the oxide (see secs. 4.4. and 4.8.). Equation (77) and (79) have to be extended with a second summation or integration to account for both logK distributions. Only when it is assumed that ΔpK is the same for all different site types a more simple relation is found. The latter assumption is however rather arbitrary. As there are no physical arguments in favour of using the two–pK_H model a good advise is *not to use* this model.

6.4. Generalized equations for multicomponent adsorption

In the presence of s.a. ions that form surface complexes with the proton sites multicomponent adsorption occurs on reference sites S_j and Eqs. (77) and (79), in general, no longer hold. Moreover, for the local adsorption the competitive or multicomponent form of Eq. (55) should be used, i.e. Eq. (55) in combination with Eq. (59). For adsorption of a proton on site S_j, on which also s.a. ions C and A can adsorb Eq. (83) results:

$$\theta_{H,j} = \frac{K_{H,j}\{H_s\}^*}{1 + K_{H,j}\{H_s\}^* + K_{C,j}\{C_{sd}\}^* + K_{H,j}K_{A,j}\{H_s\}^*\{A_{sd}\}^*} \tag{83}$$

For patchwise heterogeneous surfaces $\{H_s\}^* = \{H_s\}_p$ and $\{X_{sd}\}^* = \{X_{sd}\}_p$, (X = A, C) whereas for random heterogeneous surfaces $\{H_s\}^* = \{H_s\}_t = \{H_s\}$ and $\{X_{sd}\}^* = \{X_{sd}\}_t = \{X_{sd}\}$.

For a limited number of different sites the overall isotherm becomes:

$$\theta_{H,t} = \sum_j f_j \theta_{H,j}\,(K_{H,j}, K_{C,j}, K_{A,j}\{H_s\}^*, \{C_{sd}\}^*, \{A_{sd}\}^*) \tag{84}$$

where for each fraction f_j the $K_{X,j}$ values can vary independently.

For a continuous heterogeneity the expression for the overall complexation of protons with all the different site types is a multiple integral equation. A relevant more simple, but still complicated situation, is that of e.g. proton and metal ion adsorption on oxides. For such a situation and adsorption from an indifferent background electrolyte the integral proton adsorption equation is:

$$\theta_{H,t} = \int_{\Delta H} \int_{\Delta M} \theta_H f(\log K_H, \log K_M) d \log K_H d \log K_M \tag{85}$$

where ΔH and ΔM represent the range of the integrations, the distribution $f(\log K_H, \log K_M)$ is a two–dimensional distribution function. For mono–dentate M ion binding θ_H is given by Eq. (86):

$$\theta_H = \frac{K_H\{H_s\}^*}{1 + K_H\{H_s\}^* + K_M\{M_{sd}\}^*} \tag{86}$$

Still there is little prospect of using Eq. (85) for the analysis of ion complexation on heterogeneous surfaces, even the two–dimensional distribution function in Eq. (85) is too complicated for a routine analysis. For practical purposes Eq. (85) has to be further

simplified by making *a priori* assumptions with respect to the heterogeneity. Below some possibilities are discussed.

6.5. Patchwise heterogeneity and mineral oxides

Theoretical calculations show that the pzc of a patchwise heterogeneous surface in contact with an indifferent electrolyte solution is not only a function of the surface composition, but also of the ionic strength [32,101,102]. Therefore, for these surfaces the pzc can no longer be identified with the (near) common intersection point of the σ_s(pH) curves at a series of indifferent electrolyte concentrations. Kuo and Yen [106] in their brief review on pzc's of mixed oxides fail to recognise this important characteristic of patchwise surfaces. Although identification of the common intersection point with the pzc is wrong, the error in doing so is small if the Stern layer capacitances of both patches are similar [101]. In the presence of s.a. ions the concentration of electrolyte affects the pzc in the generic way indicated above and in a specific way depending on their affinity for the surface.

Hiemstra et al. [18, 33, 34] in their MUSIC model for the crystalline oxides use the non interacting patchwise heterogeneity model. In this model the crystal planes are the patches, each crystal plane may contain one or more types of surface oxygens, but has its own patch charge and potential. Gibbsite has a central place in Hiemstra's treatment [33, 34, 37]. Up to pH $\approx$ 10 the σ_s(pH) curve of gibbsite is determined by the singly co-ordinated groups of the edge face, above pH = 10 the doubly co-ordinated OH groups of the planar face start to contribute. The doubly co-ordinated groups of the edge face remain "inactive" due to the negative edge potential caused by the singly co-ordinated OH groups. The discrete patchwise model with independently obtained patch parameters explains the σ_s(pH) curves of gibbsite very well.

A similar success is achieved for goethite [18, 34]. Comparison of σ_s(pH) curves of goethites [34] that differ strongly in BET surface area shows that due to imperfections at the 100 face the surface group structure is different for goethites with different BET areas. Pzc values of synthetic goethites are reported to be in the range from 7.5 to 10. The variation in pzc of synthetic goethites can be understood if one assumes that the surfaces have different combinations of singly and triply co-ordinated groups. Some uncertainty is due to the fact that the $\log K_{3,1}$ value for protonation of triply co-ordinated surface oxygens is not precisely known.

Contescu et al. [105] have analysed σ_s(pH) curves of alumina samples obtained in a 0.1 M electrolyte solution. Neglecting the electrostatic interactions they found (apparent) affinity constants that are in good agreement with the predicted K_H values for Al groups shown in Table 1. Although this result is promising a critical remark can be made with respect to the procedure. For weakly heterogeneous surfaces with a local isotherm based on the one-pK_H model the determination of the affinity constant distribution as the first derivative of the overall isotherm [46, 48] may lead to a wrong result, see [32,102].

As a model for patchwise heterogeneity Gibb and Koopal [54] have studied proton adsorption on mixtures of hematite and rutile. Both hematite and rutile could be described with the pseudo-homogeneous one-pK_H SGC model. The σ_s(pH) curves of the mixtures could be predicted by weighed addition of the σ_s(pH) curves of rutile and hematite at each salt concentration. For the total differential capacitance (dσ_s/dpH) a similar additivity rule could be applied.

6.6. Random heterogeneity and mineral oxides

For a random heterogeneous surface, where the potential is uniform over the whole surface, the description of proton binding is relatively simple. The overall isotherm can be calculated using Eq. (77) or (79) with Eqs. (60) and (62) (gibbsite type sites) or Eqs. (60) and (61) (silica type sites) as local isotherm. When both gibbsite and silica type groups are present a bimodal distribution should be used. As the (smeared out) surface potential is the same over the entire surface the random heterogeneity model is well suited when little is known about the heterogeneity.

For certain continuous distribution functions and a Langmuir type local isotherm it is possible to solve Eq. (79) analytically. The thus obtained overall isotherm equations are normalised Freundlich type equations [32, 52, 53,102,107- 110], for instance:

$$\theta_{H,t} = \frac{\left(\tilde{K}_H\{H_s\}\right)^m}{1 + \left(\tilde{K}_H\{H_s\}\right)^m} \tag{87}$$

where $\tilde{K}_H$ is the affinity corresponding with the maximum in the distribution function and m its width. Equation (87) is called the monocomponent Langmuir–Freundlich (LF) equation. The major advantage of the use of the LF equation over a discrete approach is that only two parameters are required to describe the distribution function. For a discrete approach two parameters (f_j, $K_{H,j}$) are required for each site type.

When little is known about the electrostatic effects the apparent affinity distribution can be investigated rather than the intrinsic affinity distribution. For a random surface the apparent affinity is defined by Eq. (82) with ψ_s^* equal to $\psi_{s,t}$.
When only apparent affinities are considered Eq. (87) becomes:

$$\theta_{H,t} = \frac{\left(\tilde{K}_{H,app}\{H\}\right)^m}{1 + \left(\tilde{K}_{H,app}\{H\}\right)^m} \tag{88}$$

where $\tilde{K}_{H,app}$ is the apparent affinity corresponding with the maximum in the apparent distribution function with the width m. Note that this equation is equivalent to the Henderson–Hasselbalch equation that is used to describe the protonation of polyelectrolytes [111–113].

For proton adsorption on well studied systems intrinsic affinity distributions can be obtained after conversion of the $\sigma_s(pH)$ curves into $\sigma_s(pH_s)$ curves using the SGC model with a reasonable value for $C_{1,t}$. As indicated before the adequacy of the applied double layer model can be checked when adsorption data are available at a series of indifferent electrolyte concentrations. Replotting the surface charge as a function of pH_s should lead to merging of the individual curves into a master curve [44, 45]. The master curve reflects the chemical heterogeneity [46–48].

Some theoretical proton adsorption isotherms based on Eq. (87) and different types of surface groups are reported in [32,102]. Benjamin and Leckie [86] and Kinniburg et al. [14, 15] used Freundlich type equations to describe metal ion binding to ferrihydride. A discussion of this work has been given by Van Riemsdijk et al. [52, 53].

For multicomponent adsorption the situation is more complicated as explained in sec. 6.4. An often used drastic simplification is to assume that the distribution of $\log K_M$ is fully coupled (highly correlated) to that of $\log K_H$, so that the two-dimensional distribution

function reduces to a single distribution function. Similarly as for the monocomponent situation the fully coupled model leads, for certain distribution functions, to multicomponent Freundlich type equations [52, 53,107–110,116]. The multicomponent LF equation equals:

$$\theta_{H,t} = \frac{\tilde{K}_H\{H_s\}}{\sum_X \tilde{K}_X\{X_{sd}\}} \cdot \frac{\left[\sum_X \tilde{K}_X\{X_{sd}\}\right]^m}{1 + \left[\sum_X \tilde{K}_X\{X_{sd}\}\right]^m} \tag{89}$$

where the summation over X runs over all adsorbing species taking S_j as reference site, $\tilde{K}_X$ indicates the peak position of $f(\log \tilde{K}_X)$.

Rudzinski et al. [108–110] also consider the situation that the affinities lack correlation, but that the reference sites S_j are common to all species. This results in an equation that is a hybride of the multicomponent Langmuir equation and the Freundlich equation:

$$\theta_{H,t} = \frac{\left(\tilde{K}_H\{H_s\}\right)^{m_H}}{1 + \left(\sum_X \tilde{K}_X\{X_{sd}\}\right)^{m_X}} \tag{90}$$

where $\tilde{K}_X$ and m_X characterise $f(\log \tilde{K}_X)$. Equations (89) and (90) both have been used to study c.d. and s.a. ion adsorption on oxides [52, 53,108–110].

Recently a more general model, NICA, non ideal competitive adsorption, has been derived by Koopal et al. [116–118]. In this model ion specific non ideality according to Eq. (90) is combined with an intrinsic heterogeneity that applies to both c.d and s.a. ions. The NICA equation can be written as:

$$\theta_{H,t} = \frac{\left(\tilde{K}_H\{H_s\}\right)^{n_H}}{\sum_X \left(\tilde{K}_X\{X_{sd}\}\right)^{n_X}} \cdot \frac{\left[\sum_X \left(\tilde{K}_X\{X_{sd}\}\right)^{n_X}\right]^p}{1 + \left[\sum_X \left(\tilde{K}_X\{X_{sd}\}\right)^{n_X}\right]^p} \tag{91}$$

Effectively the parameter m for the width of the distribution function in the ordinary multicomponent LF equation is replaced by a product of two parameters: p representing the intrinsic affinity, n_X the ion specific non ideality. The ion specific non ideality can be due to residual heterogeneity or other non ideality effects typical for the ion studied. On the expense of one additional parameter (n_X) for each adsorbing component this model is far more flexible for multicomponent adsorption on heterogeneous surfaces than the fully coupled models. For $n_X = 1$ for all X the NICA equation reduces to Eq. (89). The NICA model has been used successfully for proton and metal ion binding to humic acids [116-118], but it is not yet applied to heterogeneous metal oxides.

The two dimensional distribution function can also be simplified by assuming a partial correlation or matching of the distributions of $\log K_H$ and $\log K_M$ [119]. The extend of matching is however an obscure function unless it boils down to fully coupled distributions. The NICA model is far more easy to handle than the equations based on partial correlation of the affinities.

REFERENCES

1. J. Lyklema, J. Colloid Interface Sci., 99 (1984) 109.
2. R.J. Hunter, Zeta Potential in Colloid Science, Principles and Applications, Academic Press, London,1981.
3. P. Debye, and E. Hückel, Physik. Z.,24 (1923) 185.
4. G. Gouy, J. Phys. 9 (4), (1910) 457; Ann. Phys., 7 (9), (1917) 129.
5. D.D. Chapman, Phil. Mag., 25 (6), (1913) 475.
6. S. Trasatti, in: Comprehensive Treatise of Electrochemistry, vol.1: The Double Layer, J.O'M. Bockris, B.E. Conway, E. Yeager, (eds.), Plenum Press, New York, Ch. 2, 1980.
7. D.C. Graham, Chem. Revs., 41 (1947) 441.
8. R. Reeves, in: Comprehensive Treatise of Electrochemistry, vol. 1. The Double Layer, J. O'M Bockris, B.E. Conway, E. Yeager (eds.), Plenum Press, New York, Ch. 3,1980.
9. D.C. Graham, J. Chem. Phys., 21 (1953) 1054.
10. S. Nir and J. Bentz, J. Colloid Interface Sci.,65 (1978) 399.
11. J. Bentz, J. Colloid Interface Sci., 90 (1982) 127. ,
12. A.E. James and D.J.A. Williams, J. Colloid Interface Sci., 107 (1985) 44.
13. G. Gunnarsson, B. Jonsson and H. Wennerstrom, J. Phys. Chem.,84 (1980) 3114.
14. P. Linse, G. Gunnarsson and B. Jonsson, J. Phys. Chem., 86 (1982) 413.
15. O. Stern, Z. Elektrochem., 30 (1924) 508.
16. Cooper, I.L. and Harrison, J.A., Electrochim Acta, 22 (1977) 519.
17. J.M. Kleyn and J. Lyklema, J. Colloid Interface Sci., 120 (1987) 511.
18. T. Hiemstra and W.H. Van Riemsdijk, Colloids Surf., 59 (1991) 7.
19. L. Pauling, The Nature of the Electrostatic Bond, Cornell Univ. Press, Ithaca, New York, 3rd ed., Ch.13–6,1967.
20. L. Bousse, N.F. De Rooij and P. Bergveld, Surf. Sci.,135 (1983) 479.
21. R.E.G. Van Hal, Advanced Packaging of ISFETs, Ph.D. Thesis, State University Twente, Enschede, The Netherlands, Ch.3,1994.
22. R.D. James and G.A. Parks, in: Surface and Colloid Science, vol.12, E. Matijevic (ed.), Plenum Press, New York, Ch. 2,1982.
23. L.K. Koopal, W.H. Van Riemsdijk and M.G. Roffey, J. Colloid Interface Sci., 118 (1987) 117.
24. J.T.G. Overbeek, J. Colloid Sci., 8 (1953) 593.
25. J.T. Davies and E.K. Rideal, Interfacial Phenomena, Academic Press, New York, London, Ch. 2,1961.
26. G.H. Bolt, in: Soil Chemistry, B. Physico-chemical Models, G.H. Bolt (ed.), Elsevier, Amsterdam, 2nd ed., Ch. 3,1982.
27. H. Ohshima and T. Kondo, Biophys. Chem.,39 (1991) 193.
28. T.W. Healy and L.R.White, Adv. Colloid Interface Sci.,9 (1978) 303.
29. L.K. Koopal, in: Coagulation and Flocculation, Theory and Applications, B. Dobias, (ed.), Surfactant Science Series, vol. 47, M. Dekker, New York, Ch. 4, 1993.
30. Westall, J. and Hohl, H., Adv. Colloid Interface Sci.,12 (1980) 265.
31. G.H. Bolt and W.H. Van Riemsdijk, in: Soil Chemistry, B. Physico-chemical Models, G.H. Bolt (ed.), Elsevier, Amsterdam, 2nd ed., Ch.13,1982.

32. W.H. Van Riemsdijk, L.K. Koopal and J.C.M. De Wit, Neth. J. Agric. Sci., 35 (1987) 241.
33. T. Hiemstra, W.H. Van Riemsdijk and G.H. Bolt, J. Colloid Interface Sci., 133 (1989) 91.
34. T. Hiemstra, J.C.M. De Wit and W.H. Van Riemsdijk, J. Colloid Interface Sci., 133 (1989) 105.
35. G.A. Parks, Chem. Rev., 65 (1965) 177.
36. R.H. Yoon, T. Salman and G. Donnay, J.Colloid Interface Sci., 70 (1979) 483.
37. T. Hiemstra, W.H. Van Riemsdijk and M.G.M. Bruggenwert, Neth. J. Agric. Sci., 35 (1987) 281.
38. A. Giatti and L.K. Koopal, J. Electroanal. Chem.,352 (1993) 107.
39. W.F. Bleam, J. Colloid Interface Sci.,159 (1993) 312.
40. R. Parsons, Handbook of Electrochemical Constants, Butterworths, London, 1959.
41. C.W. Davies, Ion Association, Butterworths, London,1962.
42. D.E. Yates and T.W. Healy, J.Colloid Interface Sci., 55 (1976) 9; J. Lyklema, Croat. Chem. Acta, 43 (1971) 249.
43. L.G.J. Fokkink, A. de Keizer, J.M. Kleijn and J. Lyklema, J. Electroanal. Chem., 208 (1986) 401.
44. J.C.M. De Wit, W.H. Van Riemsdijk, M.M. Nederhof, D.G. Kinniburgh and L.K. Koopal, Anal. Chim. Acta, 232 (1990) 189.
45. J.C.M. De Wit, W.H. Van Riemsdijk and L.K. Koopal, Environ. Sci. Technol., 27 (1993) 2015; J.C.M. De Wit, W.H. Van Riemsdijk and L.K. Koopal in: Heavy Metals in the Hydrological Cycle, M. Astruc and J.N. Lester (eds.), Selper, London, p.369, 1988.
46. M.M. Nederhof, W.H. Van Riemsdijk and L.K. Koopal, J. Colloid Interface Sci., 135 (1990) 410.
47. M.M. Nederhof, W.H. Van Riemsdijk and L.K. Koopal in: Heavy Metals in the Environment, J.P. Vernet (ed.), CEP Consultants, Ltd. Edinburgh (UK), p. 400, 1989; M.M. Nederhof, W.H. Van Riemsdijk and L.K. Koopal, Environ. Sci. Technol., 28 (1994) 1037.
48. M.M. Nederlof, J.C.M. de Wit, W.H. van Riemsdijk and L.K. Koopal, Environ. Sci. Technol., 27 (1993) 846.
49. R.K. Iler, in: Surface and Colloid Science, vol. 6, E. Matijevic (ed.), Wiley, New York, Ch.1,1982.
50. N.H.G. Penners, L.K. Koopal and J. Lyklema, Colloids Surf.,21 (1986) 457.
51. S. Ardizonne, P. Siviglia and S. Trasatti, J. Electroanal Chem.,122 (1981) 395; Siviglia, P., Daghetti, A. and S. Trasatti, Colloids Surf.,7 (1983) 15.
52. W.H. Van Riemsdijk, G.H. Bolt, L.K. Koopal and Blaakmeer, J., J. Colloid Interface Sci.,109 (1986) 219.
53. W.H. Van Riemsdijk, J.C.M. De Wit, L.K. Koopal and G.H. Bolt, J. Colloid Interface Sci., ll6 (1987) 511.
54. A.W.M. Gibb and L.K. Koopal, J. Colloid Interface Sci.,134 (1990) 122.
55. P.W. Schindler and H.R. Kamber, Helv. Chim Acta, 53 (1968) 1781.
56. W. Stumm, C.P. Huang and S.R. Jenkins, Croat. Chem. Acta,42 (1970) 223.
57. P.W. Schindler, in: Metal Ions in Biological Systems, vol.18: Circulation of Metal Ions in the Environment, H. Sigel (ed.), Marcel Dekker, New York, Ch. 7,1984.
58. Hohl, H. and Stumm, W., J. Colloid Interface Sci.,55 (1976) 281.

59. P.W. Schindler, and W. Stumm, in: Aquatic Surface Chemistry, W. Stumm (ed.), Wiley, New York, Ch. 4,1987.
60. C.P. Huang and W. Stumm, J. Colloid Interface Sci.,43 (1973) 409.
61. C.P. Huang, in: Adsorption of Inorganics at Solid/Liquid Interfaces, M.A. Anderson and A.J. Rubin (eds.), Ann Arbor Science, Ann Arbor (MI) Ch. 5, 1981.
62. C.P. Huang, Y.S. Hsieh, S.W. Park, A.R. Bowers and H.A. Elliot, in: Metals Speciation, Separation, and Recovery, J.W. Patterson and R. Passino (eds.), Lewis Publishers, Chelsea (MI) , p. 437,1987.
63. D.A. Dzombak and F.M. Morel, Surface Complexation Modelling Hydrous Ferric Oxide, Wiley, New York, 1990.
64. J.W. Bowden, A.M. Posner and J.P. Quirk, Aust. J. Soil Res., 15 (1977) 121.
65. M.J.G. Janssen and H.N. Stein, J. Colloid Interface Sci., 111 (1986) 112.
66. W. Smit and C.L.M. Holten, J. Colloid Interface Sci.,78 (1980) 1.
67. A. Foissy, A. M'Pandou, J.M. Lamarche and N. Jaffrezic-Renault, Colloids Surf., 5 (1982) 363.
68. R.O. James and T.W. Healy, J. Colloid Interface Sci.,40 (1972) 53.
69. P.W. Schindler, in: Adsorption of Inorganics at Solid/Liquid Interfaces, M.A. Anderson and A.J. Rubin (eds.), Ann Arbor Science, Ann Arbor (MI), Ch. 7, 1981.
70. D.D. Hansmann and M.A. Anderson, Environ. Sci. Technol., 19 (1985) 544.
71. M.C. Fuerstenau and K.E. Han, in: Reagents in Mineral Technology, P. Somasundaran and B.M. Moudgil (eds.), Surfactant Science Series, vol. 27, M. Dekker, New York Ch.13,1988.
72. L.G.J. Fokkink, A. De Keizer and J. Lyklema, J. Colloid Interface Sci., 135 (1990) 118.
73. R.O. James and T.W. Healy, J. Colloid Interface Sci.,40 (1972) 42.
74. R.O. James and T.W. Healy, J. Colloid Interface Sci.,40 (1972) 65.
75. G. Sposito, The Surface Chemistry of Soils, Oxford University Press, New York, 1984.
76. D.L. Dugger, J.H. Stanton, B.N. Irby, B.L. McConnell, W.W. Cummings and R.W. Maatman, J. Phys. Chem., 68 (1964) 757.
77. D.G. Kinniburgh, M.L. Jackson and J.K. Syers, Soil Sci. Soc. Am. J., 40 (1976) 796.
78. P.W. Schindler, B. Fürst, R. Dick and R. Wolf, J. Colloid Interface Sci., 55 (1976) 469.
79. R.M. McKenzie, Aust. J. Soil Res., 18 (1980) 61.
80. F.J. Hingston, A.M. Posner and J.D. Quirk, J. Soil Sci., 23 (1972) 177.
81. J.F. Ferguson and J. Gravis, J. Colloid Interface Sci., .54 (1976) 391.
82. L. Sigg and W. Stumm, Colloids Surf.,2 (1980) 101.
83. H. Motschi, Colloids Surf., 9 (1984) 333.
84. H. Motschi, in: Aquatic Surface Chemistry, W. Stumm (ed.), Wiley, New York, Ch. 5,1987.
85. M.B. McBride, Advances in Soil Science, vol.10, Springer Verlag, New York, p.1, 1989.
86. M.M. Benjamin and J.O. Leckie, J. Colloid Interface Sci.,79 (1981) 209.
87. W. Stumm, H. Hohl and F. Dalang, Croat. Chem. Acta, 48 (1976) 491.

88. J. O. Leckie, in: Metal Speciation: Theory, Analysis and Applications, J.R. Krarner and H.E. Allen (eds.), Lewis Publishers Inc., Chelsea (MI), Ch. 2, 1988.
89. K.F. Hayes and J.O. Leckie, J. Colloid Interface Sci.,ll5 (1987) 564.
90. K.F. Hayes, C. Papelis and J.O. Leckie, J. Colloid Interface Sci., 125 (1988) 717.
91. Adsorption of Inorganics at Solid/Liquid Interfaces, M.A. Anderson and A.J. Rubin (eds.), Ann Arbor Science, Ann Arbor (MI),1981.
92. J.W. Bowden, S. Nagarajah, N.J. Barrow, A.M. Posner and J.P. Quirk, Aust. J. Soil Res., l8 (1980) 49.
93. N.J. Barrow, J.W. Bowden, A.M. Posner and J.P. Quirk, J.P., Aust. J. Soil Res., 19 (1981) 309.
94. L.G.J. Fokkink, A. De Keizer and J. Lyklema, J. Colloid Interface Sci., 118 (1987) 454.
95. N.J. Barrow, Reactions with Variable-charge Soils, Kluwer Academic Publishers (M. Nijhoff), Dordrecht, The Netherlands, Ch. 3,1987.
96. F.J. Hingston, in: Adsorption of Inorganics at Solid/Liquid Interfaces, M.A. Anderson and A.J. Rubin (eds.), Ann Arbor Science, Ann Arbor (MI), Ch. 2, 1981.
97. M. Jaroniec and R. Madey, Physical Adsorption on Heterogeneous Solids, Elsevier, Amsterdam, 1988.
98. M. Jaroniec, Adv. Colloid Interface Sci., 18 (1983) 149.
99. W.A. House, Colloid Science 4, Specialist Periodical Reports, D.H. Everett, (ed.), Royal Soc. Chem., London Ch. 1,1983.
100. W. Rudzinski and D.H. Everett, Adsorption of Gases on Heterogeneous Surfaces, Academic Press, New York,1992.
101. L.K. Koopal and W.H. Van Riemsdijk, J. Colloid Interface Sci., 128 (1989) 188.
102. W.H. Van Riemsdijk, G.H. Bolt and L.K. Koopal in: Interactions at the Soil Colloid-soil Solution Interface, G.H. Bolt, M.F. de Boodt and M.H.B. Hayes (eds.), Kluwer Academic Publishers (M. Nijhoff), Dordrecht, Ch. 3,1990.
103. M.M. Nederlof, P. Venema, W.H. Van Riemsdijk and L.K. Koopal, in: Proceedings Euroclay 1991, Dresden, Germany, M. Störr, K.H. Henning and P. Adolphi, (eds.), Ernst-Moritz-Arndt-Universität, Greifswald, Germany, 795 (1991).
104. L.K. Koopal and S.S. Dukhin, Colloids Surf. A., 73 (1993) 201.
105. C. Contescu, J. Jagiello and J.A. Schwarz, Langmuir, 9 (1993) 1754.
106. J.F. Kuo and T.F. Yen, J. Colloid Interface Sci, 121 (1988) 220.
107. W.H. Van Riemsdijk and L.K. Koopal, in: Environmental Particles, Environmental Analytical and Physical Chemistry Series, vol.1, J. Buffle and H.P. Van Leeuwen (eds.), Lewis Publishers, Boca Raton/Ann Arbor, Ch.12,1992.
108. W. Rudzinski, R. Charmas and S. Partyka, Langmuir, 7 (1991) 354.
109. W. Rudzinski, R. Charmas, S. Partyka, F. Thomas and J.Y. Bottero, Langmuir, 8 (1992) 1154.
110. W. Rudzinski, R. Charmas, S. Partyka and J.Y. Bottero, Langmuir, 9 (1993) 2641.
111. A. Katchalski and P. Spitnik, J. Polym. Sci., 2 (1947) 432.
112. H.P. Gregor, L.B. Luttinger and E.M. Loebl, J. Phys. Chem., 59 (1955) 366.
113. M. Mandel, Eur. Polym. J., 6 (1970) 807.
114. D.G. Kinniburgh and M.L. Jackson, in: Adsorption of Inorganics at Solid/Liquid Interfaces, M.A. Anderson and A.J. Rubin (eds.), Ann Arbor Science, Ann Arbor (MI), Ch. 3, 1981.

115. D.G. Kinniburgh, J.A. Barker and M. Whitfield, J. Colloid Interface Sci., 95 (1983) 370.
116. L.K. Koopal, W.H. Van Riemsdijk, J.C.M. De Wit and M.F.Benedetti, J. Colloid Interface Sci., 166 (1994) 51.
117. M.F. Benedetti, C.J. Milne, D.G. Kinniburgh, W.H. Van Riemsdijk and L.K. Koopal, Environ. Sci. Technol., 29 (1995) 446.
118. M.F. Benedetti, W.H. Van Riemsdijk and L.K. Koopal, Environ. Sci. Technol., (accepted).
119. H. Moon and C. Tien, Chem. Eng. Sci., 43 (1988) 2967.

A. Dąbrowski and V.A. Tertykh (Editors)
Adsorption on New and Modified Inorganic Sorbents
Studies in Surface Science and Catalysis, Vol. 99

Chapter 3.6
Recent progress in the studies of adsorption of ionic surfactants from aqueous solutions on mineral substrates

J. Zajac and S.Partyka

Laboratoire des Agrégats Moléculaire et Matériaux Inorganiques, URA 79–CNRS,
Université des Sciences et Techniques du Languedoc,
C.C.015, 34095 Montpellier Cedex 05, France

1. INTRODUCTION

The study of adsorption of ionic surfactants at the solid–solution interface has assumed new proportions during the last decade for both practical and fundamental reasons. With the refinements of some experimental tools for probing the structure of surfactant adsorbates and the mutual interactions between the components of the adsorption system, also with the injection of concepts from statistical physics, it was possible to better understand the broad principles governing the phenomenon. This allowed bridging the gulf between the purely theoretical aspects of the field of surface chemistry and the purely empirical know–how concerning the applications of ionic surfactants in the mineral industry. The utilization of surfactants for a particular purpose, which, in the past, used to be more of an art than a science, has gained a rational approach by coupling an appreciation of the characteristics of the various types of surface–active agents currently available with a knowledge of the chemistry and physics of the interfacial phenomena in which they are used, without resorting to time– consuming and expensive trial–and–error experimentation. Nowadays the rapid growth of theoretical and experimental advances points to the need for a consolidation of ideas and for the identification of new promissing research directions and new successful applications.

Ionic surfactants can be employed in various processes in which adsorption on (or interaction with) inorganic substrates achieves desired results. The most successful applications are those that are based on potential consequences of adsorption such as ability to affect the mineral suspensions stability and modify the wetting behaviour of mineral surfaces. In many products and processes it is important to obtain stable, uniform dispersions of finely divided solids. Paints, pigments, dyestuffs, pharmaceutical preparations, drilling muds for oil wells, are examples of suspensions of colloidal–sized particles in some liquid medium. Surfactants may be used not only to disperse solids in liquids, but also to coagulate or flocculate solids already dispersed in liquid media. Colloid stability is also important in detergency, flotation, mineral separation processes based on selective coagulation, emulsion polymerization, and agricultural soil conditioning. Wetting, which commonly refers to the displacement of air from a liquid or solid surface by water or an

aqueous solution, always involves three phases, at least two of which are fluids. Therefore, modification of the wetting behaviour of minerals due to the addition of a surface-active agent must be interpreted in view of the selective adsorption of organic ions at the three interfaces present in the system. The most important applications include flotation or beneficiation of ores, enhanced oil recovery, detergency, sanitization, dyeing, printing, utilization of pesticides and herbicides.

In studies of the adsorption of inorganic or organic ions from aqueous solutions on different solid surfaces the interpretation of the results is often obscured by factors such as surface roughness, heterogeneity, porosity, or its affinity for water, which are difficult to assess and to control. *Mineral oxides* of simple geometries can provide relatively smooth surfaces with well-defined surface compositions and known surface charges. They are characterized as having high surface energies and tend to be hydrophilic and polar in nature. In aqueous solutions, mineral surfaces acquire an electric charge, which is caused by the dissociation of amphoteric surface hydroxyl groups and this is determined by the pH. These features make them close to ideal for fundamental studies. An investigation of the adsorption behaviour of such simple systems can shed light on the interaction of ionic adsorbates with many other substrates and hence leads to the development of models for the adsorption process.

The intent of this chapter is to present a brief review of simple, fundamental physicochemical principles and experimental results which are necessary to understand both the mechanism of adsorption of ionic surfactants from aqueous solutions on oxide surfaces and the action of some simple, fundamental applications. It does not enter into details in the theoretical consideration, nor does it attempt to explain complex industrial uses. Both problems have been thoroughly treated in several review articles and monographs [e.g., 1–10]. Here emphasis is placed on the contribution the adsorption calorimetry makes to the improvement of current understanding of the interactions of ionic surfactants at the mineral–water interface. All experimental data, used for the illustrative purposes throughout this chapter, were obtained at the Laboratoire des Agrégats Moléculaire et Matériaux Inorganiques.

2. MATERIALS AND EXPERIMENTAL TECHNIQUES

The adsorption of ionic surfactants at the solid–solution interface is strongly influenced by a number of factors:

(1) the nature of the solid substrate – its chemical and crystalline structure, particle size distribution, specific surface area, porosity, surface heterogeneity, charging behaviour, and hydrophilicity;

(2) the molecular structure of the surfactant being adsorbed – the structure and the charge of the polar head group, the length of the hydrophobic moiety, and whether it is straight-chain or branched, aliphatic or aromatic;

(3) the environment of the aqueous phase – its pH, ionic strength, temperature, and the presence of any additives (e.g., alcohols, urea, formamide, dioxane).

Together these factors determine the mechanism by means of which surfactant solutes may adsorb onto solid substrates from aqueous solution and very systematic studies are

needed to explore the effect of each of them on the degree of adsorption and the energetics involved. In the first place, the general research strategy consists in the comparison of the various substrates in their abilities to adsorb the same surfactant ion or the same homologous series of surfactants. Then, within each experimental series on a given substrate, important conclusions can be drawn with respect to chemical structure of the surfactant and physical properties of the liquid medium.

The complexity of the phenomenon requires the application of a variety of experimental techniques. Comparison of data from all these measurements yields greater insight into the possible mechanism of the process and its evolution with the surface coverage. The most popular tools utilized in measuring ionic surfactant adsorption include, primarily, adsorption isotherms, but also electrophoretic data and contact angle measurements [e.g., 11–21]. The reason for this tendency is that most of the studies in the past related to efforts to define the dynamics of the flotation process and to find a correlation among rise in flotation, degree of adsorption, and electrokinetic properties of mineral suspensions in solutions of an ionic collector. In most cases, the effect of adsorption is quantified by means of the standard solution depletion technique, nevertheless ellipsometry [22] and electron spectroscopy for chemical analysis (ESCA) [23,24] have been successfully tested as methods for the determination of the thickness of the adsorbed layer and the equilibrium adsorption density onto relatively simple supports like glass or mica. Adsorption isotherms are sometimes supplemented by conductivity and pH measurements or potentiometric titration. Conductivity data are used to detect changes in surfactant aggregate structure [17]. A change in pH upon adsorption indicates a change in surface charge [20], whereas the classical potentiometric titration leads to determination of the net surface proton balance in the absence and presence of surfactant [21].

An adsorption isotherm is a necessary but not sufficient way of describing the thermodynamics of ionic surfactant adsorption because a full description of the phenomenon requires knowledge of mutual interactions between all the components of the system. Such opportunity is offered by flow and batch liquid adsorption microcalorimetry [25–30].

Although large number of studies have been reported on the equilibrium adsorption of ionic surfactants at the interfaces, very little attention has been paid to the adsorption kinetics. Only a few attempts have been made to follow the time evolution of the process from the initial adsorption to the equilibrium configuration and to understand the role of the diffusion [24,25,31].

Over the last decade the surface force technique has been used to probe the nature of the forces which atomically smooth surfaces exert on each other in different solutions [32]. The effect of cationic surfactant adsorption on the surface forces, inferred from the fitted surface potentials and the measured adhesion data, has been well characterized for mica and silica glass surfaces [33–37].

Some essential discoveries concerning the organization of the adsorbed layer derive from the various spectroscopic measurements [38–46]. Here considerable experimental evidence is consistent with the postulate that ionic surfactants form localized aggregates on the solid surface. Microscopic properties like polarity and viscosity as well as aggregation number of such adsorbate microstructures for different regions in the adsorption isotherm of the sodium dedecyl sulfate/water/alumina system were determined by fluorescence decay (FDS) and electron spin resonance (ESR) spectroscopic methods. Two types of molecular probes incorporated in the solid–liquid interface under *in situ* equilibrium conditions

were chosen: pyrene and dinaphthylpropane fluorescent probes [38] and the nitroxide spin probes [39,40]. The evolution and structure of surface aggregates in the same adsorption system were also examined by excited-state resonance Raman spectroscopy [41] with the use of tris(2,2'- bipyridyl)ruthenium(II) chloride as the reporter molecule. Adsorption of cationic surfactants like dodecylpyridinum and cetylpyridinum chlorides [42], or dioctadecyldimethylammonium chloride [43] on negatively charged silica was characterized with the aid of the ESR spectra for 2,2,6,6-tetramethylpiperidinyl-1-oxy [42] and 7-doxyl-stearic acid [43], as well as the fluorescence spectra for pyrene-3-carboxaldehyde [42,43] adsolubilized in the surfactant adlayer. Recently, a number of nuclear magnetic resonance (NMR) studies have been presented [44-46]. The analysis of the adsorbate structure is based on the recorded ^2H NMR spectra of alkyltrimethylammonium bromides [44,46] or sodium alkylbenzenesulfonates [45], deuterium labeled in the moiety of the charged head-group and adsorbed on silica or alumina particles.

Other studies have opened the general possibility of observing the adsorption phenomenon by yet another sensitive technique to provide basic information on adsorbed layers, namely small-angle neutron scattering (SANS) [47,48]. For example, this technique enabled the authors [47] to look at the structure of aggregates made of silica spheres flocculated with cationic surfactants and to discuss the effect of the heterogeneity of the adsorbed layer on the formation of these aggregates. Elsewhere [48] it was possible to obtain direct structural information about a cationic surfactant adsorbed on an amorphous silica block by monitoring the intensity of neutron beams specularly reflected at the solid-liquid interface.

In reviewing a vast quantity of literature on the subject, it is possible to encounter some studies which are of little value because insufficient attention has been given to the control of important physical factors, to the potentiality of the experimental technique, or to the limitations of particular theoretical approaches. Therefore, Section 2 is exclusively devoted to description of the materials and experimental methods used in measuring the adsorption of ionic surfactant onto mineral substrates. Some experimental problems, encountered in the everyday laboratory practice, will be pointed out. Among different experimental methods, the adsorption calorimetry particularly deserves to be noted.

2.1. Solid supports

The adsorption of surfactants was studied on powdered solid samples, which were all commercial products. The following supports were considered:

1) Surface-hydroxylated amorphous silica obtained by precipitation from sodium silicate solution in Rhône-Poulenc and Aubervilliers Laboratory (France). It is a nonporous adsorbent of high purity except that it contains some traces of sodium as impurities [49-52]. This sample was used without further treatment.
2) Quartz, specified to contain 99.8% SiO_2, supplied by Sifraco (France). Ground quartz crystals were sieved and sedimented. This product was first leached repeatedly in boiling 2N HCl and thoroughly washed with deionized water until the filtrate showed no trace of chloride ion [53].
3) Zirconium dioxide obtained from T.S.K. Zirconia TZ-O (Japan) and used without further purification [54].

4) Corundum (α-aluminium oxide), specified to contain > 99% Al_2O_3, purchased from Union Carbide (USA). The sample was washed six times in deionized water in order to eliminate the traces of some 'interfacial' impurities. It was subsequently dried at 433 K in a vacuum dryer for 30 hrs [54].

Some properties of these solid samples, important in regard to the adsorption process, are presented in Table 1.

Table 1
Some basic physicochemical properties of the solid supports

Solid sample	BET specific surface area [$m^2 \cdot g^{-1}$]	Mean particle size μm	Crystalline structure	pH of the pzc
Precipitated silica	40	0.13	amorphous	2–3
Quartz	5.5	1–10	rhombohedral	1.5
Zirconia	14	0.1	monoclinic	5.5
α-Alumina	9.2	0.1–0.3	hexagonal	8

The specific surface area and porosity was determined by the nitrogen gas adsorption at 77 K using the BET adsorption model (cross-sectional area of one nitrogen molecule was taken as 16.2 Å^2). The mean particle size was observed in a scanning electron micrograph. Some of the solid samples are relatively polydisperse and the particle size range is reported in these cases. The crystalline structure was examined by X-ray diffraction analysis. The classical potentiometric titration and electrophoresis were used to determine the net surface proton balance and the electrophoretic mobility of solid particles as functions of pH in different electrolytes. The pH value corresponding to the *point of zero charge* (pzc) was calculated from the experimental results (the methods and equipments are described elsewhere [54]).

2.2. Adsorbate molecules

The adsorbate molecules, considered in this chapter, belong to four homologous series of surfactants. They also comprise *polar heads* of these surfactants, i.e., organic compounds having the same hydrophilic groups but without hydrocarbon tails. Below listed are all the solute molecules, together with their chemical formulae, the name of the producer (or the method of synthesis), the procedures applied for their purification (or the purity specified by the producer, if used as received), and the acronyms, which will be utilized afterwards:

(A) (*Anionics*) Sodium alkyl sulfates [54]; supplied by Prolabo (France) and used as received (98% purity):

1. (**SDS**) Sodium dodecyl sulfate; $n\text{-}C_{12}H_{25}SO_4^-Na^+$
2. (**SOS**) Sodium octyl sulfate; $n\text{-}C_8H_{17}SO_4^-Na^+$

(B) (*Anionics*) Sodium alkylbenzenesulfonates [54]; synthesized in the laboratory [56] and purified by recrystallization from distilled water [54]:

3. (**SOBS**) Sodium octylbenzenesulfonate; $p\text{-}C_8H_{17}C_6H_4SO_3^-Na^+$
4. (**SHBS**) Sodium heptylbenzenesulfonate; $p\text{-}C_7H_{15}C_6H_4SO_3^-Na^+$

(C) (*Cationics*) Benzyldimethylalkylammonium bromides [49–52]; purchased from Fluka (France) and purified by recrystallization from ethyl acetate and from water [50]:

1. (**BDDAB**) Benzyldimethyldodecylammonium bromide; $C_6H_5CH_2N^+(CH_3)_2\text{-}C_{12}H_{25}Br^-$

(D) (*Cationics*) Alkyltrimethylammonium bromides [49]; supplied by Sigma (France) and used as received (99% purity);

2. (**HTAB**) Hexadecyltrimethylammonium bromide; $n\text{-}C_{16}H_{33}N^+(CH_3)_3Br^-$
3. (**TTAB**) Tetradecyltrimethylammonium bromide; $n\text{-}C_{14}H_{29}N^+(CH_3)_3Br^-$
4. (**DTAB**) Dodecyltrimethylammonium bromide; $n\text{-}C_{12}H_{25}N^+(CH_3)_3Br^-$

(E) (*Polar heads*) obtained from Fluka (France) and used as received (>98% purity):

1. (**SBS**) Sodium benzenesulfonate; $C_6H_5SO_3^-Na^+$
2. (**BTAB**) Benzyltrimethylammonium bromide; $C_6H_5CH_2N^+(CH_3)_3Br^-$

Among the different properties of surfactants, it is those resulting from their amphipathic structure, the property of being adsorbed at interfaces and that of forming colloidal-sized clusters in aqueous solutions, that are the most important. The former may be characterized by the effectiveness of adsorption, whereas the latter by the *critical micelle concentration* (cmc). The *area per molecule at surface saturation*, a_0, is a useful measure of the effectiveness of the surfactant adsorption at the solution–air interface, since it corresponds to the maximum value for which adsorption can reach. When compared with its equivalent for the solid–liquid interface, this parameter may provide information on the degree of packing and the orientation of the adsorbed surfactant molecules on a solid surface. The cmc represents the maximum solubility of the single molecules in a given aqueous medium and thus plays an important role in the surfactant adsorption onto solid substrates, where single ions rather than micelles are involved. Both parameters are very sensitive to the presence of impurities and will strongly depend on purification procedure. They were determined by applying the Gibbs equation [e.g.,57] to the surface tension measurement with an electrobalance type tensiometer (Prolabo TD 2000, France). Examples are reported in Table 2.

Since surfactant molecules can aggregate into micelle–like structures on a solid surface, the enthalpies of micellization in the bulk phase are also listed in this table. They will

Table 2
Critical micelle concentration, cmc, area per molecule at surface saturation, a_0, and molar enthalpy of micellization, Dmich, for the surfactant molecules (in deionized water)

Surfactant	Solvent	Temperature [K]	cmc [mmol·kg^{-1}]	a_0 [nm^2/molec.]	$\Delta_{mic}h$ [kJ·mol^{-1}]
SDS	water	308	8.5	0.47	–6.4
SOS	water	308	100	0.47	
SOBS	water	298	11.3	0.35	–4.0
SHBS	water	298	22.6	0.35	–0.9
BDDAB	water	298	5.6	0.71	–5.3
HTAB	water	308	1.0	0.60	–23.2
TTAB	water	298	4.0	0.59	–4.7
DTAB	water	298	14.8	0.61	–1.6

be further compared with the differential enthalpies of adsorption at higher surface coverages. The enthalpic values were measured by microcalorimetry (see paragraph 2.5.).

2.3. Chemical analysis of the bulk phase

The water used throughout all experiments was deionized and purified with a Millipore 'Super Q' system. It had a pH value of about 6 and conductivity which varied between 0.05 and 0.1 $\mu S \cdot cm^{-1}$. The increase in ionic strength was effected with the salts used to buffer the system (0.1M NaBr aqueous solutions). Values of pH were determined with Tacussel electrode (France). The accuracy of the measurement was to 0.05 pH unit. When needed, the pH was adjusted by the controlled addition of 0.1N HCl or 0.1N NaOH solutions depending on the pH desired. All inorganic chemicals were of Analyzed Reagent grade.

In the case of powdered solid samples, which exhibit some residual solubility in water (e.g., silica), water saturated with soluble solid should be utilized for preparing a stock solution and then for diluting it. To this end, a given volume of water is mixed with an appropriate mass of solid in a glass mixer with a magnetic bar stirrer for 24 hr under constant temperature and pH. Then the excess of solid is repeatedly separated by filtration on a milipore filter with suction and the clear filtrate taken as solvent.

The composition of surfactant or polar head solutions is expressed in moles of solute in 1 kg of solvent, i.e., *molality*. Such an unit has two important advantages over the molar concentration. Firstly, it does not depend on the temperature and this facilitates the comparison of experimental results obtained at different temperatures. Secondly, any solution may be prepared by weighing the solute and solvent, or the stock solution and solvent in the case of dilution. The gravimetric procedure markedly increases the precision of the chemical analysis of the bulk phase.

A variety of analytical techniques are available for determining the change in concentration of the surfactant and its polar head. The refractometric technique was employed because of its universal detection capability: the detector is able to identify all compounds in a solvent which have their refractive indexes different from that of the solvent. The apparatus R– 403, belonging to the Water Associates R–400 Series Refractometers with the inlet tube and cell dead volume of 250 μl, is a recording differential refractometer for continuously and quantitatively monitoring the difference in refractive index (RI) between two liquid streams (solution and pure solvent). The concentration of the surfactant or polar head is estimated within 1–5% error from the comparison of the RI difference of the solution with those of the blanks containing known concentrations of the solute (calibration line) at constant temperature. When a phenyl or other chromophoric group is present in the solute structure (e.g., BDDAB, BTAB, SOBS, SHBS, and SBS), the UV spectroscopy allows the concentration determinations to be achieved with more precision, especially in the case of very diluted solutions (accuracy below $5 \cdot 10^{-6} mol \cdot kg^{-1}$). The UV Varian differential spectrofotometer with different cells of 0.1 to 10 mm in width was utilized to measure the absorbancy of benzyldimethylalkylammonium bromides (λ_{max} = 262.8 nm) and sodium alkylbenzenesulfonates (λ_{max} = 261.5 nm) in aqueous solvent in the wavelength range 240–340 nm. This absorbancy was compared with those of the blank solutions and the concentration of the solute was read from the least–square–fitted calibration line. In order to elucidate more precisely the exchange of the adsorbing ions with the monovalent counterions in the double layer, the concentration of Na^+ cations was determined in the supernatant using the flame absorption spectrometer (air–acetylene flame, wavelength

589.6 nm). To avoid the interference of the absorption values coming from the presence of solute molecules (surfactant or polar head), it was necessary to prepare calibration standards having the same solute concentration for each analyzed solution.

2.4. Adsorption and electrophoretic measurements

Adsorption isotherms are habitually obtained using the solution depletion method, which consists of comparing the solute concentrations before and after the attainment of adsorption equilibrium. Electrokinetic or zeta potentials are determined by two techniques: microelectrophoresis [12,14,17] and streaming potential [13,58,59]. The former is employed to measure the mobility of small particles of chemically pure adsorbents, whereas the latter is adopted to investigate the electrophoretic behaviour of less pure coarser mineral particles. A correlation between the adsorption and electrophoretic results is usually examined with the aim of sheding light on the mechanism by means of which the surfactants are adsorbed at the solution–solid interface. This implies the necessity of maintaining the same experimental conditions in both experiments. For this purpose, the same initial operational procedure is applied.

A stock quantity of buffer or salt solution of define pH and ionic strength (or pure water at free pH) was prepared, which was treated as a solvent for the preparation of the solution of surfactant. Then the solutions of the various compositions were obtained with this solution by the appropriate dilution in standard joint stoppered tubes of capacity 30 ml. Dry solid powder was weighed accurately and poured into the tubes. Each tube containing the same mass of solid sample and the same volume of aqueous solution of a given molality was equilibrated by slow rotation (avoiding the formation of foam) for 24 hr at a constant temperature. Then the solid samples were separated from the supernatants by centrifugation (13000 rpm during 20 min). A definite volume of the clear supernatant was removed from each tube with the help of a long needle glass syringe and analyzed for the solute content and pH. Simultaneously, samples of solid suspension were collected for electrophoresis experiments.

In the case of adsorption experiment carried out at constant pH, the above procedure was somewhat modified. The rotation of tubes was stopped after 8 hr and the suspension was allowed to settle for a period of time depending on the particle size of the solid sample. The pH was checked and, if necessary, readjusted to its original value. The operation was repeated until no changes in pH were observed.

The *specific amount adsorbed* of the solute, n_2^e, or the amount adsorbed per square meter of solid surface, Γ_2^e, were calculated from the experimental data using the equations

$$n_2^e = \frac{m_1^0 \cdot (C_2^0 - C_2^b)}{10^3 \cdot m_S} \qquad \text{or} \qquad \Gamma_2^e = \frac{n_2^e}{A_S} \tag{1}$$

where m_1^0 is the initial mass of solvent, C_2^0 and C_2^b are, respectively, the molalities of the initial solution (before adsorption) and the equilibrium bulk solution (after the attainment of adsorption equilibrium), m_S is the mass of solid sample, A_S is the BET specific surface area.

In studying adsorption at any interface, one is interested in determining the number of moles of the adsorbate per unit mass or unit area of the solid adsorbent since this is a measure of how much of the surface has been covered, and hence changed, by the adsorption. To find the relationship between this number of moles, n_2^s (or Γ_2^s) and the

experimentally measured quantity n_2^e (or Γ_2^e), the form of the concentration profile of component 2 up to the surface must be known. It is, however, conventional to represent the concentration as a step function according to the *surface phase model* [60]. The basic concept is that the solid–solution interface may be approximated by a thin, homogeneous layer of liquid usually called a *surface phase*. The layer is bounded on one side by the solid and on the opposite side by the homogeneous bulk solution. Following the law of conservation of mass in a closed system with respect to solute 2, after combination with Eq.(1) and simplification

$$n_2^e = n_2^s - \frac{m_1^s \cdot C_2^b}{10^3} \tag{2}$$

where m_1^s represents the mass of solvent in the surface phase per unit mass of solid. Most of the solutes used in the studies of adsorption in dilute solution possess relatively strong affinities for the solid surface, whereas the affinities of the solvents are relatively weak. Under these circumstances the product $m_1^s \cdot C_2^b$ becomes negligible, so that $n_2^e = n_2^s$ (and $\Gamma_2^e = \Gamma_2^s$ per unit surface area of solid).

The adsorption isotherm can then be plotted in terms of n_2^s (or Γ_2^s) as a function of C_2^b at a given temperature

$$n_2^s = f(C_2^b) \qquad \text{or} \qquad \Gamma_2^s = f(C_2^b), \qquad T = \text{const.} \tag{3}$$

In most cases, n_2^s (or Γ_2^s) monotonically increases with increase of C_2^b at low solute molalities. At relatively higher values of C_2^b (e.g., in the vicinity of the cmc for surfactants) it reaches a limiting steady value $n_{2,max}^s$ (or $\Gamma_{2,max}^s$) which does not increase with further increase of C_2^b. This density of adsorption at surface saturation determines the effectiveness with which the solute is adsorbed at a given temperature. The reciprocal of $\Gamma_{2,max}^s$ gives the averaged surface area per adsorbate molecule on the adsorbent.

The extent of adsorption is sometimes expressed as percentage of a total capacity of the adsorbed layer:

$$\Theta = \frac{n_2^s}{n_{2,max}^s} = \frac{\Gamma_2^s}{\Gamma_{2,max}^s} \tag{4}$$

In the literature, the experimental adsorption isotherms are plotted on three principal scales: double linear (lin–lin), linear–logarithmic (lin–log) and double logarithmic (log–log) [12,14,21,61]. The various presentations allow a more detailed analysis of the subsequent adsorption stages to be made. On a log–log scale, different regions can be explicitly distinguished in the isotherms. They are believed to reflect distinct modes of adsorption. However, the transitions between such regions are considerably more gradual in reality than they seem to be on this scale. The effects of surface heterogeneity and cooperative adsorption, which occur at very low surface coverages, show up most clearly in log–log plots. Cooperative adsorption at higher surface coverages, the plateau adsorption region in particular, markedly manifest itself only on a linear scale. The thermodynamic interpretation of the phenomenon is easier with the use of lin–log plots. Here the logarithm of the solute concentration is equal to the configurational part of the electrochemical potential of solute in the equilibrium bulk phase.

A Rank Brothers microelectrophoresis apparatus MKII with a rectangular cell was applied to measure the average velocity U at which charged colloidal particles move under

the action of a steady and weak electric field between platinum black electrodes. This velocity is determined by the balance between the electrical and viscous forces which act on the particle. At a stationary level inside the cell, where solvent is immobilized, the particle moves with a uniform velocity. Since the movement of particles is observed on a screen of monitor, the electrophoretic velocity may be calculated from the time necessary to cover a certain distance. The direction of movement permits to decide the sign of surface charge.

Sample of solid suspension in the supernatant, collected after the attainment of adsorption equilibrium, was transferred to the thermostated microelectrophoresis cell. The velocity U for at least 10 particles was measured at the two stationary levels and the average value taken; the polarity of electrodes was reversed after each velocity measurement. For a spherical particle, the following equation is satisfied:

$$U = \mu \cdot E \tag{5}$$

where E is the strength of the applied electric field and μ is called the *electrophoretic mobility* of the particle (expressed in $m^2 \cdot s^{-1} \cdot V^{-1}$). The mobility is directly related to the *zeta potential*, ζ, an important quantity associated with the electrical double layer, by the Smoluchowski's equation [57]

$$\zeta = f \cdot \frac{\mu \cdot \eta}{\varepsilon} \tag{6}$$

where η and ε are the viscosity and the dielectric constant of the suspending medium; this formula should be used with SI units. The factor f is a correction factor for the electrophoretic retardation and relaxation effects (the ion atmosphere affects the forces which act on the moving particle and decreases its mobility); it depends on the particle size, ionic strength, and ζ-potential [62–64]. The zeta potential is a potential of the charged surface at the *plane of shear* between the particle and the surrounding solution as they move with respect to each other. The plane of shear is situated at an undetermined point somewhere in the diffuse layer and it is very tempting to place it at the solution side of the Stern layer, so that $\zeta = \Psi_d$, the diffuse layer potential. However, the exact position of that plane is still the subject of some debate and the zeta potential is smaller in magnitude. In spite of this difficulty, the electrophoretic mobility, μ, can be considered as a measure of the net charge of the solid particle, i.e., the surface charge plus the charge of the adsorbed layer. It is plotted in function of the equilibrium bulk concentration or directly as a function of the amount adsorbed

$$\mu = f(\ln C_2^b) \qquad \text{or} \qquad \mu = f(\Gamma_2^s), \qquad T = \text{const} \tag{7}$$

The adsorption and electrophoretic measurements were supplemented by the qualitative observation of the flocculation of solid particles in the surfactant solutions. The turbidity of the content of each adsorption tube after adsorption, recorded at various time intervals, was compared with that of a control tube containing the same solid concentration but in pure solvent. This suspension of reference was always prepared under the same conditions as the others. A marked increase in the turbidity was taken as evidence of flocculation.

Flocculation of charged solid particles occurs with the addition of surfactant to the suspension. If surfactant ions are adsorbed on the surface and oriented so that hydrophobic

areas are produced, these areas on different particles may come together to form a micelle, even if the surfactant concentration is well below the cmc. The particles are thus held together by the powerful surface tension forces at the zone of contact until the surface remains hydrophobic. The bridges of surfactant molecules are sufficiently long to promote an open and voluminous structure of the final aggregates. As a consequence, the decrease in the surface area accessible to adsorption is small. When a twofold layer is built at higher bulk concentrations owing to hydrophobic attraction between the hydrocarbon chains, the outwardly disposed ionic head-groups render the surface hydrophilic again and the flocs redisperse. The reversibility of flocculation provides an argument for the formation of two successive layers of surfactant ions.

2.5. Microcalorimetry of adsorption

The enthalpy changes accompanying adsorption from solutions may be obtained by direct calorimetric measurements. Static calorimetry, i.e., the technique for measuring the total heat evolved when a solid is immersed in a solution of a given composition, is the method used in most experiments to date, while the flow calorimeter, in which the heat of displacement of one solution by another is measured, has rapidly been established as a valuable extension to the more conventional technique [e.g.,65–67]. In many ways the measurement of heat is easier and can be achieved with more precision than determinations of the amounts adsorbed. For basic thermodynamic reasons, heat effects should be more sensitive to the nature of the solid– solution interface. Therefore, much more reliable interpretation of the behaviour of an adsorption system may be expected while basing on the analysis of adsorption isotherms and the related heats. Only a few authors have attempted to apply such an investigation strategy to the adsorption of ionic and non-ionic surfactants [25–30,49–54,68–73] though it is evident that the lack of simultanous adsorption and heat data has left all developed thermodynamic models essentially untested.

The calorimeter 'Montcal 3' was used to measure enthalpies of dilution and adsorption. This isothermal apparatus is a specific combination of batch and flow microcalorimetric techniques. It is schematically represented in Fig.1. It is equiped with an injection system which enables the controlled introduction of reagents into the calorimetric cell. The homogeneity of the suspension is ensured by a horizontal agitator with a variable speed of rotation that can be adjusted to the nature of the solid-liquid system studied. It is thus possible to follow the process step by step along the isotherm and detect the enthalpy changes associated with successive steps. Injection of reagents, calibration processing, temperature control, and recording of the heat effects are all carried out by the appropriate microcomputer system. A detailed description of the apparatus and its functional parts, the operating principles, technical specifications, procedures for operation, and factors affecting its performance can be found in paper [74].

The calorimetric cell is initially filled with m_S grams of solid and M_P grams of solvent (pure water or buffer/salt solution); $m_1^{s\circ}$ grams of water are adsorbed per unit mass of solid. The reservoir of the injection system contains a certain volume of the stock solution of molality C_2°; the solvent used to prepare this solution must be exactly the same as that in the cell. When the termal equilibrium has been reached in the whole calorimetric system (the baseline is steady), a precision syringe pump injects a small portion of the stock solution into the suspension. The mass of solute introduced into the cell is equal to

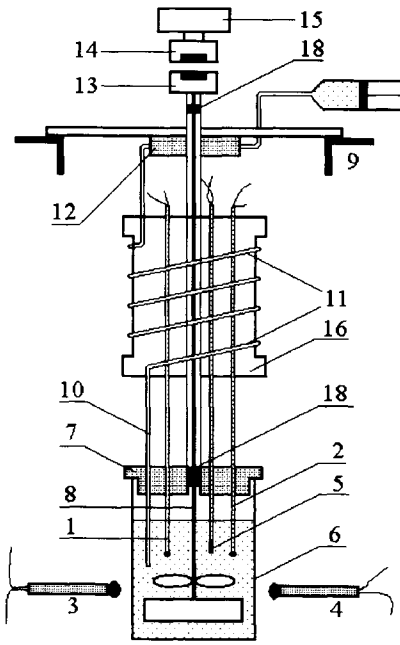

Figure 1. Liquid injection and agitation system of the Montcal microcalorimeter.

$k_o \cdot t$ and that of solvent is $(d - k_o) \cdot t$, where t is the time of injection (in min), d is the flow rate of the pump (in $g \cdot min^{-1}$), and the coefficient k_o is expressed as follows:

$$k_o = \frac{C_o M_o d}{10^3 + C_o M_o} \tag{8}$$

M_o is the molar mass of solute. The injected solute molecules are diluted in the supernatant inside the cell and a fraction of them subsequently adsorbs onto solid particles. They displace a certain amount of water pre-adsorbed at the solid-water interface, because of the limited extent of the adsorption space. At equilibrium, there are m_1^s grams of water and n_2^s moles of solute adsorbed per unit mass of adsorbent. The total operation induces a thermal effect and alters the equilibrium which is recorded as a thermal peak (after about 15–20 min the signal returns to the baseline). These data, once processed by the software, yield the related enthalpy change $\Delta_{exp}H$.

The law of mass conservation separately applied to solute 2, rearranging and combining with Eq.(2), leads to the following relationship:

$$n_2^e = n_2^s - \frac{m_1^s \cdot C_2^b}{10^3} = \frac{k_o \cdot t}{m_S \cdot M_o} - \frac{[M_p + (d - k_o) \cdot t] \cdot C_2^b}{10^3 \cdot m_S} \tag{9}$$

For given time of injection, t, n_2^e is a linear function of C_2^b and the coefficients of the linear equation correspond to two extreme states: the whole amount of solute injected in the calorimetric cell either adsorbs on the solid surface (the intercept) or remains in the solution of molality C_2^b (the slope). The partition of solute molecules between the

adsorbed phase and the bulk solution is strictly determined by the adsorption equilibrium at a constant temperature and does not depend on the path by which the adsorption system passes from its initial state to the equilibrium. In consequence, the n_2^e and C_2^b values are identified with the co-ordinates of a point where the line (9) intersects the experimental isotherm $n_2^e = f(C_2^b)$. The thermodynamic balance enables the enthalpy change during the above experiment, $\Delta_{exp}H$, to be divided into two parts, which are relevant to the displacement and dilution effects. These terms will be dependent on the choice of a reference state in the liquid phase. In the case of dilute solutions, an *infinitely dilute aqueous solution* is taken as reference and apparent molal quantities may be utilized for the solute. The dilution contribution takes the form:

$$\Delta_{dil}H = (k_o \cdot t/M_o) \cdot \left[h_2^b\left(C_2^b\right) - h_2^b\left(C_2^o\right)\right] \tag{10}$$

where $h_2^b(C_2)$ is the apparent molal enthalpy of solute in a solution of molality C_2. The value of $\Delta_{dil}H$ is measured directly with the same apparatus in a similar experiment (all the experimental conditions, like C_2^o, C_2^b, d, t, have to be the same; the only difference is that the calorimetric cell contains no solid sample). The corresponding equation for the displacement term is:

$$\Delta_{dpl}H = n_2^s \cdot m_S \cdot \left[h_2^s\left(C_2^b\right) - h_2^{b\infty}\right] + m_S \cdot (m_1^{so} - m_1^s) \cdot \left(h_1^{bo} - h_1^{so}\right) + \tag{11}$$
$$+ m_1^s \cdot m_S \cdot \left[h_1^s\left(C_2^b\right) - h_1^{so}\right] + n_2^s \cdot m_S \cdot \left[h_2^{b\infty} - h_2^b\left(C_2^b\right)\right]$$

where $h_j^s(C_2^b)$ is the partial molal enthalpy of component j (j=1,2) in the adsorbed phase being at equilibrium with a solution of molality C_2^b; h_1^{so} and h_1^{bo} are the specific enthalpies of solvent in the pure adsorbed and bulk phase, respectively; $h_2^{b\infty}$ is the apparent molal enthalpy of solute at infinite dilution. The first three terms on the right hand side of Eq.(11) successively correspond to adsorption of solute 2, desorption of solvent 1 and changes in the energetic state of solvent which remains in the adsorbed phase. Their sum represents the *integral enthalpy of displacement* (with the solute at infinite dilution as a reference). The last term is a correction expression due to difference in the composition of the equilibrium solution (C_2^b) and the reference solution ($C_2^{b\infty}$). It may be calculated from the experimental results for the dilution of a stock solution of molality C_2^b (the value at zero molality is extrapolated).

In principle, only the enthalpy of displacement is determined from the batch displacement experiment. The enthalpic value will depend on the strength of solute–solid interaction, the affinity of solvent to the support, and the molar ratio of displacement, i.e., the amount of solvent displaced by 1 mol of solute. Moreover, all these properties are functions of the state of the adsorbed phase. If adsorption of the solute occurs through either an ion exchange or an ion pairing mechanism, the integral enthalpy of displacement will also include such contributions as the enthalpy of dehydration of the adsorbing ion, the enthalpy of desorption of the pre-adsorbed counterions and their rehydration in the equilibrium bulk phase, and the enthalpic effect of the surface charge regulation upon adsorption (release or uptake of protons). In the case of cooperative adsorption of surfactants, hydrophobic interaction between hydrocarbon moieties contributes to the total interaction energy in the system.

The above experimental procedure may be repeated by the addition of further amounts of stock solution until the solid surface reaches the state of saturation, $n_{2,max}^s$ In the case

of experiment by small steps, i.e., an increase in the amount adsorbed is sufficiently small, it is possible to measure a pseudo-differential enthalpy of displacement, which gives an approximate value of the differential enthalpy of displacement. For each injection step

$$\Delta_{dpl}h^i = \frac{\Delta_{exp}H^i - \left(k_o \cdot t^i/M_o\right) \cdot \left[h_2^b\left(C_2^i\right) - h_2^b\left(C_2^o\right)\right]}{\Delta_a n_2^i} \qquad (12)$$

where $\Delta_{exp}H^i$ is the enthalpy change obtained from the integration of the thermal peak associated with the i-th injection and t^i is the time of this injection; the term of dilution $[h_2^b(C_2^i) - h_2^b(C_2^o)]$ is determined in the 'blank' dilution experiment (for the equilibrium molality C_2^i); $\Delta_a n_2^i = n_2^e(i) - n_2^e(i-1)$ is the difference between the quantities of adsorption after two successive injections and $n_2^e(j)$, j=i-1,i, is calculated using the experimental isotherm of adsorption and Eq.(9), in which the time of injection, t, is replaced by the sum $\sum_{k=1}^{j} t_k$. Since the whole adsorption region should be covered, from the beginning of the isotherm to its plateau, a surfactant stock solution at a molality much higher than the cmc should be used. A correction term in Eq.(12), arising from destruction of micelles injected into the calorimetric cell and dilution of unmicellized species, gives rise to an important contribution to the total thermal effect $\Delta_{exp}H$ and increases the uncertainty in the enthalpy of displacement evaluation. Moreover, one should be aware that the accuracy of this experimental procedure fails in the neighbourhood of the plateaus on the isotherm, where adsorption increments corresponding to the successive injections are too small to be precisely determined.

The enthalpic curves are usually plotted in terms of differential molar enthalpy of displacement, $\Delta_{dpl}h$, as a function of the corresponding amount adsorbed at a given temperature

$$\Delta_{dpl}h = f\left(n_2^s\right), \quad \text{or} \quad \Delta_{dpl}h = f\left(\Gamma_2^s\right), \quad \text{or} \quad \Delta_{dpl}h = f\left(\Theta\right), \quad T = \text{const} \qquad (13)$$

3. MECHANISMS OF THE ADSORPTION OF CATIONIC AND ANIONIC SURFACTANTS ONTO MINERAL OXIDES WITH OPPOSITELY CHARGED SURFACE SITES

It is generally accepted that the principle intermolecular forces relevant to the adsorption of ionic surfactants on highly-charged hydrophilic solid surfaces include long-range forces such as the London-van der Waals attraction and the coulombic attraction or repulsion, and short-range structural forces due to changes in the solvent structure in the vicinity of a surface. The surface charge exerts an influence on the distribution of ions in the solution; as a result, an electric double layer will form. The presence of a discrete electrical charge, borne by the surfactant molecule and by the solid surface, can result in specific adsorption of the solute occuring by ion exchange or ion pairing mechanisms.

Adsorption by dispersion forces acting between adsorbent and adsorbate molecules is important as an universal supplementary mechanism in all other types. The effect is illustrated by the ability of surfactants with long hydrocarbon tails to displace equally charged low molecular weight materials and simple inorganic ions from solid substrates [75,76].

On account of the dispersion force interactions between the alkyl chain and the support, the orientation of the adsorbate in the early adsorption stages may be quasi-parallel to the surface. However, full hydrophobic association of the chain with the surface is less probable owing to the difficulty of disrupting the 'icelike' region in the vicinity of a high concentration of hydroxyl groups.

The spectrum of adsorption mechanisms is wide and depends on the specific properties of a given adsorption system. It comprises induced dipolar or polarization effects, hydrogen bond formation, acid–base affinity, and other interactions lying somewhere between the strictly nonpolar dispersion and ion–ion coulombic forces. They can alter the extent and mode of the process. For example, if the adsorbate contains an electron-rich group and the solid support has strongly polarizing sites, attraction between them markedly enhances the energetics of adsorption [77].

The nonpolar portion of surfactant ions has an important role in promoting the adsorption process because it increases the affinity of these organic ions to the interfacial region. The effect derives from mutual attraction between the hydrophobic tails as well as their tendency to escape from an aqueous environment. That mechanism is precisely the same one which causes the spontaneous formation of micelles in aqueous solution and is known as the hydrophobic effect [78]. In the case of surfactant adsorption, it is responsible for the formation of surface aggregates. However, it is not easy to accurately predict the shape and the size of such molecular associations in the same way that the structure of bulk aggregates can be determined from the geometry of the molecule. This is because the surface imposes different restrictions on the organization of the adsorbed layer.

Such physical factors as heterogeneity [9,79,80] and charging behaviour [21,80,81] of the surface as well as the difference between the affinity of the polar head-group and that of water for the surface [9,50,52] are supposed to mostly affect the surface aggregation. In consequence, there is still some controversy about the nature of local adsorbate aggregates formed on a solid surface at low surface coverages. Three structures are usually proposed: monolayered hemimicelles [11,12,82], bilayered admicelles [5,20,80], or surface micelles [83,84], i.e., small and spherical isolated associations anchored to charged surface sites. It is difficult to predict further evolution of these molecular associations. Even direct spectroscopic studies reported on a given adsorption system are not able to dispel doubts since the proposed interpretations of the spectroscopic data are often contradictory [e.g.,86 and 87]. Moreover, the adequacy of such an experimental method is sometimes questioned because of some uncertainty concerning the location of the probe molecules in the host microstructures and their specific mutual interactions. In consequence, progress in the current understanding of the phenomenon still depends on the harmony between theoretical and experimental studies.

Redispersion of the flocculate and other evidences for the hydrophilic character of the support coated with the adsorbed surfactant in the neighbourhood of the cmc indicate that bilayer coverage represents complete saturation of the surface. Commonly, the term *bilayer* is applied to an adsorbed structure in which the surfactant molecules are oriented perpendicular to the surface and fully extended [5,9,20,37,81,89]. The hydrocarbon tails of both layers form a hydrophobic core between the heads. At both sides counterions accumulate between the ionic head-groups. The result looks like a lamellar micelle. For certain physical regimes, the adsorbed amount is only a fraction of what is expected for a tightly packed bilayer [37,48]; the structure which best fits the experimental data can

be described either as a defective bilayer (patchy bilayers) or as flattened micelles. The bilayer is also shown as an asymmetrical structure due to the different charge screening mechanisms at the inner and the outer sides of the adsorbed layer [21,81].

According to the hemimicellar reverse orientation model [34,85], as the adsorption progresses some of the oncoming molecules can interpenetrate into the hemimicellar aggregates leaving the head-groups in the bulk solution. At high adsorption densities, the ultimate structure is comparable to bilayers. The model supports spectroscopic studies in which a marked variation of properties within the hemimicellar microstructure have been observed [39–41].

Strong normal molecule–surface bonds, in conjunction with cooperative effects, are believed to cause two-dimensional condensation of the adsorbate on a patchwise-like solid surfaces [9,87,89,90]. The size of the two-dimensional aggregates is controlled by surface heterogeneity. The completion or partial completion of the monolayer should be followed by a stepwise formation of a second layer on the hydrophobic patches [9,87]. An alternate explanation is based on the conclusion that no significant structural rearrangements occur with increase in surface coverage [38]. This finding is consistent with the admicelle hypothesis [5,80]. The theory proposes that only bilayered admicelles form locally on the surface due to surface heterogeneity. The coverage of the more highly charged regions by admicelles, combined with adsorption of individual monomers, is followed by a slower filling of sites with lower charge densities.

The role of the surface heterogeneity in the ionic surfactant adsorption on charged surfaces is contested by the self-consistent field lattice theory for adsorption and association (SCFA), applied to the theoretical description of the phenomenon [21,81]. It predicts 'two- step' isotherm for adsorption on a surface with a constant charge at low salt concentrations. The first step corresponds to the compensation of the surface charge by surfactant ions adsorbed with their head-groups in contact with the surface owing to electrostatic forces. After the neutralization, the surface–adsorbate interaction quickly becomes repulsive and a great increase in the bulk phase potential is required to complete an asymmetrical bilayer. On variable-charge surfaces, the surface charge can adjust itself upon adsorption and its neutralization does not yield a pseudoplateau on the adsorption isotherm. Above the isoelectrical point, the primary hemimicellar aggregates thus grow in a direction not only perpendicular to the surface but also parallel to it.

3.1. Role of pH in adsorption

Changes in the pH of the aqueous phase usually cause marked changes in the adsorption of ionic surfactants onto charged solid substrates. According to the site-dissociation-site-binding model [57,91], the surface contains surface hydroxyl groups M–OH which can take up or release a proton:

$$M-OH_2^+ \rightleftharpoons M-OH + H^+ , \qquad K_{a1}^{int} = \frac{[M-OH]\cdot[H^+]^s}{[M-OH_2^+]} \tag{14a}$$

$$M-OH \rightleftharpoons M-O^- + H^+ , \qquad K_{a2}^{int} = \frac{[M-O^-]\cdot[H^+]^s}{[M-OH]} \tag{14b}$$

where K_{1a}^{int} and K_{2a}^{int} are the intrinsic dissociation constants; M–OH, M–O^- and M–OH_2^+ denote surface amphoteric groups in differing states of protonation. The protons invo-

lved in these reactions are assumed to lie in the *surface plane* (location of the potential determining ions) so that the surface activity of H^+, i.e., $[H^+]^s$, is estimated from the Boltzmann equation

$$[H^+]^s = [H^+]^b \cdot \exp(-e\Psi_o/kT) \tag{15}$$

where Ψ_o is the electric potential of mean force experienced in the surface plane and the superscript 'b' refers to bulk concentration. In the absence of background electrolyte, the surface charge density, σ_o, is determined by the above equilibria and thus depends on the pH of solution. Only the surfactant is responsible for the screening of the surface charge. A possible mechanism for this process is an ion pairing reaction between specifically adsorbed surfactant ions with their head-groups adhered to the surface and oppositely charged groups resulting from the appropriate dissociation of the surface amphoteric groups:

$$M - OH_2^+ + A^- \rightleftharpoons M - OH_2^+ - A^- , \qquad K_A^{int} = \frac{[M - OH_2^+ - A^-]}{[M - OH_2^+] \cdot [A^-]^i} \tag{16a}$$

$$M - O^- + C^+ \rightleftharpoons M - O^- - C^+ , \qquad K_C^{int} = \frac{[M - O^- - C^+]}{[M - O^-] \cdot [C^+]^i} \tag{16b}$$

where A^- and C^+ are the adsorbed surfactant anion and cation, respectively. The surfactant counterions reside in the *Stern layer* where the potential of mean force is Ψ_i and

$$[X]^i = [X]^b \cdot \exp(-e\Psi_i/kT) \tag{17}$$

where $X=C^+$ or $X=A^-$. As the pH of the aqueous phase is lowered, a solid surface will become more positive, or less negative, because of adsorption onto charged sites of protons from the solution, with consequent increase in the adsorption of anionic surfactants and decrease in the adsorption of cationics. Since the electrostatically adsorbed ions act as nucleation centers for surface aggregates formed through chain-chain association, a lower charge density will results in a smaller effectiveness of adsorption.

Change in the pH also may convert surfactant from one containing an ionic group capable of strong adsorption onto oppositely charged sites on the adsorbent to a neutral molecule susceptible of adsorption only through hydrogen bonding or dispersion forces. Among anionics, carboxylic acid salts are more sensitive to low pH than salts of organic phosphoric acids, and these in turn are more sensitive than organic sulfates or sulfonates [92]. Nonquaternary ammonium cationics are generally sensitive to high pH [92].

The above effects are well illustrated in Fig.2 for two adsorption systems: cationic surfactant/negatively charged silica (Fig.2a) and anionic surfactant/positively charged alumina (Fig.2b). At free pH, which corresponds to pH 8.5 before adsorption, the negative charge of silica reaches a high surface density, whereas this density is much lower slightly above the pzc, i.e., at pH 4.1. Limiting areas occupied at saturation per one adsorbed molecule of about 0.41 nm^2 (free pH) and 1.28 nm^2 (pH 4.1) can be obtained. The comparison with α_o (at the water-air interface) does not argue in favour of a complete bilayer being formed on the silica surface. However, the reversibility of flocculation in both cases suggests the formation of adsorbate structures with a bilayer character at the plateau. Hence there is a certain fraction of a solid surface which is not covered by tightly

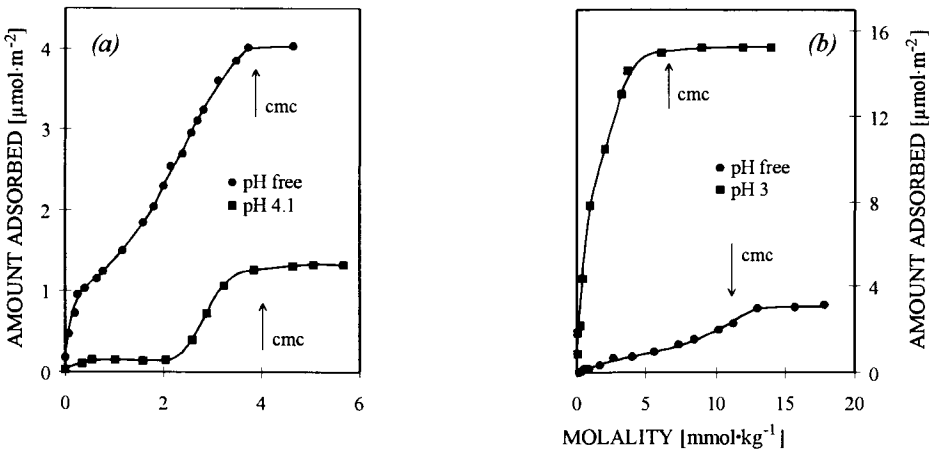

Figure 2. Adsorption isotherms of TTAB onto precipitated silica (panel a) and those of SOBS onto alumina (panel b) at 298 K and different pH values.

packed molecular associations. Whether they resemble flattened micelles or patches of bilayers has yet to be established.

The same qualitative conclusions can be drawn from the analysis of curves in Fig.2b. At free pH (pH 6.5 before adsorption), alumina sample represents a moderately-charged hydrophilic substrate because the pH value is close to the pzc. The maximum quantity of adsorption corresponds to the area of 0.52 nm^2 per one adsorbed molecule (cf. 0.35 nm^2 at the water–air interface). For pH 3 surfactant ions achieve a close-packed arrangement in the adsorbed bilayer and the density of bilayer adsorption at the plateau (0.11 nm^2/molecule) is even less than the air–water interfacial density. At the same time, the cmc is markedly diminished by a decrease in the pH. Both effects can be attributed to the appearance of a non-ionized surfactant species in a solution. The neutral form of the surfactant is less soluble in water and thus exhibits a greater affinity for a hydrophobic surface of alumina modified with grafted aliphatic chains. The decresed repulsion between uncharged heads causes a closer packing of the adsorbate in a mixed surface structure.

The mechanism of surface charge generation is locally influenced by the adsorbate–surface interaction and both surface potential, Ψ_o, and surface charge, σ_o, will vary upon adsorption. When the pH of the bulk phase is not maintained unchanged, partial neutralization of surface charge, according to Eqs.(16), shifts the equilibria (14) towards formation of additional charged sites in order to counteract the diminution in the surface potential. A rise in surface charge is accompanied by the uptake or release of protons and consequent increase or decrease in the pH of the aqueous phase. If all the ionizable surface sites are already dissociated at a given initial pH, the surface charge remains constant upon adsorption of counterions. The case of a fixed pH corresponds to a constant surface potential. Other systems fulfil the condition of charge regulation which must always lie between the limits of constant charge and potential.

In the experiments a marked change in the pH of the supernatant after adsorption was observed in all those cases where the pH was not readjusted to its initial value (free

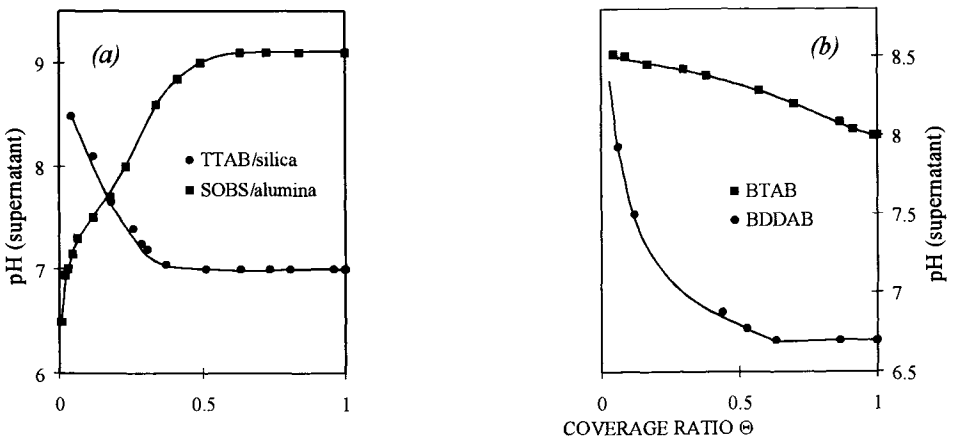

Figure 3. Variation of pH of the supernatant as a function of adsorption (pH not adjusted): (a) systems presented in Fig.2; (b) adsorption of cationic surfactant, BDDAB, and its polar head, BTAB, onto precipitated silica at 298 K.

pH). Two adsorption systems from Fig.2 are presented as examples in Fig.3a. It can be noted that the proton uptake (anionics) or release (cationics) ultimately level off in the neighbourhood of Θ=0.5. If one agrees that the surface charge is only slightly influenced by the adsorption of surfactant ions in a second layer, i.e., oriented perpendicular to the surface and fully extended, transition to a region of a constant pH will mark the end of the 'head-on' adsorption. This means that organic ions previously adsorbed through tail–tail attraction with the ionic heads oriented toward the surface also affect the mechanism of surface charge generation (e.g., by inducing an additional ionization of the neighbouring M–OH groups).

Fig.3b shows that a drop in pH due to adsorption is much greater for the surfactant than for its polar head, indicating a greater ability of the former to compensate surface charge.

A pronounced influence of the pH on the adsorption of ionic surfactants requires special attention to be paid when carrying out the experiments. For example, if the experimental results obtained in different measurements are to be compared or correlate with one another, the same solid–to–solution mass ratio has to be maintained.

3.2. Individual adsorption of ionic surfactants

The competitive character of adsorption of ionic surfactants onto charged supports from aqueous solutions is often neglected in the model considerations. It is not surprising if one takes into account that the hitherto efforts rarely go beyond the fitting of the experimental adsorption isotherms to theoretical equations. Effects arising from the displacement process can significantly modify the energetics of the surfactant adsorption. The problem, which has been already quantified in paragraph 2.5., is now discussed following the example of one cationic surfactant (BDDAB) and its polar head (BTAB) adsorbed onto precipitated silica powder [50,51]. The results of adsorption, electrophoretic and calorimetric measurements are presented in Figs. 3b, 4 and 5.

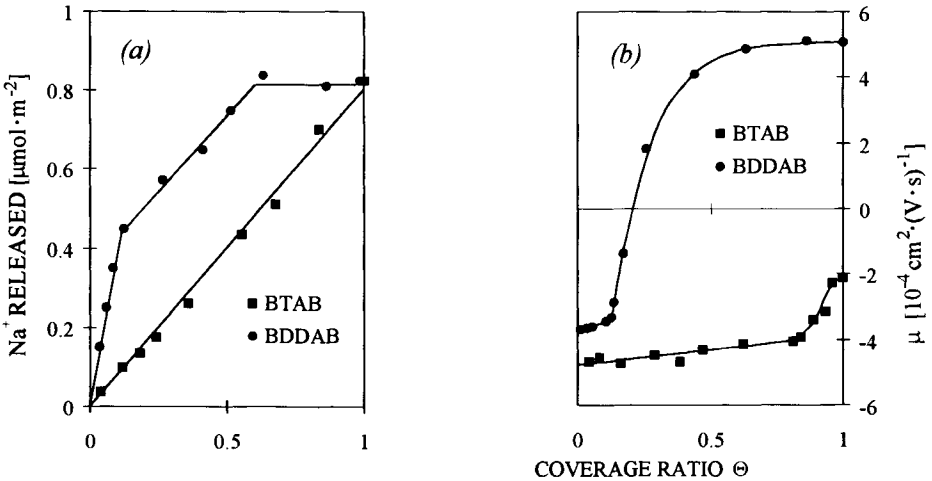

Figure 4. Adsorption of cationic surfactant, BDDAB, and its polar head, BTAB, onto precipitated silica at 298 K: (a) cation exchange between solute ions and sodium counterions upon adsorption; (b) electrophoretic mobility of silica particles against amount adsorbed.

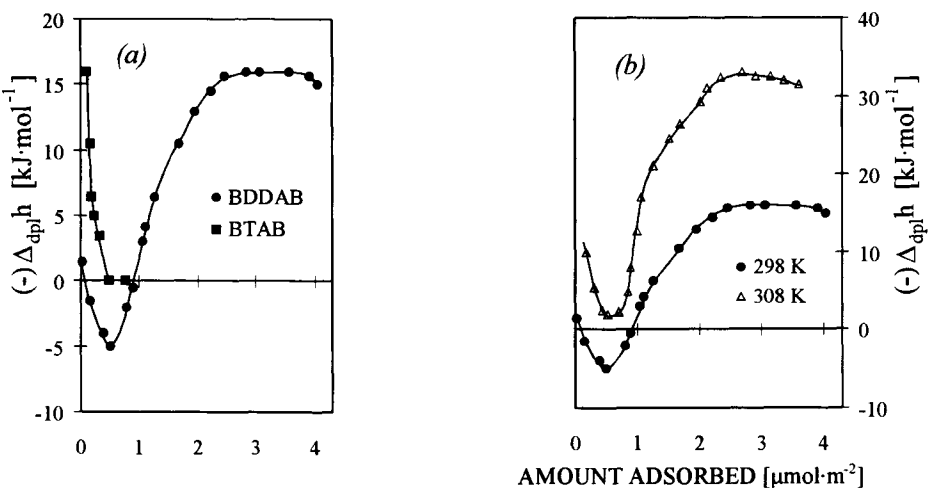

Fig.5. Differential molar enthalpies of displacement onto precipitated silica: (a) cationic surfactant and its polar head at 298 K; (b) cationic surfactant, BDDAB, at 298 and 308 K.

Silica powders are usually precipitated from sodium silicate solutions and exhibit a relatively great bulk concentration of sodium. The surface of silica was shown to trap sodium atoms. Even if the surface is etched off with HF, sodium comes from the interior after some time at room temperature [55]. Certain sodium atoms may be released to the water surrounding the negatively charged silica particles where they constitute counter cations located in either diffuse or Stern layer. As a result, there are some exchangeable sites at the silica–water interface onto which $BDDA^+$ or BTA^+ ions can adsorb via the following cation exchange mechanism:

$$Si - O^- - Na^+ + C^+ \rightleftharpoons Si - O^- - C^+ + Na^+ \qquad (18)$$

where C^+ represents either $BDDA^+$ or BTA^+. The monovalent–monovalent cation exchange does not greatly change the total surface charge, so that the electrophoretic mobility of silica particles should remain constant.

Figures 3b, 4 and 5a show that this is the only mechanism by which BTA^+ ions are adsorbed on the silica surface. The slope of the cation–exchange curve is almost equal to unity (Fig.4a) since the effectiveness of adsorption reaches about 0.8 $\mu mol \cdot m^{-2}$. Contrary to the surfactant, the polar head is not able to reverse the surface charge from negative to positive (Fig.4b). The electrophoretic mobility scarcely depends on the amount adsorbed, except for the terminal part of the adsorption interval where its negative value decreases a little. As the pH curve shows the same tendency (Fig.3b), the final rise in the neutralization efficiency of the polar head can be ascribed to effect of the double layer compression induced by the increasing ionic strength in the bulk phase.

The decreasing exothermicity of the displacement process (Fig.5a) may be related to the direct solid–adsorbate interaction and is consistent with the picture of the more active sites being covered first, i.e., the effect of surface heterogeneity [9,79,93]. The surface of silica is energetically heterogeneous and any microscopic surface area possesses a certain unsaturation, which can be satisfied by bonding with adjacent molecules or ions. The degree of unsaturation fluctuates from point to point on a surface and will result in the various strengths of proton binding to the surface hydroxyl groups. A varying affinity of protons to the surface sites represents the primary source of surface heterogenity at the oxide–water interface as being responsible for a dispersion of the K_{1a}^{int} and K_{2a}^{int} values (see Eqs.14).

The shape of each experimental curve for BDDAB reflects three different modes of adsorption. In the first adsorption region, the domain of which extends up to about 0.5 $\mu mol \cdot m^{-2}$, the surfactant adsorbs mainly by ion exchange: more than 90% of the adsorbing $BDDA^+$ enter the Stern layer by replacing Na^+ counterions; the remainder is retained directly on the negatively charged surface sites. The electrophoretic mobility of silica particles increases very slowly (Fig.4b) but it is accompanied by a pronounced decrease in the pH of the supernatant (Fig.3b). Comparison with the polar head, BTAB, indicates that the presence of an alkyl chain in the molecular structure amplifies the affinity of surfactant ions for the substrate and enables their closer approach to the surface. On this account, the compensation of the original surface charge is more efficient.

An endothermic region with a maximum at 0.5 $\mu mol \cdot m^{-2}$ can be distinguished in the enthalpic curve for BDDAB (Fig.5a). The fact that the process of displacement is driven

entropically provides an argument for a quasi-parallel orientation of the hydrophobic surfactant tail to the solid surface. Crystalline solid surfaces with an orderly arrangement of the surface atoms have been found to exert an icelike structuring of adsorbed water molecules which, through hydrogen bonding, can extend for some distance into the bulk phase [94,95]. Although there is no convincing evidence that such ordered structuring of water can be induced by the surface of amorphous silica, coulombic terms in the mineral–water interaction potential enhance a long-range effect on the arrangement and motion of the adjacent water molecules. In the presence of small or moderate concentrations of cations adsorbed specifically at silica–water interface, the additional structuring of water occurs due to the binding of free water molecules by cations [96]. Relatively small ions, such as Na^+, have net structure-making effect on water structure. Immersion experiments on the silica studied support the above conclusions: the enthalpy of immersion of an outgassed silica sample in pure deionized water was assessed at 1332 $mJ \cdot m^{-2}$ and significantly exceeded the values usually measured for this type of solid supports. Conceivably, some water molecules might be so strongly held that dewetting of a mineral surface, accomplished by alkyl chains of the adsorbing surfactant, will require much energy; the process will be accompanied by an increase in the entropy of the system [50,52].

This hypothesis may be verified by analyzing the effect of temperature on the enthalpy of displacement as shown in Fig.5b. The general shape of the enthalpic curve and the position of maximum remain unchanged. This falls in line with the temperature independence of the ion exchange mechanism. At higher temperatures water loses most of its peculiar structural properties and the strength of solid–molecule interaction decreases. The difference between the energetic state of interfacial water and that of bulk water diminishes and so does the endothermic contribution to the total enthalpy of displacement.

At the end of the first adsorption interval (0.5 $\mu mol \cdot m^{-2}$), the average surface area occupied by one adsorbed surfactant ion is equal to 3.3 nm^2. Taking into account the amorphous form of silica, the adsorbed ions can be seen as uniformly distributed over the surface; the lateral interactions between them are negligible in this region.

To sum up, in the first stage of the adsorption process, surfactants adsorb as individual ions with the ionic group directly opposite charged sites on the surface. They displace interfacial water molecules and may exchange with some other ions, which are present at the solid–water interface as pre-adsorbed counterions. On account of the energetic heterogeneity of surface sites, the differential enthalpy of displacement decreases with increasing amount of adsorption. Dewetting of a solid surface gives a positive contribution to the total enthalpy change upon adsorption of the surfactant.

3.3. Cooperative adsorption of ionic surfactants

Individual adsorption of surfactant ions occurs at low surface coverages. As the adsorption density increases, they begin to associate through lateral interaction of their hydrocarbon chains. The oncoming ions adsorb onto or adjacent to the previously adsorbed ones and this leads to adsorbate structures characterized by a higher cohesive force. Since in the intermediate adsorption region, between the individual adsorption and the bilayer formation, relatively small mineral particles covered with the surfactant link together to form flocs, it is hardly conceivable that the primary aggregates represent local bilayered admicelles.

In the case of the silica/BDDAB system, presented in Figs. 3b, 4 and 5, flocculation

occurs when the adsorption of surfactant ions ranges between 0.5 μmol·m^{-2} (Θ = 0.12) and 2.7 μmol·m^{-2} (Θ = 0.63). In this interval, the displacement of sodium cations from the adsorbed phase still occurs (Fig.4a), but the degree of exchange is much smaller than upon the individual adsorption. The pH of the supernatant monotonously decreases (Fig.3b), indicating a change in surface charge due to direct interactions between the ionic surfactant heads and the surface. Simultaneously, the net charge of silica particles sharply increases (Fig.4b); it changes sign at the amount adsorbed of 0.87 μmol·m^{-2} (Θ = 0.2) and then becomes positive owing to the excess of positive charge in the adsorbed layer. Of course, the locally formed admicelles would also contribute to the electrophoretic mobility, however, not to the extent that might first be imagined. The micelle–like nature of such aggregates, emphasized in the bilayer model [5,80,86], allows a parallel to be drawn between surfactant aggregation in solution and on the solid surface. In the bulk micelles, between 75 and 90 per cent of the micellar charge is balanced by the counterions which are strongly bound to the surface and moderate the repulsive interaction between the ionic heads. The substantial counterion adsorption at the exterior layer of head–groups would largely, but certainly not completely, cancel the contribution of the admicelles to the electrophoretic mobility.

The overall enthalpy change upon surfactant adsorption also undergoes marked modifications (Fig.5a). A continuous increase in the enthalpic value, from +5 kJ·mol^{-1} to -16 kJ·mol^{-1}, being the result of a number of competing effects, can be attributed to a gradual reorientation of the adsorbed surfactant ions toward hemimicellar arrangement consistent with the hydrophobic chains outwardly disposed and associated with one another. Based on the area per molecule a_0, and the nitrogen specific surface area of the silica, the average monolayer capacity for BDDAB can be assessed at 2.3 μmol·m^{-2} (Θ = 0.54). It is quite probable that a second surfactant layer is already starting to form in the intermediate adsorption region and the rearrangement of the adsorbed surfactant ions is continued until the final orientation with the ionic heads in the aqueous phase. The endothermic contribution, due to the local disruption of the structure of the interfacial water molecules and the release of some of them to the bulk phase, diminishes and causes the overall enthalpic effect to be more and more exothermic.

In the third adsorption region, above 2.7 μmol·m^{-2} (Θ=0.63), all the plots unequivocally indicate the completion of bilayer on the silica surface. At surface saturation, the average adsorption density corresponds to 0.38 nm^2 per one adsorbed molecule, which is approximately twice less than the air–water interfacial density.

Therefore, the hemimicelle concept is supported in this paper. All molecules adsorbed in the first individual stage may be considered as nuclei for the subsequent formation of aggregates around them. As long as the surface charge, σ_0, increases upon adsorption (changes in the pH of the supernatant), ionic heads of the adsorbed surfactants are located at the surface side. The primary hemimicellar aggregates grow in a direction parallel to the surface, imparting increasing hydrophobic character to the substrate as adsorption continues. At higher surface coverage ratios they begin to grow into larger structures with a bilayer character.

3.4. Effect of the crystalline structure of solid sample in adsorption

The transition between the monolayer and bilayer formation is rather gradual. Local inhomogeneities of the solid surface will produce wide size distributions of hemimicelles.

They will largely differ in the aggregation numbers. If within certain zones of surface these primary aggregates reach their optimal size, the local formation of a second layer will begin. This evolutionary picture is relevant to amorphous silica.

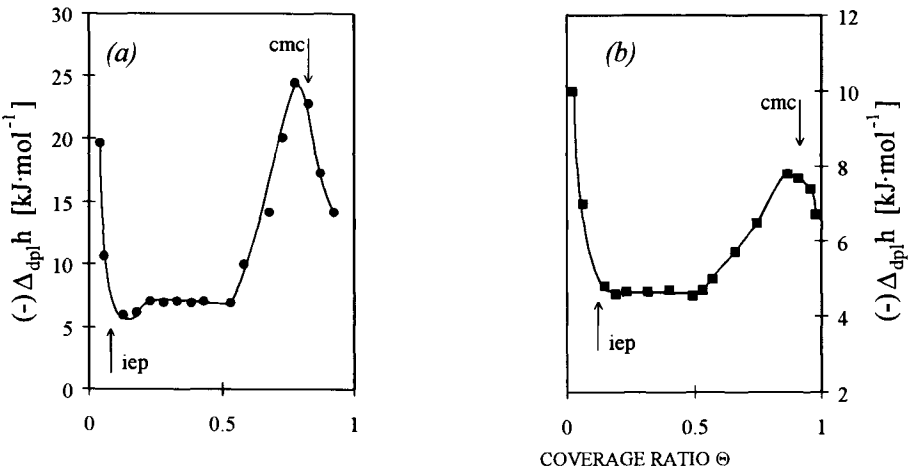

Figure 6. Differential molar enthalpies of displacement onto crystalline solid surfaces at 298 K: (a) adsorption of BDDAB onto quartz (initial pH 6); (b) adsorption of SHBS onto zirconia (initial pH 3.8).

In the case of solid supports having crystalline structures, like quartz, zirconium dioxide and α-alumina, the shape of the enthalpic curve is quite different and exhibits a distinct exothermic peak in the vicinity of the cmc (e.g., Figs. 6a and 6b). At first sight, the phenomenon seems strange, especially if all other curves are similar to those for the amorphous silica (see for example Figs. 2b, 3a and 7). An explanation based on the specific model of surface topography is advanced in this paragraph.

Powdered sample of a crystalline solid is a collection of a large number of minute crystals packed together at random orientations. Its surface consists of a considerable proportion of edges and corners, in addition to more or less plane and unisorptic patches, which can be identified with different faces of the crystallites. Consequently, the model of a patchwise-like topography [79,93] may be proposed to describe the surface heterogeneity. The patchwise-like topography of surface will result in a non-uniform distribution of surface charge.

The beginning of flocculation in the vicinity of the iep and redispersion of the flocs below but not far from the cmc confirm a bilayer character of the adsorbed structures at saturation. Comparing the overall limiting areas per one adsorbed molecule of 0.44 nm^2 (BDDAB/quartz) and of 0.39 nm^2 (SHBS/zirconia) with those at the air-water interface, the surface only partly covered with bilayer can be envisaged. In the case of quartz the bilayer coverage is much greater because this solid is farther from its pzc (initial pH 6) than the other (initial pH 3.8).

In the first region the enthalpy of displacement is exothermic and continuously decreases with increasing adsorption of the surfactant. This tendency may be interpreted in terms of surface heterogeneity interfering in the individual adsorption of surfactant ions,

which occurs through either an ion exchange or an ion pairing mechanism. The various homogeneous surface patches are filled in the sequence of the decreasing difference between adsorption energies of all the participants in the displacement process. Since local charge densities on the patches are greater than the overall surface charge density, σ_0 the lateral attraction between hydrophobic tails prevents them from adopting the orientation parallel to the surface. This explains why there is no a strong endothermic contribution to the total enthalpic change.

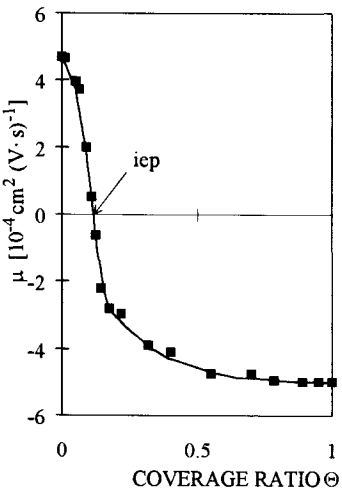

Fig.7. Electrophoretic mobility of zirconia particles at 298 K against adsorption of SHBS.

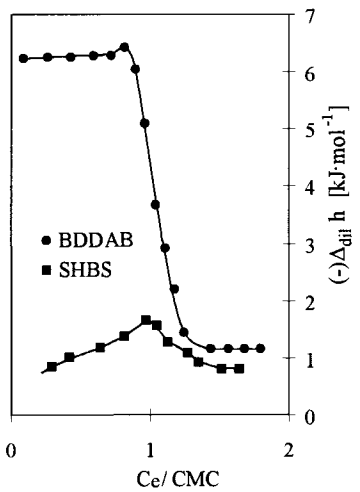

Fig.8. Differential molar enthalpy of dilution of a micellar stock solution as a function of the relative bulk molality at 298 K.

In the second region the enthalpy of displacement is a constant function of the surface coverage ratio. The driving force of adsorption chiefly derives from the hydrophobic attraction between non-polar surfactant groups. Since the surface together with the adsorbed layer is hydrophobic (flocculation of mineral particles), the adsorbate structures formed in this region represent hemimicelles. Variations of the ζ-potential (Fig.7) and those of the surface charge (Fig.3a) support the adsorption of the surfactants with their head-groups in contact with the surface. Adsorption can be regarded as the growth of the existing two-dimensional aggregates in size, increasing their aggregation numbers.

Fig.8 shows the enthalpic curves of dilution of a micellar (C_2 > cmc) stock solution in the bulk phase. One can note, between two plateaus, a transition region corresponding to the formation of micelles. The region is more extended for SHBS and the enthalpy of micelle formation is less exothermic (see Table 2). It may be that this surfactant forms smaller polydisperse micelles, of which the size, number and relative proportions are modified by the changing molality in the neighbourhood of the cmc. A steep decrease in the enthalpy of displacement in the third region (Figs. 6a and 6b) resembles this part of the bulk enthalpic curve. Thus, the hypothesis of the formation of large three-dimensional-like micelles, flattened out on the surface, may be put forward [28]. Although the process is

energetically favoured to a larger extent on the surface than in the bulk phase, all the general tendencies are preserved. The amount of adsorbed ions with the polar portion outwardly disposed increases rapidly and the surface behaves as if it were hydrophilic. In the vicinity of the cmc, the micellization starts in the bulk phase and the bulk micelles compete with those on the surface in consumption of monomers. The enthalpic effect of adsorption vanishes above the cmc as a result of a decreasing enthalpic difference between both equilibrium phases.

3.5. Influence of other physical factors on adsorption

There are several physical factors affecting the energetics of adsorption of ionic surfactants onto adsorbents with oppositely charged sites as well as its effectiveness, i.e., the amount adsorbed at surface saturation. The role of several important parameters, like the overall charge density, pH and temperature of the aqueous phase and the spatial distribution of surface charge (i.e., topography), has been discussed in the previous paragraphs.

The effectiveness of adsorption is strictly related to the orientation of the adsorbate at a given interface. For ionic surfactants the maximum packing at surface saturation is a result of the balance between two opposing tendencies: attraction between hydrophobic moieties and repulsion between their ionic heads. If adsorption is perpendicular to the solid surface in a close-packed arrangement, the maximum quantity of adsorption is determined by the effective size of the head-group and does not change with increase in the alkyl chain length. If the arrangement is perpendicular but not close-packed, or if it is not predominantly perpendicular, there may be some increase in the effectiveness of adsorption, resulting from greater van der Waals attraction between longer chains.

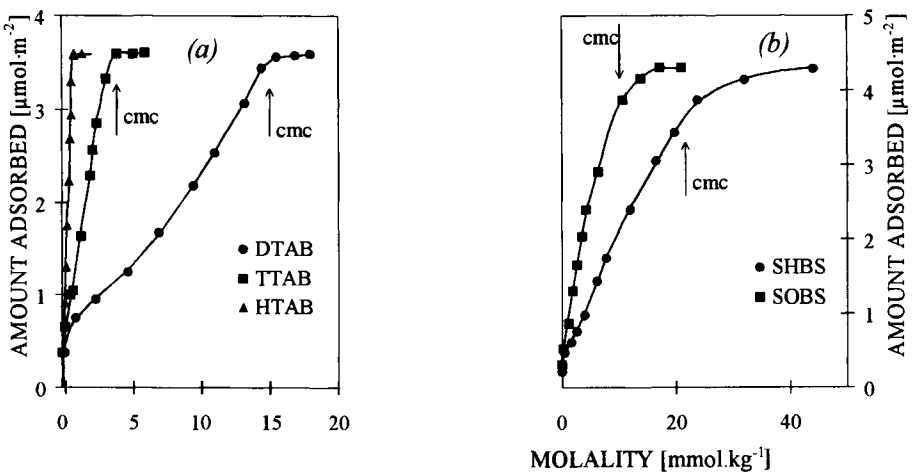

Figure 9. Adsorption isotherms of alkyltrimethylammonium bromides onto precipitated silica at 308 K (panel a) and those of sodium benzenesulfonates onto zirconia at 298 K (panel b).

Experimental results for two homologous series of cationic and anionic surfactants adsorbed onto amorphous and crystalline solids show no significant influence of the chain

length on the effectiveness of adsorption (Fig.9). Since in both cases the amount adsorbed at saturation is not great enough to cover the whole surface with a complete bilayer, the existence of tightly packed bilayer structures (patchy bilayers, flattened micelles) is confirmed once more. Differences between the isotherms within each homologous series can be ascribed to different solubilities of surfactants in water: the cmc is approximately halved by the addition of one methylene group to a straight-chain hydrophobic moiety.

In the case of precipitated silica, great endothermic contribution due to the displacement of interfacial water by the hydrophobic tails of surfactants may obscure the evaluation of the effect of the chain length on the enthalpy of displacement. As raising the temperature reduced this contribution to a great extent (see Fig.5b), the appropriate calorimetric experiments were carried out at 308 K. The results are presented in Fig.10.

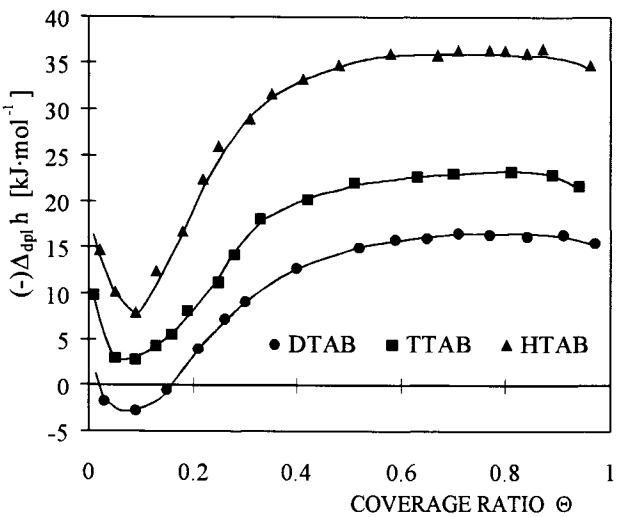

Figure 10. Differential molar enthalpies of displacement as a function of adsorption of alkyltrimethylammonium bromides onto precipitated silica at 308 K.

The enthalpy change, gained on the transfer of the monomers from the bulk solution to the interface silica–water, increases with expanding alkyl chain. This tendency at higher coverage ratios is in accordance with a rise in the enthalpy of micellization (see Table 2). In the range of individual surfactant adsorption, the differences in the enthalpy of displacement make evident a direct interaction between the surfactant tails and the surface. The energy of such hydrophobic bonding will be proportional to the number of methylene groups in the adsorbate.

An increase in the ionic strength of the aqueous phase due to addition of electrolyte (0.1M NaBr) causes an increase in the effectiveness of adsorption of DTAB onto precipitated silica (Fig.11a). The micellization in the bulk phase is thermodynamically favoured and the cmc is reduced. The effects are presumably due to the decreased repulsion between the ionic heads of the surfactant and to the salting out of the monomers by electrolyte. Since the effective size of the hydrophilic group is smaller at higher ionic strength, the effectiveness of adsorption becomes greater as a result of closer packing of the surfactant

ions in the bilayer. The initial adsorption diminishes in the presence of salt because the surfactant head-groups have to compete with salt ions for charged surface sites.

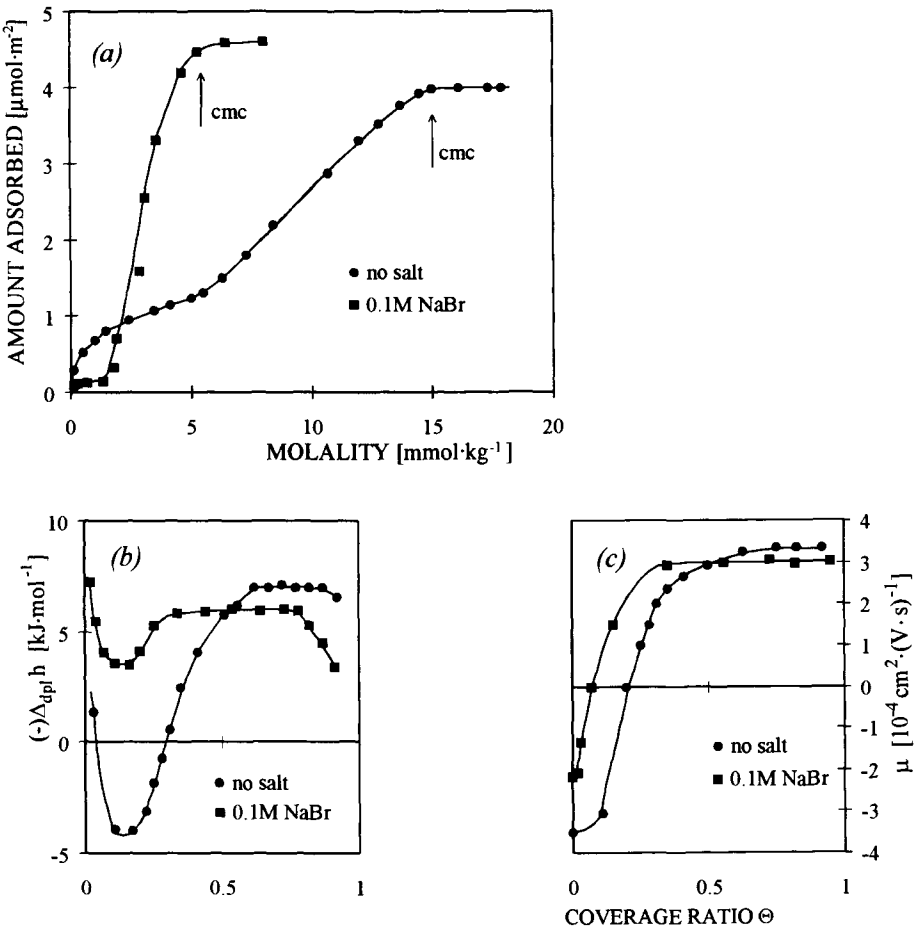

Figure 11. Adsorption of DTAB onto precipitated silica at 298 K and different ionic strengths: (a) isotherms of adsorption; (b) differential molar enthalpies of displacement; (c) electrophoretic mobilities of silica particles.

Fig.11b shows the influence of the ionic strength on the energetics of displacement. The enthalpic difference between the individual and cooperative adsorption is much lower in the case of NaBr solution. On the one hand, the electrostatic attraction between oppositely charged species is reduced by the electrolyte ions. On the other hand, the excess of sodium counterions at the silica-water interface disrupts the particular arrangement of interfacial water molecules [96] and markedly decreases the endothermic contribution owing to displacement of water. It is interesting to note that the plateau on the enthalpic curve is reached at lower coverage ratios when NaBr is added to the aqueous phase. Thus the formation of a second layer starts early. The local admicellar aggregates may even

appear on the surface as has been predicted for high ionic strengths [5,21,81]. That hypothesis explains why the enthalpic differences between both curves in Fig.11b are so large. The results of the electrophoretic measurements in Fig.11c seem to support the formation of local admicelles. The mobility of silica particles remains practically unchanged above Θ=0.35, which is congruent with the horizontal segment on the enthalpic curve.

4. SUMMARY

The adsorption of ionic surfactants onto mineral substrates is a complex phenomenon simultaneously controlled by the nature of the adsorbing species, the properties of the solid surface and the composition of the aqueous solution. As a consequence, there is no complete theoretical model which can describe, both qualitatively and quantitatively, all the experimental information available. Calorimetry of adsorption may be very useful in studying the nature of the interactions in the adsorption system, but alone it is not capable of solving satisfactorily many detailed problems which still remain to be explained. Hovewer, the evolved model of the phenomenon should be able to contain the experimental results from all the bulk, calorimetric and spectroscopic studies reported on the system.

Adsorption of the surfactant occurs successively by ion exchange, ion pairing, and hydrophobic bonding mechanisms. The latter leads to the formation of various adsorbate associations on the surface. At surface saturation, many experimental arguments support the existence of large and compact structures with a bilayer character (patchy bilayers, flattened micelles). When the overall and local densities of adsorption are sufficiently high, the fusion of these aggregates yields a compact bilayer covering the whole surface of the solid substrate. The transient surface aggregates represent monolayered hemimicelles. The orientation of the adsorbed surfactant ions with their ionic heads close to the surface, even beyond the iep concentration found in the electrophoretic measurement, is possible on account of the surface charge regulation. The surface charge, σ_0 adjusts upon surfactant adsorption and changes in the pH of the supernatant are monitored along the isotherm. On solid surfaces with patchwise-like topography (crystalline solids) the transition between the monolayer and bilayer formation is quite steep and it resembles, from the enthalpic point of view, the process of micellization in the bulk solution. On amorphous silica the primary aggregates grow in a direction both perpendicular and parallel to the surface and this transition is more gradual. At high ionic strengths, the presence of admicelles cannot be excluded.

Adsorption of ionic surfactants causes marked changes in the interfacial properties of mineral surfaces. During this process the tendency of the surface to repeal other similarly charged surfaces diminishes and ceases when the charge on the adsorbent has been neutralized. Dewetting of a mineral surface accompanies the displacement of adsorbed water molecules by surfactants, of which ionic head interacts with the surface more strongly than with water. In the case of random distribution of surface charge (amorphous silica), where the distances between the individually adsorbed surfactant ions are great, the desorption of the structured interfacial water due to the specific adsorption of a part of the hydrophobic moiety of the surfactant gives rise to the endothermic enthalpy of the process. The coverage of the surface with surfactants exposing their alkyl chains to the bulk solution results in a highly hydrophobic surface. Finely divided particles, dispersed

in the aqueous phase partly because of their mutual electrical repulsion, flocculate at some point. The flocculation is a reversible process when adsorption of surfactant ions with the head-groups oriented toward the aqueous phase renders the surface hydrophilic again.

REFERENCES

1. W.G.Cutler and R.C.Davis (eds.), Detergency: Theory and Test Methods, Marcel Dekker, New York, 1972.
2. J.Leja, Surface Chemistry of Froth Flotation, Plenum Press, New York, 1982.
3. D.B.Hough and H.M.Rendall, in: Adsorption from Solution at the Solid–Liquid Interface, G.D.Parfitt and C.H.Rochester (eds.), Chapter VI, Academic Press, London, 1983.
4. P.Somasundaran and P.Chandar, in: Solid–Liquid Interactions in Porous Media, J.M.Cases (ed.), p. 411, Technip Publisher, Paris, 1985.
5. J.H.Harwell, R.Schechter and W.H.Wade, in: Solid–Liquid Interactions in Porous Media, J.M.Cases (ed.), p. 371, Technip Publisher, Paris, 1985.
6. L.W.Lake, Enhanced Oil Recovery, Prentice Hall, New Jersey, 1989.
7. B.T.Ingram and R.H.Ottewill, in: Cationic Surfactants, D.N.Rubingh and P.M.Holland (eds.), Chapter III, Marcel Dekker, New York Basel, 1991.
8. D.W.Fuerstenau and R.Herrera–Urbina, in: Cationic Surfactants, D.N.Rubingh and P.M.Holland (eds.), Chapter VIII, Marcel Dekker, New York Basel, 1991.
9. J.M.Cases and F.Villieras, Langmuir, 8 (1992) 1251.
10. L.K.Koopal, in: Coagulation and Flocculation: Theory and Applications, B.Dobias (ed.), Chapter IV, Marcel Dekker, New York, 1992.
11. P.Somasundaran, T.W.Healy and D.W.Fuerstenau, J.Phys.Chem., 68 (1964) 3562.
12. P.Somasundaran and D.W.Fuerstenau, J.Phys.Chem., 70 (1966) 90.
13. H.C.Li and P.L.De Bruyn, Surf.Sci., 5 (1966) 203.
14. B.H.Bijsterbosch, J.Colloid Interface Sci., 47 (1974) 186.
15. M.P.Aronson and H.M.Princen, Colloid & Polymer Sci., 256 (1978) 140.
16. L.Ghosh, K.P.Das and D.K.Chattoraj, J.Surf.Sci.Tech., 2 (1986) 25.
17. W.A.Ducker, R.M.Pashley and B.W.Ninham, J.Colloid Interface Sci., 128 (1989) 66.
18. M.W.Rutland and R.M.Pashley, J.Colloid Interface Sci., 130 (1989) 448.
19. J.L.Menezes, J.Yan and M.M.Sharma, Colloids Surf., 38 (1989) 365.
20. D.Bitting and J.H.Harwell, Langmuir, 3 (1987) 500.
21. M.R.Böhmer and L.K.Koopal, Langmuir, 8 (1992) 2649, 2660.
22. H.J.Busscher, H.M.Uyen, W.J.Postma, A.van Silfhout and J.Arends, Colloid & Polymer Sci., 265 (1987) 711.
23. P.Herder, P.Claesson and Ch.Herder, J.Colloid Interface Sci., 119 (1987) 155.
24. Y.L.Chen, S.Chen, C.Frank and J.Israelachvili, J.Colloid Interface Sci., 153 (1992) 244.
25. J.Rouquerol and S.Partyka, J.Chem.Tech.Biotechnol., 31 (1981) 584.
26. F.Thomas, J.Y.Bottero, S.Partyka and D.Cot, Thermochimica Acta, 122 (1987) 197.
27. G.W.Woodbury,Jr. and L.A.Noll, Colloids Surf., 33 (1988) 301.
28. S.Partyka, W.Rudzinski, B.Brun and J.H.Clint, Langmuir, 5 (1989) 297.

29. R.Denoyel, F.Rouquerol and J.Rouquerol, Colloids Surf., 37 (1989) 295.
30. S.Partyka, M.Lindheimer and B.Faucompre, Colloids Surf., 76 (1993) 267.
31. L.Ghosh, K.P.Das and D.K.Chattoraj, J.Indian Chem.Soc., 63 (1986) 144.
32. J.N.Israelachvili and G.E.Adams, J.Chem.Soc., Faraday Trans.I, 74 (1978) 975.
33. R.M.Pashley and J.N.Israelachvili, Colloids Surf., 2 (1981) 169.
34. P.M.McGuiggan and R.M.Pashley, J.Colloid Interface Sci., 124 (1988) 560.
35. P.Kékicheff, H.K.Christenson and B.W.Ninham, Colloids Surf., 40 (1989) 31.
36. J.L.Parker, V.Yaminsky and P.M.Claesson, J.Phys.Chem., 97 (1993) 7706.
37. M.W.Rutland and J.L.Parker, Langmuir, 10 (1994) 1110.
38. P.Chandar, P.Somasundaran and N.J.Turro, J.Colloid Interface Sci., 117 (1987) 31.
39. K.C.Waterman, N.J.Turro, P.Chandar and P.Somasundaran, J.Phys.Chem., 90 (1986) 6828.
40. P.Chandar, P.Somasundaran, K.C.Waterman and N.J.Turro, J.Phys.Chem., 91 (1987) 148.
41. P.Somasundaran, J.T.Kunjappu, C.V.Kumar, N.J.Turro and J.K.Barton, Langmuir, 5 (1989) 215.
42. K.Esumi, T.Nagahama and K.Meguro, Colloids Surf., 57 (1991) 149.
43. K.Esumi, A.Sugimura, T.Yamada and K.Meguro, Colloids Surf., 62 (1992) 249.
44. E.Söderlind and P.Stilbs, J.Colloid Interface Sci., 143 (1991) 586.
45. E.Söderlind and F.D.Blum, J.Colloid Interface Sci., 157 (1993) 172.
46. E.Söderlind and P.Stilbs, Langmuir, 9 (1993) 2024.
47. K.Wong, B.Cabane, R.Duplessix and P.Somasundaran, Langmuir, 5 (1989) 1346.
48. A.R.Rennie, E.M.Lee, E.A.Simister and R.K.Thomas, Langmuir, 6 (1990) 1031.
49. M.Bouzerda, Ph.D.Thesis, University of Montpellier, Montpellier, 1991.
50. J.L.Trompette, J.Zajac, E.Keh and S.Partyka, Langmuir, 10 (1994) 812.
51. J.L.Trompette, Ph.D.Thesis, University of Montpellier, Montpellier, 1995.
52. J.Zajac, J.L.Trompette and S.Partyka, J.Thermal Anal., 41 (1994) 1277.
53. A.Berrada, Ph.D.Thesis, University of Montpellier, Montpellier 1992.
54. N.Grine, Ph.D.Thesis, University of Montpellier, Montpellier, 1990.
55. R.K.Iler, The Chemistry of Silica, Wiley, New York, 1979.
56. J.Rouvière, B.Faucompré, M.Lindheimer, S.Partyka and B.Brun, J.Chim.Phys., 80 (1983) 309.
57. R.J.Hunter, Foundations of Colloid Science, vol.I, Clarendon Press, Oxford, 1991.
58. D.W.Fuerstenau, J.Phys.Chem., 60 (1956) 981.
59. H.S.Hanna and F.Z.Saleeb, Colloids Surf., 1 (1980) 295.
60. D.H.Everett, Pure & Appl.Chem., 58 (1986) 967.
61. A.de Keizer, M.R.Böhmer, T.Mehrian and L.K.Koopal, Colloids Surf., 51 (1990) 339.
62. F.Z.Saleeb and P.L.de Bruyn, J.Electroanal.Chem., 37 (1972) 99.
63. R.H.Ottewill and J.N.Shaw, J.Electroanal.Chem., 37 (1972) 133.
64. R.W.O'Brien and L.R.White, J.Chem.Soc., Faraday Trans.II, 74 (1978) 1607.
65. A.J.Groszek (ed.), Proceedings of the BP Symposium on the Significance of the Heats of Adsorption at the Solid–Liquid Interface, BP Research Centre, Sunbury–on–Thames, 1971.
66. P.C.Gravelle, Catal.Rev.Sci.Eng., 16 (1977) 37.
67. R.Denoyel, F.Rouquerol and J.Rouquerol, J.Colloid Interface Sci., 136 (1990) 375.
68. S.Partyka, S.Zaini, M.Lindheimer and B.Brun, Colloids Surf., 12 (1984) 255.

69. S.Partyka, M.Lindheimer, S.Zaini, E.Keh and B.Brun, Langmuir, 2 (1986) 101.
70. R.Denoyel, Ph.D.Thesis, University of Provence, Marseille, 1987.
71. S.Partyka, M.Lindheimer, E.Keh and B.Brun, in: Surfactants in Solution, vol.IX, p.405, K.L.Mittal (ed.), Plenum Publish. Corporation, 1989.
72. M.Lindheimer, E.Keh, S.Zaini and S.Partyka, J.Colloid Interface Sci., 138 (1990) 83.
73. G.H.Findenegg, B.Pasucha and H.Strunk, Colloids Surf., 37 (1989) 223.
74. S.Partyka, E.Keh, M.Lindheimer and A.J.Groszek, Colloids Surf., 37 (1989) 309.
75. J.P.Law,Jr. and G.W.Kunze, Soil Sci.Soc.Am.Proc., 30 (1966) 321.
76. H.Kölbel and P.Kuhn, Angew.Chem., 71 (1959) 211.
77. L.R.Snyder, J.Phys.Chem., 72 (1968) 489.
78. Ch.Tanford, The Hydrophobic Effect: Formation of Micelles and Biological Membranes, Wiley, New York, 1973.
79. L.Lajtar, J.Narkiewicz-Michalek, W.Rudzinski and S.Partyka, Langmuir, 9 (1993) 3174.
80. M.A.Yeskie and J.H.Harwell, J.Phys.Chem., 92 (1988) 2346.
81. M.R.Böhmer and L.K.Koopal, Langmuir, 8 (1992) 1594.
82. A.M.Gaudin and D.W.Fuerstenau, Trans.AIME, 202 (1955) 66, 958.
83. Y.Gao, J.Du and T.Gu, J.Chem.Soc.,Faraday Trans.I, 83 (1987) 2671.
84. H.Rupprecht and T.Gu, Colloid & Polymer Sci., 269 (1991) 506.
85. J.T.Kunjappu and P.Somasundaran, J.Phys.Chem., 93 (1989) 7745.
86. J.H.Harwell and M.A.Yeskie, J.Phys.Chem., 93 (1989) 3372.
87. J.F.Scamehorn, R.S.Schechter and W.H.Wade, J.Colloid Interface Sci., 85 (1982) 463.
88. C.J.Tanford, J.Phys.Chem., 76 (1972) 3020.
89. J.M.Cases and B.Mutaftschiev, Surf.Sci., 9 (1968) 57.
90. J.M.Cases, J.E.Poirier and D.Canet, in: Solid-Liquid Interactions in Porous Media, p. 335, J.M.Cases (ed.), Technip Publisher, Paris, 1985.
91. J.A.Davis, R.O.James and J.O.Leckie, J.Colloid Interface Sci., 63 (1978) 480.
92. M.J.Rosen, Surfactants and Interfacial Phenomena, Wiley, New York, 1978.
93. W.Rudzinski and D.H.Everett, Adsorption of Gases on Heterogeneous Surfaces, Academic Press, London, 1992.
94. W.Drost-Hansen, J.Colloid Interface Sci., 58 (1977) 251.
95. J.L.Kavanau, Water and Solute-Water Interactions, Holden-Day, San Francisco, 1964.
96. H.Kihira and E.Matijevic, Langmuir, 8 (1992) 2855.

A. Dąbrowski and V.A. Tertykh (Editors)
Adsorption on New and Modified Inorganic Sorbents
Studies in Surface Science and Catalysis, Vol. 99

Chapter 3.7
The reaction of anions and cations with metal oxides as models for their reaction with soil

N. J. Barrow

CSIRO, Division of Soils, Private Bag, Wembley, W. A., 6014, Australia

1. INTRODUCTION

One of the reasons why the reactions between ions and metal oxides are studied is because they are thought to be important in controlling the availability of nutrients in soils or in controlling the movement of pollutants into the biosphere.

There are two strands to this argument. One is that many oxides are present in soils. Taylor et al.[1] list six iron oxides, five aluminium oxides and thirteen manganese oxides. (The term "oxide" is used loosely here to include oxyhydroxides). Of the iron oxides, goethite is most commonly found in soils of many climatic regions [2]. The presence of oxides is apparent simply from observing one off the most obvious properties of soils – their colour. Soil colour is partly related to the amounts of organic matter in the soils but also to the amount and particle size of the oxides present. Iron oxides are especially important with goethite giving the yellow-browns and haematite the reds. The names: red earth, terra rossa, terre rosse, and kraznozem, which have been applied to soils in various languages, all show the effectiveness of redness in catching peoples' attention.

The second strand of the argument is that oxides are very good at reacting with a very large range of cations and anions. Dzombak and Morel [3] list over 50 studies of reactions of inorganic cations and anions with hydrous ferric oxides. The cations studied include: Mg, Ba, Ca, Sr, Ag, Cu, Zn, Cd, Co, Ni, Mn, Pb, and Hg; the anions: PO_4, AsO_4, SO_4, SeO_3, SeO_4, VO_4, CrO_4, and $B(OH)_3$. This list makes it clear that such reactions could be very important in controlling the supply of both essential nutrients and of toxic ions to plants.

Of course, reactions between ions and oxides are important in contexts other than soil science. However, many studies have appeared in the soil science literature and these are not always well known by surface scientists. One of the purposes of this article is to bring some of these studies to attention. However the main purpose is to show how studies using simple materials such as samples of individual oxides may be used to understand behaviour of more complex materials such as soils.

2. GOETHITE: A MUCH STUDIED OXIDE

Goethite is designated α–FeO(OH) where the α denotes hexagonal close packing.

2.1. Natural goethite

The goethite which occurs in soils is rather different to the material used in many laboratory experiments. It is far from pure. It may contain manganese and other trace metals [4,5], various anions [5,6], and especially, aluminium [7–11].

Fordham, Merry and Norrish [12] described an unusual fibrous goethite for which the atomic ratios were 4:2:1 for Fe:Al:Si. This corresponds to about five percent Si by mass. Fordham and Norrish [13] found silicon contents of iron oxide pellets from a variety of soils to range between one and four percent. It is of course difficult to be sure that samples are uncontaminated but these values were believed to be free of this problem. If we are to understand the behaviour of soil goethites, we need to know how these silicon atoms are arranged. It seems unlikely that they are scattered at random through the crystal but this is difficult to investigate for the minute particles of soil goethite. Fordham et al. [12] pointed out that the silicon apparently occupied a stable position because it was resistant to extraction with oxalate. They speculated that the silicon was adsorbed on the surface of microcrystals. This suggestion is consistent with the work of Smith and Eggleton [14] who examined four samples of botryoidal goethite which varied in silica content from zero to 1.25%. The samples which contained silica were composed of fine needle–like grains with diameters as small as 30 μm. They suggested that the gaps between the grains could consist of a monolayer of silica. The sample of goethite that did not contain silica did not have this structure. Thus, the silica in soil goethites might exist as a sort of mortar between microcrystals of the oxide.

2.2. The water content of goethite

The water content of goethite is commonly greater than that calculated from the formula FeO(OH). This is true for both synthetic goethites [9,15] and for natural goethites [6,16]. One explanation is that the extra water could be H_2O molecules enclosed in the structure as suggested by Fey and Dixon [9]. In this case, the extra water could be bound in micropores between domain boundaries. Another explanation is that some of the Fe atoms of the structure are missing and the charge is balanced by extra protonation of adjacent oxygen atoms as suggested by Schulze [17]. The formula would then be written: $Fe_{1-x}O_{1-3x}(OH)_{1+3x}$ where x is the proportion of the iron atoms that are missing.

2.3. Laboratory preparation

Because natural oxides are difficult to extract from soil, most studies have used synthetic forms. The two most–commonly used oxides are ferrihydrite and goethite. Both are usually prepared by precipitation from alkaline solutions. Preparation of ferrihydrite involves little more than precipitation from solutions of Fe^{3+} salts, and while it is easily prepared, it can be argued that it is rather different to the material found in most soils which is formed from oxidation of Fe^{2+} ions. Goethite can be prepared in a number of ways but the most–widely used method involves growth of the crystals at 60°C in a highly alkaline solution [18]. However, even when the same procedures are followed, different batches of goethite can vary appreciably. For example, Hingston [19] prepared batches of goethite

which ranged in surface area from 17 to 81 $m^2 \cdot g^{-1}$. Even the best of samples prepared in this manner may be far from perfect. Most of them are aggregations of microcrystals or domains [20]. If such crystals are heated under moist conditions, the imperfections can be "healed" [15,20]. Schwertmann, Cambier and Murad [20] used temperatures of 125 – 180°C and reported that this changed a multidomainal goethite into a monodomainic one.

2.4. Titration behaviour

Goethite is a variable-charge oxide. It can gain protons at low pH and so carry a net positive charge and it can lose them at high pH and so carry a net negative charge. It follows that there is a pH value at which the net charge is zero. This point of zero charge (pzc) is one index of the properties of an oxide. Measurements of the charge and of the pzc are usually made using a titration procedure. However, equilibrium between the oxide and the titrating solution is often slow and the pH may drift over periods of days [21] (and Refs. in [3]). Part of this effect may occur because protons might be able to penetrate the crystal rather than being confined to the surface thus giving rise to a proton "cloud" in the solid phase. At high pH, the equivalent would be a cloud of vacancies in the crystal. Penetration of protons into the domainal boundaries could also be important. The slowness of the reaction is a nuisance to chemists but it is a common characteristic of many reactions with soil and must be considered as part of the system.

A wide range of values has been reported for the pzc of goethite. Zeltner and Anderson [22] assembled values which ranged from 7 to 8.8. Much of this range is due to differing contamination with carbon dioxide. Evans, Leal and Arnold [23] found that after removing carbonate, the pzc was 9.3 – a value much closer to the value of 9.48 calculated from crystallographic data [24]. Further, they reported that there was little pH drift, thus suggesting that the drift was also partly due to slow removal of carbonate from the surface by added acid.

2.5. Reaction with metal ions

The effects of pH. The effects of pH on adsorption of metal ions by oxides are remarkably consistent: as the pH is increased, reaction begins at a characteristic pH and increases rapidly so that over about 2 pH units reaction is nearly complete (Fig.1.). The sequence of reaction is similar to the sequence of their first hydrolysis constants (Fig. 1.).

Mercury differs from the other metals in that it reacts at much lower pH (Fig. 2.). However, this is indeed consistent in that its first hydrolysis constant is also much lower (negative log: 3.4). There are also large effects of chloride concentration on mercury reaction (Fig. 2.). This occurs because the strong affinity between mercury and chlorine means that the concentration of the species present in solution change with chloride concentration. Thus, this result shows that reaction does depend on the species in solution.

The effects of concentration. When metal adsorption at constant pH is plotted against solution concentration using a double logarithmic scale, linear relationships with slope less than unity are commonly obtained (Fig. 3.). This was first noted by Benjamin and Leckie [25]. In their review of a very large data set, Dzombak and Morel [3] reported that this was a common observation for metal reaction with hydrous metal oxides. This behaviour is consistent with a model in which the reacting sites are not uniform – that is, there are a few sites of high affinity, rather more of slightly lower affinity and so on.

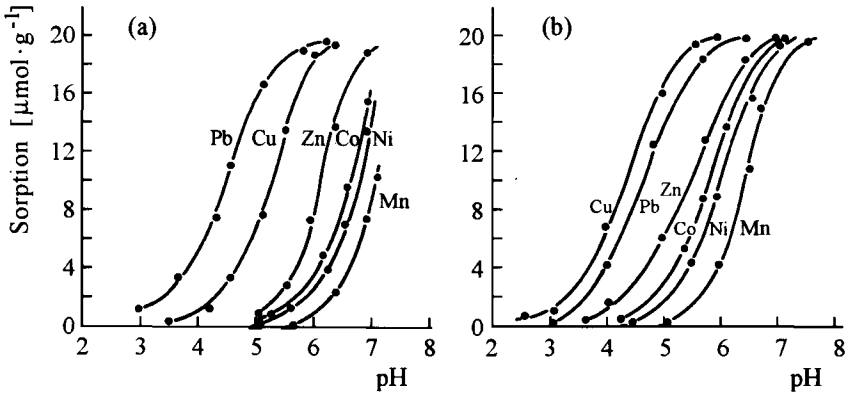

Figure 1. pH-dependence of sorption of a range of metal ions on haematite (a) and goethite (b) when they were added at a rate of 20 μmol/g of oxide [28]. The values of the negative log of the hydrolysis constants are: Pb 7.71; Cu 8; Zn 8.96; Ni 9.86; Co 9.65; and Mn 10.59 [29].

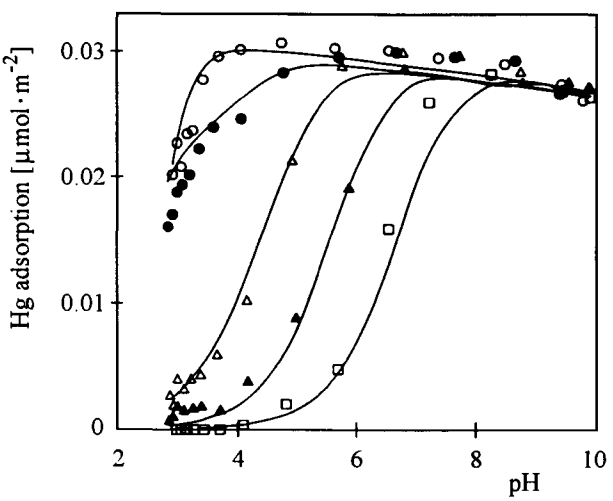

Figure 2. Effect of pH and chloride content on the adsorption of mercury by a sample of goethite [30]. The lines indicate fit of a model described in section 3.1. The concentrations of chloride are indicted as: ○ = 0μM, ● = 5μM, △ = 50μM, ▲ = 500μM, □ = 5000μM).

The effects of electrolyte concentration. Okazaki et al. [26] reported no effect of electrolyte concentration on adsorption of copper and zinc by iron and aluminium oxides. Similarly, from their own work, and from a survey of the literature, Hayes and Leckie [27] concluded that there was little effect of electrolyte concentration on metal adsorption. However, a wider view of the literature shows that there are indeed effects on surfaces which are probably negatively charged – for example, for adsorption of nickel on kaolinite [31], for zinc on soil [32], for copper, cadmium and lead on kaolinite [33] and for cadmium on soil [34]. This discrepancy probably arises because metal adsorption on oxides often

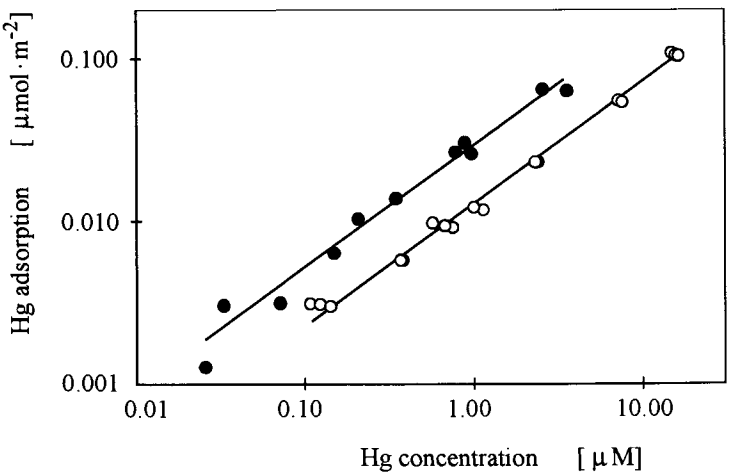

Figure 3. Relationship between mercury adsorption and mercury concentration in solution at pH 4.0 (●) and pH 9.6 (○) [30].

begins at pH values below the pzc (Fig. 1.). The surface is therefore positively charged. Increases in electrolyte concentration would decrease the positive electric potential of the surface and therefore increase reaction. However, this would be offset by decreases in the activity of the metal ions in solution so the net effect is small. It is only when reaction is with negative surfaces that both effects are in the same direction and therefore do not cancel each other.

Effects of time. As Dzombak and Morel point out [3], the rate of reaction between oxides and metal ions is often investigated in "preliminary experiments" which are not reported. The "equilibration" periods chosen from such experiments may range from a few minutes to weeks yet the data are treated as if the reaction were truly at equilibrium. Dzombak and Morel [3] accepted the idea that the reaction may comprise a rapid first step followed by a slower second step and pointed out that the second step may represent a significant proportion of the total reaction. There is an interesting dichotomy of approach to this problem. Those scientists with a chemical background tend to emphasise the rapid early reaction and attempt to treat the results using an equilibrium approach. Their difficulty is to be sure that the slow reaction has not been important in the time scale they chose yet the fast reaction is complete. Those scientists with an agriculture or soils background realise that fertilizers are applied infrequently and must supply plants for at least several months and perhaps for years. They therefore tend to emphasise the long-term slow reactions. A good example of this approach is that of Brümmer et al. [35] who showed that Ni, Zn, and to a lesser extent Cd continued to react with a sample of goethite. In a subsequent study [36], it was shown that the overall reaction was consistent with an initial adsorption of ions at a charged surface followed by diffusion of the ions into the crystal – perhaps into imperfections.

2.6. Reaction with anions

Effects of pH. The effects of pH on anion adsorption are much more diverse than those of cations. Adsorption may decrease gently or steeply with increasing pH (Fig. 4.) and there may be a pH range in which sorption increases with increasing pH. This increasing adsorption is important because it shows that the effects cannot be explained solely in terms of changes with pH in the surface for the increasingly negative charge would always decrease adsorption. It was only by studying a large range of anions that Hingston, Posner and Quirk [56] were able to discern a pattern. They noted that there were always bends in the curves near some of the pK values of the relevant acid. This is indicated for four anions in Fig 4. Similar behaviour was also observed for molybdate, tripolyphospate, pyrophosphate, and arsenate.

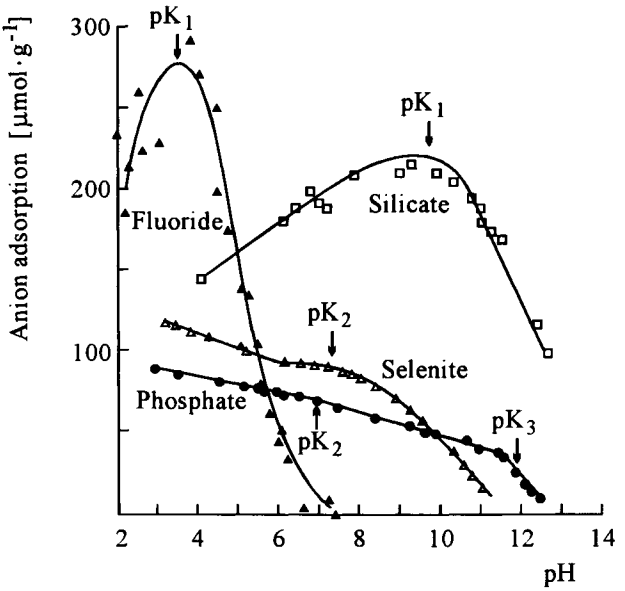

Figure 4. Adsorption of four anions by goethite. Two samples of goethite were used and the levels of addition differed for the differing anions [56].

Effects of concentration. Anions also differ from metal ions in that they appear to react with uniform sites. That is, there is no evidence for the existence of a range of sites differing in affinity. This was noted by Dzombak and Morel [3] and has recently been considered in detail by Strauss [37].

The effects of electrolyte concentration. The effects of electrolyte concentration on anion reaction depend on the pH and thus on the charge carried by the surface. At sufficiently low pH, increasing electrolyte concentration decreases adsorption. At a higher pH, it increases it (Fig. 5). There is thus a pH at which electrolyte concentration has little effect. For anions, this point of zero salt effect occurs at a lower pH than the point of zero charge of the oxide. For the data in Fig 5., the point of zero salt effect on phosphate adsorption was just above pH 4, whereas the pzc of the non-phosphated oxide was near pH 8. That is, reaction with the anion has decreased the charge on the oxide.

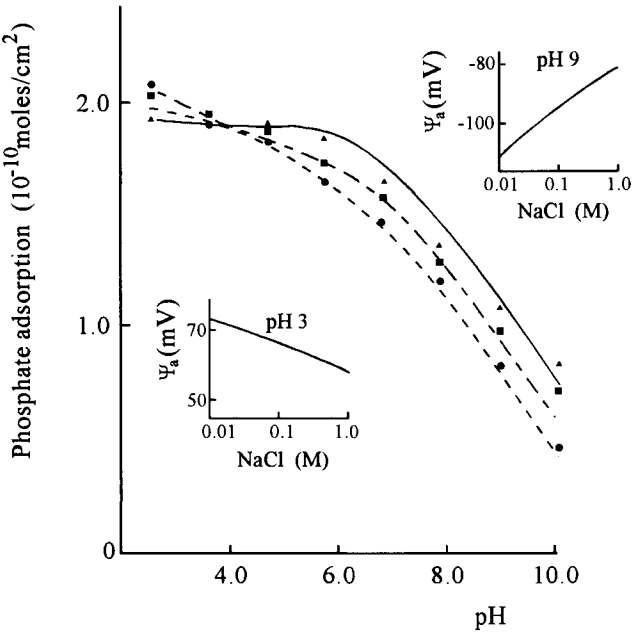

Figure 5. Effect of pH and sodium chloride concentration on the adsorption of phosphate from a solution with an initial concentration of 340 μM of phosphate and a goethite concentration of 3.1 g/l. Insets show the calculated values for the effects of salt concentration on the electric potential in the plane of phosphate adsorption. The concentration of sodium chloride was: 0.01M, 0.1M, and 1.0M [40].

Effects of time. As is the case for metal cations, many workers have assumed that anion adsorption reaches equilibrium. However, recent work by Strauss [37] with phosphate has shown that this may not be the case. He found that for a sample of goethite that had been healed by hydrothermal treatment, reaction was complete within a few hours. No further reaction was detected even after six weeks. It was only with this healed goethite that the rate of the initial reaction could be studied in isolation and it was found that reaction was faster at lower pH. This is consistent with the work of Madrid and Posner [39] and with the literature survey of Dzombak and Morel [3]. For all other samples of goethite, there was a marked continuing reaction and the poorer the crystallinity of the goethite, the more marked the reaction. These results show that phosphate reacts only with the surface of well-crystallized goethite but that it continues to react – presumably with internal surfaces of pores – of poorly crystallized goethite. As no other published studies used healed goethite, we may assume that all of the materials used were imperfectly crystallized and therefore were subject to some continuing reaction.

3. UNDERSTANDING THE REACTION WITH OXIDE SURFACES

We may attempt to understand the reaction in two ways. One is by using physical methods to investigate the bonds formed between the adsorbed ions and the surface atoms.

The results from such studies provide an input to the second way of understanding the reaction. This is to construct models which aim to describe the observed effects of pH, concentration, electrolyte concentration and time on the reaction. Such models require a reasonably realistic picture of where the adsorbed molecules reside if they are also to be realistic.

It has been agreed for some time that several anions sorb along the double octahedral chains of goethite by bonding two singly coordinated A-type OH groups [41]. They therefore form binuclear, bidentate, inner-sphere complexes. There has been some controversy about some of the other oxy-anions but Manceau and Charlet [42] recently concluded that a similar structure occurs for selenate and sulfate in addition to phosphate, arsenate and selenite.

For the metal cations, the bonding possibilities are more numerous. Spadini et al. [43] showed that, when coprecipitated, Cd takes positions that would otherwise been occupied by Fe atoms. They considered that, when sorbed, cadmium takes up positions which correspond to crystal growth sites. They observed that sorption of Cd on goethite resulted in two Cd-Fe distances and they associated these with differences in the way the Cd octahedra linked with the Fe octahedra of the goethite. These differences in the linkage could be one reason for the observed heterogeneity of oxides with respect to metal cations but not to anions. However, it is not clear whether this explanation could extend to very low surface coverage when only the most-favoured sites would be reacting.

An alternative explanation [44] for heterogeneity with respect to anions but not to cations is connected with the extra water content of goethite as mentioned earlier. If, as suggested, the formula for goethite should be written $Fe_{1-x}O_{1-3x}(OH)_{1+3x}$ where x is the proportion of the iron atoms that are missing, then we might speculate that the balancing of the charge due to missing Fe atoms is less than perfect. This would give rise to sites with an electric potential more negative than average and therefore of high affinity for cations. Depending on the location of such sites, we could expect differing values for electric potential - and hence the heterogeneity. Anions would not be affected by these sites and as the "x" in the formula would usually be less than 0.01 the decrease in maximum anion adsorption would be undetected.

3.1. Describing by modelling

Reaction of both cations and anions with oxide surfaces occurs on charged surfaces and the charge changes with pH. It is therefore essential to couple a model of ion reaction with a model of charge to give a comprehensive model. Several such models have been proposed. They differ in complexity and in effectiveness and each has their advocates. They have been reviewed and compared several times - most recently by Sposito [2], Barrow and Bowden [45], Goldberg [46]. Nevertheless, it is necessary to outline here a model which lends itself to abstraction and simplification so that it can be applied to the problems of describing the reactions in soil. This is the model of Bowden et al. [47,48] which was further developed by Barrow et al. [36] to include rate of reaction plus heterogeneity of sites when reacting with metal cations. This model is referred to as the "objective" model [2], as the "four-layer" model [45] and as the "Stern variable surface charge-variable surface potential" model [46].

Some of the ideas behind the model are represented in Fig.6. This is only a 2-dimensional representation but the structures indicated seem to be consistent with more-recent know-

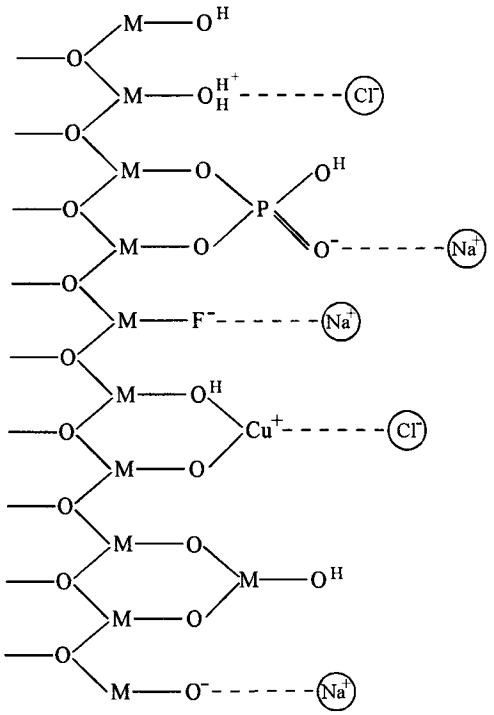

Figure 6. Diagrammatic representation of possible distribution of different ions at an interface between a metal oxide and water. M indicates a metal atom – such as Fe, —— chemical bonds, and – – – – electrostatic bonds [47].

ledge. This diagram emphasises two important points. The first is that coordination reaction with anions or cations (phosphate, fluoride or copper in the figure) does not necessarily prevent a site from reacting with electrolyte cations or anions (sodium or chloride in the figure). Mass balance equations which allocate sites exclusively to one particular reactant are thus not part of this model. This point is developed further by Barrow and Bowden [45] in regard to the status of a site after it has reacted with an anion. This model has been criticized for this structure by Sposito [2] who concluded that, as a consequence, it should not be regarded as a chemical model. This seems a curious exclusion.

The other important point is that the various ions near a surface will have their centres of charge located, on the average, at different distances from the metal ions of the oxide. For example, in Fig. 6. the fluoride ion is located closer than the phosphate ion. This means that the various ions will experience differing electric potentials and differing changes in potential with pH. Fluoride, for example, will experience a greater (absolute) potential at a given pH and a greater change in potential with pH. A new approach by Hiemstra [49] produces a similar outcome from a different direction. He argues that a certain fraction of the charge on the central ion of the complex (for example Se) can be allocated to a plane

on the solution side of the interface and the remainder to a plane on the oxide side. This gives fewer planes but the net effect should be similar to that obtained by assuming that the charge is located in a mean plane between the other two. When comparing selenate and selenite using this approach, the extra oxygen atom for a selenate complex means that a greater fraction of the charge is allocated to the plane on the solution side. This conclusion is similar to that of Barrow and Whelan [50] who concluded that the position of the mean plane of selenate sorption was further from the surface than that of selenite.

When the model is constructed so that each adsorbed ion can be allocated to a plane, each can therefore experience a different change in potential. This gives both flexibility and realism to the model. In older models, ions were constricted to fewer planes of adsorption and therefore are constrained to experiencing the changes in potential of those planes. It was usually found that, with such models, each individual reaction scheme gives the wrong shape for the effects of pH. The approach is therefore to add together two or more reaction schemes, each of which has the wrong shape, to produce an effect which approximated to the observed shape. However, when the adsorbing ions are permitted to reside in differing planes of mean potential, it is usually found that one of the solution species can be related to the amount of adsorption as indicated in the next paragraph. This subject is discussed further by Barrow and Bowden [45].

Central to this model is the definition of a term a_{is} which was called the "surface activity function" [47]. This term is defined as:

$$a_{is} = K_i a_i \exp(-z_i \psi_s / RT) \quad (1)$$

where K_i is a binding constant and is characteristic of the ion and surface concerned, a_i is the activity of the ion in solution, z_i its valency, ψ_s is the electric potential in the plane of adsorption, and R and T have their usual meaning. This equation was derived by Bowden, Posner and Quirk [47] using a thermodynamic argument. In effect, the equation attempts to divide the properties of an ion into two components – a "chemical" component specified by the activity in solution (a_i) and an electrostatic component (ψ_s). This concept has been criticized by Sposito [2]. He argued that the electrical properties that produce the chemical properties of charged species cannot be divided unambiguously into electrostatic and non-electrostatic categories. Nevertheless, analogous exponential terms occur in other models albeit with different derivations. At the least, such terms can be considered as solid-phase activity coefficients that correct for the charge of a surface species [51]. This is an important concept because it allows us to think about the effects of (say) changes in pH in terms of two components: the changes of the surface and the changes of the species present in solution.

3.2. Interpreting the terms of the model

The terms of this model can be divided into three groups: maximum surface densities, binding constants, and capacitance terms. For each ion considered there will be a permitted maximum surface density. The values might be identical as for H^+ and OH^-, or they might be different as for F^- and HPO_4^{2-}. For each ion, there will also be a specific value for the binding constant K_i. And finally there will be a series of capacitance terms which, in effect, specify the distance between the planes of adsorption (provided the electrical permittivity is constant the capacitance is inversely related to distance).

The philosophy behind this model differs from that behind other models in another important respect. The users of other models have often attempted to define constants which have significance in themselves and can be extrapolated to other situations. This was the philosophy of Dzombak and Morel [3]. However, for the model discussed, little emphasis is placed on measuring supposed constants because all models are considered to be incomplete and the supposed constants therefore unreliable [45]. Subsequent experience has supported this opinion.

Consider, for example, the terms which specify charge. As recorded earlier, measured values for pzc vary and are below the theoretical value largely because of the presence of adsorbed carbonate. In this model, the observed values for the pzc are *described* by the choice of values for K_H and K_{OH}. Analogous terms are used in other models. The values so obtained are not fundamental properties of the surface but artifacts of the preparation and treatment of the oxide. Furthermore, adding acid to such a surface will displace some carbonate and thus induce an asymmetry in the titration curves. These asymmetries are *described* by differences in the K terms for the electrolyte cations and anions. Lumsdon and Evans [52] have recently shown that different values for model parameters are needed for CO_2–free goethite.

Even in the absence of the carbonate problem, the K terms for electrolyte anions and cations (and the analogous terms for other models) need to be treated with caution. Rather than indicating differences in the affinity of cations for the surface, they probably reflect differences in the probability that a cation has a water molecule between it and the surface [53,54].

When samples of goethite of differing crystallinities are compared, the titration curves are found to reflect these differences by increased spread of the curves at pH values distant from the pzc [55]. These are *described* in this model by increases in the capacitance terms [55]. The observed behaviour probably reflects increased penetration of protons into pores between domains. In this case, we might think of the changes as reflecting changes in surface "roughness" and thus in the mean distance between planes. That this should be reflected in a capacitance term in not entirely inappropriate.

When we come to describe sorption of anions such as phosphate, we might expect that the maximum surface cover could be calculated from the known configuration of the adsorbed ions on the surface. However, this only works for goethite which has been healed [37]. For other samples of goethite, the observed maximum exceeded the theoretical even for the short reaction time of one hour. Subsequent dissolution studies strongly indicated that the difference was due to penetration of the phosphate into pores.

Thus models may closely *describe* observed behaviour but interpretation of the terms of the model is not straight forward. The argument presented is that models have generally been tested against data derived from surfaces which are rather far from the conceptual surfaces of the model. It is for this reason that I have adopted a rather pragmatic view of the models used. One could argue that there is a need to test better models against better data – for example, data generated from carbonate–free, healed goethite. That may well be so, but, when dealing with reactions with soils, we need models that apply to surfaces which are far from perfect.

3.3. How the model describes adsorption

In this section we are not concerned with how well this model describes adsorption.

There are many papers which show that it describes it very well – see Goldberg [46] for a summary. Rather we are concerned with the principles behind that description and with understanding why the various ions behave differently.

Consider first the anions. For these the behaviour is diverse. The crucial questions are: why does adsorption sometimes increase with pH (eg. silicate, Fig. 4.) and sometimes decrease (eg. selenite, Fig.4.), and why are there bends or peaks in the curves near the pK of the relevant acid?

The answers to these questions are in the interplay of the changes with pH in the ions present in solution and in the charge properties of the surface. For example, the pK for hydrofluoric acid is near 3. At pH values below this, the concentration of F^- ions increases with pH (the a_i term of equation (1)). This is opposed by the increased negative potential of the surface but because the ion is monovalent this is not sufficiently powerful (the z_i term of equation (1)) and adsorption increases. At pH values above the pK, there is decreasing scope for increases in the concentration of F^- ions; the only effect which is then relevant is that due to the increasingly negative surface potential (the ψ_s term of equation (1)). We can argue either that the F^- ions are small enough to occupy the same position as hydroxyl ions and therefore the mean position of the charge is close to the surface. Or we can argue that, unlike oxyanions, there are no oxygen atoms to affect the charge distribution [49]. In either case, the decline in potential, and hence the decline in adsorption, is steep.

Compare this with the behaviour of selenate and sulfate. For both, the pK_2 of the relevant acid is near 2. Hence both are fully dissociated over the range of pH values usually investigated. Adsorption therefore decreases with increasing pH because the only effect operating is the effect of pH on the surface potential. The resulting changes in adsorption with pH are not as steep as those for fluoride even though the ions are divalent. Again we can argue either that this is because the ions are larger and the centre of charge is further from the surface or that the oxygen atoms pull the charge distribution away from the surface. In either case, the change in potential with change in pH is less steep.

Selenite and phosphate may be treated together. For both, the pK_2 of the relevant acid is near 7. At pH values well below this, the concentration of the divalent ion increases 10–fold with each unit increase in pH. However, this effect is not sufficient to overpower the increasingly negative surface potential because divalent ions are involved. There is therefore a slow decrease in adsorption with increasing pH. Once a pH value near the pK_2 is approached, the scope for further increases in the concentration of divalent ions decreases and adsorption therefore decreases.

For silicate, the relevant acid – silicic acid (H_4SiO_4) – is very weak with pK_1 near 10 and pK_2 just above 12. The influence of these two pKs overlap so that the concentration of the divalent ion increases at first about 100–fold for unit increase in pH [38]. This is sufficient to overpower the effects of the increasingly negative surface and so adsorption increases at first (Fig. 4.). Subsequently, as the pH approaches the pKs the same effects occur as for other ions and adsorption decreases [45].

Thus the model provides a consistent explanation for the diverse effects of pH on adsorption of various anions and thus explains the observations of Hingston et al. [56]. The binding constants obtained correlate with pKs of the relevant acids (Fig. 7.). This may indicate that anions which have a strong affinity for a proton also have a strong affinity for the electrophilic metal ions of the oxide surface. Furthermore, it is consistent

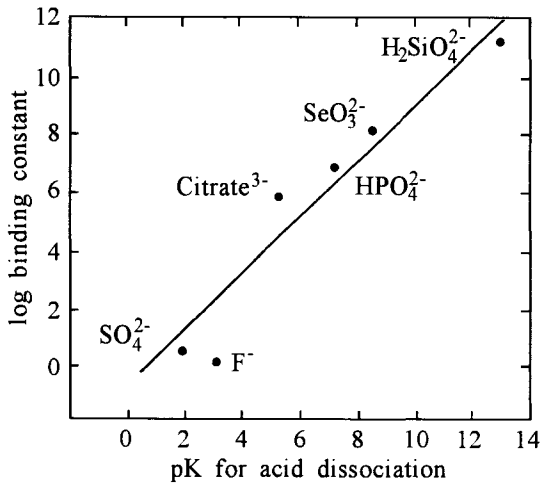

Fig. 7. Relation between the pK for the dissociation of the relevant acid and the log of the binding constant for six anions [45].

with the conclusions of Manceau and Charlet [42] that such oxyanions form binuclear, bidentate, inner-sphere complexes. The model does not specify whether the mechanism of the reaction involves an initial reaction with monovalent ions followed by a further reaction or whether there is an initial reaction with a divalent ion. It can be shown that both routes lead to similar expressions.

Suppose reaction occurs at pH=5 so that most of the phosphate is present as monovalent $H_2PO_4^-$ ions and that the reaction is represented as hydrolysis of the monovalent phosphate ions followed by reaction between the divalent ion and two sites. Suppose further that the surface gains one unit of surface charge and the net change in the solution pH is zero. The actual change in surface charge and in solution pH depends on the initial pH and on the amount of anion reacting [48]:

$$H_2PO_4^- \overset{K_2}{\rightleftharpoons} HPO_4^{2-} + H^+ \tag{2}$$

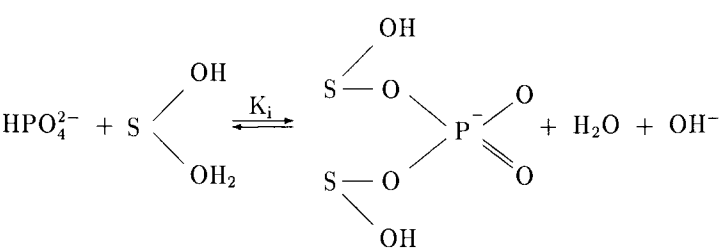

(3)

Alternatively, let us represent the reaction as an initial reaction with the monovalent phosphate ion followed by a second reaction with another site. The products are represented

as the same as before. The intermediate product formed by equation (4) is taken as being present in only small amounts:

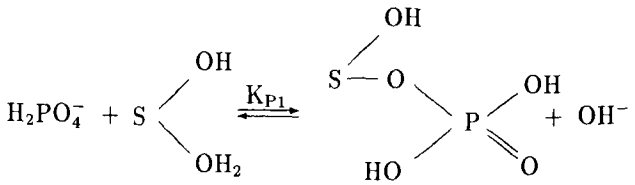

(4)

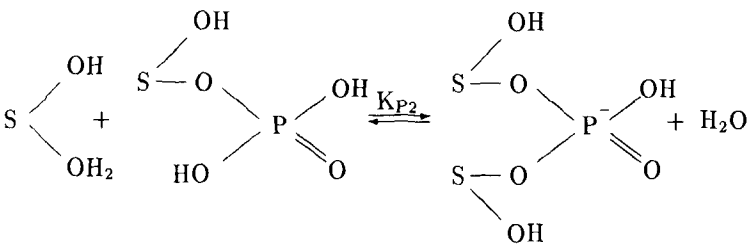

(5)

It can then be shown that $K_iK_2 = K_{P1}K_{P2}$. That is, the binding constant K_i, which is used in the model, can be specified as $K_{P1}K_{P2}/K_2$. The use of this one constant is thus consistent with binuclear, bidentate complexes but does not specify the pathway of the reaction.

Some conclusions about the pathway can be obtained by studying the rate of the reaction at different pH values. It was shown [57] that faster reaction at low pH could be taken to indicate that the process consisted of more than one step and that the rate-determining step preceded the electron transfer step and did not, of itself, involve electron transfer. The rate determining step might, for example, involve the removal of a water molecule.

Consider now the adsorption of cations. Two kinds of explanations are possible within the model. One is that reaction is dominated by the first hydrolysis product – the monovalent MOH^+ ions. Provided the pH is more than about one unit below the pK for this reaction, the concentration of MOH^+ ions increases 10-fold for each unit increase in pH. An extra effect of pH is produced from the decrease in electrical potential as the pH is increased. Thus, this explanation requires that there must be at least a ten-fold increase in the effectiveness of ions in inducing adsorption with each unit increase in pH. This is consistent with the conclusions of Kinniburgh and Jackson [58] who reported effects of pH which were more than ten-fold for reaction of cobalt, copper, zinc and cadmium with iron oxide. The values were: Co, 25 fold; Cu, 33 fold; Zn 45 fold; and Cd 50 fold.

The use of monovalent ions in models to explain the effects of pH works well. It was successfully used to model the adsorption of nickel, zinc and cadmium by goethite [50] and of mercury by goethite [30]. It also makes intuitive sense because we can imagine that the breaching of the hydration sheath, which shields the charge, by the formation of hydroxides might make the ion more vulnerable to reaction. This would then explain why ions with the greatest tendency to react at low pH have the greatest tendency to hydrolyse

– the MOH^+ ions form at a lower pH. The only problem is that there is increasing evidence that this explanation is inappropriate for soil. For cadmium at least the effect of pH is less than 10 fold for each pH unit (see later) and this rules out this explanation.

The other explanation is that divalent ions react. For most metals the concentration of these species change little with pH over the range commonly investigated. The effects of pH are then seen as entirely due to the change in electrical potential. Its effect is large because it is on divalent ions. However it is also necessary to locate the adsorbed ions close to the atoms of the reacting oxide to produce a steep change in potential with change in pH. This can also produce an effect of pH which is greater then 10–fold. The tendency for ions which hydrolyse readily to react at low pH is then explained as a correlation of affinities in a manner somewhat analogous to that for anions in Fig. 7. Dzombak and Morel [3] have reported a similar correlation between the coefficients of their model and the hydrolysis constants of cations.

4. APPLICATION TO SOIL

In many of the studies in which oxides were used, the intention was to model the behaviour of soil components. If we are to interpret these studies to understand behaviour of soil, we need to know how the materials in soil differ from the materials studied. Remember, soil is a dirty substance.

4.1. Differences between experiments with soil and experiments with oxides

Studies on soil differ from studies on pure oxides in five main ways. The reacting material in soil is impure and there may be a mixture of sorbents present; there is usually some of the reactant already present; there may be soluble organic matter in solution; the background ions differ; and the range of pH values investigated is smaller. These aspects are considered in this section.

The oxides in soil are certainly impure as indicated in section 2. The presence of silicate, phosphate, and presumably carbonate and organic compounds, means that the pzc is much lower than that of iron oxides studied in the laboratory. For top–soils with little permanent charge from clays, a common value is about pH 4. In the presence of appreciable permanent charge, it may be impossible to generate sufficient positive charge and so the mean charge remains negative even at low pH. These differences in pzc mean that we cannot assume that changes in electric potential near the surface with changes in pH will be the same as those observed with pure oxides.

Soils may also already contain some of the substance being studied. That is, one must study say phosphate sorption in the presence of the phosphate already there. This has caused some problems in the interpretations of phosphate sorption and desorption experiments [59]. This is one aspect of soil chemistry in which Western Australian soil scientists have an advantage. The very low content of phosphate in most soils simplifies such studies. Farmers, however, do not regard this as an advantage!

Soil solutions may contain some soluble organic matter. This is especially so if the soil has been treated with sewage sludge as in many experiments involving the reaction of metals with soils. The soluble organic matter can react with metals thus keeping them in solution. Reaction with the soil can only occur after the demands for this reaction are

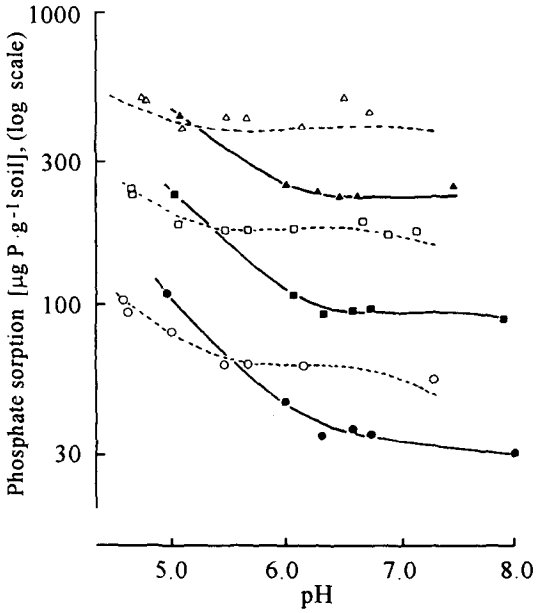

Figure 8. Comparison of the pH-dependence sorption of phosphate from a 0.01M solution of $CaCl_2$ with that from 0.01M NaCl [59].

P conc., $mg \cdot l^{-1}$	$CaCl_2$	NaCl
10	△	▲
1.0	□	■
0.1	○	●

satisfied and this gives rise to sigmoid sorption curves [60,61].

Soil solutions contain a mix of cations: mainly Ca^{2+}, Mg^{2+}, K^+, Na^+ and , at low pH, Al^{3+} and complex Al ions. In their studies, soil scientists have tended to use electrolyte solutions which they see as relevant. Often the solution used is a dilute solution of calcium chloride. This contrasts with those who have studied oxides. Their choice of background electrolyte has been motivated by a desire to use electrolytes which are close to "indifferent". Ideally, this means that neither the cation nor the anion has any affinity for the surface. In practice, it means that the affinity of both ions is small and similar. These differences in the choice of background electrolyte mean that the observed effects of pH differ. Fig. 8 shows that the decline in phosphate sorption by a soil with increasing pH is steeper when the background electrolyte is sodium chloride than when it is calcium chloride. This is because the presence of the divalent cation compresses the distribution of ions near the surface and the change with pH in the electric potential is less steep.

Soil chemists have also tended to study a limited range of pH values because of a desire to use relevant conditions. The upper limit is usually set because calcium carbonate is used to raise pH in practice. The maximum pH which can be reached depends on the calcium concentration in the solution and on the partial pressure of CO_2. In 0.01M $CaCl_2$

solutions, the value is near pH 7. Somewhat higher values are reached if the calcium concentration is lower. The lower limit also depends on practical considerations. As the pH of a soil is lowered, aluminium (and manganese) concentration in the solution increase and may reach toxic levels. Consequently, there are few studies for pH values less than about 4 in 0.01M $CaCl_2$ – or less than about 4.5 if the calcium concentration is lower. Recently, however, acid rain has lowered the pH of some European forest soils to values approaching 3. Studies on these soils are usually concerned with the harmful effects of this low pH rather than with the effects on adsorption reactions. The range of pH values in adsorption studies is therefore seldom more than about 3 units – see, for example Fig. 8. The diversity of anion behaviour as shown by Hingston et al. [56] would never have been revealed if they had confined their work to such a limited pH range.

4.2. Observations with soil – the effects of concentration

Soil scientists are very interested in the relation between the concentration of an ion in the soil solution and the amount retained by the soil. It is this relation which determines the rate of diffusion of a nutrient to a plant root and which also determines the possibilities of leaching losses from the soil.

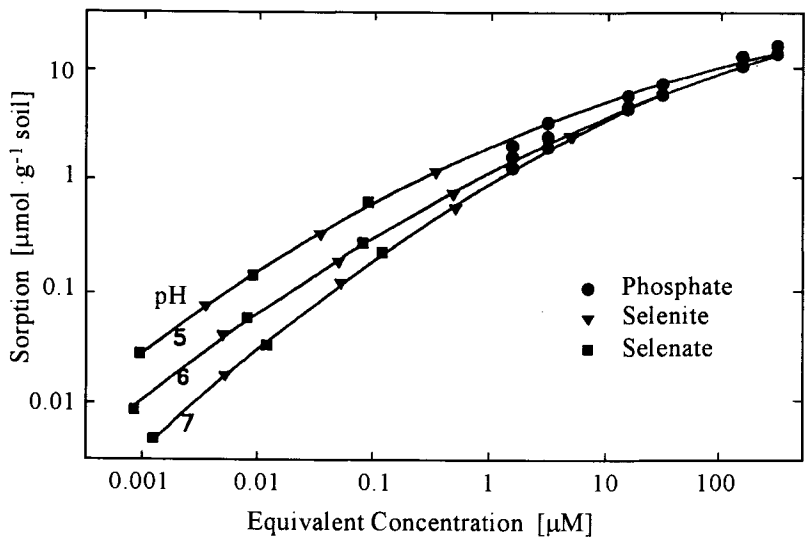

Figure 9. Logarithmic plots of sorption of phosphate, selenite and selenate by a soil at the indicated pH values. To permit plotting on a common scale, the concentrations of selenite and selenate have been multiplied by factors to account for their lower affinity. For example, the values at pH=6 for selenite were 0.05 and for selenate 0.008. The lines indicate the fit of a model based on the heterogeneity of the reacting surfaces [44].

Borrowing from surface science, they sometimes call plots of retention against concentration "adsorption isotherms". I think that this usage is a case of false immodesty. As we shall see later, the process involves more than simple *ad*sorption onto a surface; a second step which involves diffusive penetration follows. The rate of this step is affected by temperature – rather than only the position of an equilibrium and so the term is doubly

inappropriate. I prefer the more modest term of "sorption curves". The word sorption is used in a descriptive manner and without implying any mechanism. The term includes *ad*sorption.

Most studies of sorption curves involve little more that about a hundred-fold range of solution concentrations. Such a range often encompasses the interests of the experimenter and is analytically convenient. Over such a range, log log plots are usually close to linear and with a slope less than unity – that is, a Freundlich equation is appropriate and the reacting sites are therefore heterogeneous. This differs from anion adsorption by oxides which, as indicated earlier, is consistent with reaction with homogeneous sites. It is common to find that the slope of the log log plots differs between anions. That for weakly sorbing ions such as sulfate is usually greater than that for more-strongly sorbing ions such as phosphate. It seems possible that the differing anions are sampling a different part of the sorption curve. If the concentrations are adjusted to allow for the differing effectiveness of the ions in inducing reaction, the individual curves can be combined. Fig. 9 shows that the resulting log log plots are curved.

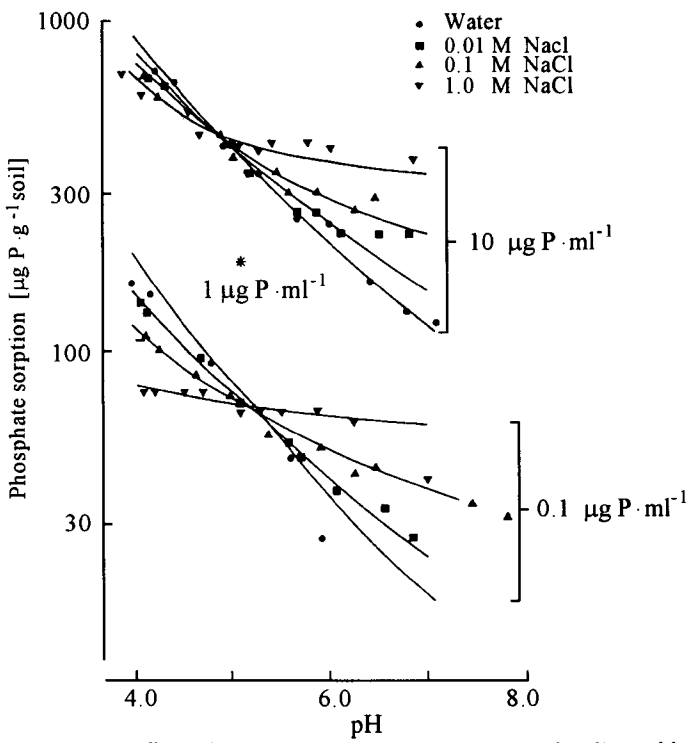

Figure 10. Effect of pH and solution concentration of sodium chloride on the sorption of phosphate at four concentrations of back-ground electrolyte in solution. The point of zero salt effect for an intermediate concentration of P has been shown by an asterisk. The lines are drawn from a fitted model [38].

This curvature only becomes apparent when a sufficient range of values is available. The curvature observed suggests that at even lower concentrations the logarithmic plots

would approach a slope of unity. That is, at very low concentrations, sorption would be proportional to concentration. This has been observed for metal sorption by soils [62,63].

4.3. Observations with soil – the effects of electrolyte

If the sorption curves pictured in Fig. 9 are caused by heterogeneity, what distribution of site properties would give rise to such curves? Sposito [64] reported that a Freundlich curve could be derived if the log of the affinity constants of a series of Langmuir equations had a distribution which was similar to a normal distribution.

In terms of equation (1), this would mean a normal distribution of log (K_i). However, it is also possible that there would be heterogeneity in the ψ_s term of equation(1). Evidence for this is obtained from a study of the effect of salt concentration on adsorption of anions. Fig. 10 shows that there are effects of salt concentration on phosphate sorption by a soil. These effects are analogous to those on phosphate sorption by goethite: at low pH, increasing salt concentration decreases sorption; at higher pH it increases sorption. There is thus an intermediate pH at which salt concentration has no effect. The value of this point of zero salt effect decreases with increasing sorption as would be expected. However, it occurs at a *higher* pH than the point of zero salt effect on pH (Fig.11).

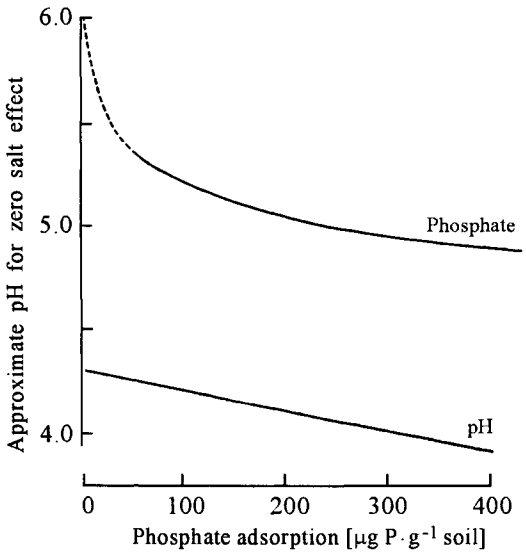

Figure 11. Effect of level of addition of phosphate on the point of zero salt effect on phosphate sorption and on the point of zero salt effect for pH [38].

Analogous effects occur with other anions (Fig. 12) and there are similar effects of level of sorption. That is, for borate, for which sorption is much weaker than for phosphate, the point of salt effect is at an even higher pH.

These effects can be explained if it is assumed that at least part of the heterogeneity of the reaction sites is in the electric potential. That is, at any given mean potential, there are some sites with a more-positive potential than the mean and some sites with a more-negative potential. This range of values of potential is assumed to be distributed

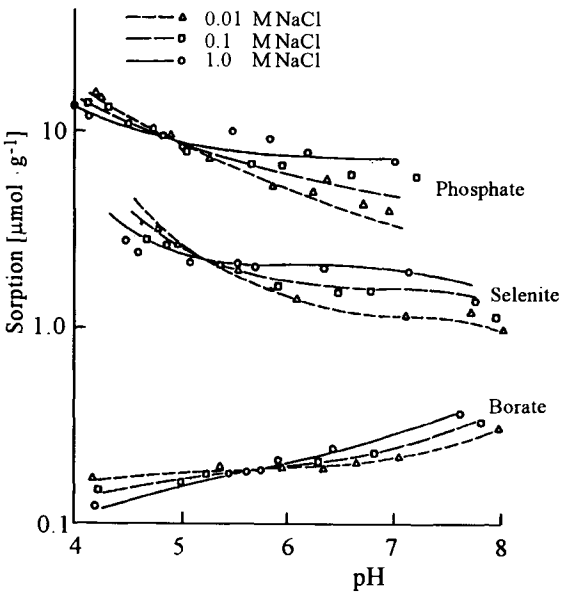

Figure 12. Observed and modelled effect of pH and of electrolyte concentration on sorption of three anions at a solution concentration of 100μM [65].

normally. Suppose that the mean potential of the soil is zero at pH=4. At that pH we would expect there to be no effect of salt concentration on pH. However if we reacted a small amount of anion with a soil at pH=4, reaction would be preferentially with sites which had a more-positive potential than the mean. Because reaction is with sites of positive potential, increasing the salt concentration would decrease sorption. We might need to raise the pH to say 6 before the mean potential of these reacted sites was decreased to zero. If we increased the amount of anion reacted, the reaction itself would lower the potential of the reacted surfaces and furthermore the reaction would spread to some less-positive sites. We would therefore not need to raise the pH quite as far before we reached the point at which the mean potential of the reacted sites was zero. Thus, if we are to model such observations, we must allocate at least part of the heterogeneity to the electric potential term of a model. It is improbable that there would not also be heterogeneity in the binding constant K_i but there is seldom information on which to allocate heterogeneity to the two sources as the two sources would have the same effect on the relation between concentration and sorption. It is therefore a modelling convention to allocate all of the heterogeneity to the potential term.

4.4. Observations with soil – the effects of pH

Subject to limitations discussed in section 4.1., the effects of pH on anions are similar to those observed using iron oxides. Thus, the sorption of phosphate and of selenite generally decrease with increasing pH (Fig. 12.) for the reasons discussed earlier. Similar principles apply for borate. However sorption increases with increasing pH because the pK for borate dissociation is near 9. The concentration of borate ions therefore increases 10-fold for each

unit rise in pH over the observed range in pH. Because the ion is monovalent, the repelling effect of the surface is insufficient to overcome the effect of the increasing dissociation and hence sorption increases with pH.

For the metal cations, the effects of pH are smaller than those observed with oxides. This can be shown by using a Freundlich equation modified to reflect the effects of pH: $S = k(c \cdot 10^{mpH})^n$. In this formulation, the coefficient m reflects the magnitude of the effect of pH on the effectiveness of a given concentration of metal in inducing sorption. If m equals one, unit increase in pH produces a ten–fold increase in the effectiveness of a given concentration in inducing reaction. If m is less than one, the effect is less than 10–fold. In unpublished work, I have obtained values for m of about 1 for Zn, about 0.85 for Ni, about 0.8 for Co and about 0.6 for Cd. Boekhold et al. [66] used a slightly different formulation but their values for m, as defined here, are abut 0.6. Naidu et al. [34] reported that the effects of pH varied between soils. The only value they quoted was equal to about 1 for m as defined here. They regarded this as particularly high. This therefore suggests that the other values were lower than one. As can be seen from the dates of these references, precise description of the effects of pH on metal sorption has only recently been attempted and presumably more data will come to hand. However, values of m less than unity do seem to occur. Such results cannot be explained by assuming that MOH^+ is the dominant ion. We have to assume that M^{2+} is the dominant ion and that the change in potential with change in pH is smaller.

4.5. Observations with soil – the effects of time and temperature

Farmers are very aware that, in most cases, it is necessary to apply rather more phosphate than was removed in produce in the previous season. Why is phosphate applied last year but remaining in the soil less effective than freshly applied phosphate? The answer is: because it has continued to react. The reaction is however, a rather strange one. By chemists' standards, it is extremely slow and continues even after many months or even years. For example, Devine et al. [67] mixed powdered phosphate with soil and found that after one year, it was 58% as effective as fresh phosphate, after 2 years 38% and after three years 20%. Geologists, on the other hand, might think this quite rapid. Nevertheless research careers are short and such a slow reaction poses research problems. Fortunately there is an easy solution. The rate of the reaction is quite sensitive to temperature and can be greatly increased by raising the temperature. By studying the reaction at say 60°C we can produce the equivalent of several years' reaction in a few days.

Because of its economic importance, far more work has been done with phosphate than with other ions. However, continuing reaction occurs with many other ions and is the norm rather than the exception. Some examples are: molybdate [68], fluoride [69], sulfate [70,71], arsenate [72], zinc [73] and chromium, cadmium and mercury [74]. It has also been shown that incubating copper with soil decreases its subsequent availability to plants [75].

Attempts to deal with this problem have varied. The simplest is to ignore it. The reaction is studied over some chosen time and the point reached is called "equilibrium". Indeed it is usual to "equilibrate" a solution with soil when what is meant is "mix". This has led to some questionable conclusions especially if the solution concentration of the reactant is decreased and desorption thereby induced. It is invariably found that the desorption limb does not follow the same track as the (ad)sorption limb. It is then concluded that

adsorption is not reversible. This is a nonsense. The essence of an adsorption reaction is that it cannot go all the way to the "right". There must be an appreciable back reaction. If that were not so, there could be no residual concentration of adsorbate in solution and it would be impossible to construct sorption curves. If sorption is observed to not be reversible, this indicates that the process involves more than *ad*sorption.

More complicated but more realistic is to measure the effect of time and to describe it. Several schemes have been tested with many of them based on interchanges between ill-defined black boxes bearing labels such as "labile" or "non labile". These and other schemes were discussed by Barrow [38]. When the rate of reaction is measured using changes in the solution concentration as an indication of the amount of reaction, the results can often be closely described by another modification of the Freundlich equation:

$$S = c^{b1}(k \cdot t)^{b2} \tag{6}$$

where S is the amount of sorption, c is the solution concentration of the adsorbate, t is time and k, b_1 and b_2 are coefficients. The term k may be related to temperature using the Arrhenius equation:

$$k = A \exp(-E/RT) \tag{7}$$

where E is an activation energy. The value of E is often about 80 kJ/mol. At this value, the rate approximately triples for each 10° rise in temperature. References to studies in which these equations are used are given by Barrow [38].

From these equations, it follows that at constant solution concentration and at constant temperature, the rate of sorption is proportional to t^{b2} where the value of b_2 ranges from about 0.05 to about 0.4 [76]. These are unusual kinetics – and they are indeed rather inconvenient. This is because the current rate of change of sorption is proportional to t^{b2-1} – that is, it depends on the time lapsed since the addition was made. This is rather difficult to incorporate into analytical models of leaching of solutes in soils. Nevertheless, such simple equations do provide a close description of the real behaviour. Our task is therefore to explain this behaviour.

5. MODELLING THE BEHAVIOUR OF SOIL

Studies with oxides provide the basis for understanding the behaviour of soil. However, in order to apply this understanding in a testable way, we have to simplify and abstract the detailed models applied to oxides. In effect, we construct a hierarchy of models with the detailed models of oxides feeding a simplified version up to the next level. The assumptions involved are as follows.

We assume: that reaction is with many variable charge surfaces (or patches); that the surfaces are heterogeneous with the heterogeneity described by a normal distribution of electrical potential; that an initial adsorption reaction on the surface of the variable charge material is followed by a very slow diffusion towards the interior of the particle; that both adsorbed and penetrated ions affect the charge of the particles and therefore the electrical potential of the surface; and that the electric potential of the adsorption plane is affected by pH and by electrolyte concentration. The equations which comprise the model were

given by Barrow [77]. They are listed in [78] and a more-robust way of dealing with the rate of the reaction was developed in work [79].

Many of the equations of the model are very simple. For example, it is assumed that the electrical potential in the plane of adsorption changes linearly with the amount of adsorption. We know that this is only an approximation but we find that in most cases it is sufficiently close to the behaviour. As explained earlier, we know that some of the heterogeneity is associated with the electrical potential. We accept that some of the heterogeneity is associated with the affinity of the sites for the ion, but, in most cases, there is no way of distinguishing these two kinds of heterogeneity and so it is convenient to lump them into the one basket. Even though the equations are simplified, manual computation would be difficult. For example, the distribution of potentials is broken into a number of discrete segments and the total behaviour is taken as the sum over the segments. There are also "chicken-and-egg" problems in that one needs to know the amount of sorption in order to calculate the electric potential of the surface – yet one needs to know the potential to calculate sorption. Computer programs are needed to solve such problems.

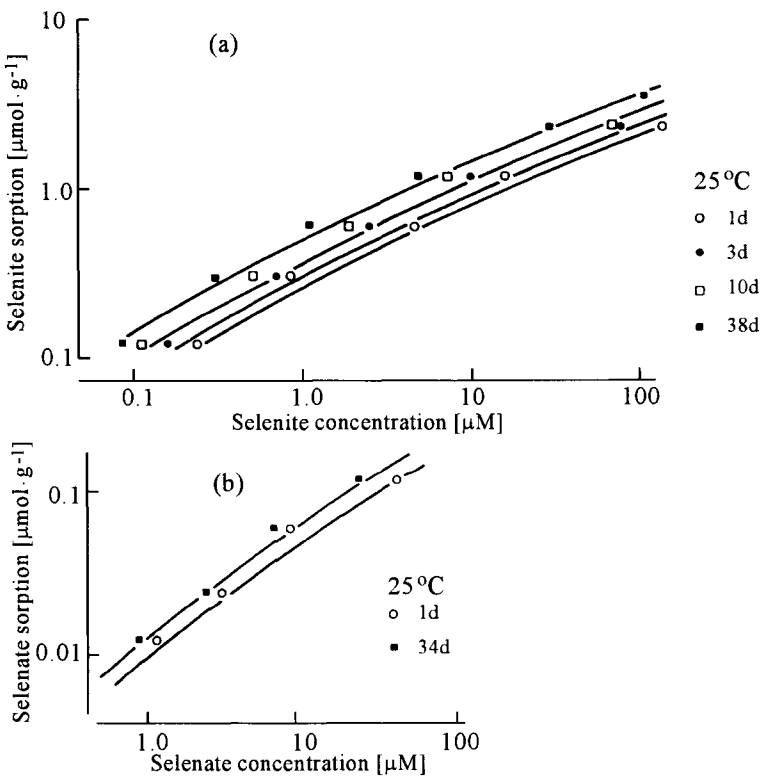

Figure 13. Effect of period of incubation on the concentration of selenite (a) and selenate (b) in solution after adding respectively selenite or selenate to a soil. Intermediate points have been omitted for clarity [80].

This model can describe most of the observations on the reaction of a large range of pollutants and nutrients with soil. These are summarised by Barrow [38] and examples of the fit of the model are given in Figs. 8–12. The present discussion will be limited to two aspects. One is the rate of the reaction.

The model explains the continuing reaction as due to diffusive penetration of the surface. The simple equation used implies that the depth of penetration is small relative to the size of the particle. Remember, we are dealing with very slow processes. For any segment, the rate is proportional to the square root of time. The observed kinetics arise partly because there is a braking effect due to the change in surface potential as a result of reaction and partly because of the smearing effect of the heterogeneity.

Figure 13 illustrates the fit of the model to the effects of time and solution concentration for selenite and for selenate sorption by a soil.

While the sorption curves are almost linear on a log log scale, the model fits a gentle curve as this is consistent with a bigger body of information (Fig. 9.). At any given level of sorption, the concentration of selenite in solution decreases with time and with increasing temperature. It is this decrease that is modelled as due to diffusive penetration. Selenate differs in that the sorption curves are steeper (as also shown in Fig. 9.) and, importantly, that the effects of time, though detectable, are much smaller. These two species therefore provide a test for the argument that apparent non-reversibility of sorption occurs because of the continuing reaction.

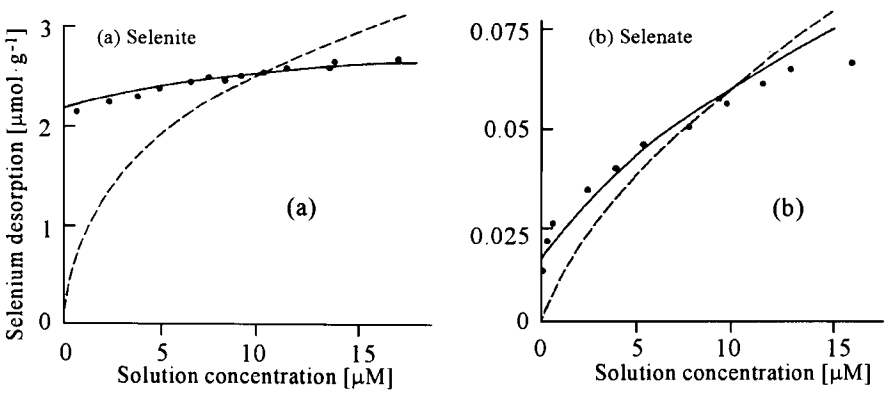

Figure 14. Desorption of selenite (a) and selenate (b), after incubation for 10 days at 60°C with selenite or selenate respectively at the levels indicated by the arrows on the vertical axis. Different levels were used so that the concentration range would be similar. The broken lines show the sorption curves [80].

Figure 14. shows that selenite desorption did not follow the same track as sorption. This is because it takes time to reverse the diffusive penetration. This was tested from the fit of the model. When the model which had been fitted to sorption data, some of which is shown in Fig. 13., was used to predict desorption, the prediction was close to the observation. In contrast, desorption of selenate was greater. This is consistent with its much slower continuing sorption reaction. The greater desorption was also predicted

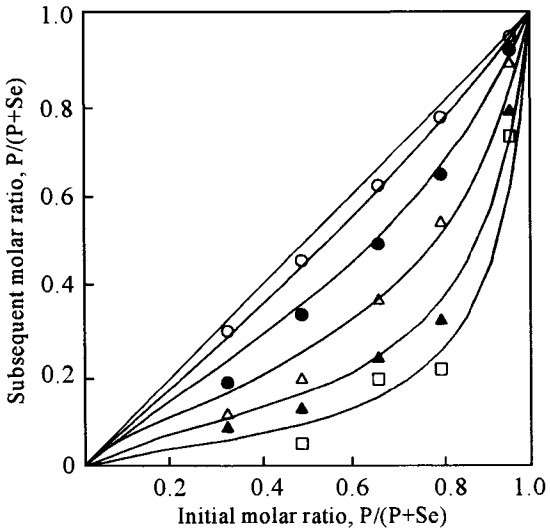

Figure 15. Observed (points) and modelled changes (lines) through time in the competition diagram for phosphate and selenite. If the anions were equally effective competitors, the points would all fall along the diagonal line. Points below the line indicate that phosphate was a more effective competitor. The times (h) were: ○, 0.25; ●, 4; △, 24; ▲, 96; □, 720.

by the model fitted to the analogous sorption data for selenate part of which is shown in Fig. 13.

The final aspect discussed is one that provides a stringent test of the model. It is the ability to describe competition for sorption between two anions through time. It is a stringent test because it requires that the interactive effects of each ion on the surface be modelled through time.

The model was able to describe the changes through time of the concentration of phosphate and selenite ions both when supplied separately and in combination [81]. It therefore mirrored changes in their competitive advantage (Fig. 15.). An important conclusion was that competition was largely through the effects of one anion in making the surface more negative and therefore less accessible to the other ion – rather than the normal chemical competition for vacant sites.

6. CONCLUSIONS

Most of the published studies on the reaction of ions with iron oxides have used samples of oxides which have been exposed to various extents to carbon dioxide. Models fitted to data from such studies do not reflect fundamental characteristics of the surface but are affected by the degree of exposure to carbon dioxide. In the case of goethite, most of the samples have consisted of multi-domainal crystals. It is only when such crystals have been "healed" by hydrothermal treatment that the true adsorption reactions of the surface can

be observed. Samples which have not been hydrothermally treated continue to react because ions diffuse into irregularities thus giving values for the apparent *ad*sorption which are too high. Because these aspects have not always been appreciated, they may have limited understanding of the fundamental characteristics of the reaction. However, one of the important reasons for studying the reaction with oxides is to understand the reaction with soil. The oxides in soils are far more "contaminated" and are very poorly crystalline. Studies with contaminated, and imperfectly crystallized iron oxides are therefore important and have provided sufficient knowledge to understand all of the observations on the reaction of ions with soil. We can now understand and closely model the effects on sorption of concentration of sorbing ion, of pH, of electrolyte concentration, and of time and temperature. We understand why different ions are affected differently by these factors and we can model the competition between ions for sorption. Finally we can also understand why desorption appears to follow a different track to sorption. To summarise: *quod erat demonstrandum* – which was the thing to be proved.

REFERENCES

1. R.M.Taylor, R.M.McKenzie, A.W.Fordham and G.P.Gillman, Oxide Minerals, in: Soils: an Australian Viewpoint, Division of Soils, CSIRO, Academic Press, Melbourne, 1983
2. G.Sposito, The Surface Chemistry of Soils, Oxford University Press, New York, 1984.
3. D.A.Dzombak and M.M.Morel, Surface Complexation Modelling Hydrous Ferric Oxide, Wiley, New York, 1990.
4. W.Stiers and U.Schwertmann, Geochim. Cosmochimica Acta, 49 (1986) 1909.
5. D.Hiller, G.W.Brümmer and D.Ackermand, Z. Pflanzen. Bodenkunde, 152 (1989) 47.
6. R.A.Kühnel, H.J.Roorda and J.J.Steensma, Clays and Clay Miner., 23 (1975) 349.
7. K.A.Norrish and H.Rosser, Mineral Phosphate, in: Soils: an Australian Viewpoint, Division of Soils, CSIRO, Academic Press, Melbourne, pp.335–361, 1983.
8. D.G.Lewis and U.Schwertmann, J. Colloid Interface Sci., 78 (1980) 543.
9. M.V.Fey and J.B.Dixon, Clays and Clay Miner., 29 (1981) 91.
10. D.G.Schulze, Clays and Clay Miner., 32 (1984) 36.
11. D.G.Schulze and U.Schwertmann, Clay Miner., 19 (1984) 521.
12. A.W.Fordham, R.H.Merry and K.Norrish, Geoderma, 34 (1984) 135.
13. A.W.Fordham and K.Norrish, Austr. J. Soil Research, 17 (1979) 283.
14. K.L.Smith and R.A.Eggleton, Clays and Clay Miner., 31 (1983) 392.
15. R.Thiel, Z. Anorg. Allg. Chem., 326 (1963) 70.
16. E.Murad, Mineralogical Magazine, 43 (1979) 355.
17. D.G.Schulze, Ph. D. Thesis, Technische Universität, München, 1982.
18. R.J.Atkinson, A.M.Posner and J.P.Quirk, J. Inorg. Nucl. Chem., 30 (1968) 2371.
19. F.J.Hingston, Ph. D. Thesis, University of Western Australia, 1970.
20. U.Schwertmann, F.Cambier and E.Murad, Clays and Clay Miner., 33 (1985) 369.
21. L.Madrid and P.de Arrambarri, Geoderma, 21 (1979) 199.
22. W.A.Zeltner and N.A.Anderson, Langmuir, 4 (1988) 469.
23. T.D.Evans, J.R.Leal and P.W.Arnold, J. Electroanal. Chem., 105 (1979) 161.

24. R.H.Yoon, T.Salman and G.Donnay, J. Colloid Interface Sci., 70 (1979) 484.
25. M.M.Benjamin and J.O.Leckie, J. Colloid Interface Sci., 79 (1981) 209.
26. M.Okazaki, K.Takomidoh and I.Yamane, Soil Sci. Plant Nutrition, 32 (1986) 523.
27. K.F.Hayes and J.O.Leckie, J. Colloid Interface Sci., 115 (1987) 564.
28. R.M.McKenzie, Australian J. Soil Res., 18 (1980) 61.
29. C.F.Baes and E.M.Mesmer, The Hydrolysis of Cations, Wiley, New York (1976).
30. N.J.Barrow and V.C.Cox, J. Soil Sci., 43 (1992) 285.
31. S.V.Mattigod, A.S.Gibali and A.L.Page, Clays and Clay Miner., 27 (1979) 411.
32. N.J.Barrow and A.S.Ellis, J. Soil Sci., 37 (1986) 303.
33. P.W.Schindler, P.Leichti and J.C.Westall, Netherl. J. Agricult. Sci., 35 (1987) 219.
34. R.Naidu, N.S.Bolan, R.S.Kookana and K.G.Tiller, Europ. J. Soil Sci., 45 (1994) 419.
35. G.W.Brümmer, J.Gerth and K.G.Tiller, J. Soil Sci., 39 (1988) 37.
36. N.J.Barrow, J.Gerth and G.W.Brümmer, J. Soil Sci., 40 (1989) 437.
37. R.Strauss, J. Soil Sci., in press.
38. N.J.Barrow, Reactions with Variable Charge Soils, Martinus Nijhoff, Dordrecht, 1987.
39. L.Madrid and A.M.Posner, J. Soil Sci., 30 (1979) 49.
40. N.J.Barrow, J.W.Bowden, A.M.Posner and J.P.Quirk, Australian J. Soil Res., 18 (1980) 395.
41. R.L.Parfitt, Adv. Agronomy, 30 (1978) 1.
42. A.Manceau and L.Charlet, J. Colloid Interface Sci., 168 (1994) 87.
43. L.Spadini, A.Manceau, P.W.Schindler and L.Charlet, J. Colloid Interfacial Sci., 168 (1994) 73.
44. N.J.Barrow, G.W.Brümmer and R.Strauss, Langmuir, 9 (1993) 2606.
45. N.J.Barrow and J.W.Bowden, J. Colloid Interface Sci., 119 (1987) 236.
46. S.Goldberg, Adv. Agronomy, 47 (1992) 233.
47. J.W.Bowden, A.M.Posner and J.P.Quirk, Australian J. Soil Res., 15 (1977) 121.
48. J.W.Bowden, S.Nagarajah, N.J.Barrow, A.M.Posner and J.P.Quirk, Australian J. Soil Res., 18 (1980) 49.
49. T.Hiemstra, in: 3rd International Conference on the Biogeochemistry of Trace Elements, Paris, 1995.
50. N.J.Barrow and B.W.Whelan, J. Soil Sci., 40 (1989) 17.
51. S.Goldberg and G.Sposito, Soil Sci. Soc. Am. J., 48 (1984) 772.
52. D.G.Lumsdon and L.J.Evans, J. Colloid Interface Sci., 164 (1994) 119.
53. I.Shainberg and W.D.Kemper, Soil Sci., Soc. Am. Proc., 30 (1966) 707.
54. I.Shainberg and W.D.Kemper, Soil Sci., 103 (1967) 4.
55. R.Strauss, G.W.Brümmer and N.J.Barrow, Europ. J. Soil Sci., in press.
56. F.J.Hingston, A.M.Posner and J.P.Quirk, J. Soil Sci., 23 (1972) 177.
57. N.J.Barrow, L.Madrid and A.M.Posner, J. Soil Sci., 32 (1981) 399.
58. D.J.Kinniburgh and M.L.Jackson, Soil Sci. Soc. Am. J., 46 (1982) 56.
59. N.J.Barrow, J. Soil Sci., 35 (1984) 283.
60. R.H.Neal and G.Sposito, Soil Sci., 33 (1982) 164.
61. N.J.Barrow and V.C.Cox, J. Soil Sci., 43 (1992) 305.
62. R.G.McLaren, J.H.Williams and R.S.Swift, Geoderma, 31 (1983) 97.
63. R.G.Gerritse and W.van Driel, J. Environ. Quality, 13 (1984) 197.
64. G.Sposito, Soil Sci. Soc. Am. J., 44 (1980) 652.

65. N.J.Barrow, Australian J. Soil Res., 27 (1989) 475.
66. A.E.Boekhold, E.J.M.Temminghoff and Van der Zee, J. Soil Sci., 44 (1993) 85.
67. J.R.Devine, D.Gunary and S.Larsen, J. Agricul. Sci., 71 (1968) 359.
68. N.J.Barrow and T.C.Shaw, Soil Sci., 19 (1975) 301.
69. N.J.Barrow and T.C.Shaw, Soil Sci., 124 (1977) 265.
70. N.J.Barrow and T.C.Shaw, Soil Sci., 124 (1977) 347.
71. B.R.Singh, Soil Sci., 138 (1984) 440.
72. E.A.Elkhatib, O.L.Bennet and R.J.Wright, Soil Sci. Soc. Am. J., 48 (1984) 758.
73. S.Kuo and D.S.Mikkelsen, Soil Sci., 128 (1970) 274.
74. M.C.Amacher, J.Kotuby-Amacher, H.M.Selim and I.K.Ishander, Geoderma, 38 (1986) 131.
75. R.F.Brennan, J.W.Gartrell and A.D.Robson, Australian J. Soil Res., 18 (1980) 447.
76. N.J.Barrow, J. Environ. Quality, 9 (1980) 644.
77. N.J.Barrow, J. Soil Sci., 34 (1983) 733.
78. N.J.Barrow, J. Soil Sci., 37 (1986) 267.
79. N.J.Barrow, J. Soil Sci., 42 (1991) 277.
80. N.J.Barrow and B.W.Whelan, J. Soil Sci., 40 (1989) 17.
81. N.J.Barrow, J. Soil Sci., 43 (1992) 421.

A. Dąbrowski and V.A. Tertykh (Editors)
Adsorption on New and Modified Inorganic Sorbents
Studies in Surface Science and Catalysis, Vol. 99

Chapter 3.8
Problems in modelling the electrical interfacial layer in metal/oxide aqueous systems

N. Kallay[a], S. Zalac[a] and I. Kobal[b]

[a]Laboratory of Physical Chemistry, Department of Chemistry,
Faculty of Science, University of Zagreb,
41001 Zagreb, P.O. Box 163, Croatia

[b]Department of Environmental Sciences, J.Stefan Institute,
61111 Ljubljana, P.O. Box 100, Slovenia

1. INTRODUCTION

Before discussing problems in modelling the electrical interfacial layer (EIL), one should answer two basic questions: What is "modelling" and what is its purpose?

In the narrow sense modelling is a simplified description of a physical phenomenon (substance or process) which serves for writing basic equations representing the properties of the system. In the broader sense the term "model" is used for theory and also includes basic equations, as well as the resulting relationships. Physical chemistry is concerned with both theoretical and experimental aspects. Figure 1 is a scheme that represents activity in a certain field. The example is given for the physical chemistry of ionic adsorption.

In principle, for one person, it is not necessary to be involved in the whole cycle; one can deal with a part of it. However, the whole community should consider all aspects of the problem if the problem is considered scientifically.

The second question was related to the purpose of modelling a physical phenomenon. Since physical chemistry is a quantitative section of chemistry and lies at the overlap between physics and chemistry, one can conclude that the purposes of modelling are:

1. To understand of specific phenomena on the basis of a few simple principles. Examples: (i) the concept of the equilibrium constant for dissociation of acetic acid. (ii) the effect of surface potential on the surface reaction enthalpy.
2. To provide the relationships which enable calculation of a certain property (physical quantity) from other measured data. Examples: (i) evaluation of the equilibrium constant of the dissociation of acetic acid from pH measurements. (ii) evaluation of surface reaction enthalpy from the temperature jump in a calorimeter, or from the temperature dependency of the point of zero charge.
3. To describe complex surface equilibrium under different conditions by introduction of a few parameters (constants). Examples: (i) calculation of the pH of a solution containing acetic acid and sodium acetate at various concentrations. (ii) in principle one should be

able to calculate the surface charge for a suspension of known composition using values of parameters such as intrinsic equilibrium constants, capacities of assumed condensors, etc.

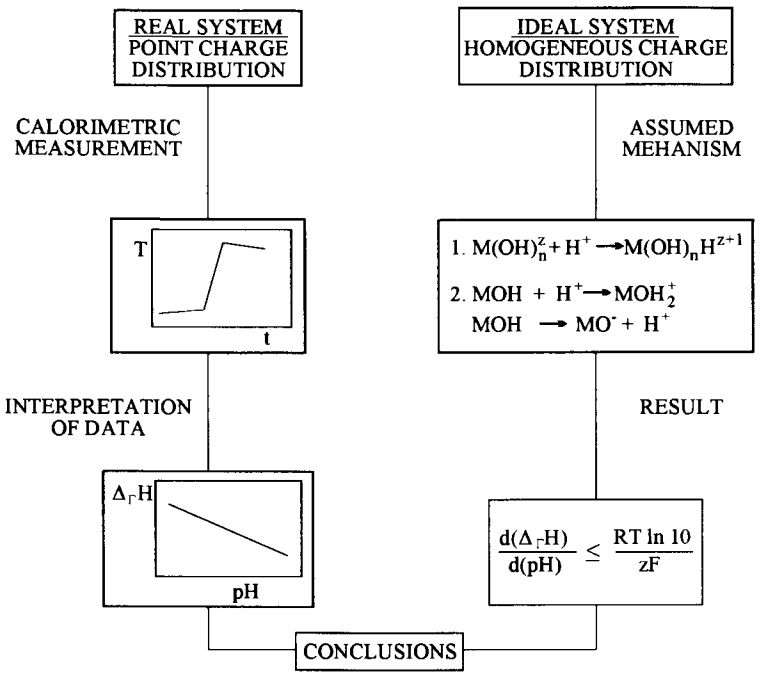

Figure 1. Schematic representation of a procedure applied to the thermochemistry of surface charging.

The above considerations indicate some different areas of research activity in the field of the electrical interfacial layer. The state of the art in this field is far from that which is common in solution chemistry. The problem is that the situation in the interfacial region is so complicated that one is forced to introduce substantial simplifications in the course of the "modelling procedure". In addition, the situation is sometimes unknown, so that one should introduce several hypotheses in treating the interfacial equilibria. With respect to the solution chemistry, the experimental data are significantly less accurate and reproducible so that several different models cannot be separated and may coexist. The choice of model used in an interpretation would depend on the taste and ability of the author. In this field it is an achievement to understand the phenomena on a semiquantitative basis; in some cases it is possible to recalculate the measurements, but data acquisition is left for the future. It would be desirable to standardise the interpretation and to produce tables with equilibrium parameters, e.g. for different oxides in order to predict their properties under different conditions (temperature, pH, electrolyte concentration, etc.). In fact, the poor reproducibility of experimental systems leads to scattering of results, even for such simple characteristics as the point of zero charge [1,2]. The apparent "advantage" of the described state of art lies in the fact that experimental data can be fitted

(interpreted) using any of a number of known theoretical concepts, and is also facilitated by the relatively large number of adjustable parameters (constants) [3,4].

In practice any theoretical concept could be refined by introducing more parameters, or by considering specific conditions representing reality. By doing so one might believe that the model is closer to the real system. The question is how far one could go with such a strategy. The answer is simple: the refinement of theory is reasonable if it has connection with the experiments. Theory may advance a few steps before experiments, but its development to the state when experimental verification is impossible has little sense. One example is the introduction of numerous parameters in the relationship describing the charging of an interface; with a sufficient number of parameters one can fit any experiment. To distinguish between two different theoretical concepts one should either improve the accuracy of measurements or introduce new experimental techniques.

This chapter is devoted to a description and interrelation of present theoretical models. The aim is to clarify the some problems and to suggest possible solutions. From the experimental point of view, one may develop new methods on the basis of existing experimental techniques, but it would be of essential interest to refine and develop new techniques, i.e. interfacial spectroscopy. The modelling of equilibria in the electrical interfacial layer involves:

1. stoichiometry of surface reactions,
2. structure of the electrical interfacial layer,
3. definition of (intrinsic) equilibrium constants,
4. mass balances (summation of the amounts of present species),
5. relationships between surface charges and corresponding electrostatic potentials (capacities, diffuse layer),
6. physical meaning of electrokinetic potential and slipping plane.

2. SURFACE COMPLEXATION MODEL

In the area of interfacial charging at the solid/liquid interface of metal oxide aqueous suspensions, the "surface complexation" or "site binding" concept is commonly used [3-20]. This concept is characterised by consideration of specific ionic reactions with surface groups, rather than assuming simple binding of ions to the surface or their accumulation at the interface (adsorption). In the past decade several different models were introduced on the basis of the surface complexation model (SCM); they differ in the assumed structure of the electrical interfacial layer (EIL) and in the proposed mechanisms and stoichiometries of surface reactions leading to surface charge.

2.1. Structure of the interfacial layer

The history of development of ideas concerning the electrical interfacial layer (EIL) originates in the mercury electrode phenomena. This concept was later applied and adapted to the metal oxide aqueous interface. The fundamental difference lies in the fact that the potential of a metal electrode is determined by an applied source of electricity, while the surface of an oxide is charged due to interactions and accumulation of ionic species at the interface. Even the simple situation at a metal oxide aqueous interface requires a relatively complicated picture of the EIL. Several different assumptions are in use. Two

of them, which are representative, are displayed on Figure 2 [4]. The double layer model (DLM) includes two layers, i.e. the inner (space between 0- and β-planes) and the diffuse layer (starting from the d-plane which is identical to the β-plane). The triple layer model (TLM) introduces a third layer, i.e. the layer between the β- and d- planes. By using the TLM one assumes that hydrated ions from the diffuse layer cannot approach the position of the β-plane.

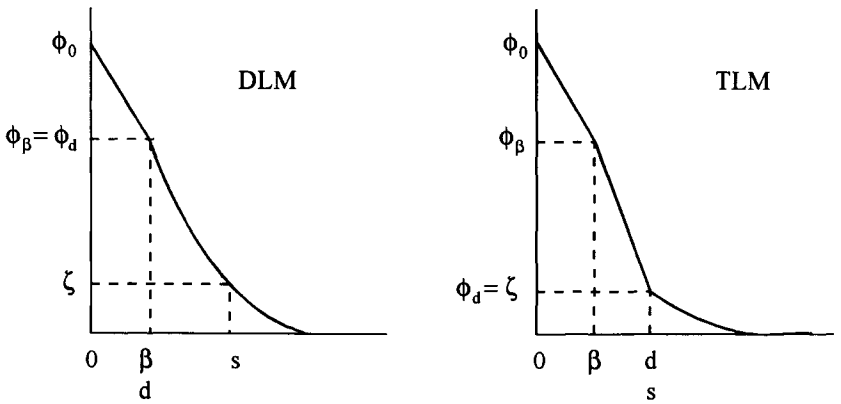

Figure 2. Schematic presentation of the electrostatic potential profile in the interfacial region according to the double layer model (DLM) and triple layer model (TLM).

In both models of the EIL several planes are assumed; the 0-plane in which surface charges are located, the β-plane characterising the position of centres of associated counterions, the d-plane which marks the onset of the diffuse layer, and the s-plane, i.e. "slipping plane" with electrokinetic ζ-potential. Other characteristic potentials (ϕ) are denoted by subscripts corresponding to specified planes. The difference between these two models could be summarised as: $\phi_0 > \phi_\beta = \phi_d > \zeta$ and $\phi_0 > \phi_\beta > \phi_d = \zeta$ (for DLM and TLM, respectively). By considering Figure 2 one can conclude that the potential drop from the 0-plane to the bulk of solution is similar so that in both models the characteristic potentials (ϕ_0, ϕ_β, ζ) should be the same. A substantial difference is that the potential drop between β- and s-planes is independent of ionic strength in the case of the TLM, while it is given by the Gouy - Chapman theory when the DLM is used. In the latter case the electrokinetic slipping plane is located within the diffuse layer so that its separation from the onset of the diffuse layer should be introduced.

The presence of organic ions or (hydrolyzed) multivalent metal ions requires an even more sophisticated approach to the EIL, and the modelling is usually more speculative. Common practice usually leaves open the problem of the point charge concept, in contrast to the homogeneous charge. Another problem which is not considered in practical applications is the structure of water in the interfacial region, which is connected to the homogeneity of the available space and the choice of the value of the relevant permittivity. The use of bulk permittivity results in an apparent value of all the space parameters of the EIL.

2.2. Mechanism and stoichiometry of surface charging

Three different concepts are in use for a description of the charging an oxide surface. Regardless of the mechanism taking place at the interface, one is in principle able to apply different stoichiometric equations for the same process. The values of the physical quantities describing the properties of a process depend directly on the way in which the reaction equation is written. This problem concerns quantities such as the extent of reaction, standard equilibrium constant, reaction enthalpy, etc. This section is devoted to relationships between thermodynamic quantities corresponding to different assumed stoichiometries. The mechanisms of the reactions are discussed in Chapter 3.6.

Adsorption concept

One approach to surface charging is the binding of potential determining ions (for oxides: H^+ and OH^- ions) on an active surface site, i.e. on a part of the surface (S). This concept is equivalent to adsorption [21,22]. The reaction equation could be then written as binding of hydronium ions, i.e. protons (reaction bp):

$$S + H^+ \longrightarrow SH^+; \quad \zeta_{bp},\ K^0_{bp},\ \Delta_{bp}H^0 \tag{1}$$

and binding of hydroxide ions (reaction bh)

$$S + OH^- \longrightarrow SOH^-; \quad \zeta_{bh},\ K^0_{bh},\ \Delta_{bh}H^0 \tag{2}$$

where ζ_r is extent of reaction, K^0_r the standard equilibrium constant and Δ_rH^0 is the standard enthalpy of reaction.

"2–pK" concept

It may be assumed that hydration of an oxide surface results in surface hydroxide groups bound to metal ions (MOH), and that these groups have amphoteric character [4,20.22,23]. The following equilibria are assumed: surface protonation (reaction p)

$$MOH + H^+ \longrightarrow MOH_2^+; \quad \zeta_p,\ K^0_p,\ \Delta_pH^0 \tag{3}$$

and surface deprotonation (reaction d)

$$MOH \longrightarrow MO^- + H^+; \quad \zeta_d,\ K^0_d,\ \Delta_dH^0 \tag{4}$$

Neutralisation (reaction n) is characterised by:

$$OH^- + H^+ \longrightarrow H_2O; \quad K^0_n,\ \Delta_nH^0,\ \Delta\zeta_n \tag{5}$$

with the equilibrium constant, K^0_n, related to the "ionic product" of water, K^0_w ($K^0_n = 1/K^0_w$).

"1–pK" concept

By applying a coordination concept one assumes protonation of only one kind of surface sites. By protonation the charge number of surface species (z) increases by one [16,17,24–26]. The actual charge of the site depends on the type of oxide, i.e. on the coordination number of the metal ion. The general reaction equation is:

$$M(OH)_n^z + H^+ \longrightarrow M(OH)_nH^{z+1}; \quad \zeta_h,\ K_h^0,\ \Delta_hH^0 \tag{6}$$

For example, charging of an alumina surface (see Chapter 3.6.) is represented by the reaction equation

$$AlOH^{1/2-} + H^+ \longrightarrow AlOH_2^{1/2+} \tag{7}$$

Surface heterogeneity

The refined treatment of surface equilibria considers different kinds of surface sites with respect to their reactivity [25–27]. Formally one may solve this problem by using any of the three above concepts by introducing two (or more) different values of the corresponding equilibrium constants. In doing so the mass balance of surface sites should be corrected appropriately.

Counterion association

Effective surface charge is reduced by association of counterions with charged surface groups. If the amphoteric (2–pK) concept is applied, the association of counterions, i.e. anions (A^-) and cations (K^+) is represented as:

$$MOH_2^+ + A^- \longrightarrow MOH_2 - A \tag{8}$$

$$MO^- + K^+ \longrightarrow MO - K \tag{9}$$

From the stoichiometric point of view, reaction equations describing association of counterions do not depend on the choice of the model; binding of one counterion to the oppositely charged surface site always occurs.

2.3. Equilibrium of surface reactions

There are two approaches to the equilibrium constants of surface reactions. Originally, the so–called "intrinsic" approach was developed [28]. For example, binding of a proton to a surface site was separated into two steps. In the first step the proton was "transferred" from the bulk of solution (aq) to the space in the vicinity of the surface site (int). This equilibrium was treated by Boltzmann statistics, so that the distribution was affected by the electrostatic potential of that space (ϕ_{int}). The second process was chemical binding with the surface site represented by so–called "intrinsic" equilibrium constant (K_{int}):

$$H^+_{(aq)} \longrightarrow H^+_{(int)}; \qquad K_1 = \exp(-zF\phi_{int}/RT) \tag{10}$$

$$H^+_{(int)} \longrightarrow H^+_{(bound)}; \qquad K_2 = K_{int} \tag{11}$$

Summation of above two reactions yields:

$$H^+_{(aq)} \longrightarrow H^+_{(bound)}; \qquad K = K_1K_2 = K_{int} \exp(-zF\phi_{int}/RT) \tag{12}$$

The second approach is to introduce activity coefficients of charged surface sites. In both cases one obtains the same result. The electrostatic contribution to the Gibbs energy depends on the charge number and on the electrostatic potential affecting the energy state of the surface species. Generally, the activity coefficient of surface species of charge number z is equal to $\exp(-zF\phi/RT)$. By applying TLM or DLM to the amphotheric (2-pK) concept, one can write the following relationships:

$$K^0_p = e^{F\phi_0/RT} \frac{\Gamma_{MOH^+_2}}{a_{H^+}\Gamma_{MOH}} \tag{13}$$

$$K^0_d = e^{-F\phi_0/RT} \frac{a_{H^+}\Gamma_{MO^-}}{\Gamma_{MOH}} \tag{14}$$

$$K^0_k = e^{F\phi_\beta/RT} \frac{\Gamma_{MOK}}{a_{K^+}\Gamma_{MO^-}} \tag{15}$$

$$K^0_a = e^{-F\phi_\beta/RT} \frac{\Gamma_{MOH_2A}}{a_{A^-}\Gamma_{MOH^+_2}} \tag{16}$$

where Γ is the surface concentration (amount of surface groups divided by surface area), a is the ionic bulk activity, while F, R and T have their usual meaning.

When treating the association of counterions one may also apply the association statistics (AS) model which is equivalent to the Bjerrum theory for ion pairing in an electrolyte solution [29,30]. However, in the case of surface association space is available only on the side of the liquid. Another difference is due to the critical distance which depends on direction and is a function of the surface potential. This theory explains why two ionic species may associate at the surface despite the fact that they do not undergo ion pairing in the bulk of solution. According to the Bjerrum theory, ions of large effective size cannot approach the critical distance and such an electrolyte is completely dissociated. At the surface the critical distance extends by increasing surface potential and once the surface potential exceeds the critical value, at which the critical distance matches the minimum separation, association at the interface proceeds.

Relations between thermodynamic quantities

The values of thermodynamic quantities associated with chemical reactions depend on the way how a reaction equation for a given process is written. Accordingly, different assumed stoichiometries for the same process would result in different values of e.g. extent of reaction, equilibrium constants, reaction enthalpies, etc. The question is trivial

so that this section includes only the equations enabling recalculation of the parameters of different models. The following equations may be used for this purpose:

$$K_h^0 = \sqrt{\frac{K_p^0}{K_d^0}} = \sqrt{\frac{K_{bp}^0}{K_{bh}^0 K_w^0}} \tag{17}$$

$$\Delta_h H^0 = \frac{\Delta_p H^0 - \Delta_d H^0}{2} = \frac{\Delta_{bp} H^0 - \Delta_n H^0 - \Delta_{bh} H^0}{2} \tag{18}$$

Index h applies to 1–pK model, while indices p and d denote protonation and deprotonation reactions when the amphoteric (2–pK) concept is applied. The assumed adsorption mechanism is characterised with indices bp and bh.

2.4. Surface charge densities

Use of the above treatment implies surface concentrations of charged species (Γ) and different kinds of surface potentials (ϕ). In solving the equilibria at the interface, one should define the surface charge densities of different postulated planes (σ). For the amphoteric (2–pK) concept the surface charge densities in the 0– and β–planes are defined as:

$$\sigma_0 = F\left(\Gamma_{MOH_2^+} + \Gamma_{MOH_2A} - \Gamma_{MOH_2^-} - \Gamma_{MO-K}\right) \tag{19}$$

$$\sigma_\beta = F\left(\Gamma_{MOH_2A} - \Gamma_{MO-K}\right) \tag{20}$$

The effective (net) surface charge density, caused by the charges fixed at the surface, (σ_s), is equal in magnitude to the charge density in the diffuse layer (σ_d)

$$\sigma_s = -\sigma_d = \sigma_0 - \sigma_\beta \tag{21}$$

An analogous treatment applies to the adsorption concept, i.e. when reactions (1) and (2) are assumed. However, for the coordination concept (1–pK)

$$\sigma_0 = F\left(\Gamma_{M(OH)_n^z} + \Gamma_{M(OH)_nH^{z+1}}\right) \tag{22}$$

Calculations of charge densities σ_β and σ_s are the similar for all possible reaction stoichiometries.

2.5. Relationships between surface charges and potentials

In the case of the double layer model (DLM) one postulates an inner layer capacitor of constant capacity C_1 with two planes 0 and β. The distance between these two planes (d) would correspond to the minimum separation between centres of charged surface groups and the centres of the associated counterions. By applying this hypothesis one can introduce the concept of the permittivity (ε) of the space between two planes and use the value of the bulk permittivity of the electrolyte. It is clear that in such a case all parameter values are artificial. The other problem is that inner capacitor is not an electroneutral system [23,31–33]. However, despite these problems, the following equation is commonly used:

$$C_1 = \frac{\sigma_0}{\phi_0 - \phi_\beta} = \frac{\varepsilon}{d} \tag{23}$$

The more "refined" triple layer model introduces one more capacitor of constant capacity C_2. The inner plane of that capacitor is the β-plane while the second, d-plane is the imaginary onset of the diffuse layer:

$$C_2 = \frac{\sigma_s}{\phi_\beta - \phi_d} \tag{24}$$

The relationship between σ_s and the potential at the onset of the diffuse layer (ϕ_d) depends on the ionic strength (I_c) and is given by the Gouy-Chapman relationship

$$\sigma_s = \sqrt{8RT\varepsilon I_c}\sinh\left(F\phi_d/2RT\right) \tag{25}$$

or

$$\phi_d = \frac{2RT}{F}\ln\left(\frac{\sigma_s}{2\sqrt{2RT\varepsilon I_c}} + \sqrt{\frac{\sigma_s^2}{8RT\varepsilon I_c} + 1}\right) \tag{26}$$

Formally, the diffuse layer could be considered as a capacitor, the capacity of which (C_{GC}) depends on ionic strength and on the surface potential ϕ_d

$$C_{GC} = \frac{\partial\sigma_s}{\partial\phi_d} = \sqrt{\frac{2F^2\varepsilon I_c}{RT}}\cosh\left(\frac{F\phi_d}{2RT}\right) \tag{27}$$

Problems in using the Gouy-Chapman theory are commonly recognised. Despite its highly approximate description of the diffuse layer, this theory is in use since it enables a complete solution of the equilibria at the charged interface, regardless of the level of approximations introduced.

3. ELECTROKINETICS

In addition to adsorption data electrokinetic measurements supply independent data useful in interpretation and also in evaluation of different theoretical models. Electrokinetic measurements yield e.g. electrophoretic mobility, which could, with more or less justification, be converted to the electrokinetic potential [5].

3.1. Meaning and use of electrokinetic potential

Questions related to the theoretical basis of the conversion of electrophoretic mobility to electrokinetic potential are directly related to the physical meaning of the latter quantity. The commonly accepted simplified picture of the slipping plane, the plane at which potential is equal to ζ-potential, introduces new assumptions regarding the structure of the interfacial layer. The high affinity of counterions for binding with charged surface groups could be explained only on the basis of a high ϕ_d value. In order to satisfy this condition, in the case of the double layer model one should locate the slipping plane within the diffuse layer and introduce the separation distance [23,34]. When the TLM is used one may simply identify the slipping plane with the onset of the diffuse layer [7]. In the latter case the potential drop between the β-plane and the slipping plane is given by the capacitance of the second capacitor.

It was believed that the effect of ionic strength on the electrokinetic potential might produce the value of the slipping plane separation. The well known method by Eversole, Lahr and Boardman is based on the assumption of constancy of the potential at the onset of the diffuse layer ϕ_d [35,36]. Since the ϕ_d value should decrease with ionic strength one can only determine the upper limit of the value of the separation distance [4]. The following form of the Gouy–Chapman theory is used for that purpose:

$$\phi_d = \frac{e^{-x_e\kappa} + \tanh(F\zeta/4RT)}{e^{-x_e\kappa} - \tanh(F\zeta/4RT)} \tag{28}$$

where x_e is the slipping plane separation, and κ is the reciprocal Debye–Hückel distance

$$\kappa = \sqrt{\frac{2F^2 I_c}{\varepsilon RT}} \tag{29}$$

Equation (28) may be converted to linear form so that x_e may be obtained from the slope according to the following relationship:

$$\ln\tanh\left(\frac{F\zeta}{4RT}\right) = \ln\tanh\left(\frac{F\phi_d}{4RT}\right) - \kappa x_e \tag{30}$$

The other approach to determination of the slipping plane separation is based on the simultaneous interpretation of adsorption and electrokinetic data, yielding a value of 6 to 10 Å for aqueous systems.

Electrokinetic measurements also yield a value of the surface charge; one simply conversts the zeta potential to the electrokinetic surface charge density by the Gouy–Chapman function via Eq. (25). This approach yields the so–called electrokinetic charge, i.e. the charge of the movable particle together with the accompanying liquid medium, and is even more speculative since its relationships to the charge density of any assumed or postulated plane is questionable.

The only quantity resulting from electrokinetic measurements, the physical meaning of which is not model dependent, is the isoelectric point. In fact, most electrokinetic results are used in the sense that the surface is positively charged "below" the isoelectric point (pH_{iep}) and negatively charged "above" that value. In addition, electrokinetic measurements are also interpreted with a semiquantitative meaning; e.g. one concludes that a higher value of electrophoretic mobility or ζ–potential corresponds to surfaces bearing a higher charge density.

3.2. Isoelectric point and point of zero charge

Despite the fact that the point of zero charge (pzc) is defined in different ways with respect to the isoelectric point (iep), both quantities are intended to characterise the condition of interfacial electroneutrality. The eloctrokinetic quantity iep represents the conditions of zero–electrokinetic charge or potential. The point of zero charge require a knowledge of the origin of surface charge and applies to conditions in which the surface charges produced by reactions with potential determining ions cancel. As an experimental quantity it is defined by the constancy of p.d. ion activities despite an increase in solid content, which means e.g. that the amount of H^+ ions that are bound to the surface is

equal to the amount of released H^+ ions (2–pK model). For oxides, potential determining ions are H^+ and OH^- ions so that the pzc, in view of 1–pK model, is defined as:

$$\Gamma_{M(OH)_n^z} + \Gamma_{M(OH)_nK^{z+1}} = \Gamma_{M(OH)_nH^{z+1}} + \Gamma_{M(OH)_nHA^z} \tag{31}$$

while for the 2–pK model the pzc is corresponds to

$$\Gamma_{MOH_2^+} + \Gamma_{MOH_2A} = \Gamma_{MO^-} + \Gamma_{MOK} \tag{32}$$

The two above equations simplify in the absence of counterion association. The values of pzc and iep coincide if no specific adsorption of other ions takes place and in addition, if counterion association is negligible or symmetrical (same amounts of associated cations and anions [4]). In such a case $\phi_0 = 0$, so that one may simply relate iep and pzc with the equilibrium constants of surface reactions.

For both 1–pK and 2–pK models the following relationship holds:

$$pH_{pzc} = 0.5 \log \frac{K_P^0}{K_d^0} = \log K_h^0 \tag{33}$$

3.3. Determination of iep and pzc

Determination of the isoelectric point by electrokinetic methods is simple. The accuracy depends on control of the conditions such as pH and in the case of electrophoresis, on the positioning of the stationary layer [5,37]. A shortcoming of common methods is that one cannot characterise conductive samples.

According to its definition, the point of zero charge is related to reactions involving potential determining ions. The common method for pzc determination is potentiometry [5]. In the case of pure oxide sample one can obtain the pzc value simply by comparing potentiometric titrations of a suspension with one performed in the absence of disperse solid phase. The problem is that one can be never sure of the purity of the sample, so that the pzc should be evaluated from the intersection of the charge functions obtained at different ionic strengths. In that case each titration provides only the relative value of surface charge density, while the common intersection point provides information on the absolute zero value of the charge density. This approach require the absence of specific adsorption of ions other than p.d. ions and negligible or symmetric surface association of counterions. In that case the pzc coincides with the iep [4]. A simplified experimental approach is to add electrolyte to suspensions at different pH values. The system which does not change pH upon electrolyte addition is that at the pzc. The main shortcoming of potentiometric pzc determination is the requirement for electrolyte addition. These methods use relatively high electrolyte concentrations so that the theoretical requirements are questionable. At high counterion concentrations one cannot simply assume negligible counterion association, or the "symmetric case" in which the amount of bound cations is the same as amount of bound anions; at high concentrations even small difference in the association affinities would lead to an undesirable disbalance. There is another problem related to drastic increase in ionic strength; the change in liquid junction potential of the reference electrode may be taken as the apparent change in pH. An additional problem is related to the accuracy with which the intersection point can be located.

Recently two methods applicable in low ionic strength conditions were developed: (i) the mass titration method [38,39], and (ii) the adhesion method for solving the problem of sample conductivity [40–42].

Adhesion method

The adhesion method was developed for determination of the isoelectric point [40,41]. In fact this method enables detection of the condition under which the potential at the onset of the diffuse layer is zero [43–45]. The principle of the method is simple: at low ionic strength colloidal particles adhere to the oppositely charged surface but they are repelled from the surface of the same charge sign. Therefore if one intends to examine the iep of a metallic surface one should use colloid particles of a charge which does not depend on the pH in the region of interest as sensor. As sensor particles one may use latex or silica particles, etc. A convenient method is the column technique [40–42]: the column is filed with grains of the metal to be examined. One changes the pH of the suspension passing through the column and measures the particle number concentration in the outlet. The light scattering technique is useful for this purpose. The logarithm of the ratio of the particle number concentrations of the inlet to the outlet suspensions is proportional to the rate constant (k) of adhesion (particle attachment) [43–45]. Figure 3. represents the determination of the isoelectric point of tin [46]. Since the adhesion method could be used for conductive samples, it was found useful in explaining the origin of charge at metallic surfaces [40,41], and also for monitoring corrosion process [42].

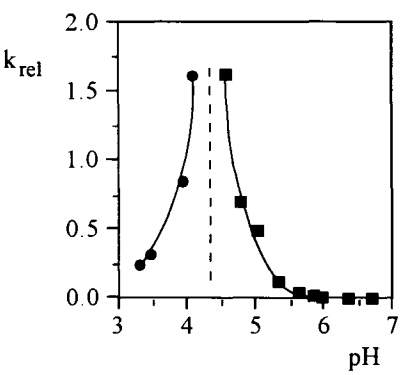

Figure 3. Determination of the isoelectric point of tin by adhesion method. Results are obtained by suspension of negative (■) and positive (●) latex particles [46].

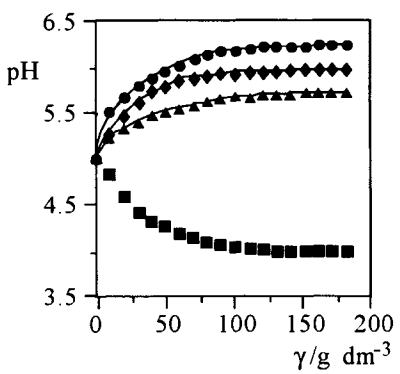

Figure 4. Effect of acidic and basic contamination, u, on the results of mass titration with a hematite suspension [47]. u/mol g^{-1}: (●) – 10^{-6}, (◆) 0, (▲) 10^{-6}, (■) 10^{-5}.

Mass titration

The mass titration method is based on work by Noh and Schwarz who showed that addition of an oxide powder to an electrolyte solution changes the pH to a constant value which corresponds to the point of zero charge [38]. The method was experimentally and

theoretically verified, but the problem is that one can never be sure of the purity of solid samples. Further work dealt with samples contaminated with acid or base [39]. Figure 4. displays the effect of acidic and basic contamination ($u/molg^{-1}$) on the experimental results with hematite [47]. It is clear that acidic contamination results in a final pH which is significantly higher than the pzc, while base produces the opposite effect. It was also shown that the resulting pH is very sensitive to small amounts of contaminants.

The problem of sample contamination was solved by performing the potentiometric acid–base titration with a concentrated oxide suspension [39]. The concentration of the solid phase should be enough high to ensure a constant pH value, i.e. the pH value corresponding to the plateau in Figure 4. Figure 5a. presents results of such an experiment obtained with a hematite suspension, while Figure 5b. was obtained by numerical simulation based on the surface complexation (SC) model combined with the Gouy–Chapman–Stern structure of the interfacial layer (DL–assumption) [47]. According to theoretical analysis based on the surface complexation model, the inflection of the function corresponds to the pzc and also provides information on the amount of acidic or basic contaminants.

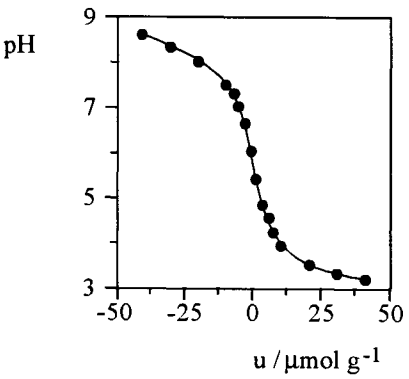

Figure 5a. Potentiometric acid–base titration of a concentrated hematite suspension [47].

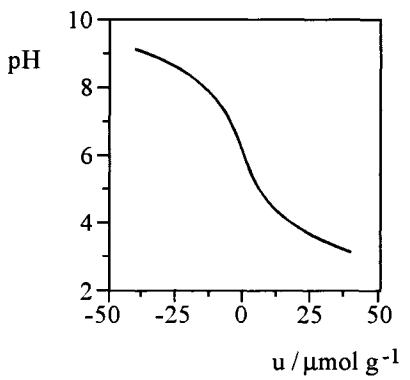

Figure 5b. Numerical simulation of the potentiometric acid–base titration based on the SC model [47].

From a theoretical point of view, this method is essentially model–independent, since at zero–charge conditions different models are equivalent and yield the same result. The main advantages of the mass titration method lies in its simplicity and accuracy. The latter characteristics are the same as those of pH measurements. As for any other potentiometry in suspension, problems could arise in control of the sedimentation potential and the electrode suspension effect. The are no additional problems such as that arising from a high electrolyte concentration since the method can be used at extremely low ionic strengths. The possibilities of the method were demonstrated in evaluation of the temperature effect on the pzc, yielding the enthalpy of surface charging [22]. Samples with higher specific area are more suitable for examination by the mass titration method.

4. CALORIMETRY

In order to better understand the equilibria in the interfacial layer, it is desirable to obtain the thermodynamic parameters of the reactions involved in the surface charging processes. It is not a simple task to determine the enthalpy of specified surface reactions. At first the mechanisms of the reactions are not always clear, and secondly the situation is often so complicated that several contributions can hardly be distinguished. In the most simple case, when association of counterions does not take place (low ionic strength), one can use measurements of the temperature dependency of the point of zero charge [48–56]. The slope of the pH_{pzc} vs. reciprocal thermodynamic temperature yields the enthalpy value dependent on the assumed stoichiometry of the processes. Application of the "adsorption" or "amphotheric" or "coordination" concept yield [22]

$$\frac{d(pH_{pzc})}{d(1/T)} = \frac{\Delta_d H^0 - \Delta_p H^0}{2R \ln 10} = -\frac{\Delta_h H^0}{R \ln 10} \tag{34}$$

Reaction enthalpies obtained from the temperature dependency of the pzc are standard values corresponding to dilute systems. Figure 6. displays the results with hematite obtained by the mass titration method, which is suitable because of its applicability at low ionic strength.

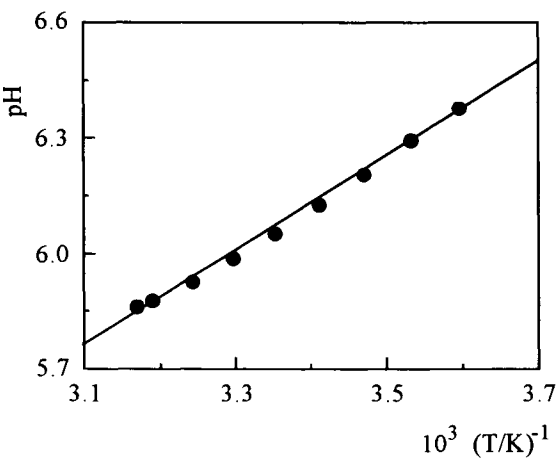

Figure 6. The dependence of pH_{pzc} value of a hematite suspension on temperature. The ionic strength (10^{-3} mol dm^{-3}) was controlled by $NaNO_3$ [68].

The direct method for enthalpy determination is calorimetry [55–67]. This technique enables the heat of surface reactions to be measured in more complicated situations, e.g. in the pH regions outside the pzc region, and also in the case of (specific) adsorption of species other than p.d. ions. However, the measured heat is a sum of the contributions of all reactions taking place at the interface, so that in interpretation of data one meets the problem of distinguishing between the different contributions. An additional problem is to account for electrostatic effects. On the other hand, one can always express the results as the enthalpy per amount of adsorbed species or per surface charge. When doing so the

result is not comparable with the standard enthalpy of a specified reaction as obtained from the dependence pzc on temperature. The problem of designing the calorimetric experiment and of the appropriate interpretation of data may be solved in simple cases, i.e. for charging of a surface by interactions with potential determining ions [22].

4.1. Determination of the standard enthalpy of surface reactions

In order to evaluate the standard enthalpy of surface reactions involving potential determining ions by calorimetry, one should first perform a theoretical analysis to find the appropriate experimental conditions. It is possible to avoid electrostatic effects by performing "symmetric" experiments, i.e. experiments in which the point of zero charge is exactly the mean value of the initial and final pH [22,55,56].

If one applies the "coordination concept" (1–pK model), the interpretation is simple [22]: one calculates the extent of reaction (6) by considering the change in equilibrium amounts of H^+ ions ($\Delta n(H^+)_{eq}$) which correspond to the difference in the final and initial pH values

$$\Delta\xi_h = n(HNO_3) - \Delta n(H^+)_{eq} = n(HNO_3) - \Delta\xi_n - c^0\left(\frac{V_2 \cdot 10^{-pH_2}}{y_2} - \frac{V_1 \cdot 10^{-pH_1}}{y_1}\right) \quad (35)$$

where $n(HNO_3)$ is the amount of added acid (which is zero if base is added), V is the volume of liquid phase, while indexes $_1$ and $_2$ denote the initial and final step of the experiment, respectively. The standard concentration is $c^0 = 1$ mol·dm^3. The hypothetical ionic activity coefficient (y) can be calculated by means of the Debye-Hückel limiting formula.

When the "amphoteric" concept (2–pK model) is applied one deals with two surface reactions [22], i.e. with protonation (3) and deprotonation (4). The extent of these reactions is same in magnitude but opposite in sign if the Nernstian equation for the surface potential holds, which is not true for real systems [69]. However, in the case of the "symmetric" experiment the protonation and deprotonation reactions are opposite in direction with the same magnitudes of their extents, regardless to the obedience of the Nernst equation. The extents of surface reactions p and d are:

$$\Delta\xi_d = -\Delta\xi_p = 0.5\left[n(HNO_3) - \Delta\xi_n - c^0\left(\frac{V_2 \cdot 10^{-pH_2}}{y_2} - \frac{V_1 \cdot 10^{-pH_1}}{y_1}\right)\right] \quad (36)$$

The neutralisation may also take place in the system, the extent of which ($\Delta\xi_n$) can be calculated by considering the change in the equilibrium amounts of OH^- ions and the amount of added base:

$$\Delta\xi_n = n(NaOH) - K_w c^0\left(\frac{V_2 \cdot 10^{pH_2}}{y_2} - \frac{V_1 \cdot 10^{pH_1}}{y_1}\right) \quad (37)$$

If acid is added to the system: $n(NaOH) = 0$.

The measured heat (Q) is the sum of surface charging and bulk neutralisation effects, so that the contribution of the latter process should be subtracted.
For reaction stoichiometry corresponding to the 1–pK model:

$$\Delta_h H^0 = \Delta_h H = \frac{Q - \Delta_n H^0 \Delta\xi_n}{\Delta\xi_h} \quad (38)$$

If the 2-pK concept is applied, one gets the difference in enthalpies of the deprotonation and protonation reactions from:

$$\Delta_{ch}H^0 = \Delta_pH^0 - \Delta_dH^0 = \Delta_pH - \Delta_dH = \frac{Q - \Delta_nH^0\Delta\xi_n}{\Delta\xi_p} \tag{39}$$

In the "symmetric" experiment the difference between the initial pH and pH_{pzc} is the same as the difference between pH_{pzc} and the final pH, so that the surface potentials of the initial and final states are same in magnitude but opposite in sign, and consequently the electrostatic contributions cancel. Accordingly, the calculated enthalpies are the standard reaction enthalpies. These standard enthalpies are defined in the same way as those which one obtains from the temperature dependency of pH_{pzc}.

4.2. Electrostatic effect

A more advanced task would be to use calorimetry for examination of the electrostatic effect on the enthalpies of surface reactions. In doing so it is necessary to account for two different contributions to the enthalpy, i.e. the "chemical", Δ_rH^0, and "electrostatic" terms

$$\Delta_rH = \Delta_rH^0 - z_rF\phi_0 \tag{40}$$

where z_r is the change in the charge number of a surface group due to reaction. The surface potential can be approximated by the Nernstian equation

$$\phi_0 = \frac{RT\ln 10}{F}(pH_{pzc} - pH)\alpha \tag{41}$$

where coefficient α represents deviation from the ideal slope. The electrostatic effect on the enthalpy of surface reaction(s) could be examined by titration in a calorimeter [70]. One adds successive portions of reagent (acid or base) to an oxide suspension. To minimise the effect of neutralisation, it is advisable to add acid to acidic and base to basic suspension. The initial pH should be close to pH_{pzc} but still far enough from the isoelectric condition so that suspension remains stable.

Interpretation on the basis of the 1-pK model is direct and simple. One uses equations (35) and (37) and calculates the extent of reaction h and of neutralisation. The latter may be neglected if the experiment is performed as mentioned above. The enthalpy could be evaluated via Eq. (38), but the value obtained is not the standard one. The plot of enthalpy vs. mean value of initial and final pH corresponds to the ϕ(pH) function. The following equation may be used for evaluation of coefficient α:

$$\alpha = -\frac{d\phi}{d(pH)}\frac{1}{RT\ln 10} \tag{42}$$

A problem in interpretation on the basis of the 2-pK model is calculation of the extent of the protonation and deprotonation reactions. The following equation describes this situation:

$$\frac{\Delta\xi_p}{\Delta\xi_d} = -10^{(1-\alpha)(2pH_{pzc} - pH_2 - pH_1)} \tag{43}$$

The ratio $(\Delta\xi_p/\Delta\xi_d)$ is defined and independent of α if one performs the "symmetric" experiment, because in that case $2pH_{pzc} - pH_2 - pH_1 = 0$. In any other case the value of coefficient α is essential and should be taken into account. The following relationship could be used for interpretation of the calorimetric titration:

$$\frac{DQ + \Delta_{ch}H^0\Delta\xi_p}{\Delta\xi_p(D+1)} = \Delta_pH^0 + \alpha\left\{\frac{[RT\ln 10(pH_{pzc} - pH)](1-D)}{D+1}\right\} \tag{44}$$

Q is the measured heat corrected for the effect of neutralisation, function D is equal to $\Delta\xi_p/\Delta\xi_d$ and is given by Eq. (43). The extent of protonation is given by Eq. (36), and the value of $\Delta_{ch}H^0(= \Delta_dH^0 - \Delta_pH^0)$ should be determined separately by the "symmetric" experiment or by measuring the dependency of pH_{pzc} on temperature. Regression analysis provides information on the values of the parameters Δ_pH^0 and α.

5. APPLICATION OF THE SURFACE COMPLEXATION MODEL

The surface complexation model may be applied for interpretation of all phenomena resulting from the equilibria in the interfacial layer. For example, one may calculate the stability coefficient of an aqueous oxide suspension at given temperature, pH and electrolyte concentration. In the first step one uses the surface complexation model, and by knowing equilibrium parameters such as equilibrium constants of surface reactions, the relevant capacitances, one calculates the potential at the onset of the diffuse layer. This potential can be further used for obtaining the electrostatic interaction energy function which in combination with the van der Waals dispersion function provides the total energy of interaction between two particles. By using Fuchs theory the stability coefficient could be obtained. On the other hand, one is in principle able to consider the complex interfacial equilibria in systems containing various electrolytes like organic acids or multivalent hydrolizible cations. The following sections describe some problems related to this subject.

5.1. Adsorption of divalent metal ions

Adsorption of divalent ions will be discussed using the example of an aqueous hematite dispersion in the presence of $Co(NO_3)_2$, $NaNO_3$ and HNO_3 or NaOH [20]. In this case the equilibrium of hydrolysis of cobalt ions was taken into account

$$Co^{2+} + OH^- \longrightarrow CoOH^+ \tag{45}$$

In the interpretation 2-pK model was employed and binding of Co^{2+} to the hematite surface was considered by three possible reaction mechanisms

$$FeO^- + Co^{2+} \longrightarrow FeO\text{-}Co^+ \quad ; \quad K_1^0 \tag{46}$$

$$2FeO^- + Co^{2+} \longrightarrow (FeO_2)\text{-}Co \quad ; \quad K_2^0 \tag{47}$$

$$FeO^- + CoOH^+ \longrightarrow FeO\text{-}CoOH \; ; \quad K_3^0 \tag{48}$$

The equlibria of these reactions are given by:

$$K_1^0 = e^{-2F\phi_i/RT} \frac{\Gamma_{FeOCo^+}}{a_{Co^{2+}}\Gamma_{FeO^-}} \tag{49}$$

$$K_2^0 = e^{-2F\phi_i/RT} \frac{\Gamma_{(FeO)_2Co}}{a_{Co^{2+}}\Gamma_{FeO^-}} \tag{50}$$

$$K_3^0 = e^{-2F\phi_i/RT} \frac{\Gamma_{FeOCoOH}}{a_{CoOH^+}\Gamma_{FeO^-}} \tag{51}$$

where ϕ_i is the electrostatic potential influencing the energy state of bound ions.

In addition to reactions involving cobalt species, protonation (3) and deprotonation (4), together with surface association of nitrate (8) and sodium ions (9) are taken into account. In doing so one deals with seven standard equilibrium constants. The parameters of basic surface reactions (3,4,8,9) were obtained by separate potentiometric experiments in absence of cobalt ions.

While interpreting the adsorption reactions in the presence of cobalt, the electrostatic effects were included by assuming several possible locations of the bound ionic species. Table 1 represents the choices used in the regression analysis.

Table 1
Assumptions used in the regression analysis (C_1 and C_2 are capacitances, 0 is 0–plane, β is β–plane)

No	MO^-	MOH_2^+	MO–Na	MOH_2–NO_3	MO–Co^+	$(MO)_2$–Co	MO–CoOH	
1	0	0	0	0	0	0	0	C_1
2	0	0	0	0	β	β	β	C_1, C_2
3	0	0	0	0	0	β	β	C_1, C_2
4	0	0	β	β	0	0	0	C_1, C_2
5	0	0	β	β	β	β	β	C_1, C_2
6	0	0	β	β	0	β	β	C_1, C_2

The regression analysis of adsorption data was performed with SCPLOT program [71] and yielded density of surface groups, seven equilibrium constants and two capacitances (only C_1 in case No. 1.). The best fit was obtained in the case No. 6 but the best agreement for the ionic strength effect was obtained for the assumption No. 4 [72,73].

It could be concluded that different assumed structures of electrical interfacial layer were not distinguished by the applied procedure. It is clear that another data are necessary for that purpose. One way would be to introduce simultaneous electrokinetic measurements and assume relationship between electrokinetic potential and the potential at the onset of diffuse layer.

There is another possibility which was applied for interpretation of adsorption of organic ions [34,74]. One measures the effect of pH on the adsorption of cobalt ions at their different total concentrations. Simultaneous electrokinetic measurements provide the concentrations at isoelectric point so that each experimental run would yield the adsorption amounts and cobalt equilibrium concentration at zero electric potential. Regardless to different

possible assumptions on the electrical interfacial layer structure one may assume that ionic species at the interface are exposed to the zero electrostatic potential at the iep conditions. Therefore, by taking only these data points one may neglect the electrostatic term in the expressions defining the equilibrium state and obtain directly values of the standard ("intrinsic") equilibrium constants. These constants may be further used for interpretation of other data points which at which the electrokinetic potential is other than zero.

REFERENCES

1. G.A. Parks, Chem. Rew., 65 (1965) 177.
2. P. Hesleitner, D. Babić, N. Kallay and E. Matijević, Langmuir, 3 (1987) 815.
3. J. Westall and H. Hohl, Adv. Colloid Intertace Sci.,12 (1980) 265.
4. N. Kallay, R. Sprycha, M. Tomić, S. Žalac and Ž. Torbić, Croat. Chem. Acta, 63 (1990) 467.
5. N. Kallay, V. Hlady, J. Jednačak-Bišćan and S. Milonjić, in: B.W. Rossiter and R.S.Baetzold (eds.), Investigation of Surfaces and Intertaces; Part A, vol. 9 of Physical Methods in Chemistry, Wiley, New York, 1993.
6. D.E. Yates. S. Levine and T.W. Healy, J. Chem. Soc., Faraday Trans. I, 70 (1974) 1807.
7. J.A. Davis, R.O. James and J.O. Leckie, J. Colloid Interface Sci., 63 (1978) 480.
8. H. Hohl, L. Sigg and W. Stumm, in: M.C. Kavanaugh and J.O. Leckie (eds.), Particulates in Water, Advances in Chemistry Series, No. 189, American Chemical Society, Washington,1980.
9. W. Stumm, R. Kummert and L. Sigg, Croat. Chem. Acta, 53 (1980) 291.
10. M.A. Anderson and A.J. Rubin, (eds.), Adsorption of Inorganics at Solid-Liquid Interfaces, Ann Arbor Science, Ann Arbor,1981.
11. R.O. James and G.A. Parks, in: E.Matijević (ed.), Surface and Colloid Science, Plenum Press, New York,1982
12. G. Sposito, J. Colloid Interface Sci., 91 (1983) 329.
13. G. Parfitt and C. Rochester (eds.), Adsorption from Solution at the Solid/Liquid Interface, Academic Press, London,1983.
14. F.M.M. Morel, Principles of Aquatic Chemistry, Wiley, New York, 1983.
15. R.E. Johnson, Jr., J. Colloid Intertace Sci.,100 (1984) 540.
16. V.H. van Riemsdijk, G.H. Bolt, L.K. Koopal and J. Blaakmeer, J. Colloid Intertace Sci.,109 (1986) 219.
17. L.K. Koopal, V.H. van Riemsdijk and M. G. Roffey, J. Colloid Interface Sci., 118 (1987) 117.
18. J. Lyklema, Structure of the Solid/Liquid Intertace and the Electrical Double Layer, in: Solid/Liquid Dispersions, Academic Press. London,1987.
19. G.H. Bolt and V.H. van Riemsdijk, in: G.H.Bolt (ed.), Physico-Chemical Models, Soil Chemistry, Elsevier, Amsterdam,1982.
20. D.A. Dzombak and F.M.M. Morel, Surface Complexation Modelling, Wiley, New York, 1990.
21. N. Kallay and D. Babic, Colloids Surf., 19 (1986) 375.
22. N. Kallay and S. Žalac, Croat. Chem. Acta, 67 (1994) 467.

23. P. Hesleitner. N. Kallay and E. Matijević, Langmuir, 7 (1991) 178.
24. W.H. van Riemsdijk, L.K. Koopal and J.C.M. de Wit, Netherlands J.Agricult.Sci., 35 (1987) 241.
25. T. Hiemstra, W.H. van Riemsdijk and G.H. Bolt, J. Colloid Interface Sci., 133 (1989) 91.
26. T. Hiemstra, J.C.M. de Wit and W.H. van Riemsdijk, J. Colloid Interface Sci., 133 (1989) 105.
27. T. Hiemstra and W.H. van Riemsdijk, J. Colloid Interface Sci.,133 (1991) 7.
28. P. W. Schindler and H. Gamsjager, Kolloid–Z. and Z. Polymere, 250 (1972) 759.
29. N. Kallay and M. Tomić, Langmuir, 4 (1988) 559.
30. M. Tomić and N. Kallay, Langmuir, 4 (1988) 565.
31. W. Smit and C.L.M. Holten, J. Colloid Interface Sci., 78 (1980) 1.
32. W. Smit, C.L.M. Holten, H.N. Stein, J. J. M. de Goeij and H.M.J. Theelen, J.Colloid Interface Sci., 63 (1978) 120.
33. W. Smit and H.N. Stein, J. Electroanal. Chem., 91 (1978) 393.
34. R. Torres, N. Kallay and E. Matijević, Langmuir, 4 (1988) 706.
35. W.G. Eversole and P.H. Lahr, J. Chem. Phys., 9 (1941) 530.
36. W.G. Eversole and W.W. Boardman, J. Chem. Phys., 9 (1941) 798.
37. R.J. Hanter, Zeta Potentials in Colloid Science, Academic Press, London, 1981.
38. J.S. Noh and J.A. Schwarz, J. Colloid Interface Sci.,130 (1989) 157.
39. S. Žalac and N. Kallay, J. Colloid Interface Sci.,149 (1992) 233.
40. N. Kallay, Ž. Torbić, E. Barouch and J. Jednaćak–Bišćan, J. Colloid Interface Sci., 118 (1987) 431.
41. N. Kallay, Ž. Torbić, M. Golić and E. Matijević, J. Phys. Chem., 95 (1991)7028.
42. N. Kallay, D. Kovačević, I. Dedić and V. Tomašić, Corrosion NACE, 50 (1994) 598.
43. G. Thompson, N. Kallay and E. Matijević, Chem.Eng.Sci., 38 (1983) No. 11.
44. N. Kallay, J. D. Nelligan and E. Matijevic, J. Chem. Soc., Faraday Trans.I, 79 (1983) 65.
45. E. Matijević and N. Kallay, Croat. Chem. Acta, 56 (1983) 649.
46. Ž. Torbić, MS Thesis, University of Zagreb, Zagreb,1990.
47. S. Žalac, MS Thesis, University of Zagreb, Zagreb,1991.
48. Y.G. Berube and P.L. de Bruyn, J. Colloid Interface Sci., 27 (1968) 305.
49. P.H. Tewari and A. Campbell, J. Colloid Interface Sci., 55 (1976) 531.
50. M.A. Blesa, N.M. Figliolia, A.J.G. Maroto and A.E. Regazzoni, J. Colloid Interface Sci., 101 (1990) 410.
51. M. Kosmulski, J. Matysiak and J. Szczypa, J. Colloid Intertace Sci., 164 (1994) 280.
52. L.G.J. Fokkink, A. de Keizer and J. Lyklema, J. Colloid Interface Sci., 127 (1989) 116.
53. L.G.J. Fokkink, A. de Keizer and J. Lyklema, J. Colloid Interface Sci., 135 (1990) 118.
54. L.S. Balistrieri and T.T. Chou, Soil Sci. Soc. Am. J., 51(1987) 1145.
55. N. Kallay, S. Žalac and G.Štefanić, Langmuir, 9 (1993) 3457.
56. N. Kallay, S. Žalac, J. Čulin, U. Bieger, A. Pohlmeier and H.D. Narres, Progr. Colloid & Polymmer Sci., 95 (1994) 108.
57. M.L. Machesky and M.A. Anderson, Langmuir, 2(1986) 582.
58. S. Partyka, M. Lindheimer, S. Zaini, E. Keh and B. Brun, Langmuir, 2 (1966) 101.

59. L.A. Noll and P.F. Jacobs, Colloids Surf., 26 (1987) 43.
60. K.A. Wierer and B. Dobiaš, J. Colloid Interface Sci., 122 (1988) 171.
61. R. Denoyel, G. Durand, F. Lafuma and R. Audebert, J. Colloid Interface Sci., 139 (1989) 281.
62. S. Partyka, W. Rudziński, B. Brun and J. H. Clint, Langmuir, 5(1989) 297.
63. M.L. Machesky and A. Anderson, Environ. Sci. Tehnol., 23(1989) 580.
64. A. de Keizer, L.G.J. Fokkink and J. Lyklema, Colloids Surf., 49 (1990) 149.
65. M.L. Machesky and P.F. Jacobs, Colloids Surf., 53 (1991) 297.
66. M.L. Machesky and P.F. Jacobs, Colloids Surf., 53 (1991) 315.
67. P. Benoit, J.G. Hering and W. Stumm, Applied Geochemistry, 8 (1993) 127.
68. S. Žalac, Doctoral Thesis, University of Zagreb, Zagreb,1994.
69. M. Blesa and N. Kallay, Adv. Colloid Interface Sci., 28 (1988) 111.
70. N. Kallay, S. Žalac, D. Kovačević, H. Lewandowski and M. J. Schwuger, to be published.
71. A. Trkov, N.Ogrinc and I. Kobal, Computers Chem., 16 (1992) 341.
72. N.Ogrinc, A. Trkov and I. Kobal, Progr. Colloid Polym. Sci., 93 (1993) 323.
73. N.Ogrinc, A. Trkov, I. Kobal and E. Matijević, Acta Chim. Slov., 41 (1994) 417.
74. N. Kallay and E. Matijević, Langmuir, 1 (1985) 195.

This Page Intentionally Left Blank

A. Dąbrowski and V.A. Tertykh (Editors)
Adsorption on New and Modified Inorganic Sorbents
Studies in Surface Science and Catalysis, Vol. 99

Chapter 3.9
Adsorption and immersional wetting on hydrophilic and hydrophobic silicates

I. Dékány

Department of Colloid Chemistry, Attila József University
H-6720 Szeged, Hungary

1. STRUCTURAL PROPERTIES OF THE SILICATE ADSORBENTS

1.1. Layer silicates

The structural units of two dimensional clay minerals are planar lattices of SiO_4, tetrahedrons, to which an octahedron layer of AlO(OH) (kaolinite) or a further tetrahedron layer of SiO_4, (illite, montmorillonite) may be attached. Accordingly, under natural conditions clay minerals of lamellar structure, with two or three layer lattice have developed. In these structures the layer charge in itself is not balanced; the neutralization of the free charges necessitates the binding of cations, and via these cations the attachment of further layers [1,2]. In the tetrahedral coordination many Si→Al substitutions, while in the octahedral coordination Al→Mg and Al→Fe substitutions occur. The negative charge building up due to their presence is compensated by the cations localized between the layers, on the surface of the silicate lamellae. These interlamellar cations (Na^+, Ca^{2+}) may be exchanged for various inorganic and organic cations. The ion–exchange capacity of minerals may vary depending upon the structure and the place of origin. However, for our study the most important characteristic of minerals with lamellar structure is that the silicate layers are arranged in a regular, parallel order, and thus their distance may be determined by X–ray diffraction [3,4]. As for the ion–exchange capacity of four layer silicates, that of non–swelling kaolinite (0.05–0.08 mequ./g) and illite (0.2–0.3 mequ./g) is the lowest, which is followed by swelling montmorillonite (0.8–1.0 mequ./g), while vermiculite, a clay mineral also able to swell has the highest ion–exchange capacity (1.3–1.5 mequ./g) [5,6]. The thickness of the layers is 9.3 – 9.6 Å, and upon swelling the basal spacing (d_L) may significantly increase due to the molecules entering the interlamellar space [7,8]. The specific surface area of layer silicates calculated from the dimensions of the unit cell is about 760–800 m^2/g. However, this extremely large specific surface area becomes accessible only in case of the sorption of molecules bringing about swelling (interlamellar adsorption)[2,9].

The surface structures of the three layer silicates studied–kaolinite, illite and montmorillonite – are essentially identical, since the surface atomic planes consist of tetrahedrons. Differences between them are due to the differences in their swelling capacities and charge

densities (ion-exchange capacity). Thus illite is important for our study as a non-swelling layer silicate with a charge density of 0.6 - 0.9/Si_4O_{10} unit. The interlamellar cations are not exchangeable, or are only partially and very slowly exchanged [10]. Montmorillonite that swells and desaggregates excellently is also a three layer clay mineral, its charge density is 0.2 - 0.4/Si_4O_{10} unit. All cations of montmorillonite are relatively rapidly exchangeable. Since the individual silicate layers are easily separated from each other, both the hydrophilic and the organophilic (hydrophobic) forms of this mineral are remarkably well dispersed in the aqueous and organic media, respectively.

Due to their apolar character, montmorillonite and vermiculite organocomplexes swell very efficiently in various organic solvents (mainly aromatic hydrocarbons), resulting in a significant increase in the basal spacing [11,12]. On the basis of geometrical considerations, the extent of the increase in the basal spacing allows conclusions to be drawn regarding the arrangement of the incorporated molecules. The publications of Weiss and Lagaly are of basic importance in this field. These authors consider this incorporation (intercalation) procedure as complex formation and assume that benzene and toluene present in the interlamellar space have a quasi-crystalline structure [13-15] or are arranged in clusters [14].

1.2. Chain silicates

One dimensional (or chain) silicates are also classified as clay minerals. Due to their internal structure their external appearance is most often fibrous, stringy, and since the unit crystal particles are usually very thin fibres, the large specific surface area and the associated characteristics make them similar to clay minerals of layered structure in many respects [16-18]. From among the minerals included in this group (sepiolite, attapulgite, palygorskite) we studied exclusively palygorskite whose composition can be given as $Si_8O_{20}(OH)_2(H_2O)_4(Mg_{5-3x}, Al_{2x})nH_2O$ [17]. According to Bradley and Nagy, the stringy, fibrous structure is a result of the alternating linkage of elements made up of two pyroxene chains [16,17]. As a result of alternating linkage, the silicate chains of 300-600 nm length surround the channels measuring 3.7×6.0 Å and parallel with the c axis, containing "zeolitic water" [18]. Palygorskite is a cation exchanging clay mineral, i.e. the Na^+ and Ca^{2+} cations bound on its surface can be exchanged not only for other inorganic cations but also for cationic surfactants.

Like layer silicates, the porous palygorskite can also be organophilized. X-ray studies, however, do not reveal any structural changes in the organocomplexes, since cationic surfactants are adsorbed only on the external surfaces. The amount of surfactant bound by ion-exchange adsorption and the extent of organophilicity can be quantified by the liquid sorption studies and microcalorimetry [19-21].

Clay minerals and their modified (organophilic) derivatives are usually readily dispersed in solvents or solvent mixtures of various polarities. The stability and structure building characteristics of the suspensions vary over a wide range, depending on the surfacial properties of the dispersed particles and the quality (composition) of the solvent (mixture). Clay minerals are of colloid dimensions, and therefore are able to adsorb significant amounts of various molecules, due to their large specific surface area. It follows from the above mentioned structural properties that sorption processes and adsorption capacity will be basically determined by the fact whether the mineral studied is of the swelling or non-swelling type [22,23]. Slabaugh and Hanson [24] were the first to deter-

mine sorption excess isotherms on industrial organophilic bentonite (Benton 34). Studying ethanol–toluene mixtures, they obtained S-shaped adsorbents. By the end of the nineteen-seventies, several papers on the liquid sorption properties of organophilic clay minerals had been published by the Department of Colloid Chemistry University Szeged (Hungary). In these studies, Dékány, Nagy and Schay – following the suggestions of Weiss and Lagaly – coupled the analysis of liquid sorption equilibrium with X-ray diffraction and proved for many systems that in the case of adsorbents with the layer structure, the volume of interlamellar liquid can be determined also by X-ray diffraction and it is in good agreement with adsorption capacity [25–29].

Illite as a non-swelling clay mineral of layer structure plays a very important role in our studies. This special role is due to the fact that both sides of the surface of the silicate lamellae are made up of SiO_4-tetrahedron planar lattices, and this structure – even when hydrophobized – is identical with the surface structure of montmorillonite and vermiculite, both of which are of the swelling type.

2. SOLID–LIQUID INTERFACIAL PROPERTIES

2.1. Adsorption excess isotherms on non-swelling clay minerals

A significant amount of experimental data have been compiled in the field of solid–liquid interfacial liquid sorption. Based on the work of Schay and Nagy [30–33] and Kipling and Everett [34–37], the systematization of the experimental observations according to Gibbs' principles opened the way to the unambiguous determination of the so-called adsorption excesses and the adsorption excess adsorbents by relatively simple experimental techniques. Namely, starting from the adsorption material balance the Ostwald-de Izaguirre equation is obtained:

$$n_1^{\sigma(n)} = n^o(x_1^o - x_1) = n_1^s - n^s x_1 = n^s(x_1^s - x_1) \tag{1}$$

where $n_1^{\sigma(n)}$ is the specific reduced adsorption excess amount, while n^o is the material amount in adsorption system and x_1^o the composition of the starting mixture. In an adsorption equilibrium, the composition is x_1, the material amount in the surface layer is $n^s = n_1^s + n_2^s$ and its composition is x_1^s.

Adsorption capacity can be calculated from excess isotherms by various methods. The best known of these is the so-called Everett–Schay function[31]:

$$\frac{x_1 x_2}{n_1^{\sigma(n)}} = \frac{1}{n_{1,o}^s}\left[\frac{r}{S-1} + \frac{S-r}{S-1}x_1\right] \tag{2}$$

which is suitable for the determination of the adsorption capacity of the pure component, $n_{1,o}^s$. In equation (2) $r = n_{1,o}^s/n_{2,o}^s$, $S = x_1^s x_2/x_2^s x_1$ is the separation factor of adsorption.

In the case of sign reversing type IV excess isotherms, equation (2) can be applied only in a narrow concentration range, therefore the application of the Schay–Nagy extrapolation method is advisable [31,33], when the values of n_1^s and n_2^s can be determined. On the other hand, the knowledge of adsorption capacities opens the way for determining the composition of the interfacial layer:

$$\Phi_1^s = \frac{n_1^s}{n_{1,o}^s} = \frac{x_1^s}{x_1^s + r x_2^s} \tag{3}$$

where Φ_1^s is the volume fraction of the surface layer. The application of Eq. (3) is essential for our purposes, since the knowledge of the adsorbents makes it possible to calculate the composition of the adsorption layer, the knowledge of which, in turn, is basically important also for the interpretation of calorimetric investigations in the binary mixtures.

The adsorption excess adsorbents in methanol(1)+benzene(2) mixtures were first determined on dialyzed kaolinite and illite and then on the samples extracted by methanol (Figs. 1,2). The adsorbent is of type II on both minerals; however, the adsorption

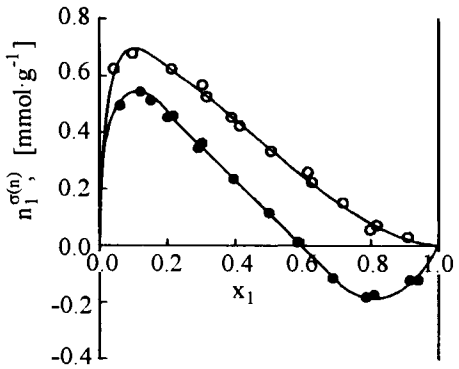

Figure 1. Adsorption excess isotherms on (○) Na-kaolinite, (●) with methanol extracted Na-kaolinite in methanol(1)+benzene(2) mixtures.

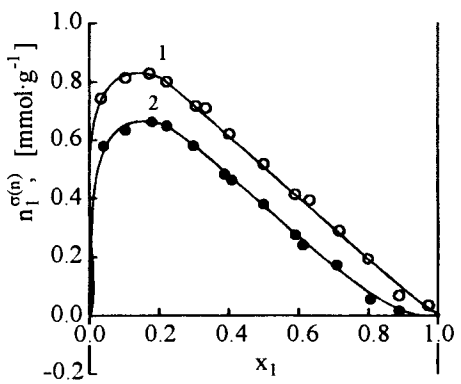

Figure 2. Adsorption excess isotherms on Na-illite in methanol(1)+benzene(2) mixtures: 1. original, 2. by methanol extracted illite.

of methanol is markedly preferential only on dialyzed kaolinite and illite, while in the methanol-treated samples the curve of the adsorbent bends as it approaches x_1 and, in the case of kaolinite, its sign is reversed. In the course of the surface treatment of kaolinite and illite, the surface is slightly hydrophobized owing to the esterification of the hydroxyl groups located on the planes and edges of the lamellae. It is when their surface is treated by cationic surfactants that the selective liquid sorption characteristics of these two minerals are basically altered. Figures 3 and 4 show the excess isotherms of kaolinite and illite organocomplexes. It is important to note that upon increasing the modification (i.e. depolarization) of the surface the adsorption of methanol is gradually repressed, and on the surface of illite - which contains a higher amount of HDP-cations - the adsorption of benzene will become significant. The change in the selective liquid sorption properties of clay organocomplexes is well characterized by the shift of the values of adsorption azeotropic composition as x_1^a approaches 0.

Given the knowledge of the material amount and surface requirement ($a_{m,i}$) of the liquid components (n_i^s) in the interfacial phase, the part of the surface on which a given i-th component is adsorbed can be calculated (i=1,2). From the adsorption isotherms, the adsorption capacity of the pure components ($n_{1,o}^s$) and the value of the so-called equivalent specific surface area ($a_{eq.}^s$) can be calculated[19].

Adsorption capacities and specific surface values of kaolinite and illite derivatives are listed in Table 1. This table also contains BET surfaces determined at a temperature of 77 K

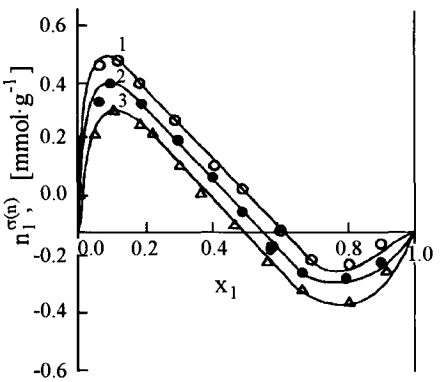

Figure 3. Adsorption excess isotherm on HDP–kaolinite in methanol(1)+benzene(2) mixtures. (1–3: increasing HDP^+–cation amount).

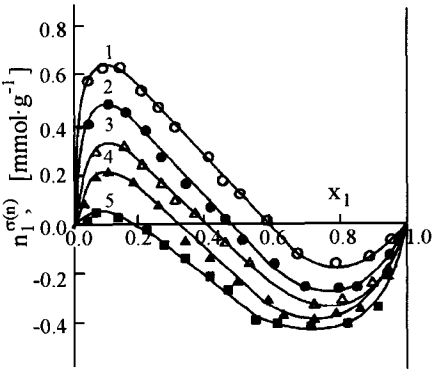

Figure 4. Adsorption excess isotherms on HDP–illite derivatives in methanol(1)+benzene(2) mixtures. 1–5: increasing HDP^+ cation surface concentration.

Table 1
Adsorption capacities, specific surface areas and immersional wetting data of different kaolinite– and illite organocomplexes

Adsorbent	HDP cation (mmol/g)	$n^s_{l,o}$ (mmol/g)	Θ_2	a^s_{eq} (m^2/g)	a^s_{BET} (m^2/g)	$\Delta_w h$ in methanol (J/mol)
Na–kaolinite	0.00	1.05	0.234	100	21	8.20
Na–kaolinite extracted	0.00	1.70	0.577	162	–	3.11
Na–HDP–kaolinite 1.	0.024	1.77	0.632	168	–	1.18
Na–HDP–kaolinite 2.	0.036	1.83	0.672	174	24	1.14
HDP–kaolinite*	0.048	2.07	0.724	190	24	0.94
Na–illite	0.00	1.06	0.00	101	44	12.50
Na–illite extracted	0.00	1.29	0.26	123	47	6.76
Na–HDP–illite1	0.097	1.84	0.57	175	35	2.77
Na–HDP–illite2	0.139	1.89	0.66	180	32	2.32
Na–HDP–illite3	0.171	1.80	0.73	171	30	2.28
HDP–illite*	0.233	1.85	0.78	170	28	2.18
HDP–DS–illite	0.233 0.016**	1.81	0.85	172	28	1.93

* HDP: hexadecylpyridinium cation, **DS: dodecylsulphate anion

from nitrogen adsorption. It is apparent that the surface calculated from the liquid sorption isotherms is 3 to 5 times larger than the gas adsorption values. It has to be noted here that the BET surface of the organophilic samples is decreased, since the silicate layers adhere to each other.

In contrast to the case of gas adsorption, the adsorption capacities determined on organocomplexes suggest disaggregation, since the maximal value of the calculated specific surface area falls in the range of 90 to 120 $m^2 \cdot g^{-1}$ for kaolinite and 170 to 190 $m^2 \cdot g^{-1}$ for illite[22].

2.2. Immersional wetting on non–swelling clay minerals

The specific immersion wetting enthalpies of kaolinite, illite and their organophilic derivatives are shown in Table 1. These data reveal that the heat of immersion in methanol is the highest in the case of the dialyzed mineral, and on increasing surface modification its value decreases[22]. The comparison of immersion wetting enthalpies relative to unit mass of the adsorbent is justified only in case if the specific surface area of the adsorbent is constant. It is also known, on the other hand, that the value of liquid sorption capacity is a function of surface modification ($\Theta_2 = n_2^s a_{m,2}/a_{eq}^s$). If a uniform treatment of immersion wetting data is desirable, it is advisable to relate the wetting enthalpy to the material amount in the interfacial phase, i.e. to use molar immersion wetting enthalpies in the calculations. In this way the changes in specific surface caused by disaggregation need not be separately monitored, since our data always refer to enthalpy changes accompanying the sorption of molar amounts of material.

The changes in molar immersion enthalpies, $\Delta_w H_m \equiv \Delta_w h$, upon the surface modification in methanol and benzene are presented in Fig. 5. In methanol, parallel with an increasing organophilicity of the surface, $\Delta_w H_m$ decreases nearly exponentially, while in benzene it increases (to a significantly lesser extent). Our experimental data can be approximated by the following exponential function[22]:

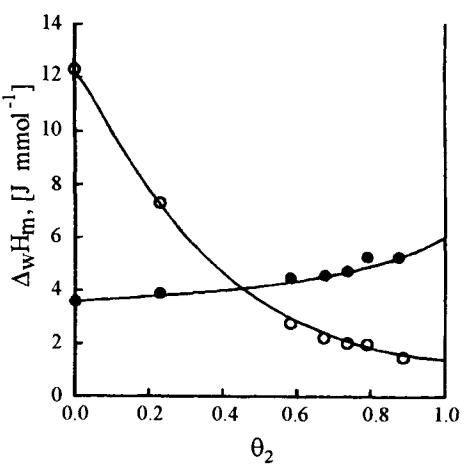

Figure 5. The molar immersional wetting enthalpy on illite organocomplexes with different hydrophobicity: (○) in methanol, and (●) in benzene.

$$\Delta_w H_m = \Delta_w H_o e^{-k\Theta_i} \quad (4)$$

where $\Delta_w H_o$ is the molar immersional wetting enthalpy determined on the original dialyzed hydrophilic mineral and k is the empiric constant characteristic of the course of the function. The k values that characterize the solid–liquid interfacial interaction described by the above equation are following: k = –2.54 in methanol, k = 0.47 in benzene.

2.3. Adsorption and immersional wetting on swelling montmorillonite organocomplexes

Since dry organocomplexes have layer structure and their basal spacing can be determined by X–ray diffraction, it is possible to gain information about the structure (more precisely, the arrangement of the interlamellar chains) of the suspended and swollen adsorbent subjected to liquid sorption studies (Table 2). The data show that in benzene, in the case of bimolecular orientation of the alkyl chains the extent of interlamellar swelling is significant, while in methanol it hardly changes with organophilicity. Since the basic difference between montmorillonite and illite is that the former is a swelling clay mineral, so–called interlamellar spaces, i.e. inner surfaces are also opened up by swelling. The adsorption capacity of montmorillonite and its organocomplexes therefore several times exceeds that of non–swelling organophilic illite.

Table 2
Interlamellar sorption and expansion data on hydrophobic montmorillonite organoclays in methanol(1)and benzene(2)

Adsorbent	organic cation (mmol/g)	Θ_2	$n^s_{l,o}$ (mmol/g)	d_L^{dry} (Å)	$d_{L,1}$ (Å)	$d_{L,2}$ (Å)
Na–montmorillonite	0.00	0.00	3.44	12.3	15.9	14.2
Na–HDP–montm.1	0.20	0.20	4.72	14.0	16.2	16.4
Na–HDP–montm.2	0.39	0.58	5.69	14.1	32.4	30.7
Na–HDP–montm.3	0.55	0.67	6.69	15.8	32.2	34.7
Na–HDP–montm.4	0.68	0.73	7.72	16.8	31.6	36.0
Na–HDP–montm.5	0.81	0.75	8.04	18.2	31.0	37.0
*HDP–montm.	0.85	0.82	8.25	18.2	31.3	38.6
*HDP–montm.	0.82	0.73	8.51	18.4	30.5	33.3
*ODP–montm.	0.82	0.84	8.33	18.2	31.9	42.0
Na–DMDH–montm.1	0.20	0.38	4.92	15.2	16.3	15.7
Na–DMDH–montm.2	0.53	0.70	8.08	26.7	34.0	42.7
*DMDH–montm.	0.83	0.84	8.90	29.1	37.7	45.1

*TDP: tetradecyl–, HDP: hexadecyl–, ODP: octadecylpyridinium cation, DMDH: dimethyldihexadecylammonium cation; $d_{L,i}$ (i=1,2)–basal spacing in benzene (i=1) and in methanol (i=2)

Adsorption capacity given for methanol, $n^s_{1,0}$ in Table 2 was calculated from type IV excess isotherms, using the Schay–Nagy method. The course of the isotherms is identical with the functions determined for organophilic illites [25–27].

The immersional wetting of montmorillonite organocomplexes in methanol and in benzene may give rise to the three types of detector signal presented in Fig. 6. Isotherm microcalorimetry of the hexadecylpyridinium derivatives in methanol and benzene yields an exothermal effect, since in these organocomplexes interlamellar swelling is not very significant. In the case of dialkylammonium derivatives a significant swelling is observed, therefore either endothermal- exothermal signals separated in time are registered within the same measurement, or immersion wetting results in an endothermal heat effect only[23].

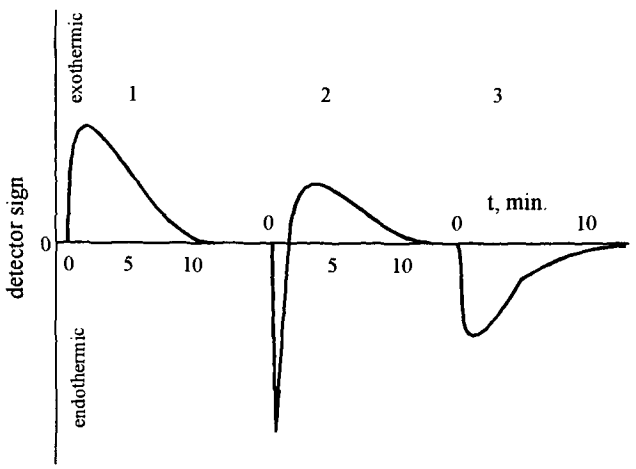

Figure 6. Exothermic and endothermic immersional wetting on swelling montmorillonite organocomplexes. 1. $\Delta_w H = -3.63 J \cdot g^{-1}$, $d_L = 3.13$nm 2. $\Delta_w H = -2.90\ J \cdot g^{-1}$, $d_L = 4.16$ nm 3. $\Delta_w H = +1.10 J \cdot g^{-1}$, $d_L = 4.51$ nm.

Fig. 7 shows the quantity of heat measurable by calorimetry as a function of the mass of the organocomplex. The points representing TDP- amd HDP-montmorillonites fall on straight lines with a positive slope, while in the case of the well swelling dialkylammonium derivatives the amount of heat measured decreases with increasing the mass of the adsorbent. The lines do not intersect in the origo since the liquid influx at m = 0 mass produces 75–80 mJ of heat in the measuring cell. The endothermal effect associated with the swelling of bentonites was first pointed out by Zettlemoyer at al. [38] and Slabaugh et al. [39–42]. They established that good swelling and gel formation result in small exothermal or exclusively endothermal effects. According to these authors, when considering the immersion wetting of swelling systems, both the interaction of polar molecules with the silicate surface and the solvatation of apolar molecules by alkyl chains, as well as the interlamellar expansion have to be taken into account. The two former interactions are always exothermal, while the latter may often be endothermal. In our view the reason for the temporal separation of the exothermal and endothermal processes presented in Fig. 6 is that interlamellar wetting may occur only in case if the silicate lamellae open up. Consequently, in the course of interlamellar wetting there may also occur a special case when

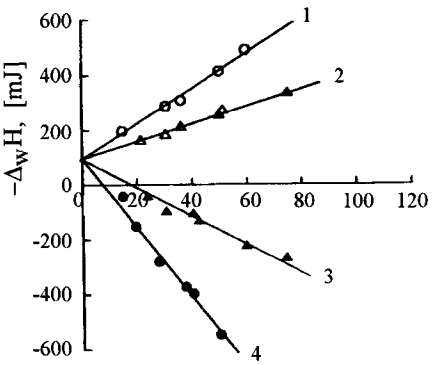

Figure 7. Enthalpy of wetting at different mass of the organo–montmorillonite in methanol. 1. TDP–, 2. HDP–, 3. DMDH–montm. 4. Benton 34.

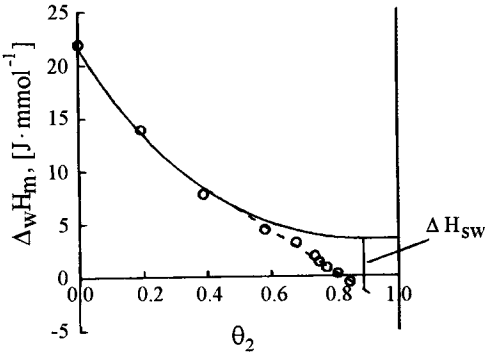

Figure 8. The molar immersional wetting enthalpy on organo–montmorillonite with different hydrophobicity in methanol (—— non–swelling illite, – – – swelling montmorillonite).

expansion along the edges of the lamellar packages is indicated by a sharp endothermal peak, and only then follows wetting in the interlayer space, appearing in the form of an endothermal effect.

Next we shall examine how an increase in the hydrophobicity of the surface affects immersion wetting enthalpy in polar solvents such as methanol. It has been pointed out already in the discussion of hydrophobic illites that molar immersion wetting enthalpy decreases exponentially with an increasing extent of hydrophobization. The same holds for swelling hydrophobic montmorillonites as well. The difference between swelling hydrophobic montmorillonite and non- swelling illite of identical hydrophobicity yields the value of swelling enthalpy, ΔH_{sw}, which is endothermal and increases with the extent of hydrophobicity.

2.4. Flow microcalorimetry on hydrophobized vermiculite

Swelling montmorillonites cannot be studied by flow microcalorimetric methods since the individual particles – due to their average lamellar diameter of 300–600 Å– pass through the sieve of the sorption measuring cell. Therefore we selected organophilic vermiculite which is made up of well–defined, crystalline lamellae (0.5–1.0 mm), and the surface structure of which is completely identical with that of montmorillonite. Its swelling can be precisely followed by X–ray diffraction measurements. Hydrophobized vermiculites are therefore excellent model systems for studies on the enthalpy balance of adsorption displacement processes on the hydrophobized surfaces and also for parallel investigations of adsorption and swelling. The excess isotherms determined on n– alkylammonium vermiculites ($n_c = 12 - 18$, the number of carbon atoms) in methanol(1)+benzene(2) mixtures are S–shaped (Fig. 9). The course of the isotherms is similar to that of the hydrophobized silicates presented above, and the azeotropic composition also decreases with increasing the number of carbon atoms in a similar manner.

Figure 10 shows basal spacing (d_L) for the liquid sorption equilibrium systems descri-

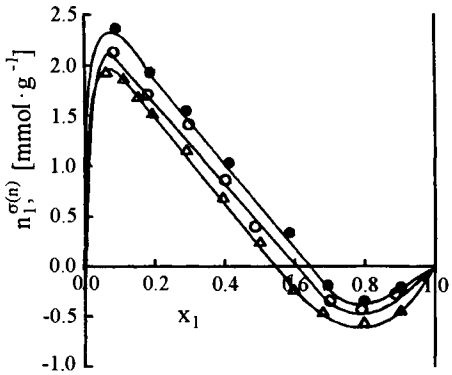

Figure 9. Adsorption excess isotherms in methanol(1)+benzene(2) mixtures vs. the number of carbon atoms in ammonium vermiculite: (●) n_c=12, (○) n_c=16, (Δ) n_c=18.

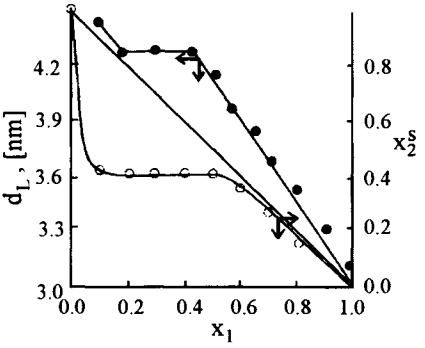

Figure 10. The mole fraction of benzene (x_2^s) in the interfacial layer and the basal spacing (d_L) in ethanol(1)+cyclohexane(2) mixtures on hexadecylammonium-montmorillonite.

bed above as a function of the composition of the bulk phase. It can be established that within the whole series of mixtures the value of d_L decreases, i.e. the alkyl chains and the silicate layers get closer to each other (Fig. 11). The composition of the interfacial layer is therefore also indicated in Fig. 10, and it is apparent that this decrease is gradual. This means that the displacement of the apolar component from the interlamellar space leads to a decrease in basal spacing. The same conclusion is demonstrated also by Fig. 11, assuming that the orientation of the alkyl chains is perpendicular.

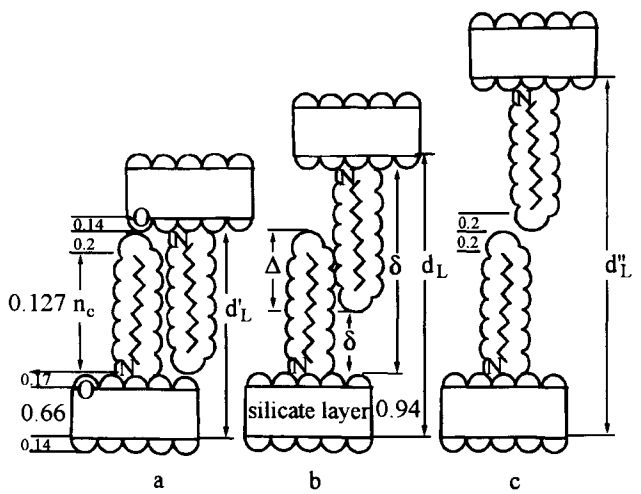

Figure 11. Orientation of the alkyl chains between the silicate layers at different swelling.

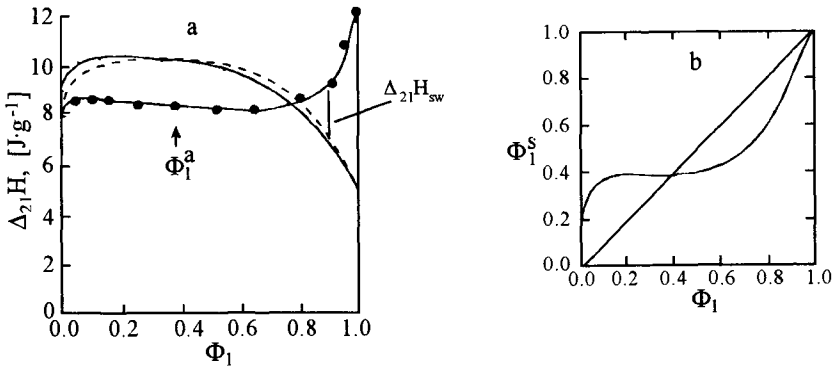

Figure 12. The integral enthalpy of displacement in methanol(1)+benzene(2) mixtures (●) experimental data, - - - calculated data, —— calculated data with ideal adsorption layer (a). $\Phi_1^s = f(\Phi_1)$ is the adsorption equilibrium diagram (b).

The integral exchange enthalpy isotherm calculated from the flow microcalorimetric measurements is shown in Fig. 12. The course of the isotherm – in case of a U-shaped adsorption excess isotherm – is determined by the composition of the interfacial phase (Φ_1^s) according to the following equation[45-47]:

$$\Delta_{21}H = \Phi_1^S \Delta_{21}H_t + \Delta_{21}H^{se} \tag{5}$$

where $\Delta_{21}H_t$ is the total integral exchange enthalpy in the range of $x_1=0$ to $x_1=1$ and $\Delta_{21}H^{se}$ is the excess enthalpy in the interfacial layer. In the case of ideal mixtures at S-shaped excess isotherms, the calculation of $\Delta_{21}H$ has to be performed in two steps. First, from $\Phi_1 = 0$ to $\Phi_1^s = \Phi_1^a$ azeotropic composition:

$$\Delta_{21}H = (\Phi_1^s \Delta_{21}H^a) / \Phi_1^a \tag{6}$$

where $\Delta_{21}H^a$ is the exchange enthalpy of the azeotropic point, the value of which can be determined from the independent immersion wetting heat in a mixture of composition Φ_1^s. The second interval covers the range from $\Phi_1 = \Phi_1^a$ to $\Phi_1 = 1$:

$$\Delta_{21}H = [(\Phi_1^a - \Phi_1^s)\,\Delta_{21}H^a] / (1 - \Phi_1^a) \tag{7}$$

It is obvious from the experimental data that the enthalpy change ($\Delta_{21}H$) calculated on the basis of Eqs. (6,7) differ from the measured data. Namely, in the case of nonideal adsorption layer and S-shaped excess isotherm an endothermal backward section should occur on hydrophobic surfaces [45-47]. According to our calculations, knowing the equilibrium composition [$\Phi_1^s = f(\Phi_2)$] and Φ_1^a, this backward section indeed occurs (Fig. 12). The experimental data, however, significantly diverge: at $\Phi \geq 0.7$, $\Delta_{21}H$ already increases and its maximal value is -12.6 J/g. We assume that the reason for this is a decrease in the swelling of the organocomplex (see Figs. 10,11). Namely, in the phase in alcohol rich interlamellar phase, the lamellae get closer to each other and the interaction among alkyl chains in the interlamellar space increases. The calculated function thus characterizes a non-swelling hydrophobic clay surface, while the experimental data describe the swelling

system. Their difference yields the swelling enthalpy, ΔH_{sw}. Figure 12 well demonstrates that this effect appears in the alcohol-rich range of composition. The expansion or contraction of silicate lamellae is well reflected by the enthalpy values presented in Fig. 13 as a function of Φ_2^s composition. It is evident that significant changes occur only beyond the azeotropic composition Φ_2^a.

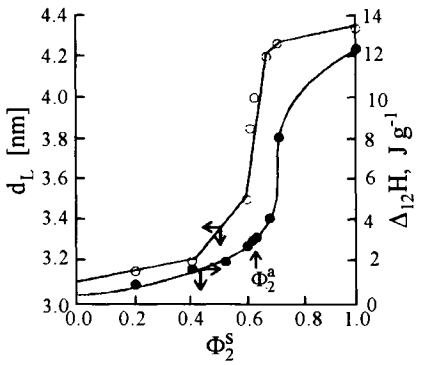

Figure 13. "Opening" of the interlamellar space. Enthalpy of displacement ($\Delta_{12}H$) and basal spacing (d_L) at different benzene volume fraction (Φ_2^s) in the adsorption layer. System: hexadecylammonium-vermiculite in methanol(1)+benzene(2) mixture.

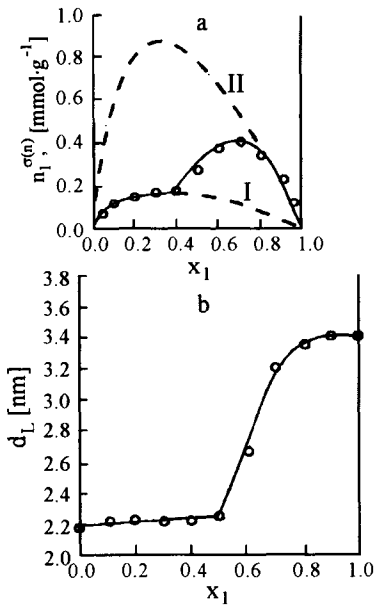

Figure 14. The adsorption excess isotherm (a) and the interlamellar expansion (b) for system: dodecylammonium-vermiculite in benzene(1)+n-heptane(2) mixtures. Dotted lines: calculated excess isotherms with non-swelling (I) and swelling (II) system.

2.5. Liquid sorption on palygorskites and their hydrophobic derivatives

From pure Na-palygorskite produced under certain conditions by cation exchange with hexadecylpyridinium-chloride (HDPCl), palygorskite organocomplexes can be prepared [50]. In this chapter we wish to show how the surface properties of palygorskite and its organophilic derivatives can be characterized on the basis of gas adsorption, liquid adsorption and immersion wetting measurements (see Table 3), since surface modification by cations affects the porosity of chain silicates, and also alters the selective liquid adsorption properties of organocomplexes and the extent of solid-liquid interfacial interaction.

We studied the surface characteristics of palygorskite and its organocomplexes first by nitrogen adsorption at standard temperature and pressure (STP). The isotherms are shown in Fig. 15. According to Brunauer's, Emmet's and Teller's classification, the isotherm determined on palygorskite is of type IV and exhibits adsorption hysteresis. An

Table 3
Results of analysis of the excess isotherms on palygorskite and hexadecylpyridinium–palygorskites in different liquid mixtures

Liquid mixtures	n_1^s	n_2^s	$n_{1,o}^s$	$a_{eq.}^s$	a_{BET}^s
	(mmol/g)			(m^2/g)	
Palygorskite					
methanol(1)+benzene(2)	5.25	0.0	5.25	499	312
ethanol(1)+benzene(2)	2.07	0.45	2.75	330	
1–propanol(1)+benzene(2)	1.20	0.35	1.59	255	
2–propanol(1)+benzene(2)	0.92	0.56	1.52	254	
HDP–palygorskite 1 (0.10 mmol HDP^+/g clay)					
methanol(1)+benzene(2)	3.62	0.51	4.59	436	254
1–propanol(1)+benzene(2)	0.68	0.85	1.64	262	
HDP–palygorskite 2 (0.19 mmol HDP^+/g clay)					
methanol(1)+benzene(2)	2.50	0.60	3.63	346	182
ethanol(1)+benzene(2)	1.05	1.10	2.70	324	
1–propanol(1)+benzene(2)	0.65	0.90	1.66	266	
HDP–palygorskite 3 (0.34 mmol HDP^+/g clay)					
methanol(1)+benzene(2)	1.95	0.88	3.63	364	141
ethanol(1)+benzene(2)	0.80	1.01	2.30	276	
1–propanol(1)+benzene(2)	0.45	1.05	1.63	261	
HDP–palygorskite 4 (0.38 mmol HDP^+/g clay)					
methanol(1)+benzene(2)	1.80	1.01	3.76	358	115
ethanol(1)+benzene(2)	0.72	1.02	2.25	270	
1–propanol(1)+benzene(2)	0.35	1.16	1.65	165	

isotherm of this kind is characteristic for markedly porous adsorbents. Part of the pores are the micropores mentioned in the discussion of structure, and another part is formed among the fibrous, stringy bundles of the mineral, in which capillary condensation takes place. Surface modification by HDP–cations brings about a change in the course of the isotherm and adsorption hysteresis does not appear. It is revealed by the Fig. 15 that with increasing surface modification the adsorption capacities gradually decrease, the reason for which is that due to organophilization, palygorskite fibres adhere more and more to each other. This fact is also expressed by a decrease in the specific surface area calculated according to the BET–equation (Table 3)[50].

The isotherms presented in Fig. 16 are shown in de Boer's representation [$V^s = f(t)$], where t is the statistical thickness of the adsorptive layer [51,52]. If a non–porous adsorbent of plain surface is considered, this representation gives a straight line starting from

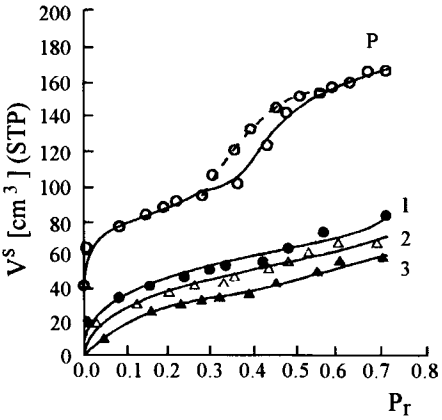

Figure 15. N_2 adsorption isotherms on palygorskite (P) and on HDP–palygorskites with increasing hydrophobicity (1–3).

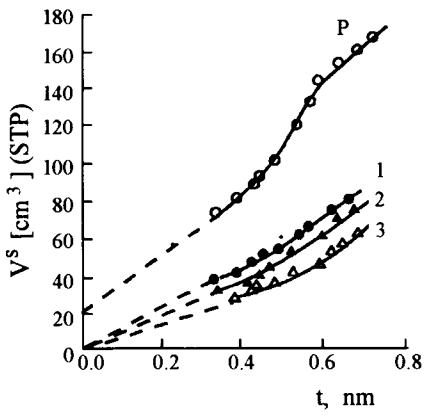

Figure 16. The de–Boer t–plot on palygorskite (P) and on HDP–palygorskites with increasing hydrophobicity (1–3).

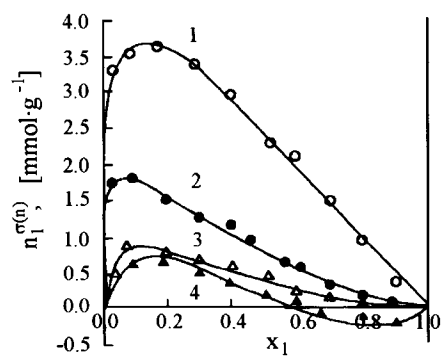

Figure 17. Adsorption excess isotherms on Na–palygorskite in alcohol(1)+benzene(2) mixtures: (○) methanol, (●) ethanol, (△) n–propanol, (▲) i–propanol.

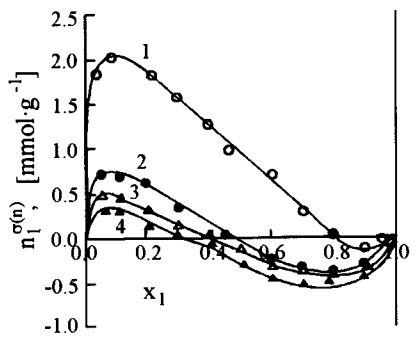

Figure 18. Adsorption excess isotherms HDP–palygorskite in alcohol(1)+benzene(2) mixtures. (○) methanol, (●) ethanol, (△) n–propanol, (▲) i–propanol.

the origo. However, as revealed by the Figure 16, in the case of natural palygorskite the line intersects the positive half of the axis indicating the presence of micropores. In the case of the HDP–palygorskite samples the $V^s = f(t)$ function starts from zero, suggesting the disappearance of micropores, since the long chains of the surfactant molecules may cover or clog these "zeolite–like" channels. It appears from a comparison of the BET–surfaces in Table 3 and the specific surfaces area calculated according to the de Boer's method that in the case of the organophilized samples the data computed according to the two

methods are in very good agreement and decrease with increasing surface modification. For palygorskite, the specific surface area according to de Boer was calculated from the slope of the first section of the function. This value (256 m^2/g) characterizes only the external surfaces and gives no information about the surface of the micropores.

We shall next examine how these surface structural characteristics affect liquid sorption in the alcohol(1)+benzene(2) mixtures. Figure 17 shows the excess isotherm determined on palygorskite. In the case of methanol(1)+benzene(2) mixtures the isotherm is of type II, indicating that methanol is preferentially adsorbed and penetrates into the micropores of the "zeolite-like" channels as well. With increasing the number of carbon atoms in the alcohol, preferential adsorption is repressed and isotherms of types III and IV are obtained. The reason for this is that, due to steric hindrance, alcohols of larger size cannot enter the micropores.

Similarly to the case of the hydrophobic clay minerals described above, isotherms determined on HDP-palygorskite are S-shaped (Fig. 18). Surface modification by HDP^+-cations has a double effect. On increasing the amount of HDP-cations the liquid sorption capacities decrease, since the micropores get clogged. On the other hand, the polarity of the surface decreases and the azeotropic composition indicates the displacement of the alcohol on the surface[50].

2.6. Adsorption and wetting on zeolites

Zeolites are silicates composed of 3-dimensional network and structurally they do not belong to the group of clay minerals. Their adsorption and wetting characteristics, however, are close to those of the chain silicates discussed above.

It is well-known in the special literature on zeolites that as a result of the partial or complete removal of aluminium, the sorption characteristics of zeolites are significantly altered. The adsorption of various polar vapours on so-called ZSM-5 zeolite was studied by Flaningen et al. in detail [53]. These authors pointed out that zeolite lattices free of

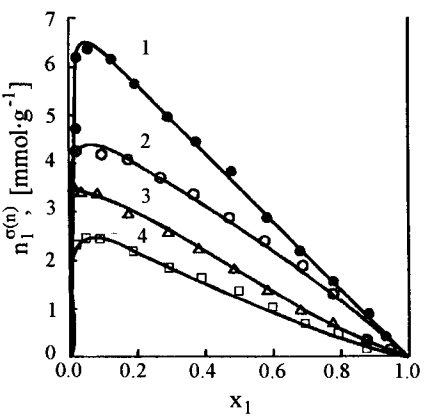

Figure 19. Adsorption excess isotherms on Na-Y zeolite in alcohol(1)+benzene(2) mixtures: (●) methanol, (○) ethanol, (△) n-propanol, (▲) n-butanol.

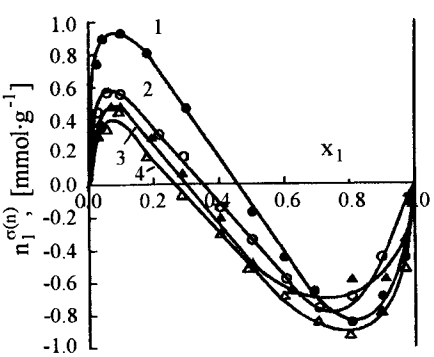

Figure 20. Adsorption excess isotherms in alcohol(1)+benzene(2) mixtures on dealuminated Y-zeolite, (●) methanol, (○) ethanol, (△) n-propanol, (▲) n-butanol.

aluminium are hydrophobic, which means that the surface energy of the zeolite crystal is significantly decreased in the course of dealuminization. In order to investigate this phenomenon in detail, we examined the sorption of mixtures of heptane and benzene, and of alcohols of various chain lengths and benzene on Na–Y and dealuminated zeolites[54].

Type II excess isotherms determined on Na–Y zeolite in the alcohol(1)+benzene(2) mixtures are presented in Fig. 19. It can be concluded from the isotherms that in a wide range of mixture compositions alcohols are preferentially adsorbed on the surface and micropores of the adsorbent. The adsorption capacities characterizing the preferentially adsorbed alcohols are listed in Table 4. Adsorption excess isotherms determined on dealuminated Y zeolite in the alcohol+benzene mixtures are presented in Fig. 20. These isotherms may be classified as type IV, which is characterized by a linear region in a rather wide intermediate composition range (in the present case, $x_1 = 0.15 - 0.55$). The adsorption capacities determined on the basis of these linear regions by graphic extrapolation are given in Table 4.

Table 4
Results of analysis of the excess isotherms on zeolites in different liquid mixtures

Liquid mixtures	n_1^s	n_2^s	$n_{1,o}^s$	V^s
	(mmol/g)			(cm^3/g)
Na–Y zeolite				
methanol(1)+benzene(2)	7.13	–	7.13	0.290
ethanol(1)+benzene(2)	4.71	–	4.71	0.276
1–propanol(1)+benzene(2)	3.64	–	3.64	0.270
1–butanol(1)+benzene(2)	2.97	–	2.97	0.273
benzene(1)+1–heptane(2)	3.16	–	3.16	0.282
dealuminated Y–zeolite				
methanol(1)+benzene(2)	1.58	1.76	4.91	0.222
ethanol(1)+benzene(2)	0.98	1.66	3.47	0.206
1–propanol(1)+benzene(2)	0.69	1.58	2.45	0.193
1–butanol(1)+benzene(2)	0.73	1.52	2.21	0.203
benzene(1)+1–heptane(2)	1.17	0.81	2.32	0.244

In the relatively wide composition range where the isotherm is linear, the molar ratio of alcohol and benzene within the interfacial phase is constant. In other words, the less polar benzene also appears in the interfacial layer and, as a result of dealuminization, ca. 70% of the total volume of the interfacial phase is occupied by benzene molecules[54]. Figure 21 shows the adsorption excess isotherms of benzene(1)+n–heptane(2) mixtures on Na–Y and dealuminated Y zeolites. On Na–Y zeolite, benzene from a benzene(1)+n–heptane(2) mixture is preferentially adsorbed in the micropores, and in the composition range of $x_1 > 0.1$ it almost completely displaces n–heptane in the interfacial phase. The volume V^s calculated from the adsorption capacity of benzene is in good agreement with that calculated from the preferential adsorption of alcohol (Table 4).

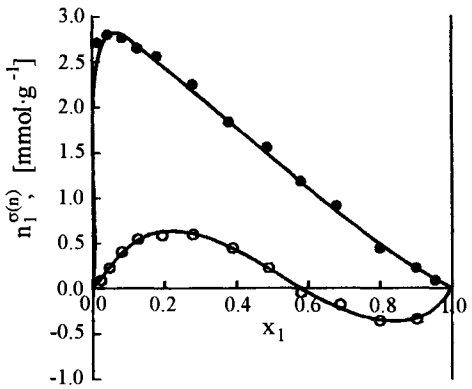

Figure 21. Adsorption excess isotherms on Na–Y (●) and dealuminated Y (○) zeolite in benzene(1)+n-heptane(2) mixtures.

When an excess isotherm is determined on dealuminated Y zeolite in benzene(1)+ n–heptane(2) mixture, again a type IV excess isotherm is obtained. In the composition range of $x_1 = 0.35 - 0.75$ the interfacial phase contains not only benzene but also n–heptane. Thus adsorption capacities determined in the mixtures of benzene and alcohols of various chain lengths, as well as in benzene(1)+n–heptane(2) mixtures unambiguously prove that for dealuminated zeolite, in the case of selective sorption of polar and apolar components of a mixture, there exists a relatively wide composition range in which a significant part of the interfacial phase is made up by the apolar component. The reason for this is that due to dealuminization the high–energy sites binding Na^+ ions disappear and the polarity of the surface is therefore decreased. On the basis of the data described above it is obvious that dealuminization of Na–Y zeolite achieves the same hydrophobizing effect as hydrophobization by cationic surfactants of clay minerals. Further information on the alteration of surface energy due to delauminization and on the depolarization of

Table 5
Immersional wetting enthalpy on Na–Y and dealuminated Y zeolites (after heating at 623 K) in different organic liquid

Liquids	Na–Y zeolite $\Delta_w H$(J/g)	Dealuminated zeolite $\Delta_w H$(J/g)
methanol	214.0 ± 2.4	41.4 ± 8.5
ethanol	196.5 ± 2.0	30.1 ± 8.7
n–propanol	190.6 ± 4.5	20.5 ± 6.7
n–butanol	175.0 ± 2.8	16.4 ± 9.7
benzene	129.5 ± 8.9	29.1 ± 6.5
n–heptane	73.4 ± 7.6	32.9 ± 7.6

the surface may be obtained by the determination of immersion wetting enthalpies. The values determined in alcohols of various chain lengths, benzene and n–heptane are listed in Table 5. The values of specific immersion wetting enthalpies ($\Delta_w H$) on Na–Y zeolite are very large in the alcohols; in benzene and n–heptane the wetting effect measured is less significant. In each liquid, the values measured on the dealuminated sample are significanly lower than those determined on Na–Y zeolite. It is clear from the data in Table 5 that on dealuminated samples the values of heat of wetting in benzene and in n–heptane are nearly identical, and do not differ significantly from the values measured in methanol and ethanol. In contrast, it can be seen that the heat effects measured on Na–Y samples in alcohols and benzene are significantly higher than those determined in apolar n–heptane[54].

REFERENCES

1. R.E. Grim, Clay Mineralogy, McGraw–Hill Book Comp., New York,1953.
2. H. van Olphen, An Introduction to Clay Colloid Chemistry, Intersci. Publ., New York, 1963.
3. U. Hofmann, K. Endell and D. Wilm, Z. Kristallogr., 86 (1933) 340.
4. H. van Olphen, J. Colloid Sci., 20 (1965) 822.
5. I. Barshad, Soil Sci. of America, 16 (1952) 176.
6. A. Weiss, A. Mehler and U. Hofmann, Z.Naturforsch., 11b (1956) 431.
7. R. Grenne–Kelly, Trans Faraday Soc., 51 (1955) 412.
8. K. Norrish, Discuss. Faraday Soc., 18 (1954) 120.
9. H. van Olphen, J. Colloid Sci., 20 (1965) 822.
10. A. Weiss, Organic Geochemistry, Springer Verlag, Berlin, 1969.
11. J.W. Jordan, B.J. Hook and C.M. Finlayson, J. Phys. Chem., 54 (1950) 1196.
12. T.R. Jones, Clay Minerals, 18 (1983) 399.
13. G. Lagaly, H. Stange, M. Taramasso and A. Weiss, Israel J. Chem., 8 (1970) 399.
14. G. Lagaly and R. Witter, Ber. Bunsenges. Phys. Chem., 86 (1982) 74.
15. T. Maramasso, G. Lagaly and A. Weiss, Kolloid–Z. Z. Polymere, 245 (1971) 508.
16. W.F. Bradley, Amer. Mineral, 25 (1940) 405.
17. B. Nagy and W.F. Bradley, Amer. Mineral, 40 (1955) 885.
18. G. Brown, Phil. Trans. Soc. London, A311 (1983) 14.
19. I. Dékány, F. Szántó, L.G. Nagy and G.Fóti, J. Colloid Interface Sci., 50 (1975) 265.
20. I. Dékány, L.G. Nagy and G. Schay, J. Colloid Interface Sci., 66 (1978) 197.
21. I. Dékány, F. Szántó and L.G. Nagy, Colloid and Polymer Sci., 65 (1978) 125.
22. I. Dékány, F. Szántó and L.G. Nagy, J. Colloid Interface Sci., 103 (1985) 321.
23. I. Dékány, F. Szántó and L.G. Nagy, J. Colloid Interface Sci., 109 (1986) 376.
24. W.H. Slabaugh and D.B. Hanson, J. Colloid Sci., 29 (1969) 460.
25. I. Dékány, F. Szántó, A. Weiss and G. Lagaly, Ber. Bunsenges. Phys. Chem., 89 (1985) 62.
26. I. Dékány, F. Szántó, A. Weiss and G. Lagaly, Ber. Bunsenges Phys. Chem., 90 (1986) 422.
27. I. Dékány, F. Szántó, A. Weiss and G. Lagaly, Ber Bunsenges. Phys. Chem., 90 (1986) 427.

28. I. Dékány, F. Szántó, L.G. Nagy and G. Schay, J. Colloid Interface Sci., 93 (1983) 151.
29. I. Dékány, F. Szántó and L.G. Nagy, Colloid and Polymer Sci., 256 (1978) 150.
30. G. Schay, in: E.Matijevic (ed.), Surface and Colloid Science, vol 2., Wiley, London, 1969, p.155.
31. G. Schay, in: D.H. Everett (ed.), Surface Area Determination, Butterworths, London, 1970, p.273.
32. G. Schay, Pure Appl. Chem., 48 (1976) 393.
33. G. Fóti, L.G. Nagy and G. Schay, Acta Chim. Hung., 80 (1974) 25.
34. J.J. Kipling, Adsorption from Solutions of Non–Electrolytes, Academic Press, London, 1965.
35. D.H. Everett, Trans. Faraday Soc., 60 (1964) 1803; 61 (1965) 2478.
36. D.H. Everett, Pure Appl. Chem., 53 (1981) 2181.
37. D.H. Everett, Progr. Colloid Polym. Sci., 65 (1978) 103.
38. A.Z. Zettlemoyer, G.J. Young and J.J. Chessick, J. Phys. Chem., 59 (1955) 962.
39. W.H. Slabaugh and P.A. Hiltner, J. Phys. Chem., 72 (1968) 4295.
40. W.H. Slabaugh and A.D. StClair, J. Colloid Sci., 29 (1969) 586.
41. W.H. Slabaugh and G.H. Kennedy, J. Colloid Sci., 18 (1963) 337.
42. W.H. Slabaugh and L.S. Carter, J. Colloid Sci., 27 (1968) 235.
43. I. Dékány, Á. Zsednai, Z. Király, K. László and L.G. Nagy, Colloids Surf., 19 (1986) 47.
44. I.Dékány , Á. Zsednai, L.G. Nagy and K. László, Magy. Kém. Folyóirat, 93 (1987) 400.
45. I. Dékány, Á. Zsednai, K. László and L.G. Nagy, Colloid Surf., 23 (1987) 41.
46. I. Dékány , Z. Király , I. Ábrahám , L.G. Nagy and K. László, Magy. Kém. Folyóirat, 93 (1987) 425.
47. I. Dékány, I. Ábrahám, L.G. Nagy and K. László, Colloids Surf., 23 (1978).
48. G. Lagaly, Clay Minerals, 16 (1981) 1.
49. K. Jasmund, G. Lagaly (eds.), Tonminerale und Tone, Steinkopft Verlag, Darmstadt, 1993, Chapter 3.
50. I. Dékány, F. Szántó, L.G. Nagy and G. Schay, J. Colloid Interface Sci., 93 (1983) 151.
51. J.H. de Boer and B.G. Linsen, Th. van der Plas, G.J. Zondervan, J. Catal., 4 (1965) 649.
52. B.C. Lippens and J.H. de Boer, J. Catal., 4 (1965) 319.
53. E.M. Flanigen, J.M. Bannett, R.W. Grose, J.P. Cohen, R.L. Patton, R.M. Kirchner and J.V. Smith, Nature, 271 (1978) 512.
54. I. Dékány, F. Szántó, L.G. Nagy and H. Beyer, J. Colloid Interf. Sci., 112 (1986) 261.

This Page Intentionally Left Blank

A. Dąbrowski and V.A. Tertykh (Editors)
Adsorption on New and Modified Inorganic Sorbents
Studies in Surface Science and Catalysis, Vol. 99
1996 Elsevier Science B.V.

Chapter 3.10
Liquid chromatography of fullerenes and study of adsorption properties of fullerenes crystals

V.Ya.Davydov

Department of Chemistry, M.V.Lomonosov Moscow State University, 119899 Moscow, Russia

1. INTRODUCTION

The discovery of stable C_{60} species which was named buckminsterfullerene or fullerene is one of the important events in chemistry [1].

The working out of preparation of fullerenes with high yield [2] was the beginning of intensive study of physicochemical, chemical, biochemical and other properties of new carbon modification [3,4]. To investigate the properties of fullerenes it is necessary to have a pure fullerenes so the separation and characterization of new modification of carbon – fullerenes have became increasingly important. The high performance liquid chromatography is the most effective method of separation and analysis of fullerenes [5–10]. For the separation of fullerenes different types of intermolecular interaction of fullerenes with the adsorbent and eluent have been exploited . The investigation of the effect of surface chemistry and eluent composition on the separation of fullerenes and their derivatives is an important problem.

Carbon containing solids is used as adsorbents for chromatography or for purification of compounds, as catalyst or supports for the preparation of catalyst. Activated carbon [11 – 13] and graphite [14] are used for the separation of fullerenes. Silica with deposited carbon layer may be used for separation in liquid chromatography [15, 16]. Carbon adsorbent namely graphitized carbon black is used in gas [17] and liquid [18] chromatography. For the separation of fullerenes carbon adsorbents are very useful, but owing to high adsorption potential of such adsorbents the large quantity of organic solvents is needed for the elution of all fullerenes and for the regeneration of chromatographic columns. As it was shown in [16] the adsorption potential of fullerenes crystals are much smaller than graphite adsorbent. So the use fullerene film on adsorbent surface makes it possible to prepare carbon containing adsorbent with smaller adsorption potential. The problem is to attach fullerene to the adsorbent surface by covalent bond. In this case the adsorbent with the attached fullerene molecules can be used in liquid chromatography.

The synthesis of polymer adsorbents containing fullerenes on the base of fullerene – melamine – formaldehyde polymer as well as on the base of fullerene – alkoxysilane xerogel are presented in [19]. These adsorbents with relatively high specific surface area are quite thermostable up to ~673 K. The main reaction for the synthesis of adsorbents was the

reaction of fullerene with aminogroups of compounds [20]. For the preparation of fullerene – containing organic aerogels and fullerene – containing silica aerogels supercritical carbon dioxide extraction was carried out [19].

The investigation of interactions of fullerene molecules with organic molecules may bring essential contribution to the study of physicochemical properties of fullerenes. The most distinctly intermolecular interactions are manifested in adsorption and chromatography based on these interactions. The study of adsorption at small coverage of different organic molecules on fullerene crystal surface makes it possible to determine thermodynamic characteristics of adsorption by means of which the intermolecular interactions can be described.

The properties of fullerene molecules arranged in surface layer of fullerene crystals can be characterized from the adsorption of compounds with different functional groups. Although the properties of free fullerene molecules are slightly different from the properties of fullerene in a crystal surface nevertheless the data on adsorption of organic compounds of different classes can be used to characterize intermolecular interaction of fullerenes with organic molecules and properties of fullerene molecules itself.

The most convenient method of study of adsorption at small coverage is gas chromatography. By this method it is possible to determine the constant of adsorption equilibrium (retention volume) and from the retention volumes at different temperatures to calculate the heat of adsorption and changing of differential standard entropy of adsorption. If the support for fullerene crystals is the adsorbent with inert and small specific surface area so the retention of compounds will be determined by intermolecular interaction of compounds with fullerene crystal surface. The deposition of fullerene crystals on support surface is quite difficult owing to small solubility of fullerene in organic solvents [21, 22] as well as small vapour pressure of fullerene [23].

For the characterization of interaction of fullerene molecules with organic compounds it is more convenient to determine not only thermodynamic characteristics of adsorption of molecule on the whole but also the contribution of different groups or fragments of molecules to these characteristics [24,25].

2. SEPARATION OF FULLERENES BY LIQUID CHROMATOGRAPHY

In arc discharge method of preparation of fullerenes [2] the mixture of fullerenes is produced. After isolation of fullerene mixture from the soot the extract containing C_{60}, C_{70}, C_{76}, C_{78}, C_{84} and other more heavy fullerenes are separated by liquid chromatography. Structure of these fullerenes are presented on Fig. 1.

For the separation of fullerenes by HPLC the stainless steel columns with Alusorb N 200, μ Bondapak 10 C18, LiChrosorb Diol, LiChrosorb SI 60 with bonded diphenylsilyl groups were used [16]. For the semi–preparative separation of C_{60} and C_{70} glass column (70×12 mm) packed by LiChrosorb SI 60 with deposited carbon layer prepared by modified method [15] was used [16].

In normal–phase liquid chromatography on silica and alumina the hydrogen bonding of fullerenes with surface hydroxyl groups of adsorbent is the most important. On separation of C_{60} and C_{70} on a column packed by alumina Alusorb N 200 from n–hexane the selectivity is 1.80 (Fig. 2 a.). The reversed–phase adsorbents such as silica with bonded diphenylsilyl

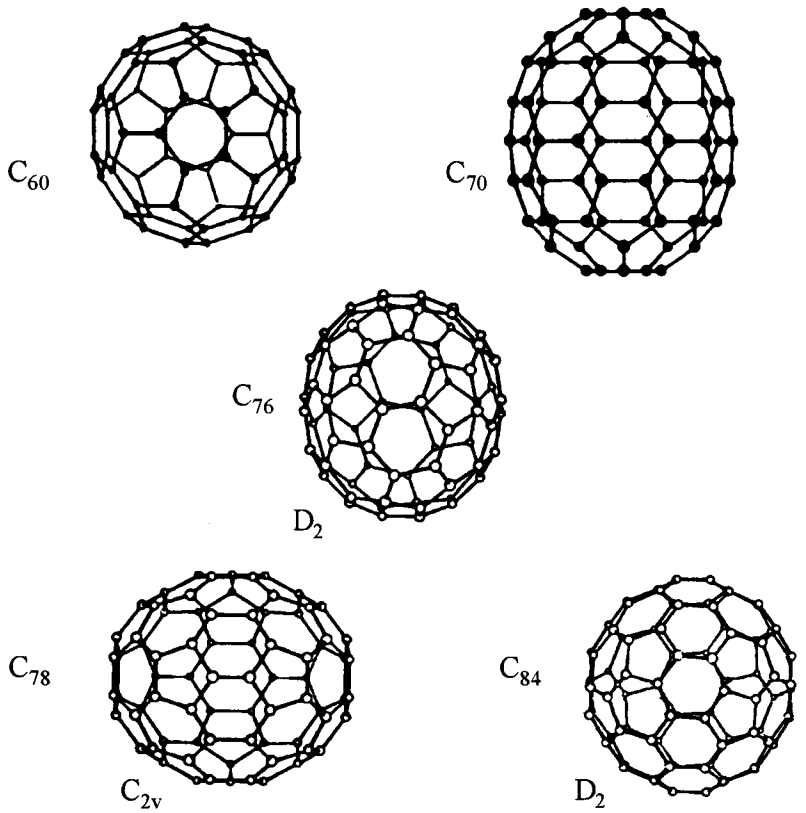

Figure 1. Fullerenes C_{60}, C_{70}, C_{76}, C_{78} and C_{84}.

groups also can be used for the separation of fullerenes. The separation on silica with bonded phenyl groups is based on a more strong interaction of fullerenes with phenyl groups of adsorbent than with n–hexane used as eluent. On separation of C_{60} and C_{70} from n–hexane on a semipreparative column packed by LiChrosorb SI 60 modified by diphenyldichlorosilane [26] the selectivity is 1.48 (Fig. 2 b.).

Excellent separation can be achieved by using silica with bonded octadecylsilyl groups and optimized composition of alcohol – hydrocarbon eluent [16]. At separation of C_{60} and C_{70} on μ Bondapak 10 C18 from mobile phase containing 70% of n–hexane and 30% of isopropanol the selectivity was 1.91 (Fig. 3 a.). For the detection UV detector at 254 nm can be used. In this case the oxide of C_{60} can be separated from C_{60} with the selectivity 1.18 and the oxide is eluted before C_{60} owing to more strong interaction of C_{60} oxide with alcohol in eluent. The determination of fullerene oxides is quite important in analysis of the purity of fullerenes.

The most convenient column for the separation of fullerenes and their oxides is the column packed by LiChrosorb Diol with eluent containing n–hexane and n–pentane. This

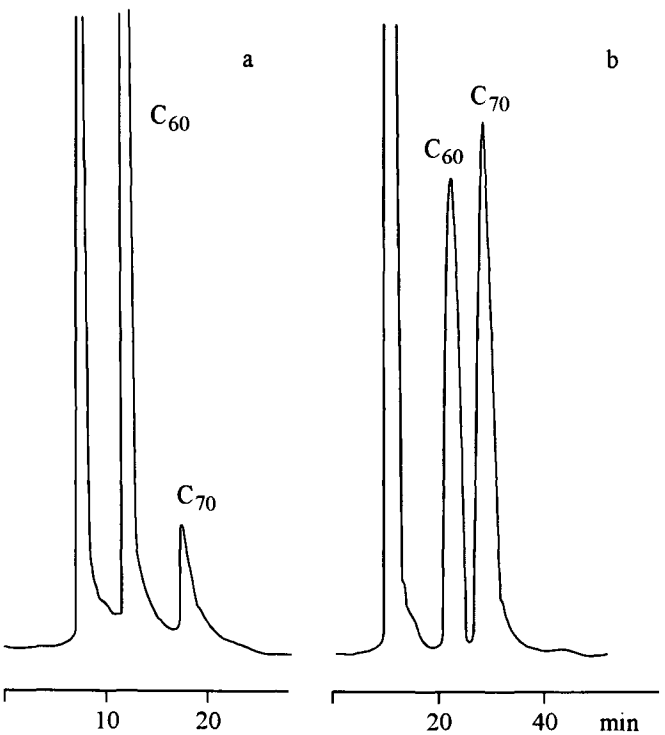

Figure 2. Separation of C_{60} and C_{70} fullerenes on Alusorb N 200 from n-hexane (column 250×3 mm, w = 0.5 ml/min) (a) and on LiChrosorb SI 60 with bonded diphenylsilyl groups from n-hexane (column 250×9 mm, w = 1 ml/min) (b).

column can be used for the separation and analysis of C_{60}, of C_{60} oxide, C_{70}, C_{76}, C_{78} and C_{84} with the selectivity relatively to C_{60} 1.33, 1.53, 2.20, 2.27 and 2.87 respectively (Fig. 3 b.). For the detection UV detector at 254 nm was used. This separation shows that the hydrogen bond of surface hydroxyl groups with fullerenes and their oxides is the most important in the separation process [16]. Oxides of fullerenes are eluted after the corresponding fullerenes.

For the purification of fullerenes from the fullerene oxides the activated alumina and silica can be used. Fulllerene oxides are adsorbed strongly on such adsorbents from solution and the oxides are removed from fullerene samples. For the preparative separation of fullerenes at present activated carbons and graphite are used [11–14]. For this purpose silica with the deposited carbon layer [16] can be used also. In this case it is very easily to regulate the pore diameter and specific surface area of adsorbents as well as particle diameter. Such adsorbents is very important for the decreasing of fullerenes loss. On preparative separation of fullerenes on LiChrosorb SI 60 with deposited carbon layer by modified method [15] on glass column first fractions contained quite pure C_{60}.

Thus silica with different surface chemistry is very useful for analytical and preparative separation of fullerenes. Silica with properly modified surface by deposition of carbon layer is useful adsorbent for preparative separation of fullerenes.

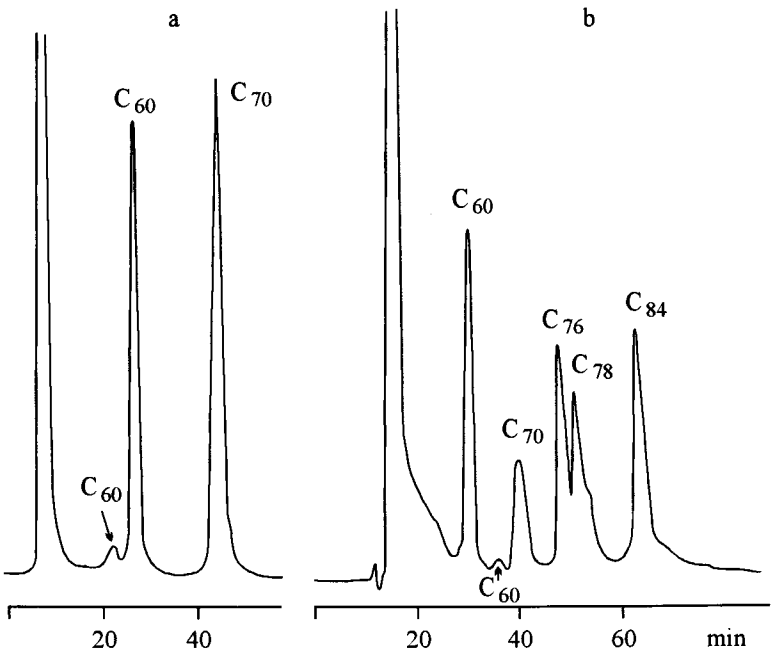

Figure 3. Separation of fullerenes and fullerene oxides on μ Bondapak C 18 from i-propanol-n-hexane (20:80) eluent (column 300×4 mm, w = 0.4 ml/min) (a) and on LiChrosorb Diol from n-hexane – n-pentane (80:20) eluent (column 250×4.6 mm, w = 0.2 ml/min) (b).

3. SILICA WITH BONDED FULLERENES

The fullerene containing silica adsorbent can be prepared by use the reaction of fullerenes with bonded to silica surface amino groups.

Silica gel with bonded aminopropyl groups (concentration of aminogroups is 0.8 mmol/g) with specific surface area s = 180 m^2/g and Silasorb Amin (CzR) with s = 200 m^2/g as initial adsorbents and fullerene C_{60} (more than 99% purity) were used for the modification of silica surface.

The surface of fullerene molecules itself in porous fullerene – containing aerogel probably are screened for the interaction with other organic molecules owing to the bonding of possible 14 aminocompounds with fullerene molecules during the reaction of polycondensation [19]. So to prepare fullerene containing adsorbent with opened for interaction of fullerene molecules with other compounds it is better to modify silica surface by 3-aminopropyltrietoxysilane and then to modify this adsorbent by fullerene molecules. In this case fullerene molecules can be attached to the surface only from one side of molecule and after reaction of modification the pore surface will be covered by fullerene molecules. The pore diameter and specific surface area of prepared adsorbent will be determined

by the corresponding values of initial silica adsorbent and by Van der Waals diameter of fullerene molecules.

Fullerene C_{60} and aminosilica react in toluene or p–xylene solutions at heating with formation of brown adsorbent. Specific surface area of silica gel and Silasorb Amin containing fullerene C_{60} after reaction of modification is increased a little in compared with the specific surface area of initial adsorbents. The values of C constant of BET equation for both adsorbents are practically the same. So the adsorption properties of these modified adsorbents are similar as well as the degree of modification by fullerene molecules.

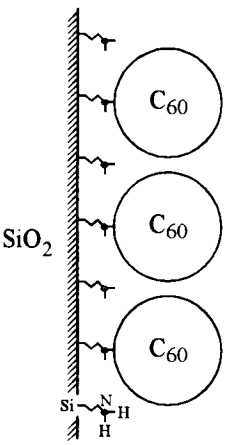

Figure 4. Arrangement of bonded C_{60} fullerene molecules on the surface of aminosilica.

The chemical attachment of fullerene molecules to the aminosilica surface does not produce the dense monolayer fullerene film on a surface of adsorbent owing to the differences in area occupied by amino group on surface of adsorbent and Van der Waals area of fullerene molecules. The concentration of free hydroxyl groups on hydroxylated silica surface is about 4 μmol/m^2 or approximately 2.6 groups / nm^2 [27]. After modification of silica by 3–aminopropyltriethoxysilane the concentration of amino groups on the surface will be approximately the same. So amino groups occupy the same area as free hydroxyl groups and the mean distance between amino groups is ~0.544 nm calculated from data [27]. Diameter of fullerene molecule can be accepted as 1.002 nm determined from closed – packed C_{60} [2]. It means that less than 20% of surface amino groups can react with fullerene C_{60} molecules (Fig. 4.).

Some information on adsorption potential of adsorbents with bonded fullerene molecules it is possible to obtain from the nitrogen adsorption isotherms. On Fig. 5 the isotherms of nitrogen adsorption on both adsorbents are presented. These isotherms coincide because of the C constant of BET equation practically the same (C constants of BET equation are 64 and 67 respectively). These values are much smaller than C on graphitized carbon black (C is ~1000) and a little smaller than on fullerene crystals (C is ~90). So the adsorption potential of such adsorbent is not very high.

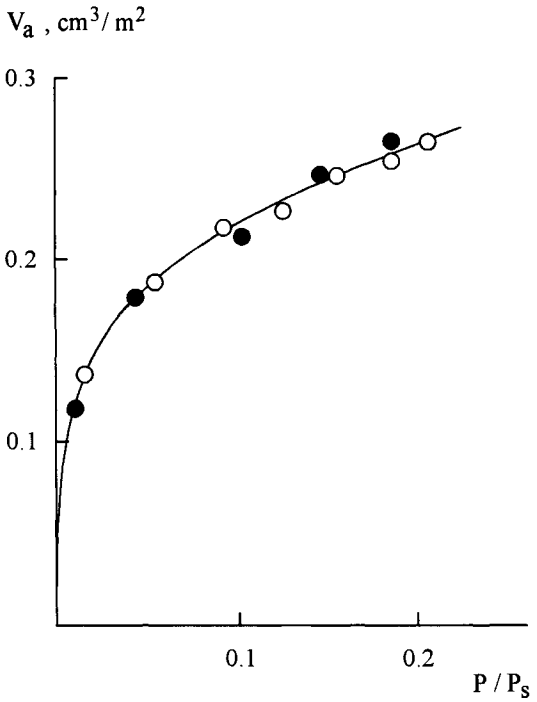

Figure 5. The isotherms of nitrogen adsorption at 77 K on aminosilica gel (filled dots) and on Silasorb Amin (open dots) with bonded fullerene C_{60}.

On separation of fullerenes on Silasorb Amin with bonded fullerene C_{60} the selectivity of adsorbent is comparable with selectivity of adsorbents used for separation of fullerenes.

Silica with bonded fullerene probably can be used for the separation of organic compounds by reversed phase liquid chromatography if the fullerene modifying layer will be stable to hydrolysis. The reaction of fullerenes with amino groups can be used for the modification of capillary columns for the separation of compounds by capillary gas chromatography.

4. ADSORPTION PROPERTIES OF FULLERENES C_{60} AND C_{70} CRYSTALS

In [16] the adsorption of organic compounds on fullerene C_{60} deposited on Chromosorb 750 was investigated. The comparison of the thermodynamic characteristics of adsorption of some organic substances on fullerene C_{60}, C_{70} crystals and on graphitized carbon black (Carbopack C HT) is of great interest.

Fullerenes C_{60} and C_{70} (more than 99% purity) were deposited on Chromosorb 750 (England) from the saturated solutions in o-dichlorobenzene. Carbopack C HT the adsorption properties of which is similar to the properties of graphitized carbon black was

used for the comparison of thermodynamic characteristics of adsorption of organic compounds on fullerenes C_{60} and C_{70} crystals and graphitized carbon black. The retention volumes of all compounds under investigation on support Chromosorb 750 itself coincide with void volumes of columns. So the retention volumes of compounds determined on Chromosorb with deposited fullerenes C_{60} and C_{70} characterize the interaction of organic molecules with surface of fullerene crystals. Thermodynamic characteristics of adsorption and the contributions of molecular groups to the adsorption equilibrium constant and to the heat of adsorption were calculated by the least-squire method.

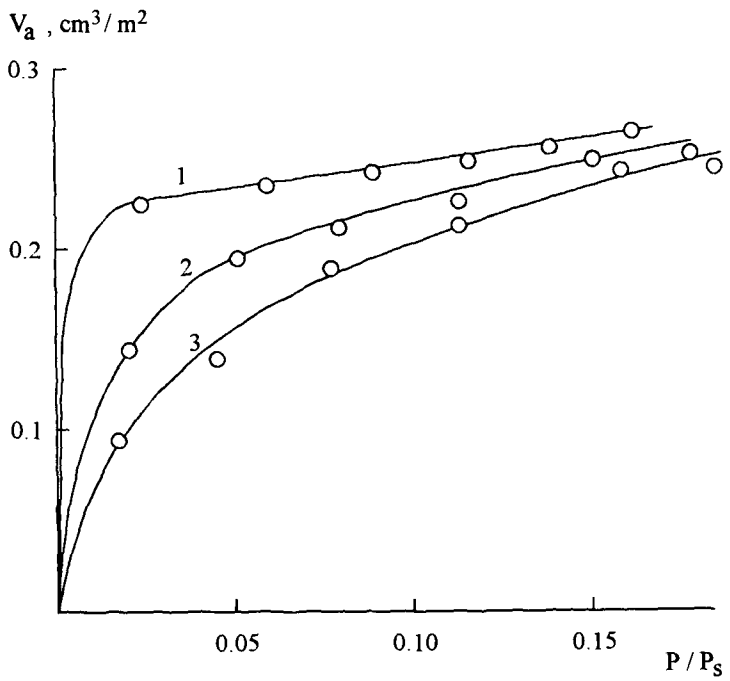

Figure 6. The isotherms of nitrogen adsorption at 77 K on Carbopack C HT (1), on Chromosorb 750 with deposited fullerene C_{60} (2) and C_{70} (3).

Fig. 6. shows the nitrogen isotherm of adsorption on Chromosorb with fullerene C_{60} and C_{70} crystals and on Carbopack C HT. Specific surface area s for Chromosorb with C_{60} is 0.52 m^2/g, with C_{70} is 0.45 m^2/g and Carbopack is 8.7 m^2/g. The constant C of BET equation for fullerenes are much smaller than for graphite . Constant C for C 60 crystals is 90, for C_{70} is 35 and for Carbopack is about 1000. These data shows that dispersion interactions of molecules with fullerene crystals will bring smaller contribution at adsorption in compared with graphitized carbon black owing to smaller concentration of adsorption centers on the surface of fullerene crystal.

The thermodynamic characteristics of adsorption of some organic compounds on fullerene crystals C_{60} and C_{70} are presented on Table 1 and those on Carbopack on Table 2. Adsorption equilibrium constant values of n-alkane and aromatic compounds on fullerenes

Table 1
The retention volumes (V_a, cm^3/m^2) at 373 K, the heats of adsorption at small coverage (q, kJ/mol) and changes of differential standard entropy of adsorption ($-\Delta\bar{S}^0$, J/mol·K) of some organic compounds on fullerenes C_{60} and C_{70}

Compound	C_{60}			C_{70}		
	V_a	q	$-\Delta\bar{S}^0$	V_a	q	$-\Delta\bar{S}^0$
n-Hexane	1.27	48±2	134±5	0.48	40±2	122±5
n-Heptane	3.99	52±6	135±6	1.16	47±2	133±5
n-Octane	11.38	52±2	126±7	2.85	50±2	134±4
n-Nonane	31.57	52±4	118±10	7.25	54±3	136±7
Benzene	0.69	37±2	110±5	0.75	26±2	79±6
Toluene	2.99	41±2	109±6	2.07	34±3	94±7
Ethylbenzene	7.53	46±2	114±7	3.84	39±4	102±11
o-Xylene	8.91	48±2	118±7	3.65	47±3	123±8
Chlorobenzene	4.57	41±3	107±9	4.06	33±4	85±10
Ether	0.69	40±2	111±6	0.59	24±2	77±5
Acetone	0.86	31±3	92±8	1.02	22±3	66±8
Methyl ethyl ketone	1.65	35±3	96±9	1.40	29±4	84±12
Ethyl acetate	2.06	37±3	100±9	1.64	32±4	88±12
n-Propanol	1.55	36±3	101±8	1.32	31±4	88±12
n-Butanol	3.33	42±4	112±12	2.20	38±4	103±12
Acetonitrile	2.30	18±3	49±9	5.72	22±5	53±13
Nitromethane	1.13	22±3	65±10	4.19	25±3	62±10
Pyridine	4.44	37±4	99±12	5.21	25±4	62±12
Triethylamine	4.33	46±4	119±11	1.56	45±5	124±14

are essentially smaller than on Carbopack and on C_{70} they are smaller than on C_{60}. Polar compounds adsorb stronger on fullerene crystals than on Carbopack owing to stronger interaction of electron-donor and electron-acceptor molecules with fullerene molecules arranged on the surface of its crystals in compared with the graphite surface of Carbopack. Fig. 7 and 8 shows the differences in the retention volumes of hydrocarbons and alcohol on C_{60}, C_{70} and Carbopack.

From the retention volumes at different temperatures the heats of adsorption at small coverage and changes of differential standard entropy of adsorption were calculated (see Table 1 and 2). The heats of adsorption are less sensitive to the properties of fullerene molecules and to the distinction in geometry of surface of fullerene crystals and surface of Carbopack.

Considering adsorption interaction of molecules with different functional groups as a whole sometimes it is difficult to reveal the details of interaction because of the increasing of contribution of one group to the interaction can be compensated by decreasing of contribution by other groups. So it is important to determine the contribution of different groups or fragments of molecules to the thermodynamic characteristics of adsorption and to consider mechanism of adsorption in accordance with these data.

Table 2
The retention volumes (V_a, cm^3/m^2) at 373 K, the heats of adsorption at small coverage (q_i, kJ/mol) and changes of differential standard entropy of adsorption ($-\Delta\bar{S}^0$, J/mol·K) of some organic compounds on Carbopack C HT

Compound	V_a	q_i	$-\Delta\bar{S}^0$
n-Hexane	3.15	41	110
n-Heptane	12.34	47	112
n -Octane	48.12	53	117
n-Nonane	195.33	60	125
Benzene	2.05	39	106
Toluene	12.44	47	112
Ethylbenzene	26.47	49	112
o-Xylene	79.36	54	117
Chlorobenzene	15.28	47	111
Ether	0.50	32	99
Acetone	0.17	28	98
Methyl ethyl ketone	0.56	33	102
Ethyl acetate	0.81	35	104
n-Propanol	0.23	31	103
n-Butanol	0.81	38	111
Acetonitrile	0.09	23	90
Nitromethane	0.11	26	96
Pyridine	2.88	44	119
Triethylamine	4.47	40	103

In liquid chromatography such consideration already used for the quantitative characterization of interaction of molecules and of its fragments with solvent and surface of adsorbent for study of mechanism of adsorption from solution [24,25].The approach that groups of the same type in different molecules bring the same contribution to the adsorption is quite well realized on adsorption from solution owing to interaction of adsorbed molecules with solvent that decreases the differences in interaction of similar groups in various molecules with adsorbent [28,29].

On adsorption from the gas phase at small coverage at gas chromatographic conditions the contribution of groups the same type in different isomer molecules will be distinguished. This distinction is used for the determination of structure of molecules by chromatoscopic method [30] . If to consider molecules of similar geometry for example the derivatives of n-alkanes and benzene it is possible to propose that groups of the same type will bring similar contribution to the adsorption from gas phase also.
The retention volume of compound (V_a) can be presented as:

$$\ln V_a = \sum(\ln V_{ai})n_i \qquad (1)$$

where V_{ai} is the contribution to the retention volume of i - groups and n_i is the number of such groups in a molecule.

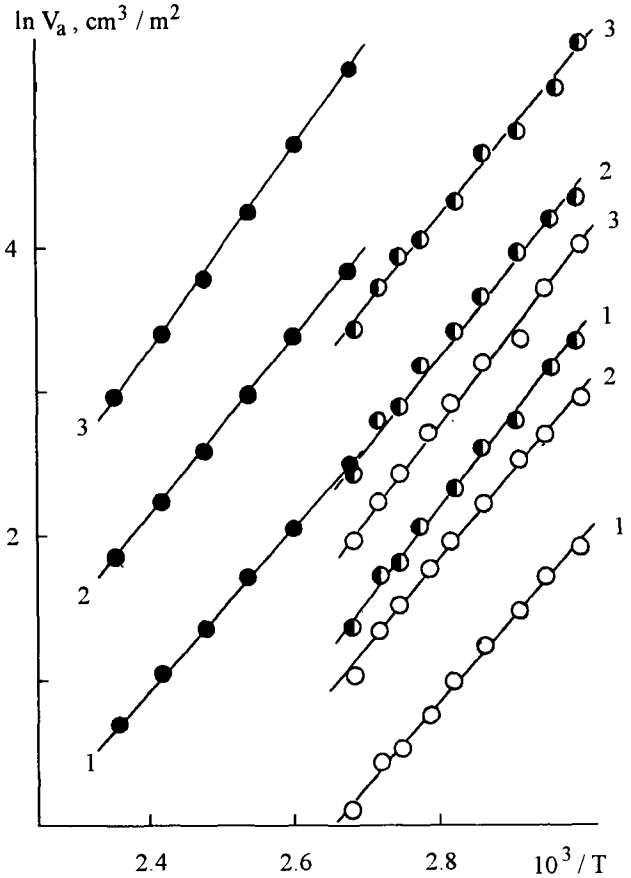

Figure 7. Effect of temperature on the retention volumes V_a (cm^3/m^2) of some n-alkanes on fullerene C_{70} (open dots), on fullerene C_{60} (half filled dots) and on Carbopack C HT (filled dots). 1: n-heptane, 2: n-octane and 3: n-nonane.

From the retention volume for some compounds consisting of different number of the same groups it is possible to determine the contribution of groups to the retention by solving system of linear equations (1).

The contribution of groups or fragments to the retention volume at different temperatures (V_{ai}) can be calculated from the retention volumes of compounds at the same temperatures (V_a) and then the contribution of groups to the heat of adsorption from equation:

$$\ln V_{ai} = q_i/RT + (\Delta\overline{S}_i^0 + R)/R \qquad (2)$$

where q_i is the contribution of i-group to the heat of adsorption.

On the other hand the heat of adsorption of compound can be presented as sum of the contribution of groups to the heat of adsorption.

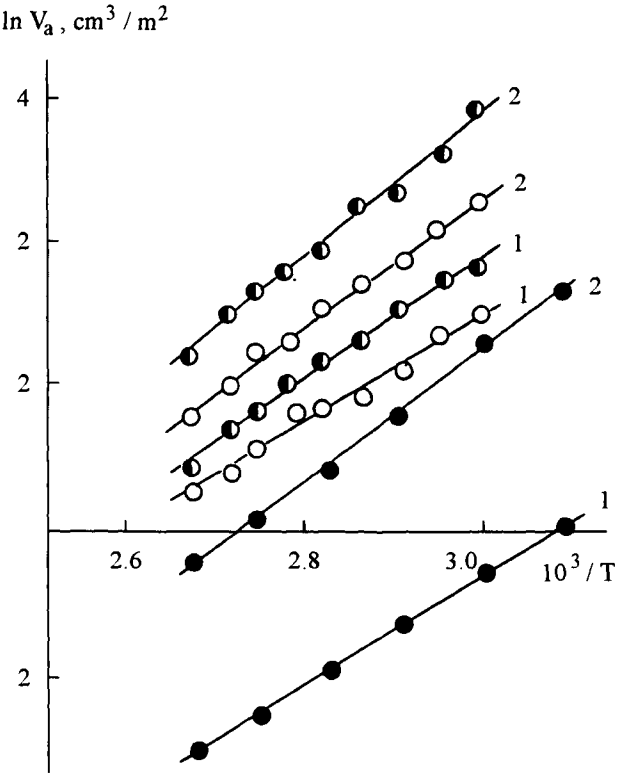

Figure 8. Effect of temperature on the retention volumes V_a (cm^3/m^2) of n–propanol (1) and n–butanol (2) on fullerenes C_{60}, C_{70} and on Carbopack (dots are the same as on Fig. 7).

$$q = \sum q_i n_i \tag{3}$$

where q_i is the contribution of i–group to the heat of adsorption and n_i is the number of group the same type. By solving the system of linear equations Eq. (3) it is possible to calculate q_i also.

In Table 3 and 4 the values of contributions of different groups or fragments of molecules to the retention volume (V_{ai}) calculated by Eq. (1) and to the heat of adsorption (q_i) calculated by Eq. (2) ($q_{i,1}$) and by Eq (3) ($q_{i,2}$) are presented. It can be seen that the contributions of polar groups (electron–donor and electron–acceptor) to the adsorption equilibrium constant are much bigger on fullerenes then on Carbopack but the contributions of hydrocarbon groups are correspondingly smaller. There is a good agreement between q_i calculated by two methods. The contribution to the heat of adsorption of molecular groups can be easily calculated from the heat of adsorption because there is no need to make intermediate calculation of the group contributions to the retention at different temperatures.

Table 3
The contributions of groups or fragments of molecules to the retention volume (V_{ai}, cm^3/m^2) at 373 K and the heat of adsorption ($q_{i,1}$ and $q_{i,2}$, kJ/mol) of some organic compounds on fullerenes C_{60} and C_{70}

Fragment	C_{60}			C_{70}		
	V_a	$q_{i,1}$	$-\Delta\overline{S}^0$	V_a	$q_{i,2}$	$-\Delta\overline{S}^0$
$-CH_3$	0.16	20±4	20.0	0.15	11±4	10.0
$-CH_2-$	2.72	2±1	2.1	2.24	5±1	4.9
-CH=	0.94	6±1	6.2	0.95	4.2±0.3	4.3
>C=	24.10	-9±4	-8	16.10	3±5	2.0
>C= (orto)	20.80	-11±8	-8	14.20	4±4	4.5
-Cl	0.26	19±4	18	0.32	9±5	9
-O-	3.51	-5±5	-3.7	5.37	-7±5	-6.5
>C=O	27.30	-8±5	-7.6	36.30	2±8	2.4
-COO-	28.70	-6±7	-4.7	33.30	6±8	6.4
-OH	1.14	14±2	14	1.53	11±3	12
-CN	14.20	-3±4	-2	38.60	12±4	12
$-NO_2$	6.98	2±3	2	28.30	14±5	15
-N=	6.06	4±4	6.2	6.60	4±3	3.3
>N-	49.90	-21±7	-20	42.70	-2±7	-1

Table 4
The contributions of groups or fragments of molecules to the retention volume (V_{ai}, cm^3/m^2) at 373 K and to the heat of adsorption ($q_{i,1}$ and $q_{i,2}$, kJ/mol) of some organic compounds on Carbopack C HT

Fragment	V_{ai}	$q_{i,1}$	$q_{i,2}$
$-CH_3$	0.15	8±3	9
$-CH_2-$	3.44	6±1	5.8
-CH=	1.13	6.4±0.1	6.4
>C=	34.7	1±4	4
>C= (orto)	45.7	4±3	5
-Cl	0.25	11±2	11
-O-	1.9	3±3	2.1
>C=O	7.36	12±4	9.6
-COO-	10.5	13±4	11.1
-OH	0.13	11±1	11
-CN	0.59	15±4	14
$-NO_2$	0.73	18±3	17
-N=	1.29	10±2	11.8
>N-	25.2	-5±4	-5

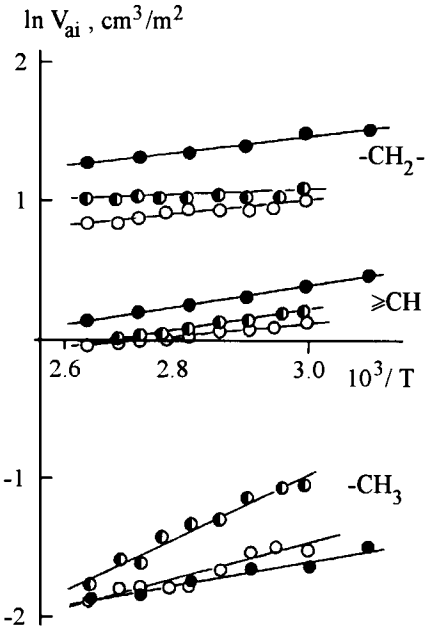

Figure 9. Effect of temperature on the contribution of $-CH_2-$, $-CH=$ and $-CH_3$ groups to the retention volume V_a (cm^3/m^2) on fullerenes C_{60}, C_{70} and Carbopack (dots are the same as on Fig. 7).

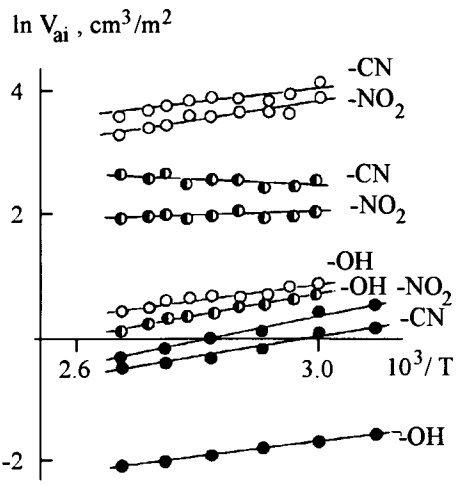

Figure 10. Effect of temperature on the contribution of –OH, –CN and $-NO_2$ groups to the retention volume V_a (cm^3/m^2) on fullerenes C_{60}, C_{70} and on Carbopack (dots are the same as on Fig. 7).

For more polar groups the contributions to the heat of adsorption on fullerene C_{60} are negative but on fullerene C_{70} only for some polar groups the contributions are negative while on Carbopack only for triethylamine the contribution of amino group to the heat of adsorption is negative. Probably it is owing to the repulsion of polar groups connected with neighbouring groups which bring addition interaction. Interesting to note the relatively large contribution of methyl groups to the heat of adsorption is realized at small contribution of these groups to the constant of adsorption equilibrium. The mobility of methyl groups are higher than methylene groups and so the last ones have large contribution to the retention volume and relatively small contribution to the heat of adsorption. The comparison data of Table 1 shows that larger retention volumes of compounds on crystals C_{60} in compared with the retention volumes on crystals C_{70} correspond to higher heats of adsorption as well as the data of Table 3 shows similar relationship between the contributions of molecular groups to the retention volumes and to heat of adsorption on C_{60} and C_{70} . The comparison of the data from Tables 3 and 4 shows that for polar groups smaller contributions to the retention volume on Carbopack correspond to larger contribution to the heat of adsorption in compared with adsorption on fullerenes. Probably it is connected with distinction in geometry of fullerene crystals surface and graphite surface and so with the effect of entropy of adsorption on adsorption process.

Figs. 9, 10 and 11 demonstrate effect of temperature on calculated ln V_{ai} for: hydrocarbon groups Fig. 9, for some polar groups Fig. 10 and for nitrogen in pyridine and triethylamine Fig. 11.

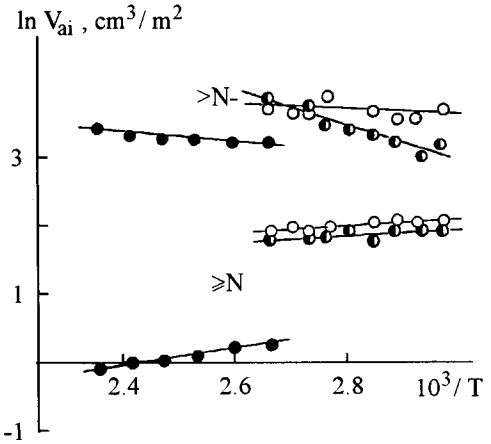

Figure 11. Effect of temperature on the contribution of >N– and –N= groups to the retention volume V_a (cm^3/m^2) on fullerenes C_{60}, C_{70} and on Carbopack (dots are the same as on Fig. 7).

Thus the thermodynamic characteristics of adsorption at small coverage of different classes organic compounds determined by gas chromatography show that surface of fullerene molecular crystals and surface of graphitized carbon black have essentially different adsorption properties. On adsorption on fullerene crystals the electron-acceptor and electron-donor properties of fullerene molecules are manifested. Adsorption data on fullerenes C_{60} and C_{70} show that properties of fullerene C_{60} and C_{70} molecules arranged in surface layer of crystals are different.

REFERENCES

1. H.W.Kroto, J.R.Health, S.C.O.Brien, R.F.Curl, R.E.Smally, Nature London, 318 (1985) 162.
2. W.Kratschmer, L.D. Lamb, K.Fostiropoulos, D.R.Huffman, Nature London, 347 (1990) 354.
3. H.W.Kroto, A.W.Allaf, S.P.Balm, Chem. Rev.,91 (1991)1213.
4. K.M.Kadish and R.S.Ruoff (eds.), Fullerenes. Resent Advances in the Chemistry and Physics of Fullerenes and Related Materials. The Electrochemical Soc. Inc., Pennington, 1994.
5. H.Ajie, M.M.Alvarez, S.J.Auz, R.D.Beck, F.Diederich, K. Fostiropoulos, D.R.Huffman, W.Kratschmer, Y.Rubin, K.E.Schriver, D.Sensharma, R.L.Whetten, J.Phys.Chem., 94 (1990) 8630.
6. J.P.Hare, H.W.Kroto, R.Taylor, Chem.Phys.Lett.,177 (1991) 394.

7. J.M.Hawkins, T.A.Lewis, S.D.Loren, A.Meyer, J.R.Health, Y.Shibato, R.J.Saykalli, J.Org.Chem., 55 (1990) 6250.
8. F.Diederich,R.Ettl,Y.Rubin,R.L.Whetten, R.Beck, M.Alvarez, S.Anz, D.Sensharma, F.Wude, K.C.Khemani, A.Koch, Science, 252 (1991) 548.
9. M.Diack, R.L.Hettich, R.N.Compton, G.Guiochon, Anal.Chem., 64 (1992)2143.
10. W.A.Scrivens, J.M.Tour, J.Org.Chem., 57 (1992)6932.
11. W.A.Scrivens, P.V.Bedworth, J.M.Tour. J. Am. Chem. Soc., 114 (1992) 7917.
12. W.A.Scrivens, J.M.Tour, J. Org. Chem., 57 (1992) 6922.
13. A.D.Darwish, H.W.Kroto, R.Taylor, D.R.M.Walton, J.Chem. Soc., Chem. Commun., (1994) 15.
14. M.Vassallo, A.J.Palmisano, L.S.K.Pang, M.A.Wilson, J.Chem. Soc., Chem. Commun., (1992)60.
15. V.Ya.Davydov, V.I.Nazarova, Vestnik Moskovskogo Universiteta, seriya 2 Khimiya, 29 (1988) 580.
16. V.Ya.Davydov, G.N.Filatova, N.M.Khrustaleva, T.M.Roshchina, in: Fullerenes. Resent Advances in the Chemistry and Physics of Fullerenes and Related Materials, K.M.Kadish and R.S.Ruoff (eds.), The Electrochemical Society Inc., Pennington, 1994,p.1588.
17. A.V.Kiselev and Y.I.Yashin, Gas Adsorption Chromatography, Plenum Plenum Press, New York, 1969.
18. J.H.Knox, B.Kaur, G.R.Millward, J. Chromatogr., 352 (1986) 3.
19. W.L.Bell, Z.Jang, S.D.Dietz, Fullerenes. Resent Advances in the Chemistry and Physics of Fullerenes and Related Matarials, (eds.) K.M.Kadish and R.S.Ruoff, The Electrochemical Society Inc., Pennington. 1994, p.92.
20. R.Mehortra, E.P.Gianelis, R.F.Ziolo, J.P.Rogalsky, Chem. Mater., 4 (1992) 236.
21. R.S.Ruoff, D.S.Tse, R.Malhotra, D.C.Lorents, J.Phys. Chem., 97 (1993) 3379.
22. N.Sivaraman, R.Dhamodaran, I.Kalliapan, T.G.Scrinivasan, P.R.Vasudeva Rao, C.K.Mathews, J.Org. Chem., 57 (1992) 6077.
23. C.K.Mathews, M.Sai Baba, N.T.S.Lakshmi, R.Balasubramanian, N.Sivaraman, P.R. Vasudeva Rao, J. Phys. Chem., 96 (1992) 3566.
24. V.Ya.Davydov, J. Chromatogr., 365 (1986) 123.
25. V.Ya.Davydov, G.N.Filatova, E.Smolcova-Keulemansova, Yu.Zima, Chromatographia, 25 (1988) 1059.
26. V.Ya.Davydov, M.Elizalde Gonzalez, A.V.Kiselev, J.Chromatogr., 204(1981)293.
27. V.Ya.Davydov, A.V.Kiselev, L.T.Zhuravlev, Trans.Faraday Soc.,60 (1964)2254.
28. V.Ya.Davydov, Zhao Zhen-Gho, Zhurn. Fiz. Khimii, 68(1994) 1084.
29. Zhao Zhen-Gho, V.Ya.Davydov, Acta Chimica Sinica, 52 (1994) 1165.
30. A.V.Kiselev, in: Physical Chemistry; Modern Problems, Ya. M. Kolotyrkin (ed.), Khimiya, Moscow,1982, No. 2, p. 180 (in Russian).

Subject Index

Activity coefficient, 650
  analytical expression, 741, 748
  global, 656
  ionic, 871
  of charged surface sites, 863
Adsorbent
  Al_{13} colloids, 320
  aluminophosphates, 3 *et seq.*
  aluminosilicates, 534
  amorphous oxides, 411–414
  calcium hydroxyapatite, 301
  carbon–mineral, 115 *et seq.*
  clay minerals, 879 *et seq.*
  co–precipitated hydroxides, 57 *et seq.*
  colloidal silicas, 93 *et seq.*
  fluorinated activated carbon fiber, 583–584
  geothite, 830
  hydrated silica–coated activated carbon (ACF), 582–583
  inorganic chemical and morphological characteristics, 479 *et seq.*
  iron oxide dispersed–ACF, 593
  modified layer silicates, 549–552
  mineral oxides, 756 *et seq.*, 797
  modified silica, 552–553
  molecular sieves, 3 *et seq.*
  natural and organosubstituted layer silicates, 554–557
  new chromatographic, 565–568
  organoderivatives of silica, 557–560
  polyhydrosiloxanes, 151–152, 285
  porous glasses, 31 *et seq.*
  silica with bonded fullerenes, 903–905
  silicates, 879, 533
  strontium hydroxyapatite, 305
  with fullerenes, 899
Adsorption
  and chromatographic studies, 411 *et seq.*
  and heat of adsorption on fullerenes, 910, 911
  and immersional wetting on clay minerals, 879 *et seq.*
  and properties of fullerenes crystals, 899, 906
  and structure of modified layer silicates and silica, 549–553
  at oxide/electrolyte interface, 381–404
  at oxide/water interface, 359–381
    model, 366–369
  at the solid–liquid interface, 649 *et seq.*
  bivalent cations on oxide surfaces, 397–404
  divalent metal ions, 873–875
  energy of ammonia, 9
  from dilute solutions, 725
  from electrolyte solutions, 729
  from multicomponent solutions, 673 *et seq.*
  from non–electrolytic binary mixtures, 649 *et seq.*
  from solutions on silica, 705 *et seq.*
  general molecular statistics
    approach, 540–549
      calculation of thermodynamic functions, 544–549
      interaction energy and adsorption potential, 541–544
      thermodynamic quantities, 540–541
  heats, 674
  multicomponent, 740
  of anions by oxides, 840–842
  of cations by oxides, 842–843

of ionic surfactants, 797 *et seq.*; *see also* adsorption of ionic surfactants
of ions on porous glasses, 40–41
of ions, 757; *see also* adsorption of ions
of metal ions by oxides, 831
of simple ions on oxide surfaces, 390–396
of supercritical fluid molecules, 24
of water on activated aluminas, 630, 638–641
on amorphous oxides, 343–352; *see also* computer simulation
on carbon–mineral adsorbents, 117–123, 130, 131, 135, 136, 139, 141, 142
on clay minerals, 879 *et seq.*
on heterogeneous surfaces, 649 *et seq.*
on hydrophilic and hydrophobic silicates, 879 *et seq.*
on modified layer silicates and silica, 549–553
thermodynamic functions, 560–565
on zeolites, 852–896
separation factor of, 881
thermodynamic characteristics of, 913
unimolecular, 266

Adsorption equilibria
on heterogeneous surfaces, 441–442
on homogeneous surfaces, 440
on silica surface sites, 707, 716, 725
with competing adsorption, 709
without competing adsorption, 707

Adsorption excess, 650, 677
on clay minerals, 881–883
on zeolites, 892–896
specific reduced, 881

Adsorption isotherm
Everett, 650
exponential, 652
for anions, 773
for cations, 773
for protons, 773
generalized Freundlich, 656, 750
integral representation, 415–418
Langmuir-Freundlich, 656, 790
on equilibrium surface, 442–444
on heterogeneous surfaces, 441–442
on homogeneous surfaces, 440
Toth, 656

Adsorption kinetics
first order, 446, 447
on heterogeneous surfaces, 437
on real surfaces, 435 *et seq.*
second order, 446, 447, 449, 451

Adsorption model
for liquid–solid interface, 651
of adsorbed layer, 731
of ionic surfactants, 799

Adsorption of ionic surfactants
critical micelle concentration (cmc), 802, 806, 820
electrophoretic mobility, 806, 817, 824
from aqueous solutions, 797 *et seq.*
influence of physical factors on, 812–824
materials and experimental techniques, 798–800
mechanism of, 810–812
microcalorimetry of, 807–810
on mineral substrates, 797
surface phase model, 804

Adsorption of ions, 734
anions, 772, 833–834
application to soil, 843–850
cations, 772, 831–832
charge determinations, 758, 767
monocomponent, 785
multicomponent, 788
on heterogeneous surfaces, 784–794
one-pK_H model of, 781
site binding model of, 767
specific adsorption charge, 762
specific, 762–763, 772, 783–784
two-pK_H model of, 784

Aggregation
effect on, 98–104
of hydrothermal treatment, 99
of medium pH, 103–104

of particle concentration, 98
of temperature, 99-103
of silica polymers, 97–98
Al_{13} colloids
adsorption of surfactants, 321–323
electrochemical interface model, 323–325
preparation, 320
surface heterogeneity , 322
Aluminophosphates
adsorption of
ammonia, amines, 7-11
porphyrins, 15–20
water, 11–15
computational study of electronic structure, 3–5
Calcium hydroxyapatite
adsorption of carbon dioxide, 314–316
adsorption of methyl iodide, 313–314
adsorption of water, 308–310
adsorption of methanol, 311–313
methods of preparation, 302
surface structure, 303–305
Calorimetry
of adsorption of ionic surfactants, 807–810
Carbon–mineral adsorbents
adsorption on, 117–123, 130, 131, 135, 136, 139, 141, 142
chemical composition of carbon deposit, 116, 117
chemical modification, 120–125, 134–136
chromatographic separation on, 125–128, 141
hydrothermal treatment, 128–133, 136, 137
methods of preparation, 116
surface heterogeneity, 116, 117
Carbon nanotubes
adsorption of aromatic hydrocarbons, 21–23
structure, 20, 21
Chemical potential
analytical expression, 737, 739
of adsorbed layer, 743
Chemisorption
alk–1–ens on modified silicas, 159–163, 170, 171, 179–183
and micropore filling, 593
benzene on chlorinated silica, 150
chemical modification of mineral surfaces, 191 *et seq.*
chlorides and oxychlorides of metals on silica and alumina, 215–228
fixed heterogeneity model in, 456–457
induced–heterogeneity model in, 457–459
kinetics on homogeneous surface 455, 456
Landsbergs model, 459
of functional olefins on modified silica, 163–169
of olefins on modified silicas, 173–179
on pyrogenic oxides
kinetic models, 253–267
main stages, 244-251
role of external and internal pore diffusion, 244, 245
structure and reactivity of modifiers, 267–277
types of surface reactions, 239–244
organometallic compounds on chlorinated silica, 148–149, 156, 158
silicon hydroxides on silica, 154–156
surface–reconstruction model in, 459–461
Chemistry of surface bounded compounds
distribution of bounded compounds on silica surface, 194–204
methods of determination, 196–199
types, 194–196
organization of bounded layers, 206–210
subject matter, 192
terminology, 192–194
Colloidal silica
adsorption on, 109–11

physicochemical properties, 104–108
surface modification, 111–112
various forms, 93–94
Computational studies
multi technique methods, 3
on the design of synthetic sorbents, 3 *et seq.*.
Computer simulation
methods, 335, 599
molecular dynamics (MD), 5–7, 338, 342
Monte Carlo (MC), 262, 340, 342, 599 *et seq.*
of adsorption on amorphous oxides, 335 *et seq.*, 343–346
above the Henry region, 349–352
adsorption potential, 343–346
at Henry's low region, 346–349
of atomic structure of amorphous silica, 338–341
of atomic structure of vitreous silica, 341–343
Concentration swing adsorption 642, 643–645
Concentration–thermal swing adsorption, 644
Contact catalysis, 437
Co-precipitated metal hydroxides
binary systems, 58–74, 80–87, 89
four component systems, 77–78,85
influence on adsorption–structural properties of
hydroxide concentration, 70–74
pH–precipitation, 66-70
temperature of co–precipitation, 80–83
mechanism of structure formation, 62–66, 75–79
specific surface area of, 86–90
synthesis of, 83–86
ternary systems, 60, 75–79
Desorption kinetics
desorption isotherms, 453–455
from heterogeneous surface, 437, 445–446
from homogeneous surface, 444
Distribution function
Gaussian, 661
of surface active sites upon reactivity, 220
Rayleigh, 661
site energy, 751
Double electrical layer
diffuse charge density, 760
diffuse layer potential, 760, 806
Donnan model of, 764, 779
electrokinetic potential, 763–764, 860
for flat surfaces, 758 *et seq.*
Gouy–Chapman (GC) model of, 758, 860, 865
of mineral oxides, 758
Stern–Donnan (SD) model of, 765–766
Stern-Gouy–Chapman (SGC) model of, 761, 865, 869
thickness of, 760
zeta potential, 806, 860, 866
Electrical interfacial layer, *see also* double layer model
calorimetry, 869–873
electrokinetics, 865–869
in metal/oxide aqueous systems, 857 *et seq.*
modelling of equilibria in, 859
potentials, 860
problems in modelling, 857 *et seq.*
structure of, 859–860
surface complexation model, 859–865, 873–875
triple layer model, 860, 865
Elovich equation, 438,439
in terms of surface heterogeneity, 449–453
Flow calorimetry, 887, 888
Gas chromatography, 503, 517, 674
and gas–solid system, 420
for studying the adsorption on solids, 553–560
integral representation of the retention volume, 420–422
Geothite
adsorption of anions by, 833–834
adsorption of cations by, 831–832

laboratory preparation, 830
natural, 830
reaction with metal ions, 831–833
water content of, 830
Heterogeneity
chemical and structural of oxide surfaces, 238, 251–253
effect on adsorption of ionic surfactants, 817
effect on surface change, 862
energetical, 490, 650
influence on gas adsorption, 490–492
equations for adsorption isotherm, 369
equations for heat of adsorption, 370–373
equations for heat of immersion, 373–376
fixed, 458, 459
induced, 458, 459
of inorganic oxides, 414–415, 423–427
of oxide surfaces, 362–366
of water/oxide interface, 362–366
primary surface, 350
structural, 660
secondary surface, 350
Heterogeneous catalysis, 435
Homogeneous catalysis, 435
Inverse gas chromatography (IGC), 465, 517
determination of
acid–base interactions on surface, 466–468, 471–474
dispersive increment of surface free energy, 469–470, 480–482
specific component of free energy of adsorption, 470, 474
surface heterogeneity of solids, 495–500
determination of thermodynamic parameters, 517–519
of non-porous carbons, 530–531
of porous carbons, 519–530
of silicates, 533–534
different possibilities of using, 517
investigation
of liquid crystal layers on silica, 514–515
of long-chain alcohol films on silica, 505–513
of modified oxides by, 483–487
Kinetics
chemisorption on heterogeneous surface, 254–267
chemisorption on homogeneous surface, 254–257
of organic compounds chemisorption, 237 *et seq.*.
on oxide surface, 237 *et seq.*.
Liquid chromatography
of fullerenes, 899 *et seq.*
separation of fullerenes by, 900–903
stationary phases for, 210
Mechanism of adsorption
water vapour on oxides, 360–362
Micropore filling
analysis and control of, 577–589
cluster-mediated, 584
mechanism in inorganic sorbents, 573 *et seq.*
Monte Carlo simulation studies, 577
of supercritical gas, 589–596
Molecular layering method, 213 *et seq.*
physicochemical fundamentals, 213–214
technology and applications, 231–233
Numerical methods
of solving the integral equation of adsorption, 418–420
Phase transitions
first-order, 614
higher-order, 614
in adsorbed layers, 599, 743
in long-chain alcohol films on silica, 508, 513, 514
in molecular sieves, 11
order-disorder, 620
second-order, 440
Polyorganosiloxanes
adsorption of benzene, n-hexane, 293, 295

adsorption of metal ions, 292, 294, 297
methods of preparation, 287–291
modification by metal complexes, 294–296
physicochemical properties, 291–294
polyhydrosiloxanes, 151–152
silica with deposited layer of, 152–154
Porous glasses
affinity chromatography on modified, 49–51
hydrothermal treatment of, 51–53
methods of preparation, 32
pore size distribution of, 34–35
structure of, 33–36
surface chemistry of, 37–43
thermal treatment of, 44–49
with controlled porosity, 31 *et seq.*
Porous structure
of hydrated silica-coated activated carbon (CAC), 582–583
pore/core size distribution, 670
pore silica distribution, 667
Pressure swing adsorption, 574, 629, 643–645
condensation swing, 578
filling swing, 578
Silicates
clay minerals, 879 *et seq.*
excess isotherms on, 883–885
solid–liquid properties, 881–896
structural properties, 879–881
wetting enthalpy on, 883–885
zeolites, 892
adsorption on, 892–896
wetting on, 892–896
Size ratio parameter
definition, 730
molecular significance, 731
Soil
modelling the behaviour of, 850–853
reaction of ions with, 829 *et seq.*
Strontium hydroxyapatite
adsorption of carbon dioxide, 314–316
methods of preparation, 302
surface structure, 305–307
Supercritical fluid extraction
studies on, 23–28
Surface
Bernal, 336, 340
charge, 759–761, 799, 813, 814, 858
corrugated Bernal, 350
diffusion of reactant, 250
fractal, 461
gibbsite type, 779
heterogeneous
patchwise model of, 262, 263, 651, 750, 785
random model of, 262, 263, 651, 750, 785
various models, 258–260
homogeneous, 733, 758, 770
isoelectric point (iep), 758, 866–869
of metal oxides, 238
type of reaction sites, 236
point of zero change (pzc), 757, 769, 801, 813, 820, 831, 866–869
silica type, 775
Surface charge *see also* Surface
and surface potentials, 864
density, 9, 40, 864, 880
of oxides, 860–862
Surface phase capacity, 649
determination methods, 652, 881
Thermal swing adsorption, 629, 642–645
Thermogravimetric analysis, 650
linear program, 666
method, 664–667
quasi-isothermal program, 666
thermal adsorption, 665

STUDIES IN SURFACE SCIENCE AND CATALYSIS

Volume 1 **Preparation of Catalysts I.**Scientific Bases for the Preparation of Heterogeneous Catalysts. Proceedings of the First International Symposium, Brussels, October 14–17,1975
edited by **B. Delmon, P.A. Jacobs and G. Poncelet**

Volume 2 **The Control of the Reactivity of Solids.** A Critical Survey of the Factors that Influence the Reactivity of Solids, with Special Emphasis on the Control of the Chemical Processes in Relation to Practical Applications
by **V.V. Boldyrev, M. Bulens and B. Delmon**

Volume 3 **Preparation of Catalysts II.** Scientific Bases for the Preparation of Heterogeneous Catalysts. Proceedings of the Second International Symposium, Louvain-la-Neuve, September 4–7, 1978
edited by **B. Delmon, P. Grange, P. Jacobs and G. Poncelet**

Volume 4 **Growth and Properties of Metal Clusters.** Applications to Catalysis and the Photographic Process. Proceedings of the 32nd International Meeting of the Société de Chimie Physique, Villeurbanne, September 24–28, 1979
edited by **J. Bourdon**

Volume 5 **Catalysis by Zeolites.** Proceedings of an International Symposium, Ecully (Lyon), September 9–11, 1980
edited by **B. Imelik, C. Naccache, Y. Ben Taarit, J.C. Vedrine, G. Coudurier and H. Praliaud**

Volume 6 **Catalyst Deactivation.** Proceedings of an International Symposium, Antwerp, October 13– 15,1980
edited by **B. Delmon and G.F. Froment**

Volume 7 **New Horizons in Catalysis.** Proceedings of the 7th International Congress on Catalysis, Tokyo, June 30–July4, 1980. Parts A and B
edited by **T. Seiyama and K. Tanabe**

Volume 8 **Catalysis by Supported Complexes**
by **Yu.I. Yermakov, B.N. Kuznetsov and V.A. Zakharov**

Volume 9 **Physics of Solid Surfaces.** Proceedings of a Symposium, Bechyňe, September 29–October 3,1980
edited by **M. Láznička**

Volume 10 **Adsorption at the Gas–Solid and Liquid–Solid Interface.** Proceedings of an International Symposium, Aix-en-Provence, September 21–23, 1981
edited by **J. Rouquerol and K.S.W. Sing**

Volume 11 **Metal-Support and Metal-Additive Effects in Catalysis.** Proceedings of an International Symposium, Ecully (Lyon), September 14–16, 1982
edited by **B. Imelik, C. Naccache, G. Coudurier, H. Praliaud, P. Meriaudeau, P. Gallezot, G.A. Martin and J.C. Vedrine**

Volume 12 **Metal Microstructures in Zeolites.** Preparation - Properties – Applications. Proceedings of a Workshop, Bremen, September 22–24, 1982
edited by **P.A. Jacobs, N.I. Jaeger, P. Jirů and G. Schulz-Ekloff**

Volume 13 **Adsorption on Metal Surfaces.** An Integrated Approach
edited by **J. Bénard**

Volume 14 **Vibrations at Surfaces.** Proceedings of the Third International Conference, Asilomar, CA, September 1–4, 1982
edited by **C.R. Brundle and H. Morawitz**

Volume 15 **Heterogeneous Catalytic Reactions Involving Molecular Oxygen**
by **G.I. Golodets**

Volume 16 **Preparation of Catalysts III.** Scientific Bases for the Preparation of Heterogeneous Catalysts. Proceedings of the Third International Symposium, Louvain-la-Neuve, September 6–9, 1982
edited by **G. Poncelet, P. Grange and P.A. Jacobs**

Volume 17 **Spillover of Adsorbed Species.** Proceedings of an International Symposium, Lyon-Villeurbanne, September 12–16, 1983
edited by **G.M. Pajonk, S.J. Teichner and J.E. Germain**

Volume 18 **Structure and Reactivity of Modified Zeolites.** Proceedings of an International Conference, Prague, July 9–13, 1984
edited by **P.A. Jacobs, N.I. Jaeger, P. Jiřů, V.B. Kazansky and G. Schulz-Ekloff**

Volume 19 **Catalysis on the Energy Scene.** Proceedings of the 9th Canadian Symposium on Catalysis, Quebec, P.Q., September 30–October 3, 1984
edited by **S. Kaliaguine and A. Mahay**

Volume 20 **Catalysis by Acids and Bases.** Proceedings of an International Symposium, Villeurbanne (Lyon), September 25–27, 1984
edited by **B. Imelik, C. Naccache, G. Coudurier, Y. Ben Taarit and J.C. Vedrine**

Volume 21 **Adsorption and Catalysis on Oxide Surfaces.** Proceedings of a Symposium, Uxbridge, June 28–29, 1984
edited by **M. Che and G.C. Bond**

Volume 22 **Unsteady Processes in Catalytic Reactors**
by **Yu.Sh. Matros**

Volume 23 **Physics of Solid Surfaces 1984**
edited by **J. Koukal**

Volume 24 **Zeolites: Synthesis, Structure, Technology and Application.** Proceedings of an International Symposium, Portorož-Portorose, September 3–8, 1984
edited by **B. Držaj, S. Hočevar and S. Pejovnik**

Volume 25 **Catalytic Polymerization of Olefins.** Proceedings of the International Symposium on Future Aspects of Olefin Polymerization, Tokyo, July 4–6, 1985
edited by **T. Keii and K. Soga**

Volume 26 **Vibrations at Surfaces 1985.** Proceedings of the Fourth International Conference, Bowness-on-Windermere, September 15–19, 1985
edited by **D.A. King, N.V. Richardson and S. Holloway**

Volume 27 **Catalytic Hydrogenation**
edited by **L. Cervený**

Volume 28 **New Developments in Zeolite Science and Technology.** Proceedings of the 7th International Zeolite Conference, Tokyo, August 17–22, 1986
edited by **Y. Murakami, A. Iijima and J.W. Ward**

Volume 29 **Metal Clusters in Catalysis**
edited by **B.C. Gates, L. Guczi and H. Knözinger**

Volume 30 **Catalysis and Automotive Pollution Control.** Proceedings of the First International Symposium, Brussels, September 8–11, 1986
edited by **A. Crucq and A. Frennet**

Volume 31 **Preparation of Catalysts IV.** Scientific Bases for the Preparation of Heterogeneous Catalysts. Proceedings of the Fourth International Symposium, Louvain-la-Neuve, September 1–4, 1986
edited by **B. Delmon, P. Grange, P.A. Jacobs and G. Poncelet**

Volume 32 **Thin Metal Films and Gas Chemisorption**
edited by **P. Wissmann**

Volume 33 **Synthesis of High-silica Aluminosilicate Zeolites**
edited by **P.A. Jacobs and J.A. Martens**

Volume 34 **Catalyst Deactivation 1987.** Proceedings of the 4th International Symposium, Antwerp, September 29–October 1, 1987
edited by **B. Delmon and G.F. Froment**

Volume 35 **Keynotes in Energy-Related Catalysis**
edited by **S. Kaliaguine**

Volume 36 **Methane Conversion.** Proceedings of a Symposium on the Production of Fuels and Chemicals from Natural Gas, Auckland, April 27–30, 1987
edited by **D.M. Bibby, C.D. Chang, R.F. Howe and S. Yurchak**

Volume 37 **Innovation in Zeolite Materials Science.** Proceedings of an International Symposium, Nieuwpoort, September 13–17, 1987
edited by **P.J. Grobet, W.J. Mortier, E.F. Vansant and G. Schulz-Ekloff**

Volume 38 **Catalysis 1987.** Proceedings of the 10th North American Meeting of the Catalysis Society, San Diego, CA, May 17–22, 1987
edited by **J.W. Ward**

Volume 39 **Characterization of Porous Solids.** Proceedings of the IUPAC Symposium (COPS I), Bad Soden a. Ts., April 26–29,1987
edited by **K.K. Unger, J. Rouquerol, K.S.W. Sing and H. Kral**

Volume 40 **Physics of Solid Surfaces 1987.** Proceedings of the Fourth Symposium on Surface Physics, Bechyne Castle, September 7–11, 1987
edited by **J. Koukal**

Volume 41 **Heterogeneous Catalysis and Fine Chemicals.** Proceedings of an International Symposium, Poitiers, March 15–17, 1988
edited by **M. Guisnet, J. Barrault, C. Bouchoule, D. Duprez, C. Montassier and G. Pérot**

Volume 42 **Laboratory Studies of Heterogeneous Catalytic Processes**
by **E.G. Christoffel,** revised and edited by **Z. Paál**

Volume 43 **Catalytic Processes under Unsteady-State Conditions**
by **Yu. Sh. Matros**

Volume 44 **Successful Design of Catalysts.** Future Requirements and Development. Proceedings of the Worldwide Catalysis Seminars, July, 1988, on the Occasion of the 30th Anniversary of the Catalysis Society of Japan
edited by **T. Inui**

Volume 45 **Transition Metal Oxides.** Surface Chemistry and Catalysis
by **H.H. Kung**

Volume 46 **Zeolites as Catalysts, Sorbents and Detergent Builders.** Applications and Innovations. Proceedings of an International Symposium, Würzburg, September 4–8,1988
edited by **H.G. Karge and J. Weitkamp**

Volume 47 **Photochemistry on Solid Surfaces**
edited by **M. Anpo and T. Matsuura**

Volume 48 **Structure and Reactivity of Surfaces.** Proceedings of a European Conference, Trieste, September 13–16, 1988
edited by **C. Morterra, A. Zecchina and G. Costa**

Volume 49 **Zeolites: Facts, Figures, Future.** Proceedings of the 8th International Zeolite Conference, Amsterdam, July 10–14, 1989. Parts A and B
edited by **P.A. Jacobs and R.A. van Santen**

Volume 50 **Hydrotreating Catalysts.** Preparation, Characterization and Performance. Proceedings of the Annual International AIChE Meeting, Washington, DC, November 27–December 2, 1988
edited by **M.L. Occelli and R.G. Anthony**

Volume 51 **New Solid Acids and Bases.** Their Catalytic Properties
by **K. Tanabe, M. Misono, Y. Ono and H. Hattori**

Volume 52 **Recent Advances in Zeolite Science.** Proceedings of the 1989 Meeting of the British Zeolite Association, Cambridge, April 17–19, 1989
edited by **J. Klinowsky and P.J. Barrie**

Volume 53 **Catalyst in Petroleum Refining 1989.** Proceedings of the First International Conference on Catalysts in Petroleum Refining, Kuwait, March 5–8, 1989
edited by **D.L. Trimm, S. Akashah, M. Absi-Halabi and A. Bishara**

Volume 54 **Future Opportunities in Catalytic and Separation Technology**
edited by **M. Misono, Y. Moro-oka and S. Kimura**

Volume 55 **New Developments in Selective Oxidation.** Proceedings of an International Symposium, Rimini, Italy, September 18–22, 1989
edited by **G. Centi and F. Trifiro**

Volume 56 **Olefin Polymerization Catalysts.** Proceedings of the International Symposium on Recent Developments in Olefin Polymerization Catalysts, Tokyo, October 23–25, 1989
edited by **T. Keii and K. Soga**

Volume 57A **Spectroscopic Analysis of Heterogeneous Catalysts. Part A: Methods of Surface Analysis**
edited by **J.L.G. Fierro**

Volume 57B **Spectroscopic Analysis of Heterogeneous Catalysts. Part B: Chemisorption of Probe Molecules**
edited by **J.L.G. Fierro**

Volume 58 **Introduction to Zeolite Science and Practice**
edited by **H. van Bekkum, E.M. Flanigen and J.C. Jansen**

Volume 59 **Heterogeneous Catalysis and Fine Chemicals II.** Proceedings of the 2nd International Symposium, Poitiers, October 2–6, 1990
edited by **M. Guisnet, J. Barrault, C. Bouchoule, D. Duprez, G. Pérot, R. Maurel and C. Montassier**

Volume 60 **Chemistry of Microporous Crystals.** Proceedings of the International Symposium on Chemistry of Microporous Crystals, Tokyo, June 26–29, 1990
edited by **T. Inui, S. Namba and T. Tatsumi**

Volume 61 **Natural Gas Conversion.** Proceedings of the Symposium on Natural Gas Conversion, Oslo, August 12–17, 1990
edited by **A. Holmen, K.-J. Jens and S. Kolboe**

Volume 62 **Characterization of Porous Solids II.** Proceedings of the IUPAC Symposium (COPS II), Alicante, May 6–9, 1990
edited by **F. Rodríguez-Reinoso, J. Rouquerol, K.S.W. Sing and K.K. Unger**

Volume 63 **Preparation of Catalysts V.** Scientific Bases for the Preparation of Heterogeneous Catalysts. Proceedings of the Fifth International Symposium, Louvain-la-Neuve, September 3–6, 1990
edited by **G. Poncelet, P.A. Jacobs, P. Grange and B. Delmon**

Volume 64 **New Trends in CO Activation**
edited by **L. Guczi**

Volume 65 **Catalysis and Adsorption by Zeolites.** Proceedings of ZEOCAT 90, Leipzig, August 20–23, 1990
edited by G. **Öhlmann, H. Pfeifer and R. Fricke**

Volume 66 **Dioxygen Activation and Homogeneous Catalytic Oxidation.** Proceedings of the Fourth International Symposium on Dioxygen Activation and Homogeneous Catalytic Oxidation, Balatonfüred, September 10–14, 1990
edited by **L.I. Simándi**

Volume 67 **Structure-Activity and Selectivity Relationships in Heterogeneous Catalysis.** Proceedings of the ACS Symposium on Structure-Activity Relationships in Heterogeneous Catalysis, Boston, MA, April 22–27, 1990
edited by **R.K. Grasselli and A.W. Sleight**

Volume 68 **Catalyst Deactivation 1991.** Proceedings of the Fifth International Symposium, Evanston, IL, June 24–26, 1991
edited by **C.H. Bartholomew and J.B. Butt**

Volume 69 **Zeolite Chemistry and Catalysis.** Proceedings of an International Symposium, Prague, Czechoslovakia, September 8–13, 1991
edited by **P.A. Jacobs, N.I. Jaeger, L. Kubelková and B. Wichterlová**

Volume 70 **Poisoning and Promotion in Catalysis based on Surface Science Concepts and Experiments**
by **M. Kiskinova**

Volume 71 **Catalysis and Automotive Pollution Control II.** Proceedings of the 2nd International Symposium (CAPoC 2), Brussels, Belgium, September 10–13, 1990
edited by **A. Crucq**

Volume 72 **New Developments in Selective Oxidation by Heterogeneous Catalysis.** Proceedings of the 3rd European Workshop Meeting on New Developments in Selective Oxidation by Heterogeneous Catalysis, Louvain-la-Neuve, Belgium, April 8–10, 1991
edited by **P. Ruiz and B. Delmon**

Volume 73 **Progress in Catalysis.** Proceedings of the 12th Canadian Symposium on Catalysis, Banff, Alberta, Canada, May 25–28, 1992
edited by **K.J. Smith and E.C. Sanford**

Volume 74 **Angle-Resolved Photoemission. Theory and Current Applications**
edited by **S.D. Kevan**

Volume 75 **New Frontiers in Catalysis, Parts A-C.** Proceedings of the 10th International Congress on Catalysis, Budapest, Hungary, 19–24 July, 1992
edited by **L. Guczi, F. Solymosi and P. Tétényi**

Volume 76 **Fluid Catalytic Cracking: Science and Technology**
edited by **J.S. Magee and M.M. Mitchell, Jr.**

Volume 77 **New Aspects of Spillover Effect in Catalysis. For Development of Highly Active Catalysts.** Proceedings of the Third International Conference on Spillover, Kyoto, Japan, August 17–20, 1993
edited by **T. Inui, K. Fujimoto, T. Uchijima and M. Masai**

Volume 78 **Heterogeneous Catalysis and Fine Chemicals III.**
Proceedings of the 3rd International Symposium, Poitiers, April 5 - 8, 1993
edited by **M. Guisnet, J. Barbier, J. Barrault, C. Bouchoule, D. Duprez, G. Pérot and C. Montassier**

Volume 79 **Catalysis: An Integrated Approach to Homogeneous, Heterogeneous and Industrial Catalysis**
edited by **J.A. Moulijn, P.W.N.M. van Leeuwen and R.A. van Santen**

Volume 80 **Fundamentals of Adsorption.** Proceedings of the Fourth International Conference on Fundamentals of Adsorption, Kyoto, Japan, May 17–22, 1992
edited by **M. Suzuki**

Volume 81 **Natural Gas Conversion II.** Proceedings of the Third Natural Gas Conversion Symposium, Sydney, July 4–9, 1993
edited by **H.E. Curry-Hyde and R.F. Howe**

Volume 82 **New Developments in Selective Oxidation II.** Proceedings of the Second World Congress and Fourth European Workshop Meeting, Benalmádena, Spain, September 20–24, 1993
edited by **V. Cortés Corberán and S. Vic Bellón**

Volume 83 **Zeolites and Microporous Crystals.** Proceedings of the International Symposium on Zeolites and Microporous Crystals, Nagoya, Japan, August 22–25, 1993
edited by **T. Hattori and T. Yashima**

Volume 84 **Zeolites and Related Microporous Materials: State of the Art 1994.**
Proceedings of the 10th International Zeolite Conference, Garmisch-Partenkirchen, Germany, July 17–22, 1994
edited by **J. Weitkamp, H.G. Karge, H. Pfeifer and W. Hölderich**

Volume 85 **Advanced Zeolite Science and Applications**
edited by **J.C. Jansen, M. Stöcker, H.G. Karge and J.Weitkamp**

Volume 86 **Oscillating Heterogeneous Catalytic Systems**
by **M.M. Slin'ko and N.I. Jaeger**

Volume 87 **Characterization of Porous Solids III.** Proceedings of the IUPAC Symposium (COPS III), Marseille, France, May 9–12, 1993
edited by **J.Rouquerol, F. Rodriguez-Reinoso, K.S.W. Sing and K.K. Unger**

Volume 88 **Catalyst Deactivation 1994.** Proceedings of the 6th International Symposium, Ostend, Belgium, October 3–5, 1994
edited by **B. Delmon and G.F. Froment**

Volume 89 **Catalyst Design for Tailor-made Polyolefins.** Proceedings of the International Symposium on Catalyst Design for Tailor-made Polyolefins, Kanazawa, Japan, March 10–12, 1994
edited by **K. Soga and M. Terano**

Volume 90 **Acid-Base Catalysis II.** Proceedings of the International Symposium on Acid-Base Catalysis II, Sapporo, Japan, December 2–4, 1993
edited by **H. Hattori, M. Misono and Y. Ono**

Volume 91 **Preparation of Catalysts VI.** Scientific Bases for the Preparation of Heterogeneous Catalysts. Proceedings of the Sixth International Symposium, Louvain-La-Neuve, September 5–8, 1994
edited by **G. Poncelet, J. Martens, B. Delmon, P.A. Jacobs and P. Grange**

Volume 92 **Science and Technology in Catalysis 1994.** Proceedings of the Second Tokyo Conference on Advanced Catalytic Science and Technology, Tokyo, August 21–26, 1994
edited by **Y. Izumi, H. Arai and M. Iwamoto**

Volume 93 **Characterization and Chemical Modification of the Silica Surface**
by **E.F. Vansant, P. Van Der Voort and K.C. Vrancken**

Volume 94 **Catalysis by Microporous Materials.** Proceedings of ZEOCAT'95, Szombathely, Hungary, July 9–13, 1995
edited by **H.K. Beyer, H.G.Karge, I. Kiricsi and J.B. Nagy**

Volume 95 **Catalysis by Metals and Alloys**
by **V. Ponec and G.C. Bond**

Volume 96 **Catalysis and Automotive Pollution Control III.** Proceedings of the Third International Symposium (CAPoC3), Brussels, Belgium, April 20-22, 1994
edited by **A. Frennet and J.-M. Bastin**

Volume 97 **Zeolites: A Refined Tool for Designing Catalytic Sites.** Proceedings of the International Symposium, Québec, Canada, October 15-20, 1995
edited by **L. Bonneviot and S. Kaliaguine**

Volume 98 **Zeolite Science 1994: Recent Progress and Discussions.** Supplementary Materials to the 10th International Zeolite Conference, Garmisch-Partenkirchen, Germany, July 17-22, 1994
edited by **H.G. Karge and J.Weitkamp**

Volume 99 **Adsorption on New and Modified Inorganic Sorbents**
edited by **A. Dąbrowski and V.A. Tertykh**